APCOM

MINING GOES DIGITAL

Editors:
Christoph Mueller
Winfred Assibey-Bonsu
Ernest Baafi
Christoph Dauber
Chris Doran
Marek Jerzy Jaszczuk
Oleg Nagovitsyn

MINING GOES DIGITAL

Proceedings in Earth and geosciences series

Volume 3

Mining Goes Digital

Editors

Christoph Mueller
MT-Silesia Sp. z o.o. Wroclaw, Poland

Winfred Assibey-Bonsu
Gold Fields Ltd., Perth, Australia

Ernest Baafi
University of Wollongong, Australia

Christoph Dauber
Technische Hochschule Georg Agricola, Bochum, Germany

Chris Doran
Mitacom Pty Ltd., Brisbane, Australia

Marek Jerzy Jaszczuk
Silesian University of Technology, Gliwice, Poland

Oleg Nagovitsyn
Kola Research Institute, Russian Federation

Table of contents

Mine planning in digital transformation

Mine operation and equipment

Mine safety in digital transformation

IoT and robotics

Emerging technology and synergies from other industries

Preface

The abbreviation "APCOM" stands for "*Applications for Computers and Operations Research in the Minerals Industry*". When the conference started in 1964, it was an informal meeting of scientists from different universities in the USA together with the "Society of Mining Engineers" (SME) of the United States. During the years the APCOM conference was performed in a mostly bi-annual rhythm. Up to today APCOM maintained its original logo formed around a punch card clearly remembering the historic origin of the conference from the times prior to the revolution caused by the era of semiconductors.

In the beginning, APCOM focused on the optimization of geostatistics and resource estimation and a number of methods used in these fields were initially presented and discussed on APCOM conferences. This field still today is an important part of any APCOM.

During the years, information technology has dramatically developed, new algorithmic methods evolved and the entire fields of electronic communication, machine automation, autonomous machines and process optimization developed. Consequently, today, APCOM is much more than a meeting of specialists in geostatistics and resource estimation: The APCOM has expanded to a conference covering all kinds of Information and Communication Technology in the mineral industry: Already in 2005 on the conference in Tuscon/AZ, the term "Mining Process Optimization" was presented as the next paradigm shift in mining after mechanization and automation, which marked another example of the continued innovative impact of the APCOM. Well ahead of the current discussions about "Digital Transformation".

In this tradition the 39th APCOM 2019 is performed in Wroclaw (Poland), a town with innovative tradition from the early times of industrialization when the town was German Breslau. A few examples can only give a glimpse of the importance of the town's historic industrial and academic achievements:

- 10 Nobel prize winners (out of 102 Germans) were born or working in Breslau.
- The first publicly owned electric power station in Germany went in operation in 1882.
- Electric public trams were introduced 1892.
- The world's biggest free span concrete hall ("Jahrhunderthalle" – "Hala Stulecia") was built in 1912 (it is an Unesco world cultural heritage site today).
- Diesel electric fast trains "Flying Silesian" featuring a top speed of 205 km/h were developed 1935 at Linke-Hoffmann Werke in Breslau, running abt. 500 km Berlin-Bytom (Beuthen) in 4 hrs 17 min!

Today Wroclaw again is a leading innovation hub in Middle-Eastern Europe hosting the internationally highly acknowledged Wroclaw University of Technology. A large number of big and small innovative companies are active not only in the area of Information and Communication Technology, but also in Chemistry, Biotechnology and Engineering. World known names like Google, Nokia, IBM, Bombardier or Volvo Buses are just few examples. Also KGHM as a world leading copper producer operates a research center in the city.

In this tradition the 39th APCOM conference titled "Mining Goes Digital" presents innovative IT related papers from Resource estimation and geostatistics, Mine Planning, Robotics, equipment automation, autonomous guidance and many other integrative aspects of digital transformation in the minerals industry. A few papers also provide inputs from other industries into the mining community to create potential synergies. This evolution of the APCOM from its origins in resource estimation to a general mining IT related conference

also emphasizes the importance of a holistic view on the optimization of the overall mining operations from the resource to the preparation plant in the era of digital transformation.

In this view, the APCOM conference in Wroclaw also marks a change in the appearance of the conference logo: The original APCOM logo was changed slightly: The attentive reader may have observed that the original punchcard was exchanged by a more up-to-date symbolic PCB layout and an upgraded font set. So the APCOM can be recognized as "the" leading international event for Information Technology in mining for many years to come.

Dr. Christoph Mueller
Chairman of the 39th APCOM 2019

Editors

Dr. Christoph Mueller

Dr. Christoph Mueller, born 1963, after his engineering studies and an additional education in technical software engineering at Siemens got his PhD in Electronics and Telecommunications.

Since 1992 Christoph Mueller works mainly with automation projects for mobile machinery in the raw material industries. From 1997 he is operating his own companies specialized on successfully turning innovations into operational benefits in major mining process optimization and machine automation projects. Currently, these companies in Germany and Poland are working mainly with functional safe machine automation, driver assistance systems and autonomous operation in areas as mining and tunneling, agriculture or airport equipment.

Dr. Winfred Assibey-Bonsu BSc(Mining); PhD(Eng) Wits Univ.; EDP, Wits Business School, FSAIMM, MSACNASP

Current Position: Group Geostatistician and Evaluator, Gold Fields Ltd, Corporate Technical Services, Perth, Australia.

Employment post PhD studies; Gold Fields of South Africa, 1991 to 1994; Gencor Limited, 1994 to 1998; Gold Fields Limited, 1998 to date.

Winfred's experience includes mineral resource assets assessment for mining companies as well as new business associated work including prospects in South Africa, Australia, South America, Zaire, Ghana, Ivory Coast, Philippines, Ethiopia, Tanzania, Cuba, Dominican Republic, Russia, Finland, Romania, Papua New Guinea.

Winfred is a dedicated family man with wife and four children. He enjoys reading and soccer.

Dr. Ernest Baafi

Ernest Yaw Baafi holds PhD in Mining Engineering from University of Arizona, MS in Mining Engineering from Penn State University, US and BE, ACSM from Camborne School of Mines, Cornwall, UK. He is Associate Professor in Mining at University of Wollongong, Australia where he is currently the Academic Program Director in Mining Engineering. His primary field of research is the application of computers and operations research methodologies to system evaluation and design. His current research activities include geostatistical ore reserve estimation, mine system simulation, logistics and optimisation. He is the current Chair of the International Council of Application of Computers and Operations Research in the Minerals Industry (APCOM), representing the Australasian Institute of Mining and Metallurgy (AusIMM) on the Council.

Prof. Dr. Christoph Dauber

Born in 1954, Prof. Dauber has studied Mining Engineering at the RWTH Aachen, where he obtained his Ph.D. about refrigeration techniques for deep hard coal mines. 1982 he joined RAG, the biggest hard coal mining company in Germany, and started as a deputy and undermanager. An exchange of engineers gave him the opportunity to work for six month in two Australian coal mines. Seven years he acted as the production manager of the hard coal mines Ewald and Walsum, before he joined the central technical department. Being the responsible manager for central technical support and supply he initiated and accompanied

a couple of operational innovations. 2008 he become a professor at the THGA in the field of mining technology. Additionally he held the position of a Vice President responsible for research and development. Since 2015 he works as a part-time professor for the THGA.

Dr. Chris Doran

Dr. Chris Doran is a Mining Technology Consultant at Mitacom, a company specialising in technology services related to mobile equipment safety and automation for minerals and resource industry clients in Australia, Southern Africa and South America, including development of requirements for collision avoidance and introduction of advanced technologies and automation systems into mining operations. Dr. Doran is a key participant in several industry programs to improve mobile equipment safety, promote interoperability, a driving innovation between mining houses, mobile equipment manufacturers (OEMs) and technology providers. He is also an active contributor to the development of national and international standards for safety and interoperability in the field of earthmoving and mining.

Prof. Dr. Marek Jerzy Jaszczuk

Professor Marek Jaszczuk PhD, DSc is employed at the Department of Mining Mechanization and Robotics of the Faculty of Mining and Geology of the Silesian University of Technology in Gliwice, Poland. His subject covers issues related to the identification of external and internal loads of mining machinery, especially shearer-loaders, armored face conveyors and hydraulic roof supports, as well as the interaction of mining machines with their natural environment. He is the author and co-author of original mathematical models and software for computer-aided design of cutting drums for longwall shearers and multi-criteria optimization of design features of the hydraulic roof supports. For the solutions resulting from the research he and his team won the Team Award of the Prime Minister for the outstanding national scientific and technical achievement and the 1st degree Award of the Minister of Labour and Social Policy. They have also been awarded medals of prestigious innovation exhibitions at home and abroad, including: Warsaw, Brussels, Nuremberg, Seoul, Kuala Lumpur and SuZhou.

He is the author and co-author of 4 academic textbooks, 5 monographs, over 90 articles in domestic and foreign journals, over 50 papers delivered at national and international conferences and the scientific editor of 5 monographs. He gained 15 patents for innovative solutions.

Oleg Nagovitsyn, Dr. Eng.

Oleg Nagovitsyn, Dr. Eng. is Deputy Director of the Mining institute of the Kola Science Centre of the Russian Academy of Sciences.

Oleg Nagovitsyn's scientific activity is connected with the studies aimed at development of the software which realizes the functions of a mining-and-geological information system for the mining and mineral processing. The geo-information system is based on the application of subject-oriented databases, visualization and integration; spatially related geological, technological, geophysical, geomechanical and monitoring data which form a single geo-information space of the mining and processing enterprise. The practical significance of the studies lies in the fact that the developed software, educational and methodological materials realize the computer technology of geological modeling, design and planning of mining operations.

Committees

SCIENTIFIC COMMITTEE

Marek Andrzejewski, *Director Energomechanical Department, KGHM Polska Miedź S.A. (PL)*
Małgorzata Malec, Ph.D. Eng., *KOMAG Institute of Mining Technology, Gliwice (PL)*
Prof. Dr hab. Wojciech Moczulski, *Silesian University of Technology, Gliwice (PL)*
Prof. Dr. Jürgen F. Brune P.E., *QP, Colorado School of Mines (US)*
Prof. Józef Jonak, Phd, DSc (Eng), *Lublin University of Technology (PL)*
Prof. Krzysztof Tchon, *Professor of Control Engineering and Robotics, Wroclaw University of Technology (PL)*
Prof. Teresa Orłowska-Kowalska, D.Sc., Ph.D., *Wroclaw University of Technology (PL)*
Professor Marek Jerzy Jaszczuk Ph.D., Dsc, *Silesian University of Technology, Gliwice (PL)*
Dr. hab. inż. Anna Timofiejczuk, *Professor of Silesian University of Technology (PL)*
Prof. dr hab. inż. Bogdan Miedziński, *Electrical Department, Wroclaw University of Technology (PL)*
Dr. hab. inż. Jan Blachowski, *Faculty of Geoengineering, Mining and Geology, Wroclaw University of Technology (PL)*
Prof. dr hab. inż. Jan Palarski, *Professor of Mining Engineering, a head of The Chair of Clean Mining Technologies, The Technical University of Silesia (PL)*
Dr. inż. Jerzy Kicki, *AGH (PL)*
Krzysztof Stankiewicz, Ph.D. Eng., *KOMAG Institute of Mining Technology, Gliwice (PL)*
Prof. dr hab. inż. Piotr Dudziński, *Department of Mechanical Engineering, Wrocław Univeristy of Technology (PL)*
Dr. Sukumar Bandopadhyay, *Professor of Mining Engineering at the University of Alaska Fairbanks (US)*
Dr. hab. inż. Violetta Sokola-Szewioła, *Professor at Silesian University of Technology (PL)*
Dr. hab. inż. Radosław Zimroz, *Professor of Faculty of Geoengineering, Mining and Geology, Wroclaw University of Technology (PL)*
Dr. Ernest Baafi, *University of Wollongong (AUS)*
Dr. Hooman Askari-Nasab, *University of Alberta (CA)*
Javad Sattarvand, *University of Nevada, Reno (US)*
Kadri Dagdelen, Ph.D., *Colorado School of Mines, Mining Engineering (US)*
Prof. Roussos Dimitrakopoulos, *McGill University (CA)*
Prof. Dr.-Ing. Oliver Langefeld, *TU Clausthal (DE)*
Prof. dr hab. inż. Monika Hardygóra, *Faculty of Geoengineering, Mining and Geology, Wroclaw University of Technology (PL)*
Dr hab. inż. Jan Kudełko, *Faculty of Geoengineering, Mining and Geology, Wroclaw University of Technology (PL)*
Prof. dr hab. inż. Andrzej Typiak, *Faculty of Mechanical Engineering, Military University of Technology | WAT (PL)*
Professor Håkan Schunnesson, *Luleå University of Technology, Sweden*
Dr. Sean Dessureault, *Entrepreneur and Innovation Evangelist, USA*

INTERNATIONAL COMMITTEE

Andrzej H. (Andrew) Issel, *Director Resource Estimation & Reporting, Freeport McMoRan Inc. (USA)*

Claudia Haney, *Senior Manager Accenture Strategy – Resources (DE)*

Prof. Dr. Christoph Dauber, *Mining and Mineral Resources, Technical University Georg Agricola, Bochum (DE)*

Ernesto Vivas, *Hexagon Mining*

K.H. Wennmohs, *(DE)*

Klaus Boede, *Hochtief Polska (PL)*

Oleg Nagovitsyn, *Kola Research Institute (RUS)*

Jörgen Appelgren, *Epiroc (S)*

Claudia Monreal, *Core MiningStudies (CDN)*

Peter Salditt, *President Underground Mining, Komatsu (USA)*

Dr. Chris Doran, *Managing Director, Mitacom Pty Ltd., Brisbane (AUS)*

PAPER PEER REVIEWERS

Lawrence E. Allen, *Senior Director Resource Modeling Technology, Newmont Mining Corporation, USA*

Dr. Hooman Askari-Nasab, *University of Alberta, Canada*

Dr. Winfred Assibey-Bonsu, *Corporate Technical Services, Gold Fields Ltd., Perth, Australia*

Dr. Mehala Balamurali, *Reserach Fellow, Australian Centre for Field Robotics, University of Sydney, Australia*

Prof. Dr. Jürgen F. Brune P.E., *QP, Colorado School of Mines, USA*

Dr. Ernest Baafi, *University of Wollongong, Australia*

Dr. Jacqui Coombes, *Head of Innovation, Snowden Group, USA*

Kadri Dagdelen, Ph.D., *Colorado School of Mines, Mining Engineering, USA*

Dr. Sean Dessureault, *Entrepreneur and Innovation Evangelist, USA*

Prof. Dr. Christoph Dauber, *Technical University Georg Agricola, Bochum, Germany*

Dr. Chris Doran, *Managing Director, Mitacom Pty Ltd, Brisbane Australia*

Claudia Haney, *Senior Manager Accenture Strategy – Resources, Germany*

Andrew Issel, *Director Resource Estimation & Reporting – PTFI, Freeport McMoRan Inc., USA*

Professor Marek Jerzy Jaszczuk Ph.D., Dsc, *Silesian University of Technology, Gliwice, Poland*

Prof. Dr.-Ing. Oliver Langefeld, *TU Clausthal*

Oleg Nagovitsyn, *Kola Research Institute, Russian Federation*

Arja Jewbali, *Senior Director Resource Modeling Services, Newmont Mining Corporation, USA*

Dipl. Ing. Christoph Mueller Ph.D., *MT-Silesia Sp. z o.o., Poland*

Harry Parker, *Consulting Mining Geologist and Geostatistician, Wood plc*

Professor Håkan Schunnesson, *Luleå University of Technology, Sweden*

Dr hab. inż. Violetta Sokola-Szewioła, *Professor at Silesian University of Technology, Poland*

Prof. Krzysztof Tchon, *Professor of Control Engineering and Robotics, Politechnica Wroclawska, Poland*

Prof. dr hab. inż. Andrzej Typiak, *Faculty of Mechanical Engineering, Military University of Technology | WAT, Poland*

Prof. Dr hab. Wojciech Moczulski, *Silesian University of Technology, Gliwice, Poland*

LOCAL ORGANIZATION TEAM

Dipl. Ing. Christoph Mueller Ph.D., *MT-Silesia Sp. z o.o. (PL)*

Pola Cybulska, *MT-Silesia Sp. z o.o. (PL)*

Szymon Kochanik, *MT-Silesia Sp. z o.o. (PL)*

Monika Oleksyszyn, *MT-Silesia Sp. z o.o. (PL)*

Rafal Sztandera, *MT-Silesia Sp. z o.o. (PL)*

THE APCOM COUNCIL

Dr. Kadri Dagdelen, *Representing Colorado School of Mines, USA*

Dr. Ernest Baafi, *Representing Australasian Institute of Mining and Metallurgy, Australia*

Dr. Sukumar Bandopadhyay, *Representing Society of Mining, Metallurgy and Exploration, Inc., USA*

Dr. Victor Tenorio, *Representing University of Arizona, USA*

Dr. Christina Dohm, *Representing South African Institute of Mining and Metallurgy, South Africa*

Dr. Roussos Dimitrakopoulos, *Representing Canadian Institute of Mining, Metallurgy and Petroleum, Canada*

Dr. Antonio Nieto, *Representing University of Witwatersrand, South Africa*

Dr. Julia Ortiz, *Representing Queens University in Ontario, Canada*

Dr. Andrej Sublj, *Representing Institute of Mining, Geotechnology and Environment, Slovenia*

Dr. Wang Yuehan, *Representing China University of Technology, China*

Dr. Joao Felipe Costa, *Representing Universidade Federal do Rio Grande do Sul (UFRGS), Porto Alegre, Brazil*

Sponsors

SILVER

COPPER

ORGANIZERS

A-LA-CARTE SPONSORS

SUPPORTERS

Society of Mining Professors
Societät der Bergbaukunde

IREDES KOMAG HOCHTIEF

Wrocław University of Science and Technology PAN POLSKA AKADEMIA NAUK Politechnika Śląska

MEDIA PARTNERS

IM INTERNATIONAL MINING Inżynieria Górnicza KWARTALNIK SPECJALISTYCZNY GEORESOURCES Portal for Mining, Tunnelling, Geotechnics and Equipment

General aspects of digital transformation in mining

The so-called "Green Paradox"

Ansgar B. Bendiek
HOCHTIEF PPP Solutions GmbH, Germany

Maximilian P. Bendiek
Technical University Clausthal, Germany

ABSTRACT: Global warming is rising; humanity must act urgently. Some countries have limited their CO_2 emissions through the Kyoto Protocol. Despite this, projections for global CO_2 emissions are to go up in 2018 by 2.7%. In the so-called "Green Paradox", Sinn 2012 is promoting a supply side approach to reduce global warming. The temporal allocation of resource production is a portfolio optimization issue. The basic assumption made by Sinn is that resource owners behave as described by Hotelling, 1931. For the world petroleum market, it is being demonstrated that only the behavior of a part of the producers (e.g. Saudi Arabia) can be explained by the theory established by Hotelling. Therefore, the supply side approach outlined by Sinn, a tax on oil production, which is now high and declines over time, would incentivizes a constant increase in the oil production, which would increase CO_2 emission further.

1   INTRODUCTION

The Global warming is rising; humanity must act urgently. Some countries have limited their CO_2 emissions through the Kyoto Protocol. Despite this, projections for global CO_2 emissions are to go up in 2018 by 2.7%. In 2017, they increased by 1.6%, having flattened out between 2014 and 2016. The reasons? The use of oil and gas keeps growing, and some countries are still using coal to fuel much of their economic growth (Figueres, 2018). The Global Carbon Project released the findings on 5 December at the 24th Conference of the Parties to the United Nations Framework Convention on Climate Change (COP24) in Katowice.

In the so-called "Green Paradox" (Sinn 2012), Sinn deals with a solution to global warming. He describes what is generally acknowledged, the reduction in demand for fossil energy in the Kyoto countries has resulted in a temporary reduction in the world market price and caused an increase in demand in those states (US and China) that do not reduce emissions. The obvious solution would be a reduction in CO_2 emissions by a global CO_2 tax on the demand side (as it is poorly practiced in the EU).

However, Sinn is promoting a supply side approach. His argument is that ultimately the resource owners determine how much carbon is produced. To reduce CO_2 emissions, the production volumes must be shifted into the future. The temporal allocation of resource production is a portfolio optimization issue. He proposes some measures so that resource owners will reduce their production volumes today and shift it into the future. The main measure is a tax that should be high today and being reduced over time. This makes it more attractive for the resource owners to reduce their production today and benefit from higher prices in the future. The underlying concept is that of a warehouse.

For the most important market for fossil energy, the world petroleum market, it is investigated whether the resource owners behave as described by (Hotelling, 1931), which is the basic assumption made by Sinn. It is being demonstrated that only the behavior of a part of the producers (e.g. Saudi Arabia) can be explained by the theory established by Hotelling.

It is shown that, marginal cost providers (US shale oil producers) that are crucial for price setting do not behave as described by Hotelling.

The marginal cost providers increase their supply today and in the future with an increasing oil price (positive supply elasticity). The Hotelling calculus, taking less from the "warehouse" today, and selling these quantities later (negative supply elasticity), is not a concept being observed for them. Therefore, the supply side approach outlined by Sinn, a tax on oil production, which is now high and declines over time, would incentivize a constant increase in the oil production, which would increase CO_2 emission further.

2 THE HOTELLING RULE

Resource owners are faced with the alternative of leaving their assets as carbon in the soil or mining the resource and investing the resulting surpluses in the capital market. As fossil fuels become increasingly scarce as production progresses, untouched resources are becoming more and more valuable: the resources therefore generate a return in the form of ongoing increases in value. On the other hand, there is the capital market return if the resource is mined today and the proceeds are invested on the capital market. This consideration goes back to the fundamental work of the American economist Hotelling in 1931. Sinn assumes that all resource owners follow this simple decision-making principle.

3 RESOURCE ECONOMICS

The basic model for the economic theory of exhaustible resources, which was used both as an explanatory approach to the behavior of non-renewable resource providers and to explain and forecast the price of oil, was developed by (Hotelling, 1931) and has since been empirically tested, criticized and further developed many times.

In its basic model, Hotelling considered the production decisions of raw material producers over time. Their goal is to maximize the present value of their current and future profits from producing the resource in the deposit.

The time path of the price development results from the producer's decisions regarding the production volume. The producer can invest the yields generated by the current production (p0 per unit produced) on the market at the market interest rate and receives $p0 \times (1 + r)$ monetary units from this in the following period. If the following applies to the price of the raw material in the next period: $p1 = p0 \times (1 + r)$, the producer would be indifferent between today's and tomorrow's production. If, on the other hand, $p1 < p0 \times (1 + r)$ applies, the producer will opt for today's production because it will generate higher profits than tomorrow's production. However, if all suppliers behave accordingly and already produce today, the supply of the corresponding raw material would increase and today's price (p0) would fall.

According to (Watkins, 2006) and (Fattouh, 2007), the Hotelling model is primarily suitable for analyzing the production strategy of individual oil suppliers rather than the overall market.

(Anderson, Kellogg, & Salant, 2014) showed that the actual production decisions of oil producers in Texas and, accordingly, the production volumes there as a whole cannot be explained by the theory of Hotelling.

(Adelman, 1990) in turn rejected Hotelling's assumption of a static resource stock. Instead, in his model he took into account increases in recoverable reserves through investments in the further development of already developed resources and the exploration and development of new resources. According to his model, price development depends less on the scarcity rent than on the development of marginal costs, the replacement of old resources by new ones.

(von Wahl, 1991) shows that, in accordance with the theorem of cost theory, the development of new resources leads to an increase in the optimal size of the operation and thus in the production volume as marginal revenues rise.

4 THE SO-CALLED "GREEN PARADOX"

(Stern, 2006) has argued that policymakers should try to slow climate change on the demand side through a carbon tax, i.e. a tax on carbon input and output.

However, this assumption is according to (Sinn H.-W., 2008) far away from reality. How supply really reacts to demand reductions depends on the intertemporal decision calculation of resource owners, and this has little to do with the static supply reactions found in reproducible goods.

If the extraction costs are negligible, so that the Hotelling rule applies (rate of price increase = interest), the absolute price wedge rises accordingly at a rate equal to the interest rate, which implies its constancy in present values. Consequently, there is no variation in the extraction path (Sinn H.-W., 2008). Therefore, with negligible extraction costs, a constant value tax will have no effect on fossil fuel consumption.

But it is unlikely that governments will agree to levy a value tax at a constant rate. What if resource owners expect the tax rate to rise over time due to increasing temperatures and public awareness of CO_2 emissions? As it was shown in (Sinn H.-W., 1982), in this case they will increase their sales in the present to escape the future tax burden. Climate change will therefore accelerate, a phenomenon that could be described as a "green paradox" (Sinn H.-W., 2008).[1]

In sum, Sinn comes to the conclusion that since demand policy is ineffective in its current form because it makes completely unrealistic assumptions about supply, the question arises as to what effective policy measures look like. Such policy measures must be derived with explicit consideration of the temporal dimension of supply decisions.

5 STRUCTURE OF THE WORLD OIL MARKET

Today, the world's oil reserves are almost entirely in the hands of National Oil Companies (NOCs). In 2007, 88 percent of the world's oil reserves were controlled by NOCs. In contrast, private oil companies (Investor Owned Companies, IOC) had access to about 6 percent of the world's oil sources.

Until the first oil price crisis in 1973 (Mineralölwirtschaftsverband e.V., 2013), a few multinational, private-sector companies from western industrial countries held a high market share on the global oil market. After the expiry of the license agreements and the nationalization of the oil reserves as well as a substantial increase in the proven oil reserves, the situation shifted decisively. Access to oil is now almost completely (2007: 88 percent) controlled by states or state-owned enterprises, so-called NOCs, in the countries in whose territory the oil reserves are located. Only around 6 percent of the world's oil reserves are still available to the IOCs for production through licensing agreements. Another up to 10 percent of the oil reserves controlled by the NOC are negotiable in principle within the framework of joint ventures between the IOC and the NOC.

Table 1.   Access to oil resources in 1970 and 2007 (Source: Mineralölwirtschaftsverband e.V., 2013).

	1970		2007
Investor Oil Companies (IOC)	85%	IOC	6%
Russia	14%	NOC, negotiated	10%
National Oil Companies (NOC)	1%	Russia	6%
		NOC, negotiated	78%

---

1. The green paradox does not only occur with rising value tax rates and negligible extraction costs. According to Sinn H.-W., 2008, a generalization to the case of extraction costs and other demand-limiting measures is possible.
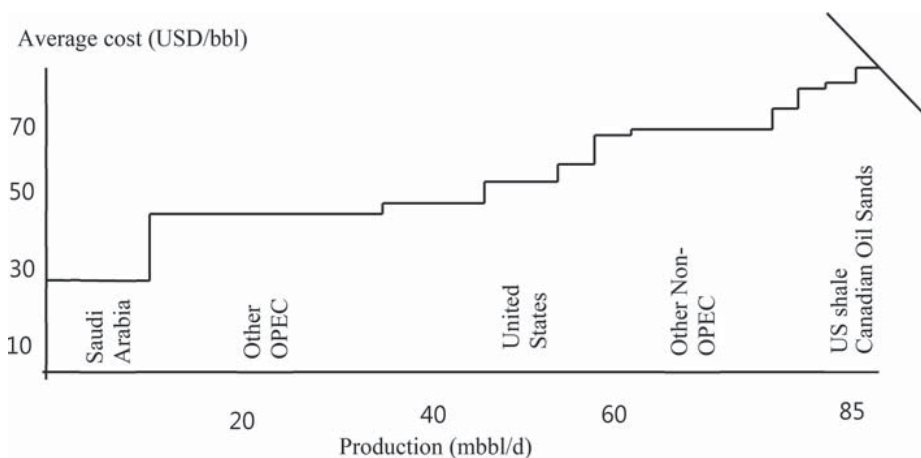
Figure 1.   Global cost curve 2014, schematic illustration.

6   SUPPLY FUNCTION

The supply cost function (Figure 1) is a schematic illustration of the average production costs in 2014 for existing production. The main beneficiaries of high oil prices are the oil-producing countries, above all the members of OPEC. The gap between the world market price and the average production costs for crude oil has been widening for several years. As a result, the oil states are generating increasingly higher revenues. This is particularly evident in Saudi Arabia, where production costs are particularly low at around USD 25 per barrel. Oil sands and US shale oil are at the top of the cost curve and are the so-called border suppliers.

After the drop-in oil prices at the beginning of 2015, Canadian oil sands, parts of shale oil production are uneconomical.

The long-term supply function established on the basis of discrete partial supply quantities is brought to an intersection with the continuous demand function (assuming an atomistic demand function) (von Wahl, 1991). Under the previously set condition of the ideal market at the intersection of the two functions, one obtains a) the competitive or equilibrium price (as a unit price) for all supply and demand quantities in the competitive part of the market spectrum (to the left of the intersection) and b) the competitive supply quantity.

7   PRICE DEVELOPMENT

From the middle of the past decade to 2014, there was a worldwide boom in raw materials, triggered in particular by rising demand from Asia. This resulted in enormous investments in the development of new oil fields. Especially in the USA, supply has increased due to tech-nologies such as fracking, but production has also increased in the Middle East and Russia.

In the summer of 2014, the North Sea variety Brent cost over 100 dollars per barrel (159 liters). In the meantime, the price of the world's most important raw material has risen again to around 65 dollars following a crash to below 30 dollars at the beginning of 2016. Because oil is traded worldwide, the price in the USA and Asia has fallen almost as sharply as in Europe.

According to the US Energy Agency (EIA), global consumption amounted to 96 million barrels per day in 2014, production to just under 94 million barrels, and the opposite was true in 2015. An important reason for this was that Saudi Arabia decided in autumn 2014 not to produce less despite falling prices due to overproduction. This sent the oil price onto the accelerated downward spiral. Currently, global oil production continues to exceed demand. Stocks are filling continuously.

Table 2. Studies on price elasticity of oil supply according to (Schlothmann, 2016) and (Golombek, 2018).

Study	Short-term price elasticity	Long-term price elasticity	Countries	Investigation period
Gately (2004)	0,03–0,05	0,15–0,58	Non-OPEC	Assumptions until 2020
Brook et al. (2004)	0,04	0,35	Non-OPEC	1971–1997
Krichene (2007)	Inelastic to negative		World	1970–2005
Hansen and Lindholt (2008)	0,02	−0,32	OPEC	1974–2001
	−0,04	0,38	Non-OPEC	1974–2002
Askari and Krichene (2010)	−0,014	−0,48	World	1970–2008
Golombek et al. (2018)		−0,79	OPEC	1986–2016
		0,32	Non-OPEC	1986–2017

8 BEHAVIOR OF SUPPLIERS

In order to examine whether the various suppliers behave in accordance with the Hotelling rule, it is appropriate to consider the elasticity of supply. The price elasticity of the offer indicates the percentage by which the quantity offered changes if the oil price changes by 1%. If it is negative, the supply goes down if the oil price rises. This would correspond to the behavior assumed by the Hotelling rule.

Table 1 shows the results of (Schlothmann, 2016), which summarizes recent studies on the price elasticity of oil supply in the short and long term. A study recently prepared by Golombek 2018 was added.

As can be seen in Table 2, the authors concluded regarding the long-term price elasticity of supply. While the very low short-term elasticity shows that the oil supply hardly reacts to changes in oil prices in the short term, i.e. behaves in elastically, the long-term price elasticity shows that it is positive in the non-OPEC countries. Whereas the long-term price elasticity of OPEC seems to be negative, i.e. an increase in the oil price leads to a reduction in production. This means e.g. an 1% increase in the oil price goes along with a reduction in production by e.g. 0.79% (with an elasticity of −0.79).

9 CONCLUSION

In this publication, based on the state of research, it was demonstrated that only the behavior of a part of the suppliers (e.g. for Saudi Arabia) can be explained by the theory developed by Hotelling. It was shown that in particular the marginal cost providers (US shale oil producers), which are decisive for price formation; do not behave as described by Hotelling. These marginal cost suppliers increase their production with rising prices (positive supply elasticity). The Hotelling calculation of withdrawing less from resources today so that these quantities can then be produced later (negative supply elasticity) cannot be observed with these suppliers. A high tax on oil production today and decreasing over time, as proposed by Sinn, would thus create incentives for a constant increase in production volumes, thus further increasing the amount of CO_2 contrary to the theory of the Green Paradox.

REFERENCES

Adelman, M. (1990). *Mineral Depletion, with special reference to petroleum.* The Review of Economics and Statistics, Vol. LXXII, Nr.1.

Anderson, S., Kellogg, R., & Salant, S. (2014). *Hotelling Under Pressure.* NBER Working Paper, Nr. 20280.

Erber, G. (14/2015–68. Jahrgang). *Der Ölpreis auf den Weltmärkten – ein Oligopolspiel mit ungewissem Ausgang.* München: ifo Schnelldienst.

Fattouh, B. (2007). *The Drivers of Oil Prices: The Usefulness and Limitations of Non-Structural Model, the Demand–Supply Framework and Informal Approaches.* London: University of London, School of oriental and African studies, Centre for financial and management.

Figueres, C. (2018). Emissions are still rising: ramp up the cuts in. *Nature, 564*, pp. 27–30.

Golombek, R.I. (2018). *OPEC's market power: An empirical dominant firm model for the oil market in: Energy Economics 70 (2018) 98–115.* Elsevier.

Hotelling, H. (1931). *The Economics of Exhaustible Resources.* Vol. 39 (1931) Nr. 2, S. 137–175: The Journal of Political Economics.

IEA. (2017). *IEA Database, CO_2 Emissions from Fuel Combustion,* verfügbar unter: http://www.iea.org/ publications/freepublications/publication/CO2EmissionsfromFuelCombustionHighlights2017.pdf.

Mineralölwirtschaftsverband e.V. (2013). *Wahrnehmung und Realität Ein Beitrag zur Versachlichung der Debatte um Rohöl, Raffinerien und Kraftstoffe.* Braunschweig: Oeding print GmbH.

Schlothmann, D. (2016). *Kurz- und langfristige Angebotskurven für Rohöl und die Konsequenzen für den Markt.* Freiberg: Dissertation, Technischen Universität Bergakademie Freiberg.

Sen, A. e. (9 Dec 2014). *In Focus: Survival of the fittest.* München: UniCredit Energy Weekly.

Sinn, H.-W. (1982). *Absatzsteuern, Ölförderung und das Allmendeproblem.*, in: H. Siebert, Hrsg., Reaktionen auf Energiepreisänderungen, Lang, Frankfurt und Bern, 83–103.

Sinn, H.-W. (1984). *Common Property Resources, Storage Facilities and Ownership Structures: A Cournot Model of the Oil Market.* Economica 51, 1984, pp. 235–252.

Sinn, H.-W. (2008). *Das grüne Paradoxon: Warum man das Angebot bei der Klimapolitik nicht vergessen darf.* München: Ifo Working Paper No.54.

Sinn, H.-W. (2015). *The Green Paradox: A Supply-side View of the Climate Problem.* München: CESIFO WORKING PAPER NO. 5385.

Stern, N.e. (2006) *Stern Review: The Economics of Climate Change, HM Treasury.* London.

von Wahl, S. (1991). *Bergwirtschaft, Band III.* Essen: Verlag Glückauf GmbH.

Watkins, G. (2006). *Oil Scarcity: What have the last three decades revealed?* Vol. 24 (2006), Nr. 5, S. 508–514.: Energy Policy.

Digital technology trends and their implementation in the mining industry

L. Barnewold

Institute Mineral Resources Engineering RWTH University, Aachen, Germany

ABSTRACT: The actual process of the technologically induced change (i.e. digital transformation) is referred to as "digitalization", and vague terms like those that "Industry 4.0" are used to describe the necessary and inevitable change to all business sectors because of the evolution and revolution of currently used technologies. This work focuses on the systematical identification of those digital trends for the mining industry by using co-word analysis together with text mining algorithms from expert articles. Network analyses are used to investigate the relations between the significant trends. Furthermore, a method to detect the implementation level of individual trends in active mines is introduced. The methodology was able to identify a variety of digital trends and their relevance, such as "automation" and basic technologies such as "big data", "internet of things", "artificial intelligence" and "machine learning" which can be used as orientation points for future digital transformation processes.

1 INTRODUCTION

Looking at the last 200 years, steam engines, electricity or the use of computers represent important technological inventions. Each technical achievement influenced the industrial landscape for a certain period and led to strong industrial growth, but also to a high degree of change. Today we are faced with such a technological development again. The so-called forth-industrial revolution, "digital transformation" or simply "Industry 4.0" plays an important role in every business sector and will be a basis for the future industrial development. (Paul 2016) In contrast to the previous technical evolutions, a unique and clear core technology is not discernible. Rather, it consists of a complex network of the most diverse approaches and technologies. The complexity and inflationary use results in an ambiguity of the mentioned terms. (Bassi 2017; Chiarello *et al.* 2018) Future developments and trend analyses for the mining industry were already been carried out in previous work, Stanway *et al.* (2015) deals with the general direction and structure of innovative processes and trends in the mining industry and thus more with influencing factors that encourage the implementation of trends (Boudreau-Trudel *et al.* 2015). Other work focuses on specific technologies, such as for example new machinery in mobile open pit equipment section in Lumley (2012), Lumley *et al.* (2012), the SX-EW method in copper processing in Ericsson (2012) or new filtering technologies presented by Palmer (2016). These trends are focusing more on mechanical developments of new machinery and new basic processes. A discussion of digital technologies is mainly used in direct relation to detailed existing processes, especially for the processing and beneficiation industries. (Jämsä-Jounela 2007; Groenveld and Rozou 2016; Ofstie and Kargutkar 2015; van Duin *et al.* 2013). However, an overview of all digital trends relevant to the mining industry from reliable sources do not exists. Due to this, the research question was formulated as:

> Which digital trends are currently relevant for the mining industry and how can they be systematically captured?

This paper deals with the identification of current digital trends directly related to the "Industry 4.0" discussion. In order to ensure a certain relevance of the trends and a

reproducibility of the analysis at any time, a general systematics for the determination will be developed in the following.

In order to assess the significance of individual trends for the mining industry, it is important to have an overview of the use of technology in active mining operations. A research using conventional search engines is difficult due to the lack of search approaches (such as the name of the mines). This leads to the second research question of this work: How can the degree of implementation of digital trends be determined from reliable sources?

The developed method will allow stakeholders of the mining industry to evaluate the landscape of digital trends for the mining industry at any time and use this as a general orientation for future developments on the sector. The analysis regarding the implementation level of individual technologies will make the progress visible in the industry and will allow the classification of individual mining operations on a larger scale.

2 METHOD

The methodology developed to identify digital trends and links in the mining industry is based on a co-word analysis and consist of three steps (see Figure 1a). The basic instruments used for this investigation are text-mining algorithms, which are programmed based on the data mining software Rapidminer. Text Mining turns unstructured text datasets in structured tokenized data and is used to search for hidden knowledge and semantic information. This method allows to analyze a high range of research papers in a short time. (Liddy 2000) (Salloum *et al.* 2018, pp. 375–376).

2.1 *Text sources*

The input data is generated from two different sources. Assuming that leading management consulting firms are an indicator for future developments and trends in the industry, all published reports, white paper and case studies of the top rated consulting firms by the business magazine "Forbes" are taken as a first input source. Additionally, the collection of technical documents, conference papers and articles with the focus on the mining sector from the online library "onemine.org" represents the second source. Especially all papers from 2010 up until today in English are used for the investigation of the implementation level in the mines.

2.2 *Defining keywords*

In a first step, all consulting papers are reviewed for digital technologies associated with the future development of the mining industry. The identified trends are sorted according to synonyms, such as "computer" and "PC" into sub groups. In a next step, these groups are organized in main categories again.
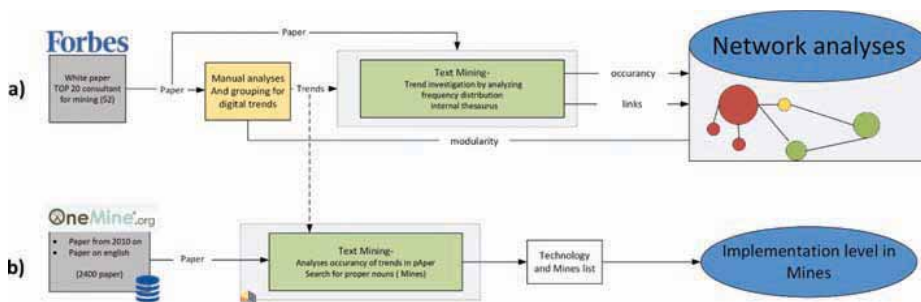
Figure 1.   Methodology used to identify trends in expert articles.

2.3 *Extracting and quantifying digital trends*

Secondly, the identified trends are extracted and quantified by a text-mining algorithm from the consulting papers. This is done by on a standard machine with two cores @ 2.3 GHz and 8 GB ram. The algorithm analyzes the respective trends according to the occurrence in a single paper (Term Occurrence) and total number of words in respective paper. From this data the nominal term frequency is calculated, which allows to compare the term frequency (TF) from different papers with different length. The binary term occurrence (BTO) can be used to determine the number of articles in which the respective trend was mentioned. The paper frequency (PF) results from the total number of articles and the BTO.

Content relations between individual trends help to classify these and draw a superordinate picture of all relations of current digital technologies. The links are extracted from the consulting paper by using the order of words in the text to draw a conclusion on which trends are mentioned together and might have a direct connection. To increase the validity of these connections, semantic relatedness from Wikipedia are used to complete the network. Particularly, the direct links to related topics or terms and assigned categories are of great interest and investigated for more connections. Detailed information about the usage of Wikipedia related text-mining is provided by Gabrilovich and Markovitch (2007) and Simanovsky and Ulanov (2011). The algorithm were run on a 4 cores @ 3.4 GHz and 32 GB machine.

Trends and the links between the trends can be seen as a big network. The resulting complex is further investigated in networking analyses, by focusing on the key parameters weighted degree, centrality as well as layout analytics, which were discussed in Cherven (2015) and Opsahl *et al.* (2010). The open source program Gephi is used to visualize the network and to highlight the links between the trends in a networking structure. Nodes and edges characterize these structures. In this case, the nodes are represented by the individual trends. Edges show the relation between two trends. (Chiarello *et al.* 2018). A forced-directed algorithm (Force Atlas 2 by Jacomy *et al.* (2014)), which takes attraction and repulsion of the single trends and their connections in consideration was used for the layout of the network.

As mentioned in the introduction, a reliable and extensive database is necessary to analyze the implementation level of new digital technologies. In this case, articles from the onemine. org database are used together with a text mining method (see Figure 1b), which filters the paper for the identified trends. The resulting papers are then searched for all proper nouns and, in a next step, analyzed for mine operation names. The mine and the mentioned trend can then be linked.

3 RESULTS

3.1 *Data collection from the database*

The Forbes list for metals and mining consulting consists of 13 international acting companies. Eight of these companies offer 28 mining related online white papers in total. 26 papers from seven companies address directly digital mining trends. The request on "onemine.org" database focuses on all research papers published after 2010 in English via seven professional mining organizations. This resulted in 2400 individual papers.

By analyzing the consulting papers, 209 digital trend terms were recognized. After eliminating duplicates and use of a uniform spelling, 107 individual terms were identified. Furthermore, the trends were divided into 21 synonym groups and finally clustered in the five categories that are shown in Table 1.

3.2 *Extracted digital trends*

The text-mining algorithm took around 3 min. In a first run the term occurrence (TO) of the single trends were calculated for every paper, where 820 mentions in all 26 papers were detected. Figure 2 shows the top 20 trends with the highest TO in all consulting white papers. In detail, the results show a significant peak for the term "automation" with 153 mentions.

Table 1. Categorization of determined trends.

Category	Number of trends
Automation and robotics	22
IT infrastructure	18
Advanced process control	24
Advanced simulations	23
Data analytics	20
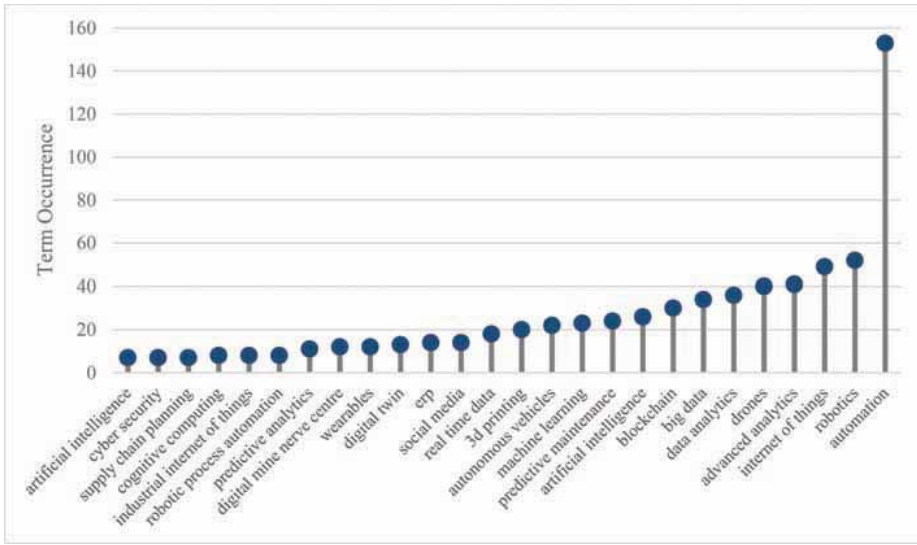
Figure 2. Top 20 of the most frequently cited trends.
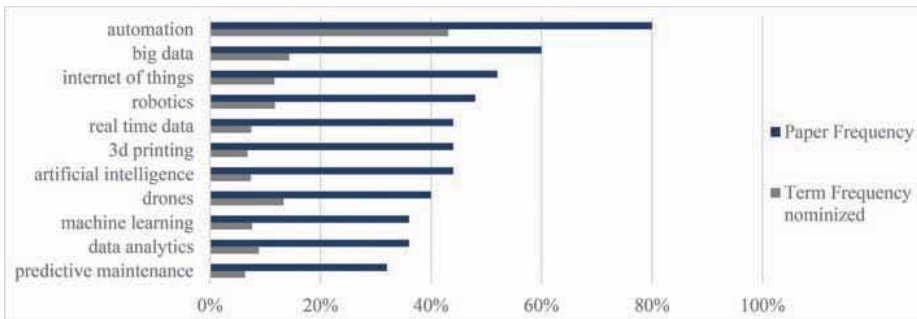
Figure 3. Term and paper frequency of eleven trends.

The terms "robotics" and "internet of things" are named 52 and 49 times followed by "advanced analytics" and "drones".

As already discussed in the method section, the TF, especially the nominal TF, gives an expanded view on the trends and allows further analyses. When looking at the average of the nominal TF together with the PF the picture from the term occurrence can be validated as seen in Figure 3. "Automation" occurs in 80% of all papers with a high FT value. Different from the previous section, big data plays a significant role in 60% of the manuscripts with the second highest TF. In total, the diagram shows a connection between TF and PF in most cases. The term "drones" is mentioned in 40% of the white paper but with only 13% of a nominal TF.

3.3 Network of identified digital trends

The algorithm for internal and Wikipedia related links took an average calculation time of 30 min. In total 1389 undirected links between the trends were detected. The dataset is visualized as a network structure in Figure 4. Additional properties of the nodes, as the size and color represent the weighted degree and categories of the trend. The position and distance of the nodes indicates how related these trends are. The trends "artificial intelligence", "internet of things", "machine learning" and "virtual reality mine training" are based in the middle and act as a central points of the diagram.

The analyzed weighted degree of every single node, shows again, "automation" as a leading trend with 52 relations, followed by "artificial intelligence" (35), "machine learning" (37), "3D printing" (31) and "virtual reality mine training" (24). This correlates to the positions of the trends and reflects the central role of these nodes in the network.

3.4 Extracting trends and mine names from research database

The algorithm for analyzing the onemine datatbase were executed on a 4 cores @ 3.4 GHz and 32 GB machine and took in the average 25 min. In total 2400 paper were analyzed and 25 individual trends in 164 paper were recognized. In the filtered papers, proper name lists were created and 92 papers with a possible mine name citation were detected. By reviewing
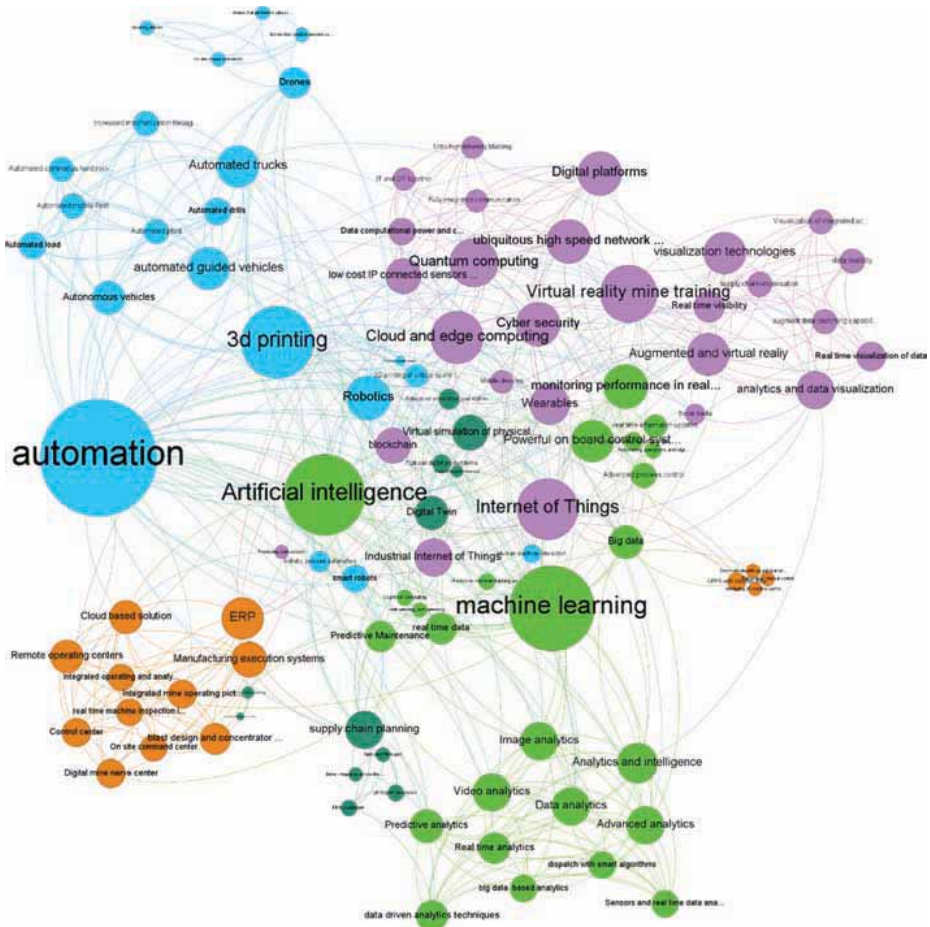
Figure 4. Network structure of all trends with the weighted degree as node size.
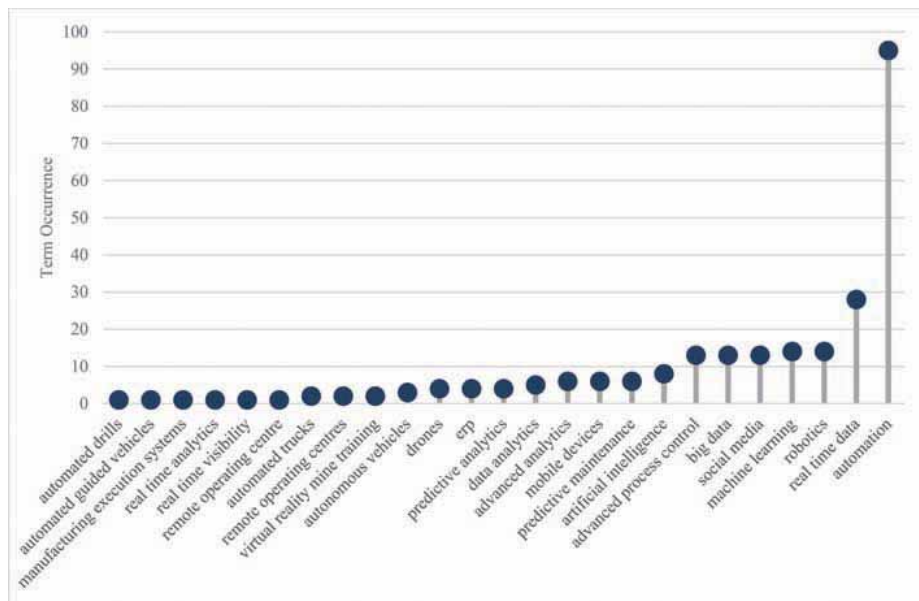
Figure 5. Term occurrence of the recognized trends in the onemine database.

the papers again manually, 65 papers with 158 mining operations were identified. The TO from all papers are shown in Figure 5. Especially "automation", "real time data", "advanced process control" and "machine learning" show high values.

4 DISCUSSION

Even though the identified trends come from a number of experts of the industry, the trends only can be seen as indictors for the industry. The analysis does not leave any statement about the technical benefit as well as urgency or relevance for a single mining operation. Moreover, this analyses gives an overview about discussed digital technologies for the mining industry and where possible potential is seen by experts. The examined scientific articles confirm the significance of the analysis, since the same trends are seen as trend-setting. Additionally, the named trends, like "automation", "IoT", "big data", etc. are reflected in the trend analysis for the manufacturing or logistic industry and play a significant role there (cf. TippingandKauschkeTipping and Kauschke (2016), Kovacs and Kot (2016), Tao et al. (2017), Grazia Speranza (2018)). This also supports the importance of this development in the mining industry.

4.1 *Which digital trends are currently relevant for the mining industry and how can they be systematically captured?*

As seen in the results section, automation is the significant trend, which will or already does affect the mining industry. The high degree of automation highlights the complex connection to other terms, which are effected by, or affect an automated process. An essential reason for the dominance of automation is also the manifold use of this technology, e.g. process automation in beneficiation processes, automation of machines up to the close relation to autonomies. Same tendency is reflected in the results of terms "Internet of things", "real time data", "artificial intelligent", "machine learning" and "3D printing". Different to automation, all trends are centrally positioned in the network. This shows how important these trends are as fundamental technologies in the future development of the mining industry.

Automation, on the other hand, is positioned not directly in the center of the network, what leads to the fact, that automation has influenced many other technologies but is not a basic technology for the near future.

The Term "big data" has the second highest PF and TF with over 60%. However, the TO of "big data" correlates quite low to other terms. This is due to the fact, that big data is named in a lot of papers, but not with a special focus. Nevertheless, "big data" is seen as a major trend in the mining industry by the consulting experts. Drones plays a significant role in 40% of all papers with a relative high TF. This results from some special issue papers with focus on UAVs or Drones. Terms that are directly linked to "ERP", "data analytics" or "drone" have a more satellite-based position, which suggests an independent development of this technology.

4.2 *How can the degree of implementation of digital trends be determined from reliable sources?*

The results from the developed algorithm show that in a short time frame a high variety of papers can be analyzed. Compared to a normal manual literature review with conventional search engines, the considerable papers could be reduced by 44%. Besides this, the 201 manual request for every single trend in the database is not necessary which saves a lot of time during a literature review. Nevertheless, this algorithm does not clearly identify mines in connection with used digital technology trends. The guessed mines from the proper noun list, generated by the algorithm are not 100% reliable, due to that the name of the mines often come from landscapes, people's names or regions. Additions like mine or operation helps to identify a mine, but are not used in every case. The algorithm can be improved by using neuronal networks as Poria *et al.* (2016) show for opinion mining. An overview of the implementation level of digital trends in active mining operations is not useful to create a ranking or to compare different operations, due to total different infrastructure, used equipment and available infrastructure. This overview can rather be seen as a self-evaluation to identify options and possible improvement for the own operation.

5 CONCLUSION

The developed text-mining method is a timesaving and therefore easily repeatable methodology for performing trend analyses independent of the data source. In this paper, recent digital trends were extracted from consulting papers of the TOP 20 consulting agencies. The results draw a clear picture of the leading technologies, "automation", "internet of things" or "real time data", which are and will be significant for the mining industry in the next years. The identified technologies play an important role for the manufacturing and logistics industry, which underlines the relevance and reliability of the data source. An overview about the implementation level in the mining sector helps to asses the value of a certain technology for the industry. Data is rarely available and difficult to search in existing databases. For this purpose, a text-mining algorithm was developed which searches document sets for given keywords and associates them with the mining operation names mentioned. Future work will focus on improvements of the proper noun recognition and drawing a detailed picture of the implementation level of trends in the mining industry.

REFERENCES

Bassi, L. 2017. Industry 4.0. Hope, hype or revolution? *In:* 2017 IEEE 3rd International Forum on Research and Technologies for Society and Industry – Innovation to Shape the Future for Society and Industry (RTSI) 2017. Piscataway, NJ: IEEE, 1–6.

Boudreau-Trudel, B., Nadeau, S., and Zaras, K. 2015. Innovative Mining Equipment. Key Factors for Successful Implementation. *American Journal of Industrial and Business Management,* 05 (04), 161–171.

Cherven, K. 2015. *Mastering Gephi network visualization. Produce advanced network graphs in Gephi and gain valuable insights into your network datasets*. Birmingham, UK: Packt Publishing.

Chiarello, F.*, et al.* 2018. Extracting and mapping industry 4.0 technologies using wikipedia. *Computers in Industry,* 100, 244–257.

Ericsson, M. 2012. *Mining technology – trends and development*. 1st ed. Bruessel: European Commision.

Gabrilovich, E., and Markovitch, S. 2007. Computing semantic relatedness using Wikipedia-based explicit semantic analysis. *In: Proceedings of the 20th international joint conference on Artificial intelligence*. Hyderabad, India: Morgan Kaufmann Publishers Inc, 1606–1611.

Grazia Speranza, M. 2018. Trends in transportation and logistics. *European Journal of Operational Research,* 264 (3), 830–836.

Groenveld, D., and Rozou, M. 2016. Advanced Process Control for grinding circuits. *In:* 2016.

Jacomy, M.*, et al.* 2014. ForceAtlas2, a continuous graph layout algorithm for handy network visualization designed for the Gephi software. *PloS one,* 9 (6), e98679.

Jämsä-Jounela, S.-L. 2007. Future trends in process automation. *Annual Reviews in Control,* 31 (2), 211–220.

Kovacs, G., and Kot, S. 2016. New logistics and production trends as the effect of global economy changes. *Polish Journal of Management Studies,* 14 (2), 115–126.

Liddy, E.D. 2000. Text Mining. *Bulletin of the American Society for Information Science and Technology,* 27 (1), 13–14.

Lumley, L. 2012. Understanding Trends in Performance of Open Cut Mining Equipment. *In:* The Australasian Institute of Mining and Metallurgy, ed. Project Evaluation Conference, 24–25 May 2012, 203–224.

Lumley, L., Trott T, and Lewis, M. 2012. Reversing the Trend in Open Pit Mining Equipment Output. *In:* The Australasian Institute of Mining and Metallurgy, ed., 18.-19 September 2012 2012. Perth, 75–82.

Ofstie, D., and Kargutkar, B. 2015. Digital transformation in metallurgical facility design, construction and operations. *In: COM 2015. Hosting AMCAA: 54th Annual Conference of Metallurgists hosting America's Conference on Aluminium Alloys: August 23–26, Fairmont Royal York Hotel, Toronto, ON, Canada: proceedings.* Westmount, Québec, Canada: Canadian Institute of Mining Metallurgy and Petroleum.

Opsahl, T., Agneessens, F., and Skvoretz, J. 2010. Node centrality in weighted networks. Generalizing degree and shortest paths. *Social Networks,* 32 (3), 245–251.

Palmer, J. 2016. Operation results and future trends of filtration technology in mineral processing. *In:* 2016.

Paul, H. 2016. *Industrie 4.0. Annäherung an ein Konzept*. Dortmund: Gelsenkirchen: IAT.

Poria, S., Cambria, E., and Gelbukh, A. 2016. Aspect extraction for opinion mining with a deep convolutional neural network. *Knowledge-Based Systems,* 108, 42–49.

Salloum, S.A.*, et al.* 2018. *Using Text Mining Techniques for Extracting Information from Research Articles*: Springer, Cham.

Simanovsky, A., and Ulanov, A. 2011. Mining Text Patterns for Synonyms Extraction. *In:* F. Morvan, ed. 2011 22nd International Conference on Database and Expert Systems Applications (DEXA) 2011. Piscataway, NJ: IEEE, 473–477.

Stanway, G.*, et al.* 2015. Understanding the State of Innovation in the Iron Ore Industry. *In:* The Australasian Institute of Mining and Metallurgy, ed. Iron Ore Conference, 13–15 July 2015. Perth, 631–645.

Tao, F.*, et al.* 2017. Advanced manufacturing systems. Socialization characteristics and trends. *Journal of Intelligent Manufacturing,* 28 (5), 1079–1094.

Tipping, A., and Kauschke, P. 2016. *Shifting patterns. The future of the logistics industry*. 1st ed. Sydney: PwC.

van Duin, S., Meers, L., and Gibson, G. 2013. Hard automation trends in Australian underground coal mines. *In:* F. Hassani, ed. *Building the future in automation and robotics. 30th International Symposium on Automation and Robotics in construction and Mining (ISARC 2013), Montreal, Quebec, Canada, 11–15 August 2013; held in conjunction with the 23rd World Mining Congress*. Red Hook, NY: Curran.

Virtual reality mine: A vision for digitalised mining engineering education

R. Suppes & Y. Feldmann
Institute of Mineral Resources Engineering, RWTH Aachen University, Aachen, Germany

A. Abdelrazeq & L. Daling
Cybernatics Lab IMA & IfU, RWTH Aachen University, Aachen, Germany

ABSTRACT: Virtual Reality (VR) is becoming increasingly popular in domains such as tertiary education and industrial training. For prospective mining engineers, a comprehensive understanding of complex 3D processes is crucial but is difficult to convey in traditional ways. The benefits of VR are the possible direct 3D immersion into locations that are remote, too costly to visit and/or unsafe. To improve future graduate education, an informative and interactive underground VR environment is being developed by RWTH Aachen University and TalTech University, called the VR-Mine. It is based on the concepts of blended learning, gamification and flipped classroom, and focusses on the topics health and safety, and principles of underground mining. Furthermore, it could help increasing the industry's health and safety standards with specialised training in safe environments. The vision of the project is to create a comprehensive VR mining environment where all process-related aspects of a mine's life can be explored.

1 INTRODUCTION

Due to the growing world population and the associated increasing demand for mineral raw materials, the education of mining engineers continues to have a high international relevance. In Germany alone, over 720 million t of mineral raw materials are produced annually (D-EITI, 2018). To date, literature from past decades (e.g. by Tamrock (1984), Goergen and Heckschen (1987), Reuther (1989), Bauer (2002)) is primarily used as basic teaching material in tertiary education. The advent of modern technologies such as virtual reality (VR) allows teaching and training not only to be interactive but also to be experienced by the user. VR is a computer-generated 3D world into which the user immerses completely with the aim of feeling physically present (Steuer 1992). Today, VR devices have become affordable for the broad public. For these reasons, VR is becoming increasingly popular in different domains such as industrial training, academic research and tertiary education. Its use in education can be regarded as a natural development of computer-aided instruction or training and can generate motivation (Freina and Ott 2015). Pantelidis (2009) concludes that VR as a new, digital learning experience can change the way in which knowledge is taught, learned and experienced. On top of that, early studies on this topic show that a VR environment can stimulate learning and understanding because it offers a close coupling between symbolic and experiential information (Bowman *et al.* 1998). In this context, it can be stated that the potential of digital teaching and learning formats in mining engineering has hardly been exploited yet.

The challenges in the field of tertiary education in mining engineering are diverse: in particular, the challenging transferability of theoretical knowledge into practical work represents a problem that has not yet been sufficiently solved with conventional teaching methods. To improve future graduate education, an informative and interactive underground VR environment is being developed in a research project, called the VR-Mine. It is based on

the scheelite mine in Mittersill (Austria). The project's research consortium consists of the Institute of Mineral Resources Engineering (MRE) and the Chair of Information Management in Mechanical Engineering (IMA) of the RWTH Aachen University (RWTH, Germany), the TalTech University (Estonia) and the mining company WOLFRAM Bergbau und Hütten AG (Austria). For prospective mining engineers, a comprehensive understanding of complex 3D processes as well as technical-human-environmental interdependencies are a crucial skillset. Furthermore, geological conditions in 3D deposits, the planning of mine workings based on these conditions and specific process steps such as rock blasting or the disposition of machines in artificially ventilated rooms have to be imagined. In general, there is limited access to active mines because of the oftentimes remote locations and the high safety requirements, resulting from the specific hazards associated with mining. The aforementioned basic literature is rarely updated, usually deals with the same topics for decades and is limited to a static representation. In mining engineering, taught aspects are oftentimes site-dependent and vary greatly, therefore requiring an individual adaptation of the visual materials. Here, VR can contribute to answering questions using concrete examples and to creating a holistic process understanding. In this context, the benefits of VR are the possible direct 3D immersion into locations that are remote, too costly to visit and/or unsafe. Chou (1998) notes that the success of simulations lies primarily in the promotion of the learner's self-determination, unique learning experiences, support for new teaching approaches, and the development of cognitive skills. Established models from didactics or pedagogy, e.g. from Warwitz (1974) (see Figure 1), already show learning as a multidimensional process. Although simulations are a representation of real scenarios, the functions going beyond it stand out in particular: selected scenarios can be standardised and lived through as often as desired (Aldrich 2004). The use of VR in teaching, as opposed to conventional teaching, offers another advantage: beside a cognitive stimulation, the integration of affective and psychomotor elements allows other senses and therefore other learning types to be stimulated. The results of the research, amongst others by Herrmann (2004), and Jones and Bursens (2018), are used in this research project to focus on the learning individual's specific experiences, skills and abilities. But there is not only an enormous potential for the use of VR on the side of the students' learning success. A shift in the teacher's role to a mentor or coach is desired for a contemporary approach. This triggers a change in the traditional role of the teacher as an 'expert' who traditionally engages in the form of frontal teaching (Youngblut 1998).

Considering the long run, the VR-Mine could be further extended: aspects as the assessment of a mining project's feasibility or the visualisation of the development steps of a sustainable reclamation could also be implemented. The user could select specified scenarios and observe the pertinent processes. In the end, a 3D animation of a mineralogical deposit is envisaged into which the user can immerse and interact with the mining processes related to the entire life of mine cycle. The VR-Mine concept could then be transferred to teaching in other locations or similar subjects worldwide. The potential is great since in Europe alone more than 40 universities with relevant programmes could apply the concept.
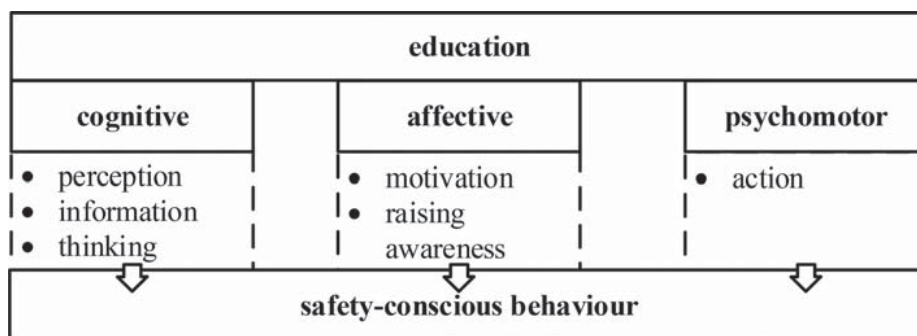
Figure 1.   Learning model, example of safety-conscious behaviour (adapted from Warwitz (1974)).

2   METHODOLOGY

The VR-Mine is being created with the Unity game engine. It is accessible by means of Head-Mounted Displays (HMD) and controllers and was designed with the help of photogrammetry in combination with modelled environments to convey a realistic impression of the mine. In addition to the possibility of interaction with the virtual environment, it contains a database so that students can inform themselves about specific aspects at various locations. The theory is supplemented by 360°/conventional video sequences of specific processes and mining expert interviews at suitable points of the story line to refine the understanding of practical applications. Furthermore, the students can play through certain processes in the sense of a gamification (e.g. selection of a suitable drill pattern based on given parameters as rock strength). This chapter describes the critical considerations that were taken into account to create the VR-Mine.

2.1   *General considerations*

First and foremost, the understanding of processes and the students' abilities to provide transfer knowledge should be activated and the reference of the taught contents to the real world facilitated. This means that higher taxonomy levels going beyond the mere reproduction of knowledge according to Bloom (1974), and taken up by Marzano and Kendall (2007), are explicitly addressed. The adaptation of lectures and exercises with respect to a flipped classroom is an essential component of the project. The developed approaches are applied in the graduate courses 'principles of underground mining' and 'health and safety', both of which demand a high degree of process understanding. In the VR-Mine, the students must solve virtually presented problems and thereby cooperatively engage in a discourse with each other and the teacher. In addition, the immersion creates transparency over comprehensive processes for even complex situations are designed interactively. Through the perceived physical presence in the VR environment, students are given the feeling of closeness to reality in order to activate affective learning. Regarding the students' motivation, it is expected that the creation of references that are relevant to the job has a positive effect. Ultimately, the low-cost repeatability of the problems to be solved in the VR world, in contrast to a laboratory, allows self-determined learning.

2.2   *Technical considerations*

Following from the general considerations, it can be stated that the requirements for the VR-Mine in terms of realism and computing power are high. For these reasons, low-cost cardboard solutions with smartphones are excluded as they do not allow the depiction of detailed and interactive environments due to their lack of computing capacity. Cave Automatic Virtual Environments (CAVE) systems are not considered either as they offer a lower degree of immersion compared to HMD and they are still considerably more expensive. A disadvantage of these systems is that they must be permanently installed in a sufficiently large room and are therefore not semi-mobile. (Freina and Ott 2015) This does not allow transportation and usage elsewhere if required.

2.3   *Basics of the learning concept*

The basis of the learning concept is the change 'from teaching to learning', in which research and learning formats are increasingly merging (Wildt 2009). The focus is on making learning sustainable and on enabling 'deep' learning in which the learner becomes active. According to Ertl and Mandl (2004), learning situations must be created in a way that they are situated and structured on the basis of external problems, take place in multiple contexts, and enable learning in a social context and from multiple perspectives. The following research questions on higher taxonomy are to be answered in the course of the VR-Mine's application in teaching:

- To what extent can reality be replaced by VR?
- Can the VR world generate a feeling for real processes?
- To what extent can internships in mining be replaced for a basic process understanding?
- Can VR be used to trigger affective learning through emotions?
- Can the VR world create uncertainty amongst students?

2.4 *Implementation of scenarios*

A test run of the concept is to be carried out first in the summer semester 2019 and then in regular teaching from the winter semester 2019/2020: first, the concept will be tested in the European Mining Course (EMC). The EMC is an international graduate programme in which a group of approx. 20 (inter-)national students spend their 2nd semester at RWTH Aachen University together with mining engineering students. Second, the lessons learned from the test phase are to be used to adapt the learning concept. Subsequently, the concept will be integrated into the mining engineering courses of RWTH Aachen University and TalTech University. The courses will then be evaluated in order to further elaborate the concept.

2.5 *Evaluation*

The test lectures will be evaluated to run through two cycles of concept adaptation and continuous quality assurance. For this purpose, an evaluation tool has been developed to support regular adjustments and uncover weaknesses and possibilities for improvement of the overall concept.

The evaluation concept is based on the Four Levels of Evaluation model by Kirkpatrick (1959) (see Figure 2). In addition, it includes the iterative realisation of the VR solution in the evaluation process. The first evaluation cycle focuses on the effect of the VR application on the students. Since an effective implementation of VR in mining engineering education depends largely on the acceptance and use by the teaching staff, the second evaluation cycle deals with the evaluation and assessment of the teachers. By combining both evaluation cycles, not only can measures and processes be improved at the same time, but essential findings and questions can also be derived in the current discourse on the usability of VR measures in mining engineering education. The evaluation aims at the following questions:

- **Level 1:** How do students and teachers react to the learning concept?
- **Level 2:** Can a positive effect of the use of VR on the learning outcomes be observed?
- **Level 3:** How well is the transferability of experiences from the VR environment perceived and to which extent can reality be depicted?
- **Level 4:** Which long-term effects of the concept can be expected and where are the limits of the concept?
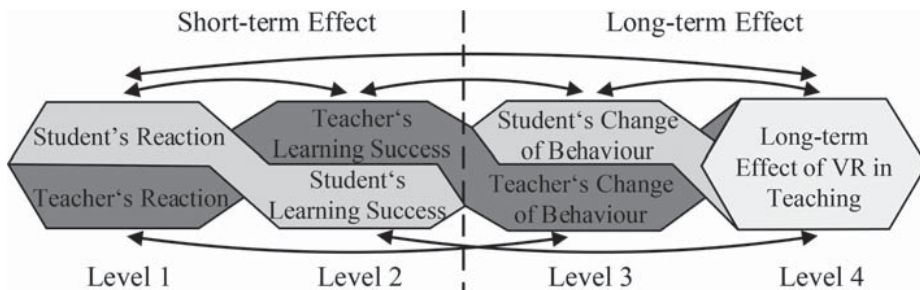
Figure 2.   Four Levels of Evaluation model (adapted from Warwitz (1974)).

2.6 *Transfer*

After the finalisation of the learning concept, recommendations for the VR-Mine's use in teaching will be given. Beyond the end of the project, the long-term effectiveness of the project results is to be tested by consolidating the learning concept in the teaching of the afore-mentioned courses and by a curricular anchoring. A dissemination of the project results is anticipated to lead to further applications and developments of the findings in relevant courses of other universities.

3 RESULTS

The presented approach combines didactic teaching concepts with a VR application in graduate mining engineering education. The level of detail and realism as well as the design for self-learning is unique so far. The components of the VR-Mine are divided into three areas: thematic content, technical design and didactic concept.

3.1 *Thematic content*

The two selected courses 'principles of underground mining' and 'health and safety' have been identified as courses where the use of VR is sensible and offers added value. The content is divided into 12 different chapters in a storyline. The user can either experience the entire content chronologically in a coherent story or select a specific chapter from the interface. The storyline has several decision points at which the user's decision influences further actions. An example of the interactive structure is given in Figure 3.

The chapter related to principles of underground mining presents the underground blasting cycle. Here, the user has the possibility to choose between different drill patterns, types of explosives, drill hole fillings, detonators (see Figure 3), and drill hole parameters. Each decision option is stored together with the necessary technical information and influences the digitally displayed blasting result which then can be examined virtually and again is stored with information of the origin. Additionally, the user can repeat the operation at will to optimise the outcome. The course health and safety contains the factors influencing productivity, and occupational health and safety. In addition, hazard assessments and safety-conscious behaviour are focussed topics. Case study examples of accidents are incorporated to learn about their course and discuss possible measures to prevent similar accidents.

3.2 *Technical design*

The choice of hardware considers the required high degree of realism, immersion and interaction. The VR-Mine is presented with high-quality 3D graphics including large-sized models (see Figure 4) with different interactions taking place between the user and the models. Based on these different reasons, the VR-Mine is being development to run on a high-end PC-based HMD. The Oculus Rift was chosen as HMD with a resolution of 2160×1200 and a 90 Hz refresh rate. The Oculus touch controllers conform the hand and allow finger
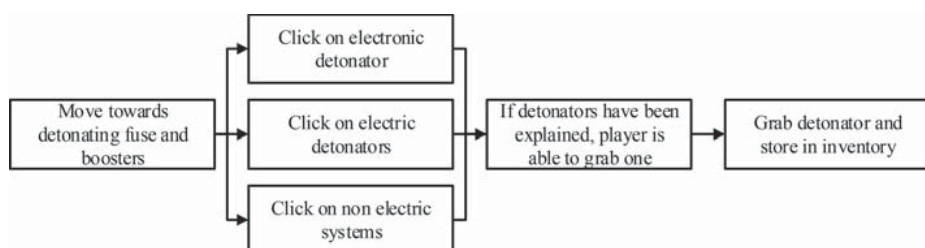
Figure 3. Interactive process of selecting a suitable detonator.

Figure 4.   Interactive digital model of a scaler.

Figure 5.   Screenshot from the VR-Mine showing the user driving a scaler in front of the mine entrance.

recognition. Its benefits are the possible interactions such as pointing, lifting the thumb up and grabbing objects.

To ease the porting process for future different platform, the Unity 3D game engine was adapted for the software development. The VR-Mine application is composed of several modules (i.e. Game Objects) within a Unity scene. The scene development is intensively based on the provided Oculus Rift software development kit. The scenes require visualising the mine as close as possible to reality to realistically depict actual colours, textures and geometry of the walls and faces. In order to do so, photogrammetry in combination with a modelled environment is being used (see Figure 5).

3.3   *Didactic concept*

The VR-Mine is designed interactively and offers gamification-based learning. In this way, contents are conveyed very close to professional practice and self-determined learning is supported. Due to integrated explanations, the students can use the VR-Mine during their self-study phase.

Teaching with the VR-Mine is done within the framework of a flipped classroom concept: students independently make appointments in the VR laboratory to visit the VR-Mine. In these sessions, the students can go through specified chapters based on the curriculum to study the relevant topics that will be dealt with elaborately during the presence phase. To achieve the desired learning outcomes for the students, explanations are integrated into the VR-Mine at suitable points, which can be queried via a menu or appear in the course of the story line. The story line contains different subject areas and thus guides the students through thematically delimited sequences. Self-tests are implemented at suitable points to reveal any gaps in knowledge. This way the students receive direct feedback on their learning success. As a final element, a reference work for the most important mining terminology is implemented in the VR-Mine where the user can look up basic mining terminology.

After the independently organised self-study phase, a lecture is offered. The lecture serves to answer questions of the students that have arisen during the self-study phase and to further deepen the knowledge of the subjects. Students can take screenshots in the VR-Mine and add comments to them, which later serves as a basis for discussions in the lectures. This cycle of self-study and presence phase is continuously repeated throughout the semester.

4 DISCUSSION

In the long run, the VR-Mine shall be implemented into the curricula of the mining engineering programmes at RWTH Aachen University and TalTech University and its content shall be further develop. Also, a portfolio of different mine types shall be created. Once the VR-Mine will have been curricularly implemented, the long-term effects on the set learning outcomes in examinations and the way teachers adopt the new learning concept shall be evaluated. This is to study the effectiveness of the implemented 'from teaching to learning' approach as well as the expected benefits of the application of VR in mining engineering education. It is envisaged to digitalise all teaching contents of the mining engineering programmes where applicable to set the education in a modern context. On top of that, it is expected that the possibility to visit various mining locations and the possibility to interact with the VR environment will prepare prospective mining engineering for the job market in a better way than conventional teaching. In a further step, the project results will be disseminated to generate positive effects of the ideas and finings at other universities and in the industry. Lastly, the adaptation of the VR-Mine for training of workforce in mining companies shall be investigated under consideration of aspects such as the reduction of accidents and cost-effectiveness.

5 CONCLUSION

The education of mining engineers at tertiary level continues to have great international relevance due to the growing world population and the associated growing demand for mineral raw materials. This paper describes the development of a virtual reality mining environment, called the VR-Mine, to tackle problems that are associated with mining engineering education. The technology has been chosen due to the possible immersion, which is crucial when it comes to understanding the complex 3D processes of underground mining. In addition, VR can make a significant contribution to satisfying the aforementioned requirements as a creativity-enhancing interactive setting with complex simulations in mining engineering. In particular, intra-individual motivational aspects are taken into account, which are expected to have a positive influence on current challenges such as non-adaptable basic literature and the students' lack of practical experience. So far, the didactic concept has been finalised, a basic version of the VR-Mine has been built and a trial period in lectures is foreseen for the summer semester 2019. The vision of the VR-Mine is to create a comprehensive 3D depiction of a mineralogical deposit into which the user can immerse and interact with the mining processes related to the entire life of mine cycle.

REFERENCES

Aldrich, C., 2004. *Simulations and the future of learning. An innovative (and perhaps revolutionary) approach to e-learning*. San Francisco: Pfeiffer.

Bauer, M.J., 2002. *Arbeits- und Gesundheitsschutz. Arbeitsblätter zu den Seminaren bzw. zur Vorlesung und zu den Übungen*. 1st ed. Aachen: Mainz.

Bowman, D.A*., et al.,* 1998. The Educational Value of an Information-Rich Virtual Environment. *Presence: Teleoperators and Virtual Environments,* 8 (3), 317–331.

Chou, C., 1998. *The effectiveness of using multimedia computer simulations coupled with social constructivist pedagogy in a college introductory physics classroom.* Dissertation: Teachers College-Columbia.

Deutschland – Extractive Industries Transparency Initiative, 2018. *Gesamtdeutsche Rohstoffproduktion* [online]. Available from: http://www.rohstofftransparenz.de/daten/gesamtdeutsche_rohstoffproduktion/ [Accessed 8 January 2019].

Ertl, B., and Mandl, H., 2004. *Kooperationsskripts als Lernstrategie*. München: Institut für Pädagogische Psychologie; Ludwig-Maximilians-Universität München.

Freina, L., and Ott, M., 2015. A Literature Review on Immersive Virtual Reality in Education: State Of The Art and Perspectives. *In:* I. Roceanu, ed. eLSE 2015 – The 11th International Scientific Conference "eLearning and Software for Education", 23.4–24.4.2015 2015, 133–141.

Goergen, H., and Heckschen, P., 1987. *Festgesteinstagebau*. Clausthal-Zellerfeld: Trans Tech Publ.

Herrmann, U., 2004. Gehirnforschung und die Pädagogik des Lehrens und Lernens: Auf dem Weg zu einer "Neurodidaktik"? *Zeitschrift für Pädagogik,* 50 (4), 471–474. Available from: https://www.pedocs.de/volltexte/2011/4820/pdf/ZfPaed_2004_4_Herrmann_Gehirnforschung_Paedagogik_des_Lehrens_D_A.pdf [Accessed 8 January 2019].

Jones, R., and Bursens, P., 2018. Die Effekte von aktivierenden Lernumgebungen. Wie Simulationen affektives Lernen fördern, 37–51. Available from: https://www.researchgate.net/profile/Rebecca_Jones81/publication/319430549_Die_Effekte_von_aktivierenden_Lernumgebungen_Wie_Simulationen_affektives_Lernen_fordern/links/5ab12b120f7e9b4897c37afb/Die-Effekte-von-aktivierenden-Lernumgebungen-Wie-Simulationen-affektives-Lernen-foerdern.pdf [Accessed 8 January 2018].

Kirkpatrick, D.L., 1959. Techniques for Evaluation Training Programs. *Journal of the American Society of Training Directors* (13), 21–26.

Marzano, R.J., and Kendall, J.S., 2007. *The New Taxonomy of Educational Objectives*. 2nd ed. Thousand Oaks, CA: Corwin Press.

Pantelidis, V., 2009. Reasons to Use Virtual Reality in Education and Training Courses and a Model to Determine When to Use Virtual Reality. *Themes in Science and Technology Education,* 2 (1–2), 59–70.

Reuther, E.-U., 1989. *Lehrbuch der Bergbaukunde, mit besonderer Berücksichtigung des Steinkohlenbergbaus*. 11th ed. Essen: Glückauf.

Steuer, J., 1992. Defining Virtual Reality. Dimensions Determining Telepresence. *Journal of Communication,* 42 (4), 73–93.

Tamrock, 1984. *Handbook on Surface Drilling and Blasting*. Tampere, Finland.

Warwitz, S.A., 1974. *Interdisziplinäre Sporterziehung: didaktische Perspektiven und Modellbeispiele fachübergreifenden Unterrichts*: Hofmann.

Wildt, J., 2009. Forschendes Lernen: Lernen im "Format:" der Forschung. *Journal Hochschuldidaktik,* 20 (2), 4–7. Available from: http://www.zhb.tu-dortmund.de/hd/journal-hd/2009_2/journal_hd_2009_2_wildt.pdf [Accessed 17 December 2018].

Youngblut, C., 1998. *Educational Uses of Virtual Reality Technology*. Alexandria, Virginia: Institute of Defense Analyses.

Investing in engineering, research and education in Africa to derive a roadmap for ensuring local digital mining success

Winfred Assibey-Bonsu

Gold Fields Ltd., Corporate Technical Services, Perth, Australia

ABSTRACT: This paper demonstrates that without a suitable pool of qualified mining professionals, appropriate research and long-term strategic funding, mining innovation and the move towards digital mining will all suffer. Through support of local tertiary engineering education and digital mining research centres in the developing world, we not only immediately broaden the talent pool available to the discipline, but also achieve diversity and creativity in ideas and problem solving. Benefits are tangible and will be seen to bear significant fruit in the medium to long-term, not only to students, countries and regions, but also for large mining houses, junior exploration companies, shareholders and other stakeholders.

1 INTRODUCTION

Africa is richly endowed with many of the minerals and natural resources required both locally and worldwide for innovation, technology and sustainable economic development into the 21st century and beyond. As a major supplier of many of these minerals, there is little doubt that the mining industry has and will continue to be one of the major engines driving Africa's economy.

Investment and funding of high level technical, mining engineering education and digital mining research in the industry, will ensure both its survival as a critical economic cog and to drive the growth and diversification required for long-term success. Decisions on such investments and funding for the future must therefore be strategic with long-term focus.

This paper puts in perspective the trends and challenges facing the mining industry, including those relating to digital mining. It considers how investment by certain major mining countries into mining engineering education, research and digital mining innovation, have generated billions of dollars of total exports, contributing materially towards industrialisation, growth, employment and GDP.

In a case study revolving around the two major African mining countries of South Africa and Ghana, suggestions are made as to how governments in major African mining countries could enter partnerships with industry, academic institutions and others, to facilitate education and research solutions. These include those relating to digital mining innovation, mining engineering and other engineering disciplines. Some current digital mining initiatives being implemented in industry are reviewed.

In tandem with the advancement of education and technology has come the explosion of opportunities for young people to build their careers across a multitude of industries, most especially in the developed world. The paper further discusses how major mining countries are either struggling to maintain current enrolment numbers in mining engineering, and/or the funding and research infrastructure necessary to further develop keen minds, with the aim of providing suggestions as to how Africa and the developing world could avoid this mining expertise gap.

2   THE IMPORTANCE OF MINERALS TO THE ECONOMY OF SOME MAJOR MINING COUNTRIES

Figure 1 below [8] demonstrates a general positive trend of how four major mining countries are faring in respect of their mineral export contributions as a percentage of total exports. At 48 per cent, mining contributed the largest proportion of export revenue for Ghana in 2016. The figure further depicts that since 2007 Australia's mining export contributions have exceeded 50% of total.

A report by the World Gold Council found that gold mining contributed some USD78 billion in gross economic value added and 530,000 direct jobs in the 15 leading gold producing countries [7]. Additionally, large numbers of indirect jobs are also generated. For example, in Ghana, one mining position supports an estimated 28 other jobs and livelihoods in the country and in Peru about 19 jobs. In South Africa, mining supports about 1.4 million direct, indirect and induced jobs, and each of these supports on average around nine dependents [7].

Digital mining success is premised on other important considerations receiving the requisite attention, such as taking into account those communities directly impacted through mining activities. A shared value approach to promoting community development is based on three key areas: (i) Preferential community employment, (ii) Preferential community procurement, and (iii) Water security. A practical example would be how Gold Fields Limited operates within Ghana, where the following milestones have been accomplished in its 25 years of operating there [6]:

1. Community spend: – Gold Fields' Ghana Foundation started in 2004 and has spent USD 47 million to date.
2. Employment: – the current workforce includes around 7,570 people. The dependency ratio is approximately 8–15, leading to support of 70,000 to 100,000 people.
3. In country procurement: – support of local economy is good, with 90% of supplier spend staying in Ghana, and 25% of the supplier spend is now within the host community.
4. Government revenue: – Gold Fields has paid USD 1.2 billion in taxes since 1998, plus an additional USD 100 million in shareholder payments to the government.
5. Infrastructure: – Gold Fields has assisted by rehabilitating over 100 km of public roads, including the upgrading of the Tarkwa to Damang road for USD 22 million. Further support to communities has, amongst others, included connecting them to the energy grid.
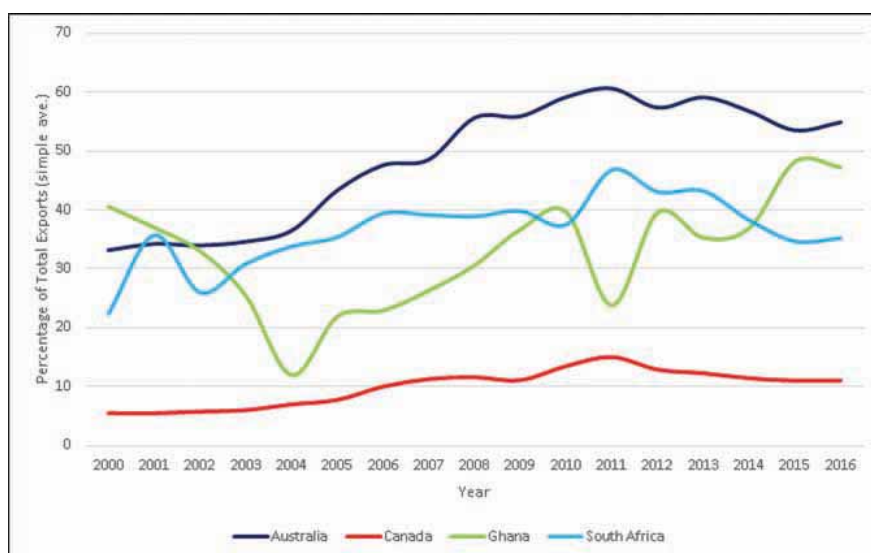
Figure 1.   The importance of minerals to the economy of some major mining countries [8].

3 THE CHALLENGES FACING THE MINING INDUSTRY

The peaks and troughs in commodity prices have in many cases led to the industry cutting costs in those areas not directly affecting production, together with reducing invaluable knowledge, experienced skills and those areas of output carrying the highest costs. In many cases this directly impacted research and development (R&D) together with exploration, all prime feeders in ensuring a medium and long-term future. When prices recovered, the focus usually shifted to ensure a return for investors and lengthen the life of operations by returning to now profitable areas, plus increasing exploration spend. As R&D and innovation are pre-dominantly long-term endeavors, they were usually treated as 'nice to haves', with production and stay-in-business capital obviously taking priority. This approach has damaged the long-term viability of much of the mining industry, where it now lags many others in terms of its creativity and innovativeness in moving to the requirements for successful enterprise in the 21st Century and beyond. Adoption of new technology to address the lag and move towards a digital future is now one of the key elements of many of the major mining Companies and is seen as a cornerstone together with exploration, in ensuring that costs are curtailed, with productivity and safety improved. This is seen to position those Companies as leaders in their fields and commodities, through providing them with a competitive advantage. Although much emphasis is placed on incorporating existing technological and digital solutions into the operations, there is also a drive through Centres of Excellence, Universities and other high-level research and innovation institutions, to leap frog into a new era.

For those that successfully bridge the gap into a digital future, the benefits are indeed tangible: The potential economic impact of current and future technologies from Mckinsey analysis [4] are estimated to be in the region of about USD370 billion per year worldwide by 2025, or approximately 17% of the anticipated cost base, with assumptions based on a high-adoption rate of 80% in operations management and 100% in equipment maintenance.

A 2018 Deloitte report highlighted the various challenges faced by the mining industry in this current and future industrial revolution, driven primarily through adoption of digital technologies. A Thermofisher blog [17] summary of the Deloitte report aptly highlights the 10 major issues, namely:

1. "Bringing digital to life: Miners need to understand how digital technologies, including autonomous vehicles, drones and Internet of Things (IoT), may influence the way they do business.
2. Overcoming innovation barriers: Mining companies are traditionally risk averse, with innovations involving high start-up costs often being dismissed. Desire for competitive advantage has also resulted in non-collaboration.
3. The future of work: While digital solutions will empower employees to make better decisions, they will also create some challenges as manual jobs are automated. Mining companies need to consider how to create new employment opportunities, and how to retrain people to learn technology and tools faster.
4. The image of mining: Mining companies need to take proactive steps to address, and change, the industry's reputation.
5. Transforming stakeholder relationships: The mining industry must adapt new approaches to the communities in which they operate to meet various stakeholders increasing demands.
6. Water management: As concerns about water availability grow, mining companies must find more innovative ways to reduce, reuse, and recycle water in water–scarce regions
7. Changing shareholder expectations: High commodity prices have traditionally meant the industry overspending. As shareholder expectations grow, mining companies need to re–establish their credibility with their stakeholders
8. Reserve replacement woes: Depleted reserves currently plague the industry. Due to capital intensity requirements and rising costs, mining companies are struggling to free up the exploration and development budgets required to exploit new resources and engage in new acquisitions.

9. Realigning mining boards: To transition to "the mine of the future", mining companies need to ensure that their boards embrace the full power of digitisation and innovation to help drive the technological changes the industry requires.
10. Commodities of the future: To assess which commodities to invest in, and which to divest, miners need to track fluctuating consumer demands, global demographic and economic shifts, the effects of environmental change, and the emergence and adoption of new technologies. An example being the demand for lithium, graphite, and cobalt, resulting from the growth of electric vehicles."

Future engineers will be required to be highly trained and digitally conversant professionals, and although beliefs in many industries are that fewer people will be required to achieve more, the mining industry will most likely require more relevant expertise and experience, rather than fewer if it is to thrive moving forward.

4 THE ROLE OF THE MINING ENGINEER

The role of the extractive engineering profession has evolved in line with how the world itself has advanced, during especially the last half century. The education required 50 years ago, although in many aspects still relevant today, has progressed exponentially, with technology and computer expertise amongst the few of many extra skills the modern engineer is required to master. In line with how the world has developed, so have also the opportunities for the most gifted learners, making attraction and retention into the industry a particularly challenging issue. This requires a new mindset and approach to how we address the education, skills and mining expertise professionals will need to succeed in the 21st century and beyond.

The engineering circle or wheel of design and project value development with time as highlighted by Stacey et al. [14] and summarised in Figures 2 and 3 below, illustrate the intrinsic value of ensuring success through efficient and effective professional inputs.

The two figures show various stages of mining projects and require consideration together, covering the exploration and scoping, the prefeasibility stage, feasibility stage, implementation of the project followed by mining production. Each stage requires critical skills, where for example step 4, the Prefeasibility (or concept formulation) of the project, is the stage in which the most value is created. It requires the most innovative, high level and experienced skills that can be brought to bear. If there is poor definition in this stage, the project is unlikely to deliver value, even if it is extremely well implemented and operated.

The critical skills required for these stages demand high level relevant 21st century and beyond 'professional engineering' skills. It demonstrates very clearly the importance of
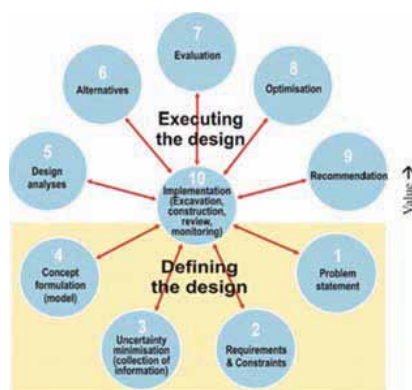
Figure 2. Engineering circle (Design process).
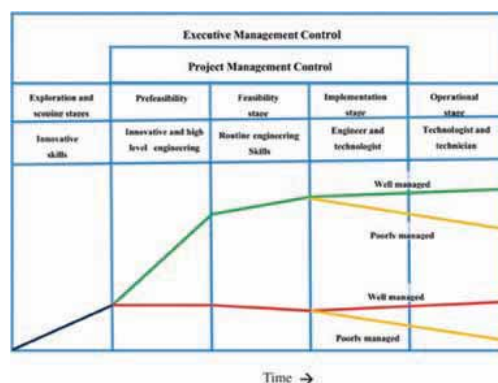
Figure 3. Project value development with time (Schematic project timeline).

mining engineering graduates to the future of the mining industry. These graduates provide the significant 'thinking' skills and injection of appropriate innovation and technology, during both the Project's Prefeasibility and Feasibility stages, and for operational delivery.

The mining profession, from education, R&D and innovation, to exploration, is changing in ways other industries (including manufacturing) already have. The major players have recognised this, with some already pioneering new technology and methods, benefitting not only themselves, but also the industry, society and the world at large.

To be in this race Africa needs the institutions, equipment, research and funding, to develop and harness the tremendous potential of the human talent pool and natural resources it has been blessed with.

5   THE DECLINE OF MINING ENGINEERS IN THE DEVELOPED WORLD

Mining engineering and associated skills are and continue to be in decline, with this being again illustrated by Stacey et al. [14], showing that the world's mining engineering education and research sphere was in crisis. This skills shortage problem in mining engineering and related disciplines is not new, though has continued to deteriorate for much too long and has reached crisis levels in some countries.

The skills shortage in Australia appears to be one of the worst affected, with the Mineral Council of Australia already predicting in 2014 the need for an additional 86,000 mining professionals and skilled mine workers by 2020 [9].

A list of employment statistics (1982 to 2015) from Graduate Careers Australia [15] showed that mining engineers were the most employable and highest paid engineers, so money does not appear to be the issue.

Although the mining and resources sector accounts for two-thirds of the Australia's export income, young Australians are not currently very keen to join the industry.

In 2017, 171 people were expected to graduate from Australian mining engineering courses, which is to fall to 98 this year (2018), with the numbers predicted to fall further by 2020 [15].

North America has not been immune to the shortages, with data from the Canadian Mining Industry Human Resources Council indicating that 40% of the professional and technical component of the mining workforce was at least 50 years old already in 2014, and that one-third of those workers were eligible to retire by 2015 [9]. There is already a 'missing generation' in the mining sector, with most employees over 50 or under 35. In the USA, specialised geoscience programmes at colleges and university have fallen from a high of 25 in 1982 to 14 in 2014, from which only 11% of undergraduates and 4% of postgraduates chose to go into mining [9]. A HSBC 2014 report noted that "50% of U.S. geoscience professionals, including engineers, are just 10–15 years from retirement", which is mirrored in Canada and South Africa [9].

Canada has had some recent success in addressing its own skills shortage, with mining and minerals engineering programmes being the fastest growing engineering disciplines between 2009 and 2013 at +56%. Latest figures for 2016 unfortunately also showed the greatest decline, with enrolment down 11.8%. The recent overall successes of education in Canada may mean that students graduating might experience increased difficulty in procuring entry level jobs and internships within the sector [5]. The mining sector must work hard in a joint effort with academic institutions to address this situation before it leads to another "lost generation" in the industry. These trends are illustrated in Figure 4 below.

Reliance on external skills will prove ever costlier and more difficult to obtain, and as mines cannot operate without mining engineers, who are required for regulatory as well as practical purposes, the implications are clear.

Reasons for the decline are varied, but the solutions are clear, if Africa is to reach its full potential in multiplying the mineral wealth so generously bestowed upon it, then local mining education and research must be seen to be a critical component for achieving this. Through sufficient government and industry support and assistance, African tertiary institutions will be able to provide the skills, expertise and research in support of these objectives.
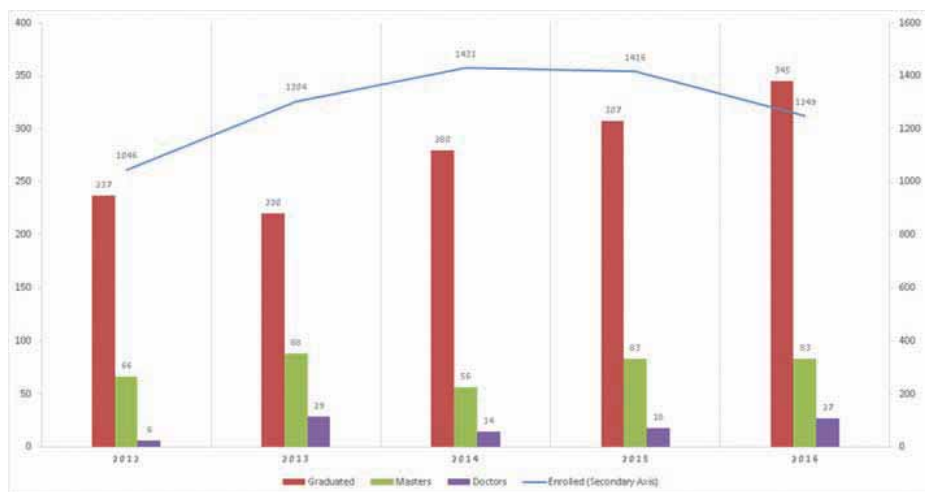
Figure 4.   Current Canadian mining engineering situation [5].

6   COLLABORATIONS AND RESEARCH CENTRES AND SOME ECONOMIC OUTCOMES

Canada and Australia have world class R&D mining centres, including Canada's 10-year old Centre for Excellence in Mining Innovation (CEMI), Australia's 20-year old Minerals Research Institute of Western Australia (MRIWA), The Australian Centre for Sustainable Mining Practices (ACSMP), and many others. South Africa have again re-embraced the challenge and in 2018 opened their own version, the Mandela Mining Precinct (MMP).

Figure 5 below illustrates how Australia identified how to leverage its mineral wealth together with the opportunities available through the implementation of the necessary interventions, including R&D, to promote growth and reduce barriers [8]. Through transitioning its economy more towards mining it benefitted from all the related linkages and other positives that accompany the process, including development of relevant expertise (knowledge economy) and related industrial aspects. The mining industry is now Australia's main economic engine, generating $112 billion or 50% of Australia's total exports in 2007 and increasing at over $1billion a year. Tax contributions exceeded $7 billion in 2007 and it is estimated that the industry accounts for over 19% of Australia's fixed and natural capital [14] & [2].

As is well known, Canada has also long been a top mining nation in mineral production, mining finance, mining services and supplies, and sustainability and safety. However, there are signs that this leadership position is slipping, which has the potential to jeopardise Canada's ability to attract FDI and seize new opportunities for growth.

Australia's mining supply sector has surpassed Canada's in 2015. Mining innovation dollars are steadily flowing out of Canada to countries such as Australia, Germany and South Africa [16]. In response, Canadian initiatives have also advanced further, with a new 'supercluster' proposal, CLEER (Clean, Low-energy, Effective, Engaged and Remediated), aimed at powering clean growth through mining innovation. If successful, this initiative would tackle the challenges of water use, energy intensity and environmental footprint, with aggressive targets of at least a 50% reduction in each area by 2027. Additionally, the research initiative would make several key contributions to the Canadian economy [16].

Africa is already a resource rich continent and dependent upon mining for a considerable period, with the challenge being to leverage those resources further, to not only diversify the economy, but also grow mining's contribution to its full potential (linkages included). In the long-term, this is best served through quality education, R&D and innovation.
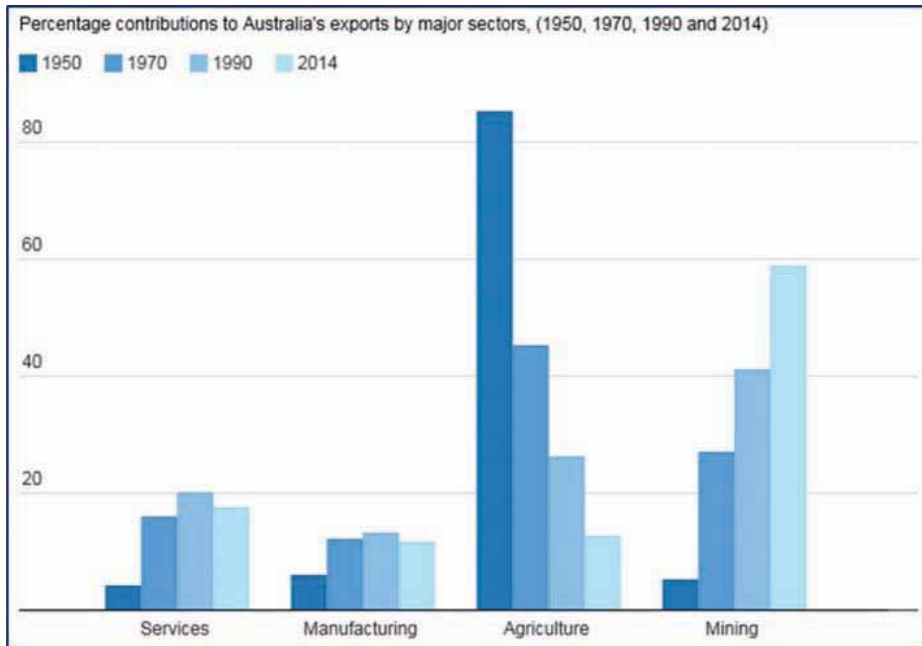
Figure 5. Australian contributions to exports and growth in mining.

7 GLOBAL SPENDING ON RESEARCH AND DEVELOPMENT (R&D) AS A PERCENTAGE OF GDP

The United Nations Educational, Scientific and Cultural Organization's (UNESCO) institute for statistics (UIS) paint a bleak picture of R&D spend in the world today, as illustrated in Figure 6 below [19], which may to a degree explain why developed countries remain developed, whilst developing ones are always playing 'catch-up'.

It notes that global spending on R&D has reached a record high of almost US\$ 1.7 trillion, with about 10 countries accounting for 80% of spending [19]. As part of the Sustainable Development Goals (SDGs), countries have pledged to substantially increase public and private R&D spending as well as the number of researchers by 2030, though will this be achieved? It needs to be noted that the top 15 countries have strong spending by the business sector in common as an underlying factor for success. African countries should aim to move up of the curve and close the gap for the benefit of all.

If there is no investment in research by an industry, there is no long-term future for that industry. Investment in research is an investment in the long-term success of an industry, and decisions on such investments must therefore be strategic.

The situation as pointed out by Stacey et al. [14], highlighted the sorry state of mining research and dearth of researchers in South Africa compared to its peers in Canada and especially Australia. It further highlighted the hundreds of millions of dollars spent in the previous decade in Australia on R&D beginning to bear significant fruits, with it seen as a leading provider of mining expertise resulting in billions of dollars of exports from the mining technology and services sector alone.

As touched on previously, subsequent developments in South Africa have included incentives for business from Government for the investment in R&D activities, with most recently the opening of the Mandela Mining Precinct (MMP), with significant funding and support promised. One of the aims is to help strengthen, modernise and grow the mining industry thus improving its contribution to GDP, which has dropped from 21% in 1970 to 7,4% in 2017. The MMP is in line with South Africa's commitment to increasing its investment in research and development to 1.5% from the current 0,77% of GDP [3].
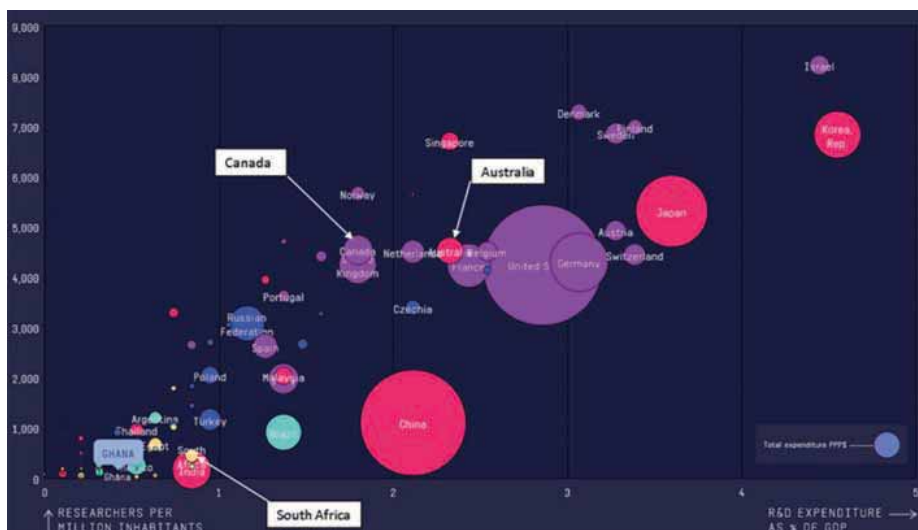
Figure 6. Researchers per million inhabitants and R&D as% of GDP.

8   MINING ENGINEERS IN THE FOURTH INDUSTRIAL REVOLUTION

In a pre-AGM address to the South African Chamber of Mines in 2017, Prof C. Musingwini, the head of the School of Mining Engineering at the University of the Witwatersrand ("Wits"), spoke of "The role of the mining industry during this difficult time in our academic environment and how tertiary institutions can continue to support the mining industry's skills pipeline" [11]. In reference to the four Mining Engineering Schools in South Africa (Universities of Johannesburg ("UJ"), Pretoria ("UP"), South Africa ("UNISA") and Witwatersrand ("Wits")), he outlined how in 2015 the Heads of these 4 schools established a Mining Engineering Education South Africa (MEESA) initiative to strengthen collaboration, so as to serve the country better and also produce engineers with the required skills set for the 4th industrial revolution, or "Mining 4.0". MEESA collaborates on many fronts, in teaching, research and service activities, also including joint participation in Mine Health and Safety Council (MHSC) research projects and research projects identified by the Mining Phakisa process inclusive of the Mining Precinct. In his speech, he further outlined how tertiary education needed to produce mining engineers with skill sets that can not only cope, but also drive systems in the 4th industrial revolution, requiring graduates with high Intelligence Quotient ("IQ"), Emotional Intelligence ("EQ"), Creative Quotient ("CQ") and Adaptive Quotient ("AQ"). In this regard, Wits itself is refining the curriculum, planning to include digital technologies, autonomous systems, data analytics and entrepreneurship, to name but a few. Once suitable approvals are received from the relevant university channels, the redesigned curriculum should gradually roll out from 2019.

   In light of industry requirements and technological advancements, Wits is not alone in continuously reviewing and improving its offerings, with the University of Johannesburg replacing it's BTech/National Diploma with a new Bachelor of Engineering Technology degree, with first graduates expected at the end of 2019. The University of Pretoria is similarly looking to address various portions of its curricula in relation to the demands of the 4th Industrial Revolution, which requires the Department to re-evaluate its approach to educating and training the next generation of mining engineers. These changes will commence from 2020, including the management of its planned student numbers. After several years of significant growth in undergraduate student numbers, followed by a slump in mining student numbers worldwide, it decided to reduce the Department's first-year intake. Its design capacity is 50 final-year students, and its strategic intent is to have 200 undergraduate and 100 postgraduate students by 2025.

Enrolled total undergraduate and postgraduate students at Wits, UMaT ("University of Mines and Technology" in Ghana) and UP are graphically illustrated in Figure 7 below. Students from UNISA and UJ, although not included due to lack of data and changes in the degree offering, do however contribute to the discourse [20].

The slight decline for Wits undergraduates is probably as a result of a slight strengthening of first year admission criteria, whilst those at UP are aligned with their long-term plans to manage its numbers in accordance with its capabilities/space. Although UP still has some way to go in reaching it's 2025 target for postgraduates, Wits has increased markedly, which may go some way in explaining its movement up the QS World university rankings (Mineral & mining engineering ratings) over the last few years: Although primarily driven through MSc students, these provide a useful feeder into PhD programmes.

Figure 8 that follows, looks at actual completed degrees of undergraduates, Masters and Doctorates at specifically Wits and UMaT. Although there are one or two drops in places,
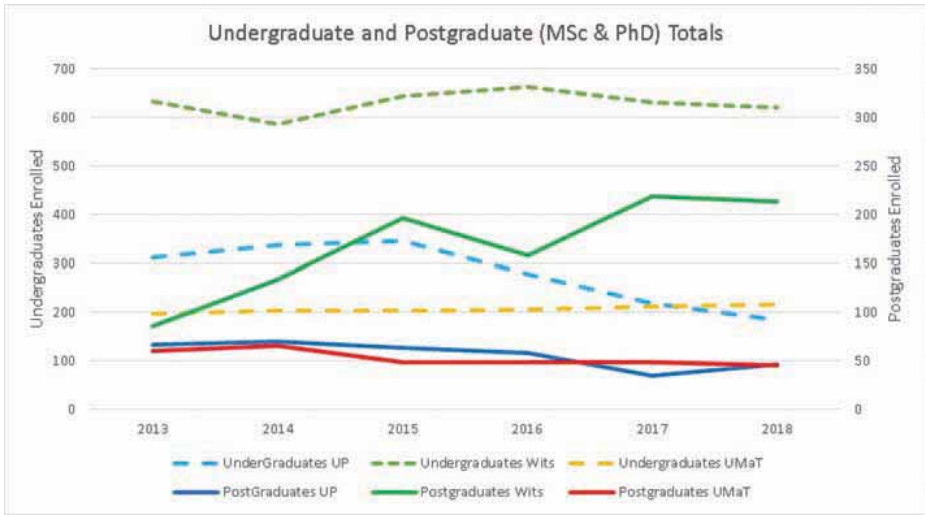
Figure 7.   Total undergraduate and postgraduate (MSc/PhD) students at selected African universities.
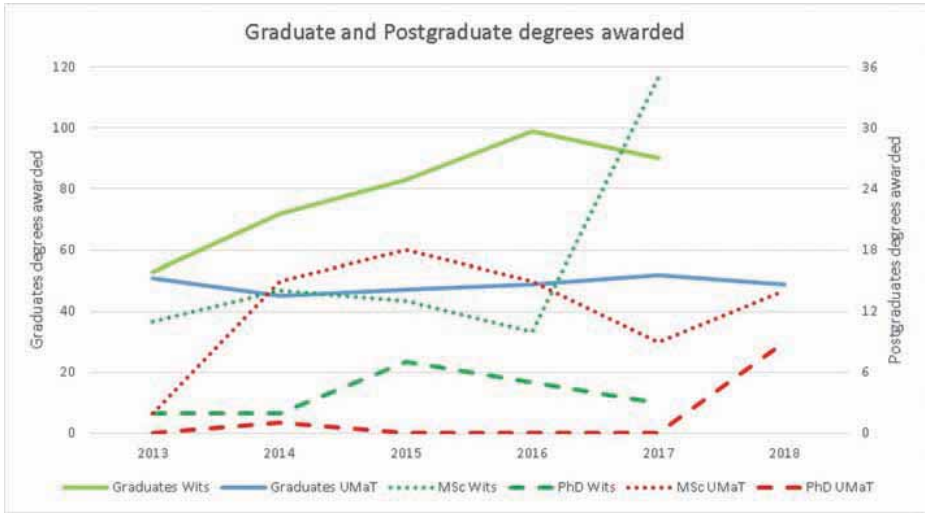
Figure 8.   Total undergraduate and postgraduate (MSc & PhD only) students awarded at Wits and UMaT.

33

overall both universities have stable to increasing numbers of degrees awarded. Given the high number of MSc degrees awarded at Wits during 2017, it would be logical to deduce that some of these will lead to an increase in the number of PhD degrees awarded in the years ahead [20].

As mentioned, all the universities are catering for the challenges of the 4th industrial revolution, together with an increased emphasis on research and innovation, much of which is specific to current and future industry requirements. In this regard their collaboration both locally and internationally, with industry, universities and others, are designed to strengthen their offerings whilst ensuring wide based support.

Although the South African universities appear to be well supported by both government and industry mechanisms, including research chairs and other additional staff, which supports staff retention and the long-term objectives, adequate industry support for UMaT in Ghana appears lacking, especially in respect to the funding of research equipment and facilities. Additionally, UMaT suffers from a high staff turnover, most probably driven by improved opportunities offered from industry.

The observed relationship between strong universities and mining performance is one of the benefits of investing in education and is a foundation of unlocking the up and downward linkages the industry has to offer the economy and the other various invested stakeholders. For several years, the QS World University Rankings by Subject has been compiling a list of top universities based on various criteria. In the Minerals and Mining Engineering fields for 2018, Australian Universities held 4 of the top 10 positions, with Canada and USA universities 2 each, and Germany and Chile 1 each [18]. This indicates how the major mining countries proactively and intentionally invest and fund their mining engineering universities, with the long-term and strategic objective of value creation. Africa should endeavour to follow suite and indeed where not already the case, to collaborate closely with these top mining institutions. As noted earlier, Wits has been steadily climbing these rankings, reaching 15th position in the 2018 iteration of the list [18].

9   CURRENT AND FUTURE INITIATIVES

As previously touched on, there is a race amongst many of the major global miners to embrace the benefits of innovation and technology, to achieve a competitive advantage through digital mining in the fourth industrial revolution. Examples are many, but a few include:

1. Rio Tinto is busy with automation initiatives as part of the "Mine of the Future" project launched in 2008, which included setting up a centre to monitor operations remotely near Perth airport, more than 1,500 kilometres away from site. Efficiency opportunities already achieved have apparently helped reduce costs by $80 million, with a commitment to deliver $500 million of additional free cash flow from 2021 onwards [13]. Driverless autonomous trucks already haul over a quarter of both ore and waste material, and with 80 of 400 haul trucks already autonomous, this is expected to increase going forward. These future additions to the autonomous truck fleet are being studied and are expected to contribute to the $5 billion productivity programme. Plans are also being considered to double its fleet of autonomous production drill rigs [10]. In October 2018, the first long-haul journey was completed with a completely autonomous locomotive, with plans to have a network of such driverless trains in Western Australia. The subsequent BHP runaway train incident may have raised some safety concerns in the short-term.
2. Goldcorp recently began using IBM's cognitive computing system, which can learn from interactions with data and humans and has the potential to transform every facet of the mining process.
3. Barrick Gold has begun to work with Cisco Systems to embed digital technology at its Cortez mine in Nevada, with the aim of improving decision-making and performance.
4. Ongoing Gold Fields' Innovation and Technology projects currently in operation include surface remote control of underground loaders, and drone technology for surveying.
5. Vale's massive S11D iron ore mine in Brazil, has one of the lowest cash costs per tonne, partly because of increased operational efficiency achieved through investments in

Figures 9 and 10.   Rio Tinto remote control room and autonomous trucks.

Figures 11 and 12.   Rio Tinto autonomous drill rigs and locomotive.

    innovation and technology. These include cutting fuel costs by using a truckless solution
    for conveying ore, reducing water consumption by up to 93% through using the humidity
    in the ore itself to remove impurities, and through using an advanced automation and
    control system [12].

6. BHP has improved both safety and profitability by using drones fitted with military-grade
    cameras and are able to transmit real-time aerial footage and 3D maps. The company esti-
    mates that it is saving $5 million a year at its Queensland sites alone by replacing planes
    with drones for some survey work. The drones are used in several other processes, from
    ensuring areas are clear before blasting and tracking blast fumes [12].

    The benefits of asset optimisation tools can be significant. Separate analysis by PwC esti-
mated that companies could lower maintenance costs by between 20 to 40 percent, increase
asset utilisation by up to 20 percent, reduce capital expenses by between 5 and 10 percent,
whilst also improving environmental health and safety [12].

    Figures 9–12 below [21] illustrate remote control rooms, together with autonomous trucks,
drill rigs and locomotive.

10   CONCLUSIONS

Mining and mining engineering are one of the oldest and most durable industries and pro-
fessions, with the oldest Mine on archaeological record being some 43,000 years old and
interestingly located in Africa (Swaziland). Mining will survive many of the current indus-
tries and those yet to come, continuing to provide a return for all stakeholders associated
with it. It is now a highly complex and technology driven business, where engineering skills
and knowhow not only determine success, but also safety, the environment and many other

aspects. Autonomous machines, mining of the seabed, proposals for mining asteroids and meteorites, current mines at depths of 4 km, all in sometimes remote and inhospitable locations, all require engineers, researchers and innovators of a calibre comparable to what is found nowhere else. Africa can, will and does provide these engineers, researchers, innovators and leaders in the industry, with its legacy etched in the very stone by the output it produces. Many African mining and other engineers already travel the world, contributing not only to their own growth and experience, but also to those companies they work for and those countries they work in.

To appreciate and recognize this also involves the collaboration and investment that the continent requires in both universities and research centres. With digital mining one of the main drivers in the fourth industrial revolution, the requirement for a sustained pool of local researchers, innovators, engineers and technicians is obvious. To contribute in this revolution, Africa needs the tools, equipment and cooperation to not only add, but also assist in driving the conversation. The retention, development and specialisation of the expert educators and researchers, together with those that graduate, are key to a bright mining future. Failure to support universities and centres of R&D, innovation and excellence in the developing world, by government, industry and others, will ultimately lead to total dependency upon expertise and direction from countries in North America, Europe and Australia. This dependency will not only be down to the expertise, worse still it will be on their availability, which in a resources boom scenario together with a low number of professionals could be limited, leading to loss in opportunity for country and continent. Lack of African mining engineers will also affect the continent's effective contribution to the digital mining revolution and will negatively impact the discovery and development of the continent's extensive natural resources. This will have an obvious global negative impact, as Africa is richly endowed with many of the minerals and natural resources required both locally and worldwide for innovation, technology and sustainable economic development into the 21st century and beyond.

Regulatory and tax incentives should be structured to ensure that industry supports the long-term objectives of extraction to the benefit of investors and local stakeholders alike, especially so as seen in the South African context. UMaT in Ghana could benefit from more industry support, though unlike South Africa lacks a larger and stronger commodity and industry base to suitably assist. Although initiatives are aligned to diversify the economy and multiply Ghana's wealth, it requires an investment in mining and engineering education and research to reach such milestone in the most effective, efficient and economic manner. The various stakeholders in Ghana will need to suitably address the situation and reach a Ghanaian solution that benefits all, which needs to be strategic and long-term in nature, as lack of funding and high university staff turnover will most likely be an impediment to growth.

Many of the universities are already adapting to the challenges the future holds and are blessed with the youthful talent keen to become involved. Through increased and sustained investment by government, private industry and others, together with fostering ever closer relationships with like-minded institutions and organisations that see a brighter and more prosperous future through sharing and cooperation, African universities will not only ensure that they provide sufficient expertly trained professionals, but also the innovations and research to assist them, whilst adding to the global discourse in ensuring digital mining is a success for not only this generation, but also those that follow. The key to prosperity is intimately linked to not only the quantity and quality of the technicians, engineers and innovators that can be produced within the minerals industry, but also the facilities provided to this pool of pioneers to explore, utilise and grow their talents.

REFERENCES

[1] Australian Bureau of Agricultural and Resource Economics, Australian Commodities Statistics, and Department of Industry and Science.
[2] Chamberlain, B. 2007. CSIRO Minerals Down Under national research flagship. The AusIMM Bulletin, vol. no. 5, September/October 2007, p. 12.

[3] CSIR. 2018. Retrieved from: https://www.csir.co.za/modernising-mining-through-partnerships-and-transformation.

[4] Durrant-Whyte, H. et al. 2015. How digital innovation can improve mining productivity. McKinsey & Co. Retrieved from: https://www.mckinsey.com/industries/metals-and-mining/our-insights/how-digital-innovation-can-improve-mining-productivity.

[5] Engineers Canada Website. Retrieved in 2018 from https://engineerscanada.ca/reports/canadian-engineers-for-tomorrow-2016#data-tabulations-engineering-enrolment-and-degrees-awarded

[6] Gold Fields Limited. 2018. Company Website and personal correspondence.

[7] Holland, N. 2014. "Gold mining and shared value: Contributing to development and communities." GREAT insights Magazine, Volume 3, Issue 7. July/August 2014. Retrieved from: https://ecdpm.org/great-insights/extractive-sector-african-perspectives/sharing-benefits-gold-mining/. ICMM (2007) and McMahon and Moreira (2014).

[8] ICMM. Data UNCTAD. 2018. Retrieved from http://data.icmm.com/.

[9] Kosich, D. 2014. "Shrinking mining professional ranks may impact investors". Retrieved from https://republicofmining.com/2014/07/29/shrinking-mining-professional-ranks-may-impact-investors-hsbc-by-dorothy-kosich-mineweb-com-july-29-2014/ & http://www.canadianminingjournal.com/news/comment-mining-industry-talent-forecast.

[10] Mining.com. Retrieved from: www.mining.com and https://www.mining-technology.com/features/mining-robots-rio-tinto-doubles-autonomous-drilling/.

[11] Musingwini C. 2017. Professor and Head of the Wits School of Mining Engineering, "The role of the mining industry during this difficult time in our academic environment and how tertiary institutions can continue to support the mining industry's skills pipeline", Chamber of Mines (now Minerals Council) of South Africa, 23 May 2017, Pre-AGM Dinner Speech.

[12] PWC. 2017. Mine 2017. Retrieved from https://www.pwc.com/gx/en/mining/assets/mine-2017-pwc.pdf.

[13] Rio Tinto Media Release. 2018. "Rio Tinto's iron ore business delivering value through additional flexibility". Retrieved from: https://www.riotinto.com/documents/180618_Rio_Tintos_iron_ore_business_delivering_value_through_additional_flexibility.pdf.

[14] Stacey, T.R. et al. 2008. "Technical skills—a major strategic issue". The Journal of The Southern African Institute of Mining and Metallurgy.

[15] Stirling, D. (Chair of the Monash Mining & Resources Advisory Board). 2018. "Mining engineering graduates in short supply". Monash University Lens. Retrieved from: https://lens.monash.edu/2018/04/16/1346398/mining-story.

[16] The Mining Association of Canada (MAC). 2017. Facts and Figures of the Canadian Mining Industry.

[17] Thermofisher blog summary of Deloitte report. 2018. Retrieved from https://www.thermofisher.com/blog/mining/2018-deloitte-report-mining-industry-trends-and-challenges/ & Deloitte 'Tracking the trends 2018' report: http://www.mining.com/wp-content/uploads/2018/01/Deloitte-Tracking-the-Trends-Global-Mining-Study-FINAL.pdf?kui=rzrUq_cVzFSMfpMQ8K4YFw#_ts=1519224874 780; https://mineralsmakelife.org/resources/minerals-mining-the-forefront-of-tech-innovation/.

[18] Topuniversities.com. 2018. Retrieved from: https://www.topuniversities.com/university-rankings/university-subject-rankings/2018/engineering-mineral-mining.

[19] UNESCO Institute for Statistics (UIS). Retrieved from: http://uis.unesco.org/apps/visualisations/research-and-development-spending/.

[20] University websites and personal communication. 2018.

[21] Various. Retrieved from: http://www.abc.net.au/news/2015-10-18/img_0266.jpg/6864164; www.mining.com; https://www.mining-technology.com/features/mining-robots-rio-tinto-doubles-autonomous-drilling; http://www.mining.com/rio-tinto-back-on-track-to-haul-iron-ore-in-driverless-trains-beginning-next-year/. Image: Christian Sprogoe Photography|Rio Tinto.

The application of correlation models for the analysis of market risk factors in KGHM capital group

Łukasz Bielak & Paweł Miśta
KGHM, Lubin, Poland

Anna Michalak
Faculty of Geoengineering, Mining and Geology, Wrocław University of Science and Technology, Wrocław, Poland

Agnieszka Wyłomańska
Faculty of Pure and Applied Mathematics, Wrocław University of Science and Technology, Wrocław, Poland

ABSTRACT: Mining companies to properly manage their operations and be ready to make business decisions are required to forecast potential scenarios for main market risk factors. Regardless of the typical uncertainty related to asset price projections, the main challenge is to properly quantify dependencies/relations among main risk factors and its stability over time. From the KGHM perspective, Polish copper and silver mining company, main market risks can be divided into four baskets: base metals (copper, nickel), precious metals (gold, silver), exchange rates (EURUSD, Dollar Index, USDPLN) and interest rates (LIBOR). Detailed studies of the risk factors dependency structure and finding proper correlation models may enable building more adequate forecasts, especially for stress test scenarios. In the literature one can find different approaches in the considered issue. In this paper we concentrate on the relations between mentioned factors and using mathematical/statistical methods we propose a models that takes under consideration the dependences between them.

1 INTRODUCTION

Risk measurement is an integral and very important part of market risk management process.
    Proper determination of market risk exposure and exposure change dynamics allows for the selection and application of appropriate tools, by means of which this risk can be properly shaped and managed. KGHM as a mining company is exposed on significant market risk driven by mainly metals prices and exchange rates. For planning and sensitivity analysis purposes there are prepared several potential price deck scenarios which are based on certain given correlations between main risk factors. Confirmation of dependence between risk factors or improvement of used methodology to reflect dynamic characteristic of such relations may help in improving of the usability of the price deck scenarios that are prepared. In the literature there are known many measures that can help to describe the dependence between variables and indicate the strength of the relationship between them. One of the most classical one is the Pearson correlation coefficient which indicates the linear relationship between variables. The classical measure was introduced in 1895 and it is the most often used in the problem of the data dependence description because of its simple form. However, this measure indicates only the linear dependence between data and might be misleading in case of the nonlinear relation [1]. Thus one can find different alternative measures used in this context. Among all measures of association between data the Kendall's rank correlation seems to be the most popular. It can be used in the nonlinear relationship between variables, it does not depend on their scale and is robust of outliers. Especially the last feature of the

Kendall'r rank correlation caused it to be used frequently in the real data analysis [2–4]. It is especially important in the analysis of variables with non-Gaussian behaviour often demonstrated in the real time series. The other measure of relationship that need to be mentioned is the Spearman correlation. The Spearman correlation between two variables is equal to the Pearson correlation between the rank values of those two variables; while Pearson's correlation assesses linear relationships, Spearman's correlation assesses monotonic relationships (whether linear or not) [2].

In the more advanced statistical analysis one can also consider other measures of dependence adequate especially for processes with infinite variance. We only mention here the codifference [5–7], covariation [5,8–10] and fractional lower order covariance [11–12]. All of them are used in the practical applications and can be alternatives to the classical measures of dependence.

Beyond the aforementioned measures of dependence, in the literature there are considered weighted correlation coefficients [13–14], to obtain reliable full-rank dependence measures which take under consideration the fact that present observations weight more than past measurements. Therefore the weighted correlation coefficients can characterise the dynamics of the dependence structure in the better way than the classical measures [13]. It should be mentioned, the idea of weighted correlations is not new [14–17]. The study of the optimal weights, aimed at avoiding unwelcome side effects has been mostly overlooked in the literature.

In this paper we analyse three selected correlation coefficients presented in [13], namely classical Pearson correlation coefficient, Kendall's rank correlation and exponentially weighted Pearson correlation coefficient. We apply them in order to find the relationship between main market risk factors of KGHM capital group. We indicate that three mentioned correlation coefficients can give different information about the structure of dependence dynamics of the selected risk factors. We analyse the relationship as a function of time in order to indicate it changes when the unexpected events on the market appear. The main result of the paper is to demonstrate that the main market risk factors of KGHM capital group are strongly correlated and different measures of relationship change over time. However, the weighted correlation coefficient is more sensitive on the market changes with respect to the measures that take under consideration all observations with the same weights. Thus in order to enable using the examined relation for forecasting purposes it is crucial to build models taking under account this kind of correlation measures.

The rest of the paper is organized as follows: in section 2 we present the main market risk factors of the KGHM capital group and indicate their specific behaviour. Section 3 is devoted to the measuring of the dependence dynamics of the selected marker risk factors. We introduce three analysed measures of dependence and in section 4 indicate their behaviour for the analysed time series taking into account parameters of selected measures such as the weight factor in the weighted Pearson correlation coefficient or the way of their determining (data frequency). All analysed factors influence the behaviour of the structure of dependence dynamics. Last section concludes the paper.

2 MAIN MARKET RISK FACTORS OF KGHM CAPITAL GROUP

In this section we present briefly the main market risk factors of KGHM capital group that are analysed in the following sections. In our analysis we take under consideration the following factors: copper (Cu) price, gold (Au) and silver (Ag) prices, nickel (Ni) price, EURUSD and USDPLN exchange rates and LIBOR. Due to lack of space we present only selected time series of the risk factors that will be analysed in following sections, namely Cu, Ag, Au and USDPLN. In Fig. 1 we demonstrate their behaviour along time. In this paper we examine the daily real time series from 1st of January 2000 to 31st of March 2017.

As one can see, the data exhibit very specific behaviour. In Fig. 2, we present the logarithmic rates of return for selected risk factors. They change dynamically over time and in many cases the variance of the data is very high, especially for metals. Moreover, one can see non-Gaussian behaviour of the analysed time series. Volatility clustering appears in similar
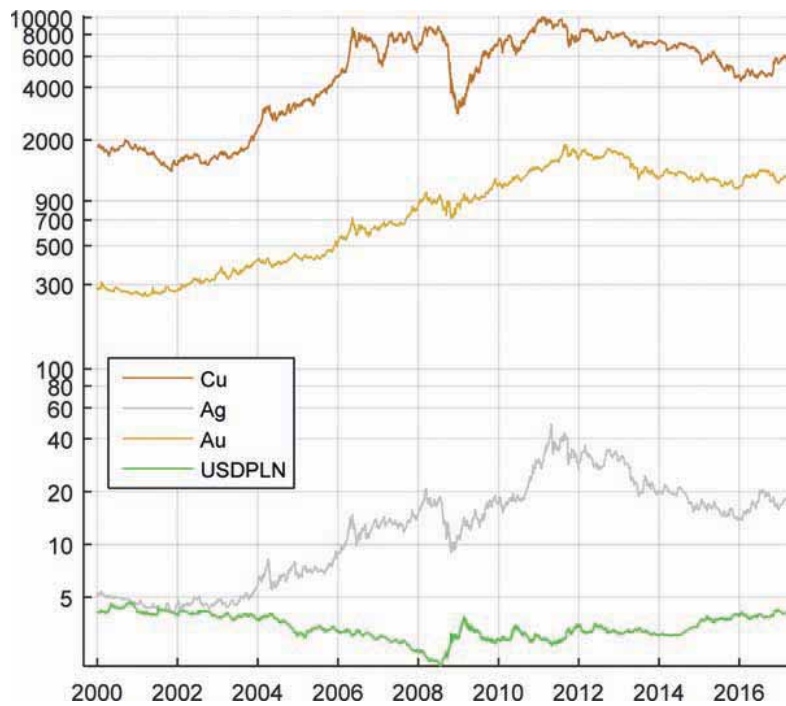
Figure 1. The time series related to four selected risk factors.
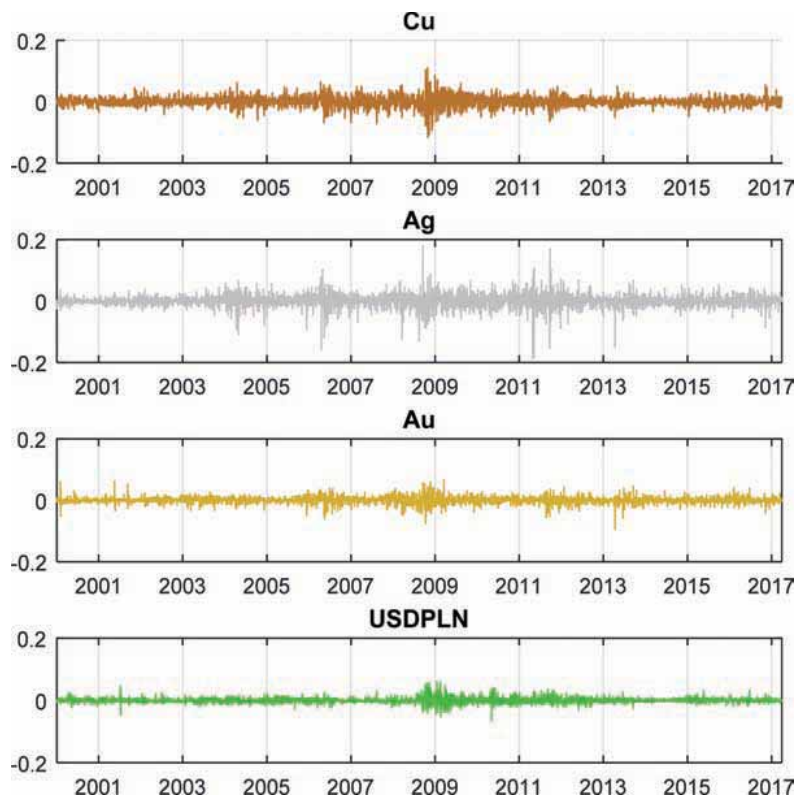
Figure 2. The logarithmic rates of return related to four selected risk factors.

40

sections of time what can mean that one may suspect there is a strong relationship between the presented market risk factors. Thus in the next section we examine the real time series in the context of their dependence dynamic expressed in the terms of different measures of dependence. The relationship between the main risk factors will be analysed as a function of time. Therefore one can observe the significant changes of the risk factors (caused by changes on the market) influence the changes of the relationship between them.

3 MEASURING THE RELATIONSHIP BETWEEN MAIN MARKET RISK FACTORS OF KGHM CAPITAL GROUP

As it was mentioned, in this section we analyze the relationship between the main market risk factors of the KGHM capital group. First, we make the visual inspection of the relationship between them and in Fig. 3 we present correlogram-like picture. On the diagonal of the matrix we indicate the risk factors. More precisely, the n-th diagonal indicates which row and each column corresponds to given factor. In the upper triangular matrix we present the scatter plots of the given factors indicating their relationship. Based on this we can perfectly select which market risk factors of KGHM capital group are the most dependent. In the further analysis they are taken under consideration. In the bottom triangular matrix we demonstrate the scatterplots for the logarithmic returns of the analyzed risk factors. In the
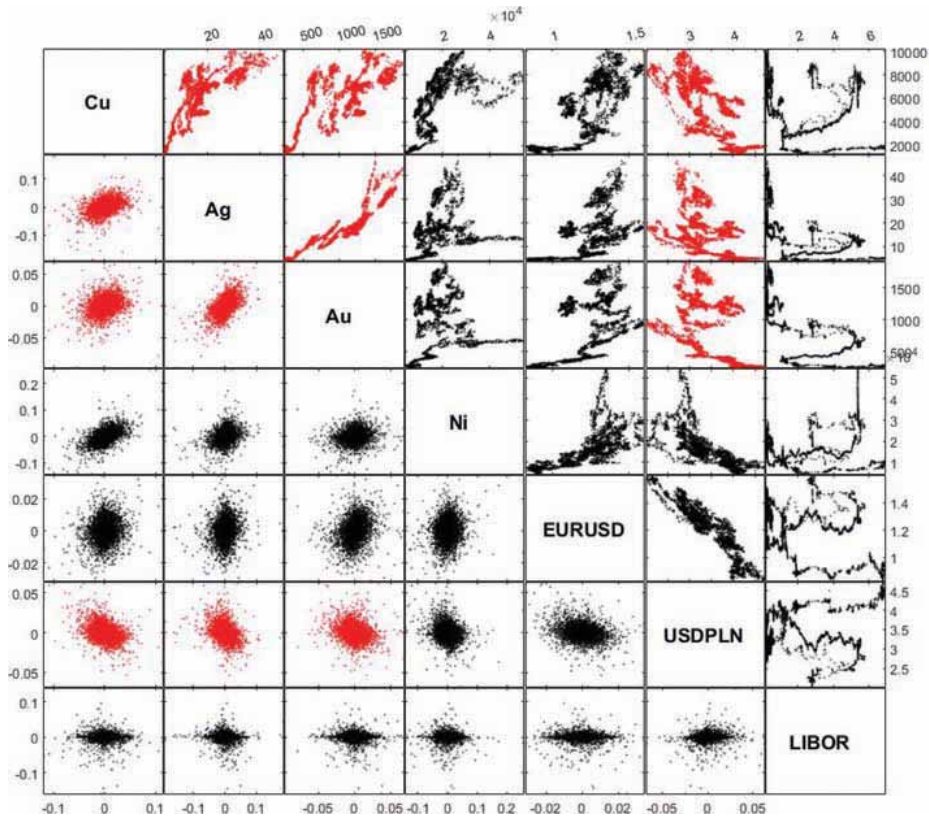
Figure 3. The correlogram-like picture. On the diagonal of the matrix we indicate the market risk factors. The n-th diagonal indicates which row and each column corresponds to given factor. In the upper triangular matrix we present the scatter plots of the given factors indicating their relationship. The selected market risk factors are marked in red. The bottom triangular matrix we present the scatterplots for the logarithmic returns.

further analysis we calculate the selected measures of dependence for logarithmic returns of the selected risk factors. In Fig. 3 we highlighted those factors for which the relationship seems to be the strongest by visual inspection. Based on Fig. 3 we have selected four market risk factors: Cu, Ag, Au and USDPLN. They are presented in Fig. 1. They seem to be related however the dependence have different character. For some time periods we observe the positive relationship between the selected factors while for some cases—negative. In the further analysis we quantify the dependence and prove our assumption by using the appropriate correlation coefficients.

After visual inspection, we propose to quantify the relationship between the selected market risk factors. We propose to take under consideration three different measures of dependence. The first one is the classical Pearson correlation coefficient [1]. In statistics, the Pearson correlation coefficient is a measure of the linear relation between two variables X and Y. According to the Cauchy–Schwarz inequality it has a value between +1 and −1, where 1 is total positive linear correlation, 0 is no linear correlation, and −1 is total negative linear correlation. This is the most classical dependence measure and its empirical version for two time series $x = (x_1, x_2, ..., x_n)$ and $y = (y_1, y_2, ..., y_n)$ is defined as follows [13]:

$$\rho_{xy} = \frac{\sigma^2_{xy}}{\sigma_{xx}\sigma_{yy}}, \tag{1}$$

where σ_{xy} is the empirical covariance of the vectors x and y defined as:

$$\sigma^2_{xy} = \frac{1}{n}\sum_{i=1}^{n}(x_i - \bar{x})(y_i - \bar{y})$$

and $\bar{x}, \bar{y}$ are sample means of vectors x and y, respectively. Moreover σ_{xx} is the sample standard deviation of vector x and σ_{yy} – of vector y. The Pearson correlation coefficient is easy to calculate thus it is often used in the real applications. But is should be noted that this measure has few important disadvantages. The first one is that the Pearson correlation coefficient captures the linear relationship between variables and is insufficient for nonlinear relations. It depends on the unit of the measurements and does not change when there is a nonlinear transformation of the considered variables. The Pearson correlation coefficient is not robust to the outliers and is equally sensitive for all observations and generally is defined when the observations comes from the finite-variance processes [13]. In our analysis we calculate the Pearson correlation coefficient (as well as the Kendall's rank correlation) as a function of time, i.e. we calculate the parameter according to formula (1) for logarithmic returns of the real time series from given window length. Then, the time is moving and the next value of the correlation is obtained for data from the next time periods for the same window length.

In order to capture the non-Gaussian behaviour of the given data we propose to calculate the Kendall's rank correlation [2–4]. It describes nonlinear but monotonic relationship between two data sets and does not depend on the scale of the considered variables. This measure is robust to outliers and thus can be applicable for data with infinite variance. The Kendall's rank coefficient does not depend on the distribution of the variables. If we consider two time series $x = (x_1, x_2, ..., x_n)$ and $y = (y_1, y_2, ..., y_n)$, then the Kendall's rank coefficient is defined as follows [18]:

$$\tau_{xy} = \frac{2}{n(n-1)}\sum_{u=1}^{n-1}\sum_{v=1}^{n}d^x_{ij}d^y_{ij}, \tag{2}$$

where $d^x_{ij} = sign(x_i - x_j)$ and $d^y_{ij} = sign(y_i - y_j)$. In the literature one can find different modifications of the Kendall's rank coefficient, see for instance [19].

In the analysis of many real data, especially financial time series, the crucial is to consider observations from different periods with different weights and analyse not the raw

data itself but the weighted ones. The simplest case is to assign smaller weights for observations from the past periods than from the current period (not far from the present time point). In the literature one can find different modifications of the classical measures of dependences in this direction [14–17]. In this paper we take under consideration the exponentially weighted Pearson correlation coefficient [13]. In general, the weighted Pearson correlation coefficient for two time series $x = (x_1, x_2, \ldots, x_n)$ and $y = (y_1, y_2, \ldots, y_n)$ is defined as follows:

$$\rho_{xy}^w = \frac{\left(\sigma_{xy}^w\right)^2}{\sigma_{xx}^w \sigma_{yy}^w},$$

(3)

where

$$\left(\sigma_{xy}^w\right)^2 = \sum_{i=1}^n w_i\left(x_i - \overline{x^w}\right)\left(y_i - \overline{y^w}\right), \qquad \sigma_{xx}^w = \sqrt{\sum_{i=1}^n w_i\left(x_i - \overline{x^w}\right)^2}, \qquad \overline{x^w} = \sum_{i=1}^n w_i x_i.$$

In the same way we define the σ_{yy}^w and $\overline{y^w}$. In the above equations the vector $w = (w_1, w_2, \ldots, w_n)$ represents the weights, i.e. for each $i = 1, 2, \ldots, n$ $w_i \geq 0$ and $\sum_{i=1}^n w_i = 1$. In our analysis we propose to take the exponential weights, i.e. $w_i = w_0 exp\,(\alpha i)$, where $w_0 > 0$ is such that the following is fulfilled:

$$\sum_{i=1}^n w_0 exp\left(\alpha i\right) = 1.$$

When $\alpha = 0$, then the weights are uniform and the exponentially weighted Pearson correlation coefficient reduces to the classical Pearson correlation coefficient.

4 REAL TIME SERIES ANALYSIS

In this section we present the real time series analysis using the presented methodology. For the selected market risk factors we will analyze the introduced dependence measures with respect to time in order to describe its dynamic related to unexpected market events. The Cu price will be compared with the other three risk factors selected in the previous section. The measures of dependence are calculated for the logarithmic returns of real time series. In order to check how sensitive are the analyzed correlation parameters for the frequency of the data for each pair of the risk factors we analyze three different frequencies: daily, weekly and monthly. The weekly data are calculated as the mean of the daily time series corresponding to given week, while the monthly data are calculated as the mean of the daily time series corresponding to given month.

In each considered case we calculate the correlation coefficients based on data from period of time corresponding to 10 years. For the daily data we shift the window for 5 days, while for the weekly correlation coefficients—for one week and for the monthly—for one month. For each pair of risk factors we present the same analysis. On left-top panels of the Figs. 4–6 we demonstrate the classical Pearson and Kendall's rank correlations for daily, weekly and monthly data. On the right-top panels we present the exponentially weighted Pearson correlation coefficient with $\alpha = 0.03$ while on the bottom panel we compare the classical Pearson and Kendall's rank coefficients for daily data with the exponentially weighted Pearson correlation coefficient for three different vales of the α parameter, namely: 0.1, 0.03 and 0.01. As one can observe on Figs. 4–6 the classical Pearson and Kendall's rank correlations are not sensitive on the significant changes on the market and do not indicate properly the dynamic of the dependence between analyzed market risk factors. They are very smooth for three methods of their determining (daily, weekly and monthly).
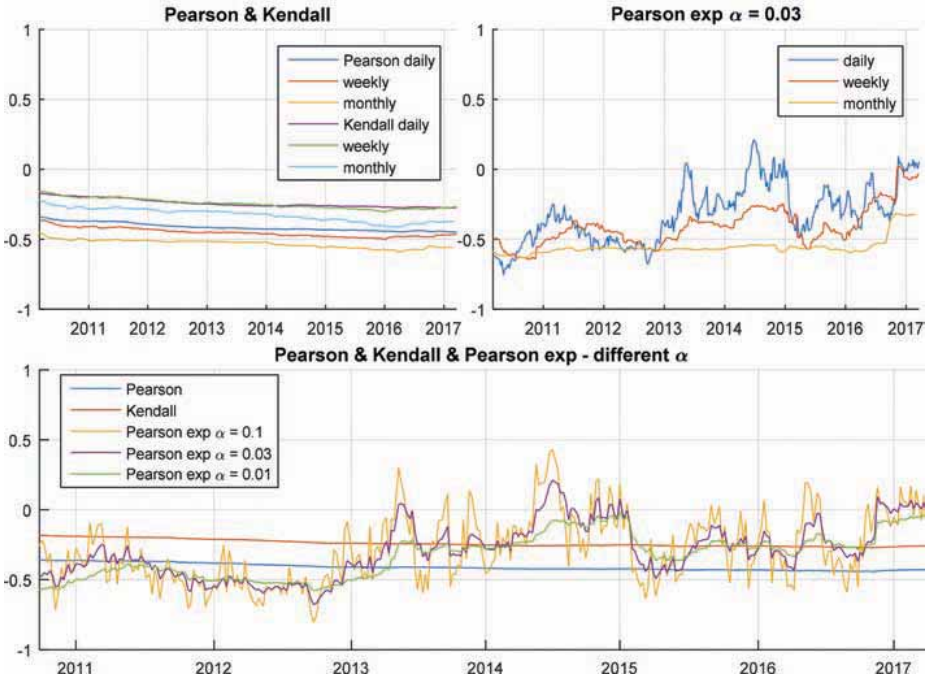
Figure 4. Cu-USDPLN. Left-top panel: the classical Pearson and Kendall's rank correlations for daily, weekly and monthly time series. Right-top panel: the exponentially weighted Pearson correlation coefficient with $\alpha = 0.03$ for daily, weekly and monthly data. Bottom panel: the comparison between classical Pearson and Kendall's rank correlation coefficients and exponentially weighted Pearson correlation coefficient for daily data for three different values of α parameter: *0.1, 0.03* and *0.01*.

The exponentially weighted Pearson correlation coefficient seems to be more sensitive for the significant changes in the real data and their relationship. Based on this dependence measure one can observe the dynamic of the correlation. By using this measure we can easily indicate the periods of time when the dependence between factors is positive and negative. The best results one can observe when the exponentially weighted Pearson correlation coefficient is determined for the daily data. In such a case the significant changes of the structure of dependence is easily to observe. For weekly and monthly data the measures of dependence are more smooth than for the daily data-approach. This simple analysis demonstrates there is need to consider the weighted correlation coefficients and consider observations from different periods with different weights for daily data. This approach seems to be crucial in the problem of analyzing the dynamic of dependence for main market risk factors.

As one can see in Fig. 4, the Pearson and Kendall's rank correlations (for all data frequencies) are negative, which indicate the negative relationship between Cu price and USDPLN exchange rate. However, the exponentially weighted Pearson correlation coefficient is a little above zero in 2014. This measure of dependence calculated for daily data clearly indicate the change in the relationship between analyzed factors.

One can see in Fig. 5 all analyzed measures of dependence are positive and their values are around 0.5 which indicates strong positive relationship between the risk factors. However the exponentially weighted Pearson correlation coefficient for daily data falls below zero in 2016. The other measures of dependence do not indicate this event.

For the Cu-Au the classical measures of dependence are always positive. The exponentially weighted Pearson correlation coefficient falls below zero for daily data in 2014 and 2016. This negative correlation corresponds with the behaviour of the data in Fig. 1.
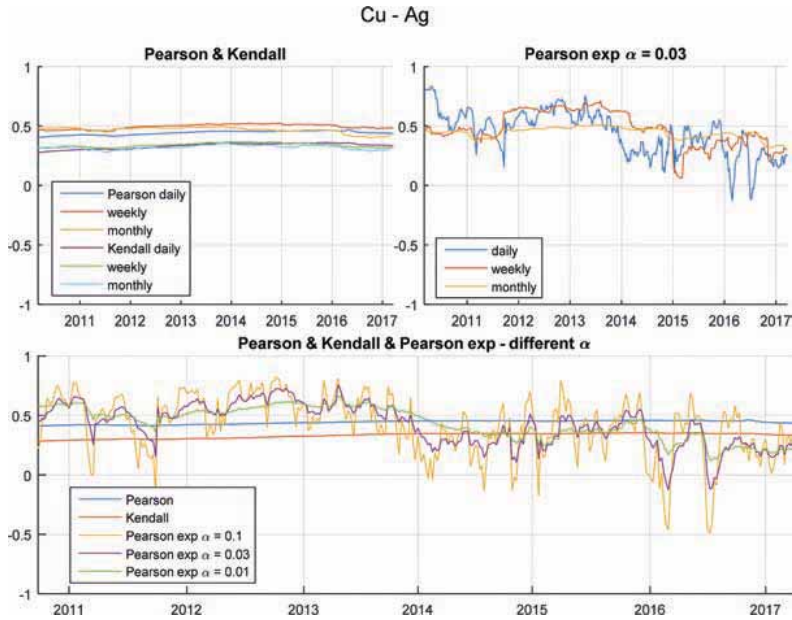
Figure 5.   Cu-Ag. Left-top panel: the classical Pearson and Kendall's rank correlations for daily, weekly and monthly time series. Right-top panel: the exponentially weighted Pearson correlation coefficient with $\alpha = 0.03$ for daily, weekly and monthly data. Bottom panel: the comparison between classical Pearson and Kendall's rank correlation coefficients and exponentially weighted Pearson correlation coefficient for daily data for three different values of α parameter: *0.1, 0.03* and *0.01*.
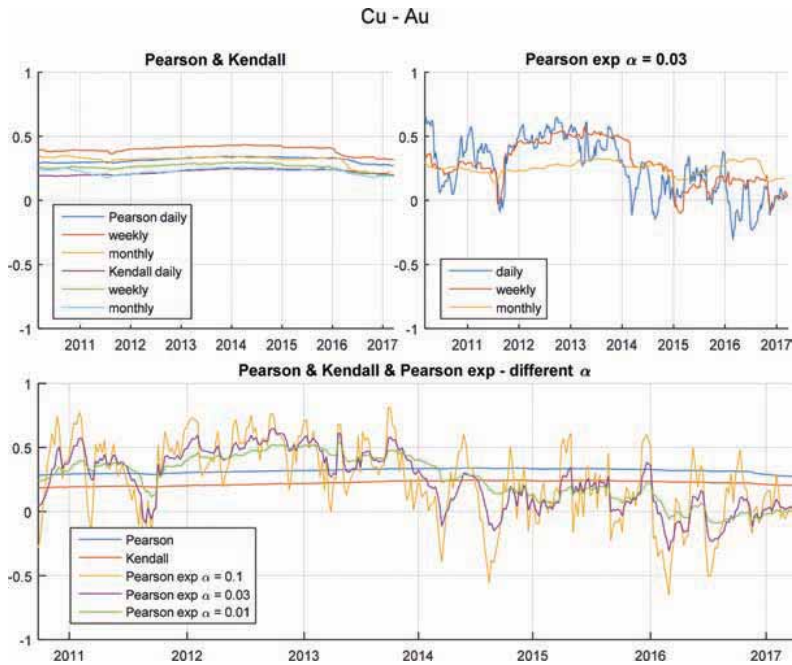
Figure 6.   Cu-Au. Left-top panel: the classical Pearson and Kendall's rank correlations for daily, weekly and monthly time series. Right-top panel: the exponentially weighted Pearson correlation coefficient with $\alpha = 0.03$ for daily, weekly and monthly data. Bottom panel: the comparison between classical Pearson and Kendall's rank correlation coefficients and exponentially weighted Pearson correlation coefficient for daily data for three different values of α parameter: *0.1, 0.03* and *0.01*.

5 CONCLUSIONS

In this paper we have considered the different approaches used in the parametrization of the relationship of the main market risk factors of KGHM capital group. Based on the visual inspection and the correlogram-like picture we have selected four market risk factors that are mostly dependent. We have proposed three approaches to quantify the dependence structure for analyzed data, namely classical Pearson, Kendall's rank correlations and exponentially weighted Pearson correlation coefficient. Based on the mentioned measures of dependence determined as functions of time we have indicated their differences based on the real time series analysis. The main result of this paper is the fact that the weighted correlation coefficient seems to be the most appropriate in the description of the structure of dependence for analyzed market risk factors. Moreover, the correlation coefficients calculated for daily data demonstrate proper dynamic of the dependence which corresponds with the behavior of the data caused by market events. The presented approach can be a base for analyzing the models which take under consideration the dependence of the data expressed in terms of non-classical measures of dependence. One of the most important questions, which can be addressed here is whether there are regime changes of relations between risk factors and if they exists how it can be used for forecasting purposes.

REFERENCES

[1] P.J. Brockwell, R.A. Davis, Introduction to Time Series and Forecasting, Springer, 2002.

[2] W.W. Daniel, Kendall's tau, Applied Nonparametric Statistics (2nd ed.). Boston: PWS-Kent. 365–377. 1990.

[3] M. Kendall, J.D. Gibbons, Rank Correlation Methods. Charles Griffin Book Series (5th ed.). Oxford: Oxford University Press, 1990.

[4] D.G. Bonett, T.A. Wright, Sample size requirements for estimating Pearson, Kendall, and Spearman correlations, Psychometrika. 65 (1), 23–28, 2000.

[5] G. Samorodnitsky, M.S. Taqqu, Stable Non-Gaussian Random Processes, Chapman & Hall, 1994.

[6] D. Rosadi, M. Deistler, Estimating the codifference function of linear time series models with infinite variance, Metrika 73(3), 395–429, 2011.

[7] A. Wyłomańska, A. Chechkin, I.M. Sokolov, J. Gajda, Codifference as a practical tool to measure interdependence, Physica A 421, 412–429, 2015.

[8] C.M. Gallagher, A method for fitting stable autoregressive models using the autocovariation function, Statistics & Probability Letters 53, 381–390, 2001.

[9] P. Kruczek, A. Wyłomańska, M. Teuerle, J. Gajda, The modified Yule-Walker method for alpha-stable time series models, Physica A 469, 588–603, 2017.

[10] G. Żak, M. Teuerle, A. Wyłomańska Agnieszka, R. Zimroz, Measures of dependence for alpha-stable distributed processes and its application to diagnostics of local damage in presence of impulsive noise, Shock and Vibration, vol. 2017, Article ID 1963769, 9 pages, 2017.

[11] M. Shao, C.L. Nikias, Signal processing with fractional lower order moments: stable processes and their applications, Proceedings of the IEEE 81(7), 986–1010, 1993.

[12] G. Żak, A. Wyłomańska, R. Zimroz, Periodically impulsive behaviour detection in noisy observation based on generalised fractional order dependency map, Applied Acoustics 144, 31–39, 2019.

[13] F. Pozzi, T. Di Matteo, T. Aste, Exponential smoothing weighted correlations, Eur. Phys. J. B 85, 175, 2012.

[14] A. Meucci, Risk and Asset Allocation, Springer, 2005.

[15] R. Litterman, K. Winkelmann, Estimating covariance matrices, in Goldman Sachs, Risk Management Series, 1998.

[16] D. Quade, I.A. Salama, A survey of weighted rank correlation, in Order Statistics and Nonparametrics: Theory and Applications, edited by P.K. Sen, I.A. Salama, Elsevier, 1992.

[17] J. Svensson, The asymptotic spectrum of the EWMA covariance estimator, Physica A 385, 621–630, 2007.

[18] M.G. Kendall, A new measure of rank correlation, Biometrika 30, 81–93, 1938.

[19] M.G. Kendall, Rank Correlation Methods, Charles Griffin & Co Ltd., 1948.

Improvement of investment processes in mining company by implementation of project management system

M. Wach
KGHM Polska Miedź S.A., Lubin, Poland

I. Chomiak-Orsa
Wrocław University of Economics, Wrocław, Poland

ABSTRACT: The paper presents the experience gained from implementing Project Management System in investment processes of mining company on an example of KGHM Polska Miedź S.A. The customized system architecture has been developed to effectively support project management area negatively influenced by the extensive planning phases, delayed reporting, hampered portfolio management and hard accessible data sources. Specific attention is paid to the positive impact Project Management System has on project managers, project management offices and decision-making processes on strategic level. Expansion of Business Intelligence tools and databases led to further development including: balancing and consolidation of portfolios, electronic documentation workflow and detailed statistical reports. Research has been set up to incorporate predictive analysis capable of estimating real budget, scope and time required for successful completion of project's tasks.

1 INTRODUCTION

In the second half of the year 2010 KGHM Polska Miedź S.A. initiated works aimed at development and introduction of a dedicated IT platform for company's investment structures. The platform would serve as a comprehensive tool for Enterprise Project Management (EPM). EPM does not possess a unified definition, but some of its features are commonly mentioned in various publications regarding that subject. Hornby (2000) describes it as "(…) a number of initiatives aimed at improving management effectiveness beyond a single project and the strict domain of an individual project management. These include consolidation of multiple projects using advanced project management software, elevation of a project office to departmental level, and project management competency improvement (…)". Crawford (2010) describes the main role of EPM as "linking corporate strategy to programs and projects" so that "strategy document produced by senior management can be converted into the projects and programs that carry out that strategy". The above characteristics reflect in KGHM's approach to carry out investments, that are entirely centered around managing projects. The company's investment budget is divided into project portfolios assigned to KGHM's divisions (mines, smelters etc.). These divisions utilize the products of these projects solely for their own purpose, with an exception of the Central Division that possesses multiple portfolios consisted of projects that benefit the whole company like e.g. resource exploration projects. In 2010–2014 period project management had a growing importance as a result of upcoming implementation of the new project methodology. It was necessary to create a customized Project Management System to effectively oversee all portfolios and meet the assumptions of EPM.

2 REASONS OF IMPLEMENTATION

By the time the works on the Project Management System began, multiple reasons indicating a need to create this kind of system had been identified and characterized. The most important issues Project Management System had to address can be divided into three key areas: managing investment projects, supporting investment decision-making processes and facilitating the access to project information for the stakeholders.

2.1 Project management

In terms of project management, the main objective was to facilitate work done by Project Managers (PMs) during a projects' lifetime. Instead of contracting PMs from outside of the company, KGHM tends to entrust the task of project managing to its own employees, who are specialist in the given field. Müller & Turner (2007) claim that managers from local teams who are involved in the wider lifecycle of a project tend to be more successful. Moreover, singularity of the business conducted by the KGHM in the region supports this approach, as there is a deficiency of professional PMs experienced in underground mining. On the other hand, it can be observed, that local PMs, especially these beginning their work with projects, might be under-skilled in the sense of scheduling, accounting and reporting, as well as lacking the general comprehension of investment processes. From a financial point of view, cost incurred on software licensing related to carrying out all project activities was disproportionate to the amount of work done. For example, 30% of SAP ERP licenses possessed by the company were used solely for the purpose of managing projects. Both these negative issues were planned to be resolved by integrating already existing systems into one platform that reduces licensing cost and simplifies all management activities including the access to accounting, purchases and contract management. For this reason, the system was perceived by the management as an useful tool to enhance bottom-up planning, that can translate into increased accuracy of scope, budget and time required to deliver project's products as well as shortening the period of transition to project implementation phase.

2.2 Planning and reporting

Apart from facilitating project management, the system was meant to positively impact budgeting and reporting abilities of the company and in this way to improve decision-making process. Reduction of time needed to prepare customized reports based on real time information was one of the main objectives when introducing the system. At that time reporting was based primarily on the information gathered by PMs and send to local planning departments, that merged these reports into full information about divisional investments. This basic approach was highly sensitive to human errors, lack of data integrity and complexity of tools needed in cross-checking the reports reaching the Central Division. IT tools utilized at that time were incapable of producing real time information and establishing communication with accounting systems like SAP ERP. The Project Management System had been planned as a means to enforce a single, company-wide model of planning and managing investments. Although the investment policies established around the company were followed, they left too much space for individual tool choice and data inconsistency. The growing number of investment tasks required quick introduction of company-wide standard in documentation and reporting. Moreover, a new project management methodology had not been fully developed yet, as it closely followed the introduction of the Project Management System.

2.3 Communication

The third issue that had to be addressed, was the difficulty in accessing project information by projects stakeholders and poor communication within the projects. An IT solution

was needed to allow an undisturbed access to project documentation, limited only by the roles users hold in the project or company organization structure. Moreover, paper based document workflow utilized at the time was already outdated, highly time consuming and required to be replaced by electronic workflow of documents and tasks as soon as possible.

3 SYSTEM ARCHITECTURE AND FUNCTIONALITIES

3.1 *Architecture*

The architecture of the Project Management System has been based on Microsoft Project Server 2010 and SharePoint Server 2010. Both products through their core functionalities support project management and communication in big organizations. The main technical challenge was to create efficient connection with SAP ERP system, that was already utilized to support financial processes. Because the Project Management System required much more flexibility then SAP ERP in terms of data modification, a dedicated application has been developed to link both systems and ensure their compatibility.

The role of SAP ERP in accounting services remained unaffected, but it has been moved to the background so it no longer needs to be directly accessed by the PMs. Apart from SAP ERP, there are two other systems operating within the company that require data exchange with Project Management System, these are: Contract Management System that store all the information regarding signed contracts and Purchase Support System that allows to manage procurement and purchase procedures. MS BizTalk Server has been chosen as a mean of communication between internal and external elements of the environment. The customized application guarantees safety of communication and prevents creating records in external systems without user consent and control. A simplified system architecture scheme is presented in Figure 1.
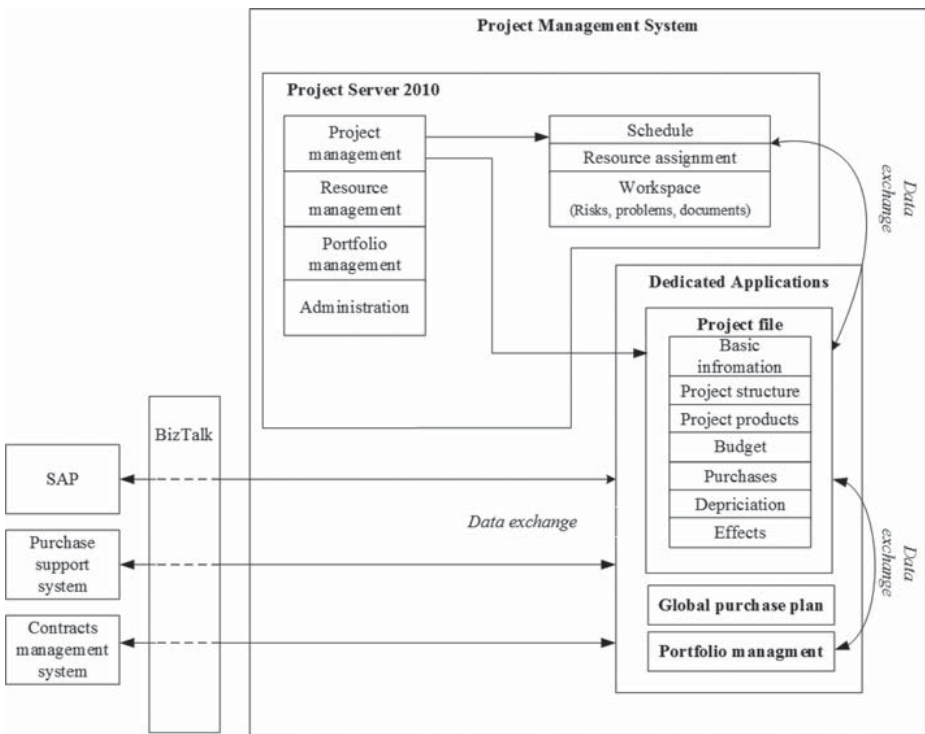
Figure 1.   Project management system architecture.

Project's website and dedicated applications utilize SharePoint platform as the interface to input and present project data. From the user point of view, access to the system is enabled via web browser with the additional ability to create detailed schedule in MS Project. Project Management System allows its users to conduct all necessary operations related to project management, including:

- **Creating and submitting project application form** – inputting of basic information describing project (project ID, classification, length, source of financing), creating project schedule with budget and dependencies assigned to tasks, establishing depreciation plan based on capital expenditures (CAPEX) planned in the schedule, assigning project roles to other users of the system, creating the accounting structure in SAP ERP based on products included in the schedule.
- **Managing an ongoing project** – managing project documentation using file repository, analyzing project data (budget deviations), creating and submitting standardized reports based on uploaded data, managing the schedule and accounting records, overviewing purchases.
- **Filing application for change in the project** – creating modified instances of project, storing past versions containing complete project data for future analysis, keeping the log of all modifications, submitting project's changes using electronic workflow without interfering with current work.
- **Managing portfolios** – creating customized portfolio views, accessing portfolios' projects to check detailed information and project documentation, monitoring projects' statuses, consolidating single reports into aggregated portfolio reports (introduced in 2nd phase of system development), supporting and training PMs in a proper system operation.

Thanks to the dedicated applications included in the architecture, all of the processes required by company's standards have been successfully incorporated into Project Management System, including those not supported by MS Project Server. This approach allows a step-by-step development of the system, which is particularly useful when significant changes in external systems occur or additional functionality is required.

4 POSITIVE ASPECTS OF SYSTEM INTRODUCTION

4.1 *Standardization*

Introduction of the system was carried out in the second half of year 2014 after conducting series of trainings dedicated to present and future PMs. The initial challenge was transferring all available data related to ongoing projects into the system. This phase showed first positive signs of structured approach to managing projects. Predefined scheduling rules given to PMs resulted in construction of detailed schedules with interdependencies between tasks and elementary budgets assigned to them. Up to that point investments were carried out mostly as investment tasks not full projects and were focused mainly on distribution of money in time. Less attention was paid to control preparatory processes. Since the introduction of the system, PMs have been obliged to accurately plan non-financial tasks. It gives the possibility to track projects implementation at any point in time, spot scope deviations in advance and make more accurate budget assumptions. PMs have become more aware of the time required to complete particular tasks. As a result, required formal changes were applied earlier, though implementation delays still remain an issue. Standardized guidelines regarding scheduling and its relation to accounting structure held in SAP ERP resulted in more cautious planning of partial products and more detailed invoicing by contractors. The main advantage of these requirements is the ability to track and report progress of expenditures made on particular products not the whole project. Additionally, PMs become more aware of accounting structure of their projects, what reduces number of mistakes and amount of resources committed to correcting them in financial departments. The accounting structure in SAP ERP is now

generated automatically on the basis of the schedule and all accounting actions required from PMs can be performed in one system. In this way, implementation of the system fulfilled the requirements regarding simplifying accounting responsibilities of PMs.

4.2 *Project supervision*

Introduction of the system significantly benefitted controlling and reporting processes, facilitating duties of Local Project Management Offices (LPMOs) and Central Project Management Office (CPMO) as well as PMs. At the moment PMs utilize two basic reports available in the system. The first converts a schedule into a budget plan, allowing PM to overview budget distribution in time and control its deviations. This report is very useful during change processing or applying for funds when project has not been approved yet. The second report called State of the Project Report (SPR), is the most important reporting tool related to project management utilized within the company. It is a base for both financial and technical verification of projects. Beside project details and financial data uploaded from the system, PMs have to give their own comments on the essential project parameters using standardized survey. The survey contains statements on budget and scope estimation, state of signed contracts, involvement in purchase processes, project's products delivered or delayed and upcoming milestones. This reporting tool provides two major advantages in comparison to the previous solutions. Because of the connection with accounting database, all the financial data is consistent and cannot be modified by PMs so all mistakes like e.g. copying incorrect data are eliminated and budget plans are always reliable and up-to date. PMs can report their own budget estimation as an addition to real data, but only with regard to the future. The other advantage is the ability to automatically consolidate these reports into a single report dedicated to portfolio or program. In this way Portfolio Owners and program directors acquired a quick and useful tool to check the status of all elementary projects under their management. They can now monitor combined actual spending, processed changes, causes of delays or milestones achieved in projects and prepare for the upcoming issues that have to be resolved on higher management level.

Along with increasing number of projects entered into the system, CPMO started to conduct so called "projects reviews". These are periodic meetings with project teams working on the strategic projects or programs. Project Management System allows for easily checking of the information given by PMs or Program Directors against data uploaded from the system, verify the quality of project management in reference to planned schedule and discus technical sides of the projects.

4.3 *Skill improvement*

The system is functioning not only to control PMs, it has also proved to be very useful in raising their professional skills. As it was mentioned before, many PMs are specialists in their respective fields, but have little experience in managing projects according to the methodology. Requirement of keeping projects entered into the system up to date and supervising workflow when processing changes, gave them better understanding of project management and investment processes. A clear set of instructions, standardized procedures and always available support from the PMOs allowed them to gain the experience much faster. In order to enhance training process, e-learning site and testing environment is available. There they can work on training copy of the system with all functionalities and data inherited from the real system. It has been observed, that PMs working in the same departments started to support each other and share their knowledge partially relieving PMOs from training duties. In more problematic or complicated situations, the system proved to be very useful, as it plays the role of common workspace. PMOs can access any project and instantly help PMs with all pressing issues or in time limited situations to fast track any changes that have to be processed. All the positive aspects regarding PMs raising abilities are reflected in faster and more professional way of managing projects and cooperating with company's departments reliant on data exchange with investment projects.

4.4 *Coordination of processes*

One of these closely cooperating departments is the Department of Purchases. As a part of the system, the Global Purchase Plan has been developed as a dedicated application. This functionality aggregates all tasks marked as investment purchases in projects' schedules. It serves the Department as an initial plan for the upcoming purchase procedures. The actual purchase process is conducted via external Purchase Support System, that sends to Project Management System a current status of the procurement. This online information helps PMs assess the situation in their projects without engaging purchase operators. After purchase is completed and respective contract signed, system allows PM to generate orders in SAP ERP and register invoices which together with contract details are assigned to particular tasks. From the controlling point of view it gives the possibility to analyze expenses from additional angles. For example, system allows for easily tracking of all the expenditures under a particular contract to better control its financial limit, especially when these expenditures are scattered among different projects.

4.5 *Strategic programs*

Introduction of the system resulted in important improvements in management of the strategic programs. Prior to the implementation, there were only two programs run by the company, that could be characterized as strategic. One of them still continues, three more have already started and five are currently at various stages of planning. The system has significantly simplified the process of controlling and coordinating component projects. Program Offices (PO) established to support Program Directors, now have the possibility to create combined program schedules linking component projects. All basic information is accessible without time consuming communication with large group of PMs and waiting for their responses. Report that consolidates SPRs presents PO with the most pressing matters in every component project. Managing combined budget has become more transparent, as all the expenditures are registered and reported without delays. Three-way communication with PMOs and PMs has been facilitated allowing them to work simultaneously on the same data if required. Decision-making process has been shortened, as the Program Director can respond to answers addressed by his superiors in a matter of hours or even instantly depending on the complexity of the required information.

4.6 *Data analysis*

Since all project data is stored in databases and accessible in raw form, it has become possible to create a large variety of detailed analytical reports or even set up scientific studies. This ability has been used e.g. to automatically detect mistakes made in project schedules. A dedicated report indicates loose, disconnected tasks, wrong assignment of task type or incorrect parameters of milestones and project products. This report proved to be very useful, when e.g. "KGHM 4.0" Program was founded and over 40 project schedules had to be created by large group of PM with different level of experience in operating the system. Checking the correctness of these schedules was done automatically, so the only role of PO and PMO was to inform and instruct PMs about the parts that required reworking.

5 SYSTEM DEVELOPMENT

The second phase of system development began in 2016 and is planned to be finished by the end of 2019. The main directions of works include: transition to MS Project Server 2016, extension of functionalities regarding portfolio management, introduction of electronic documentation workflow, incorporation of R&D projects and development of analytical reports.

The platform requires an update, as a loss of efficiency has been observed with growing number and volume of projects located on the server. Future limitations in technical support and incompatibility with software supplied to the employees have been also taken into

account. The other works described in this chapter result from the experienced gathered after the implementation of the system or modifications of current functionalities that had been planned beforehand.

5.1 *Portfolio management*

Among current works, portfolio management is the one perceived as the biggest challenge. Functionalities implemented within first version of the system facilitated portfolio management to some extent, but it is still lacking sufficiently specialized tools. As a result, part of the work has to be done manually by the Department of Portfolio Management and LPMOs. The currently available solution allows to aggregate data from the projects but do not support its further management—versioning, prioritizing, reserve planning and budget balancing. A sub-team has been formed within the development project to supervise works on this new functionality. At the moment it is in the final phase of development. New application gathers budget data from all divisional portfolios allowing General Director of Investments to prioritize projects. This operation includes e.g. blocking changes in projects with strategic importance for the company or decreasing budget previously assigned to others. Each divisional portfolio is given a budget cap for five upcoming years and is forwarded to Portfolio Owners. In their respective divisions, Portfolio Owners can distribute available budget among projects or even cancel some of them to meet the limitations. The final forms of the divisional budgets are send back to General Director of Investments via Department of Portfolio Management and combined into company's budget.

5.2 *Electronic documentation workflow*

The current version of the system covers project management process starting from the point when the whole project plan is already approved and ready to be entered into the system. In the last few years it has been observed, that the planning phase and preparation of necessary documents cause PMs too many problems due to difficult communication with all stakeholders and managers, whose consent is required to launch a project. Works on 2nd version of the system include introduction of electronic documentation workflow intended for planning phase, that results in creation of complete project proposal. This process will cover: defining the project, verification by the client and PMO, issuing of specialists' opinions, budget approval, assignment and approval of project roles and finally project activation.

5.3 *KGHM 4.0 and future challenges*

In 2018, development of Project Management System has been incorporated into "KGHM 4.0" – new strategic program, that is partially based on the assumptions of Industry 4.0. This program combines over 50 IT projects with main objective to ensure consistent management of production area and maximization of data utility to improve productivity and efficiency. Therefore an attention has been paid to launch projects that set new standards and provide technical abilities to take data processing and analysis to a higher level by e.g. introducing data governance and big data or establishing Center of Advanced Data Analysis. Awareness of the expected outcome of these projects initiated scientific research that aims to utilize data from Project Management System in order to conduct predictive analysis. These analysis are expected to support project management and high-level decision-making process by appraising reality of project assumptions and thus assigning more realistic time and budget to particular tasks. Figure 2 shows cumulated CAPEX incurred in mining divisions in comparison to its plan on the example of year 2018. The gap between plan and its execution is growing with the progress of the year, causing control, report and management issues, hereby proving underestimation of time required to complete the investments.

Analytically improved time and budget estimation can be useful in reducing presented gap and limiting negative impact of sudden budget peak in December that is shown in Figure 3. Highlighted peaks result from the PMs' tendency to avoid project or task extension
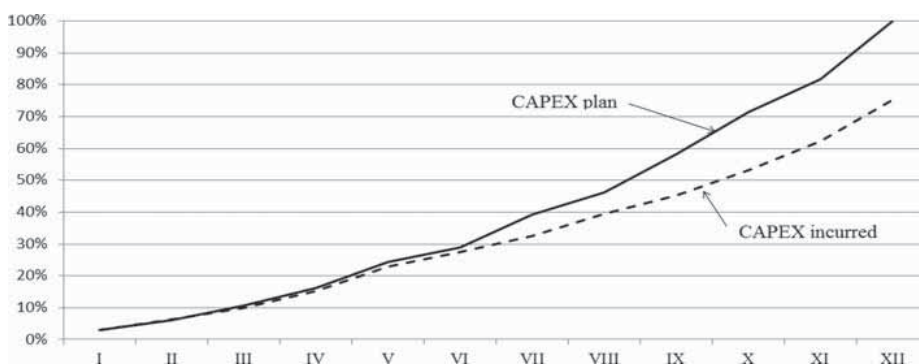
Figure 2. Cumulated CAPEX incurred and planned in mining divisions of KGHM in 2018.
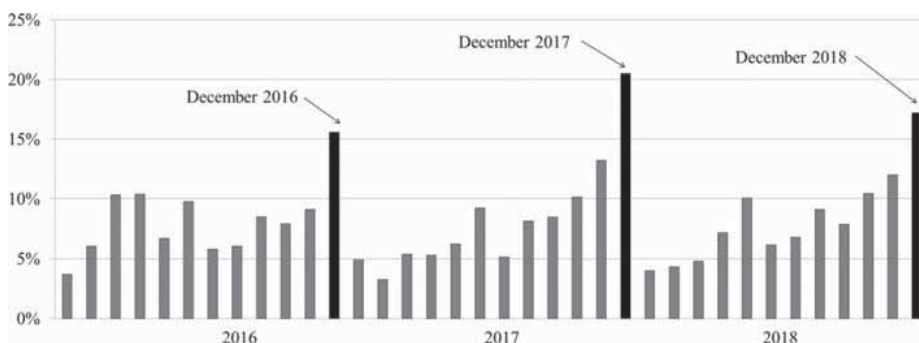
Figure 3. Monthly distribution of CAPEX plan in years 2016–2018 in mining divisions of KGHM.

to subsequent years. Predictive analysis should provide PMs with more realistic assumptions and enhance distribution of budget between adjacent months.

Two project management processes still remain outside the scope of system development and create the space for future works. Both risk and resource areas are managed within the organization, but mostly by specialized services (risk) or its owners (resources). They closely cooperate with PMs, who give their input regarding project needs and remain responsible for updating project data regarding these subjects. Both processes are intended to be incorporated into the system but first they require appropriate changes in company policies.

6   SUMMARY

Introduction of Project Management System in 2014 was a milestone for the KGHM's investment structures. It fulfilled the initial business assumptions that included: facilitation of project management, efficient project supervision based on real time data, shortening of project initiation phase and simplified portfolio management.

System architecture based on Microsoft Project Server 2010, SharePoint Server 2010 and dedicated applications has been designed to exchange data with external systems already operating in the company via MS BizTalk Server. By that means selected accounting, purchasing and contract management features together with project management functionalities have been combined into one IT tool that enabled all actions required from Project Managers to be performed in a single system.

Apart from initial assumptions, additional positive aspects have been observed after the introduction of the system, among them can be distinguished: higher quality and reliability of reporting, increased professional skills of project managers, comprehensive support

for program management, extended database with historical data and convenient access to project information for authorized stakeholders.

After two years of gathering experience from the first implementation, the second phase of system development was commenced. Its main goal is the removal of technical flaws of the first version of the system and addition of advanced features. The platform requires an update, as a loss of efficiency has been observed with growing number and volume of projects located on the server. Future limitations in technical support have been also taken into account. After enabling successful transfer of projects into the system, development works aim toward advanced utilization of the possessed data. The system architecture allows further extensions to be introduced gradually, resulting in different stage of completion of current works. Documentation workflow and advanced portfolio management are expected to be fully implemented in upcoming months, what will result in acceleration of planning processes. Significantly more time is required to introduce predictive data analysis or risk and resource management. On the other hand, much bigger impact on projects' efficiency is expected from these functionalities. Current long term budget plans require higher accuracy to ensure optimal use of financial resources. Fully manageable and controlled investment process supported by data analysis of historical data can significantly contribute to success of local and strategic investments in KGHM.

REFERENCES

Crawford, J.K. 2010. *The enterprise PMO as strategy execution office*. Paper presented at PMI® Global Congress 2010—North America, Washington, DC. Newtown Square, PA: Project Management Institute.

Hornby, R. 2000. *Building effective enterprise project management (EPM)*. Paper presented at Project Management Institute Annual Seminars & Symposium, Houston, TX. Newtown Square, PA: Project Management Institute.

Müller, R. & Turner, R. 2007. The Influence of Project Managers on Project Success Criteria and Project Success by Type of Project. *European Management Journal* 25(4):307.

Resource estimation and geostatistics

An approach for drilling pattern simulation

G. Usero & S. Misk
Regional Director Latin America, Geovariances, Belo Horizonte, Brazil
Geovariances, Belo Horizonte, Brazil

A. Saldanha
MCB Serviços de Mineração, Belo Horizonte, Brazil

ABSTRACT: Drilling is one of the most relevant expenditure in the mining industry. This cost depends on location, geology feature and complexity of the operation, but in general, it could typically cost 150 to 300 USD/meter. This paper presents an approach to assess the geological and financial risk related to different drilling patterns with the use of conditional simulations. The methodology has been successfully applied in different operating mines and mineral exploration projects located in different geological contexts and for commodities such as iron, bauxite, niobium, zinc, copper and gold. The first step of perform a set of conditional simulations using the real dataset available. From the total realizations some are selected, based on a cluster analysis, as the simulated realities that will form the basis of the study. The selected realizations are resampled in different patterns (at least five) and these virtual drilling patterns are then used as an input for additional conditional simulations. The result of the conditional simulations with the virtual drilling patterns are then rescaled to the production increments, based on the actual production of the operating site or the production forecast of the mineral exploration projects. The increments used are consistent with monthly or quarterly and annual production, and the risk assessment is performed within a confidence interval of 90% of the simulated results according to the methodology proposed by Harry Parker. From this study, the degree of accuracy related to each drilling pattern is assessed and used as a guide for additional drilling campaign, based on the risk that the company is willing to take and budgetary forecast.

1 INTRODUCTION

An appropriate mineral resource estimation requires enough geological knowledge of the target which may be achieved through an adequate drilling mesh in order to assess the unique geological, chemical, mineralogical and structural characteristics of each mineral occurrence (JORC 2012). Since drilling plays an important role in budget constraint, it is crucial for the mining companies to be able to assess the relevant quantity of drillholes required to be within an acceptable risk boundary.

One of the main challenges faced by companies, especially during early stage mineral exploration programs, is to define the drilling pattern/densities that are adaptive for a robust mineral resources classification, considering that just a few drillholes are available and consequently the geological knowledge of the deposit is yet sparse. A possible approach is to use the available data to perform conditional simulations to create possible and equiprobable realities that represent the scant dataset available and may be used as a starting point to assess the risk related to different drilling pattern/densities.

Although the methodologies for an appropriate risk assessment are still under research and debated, geostatistical conditional simulations have been considered as the best practice by various mining codes and consequently for robust mineral resources classification. Geostatistical simulation generates stochastic models that accurately represent the actual distribution and spatial variability of the variables of interest: grades,

thickness proportions, etc (Audet and Ross, 2007; Wawruch and Betzhold, 2005 and Dohm, 2005).

This paper presents a combination of drilling pattern simulation techniques associated with the mineral resources classification methodology proposed by Verly at al. (2014), which uses the geostatistical conditional simulations and the concept of confidence intervals (CI) and production increments for risk assessment. This combination of methodologies has been successfully applied in different operating mines and commodities such as, gold, bauxite, iron and niobium and it assisted mining companies in optimizing their drilling program, based on the risk evaluation and mineral resources classification, even during the early stages of mineral exploration.

Its main applicability is to assess the risk associated to a range of drilling patterns/densities to support decision-making for additional drilling campaigns to convert the resource into measured and indicated.

2 METHODOLOGY

2.1 *General workflow*

The workflow of this study is fully performed with Isatis® (Bleines 2012) and consists of a three-step process:

1. Conditional simulations are performed on the available drillhole dataset to create different plausible scenarios;
2. A representative subset of scenarios is then identified, and various sampling patterns defined for each scenario allowing to generate virtual drillholes;
3. Conditional simulations are performed on each virtual drilling mesh in order to compute the dispersion of different simulated attributes within a confidence interval of 90%, considering monthly/quarterly and annual production increments, according to the classification methodology proposed by Verly at al. (2014).

The resource classification mentioned above uses the distribution of the set of simulations to assess the risk associated to the deposit of interest and then the following rules are applied:

– Measured: ± 15% with 90% Confidence Interval (CI) on a quarterly or monthly production increment;
– Inferred: ± 15% with 90% CI on an annual production increment;

This methodology indicates the risk level associated to each attribute and it is possible to assess, locally and globally, the uncertainty (risk) related to each drillhole spacing. As a result, the company may define the optimum drilling pattern considering mineral resources classification and the risk that the company is willing to take.

2.2 *Case study*

The studied deposit consists in a bauxite deposit from one of the major bauxite regions in the world. The sediments beneath the bauxitic formation are composed of alternating c1ayey, silty and sandy layers of a weathered c1astic sediment consisting of kaolinite, quartz and a small quantity of iron and titanium oxides. The terrain forms gently undulating plateaus.

The raw data consist of 388 vertical drillholes and 5801 samples (see Figure 1). The study was carried out on a fictitious dataset of a domain 'D' and the variables of interest are the grade 'v1' and the thickness 'v2'. The study was set on a 2D environment, but it could be done on 3D environment as well.

2.3 *Perform conditional simulations on the available dataset*

As the study was implemented on a 2D environment, the first step is to calculate the accumulation of the grade variable v1 (acc_v1) and to define the thickness v2 considering only
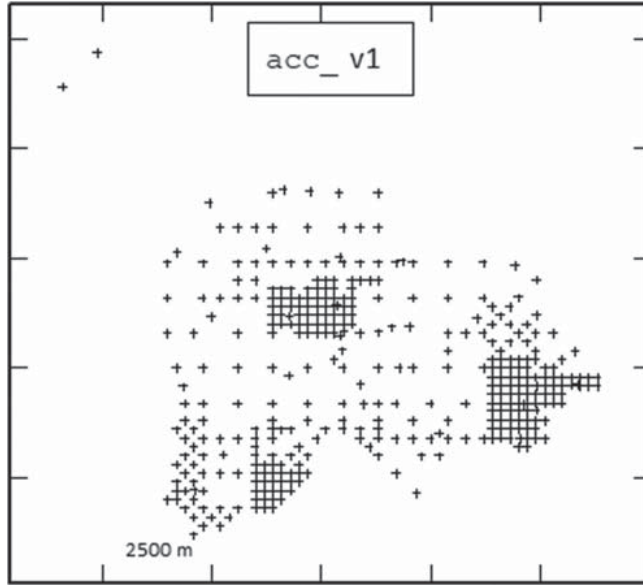
Figure 1.   Map of the dataset.

the samples within the domain D. The accumulation of a grade variable is calculated along each drillhole as a new variable in a point file. The accumulation is the result of the following Equation 1:

$$accumulation = \sum_{i=1}^{n} V_i L_i \qquad (1)$$

where Vi is the grade variable to compute the accumulation; and Li is the analyzed length of a drillhole which is the sum of the length of the selected samples for which the grade variable is defined (Bleines 2012).

With the variographic modelling of the gaussian variables, and a search neighborhood "SN", the next step consists in performing the conditional co-simulation of the variables acc_v1 (gaussian) and thickness (gaussian) on a 50×50 m grid (Figure 2). The total amount of realizations is 100.

2.4   *Create virtual drillholes from the simulations*

With the results of the simulations, five scenarios were selected among the set of realizations of each variable (acc_v1 and thickness), to create five possible realities that will be the basis for the study from this stage onwards.

Such selection was done with an Isatis® tool named "Simulation Reduction" that was developed by a joint consortium of Geovariances and the CERNA (Centre of industrial economics of MINES ParisTech) which created an efficient method for selecting the best subset of a predetermined size, k, from an original set of N simulations. The k simulations selected are no longer equiprobable: some simulations represent "typical" deposits that are likely to occur; other ones are less likely and some other ones are outliers (Armstrong *et al.* 2013).

Due to the co-simulation of acc_v1 and thickness v2, the same five scenarios were chosen for both simulations among the set of realizations. The results obtained with the respective probabilities for each scenario are listed in the Table 1, presented below:

Finally, from the previous stage, the virtual drillholes were defined, from the five realizations of the grade v1 and the thickness v2, by resampling each selected realizations with a

61
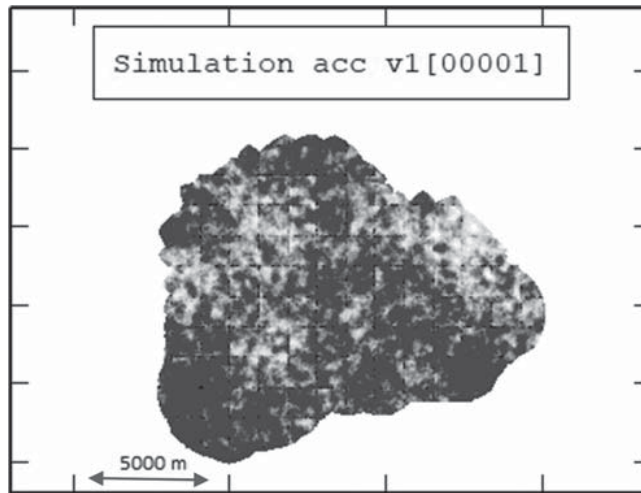
Figure 2.   One realization from the conditional simulation of the variable acc_v1. Plant view.

Table 1.   Probabilities for each realization.

Best Simulations Combination for acc_v1 & thickness	8	25	12	33	77
Best Simulations Probabilities:	0.07	0.29	0.16	0.37	0.11

range of spacing: 100×100 m, 100×150 m, 100×200 m, 100×250 m, 100×300 m and 100×350 m as exemplified by Figure 3.

2.5   *Conditional simulations of each virtual drillhole and risk analysis*

To highlight the impact of the drillhole spacing, independent variograms have been adjusted for each drilling mesh, but the same SN has been used for all simulations.

The results of the simulation of the variables v1 and thickness, for each drilling mesh, are then rescaled to production increments of one year and quarterly that are created by gathering the simulated blocks up to the tonnage equivalent to a year or a quarterly production of the operation. The dispersion of the simulations is calculated within a confidence interval of 90% considering the production basis. Nevertheless, grouping small block units into bigger units remains an issue when the quarterly/yearly lots have not yet been defined, which is the case at early exploration stages. A possibility could be to choose between two extreme situations:

– The unit (month, quarter or a year) is made of a set of contiguous simulated blocks: the volume of the unit is defined by merging n volumes of small simulated blocks. Averaging these simulated blocks that contemplates the volume production increment of a year, mouth or quarter gives the experimental distribution of the grade on which confidence intervals may be calculated;

– The unit is made of a blending of blocks coming from different areas. By considering the case where these areas are far from one another, the quantities of the blocks are independent. The distribution of the unit may then be considered as Gaussian, with a variance over the period that is the variance of one block divided by the number of blocks making up the unit. Aiming at getting the relative standard deviation of the lot less than a given threshold determines the threshold of the standard deviation of the small blocks, contributing to the measured or indicated resources.

Figure 3.   Virtual drillholes for one of the selected virtual realities. Plant view.

In a 2D study, the mean thickness (global or local) of the deposit or the domain should be known to calculate the volume of each simulated block and to group it into bigger units that corresponds to production units.

The variance of the 100 realizations of each drilling spacing is calculated within a 90% CI, using the quantiles of 5% (Q05) and 95% (Q95) and the mean of simulations (see Figure 4) as shown Equation $Accuracy\,(IC\,90\%) = Q95 - Q05\,/\,The\;mean\;of\;simulations * 2$ (2):

$$Accuracy\left(IC\,90\%\right) = \frac{Q95 - Q05}{The\;mean\;of\;simulations * 2} \qquad (2)$$

Assuming a normal distribution, the accuracy can also be calculated as follows Equation 3 (Verly et al. 2014):

$$Accurancy\left(IC\,90\%\right) = 1.645 * \sigma_t / The\;mean\;of\;simulations \qquad (3)$$

where σ_t is the standard deviation of the simulations.
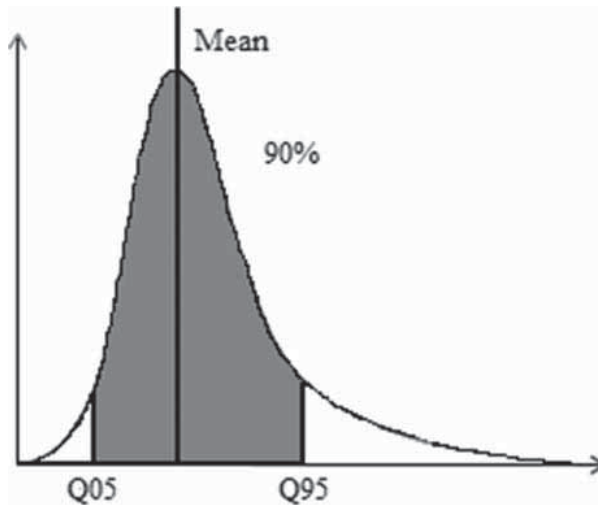
Figure 4.   Confidence Interval of 90% in an asymmetric distribution of the rescaled simulations.
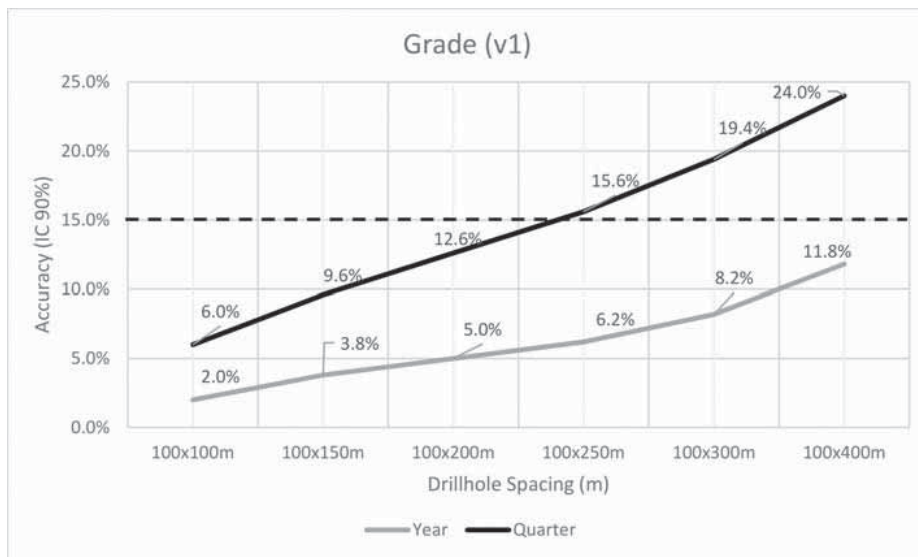
Figure 5.   Mean of the accuracy around the mean within a 90% CI from the five scenarios rescaled into quarter and annual basis – Grade (v1).

Finally, the analysis on a 90% CI within a quarterly or annually basis gives the risk assessment attached by each drillhole spacing to classify the resource as measured or indicated. Since the result of accuracy, rescaled to the production increments and for the same patterns are very similar for the five tested realizations, the Figure 5 and Figure 6 show the mean of the results.

As proposed by Verly *et al.* (2014), the mesh 100×200 m is enough to classify the mineral resources for this ore body as measured and the mesh 100×400 to classify as indicated, as shown in Table 2.
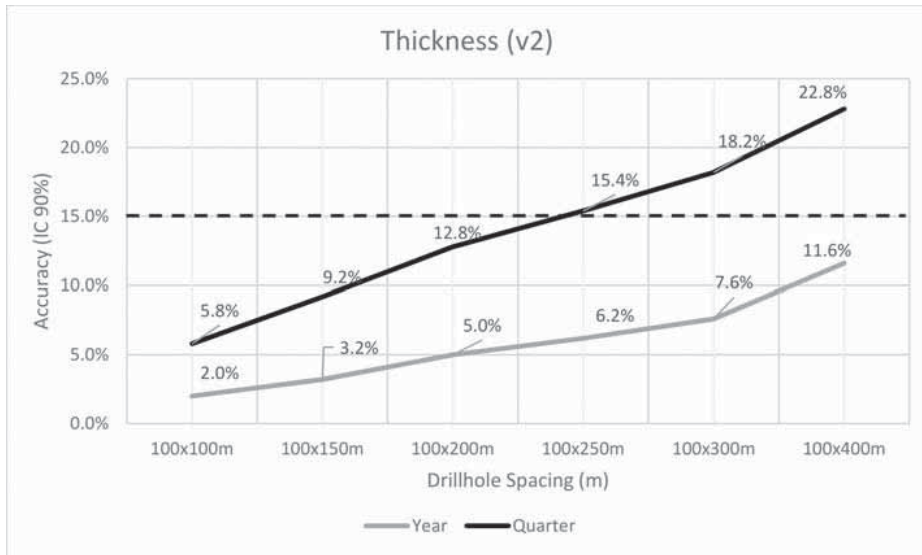
Figure 6. Mean of the accuracy around the mean within a 90% CI from the five scenarios rescaled into quarter and annual basis – Thickness (v2).

Table 2. Illustrates the drilling pattern that gives the level of confidence in resource classification.

| | | Drillhole spacing (m) | |
		Grade (v1)	Thickness (v2)
Resource	Measured	100×200	100×200
Classification	Indicated	100×400	100×400

3 CONCLUSION

Considering that the value of mining companies, the investments and benefits to shareholders revolve around millions of dollars, it is critical to quantify the level of confidence on resources estimation and classification to have a reliable estimation of the mining assets. As the drillholes represent a sample of the reality to be understood, and the level of geological knowledge impacts on the mineral resources estimation and classification, there is a genuine need for companies to assess the pattern of drillholes that are suitable for a robust economic evaluation of an operating mine or mineral exploration project.

In this paper, an approach integrating drilling spacing simulation techniques with the resource classification proposed by Verly *et al.* (2014) is described and its applications explored. The approach is based on conditional simulations, which take into account the spatial variability of the studied variables, and the uncertainty analysis associated with each drilling mesh and production volume is computed for resource classification.

With the proposed approach, it is possible for the mining companies to estimate the risk attached to a range of drilling patterns, even during the early stage exploration program, in order to create a systematic drilling campaign considering the risks and the impact on the mineral resources classification of each drilling pattern. The results of the combined method is a guideline for the companies to support their decision making for additional drilling campaigns, thus reducing geological uncertainty and converting the resources into measured or indicated.

REFERENCES

Armstrong, M., Ndiaye, A., Razanatsimba, R., Galli, A. (2013). Scenario Reduction Applied to Geostatistical Simulations. *In: Mathematical Geosciences*, February 2013, vol. 45, Issue 2, pp. 165–182.

Audet, M. and Ross, A.F., 2007. Koniambo lateritic Ni-Co deposits, New Caledonia – A case study from geological modelling to mineral resource classification, *in Orebody Modelling and Strategic Mine Planning*, second edition (ed: R. Dimitrakopoulos), pp. 235–244. (The Australasian Institute of Mining and Metallurgy: Melbourne).

Bleines, C., Deraisme, J., Geffroy, F., Perseval, S., Rambert, F., Renard, D., Touffait, Y., and Wagner, L. 2012. *ISATIS software manual. Geovariances and Ecole des Mines de Paris*. 531 pp.

Dohm, C. 2005. Quantifiable mineral resource classification – A logical approach, *in Geostatistics Banff 2004* (eds: O. Leuangthong and C. Deutsch), 1:333–342 (Springer: Dordrecht).

Joint Ore Reserves Committee (JORC), 2012. *Australasian Code for Reporting of Exploration Results, Mineral Resources and Ore reserves* (JORC Code).

Verly, G., Postolski, T., and Parker, H.M. 2014. Assessing uncertainty with drillhole spacing studies: applications to mineral resources, *In AusIMM: Orebody Modelling and Strategic Mine Planning* 2014, Paper No. 72, 23 pp.

Wawruch, T., Jorge, F. and Betzhold, J.F., 2005. Mineral Resource classification through conditional simulation, *in Geostatistics Banff* 2004 (eds: O. Leuangthong and C. Deutsch), 1:479–489 (Springer: Dordrecht).

Application of Locally Varying Anisotropy (LVA) kriging at the Grasberg porphyry Cu-Au-Ag deposit, Papua, Indonesia

Andrew Issel, Adam Schwarz, Ken Moss & Rick Rossi†
Freeport-McMoRan, Inc. Phoenix, Arizona, USA

ABSTRACT: The Grasberg porphyry Cu-Au-Ag deposit in Papua, Indonesia is primarily hosted by a funnel shaped body of Pliocene intrusive rocks known as the Grasberg Intrusive Complex (GIC). Cu-Au-Ag mineralization exhibits concentric grade contours in plan view and extends over a vertical depth of 1,500 m. Traditional geostatistical tools measure the spatial continuity between sample locations as a function of Euclidean distance and direction. Complex geometries often violate first- and second-order stationarity assumptions. The circular pattern of grade continuity at Grasberg challenges traditional linear estimation methods limited by a fixed anisotropy for a domain of interest. Locally Varying Anisotropy (LVA) kriging overcomes this limitation, removing anisotropy by multidimensional scaling according to a defined anisotropy grid. Implementation of LVA kriging to estimate block grades at the Grasberg porphyry Cu-Au-Ag deposit began in 2013 and continuous improvement efforts have focused on correctly modeling the anisotropy grid, known as the LVA field. The LVA field is the most important input to the LVA estimation process, as it defines the direction and magnitude of continuity of the attribute under consideration. The LVA field for Grasberg evolved from a perfect circle used for all three metals to a grid interpolated from guiding polylines on each level that are individualized for each metal. Progress is substantiated by cross validation techniques. The resulting models display grade distributions that better reflect field observations, and have improved the reliability of resource estimates for this complex domain.

1 INTRODUCTION

Traditional geostatistical tools such as the variogram, covariance, and correlogram measure the spatial continuity between sample locations as a function of both distance and direction. However, distance and direction are straight-line or vector or Euclidean measures. Nonlinear geologic features (e.g. anticlines, folded strata, fluvial reservoir channels, porphyry deposits with concentric grade contours) present formidable challenges for geostatistical estimation because of the curvilinear features. In geostatistical terms, complex geometries often violate first-order stationarity (the mean is invariant of location in the estimation domain) and the second-order stationarity (the covariance is invariant of location in the estimation domain) assumptions. Locally varying anisotropy (LVA) kriging offers an alternative.

LVA kriging was adopted by Freeport-McMoRan (FCX) to model block grades of Cu, Au, and Ag at the supergiant Grasberg porphyry deposit in Papua, Indonesia in 2013. In the subsequent years, several improvements to the estimation framework and workflow have been implemented. This paper describes the evolution of the LVA estimation workflow applied at the Grasberg deposit.

2 LOCALLY VARYING ANISOTROPY KRIGING

The LVA kriging methodology, developed by Boisvert (2010) and employed by FCX for resource estimation at the Grasberg deposit, starts with the construction of a 3D LVA field.

The LVA field specifies the local orientation and aspect ratio of the anisotropy field at each grid cell (block center) location, which varies throughout the model space. Copper, gold and silver at Grasberg have circular continuity in plan view but near vertical continuity in cross section, so the local anisotropy is defined by a horizontal direction (rotation about z-axis) and aspect ratios of the horizontal (major: semi-major) and vertical (major: vertical) anisotropy.

Rather than using the Euclidean or linear straight line distance between points to calculate variogram lag distances, the LVA method considers the "shortest path distance" (SPD). The SPD is calculated by representing the space in the 3D model volume as a graph (Boisvert and Deutsch, 2011). The local anisotropy (direction and anisotropy ratio) is specified at each cell in the grid (the LVA field), providing the road map to follow between points. The length between the points is measured by summing up the edge lengths of all vertices traversed through the LVA field (Fig. 1).

Boisvert's (2010) LVA variogram calculation program employs the Dijkstra algorithm to find shortest path distance between locations. This nonlinear path is a non-Euclidean distance metric that conforms to the anisotropic minimum distance. To ensure a positive definite kriging system of equations, multidimensional scaling or landmark isometric mapping (ISOMAP) is employed (Boisvert, 2010; Boisvert and Deutsch, 2011). Essentially, multidimensional (or "q-dimensional") scaling transforms the initial grid of cells into a new set of coordinates in hyper dimensional space so that the anisotropic minimum path distance is transformed into a straight line path. This removes all anisotropy from the original space, and the Euclidean distance metric of the q-dimensional space permits a positive definite covariance matrix for applying kriging. The data and grid locations are embedded into the q-dimensional space and an isotropic variogram can be calculated and modeled.

Numerous variogram models (e.g., spherical, exponential, Gaussian, hole-effect, etc.) have been shown to produce a positive definite kriging system of equations in two- and three-dimensional space. The exponential model is positive definite in n-dimensional space, and thus, it is the preferred model to use in the hyper-dimensional space of LVA kriging.
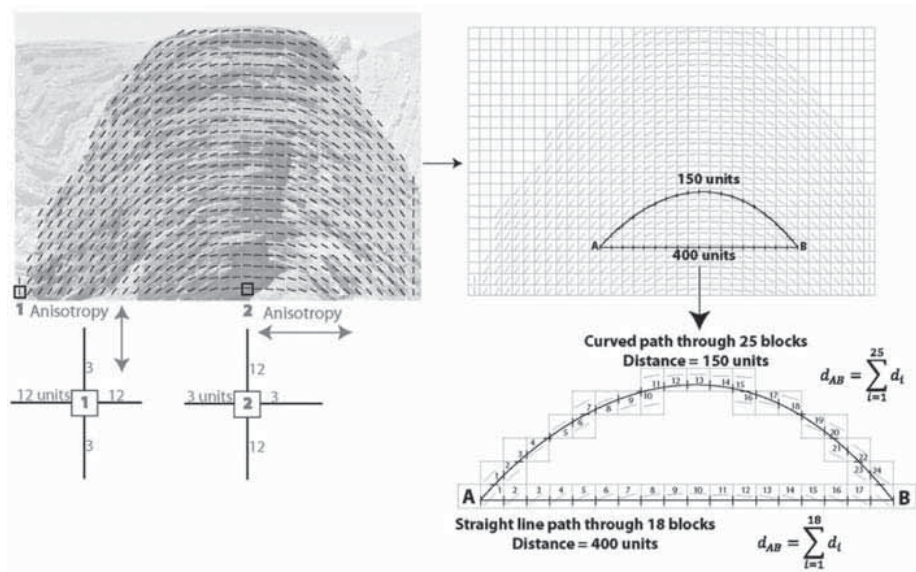
Figure 1. Illustration of geologic anisotropy and the concept of anisotropic shortest path distance from Boisvert and Deutsch (2011). Left: An anticline overlain with a 2D LVA grid. Locations 1 and 2 illustrate how the anisotropic distance in each cell depends on LVA. At point 1 a horizontal path has an anisotropic distance of 12 units whereas a vertical path is 3 units. Right: Two potential paths between points A and B, where the curved path is shorter according to the anisotropic shortest path distance (the path used in LVA kriging), while the horizontal path is shorter according to Euclidean distance.

Kriging is performed in the q-dimensional space, and the space is then back-transformed to the original grid coordinates. The LVA kriging programs used by FCX at Grasberg were built by Boisvert (2010), who modified GSLIB (Deutsch and Journel, 1992) open-source software. Specifically, the GSLIB programs modified are GAM3, a variogram calculation program and KT3D, a three-dimensional kriging program. GAM3 was modified to GAM3_LVA and performs the multidimensional scaling and then calculates the resulting isotropic omni-dimensional variogram. KT3D was modified to KT3D_LVA and reads in the hyper dimensional rescaled coordinates and performs the kriging.

3   GRASBERG RESOURCE ESTIMATION

3.1   *Motivation for adopting LVA*

The motivation for adopting LVA for estimation at Grasberg derives from the complex, non-linear geometry of grade continuity in the ore zone, which is a direct reflection of the geologic evolution of the deposit. There are also mine planning considerations. In 2019, mining at Grasberg will transition from open pit operations, where blasthole assays are available prior to mining, to underground block caving where only the long term resource model will guide production grade forecasting. Not only is it important to calculate the correct grade-tonnage curve for long term planning, it is critical to produce the most accurate and realistic spatial distribution of grades in the resource model. Linear ordinary kriging cannot sufficiently reproduce the circular grade continuity of the primary mineralized domain in the deposit. LVA kriging is far more effective for replicating the curved nature of mineralization.

3.2   *Geology of the Grasberg deposit*

The Grasberg Cu-Au-Ag deposit, located in the central highlands of Papua, Indonesia, is one of the largest porphyry Cu-Au deposits in the world, containing over 5 billion metric tonnes of material at around 0.6% Cu and 0.5 ppm Au for an estimated 32 million metric tonnes of copper and 96 million troy ounces of gold (Leys et al., 2012). Mineralization at Grasberg is hosted primarily by Pliocene intrusive rocks that were emplaced in a tightly folded and faulted sequence of Tertiary carbonate rocks. These carbonate rocks also host substantial skarn deposits within the Ertsberg-Grasberg District (Fig. 2; Leys, et al., 2012).

The Grasberg intrusive rocks were emplaced in three main stages collectively referred to as the Grasberg Intrusive Complex (GIC) (MacDonald and Arnold, 1994). The first stage, the Dalam, makes up the bulk of the GIC and forms an upward flaring, funnel shaped package of monzodioritic intrusions, subvolcanic breccias and volcanic rocks. An early stage of alteration, veining and Cu-Mo mineralization is associated with a deep porphyry intrusion of Dalam age known as the Gajah Tidur porphyry. The second stage, the Main Grasberg Intrusion (MGI), is a pipe-like diorite plug positioned just north of the central axis of the Dalam phase rocks. The bulk of the Cu-Au mineralization in the Grasberg deposit is associated in time and space with the MGI. The third and final stage, the Kali, is a barren, wedge-shaped intrusion thickening from the center of the GIC to the southeast, truncating older mineralization.

High grade Cu-Au mineralization is hosted in a quartz-magnetite vein stockwork centered on the MGI with Cu-Au-Ag grade contours decreasing outward in a concentric pattern that reflects the temperature gradient at the time of mineralization (Fig. 3). The MGI stage of mineralization produced an ore column approximately 1,500 m in vertical extent. Mineralization also extends along radial structures that locally disrupt the relatively stable concentric grade contours.

3.3   *Process summary*

Figure 4 illustrates the LVA kriging workflow developed for the Grasberg deposit. Individual aspects of the process will be described in more detail in the following sections. The LVA process at FCX begins by defining mineralization controls. Polylines outlining the
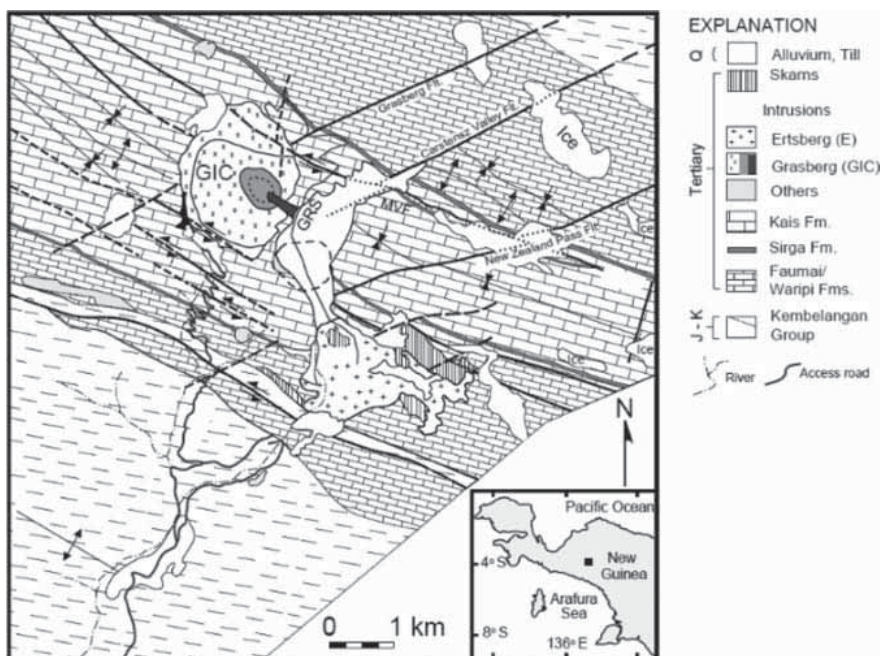
Figure 2. Location and geological map of the Grasberg deposit in the Ertsberg-Grasberg mining district, Papua, Indonesia modified from Sapiie and Cloos (2004). The Grasberg deposit is in the upper left quadrant of the map area labeled "GIC".
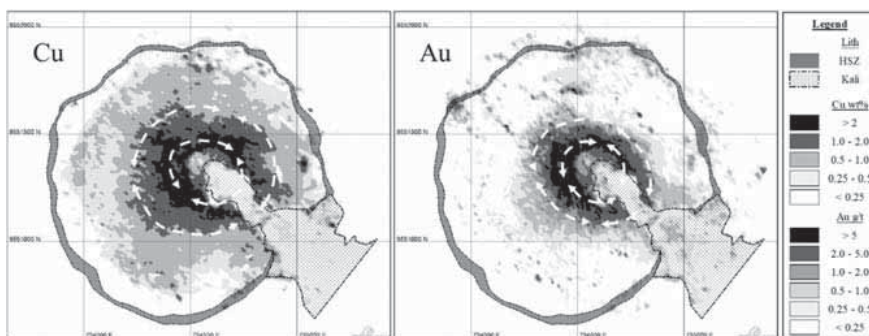
Figure 3. Plan view at 3,600 m elevation of Cu and Au grades in the Grasberg deposit. Dashed lines with arrows illustrate the circular continuity of Cu and Au grades.
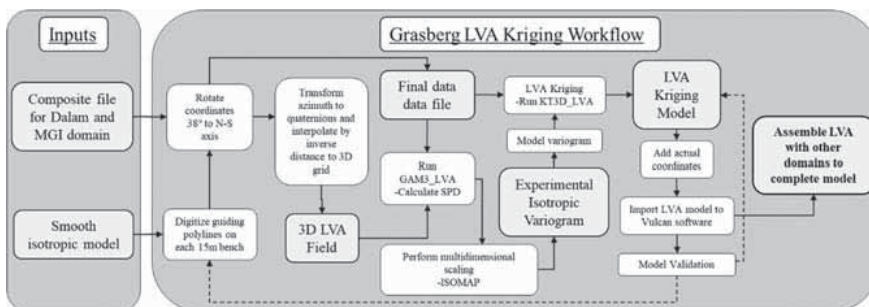
Figure 4. Flow chart of the LVA estimation process applied in the Dalam-MGI domain at Grasberg.

mineral controls are digitized in plan for each level, following the circular grade contours of an isotropic model of Cu and Au. The polylines are converted to quaternions and interpolated into each block, creating the LVA field. The LVA variogram program calculates the SPD between all points and embeds the points in multidimensional space, and an exponential variogram model is fit to the output. LVA kriging is performed in the multidimensional space which has taken into account the SPD following mineral controls. Parameter files for the programs are batched together into a script file to simplify the process. Estimation parameters are optimized by iterating various parameters and running k-fold validation. Standard model validation techniques such as swath plots, comparison with other estimation techniques and visual inspection are completed prior to inserting the LVA results into the final resource model.

3.4 *LVA field evolution*

Defining the LVA field is the most critical aspect of the workflow, as the multi-dimensional scaling and calculation of the isotropic variogram are all dependent on the SPD specified by the LVA field. Several methods have been proposed for inferring the LVA field, including from drill hole data, image processing, structural models, simulations, gradients, or from geologic interpretation (Lillah and Boisvert, 2015). The vast number of assays and advanced nature of the geologic interpretation of the Grasberg led FCX to choose to define the LVA field from the Cu and Au grade distribution. In this context, improvements to the LVA field for estimation in the GIC has been the focus of improvements to the estimation workflow. It has evolved from a simple circular geometry applied for all three metals to more complex geometries that better reflect local mineral controls for each metal.

3.4.1 *2012–2014*
FCX began exploring the LVA method in 2012 after discussions with academics from the Centre for Computational Geostatistics (CCG) at University of Alberta at APCOM in Wollongong, Australia in 2011. In order to prove that the method could be effective, a simplified, perfectly circular LVA field was constructed. The center of the circle was defined and the LVA field was created by finding the perpendicular vector for each block from the circle's centroid location. Each block's perpendicular vector to the centroid forms its strike angle (or "angle1" in GSLIB parlance), the rotation around the z-axis (Fig. 5a). During this exploratory stage of the method application at Grasberg, the same LVA field was applied for all three metals, Cu, Au and Ag. Applying the circular LVA field for kriging showed that the circular grade continuity was far better replicated with LVA kriging then by the traditionally applied linear ordinary kriging, and the proof-of-concept study was positive enough to warrant additional work on the method.

3.4.2 *2014–2017*
Prior to using the LVA kriging model to develop mine plans, more effort was devoted to creating an LVA field that would reflect local mineral controls in more detail. The decision was made to use the grade contours of the existing models to guide the anisotropy paths for the LVA field. Two polylines were digitized on each level: 1) an inner polyline of generally elliptical shape that followed the Au grade contours, and 2) an outer polyline of irregular, circular shape that followed the Cu contours. Importantly, the post-mineralization barren Kali dike was treated as though it did not exist; the polylines pass smoothly through the Kali, connecting up the matching parts of the grade contours in the Dalam and MGI (Fig. 5b).

The two anisotropy-guiding polylines were digitized for all 15 m high levels from 2,387.5 m to 4,322.5 m elevation, then input into a semi-automatic LVA field generation program called SPFIT, developed by researchers at the Center for Computational Geostatistics at the University of Alberta (Dr. Jeff Boisvert and his student, Maksuda Lillah). SPFIT computes the azimuths or strikes for each block in a 2D grid, guided by one or more user-supplied polylines that mimic the anisotropic geometry of the variable under consideration. The azimuth grids for each level were collated into a single 3D LVA field file for input into GAMV_LVA and KT3D_LVA.
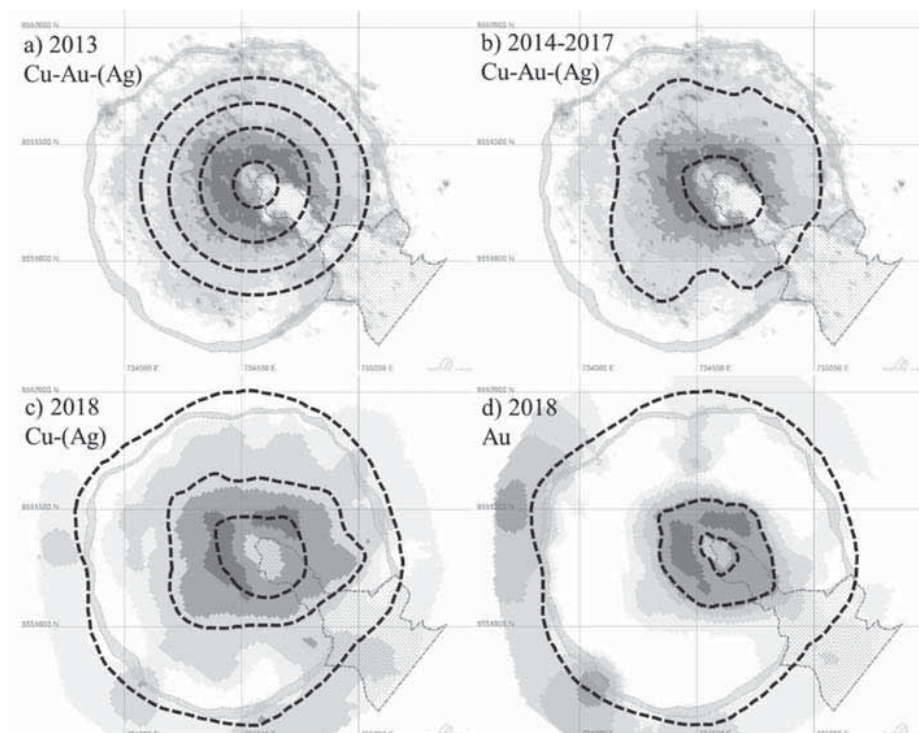
Figure 5. Evolution of the LVA field applied for estimation at Grasberg.

The results of this work showed much better replication of the local spatial distribution of grades due to the improved LVA field. The LVA estimate was validated using standard approaches and for the first time, the model was used for mine design and reporting of reserves and resources in December 2014.

3.4.3 *2018*

In order to more accurately reflect the differences between spatial distributions of Cu and Au, the LVA field generation method was revisited in early 2018. Dr. Boisvert was again engaged to write a program that generates a 3D LVA field from 2D level polylines, but with more flexibility in the number of polylines used to control the anisotropy field. Guiding polylines were digitized on each level for Cu and Au, individually. A smooth isotropic search model with a high number of samples was used as the basemap for the polyline interpretation (Fig. 5a, b).

The program requires a minimum of one polyline per level to guide the interpolation of the LVA field into each grid cell on that level. It calculates the azimuth of each line segment making up the polyline, and uses quaternion averaging by inverse distance squared to interpolate the azimuth of the LVA field at each block centroid. Cu and Ag are more highly correlated than Cu and Au, so the Cu LVA field was used in the Ag estimation.

3.5 *Variography and Kriging*

After the LVA field is constructed, the next step is to calculate and model the isotropic variogram, and perform the kriging. Prior to 2018, the LVA variogram calculation and kriging was performed in a step by step process, running one program at a time until the estimation was complete. In 2018, a bash script was written that incorporates all the GSLIB and CCG programs that perform coordinate rotations, variography, kriging and output model formatting. The scripting has streamlined the workflow and added more integrity to the process.
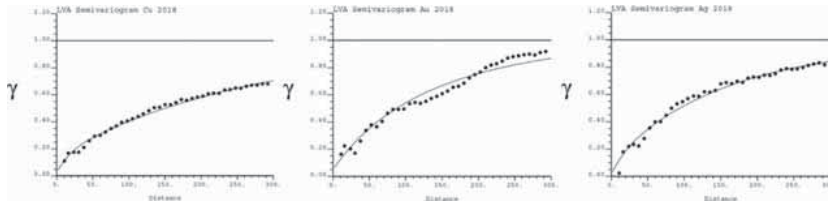
Figure 6.   Isotropic variogram models for Cu, Au and Ag within the GIC estimation domain.

The bash script is called LVA_(metal)_2018.sh, and it runs four programs in succession:

1. rotcoord – rotates X and Y coordinates in data file 38 degrees to align the data with the north-south estimation grid required by the LVA programs.
2. gamv_lva – calculates the omnidirectional experimental variogram after finding the shortest path distances and conducting multidimensional scaling.
      After gamv_lva is completed, the isotropic variogram is modeled before performing the LVA kriging (Fig. 6).
3. kt3d_lva – performs LVA kriging.
4. merge_ult – adds the native block coordinates to the model output file from kt3d_lva. The model file can then be imported directly to a Vulcan block model file.

4   MODEL VALIDATION

To fine tune the anisotropy ratios of the LVA field and the number of samples to use in estimation, a technique known as k-fold validation was applied. K-fold validation is a type of cross-validation or jackknifing approach to test the effect of changing estimation parameters. The process is as follows:

1. 20% of the drill holes in the data file are randomly selected and removed from the dataset.
2. Estimates are made at the data locations of this 20%, using only the 80% of drill holes that remain.
3. Perform steps 1 and 2 "k" number of times, with a different 80/20 split of the data each time.
4. Results are then summarized with statistics such as Mean Squared Error, Correlation Coefficient, and Slope of Regression.

For our studies, we ran the validation 8 times (8-fold) each for Cu and Au for the three parameters that were tested: 1) horizontal anisotropy ratio, 2) vertical anisotropy ratio, and 3) maximum number of samples. The results of the cross validation were plotted for each parameter, and the optimal parameter value was chosen based on the value that maximized the correlation between estimated and actual values (Figs. 7, 8). The horizontal anisotropy and number of samples parameters were updated after the validation exercise and applied in the 2018 LVA kriging runs:

LVA parameter	Pre-2018	2018
Horizontal anisotropy ratio	0.2	0.15
Vertical anisotropy ratio	1	1
Maximum number of samples	10	25

Traditional model validation methods were also applied, such as swath plots, comparison of results to other accepted methods, and visual inspections of level plans and sections. The swath plots show excellent agreement between the nearest neighbor assignment and the LVA kriging estimates, indicating that the LVA estimate closely reflects the underlying data
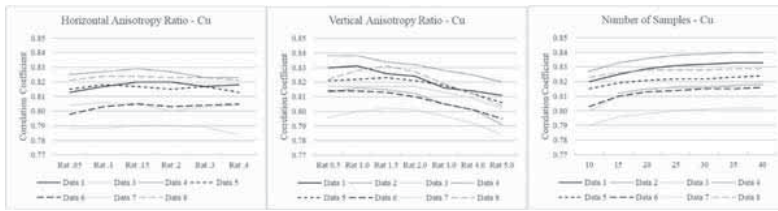
Figure 7. Cu cross validation correlation results, iterating three parameters: 1) Horizontal Anisotropy Ratio, 2) Vertical Anisotropy and 3) Number of Samples.
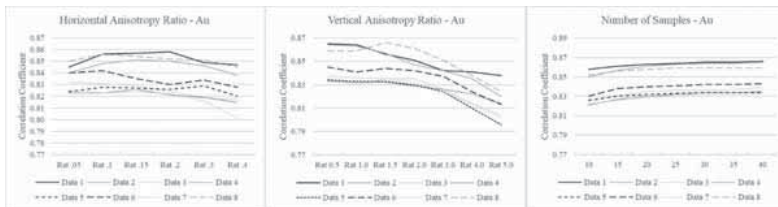
Figure 8. Au cross validation correlation results, iterating three parameters: 1) Horizontal Anisotropy Ratio, 2) Vertical Anisotropy and 3) Number of Samples.
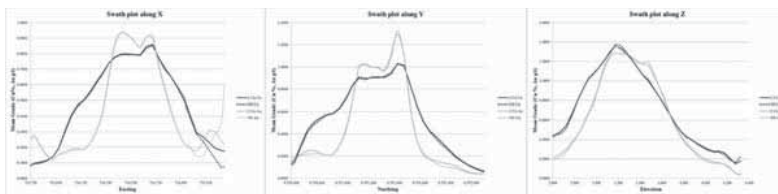
Figure 9. Swath plots of LVA Cu and Au estimates and Cu and Au nearest neighbor assignments.
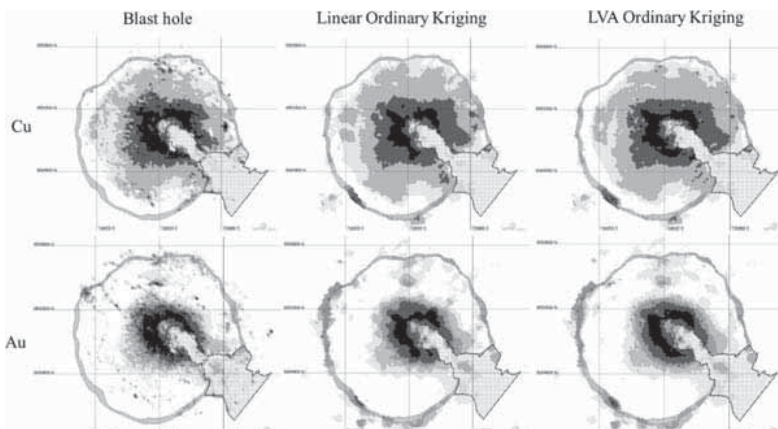
Figure 10. Visual comparison on the 3,600 m elevation of the blasthole model, linear ordinary kriging, and LVA ordinary kriging.

(Fig. 9). Local differences occur on the low grade edges of the deposit where data are sparse, but these will not affect the mine plan.

Figure 10 shows maps of the 3,600 m elevation comparing the blast hole model to models produced by linear ordinary kriging and LVA ordinary kriging. The goal of the LVA is to better reproduce the true spatial pattern of grades as observed from the blast holes. LVA kriging reproduces the circular grade pattern better than linear kriging. Note that the linear ordinary kriging and LVA ordinary kriging models did not use blast holes in the estimation data set.

5 CONCLUSIONS

The model of the Grasberg porphyry deposit estimated by LVA kriging closely mimics the spatial distribution of Cu, Au and Ag grades that characterize the deposit. High grade mineralization hosted in a central quartz-magnetite vein stockwork has a strong trend with Cu-Au-Ag grade contours decreasing outward in a concentric pattern. This pattern reflects the lateral temperature gradient at the time of mineralization which controlled the precipitation of Au and Ag bearing Cu-sulfides. The LVA estimation method dampens the impact of the outwardly decreasing grade trends by directing the search path along the circular continuity. The goal of the estimation was not only to calculate the correct grade-tonnage curve for long term planning, it was also critical to have the resource model accurately and realistically represent the local spatial distribution of grades to support the block cave design. Other tested methods that use linear anisotropy (directional search ellipsoid, pie slice selection, local directional anisotropy, spherical isotropic, octant search) cannot adequately follow the circular grade continuity of the primary mineralized domain. In this context, LVA kriging was chosen as the solution for estimation in the GIC, and has proven effective.

REFERENCES

Boisvert, J.B., 2010. *Geostatistics with Locally Varying Anisotropy*. Ph.D. Dissertation, University of Alberta, Edmonton, Alberta.

Boisvert, J.B., and Deutsch. 2011. Programs for kriging and sequential Gaussian simulation with locally varying anisotropy using non-Euclidean distances. *Computers & Geosciences* 37: 495–510.

Deutsch, C.V. and Journel, A.G. 1992. *GSLIB: Geostatistical Software Library and User's Guide (2nd Ed.)*, Oxford University Press, New York.

Leys, C.A., Cloos, M., New, B.T.E., and MacDonald, G.D. 2012. Copper-gold ± molybdenum deposits of the Ertsberg-Grasberg District, Papua, Indonesia. In Hedenquist, J.W., Harris, M., and Camus, F., (eds.) *Society of Economic Geologists Special Publication 16*: 215–235.

Lillah, M., and Boisvert, J.B. 2015. Inference of locally varying anisotropy fields from diverse data sources. *Computers & Geosciences* 82: 170–182.

MacDonald, G.D., and Arnold, L.C. 1994. Geological and geochemical zoning of the Grasberg Igneous Complex, Irian Jaya, Indonesia. *Journal of Geochemical Exploration* 50: 143–178.

Sapiie, B., and Cloos, M. 2004. Strike-slip faulting in the core of the Central Range of West New Guinea, Ertsberg mining district, Indonesia. *Geological Society of America Bulletin 116:* 277–293.

Multivariate geostatistical simulation using principal component analysis

M. Bolgkoranou & J.M. Ortiz

The Robert M. Buchan Department of Mining, Queen's University at Kingston, Ontario, Canada

ABSTRACT: Multivariate geostatistical simulation is aimed at reproducing the statistical relationships between variables and their spatial distribution. We present a methodology whereby grades and a filler variable are transformed to log-ratios, to impose the sum to 100%. Then, these log-ratios are linearly transformed to Principal Components. Sequential Gaussian Simulation is performed and the simulated factors are then back-transformed to simulated log-ratios, and these are back-transformed to grades. An application to a Nickel laterite deposit is presented. Spatial dependences are checked by use of cross-variograms and Sequential Gaussian Simulation is used to impose the spatial continuity of the factors of the log-ratios transformed grades. This confirms that PCA tends to spatially decorrelate the factors, allowing for the independent simulation of each PCs, instead of requiring a co-simulation. The results of SGS showed that the simulated grades resulting from the proposed approach reproduce reasonably well the spatial and statistical relationships between the grades.

1 INTRODUCTION

Multivariate geostatistics is used to take advantage of spatial relationships between variables, in order to improve the estimation of a variable using secondary variables, or to jointly simulate a set of correlated variables, preserving their relationships in the models.

There are many methods available to create multivariate models. Sequential Gaussian cosimulation requires a linear model of coregionalization (Verly, 1993), which imposes constraints into the modeling of the direct and cross-variograms, making it unflexible. Other approaches try to avoid this burder by simplifying the cross correlation model by using collocated co-kriging to infer the conditional distributions during simulation (Almeida and Journel, 1994), or by attempting to decorrelate the data through the use of minimum/maximum auto-correlation factors (Desbarats and Dimitrakopoulos, 2000), stepwise conditional transformation (Leuangthong and Deutsch, 2003), or diagonalization approximation (Mueller and Ferreira, 2012).

Principal Component Analysis (PCA) is one of the most commonly used method for multivariate data analysis, due to its mathematical simplicity and to its simple interpretation (Wackernagel, 2003). A linear transformation takes place, in which a set of correlated variables are transformed into uncorrelated (orthogonal) factors (Hotelling 1933; Johnson and Wichern, 1982). The factorization occurs with collocated data, which does not necessarily remove the spatial correlation that may exist between non-collocated data, either from a single variable or between variables (Suro-Perez and Journel, 1991). PCA has been used in geology and soil science before and is a well-established technique in statistical analysis (Davis, 1986; Webster and Oliver, 1990; Goovaerts, 1997).

PCA can be used to reduce the co-kriging of N variables, into the kriging of N uncorrelated principal components (Davis and Greenes, 1983; Goovaerts, 1997). Furthermore, PCA can be used as a compression tool, if only the first few principal components are retained, reproducing most of the variability of the original variables (Wackernagel, 2003).

In this paper, we present a detailed methodology to apply PCA, as a simple decorrelation approach of a compositional dataset, and show its application and performance in a Nickel laterite deposit.

2 NOTATION

In this paper, the original variable is successively transformed several times, so, we provide notation to help the reader:

- $p-1$ is the dimension of the original vector variable.
- p is the dimension of the vector variable after adding the filler to complete 100%.
- n is the number of data samples.
- $X^{original}$ is the $(p-1)$ dimensional vector with the original variable.
- X is the (p) dimensional vector with the original variable, including the filler variable.
- Z is the $(p-1)$ dimensional vector of additive log-ratios.
- F is the $(p-1)$ dimensional vector of principal components computed from the log-ratios.
- Y is the $(p-1)$ dimensional vector of normal scores of the principal components computed from the log-ratios.

3 METHODOLOGY

The proposed methodology requires three sequential transformations of the data prior to simulation. The general methodology is illustrated in Figure 1.

The original variables are the grades (in %) from chemical analyses for a number of samples over the domain of interest. The original grades are noted as:

$$X^{original}\left(u_\alpha\right) = \left(X_1\left(u_\alpha\right), X_2\left(u_\alpha\right),..., X_{p-1}\left(u_\alpha\right)\right) \qquad \forall \alpha = 1,...,n \qquad (1)$$

Since the grades form a composition, we need to complete the vector with a filler variable, to have the set of variables that sum to 100%:

$$R\left(u_\alpha\right) = 100\% - \sum_{i=1}^{p} X_i\left(u_\alpha\right) \qquad \forall \alpha = 1,...,n \qquad (2)$$

The vector needs to be updated, by adding the filler variable:

$$X\left(u_\alpha\right) = \left(X_1\left(u_\alpha\right), X_2\left(u_\alpha\right),..., X_{p-1}\left(u_\alpha\right), R\left(u_\alpha\right)\right) \qquad \forall \alpha = 1,...,n \qquad (3)$$
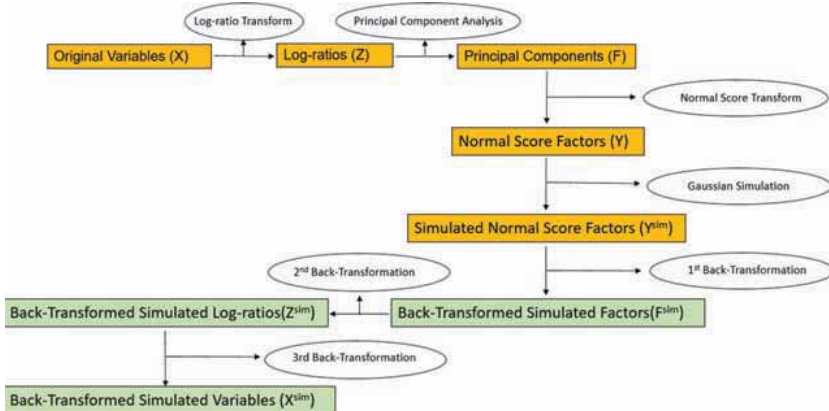
Figure 1. Flowchart of the proposed methodology.

Notice that this approach requires all variables to be informed at all locations, that is, the dataset must be homotopic. Samples with missing variables are common in geological data sets for many reasons. The missing data must be imputed (inferred) to permit the measured data to be used to their full extent. Imputation methods for geological data should address spatial structure and multivariate complexity. If some variables are missing, an imputation process should be applied (Silva and Deutsch, 2016).

3.1 Log-ratio transform

Geological data are frequently reported in terms of the grades of different elements or the mineralogical proportions present in the rock. These sets of variables form a closed array or a composition, as their sum must add to the whole of the material. If all elements are considered, they should sum to 100%. If mineralogical proportions are used, they should add up to 1. This translates in a dependence between the variables, as there is always one less degree of freedom in the system, than variables available. Correlations are also distorted by this dependence, and this can lead to wrong inference and interpretations (Pawlowsky-Glahn and Olea, 2004). This also occurs with sub-compositions, that is when only a subset of all the variables that form the composition are used (Pawlowsky-Glahn and Egozcue, 2006).

Considering the data $\{X(u_\alpha), \alpha = 1, \ldots, n\}$ form a composition, compositional data analysis solves this closure problem by applying a **log-ratio transformation** of the data, so that any further statistical manipulation respects the constraint that the sum adds to 100% (Pawlowsky-Glahn and Egozcue, 2006).

The three most important transformations are:

1. Additive log-ratio (**alr**): it is the logarithm of the ratio between each component and one of the variables, in our case, the filler variable, and was introduced by Aitchison (1982) (see also Pawlowsky and Egozcue, 2006; Aitchison, 1986);
2. Centered log-ratio (**clr**): it is the logarithm of the ratio between each component and the geometric mean of the parts, and was also introduced by Aitchison (1982); and
3. Isometric log-ratio (**ilr**): it is obtained by projecting the composition over an orthonormal basis with $(p - 1)$ dimensions. It was introduced by Egozcue et al. (2003).

In our methodology, we used the **alr** transform, therefore, the data are transformed to a new vector variable, as follows:

$$Z(u_\alpha) = \left(log\left(\frac{X_1(u_\alpha)}{R(u_\alpha)} \right), log\left(\frac{X_2(u_\alpha)}{R(u_\alpha)} \right), \ldots, log\left(\frac{X_{p-1}(u_\alpha)}{R(u_\alpha)} \right) \right) \qquad \forall \alpha = 1, \ldots, n \quad (4)$$

The p dimensional vector $X(u_\alpha)$, becomes a $(p - 1)$ dimensional vector $Z(u_\alpha)$.

3.2 Principal component transform

The next step is to transform the log-ratios obtained in the previous step to linearly uncorrelated factors by using Principal Component Analysis. This **principal component transformation** finds a set of orthogonal linear axes that passes through the multivariate mean of the log-ratio transformed variables, and is such that the variance of the projections of the original log-ratios onto the first axis (called first principal component) is maximized. Axes corresponding to subsequent principal components are determined orthogonal to the previous ones, and with maximum variance (Howarth, 2017).

Principal components are found after an eigen-decomposition of the covariance matrix of the variable of interest (Wackernagel, 2003). The steps required are:

- Compute the mean vector of the variables in vector Z:

$$m = \left(m_{Z_1}, m_{Z_2}, \ldots, m_{Z_{p-1}} \right) \tag{5}$$

where:

$$m_{Z_i} = \frac{1}{n} \sum_{\alpha=1}^{n} Z_i(u_\alpha) \quad \forall i = 1,\ldots,p-1 \tag{6}$$

- Calculate the covariance matrix:

$$C_Z = \frac{1}{n}(Z-m)^T \cdot (Z-m) \tag{7}$$

- Decompose the covariance through an eigen-decomposition:

$$C_Z = Q \cdot \Lambda \cdot Q^T \tag{8}$$

where Q is a matrix where the columns correspond to the eigen-vectors of C_Z, Λ is a diagonal matrix where the terms in the diagonal are the eigen-values of C_Z, sorted in decreasing order.
- Determine the factors (principal components) F: the principal components are obtained by multiplying the data matrix by the eigen-vectors:

$$F = (Z-m) \cdot Q \tag{9}$$

- Although the goal of PCA is to decompose the original variable into decorrelated components, notice that the data can be reconstructed from these principal components:

$$Z = F \cdot Q^T + m \tag{10}$$

The $(p-1)$ dimensional vector $Z(u_\alpha)$ becomes a $(p-1)$ dimensional vector $F(u_\alpha)$. Data compression can be achieved in the last step of the process described above, by retaining only the first $k < (p-1)$ principal components, that is, an approximate reconstruction is obtained as: $Z^{comp} = F' \cdot (Q')^T + m$, where F' are the first k principal components, and Q' corresponds to the first k columns of the matrix of eigen-vectors, hence, these are the eigen-vectors corresponding to the first k highest eigen-values. In our case, compression was not used.

3.3 *Normal score transform*

In order to spatially simulate the principal components, and assuming these are independent from each other, a multigaussian geostatistical simulation method can be used (Chiles and Delfiner, 2012). These methods require a **normal score transformation** to satisfy the requirement of gaussianity. Although in theory a multigaussian assumption is needed, in practice only the univariate condition is imposed through a quantile or polynomial transform.

For each component of the vector of principal component factors, a univariate transformation is performed as follows:

$$Y_i = \varphi_i(F_i) \quad \forall i = 1,\ldots,p-1 \tag{11}$$

where φ_i is the transformation function for variable i.

3.4 *Gaussian simulation*

Variables transformed to normal scores can now be simulated using any of the available multigaussian simulation methods available in the geostatistical toolbox. The simulation can proceed independently for each variable Y_i, $i = 1, \ldots, p-1$, under the assumption that the normal scores of the principal components are independent, that is, their collocated values are linearly decorrelated and they do not show spatial correlation or non-linear correlation.

This can be easily checked by plotting scatterplots and displaying the experimental direct and cross-variograms.

The simulation process will return as output a suite of L realizations of the normal scores of the principal components, over a lattice of locations u defined over the simulation domain D:

$$\left\{ Y_{i,l}^{sim}(u), u \in D \right\} \quad \forall i = 1,\ldots,p-1; \forall l = 1,\ldots,L \tag{12}$$

These realizations reproduce a histogram following a standard normal distribution, honor the data at sample locations $\left(Y_i(u_\alpha), \forall i = 1,\ldots,p-1; \forall \alpha = 1,\ldots,n \right)$, and reproduce the spatial continuity imposed by the variogram model (Deutsch and Journel, 1998).

3.5 *Back-transformations*

The resulting simulated values need to be brought back to their original units by applying the corresponding normal score, principal component and log-ratio back-transformations.

The first back-transformation brings the Gaussian simulated values back to principal components, by using the inverse of the transformation function for each principal component.

$$F_{i,l}^{sim}(u) = \varphi_i^{-1}\left(Y_{i,l}^{sim}(u) \right) \tag{13}$$

The second back-transformation reconstructs simulated log-ratios, from the simulated principal component variables, at every location in the simulation lattice. These are obtained by multiplying the vector of simulated principal components by the transposed matrix of eigen-vectors and adding back the vector of means of the log-ratios.

$$Z_l^{sim}(u) = F_l^{sim}(u) \cdot Q^T + m \tag{14}$$

Finally, the third back-transformation brings the simulated vector of log-ratios, which is a $p-1$ dimensional vector, to the original grades, including the filler variable. This is achieved by determining the closure of the exponentials of the simulated log-ratios.

$$X_l^{sim}(u) = alr^{-1}\left(Z_l^{sim}(u) \right) = C\left[\exp\left(\left[Z_l^{sim}; 0 \right] \right) \right] \tag{15}$$

4   APPLICATION TO A NICKEL LATERITE DATASET

Six geochemical variables corresponding to grades in % of a Nickel laterite deposit are available at 9990 locations in the database: $X_1 = Ni$; $X_2 = Fe$; $X_3 = MgO$; $X_4 = SiO_2$; $X_5 = Al_2O_3$; $X_6 = C_r$.

A filler variable $R = 100\% - \sum_{i=1}^{6} X_i$ is calculated to ensure closure. Then, the additive log-ratios (alr) are computed with respect to the filler variable. Location maps of the samples are presented in Figure 2, as well as the basic statistics of the grades (Figure 3). Scatterplots between the log-ratios (for collocated locations) are shown in Figure 4.

Given that the data are preferentially sampled in specific areas, declustering is required to obtain the representative distribution of the grades (Pyrcz and Deutsch, 2003). Cell declustering is used to determine the weights associated to each sample, based on their location.

Principal component analysis is applied over the log-ratios.

Direct and cross-variograms of the normal scores of the principal components are computed to check the spatial decorrelation obtained by means of the decomposition into principal components. The cross-variograms are displayed in Figure 5. They show that in the horizontal plane there is no spatial correlation. Vertically, very low cross-correlation exists up to 30 m. Beyond that distance, some correlation appears, which is deemed to a trend in the grades.

The direct variograms are fitted with nested licit variogram models. The parameters for the variogram models are summarized in Table 1.
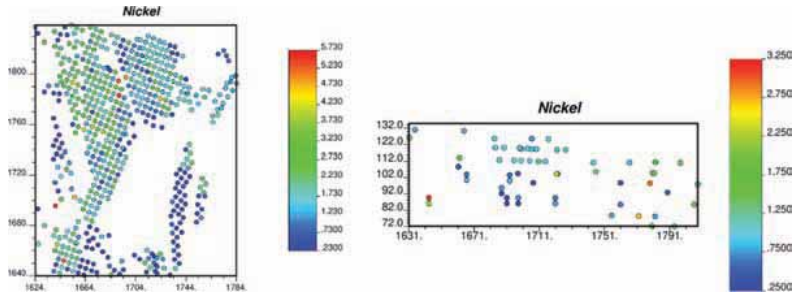
Figure 2: Location maps of the samples in XY (Z = 97 m) and in XZ (Y = 1740 m), for Nickel.
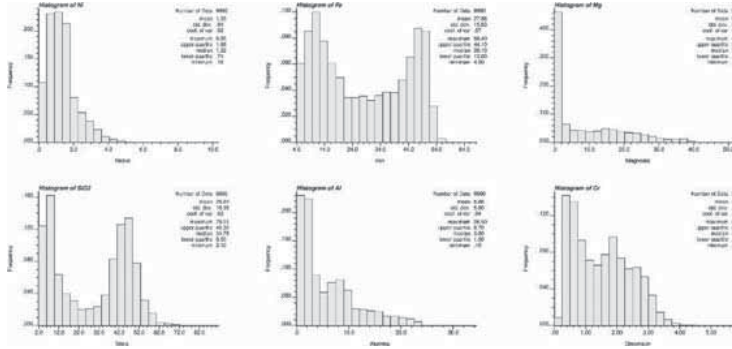
Figure 3. Histograms and basic statistics of the grades.
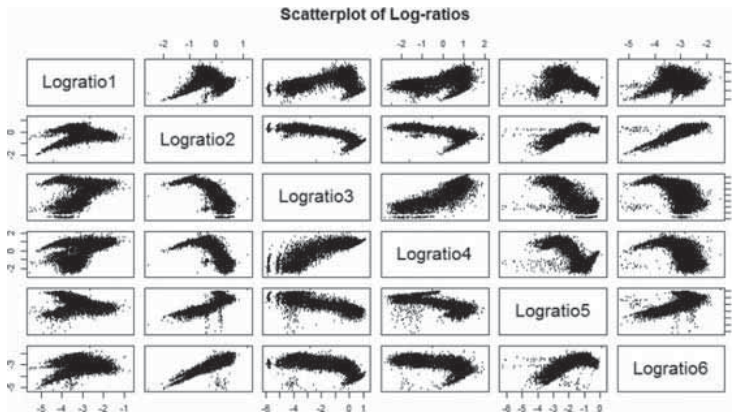
Figure 4. Matrices of log-ratios.
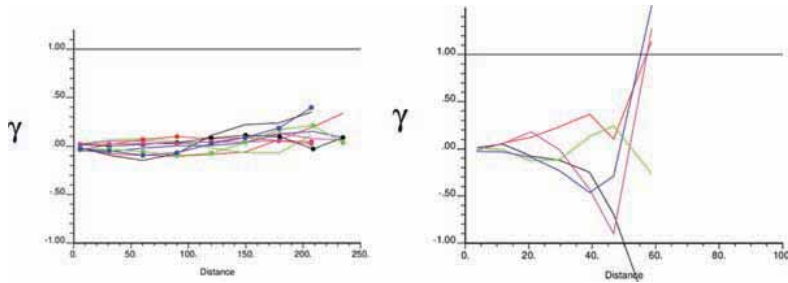
Figure 5. Cross-variogram of normal scores of PC1 (purple), PC2 (red), PC3 (black), PC4 (red), PC5 (green), PC6 (blue) in two orthogonal horizontal directions (left) and in the vertical direction (right).

Table 1. Parameter of the variogram models of each normal score of PC.

| | Nugget effect | Spherical | | | | Spherical | | |
		Sill	Rotation	Ranges		Sill	Rotation	Ranges
PC1	0.2	0.6	0°/0°/0°	50/100/20		0.2	0°/0°/0°	150/infty/20
PC2	0.3	0.7	0°/0°/0°	70/40/20				
PC3	0.3	0.7	130°/30°/0°	55/50/20				
PC4	0.4	0.6	130°/10°/0°	70/58/18				
PC5	0.4	0.6	0°/0°/0°	70/70/20				
PC6	0.4	0.6	0°/0°/0°	120/60/20				

Table 2. Definition of the grid system.

Coordinate	Number of nodes	Initial coordinate	Spacing
X	38	1623.6	5
Y	41	1640.2	5
Z	15	71.2	5
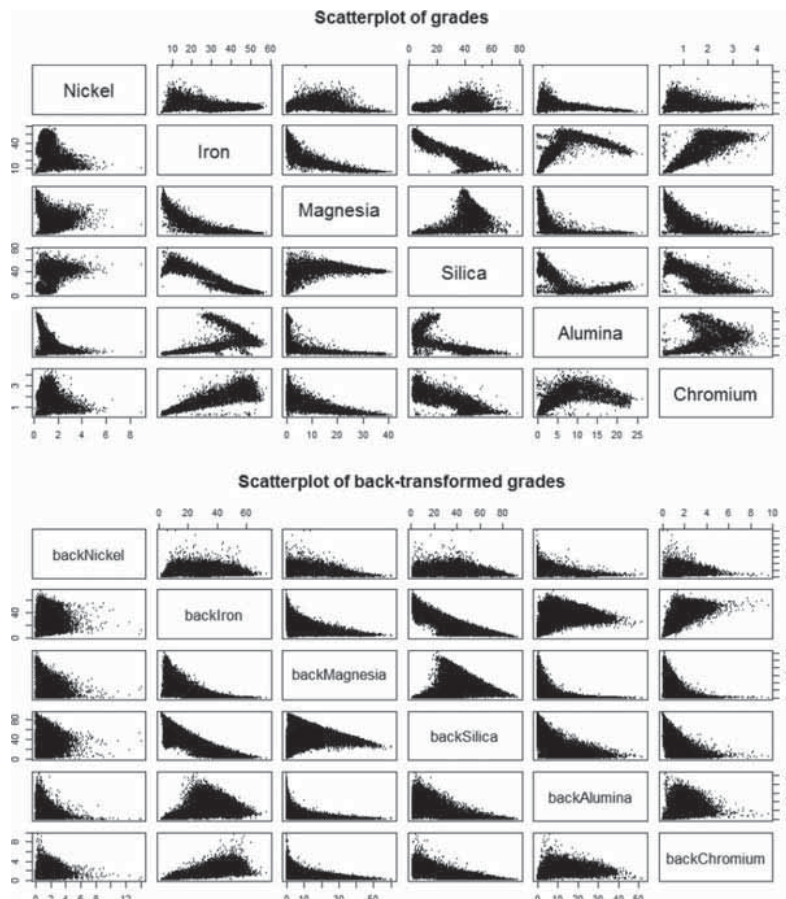
Figure 6. Scatter plots of original grades and back-transformed simulated grades.

Afterwards, Sequential Gaussian Simulation was independently performed for each Principal Component. The simulation is performed to create 5 realizations over the grid of nodes shown in Table 2.

The simulated principal components are back transformed to log-ratios, and these log-ratios are back-transformed to grades. The plots of pairs of the back-transformed grades are calculated and compared with the corresponding sample scatter plots (Figure 6).

Results show that statistics of the distribution of simulated grades are reasonably close to the original sample grades, and even some complex relationships are preserved. This is mainly controlled by conditioning, and not directly imposed by the proposed method which only captures linear relationships. Care should be taken to ensure that statistics are preserved at every step of the methodology, to avoid biasing the results. More realizations would likely lead to a better characterization of the univariate and bivariate distributions.
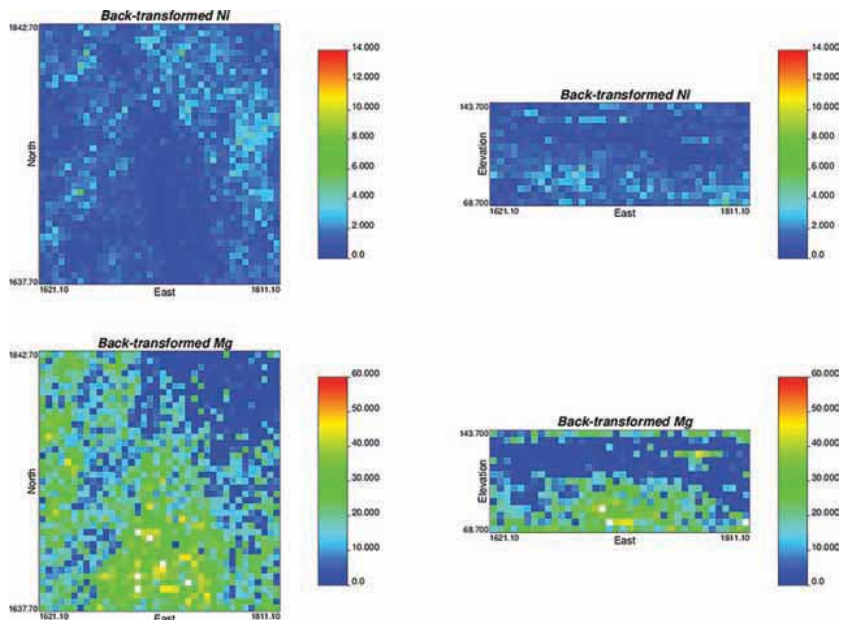
Figure 7. Plan view and cross section of a single realization of back-transformed simulated Nickel and Magnesia.
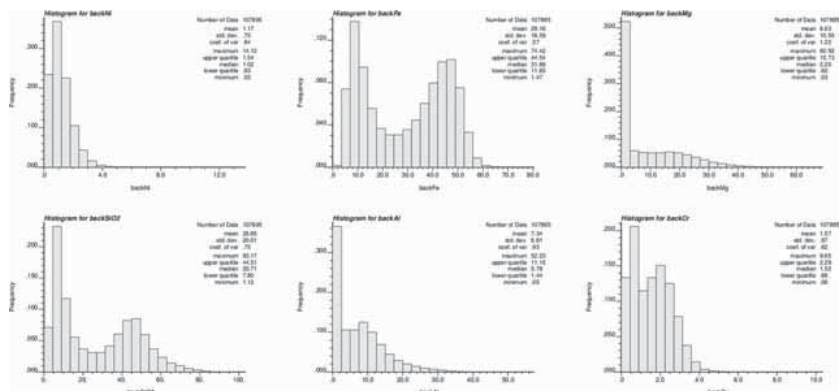
Figure 8. Histograms and basic statistics of the back-transformed simulated grades.

5 CONCLUSIONS

Principal component analysis is an orthogonal transformation that can be used to convert a set of correlated variables into a set of almost linearly uncorrelated components. In this paper, we show a detailed methodology to apply principal component analysis to a set of geochemical variables from an exploration campaign of a Nickel laterite deposit. The method requires dealing with the compositional nature of the data, thus requiring a transformation of the grades into log-ratios. These log-ratios are then decorrelated using PCA. The decorrelation is checked by computing cross variograms between the principal components, which confirms that almost all linear correlation is removed by the transformation into principal components. These principal components are then independently simulated using sequential Gaussian simulation, which in turn requires a normal score transformation of the data.

The methodology is therefore presented as a sequence of three transformations: a logratio transformation using the additive approach, a decorrelation using principal component analysis, and a normal score transformation to use Gaussian simulation. The simulated results must be back-transformed to bring them back from Gaussian simulated deviates, into simulated principal components, then into log-ratios and finally, into simulated grades.

Results are checked to ensure the correlation statistics are preserved, which is confirmed by the scatter plots of the simulated variables, where correlation coefficients are well preserved, and the general correlation structure is reproduced. The method cannot capture some non-linear features of the relationships, which is expected due to its linear nature. Overall, results are satisfactory, confirming that PCA is a suitable approach to model spatially correlated variables.

REFERENCES

Aitchison, J. 1982. The statistical analysis of compositional data (with discussion). *Journal of the Royal Statistical Society, Series B (Statistical Methodology)* 44 (2): 139–177.

Aitchison, J. 1986. The statistical analysis of compositional data. *Monographs on Statistics and Applied Probability*, London, Chapman & Hall Ltd., 416 p.

Almeida, A.S. & Journel, A.G. 1994. Joint simulation of multiple variables with a Markov-type coregionalization model. *Mathematical geology* 26(5): 565–588.

Chiles, J.-P. & Delfiner, P. 2012. *Geostatistics – Modeling Spatial Uncertainty*, Second Edition. Willey, 699 p.

Davis, B.M. & Greenes, K.A. 1983. Estimating using spatially distributed multivariate data: An example with coal quality. *Mathematical Geology*, 15(2): 287–300. https://doi.org/10.1007/BF01036071.

Davis, J.C. 1986. *Statistics and Data Analysis in Geology*, 2nd Edition, John Wiley & Sons, New York, 646 p.

Desbarats, A.J. & Dimitrakopoulos, R. 2000. Geostatistical simulation of regionalized pore-size distributions using min/max autocorrelation factors. *Mathematical Geology* 32(8): 919–942.

Deutsch, C.V. & Journel, A.G. 1998. GSLIB: Geostatistical Software Library and User's Guide, Oxford University Press, New York, 2nd edition.

Egozcue, J.J., Pawlowsky-Glahn, V., Mateu-Figueras, G. Barcelo-Vidal C (2003) Isometric Logratio Transformations for Compositional Data Analysis, Mathematical Geology 35 (3): 279–300 https://doi.org/10.1023/A:1023818214614.

Goovaerts, P. 1997. *Geostatistics for natural resources evaluation*. New York, N.Y.: Oxford University Press.

Hotelling, H. 1933. Analysis of a complex of statistical variables into principal components. *Journal of Educational Psychology*, 24: 417–441, 498–520.

Howarth, R.J. 2017. *Dictionary of Mathematical Geosciences – With Historical Notes*, Springer, 893 pages. DOI 10.1007/978-3-319-57315-1.

Johnson, R.A. & Wichern, D.W. 1982. *Applied multivariate statistical analysis*. Englewood Cliffs, NJ, Prentice-Hall.

Leuangthong, O. & Deutsch, C.V. 2003. Stepwise conditional transformation for simulation of multiple variables, *Mathematical Geology* 35(2):155–173.

Mueller, U.A. & Ferreira, J. 2012. The U-WEDGE transformation method for multivariate geostatistical simulation, *Mathematical Geosciences* 44(4): 427–448.

Pawlowsky-Glahn, V. & Olea, R.A. 2004. *Geostatistical Analysis of Compositional Data*, Oxford University Press, 181 p.

Pawlowsky-Glahn, V. & Egozcue, J. 2006. *Compositional data and their analysis: an introduction*. Geological Society, London, Special Publications, pp. Geological Society, London, Special Publications 2006, v.264; p1–10.

Pyrcz, M. & Deutsch, C. 2003. Declustering and debiasing, downloaded from http://www.gaa.org.au/pdf/DeclusterDebias-CCG.pdf (February, 2019).

Silva, D. & Deutsch, C. 2016. Multivariate data imputation using Gaussian mixture models. *Spatial Statistics*.

Suro-Perez, V. & Journel, A.G. 1991. Indicator Principal Component Kriging, *Mathematical Geology*, 23(5): 759–788. https://doi.org/10.1007/BF02082535.

Verly, G. 1993. Sequential Gaussian co-simulation: a simulation method integrating several types of information, *Geostatistics Troia '92*, A. Soares (ed.), volume 1, 543–554, Kluwer Academic Publishers, Dordrecht.

Wackernagel, H. 2003. *Multivariate geostatistics*. Third Edition. Berlin, Springer. 387 p.

Webster, R. & Oliver, M.A. 1990. *Statistical methods in soil and land resource survey*, Oxford University Press, New York, 316 p.

Application of ASTER multispectral data and hyperspectral spectroscopy for phosphate exploration

N. Mezned

Mineral Resources and Environment Laboratory, Department of Geology, Faculty of Science of Tunis, University of Tunis El Manar, Tunisia
Higher Institute for Preparatory Studies in Biology and Geology Soukra, Institution of Agricultural Research and Higher Education, Tunisia

A. Fatnassi & S. Abdeljaouad

Mineral Resources and Environment Laboratory, Department of Geology, Faculty of Science of Tunis, University of Tunis El Manar, Tunisia

ABSTRACT: Reflectance spectroscopy and ASTER data have proven their capabilities for remote mineralogical mapping and ore exploration. In this context, a new methodology based on the use of ASD hyperspectral spectroscopy and ASTER multispectral data is proposed for the exploration of phosphates in a specific geological and abruptly topographical context in Tunisia. The contribution of this study consists in mapping sedimentary phosphates in the Chaketma mine site in the Centre West of Tunisia using all ASTER VNIR, SWIR and TIR data. Resulting maps from the processing of ASTER data using MF method highlighted already delimited phosphate perspectives as well as other no prospected phosphate outcrops. XRD analysis results as well as ASD hyperspectral spectra were used for the validation purposes. Given the abrupt landscape of the site, the contribution of this approach is well highlighted. Moreover, these results allow to better mark out phosphates and minimize the impact of their exploitation on environment.

1 INTRODUCTION

Phosphate constitutes an important and a necessary resource for the development in Tunisia, as it is very considered in worldwide. Due to the inaccessibility of the most mineral deposits, prospecting has completed only 14% of basic investigations. In addition, laboratory analyzes as well as the field work are cumbersome, punctual and costly. Therefore, the remote sensing technique becomes very useful for the rapid detection and mapping of different surface states, especially mineralization. Remote sensing at moderate cost facilitates the observation, analysis and management of natural resources. It shows a considerable contribution compared to traditional techniques which always remain complementary. Particularly, reflectance spectroscopy has proven its capabilities for remote mineralogical identification. Indeed, due to their absorption features in the Short Waves Infra-Red SWIR region, carbonates were identified and quantified in several previous studies (Clarck, 1999; Gomez et al., 2008; Alayet et al., 2017). Moreover, Aster VNIR (Visible and Near InfraRed) and SWIR multispectral satellite images have been widely used for mineral mapping and ore exploration such us bauxite, iron oxides, gold (Houssainjani et al., 2015). Aster SWIR data have been recently used for targeting rock phosphate (Guha et al., 2018). Aster derived emissivity and temperature has however been used for quartz and igneous rock mapping (Pasricha et al, 2018). Testing the ability of ASTER VNIR, SWIR and particularly TIR data for sedimentary phosphate exploration and mapping is absent in the literatures.

In this context, we propose a new methodology based on the use of hyperspectral spectroscopy and ASTER multispectral data for the exploration of phosphates in a specific geologic and abruptly topographic context in Tunisia. The contribution of this study consists in mapping sedimentary phosphates in the Chaketma mine site in the center west of Tunisia using ASTER VNIR, SWIR and TIR data. These results allow to better mark out phosphates and minimize the impact of their exploitation on environment.

2 STUDY MINE SITE

The mine of Chaketma (Fig. 1) is located in the center west of Tunisia, 200 km southwest of the capital, Tunis and 4 km from the village of Rouhia. The phosphate of the Chaketma mine belong to the category of sedimentary phosphates. This facies which is the most common comes from three main petrographic constituents: granules (pseudo-oolites), nodules and organic debris (coprolites) (Chaabani, 1978; Sassi, 1974). In 2012, the company of "Celamin Holdings" formalized the Chaketma project, which consists of 6 individual phosphate prospects as following: Kef El Louz, Sidi Ali Ben Oum Ezzine, Gassaa Kebira, Gassat Ezarbat, Kef EL Aguereb and Douar Ouled Hamouda. Indeed, the company has intersected thick mineralized zones of an average of more than 15 meters at favorable depths, surface outcrops in areas and qualities that generally exceed 20% of pentoxide phosphorus "P_2O_5" (Celaming Holding, 2012). The estimated mineralization in the 6 perspectives of the Chaketma mine is 176 Mt at 19.5% P_2O_5. This would generate about 79 Mt of phosphate at 30% P_2O_5 content (Craighead, et al., 2012). Tunisian Mining Service TMS (2012) has published a geological map of the Chaketma mine site which shows phosphate outcrops (Fig. 2).

1: Gassaa Kbira
2: Douar Ouled Hamouda
3: Kef El Aguereb
4: Sidi Ali Ben Oum Ezzinze
5: Kef Elouz
6: Gassat Ezarbat
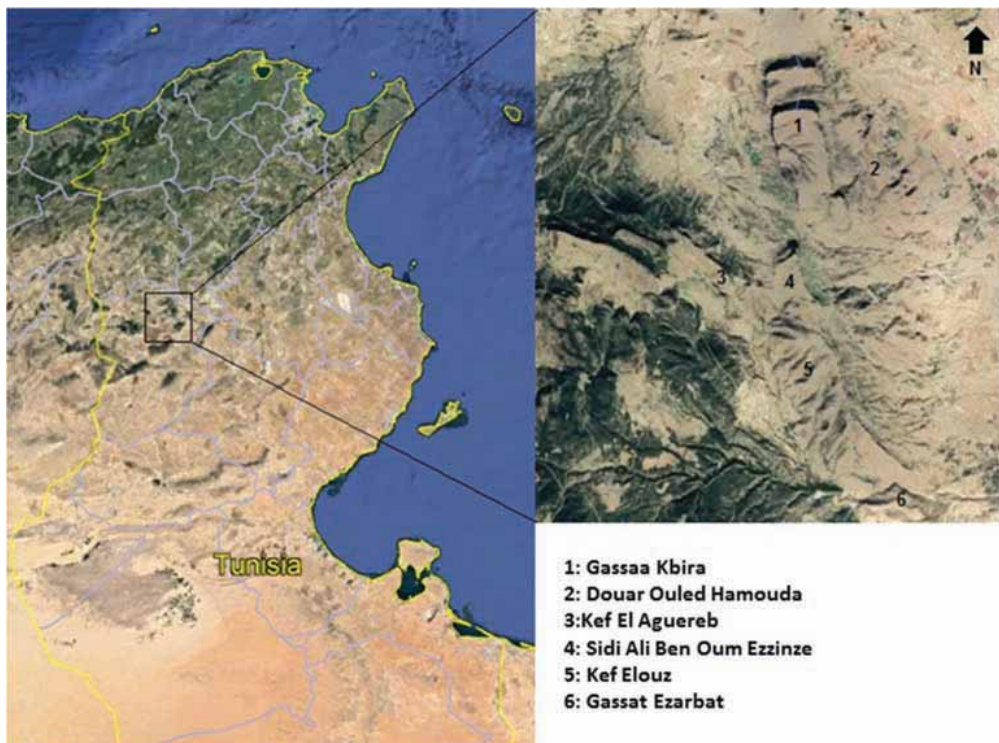
Figure 1.   Chaketma mine site location in the Centre West of Tunisia, in the North Phosphate Basin. Numbers indicate the location of different perspectives: (1) Gassaa Kebira, (2) Douar Ouled Hamouda, (3) Kef EL Aguereb, (4) Sidi Ali Ben Oum Ezzine, (5) Kef El Louz and (6) Gassat Ezarbat.
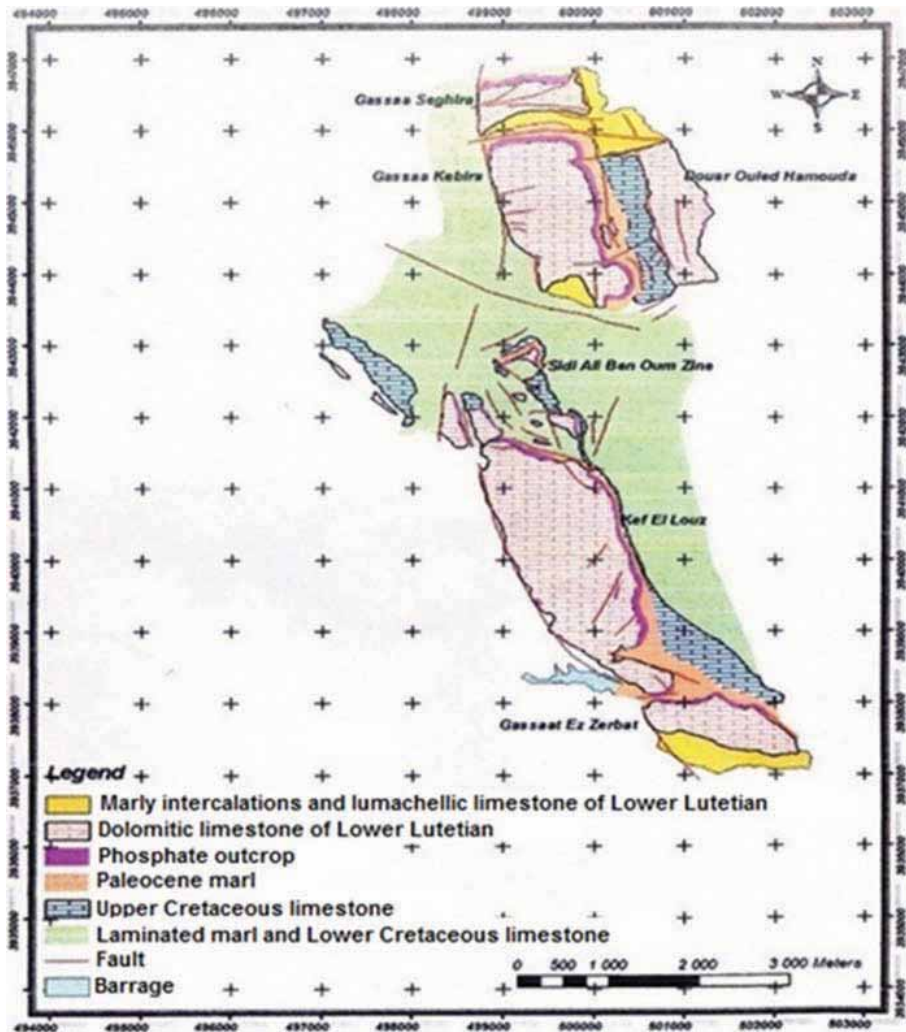
Figure 2. The geological map of the Chaketma mine (TMS, 2012).

3 METHODOLOGY

The methodology (Fig. 3) proposed in this study was applied using Aster multispectral data for phosphate mapping purpose. Thus, a field campaign was firstly achieved in 2017 for phosphate sampling. Thus, twenty five samples were gathered from the first 3 cm of ground surface in the Chaketma site. Each sample was the subject of both mineralogical analysis and reflectance measurement, after homogenization and quartering. The mineralogical analysis was performed using a PANalytical X'Pert PRO X-ray Diffractometer. Thus, the mineralogical composition of each sample was identified and the percentage of different minerals was determined. However, ground spectral measurements were taken under natural light on the field with the ASD FieldSpec HiRes spectrometer (Analytical Spectral Devices, Boulder, Co., USA). This spectrometer was fitted with 10° field of view fiber optics and operated in the 350–2500 nm spectral regions with sampling intervals of 1 nm. The absolute reflectance factor for field measurements was provided by a white spectralon panel (5×5 cm). Thus, surface reflectance measurements were taken at the 25 sites over each sample point location.

Moreover, multispectral data was pre-processed before phosphate mapping. Indeed, the ASTER (Advanced Spaceborne Thermal Emission and Reflection) data, which was acquired
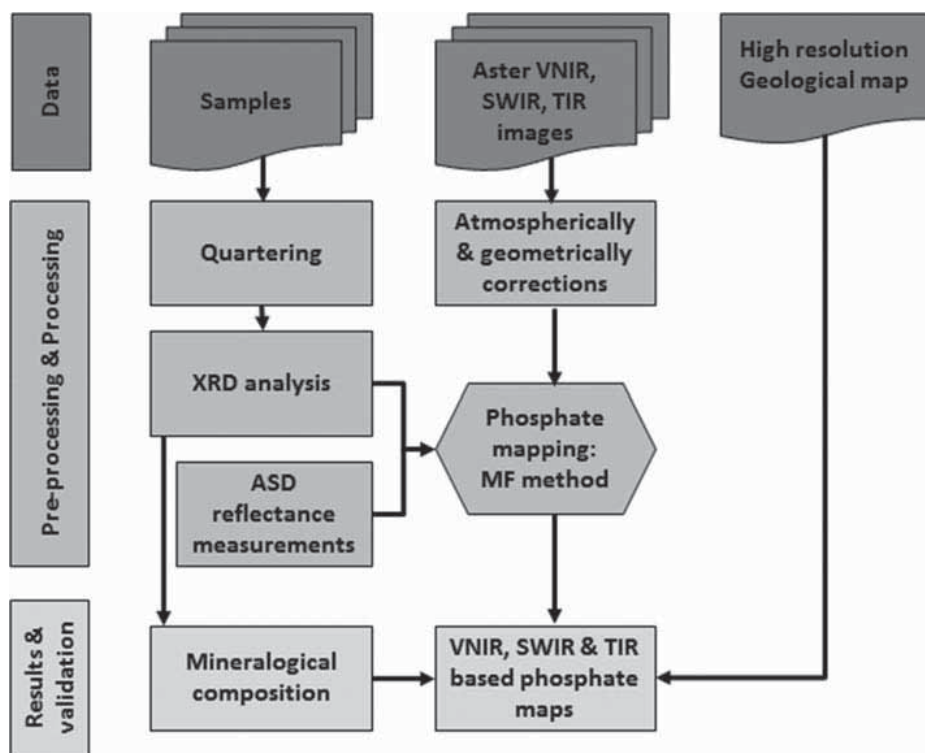
Figure 3.   Methodological flowchart.

on September 28, 2007, was used in this study. ASTER sensor provides seasonal coverage of the overall weight to a spatial resolution of 15 m for the VNIR, of 30 m for the SWIR (Short Waves InfraRed), and 90 m for the TIR (Thermal InfraRed). All images were georeferenced to UTM zone 32 North projection with WGS84 datum. An image subset was derived after that for VNIR and SWIR images and was radiometrically normalized using the Internal Average Relative Reflection (IARR) to estimate surface spectral reflectance. This methodology was previously well presented and introduced as an efficient method for similar areas (Hosseinjani et al., 2005; Hosseinjani et al., 2011; Guha et al., 2018). The TIR image was calibrated using in-scene-atmospheric correction (ISAC) method (Guha et al., 2015) and an emissivity normalization method was after that implemented for deriving ASTER based emissivity (Guha, 2014).

Matched Filtering MF algorithms were implemented on the normalized three VNIR, SWIR and TIR data using image derived spectra in order to map phosphate outcrop for ore exploration. The principle of the MF algorithm consists on the maximization of the response of the known end member and the suppression of the response of the background materials by mathematically projecting each pixel vector onto a subspace, which is orthogonal to the background spectra (Liu, 2005). All endmembers were selected using PCA (principal component analysis) statistical analysis (Theseira, 2003). Resulting maps were compared to delineate phosphate outcrop and their abundances.

4   RESULTS AND DISCUSSION

4.1   *Phosphate ore characterization*

The depiction of X-ray diffractograms, resulting from XRD analysis, revealed the mineralogy of the different samples. All samples have shown the presence of both calcite ($CaCO_3$) and dolomite ($Ca\,Mg\,(CO_3)^2$) carbonates, as dominant minerals, with important concentrations.

The nature of the geological context of the Chaketma region can explain the high concentration of these minerals, with a maximum around 97% and around 68%, respectively for dolomite and calcite. Quartz (SiO_2) is also present with a relative important percent around 30%. The principal mineral indicating the presence of phosphate is the fluorapatite ($Ca_5 (PO_4)^3F$) which reaches 27.21%, particularly in the sector of Sidi Ali Ben Oum Ezzine.

Reflectance spectroscopy has confirmed the presence of this mineralogical composition within samples based on their absorption features detected between visible (VIS) and shortwave infrared (SWIR) (350–2500 nm). Indeed, carbonates were revealed based on vibrational absorption feature in the SWIR region at 2336 nm due to CO_3^{2-} ion (Alayet et al., 2017). Particularly, dolomite (MgCaCO3) presents a displaced carbonate absorption feature at 2326 nm instead of 2336 nm, compared to the calcium carbonate (CaCO3), with an absorption minimum at 2270 nm instead of 2298 nm (Fig. 4). According to Lane et al. (2007), fluoroapatite is known for sharp absorption bands at 3470 and 3980 nm with the presence of water bands around 1400, 1900 and 3000 nm. Guha et al. (2018) presented some diagnostic spectral features of rock phosphate such as the flatness of the spectra of rock phosphate as compared to the spectrum of dolomite around the spectral range from 2200 to 2400 nm, the absence of the dolomite characteristic absorption minimum at 2300 nm, and the presence of a subtle absorption kink at 2200 nm. In our study, we confirm this funding. Moreover, the spectrum of a fluoroapatite sample, which was collected from a Tunisian carbonate geologic context, revealed the presence of the same absorption feature around 2209 nm. We particularly show that the absorption kink at 2209 nm that characterizes the presence of fluoroapatite is still detected in presence of both high grade enriched dolomite and calcite carbonates (Fig. 4).

4.2 *Phosphate mapping*

Using the first three PCs (principle component), three endmembers could be identified from VNIR image and four endmembers from both SWIR and TIR images. These endmembers are identified as rock phosphate outcrops, dolomite (a low grade carbonate bearing phosphate), soils and vegetation. The rock phosphate derived SWIR image spectrum was compared to the ASD measured spectrum before ASTER SWIR data processing. The matched filtering results, conducted on all ASTER images using image derived endmembers, show endmember fraction maps. Only rock phosphate maps are listed and discussed. In these maps, the white color reveals a high content of phosphate and the black color indicates a low content. The accuracy of estimated endmember proportions is evaluated according to the comparison of the spatial
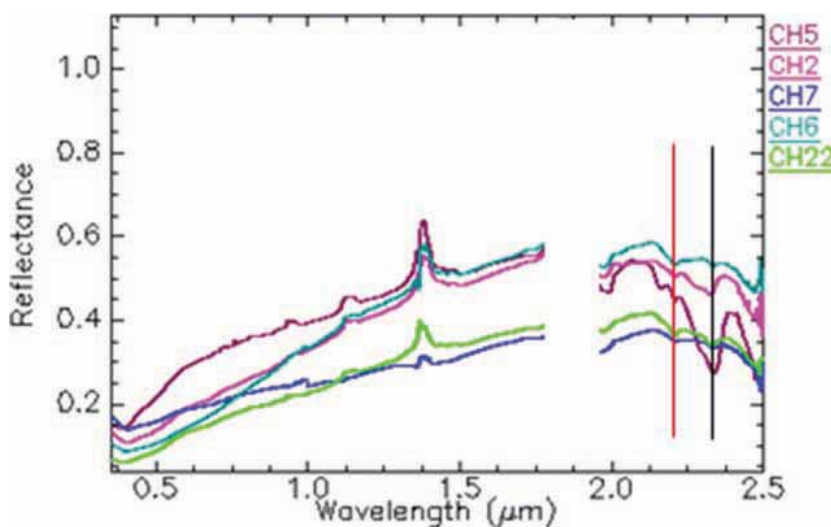
Figure 4. ASD reflectance spectra of some collected samples. Black line indicates the absorption feature at 2336 nm due to CO_3^{2-} ion. Red line indicates however, the absorption kink at 2209 nm.

distribution of phosphate outcrop with a geologic map which was done by the Tunisian Mining Service TMS Company after a detailed field and laboratory work. Phosphate Rocks are detected in the different perspectives of Gassaa Kebira and Kef Ellouz, already identified and revealed in the geological map (TMS, 2012). However, other no prospected phosphate outcrops, were detected and appear up the slope of the Oum Esseba Mountain. Given this abrupt landscape, the contribution of this approach is well highlighted. These perspectives as well as the new highlighted regions were delineated in the map (Fig. 5a; Fig. 5b), which was gener-
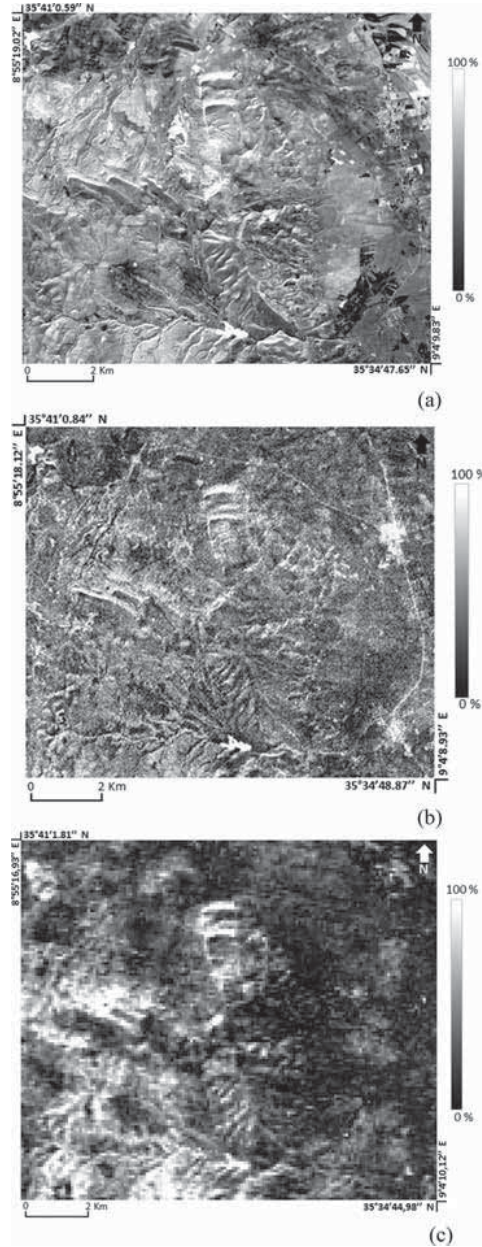
Figure 5. Chaketma phosphate maps: (a) map 891*767 pixels resulting from the Matched Filtering of ASTER VNIR data, (b) 447*385 pixels resulting from the Matched Filtering of ASTER SWIR data and (c) 150*130 pixels resulting from the Matched Filtering of ASTER TIR data.

ated from the processing of ASTER TIR data. This result highlights the contribution of our approach using the TIR data for the first time for phosphate mapping (Fig. 5c).

The validation of the different maps was conducted through the comparison of the phosphate perspectives delineated in Aster VNIR, SWIR and TIR maps and the geological map (TMS, 2012) and the perspective map (Celamin Holding, 2012). Thus, a Kappa coefficient was calculated for all maps and revealed that the proposed approach is efficient. Indeed, the different results generated from the matched filtering of the VNIR, SWIR and TIR data show a calculated kappa coefficient equal to 0.89, 0.95 and 0.86, respectively.

5 CONCLUSION

In study, a new methodology based on the use of hyperspectral spectroscopy and ASTER multispectral data is proposed for the exploration of phosphates in a specific geologic and abruptly topographic context in Tunisia. Testing the ability of all ASTER VNIR, SWIR and particularly TIR data for a sedimentary phosphate exploration and mapping is absent in the literatures. Thus, the contribution of this study consists in mapping sedimentary phosphates in the Chaketma mine site in the center west of Tunisia using ASTER VNIR, SWIR and TIR data. Resulting maps from the processing of All ASTER data using MF method highlighted phosphate rocks in the different perspectives of Gassaa Kebira and Kef Ellouz, already identified and revealed in the geological map (TMS, 2012). However, other no prospected phosphate outcrops, were detected and appear up the slope of the Oum Esseba Mountain. Given this abrupt landscape, the contribution of this approach is well highlighted. Moreover, these results allow to better mark out phosphates and minimize the impact of their exploitation on environment.

ABBREVIATIONS

ASD: Analytical Spectral Devices
ASTER: Advanced Spaceborne Thermal Emission and Reflection Radiometer
MF: Matched Filtering
PC: Principle Component
PCA: Principle Component Analysis
SWIR: Short Waves and InfraRed
TIR: Thermal InfraRed
TMS: Tunisian Mining Service
VNIR: Visible and Near InfraRed
XRD: X-Ray Diffraction

REFERENCES

Alayet, F. Mezned, N. Sebai, A. Abdeljaouad S. 2017. *Continuum removed band depth analysis for carbonate mining waste quantification using XRD and Hyperspectral spectroscopy in the north of Tunisia.* Journal of Applied Remote Sensing, SPIE. 11(1):016021.

Celamin Holdings. 2012. *Maiden JORC Ressource: 37 millions de tonnes au projet Chaketma phosphate.* C. Holdings (Éd.), ASX announcment. Celamin Holdings.

Chaabani, F. 1978. *Les phosphorites de la coupe de Foum Selja (Metlaoui, Tunisie), une série sédimentaire séquentielle a évaporite du paléocène.* thèse 3 ème cycle.

Craighead, G., & Woolfe, T. 2012. *Delivering on phosphate development opportunities*. Celamin Holdings.

Clark, R.N. 1999. *Spectroscopy of rock and minerals, principles of spectroscopy*, In A. Rencz (Ed.), Manual of remote sensing. New York: J. Wiley and Sons Inc.

Gomez, C., Lagacherie, P. & Coulouma G. 2008. *Continum Removal versus PLSR method for clay and calcium carbonate content estimation from laboratory and airborne hyperspectal measurements*. Geoderma, 141–148.

Guha, A., singh, Kr., Reshma, V., Kumranchat, Jeyaseelan & Dhanamjaya. 2018. *Reflectance spectroscopy and ASTER based mapping of rock-phosphate in parts of Paleoproterozoic sequences of Aravalli Group of rocks, Rajasthan, India*. Ore Geology Reviews.

Guha, A., Kumar, K.V. & Ravi, S. 2015. *Reflectance Spectroscopy of Kimberlites – in parts of Dharwar Craton, India*. Arabian Journal of Remote Sensing. 8(11).

Guha, A. 2014. *Integrated approach of using ASTER-derived emissivity and pixel temperature for delineating different granitoids – a case study in parts of Dharwar Craton, India*. Journal of Geocarto International.

Hosseinjani Zadeh, M. & Tangestani, M. 2011. *Mapping alteration minerals using sub-pixel unmixing of ASTER data in the Sarduiyeh area, SE Kerman, Iran.* INT. J. Digital earth.

Lane, M.D., Dyar, M.D. & Bishop, J.L. 2007. *Spectra of Phosphate Minerals as Obtained by Visible-Near Infrared Reflectance, Thermal Infrared Emission, and Mössbauer Laboratory Analyses*. 38th Lunar and Planetary Science Conference, (Lunar and Planetary Science XXXVIII), held March 12–16, 2007 in League City, Texas. LPI Contribution No. 1338, p. 2210.

Liu, 2005. *Classifying multi-temporal Landsat TM imagery using Markov random fields and support vector machines*. In 3rd Intl Workshop on the Analysis of Multitemporal Remote Sensing Images.

Pasricha, K., Guha, A., Sanjit & Kumranchat. 2018. *Comparative Analysis of Potentials of ASTER Thermal Infrared Band Derived Emissivity Composite, Radiance Composite and Emissivity Temperature Composite in Geological Mapping of Proterozoic Rocks in Parts of Banswara, Rajasthan*. Journal of the Indian Society of Remote Sensing.

Sassi, S. 1974. *La sédimentation phosphatée au Paléocène dans le Sud et le Centre Ouest de la Tunisie*. Doctorat d'Etat ès-Sciences, Orsay Paris France.

Theseira, M.A., Thomas, G., Taylor, J.C., Gemmell, F. & Varjo, J. 2003. *Sensitivity of mixture modelling to endmember selection*. Int. J. Remote Sens. vol 24, n°. 27, 1559–1575.

Multivariate Gaussian process for distinguishing geological units using measure while drilling data

K.L. Silversides & A. Melkumyan
Australian Centre for Field Robotics, The University of Sydney, Sydney, NSW, Australia

ABSTRACT: Banded iron formation hosted iron ore deposits are typically stratigraphically modelled using exploration drilling. This drilling has a large horizontal spacing, resulting in a coarse model resolution. Production blast holes are drilled at a higher horizontal resolution, but rarely include detailed information. Measure While Drilling (MWD) data is available, however it only provides information about the relative hardness or strength. There is often a large overlap in the MWD data for adjacent rock units, making manual classification difficult. A Gaussian Processes model was used to automatically label MWD points from two adjacent geological units. For a shale to ore contact, the trained GP had an accuracy of 79%. When distinguishing between two ore units, the GP had an accuracy of ~96% for the library and ~83% for the cross-validation data. Therefore this method can provide additional detail about the location of the contact between geological units for modelling.

1   INTRODUCTION

The banded iron formation hosted iron ore deposits of the Hammersley Region of Western Australia are typically stratigraphically modelled using exploration drilling (De-Vitry et al. 2010; Jones et al. 1973). While these data sources are dense down hole, ~0.1–2 m resolution, the exploration holes are typically drilled with a horizontal spacing of ~50 m. This results in a coarse resolution in the modelling of the contacts between different geological units, with the accuracy decreasing away from the exploration holes. This presents an opportunity to increase the local accuracy of these models using production data.

Production blast holes are drilled at a much higher horizontal resolution (~5 m), but the detailed information collected on the exploration drill holes is rarely obtained. Measure while drilling (MWD) data is available, however it can only provide information about the relative hardness or strength of different geological units. MWD parameters include penetration rate (PR), force on bit (FOB) and torque. The data is collected at 10 cm intervals. PR alone cannot be used to distinguish units, as it is also dependent on the energy inputs. An increase in PR can be due to either a softer rock or an increase in the energy provided by the drill, i.e. through increasing torque or FOB. Several measures, such as adjusted penetration rate (APR) (Zhou et al. 2011) and specific energy of drilling (SED) (Teale 1965), have been created to combine MWD parameters. However these reduce the dimensionality of the data to a single quantity, causing a loss of information. When the natural logarithms of the MWD parameters are plotted for two adjacent rock units, it is difficult to manually classify the regions due to the large overlap between the units. However, a machine learning algorithm can distinguish regions that are dominated by a single unit.

This study uses data from stratified BIF-hosted iron ore mines that contain banded layers of shale and mineralised BIF (Thorne et al. 2008; Dalstra & Rosiere 2008). The ore is consistently harder than the larger shale bands, however the differences in the MWD values between different ore units is much harder to identify. Our MWD based GP identification method is tested in two cases. The first is the shale to ore contact at a typical Marra Mamba style deposit containing the West Angelas Shale and Mount Newman Member iron ore. The

second is the contacts between several ore units in the Dales Gorge Member at a typical Brockman style deposit. The first case contains a soft to hard contact that has been successfully automatically identified using Gaussian Processes on APR signatures (Silversides & Melkumyan 2018). However, the second test contains much more subtle changes between the units and the same technique was not successful in classifying these units.

2 BACKGROUND

In this paper two different approaches using Gaussian Processes (GPs) are presented. A Gaussian Process is defined mathematically as an infinite collection of random variables, any finite number of which has a joint Gaussian distribution (Bishop 2006; Rasmussen & Williams 2006). This is a probabilistic method of modelling functions that represent quantities of interest within a data set. Applying GPs involves two steps: training and inference.

GPs are trained by optimising the hyperparameters that are defined by a given covariance function. This covariance function partially describes the general characteristics of the relationship between the inputs and outputs, such as the level of smoothness. This study uses the multiple length-scale squared exponential covariance function, which can be expressed as:

$$k\left(x_i, x_j\right) = \sigma_0^2 \exp\left[-\sum_{k=1}^n \frac{\left|x_{ik} - x_{jk}\right|^2}{2l_k^2}\right] \tag{1}$$

where l_i is the characteristic length-scale for each variable in the input (PR, FOB, torque etc.). The trained GP is then used to predict the values of the function of interest at new locations.

Mathematically, the GP uses a given training set $D = \{x_i, y_i\}_{i=1}^N$ consisting of N input points $x_i \in R^D$ and the corresponding outputs $y_i \in R$ to compute the predictive distribution $f\left(x_*\right)$ at a new test point x_*. A multivariate Gaussian distribution over the space of function variables $f\left(\mathbf{x}\right)$ maps the input to output spaces. Mathematically the GP specified by its mean function $\mu(x)$ and covariance function $k\left(\mathbf{x}, \mathbf{x}'\right)$, so that $f\left(\mathbf{x}\right) \sim GP\left(\mu\left(\mathbf{x}\right), k\left(\mathbf{x}, \mathbf{x}'\right)\right)$. If the training set is $\left(\mathbf{X}, \mathbf{f}, \mathbf{y}\right) = \left(\{x_i\}, \{f_i\}, \{y_i\}\right)_{i=1}^N$ and the test points $\left(\mathbf{X}_*, \mathbf{f}_*, \mathbf{y}_*\right) = \left(\{x_{*i}\}, \{f_{*i}\}, \{y_{*i}\}\right)_{i=1}^N$, the joint Gaussian distribution is:

$$\begin{bmatrix} y \\ \mathbf{f}_* \end{bmatrix} \sim N\left(\mu, \begin{bmatrix} K\left(X, X\right) + \sigma^2 I & K\left(X, X_*\right) \\ K\left(X_*, X\right) & K\left(X_*, X_*\right) \end{bmatrix}\right) \tag{2}$$

where $\mathbf{f}_* = f\left(x_*\right)$ is the predicted function without noise. During training the log of the marginal likelihood (l ml) is maximised with respect to the hyper-parameters θ, where:

$$\log p\left(\mathbf{y}|\mathbf{X}, \theta\right) = -\frac{1}{2}\mathbf{y}^T\left[K\left(X, X\right) + \sigma^2 I\right]^{-1}\mathbf{y} - \frac{1}{2}\log\left|K\left(X, X\right) + \sigma^2 I\right| - \frac{N}{2}\log 2\pi. \tag{3}$$

The predictive distribution for any test points can then be obtained as $p\left(f_i|\mathbf{X}_*, \mathbf{X}, \mathbf{y}\right) = N\left(\boldsymbol{\mu}_*, \boldsymbol{\Sigma}_*\right)$ where:

$$\begin{aligned} \boldsymbol{\mu}_* &= K\left(X_*, X\right)\left[K\left(X, X\right) + \sigma^2 I\right]^{-1} y \\ \boldsymbol{\Sigma}_* &= K\left(X_*, X_*\right) - K\left(X_*, X\right)\left[K\left(X, X\right) + \sigma^2 I\right]^{-1} K\left(X, X_*\right) + \sigma^2 I \end{aligned} \tag{4}$$

3 METHOD

MWD training data was selected using the existing manual labelling in the corresponding exploration holes. If an exploration hole was within 5 m of a blast hole, the geological interpretation
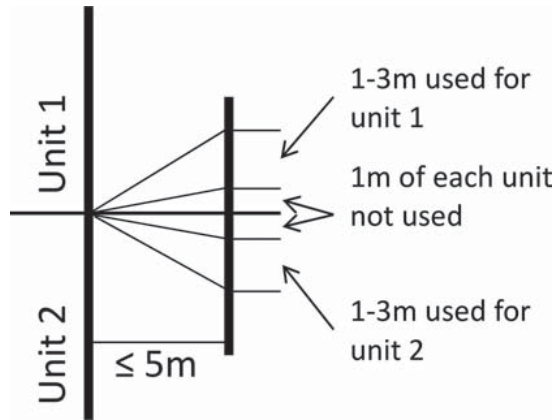
Figure 1.   Using an exploration hole to label the MWD data from a nearby blast hole.

in the exploration hole was used to estimate the contact depth in the blast hole. For the two units on either side of the contact, the data was collected in the interval 1 to 3 m from the contact (Fig. 1). The first metre on each side of the contact was not used to allow for errors in the labelling. The next two metres were used as examples of MWD points close to the contact. The entire unit was not used as there can be significant differences throughout these units due to the banded nature of the deposit. Using the data close to the transition makes the training library more specific for this particular change.

MWD data points above (unit 1) and below (unit 2) the contact were given training labels of 1 and −1, respectively. The library points were used to train a GP with a multiple length-scale squared exponential covariance function. The inputs were the natural logarithms of the PR, FOB and torque. For library validation, this GP was then used to process both the training library and other labelled data (cross-validation). Due to space limitations this is only demonstrated using the ore units. 4000 points were available for each class. They were randomly assigned to four groups of 1000 labelled G1 to G4. These groups were used to create different libraries that contained 2000 points from each class, leaving 2000 points for the cross-validation.

The trained GP was then used to process all MWD points within ±5 m of the existing, exploration based surface. For each point the GP provided an output consisting of a mean and standard deviation (SD). Only the points where the GP provided a relatively confident classification were used. If output > 0 and output – SD/2 > 0 were true the point was assigned to unit 1. If output < 0 and output + SD/2 < 0 the point was assigned to unit 2.

The results for each hole were then post-processed using two steps to reduce noise and inconsistencies in the labelling down the hole. The first step was removing any points that did not have two other points of the same category within 0.5 m. Step 2 was applied to ensure consistency in the classifications down the hole. If a point was labelled as unit 1 the points located above it (below it for unit 2) were considered. If less than 80% of these points were of the same unit the point was discarded. To validate the results, they were compared to the existing, exploration based surface and the labelled points were checked for consistency between nearby holes.

4   RESULTS

A total of 7083 MWD points were labelled from blast holes drilled in the shale and ore units in the Marra Mamba style iron ore deposit. The labels were taken from the manually labelled exploration holes as described above (Fig. 1). 2000 of these MWD points (1000 each of shale and ore) were used for training a multivariate GP. This trained GP was then applied to the

remaining points that were not used in the library to conduct automated labelling. To reduce noise and inconsistencies in the results, the two post processing steps that compare the points within each hole were applied as described above. This post-processing produces more consistent results; however it also decreases the number of points that are labelled.

This test resulted in 436 MWD data points from 31 holes being labelled as either ore or shale. Of these 346 points (79%) were correctly labelled. Figure 2 compares the original exploration based labels to the new GP labels. While the number of points is reduced due to only using the points that could be confidently labelled by the GP, the points that remain are mostly correct. For this test only points which could be labelled from nearby exploration holes were used, this was to ensure that a ground truth was available. However, once trained on the labelled data, this method can be expanded out to process and label all available MWD.

For case 2, the data used was from two adjacent Dales Gorge hosted ore units. MWD points that had been labelled using the exploration data were grouped into four groups (G1 to G4) that each contained 1000 points from each geological unit. These groups were combined in pairs to create six different libraries. A GP was then trained for each library and used to process both the library points and a cross-validation data set that consisted of the
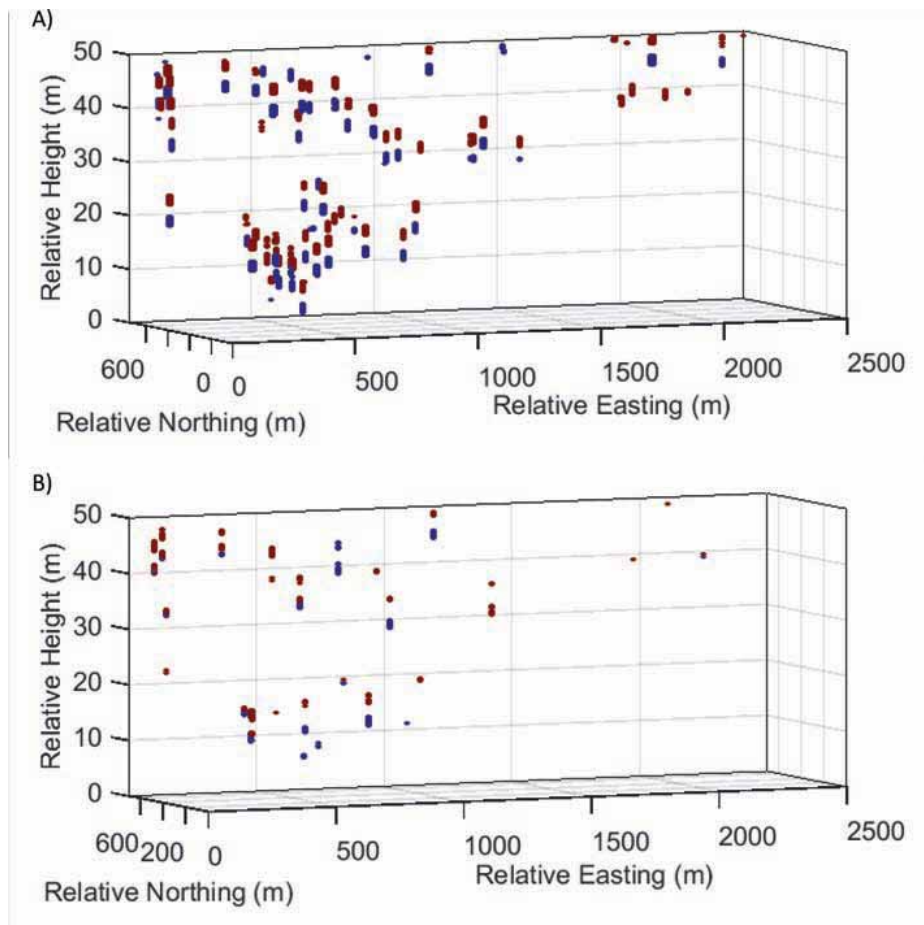
Figure 2. Labelled MWD points for the shale to ore contact. A) The labels used as the ground truth, which were obtained from the exploration holes. B) The labels from the GP for the same holes as in (A). While the GP identifies only a small proportion of the points, they are generally correct. The red points are those labelled as unit 1 (above) and the blue as unit 2 (below). Note that the Z axis is stretched to allow for the densely spaced downhole points to be better observed.

groups that were not used in the library. The post-processing steps were not used in this case as the points were considered individually instead of per hole. When comparing the GP labelled points with the original labels, this method had an accuracy of ~96% for the library and ~83% for the cross-validation data (Table 1). Therefore the libraries were being successfully trained and can provide a useful output. Due to the similarity between the two ores, the percentage of points labelled is low, ~51% for the training library and ~39% for other data. This would be further reduced by the post-processing steps on a normal data set. While the large reduction in data is not desirable, it is partly offset by the high downhole density of the MWD.

When an ore to ore contact for a section of the second deposit is labelled with a trained GP (Fig. 3A) enough data is labelled that the overall shape of the contact and the locations of the units can be seen. When nearby holes are visually compared most are reasonably consistent. However, there are some holes that clearly conflict with their neighbours. Comparing the GP labelled points to a surface based on the exploration data (Fig. 3B) reveals areas where the MWD results conflict with the existing surface and others where they are consistent with the existing surface. Due to the coarse nature of the exploration based surface the MWD results are not expected to always agree with it. Where the MWD points are consistent with each other but in conflict with the surface they can potentially be used to improve the location of the contact surface. Some individual holes are not consistent with either the surface or the surrounding holes. Further cleaning that uses multiple holes could potentially be used to reduce these errors.

While the percentage of points labelled is relatively low, the methodology presented in this paper requires very little user time. The points for the library examples are labelled based solely on the existing exploration labelling and do not require additional manual input. The training and inference steps are then done automatically using this library. In comparison, manually labelling these holes would not only be time consuming, but the lack of visual separation between the data from two units would make it very difficult and subjective.

The GP-based classification methodology proposed here is a binary classification approach which is trained using a library of points from the two adjacent stratigraphic units. It does not have any way of identifying that a point does not belong to either unit. Many other units have similar properties and result in similar MWD values, particularly the ore units. This means that the GP results need to be restricted to the area in close proximity to the contact to prevent a large amount of incorrect classifications and noise. As this methodology is designed to provide finer grained detail for an existing deposit, it is assumed that such a

Table 1.   For each of the libraries the percentage of points where the GP has a certain output and labelled the point (percent labelled), the percentage of the total points which were labelled and correct (percent all correct) and the percentage of the labelled points that were correct (percent of labelled correct) were determined. This was done on the points used to train the GP (library checking) and the other labelled points (cross-validation). Both the library and cross-validation data sets contained 2000 points from each class, 4000 in total.

| Library | Library checking | | | Cross-validation | | |
	Percent labelled	Percent all correct	Percent of labelled correct	Percent labelled	Percent all correct	Percent of labelled correct
G1, G2	51.1%	48.7%	95.3%	38.3%	32.3%	84.4%
G2, G3	55%	53.2%	96.7%	42.6%	35.1%	82.4%
G3, G4	53.6%	51.7%	96.4%	41.7%	34.3%	82.2%
G1, G3	50.1%	48.5%	96.7%	37.2%	31.4%	84.2%
G1, G4	47.0%	45.6%	96.9%	35.2%	29.9%	84.9%
G2, G4	49.1%	46.8%	95.2%	39.0%	32.4%	83.1%
Average	51.0% ± 4.0%	49.1% ± 4.1%	96.2% ± 1.0%	39.0% ± 3.8%	32.6% ± 2.7%	83.5% ± 1.4%
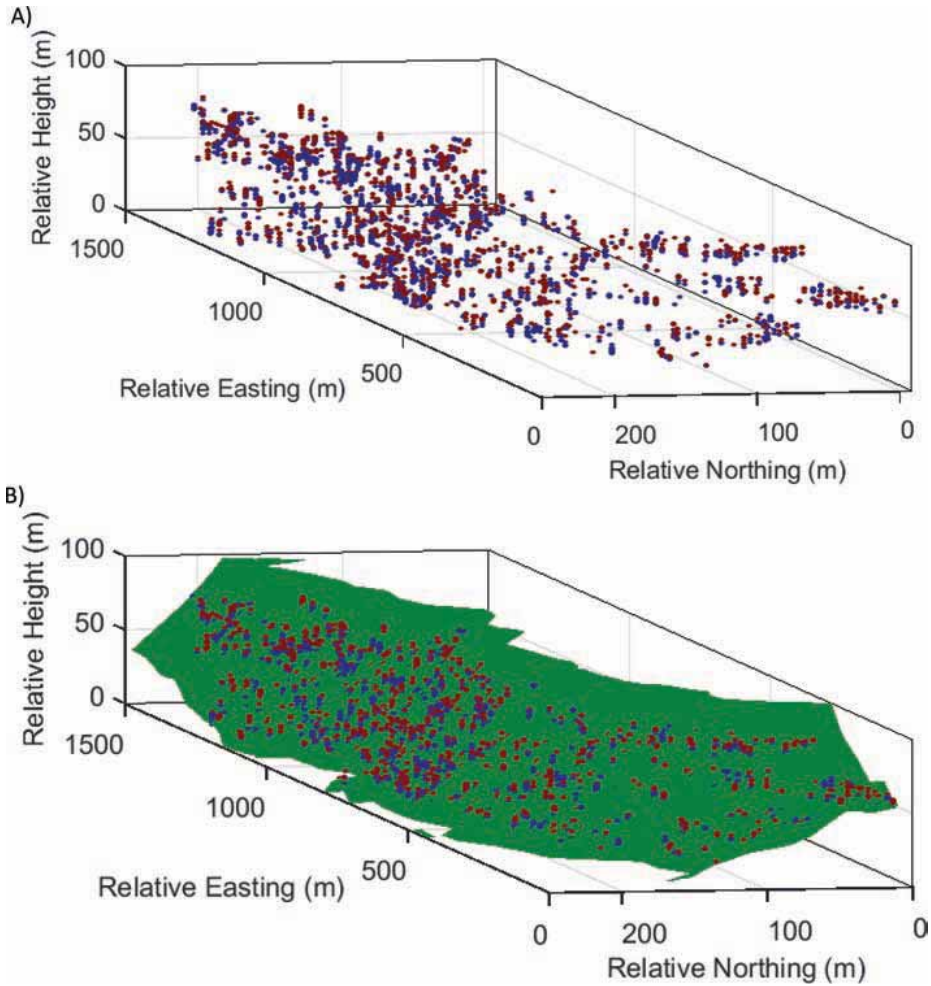
Figure 3. (A) GP labelled MWD points for an ore to ore contact. (B) Comparing A to a surface based on the exploration data. The red points are those labelled as unit 1 (above the contact) and the blue as unit 2 (below the contact).

limiting surface exists. We have used a limit of ±5 m, however this can be adjusted based on both the accuracy of the surface used for limiting the data and the width of the geological units being identified.

5   CONCLUSIONS

The multivariate GP methodology presented in this paper is capable of automatically identifying unit contacts using MWD data in iron ore mines. Unlike APR based methods, the approach proposed in this paper can be used to distinguish two geological units that only have subtle differences in their MWD. We successfully identified both a shale to ore and ore to ore contact. While the similar properties of the two ore zones causes a lot of data to be unlabelled, the large amount of data collected allows for useful information to be provided about the local features of the contact. Therefore the proposed methodology can provide additional detail about the location of the contact between geological units for modelling.

REFERENCES

Bishop, C.M. *2006 Pattern Recognition and Machine Learning* Berlin: Springer.

Dalstra, H.J. & Rosiere, C.A. 2008 Structural controls on high-grade iron ores hosted by banded iron formation: a global perspective. In Hagemann, S., Rosiere, C., Gutzmer, J. & Beukes, N.J. (eds.) *Banded Iron Formation-Related High-Grade Iron Ore.* Littleton, CO: Society of Econimic Geologists, INC.

De-Vitry, C., Vann, J. & Arvidson, H. 2010 Multivariate iron ore deposit resource estimation – a practitioner's guide to selecting methods. *Transactions of the Institution of Mining and Metallurgy Section B,* 119: 154–165.

Jones, H., Walraven, F. & Knott, G.G. 1973 Natural gamma logging as an aid to iron ore exploration in the Pilbara region of Western Australia. *Australasian Institute of Mining and Metallurgy Annual Conference.* Perth, Australia.

Rasmussen, C.E. & Williams, C.K.I. 2006 *Gaussian Processes for Machine Learning,* Massachusetts: MIT press.

Silversides, K.L. & Melkumyan, A. 2018 Characterising Measure While Drilling data responses to changes in rock hardness. IN Hron, K., Bábek, O., Fišerová, E. & Van Den Boogaart, R. (eds.) *The 19th Annual Conference of the International Association for Mathematical Geosciences (IAMG2018).* Olomouc, Czech Republic.

Teale, R. 1965 The concept of specific energy in rock drilling. *International Journal of Rock Mechanics and Mining Sciences,* 2: 57–73.

Thorne, W., Hagemann, S., Webb, A. & Clout, J. 2008 Banded iron formation-related iron ore deposits of the Hammersley Province, Western Australia. IN Hagemann, S., Rosiere, C., Gutzmer, J. & Beukes, N. (eds.) *Reviews in Economic Geology: Banded Iron Formation-Related High-Grade Iron Ore.* Westminster, CO, USA: Society of Economic Geologists.

Zhou, H., Hatherly, P., Ramos, F. & Nettleton, E. 2011 An Adaptive Data Driven Model for Characterizing Rock Properties from Drilling Data. *2011 IEEE International Conference on Robotics and Automation (ICRA).* Shanghai, China.

Machine learning classification of geochemical and geophysical data

L. Huang
The University of Sydney, Sydney, NSW, Australia

M. Balamurali & K.L. Silversides
Australian Centre for Field Robotics, The University of Sydney, Sydney, NSW, Australia

ABSTRACT: Accurate classifications in downhole exploration data are essential for exploration, geological modelling and prediction of mining outputs. These holes are typically interpreted manually, which is slow, subjective and prone to error. Machine learning techniques can potentially automate these classifications. Our test deposit contains the shale dominated West Angelas (WA) Member, and banded iron formation and iron ore in the Mount Newman (MN) Member. Deep learning using autoencoders, Support Vector Machine (SVM) and k-means were applied to classify stratigraphy and rock type using mineral groups or geochemical assays. Autoencoder produced accuracies of 83.2–95.1%, K-means accuracies of 30.4–58.8%, and SVM accuracies of 81.6–88.5%. Geochemical assays were a better indicator of stratigraphy. Autoencoder and SVM produced significantly better results than k-means. This was probably due to k-means not using training data. Although they gave similar results, autoencoder is preferable to SVM for this application as it can handle more than two categories.

1 INTRODUCTION

Accurate classifications in downhole exploration data are essential for exploration, geological modelling and for prediction of mining outputs such as ore tonnages. The data is typically divided into groups based on properties such as stratigraphy and ore or waste designations. While interpreting data from these holes is typically done manually, the process is slow and subjective and is prone to error. Different machine learning techniques can potentially automate some of these classifications. Many different types of machine learning exist, and methods such as Gaussian Processes (Silversides & Melkumyan 2016), t-SNE (Balamurali & Melkumyan 2016) and continuous profile model (Nathan et al. 2017) have been applied to deposits that are similar to our test case. One way of grouping these methods is by the way that the model is trained, for example supervised or unsupervised learning.

This study aimed to investigate the usefulness of different types of machine learning methods to identify geological features from exploration hole data. Three classification methods were used: deep learning using autoencoders, support vector machine (SVM) and k-means. These methods were done as semi-supervised training, supervised training and clustering without training data respectively.

Our test case is a banded iron formation (BIF) hosted iron ore deposit in the Mamma Mamba Iron Formation in the Hammersley Region of Western Australia. This deposit contains two significant stratigraphic units. These are the West Angelas (WA) Member, which is shale dominated, and the Mount Newman (MN) Member, which is a BIF that is mineralised to iron ore in some locations (Clout 2006; Lascelles 2000). The rock can be generally divided into three classes, ore BIF and shale. In this study we use different machine learning methods

to label samples with these classes. Two different data types were used, the geochemical assays and the manually identified material groups present in each sample.

2 BACKGROUND

2.1 *K-means*

K-means clustering involves separating n observations into k clusters to minimise the within-cluster sum of squares (WCSS) (Steinhaus 1957). At the same time the between-cluster sum of squares (BCSS) should be maximised. In this study, Squared Euclidean distance was used to find the distance between data points and every centroid, where every centroid is the random number of n samples. The whole process of k-means is calculating the distances between different data repeatedly to find out the best classification that minimises the WCSS and maximises the BCSS in unsupervised method.

2.2 *SVM*

Support vector machine (SVM) (Melgani & Bruzzone 2004; Liu et al. 2016) can be used for supervised classification and regression. SVM uses the construction of hyperplanes in high-dimensional or infinite-dimensional space and a functional margin that indicates the distance from hyperplane to the nearest training-data point of any class. When training the SVM the functional margin should be maximised and the generalization error of the classifier minimised. SVM uses a kernel function to define dot products in order to simplify the computation in the original space. The formula: $\sum_i \alpha_i k(x_i, x) = c$ relates the points x in the feature space where c is a constant. This means the relative closeness of test points and data points can be calculated by the sum of this kernel function.

2.3 *Deep learning using autoencoder*

An autoencoder is a type of neural network that can be used as an method for training a deep learning neural network. Autoencoders reduce the dimension of the inputs to lower-dimensional code and then produce new features that have same number of input features in an unsupervised manner (Bengio 2009). The learning is done by using 3 components: encoder, code and decoder. The encoder compresses the input and produces the code, the decoder then reconstructs the input only using this code. For learning new features autoencoders do not use explicit training labels, thus the process can be considered an unsupervised learning technique. However, as autoencoders produce their own labels from the input samples this is generally considered as self-supervised or semi-supervised method.

In this study, two autoencoders are used for the deep learning. The features extracted from the hidden layer of the first autoencoder are used as inputs to the second autoencoder. Extracted features from the second autoencoder are used to train a classification layer with the corresponding class labels. Therefore the deep net was created by stacking two autoencoders and a classification layer. Then the deep net was used to predict the labels for the test samples.

2.4 *Data*

The data used in this paper is available through the Western Australian Department of Mines and Petroleum (WAMEX A95838 2012) and has been previously studied in Nathan et al. (2017). Drill hole data was obtained from 11 exploration holes, with a total depth of 662 m. The data includes geochemical assays (Fe, Al_2O_3, P, SiO_2, Mn, MgO, K_2O, TiO_2, S, As, Co, Cu, Pb, Ni, Zn, Ba, Cr, Sn, V, Cl and loss on ignition (LOI)) and mineralogy (grouped into BIF, shale, goethite and hematite) sampled at 2m intervals. Each of these intervals had a manual classification for the ground truth.

3 METHOD

In this study the three machine learning methods autoencoder, SVM and k-means were used to classify the 2 m intervals in three different tests based on different training data. These methods were done as semi-supervised training, supervised training and clustering without training data respectively. Due to the small dataset 90% of the points were used for training and the remainder for testing. The tests were repeated ten times, each time using a different 10% of the data for testing.

The Test 1 used the mineral groups to classify each interval as either WA or NM. For each 2m interval the percentages of each mineral group were used as the inputs and the lithology the output. 207 of these intervals were labelled as either WA (106) or NM (101). Only these intervals with a ground truth were used in the training and testing.

Test 2 used the geochemical assays to classify the intervals as shale, BIF or ore. The ten dominant geochemical species (Fe, Al_2O_3, P, SiO_2, Mn, MgO, K2O, TiO_2, S and LOI) were used as the inputs. Only 136 data points contained both assays and labels. SVM was not used in this test as it is optimised for two categories and cannot be directly applied to separate these three classes.

Test 3 used the same ten geochemical assays for the 207 data points from Test 2; however this time the aim was to classify the intervals as either WA or NM.

4 RESULTS AND DISCUSSION

For Test 1, k-means produced a much lower accuracy than autoencoder and SVM, which had similar results (Table 1). Therefore the most obvious clustering of the data does not necessarily match the labels that the user is interested in when training data is not used. This may be due to the many zero values within the mineral group data.

For Test 2, autoencoder again performs better than k-means (Table 2). An analysis of the results revealed that the highest accuracies were for shale, as BIF and ore are easier to misclassify due to their higher similarity. When comparing these results to Test 1, both methods had a better result for Test 2. Therefore the geochemical assays contain more information that is relevant to the rock type than the mineral groups have for the lithology. Another difference between the data sets is that the geochemical assays are not dominated by zeros like the material groups.

K-means was again the least accurate method for Test 3 (Table 3). The specificity was zero, as no NM samples were correctly classified. The accuracy of SVM (88.5%) was again similar to the accuracy of autoencoder (88.4%). In addition, the sensitivity of SVM was higher than for the autoencoder. Figure 1 plots the distributions of the geochemical assays

Table 1. Results from Test 1, using mineral groups to identify lithology

Method	Accuracy (%)	Sensitivity (%)	Specificity (%)
Autoencoder	83.2	83.9	83.3
K-means	30.4	22.9	34.3
SVM	81.6	85.9	78.7

Table 2. Results from Test 2, using geochemical assays to identify rock type

Method	Accuracy (%)	Sensitivity (%)	Specificity (%)
Autoencoder	95.1	97.8	92.5
K-means	58.8	36.8	68.4

Table 3. Results from Test 3, using geochemical assays to identify lithology

Method	Accuracy (%)	Sensitivity (%)	Specificity (%)
Autoencoder	88.4	89.6	88.5
K-means	31.9	39.5	22.6
SVM	88.5	93.2	86.6
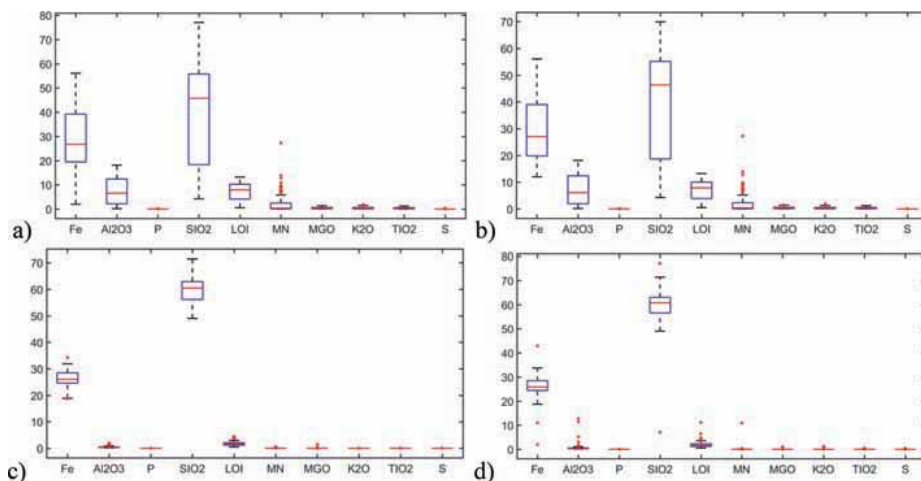
Figure 1. The distribution of the geochemical assays of: (a) Points manually labelled as WA. (b) Points labelled by the autoencoder as WA. (c) Points manually labelled as NM. and (d) Points labelled by the autoencoder as NM.

for points when they are labelled manually and using autoencoder. The dominant geochemical assays for WA include SiO_2, Fe, LOI and Al_2O_3, with median assays of 45wt%, 25wt%, 8wt% and 5wt% respectively. In contrast, NM is dominated by only Fe and SiO_2, with medians of 59wt% and 25wt% respectively. There is also a small amount of LOI. The different WA groups have similar assays (Figures 1 (a) and 1(b)), with the only significant change occurring in the top quartile of the silica. While the overall medians have also stayed the same for the NM, the autoencoder results have more outliers, particularly in the Fe and Al_2O_3. The misclassifications tended to occur at the base of the WA. This section contains less shale and more iron ore than the rest of the member, and is sometimes more similar to the NM than the rest of the WA.

The accuracy of Test 3 (Table 3) was higher than that of Test 1 (Table 1) for all methods. This indicates that the geochemical assays contain more information that is useful for separating the WA and NM. However, the accuracy of Test 3 (Table 3) was lower than Test 2 (Table 2), which indicates that the geochemical assays are a better indicator of rock type than lithology.

For all tests, autoencoder and SVM had significantly better results than k-means. This is due to k-means not using training data. Although they had similar results, autoencoder is preferable to SVM for this application as it can handle more than two categories. Therefore for this problem is the best of the tested methods.

5 CONCLUSION

Deep learning using autoencoder, SVN and k-means were successfully applied to both geochemical assays and mineral groups to determine the rock type or lithology. Autoencoder

and SVM had significantly better results than k-means, probably due to k-means not using training data. This indicated that for this type of data it is better to use a supervised or semi-supervised method. In Test 2 the highest accuracies were for shale, as BIF and ore are easier to misclassify due to their higher similarity. Test 3 had higher accuracies than Test 1, indicating that geochemical assays are a better indicator of WA or MN. Although they had similar results, autoencoder is preferable to SVM for this application as it can handle more than two categories. Overall, deep learning using autoencoder produced a high accuracy and is an effective machine learning technique to use when to classifying this type of geological and geochemical data.

REFERENCES

Balamurali, M. & Melkumyan, A. 2016. "t-SNE based visualisation and clustering of geological domain," in International Conference on Neural Information Processing. Springer, 2016, pp. 565–572. In Hirose, A., Ozawa, S., Doya, K., Ikeda, K., Lee, M. & Liu, D. (eds.) *Neural Information Processing. ICONIP 2016. Lecture Notes in Computer Science.* Springer, Cham.

Bengio, Y. 2009. *Learning Deep Architectures for AI. Foundations and Trends in Machine Learning 2*.

Clout, J.M.F. 2006. Iron formation-hosted iron ores in the Hamersley Province of Western Australia. *Transactions of the Institution of Mining and Metallurgy Section B,* 115: 115–125.

Lascelles, D.F. 2000. Marra Mamba iron formation stratigraphy in the eastern Chichester range, Western Australia. *Australian Journal of Earth Sciences*: 799–806.

Liu, P., Choo, K., Wang, L. & Huang, F. 2016. SVM or deep learning? A comparative study on remote sensing image classification. *Soft Computing,* 21: 7053–7065.

Melgani, F. & Bruzzone, L. 2004. Classification of hyperspectral remote sensing images with support vector machines. *IEEE Trans Geosci Remote Sens,* 42: 1778–1790.

Nathan, D., Duuring, P., Holden, E.J., Wedge, D. & Horrocks, T. 2017. Learning characteristic natural gamma shale marker signatures in iron ore deposits. *Computers & Geosciences,* 106: 77–88.

Silversides, K.L. & Melkumyan, A. 2016. Gaussian Processes based fusion of multiple data sources for automatic identification of geological boundaries in mining. In Hirose, A., Ozawa, S., Doya, K., Ikeda, K., Lee, M. & Liu, D. (eds.) *Neural Information Processing. ICONIP 2016. Lecture Notes in Computer Science.* Springer, Cham.

Steinhaus, H. 1957. Sur la division des corps matériels en parties. *Bull. Acad. Sci. (in French),* 4: 801–804.

Wamex A95838 2012. Wee One Annual Technical Report. http://geodocs.dmp.wa.gov.au/search.jsp?Report_Ref=A95838&cabinetId=2301.

Covariance table and PPMT: Spatial continuity mapping of multiple variables

J. Kloeckner, C.Z. da Silva & J.F.C.L. Costa
Universidade Federal do Rio Grande do Sul, Porto Alegre, Brazil

ABSTRACT: In most mining projects often multiple variables, which may be correlated, are required to build models. The relationship among variables has a significant impact on processing plant performance. Therefore, such relationships should be accounted for so that the final model is representative of the reality in the deposit. The projection pursuit multivariate transform is a modern approach that simplifies multivariate geostatistical modeling while assuring multigaussianity. Even though, it simplifies significantly multiple variables modeling, it remains a laborious and crucial step: calculate and fit a semivariogram model to each and every variable for geostatistical estimation and simulation methods. We propose a methodology using a covariance table to map automatically spatial continuity to replace the traditional covariance explicit defined model. A three dimensional case study of an iron ore deposit illustrates the practical applicability for the work flow proposed. The results are satisfactory, validated by the standard simulations verification.

Keywords: covariance table, PPMT, multivariate data

1   INTRODUCTION

The geostatistical modeling is crucial for a complete understanding of the geological phenomenon. A key feature for the modeling process is the spatial continuity within the deposit, which affects all the planning and exploration stages of the mining endeavour. Traditionally, the spatial continuity model is obtained through the semivariogram, which is valid within a domain along all spatial directions. Although widely used, this approach demands human effort that can be highly laborious and subjective for a multiple variables data set. Numerous methods propose an automatic semivariogram model fitting. However, such methodologies are based on the parameters that are subject to the analyst adjustment. This way, the main goal of this study is to reduce the human laborious tasks to as little as possible if desired.

This is achievable through the use of covariance table (CT) instead of the explicit covariance model. The covariance table proposed is obtained through a three-steps work flow: interpolating the data set to fill it up a regular grid; auto convolute the gridded data via a fast Fourier transform algorithm; back transform the model to spatial domain ensuring positive definiteness condition. The projection pursuit multivariate transform (PPMT) to deal with multivariate relations amongst variables. The projection pursuit multivariate transform is a modern approach to transform multivariate data of any distribution shape, size and dimension to an uncorrelated multivariate Gaussian distribution. Thereby, geostatistical simulation can be performed independently. After, PPMT back-transform restores the original multivariate correlation of individual independent simulations. In doing so, the PPMT simultaneously simplifies multivariate geostatistical modeling while assuring multigaussianity.

This paper is organized in four sections. The first one explains briefly the PPMT method and how it was applied in this study. In the second section, we propose the workflow to automatically obtain the CT for each variable and its essential step named base model to extract the covariance (BMEC). The third section presents the methodology. In the fourth section,

we present a case study in an iron ore deposit illustrating the practical application for the work flow proposed.

2 PROJECTION PURSUIT MULTIVARIATE TRANSFORM

In mining projects very often it is required to characterize multiple correlated attributes. The relationship between variables must be accounted for so that the final model is representative of the geological phenomenon. The multivariate relationships imply the use of co-simulation (Verly, 1983) techniques, which in turn demand the simultaneous modeling of the direct and cross covariance functions for all variables considered. Also, traditional co-simulation methods are performed under the Gaussian formalism. Assuming that the attributes are multivariate Gaussian allows all relationships to be fully parameterized by the covariance matrix. Even though, the traditional approaches allow obtaining realistic models, the covariance modeling is extremely tedious with more than two variables, and geological attributes rarely are multivariate Gaussian in nature. So, prior to the co-simulation (Verly, 1983) process, nscore (Journel and Huijbregts, 1976) transformation is often applied on the variables, so that the Gaussian formalism may be used. However, the nscore transform only ensures that the variables are univariate Gaussian, even though this is a necessary condition, it is not sufficient. Generally, the bivariate Gaussianity is verified and if valid, the multivariate Gaussianity is assumed. This assumption, on the other hand, in some cases may not be met. An alternative is to use *P*rojection pursuit multivariate transform (Barnett et al., 2014). (PPMT), which transforms any number of variables to be multivariate Gaussian and uncorrelated, enabling the independent modeling of each attribute considered while reproducing the multivariate complexities on the final model (Manchuk et al., 2017). The PPMT approach involves 3 stages: a pre-processing stage where the properties of the data matrix are made sure to be suitable for the projection pursuit algorithm; then the projection pursuit is performed on the data matrix while *Gaussianizing*, as the process is called in the literature, the data; finally the data may be back-transformed once the geostatistical model has been built (Barnett et al., 2014). Each phase will be briefly explained, for further details on PPMT methodology refer to (Barnett et al., 2014) and (Manchuk et al., 2017).

2.1 *Pre-processing*

Considering a random vector **U** of the *N* multiple attributes, a normal score transformation is applied to remove all marginal complexities from the data (Barnett et al., 2014). Then, the normal scored data **Y** are made orthogonal, ergo, uncorrelated through a *sphering* process, according to equation 1:

$$X = S^{-\frac{1}{2}}Y,$$ (1)

where $S^{-\frac{1}{2}}$ is the sphering matrix obtained through equation 2:

$$VD^{-\frac{1}{2}}V^{T}$$ (2)

V and **D** are the eigenvector and eigenvalue matrices, respectively.

2.2 *Projection pursuit*

According to (Manchuk et al., 2017), considering a vector $\boldsymbol{\theta}$ and the projection **p** of the *sphered* data **X** upon $\boldsymbol{\theta}$, if **X** is multivariate Gaussian then the projection **p** shouldalso be Gaussian. So, for this phase of the PPMT algorithm is defined a projection index $I(\boldsymbol{\theta})$ that measures the non-Gaussianity of the projection (Manchuk et al., 2017). That is, if $I(\boldsymbol{\theta}) = 0$ then **p** is Gaussian. The aim of this step in the PPMT algorithm is to perform an optimized

search so that $I(\boldsymbol{\theta})$ is a maximum, meaning that the projection is strongly non-Gaussian. Once the maximum value of $I(\boldsymbol{\theta})$ is obtained the projected data $\mathbf{X}$ is *Gaussianized* leading to $\mathbf{X}^*$, so that the projection is univariate Gaussian. Then, the search begins once again, for another maximum value of $I(\boldsymbol{\theta})$, and the data is once again *Gaussianized*, and so on. The procedure is repeated until the data are multivariate Gaussian. The stopping criteria for the PPMT algorithm is based on bootstrap sampling (Barnett et al., 2014) and (Manchuk et al., 2017). Once the data are multivariate Gaussian the geostatistical modeling may proceed as usual, independently for each projection obtained.

2.3 *Back-transformation*

The back-transformation is the reverse operation applied at each iteration in the *Gaussianization* process, so the more iterations performed on the forward transform the more reverse operation performed on the back-transform. After all iterations have been reversed, the sphering and normal score should be back-transformed (Manchuk et al., 2017).

3 COVARIANCE TABLE

Covariance table (CT) is a set of information that can be used to describe the spatial correlation in kriging and geostatistical simulation (Chu, 1993), (Deutsch and Journel, 1998), (Yao and Journel, 1998), (Yao, 2004) and (Pyrcz and Deutsch, 2006). We propose to generate a CT that describes the spatial phenomena by: (1) building a base model to extract the covariance (BMEC) by estimating values from the data set to fill up a regular grid; (2) this grid is then auto convoluted via FFT algorithm (Johnson and Frigo, 2008) to obtain the spectral density table (frequency domain); and (3) we back transform the spectral density table into CT (spatial domain). Figure 1 illustrates the workflow to obtain the proposed CT from a data set to a simulation case. To apply the technique on an estimation case, the work flow would be the same.

In Figure 1 and throughout this paper, the BMEC was built using nearest neighbor estimation (NN), because it is a very simple estimator and it preserves the declustered data set variance. For sparse data, e.g. in mining feasibility studies, NN will duplicate several times the data and the CT will be smoother than it should. However, BMEC is a concept which allows us to explore further estimation techniques, such as artificial neural network (ANN). Given their ability to recognize
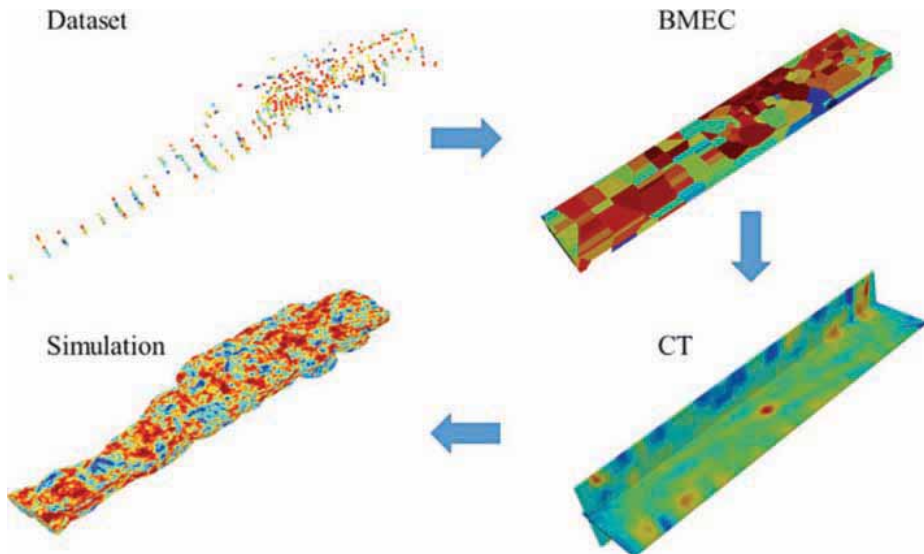
Figure 1.   Work flow to obtain the proposed CT from a data set.

patterns in data, ANNs have been proposed as an alternative method for spatial interpolation (Öztopal, 2006) and (Carvalho et al., 2007). The ANN approach makes no assumptions regarding stationarity, obviates the need to specify a covariance model (Rigol et al., 2001), and can provide multiple realizations of the estimated field (Rizzo and Dougherty, 1994). This method can reduce drastically the user influence or even allow a fully automatic workflow. This workflow also addresses a less subjective methodology. The CT is defined as:

$$C_z(h) = \frac{1}{N(h)} \sum_{\alpha=1}^{N(h)} z(u_\alpha) z(u_\alpha + h) - m_{z_{-h}} m_{z_{+h}}, \tag{3}$$

where $m_{z_{-h}}$ and $m_{z_{+h}}$ denote, respectively, the mean of the tail and head values, and $N(h)$ denotes the number of pairs that can be found at one lag h.

3.1 *Fast Fourier Transform and convolution*

The Fourier transform (FT) is a mathematical operation which allows us to transform a function from spatial domain to frequency domain (Yoo, 2001). This transformation points out, in frequency domain, periodical characteristics of this function. FT of the function $z(u)$ is defined as:

$$\mathscr{F}\left[z(u) \right] = \int z(u) e^{-i\omega u} du \tag{4}$$

where $\mathscr{F}[\cdot]$ is the operator for the Fourier transform. Convolution is an operation on two functions (or auto convolution for the same function) to produce a third function that expresses how the shape of one is modified by the other. It can also be used to amplify the shape of the same function. Covariance of $z(u)$ is defined in one dimension as the convolution product (Bracewell and Bracewell, 1986):

$$C_z(h) = \int_{-\infty}^{\infty} z(u) z(u+h) du = z(u) * z(-u). \tag{5}$$

Applying Fourier transformation in (5) we obtain the spectral density of $z(u)$ in the frequency domain as follows:

$$s_z(\omega) = \mathscr{F}\left[C_z(h) \right] = \mathscr{F}\left[z(u) \right] * \overline{\mathscr{F}}\left[z(u) \right] = Z(\omega)^2, \tag{6}$$

Therefore $Z(\omega) = \mathscr{F}\left[z(u) \right]$, and $\overline{\mathscr{F}}\left[z(u) \right]$ and is the complex conjugate. $s_z(\omega)$ stands for spectral density and, it can be used to perform spectral simulation (Yao, 2004) orit can be back-transformed into CT in the spatial domain. In practice, we normally have a data set
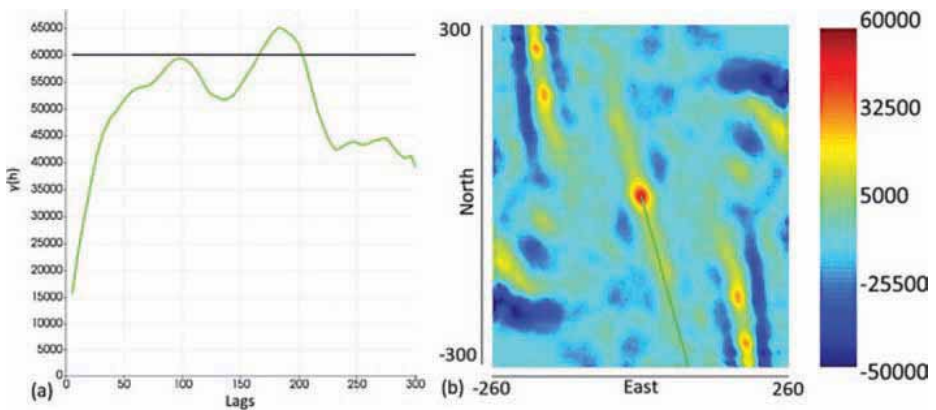
Figure 2.   The semivariogram model for the principal direction (a) and its respective CT (b).

109

with a list of values of $z(u)$ for a discrete set of u's. To obtain the FT pair for one variable, meaning forward and back transform Fourier equations, $z(u_\alpha)$ must be sampled in uniform steps (Yoo, 2001). Thus from a real data set available it is not trivial to perform fast Fourier transform FFT algorithm. For that reason, we propose to estimate values that reproduce samples spatial continuity property in a regular grid (BMEC).

3.2 *Conditioning the covariance table*

Given that covariance models must honor conditional negative definiteness to provide licit values for any lag and direction, and the proposed method does not guarantee a conditional negative definite CT, we need to overcome this issue. Figure 2 shows an example of a semi-variogram model and its respective CT that does not honor conditional negative definiteness.

To solve it the Bochners theorem is used. It defines the general form of a continuous conditional negative definite function $C(h)$, without taking the nugget effect into account, for $h = 0$:

$$C(h) = \int_{-\infty}^{\infty} cos(\omega h)\, dS(\omega), \tag{7}$$

under the constraints that $dS(\omega) > 0$ and $\int_{-\infty}^{\infty} dS(\omega) = C(0) < \infty$. $S(\omega)$ is the spectral cumulative distribution function. In practice, the CT is corrected for conditional negative definiteness by transforming all negative real values to zero and then standardizing all spectrum values to sum to the variance desired (Pyrcz and Deutsch, 2006).

4 METHODOLOGY

Once all the fundamental theory have been presented, it is possible to describe the proposed work flow. The first step is to make all variables $z_1, z, ..., z_N$ independent from each other through PPMT method. This is the key step to overpass cross CT. What would make the entire workflow more laborious. The second step is to apply the proposed CT method for each independent variable. The third step is to simulate each independent variable using any geostatistical simulation method based on covariance. The fourth step is to back transform each realization to make the multiple variables as they were originally correlated. Figure 3 illustrates the entire step by step methodology for a multiple variable data set simulation case.
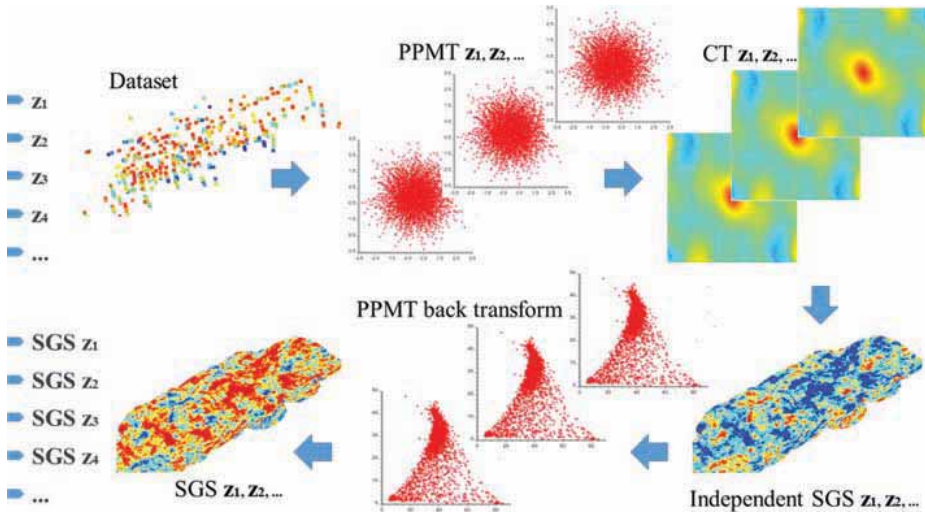
Figure 3. Step by step for the proposed methodology.

The methodology can be used as a fully automatic workflow. However, human interaction with a spatial continuity model may be useful, because it can provide interpretation and uncertainty analysis if desired. A possible input from the geo-modeler is to impose a preferential direction when building the BMEC. The CT extracted from it will reproduce those anisotropy directions. Another potential problem is the size of the CT. For a very large area, or even inclined boreholes, the CT requires to compute covariances for all distances. An analytic form of covariance is needed for those cases.

5 CASE STUDY

For the case study, a three dimensional multivariate data set from an iron deposit in Brazil was used. However, due to the extension of the data set it was chosen to work with the two main variables: Fe (%) and Si (%). Figure 4 shows the location map for the Fe (%) samples, covering an area of 5000 m × 1000 m and 300 m deep. The Si (%) samples are collocated with Fe (%). Figure 5 shows the scatter plot and the statistical summary for Fe (%) and Si (%). The variables have a strong negative correlation (−0.99). As explained in the methodology section, the next step is to decorrelate Fe (%) and Si (%). After, the variables are normal score transformed and the PPMT transformation is applied. Figure 5 also shows the scatter plot of the independent variables completely uncorrelated.

For each uncorrelated variable, one CT is generated. Both CTs are three dimensional grids. The CT extracted from the Fe (%) BMEC and from Si (%) BMEC are shown in Figure 6 in horizontal plan view at $z = 0$. The red line in both CTs mark the major range and the semivariogram extracted from both CTs for the major anisotropy are presented for Fe (%) in Figure 9 and for Si (%) in Figure 10 when compared with SGS ergodic fluctuations results.

The Bochners theorem for conditional negative definiteness was not performed for this example, given that all CTs generated satisfactory results. For each case, 20 realizations were generated. The SGS using the CT was performed for both independent variables. From those resulting realizations the PPMT back transform was applied, so the final model would be in the original data space. Figure 7 shows the scatter plot for the resulting correlated realizations. The results show that the original correlation between variables (−0.99) is preserved (−0.98).

Figure 8 shows one realization map for Fe (%) and one for Si (%). Figure 9 shows the variogram extracted from the Fe (%) CT for the major anisotropy direction in comparison with the
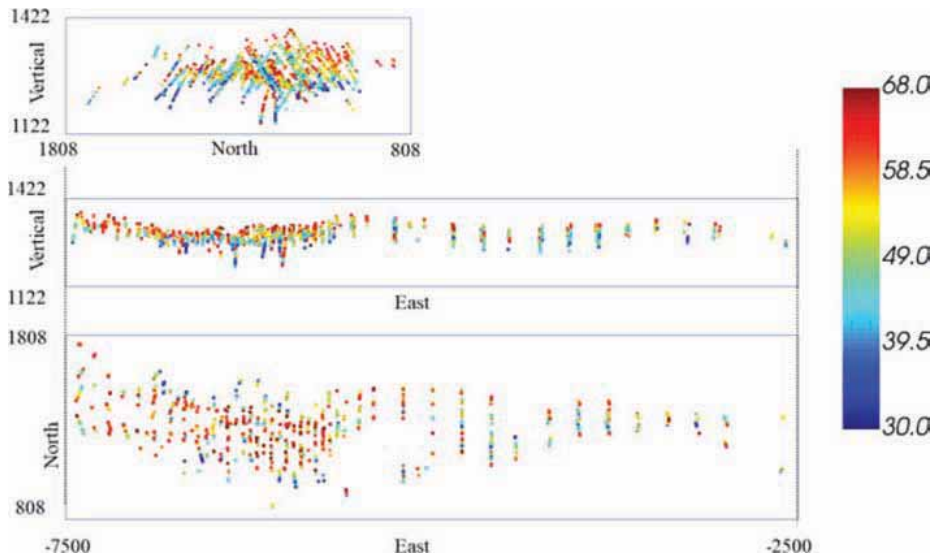
Figure 4. Location map for the Fe (%) variable, covering an area of 5000 m × 1000 m and 300 m deep (Samples for Si (%) are collocated with Fe (%).
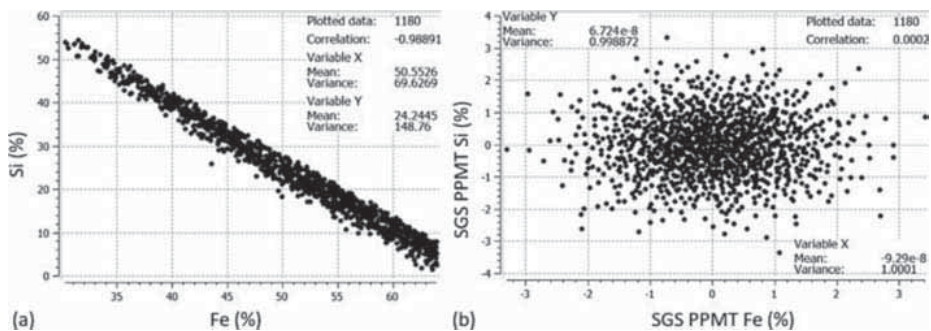
Figure 5. Scatter plot for the Fe (%) and for Si (%) (a) and scatter plot of Fe (%) and Si (%) after PPMT transform (b).
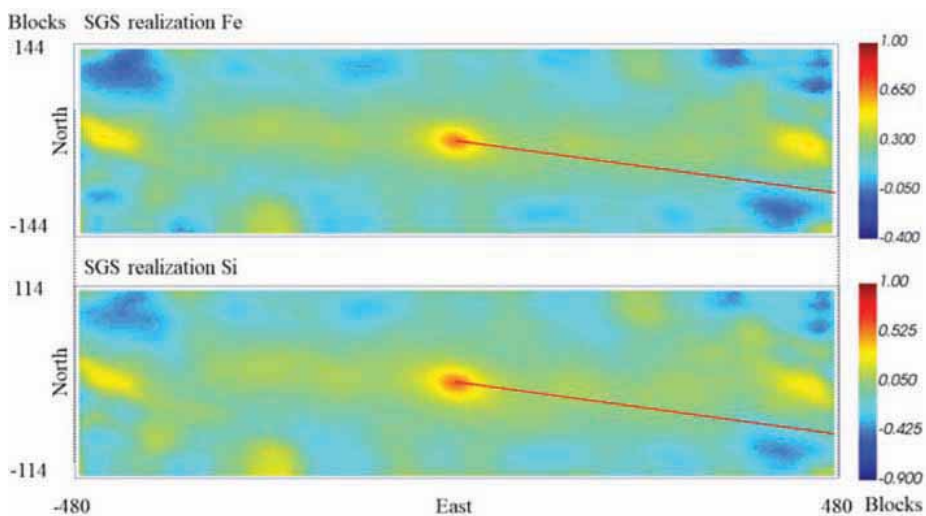
Figure 6. CT from the Fe (%) BMEC (a) and from Si (%) BMEC in plan view at $z = 0$.
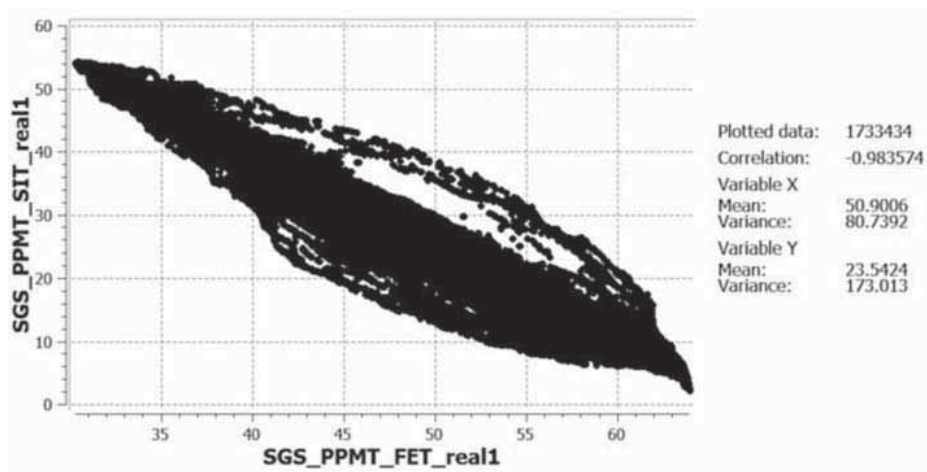
Figure 7. Scatter plot for one realization of Fe (%) and one of Si (%) after PPMT back transform.
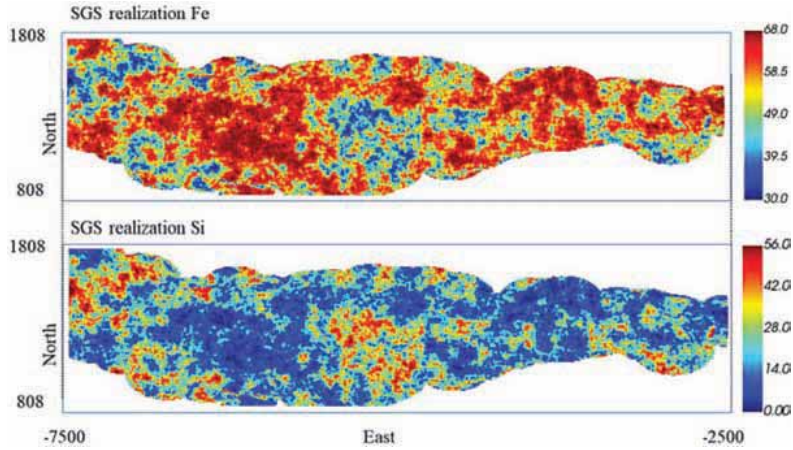
Figure 8. Realization map through SGS for Fe (%) (a) and realization map for Si (%).
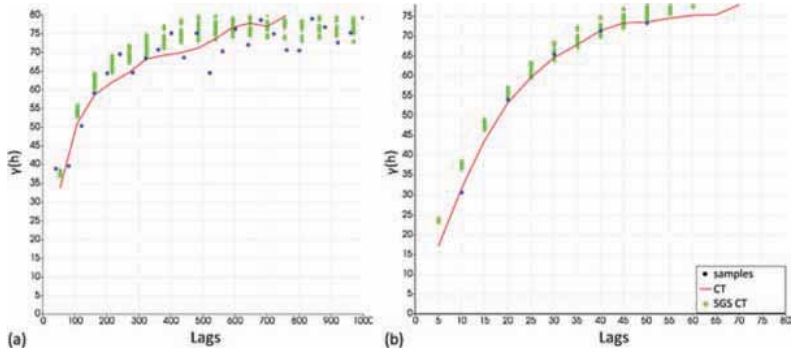
Figure 9. The semivariogram models for Fe (%) in the major range (a) and minor range (b).
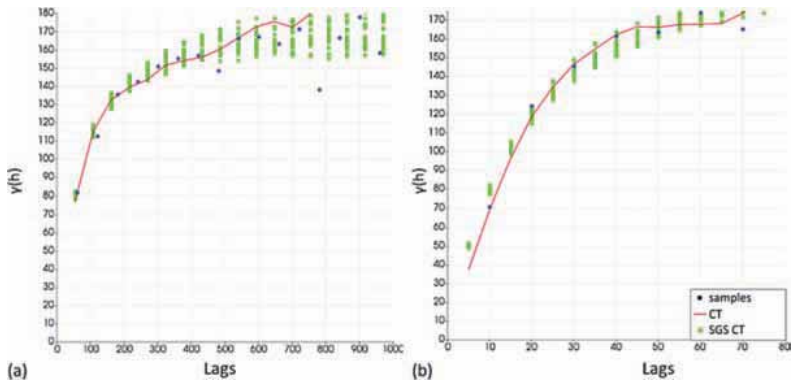
Figure 10. The semivariogram models for Si (%) in the major range (a) and minor range (b).

ergodic fluctuations of the SGS realizations and the Fe (%) experimental variogram (obtained through the sparse data). Figure 10 shows the semivariogram extracted from the Si (%) CT along the major anisotropy direction in comparison with the ergodic fluctuations of the SGS realizations and the experimental variogram Si (%). In both cases the CT and results are very close from the experimental variogram, indicating the robust methodology proposed.

113

The results shown that the methodology proposed produces a satisfactory result for the case study. It is noted that the simulation back transformed mean of the variables reproduces the original mean of the data very well. However, the samples variances are not well reproduced, +16% for Fe and −14% for Si. The BMEC is a work in progress but it opens a different approach to build a robust CT with new BMEC's to be explore.

6 CONCLUSION

The technique based on extracting a covariance table (CT) from a base model to extract covariance (BMEC) was found to obtain good results. The statistical validation of the method and the speed of obtaining a spatial continuity analysis are good indicators that is possible to substitute the traditional variogram modeling. Projection pursuit multivariate transform (PPMT) to make any number of variables to be multivariate Gaussian and uncorrelated, enabling the independent acquisition of CT for each attribute considered, while reproducing the multivariate complexities on the final model. This CT is obtained through a three steps workflow: interpolating the data set to fill up all grid nodes in a regular grid, auto convolute via FFT algorithm and back transform to spatial domain. The BMEC represents a simple solution to a complex problem comparing with previous methods that proposed CT usage. The proposed method does not suppress previous modeling phases, such as choosing stationary domain, but it is a fast automatic spatial continuity method to compute covariances. For a future work a more complete comparison between the current methodology with the proposal in this paper will be done.

REFERENCES

Barnett, R.M., Manchuk, J.G., and Deutsch, C.V. (2014). Projection Pursuit Multivariate Transform. *Society of Petroleum Engineers*, 21(6):337–359.

Bracewell, R.N. and Bracewell, R.N. (1986). *The Fourier transform and its applications*, volume 31999. McGraw-Hill New York.

Carvalho, A.R., Carvalho, J.C., Shiguemori, E.H., Da Silva, J.D.S., and Ramos, F.M. (2007). Neural network based models for the retrieval of methane concentration vertical profiles from remote sensing data. In *Anais XIII Simposio Brasileiro de Sensoriamento Remoto. Florianopolis, Brasil*, volume 21, page 6.

Chu, J. (1993). *Conditional fractal simulation, fast sequential indicator simulation, and interactive variogram modeling*. PhD thesis, Stanford University.

Deutsch, C.V. and Journel, A. (1998). Geostatistical software library and users guide. *Oxford University Press, New York*.

Johnson, S.G. and Frigo, M. (2008). Implementing FFTs in practice. *Fast Fourier Transforms*.

Journel, A.G. and Huijbregts, C.J. (1976). Mining geostatistics.

Manchuk, J.G., Barnett, R.M., and Deutsch, C.V. (2017). The reproduction of secondary data in projection pursuit transformation. *Stochastic Environmental Research and Risk Assessment*, 31(10):2585–2605.

Öztopal, A. (2006). Artificial neural network approach to spatial estimation of wind velocity data. *Energy Conversion and Management*, 47(4):395–406.

Pyrcz, M.J. and Deutsch, C.V. (2006). Spectral corrected semivariogram models. *Mathematical Geology*, 38(7):891–899.

Rigol, J.P., Jarvis, C.H., and Stuart, N. (2001). Artificial neural networks as a tool for spatial interpolation. *International Journal of Geographical Information Science*, 15(4):323–343.

Rizzo, D.M. and Dougherty, D.E. (1994). Characterization of aquifer properties using artificial neural networks: Neural kriging. *Water Resources Research*, 30(2):483–497.

Verly, G. (1983). The multigaussian approach and its applications to the estimation of local reserves. *Journal of the International Association for Mathematical Geology*, 15(2):259–286.

Yao, T. (2004). Reproduction of the mean, variance, and variogram model in spectral simulation. *Mathematical geology*, 36(4):487–506.

Yao, T. and Journel, A.G. (1998). Automatic modeling of (cross) covariance tables using fast fourier transform. *Mathematical Geology*, 30(6):589–615.

Yoo, Y. (2001). Tutorial on fourier theory. *Retrieved June*, 17:2007.

Optimal drill hole spacing for resource classification

Marek Nowak
SRK Consulting Canada Inc., Vancouver, BC, Canada

Oy Leuangthong
SRK Consulting Canada Inc., Toronto, ON, Canada

ABSTRACT: Regulatory bodies around the world have relied on similar definitions for mineral resource categories, and subdivide mineral resources in order of increasing geological confidence: Inferred, Indicated and Measured. Major investment and development decisions are based on a correct assignment of a resource to a proper category. The progression to mineral reserves reporting requires at least the categorization of Indicated and/or Measured resources. As such, the assignment of a mineral resource to an Indicated category should be recognized as a necessary step to advance towards the feasibility of a project.

Allocation of mineral resource categories often relies on some geostatistical tools, of which drill hole spacing is perhaps most common. This paper looks at procedures to determine the optimal drill hole spacing required for allocation of a portion of resources to an Indicated category in metal deposits. These procedures are differentiated into two main groups based on their simplicity and stage of application: (1) general assessment of adequate drill hole spacing; and (2) local assessment of uncertainty on estimated grade within large panels representing monthly or quarterly production. At an early exploration stage general assessment of optimal drill hole spacing for an assignment to an Indicated category is quite adequate. On the other hand, at a pre-feasibility stage simulation studies represent the best tool for resource categorization. Practical examples from a case study the authors have worked on will be presented.

1 INTRODUCTION

Mineral resource estimation models are always sub-divided in order of increasing geological confidence into Inferred, Indicated, and Measured categories. The definitions of mineral resource categories are very similar between the Canadian Institute of Mining (CIM), The Australasian Code for Reporting of Mineral Resources and Ore Reserves (JORC), and the South African Code for Reporting of Mineral Resources and Mineral Reserves (SAMREC). The established standards for reporting on resource categories are based on a Qualified Person's (QP) assessment of geological and grade continuities and, in general, are often based on the QP's subjective assessment of confidence on the estimated tonnage and grade.

Important, and often costly, investment decisions rely on this assignment of resources into different classification categories. At an early exploration stage, resources are usually allocated to an Inferred category. With each additional drill campaign, the portions of the Inferred category resources can be upgraded to Indicated or Measured categories. Once a resource has been assigned to an Indicated or higher category, it has the potential to be converted to a Probable Reserve. The conversion to the reserves is not possible for an Inferred category resource. Therefore, the assignment of a mineral resource to at least an Indicated category is a necessary step to advance towards the feasibility of a project and eventually towards mine development and construction.

To assign a mineral resource to an Indicated category, the geological and grade continuity must be established directly from available data. Spatial distribution of the data should allow confident interpretation of the geological framework. It should also reasonably reflect the continuity of the mineralization. For this purpose, there are a number of factors that can be applied by QPs for resource classification:

- Data quality
- Structural setting
- Geological continuity
- Drill hole spacing
- Grade continuity, often based on variogram analysis
- Applied cut-off for resource reporting
- Data used to estimate a block:
  - Number of drill holes
  - Number of samples
  - Number of octants
  - Average distance to informing composites

The most often discussed and used component for resource classification is drill hole spacing. This is evident from NI 43-101 reports the authors reviewed. Management of exploration companies often ask the authors what drill hole spacing would be necessary for allocation of resources to at least an Indicated category. The answer is never straightforward. Allocation to an Indicated category is subjective—assignment to the category is often open to interpretation and potential modifications.

Fortunately, there are geostatistical tools that can make the assignment to an Indicated category less subjective. This paper focusses on two primary groups of methods: (1) those aimed at a general assessment of drill hole spacing and may be applicable at early stages in a project; and (2) those aimed at local assessments of drill spacing while accounting for local grade variability which may be more relevant for intermediate to advanced studies. Finally, an approach to design the location of infill drill holes for the purposes of classification upgrading is proposed. This may be important as a project advances towards feasibility and the focus of an infill drill campaign may be to strategically drill in areas to upgrade Inferred areas to an Indicated category. The examples presented in this paper are based on a low grade gold deposit in Nevada, US. For this presentation the grades have been modified by a constant factor.

The compiled methods and procedures laid out in this paper were specifically chosen for their practicality and accessibility to the general mining practitioner. The authors recognize that other, more advanced approaches have been proposed; however, many of them are not considered standard in the industry at this time.

2 GENERAL ASSESSMENT OF DRILL HOLE SPACING

One of the simplest tools often used for an assessment of drill hole spacing for the Indicated category is an indicator variogram (Journel, 1983; Journel, 1985). Drill hole composite assay data are converted to 0/1 indicators based on a predefined cut-off, similar to the cut-off used for resource reporting. If a composite assay is higher or equal to the cut-off it is converted to a value of one. Otherwise the assay is given a value of zero. A modelled range of continuity from a variogram calculated on the indicators is the first pass assessment of necessary drill hole spacing for the Indicated category. It is usually applied at early stages of an exploration project. A 2/3 of the modelled range of continuity is often given for the drill hole spacing. For example, as shown in Figure 1(a), the range of continuity is approximately 250 ft, which indicates drill hole spacing of approximately 160 ft.

Another, less known, tool is based on a technique called "p-gram" (Srivastava, 2004; Leuangthong and Nowak, 2015). To construct p-grams, composites above a predefined cut-off grade are coded with an indicator variable. Using a process similar to indicator variography,
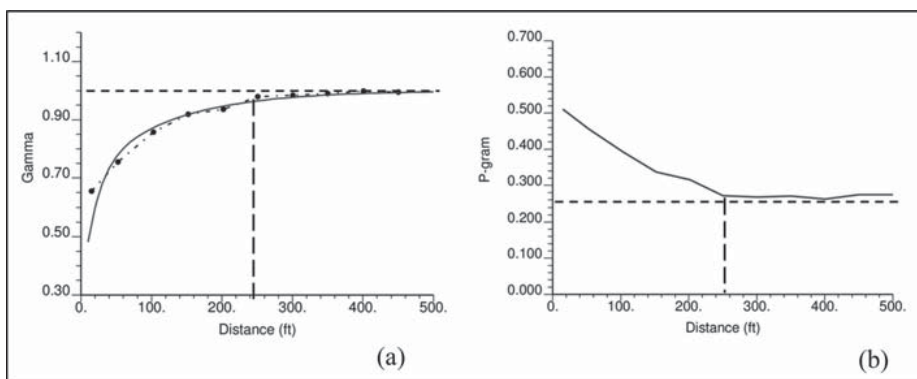
Figure 1. Indicator variogram and p-gram in one of the major domains of the deposit: (a) Experimental and modelled indicator variogram; (b) Experimental p-gram.

the data are paired over a series of lag distances. In an indicator variogram half of the average of the squared differences between the "head" end and the "tail" end of the pair are calculated. For a p-gram, only those pairs for which the tail is in ore, i.e. with an indicator one, are considered. For each p-gram lag the proportion of pairs, with head and tail equal to one, i.e., that start and finish in ore is determined. The higher the proportion, the greater continuity of the high grade assays. The results, when plotted against the lag distance, represent the average probability that two samples separated by a particular lag distance will both be above the cut-off. The plotted curve can be considered similar to a traditional correlogram in that it has a nugget, sill and range. The range is the lag distance at which the curve levels off at the sill.

Figure 1(b) shows the continuity of assay grades above a threshold identical to the one used in the indicated variogram. The range of the continuity can be indicated up to a distance where plotted curve roughly levels off at 250 ft. In this specific example, the range is almost identical to the range defined from the indicated variogram. Therefore the confirmed drill hole spacing needed for an Indicated category assignment is 160 ft. In both instances, the authors have found that an omnidirectional calculation of either the indicator variogram or p-gram yields generally stable results and affords the ability to define a reasonable drill hole spacing for this purpose. This approach should be modified in cases of strong structural controls, such as faults, or strong anisotropy. Unlike the example shown herein, the results are usually not identical; however, experience over a range of projects has shown that the two metrics do tend to give similar drill hole spacings to define an Indicated category. Further, the p-gram measure may be perceived more favourably because it focuses solely on the grade continuity within the economic portion of the domain (as defined by the threshold applied).

3 LOCAL ASSESSMENT OF DRILL HOLE SPACING

Unlike the general approaches using indicator variograms or the p-gram, the methods under this category try to account for the local grade variability within reasonably large panels or production periods. Confidence intervals and the uncertainty of grades within these large panels form the basis for assignment to an Indicated category. Two approaches to calculating the local confidence interval will be discussed here: (1) a kriging-based approach adjusted for local data, and (2) a modified simulation approach that uses the local simulated statistics.

3.1 *Kriging based assessment*

To the authors knowledge, the main geostatistical tool discussed here originated from studies developed by Harry Parker, though others have used similar approaches based on confidence intervals (Dohm, 2004; Wawruch and Betzhold, 2004, Arik, 2002). The main procedure can be designed as follows:

1. Estimate metal grade in large panels representing monthly or quarterly production. Only data located in or very close to the panels are used to estimate the grade of the panels by kriging.
2. Calculate uncertainty on the estimated panel grade. As shown in formula (1) the uncertainty is calculated from kriging variance (*OKVar*), declustered variance of the data used for the estimation (*VarDat*), and the estimated grade (*EstGr*).

The kriging variance is based on a variogram model standardized to sill of 1.0. To calculate the uncertainty on the estimated panel grade the kriging variance is adjusted for local variability by a squared coefficient of variation (*VarDat/EstGr²*). If a panel represents monthly production, uncertainty on the estimated panels within one year period can be calculated as follows:

$$VarKr = \left(OKVar * \frac{VarDat}{EstGr^2} \right) \Big/ 12 \tag{1}$$

Here, it is assumed that during a period of one year 12 panels of similar grade would be mined, and that that there is independence between the panels. Checking the independence between the panels is critical in this model. Considering that the indicator variogram model presented in Figure 1 shows the first range of continuity of 60 ft, which is much less than the panel size of 560 ft, and considering that drill hole spacing is around 100–150 ft the assumption of independence in this case is acceptable (Murphy et al., 2004). Suggested confidence limits often used for Indicated category represent a 90% chance that the true average grade is within ±10% to ±15% for annual production. Considering that a distribution of estimated grades from large panels can be approximated to a normal distribution, classical confidence limits can be derived from the formula:

$$Relative\ 90\%\ confidence\ limit = \pm\ 1.645 \times \sqrt{VarKr} < 15\% \tag{2}$$

Figure 2 (a) shows a bench in an open pit with Indicated category blocks originally assigned from drill hole spacing. The smaller grey blocks clustered around drill holes reflect the blocks classified as Indicated by applying fields populated in the 3D block model during estimation. The blocks were assigned to the Indicated category if two drill holes were found within the range of the modelled variogram or if a single drill hole was found within 75% of the variogram range. Figure 2(b) shows monthly production panels assigned either to the Indicated or to the Inferred category based on the local variability procedure described above. Results using the monthly production panels show some areas are neither classified as Indicated nor Inferred, despite the presence of drillholes (e.g. bottom left corner near block B). In this example, some areas informed by drillholes may have been excluded for a number of reasons such as less than 50 percent of the panel was below topography and/or overburden, or a substantial portion of the panel is located outside of the pit area.

A comparison of the typical classification assignment (small blocks in Figure 2(a)) to the superimposed panels from Figure 2(b) shows that while some block and categories are very similar, there are other areas that are different. For example, panel A was assigned to the Indicated category although only a small portion of that panel would be assigned to that category based on drill hole spacing alone [Figure 2(a)]. The opposite case is for panel B which has been assigned to the Inferred category although based on drill hole spacing the block would be largely assigned to the Indicated category. These differences are related to grade variability within the panels, and their corresponding impact on drill hole spacing.

To assess adequate drill hole spacing and proceed with additional drilling, panels assigned to an Indicated category can be grouped into low and high grade variability panels. In the low grade variability panels, drill hole spacing is typically larger while in the high variability panels drill hole spacing is typically smaller. The grade variability can be derived from declustered variance of the data used for panel estimation. Kriging weights can be used to calculate the declustered variance of the data v_i as presented in the following formula:
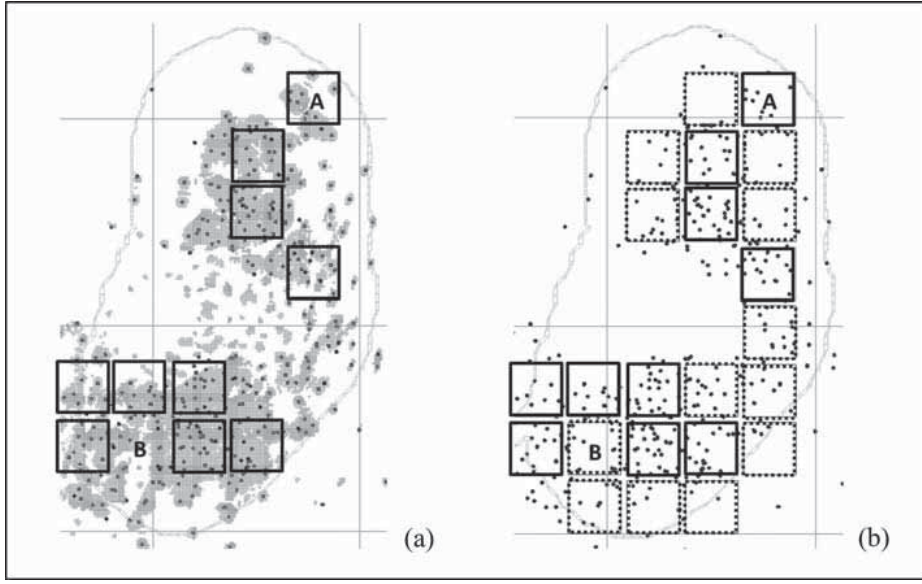
Figure 2. Indicated and Inferred categories on an open pit bench: (a) Indicated category blocks from a drill hole spacing criteria applied to the block model and panels assigned to an Indicated category from local variability assessment; (b) all panels assigned to Inferred (dashed line) and Indicated (thick line) categories from local variability assessment.

$$VarDat = \frac{\sum_{i=1}^{n} krwt_i * (v_i - \mu)^2}{\sum_{i=1}^{n} krwt_i} \qquad (3)$$

where $krwt_i$ represents the accumulated kriging weight for sample i.

Based on a number of drill holes in those panels, average drill hole spacing can be calculated in both the high and the low grade variability panels. This drill hole spacing can be applied for necessary infill drilling in panels assigned to an Inferred category.

3.2 Local statistics from simulation

The second approach to access local statistics for risk assessment is to use conditional simulation (Isaaks, 1990; Journel, 1993; Goovaerts, 1997; Chilès and Delfiner, 1999; Deutsch, 2002; Murphy et al, 2004). While simulation is preferred, from the standpoint of quantifying both local and global uncertainty, it is somewhat more complicated and time consuming than the conventional kriging approach. Some commercial software packages provide options for simulating point grades. Sequential Gaussian simulation methodology is the most popular for this type of work, though Turning Bands is also a practical option depending on the commercial platform. In essence, points are simulated and these simulated points can be averaged in a block or a panel resulting in simulated block or panel grades. Instead of having just one block model with estimated panel grades as in the kriging approach above, multiple (e.g. 100) equally likely panel models (realizations) can be designed that honour drill hole data, assay variability, and the spatial continuity of the grades.

Monthly production panel simulated grade values can be derived from each realization. This results in a full distribution of potential average grades in each panel (Figure 3). This time, instead of relying on kriging variance and data variance as given in formula (1), the uncertainty on the estimate can be directly derived from the conditional mean and standard deviation of the simulated panel grades.

The relative 90% confidence limit can be calculated as in formula (2):

$$\sigma_r = \frac{Panel\ Standard\ Deviation}{Panel\ Mean} \times 100\%$$

$$Relative\ 90\%\ confidence\ limit = \pm \frac{1.645 \times \sigma_r}{\sqrt{12}} < 15\%$$

As in the kriging-based approach, this still assumes an underlying normal distribution for an annual production of 12 months with similar grade distributions. The simplicity of this approach is that it avoids the construction of a large scale model to assess multiple periods of annual production in order to make confidence interval statements relevant for an Indicated category assignment. The assumption of normality permits assignment of the monthly panel to an Indicated category assuming independence between 12 monthly panels of similar distributions.
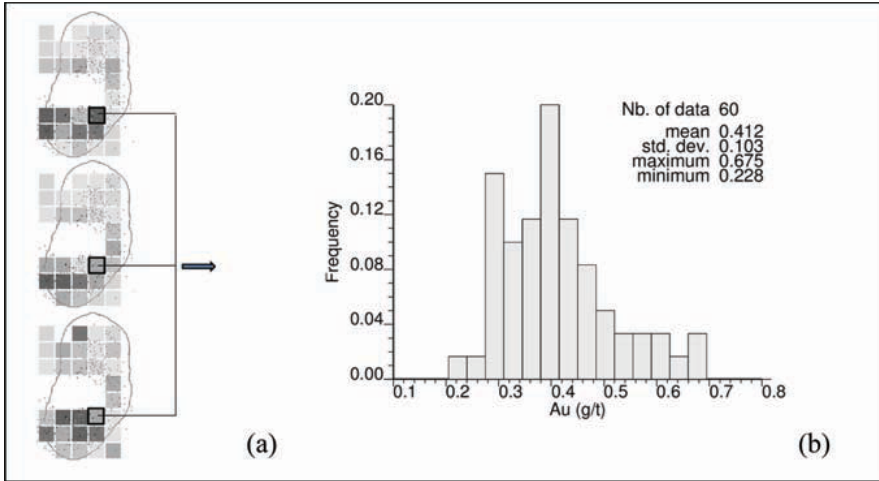
Figure 3. (a) Simulated panel grades in three realizations; (b) Distribution of the simulated panel grades in one panel with its conditional mean and standard deviation.
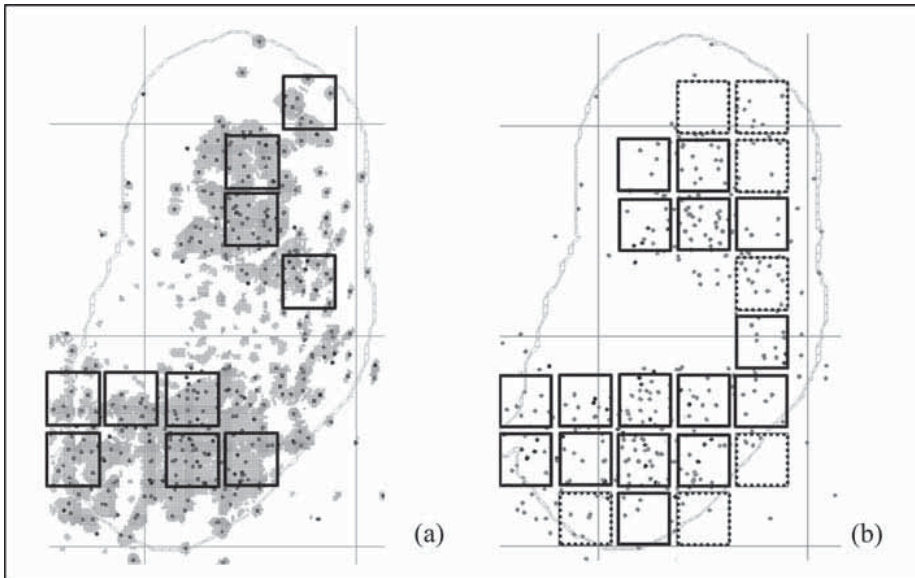
Figure 4. Indicated and Inferred category on an open pit bench within the pit area: (a) Indicated category blocks and panels; (b) panel categories based on simulation: Inferred (dashed line) and Indicated (thick line).

Figure 4 shows the comparison of the Indicated category panels from the kriging based approach (Figure 4a, reproduced from Figure 3a) and the simulation approach (Figure 4b). Overall, more panels are assigned to the Indicated category than defined from either the drill hole spacing or from the kriging approach. This result indicates that, in this case study, the assignment to the Indicated category from drill hole spacing was conservative, in the sense that it would not be necessary for additional in-fill drilling in the center of the deposit. More specifically, the simulation approach resulted in 20% increase of the volume assigned to the Indicated category.

4 PRECISE ALLOCATION OF ADDITIONAL DRILL HOLES

With progressively more localized assessments of drill hole spacing requirements comes the ability to extend the simulation approach to further the planning of the next drill campaign. Specifically, the simulation methodology provides a much more precise assessment of necessary infill drilling, with a suggested location of the infill drill holes, for upgrading from Inferred to Indicated category. This is an important question at the forefront of most drill campaigns as a mining exploration project advances from pre-feasibility to feasibility and development.

The procedure, albeit quite straightforward, requires a few more steps than described in the previous section:

1. Construct a reference model in a studied domain. This can be done using sequential Gaussian simulation. The model is a representative realization with similar statistics to actual drill hole data in the domain.
2. Simulate the drilling of the deposit, by sampling from the reference model. The sampling is chosen at locations with sparse drilling and within panels allocated to the Inferred category.
3. Re-simulate the grades with the additional "holes" and average the simulated grades within the panels.
4. For each panel calculate the relative 90% confidence limit from the distribution of the re-simulated panel grades.
5. If the relative confidence limit is lower than 15% the panel is assigned to the Indicated category.
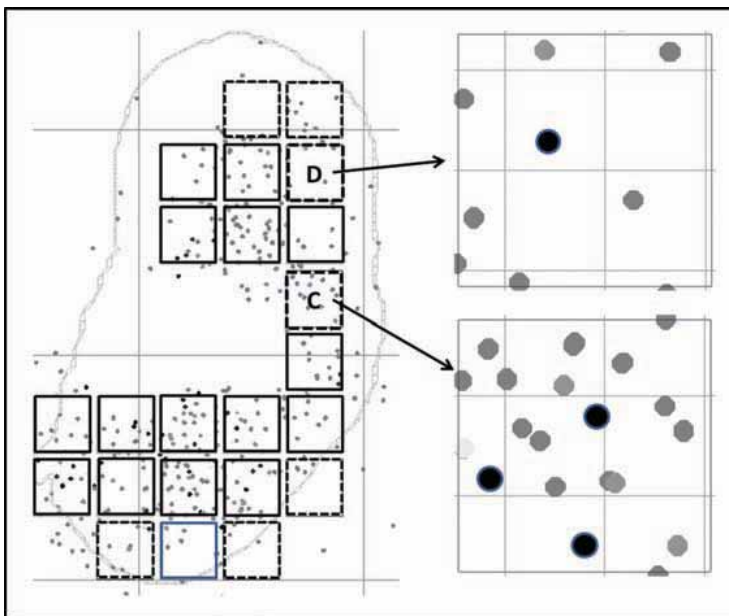
Figure 5.   Two panels with additional "drill holes" shown as black circles and re-assigned to an Indicated category.
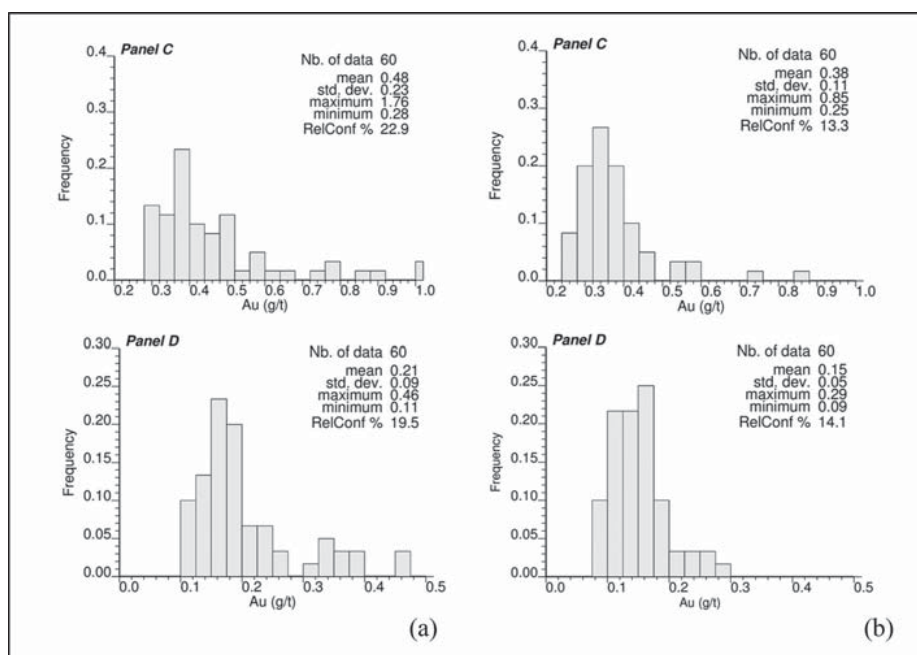
Figure 6. Distributions of simulated panel grades: (a) from current drilling; (b) from additional drilling. Panels with the additional drilling have been re-assigned to an Indicated category.

Figure 5 shows two panels on the bench that have been assigned to an Inferred category. Both panels have been sampled with additional "holes". In panel C it was necessary to drill three additional "holes" and in panel D only one "hole" to re-assign the panels into an Indicated category. Figure 6 shows the distributions of the panel means before and after additional "holes". Notably, in Figure 6(a) the distributions steer away from an assumption of normality that was applied when calculating relative confidence limits. With additional drilling long tails in the distributions are less evident and there is a large drop in a coefficient of variation.

5 DISCUSSION

A typical allocation of resources to an Indicated category is often based on density of drilling and on ranges of metal continuity defined from variograms. Variogram models do not take into account local statistical characteristics of grades. The variogram models at best define an average continuity in a studied domain and at worst may improperly define the continuity in more challenging structural settings.

Most notably, changes in local variability of grades contribute to improper assessment of drill hole spacing for an assignment to an Indicated category. Simulating grades for resource categorization represents the best attempt to steer away from very general and often subjective approach and focus on statistical characteristics often overlooked when using simple tools such as indicator variograms.

Estimating confidence limits for a mean of a panel grade can be calculated using normal distribution theory. Normality checks can be made by a comparison of 5th and 95th theoretical percentiles to the same percentiles from the simulation. It is possible for the panel grades to deviate from normality, as was actually shown in Figure 6. If simulated panels represent the volume mined in one year production periods, the confidence limits would not have to be based on the normal distribution theory. It would be sufficient to calculate a proportion of panel averages that fell within ±15 percent, and calculate the confidence limits directly.

Often overlooked local variability of metal grades, when allocating blocks to resource categories, can potentially be used as an additional criterion for an assignment to an Indicated category. A resource geologist could simply calculate coefficients of variations of grades in large panels and link them to blocks located in those panels. Blocks originally assigned to an Inferred category and located in low grade variability areas may be re-assigned to an Indicated category. On the other hand, blocks located in the high grade variability environment can be considered for re-assignment to an Inferred category.

There are more advanced approaches than those presented here. For example, Pinto (2015, 2016) considered the calculation of confidence intervals of the panel as a moving window formulation, thereby allowing for smoother boundaries between classification categories. Silva et al. (2018) presented a framework to place additional drill holes subject to physical constraints (location, drilling angles, depth limitations) and budget considerations. These approaches, while more advanced and sophisticated, have yet to become common practice in the mining industry. They also require a degree of comfort with advanced geostatistics and the development of prototype software for implementation, that a general practitioner in the mining industry may find them to be inaccessible at this time.

6   CONCLUSIONS

In general, drill hole spacing is most often used by resource geologists for an assignment of resources to categories. The categories are rarely based on more than drill hole spacing and ranges of continuities defined from variogram models. Potential commercial development of a deposit relies on consecutive drill campaigns that focus on resources assigned to an Inferred category. Application of the approaches discussed in this paper could lead to substantial savings, with the potential to reduce the number of holes drilled.

The geostatistical tools discussed here are an improvement on a typical approach applied by resource geologists, because they take into account the local data variability. A seasoned resource geologist instinctively knows that in areas with lower grade variability drill hole spacing can be wider than in higher grade variability for an assignment to an Indicated category. Simulating grades in large panels and translating those results to yearly production may result in larger areas assigned to an Indicated category than on drill hole spacing alone.

REFERENCES

Arik, A., Comparison of resource classification methodologies with a new approach, APCOM 2002: 30th International Symposium on the Application of Computers and Operations Research in the Mineral Industry Phoenix, Arizona, 2002, pp. 57–64.

Chilès, J.P., and Delfiner, P., Geostatistics: Modeling Spatial Uncertainty, John Wiley & Sons, New York, 1999.

Deutsch, C.V., Geostatistical Reservoir Modeling, Oxford University Press, New York, 2002.

Dohm, C., "Quantifiable Mineral Resource Classification: A Logical Approach", in O. Leuangthong and C. Deutsch, eds., Geostatistics Banff 2004, vol. 1, Springer Science+Business Media, pp. 333–342.

Goovaerts, P., Geostatistics for Natural Resources Evaluation, Oxford University Press, New York, 1997.

Isaaks, E.H., The Application of Monte Carlo Methods to the Analysis of Spatially Correlated Data, PhD Thesis, Stanford University, Stanford, CA, 1990.

Journel, A.G., Recoverable reserves estimation—the geostatistical approach, Mining Engineering, 1985, Vol. 37 (6), pp. 563–568.

Journel, A.G., Nonparametric-estimation of spatial distributions, Journal of International Association for Mathematical Geology, 1983, Vol. 15 (3), pp. 445–468.

Journel, A.G., Modeling Uncertainty: Some Conceptual Thoughts, Geostatistics For the Next Century, Kluwer Academic Publications, 1993, p. 30–43.

Leuangthong, O. and Nowak, M., Dealing with high-grade data in resource estimation, SAIMM Journal, January 2015, Vol. 115, pp. 27–36.

Murphy, M., Parker, H., Ross, A., and Audet, M.A., "Ore-Thickness and Nickel Grade Resource Confidence at the Koniambo Nickel Laterite (A Conditional Simulation Voyage of Discovery)", in O. Leuangthong and C. Deutsch, eds., Geostatistics Banff 2004, vol. 1, Springer Science+Business Media, pp. 469–478.

Pinto, F.A.C., Guide to data spacing and uncertainty, CCG Guidebook Series, Vol. 19, University of Alberta, 2015, 62 p.

Pinto, F.A.C., Advances in Data Spacing and Uncertainty, M.Sc. Thesis, Civil and Environmental Engineering, University of Alberta, 2016, 177 p.

Silva, D.S., Jewbali, A., Boisvert, J.B. and Deutsch, C.V., Drillhole placement subject to constraints for improved resource classification, 2018, CIM Journal, Vol. 9 (1), pp. 21–32.

Srivastava, R.M., personal communication regarding P-Gram statistic, 2004.

Wawruch, T. and Betzhold, J.F., "Mineral Resource Classification Through Conditional Simulation", in O. Leuangthong and C. Deutsch, eds., Geostatistics Banff 2004, vol. 1, Springer Science+Business Media, pp. 479–490.

Geostatistical simulation with heterotopic soft data without the LMC

C.P. Araújo, M.A.A. Bassani & J.F.C.L. Costa

PPGE3M-Post-Graduation Program in Mining, Metallurgical and Materials Engineering,
Federal University of Rio Grande do Sul, Porto Alegre, Rio Grande do Sul, Brazil

ABSTRACT: To integrate the multiple variables, traditional methodologies suggest modelling the cross variograms and co-simulation using the Linear Model of Coregionalization (LMC), that is difficult task. This framework combines two approaches: Bayesian Updating and Sequential Gaussian Simulation considering all information regarding the relationship of the multiple variables without modelling the LMC. Firstly, at each soft data location, hard and soft data were incorporated using Bayesian Updating, which considers multivariate correlations between variables, to build a conditional distribution. Secondly, n-possible values are drawn from these conditional distributions and imputed as hard data. Next, Sequential Gaussian Simulation was performed to complete all the grid nodes using the original and previously simulated hard data. The simulated models were compared with the models obtained by Sequential Gaussian Simulation (SGS) using only the original hard data. The results show the soft data addition improve the accuracy of the models once an appropriate methodology is used to incorporate them.

Keywords: complete heterotopic, bayesian updating, soft data, linear model of coregionalization, simulation

1   INTRODUCTION

In the mining industry, it is common to have samples obtained from different drilling campaigns, sources and periods of time, implying different quality and quantity of these samples. During the exploration stage, the samples are limited and sparse, but have high quality. These samples are usually obtained with diamond drill holes (DDH). These samples are called hard data. Throughout the production stage, mitigating the uncertainty of a geological attribute comprises the reduction distances between samples. These samples have larger sampling errors and are called soft data.

An important type of soft data has gained popularity recently. These data are obtained with sensors, such as Portable X-ray fluorescence. These data contain noise, but are numerous and fast to obtain. Neves et al. (2018) integrated these data to update grade models using direct sequential simulations with point distributions (DSS). They considered the sensor data as a histogram of possible values (called point distribution) including their uncertainty. The point distribution was obtained with a calibration between the sensor and hard data. This calibration requires that a subset of the dataset is isotopic (the hard and soft data are sampled at the same locations), which is the main limitation of the method. In this paper, we are interested in datasets that are completely heterotopic (there is no soft datum sampled at the same location of a hard datum).

To integrate the multiple variables with spatial correlation, traditional methodologies suggest modeling the direct and cross variograms using the linear model of coregionalization (LMC) to assign weights to correlated values in cokriging. The problem is that the LMC is difficult to model when more than two variables are considered.

Some simplifications of the LMC were proposed in the literature. Almeida and Journel (1994) suggested a Markov Model of coregionalization for modeling the cross-covariances. In the Markov Model, the cross variogram model is either proportional to the variogram of the primary variable (MM1) or the secondary variable (MM2). These Markov Models are usually used with collocated cokriging, which uses only the collocated secondary datum for estimation. The problem with collocated cokriging is that the variance is inflated (Deutsch and Journel, 1998). To avoid variance inflation, Babak and Deutsch (2009) proposed to use the secondary data at the location being estimated and at the locations of the primary data. This approach is denoted as intrinsic collocated cokriging (ICCK). The limitation of collocated and intrinsic collocated cokriging is that the secondary data must be sampled at all the nodes of the grid. We are interested in situations where the secondary data is more sampled than the primary data, but it does not cover the entire grid. One alternative is to perform the simulation hierarchically (Almeida and Journel, 1994). In this case, the secondary is simulated first and used as secondary information with ICCK in the simulation of the primary variable. However, this approach demands more computer memory and processing time than simulating directly the primary variable.

In situations where the secondary data are more sampled than the primary, multiple imputation (MI) techniques are available and consist of simulating first at the locations of the secondary and second at the nodes of the simulation grid (Barnett and Deutsch, 2015; Soares et al, 2017; Silva e Deutsch, 2018). Barnett and Deutsch (2015) proposed two multiple imputation methodologies: parametric and non-parametric to impute missing geological data based on Bayesian updating to generated isotopic datasets. The parametric method assumes that the joint distribution is multivariate Gaussian while the non-parametric calculates the joint distribution from the scatter plots. Similarly, the methods used by Soares et al. (2017) and Silva and Deutsch (2018) used the scatter plots to obtain the joint distribution. The problem is that building a scatter plot requires a subset where the primary and secondary data are isotopic. As a result, these methods are not applicable when the data set is completely heterotopic. In this context, the parametric approach proposed by Barnett and Deutsch (2015) was used.

The parametric approach (Barnett and Deutsch, 2015) requires the coefficient of correlation between the primary and secondary variable. When these variables are completely heterotopic, the coefficient of correlation may be obtained by extrapolating the experimental cross correlogram (Minnitt and Deutsch, 2014) to the zero distance. In this paper, we combine the approach of Minnitt and Deutsch (2014) to obtain the coefficient of correlation with the parametric multiple imputation method of Barnett and Deutsch (2015). The parametric method presented by Barnett and Deutsch (2015) uses Bayesian Updating to account for the secondary data. Bayesian Updating is a form of collocated cokriging (Doyen, 1996; Deutsch and Zanon, 2004; Ren, 2007) and does not require the LMC, only the coefficient of correlation between the primary and secondary variable. We assume that obtaining the coefficient of correlation is easier than modeling the LMC.

As data sources do not have the same quality and are totally heterotopic and spatially correlated, it is difficult to establish the correlation between these data types. Minnitt and Deutsch (2014) suggested to infer their statistical relationships using the experimental cross-correlogram values extrapolated so the correlation coefficient at zero lag can be obtained.

This work proposes a framework to simulate hard and soft data considering all information regarding the relationship of the multiple variables without modelling the LMC (linear model coregionalization). This framework combines two approaches: Bayesian Updating and Sequential Gaussian Simulation. The simulated models were compared with the models obtained by Sequential Gaussian Simulation (SGS) using only the original hard data. To illustrate the methodology, we used a modified version of the Walker lake dataset (Isaaks and Srivastava, 1989).

2   METHODOLOGY

This framework combines two approaches: Bayesian Updating (BU) and Sequential Gaussian Simulation (SGS). Firstly, at each soft data location, the hard data values are

simulated both the hard and soft data as conditioning information through Bayesian Updating. Details of this methodology are found in Barnett and Deutsch (2015). The result is a set equally probable datasets where the primary variable is available at their original locations and at the locations of the secondary. These datasets are used to condition the realizations of the grid nodes. Each dataset conditions one realization (this framework is called Multiple Imputation by Barnett and Deutsch, 2015). Next, Sequential Gaussian Simulation was performed to complete all the grid nodes using the datasets simulated previously. To perform the proposed workflow the steps needed are the following:

Step 1: Normal score Transform: The Bayesian Updating and Sequential Gaussian Simulation assume that the data are standard multivariate Gaussian. The normal score transforms the data that so that the transformed data are univariate Gaussian.

Step 2: Inference of coefficients of correlation: The relationship between the variables is considered linear and characterized by correlation coefficients. To infer the correlation between the variables, we extrapolated the experimental cross-correlogram to obtain the correlation coefficient at zero lag. In this case study, the correlation coefficients obtained resulted in a positive definite correlation matrix. However, this methodology does not guarantee the positive definiteness of the correlation matrix and some correction may be required. A method for correcting a non-positive definite matrix is found in Kumar and Deutsch (2009).

Step 3: Simulate n values at each soft datum location (unsampled hard data location) from the conditional distributions obtained by Bayesian Updating. The conditional distributions are called posterior distributions and are the result of merging the prior and likelihood distributions. The prior distributions are Gaussian and parameterized by the simple kriging mean and variance of the hard data (original and previously simulated). The likelihood distribution uses the collocated secondary data and is parametrized by the estimate and variance obtained by linear least squares regression. The hard data value is sampled from the posterior distribution, which integrates information from both the primary (through the prior distribution) and secondary data (through the likelihood).

Step 4: Sequential Gaussian Simulations: used to perform stochastic sequential simulations using two types of the hard data and n values inferred by Bayesian updating.

Step 5: Normal score back transform the Gaussian realizations to the original units.

3 RESULTS

3.1 *Case study*

The dataset mimicks the sampling configuration proposed by Neves et al. (2018) in the framework of Real-time mining concept (Osterholt and Benndorf, 2015). A synthetic 2D data-set was created to mimicking a copper mine. The key idea is to use all information available sampled by different techniques. The variable of interest (primary) is Copper grade (Cu_DDH) and the secondary variables are Copper (Cu_Chip) collecting face chip samples and Copper (Cu_XRF) obtained by Portable X-ray fluorescence. The samples are comprised by: hard data (Cu_DDH) and soft data (Cu_Chip and Cu_XRF) are totally heterotopic but soft data are collected in the same location (totally isotopic). The primary variable data was sampling by 20×20 meters and secondary variables 5×5 meters. Figure 1 shows the locations maps of the variables.

Table 1 shows the statistics for the three variables which will be combined to build the grade models: primary variable (Cu_DDH), considered precise and accurate but sparse and scarce, considered as hard data. The secondary variable are collected face chip samples (Cu_Chip) and are imprecise and inaccurate. The las copper values were measurement sampled by portable X-ray fluorescence (Cu_XRF), fast and abundant monitoring of system to derive ore grades as soft data.

Figure 2 shows the univariate gaussian histogram of the primary (Fig. 2a) and secondary variables (Fig. 2b and Fig. 2c) obtained by the normal transformation required to perform
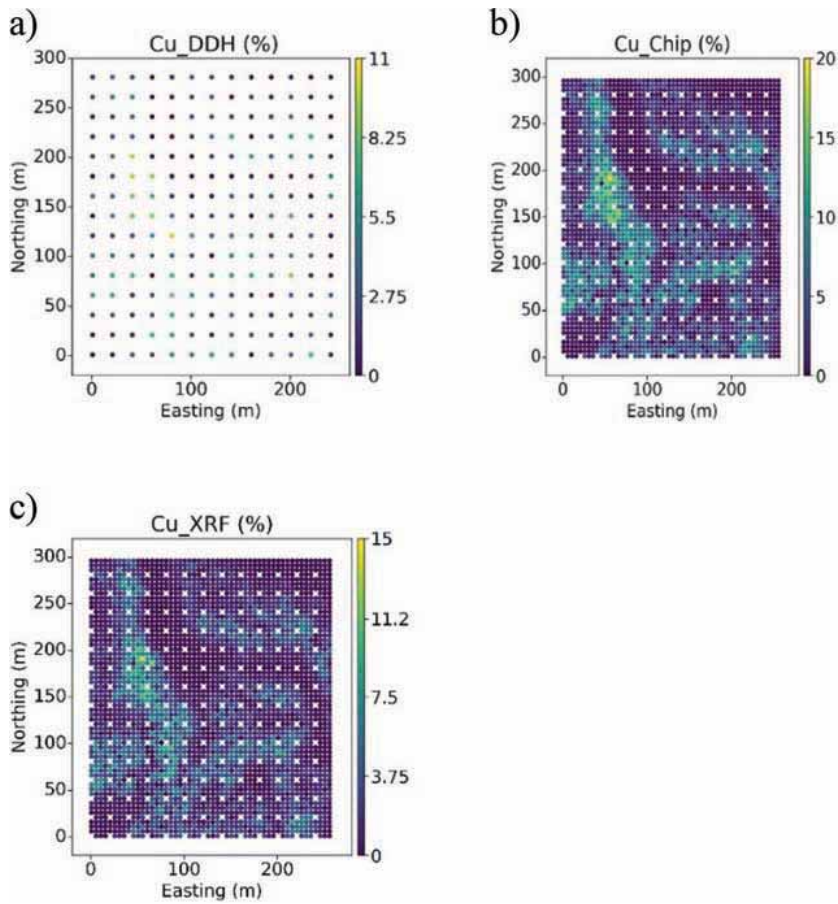
Figure 1.   Location map (a) primary variable, (b) and (c) secondary variables.

Table 1.   Statistics for the available data.

Dataset	Cu (%) (Primary variable) good quality, sparse data, limited borehole data	Cu_Chip (%) (Secondary variable) poor quality, abundant data, RC or channels/chip samples	Cu_XRF (%) (Secondary variable) poor quality, abundant and fast acquisition data, FRX measurements
Sampling spacing	20×20 m	5×5 m	5×5 m
Number of samples	195	2925	2925
Mean	2.73	3.46	2.06
CV	0.89	0.92	0.96
Variance	5.90	10.17	3.92
Standard Deviation	2.43	3.19	1.98
Min.	0.00	0.00	0.00
Max.	10.13	19.61	14.81

the Bayesian Updating and Sequential Gaussian Simulation. The results show the data after transformation are normally distributed (zero mean, unit variance).

Figure 3 shows the correlation of the all variables calculated by cross-correlograms. When it was compared the primary data (Cu_DDH) against soft (Cu_Chip), the correlation is
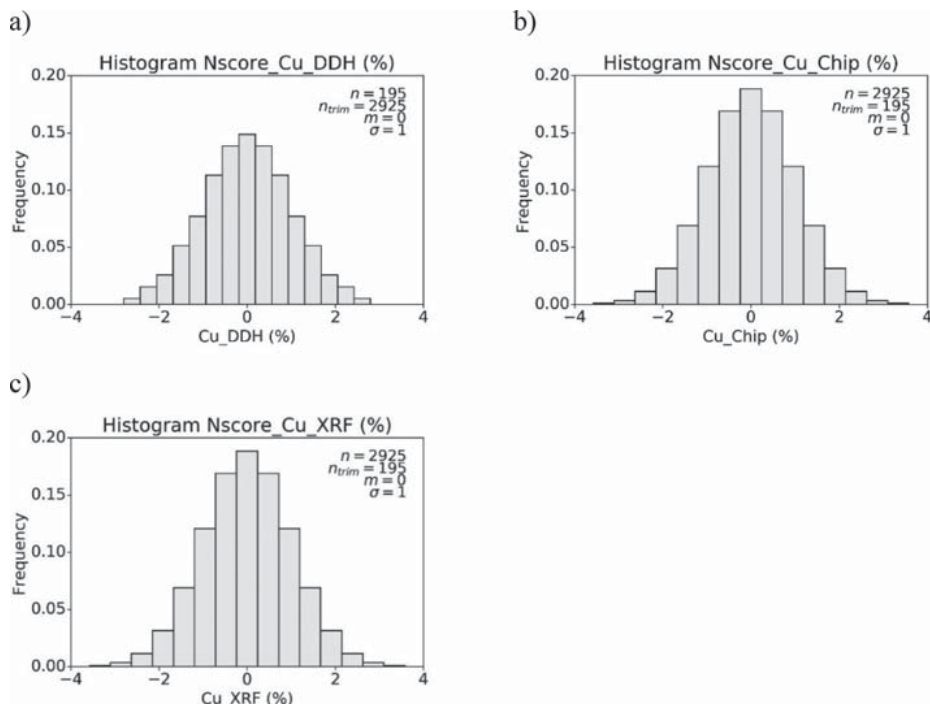
Figure 2.   Histogram Nscore unit of variables a) Primary variable (Cu_DDH), b) Secondary variable (Cu_Chip) and c) Secondary variable (Cu_XRF).
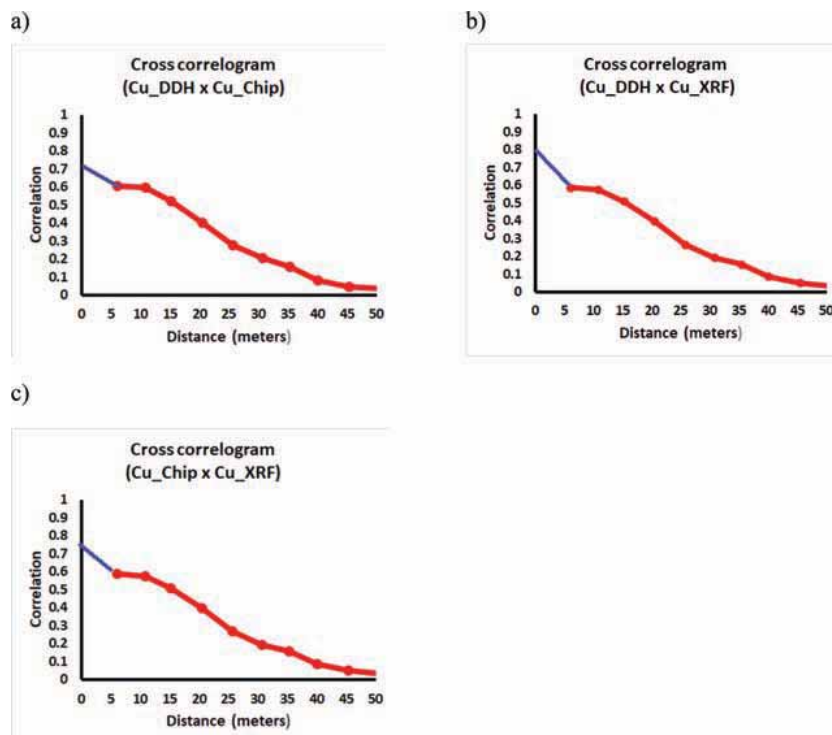
Figure 3.   Cross-correlogram between hard and soft data, correlation fit (red line) and extrapolation (blue line) a) Cu_DDH × Cu_Chip, b) Cu_DDH × Cu_XRF and c) Cu_Chip × Cu_XRF.

approximately 0.75 (blue line), hard data (Cu_DDH) with soft data (Cu_Chip) is close to 0.80 (red line), soft data (Cu_Chip), with data (Cu_XRF) is near to 0.75 (black line). In general, the variables have a moderate correlation. It indicates the soft and uncertain data can improve the models obtained by stochastic simulation.

The variogram model was fitted to the experimental variogram of the normal score of the primary variable. Equation 1 defines the variogram model of the primary variable (normal score):

$$\gamma_{Cu}(h) = 0.10 + 0.90 \cdot \text{Sph}(1) \cdot \left(\frac{157.5}{66\,\text{m}}, \frac{67.5}{40\,\text{m}} \right) \tag{1}$$

3.2 *Validations*

To validate the simulated datasets obtained with Bayesian Updating, their spatial covariance and histogram were compared with the histogram and variogram of the original data. These simulated values are at the locations where the secondary data had been sampled. Figure 4 shows the experimental variograms along the major and minor directions, where the red line represents the variogram model (Eq. 1) and the black lines represent the experimental variograms of the data simulated by Bayesian Updating. The models are similar; meaning the inferred data have the same spatial continuity of the hard data.

Figure 5 compares the histogram of original (red line) and simulated (by Bayesian updating) data (black lines). The simulated values reproduced the histogram of the original data.
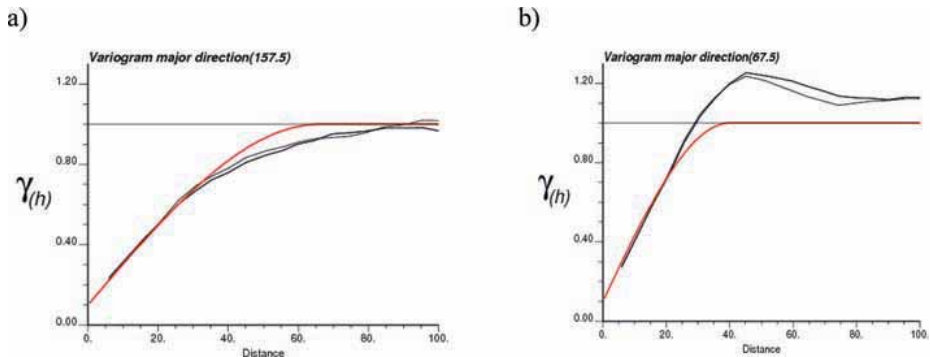
Figure 4. Experimental (black line) data inferred by Bayesian Updating and modeled variograms of the hard data (red line) a) Major direction, b) Minor direction.
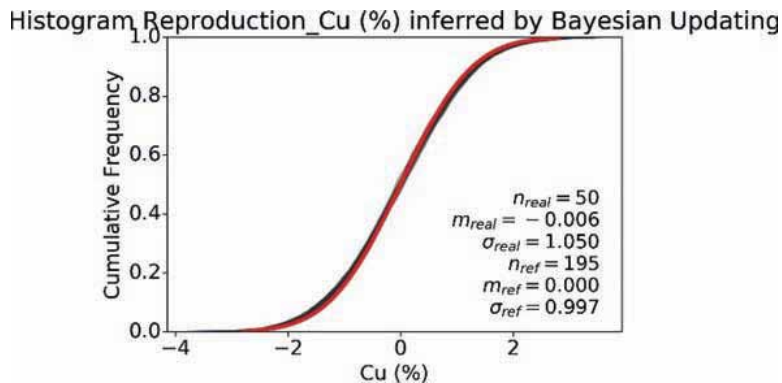
Figure 5. Histogram reproduction hard data (red line) and Bayesian Updating data (black lines).

The simulated datasets were used as conditioning information to simulate the entire grid using Sequential Gaussian Simulation. This methodology was compared against realizations that used only the original hard data to condition the simulations. Figures 6a-b compare the histogram reproduction of the simulations using only the original data, and using the simulated datasets with Bayesian Updating, respectively. The histograms of the realizations that considered both original and simulated values have lower spread. The result indicates that the integration of secondary data through Bayesian Updating reduced the global uncertainty.

Figure 7 compares the variogram reproduction of the final models obtained by Sequential Gaussian Simulation using only hard data (Fig. 7a) and Bayesian updating data with Sequential
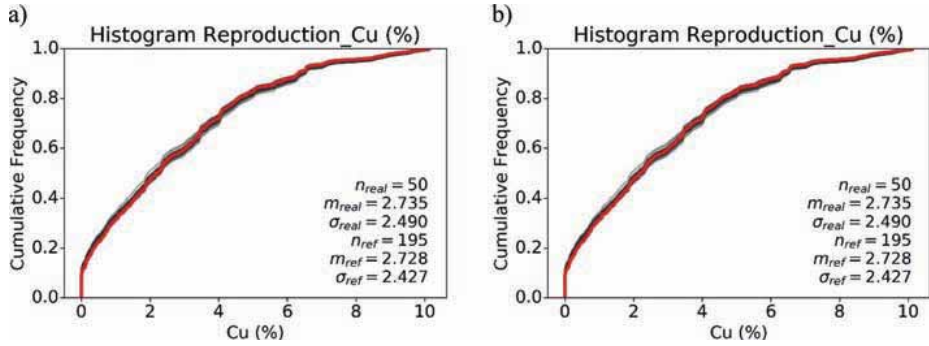
Figure 6. Histogram reproduction hard data (red line) and realizations (black line) a) Sequential Gaussian Simulation only hard data and b) Bayesian updating with Sequential Gaussian simulation.
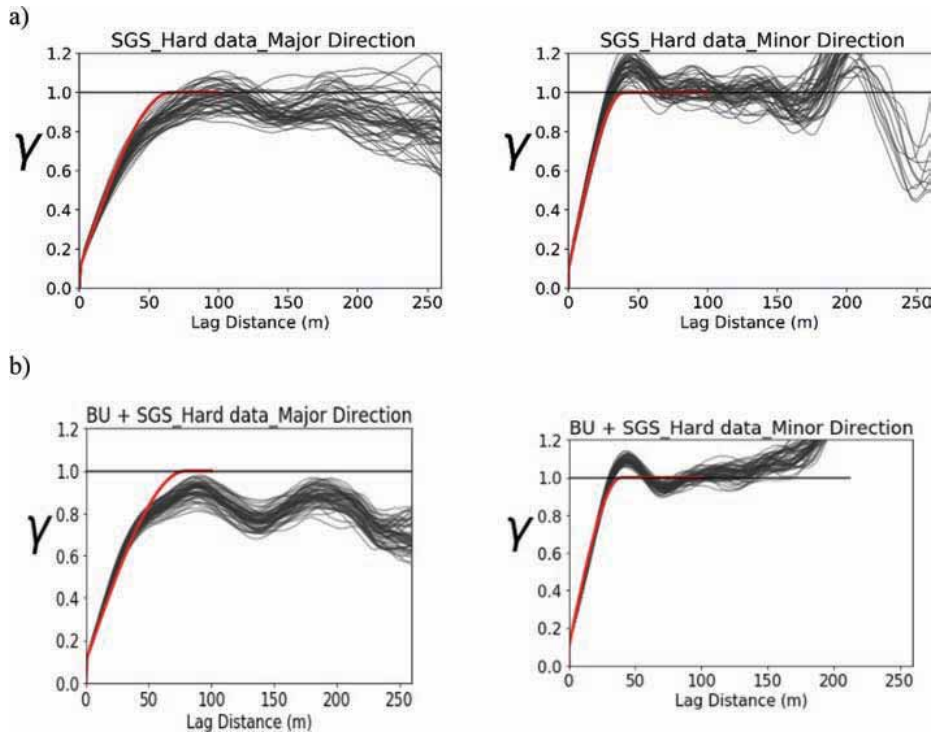
Figure 7. Experimental (black line) and modeled variograms of the hard data (red line) in the major (left side) and minor direction (right side) a) Sequential Gaussian Simulation using only hard data and b) Bayesian updating with Sequential Gaussian simulation.
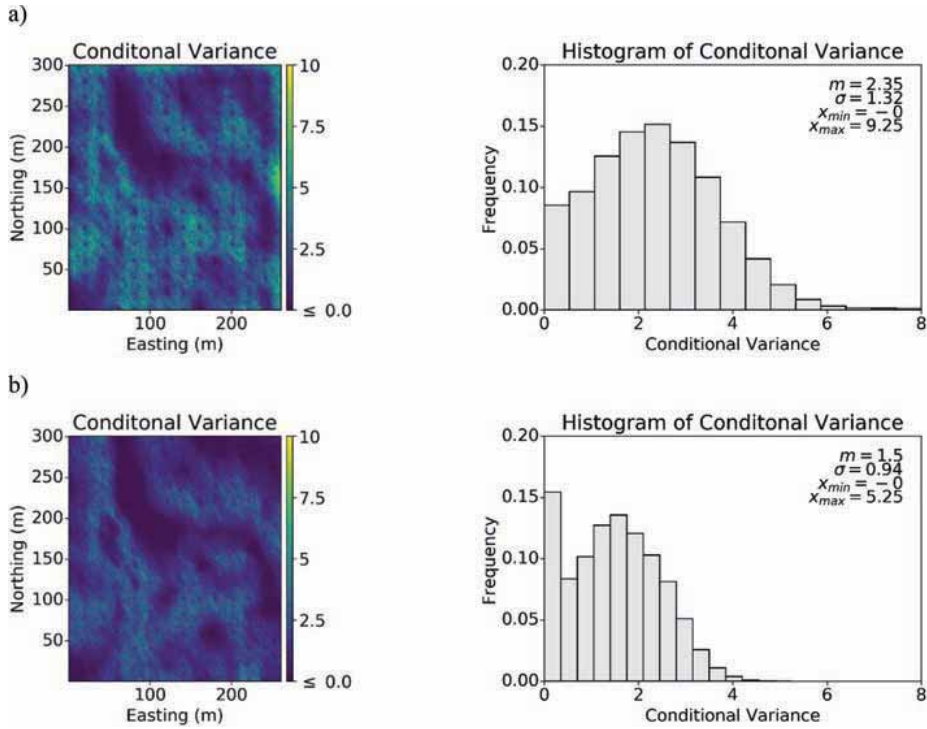
Figure 8. Conditional variance location map and histogram using a) Sequential Gaussian Simulation only hard data and b) Bayesian updating with sequential Gaussian simulation.

Gaussian Simulation (Fig. 7b) in the minor and major directions. The results showed that the spatial continuity was reproduced in both methodologies.

Figure 8 shows the location map and the histogram of the conditional variance of the models. The average conditional variance obtained using sequential Gaussian simulation only hard data are higher (Fig. 8a) compared to the model obtained via Bayesian updating with sequential Gaussian simulation (Fig. 8b). The conditional variance of the final models decreases by 31% (from 2.35 to 1.60) due to the influence of the soft data. The main reason for that is the Bayesian updating uses the information provided by the secondary data, reducing the uncertainty and improving the accuracy of the final model.

4 CONCLUSIONS

Differences in data quality are significant for the geostatistical framework adopted. This difference has to be considered to integrate the three sources of information, i.e. hard data, soft data and uncertain data. Classical approaches to integrate hard and soft data require cokriging and cosimulation algorithms based on modeling the LMC, which sometimes is a difficult task. This paper demonstrated an approach using Bayesian Updating to incorporate soft and uncertain data into stochastic simulations to integrate the samples with error (soft data) and uncertainty in the stochastic simulation process.

The results indicate that soft data may improve the models obtained via stochastic simulations. The idea to incorporating different types of data using Bayesian Updating was satisfactory. The inferred data reproduce the distribution and the spatial continuity structure of the hard data. The final models generated with additional information reproduce the statistics and spatial continuity of the hard data and the uncertainty in these models was reduced.

ACKNOWLEDGMENTS

REFERENCES

Almeida, A.S., & Journel, A.G. 1994. Joint simulation of multiple variables with a Markov-type coregionalization model. *Mathematical Geology*, *26*(5), 565–588.

Babak, O., & Deutsch, C.V. 2009. An intrinsic model of coregionalization that solves variance inflation in collocated cokriging. *Computers & geosciences*, *35*(3), 603–614.

Barnett, R.M. and Deutsch, C.V., 2015. Multivariate imputation of unequally sampled geological variables. *Mathematical Geosciences,* 47(7), pp. 791–817.

Deutsch, C.V. and Zanon, S.D., 2004, January. Direct prediction of reservoir performance with Bayesian updating under a multivariate Gaussian model. In *Canadian International Petroleum Conference*. Petroleum Society of Canada.

Doyen, P.M., Den Boer, L.D., & Pillet, W.R. 1996, January. Seismic porosity mapping in the Ekofisk field using a new form of collocated cokriging. *In SPE Annual Technical Conference and Exhibition*. Society of Petroleum Engineers.

Isaaks, E.H. 1989. The application of Monte Carlo methods to the analysis of spatially correlated data.

Kumar, A. and Deutsch, C.V. 2009. Optimal correction of indefinite correlation matrices. CCG Annual Report 11, Paper 401.

Minnitt, R.C.A., & Deutsch, C.V. 2014. Cokriging for optimal mineral resource estimates in mining operations. *Journal of the Southern African Institute of Mining and Metallurgy*, *114*(3), 189–189.

Neves, J., Pereira, M.J., Pacheco, N., & Soares, A. 2018. Updating Mining Resources with Uncertain Data. *Mathematical Geosciences*, 1–20.

Osterholt V, Benndorf J, 2015. Real-time mining process flow analysis. Published document of European Programme Horizon 2020 funded project Real-Time Mining. Published under www.realtimemining.eu on 05/11/2015.

Ren. W. 2007. Exact downscaling in reservoir modeling (PhD thesis). Edmonton (AL): University of Alberta.

Silva, D.S. and Deutsch, C.V., 2018. Multivariate data imputation using Gaussian mixture models. *Spatial statistics*, 27, pp. 74–90.

Soares, A., Nunes, R. and Azevedo, L., 2017. Integration of uncertain data in geostatistical modelling. *Mathematical Geosciences*, 49(2), pp. 253–273.

Application of localized multivariate uniform conditioning and conditional simulation for a stockwork niobium deposit

L. Bertossi
CMOC US, Phoenix, USA
Sr. Geologist Modeler, MAusIMM, Brazil

D. Raposo, J. Watanabe & S. Silva
CMOC Brasil, Ouvidor, Brazil

G. Usero
Regional Director, Geovariances, Belo Horizonte, Brazil

ABSTRACT: Linear estimation approaches as Ordinary Kriging and Simple Kriging are widely used and successfully applied to estimate mineral resources in the mining industry, although it may generate a biased estimate of metal tonnage and ore recovery after a cutoff application. The bias is more evident in narrow veins or deposits with tight mineralization that are modeled with small blocks when the data spacing is much larger than the SMU size.

Uniform Conditioning (UC) can be used as an alternative to generate unbiased estimates for the evaluation of the potential of selective mining. The Localized Uniform Conditioning (LUC) technique has been applied to enrich the UC distribution by localizing the results at the SMUs scale. A complementary workflow using Conditional Simulations is also applied in this study to access the grade fluctuations at the SMU scale.

1   INTRODUCTION

In some kinds of deposits well covered by sample with normal distribution grades, all linear estimation, including ordinary kriging, can correctly predict the grade and the tonnage, with a low conditioning bias. However, in deposits poorly sampled with a lognormal underlying grade distribution, liner estimation will provide a biased estimate of metal tonnage and it can produce smoothed assessment of the recoverable resources when applied to a small block model which is not supported by dense data spacing (Armstrong and Champigny, 1989; Ravenscroft and Armstrong, 1990; Pan, 1998).

Uniform conditioning (Rivoirard, 1994) is one of the methodologies widely used in the mining industry for modelling the recoverable resources above cut-off grades, the advantage of UC is that it can be used in a widely spaced data, across domains that are not strictly stationary, provided that there is a sufficient data for conditionally unbiased estimate of the panel mean grade (Rivoirard, 1994; Hansmann, 2016).

The drawback of the conventional Uniform Conditioning (UC) method is its inability to predict a spatial location of the economically extractable mineralization (Abazlov, 2014), in other words, UC does not estimate grades directly, it calculates the tonnage and the mean of recoverable resources distributed in a large panel. Abzalov (2006), proposed a method for modelling grades of selective mineable units (SMU) called Localized Uniform Conditioning (LUC), it enhances the UC approach by localizing the model panel results, representing a partitioning of this panel.

According to Hansmann 2016, UC and the add-on LUC has been successfully applied in several different types of deposits, indicating that the method is applicable on a normal

distribution as well as, on skew lognormal distributions, which are: 1) – porphyry copper-gold deposit in Chile and Peru (Deraisme *et al.*, 2008; Deraisme and Assibey-Bonsu, 2011; Millad and Zammit, 2014), 2) – gold deposits, Australia (Assibey-Bonsu, 1998; Humphreys, 1998), 3) – iron ore deposit, Australia (De-Vitry *et al.*, 2007) and 4) – Bauxita and Iron ore deposits, Australia (Abazlov, 2014).

Another non-linear estimation technique, Indicator Kriging and different kinds of simulations as, Sequential Gaussian Simulation and Turning Bands Simulation can produce, in general, a satisfactory recoverable resources model, however those approaches are still very time consuming.

2   MINE GEOLOGY

Niobium mineralization within the Boa Vista project is associated exclusively with nelsonite veins. These veins, comprising a magnetite-apatite-carbonate rock host the niobium mineralization in the form of pyrochlore. Nelsonite occurs as a complex stockwork of veins and stringers with variable thickness and orientation, frequently in association with carbonatite stringers and veins. The carbonatites are not well mineralized with niobium, but field relationships suggest that there are instances where nelsonite bodies appear to have fractionated from original carbonatitic magmas.

The nelsonite stringers are hosted within a variety of pre-existing lithologies including amphibolite and fenite, a metasomatically altered rock believed to originally comprise phyllite.

The geometry of the mineralized zone and the nature of the distribution of mineralized veins result in a grade distribution in space that shows strong trends. Vertically within the mineralized zone, the average Nb_2O_5 grade increases with depth, as the trumpet narrows into a more concentrated zone dominated by carbonatite and thick nelsonite dykes. The Nb_2O_5 grade also decreases radially from the central feeder zone towards the limits of the drilled volume. These trends are also consistent with the results of exploratory de-clustering statistics; the de-clustered average grade falls consistently within the increasing cell size, revealing that the higher-grade central core zone has been more densely drilled than the lower-grade peripheral zones. The presence of these trends compel the use of a grade-related domain to delimit a central mineralized zone where the niobium grades are sufficiently stationary to permit the determination of reasonable structured interpretable variograms.

3   CASE STUDY

The objective of this case study is to access the mineable resources in a high complex Niobium deposit, in a multivariate case using Uniform Conditioning (UC) and localize the panel result in SMU scale using the Localized Uniform Conditioning (LUC). Additionally, the global results and the annually mine plan results are compared against a Conditioning Simulation model that enables to access the grade fluctuation in 100 equiprobable realizations. In the present case, the Turning Bands (TB) algorithm is chosen for its accuracy and computational efficiency. As the Nb_2O_5 is the main variable and only one with economic interest, the Turning bands univariate simulation is used to access the fluctuation grades and compare with LUC Nb_2O_5 grades.

4   DESCRIPTION OF CASE STUDY DATA AND DE-CLUSTER

The area of the study is approximately 600 m (N-S) by 800 m (E-W) and the vertical extent over which niobium mineralization has been identified is approximately 600 m. Two data set are used in this study, the exploration diamond drilling (DDH) and the grade control reverse circulation (RC) drilling. The exploration drillhole dataset is a majority drilling in spacing between 25×25 m. and 50×50 m. The sampling intervals range from 1.25 m. to 2.5 m. and the grade control spacing is between 5×5 m. and 10×10 m. while the sampling in 1.25 meters

interval. The Qa/Qc protocol consists of 5% samples inserted in all batches, such as: blanks, standards, duplicates and includes both DDH and RC. The grade control drilling usually covers up to 12 months in the mine plan.

Checking whether both datasets have similarity in terms of Nb_2O_5 grade, P-P plot was used to compared both distributions in an area predefined covered by exploration and grade control drilling. The results show that both distributions have a very similar shape, despite the DDH and RC have a quite different sampling support.
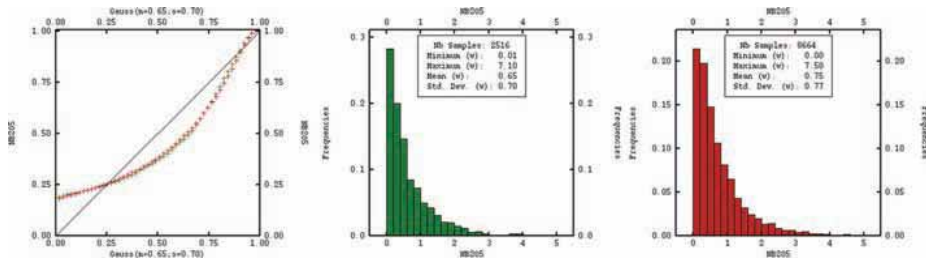
Figure 1. (Left) P-P Plot compares the two distributions, (Center) Nb_2O_5 sample histogram for DDH, and (Right) Nb_2O_5 sample histogram for RC, all in the same predefined area.
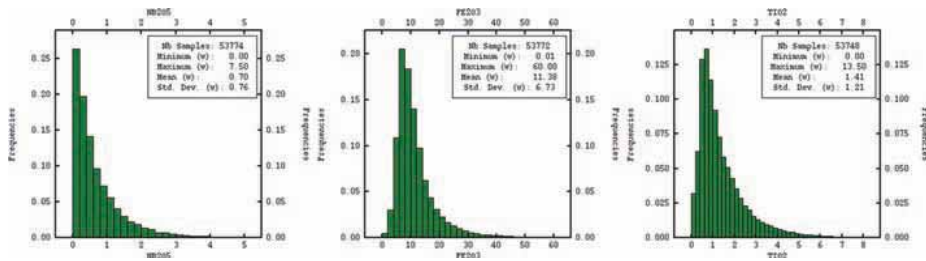
Figure 2. Sample histogram of the target variable Nb_2O_5, Fe_2O_3 and TiO_2, DDH and RC data.

Table 1. Matrix correlation between the interest target variable Nb_2O_5, Fe_2O_3 and TiO_2, DDH + RC data.

Variable	Nb_2O_5	Fe_2O_3	TiO_2
Nb_2O_5	1	0.73	0.45
Fe_2O_3	0.73	1	0.65
TiO_2	0.45	0.65	1
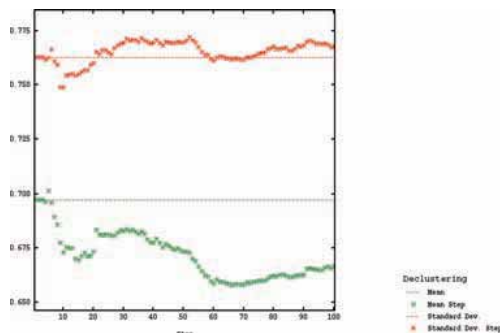
Figure 3. Cell de-clustering results for Nb_2O_5 data for the Boa Vista fresh rock samples within the mineralized envelope.

This study assumes that both datasets will be used together to perform further estimates. These grade control data are considered very desirable for assessing the semivariance at short ranges, however most of the grade control drilling is located in and around the nelsonite veins and it is comparatively high-grade relative to material that has been intersected within the core zone of the complex.

The principal element of interest is Nb_2O_5. The secondary ones are Fe_2O_3 and TiO_2 because these are related to nelsonite mineralization and have some significance for metallurgical recovery processes. In order to represent the correlation between those elements, a multivariate Localized Uniform Conditions (MLUC) is applied in order to reproduce the correlation between the variables.

Prior to attempting any variography, the Nb_2O_5 data within the Fresh Rock domain were subjected to a de-clustering analysis using a moving windows process. All Fresh rock data were declustered using an isotropic cube-shaped window. Within Figure 3, there is a local 'plateau' within the decluster curve corresponding to a window size of approximately 15 m × 15 m × 15 m (step 15). The data were declustered at this window size and decluster weights were calculated and stored. This plateau is interpreted to represent the removal of a local and small-scale cluster effect that is a consequence of the close-spaced grade control data.

5 NORMAL SCORE AND GAUSSIAN ANAMORPHOSIS

As the discrete Gaussian model (DGM) for change of support is part of the UC workflow, it is necessary to test the applicability of DGM. Checking ratios of grade indicator variograms can theoretically test the applicability of the diffusive mode (Rivoirard, 1994). The common 'diffusion model' is one in which higher grade zones transcend into low grade zones through intermediate grades. This model has so been called 'edge effects' and it is the most common description of real grade distributions. The Figure 4 shows the ratio of the square root of the variogram to the madogram of the Nb_2O_5 normal score transformation. The value of
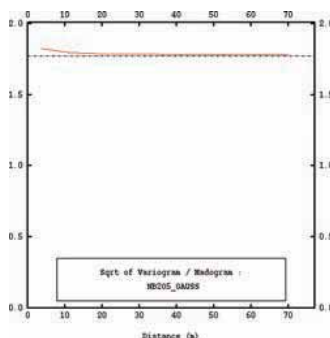
Figure 4.   Square root of variogram/madogram for Gaussian transformation of Nb_2O_5.
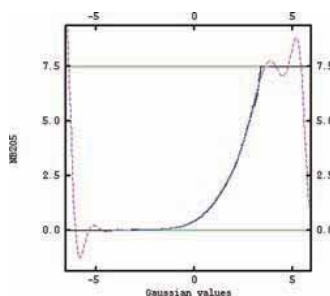
Figure 5.   Gaussian anamorphosis model with hermite polynomials for Nb_2O_5.

137

this ratio is approximately constant at 1.77, which is the square root of π. Theory shows that for bigaussian data, this relationship holds true and this result shows that the normal score transformation of Nb_2O_5 is approximately bigaussian.

The next step is to perform a Gaussian anamorphosis, calculating the normal scores values of the grades and fit a set of Hermite polynomials to describe the relationship between the sample grades and their corresponding normal scores values. Hansmann (2016) says that the number of Hermite coefficient used to fit the anamorphosis model, can vary, and the optimum number depends on how well the polynomial set fits the underlying distribution. It is recommended to use less than 100 coefficients, although in this study 30 coefficients were sufficient, see Figure 5.

6 VARIOGRAPHIC ANALYSIS

Two different variographic analysis were performed to carry out the estimation for both approaches.

Summing up, there are two important differences:

- First, for multivariate LUC (MLUC) a variogram model of the raw grades was used.
- Second, for MLUC a cross variogram with 3 variables Nb_2O_5, Fe_2O_3 and TiO_2 was adjusted, while for the simulation, only a Nb_2O_5 was modeled.

MLUC requires a calculation of change of support coefficients on the SMU support and cokriging of the panels for the 3 variables Nb_2O_5, Fe_2O_3 and TiO_2, where Nb_2O_5 was the main variable.

For Nb_2O_5 conditioning univariate TB simulation, the process is the following:

- Normal score transformation;
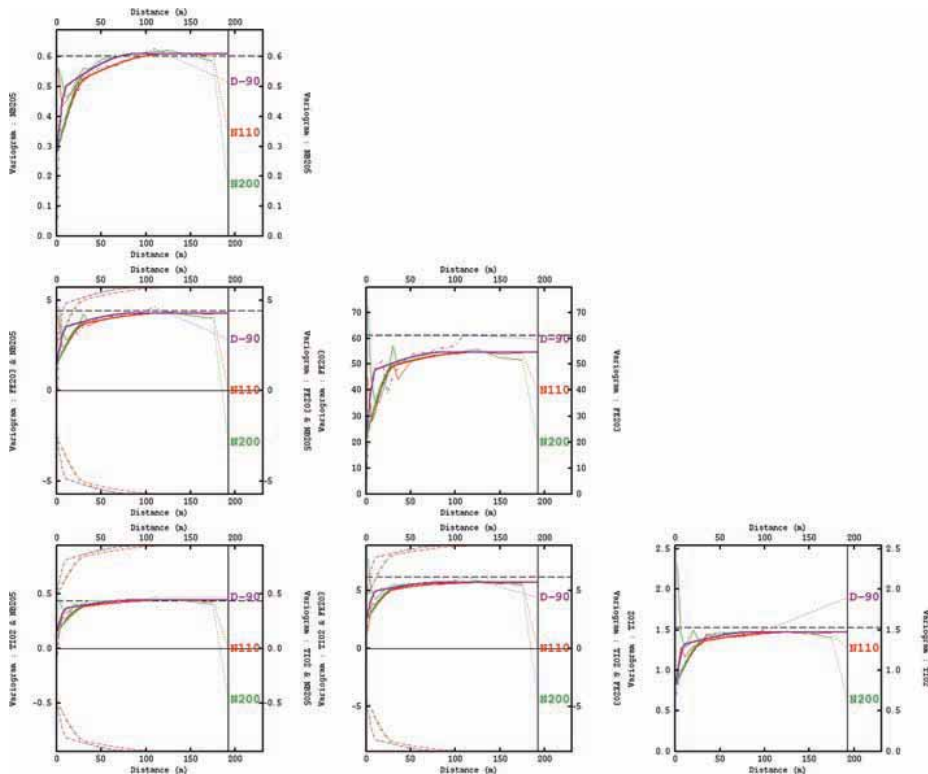
Figure 6.   Experimental and fitted cross variogram for Nb_2O_5, Fe_2O_3 and TiO_2.
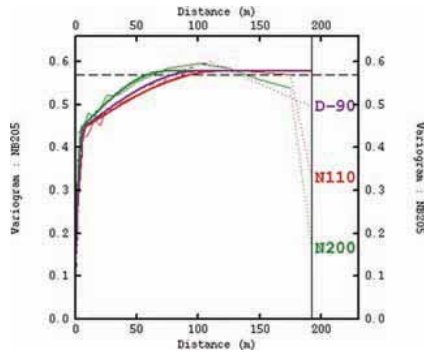
Figure 7. Normal experimental and fitted variogram for Nb_2O_5.

- A weighted variogram model of Gaussian Nb_2O_5 grade is used for TB simulation.

The cross-variograms and the Gaussian variogram, for both approaches are interpreted as follows:

- The short-range high variance structures, including the nugget variance are believed to represent the dominant influence of the stockwork of veins, with narrow zones of high-grade material interspersed with low-grade, almost barren rock;
- The anisotropic, longer range structure represents the dominant orientation of the feeder structures at depth, whilst the longer ranges in the vertical variogram include a component of drift reflecting the transition from high-grade narrow mineralization at depth to more widely dispersed, lower grade mineralization at shallow depths within the mineralized envelope.

7 CHANGE OF SUPPORT

For Uniform Conditioning the block anamorphosis determines the value of the coefficient *r*, which is used to determine the variance reduction of support. The change of support coefficients is calculated for (Deraisme and Bonzu, 2011):

- The SMU support, $10 \times 10 \times 5$ meters, from the variance computed from each variogram model of raw data.
- The kriged panel, $30 \times 30 \times 10$ meters, from the theorical dispersion variance of the cokriging of the panel. To account for the heterogeneity of the cokriging configurations, the panel can be classified according to the variance of the main variable, Nb_2O_5, with a value of the class.

For Turning Bands univariate simulation uses a regular node support $2.5 \times 2.5 \times 2.5$ meters, to simulate 100 realizations, the Gaussian value obtained is converted in raw data using the Gaussian point anamorphosis. To compare both approaches in the same SMU support, the mean of nodes inside each SMU was assigned.

8 UNIFORM CONDITIONING AND LOCALIZATION

UC technique involves calculating a conditional expectation of a non-linear function $\Psi(Z(v))$ of block (v) with respect to the corresponding panel grade Z(V), (Rivoirard, 1994; Wackernagel, 2002). The conventional UC method estimates the tonnage and grade of mineralization which can be recovered using SMU of size (v) at chosen cut-off value. It assumes that the grade of the panel Z(V) is known. In practice, as the true panel grade Z(V) is not available, it is substituted in the UC model by the Z(V)*panel grade estimated by Ordinary Kriging (Abzalov, 2016).

To simplify the planning and mining engineering studies, the Uniform Conditioning estimates have been 'localized'. This estimation approach is an addition to the conventional Uniform Conditioning process. The Grade-Tonnage relationships inside each panel are discretized into a set of SMU grades that respects the estimated Uniform Conditioning Grade Tonnage relationships. These SMU grades are then located within each panel using a linear estimate of the SMU grades to reveal the likely locations of the highest-grade SMUs and lowest grade SMU's. This approach has been described by Abzalov 2006.

The panel grade estimate, using co-kriging was performed in the panel level in order to minimize the conditional bias while retaining some local variability, the panel size is similar to the long-term sample space. The discretization and the neighborhood definition were chosen using quantitative kriging neighborhood analysis QKNA, (Vann, et al., 2003). The UC conditioning was performed using the panel model and the DGM, for the main variable was chosen 61 regular cut-off grades (0 to 6) were chosen. The UC post-process (LUC) was carried to localize the grades using the SMU model which was estimated using the same approach used for the panel estimate.

9 TURNING BAND UNIVARIATE SIMULATION

Geostatistical simulation produces a model of uncertainty that is represented by multiple sets of possible values distributed in a space; one set of possible outcomes is referred to as a realization (McLennan and Deutsch, 2004). In this study, the fluctuation of 100 realizations is used to check the localized uniform conditioning estimate.

The Turning Bands algorithm, used in this study, consists in drawing many lines in space, with random or, preferably, quasi-regular orientations, and simulating a one-dimensional random field along each line (Lantuéjoul, 1994, 2002). By adequately choosing the covariance function of such one-dimensional random fields, their superposition provides a multidimensional random field with the target covariance function, the distribution of which is practically Gaussian by virtue of the central limit theorem. The application of the method is therefore controlled by the number of lines used and by the method used to simulate the basic one-dimensional random fields

For Nb_2O_5 Turning Bands simulation, 400 bands were chosen to create a multidimensional simulation, it was performed in a node level using the same neighborhood strategy defined by QKNA and applied in the UC workflow. Finally, the normal scores simulated results were retro-calculated to raw and averaged in order to calculate simulations to the SMU grades.

The quality of the turning band simulation was checked using the Minimum Acceptance Criteria for Geostatistical Realizations (Leuangthong, *et al.*, 2004), in a nutshell, it consists in the fact that the simulation must reproduce the those following steps:

- data values at their location,
- distribution of the attribute of interest, and
- the spatial continuity characterized by the variogram model.

10 DISCUSSION

The performance of two popular algorithms: 1) – Multivariate Uniformed Conditioning (and the add-on localized) that estimates the conditional distribution of metal and tonnage above a cut-off within a mining panel and; 2) – Turning Bands which performs simulations in a multi-dimensional space through a series of one-dimensional simulations were tested in this study through a real case.

The set of 100 realizations obtained via TB were plotted in a grade tonnage curve and then compared with the UC and the LUC. It demonstrates that the UC and the LUC were able to correctly predict the recoverable tonnage of the deposit, since those curves match in every cut-off grade (from 0 to 3% Nb_2O_5) with the fluctuation curves derived as a result of the simulation, see Figure 8.
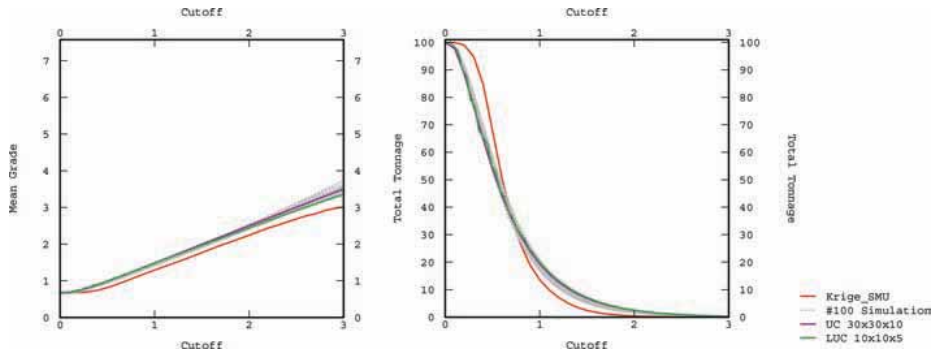
Figure 8.   Global grade tonnage curve of UC, LUC and 100 realizations.

The Ordinary Kriging used to localize the Panel grades in the SMU was also plotted in the grade tonnage curve. The Ordinary Kriging can estimate the in-situ resources (0% NbO_5 cut-off grade) but it fails to correctly predict the grade tonnage distribution in every cut-off grade applied. Using the current economic cut-off grade for this project, to perform a selective mining operation, delivering a head grade of 1% Nb_2O_5 above 0.5% Nb_2O_5%, the OK is approximately 0.82% Nb_2O_5. The UC and the LUC seeks to increase this grade by 20% to 1.02% Nb_2O_5, by simultaneously excluding about 25% of the total material, characterized below 0.5% Nb_2O_5. It can change drastically the successful of the project, especially in a selective mine operation.

These results show that the UC gives a better result than a linear estimate, the OK does not closely conform to the actual values obtained via simulation. The low performance of a linear estimate and the grade smoothing observed in the Ordinary Kriging grade tonnage distribution, can be interpreted as a result of the Niobium lognormal distribution. The lack of data, specially where the deposit is not covered by grade control drilling, can also contribute to the outperforming UC in term of estimate recovery. A high nugget effect and small block size in the estimate can also amplify this conditioning bias.

Comparing the effect of the recovery estimate where there is a good data coverage, the grade tonnage curve was built above level 750, in an area fully covered by grade control drilling (10×5 m), see Figure 9.

In this upper position of the deposit, the performance of a linear estimate is slightly better than the area with a relatively poor data coverage, however some smoothing effect still impacts on the grade tonnage curve. According to Hansmann (2016), in case of normally distributed grades, where there is a good coverage, Ordinary Kriging performs well for determining the recovery resource. In this specific case study, despite the good coverage of data (Grade Control Drilling) above level 750, the following deposit particular characteristics: 1) – the lognormal distribution of Nb_2O_5, 2) – short-range variability and 3) – the high nugget, were causing a lack of the recovery resources adherence compared with the TB simulation. However, mining reconciliation is in progress and it has been shown that de metal difference between the ore mined based on new areas of grade control drilling versus LUC model were –5% in Q3–18 and +6% in Q4–18.

To locally check the accuracy of the UC and the LUC against the TB simulation, the SMU blocks were coded with the current annual Life of Mine designed pit. The range of all 100 realizations were plotted and the 90% interval confidence was calculated using the follow equation.

$$ACCURACY\,(IC\,90\%) = Q95 - Q05 / The\,mean\,of\,simulations * 2$$

For each single year in the Life of Mine with exception of the year 2026, the LUC result lies between the percentile P0.05 and P0.95, although the year 2026 is outside the 90% IC, it is still in range of the all 100 realizations, see Figure 10.

141
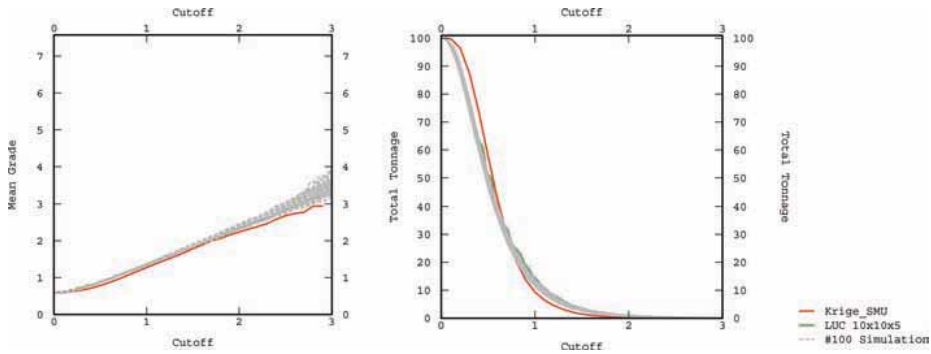
Figure 9.   Grade tonnage curve of LUC and 100 realizations, above the level 750.
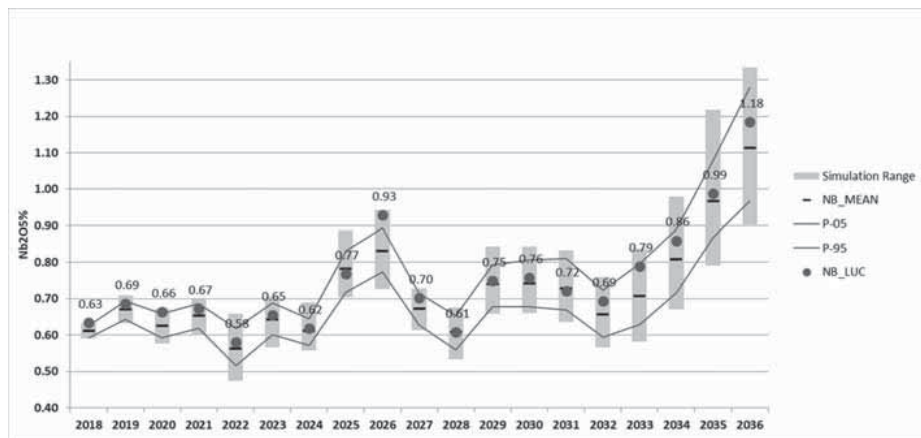
Figure 10.   Nb$_2$O$_5$ grade variation obtained from 100 realizations and the LUC throughout the life of mine.

11   CONCLUSIONS

When the deposit being studied has a lognormal distribution, a high nugget effect and a short-range variogram combined with a high-selectivity operation and limited number of drillholes that lead to a substantial support difference between the panel (limited by the drilling mesh) and the SMU size, in-situ resources estimation with linear methods such as Ordinary Kriging are not effective for a reliable estimation of the contained metal in such deposit. For an accurate estimation of the contained metal, the concept of Recoverable Resources need to be applied with the use of non-linear techniques such as Uniform Conditioning and Conditional Simulations (SMU scale) that provide practical and reliable alternative for the assessment of the recoverable resources.

Univariate Turning Bands does not explicitly use the correlations between the main and auxiliary variables as the Localized Multivariate Uniform Conditioning, besides this, Multivariate Localized Uniform Conditioning grade tonnage distribution lies within the range of 100 grade tonnage curves obtained by using conditional simulation. The results achieved by two different approaches, Localize Multivariate Uniform Conditioning and Turning Band Simulation, provides a more accurate global estimate of grade and tonnage over the in-situ linear estimation performed with Ordinary Kriging.

Although the Turning Bands Simulation is known for its accuracy and computational efficiency, the Localize Multivariate Uniform Conditioning is less time consuming and has an easier workflow implementation. Nevertheless, only the simulation approaches can quantify

the uncertainty related to grades, contained metal and tonnage and thus provides a better understanding of the geological and financial risks associated with the deposit.

ACKNOWLEDGEMENTS

REFERENCES

Abzalov, M.Z. 2006. Localised uniform conditioning (LUC): a new approach for direct block modelling. Mathematical Geology, vol. 38, no. 4. pp. 393–411.

Abzalov, M.Z. "Localized uniform conditioing (LUC): Method and application case studies". In: The journal fo the South African Institute of Mining and Metallurgy 114 (2014), pp. 205–211.

Armstrong M. and Champigny N. 1989: A study on kriging small blocks. CIM Bull., 82, 128–133.

Deraisme, J., Rivoirard, J., and Carrasco Castelli, P. 2008. Multivariate uniform conditioning and block simulations with discrete gaussian model: Application to the Chuquicamata deposit, Proceedings of the VIII International Geostatistics Congress (Geostats 2008), Santiago, Chile, 1–5 December 2008. Gecamin, Santiago. pp. 69–78.

Deraisme, J. and Assibey-Bonsu, W. 2011. Localised uniform conditioning in the multivariate case—An application to a porphyry copper gold deposit. Proceedings of the 35th International Symposium on Application of Computers and Operations Research in the Minerals Industry (APCOM), Wollongong, Australia, 24–30 September 2011. Baafi, E.Y., Kininmonth, R.J., and Porter, I. (eds.). Australasian Institute of Mining and Metallurgy, Melbourne.

De-Vitry, C., Vann, J., and Arvidson, H. 2007. A guide to selecting the optimal method of resource estimation for multivariate iron deposits. Proceedings of Iron Ore2007, Perth, Australia. Australasian Institute of Mining and Metallurgy, Melbourne. pp. 67–77.

Hansmann, K. When should uniform conditioning be applied?. J. S. Afr. Inst. Min. Metall, Johannesburg, v. 116, n. 7, p. 645–654, July 2016.

Harley, M. and Assibey-Bonsu, W. 2007. Localised uniform conditioning: How good are the local estimates? Proceedings of the 33rd International Symposium on Application of Computers and Operations Research in the Minerals Industry (APCOM), Santiago, Chile, 24–27 April 2007. Magri, E.J. (ed.). Gecamin, Santiago. pp. 105–112.

Lantuéjoul, CH. 1994. Non conditional simulation of stationary isotropic multigaussian random functions. In: Armstrong, M., Dowd, P.A. (Eds.), Geostatistical simulations. Kluwer, Dordrecht, The Netherlands, pp. 147–177.

Lantuéjoul, CH. Geostatistical Simulations. Models and Algorithms. Springer-Verlag Print, 2002. Berlin. ISBN 3-540-42202-1.

Leuangthong, O., McLennan, J.A., Deutsch, C.V., 2004. Minimum acceptance criteria for geostatistical realizations. Natural Resour. Res. 13 (3), 131–141.

Millad, M.G. and Zammit, K.M. 2014. Implementation of localised uniform conditioning for recoverable resource estimation at the Kipoi Copper Project, DRC. Proceedings of the Ninth International Mining Geology Conference. Australasian Institute of Mining and Metallurgy, Melnourne. pp. 207–214.

Pan G. 1998: Smoothing effect, conditional bias and recoverable reserves. CIM Bull., 91, 81–86.

Ravenscrof P.J. and Armstrong M. 1990: Kriging of block models-the dangers re-emphasized. In: Proc. 22nd APCOM, Berlin, Germany, vol. II, pp. 577–587.

Rivoirard J. Introduction to Disjunctive Kriging and Non-Linear Geostatistics. Oxford, 1994.

Vann, J., Jackson, S., Bertoli, O., 2003. Quantitative kriging neighbourhood analysis for the mining geologist—a description of the method with worked case examples. In: Dominy, S. (Ed.), Proceedings of the 5th International Mining Geology Conference. Australasian Institute of Mining and Metallurgy, Melbourne, Australia, pp. 215–223.

Wackernagel H. 2002: Multivariate Geostatistics: an introduction with applications. Springer Verlag, Berlin, Germany, 388 pp.

MILP framework for open pit and underground mining transitions evaluation

B.O. Afum
Mining Optimization Laboratory, Laurentian University, Sudbury, Canada
University of Mines and Technology (UMaT), Tarkwa, Ghana

E. Ben-Awuah
Mining Optimization Laboratory, Laurentian University, Sudbury, Canada

ABSTRACT: The strategic decisions to exploit a mineral deposit extending from the surface to great depth are essential to the financial and sustainability benefits of any mining project. Mining option strategies for resource extraction include: (a) independent open pit mining; (b) independent underground mining with crown pillar; (c) simultaneous open pit and underground mining with crown pillar; (d) sequential open pit and underground mining with crown pillar; and e) combinations of (c) and (d). This research investigates the extraction strategy that maximizes the Net Present Value (NPV) of a resource using a Mixed Integer Linear Programming (MILP) optimization framework. The MILP model determines the best extraction strategy for a given ore body and further determines the mining and processing schedule, positioning of the required crown pillar, and the schedule for underground capital and operational developments. The model is implemented for a synthetic copper case study.

1 INTRODUCTION

Decisions made at the prefeasibility stage of a mining project are essential to the commencement and sustainability of the project. Important decisions including the selection of a suitable mining option(s) for exploiting the deposit improves the confidence of mine management and investors when their correctness and accuracy are done right from the onset of the mining project. The decision on the choice of mining option(s) becomes complicated when the deposit is deep-seated and exhibits significant outcrops. The potential of such a deposit to be exploited by open pit (OP) or underground (UG) mining or both (OPUG) could lead to several variations of mining options. To generate early revenue, the portion of the deposit closer to the surface is often exploited by open pit mining option while the deeper portions are exploited with underground mining option. In OP mining, the incremental stripping ratio and overall mining cost with depth makes UG mining profitable beyond a certain depth. This depth has been referred to by several authors as the transition depth or point (Bakhtavar et al., 2009, Dagdelen and Traore, 2014, De Carli and de Lemos, 2015, King et al., 2016, MacNeil and Dimitrakopoulos, 2017, Opoku and Musingwini, 2013, Ordin and Vasil'ev, 2014, Roberts et al., 2013, Ben-Awuah et al., 2016, Ben-Awuah et al., 2015).

The choice of the most economic mining option(s) can be implemented through an optimization approach. The optimization process becomes complicated when the transition point acts as the unmined crown pillar together with the integration of both capital and operational developments. This leads to several variations of the optimal mining option(s): (a) independent OP mining; (b) independent UG mining with crown pillar; (c) simultaneous OPUG mining with crown pillar; (d) sequential OPUG mining with crown pillar; and e) combinations of (c) and (d). The decision to adopt any mining option strategy will primarily depend on the project economics and the geology of the mining area. Traditionally,

the outcrop portion of the deposit is optimized for OP mining and during the OP mining operation, the deep-seated portion below the bottom of the open pit is evaluated for UG mining. This approach leads to missed financial and sustainability opportunities because it often leads to sub-optimal solutions.

A mathematical programming framework for determining the extraction strategy for any deposit that has the potential to be exploited with several variations of mining options in the presence of a suitable crown pillar, capital development (shaft/decline) and operational developments (level, ore drives and crosscuts) has been developed. Integrating three-dimensional (3D) crown pillar positioning into the optimization process allows the OP and UG mining options the fair opportunity to economically compete for selection.

This paper presents a Mixed Integer Linear Programming (MILP) framework for solving the open pit and underground mining transition problems. The model determines a suitable optimized mining option and strategy for extracting a deposit that is potentially amenable to either or both open pit and underground mining option. A synthetic copper dataset is used as a case study to implement the model for evaluation. Sensitivity analysis is further conducted to assess the influence of selected technical and economic parameters to changes in the mining options.

The next section of this research paper covers a summarized literature review on open pit to underground mining transition with highlights on research gaps. Section 3 discusses the assumptions and notations used in the proposed MILP model. Section 4 introduces and explains the proposed integrated MILP model for the open pit to underground mining transition complex. Section 5 documents the implementation of the MILP model for a synthetic copper deposit while Section 6 outlines the research conclusions and recommendations.

2 SUMMARY OF LITERATURE REVIEW

Strategic open pit and underground mining interface optimization models have been developed based on determining the transition depth between open pit and underground mining. These existing models focus on investigating how an underground mining operation can be exploited after the open pit mine life and/or finding the transition depth. Acknowledging notable challenges and shortfalls, several researchers have employed techniques, algorithms and/or models to determine the transition depth (Bakhtavar et al., 2009, Dagdelen and Traore, 2014, De Carli and de Lemos, 2015, King et al., 2016, Opoku and Musingwini, 2013, Ordin and Vasil'ev, 2014, Roberts et al., 2013, MacNeil and Dimitrakopoulos, 2017) and the ore block extraction strategy (Ben-Awuah et al., 2016, De Carli and de Lemos, 2015, King et al., 2016, MacNeil and Dimitrakopoulos, 2017, Whittle et al., 2018).

Optimizing the location of a crown pillar is a key factor in the optimal resource extraction evaluation process for deposits amenable by both open pit and underground mining. Finding the most suitable location of the crown pillar in a combined OPUG mining operations is one of the most interesting problems for mining engineers today (Bakhtavar et al., 2012). The transition from open pit to underground (OPUG) mining involves a complicated geomechanical process. Recent formulations of the OPUG mining transition complexes produces near optimal solutions at minimal level of confidence, and do not integrate the positioning of a 3D crown pillar, capital and operational developments into the optimization process.

Kurppa and Erkkilä (1967) assessed the simultaneous extraction between open pit and underground (OPUG) mining during the operations of the Pyhasalmi mine. They indicated that, simultaneous mining was possible due to the geometry of the orebody being worked. Luxford (1997) argued that, cost usually drives the decision to make the transition because as the open pit waste stripping cost keeps increasing with depth, there comes a time when the underground mining cost will be less than the open pit mining cost. Ben-Awuah et al. (2016) investigated the strategy of mining options for an orebody using a mathematical programming model. The research evaluated the financial impacts of applying different mining options separately or concurrently to extract a given orebody. The formulation maximizes the NPV of the reserve when extracted with: (1) open pit mining, (2) underground mining, and (3) concurrent open pit and underground mining (Ben-Awuah et al., 2015). The positioning

of a crown pillar together with capital and operational development requirements were not incorporated into this model.

King et al. (2016) incorporated crown and sill pillar placement into their OPUG transition studies to separate the open pit from the underground mine. In their model, the location of the crown pillar was simulated, and preselected to divide the deposit into OP and UG mining zones before running an optimization for the OP mining zone and planning for the UG mining zone. MacNeil and Dimitrakopoulos (2017) investigated the transition decision at an operating open pit mine within the context of a mining complex comprising five producing pits, four stockpiles and one processing plant. In their research, MacNeil and Dimitrakopoulos (2017) priori identified the crown pillar envelope for a gold deposit and evaluated four crown pillar locations within this envelope leading to four distinct candidate transition depths. Decomposing the OPUG optimization process into scenarios has the tendency to compromise the global optimal solution.

A mathematical model that solves the transition problem was developed by Whittle et al. (2018) after modifying the normal pit optimization model based on the maximum graph closure algorithm (Lerchs and Grossman, 1965). The modifications allow the algorithm to account for the underground mining value of a block, and the requirement for a specified 2D crown pillar location above the underground mine. The algorithm of Whittle et al. (2018) is based on what they called the "opportunity cost approach", thus, if a given block is mined by open pit method, its open pit value is gained while its value that would have been obtained by extracting it using underground mining methods is lost. According to Whittle et al. (2018), the optimization approach does not control the mining sequence with time and produces a near optimal value for the mining project. Future works were therefore recommended to improve on their model.

In this research study, we have developed, implemented, and tested a MILP optimization framework for evaluating the extraction strategy for a deposit. The MILP model maximizes the Net Present Value (NPV) of the resource and determines the best extraction strategy for a given ore body amenable to different mining options. The model further determines the mining and processing schedule, the location of the required crown pillar, and the schedule for underground capital and operating developments (shaft/decline, levels, ore drives and crosscuts) for the optimal extraction option.

3 ASSUMPTIONS AND NOTATIONS

It is assumed that the size of the Selected Mining Units (SMUs) for open pit mining is equivalent to the stope sizes for underground mining. In the MILP framework, the SMUs are represented by mining blocks in general, or mining-cuts in specific relation to open pit mining or mining-stopes for underground mining. The location of each mining block or mining-cut or mining-stope is represented by the coordinates of the centroid. It is assumed that a crown pillar is required for the exploitation of the orebody by underground mining. The size of the crown pillar is estimated to be one vertical length of a stope or bench; thus, one bench or level in the block model will represent the crown pillar. For underground mining, ore extraction is achieved by a retreating method. Some of the notation of indices and parameters are as follows:

3.1 *Indices*

A general parameter f can take four indices in the format of $f_{k,l}^{a,t}$. Where:

$j \in \{1, ..., J\}$ index for open pit mining-cuts in the model.
$p \in \{1, ..., P\}$ index for underground mining-stopes in the model.

3.2 *Parameters*

$v_j^{op,t}$ the open pit (*op*) discounted revenue generated by selling the final product within mining-cut j in period t minus the discounted extra cost of extracting mining-cut j as ore and processing it.

$v_p^{ug,t}$ the underground (*ug*) discounted revenue generated by selling the final product within mining-stope *p* in period *t* minus the discounted extra cost of extracting mining-stope *p* as ore and processing it.

$q_j^{op,t}$ the open pit (*op*) discounted cost of mining all the material in mining-cut *j* in period *t* as waste.

$q_p^{ug,t}$ the underground (*ug*) discounted cost of mining all the material in mining-stope *p* in period *t* as waste.

g_j average grade of element in ore portion of mining-cut *j*.

g_p average grade of element in ore portion of mining-stope *p*.

o_j ore tonnage in mining-cut *j*.

o_p ore tonnage in mining-stope *p*.

r processing recovery; the proportion of mineral commodity recovered.

sp selling price of mineral commodity in present value terms.

sc selling cost of mineral commodity in present value terms.

pc extra cost in present value terms per tonne of ore for mining and processing in period *t*.

cm_l^t cost per bench or level *l* in present value terms of mining a tonne of rock material by open pit mining in period *t*.

cm^t cost in present value terms of mining a tonne of rock material by underground mining in period *t*.

4 THE INTEGRATED MILP MODEL

An integrated MILP model is formulated to determine the time and sequence of extraction of ore and waste blocks over the mine life for open pit and/or underground mining. The proposed MILP model interrogates the orebody and determines the best mining option that produces an optimal extraction sequence to maximize the Net Present Value (NPV) of the mining project. The mining options could either be open pit mining or underground mining or a combination of both open pit and underground mining. The model further determines the capital and operational development schedules required to extract the orebody by underground mining. The NPV of the extraction strategy is maximized in the presence of technical, geotechnical, geological, and economic constraints to enforce the mining sequence, grade blending requirements, capital and operational developments, and mining and processing capacities.

4.1 *Modeling the economic block value*

The economic block values are defined based on the SMUs, thus, mining-cuts for open pit mining and mining-stopes for underground mining. The value of the block is a function of the recovered quantity of mineral present in the block (processing recovery), the discounted revenue from selling the commodity, and the discounted mining, processing and selling costs.

The discounted revenues generated by selling the final product within block *k* being extracted in period *t* by open pit mining $v_j^{op,t}$ and underground mining $v_p^{ug,t}$ are respectively given in Equations (1) and (2). Similarly, the discounted costs of mining all the material within block *k* being extracted in period *t* by open pit mining $q_j^{op,t}$ and underground mining $q_p^{ug,t}$ are respectively given in Equations (3) and (4).

$$v_j^{op,t} = \sum_{j=1}^{J} o_j \times g_j \times r \times (sp - sc) - \left(\sum_{j=1}^{J} o_j \times pc \right) \qquad (1)$$

$$v_p^{ug,t} = \sum_{p=1}^{P} o_p \times g_p \times r \times (sp - sc) - \left(\sum_{p=1}^{P} O_p \times pc \right) \qquad (2)$$

$$q_j^{op,t} = (o_j + w_j) \times cm_l^t \tag{3}$$

$$q_p^{ug,t} = (o_p + w_p) \times cm^t \tag{4}$$

4.2 Objective function

The objective function of the MILP model maximizes the NPV of the mining project for combined open pit and underground mining options. During optimization, if OP only or UG only is selected, the objective function of the unselected mining option becomes zero. The objective function of the MILP model maximizes the NPV of the mining project for both open pit and underground mining. The quantity of ore processed is controlled by the continuous decision variables for open pit and underground mining respectively. Similarly, the quantity of rock material extracted by open pit and underground mining are also controlled by the continuous decision variables respectively. The continuous variables ensure fractional extraction and processing of the mining-cut or mining-stope in different periods of the mine life.

4.3 Constraints

The components of the constraints are grouped as follows: a) OP mining constraints; b) UG mining constraints; c) interaction of OP mining with UG mining constraints; d) crown pillar constraints; e) capital development constraints; f) operational development constraints; and g) non-negativity constraints. Acceptable upper and lower targets are defined for the mining, processing, developments, and plant head grade requirements. The mining capacity is a function of the ore reserve and the designed processing capacity which is also based on the available mining fleet acquisition for the operation. The processing capacity constraints define the ore production schedule in each period and further ensures the run-of-mine (ROM) material satisfies the quantity specification of the processing plant.

4.3.1 OP mining constraints
The OP mining constraints are deployed to control the open pit mining operations. The set of constraints include mining and processing capacities, grade blending, ore and mining-cut tonnages, available reserve, and vertical block precedence relations.

4.3.2 UG mining constraints
The UG mining constraints control the underground mining operation. These constraints include the mining and processing capacities, grade blending, ore and mining-stope tonnages, available reserve, and lateral block precedence relations.

4.3.3 Interaction of OP mining with UG mining constraints
The interaction of OP mining with UG mining constraints ensure that each mining block is extracted by only one mining option or left as unmined block in the crown pillar. The constraints further include a combined processing capacity that represents the contribution of ore production from both OP and UG mining operations.

4.3.4 Crown pillar constraints
The crown pillar constraints control the positioning of the required crown pillar. These constraints define the relationship of the location of the open pit and underground mining operations. The constraints ensure that the crown pillar is located at the bottom of the open pit mine, is always located above the underground mining, and stays unmined throughout the mine life.

4.3.5 Capital development constraints
These constraints ensure that the required capital development is considered when underground mining is the preferred extraction option. These set of constraints define the capital development requirements for the underground mining which involve the total length of capital development (shaft) and the relationship with the required operational developments.

4.3.6 *Operational development constraints*

These constraints ensure that the required operational developments are considered when underground mining is the preferred option for extracting the ore body. These set of constraints define the operational development requirements including the type and length of each operational development (level, ore drive, crosscuts) and lateral precedence relations with the block extraction sequence.

5 COMPUTATIONAL IMPLEMENTATION OF THE MILP MODEL

5.1 *Preparation of the model*

The formulated MILP model was implemented with an experimental case study. MATLAB 2018a (Mathworks, 2018) environment was used to define the modelled framework and IBM ILOG CPLEX Optimization Studio (ILOG, 2015) was integrated into MATLAB to solve the MILP at a gap tolerance of 5%. The model was tested on an Intel(R) Core™ i7-7700HQ CPU Dell computer @ 2.80GHz, with 32 GB RAM.

In open pit mining, the ore is exploited from the top to the bottom with a 45° slope to ensure the geotechnics of the mine is controlled. A cross-section of the block model showing the precedence of block extraction for the open pit mine is shown in Figure 1. In Figure 1, to extract block 1, blocks 2, 3 and 4 needs to be extracted. However, to extract block 4, blocks 7, 8 and 9 must be priori extracted while to extract block 9, blocks 14, 15 and 16 must be priori extracted. It therefore follows that to mine block 1, all the shaded regions with blocks 1 to 16 must be afore-mined.

However, in underground mining, the block model of the deposit is prepared by citing the location of the main capital development (shaft) and defining the location of the operational developments (levels, ore drives and crosscuts) on each level. The level development links the shaft or decline to the ore drives through the centroid of each block. The crosscut developments extend from this ore drive to the ends of the minefield through each block, acting as stope drives. At this stage, the extraction method (retreating or advancing) is established for the ore body. Figure 2 is a schematic representation of the block model showing the underground operating developments. The arrows show a retreating mining method for the ore extraction sequence on a typical level.

5.2 *Case study—synthetic copper deposit*

The Mixed Integer Linear Programming (MILP) model was implemented and tested on a synthetic copper deposit. The copper dataset is represented by a geologic block model which is a 3D array of cubical blocks containing 605-unit blocks. These unit blocks represent the
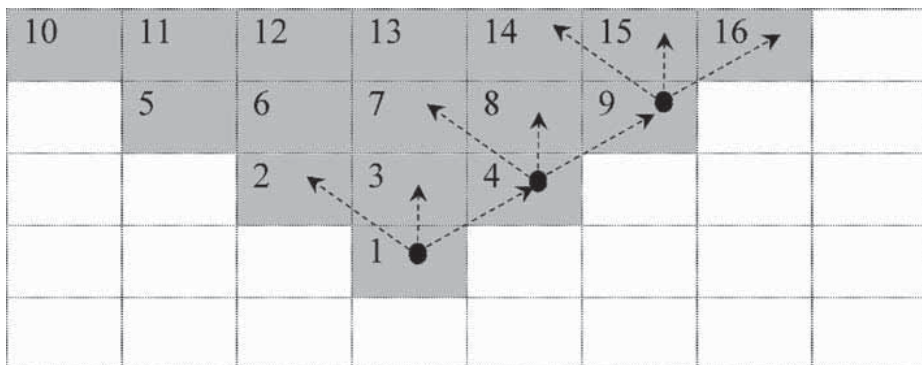
Figure 1.   A cross-section of the block extraction precedence for OP mining in the MILP model.
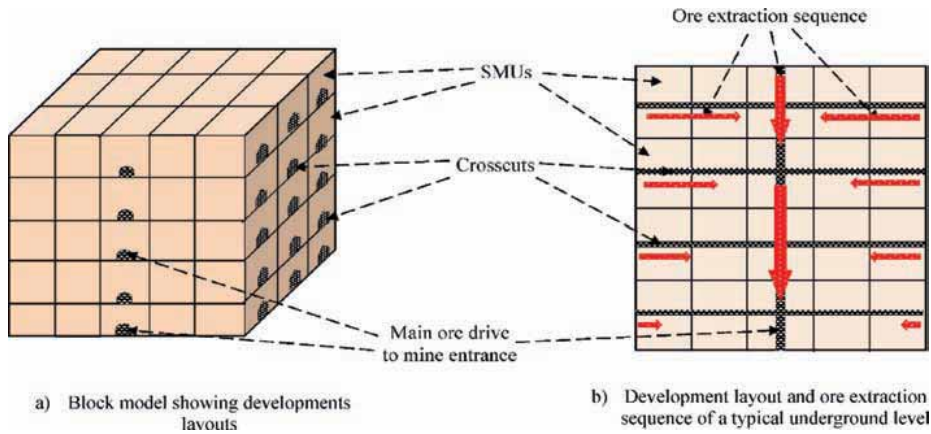
Figure 2. Isometric view of the block model and development layout of an underground level.
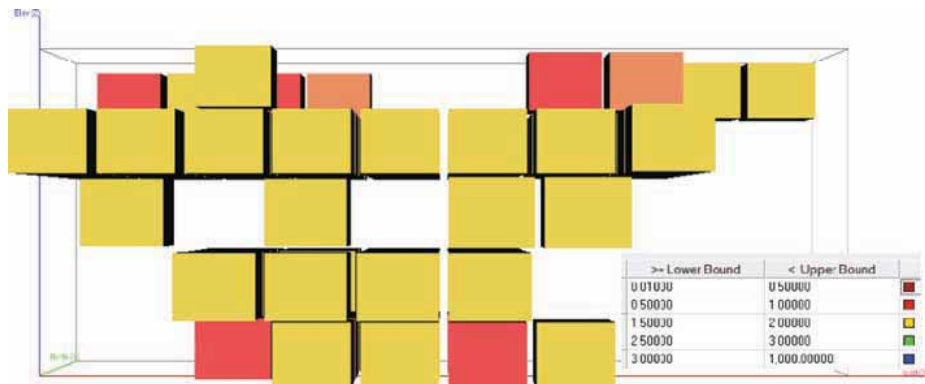
Figure 3. Layout of the synthetic copper deposit showing mineralized blocks.

Selective Mining Units (SMUs) for OP and UG mining. The ore body in the block model is irregularly shaped with a total mineral resource of 116.10 Mt at an average Cu grade of 1.05%, minimum grade of 0.72% and maximum grade of 3.0%. Figure 3 shows the layout of the synthetic copper deposit showing mineralized blocks. Table 1 and Table 2 respectively show the statistical description and distribution of the quality and quantity of metal in the deposit. The quality of the copper deposit is shown by a few blocks occurring at the top portions of the ore body with higher metal contents. The bottom portions of the deposit show a similar mineralization while low quality ore blocks occur in the middle sections. The copper distribution in the deposit suggests it could be exploited with open pit mining for earlier financial benefit. However, the incremental cost of open pit mining with depth may cause underground mining to compete as the better option at a certain depth during the mineral exploitation process. Therefore, the essence of evaluating this deposit with the proposed MILP framework.

5.2.1 *Economic and mining data*

The yearly processing capacities are determined based on the proposed plant capacities for the mine while the yearly mining capacities are deduced from the ore and waste proportions of the deposit. An incremental bench cost of $4.0 per 15 m bench was used as the open pit mining variable cost as the pit extends downwards. The economic, mining and processing data used for evaluating the copper deposit as summarized in Table 3 were estimated using data obtained from CostMine (2016) and pre-feasibility reports of two mining companies in Canada (Centerra Gold Inc. and Premier Gold Mines Limited, 2016).

Table 1. Statistical description of the synthetic copper deposit.

No.	Description	Value
1	Total mineralized material (Mt)	116.10
2	Minimum value of Cu (%)	0.719
3	Maximum value of Cu (%)	3.000
4	Average value of Cu (%)	1.051
5	Variance (%²)	0.394
6	Standard deviation (%)	0.628
7	Number of levels/benches	5

Table 2. Distribution of the metal quality and quantity in the deposit.

Level no.	Total metal content (% × million)	Total ore tonnage (t × million)	Value
1	19.10	12.15	9
2	40.22	52.65	39
3	4.05	5.40	4
4	15.74	20.25	15
5	42.84	25.65	19

Table 3. Economic, mining and processing data for evaluating the copper deposit.

No.	Parameter	Value
1	Open pit mining cost ($/t)	8.0
2	Underground mining cost ($/t)	300.0
3	Processing cost ($/t)	15.0
4	Selling cost ($/lb)	1.5
5	Selling price of copper ($/lb)	3.5
6	Discount rate (%)	10.0
7	Processing recovery (%)	95.0
8	Max open pit (OP) processing capacity (Mt/year)	8.0
9	Min open pit (OP) processing capacity (Mt/year)	0.0
10	Max open pit (OP) mining capacity (Mt/year)	20.0
11	Min open pit (OP) mining capacity (Mt/year)	0.0
12	Max underground (UG) processing capacity (Mt/year)	3.0
13	Min underground (UG) processing capacity (Mt/year)	0.0
14	Max open pit & underground (OPUG) processing capacity (Mt/year)	8.0
15	Min open pit & underground (OPUG) processing capacity (Mt/year)	0.0
16	Max underground (UG) mining capacity (Mt/year)	3.0
17	Min underground (UG) mining capacity (Mt/year)	0.0
18	Incremental bench cost ($/15 m)	4.0
19	Operating development cost ($/m)	7000
20	Capital development cost ($/m)	15,000
21	Max operating development (m/year)	5000
22	Max capital development (m/year)	30

5.2.2 *Results and discussions*

Evaluation of the copper deposit with the integrated Mixed Integer Linear Programming (MILP) model indicates that a combined sequential and simultaneous open pit and underground (OPUG) mining operation is the preferred mining option with the highest Net Present Value (NPV) of $265.89 billion. The integrated MILP model was modified to evaluate the ore body for an independent open pit (OP) mining option and an independent underground

(UG) mining option with the required crown pillar, capital and operational developments. The NPV of the OPUG mining option is about 14.4% better than an independent OP mining option and about 24.1% better than an independent UG mining option. The evaluated results are shown in Table 4. The copper deposit is therefore best exploited with a combined open pit and underground (OPUG) mining option for a mine life of 19 years with Level 3 acting as the unmined crown pillar.

With a total ore production of 100.05 Mt from the combined OPUG mining option with crown pillar, the OP mining operation contributes 64.80 Mt of ore while the UG mining operation contributes 35.25 Mt of ore. The remaining 15.95 Mt of the available mineral resource is either left in the crown pillar (5.40 Mt) or left as unmined low-grade stopes (10.55 Mt). In a more practical underground mine, where the crown pillar is recovered ("robbed") during the operational life of mine, the 5.40 Mt of ore deposit will be mined to further improve the total net present value (NPV) of the project if the ore quality is economical.

A sectional view through the ore body showing the open pit limit, location of the required crown pillar, an unmined low-grade stope and the mineralized zone extending beyond the bottom of the open pit limit is shown in Figure 4. The crown pillar is located on Level 3; thus, the first 2 levels (or benches) are extracted by open pit mining while Levels 4 and 5 are extracted by underground mining.

The ore and rock extraction schedules for the combined open pit and underground mining (OPUG) option with a crown pillar are shown in Figure 5 and Figure 6 respectively. The ore is extracted by an independent open pit mining option in the first 2 years of the mine life before underground ore production begins simultaneously from the 3rd year through to the 12th year. The ore production schedule switches completely to an independent underground mining option in the remaining 2 years of the mine life. In summary, the ore extraction profile for the combined OPUG mining option is a blend of sequential and simultaneous open pit and underground mining options for a mine life of 14 years. Due to the outcrop of the ore

Table 4. Results from the integrated MILP model for the case study.

Mining option	Net present value ($b)	NPV of OPUG compared (%)	Processed ore tonnage (Mt)	Resource depletion (%)
Open pit mining	227.73	−14.4	116.00	100.0
Underground mining	201.72	−24.1	103.95	89.6
Combined open pit and underground mining	265.89	–	100.05	86.3

Figure 4. A sectional view through the block model showing the open pit limit, crown pillar and underground mining regions for the case study.
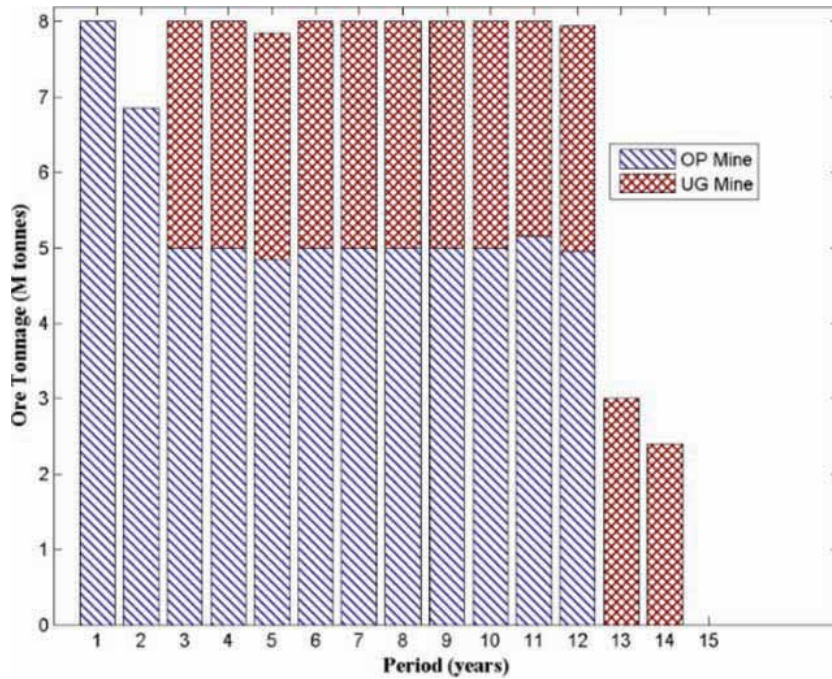
Figure 5. Yearly ore production schedule for the OPUG mining option.
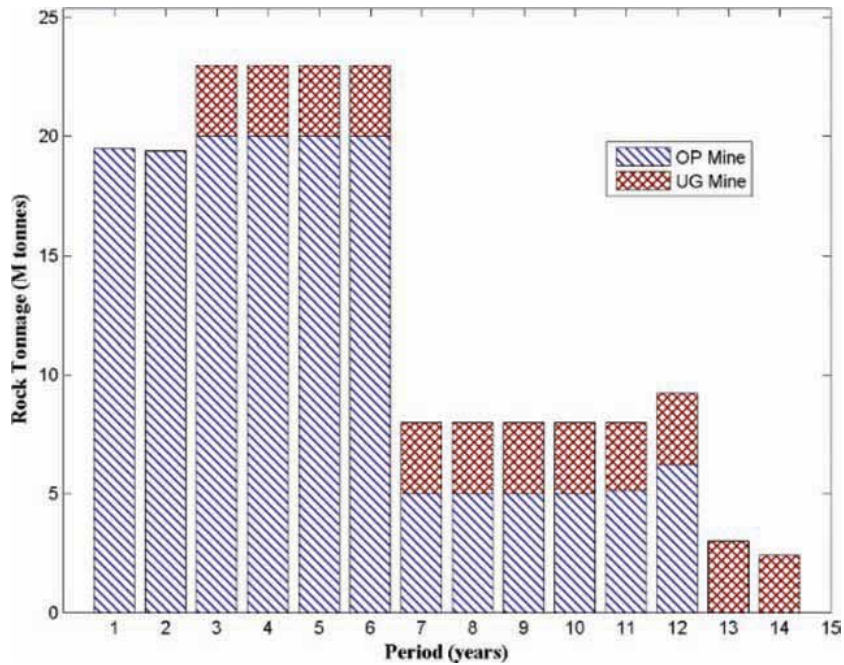
Figure 6. Yearly rock production schedule for the OPUG mining option.

body, the ore extraction schedule in the first year of the mine life satisfies the full capacity of the plant requirement of 8.0 Mt.

The average grade of Cu ore processed in each period for the combined open pit and underground mining option with a crown pillar is shown in Figure 7. In Figure 7, the yearly
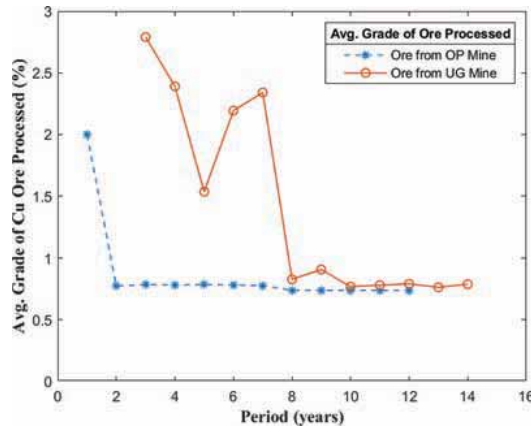
Figure 7. Average grade of ore processed in each year for OPUG mining option.
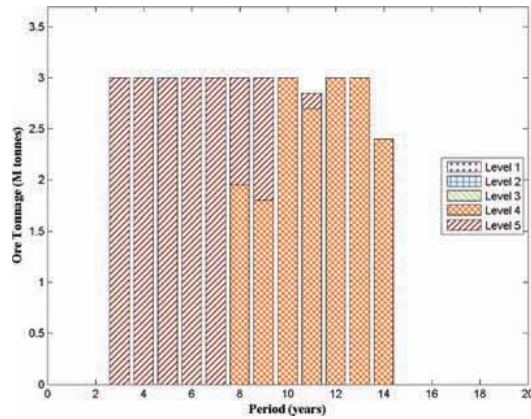
Figure 8. Ore tonnage per level extracted in each year for the underground mining operation in the OPUG mining option.

average grade of processed ore for the underground mining operation is generally higher compared to the open pit mining operation. This shows that underground mining prioritizes the extraction of high-grade ores to cover the high cost of mining by generating higher revenues. It is convincing that the grade blending constraints of the MILP model prioritizes higher grades over lower grades in exploiting the mineral deposit by any of the mining options. Thus, the open pit mining operation targeted the outcropped high-grade ore while the underground mining operation targeted the deep-seated high-grade ore.

To highlight the nature of the underground mining operation and obtain further information on the required exploitation method, the levels contributing to the mineral extraction schedule are shown in Figure 8. With the crown pillar located on Level 3, ore extraction by the underground mining operation started on the last level, Level 5, from the 3rd year through to the 7th year of the mine life before continuing with ore production from Level 4 to the end of mine life. With this knowledge on the mining sequence from each level (Figure 8) and the geotechnics of the rock formation, any suitable underhand method of ore extraction could be further evaluated and selected as the appropriate underground exploitation method to develop this deposit. The operational development schedule for the underground mine is shown in Figure 9. With a total operational development capacity of 10,000 m per year, advancement starts immediately after completion of the capital development (shaft) in the 3rd year but ends in the 6th year before commencing again from year 8 to 12.

154
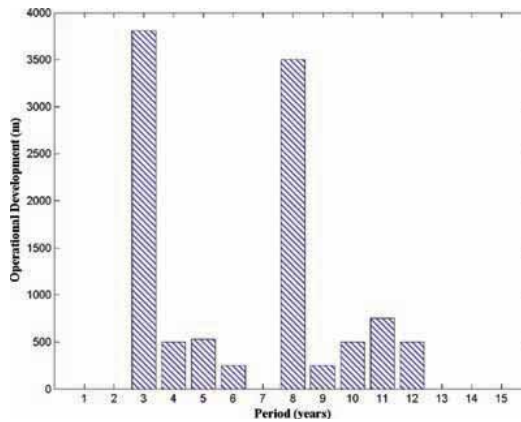
Figure 9. Operational development schedule for the underground mining operation in the OPUG mining option.
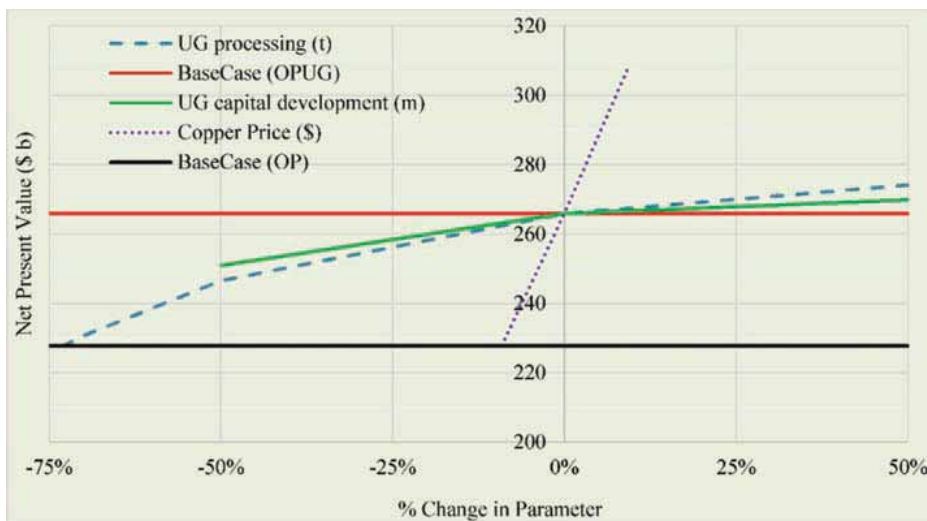
Figure 10. Sensitivity assessment of selected technical and economic parameters used in the MILP model.

5.2.3 *Sensitivity analysis*

The sensitivity of the results to gold price, underground processing capacity and underground capital development (shaft) is evaluated with the MILP model. This sensitivity analysis was conducted to examine the selected technical or economic parameters that influence the choice of mining option(s) for the deposit. The sensitivity plot is shown in Figure 10. In Figure 10, the MILP model is very sensitive to the market price of copper followed by the quantity of ore processed from the UG mining operation and the completion rate of capital development.

For this case study, about 9% decrease in the copper price (from $3.18 to $2.89 per lb) will change the optimal mining option from combined OPUG mining to an independent OP mining option for a reduced NPV of $227.73. Similarly, when the underground processing capacity decreases by about 73% (0.81 Mt), the combined OPUG mining will change to an independent OP mining option. This copper deposit is however less sensitive to the completion rate of underground capital development (shaft) as it did not cause a change in mining option within the changes tested.

155

6 CONCLUSIONS AND RECOMMENDATIONS

An integrated Mixed Integer Linear Programming (MILP) model for evaluating the extraction of a mineral deposit has been developed, implemented, and tested on a synthetic copper dataset. The proposed MILP model interrogates a deposit and determines the optimal extraction strategy for a combination or one of the mining options: (a) independent open pit mining, (b) independent underground mining with crown pillar, (c) simultaneous open pit and underground mining with crown pillar, (d) sequential open pit and underground mining with crown pillar, and (e) combinations of simultaneous and sequential open pit and UG mining with crown pillar. The location of the 3D crown pillar together with the required capital and operational development schedules are decided by the optimization process. The MILP model is applicable to all types of deposits and for any preferred direction of mineral extraction sequence. The capital development can either be a shaft, decline or both and during optimization, depending on the optimal mining option, the capital development can either commence from the surface, bottom of the open pit mine or both.

To implement the MILP model, the block model was organized by first selecting a preferred ore extraction method on a level (advancing or retreating) and siting the possible location of the underground capital and operational developments based on the philosophy and geotechnical understanding of the mine. As in practice, the MILP model requires that an incremental cost for open pit mining is defined per depth (m) for block extraction. Thus, the cost of open pit mining increases with depth until underground mining becomes preferable to open pit mining. This concept allows the optimizer to decide when to stop the open pit mining operation, introduce a crown pillar and start the underground mining operation in the presence of both capital and operational developments.

The results from the case study showed a combined sequential and simultaneous open pit and underground mining option (OPUG) with crown pillar was selected as the optimal mining option to exploit the deposit. The ore and rock extraction schedules for the open pit and underground mining operations together with the operational and capital development schedules were determined for the synthetic copper project. The output of the model in mapping-out the ore extraction per level in each period further provides more insight into the mining sequence for selection of the appropriate underground mining method. A sensitivity analysis conducted on selected technical and operational parameters indicate that the determination of the optimal mining option using the MILP model is very sensitive to the selling price of copper, followed by the quantity of ore processed by the underground mining operation and the completion rate of the underground capital development (shaft).

The authors recommend that stockpile management and geotechnical information be incorporated into the MILP model to ensure the outputs of the model is exhaustive and realistic. Similarly, it is necessary to extend the model from its current deterministic approach to a stochastic framework to address the impact of grade uncertainty in the choice of mining option and project evaluation.

REFERENCES

Bakhtavar, E., Shahriar, K. & Mirhassani, A. 2012. Optimization of the transition from open-pit to underground operation in combined mining using (0–1) integer programming. *J South Afr Inst Min Metall* 112, 1059–64.

Bakhtavar, E., Shahriar, K. & Oraee, K. 2009. Transition from open-pit to underground as a new optimization challenge in mining engineering. *Journal of Mining Science,* 45, 485–494.

Ben-Awuah, E., Otto, R., Tarrant, E. & Yashar, P. 2016. Strategic mining options optimization: Open pit mining underground mining or both. *International Journal of Mining Science and Technology,* 26, 1065–1071.

Ben-Awuah, E., Richter, O. & Elkington, T. 2015. Mining options optimization: Concurrent open pit and underground mining production scheduling. *37th International Symposium on the Application of Computers and Operations Research in the Mineral Industry.* Fairbanks, Alaska: SME.

Centerra Gold Inc. & Premier Gold Mines Limited 2016. Centerra gold and premier gold announce feasibility study results on the hardrock project. *In:* Pearson, J.W. & Gollat, M. (eds.). CenterraGold and Premier Gold Mines Limited.

Costmine 2016. Mine and mill equipment costs: An estimator's guide. Washington, USA: CostMine Division of InfoMine USA, Inc. in cooperationg with Aventure Engineering, Inc.

Dagdelen, K. & Traore, I. Open pit transition depth determination through global analysis of open pit and underground mine scheduling. *In:* Dimitrakopoulos, R., ed. Proceedings of Orebody Modelling and Strategic Mine Planning, 2014 Perth, Australia. Australasian Institute of Mining and Metallurgy, 195–200.

De Carli, C. & De Lemos, P.R. 2015. Project optimization. *REM: R. Esc. Minas,* 68, 97–102.

Ilog, I. 2015. Cplex reference manual and software. 12.6.3.0 ed. Pullman, WA, USA: ILOG S.A. and ILOG Inc.

King, B., Goycoolea, M. & Newman, A. 2016. Optimizing the open pit-to-underground mining transition. *European Journal of Operational Research,* 257, 297–309.

Kurppa, R. & Erkkilä, E. Changing from open pit to underground mining at pyhasalmi. Rock Mechanics Symposium, 1967 Helsinki. 239–247.

Lerchs, H. & Grossman, I.F. 1965. Optimum design of open-pit mines. *The Canadian Mining and Metallurgical Bulletin,* 58, 47–54.

Luxford, J. 1997. Surface to underground-making the transition, in proceedings of the international conference on mine project development. *In:* Barnes, E. (ed.) *The Australasian Institute of Mining and Metallurgy.* Sydney: AusIMM.

Macneil, J. a. L. & Dimitrakopoulos, R. 2017. A stochastic optimization formulation for the transition from open pit to underground mining. *Springer*, 21.

Mathworks, I. 2018. Matlab software. *In:* Mathworks (ed.) 9.4.0.813654 (R2018a) ed.: Mathworks Inc.

Opoku, S. & Musingwini, C. 2013. Stochastic modelling of the open pit to underground transition interface for gold mines. *International Journal of Mining, Reclamation and Environment,* 27, 407–424.

Ordin, A.A. & Vasil'ev, I.V. 2014. Optimized depth of transition from open pit to underground coal mining. *J Min Sci,* 50, 696–706.

Roberts, B., Elkington, T., Van Olden, K. & Maulen, M. 2013. Optimising combined open pit and underground strategic plan. *Mining Technology.* Maney on behalf of the Institute and The AusIMM.

Whittle, D., Brazil, M., Grossman, P.A., Rubinstein, J.H. & Thomas, D.A. 2018. Combined optimisation of an open-pit mine outline and the transition depth to underground mining. *European Journal of Operational Research,* 000, 1–11.

Multi-collocated cokriging: An application to grade estimation in the mining industry

N. Madani

School of Mining and Geosciences, Nazarbayev University, Astana, Kazakhstan

ABSTRACT: Geostatistical modeling of cross-correlated variables in deposits is of paramount importance for mineral resource evaluation. The resulting constructed block model is expected to re-establish this correlation among the variables. Independent estimation, however, may be inadequate as the data correlation is not taken into account precisely. To tackle this problem, cokriging approach can be used. Nevertheless, cokriging system may be unstable when dealing with numerous amount of sample points. Reducing the size of cokriging system can be introduced as a choice, to circumvent this difficulty, by considering a sub-set of data. Multi-collocated cokriging in this respect, as an offshoot of collocated cokriging approach provides much trustworthy results. In this study, three searching strategies are selected to estimate the gold grade in a deposit. The results showed that Multi-collocated cokriging in the case of moving neighborhood bear resemblance to Multi-collocated kriging in the case of unique neighborhood.

1 INTRODUCTION

Cokriging is used in the earth sciences for predicting coregionalized variables at locations where no observation is available. Application fields include mineral resource assessment (Journel & Huijbregts, 1978, Pan et al. 1993, Gálvez & Emery, 2011), petroleum reservoir modeling (Xu et al. 1992, Hohn, 1999) groundwater hydrology (Boezio et al. 2006, Dalla Libera et al. 2017, Olea et al. 2018). Cokriging is of particular importance when the variable of main interest (hereafter called primary variable) is sparsely sampled and is correlated with one or several secondary variables that are available extensively at the locations where the primary variable must be predicted (Vargas-Guzmán & Jim Yeh, 1999, Wackernagel, 2003). However, in such a case, applying cokriging may be problematic due to the computational requirements caused by the large number of data to process (Emery, 2009, Chilès and Delfiner, 2012). This situation motivates the need to reduce the number of data to be used in the cokriging system, by considering the data located in a neighborhood of the target location and dropping out all the remaining data. In this respect, several strategies have been proposed to select the neighboring data, such as the strictly collocated cokriging approximation (Xu et al., 1992), where a single data of each secondary variable (the one situated at the target location) is retained, or the multi-collocated approximation (Rivoirard, 2001), which also incorporates the secondary data that are collocated with the primary data. These two neighborhoods have been extensively applied in petroleum reservoir modeling, wherever the secondary variable (e.g. seismic) exhaustively available at target locations, contributing to the modeling process of porosity and permeability (Pyrcz and Deutsch, 2014). Madani & Emery (2018) showed that multi-collocated cokriging outperforms the collocated cokriging in terms of variance of estimation error. However, the application of both cokriging systems in mining industry is somehow neglected due to unavailability of exhaustive secondary data. Instead, borehole information obtaining from mineral deposits may show different sampling patterns, in which some variables share some sample locations, namely "partially heterotopic" (Wackernagel, 2003, Goovaerts, 1997, Rossi and Deutsch, 2014). In this respect,

the secondary variable, which represents more availability, is of paramount importance for estimation of primary variable, particularly if there exist an interdependency characteristics between them. Hierarchical cokriging procedure, in this paper, introduces an innovative algorithm to estimate the variables in turn, rather than simultaneously. This methodology integrates multi-collocated cokriging to estimate the primary variable beyond the secondary variables that is estimated beforehand in hierarchical sequence. The goal of this paper is threefold: First, it is of interest to provide a background about the co-estimation methodologies, theory behind and the algorithm proposed. Second, a real case study is presented from a copper deposit that gold grade as the primary variable is estimated, based on the proposed algorithm, condition to the primary variable, copper grade which already estimated. Last, the results are then compared with traditional cokriging approaches and relevant discussion is provided as conclusion.

2 METHODOLOGY

2.1 Ordinary cokriging system

Ordinary cokriging is an extension of ordinary kriging, allows predication of primary and secondary variable by taking into account their cross-correlated structures (Wackernagel, 2003; Chilès and Delfiner, 2012). Stationary characteristics of mean values are restricted to a local neighborhood centered on the location x being estimated. The ordinary cokriging system for prediction of primary variable, Y_1 in the case of a single secondary variable, Y_2 considering the direct and cross-covariance are defined as (Goovaerts, 1997):

$$
\begin{cases}
\sum_{\beta_1=1}^{n_1(x)} \varphi_{\beta_1}^{OCK}(x) C_{11}\left(x_{\alpha_1}-x_{\beta_1}\right) + \sum_{\beta_2=1}^{n_2(x)} \varphi_{\beta_2}^{OCK}(x) C_{12}\left(x_{\alpha_1}-x_{\beta_2}\right) + \mu_1^{OCK}(x) = C_{11}\left(x_{\alpha_1}-x\right) \\
\qquad \alpha_1 = 1,\ldots,n_1(u) \\
\sum_{\beta_1=1}^{n_1(x)} \varphi_{\beta_1}^{OCK}(x) C_{21}\left(x_{\alpha_2}-x_{\beta_1}\right) + \sum_{\beta_2=1}^{n_2(x)} \varphi_{\beta_2}^{OCK}(x) C_{22}\left(x_{\alpha_2}-x_{\beta_2}\right) + \mu_2^{OCK}(x) = C_{21}\left(x_{\alpha_2}-x\right) \\
\qquad \alpha_2 = 1,\ldots,n_2(u) \\
\qquad\qquad\qquad \sum_{\beta_1=1}^{n_1(x)} \varphi_{\beta_1}^{OCK}(x) = 1 \\
\qquad\qquad\qquad \sum_{\beta_2=1}^{n_2(x)} \varphi_{\beta_2}^{OCK}(x) = 0
\end{cases}
\tag{1}
$$

where $\varphi_\alpha^i (i=1, 2)$ is the weight assigned to the data $Y_i(x_{i,\alpha})$ of the i-th variable Y_i at the α-th data location $x_{i,\alpha}$ ($\alpha=1, \ldots n_i$) of this variable, x is the location targeted for prediction; μ_1^{OCK} and μ_2^{OCK} represent the Lagrange parameters, accounting for the two unbiasedness constraints; C_{ij} is the direct ($i=j$) or cross ($i \neq j$) covariance between variables Y_i and Y_j (i, j = 1, 2). The previous equations can be generalized to the case with more than one secondary variable, at the price of heavier notation, which will not be considered in this work. Note that the numbers of data are not necessarily the same for the primary and secondary variables, a case known as a heterotopic sampling design (Wackernagel, 2003) in opposition to the isotopic (equally-sampled) case.

Different neighborhood strategies can be used to reduce the number of data for cokriging. For instance, a single search strategy selects the data locations that are geographically the closest to the target location x, irrespective of which variables are known at those locations.

2.2 Ordinary multi-collocated cokriging system

In multi-collocated cokriging system, the secondary variable is retained at both target location x and sample locations, wherever the primary variable is available and share same coordinates with secondary variable. In the case of a single secondary variable, the cokriging predictor and the error variance are built up with (Rivoirard, 2001; Wackernagel, 2003; Chilès and Delfiner, 2012):

$$\begin{cases} \sum_{\beta_1=1}^{n_1(x)} \varphi_{\beta_1}^{OMCK}(x) C_{11}\left(x_{\alpha_1}-x_{\beta_1}\right) + \sum_{\beta_2=1}^{n_2(x)} \varphi_{\beta_2}^{OMCK}(x) C_{12}\left(x_{\alpha_1}-x_{\beta_2}\right) + \varphi_2^{OMCK}(x) C_{12}\left(x_{\alpha_1}-x\right) \\ \quad + \mu^{OMCK}(x) = C_{11}\left(x_{\alpha_1}-x\right) \qquad \alpha_1 = 1,\ldots,n_1(u) \\ \sum_{\beta_1=1}^{n_1(x)} \varphi_{\beta_1}^{OCK}(x) C_{21}\left(x_{\alpha_2}-x_{\beta_1}\right) + \sum_{\beta_2=1}^{n_2(x)} \varphi_{\beta_2}^{OCK}(x) C_{22}\left(x_{\alpha_2}-x_{\beta_2}\right) + \varphi_2^{OMCK}(x) C_{22}\left(x_{\alpha_1}-x\right) \\ \quad + \mu^{OCK}(x) = C_{21}\left(x_{\alpha_2}-x\right) \qquad \alpha_2 = 1,\ldots,n_2(u) \\ \qquad\qquad \sum_{\beta_1=1}^{n_1(x)} \varphi_{\beta_1}^{OCK}(x) + \sum_{\beta_1=1}^{n_1(x)} \varphi_{\beta_2}^{OCK}(x) + \varphi_2^{OMCK}(x) = 1 \end{cases} \qquad (2)$$

with the same notations as in the previous subsection.

2.3 *Coregionalization modeling*

Solving the cokriging system in both cases, requires the knowledge of the direct and cross-covariances between the primary and secondary variables. In this respect, the linear model of coregionalization is widely used to fit such covariances, owing to its mathematical simplicity and tractability (Journel and Huijbregts, 1978; Goovaerts, 1997; Wackernagel, 2003). In this model, the direct and cross-covariances $C_{ij}(h)(i,j=1,2)$ are defined as weighted sums of L basic covariances, also called basic nested structures:

$$C_{ij}(h) = \sum_{l=1}^{L} b_{ij}^l c_l(h) \qquad (3)$$

where, for each structure $(l=1,\ldots L)$, $(b_{ij}^l)_{i,j=1,2}$ is a 2×2 real-valued, symmetric, positive semi-definite matrix (coregionalization matrix) and $c_l(h)$ is a permissible stationary covariance model (basic nested structure). In practice, such a model can be fitted to a set of experimental direct and cross-covariances by means of semi-automated algorithms (Goulard and Voltz, 1992; Emery, 2010).

2.4 *Proposed algorithm*

The multi-collocated cokriging is subjected to availability of the secondary variable at target locations. This requirement is frequently met in oil reservoir characterization, since the secondary variable (e.g. seismic) is exhaustively available entire the region. Taking into account this valuable information, the primary variable such as porosity and permeability can be modeled in 3-dimension by multi-collocated cokriging. However, in the mining industry, the secondary information may be rarely available exhaustively at target location and instead, one, commonly is dealing with different sampling patters such as heterotopic, in which the primary and secondary variables share partially some locations and leading to more availability of secondary variable. In this case, an algorithm proposed in this study, namely hierarchical searching strategy, in order of utilizing the multi-collocated cokriging system for mining applications. This theory is inspired from hierarchical joint simulation algorithm already proposed by Almeida and Journel (1994) for simulating the variables in turn rather than simultaneously taking into account the collocated cokriging. Interested readers are referred to Goovaerts (1997) for more information about the latter approach. Based on this, the proposed algorithm for cokriging of two variables in multi-collocated cokriging, proceeds as follows:

1. Define the hierarchy of variables, starting with the most important or better auto-correlated variable with more availability, Y_2
2. Estimate Y_2 at target locations x by ordinary kriging to define the parameters of conditional cumulative distribution function of the secondary variable Y_2 at all the target locations. The conditioning information in this step is just the values of secondary variable.
3. Use ordinary multicollocated cokriging to estimate Y_1 taking into account the information available from Y_2, already estimated at target locations and also the original Y_2 accompanying the primary variable Y_1 at sample locations.

This procedure needs modeling the full matrix of cross-covariance functions. In second step, only the direct variograms of secondary variable is enough for accomplishing this step. The simple cokriging systems also can be substituted for ordinary cokriging systems in the case that the mean values for both variables are perfectly known in the study area. This algorithm is implemented in a copper deposit as a case study, aiming at estimation of gold grade taking into account the copper grade as secondary variable which is more available. The results are then compared with traditional ordinary cokriging approaches, considering the isotopic searching strategy.

3 ACTUAL CASE STUDY

The case study belongs to a copper deposit obtained from borehole campaign. Two variables are available at sample locations, Copper (Cu) and Gold (Au). Au is undersampled in relation to Cu, indicating the partially heterotopic sampling pattern. In order to preserve the confidentiality of data set, the name and location of deposit are not disclosed. Following the proposed algorithm, the copper grade can be considered as secondary variable due to more availability and gold grade can be taken into account as primary variable or target variable to be estimated in the region. Since the sampling pattern is irregular, it is required that the dataset is declustered to provide more representative statistical parameters. To do so, cell declustering is chosen based on dimension of 50 m*50 m*12 m. The declustered statistical parameters are illustrated in Table 1. Figure 1 also shows the declustered histogram distribution. Shape of distribution in copper grades approximately follow the log-normal distribution and in gold grades follow exponential distribution, respectively.

In order to check the bivariate relation between the underlying variables, correlation coefficient is computed through the isotopic locations, wherever both information are accessible as $\rho = 0.76$. Scatter plot, showing interrelationship of gold grade versus copper grade, accompanying with relatively high correlation coefficient (Fig. 2), shows that there exist a satisfying

Table 1. Declustered statistical parameters for copper and gold grades.

Parameter	Au (ppm)	Cu (%)
Number of data	902	2376
Mean	2.79	0.90
Variance	34.95	0.342
Minimum	0	0.12
Maximum	68.82	7.24
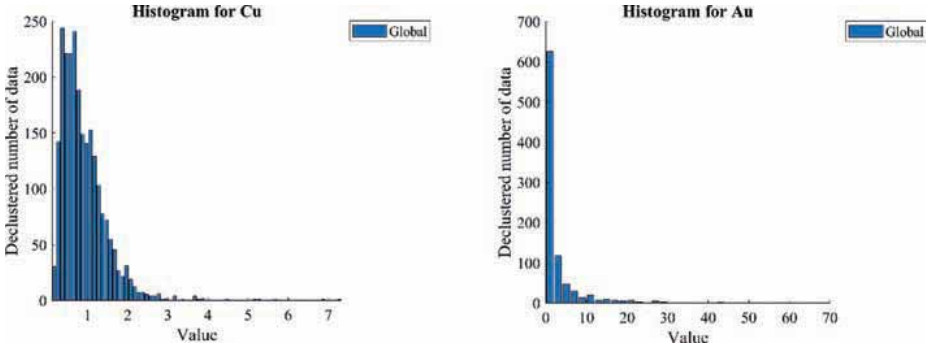
Figure 1. Diclustered histogram of copper and gold grades.
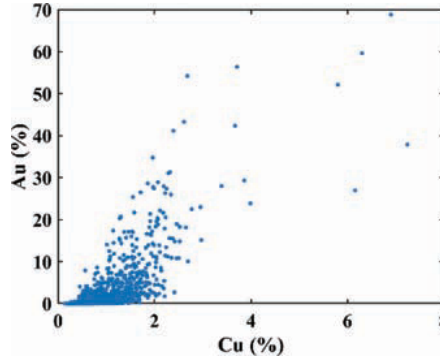
Figure 2.   Scatter plot between copper and gold grades with correlation coefficient, 0.76.

dependency between two primary and secondary variables and, consequently motivates one to utilize cokriging algorithms rather than independent kriging modeling.

3.1   Joint estimation of gold and copper grades

In this section, it is of interest to estimate the gold and copper grades in the region following the proposed algorithm presented in Section 2.4.

Step 1:   because of more availability of copper grade, this variable is selected as secondary variable and gold grade as primary variable. The idea is then using gold grade as target variable for estimation.

Step 2:   the copper grade is then estimated by ordinary kriging system (Section 2.1) independent of gold grade, taking into account the spatial continuity obtained from direct variogram analysis of copper values itself. Since no special anisotropy detected in horizontal plane, one omni-directional variogram in plan and one vertical variogram are accounted for describing the spatial distribution of copper grade. For theoretical variogram inference, a model composed of one nugget effect and two spherical structures (Eq. 4) are fitted to experimental points (Fig. 3). The fitting can be implemented based on manual or semi-automatic process (Emery, 2010, Goulard & Voltz, 1992).

$$\gamma(h) = 0.083 + 0.19Sph(15m,15m,180m) + 0.1Sph(100m,100m,180m) \qquad (4)$$

Once the variogram model is inferred, the ordinary cokriging system is solved and the copper grade are estimated at target locations. In this respect, a 3D grid is created consisting of 33,792 node numbers and 12.5 m*12.5 m*11 m of support dimension for each, to entirely cover the sampling region. The neighborhood is moving with conditioning up to 100 surrounding data characterized by radiuses equal to 200 m, derived from the variogram analysis. The produced map for elevation 125 m is depicted in Figure 4.

Step 3:   once the estimated values of copper grade (i.e. secondary variable) are attained in all the target blocks, ordinary multi-collocated cokriging algorithm can be applied for estimation of gold grade (i.e. primary variable). In this regard, the copper values are considered not only at target locations (output of step 2), but also they need to be acknowledged at sample locations. Solving this reduced cokriging system, likewise requires the direct and cross-variograms of primary and secondary variable inferred from the data available at sample locations. The problem for cross-variogram in this case is related to the type of sampling pattern. Since the dataset is heterotopic, computation of this function, entails removing some of sample points, in which just the copper grade is

162
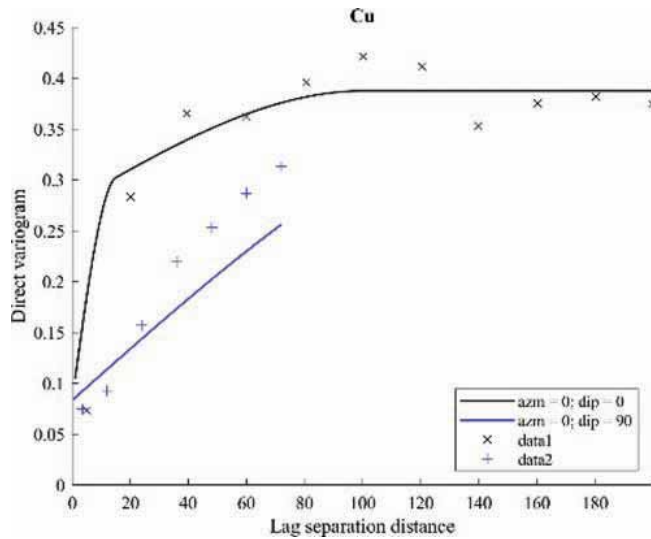
Figure 3. Variogram analysis for copper grade; cross points represent the experimental variogram and solid lines introduce the theoretical fitted variogram model.
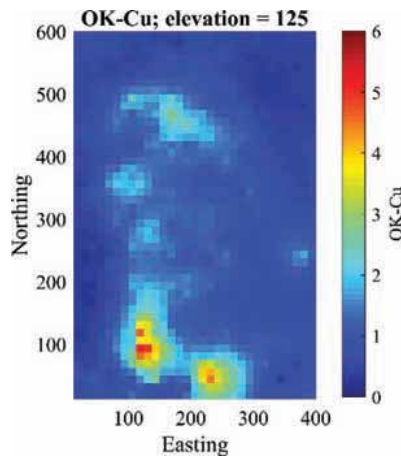
Figure 4. Section plan for estimation of copper at target location irrespective of gold grade at elevation: 125 m.

available; leading to loose valuable information. To circumvent this difficulty, the direct and cross-covariances, instead are highly advocated to be employed for such a joint spatial continuity modeling, for which all the sample points, including those which share only the secondary variable can also be retained. Figure 5 shows the direct and cross-covariances obtained from gold and copper grade at sample locations preserving the heterotopic characteristics of pattern. Following the same instruction as stated in step 2 for direct variogram fitting of copper grade, the semi-automatic procedure is used for fitting the direct and cross-covariance structures, thanks to the linear coregionalization model condition, including one nugget effect and one spherical model:
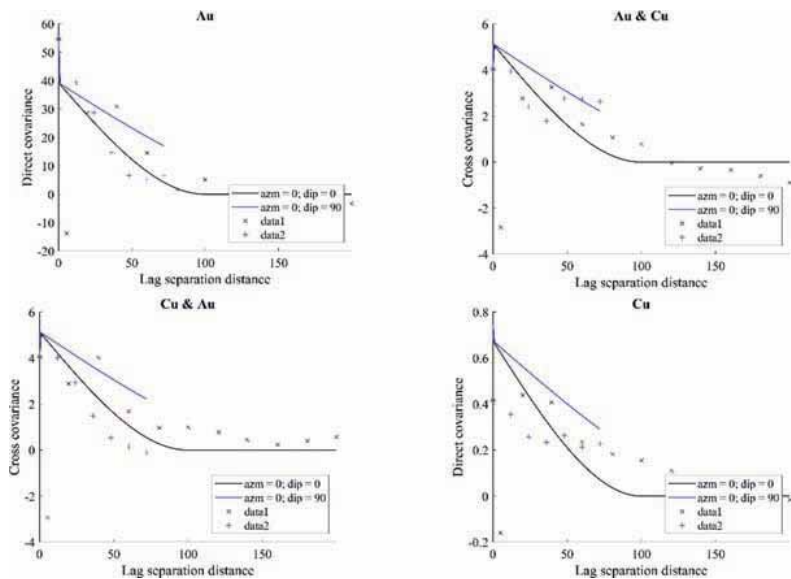
Figure 5. Direct and cross-covariances obtained from two variables, gold and copper grades taking into account their heterotopic sampling pattern.

$$\begin{pmatrix} Cov_{Au} & Cov_{Au/Cu} \\ Cov_{Cu/Au} & Cov_{Cu} \end{pmatrix} = \begin{pmatrix} 15.37 & -1.06 \\ -1.06 & 0.07 \end{pmatrix} nugget + \begin{pmatrix} 39.24 & 5.14 \\ 5.14 & 0.67 \end{pmatrix} Sph(100m, 100m, 180m) \quad (5)$$

Positive semi-definite condition of the sill matrix was also examined. This implies that the fitted linear model of coregionalization is mathematically sound and the direct and cross-covariances can be used for establishing the ordinary multi-collocated cokriging system. To do so, the same moving neighborhood characterization as it was used for estimation of the copper grade, is considered in this case. A neighborhood with conditioning up to 100 surrounding data characterized by radiuses equal to 200 m, derived from the direct and cross-covariances. In order to make a comparison, a unique neighborhood in ordinary multi-collocated cokriging system is also considered for benchmarking. In this cokriging paradigm, which is theoretically sound, one uses all the conditioning data for estimation process, for which it does not lead to a loss of accuracy that may happen in moving neighborhood (Emery, 2004). However, the computation restrictions is one reason to switching from unique to moving neighborhood in usual co-estimation workflows. Conventional cokriging system also is taken into account for further testing the algorithm. To do so, an isotopic searching strategy is opted, in which 100 closest sampling points containing both the primary and secondary variables are attended in a moving neighborhood. This practice is indeed typical in block modeling for mineral resource estimation in mining industry.

Figure 6 illustrates the produced maps for the target variable, gold and also secondary variable, copper. In all the maps, the results of estimated gold grades in ordinary multi-collocated cokriging for the case of moving neighborhood bear relatively resemblance to the case of ordinary multi-collocated cokriging with unique neighborhood. In copper grade, however the results are exactly the same in two underlying maps, because two methods use the same estimated copper grade values as secondary information which already was produced through step 1 by ordinary kriging. The outputs for traditional ordinary cokriging system with isotopic searching strategy is, however somehow different in some areas. For instance, in coordinate (East: 200 m and North: 450 m), the latter approach is failed to estimate the high values of gold and copper grade. Nevertheless, the smoothing effect in all the cases show the same outcome due to (co)-kriging assumptions. Another examination over the three methodologies relates to
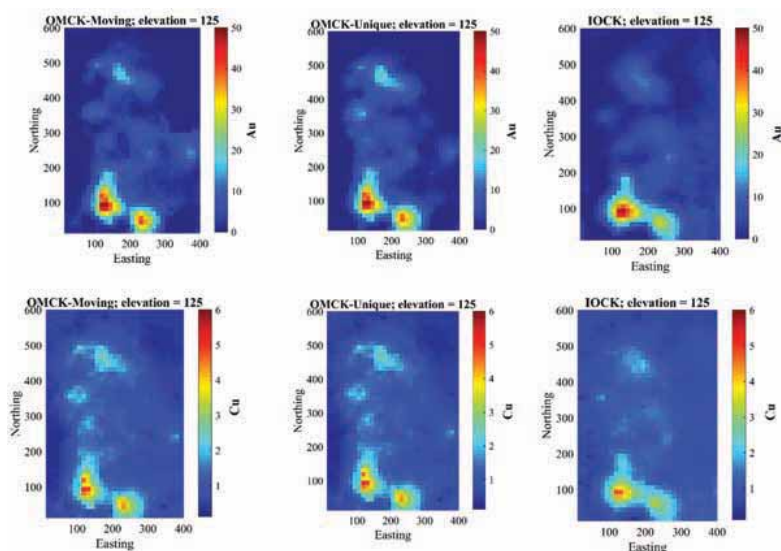
Figure 6. Cokriging maps obtained from ordinary multicollocated cokriging (left: moving neighborhood (OMCK – Moving) and middle: unique neighborhood (OMCK – Unique) and right: traditional ordinary cokriging (isotopic search – moving neighborhood (IOCK)); first row: estimated gold grade and second row: estimated copper grade.
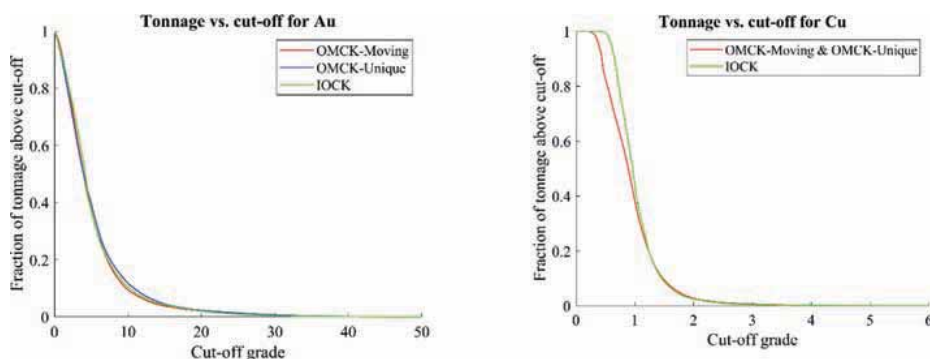
Figure 7. Grade-tonnage curves for estimated gold and copper grades.

the ability in precisely calculation of estimation variance. Application of variance map in mining industry, for instance, involves the mineral resource categorization based on international standards. This parameter is an index of data configuration, ranking the resource blocks model on the basis of available information (e.g., borehole data) and level of confidence (Rossi and Deutsch, 2014). The ordinary multi-collocated cokriging variances in both cases of moving and unique neighborhoods are then computed block-by-block and compared with the variance measures obtained from traditional ordinary cokriging algorithm with isotopic search and moving neighborhood. In Figure 7, the fraction of tonnage-cut off grades are illustrated as well. The differences among the values are not very significant for three methodologies.

Figure 8 depicts the distribution of cokriging variance in boxplot. As can be seen, the ordinary multi-collocated cokriging resulted in minimum variance, while the isotopic ordinary cokriging produces the maximum variance. The output for cokriging variance in multi-collocated cokriging with moving neighborhood is approximately closer to ordinary multi-collocated cokriging with unique neighborhood. This results corroborate the trustworthy in cokriging variances

165
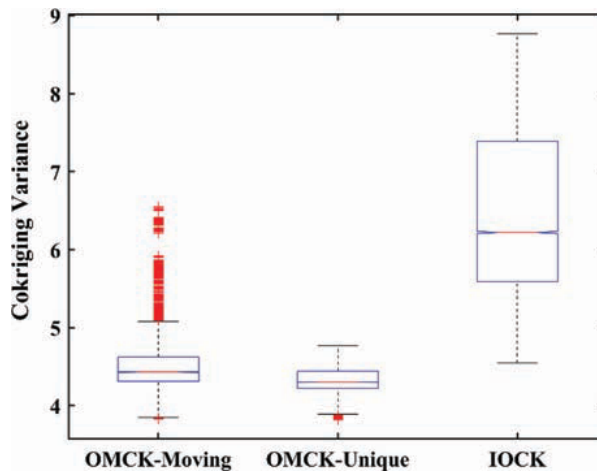
Figure 8. Cokriging variances obtained from ordinary multi-collocated cokriging with both moving and unique neighborhood and traditional ordinary cokriging with isotopic search and moving neighbourhood.

and show that although ordinary multi-collocated cokriging is able to manage the minimum amount of variance, however the moving neighborhood also in an acceptable level of accuracy following the same variability as unique neighborhood in this type of cokriging system.

4 CONCLUSION

Cokriging is of paramount importance in the case when one is dealing with estimation of cross-correlated variables. Reproducing the intrinsic interdependency among the variables entails employing some sophisticated geostatistical algorithms that not only they are mathematically sound, but also can meet the requirements of industry. A hierarchical approach in this paper is presented for integration with multi-collocated cokriging system for estimation of primary variable while the secondary variable is exhaustively available at target locations. This algorithm can be of particular interest for modeling the variables with heterotopic sampling pattern, in which the secondary variable is more available at sampling locations. Following the proposed algorithm, the secondary variable first should be estimated at all target locations and then be taken into account for estimation of primary variable by ordinary multi-collocated cokriging. This workflow implemented and tested through a copper deposit, in which the primary or target variable for estimation is gold grade and secondary variable with more availability is copper grade. The results are then compared with traditional cokriging approach that is very common tool in mining industry. Comparison of estimated maps and variance results explained that first of all, multi-collocated cokriging outperforms the traditional approaches of cokriging method that is very common in mining industry and second, moving neighborhood in multi-collocated cokriging system produces the closest results to unique neighborhood. It is highly recommended to use this hierarchical approach in mining industry especially whenever is dealing with mineral resource categorizations.

REFERENCES

Almeida, A.S., Journel, A.G., 1994. Joint simulation of multiple variables with a Markov-type coregionalization model. *Mathematical Geology 26(5):* 565–588.
Boezio, M.N.M., Costa, J.F.C.L., Koppe, J.C., 2006. Kriging with an external drift versus collocated cokriging for water table mapping. Transactions of the Institutions of Mining and Metallurgy, Section B: Applied Earth Science 115(3): 103–112.

Chilès, J.P., Delfiner, P., 2012. Geostatistics: Modeling Spatial Uncertainty. Wiley, New York.

Dalla Libera, N., Fabbri, P., Mason, L., Piccinini, L., Pola, M., 2017. Geostatistics as a tool to improve the natural background level definition: An application in groundwater. *Science of the Total Environment 598*: 330–340.

Emery, X., 2004. Testing the correctness of the sequential algorithm for simulating Gaussian random fields. *Stochastic Environmental Research and Risk Assessment 18(6)*, 401–413.

Emery, X., 2009. The kriging update equations and their application to the selection of neighboring data. *Computational Geosciences 13(3):* 269–280.

Emery, X., 2010. Iterative algorithms for fitting a linear model of coregionalization. *Computers & Geosciences 36(9):* 1150–1160.

Gálvez, I., Emery, X., 2011. Multivariate resources modelling: which data are relevant for cokriging? *In:* Beniscelli, J., Kuyvenhoven, R., Hoal, K.O. (eds.), *Proceedings of the 2nd International Seminar on Geology for the Mining Industry. Gecamin Ltda*, Santiago, Chile, pp. 10.

Goovaerts, P., 1997. Geostatistics for Natural Resources Evaluation. Oxford University Press, New York.

Goulard, M., Voltz, M., 1992. Linear coregionalization model: tools for estimation and choice of cross-variogram matrix. Mathematical Geology 24(3): 269–286.

Hohn, M.E., 1999. Geostatistics and Petroleum Geology, 2nd edn. Kluwer Academic, Dordrecht, The Netherlands.

Journel, A.G., Huijbregts, C.J., 1978. Mining Geostatistics. Academic Press, London.

Madani, N., Emery, X. (2018). "A comparison of search strategies to design the cokriging neighborhood for predicting coregionalized variables". *Stochastic Environmental Research and Risk Assessment,* DOI: 10.1007/s00477-018-1578-1. In press.

Olea, R.A., Raju, N.J., Egozcue, J.J., Pawlowsky-Glahn, V., Singh, S., 2018. Advancements in hydrochemistry mapping: methods and application to groundwater arsenic and iron concentrations in Varanasi, Uttar Pradesh, India. *Stochastic Environmental Research and Risk Assessment 32(1)*: 241–259.

Pan, G., Gaard, D., Moss, K., Heiner, T., 1993. A comparison between cokriging and ordinary kriging: Case study with a polymetallic deposit. *Mathematical Geology* 25(3): 377–398.

Pyrcz M, Deutsch CV (2014) Geostatistical reservoir modeling. Oxford University Press, New York.

Rivoirard, J., 2001. Which models for collocated cokriging? *Mathematical Geology 33(2)*: 117–131.

Rossi M, Deutsch CV (2014) Mineral resource estimation. Springer, New York

Vargas-Guzmán, J., Jim Yeh, T.C. 1999. Sequential kriging and cokriging: two powerful geostatistical approaches. *Stochastic Environmental Research and Risk Assessment* 13(6): 416–435.

Wackernagel, H., 2003. Multivariate Geostatistics: an introduction with Applications. Springer, Berlin.

Xu, W., Tran, T.T., Srivastava, R.M., Journel, A.G., 1992. Integrating seismic data in reservoir modeling: the collocated cokriging alternative. *In: 67th SPE Annual Technical Conference and Exhibition. Society of Petroleum Engineers, SPE paper 24742*, pp. 833–842.

Xu, W., Tran, T.T., Srivastava, R.M., Journel, A.G., 1992. Integrating seismic data in reservoir modeling: the collocated cokriging alternative. *In: 67th SPE Annual Technical Conference and Exhibition. Society of Petroleum Engineers, SPE paper 24742*, pp. 833–842.

Recursive convolutional neural networks in a multiple-point statistics framework

Sebastian Avalos & Julian M. Ortiz

The Robert M. Buchan Department of Mining, Queen's University, Canada

ABSTRACT: This work proposes a new technique for Multiple-Point Statistics simulation based on a Recursive Convolutional Neural Network approach (RCNN). A study on the architecture of the network is done to ensure that the spatial structure of the phenomenon inferred from a training image and its associated uncertainty are properly captured. A sensitivity analysis over the main architecture parameters is performed on a two dimensional binary image. Statistical and spatial metrics are determined to quantify the impact of each parameter as well as the ability to capture the underlying phenomenon.

Keywords: Geostatistics, Deep Learning, Training Image, Categorical Variable

1 INTRODUCTION

Multiple-point statistics (MPS) simulation has seen an explosive development since Strebelle's seminal paper in 2002 (Strebelle, 2002). Many different approaches have been proposed (Arpat & Caers, 2007; Mariethoz et al., 2010; Parra & Ortiz, 2011) and some have reached industrial applications (Mariethoz et al., 2010). The methods associated to MPS are intimately related to image and texture analysis (Daly, 2004; Parra & Ortiz, 2011; Zahner et al., 2015). Excellent reviews of multiple-point simulation methods are available (Tahmasebi, 2018) and further theoretical and practical details can be found (Mariethoz & Caers, 2014).

This paper is motivated by the possibilities offered by deep learning methods, particularly Convolutional Neural Networks (CNNs) (LeCun et al., 1998) which have shown extraordinary performances in image analysis, including classification, reconstruction, segmentation, labeling and more (Dosovitskiy et al., 2015; Eilertsen et al., 2017; Gatys et al., 2016; He et al., 2016). The main aim is to create a bridge between CNNs and MPS. This is done by proposing a Recursive Convolutional Neural Network (RCNN) approach that enables the architecture to learn features of an underlying phenomenon from a training image and then perform simulations on different domains reproducing the phenomenon complexity.

2 RELATED WORK

MPS simulation provides a framework for spatial modeling of variables in geoscience problems. The reproduction of complex patterns and spatial uncertainty assessment are their main goals. They can be applied for continuous or categorical variables and the methods can be extended to the multivariate case, suiting applications in diverse fields (oil and gas, hydrological reservoirs, ore deposits).

CNNs belong to a set of deep learning architectures with great abilities on image analysis. Their features extraction properties, from raw images, have made them suitable for a variety of image analysis applications. Connecting neural networks with MPS is not new (Caers & Journel, 1998) however deep learning techniques have only recently been connected to MPS (Laloy et al., 2018).

CNNs are a natural extension of neural networks to inputs in a grid-like topology. Usually, the nature of inputs vary from temporal 1D/2D data, RGB images (3D) and Videos (4D) while the nature of outputs are either a probability vector, for classification tasks, or a continuous vector, for regression problems.

Their main feature of sharing inner parameters across the network leads to architectural properties of scale, shift and distortion invariance, making them a powerful tool for image feature extraction. Those properties mean that regardless where and how a specific raw feature appears in the image, a suitable and well-trained CNN is able to capture that feature. Once features are extracted, images can be classified, segmented or even reconstructed.

CNNs are composed by a *feature extraction* block and a *classification* block (Fig. 1). The first block receives a grid-like topology input and extracts representative features in a hierarchical manner. The second block receives the top hierarchical feature and delivers a final matrix of prediction.

From now on, a two dimensional image grid-like topology is used to illustrate and describe the inner process of a CNN. The building blocks of the feature extraction section are:

X: Input image. Dimensions $\left(in_x, in_y, in_d\right)$, where x and y are spatial dimensions while d is the respective depth.

W_m: Filter. Dimensions $\left(w_x^{(m)}, w_y^{(m)}, w_d^{(m)}, w_c^{(m)}\right)$, where x and y are spatial dimensions, d is the corresponding depth and c the number of channels in the filter.

B_m: Bias vector.

H_m: Hidden layer. Dimension $\left(h_x^{(m)}, h_y^{(m)}, h_d^{(m)}\right)$, with x and y spatial dimensions and d is the depth.

where H_m results of convolving W_m over $\boldsymbol{H}_{m-1}$, adding a bias vector b_m and then passing the temporary result through (1) a Batch-Normalization function, (2) a non-linear activation function and (3) a pooling function as:

$$
\boldsymbol{H}_m = \begin{cases} X & \text{if } m = 0 \\ pool\left(g\left(BN\left(\boldsymbol{W}_m \boldsymbol{H}_{m-1} + \boldsymbol{b}_m\right)\right)\right) & \text{if } 0 < m \leq M \end{cases} \tag{1}
$$

A convolution is understood as the process of sliding the filter over the input while performing the sum of an element-wise multiplication between the filter values and the corresponding section of the input. The input size $\left(in_x, in_y, in_d\right)$ is fixed and the user must define the two dimensional size of every filter $\left(w_x^{(m)}, w_y^{(m)}\right)$ and the respective number of channels $w_c^{(m)}$. Each channel creates a feature map in the hidden layer, so there will be as many features maps $h_d^{(m)}$ as channels in the filter $w_c^{(m)}$. The $w_d^{(m)}$ corresponds to the number of previous feature maps. Every feature map must be taken into account for an adequate feature extraction so $w_d^{(1)} = in_d$ and $w_d^{(m)} = h_d^{(m-1)}$.
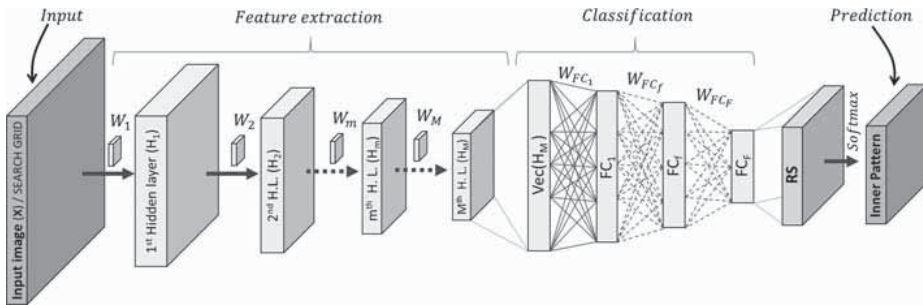
Figure 1. CNN architecture showing the features extraction and classification zones together with main notations.

Activation functions, $g(\cdot)$, a set of non-linear transformations are required to suitably extract features. They are applied element-wise over each feature map in the hidden layers. Some activation functions are *Sigmoid*, *TanH* and *ReLU*. Each activation function has an active zone, that is, an interval where the derivative of the function is not zero.

The Batch Normalization function (BN) (Ioffe & Szegedy, 2015) normalizes $(W_m H_{m-1} + b_m)$ before passing it through the activation function by subtracting the mean and dividing by their respective standard deviation over each feature map. This process has three main properties: (1) it avoids vanishing gradient problems during training, by adjusting the input values to the active zone; (2) it accelerates the training process; and (3) it serves as a regularization method.

The pooling function, $pool(\cdot)$, seeks to reduce the size of the representative hidden layer by taking small regions of each feature map. Several functions exist including the widely used *max pooling*, and others such as *average pooling*, *min pooling* and *L2-norm pooling*. They are usually applied to go from a moving window of (2, 2) to a single value (size (1, 1). *Max pooling* keeps only the maximum value among the nodes in the small region. This pooling function significantly reduces the number of learning parameters, improving statistical efficiency and reducing the memory storage consumption (Goodfellow et al., 2016).

The classification section is composed by a set of feedforward networks (Hornik et al., 1989) whose building blocks are:

W_{FC_f} : weight matrix. Dimensions $\left(n_{FC}^{(f)}, n_{FC}^{(f-1)}\right)$ corresponding to the previous fully connected layer size and the next fully connected desired size.

B_f; bias vector.

FC_f; hidden fully connected layer. Dimensions $\left(n_{FC}^{(f)}, 1\right)$.

where FC_f results of a matrix multiplication between W_{FC_f} and FC_{f-1}, adding a bias vector b_f and then passing the temporary result only by (1) a Batch-Normalization function and (2) an activation function as:

$$FC_f = \begin{cases} Vec(H_M) & \text{if } f = 0 \\ g\left(BN\left(W_{FC_f} FC_{f-1} + b_f\right)\right) & \text{if } 0 < f \leq F \end{cases} \tag{2}$$

The first feedforward network FC_0 corresponds to a vector-representation $Vec(H_M)$ of the last hidden layer in the feature extraction block. The BN and activation functions act exactly as presented before.

When categorical distributions are required, the final layer FC_F must have the same dimensions as the number of categories. Let K be the number of categories, $n_{FC}^{(F)} = K$, and $s_k \in \{s_1, ..., s_K\}$ the non-normalized conditional probability of each class in FC_F. By passing FC_F through a softmax function:

$$\hat{p}(k) = \frac{e^{s_k}}{\sum_{c=1}^{K} e^{s_c}} \tag{3}$$

the expected conditional probabilities for each class are obtained. When P continuous points are required to be predicted, a usual technique is to apply another fully connected layer $FC_{F+1} = g\left(W_{FC_{F+1}} FC_F + b_{F+1}\right)$ where $W_{FC_{F+1}}$ has dimensions $\left(P, n_{FC}^{(F)}\right)$ and the activation function depends on the nature of the predicted variable, that is, if the expected output is in the range $[0,s] s \in \mathbb{R}^+$ a ReLU function seems suitable, while outputs with a normal gaussian distribution would be better treated with a Sigmoid or TanH function.

Inner parameters $\left(\Theta = \{W, b\}\right)$ are initialized as random values from a normal gaussian truncated function. Optimum Θ values are obtained as result of training the CNN by applying the Adam optimizer (Kingma & Ba, 2014) algorithm. The loss functions to minimize during training (Eq. (4)) for categorical variables, considering the predicted probability of each class (Eq. (3)) and the real probability $p(k)$, is the negative log-likelihood of the Cross Entropy

(*CE*), and for continuous values the Mean Squared Error (*MSE*) between each predicted value $\hat{y}_k$ and the real one y_k:

$$CE : \mathcal{L}(\Theta) = -\sum_{k=1}^{K}(\log \hat{p}(k)) \cdot p(k) \quad MSE : \mathcal{L}(\Theta) = \frac{1}{P}\sum_{k=1}^{P}(\hat{y}_k - y_k)^2 \qquad (4)$$

3 THE RECURSIVE CONVOLUTIONAL NEURAL NETWORK APPROACH

Let SG $(sg_x, sg_y, 1)$ and IP $(ip_x, ip_y, 1)$ be the search grid and inner pattern, whose dimensions sg_x, sg_y, ip_x and ip_y are odd positive integers to ensure the existence of a collocated center (Fig. 2. Left). In MPS terms, the SG is the neighbourhood (template) that contains the data event d_n (conditioning data).

The main idea is that a first CNN_1 is trained to predict a conditional cumulative distribution function (ccdf) of each node inside an IP by receiving, as input, a data event (d_n) embedded in a SG (Fig. 2. Left). Then a second CNN_2 is trained to predict the same ccdf but now knowing the same input and the IP predicted by the previous CNN_1. The third CNN_3 is trained using same input and the two previously predicted IP by CNN_2 and CNN_1. The process can be done again (Fig. 2. Right) giving the *recursiveness* property to the RCNN approach. The idea behind the recursiveness is the improvement on results quality by taking into account the previously simulated information.

The input must be preprocessed as the phenomenon representation matters in order to efficiently and effectively capture complex inner features (Goodfellow et al., 2016). The input has known nodes with categories $s_k \in \{s_1,...,s_K\}$ and unknown nodes treated as zeros. One way to go is to assume unknown nodes as another category s_0 and then assigning to each s_k category the associated value in the range [0,2], in equidistant K intervals. In the binary case ($K = 2$) the result transformation is $[s_0, s_1, s_2] = [0,1,2]$. Using the notation of Section 2, the size of FC_F is imposed, $n_{FC}^{(F)} = ip_x \times ip_y \times K$, so it can be reshaped into a matrix $\mathbf{RS}$ with dimensions (ip_x, ip_y, K). At each location $(a,b) \in \mathbf{RS}$, a vector $v_K = [s_1,...,s_K]$ is passed through Eq. (3) to obtain the expected conditional probability of each state s_k as:

$$\hat{p}(k \mid \mathbf{RS}_{a,b}; (X,\Theta)) = \frac{e^{s_k(\mathbf{RS}_{a,b};(X,\Theta))}}{\sum_{c=1}^{K} e^{s_c(\mathbf{RS}_{a,b};(X,\Theta))}} \qquad (5)$$

Once $\mathbf{RS}$ has passed through the softmax function, the final predicted category, at each location (*a*, *b*), of the inner pattern can be obtained by taking the most probable category as:

$$IP_{a,b} = \underset{k \in K}{\arg\max}\, \hat{p}(k \mid \mathbf{RS}_{a,b}; (X,\Theta)) \qquad (6)$$
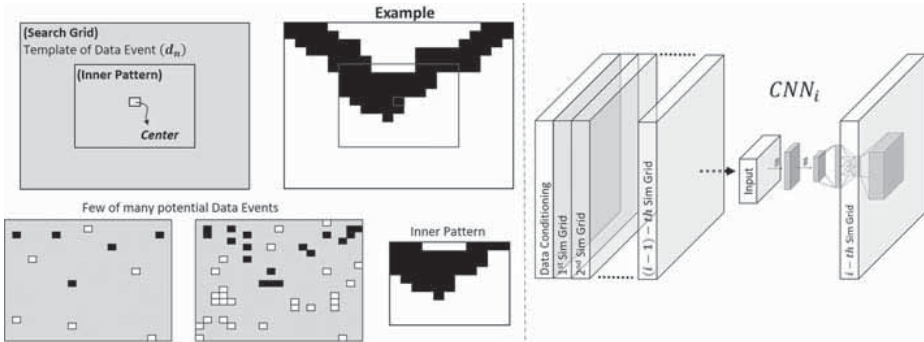
Figure 2.   (Left) Illustration of search gird and inner pattern concepts together with a simple 2D binary example. (Right) Scheme of the CNN_i in a RCNN architecture.

Let D be the domain to simulate and N the number of CNNs to be used, the RCNN architecture is expressed as:

$$X^i = \begin{cases} SG(D^0) & \text{if } i = 1 \\ \begin{bmatrix} X^{i-1} & SG(D^{i-1}) \end{bmatrix} & \text{if } 1 < i \leq N \end{cases}$$

$$H^i_m = \begin{cases} X^i & \text{if } m = 0 \\ MaxPool_{2x2}\left(ReLU\left(BN\left(W^i_m H^i_{m-1} + b^i_m \right) \right) \right) & \text{if } 0 < m \leq M^i \\ ReLU\left(BN\left(W^i_m H^i_{m-1} + b^i_m \right) \right) & \text{if } m = M^i \end{cases} \tag{7}$$

$$FC^i_f = \begin{cases} Vec\left(H^i_M \right) & \text{if } f = 0 \\ ReLU\left(BN\left(W^i_{FC_f} FC^i_{f-1} + b^i_f \right) \right) & \text{if } 0 < f \leq F^i \end{cases}$$

$$RS^i = reshape\left(FC^i_F, \left(ip_x, ip_y, K \right) \right)$$

$$IP^i = \underset{k \in K}{\arg\max}\, \hat{p}(k \mid RS^i; \left(X^i, \Theta^i \right))$$

where the CNN_i has M^i hidden layers and F^i fully connected layers. All activation functions are $ReLU$ and all hidden layers in the feature extraction zone have a max pooling function of 2×2 except he last one.

The RCNN training algorithm starts by creating $N + 1$ simulation grids (domains), namely $D^0, D^1, ..., D^N$, whose dimensions are equal to the TI and then extracting a random percentage of hard data $\left(perDC, \text{ suggesting } perDC \in [0.1, 5.0] \right)$ from the TI and assigning them to all D^i. The simulation process, explained later, is carried. Once all D^i are simulated, every pair-list database (DB^i) of input-output as $X^i \leftrightarrow IP^{Real}$ is created in order to train the respective CNN_i. This is done by extracting $\forall i SG(D^i)$ in order to create $\mathbf{X}^i$ and the respective collocated IP^{Real}. Using the CE of Eq. (4) and notation of Eq. (5), the loss function of each CNN_i is:

$$\mathcal{L}_i(\Theta^i) = -\sum_{a=1}^{ip_x} \sum_{b=1}^{ip_y} \sum_{k=0}^{K} (\log \hat{p}(k \mid RS_{a,b}; (X^i, \Theta^i))) \cdot p(k \mid IP_{a,b}^{Real}; (X^i)) \tag{8}$$

Eq. (8) represents the sum of all CE in IP between the predicted conditional probability (Eq. (5)) and the real probability $p(k)$ from IP^{Real}. Any location (a, b), whose category in IP^{Real} is k, has a real probability vector of $[0..1..0]$ with 1 at the k-position, so Eq. 8 is highly simplified when calculated. Each CNN_i receives a mini-batch of m samples from DB^i and estimates the gradient with respect to the loss function, $\nabla_\Theta \mathcal{L}_i(\Theta^i) \approx \nabla_\Theta \left[1/m \sum_{k=1}^{m} \mathcal{L}_i(\Theta^i; X^i_k) \right]$, and performs a parameter update $\Theta^i_t \leftarrow \Theta^i_t + \Delta\Theta^i$ by inferring the updated direction $\Delta\Theta^i$ with respect to the gradient $\nabla_\Theta \mathcal{L}_i(\Theta^i)$ by using the Adam Optimizer (Kingma & Ba, 2014). After all CNN_i have been trained by all mini-batches, the first epoch is completed. The entire process is carried out again as many times as the number of epochs previously defined, or until the entire network shows signs of convergence.

The RCNN simulation process begins by migrating the conditioning data to the closet node at each D^i. First D^1 is fully simulated, then D^2 until D^N is completely informed. The sequence of nodes to be simulated at each D is given by the same random path, previously defined. Following that path and at unknown locations over D^i, the collocated SG associated to $D^{i-1}, D^{i-2}, ..., D^0$ are extracted, concatenated and fed into the CNN_i to obtain the IP^i. Then, instead of freezing all IP^i values in D^i, only a random percentage of them are selected and frozen at unknown locations. Particularly, the unknown center is always simulated. The percentage of random values used across this paper is 50%.

172

4 EXPERIMENTS

By exploring a two dimensional binary case and performing parameter sensitivities, the RCNN approach is illustrated and a simple guide of RCNN architecture definition is provided. Figure 3 (Left) shows a binary random field with 250 by 250 pixels used as a TI. Another image, Figure 3 (Center), with the same structural features is used as Ground Truth (GT). The TI is used to train the RCNN while the GT is used to extract conditioning data and assess performance. During simulations, 1% of conditioning data (Fig. 3 (Right)) are randomly extracted and used by all realizations. Then, realizations are compared with GT in order to understand the impact of the TI, and the relevance of hard data and the RCNN architecture.

The base case, that serves as a reference in the sensitivity analysis, consists of a RCNN with 4 nested CNNs all with the same architecture, following the structure of Figure (7) with 4 hidden layers ($M^i = 4$), 3 fully connected layers ($F^i = 3$) and two categories ($K = 2$). The rest of the inner parameters are:

$\mathbf{X}^i$:   Search Grid (input image). Dimensions: $\left(sg_x, sg_y, sg_d\right) \leftarrow (23, 23, i)$

$\mathbf{W}_m^i$:   Filter. Dimensions: $\left(w_x^{(m)}, w_y^{(m)}, w_d^{(m)}, w_c^{(m)}\right) \leftarrow \left(3, 3, w_d^{(m)}, 128\right)$

$\mathbf{H}_m^i$:   Hidden layer. Dimension: $\left(h_x^{(m)}, h_y^{(m)}, h_d^{(m)}\right) \leftarrow \left(h_x^{(m)}, h_y^{(m)}, 128\right)$

$\mathbf{W}_{FC_f}^i$:   Weight matrix. Dimensions: $\left(n_{FC}^{(f)}, n_{FC}^{(f-1)}\right) \leftarrow \left(3000, n_{FC}^{(f-1)}\right)$

$\mathbf{FC}_f^i$:   Hidden fully connected layer. Dimensions: $\left(n_{FC}^{(f)}, 1\right) \leftarrow (3000, 1)$

$\mathbf{IP}^i$:   Inner pattern (output). Dimensions: $\left(ip_x, ip_y, 1\right) \leftarrow (23, 23, 1)$

Although bias vectors are not depicted in the previous expressions, they are used. The dimensions $w_d^{(m)}, h_x^{(m)}, h_y^{(m)}$ and $n_{FC}^{(f-1)}$ are not defined since they depend on m or f. Over the previous architecture, the set of parameters $\left\{\left(sg_x, sg_y\right), \left(ip_x, ip_y\right), h_d^{(m)}, n_{FC}^{(f)}\right\}$ are tuned independently in order to capture their impact over the final simulated domain.

A variety of metrics are used to compare each hyper-parameter combination (Table 1) based on their ability to reproduce the spatial complexity of the phenomenon *Visualizations:* one random realization, the *E*-type over a hundred realizations and the respective local
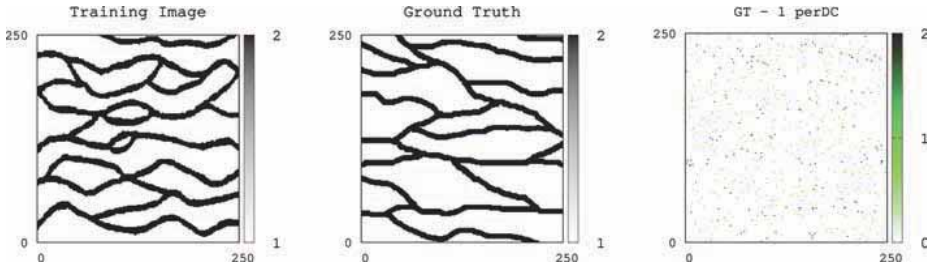
Figure 3. Binary structure channels. (Left) Training Image. (Center) Ground Truth. (Right) 1% of hard data randomly selected from ground truth.

Table 1. Set of values for each parameter sensitivity.

Parameters	Values						
$sg_x \times sg_y \wedge ip_x \times ip_y$	11×11	15×15	19×19	23×23	27×27	31×31	35×35
$\forall m\, h_d^{(m)}$	16	32	64	128	256	384	512
$\forall f\, n_{FC}^{(f)}$	100	500	1500	3000	5000	6250	7500

variance map. *Variograms*: horizontal and vertical experimental variograms over the TI, GT and each realization are compared, providing a measure of the two-points statistics. *Binary proportion* (**BP**): the number of channel nodes (pixels) over the total number of nodes in the simulation grid. *Pixel Error*: having obtained the *E*-type over a hundred realizations, a threshold based on the GT binary proportion can be applied to obtain the final categorical prediction (**T**) as:

$$T_{i,j} = \begin{cases} s_1 & if \ (E-type_{i,j}-s_1) < BP(s_2)/100, \\ s_2 & otherwise. \end{cases} \tag{9}$$

The pixel error is then the average of the absolute difference between the GT and **T**. This metric measures the accuracy of the RCNN to replicate exhaustively the GT.

5   RESULTS

5.1   *Sensitivity over search grid and inner pattern*

The sensitivity range, for SG and IP size, goes from 11×11 to 35×35. As 1% of randomly distributed hard data is used, the amount of expected informed nodes at SG are 1 and 12 for 11×11 and 35×35, to infer 121 and 1225 nodes at IP, respectively.

Visual results show that increasing the SG/IP size leads to a better pattern inference. By using small SG/IP, connectivity is not achieved. In that sense, using a SG of 19×19 (~4 informed nodes) or bigger seems to be enough to capture connectivity. Similar responses are shown in the variographic analysis. Indeed, while 11×11 fails to reproduce the two point statistics, the 19×19 clearly improves this. However, good variogram reproduction is only achieved at 31×31. It is worth mentioning that all realizations follow the variographic behaviour of the ground truth. The statistical metrics confirm the previous trend.

5.2   *Sensitivity over hidden layer depths*

The sensitivity range over h_d goes from 16 to 512. The increase on the number of feature channels h_d leads to a loss of continuity in the structure. Indeed, the variance map with $h_d : 512$ shows less connectivity of the channels structure than $h_d : 16$. From a variographic perspective, using $h_d : 16$ leads to realization with spatial correlation similar to the GT, while larger h_d shows a worse variogram reproduction. The statistical metrics confirm the trend, and RCNN with $h_d : 16$ achieves the closest binary proportion respect to the GT.

5.3   *Sensitivity over fully connected sizes*

The sensitivity range over n_{FC} goes from 100 to 7500. From a visual perspective, the best result in terms of structure continuity and shape is achieved by $n_{FC} : 5000$. By using more or fewer nodes at the fully connected zone, the RCNN loses structure connectivity. The variographic analysis supports the visual analysis. Indeed, the best variogram reproduction is achieved with $n_{FC} : 5000$, followed by $n_{FC} : 100$. The statistical metrics support the conclusion that $n_{FC} : 5000$ achieves the best results, with the lowest pixel error and the binary proportion closest to the GT

All previous sensitivity analyses have been carried out by varying each variable independently, leading to the following set of optimum parameters:

$$\left(sg_x, sg_y\right) \equiv \left(ip_x, ip_y\right) \leftarrow (19,19) \qquad h_d \leftarrow 16 \qquad n_{FC} \leftarrow 5000 \tag{10}$$

Using the previous optimum parameters, a simulation with 100 realizations is carried out and results over the last domain (D^4) are shown in Figure 4.
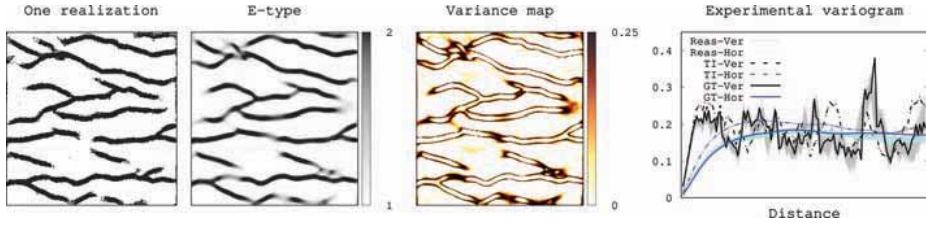
Figure 4. One realization, E-type, variance map and variographic analysis over D^4, using optimum parameters.
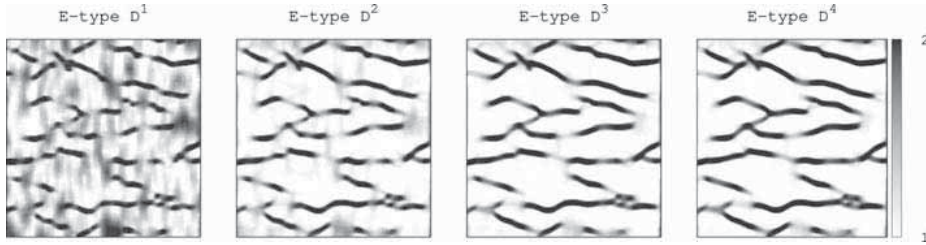
Figure 5. E-types over each domain using 100 realizations using the base case.

5.4 *Recursiveness*

Section 3 discusses the theoretical benefits of the recursive approach, where CNN_1 is trained to infer the closest IP from a finite number of hard data while $CNN_{i|i>1}$ learns how to remediate the lack of previous information by improving the quality of the inferred IP.

D^1 has some artefacts due to the lack of information but on D^4 the structures get connected and almost every artefact has been erased. Realizations go from failing to reproduce the two-points statistics at D^1 to suitably reproduce the GT variogram at D^4. The pixel error decreases considerably from D^1 to D^4. The binary proportion does not seem to improve after D^2. Figure 5 shows E-types at each domain using 100 realizations and the base case parameters.

6 CONCLUSIONS

RCNN, a Recursive Convolutional Neural Network approach to perform Multiple-Point Statistics simulations was presented. The focus was mainly on the architecture of RCNN, and the training and simulation methodology to provide a clear understanding of the novel approach and a simple guide to define CNN inner architectures. Excellent results were achieved over a two dimensional binary case, showing the benefits of bringing deep learning techniques into the classical MPS framework.

By means of visualizations, variographic analysis and statistical metrics of continuity, the relevance of the amount of neurons at the classification zone has been stablished suggesting 5000 neurons, as well as the advantage of keeping a simple model with a depth in the hidden layers in the extraction feature zone of 16, and a search grid and inner pattern of 19×19.

Although no sensitivities on the amount of nested CNN were carried out, the benefits of using a RCNN with 4 nested CNN were clearly established suggesting the further use of at least four recursive CNN. Results are promising and further work must be carried out to achieve better results with less information.

ACKNOWLEDGMENTS

REFERENCES

Arpat, G.B. & Caers, J. *Conditional simulation with patterns*. Mathematical Geology, 39 (2):177–203, 2007.

Caers, J. & Journel, A.G. *Stochastic reservoir simulation using neural networks trained on outcrop data*. In SPE Annual Technical Conference and Exhibition. Society of Petroleum Engineers, 1998.

Daly, C. *Higher Order Models using Entropy, Markov Random Fields and Sequential Simulation*. In O. Leuangthong and C. Deutsch, editors, Geostatistics Banff 2004 (Quantitative Geology and Geostatistics, vol. 14), pages 215–224, 2004.

Dosovitskiy, A., Springenberg, J., & Brox, T. *Learning to generate chairs with convolutional neural networks*. In Proceedings of the IEEE Conference on Computer Vision and Pattern Recognition, pages 1538–1546, 2015.

Eilertsen, G., Kronander, J., Denes, G., Mantiuk, R., & Unger, J. *HDR image reconstruction from a single exposure using deep CNNs*. ACM Transactions on Graphics (TOG), 36(6):178, 2017.

Gatys, L., Ecker, A., & Bethge, M. *Image style transfer using convolutional neural networks*. In Proceedings of the IEEE Conference on Computer Vision and Pattern Recognition, pages 2414–2423, 2016.

Goodfellow, I., Bengio, Y., & Courville, A. *Deep learning*. Vol. 1. MIT press Cambridge, 2016.

He, K., Zhang, X., Ren, S., & Sun, K. *Deep residual learning for image recognition*. In Proceedings of the IEEE conference on computer vision and pattern recognition, pages 770–778, 2016.

Hornik, K., Stinchcombe, M, & White, H. *Multilayer feedforward networks are universal approximators*. Neural networks, 2(5):359–366, 1989.

Ioffe, S. & Szegedy, C. *Batch normalization: Accelerating deep network training by reducing internal covariate shift*. arXiv preprint arXiv:1502.03167, 2015.

Kingma, D. & Ba, J. *Adam: A method for stochastic optimization*. arXiv preprint arXiv:1412.6980, 2014.

Laloy, E., Herault, R., Jacques, D., & Linde, N. *Training Image Based Geostatistical Inversion Using a Spatial Generative Adversarial Neural Network.* Water Resources Research, 54(1):381–406, 2018.

LeCun, Y., Bottou, L., Bengio, Y., & Haffner, P. *Gradient-based learning applied to document recognition*. Proceedings of the IEEE, 86(11): 2278–2324, 1998.

Mariethoz, G. & Caers, J. *Multiple-point geostatistics: stochastic modeling with training images*. John Wiley & Sons, 2014.

Mariethoz, G., Renard, P. *The direct sampling method to perform multiple point geostatistical simulations*. Water Resources Research, 46(11), 2010. W11536.

Parra, A. & Ortiz, J. *Adapting a texture synthesis algorithm for conditional multiple point geostatistical simulation*. Stochastic Environmental Research and Risk Assessment, 25(8):1101–1111, 2011.

Strebelle, S. *Conditional simulation of complex geological structures using multiple point statistics*. Mathematical geology, 34(1):1–21, 2002.

Tahmasebi, P. *Multiple Point Statistics: A Review*. Handbook of Mathematical Geosciences, page 613, 2018.

Zahner, T., Lochbuhler, T., Mariethoz, G., & Linde, N. *Image synthesis with graph cuts: a fast model proposal mechanism in probabilistic inversion*. Geophysical Journal International, 204(2):1179–1190, 2015.

Grade estimation in a tabular deposit using unstructured grids

M.A.A. Bassani, C.P. Araújo & J.F.C.L. Costa
Federal University of Rio Grande do Sul, Porto Alegre, Brazil

ABSTRACT: Tabular deposits are known to have two dimensions much larger than a third one (e.g., bauxite deposits, gold reefs, coal strata). Grade estimation in these deposits is often performed at regular Cartesian grids, whose blocks have the same size. The problem is that regular Cartesian grids do not adapt well to the geological solid used to define the shape and volume in this kind of mineral deposit. Better modeling of the geological solid may be obtained with unstructured grids, whose blocks have different sizes. This work presents the use of these grids for grade estimation in a bauxite deposit. The methodology to build the unstructured grid is shown. Then the grades were estimated in the unstructured grid by ordinary kriging. The resulting grade model was checked by visual inspection, swath plot, and cross validation. Results showed that the estimates reproduced the trend of the data and were globally unbiased.

1 INTRODUCTION

Most geostatistical software tools work with regular Cartesian grids, whose blocks have the same size and shape. Grids are often denoted as block models in the mining industry. The problem is that regular Cartesian grids usually do not fit well the geological solid of tabular deposits. Tabular deposits are deposits whose dimensions along two directions are much larger than the dimension in a third direction (i.e., bauxite and coal deposits). For grade estimation in these deposits, many users work with block models in two dimensions.

The estimates in 2D block models are performed with the variables accumulation (product of grade and thickness) and thickness (Krige 1978, Bertoli *et al.* 2003, Marques *et al.* 2014). The grade estimates are obtained by dividing the accumulation estimates by the thickness estimates. This approach eliminates the vertical component (Z), resulting in a two-dimensional (2D) model. The problem with this method is that a 2D block model does not allow the mine planner to take into account the vertical selectivity during mining planning. As a result, the mine planner may not use a 2D block model to test mining scenarios with different vertical selectivity.

A common approach used in petroleum geostatistics involves transforming the coordinates to the depositional space and fitting a regular Cartesian grid in the depositional space (Mallet 2002, Mallet 2004, Caumon et al. 2004, Pyrcz & Deutsch 2014). Geostatistical modeling is then performed in the depositional space. Finally, the grid is back-transformed to the real space. This approach results in a grid whose number of cells (blocks) in the vertical direction is the same. The problem with this approach is that the volumes of the blocks vary a lot after the grid is back-transformed to the real space. This variation in the volume of the blocks is not desired for mining planning when the vertical selectivity is roughly constant.

Another possibility is to use an unstructured grid, which may have a different number of cells (blocks) in any direction. Moreover, the unstructured grid is very flexible, as its cells may have different sizes and shapes. Unstructured grids have been used in the petroleum industry to obtain more realistic models (Manchuk 2010). However, they have been little used in the mining industry.

This work presents a case study of grade estimation using an unstructured grid in a tabular mineral deposit. The methodology for building the unstructured grid is presented. The case study used data obtained from a bauxite deposit in Brazil. The estimates were performed

using ordinary kriging. The grade model was checked by visual inspection, swath plots, and cross validation.

2   DATA SET PRESENTATION

The data are derived from a bauxite deposit in Brazil, and the variable of interest is Recoverable Alumina (AA). Figure 1 shows a location map of the data. The sparsest sampling spacing is roughly 200×200 meters along the X and Y directions while the densest sampling spacing is about 25×25 meters along the X and Y directions. Furthermore, the area contains intermediate sampling spacings of 100×100 meters and 50×50 meters along the X and Y directions. The samples were obtained from vertical drill holes, and the sampling length is 0.5 meter.

Cell declustering (Deutsch & Journel 1998) was performed in two dimensions. Pyrcz & Deutsch (2014) recommend performing cell declustering in two dimensions when the drill holes are vertical and fully intersect the formation. The cell size is 200 m along the X and Y directions and corresponds to the sampling spacing in the sparsely sampled areas. Figure 2 shows the Qq-plot between the original and declustered histograms of AA. The points in Figure 2 are close to line y = x and show that the two distributions are similar.
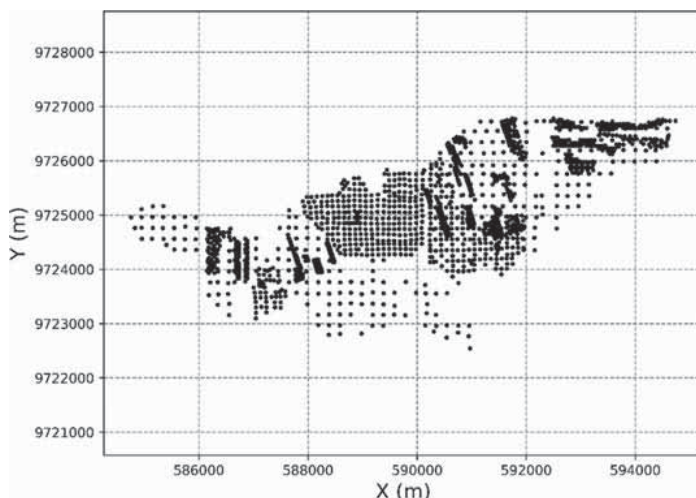
Figure 1.   Location map of the samples.
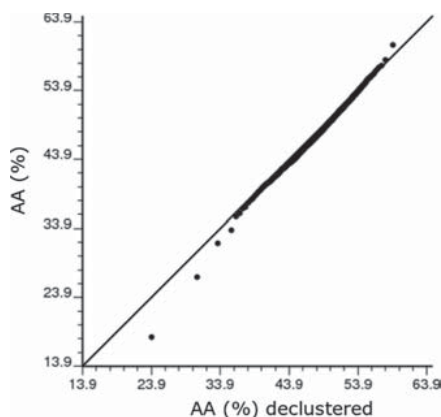
Figure 2.   Qq-plot between the original and declustered histograms of AA.

3 CONSTRUCTION OF UNSTRUCTURED GRID

The construction of the unstructured grid requires the surfaces of the top and base of the ore seam. These surfaces were obtained through the estimation of the Z coordinate of the top of the seam (Z_{top}) and Thickness. The estimated Z coordinate of the base (Z_{base}) was obtained as the estimates of Z_{top} minus the estimates of Thickness. Obtaining Z_{base} as Z_{top} minus Thickness mitigates the problem of obtaining estimates of Z_{base} greater than the estimates of Z_{top}.

The variogram models were fitted to the experimental variograms. The experimental variograms were standardized, so the sill equals one. Equations 1 and 2 describe the variogram models of Z_{top} and Thickness, respectively:

$$\gamma_{Ztop}(h) = 0.02 + 0.68 \cdot Sph\left(\frac{EW}{2000\,m}, \frac{NS}{1400\,m}\right) + 0.30 \cdot Sph\left(\frac{EW}{4000\,m}, \frac{NS}{1600\,m}\right) \quad (1)$$

$$\gamma_{Thickness}(h) = 0.50 + 0.20 \cdot Sph\left(\frac{EW}{90\,m}, \frac{NS}{90\,m}\right) + 0.30 \cdot Sph\left(\frac{EW}{800\,m}, \frac{NS}{800\,m}\right) \quad (2)$$

Z_{top} and Thickness were estimated using ordinary kriging. Point kriging was performed in a 2D grid with an areal resolution of 25×25 m. Figures 3a–c show the estimates of Z_{top}, thickness, and Z_{base} together with the data, respectively.

The unstructured grid used here discretizes the volume of the ore seam with cells that are irregular hexahedrons. Manchuk (2010) used unstructured grids whose cells were tetrahedrons. We chose to use hexahedrons because they represent better the selective mining unity (SMU). The algorithm to build the unstructured grid involves the following steps:

I. Get the Z coordinates of the 8 vertices that define the top and base of the ore seam and calculate the average thickness (average of the 4 vertical edges);
II. Calculate how many cells fit inside the average thickness based on the desired vertical resolution. The number of cells along Z is the closest integer to the fraction between the average thickness and the vertical resolution. If the average thickness is less than half the vertical resolution, no grid cell is built in this place;
III. Build the irregular grid with the number of cells calculated at step II.
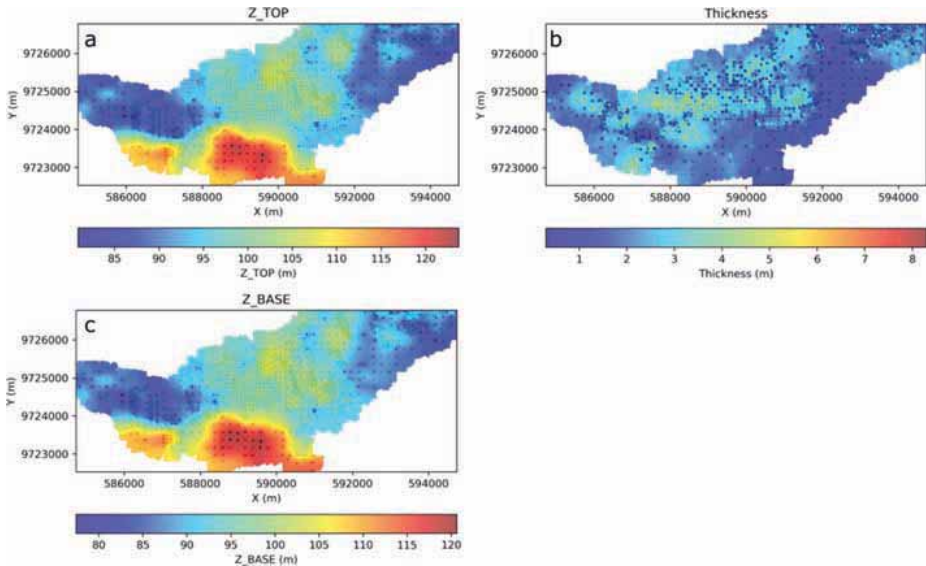
Figure 3.   Estimates of Z_{top} (a), Thickness (b) and Z_{base} (c).

179

Figure 4 shows a straightforward example. Suppose the vertical resolution is 0.5 meters, the thickness of one corner is 1 meter, and the thickness of the other corner is 1.2 meters (Fig. 4a). The resulting irregular grid will contain two cells. The corner with the smallest thickness will have cells with vertical edges of 0.5 meters and the corner with the largest thickness will have cells with vertical edges of 0.6 meters (Fig. 4b).

Figures 5a–b shows an arbitrary view and cross section of the unstructured grid, respectively. The unstructured grid reproduced the curvilinear features of the estimated surfaces.

The unstructured grid was compared with a regular Cartesian grid. The regular Cartesian grid was built using blocks of $25 \times 25 \times 0.5$ m. The blocks inside the geological surfaces were selected. Figures 6a–b show a cross section of the regular Cartesian grid and the unstructured grid, respectively. The unstructured grid reproduces better curvilinear features, as expected.
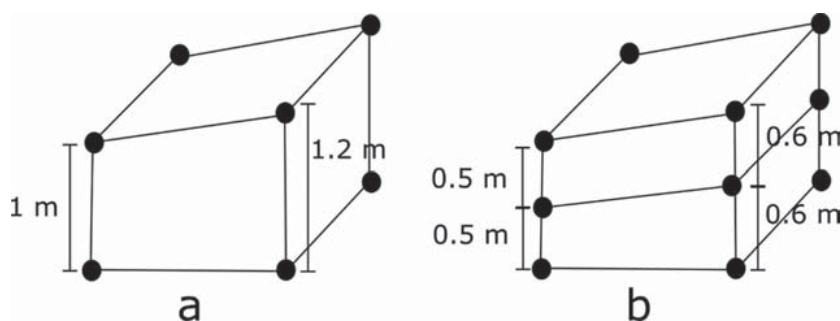
Figure 4. Schematic illustration of surfaces of top and bottom of ore seam (a) and irregular grid built using a vertical resolution of 0.5 meters (b).
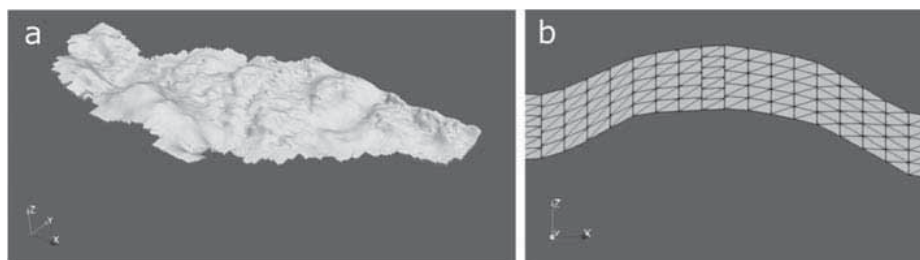
Figure 5. Arbitrary view (a) and cross section (b) of the unstructured grid. The vertical exaggeration is 25:1.
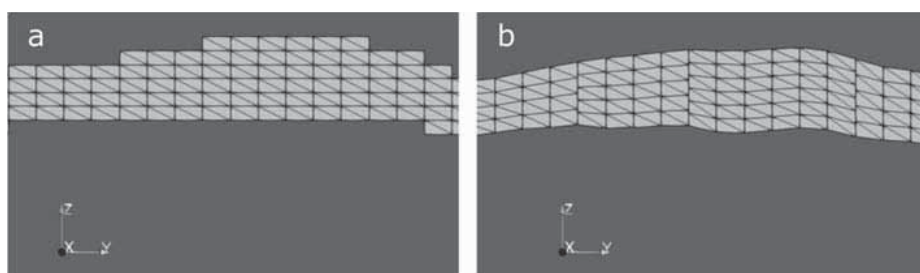
Figure 6. Cross section of the regular Cartesian grid (a) and unstructured grid (b). The vertical exaggeration is 25:1.
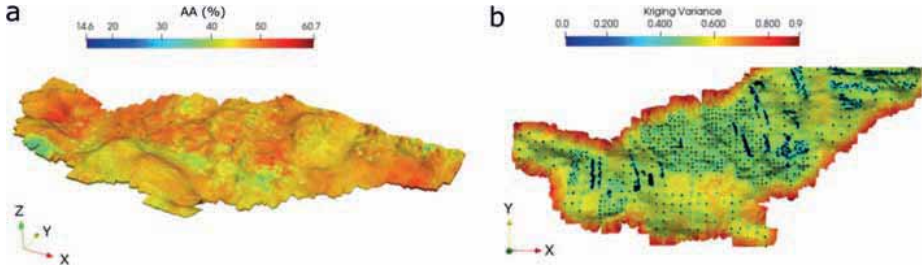
Figure 7. Estimates of AA (a) and kriging variance (b).

4 GRADE ESTIMATION IN UNSTRUCTURED GRID

The grade estimation in the unstructured grid involves three main steps: (i) change of coordinates, (ii) variogram analysis and modeling and (iii) estimation in unstructured grid.

4.1 *Change of coordinates*

The Z coordinates of the data set and of the unstructured were changed to stratigraphic Z coordinates. The stratigraphic coordinates were calculated as the Z coordinates minus the Z coordinate of the top of the seam. The experimental variograms and estimates were performed using the stratigraphic coordinates.

4.2 *Variogram analysis and modeling*

The experimental variograms were calculated using the stratigraphic coordinates. The variogram model was fitted to the experimental variograms. The experimental variograms were standardized, so the sill equals one. Equation 3 describes the variogram model of AA:

$$
\begin{aligned}
\gamma(h) = {}& 0.10 + 0.62\ Sph\left(\frac{NS}{60\ m}, \frac{EW}{60\ m}, \frac{vert.}{1.30\ m}\right) + 0.18\ Sph\left(\frac{NS}{700\ m}, \frac{EW}{700\ m}, \frac{vert.}{8.5\ m}\right) \\
& + 0.10\ Sph\left(\frac{NS}{5000\ m}, \frac{EW}{5000\ m}, \frac{vert.}{9\ m}\right)
\end{aligned}
\tag{3}
$$

The major direction of spatial continuity is horizontal while the minor direction of spatial continuity is vertical

4.3 *Estimates in unstructured grid*

The estimates were performed using ordinary block kriging. The block discretization was $5 \times 5 \times 1$. The shape of the irregular hexahedron cells were considered to calculate the covariances point-to-block and the kriging variance. Figure 7a shows an arbitrary view of the estimates in the unstructured grid. Figure 7b shows a plan view of the kriging variance together with the data (black points in Fig. 7b). The kriging variance is lower in the areas near the data, as expected.

5 MODEL VALIDATION

The grade model was checked with visual inspection, swath plot, and cross validation. Visual inspection consists of comparing visually the grade model with the samples. Figure 8 shows the grade model and the data using the same color scale. The high grade estimates are close to the high grade samples, as expected.
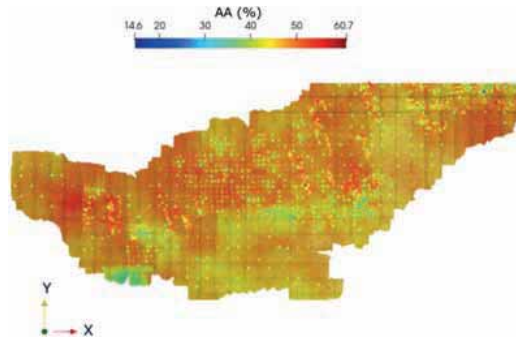
Figure 8.   Grade model and samples.
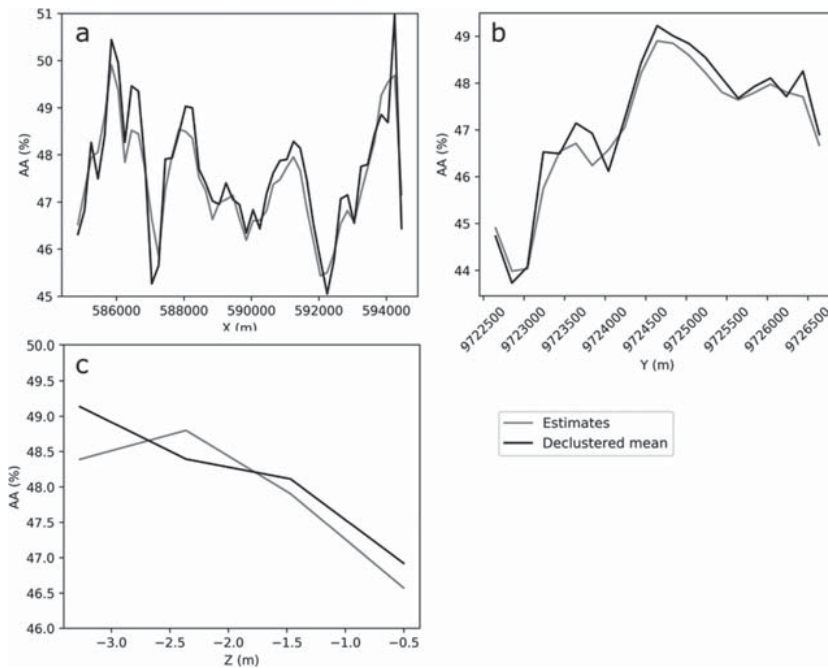
Figure 9.   Swath plots along the X (a), Y (b), and Z (c) directions.

Swath plot consists of first defining a series of swaths or slices along the X, Y, and Z directions. Then, the average grade of the model and the declustered average grade of the samples within the slices are compared. The samples were declustered with a nearest neighbour estimate. Figures 9a–c show the swath plots along the X, Y, and Z directions. The stratigraphic Z coordinate was used for the swath plot along the Z direction. The local mean of the estimates is consistent with the local mean of the data (see Fig. 9).

In the cross validation, first one sample at a particular location is removed. Second, the value is estimated at that location using the remaining samples. The same estimation parameters used in the estimation of the block model were used in the cross validation. The estimation error (the difference between the estimated and true value) was calculated. Furthermore, the estimated and true values were compared using a scatter plot.

Figure 10a shows the histogram of the estimation error obtained with cross validation. The histogram is symmetric and the mean is close to zero. This result indicates that the estimates are global unbiased. Figure 10b shows the scatter plot between the true and estimated values together
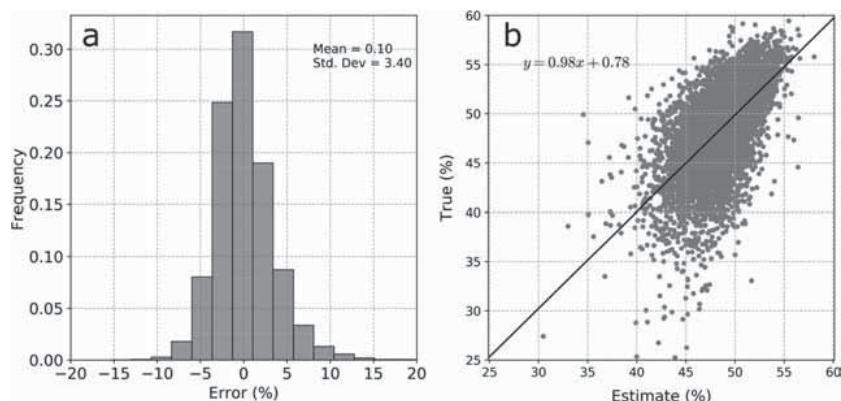
Figure 10. Histogram of estimation error (a) and scatter plot between estimated and true values (b) obtained with cross validation.

with the linear regression y = ax + b (black line in Fig. 10b). The slope of the linear regression is 0.98, which is very close to one. This result shows that the estimates have low conditional bias.

6 CONCLUSIONS

The paper shows a case study of grade estimation in a bauxite deposit using an unstructured grid. The methodology for the construction of the unstructured grid is explained. The unstructured grid is built using irregular hexahedrons whose average height is close to the vertical mining selectivity. The unstructured grid was compared visually to a regular Cartesian grid. The unstructured grid reproduced better the curvilinear shapes of the geological solid than the regular Cartesian grid.

The unstructured grid was populated with grade estimates. The estimates were performed with ordinary kriging. The estimates were consistent with the data and reproduced the trend of the data. Cross validation results show that the estimates were globally unbiased and had little conditional bias. The case study demonstrates that unstructured grids are suitable for grade estimation in tabular deposits.

REFERENCES

Bertoli, O., Vann, J., & Dunham, S., 2003. Two-dimensional geostatistical methods—theory, practice and a case study from the 1 A shoot nickel deposit, Leinster, Western Australia. In *Proceedings of the 5th international mining geology conference. The Australian Institute of Mining and Metallurgy, Melbourne* (pp. 189–195).

Caumon, G., Grosse, O., Mallet, J.L., 2004. High resolution geostatistics on coarse unstructured flow grids. In: Leuangthong O., Deutsch, C.V. (editors). Geostatistics Banff 2004. Springer, New York, pag. 703–712.

Deutsch, C.V., & Journel, A.G., 1998. Geostatistical software library and user's guide. *Oxford University Press, New York*.

Krige, D. (1978). Lognormal-de Wijsian geostatistics for ore evaluation. Johannesburg, South African Institute of Mining and Metallurgy. *Monograph Series*, *1*.

Mallet, J.L., 2002. Geomodeling. Applied geostatistics. Oxford University Press, New York.

Mallet, J.L., 2004. Space-time mathematical framework for sedimentary geology. Mathematical Geology, 36, 1, pag. 1–32.

Manchuk, J.G., 2010. Geostatistical modeling of unstructured grids for flow simulation. PhD thesis, University of Alberta, CA.

Marques, D.M., Rubio, R.H., Costa, J.F.C.L., & Silva, E.M.A.D., 2014. The effect of accumulation in 2D estimates in phosphatic ore. *Rem: Revista Escola de Minas*, *67*(4), 431–437.

Pyrcz, M.J., & Deutsch, C.V., 2014. *Geostatistical reservoir modeling*. Oxford university press.

Influence of drilling spacing on the mineral resources uncertainty

C.J.E. Silva, M.A.A. Bassani & J.F.C.L. Costa
*PPGE3M-Post-Graduation Program in Mining, Metallurgical and Materials Engineering, Federal
University of Rio Grande do Sul, Porto Alegre, Rio Grande do Sul, Brazil*

ABSTRACT: Rock cores from drilling works in mineral research activities are the main ore
modeling information and consume most of the budget. Data spacing should be optimized to
reduce uncertainties in the geologic model and mineral resource inventory. This paper inves-
tigates how the uncertainty of the mineral resources is influenced by distinct data spacings
through a case study on a bauxite mineralization in Brazilian Amazon plateau. The results
showed that the uncertainty of the mineral resource decreases as the data spacing decreases.
Depending on an acceptable uncertainty level, wider data spacings may be selected. This
optimal drilling data spacing may be defined using the uncertainty in the mineral resource
estimation, which is demonstrated in this case study.

1   INTRODUCTION

Mineral exploration aims at having a mineral resource statement, which plays a key role
to decide whether the mining project is feasible. These statements follow modern reporting
codes standards (CRIRSCO 2013). The Mineral Resources are classified as Measured, Indi-
cated or Inferred depending on the confidence of their estimation. Furthermore, the codes
encourage the quantification of the risk and uncertainty of the mineral resources. Usually,
the uncertainty of the resource model is lower where the data are more densely sampled.
However, a denser sampling grid is more expensive. In this paper, mineral resource is defined
as the tonnage and grade above a given cut-off and we aim to quantify the relationship
between data spacing and the uncertainty of the mineral resources. This relationship helps
the project manager to select the most appropriate data spacing. The appropriate data spac-
ing is that which results in an acceptable uncertainty of the resources and adheres to the
project's budget.

2   BACKGROUND TO GEOSTATISTICS

Geostatistical simulation is a method for characterizing uncertainty in earth sciences mod-
eling. It allows the generation of multiple equally probable realizations that honor the input
data, histogram, and variogram (Wild & Deutsch 2013). These realizations provide a meas-
ure of uncertainty about the phenomenon being modeled (Journel & Kyriakidis 2004).

The principle of sequential simulation, under a hypothesis of a multigaussian random
function, defines the Sequential Gaussian Simulation (SGS) (Isaaks 1990). When using SGS,
the data must be normally distributed. A normalization can be achieved by a normal score
transformation (Deutsch & Journel 1998). More details about mathematical proofs, param-
eters and applications of SGS can be found in several books (Goovaerts 1997, Deutsch &
Journel 1998, Journel & Ying 2001, Sinclair & Blackwell 2004).

Relevant works address the use of geostatistical simulation to measure the uncertainty and
its relation to data spacing (Wild & Deutsch 2013, Deutsch & Beardow 1999, Boucher et al.
2004, Journel & Kyriakids 2004, Pilger et al. 2001, Koppe et al. 2017). The methodology used
to develop our case study is similar to that used by Wild & Deutsch (2013).

3 METHODOLOGY

The methodology investigates how the uncertainty of the mineral resources is influenced by distinct data spacings and consists of the following steps (Fig. 1):

1. Exploratory Data Analysis and declustering;
2. Stratigraphic Correction;
3. Variogram analysis and modeling
4. Simulate realizations for reference distribution;
5. Sampling the simulated Reference Model at regular spacings n times to obtain databases with regular data spacing;
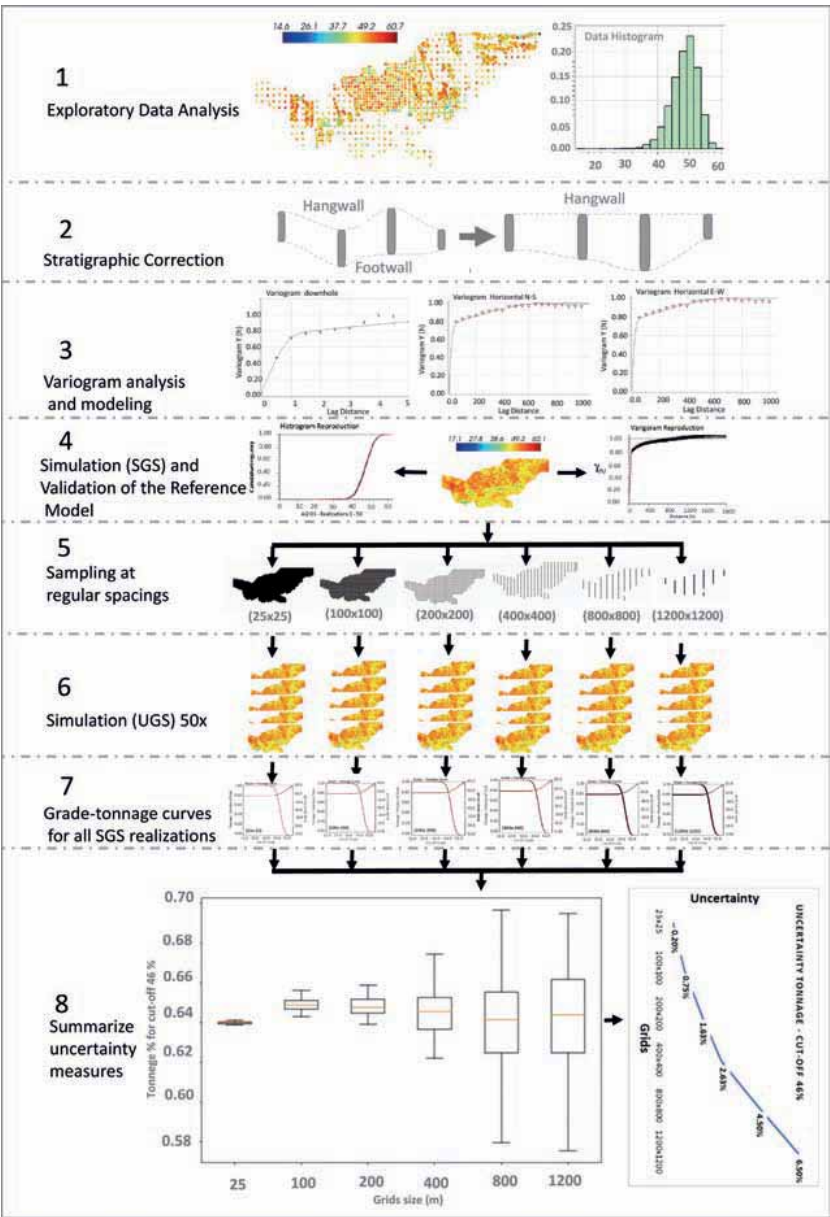
Figure 1.   Flowchart of resource uncertainty.

6. Geostatistical Simulation using the n databases with regular spacing;
7. Calculation of grade-tonnage curves for all the realizations;
8. Summarize uncertainty measures.

3.1 *Exploratory data analysis*

This case study uses a database of a large mine in one of the greatest bauxite plateaus of the Brazilian Amazon. The data cover approximately an irregular area of 10 km on the east-west axis and 4.5 km on the north-south axis. There are 4 drilling grids: 200×200, 100×100, 50×50 and 25×25 meters along the X and Y directions.

The bauxite mineralization is formed by lateritic processes typical of tropical zones and started in the early Cenozoic age, acting over immature sandstones and mudstones forming extensive layers at kilometric plateau formations. The capping of non-mineralized clay varies from 0.5 to 12 meters.

One main seam of bauxite ore in the database was chosen for the case study. This mineralized seam has an average thickness of 1,5 meters. Furthermore, this seam contains 2784 drill holes with 7609 geochemical samples at an average length of 0.5 meters.

The chemical species analyzed include available alumina (Al_2O_3 – related to gibbsite content representing the most important chemical analyses for bauxite). Summary statistics of the Al_2O_3 are in Table 1.

To avoid the bias effect in the histogram due to the irregular sampling grids, with a higher density of sample points at some places than in others, cell declustering was performed. The software declus (Deutsch 1989, Deutsch & Journel 1998) was used, and resulted in an weighted average Al_2O_3 content of 47.25%.

3.2 *Stratigraphic correction*

Mainly large mineralized layers constitute mineral deposits such as bauxite, coal, manganese and some nickel laterites. These layers formed by sedimentation or weathering processes may pass through several subsequent geological events such as folding, erosions and/or basin formation (Rubio et al. 2015). One of the most common problems for this kind of deposit is the spatial continuity analysis. This spatial continuity may be worsened by the combination of samples from different stratigraphic levels. (Rubio et al. 2015).

A vertical coordinate will be defined as the relative distance between a correlation top and correlation base grid. This vertical coordinate will make possible to infer measures of horizontal correlation using samples at the same stratigraphic level and to preserve the geologic structure in the final numerical model (Deutsch 2002). The new vertical coordinates can be calculated using the Equation 1 (Deutsch 2002), this represent the stratigraphic correction coordinates performed using as references hangwall distance (Fig. 1).

$$Z(i)str = Z(i) - Z(i)t \qquad (1)$$

where: $Z(i)str$ = Z elevation after stratigraphic correction in sample (i); $Z(i)$ = actual Z elevation in sample (i); and $Z(i)t$ = top layer Z elevation in sample (i);

Table 1. Al2O3 statistical summary.

Number of data	7609
Maximum	60.71%
Minimum	14.62%
Mean	48.50%
Median	49.00%
Variance	18.90
Skewness	4.35
kurtosis	6.24

As a test, the stratigraphic correction for the footwall, hangwall and average of the mineralized layer was carried out and the variography and cross validation using ordinary kriging of them were made in opposition to the real coordinates. The stratigraphic correction by the hangwall of the layer was adopted because it presented the smallest variance of the error obtained by cross validation.

3.3 Variogram analysis and modeling

The spatial continuity model was fitted to the original and normal. Equation 2 describes the variogram model of the original data. The variogram model of the normal score was used to condition the geostatistical simulations and is described in Equation 3:

$$2\gamma = 0.95 + shp \left\{ 13,68 \left(\frac{(N-S)/0^0)}{65\,m} + \frac{(E-W)/0^0)}{65\,m} + \frac{(N-S)/0^0}{1.1\,m} \right) \right.$$
$$\left. + 4.37 \cdot \left(\frac{(N-S/0^0)}{840\,m} + \frac{(E-W/0^0)}{840\,m} + \frac{(N-S/0^0)}{10\,m} \right) \right\} \tag{2}$$

$$2\gamma = 0.05 + shp \left\{ 0.72 \left(\frac{(N-S/0^0)}{50\,m} + \frac{(E-W/0^0)}{50\,m} + \frac{(N-S)/0^0)}{1.4\,m} \right) \right.$$
$$\left. + 0.23 \cdot \left(\frac{(N-S)/0^0)}{760\,m} + \frac{(E-W)/0^0}{760\,m} + \frac{(N-S)/0^0)}{10\,m} \right) \right\} \tag{3}$$

3.4 Simulate realizations of the reference distribution

The geostatistical simulations were performed using Sequential Gaussian Simulation (SGS). The software usgsim (Manchuk & Deutsch 2010) was used to perform the simulations. Fifty realizations were generated at $5 \times 5 \times 0.5$ meters grid and validated.

The validation consisted of comparing the histograms and variograms of the realizations to the histogram and variogram of the data (Goovaerts 1997). The realizations reproduced the histogram and variogram of the data (Fig. 1). One realization was selected and assigned as a true or reference model of the mineralized layer (Fig. 1).

3.5 Sample the simulated reference distribution at regular spacings

Once obtained as an imputed model reality the mineral deposit, sampling is performed at this model mimicking the drilling spacing desired for study. Therefore, six databases with distinct regular data spacing were obtained: (i) $25 \times 25 \times 0.5$; (ii) $100 \times 100 \times 0.5$; (iii) $200 \times 200 \times 0.5$; (iv) $400 \times 400 \times 0.5$; (v) $800 \times 800 \times 0.5$, and (vi) $1200 \times 1200 \times 0.5$ meters along the X, Y and Z directions, respectively (Fig. 1).

3.6 Simulation of n grids

The 50 realizations were performed for each of this six distinct drilling spacing obtained previously with the same parameters employed previously to generate the reference simulation (Fig. 1). The realizations were block averaged to block size of $25 \times 25 \times 0.5$ meters, which is the selective mining unity (SMU).

3.7 Stochastic simulation transfer function

The stochastic simulation is used for assessing uncertainty in the global resources. Grade-Tonnage curves are used as the transfer function which informs the uncertainty of the mineral resources (Figs. 1, 3).
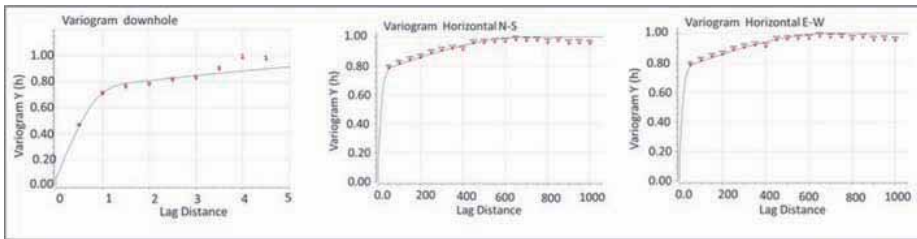
Figure 2.   Variograms of normalized data.
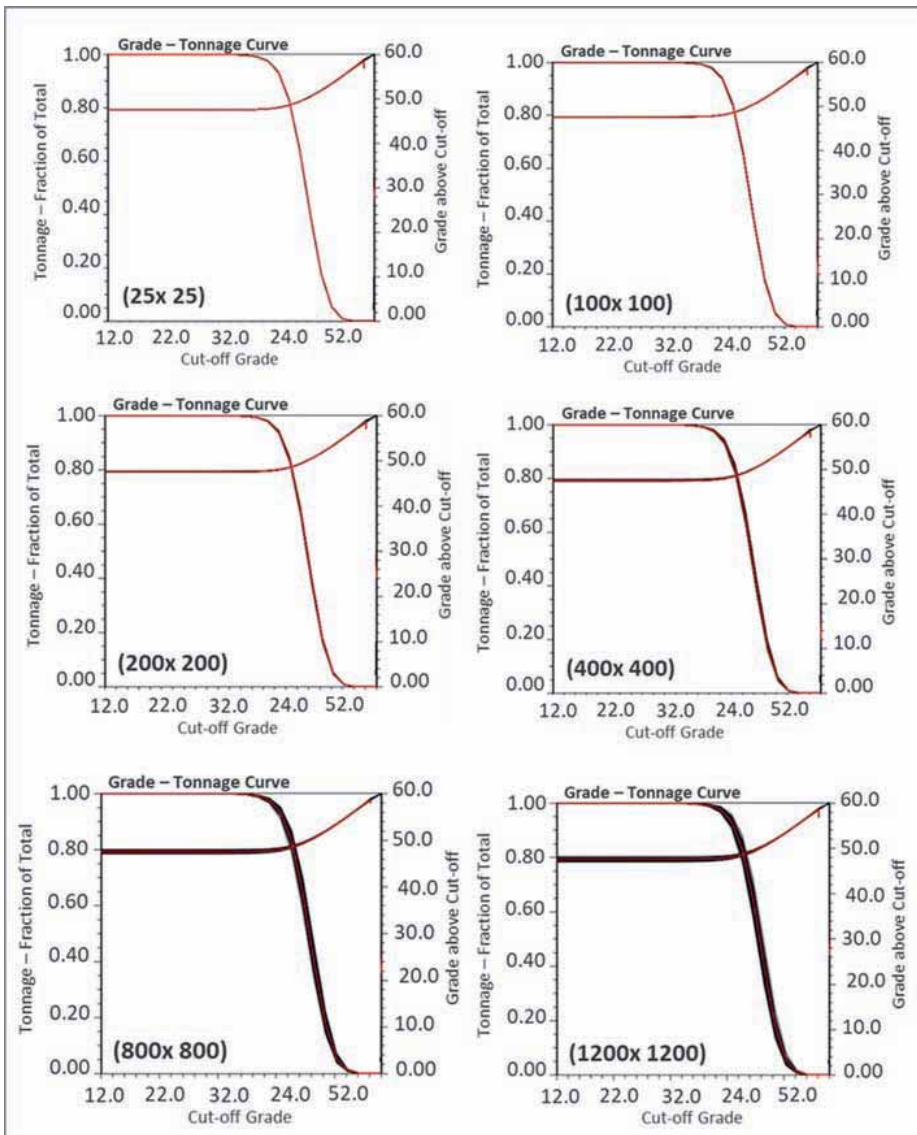
Figure 3.   Grand tonnage curve of the all SGS.

Grade-Tonnage curves are a graphical representation of the impact of cut-off grades on the mineral resources. The Grade-Tonnage Curves display the tonnage and grade above cut-off grade for a series of cut-offs. As the criteria for ore classification becomes more selective,
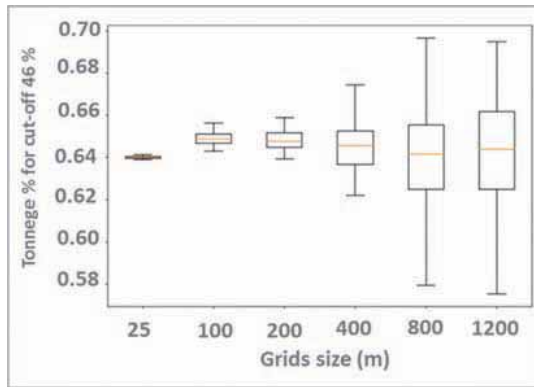
Figure 4.   Box plot for cut-off 46%.

the tonnage above the cut-off grade of the deposit decreases. Conversely, as the cut-off grade is lowered, the tonnage of the deposit increases. This is simply because the standard used to distinguish between ore and waste has become less selective. As the cut-off grade increases, so does the average grade of the ore mined. The curves ultimately show how the average grade and tonnage of a material delivered to a certain process are dependent on the cut-off grade selected.

Grade-tonnage curves are applicable throughout various stages of deposit evaluation. During exploration, for example, they can be a significant tool used to estimate the general size of a resource in tons of metal, using exploration data to generate the estimates. The grade and tonnage data used to create the curves are compiled with several assumptions, which should be taken into consideration when using the curves. Such assumptions are that the deposit is correctly classified, the data represents the complete *in situ* resource. Certain sources of error that can be prevalent when creating the curves include mixed geological environments, which may also be poorly known, the use of multiple mining methods, and incomplete estimates/errors in data recording.

3.8   *Summarize uncertainty measures*

The size of the band formed by the spreading of the grade-tonnage curves is a qualitative measure of the uncertainty associated to the mineral resources. Thus, the narrower the band formed by the scattering of these curves, the lower the uncertainty; in turn, the wider the band, the greater the uncertainty.

Cut-off grade is the minimum grade required in order for a mineral or metal to be economically mined (or processed). Material found to be above this grade is considered to be ore, while material below this grade is considered to be waste. By setting a value cut-off in the grade-Tonnage curve, it is obtained the value of the tonnage and average content for that cut-off. Thus, it is possible to identify in a quantitative way the degree of uncertainty coming from the resources simulations. Various measures are used to summarize like the standard deviation, coefficient of variation, 90th (P90) and 10th (P10) percentiles, and relative uncertainty (P90–P10)/P50) (Deutsch et al. 2007) (Figs. 1, 4).

4   RESULTS OF THIS STUDY CASE

The expected result on this case study was the generation of the grade-tonnage curves through 50 realizations for 6 databases with different data spacings. Figure 3 presents the grade-tonnage curves obtained with the different data spacings: (i) $25 \times 25 \times 0.5$; (ii) $100 \times 100 \times 0.5$; (iii) $200 \times 200 \times 0.5$; (iv) $400 \times 400 \times 0.5$; (v) $800 \times 800 \times 0.5$, and (vi) $1200 \times 1200 \times 0.5$. Analyzing these graphs, it is well known that the denser the sampling mesh, the smaller the curve spread band, and the larger the sampling mesh, the larger the curve spacing band. This quali-

tatively states that the uncertainty relative to the mineral resources is inversely proportional to the sampling density (Figs. 4, 5).

Considering the Al2O3 cut-off grade as 46% and adopting the difference between the P10 and P90 as the measure of uncertainty at 80% confidence limit. We can obtain the measure of uncertainty associated with the different data spacings (i) $25 \times 25 \times 0.5$; (ii) $100 \times 100 \times 0.5$; (iii) $200 \times 200 \times 0.5$; (iv) $400 \times 400 \times 0.5$; (v) $800 \times 800 \times 0.5$, and (vi) $1200 \times 1200 \times 0.5$. Respectively, the obtained uncertainty was 0.20%, 0.75%, 1.63%, 2.63%, 4.50% and 6.50% for the tonnage above cut-off (Fig. 5) at 80% confidence limit. These results show an almost linear increase in uncertainty as the data spacing increases. The same way, the uncertainty of grade average curve with cut-off above 46% relative to those grids, is 0.008%, 0.033%, 0.051%, 0.111%, 0.234% and 0.247% (Fig. 6). As checked, a characteristic of the ore is a low variation in its average grade.

We also evaluated the uncertainty for the selective mining unity (SMU) scale. The uncertainty was measured using the probability to be around 15% of the mean. The mean is the
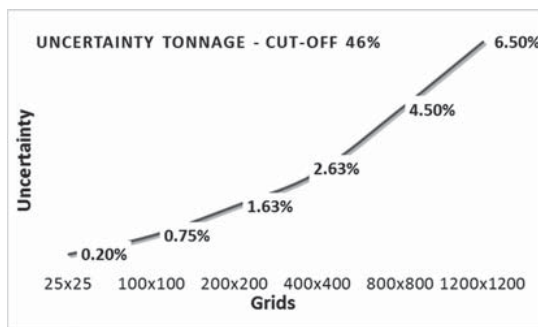
Figure 5.   Uncertainty (defined as the P90–P10) off tonnage mass with cut-off 46%.
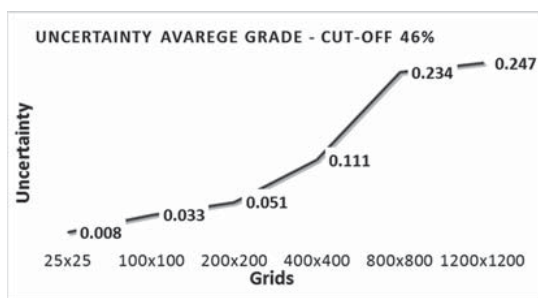
Figure 6.   Uncertainty (defined as the P90–10) of average grade with cut-off 46%.
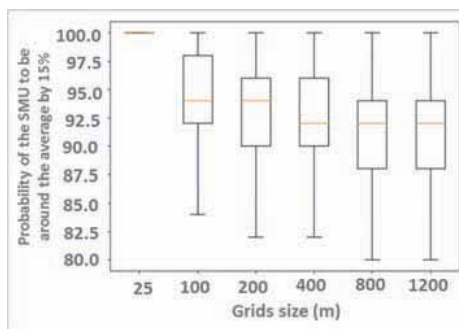
Figure 7.   Boxplot—probability of the SMU to be around the average by 15%.

mean over all the realizations for each block (E-type). The higher the probability to be around 15% of the mean, the lower the uncertainty. The minimum probability to be around 15% of the mean represents the worst case (highest uncertainty). For the 25×25 m data spacing, the minimum probability to be around 15% of the mean is nearly one hundred (Fig. 7). The result indicates that the difference between the true and E-type will not be higher than 15% using the data spacing of 25×25 m. As the data spacing increases, the probability to be around 15% of the mean decreases. The minimum probability around 15% of the mean for the data spacings of 100×100, 200×200, 400×400, and 800×800 m were roughly 84, 82, 82, 80 and 80%. Moreover, the result indicates that the data spacing affects more grade uncertainty at smaller scales. Although large data spacings justify the global resources delineation, the same may not happen for the prediction of resources in SMU scale.

5 CONCLUSIONS

The sampling density directly affects the uncertainty associated to the mineral resources calculations.

Each type of mineral deposit and commodity studied has its own intrinsic characteristics. The uncertainty of the mineral resources helps managers make better business decisions. For instance, if the mining company wants to avoid risks, it may prefer to invest in projects with little uncertainty.

This paper presents a methodology to evaluate the influence of the data spacing on the uncertainty of mineral resources. A case study with data derived from a bauxite deposit illustrates the methodology.

REFERENCES

CRIRSCO. (2013, November). crirsco.com. Retrieved from crisco.com: crisco.com/templates/international_reporting_template_november_2013.pdf.

Deutsch, C.V. (1989). DECLUS: A Fortran 77 program for determining optimum spatial declustering weights. *Computers & Geosciences* 15(3), 325–332.

Deutsch, C.V. (2002). *Geostatistical reservoir modeling*. New York: Oxford University.

Deutsch, C.V. (2011). *Guide to Best Practice in Geostatistic*s, Version 1.0. Edmonton, Canada: Centre for Computational Geostatistics, University of Alberta.

Deutsch, C.V., & Journel, A.G. (1998). *GSLIB. Geostatistical Software Library and User's Guide*. New York: Oxford University Press.

Goovaerts, P. (1997). *Geostatistics for Natural Resources Evaluation*. New York: Oxford University Press.

Isaaks, E.H. *The application of Monte Carlo methods to the analysis of spatially correlated data*. USA: Stanford University, 1990. 213p. (PhD. Thesis).

Isaaks, H.E., & Srivastava, M.R. (1990). *An Introduction to Applied Geostatistics*. New York: Oxford University Press.

Journel, A.G., & Kyriakidis, P.C. (2004). *Evaluation of mineral*. New York, NY: Oxford University Press.

Journel, A.G., & Ying, Z. (2001). The theoretical links between Sequential Gaussian Simulation, Gaussian Truncated Simulation and Probability Field Simulation. *Mathematical Geology*, Vol. 33, No. *1, 31–40.*

Koppe, V.C., Rubio, R.H., & Costa, J.C. (2017). A Chart for Judging Optimal Sample Spacing for Ore Grade Estimation. *Natural Resources Research* (2017) V.26, 191–199.

Manchuk, J.G., & Deutsch, C.V. (2010). Updated Ultimate SGSIM. *CCG Annual Report 12*, paper 401.

Olea, R.A. (1999). Geostatistics of engineers and earth scientists. Boston. Kluwer Academic Publishers.

Pilger, G.G., Costa, J.F.C.L., & Koppe, J.C. (2001). Additional samples: where they should be locat-ed. *Natural resources research,* 10(3), 197–207.

Rubio, H.R., Koppe, V.C., Costa, J.C., & Cherchenevsk, P.K. (2015). How the use of stratigraphic coordinates improves grade estimation. Fonte: *Rem: Rev. Esc. Minas [online]*. 2015, vol. 68, n. 4 [cited 2019-01-07], pp. 471–477: <http://www.scielo.br/scielo.php?script=sci_arttext&pid=S0370-44672015000400471&lng=en&nrm=iso>.

Sinclair, A.J., & Blackwell, G.H. (2004). *Applied mineral inventory estimation*. Cambridge: Cambridge University Press.

Wild, B.J., & Deutsch, C.V. (2013). Methodology for quantifying uncertainty versus data spacing applied to the oil sands. *CIM Journal*, p. 211–219.

Evolving estimation techniques for an evolving world class stratiform copper deposit at Kamoa-Kakula, Democratic Republic of the Congo

G. Gilchrist
Ivanhoe Mines, Johannesburg, South Africa

ABSTRACT: The supergiant Kamoa-Kakula copper deposit is a greenfields discovery made by Ivanhoe Mines in the Western Forelands area of the Central African Copperbelt in the Democratic Republic of the Congo. Over ten years, progressive collection of significant geological data and completion of nearly 1500 drillholes has led to an evolving modelling methodology to include greater geological control, meet the needs of advancing mining studies, and to solve the difficulties posed by stratigraphic and mineralisation units extensive over many kilometres but some only a few metres to tens of metres thick. Innovative modelling routines, combining Datamine and Leapfrog functionality, has led to a full three dimensional (3D) model honouring vertical grade profiles, known controls on mineralisation, and accurately representing the geometry and relationships of numerous stratigraphic and mineralised units. Information now captured in the model has aided mining and metallurgical optimisation, which has added significant value to the project economics.

1 INTRODUCTION

The Kamoa-Kakula copper deposit is a greenfields discovery made by Ivanhoe Mines in the Western Forelands area of the Central African Copperbelt (CACB) in the Democratic Republic of the Congo (DRC), discovered in an area previously considered unprospective for large copper deposits just 25 km west of the Kolwezi Cu-Co district. Ten years later, nearly 1500 drillholes have defined the largest copper deposit ever discovered in Africa, extending 28 km north-south and 23 km west-east, and with characteristics similar to the Kupfeschiefer copper deposits in Poland. At a 1% cut-off, the deposit boasts an Indicated Resource of 1387 Mt at 2.64% Cu and an Inferred Resource of 316 Mt at 1.76% Cu. Mine development has commenced and the project has attracted international investment.

Since its discovery, mapping, geophysical surveys and a growing drillhole database have allowed for significant advancements in the geological understanding of the deposit, in particular the controls on mineralisation. Traditionally, understanding geological processes is a key focus during the exploration phase, but emphasis tends to shift to ensuring the geometry is correct once resource estimation and mine planning commence. In the modelling approach developed at Kamoa-Kakula, both the geological processes controlling mineralisation and accuracy in geometry are combined to produce a high quality resource model. This is achieved without making the model so complex that it is impractical to update on a regular basis.

2 GEOLOGY

2.1 *Regional geology*

The CACB is the world's premier sediment-hosted copper province. It is contained in the Katangan basin, an intracratonic rift that records onset of growth at ~840 Ma and inversion at

~535 Ma (Selley et al. 2018). The succession is divided into three regionally mappable groups, which from oldest to youngest are named the Roan, Nguba, and Kundelungu Groups.

Most of the known CACB deposits in the DRC are hosted by dolomitic rocks of the Mines Subgroup in the lower part (Roan Group) of the succession (Francois 1973, Cailteux et al. 2005), whereas Kamoa occurs at the base of a stratigraphically higher diamictite, the Grand Conglomérat of the basal Nguba Group (Broughton & Rogers 2010, Schmandt et al. 2013).

Timing of mineralisation in the CACB has been a matter of debate for decades. In the context of exploration, however, the absolute timing of mineralisation is less crucial, as the distribution of deposits is fundamentally controlled by chemical (reductant) and permeability (aquifer) considerations upon which ore fluids were superimposed (Selley et al. 2018). Incorporation of these controls during grade estimation has been a key objective.

2.2 *Local geology*

At Kamoa, haematite-bearing sandstone and siltstone of the Mwashya Subgroup (upper Roan Group) form the oxidised lower strata, and the pyritic rocks of the basal diamictite and interbedded siltstone-sandstones form the reduced host rock (Twite et al. 2018).

Although often associated with glacial origins, the diamictites of the Grand Conglomérat at Kamoa are interpreted as the deposits of cohesive debris flows, with the sandstone and siltstone units the product of turbidity flows in a rapidly subsiding and evolving rift (Kennedy et al. 2018). The abundance of framboidal pyrite, which can only form under anoxic conditions, suggests there was little shallowing of the basin even with the substantial sedimentary input (Kennedy et al. 2018). This pyrite played a critical role in providing the reductant for copper sulphide mineralisation in diamictites and siltstone units at the base of the Grand Conglomérat (Schmandt et al. 2013).

The mineralisation at Kamoa is broadly stratiform, but zones of elevated copper grades appear to be related to inferred growth faults that were active during sedimentation, underscoring an important link between extensional fault architecture and localisation of orebodies. These are marked by abrupt changes in stratigraphic thickness, steepened bedding and rotated mesoscopic faults (Twite et al. 2018). Syn-sedimentary normal faults have been documented as first-order ore controls at several deposits in the Zambian Copperbelt, such as Mwambashi B, Chambishi, Konkola, Musoshi and Fishtie (Selley et al. 2005, Hendrickson et al. 2015).

Units are deformed into dome and basin patterns, resulting from the interference of NE-, ENE-, and WNW-trending, mainly gentle to open, upright folds. This relatively weak deformation contrasts greatly with the complex strain patterns of the neighbouring Kolwezi system (Selley et al. 2018). A much younger extensional fault set, known as the West Scarp Fault, transects the project in an approximate north-south orientation (west block down) to the west of Kamoa and separating Kakula from Kakula West. This is the only brittle fault system identified to date on the project with significant offset.

2.3 *Mineralisation*

Copper mineralisation at Kamoa-Kakula is typically bottom-loaded, with a vertical transition from chalcocite at the base progressing upwards through bornite, chalcopyrite and pyrite. Mineralising fluids in the CACB have been modelled by Muchez & Corbella (2016) to advance slowly, laterally and across stratigraphic layers away from the fluid source, driving the reactions between a copper-rich fluid and the host rock reductant (anhydrite or pyrite), precipitating copper sulphides. This mineralising front is also capable of dissolving some of the earlier copper sulphides, with the stratigraphically lower, more copper-rich sulphides partially replacing the overlying, more copper-poor sulphides (Twite et al. 2018). A characteristic zonation develops whereby pyrite is replaced by chalcopyrite, chalcopyrite by bornite, and bornite by chalcocite. This zonation is evident at Kamoa-Kakula (Fig. 1) and elsewhere on the CACB (Van Langendonck et al. 2013).

The vertical position of mineralisation relates to the location of the reductant/s and proximity to the Roan aquifer. Although broadly stratiform, mineralization does transgress stratigraphy when a lower reductant narrows or pinches out (Fig. 2). Mineralisation is strongest, and the bottom-loaded profile is best developed when the reductant is in direct, or very close contact, to the Roan aquifer.
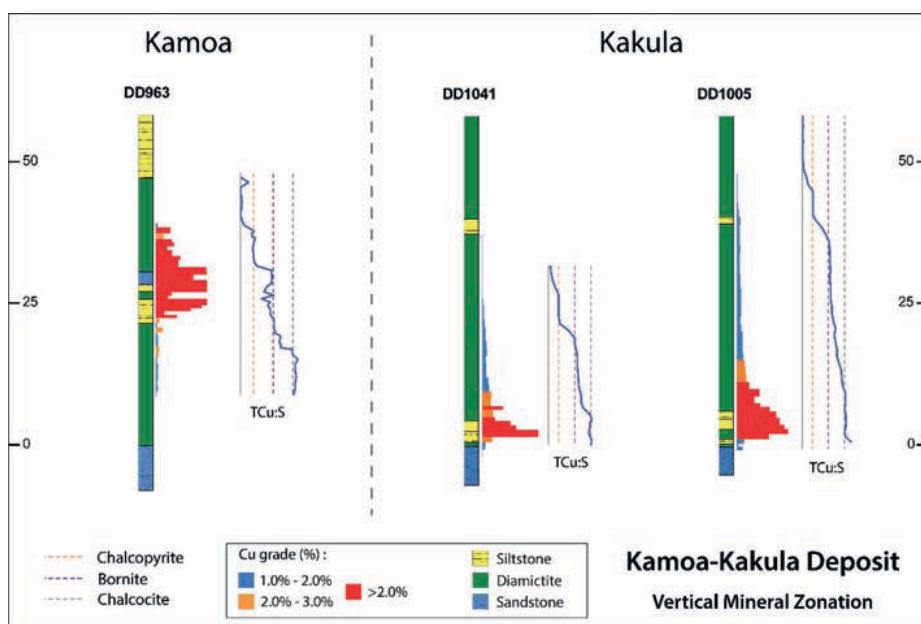
Figure 1.   Example grade profiles and sulphide species from Kamoa and Kakula deposits illustrating the well-defined vertical transition chalcocite-bornite-chalcopyrite-pyrite.
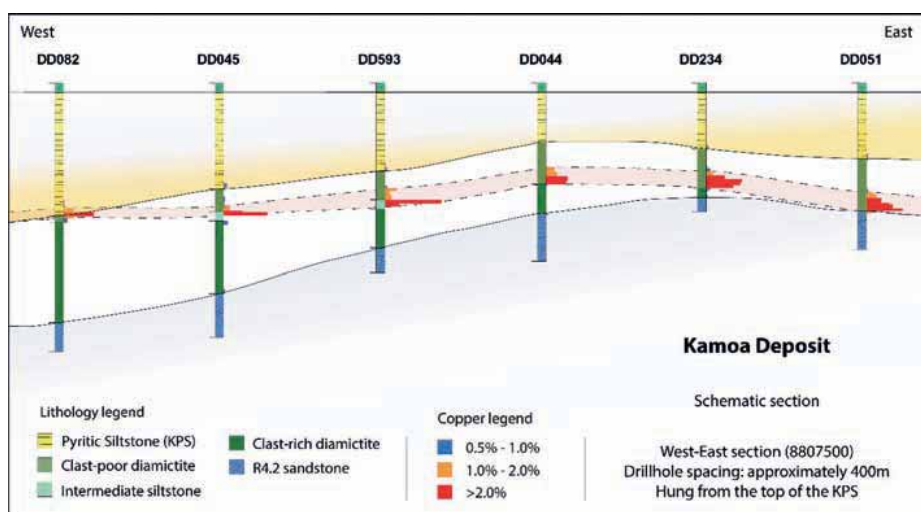
Figure 2.   Transition of the mineralized horizon from within the Kamoa Pyritic Siltstone (KPS) (west) to occurring directly on the Roan aquifer (east).

3 RESOURCE MODELLING

3.1 *Initial models*

Initial modelling in 2009 utilised just 46 drillholes on a 400 m to 800 m spacing, with the mineralised horizon defined using a 1% Cu cut-off, with a minimum 3 m downhole thickness to ensure the mineralised horizon could be considered mineable utilising underground methods. In low grade areas, where the 1% cut-off was <3 m, the interval was diluted to 3 m to introduce lateral dilution into the model. Drillholes were composited across the full mineralised interval to define a single average value per drillhole.

A 100 m by 100 m block model was created within the modelling limits and draped onto a surface modelled using trend-surface analysis within individual fault blocks, whereby a first- or second-order polynomial trend surface was fitted to the drill data, and the residuals from this surface modelled using two-dimensional inverse distance squared (ID2) weighting. Copper grade was back-calculated from estimates of true thickness and metal accumulation (Cu% * true thickness), also using ID2 at a datum elevation. When used at Kakula, density weighting was also applied as the higher grades materially impacted the density. A single block was defined in the vertical orientation, with the block height set to the estimated vertical thickness (Fig. 3).

This two dimensional (2D) gridded seam model approach is commonly used in early-stage projects with limited and wide-spaced drilling. The approach was continued through a number of updates. Advantages to this approach include:

– File sizes are very small and easy to use
– Estimation is rapid
– Grade trends can be easily plotted without the need for further post-processing
– They are well suited to early-stage engineering studies

The initial 2D approach used did have a number of disadvantages:

– The vertical grade profile and trend in sulphide species was lost when the full width composite (average value) was defined
– Mining heights were hard-coded into the mineralised horizon definition; no optimisation of the vertical mining height was thus possible without the entire modelling process being repeated at different cut-offs or minimum and/or maximum mining height considerations
– Trend surfacing to define the correct vertical position of blocks led to a dimpled surface and 'drag' folds developing along faults as, away from data, the surface continually returned to the regionally defined trend.
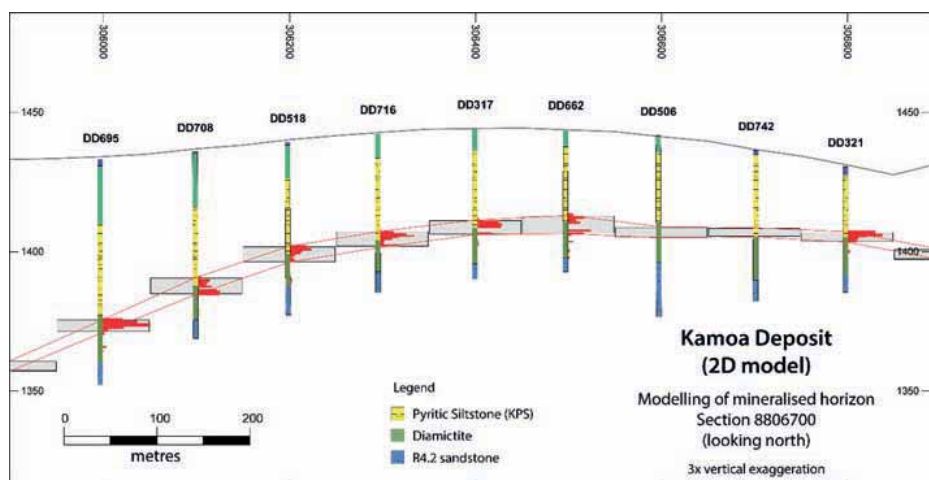
Figure 3.   Two dimensional model in the correct three dimensional space, but with only a single block defining the mineralized horizon.

- Only a single mineralised horizon was defined for each drillhole, even if two or more horizons were evident
- Where mineralisation transgressed stratigraphy, the 2D modelling approach aligned mineralised horizons located in different stratigraphic positions for estimation
- Estimation using ID2 did not incorporate geological controls known from syn-sedimentary growth faults.

Later improvements to the 2D model were made possible through the addition of significant drilling to close the drill grid to 100 m or 200 m, resulting in an improved understanding of the project geology and controls on mineralisation. Improvements included the introduction of non-vertical faults, the use of an innovative smoothing routine in Datamine utilising the 'centre-of-gravity' points for individual wireframe triangles to reduce the dimpling effects, and a time-consuming process drawing control strings along fault block edges. Grade estimation gradually incorporated greater geological controls through the use of anisotropic searches aligned with trends evident in the variography and thickness trends of stratigraphic units.

Dilution skins were added for improved mining study results. The initial steps towards 3D modelling was incorporated into the Kakula model, where five stacked gridded models introduced limited vertical grade variability at 1%, 2% and 3% copper cut-offs.

To enable the construction of a full 3D model constrained within stratigraphic and mineralised horizon wireframes, certain key challenges to modelling had to be overcome:

- Stacked stratigraphic units representing changes in basin depositional environments are extensive over kilometres, but some only a few metres thick
- Gentle folding, extensional and compressional faulting, and erosion on elevated domes had to be accounted for, as did localised onlapping of stratigraphic units
- A large data set (nearly 1500 drillholes) made manual coding exercises time consuming and ruled out surface creation through sectional interpretation and joining of interpreted strings.

3.2   Overcoming surface modelling constraints

The development of uneven surfaces, pinch outs and abnormal thinning or thickening of units was overcome through internal testwork (Nielsen 2014) through combining key functionality of Datamine and Leapfrog modelling software.

Modelling a surface in Leapfrog using just point data is susceptible to the same dimpling effect and pinch-outs encountered using the trend modelling approach in Datamine. The use of structural data in Leapfrog, where dip and dip direction are defined at specific coordinates, effectively defines a trend surface at each individual drillhole. Surfaces generated from structural data are smoother and honour the expected trends far more effectively. The challenge is to determine the appropriate dip and dip direction for each drillhole position.

The contacts from each stratigraphic or mineralised unit are identified in Datamine and exported to Leapfrog. A reliable marker horizon is identified and modelled from the point data to create a reference surface for individual fault blocks. This surface is dimpled, but is a good general representation of the marker horizon. The wireframe is exported to Datamine, where the ANISOANG function is used to determine the dip and dip direction of each triangle of the wireframe. These values are estimated into a block model, with the estimated dip and dip direction tagged back to the point data and reimported into Leapfrog as structural data (Fig. 4). A key step, to prevent pinch outs or the creation of abnormal thinning or thickening between layers, is the assignment per drillhole of the identical dip and dip direction for each unit modelled.

Surfaces modelled with the structural data are smooth (Fig. 5), realistic and successful when tested by drilling, and require very little control along fault surfaces. The contact points and the dip and dip direction used are generated in Datamine through a process that can be carefully monitored and adjusted; the user retains full control of the modelling. The process is robust, and largely automated through scripted modelling routines, creating a high quality
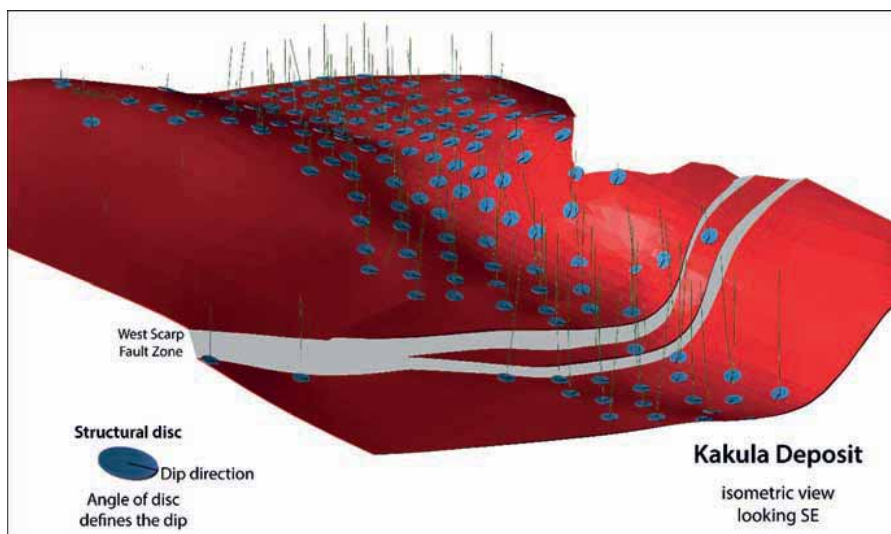
Figure 4.   Structural discs used control the modelling of the mineralized horizon at the Kakula deposit.
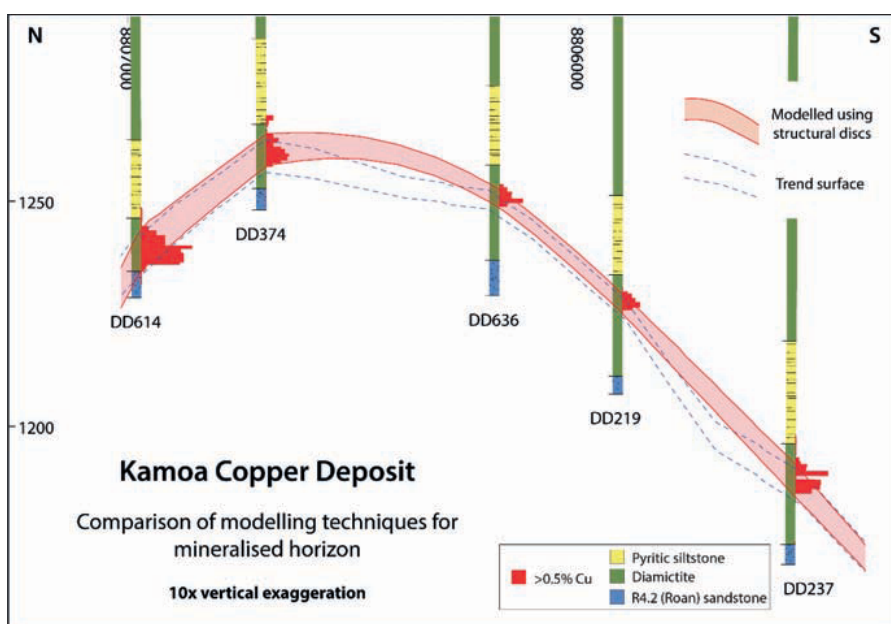
Figure 5.   Comparison of the Datamine trend surface modelling and the improved surface creation utilizing structural discs in Leapfrog. Note the 10x vertical exaggeration to highlight differences.

boundary model for resource estimation without a reliance on manual digitisation. Stratigraphic relationships defined in Leapfrog allow the stratigraphic and mineralised units to be exported as 3D volumes, used to code and constrain the block model in Datamine.

3.3   Three dimensional modelling

With the creation of high quality surfaces for stratigraphic and mineralised units, it is possible to use this information to constrain a full 3D block model and estimation. A block size of 50 m

by 50 m by 1 m was used to fill the wireframe solids, complementing the 1 m composite sample length from the drillholes. Boundaries between units are used to constrain grade estimation, to prevent estimation across reductants of different character. Key geotechnical units, most notably the pyritic siltstones, are coded into the model, and provide valuable input to mine planning.

In developing 3D models, a key objective was to retain the vertical and lateral variation evident to allow for optimisation of the mine design and schedule to maximise returns. Unlike the earlier 2D models, no mining constraints were hard-coded into the models, ensuring flexibility to optimise cut-off grade.

The challenge in grade estimation is twofold:

– Retain the vertical bottom-loaded grade profile given the folding and thickness variations within the mineralised horizon.
– Incorporate trends from stratigraphic modelling that will be used to control the search orientation angles during estimation.

The bottom-loaded grade profile evident in drillholes is typically retained between drillholes even though the thickness of the mineralized horizon can vary. This, combined with the gently folded basin and dome geometry, required the data to be transformed prior to estimation. A dilational transform, applied only to elevation, converted the measured co-ordinates for both blocks and informing drillholes per domain to a scaled position relative to the maximum thickness of each domain to match up the roof, middle and floor of each horizon (Fig. 6). This is a technique adapted from bauxite and nickel laterite estimation (Audet & Ross 2009, Vigar et al. 2009).
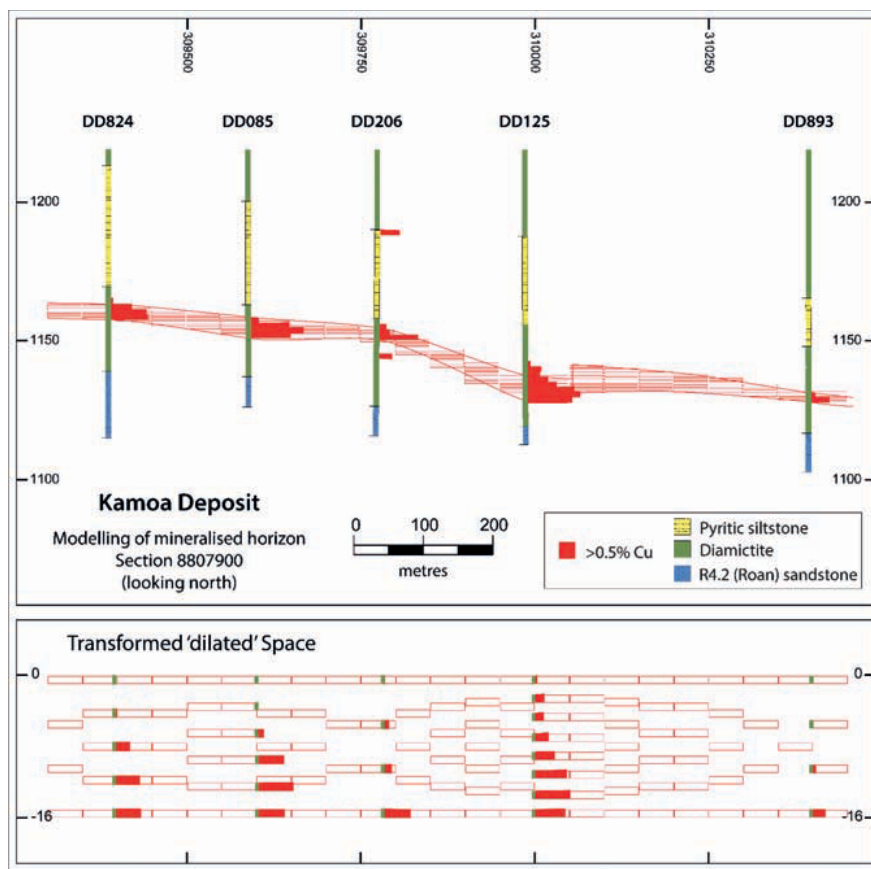
Figure 6.   Dilation of the drillholes and block model to correctly align the grade distribution between holes of varying thickness.

Variography and grade estimation using ordinary kriging occur in transformed space, with both constrained vertically by a third, to a quarter of the maximum domain thickness. This ensures samples occurring laterally within the same position in the dilated profile gain prominence over those occurring in a different vertical position in the grade profile. This honours the strong vertical grade and sulphide species zonation evident at Kamoa-Kakula, allowing full vertical optimisation and material selection to be made.

A link between extensional fault architecture and localisation of orebodies is known in the CACB. Thickness changes in modelled units were used to guide the search orientations during estimation, in a Datamine process known as 'dynamic anisotropy'. This process allows the search orientation to change from block to block across the deposit based on trends incorporated into the block model, ensuring that known geological controls affect the estimate of grade.

There are significant benefits to using the 3D modelling approach:

– The vertical grade definition allows for optimisation studies during mine planning and scheduling
– The resource model only needs to be built once as no engineering constraints are built into the model to limit its flexibility; no additional dilution models need to be constructed
– The modelling approach can effectively model numerous mineralised horizons at different vertical (and lateral) positions within the stratigraphic profile. Variography and estimation thus occur within horizons that share lithological or mineralisation characteristics; estimated block grades do not use samples from cross-stratigraphic positions.
– In addition to copper grades, processing, smelter and marketing studies can rely on information in the model including copper sulphide species, arsenic, iron and sulphur grades.

The improved model definition does create some challenges:

– Reporting the resource is complex as areas occur where two or more mineralised horizons overlap. Given the limited selectivity of underground mining techniques, isolated blocks above cut-off were not considered economically extractable, and were excluded from the Mineral Resource. Reporting also considers minimum mining heights.
– Processing time for the estimate is significantly longer than the 2D model, with much larger file sizes created as outputs.
– Displaying grade trends across stratigraphic or mineralised units requires post-processing of the model to create a 2D equivalent.

4 CONCLUSION

During the exploration phase, an emphasis is placed on understanding geological processes. Once resource estimation and mine planning commence, the emphasis is placed on ensuring the geometry is correct. In the modelling approach developed at Kamoa-Kakula, both the geological processes and accuracy in geometry are combined to produce a high quality resource model.

The modelling approaches have progressively improved to include more detailed information and geological control in the grade estimates. Models have also aligned with evolving requirements from advancing mining studies, and have added significant value to project economics.

Models have progressed from a simplified 2D model using isotropic ID2, to a full 3D model estimated in transformed space using ordinary kriging with dynamic anisotropy to ensure vertical and lateral grade trends evident in the vast drillhole database are replicated in the estimated block model grades.

Prior to the inclusion of close-spaced grade control information, resource models using wider spaced drilling and estimated using ordinary kriging will likely be a smoother representation of the block grade distribution than encountered in reality. Many factors inherent to the Kamoa deposit, and Kakula in particular, mitigate this risk:

– The mining cut-off applied in planning and scheduling is well below the average grade of the majority of blocks included in the mining cut
– The deposit has strong geological controls which have been incorporated into the estimation
– The copper grade distribution is not strongly skewed
– The mine plan only incorporates underground mining with a minimum selectivity of at least 100 m by 100 m, approximately half the current drillhole spacing.

A full grade control programme is planned to further mitigate this risk. Other estimation techniques are being considered, including simulation, to test the effect of smoothing inherent in kriging, and to quantify the impact of contact dilution across the deposit.

Although the modelling process has become more complex, a full resource update with revised structural interpretation takes a single geologist two weeks to complete. Interim updates, with an unchanged structural model, can be completed in one to three days depending on computing power.

REFERENCES

Audet M. and Ross A. 2009. Koniambo Lateritic Ni-Co Deposits, New Caledonia—A Case Study from Geological Modelling to Mineral Resource Classification. *Orebody Modelling and Strategic Mine Planning International Symposium*.

Broughton, D. & Rogers, T. 2010. Discovery of the Kamoa copper deposit, central Africa Copperbelt, D.R.C. *Soc. Econ. Geol. Spec. Publ.* 15, 287–298.

Cailteux, J.L.H., Kampunzu, A.B., Lerouge, C., Kaputo, A.K. & Milesi, J.P. 2005. Genesis of sediment-hosted stratiform copper-cobalt deposits, Central African Copperbelt. *J. Afr. Earth Sci.* 42, 134–158.

François, A. 1973. L'extrémité occidentale de l'arc cuprifère Shabien. Etude géologique, *Gécamines, Likasi (Shaba-Zaïre)*. pp. 65.

Hendrickson, M.D., Hitzman, M.W., Wood, D., Humphrey, J.D. & Wendlandt, R.F. 2015. Geology of the Fishtie deposit, Central Province, Zambia: iron oxide and copper mineralization in Nguba Group metasedimentary rocks. *Miner. Deposita* 50, 717–737.

Kennedy, K., Eyles, N. & Broughton, D. 2018. Basinal setting and origin of thick (18 km) mass-flow dominated Grand Conglomérat diamictites, Kamoa, Democratic Republic of Congo: resolving climate and tectonic controls during Neoproterozoic glaciations. *Sedimentology*.

Muchez P. & Corbella M. 2016. Reactive transport modelling of ore mineral zoning and the paragenesis of copper sulfides in sediment-hosted stratiform ore deposits, the Katanga Copperbelt (DRC). *Geologica Belgica,* 19, 219–223.

Nielsen S. 2014. Kamoa Copper Project modelling. Leapfrog Geo User Forum. Johannesburg, 9 December 2014.

Schmandt, D., Broughton, D., Hitzman, M.W., Plink-Bjorklund, P., Edwards D. & Humphrey, J. 2013. The Kamoa copper deposit, Democratic Republic of Congo: stratigraphy, diagenetic and hydrothermal alteration, and mineralization. *Econ. Geol.* 108, 1301–1324.

Selley D., Scott R., Emsbo P., Koziy L., Hitzman M.W., Bull S.W., Duffett M., Sebagenzi S., Halpin J. & Broughton D. 2018. Structural Configuration of the Central African Copperbelt: Roles of Evaporites in Structural Evolution, Basin Hydrology, and Ore Location. *SEG Special Publications,* no. 21, pp. 115–156.

Twite F., Broughton D., Nex P., Kinnaird J. & Gilchrist G. 2019. Lithostratigraphic and structural controls on sulphide mineralisation at the Kamoa copper deposit, Democratic Republic of Congo. *J. Afr. Earth Sci.* 151, 212–224.

Van Langendonck, S., Muchez, P., Dewaele, S., Kaputo Kalubi, A. & Cailteux, J. 2013. Petrographic and mineralogical study of the sediment-hosted Cu-Co ore deposit at Kambove West in the central part of the Katanga Copperbelt (DRC). *Geologica Belgica*, 16, 91–104.

Vigar A.J., Jiang G., Morgan M., MacDonald G., Smith L., Taylor I., Recklies M. & Grobler C. 2009. Resource Estimation for the Aurukun Bauxite Deposit. *Seventh International Mining Geology Conference*.

Critical review of mineral resource classification techniques in the gold mining industry

S.K.A. Owusu & K. Dagdelen
Mining Engineering Department, Colorado School of Mines, Golden, Colorado, USA

ABSTRACT: This paper investigates the different classification techniques used by the gold mining industry professionals to classify mineral resources into measured, indicated and inferred categories. The research is based on forty-five (45) public disclosure reports from System for Electronic Document Analysis and Retrieval (SEDAR) and one general classification guideline of a major gold producer unlisted on SEDAR. The survey includes public documents categorized by various geologic types of deposits and companies considered as major, mid-tier and junior gold mining operators. It encompasses 19 NI 43-101 technical reports filed in 2018 and 26 reports filed between 2006 and 2017. The purpose of the research is to explore and understand how the different mining companies perform classification of mineral resources in terms of the requirements used and different deposit type consideration. The paper summarizes the survey results, discusses the general implications and the need for developing more formal approach to mineral resource classification.

1 INTRODUCTION

1.1 *Purpose of the study*

Capital-intensive investment decisions are made in the mining industry with respect to confidence levels displayed in the mineral resources and reserves. The quality and quantity of materials estimated to be mined from a deposit have economic implications on the production schedule. The uncertainties with regards to the composition of a deposit may result in unreliable estimates and misclassification of resources. Although the various industry mineral resource reporting standard codes provide guidelines to be followed in generating classification reports, different mining companies use various procedures because each Competent Person (CP) or Qualified Person (QP) uses different assumptions, since none of the codes provides consistent assumptions to be adopted for reporting purposes. This has created classification categorization inconsistencies, leading to the disclosure of mineral resource reports with different accuracies in the industry. Mineral resource classification is a key requirement for public reporting of economic assessment and investor confidence in a mineral project.

1.2 *Mineral resource definitions and standards*

To protect investors and mineral project advisors from misleading public disclosure of mineral resources, the Council of Mining and Metallurgical Institutes (CMMI) introduced classification standard codes in 1994 to provide guidelines to categorize mineral resources into measured, indicated and inferred classes in decreasing order of geological confidence reposed in the blocks in a deposit. The authenticity of the available data for estimation and classification determines the geological confidence assigned by the CP or QP. The main factors that are evaluated to justify the credibility of a data include nature, quality, quantity and distribution. The distribution of most earth science data are skewed or lognormal. Effective and credible resource estimation and classification lead to reliable mine designs, production schedules, robust business plans and financial forecasts. Forty-five (45) different public

disclosure reports on System for Electronic Document Analysis and Retrieval (SEDAR) (www.sedar.com) were reviewed with respect to gold mining companies considered as major, mid-tier and junior categories. The survey covered 20 junior, 20 mid-tier, and 5 major companies in North America, South America, Asia, and Africa.

The Council of Mining and Metallurgical Institutes (CMMI) in 1994, formed a working group of representatives from different organizations to standardize mineral resource definitions. In 2000, the committee became the Combined Reserves International Reporting Standards Committee (CRIRSCO) and introduced a concept that Measured and Indicated mineral resources had to support mine planning. The main reporting codes produced by the member CRIRSCO institutions are the Canadian National Instrument 43-101 (NI 43-101) Code, the Australasian Joint Ore Reserves Committee (JORC) Code, the South African Mineral Resource Committee (SAMREC) Code and the American Society for Mining, Metallurgy and Exploration (SME) Guide, 2007. Other reporting codes include the Europe and United Kingdom (PERC) Code, the Brazil (CBRR) Guide, Chile and Peru (CMC) Guide, the Kazakhstan (KAZRC) Guide, the Mongolia (MRC) Code, and the Russia (NAEN) Code. The common goal of the various standard reporting codes is to ensure competence, materiality and transparency, Shaw et al (2006).

The principle of competence unreservedly assumes that the estimation and classification are done correctly, according to the current accepted practice. The transparency requires that the information contained in a public report should be accurate and sufficient. The materiality requires that all the relevant information needed by investors and their professional advisors to enable them to make informed business decisions should be contained in the public report. However, none of the standard codes specifies the consistent procedures to be followed by QPs in ensuring these three key inputs are included in public reporting of mineral resources.

1.3 *System for Electronic Document Analysis and Retrieval (SEDAR)*

SEDAR is an official webpage developed by the Canadian Securities Administrators to provide access to most public securities documents and information. The statutory objective of the webpage is to enhance investor awareness of the respective business and to promote confidence in the transparent operation of capital markets in Canada. The Canadian Institute of Mining Definition Standards on Mineral Resources and Reserves (CIM Definition Standards) established the guidance on the definitions for mineral resources, mineral reserves, and mining studies used in Canada (www.cim.org). The Canadian Securities Administrators (CSA) developed the NI 43-101 reporting code and it came into force in 2001. The code was established to provide best practice standards and guidelines for public disclosure of mineral resources and reserves reports in Canada. It was amended in 2005, 2011 and 2014.

The NI 43-101 reporting code focuses on improving the standards of practicing governing operating activities and the need for good public disclosure. It provides some specific requirements for reporting mineral resource estimates and classification to meet standard public disclosure. The guideline enforces the QPs to provide information that are comprehensive in their technical reports on exploration information, mineral resources and mineral reserves. However, the guideline is not prescriptive in terms of geological details, as the quantity of geological information needed to categorize mineral resources were not provided. The quality of reports vary as industry practices and assumptions considered by various QPs differ. Currently, there is no one particular document that specifies the acceptable industry practice and assumption to be followed by all QPs. Considering same mineral deposit, different QPs employ different assumptions and techniques to generate the estimation and classification with the same project drilling data. At each stage of the estimation process, different expertise skills are applied. Due to different approaches used by different industry professionals to analyze and interpret geologic data, there are various misleading public reports in the mining industry. The definition of each classification category can be found on www.cim.org.

2 CLASSIFICATION METHODS

Mineral resource classification is important to mining companies, investors, and financial institutions, as investment decisions are usually based on grade, tonnage and confidence assigned to deposits. However, the approach used to perform classification remains subjective because of lack of formal standards. The various public reporting codes do not categorically recommend the method or threshold needed to be used for classification, as the process depends on the judgement of the responsible CP or QP. The industry's best practice for classification is assessing and quantifying the uncertainty and risk associated with mineral resource estimation. The two basic methods used to perform classification tasks are the geometric and geostatistical techniques. In the survey, the geometric classification method was discovered to be mostly used in the mineral industry. Classification is commonly performed on a block-by-block basis, but the volumes are chosen reasonably large and contiguous, because one often believes that confidence in the grade should not change abruptly between adjacent blocks, Deutsch et al (2016).

2.1 *Geometric methods*

The geometric methods of mineral resource classification consider the amount, proximity and location of data available for estimation of a block. In the review of the recent classification reports, the geometric information used by the industry professionals included the dimensions of ellipsoidal search (ES), number of drill holes (NDH), minimum number of samples per estimate (NS), distance to nearest drill hole (DNDH), average drill hole spacing (DHS), and de-clustering by octant search (OS). The survey of the classification reports showed that each QP unilaterally selected the information to be considered in assigning confidence levels to blocks, as there are no standards to determine the needed information to be used for a particular type of deposit. The quantity of information to be used for classification is unrestricted, hence various QPs in the industry make different assumptions in assigning parameters to define the classification categories. Considering the minimum distance between a block's centroid and the composite samples for estimation, some QPs assigned different percentages of the variogram sill range while others assumed different values, based on their understanding of the deposits. Examples of the different assumptions made by the QPs in the reviewed technical reports can be found in the survey results in the next section. Generally, the geometric classification method does not consider the spatial continuity of the data in characterizing uncertainty associated with the estimation of the grades.

2.2 *Geostatistical methods*

The geostatistical classification methods are used to quantify risk on a given future production period. It is an effective and efficient method used to model geologic and grade uncertainty in mineral deposits. According to Deutsch et al (2016), desire to have purely probabilistic criteria based on sound estimates of uncertainty are understandable. The probabilistic techniques rely on classifying the blocks either by using KV directly or characterizing uncertainty of grade estimates, tonnages, and quantity of metals based on confidence intervals, kriging variance, and/or conditionally simulated realization of grades. After reviewing the recent NI 43-101 public reports, it was evident that the industry players have not embraced the geostatistical techniques. Although it makes sense, characterizing uncertainty of grade estimates, tonnages and quantity of metals based on confidence intervals, kriging variance and/or conditionally simulated realization of grades were applied by only few companies in the mining industry.

2.2.1 *Kriging variance approach*
Kriging is a minimum variance estimator which minimizes the squared error between the estimated value and the unknown true value. The error variance generated from the

estimation is the kriging variance (KV). The KV takes into account geostatistical parameters which combine both geometric and geological inputs in characterizing the uncertainty associated with the estimated parameter. The consideration of the spatial structure of the estimated variable and the redundancy between samples are the purposes of using kriging variance as the criterion for classification. In the process of assigning confidence levels, estimated blocks with high kriging variance have lower confidence than those with lower kriging variance. Emery et al (2006) suggest the establishment of KV thresholds for measured, indicated and inferred mineral resources classification categories based on a given desired number of drill holes, spacing and the variogram model in a given domain. Classifying each block into a specific measured, indicated and inferred mineral resource category is done on the basis of KVs associated with each block and these previously determined thresholds.

2.2.2 *Classification based on 90% confidence interval*

This technique involves calculating the 90% confidence intervals (CI) on the tonnage, grade and metal content within quarterly and annual production blocks either through KV or geostatistical conditional simulations. A recognized mining industry practice in the application of this technique is the ability to determine the drill hole spacing to be enough in the prediction of tonnage, grade and metal content within ±15% relative precision at 90% confidence interval within a quarterly or annual production rates. Measured resource considers quarterly production period and indicated resource corresponds to annual production period. For the detail description of mineral resource classification based on 90% confidence intervals, please refer to Verly et al (2014).

3 SURVEY RESULTS AND DISCUSSIONS

3.1 *Survey details*

This paper focuses on the review of 45 NI 34-101 technical reports of gold deposits which were obtained from System for Electronic Document Analysis and Retrieval (SEDAR) website plus one major gold mining company's publicly available general classification guidelines. The purpose of the survey was to investigate the current different techniques used to classify gold deposits into measured, indicated and inferred categories. After evaluating the different reports, it was realized that the mineral industry players use different procedures to categorize blocks into different classes, confirming irregular methodology used in the classification of mineral resources. A summary table was created to include the following information as formally described in the various NI 43-101 reports: publication date, company name, location, continent, state or province, commodity type, operation type, deposit type, interpolation method, classification criteria, classification technique, specific gravity method, domaining and boundary applications.

The public disclosure reports were grouped with respect to companies considered as major, mid-tier and junior gold mining operators. The investigations covered twenty (20) junior, twenty (20) mid-tier, and five (5) major gold mining companies in North America, South America, Asia and Africa. Also, the general classification guidelines of a major gold mining company unlisted on SEDAR was reviewed. Tables 1–4 show details of the number of NI 43-101 reports that were surveyed in terms of continent, country, company category, company name, deposit type and operation type. The overall investigations were based on; classification reports for same deposit type for same company, classification reports for same deposit type for different companies, classification reports from different consultants on same deposit type for different companies, and different classification estimation passes for same mining district and mineralized belt.

After critical look at the classification guidelines used by the various companies from SEDAR, forty-three (43) of the reports applied geometric methods and two (2) applied combined geostatistical and geometric methods. The major gold mining company unlisted on SEDAR also applied both geostatistical and geometric techniques. The abbreviations used in

Table 1. Number of technical reports by continent, country and company category.

Continent	Count	Percentage
North America	27	60.0
South America	11	24.4
Africa	6	13.3
Asia	1	2.2

Country	Count	Percentage
United States	16	35.6
Canada	11	24.4
Mauritania	5	11.1
Chile	4	8.9
Mexico	2	4.4
Brazil	2	4.4
Argentina	1	2.2
Burkina Faso	1	2.2
Dominican Republic	1	2.2
Guyana	1	2.2
Mongolia	1	2.2

Company category	Count	Percentage
Major	6	13.0
Mid-tier	20	43.5
Junior	20	43.5

Table 2. Number of technical reports by deposit type and operation type.

Deposit type	Count	Percentage
Greenstone Belt, Orogenic	16	35.6
Gold-Copper Porphyry	6	13.3
Epithermal Low Sulfidation	9	20.0
Carlin-Type	4	8.9
Lode and Placer	4	8.9
Gold Porphyry	2	4.4
Epithermal High Sulfidation	2	4.4
Placer Gold	1	2.2
Breccia Pipe	1	2.2

Operations type	Count	Percentage
Surface	29	64.4
Underground	8	17.8
Surface and Underground	7	15.6
Unknown	1	2.2

the tables are; Drill Hole Spacing (DHS), Distance to Nearest Drill Hole (DNDH), Number of Samples (NS), Number of Drill Holes (NDH), Ellipsoidal Search (ES), Octant Search (OS), Drill Hole Intercept (DH Intercept), and Kriging Variance (KV).

Generally, the parameters used differed even in the case of same type of deposit. For example, using the variogram range as a measure of search neighborhood, companies used different percentages of the variogram range, for example, 95%, 90%, 80%, etc. After critical study of the table and realizing different parameters used, one can conclude that different

Table 3. Number of technical reports per each gold mining company.

Company	Count	Percentage
Kinross Gold	16	34.8
Barrick Gold	6	13.0
Coeur Mining	3	6.5
New Gold	3	6.5
Centerra Gold	2	4.3
Osisko Mining	2	4.3
Agnico Eagle	1	2.2
Allegiate Gold	1	2.2
Brigus Gold	1	2.2
Goldcorp Mining	1	2.2
Guyana Goldfields	1	2.2
Parallel Mining	1	2.2
Wallbridge Mining	1	2.2
Newmont Gold	1	2.2

Table 4. Different classification techniques applied in the technical reports.

Classification technique	Count	Percentage
DHS	2	4.4
CNDH	2	4.4
NDH	0	0.0
NS + CNDH	2	4.4
DHS + NDH	3	6.7
NDH + ES	1	2.2
NDH + NS	2	4.4
NS + ES	3	6.7
NS + OS	3	6.7
DHS + CNDH	1	2.2
NDH + CNDH	4	8.9
DHS + NDH + CNDH	1	2.2
DHS + NS + OS	1	2.2
NDH + CNDH + ES	2	4.4
NDH + NS + CNDH	5	11.1
NDH + NS + OS	1	2.2
DH Intercept + NS	6	13.3
KV + CNDH + NDH + NS	2	4.4
Unknown	2	4.4

assumptions made by different QPs lead to potential discrepancies in public reporting of mineral resources. A gold deposit categorized by QP-A as measured may not pass the classification test for inferred by QP-B. In the public domain, it is difficult for investors to justify the correct reports from the misleading ones. The current industry practices lack consistency, resulting in various forms of implications, hence the need for the development of more formal methods.

3.2 Geostatistical techniques applied in the reports

Although geostatistical methods are considered to be providing the best techniques available to model geologic and grade uncertainty in mineral deposits, it is evident from the survey and from Table 5, that the industry professionals do not commonly use these methods and

Table 5. Geostatistical with geometric classification parameters applied to different deposits.

Deposit type	Parameter	Measured	Indicated	Inferred
Gold-Copper Porphyry	KV		≤0.66	≥0.66
	OS			
	CNDH	≤1/2 sill range	≤3/4 sill range	≤sill range
	NDH	≥3	≥3	
	NS	≥8	≥8	≥5
Orogenic Gold Deposit	KV		≤10	≥10
	OS	≥3	≥2	≥1
	CNDH	≤1/2 sill range		
	NDH			
	NS	≥12	≥8	≥4
All Deposits (Major gold company unlisted on SEDAR)	NS/H	≤1	≤1	≤1
	CNDH	2–3 times drill spacing	2–3 times drill spacing	2–3 times drill spacing
	NDH	≥3	≥3	≥3
	NS	≥3	≥3	≥3
	% Est. Error	± 15%	± 15%	± 30%
	% Confidence	90% over quarterly period	90% over annual period	90% over annual period

even when they are used, the geostatistical methods also include assumptions on geometric parameters.

3.3 *Geometric techniques applied in the reports*

Considering the details of the survey, no single technique was considered for a specific type of deposit, as the various project QPs made different assumptions for same type of deposits. Most of the companies used different classification parameters or requirements for similar type of deposit in different locations, as shown in Table 6. From the survey on the technical reports, only two companies followed a consistent classification method for all its deposits, regardless of the jurisdiction.

3.4 *Discussion*

The research has shown that the gold mining industry players prefer the geometric method, since few reports applied geostatistical methods for classification. The geometric method is simple and faster to apply. Hence, there is the need to research into generation of an easier and timely geostatistical classification framework to attract the interest of the gold industry players. A good and reliable resource estimation is important in the mineral extractive industry. During the survey, it was observed that different QPs applied different interpolation approaches on same type of deposit. Different grade capping approaches were applied by different QPs. These included capping before compositing, capping after compositing, capping per geological domain, and average capping value for all geological domains. Each capping approach can lead to variation of the average grade of a deposit. Different block modeling approaches were identified in the survey. These included single block model for surface and underground operations of same deposit, multiple block models for surface and underground operations of same deposit, different block models for different geological domains, and same block model for different geological domains. Also, an estimation pass for mineral resource classification is very crucial in predicting blocks that belong to Measured, Indicated and Inferred categories. In the survey, different QPs from same mining company applied different assumptions for similar type of deposits. There was no consistency in the creation of the parameters used for estimation passes for classification.

Table 6. Geometric classification parameters applied to different deposit types.

Deposit type	Parameter	Measured	Indicated	Inferred
Breccia pipe	DHS			
	CNDH	≤55	≤110	≤200
	NDH	≥3	≥1	≥1
Carlin-type	DHS	≤35 ft	≤75 ft	≤150 ft
	CNDH	≤30 ft, 80% sill range	≤80%–90% sill range	≤90% sill range
	NDH	≥2	≥1–2	≥1–2
	NS	≥2–3, with intercept	≥1–2	≥1–2
	ES		≤80% sill range	≤90% sill range
Epithermal high sulfidation	DHS			
	CNDH		≤20 m–35, ≤40 m–70	≤23 m–65, ≤70 m–110, ≤180 m
	NDH	≥1–2	≥1–2	≥1–2
	NS	≥1, with intercept	≥1–2	≥1–2
	ES			
Epithermal low sulfidation	DHS	≤75 ft	≤200 ft	≤300 ft
	CNDH	≤50 ft, ≤95 ft, 70% sill range	≤135 ft, ≤140 ft, 80% sill range	≤300 ft, 95% sill range
	NDH	≥3–5	≥2–3	≥1–2
	NS	≥4–8, ≤9–15	≥3–6, ≤7–12	≥1–5, ≤7–15
	ES	≤40 ft	≤100 ft	≤300 ft
Gold-Copper Porphyry	DHS	≤50 m	≤80 m	
	CNDH	≤10 m–35 m, 50%–60% sill range	≤40 m–50 m, 75–80% sill range	≤50 m, 90%–100 sill range
	NDH	≥1–≥3	≥1–≥3	≥1
	NS	≥4	≥4, ≥8	≥4–5
	ES	≤50 m–75 m	≤70 m–100 m	
Greenstone belt	DHS	≤25 m	≤25 m, 50 m	≤100 m, 120 m
	CNDH	≤20	≤20–30	
	NDH	≥2	≥3	≥2
	NS	≥16	≥16	≥8
	ES	≤50 ft	≤100 ft	≤500 ft
Lode and placer	DHS		40 m × 40 m	80 m × 80 m
	CNDH	≤30.5 m, ≤100 m	≤61 m, ≤36.6 m, ≤200 m	≤68.6 m, ≤76 m, ≤400 m
	NDH	≥3	≥1–2	≥1–2
	NS	≥3, ≥6	≥2, ≥3	≥3
Mesozonal orogenic	DHS	≤25 m	≤100 m	
	CNDH	≤30 ft, ≤50 ft	≤75 ft, ≤100 ft	
	NDH	≥1, ≥3	≥2	
	NS	≥6	≥4	
	ES		≤80% sill range	≤90% sill range

4 CONCLUSION

The investigation has served as a basis for identifying how different Qualified Persons apply different assumptions and approaches to categorize mineral resources into measured, indicated, and inferred in the gold mineral industry. The various mining companies considered in this survey did not apply consistent parameters for their estimation and classification

methods for same type of deposit, as the individual resource estimator used different knowledge and experience to generate the classification requirements. This has proved that the industry lacks standard procedure to be followed by all QPs. Although, all the QPs followed the NI 43-101 guidelines, the different approaches used could result in misleading public reports, since there was no right or wrong approach until mining production period. In addition, a single judgement by a QP of a project has major influence on the prospect of economic extraction. This makes QPs assumptions play important role in determining the resource uncertainty associated with economic viability of deposits. To champion the cause of addressing the inconsistency and misclassification problems, the industry needs to investigate into acceptable limits for assumptions made by different QPs in the estimation and classification of mineral resources, particularly in terms of geology and deposit type.

REFERENCES

Deutsch, C.V., Leuangthong, O. & Ortiz, J.M. 2016. A case for geometric criteria in resources and reserve classification. *CCG Annual Report* 08: Paper 301.
Ortiz, J.M., and Emery, X. 2006. Geostatistical estimation of mineral resources with soft boundaries: a comparative study. *Journal of the South African Institute of Mining and Metallurgy* (ISI), 106(8): 577–584.
Shaw, W.J., Godoy, M.C., Muller G & Larrondo, P. 2006. An approach to more objective classification of mineral resources. *6th International Mining Geology Conference, AusIMM*. NT: 85–89.
Verly, G., Postolski, T. & Parker H.M. 2014. Assessing uncertainty with drill hole spacing studies: applications to mineral resources. *Orebody modelling and strategic mine planning symposium 2014, AusIMM*. Melbourne: 109–118.

Transforming exploration data through machine learning

I.W.S. Whitehouse
Geobank, Australia

W. Slabik
MICROMINE, Australia

ABSTRACT: The application of machine learning to the process of collecting and analysing geological data in mineral exploration has the potential to transform the way explorers operate.

The traditional process of plan – drill – observe – measure – analyse can be slow and lead to costly re-drill or re-sample programs. A common issue faced by exploration companies is the inconsistency in the way data has been collected and categorised. This complicates the task of data modelling when undertaking economic viability studies. Using machine learning, data can be cleansed and validated prior to starting the modelling process.

There are several ways to streamline the process for the resource geologist, the first being feature identification through imagery. High quality DSLR cameras provide a tool for exploration companies to collect high quality imagery of core and chip trays. Machine learning algorithms can recognize features in the images such as colour, structures, veins, particle size and hand-written text. It is feasible for this data to be automatically collected and stored in a database.

Drill hole databases record rock interval attributes like rock code, hardness, colour, grade, location, and geophysical measurements. These attributes could be used as a lithological signature to identify other instances of similar signatures within the database. This technique could be used for data consistency testing or to discover new information within the dataset.

Finally, to illustrate the power of machine learning, a small research project is presented that successfully identified the regions of core tray imagery that contained drill core.

1 INTRODUCTION

Machine Learning (ML) is the field of study that gives computers ability to learn without being explicitly programmed (Géron, 2017). Instead of designing computer programs with explicit complex logic, the programs use input data to self-learn patterns to generate the desired output. The beginnings of machine learning and artificial intelligence (which ML is part of) date back to the early 1950s when Marvin Minsky and Dean Edmonds built the first computer machine capable of learning, (http://cyberneticzoo.com/mazesolvers/1951-maze-solver-minsky-edmonds-american/). However, technological limitations made it impossible to design and build a practical system that could help with complex problems. In 1996, when IBM developed a chess playing ML system that beat the reigning world champion (https://www.ibm.com/blogs/think/2017/05/deep-blue/), a significant development milestone in ML was achieved. This was followed by the introduction of AlexNet – machine learning neural network (Krizhevsky, A., Sutsskever, I., Hinton, G. 2012) which won the 2012 ImageNet competition in which a program had to label 150,000 photographs (http://image-net.org/challenges/LSVRC/2012/). AlexNet proved that computers can learn difficult patterns. These developments in ML design and massive advancements in computer processing speeds since the 1950s, means ML solutions are now able to accurately process information in real time.

Machine learning has already been used within the mining industry. But the application of this technology to geology, and to geological samples and observations is very limited. This paper undertakes a high-level review of the machine learning technology that could be applied to geological data. It highlights areas where the technology could add value to a resource business. And finally, it demonstrates the effectiveness of the technology by presenting a research project that was able to successfully isolate the areas of core within core tray imagery.

2 AN OVERVIEW OF MACHINE LEARNING

Machine learning algorithms use input data to learn patterns and use inference to build mathematical models. These models are used to make predictions or decisions on the input data (Bishop, 2006).

There are four main types of machine learning systems: supervised, semi-supervised, unsupervised, and reinforcement learning. Supervised learning algorithms create models using training data that contains inputs and labels. The iterative optimization of an objective function allows supervised learning algorithms to learn and predict the output from input data (Mohri et al, 2012) to the point where it can correctly determine the output for data not in the initial training dataset.

In unsupervised learning, no labelled data is used. Instead the system attempts to learn by following the output of functions. Clustering is an example of unsupervised learning where an algorithm tries to detect similar features in input data and group them into unlabelled groups. For example, if this style of algorithm was used to sort multiple pictures of a group of people, the algorithm would group similar images and each group would contain images of the same person.

The semi-supervised learning is a combination of supervised and unsupervised learning. Face recognition algorithms are a good example of this ML type. Using our earlier example, the unsupervised part of the algorithm detects and groups similar human faces from the set of pictures. If the user then labels the whole set of pre-grouped images, then this second part of the process is supervised, and the overall classification for the algorithm becomes semi-supervised.

The last type of reinforcement learning is where an algorithm learns by experimentation. The algorithm requires a scoring function to determine if it is making good or bad decisions. When this ML type is used to teach an algorithm for a self-driving car, the function gives a high score when the vehicle is driving within marked road lines, but if the car unintentionally goes outside the lines (it is not deliberately changing lanes) it receives a low score. This reliance on learning from bad decisions makes it difficult to practice reinforcement learning methods in the real-physical world. However, there have been some good results using this type in the virtual world. For example, OpenAI has prepared a reinforcement learning algorithm that can compete with some of the best players in a complex strategic game (https://blog.openai.com/openai-five/). This opens the possibility of using this ML type in the mine environment by training an algorithm on high quality digital twins of the mine.

Deep learning algorithms analyse an image by examining it through a series of layers (sometimes also called filters). The lower layers define the simple features while the higher layers composite the lower layers to create more abstract features (Bengio, 2015). For example, the first presentation layer may abstract the pixels and encode edges within the image. The next layer might combine arrangements of edges together. The third layer might encode the combined edges into wheels, a cab, or a tray. The final layer might recognise the image contains a haul truck.

Most deep learning algorithms are based on artificial neural networks. The design of artificial neural networks was inspired from the biological neural networks of animal brains (Coolen et al., 2005). An artificial neural network contains connected nodes called artificial neurons which are analogous to the neurons in a biological brain. Just like the synapses in a biological brain, the connections transmit a signal from one node to another. The signal is normally a real number, and the node computes a sum of the inputs with a non-linear function. The connections are called edges, and the nodes and the edges are weighted to adjust the

learning process. The weighting effects the strength of the signal at the connection. A node might filter data by only allowing values above a threshold to continue. Nodes, or artificial neurons, are arranged into layers with each layer typically performing a style of transformation (Bengio, 2015).

Convolutional Neural Network (CNN) is a neural network pattern that resembles the organisation of an animal's visual cortex. In the visual cortex individual neurons only respond to stimuli within a restricted region (called the receptive field) in the field of view. The receptive fields overlap to give the animal a full coverage of the field of view. The major advantage of this structure is the algorithm does not require human help with feature design. They have been in wide use since early 1990s. One of the first use cases was zip code reading system for United States Postal Service developed by Bell Labs (Chollet, 2017). In recent years CNNs have become a dominant computer vision technology which is enabling rapid growth of automation and robotics.

A machine learning network called Mask R-CNN, developed by Facebook's AI research team (Region based Convolutional Neural Network mask regions with Convolutional Neural Networks), is used for object detection and segmentation. Mask R-CNN is an approach to solve the problem of instance segmentation where objects in an image are detected and delineated. Instance segmentation is the combination of two problems: object detection and semantic segmentation. Object segmentation finds and classifies a variable number of objects in an image. While semantic segmentation is understanding an image at the pixel level (https://research.fb.com/publications/mask-r-cnn/). For example, which parts of a loaded haul truck image are the truck and which parts of the image are the ore.

3   POTENTIAL APPLICATIONS

Many areas of the mining value chain could benefit from machine learning. This is particularly true for the collection and initial analysis of geological observations and measurements.

Once a company has identified a resource target, they will invest large amounts of time and money in discovering the physical distribution of the mineralization. The primary data collection methods are outcrop or surface sampling, trench sampling and samples collected from drill rigs. Samples from these methods are often chemically analysed and are described by observations. The companies use this data to determine if the deposit is economically viable using technical and business modelling techniques.

Samples are commonly photographed with a digital single lens and reflex mirror (DSLR) camera as part of the collection procedure. A deposit commonly has a photo library of images of thousands of meters of drill core. These photos are normally poorly annotated with metadata and are simply used by the geologist as a visual reference to the sample to save them the effort of looking at the physical sample (if it still exists).

The sample photos are normally photos of drill core or chips. Drill chips (Figure 1) are the samples created by drilling techniques where a drill-bit fragments the rock and compressed air lifts these fragments to the surface. Core samples are cylinders of rock cut as a diamond tipped steel sleeve (the drill-rod) cuts down into the rock. Photos of drill cores (Figure 2) are normally photos of storage trays containing a length of the core (for example, 5 meters of core). To associate the part of a core tray photo with a drill hole interval, the strips of core in the photograph must be extracted. This is a tedious manual process.

Core tray photos often contain metadata. The hole name and depth measurements are often written on the tray or on blocks placed in the tray along with the core (Figure 3). Extracting this data and storing it along with the core images allows the location of the images in 3-dimensional space.

The logging of core is a time-consuming process and geologists can waste valuable time logging core from uneconomic areas. Having a system that can identify zones of interest within a core and direct a geologist to review those zones provides a more efficient utilisation of the geological team's time. By directing senior geological staff to view key zones of mineralisation, the overall quality of the logging will improve. Currently, the geologists logging

Figure 1. A photograph of drill chips.
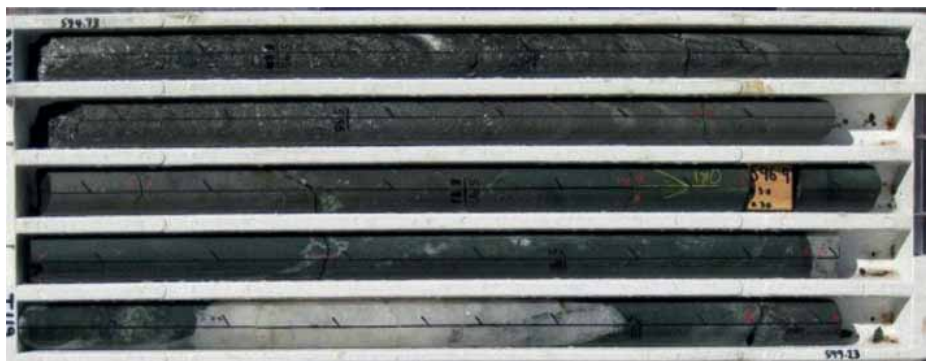
Figure 2. A photograph of a core tray.
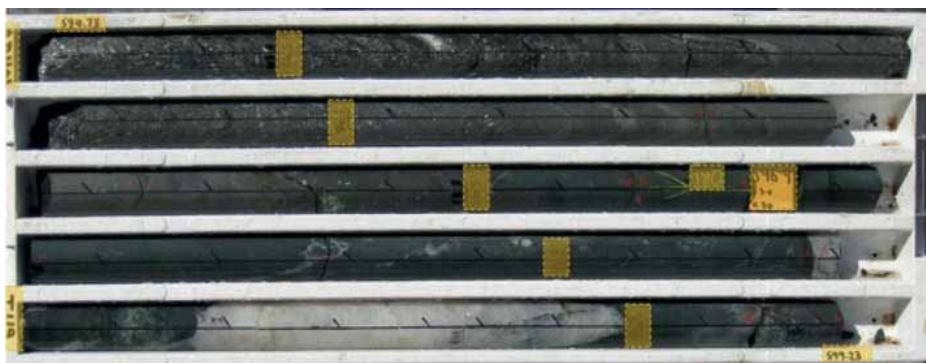
Figure 3. Metadata such as the drill hole identifier and depth values can be extracted from the core tray images.

the core are often junior members of staff and their lack of experience can mean important features are overlooked or misclassified. Inconsistent logging can have a flow-on effect to the quality of the geological models produced.

Mineralisation is controlled by geological features. Errors in the modelling of the geology will cause errors in the understanding of the mineralisation distribution. This is particularly true when computers are increasingly relied on to build the geology model. An artificial intelligence technique called implicit modelling uses algorithms to generate the geological shapes. Although inconsistent logging will impact the quality of a human created model, a human has some capacity to generate models that account for the inconsistencies. However, a computer-generated implicit model based on the same data will simply follow the input data and produce a model that is inherently wrong. As companies become more reliant on computer generated models, the possibility of lower quality models caused by low quality input increases.

The concept of geological consistency extends to stratigraphic sequences. Often there is an expected lithological order down a hole and the geologist assumes to see rocks within a drill hole in this order. If this sequence is not observed, it could indicate the geological sequence has been disrupted by folding or faulting, or there is an error in the logging. Artificial intelligence can be used to identify drill holes that fail to conform to the expected pattern. Such holes could be flagged for review by senior staff.

Understanding the engineering strength of a rock effects the stability of the mine. Rocks with lower strengths require lower angles for pit walls and greater support underground. Major factors in determining the rock's strength are understanding the joint patterns, density, geometry and joint infill. The geotechnical properties of the rock not only effect the safety of the mine but also its economic viability. It is therefore highly advantageous to train a computer system to identify and measure joints and fractures in the rock from core imagery.

As the mining industry becomes more automated, the need for equipment to monitor itself and correct its actions based on monitoring results increases. An example of this is an automated blast rig drilling on a coal deposit. The blast holes are drilled so explosive charges can be used to fracture the rock overlying the coal. This makes it easier for equipment to remove this overburden. The blasting should not extend into the coal seam. The holes drilled for blasting should stop before the coal is reached. Having drill rigs that can detect the approaching top of a coal seam and so stop drilling is helpful.

Often when a hole is drilled, geophysical instruments are lowered down the hole to take measurements of the surrounding country rock. These measurements provide a valuable source of objective data. Certain strategic horizons have very pronounced geophysical signatures. This is particularly true for coal seams. These signatures could be used to help identify known coal seams.

The geophysical traces are useful in correcting the depth of samples and observations. As the hole is drilled, the sample depth is estimated. Unfortunately, drill cores fracture or sections of the core can be destroyed in the drilling process. This makes the depth estimations difficult. By comparing the geophysical traces of the surrounding country rock with the rock in the core, it is possible to adjust the depth of observations and samples to a value closer to the real collection depth. This process is currently undertaken manually.

4 CASE STUDY

Not only can machine learning assist in the areas of process efficiencies, data quality and prediction, but it can be used to extract information from historic photographic datasets. Core tray imagery contains a wealth of textural, mineralogical and geotechnical information. However, this data source is poorly utilised because of the arduous manual process of clipping the regions of core from each core tray image.

MICROMINE Pty Ltd (MICROMINE) undertook a research project as part of the Newcrest Crowd "Get 2 the Core" online competition. Machine learning was applied to extract the core outline from core tray images. The spatial extent of the tray in each image was determined and within that region, the rows containing the core were isolated. Masking core tray images to isolate just the core is difficult because the tray boxes can be made from a

variety of materials, the images are highly variable in terms of resolution, aspect ratio, quality and the relative position of the tray within the image is inconsistent.

Transfer learning was utilised to quickly train a Mask R-CNN model to deal with the core tray data. This negated the need to label thousands of core trays to train the machine. More traditional edge detection techniques were used to mask the core bounding box (Figure 4 and Figure 5).

Figure 4.   The raw image of a core tray.
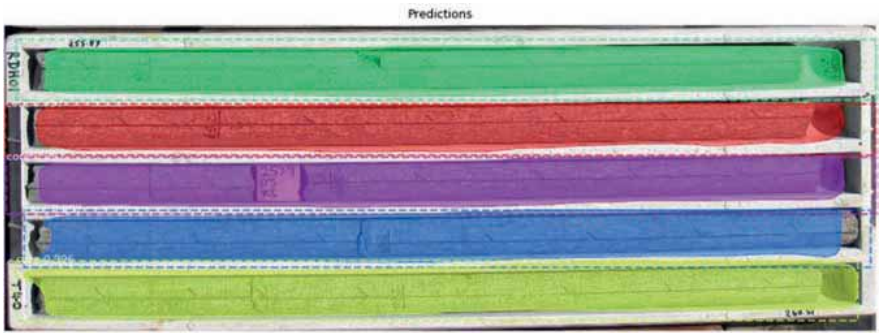
Figure 5.   The core image in Figure 3 with areas identified by machine learning as core masked by colour regions.
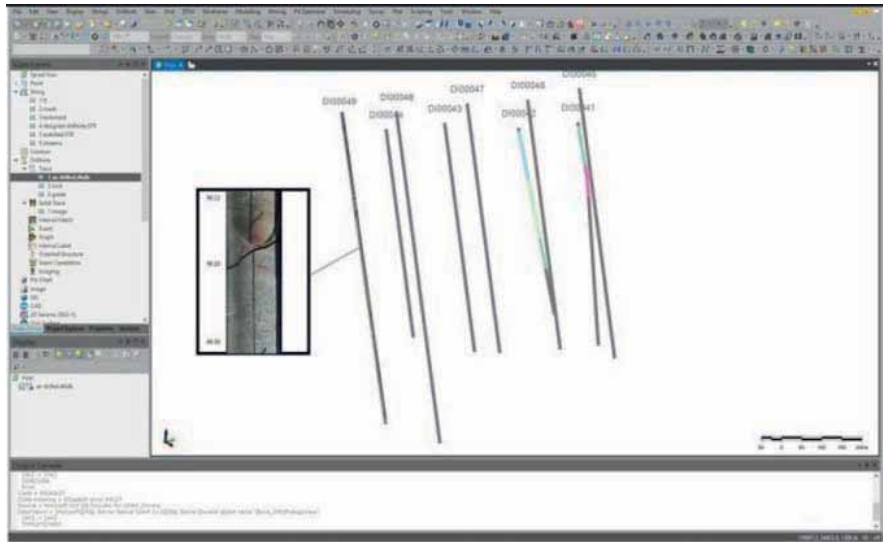
Figure 6.   A representation of how clipped core images could be shown in a sectional view.

When the algorithm was run against a test dataset, a success score of over 98% was achieved. MICROMINE plans to commercialize this machine learning technology. The vision is to develop technology that transforms the core tray photos into continuous drill core images for each hole (Figure 6).

MICROMINE currently has technology that can do this. It can join and present 2-dimensional core images on 3-dimensional drill hole strings. Using the technological developments described in this paper, the manual imaging clipping and labeling processes will be replaced by ones controlled by machine learning.

The accuracy of automatically positioned clipped core images is unknown. Determining this accuracy is a subject for later investigations.

5   CONCLUSION

The development of machine learning and the ability to use pre-trained algorithms allows the rapid development and deployment of this technology to drill hole data. The technology has already been successfully tested in a project that separated the core and non-core components in core tray imagery. But similar image processing techniques could be developed to recognize features such as colour and geological structures. Isolating this data and storing it in databases along with related observations and measures will deliver value to the geologist.

Machine learning can also be applied to non-image data to make geological predictions during drilling and to check the quality and consistency of manual and electronically collected data. This includes the use of geophysical and geochemical signatures to help in the isolation and identification of lithological units.

Machine learning is becoming an important tool to the geologist and will improve the quality and consistency of the data available to processes within the mining chain of activities. If the technology can be effectively applied, the efficiency gains will improve mine profitability through reduced cost, time and increased data quality.

REFERENCES

Bengio, Yoshua; LeCun, Yann; Hinton, Geoffrey 2015. "Deep Learning". Nature. 521 (7553): 436–444. Bibcode:2015 Natur.521.436 L. doi:10.1038/nature14539. PMID 26017442.
Bishop, C.M. 2006, Pattern Recognition and Machine Learning, Springer, ISBN 978-0-387-31073-2.
Chollet, F. 2017. "Deep Learning with Python". O'Reilly Media.
Coolen, A.C.C, R. Kuehn, P. Sollich 2005. "Theory of Neural Information Processing Systems". Oxford University Press.
Dimitri P. Bertsekas 2012 Dynamic Programming and Optimal Control: Approximate Dynamic Programming, Vol.II", Athena Scientific.
Dimitri P. Bertsekas and John N. Tsitsiklis 1996 Neuro-Dynamic Programming, Athena Scientific.
Geron, A. 2017 "Hands-On Machine Learning with Scikit-Learn and TensorFlow". O'Reilly Media, Inc, USA.
Krizhevsky, A., Sutsskever, I., Hinton, G. 2012. "*ImageNet Classification with Deep Convolutional Neural Networks*". https://papers.nips.cc/paper/4824-imagenet-classification-with-deep-convolutional-neural-networks.pdf.
Mohri, Mehryar; Rostamizadeh, Afshin; Talwalkar, Ameet 2012. Foundations of Machine Learning. The MIT Press. ISBN 9780262018258.
Russell, Stuart J.; Norvig, Peter 2010. Artificial Intelligence: A Modern Approach (Third ed.). Prentice Hall. ISBN 9780136042594.
Poole, David; Mackworth, Alan; Goebel, Randy 1998. Computational Intelligence: A Logical Approach. New York: Oxford University Press. ISBN 978-0-19-510270-3.
Yann LeCun, Yoshua Bengio & Geoffrey Hinton Nature 521, 436–444 (28 May 2015). doi:10.1038/nature14539.

Rock mass characterization using MWD data and photogrammetry

S. Manzoor, S. Liaghat, A. Gustafson, D. Johansson & H. Schunnesson
Division of Mining and Geotechnical Engineering, Luleå University of Technology, Luleå, Sweden

ABSTRACT: Measurement while drilling data are produced in enormous quantity in underground and surface mines across the world. The data comprise parameters recorded during the drilling process, including penetration rate, rotation pressure, feed pressure, percussive pressure, damping pressure and flush pressure. MWD data are shown to be very useful for rock mass characterization, blasting applications and geological modelling of the rock mass. In this study, an open pit mine in Austria was selected for data collection as a part of SLIM project. The MWD data collected from drilling rigs were processed to identify different zones of rock mass, i.e. weak, fractured or competent rock. The results were compared to 3D images obtained by close-range terrestrial digital photogrammetry for validation; which showed a close agreement with each other. The method can be used to characterize the rock and to modify the charging of explosives in the boreholes for improved blasting results.

1 INTRODUCTION

Measurement while drilling (MWD) is a technique that monitors relevant drill process parameters, which usually include penetration rate, percussive pressure, rotation pressure, feed pressure, damping pressure and flush pressure during the drilling operation. The technique increases the available information about the rock mass and improves the characterization of the rock mass (Khorzoughi, 2013). In particular, MWD technique provides a better description of the hidden volume of the rock mass compared to other exploration methods (Segui & Higgins, 2002). The most important aspect of MWD is that it collects information with reduced time and cost compared to other methods like core drilling or geophysical surveys (Khorzoughi, 2013). The technique was introduced in the oil industry in 1911 to diminish the uncertainties involved in drilling operations and was applied to mining in the 1970s (Segui & Higgins, 2002). Since then, many researchers have applied this technique to improve different mining operations.

Leighton (1982) used drill monitoring technique to optimize fragmentation, reduce blast damage and increase slope stability by improving the blast design. Similarly, Piyush et al. (2016) used MWD to improve the blast design and its results. Schunnesson (1996) interpreted the MWD parameters to identify the fracture zones along the borehole in a railway tunnel and calculate rock quality designation (RQD). Ghosh et al. (2018) assessed the chargeability of production boreholes by analyzing the MWD parameters. Drill monitoring parameters have also been used for real-time assessment of the unconfined compressive strength of the rock mass (Rodgers et al., 2018). Information extracted from MWD data can be used for better blast design, resulting in less ore dilution, improved fragmentation size and better muckpile diggability (Khorzoughi, et al., 2018). A combination of MWD data and excavation design parameters in underground constructions can predict the blast-induced excavation damage zone quite well (Van Eldert, et al., 2018).

MWD data have often been used to relatively characterize the rock mass (Khorzoughi, 2013; Van Oosterhout, 2016; Khorzoughi, et al., 2018) but established methods for rock mass characterization has rarely been used to validate results. These methods vary from traditional

one-dimensional scanline and two-dimensional window surveys using compass-clinometer technique (Gaich, et al., 2006; Sturzenegger & Stead, 2009) to modern photogrammetry and laser scanning techniques (Ferrero, et al., 2009). In the last two decades, aerial and close-range terrestrial digital photogrammetry (CRTDP) has evolved as a powerful tool widely used for 3D topographic modelling and rock mass characterization (Westboy, et al., 2012). Wolf & Dewitt (2000) used the term 'close-range' for a distance between camera and object up to 300 m. CRTDP is gaining widespread application as a mapping tool to characterize natural and man-made rock slopes in 3D (Sturzenegger & Stead, 2009). It is a useful tool for comprehensive surveys of the geometrical-structural layout of the rock face, even in remote sites (Firpo, et al., 2011). Sturzenegger & Stead (2009) document the following advantages with this technique:

– It provides more representative data than other conventional methods, as it is not restricted to the base of the outcrop;
– It makes it easier to access steep and high rock faces;
– It is safer in poor rock conditions, as the surveyor does not need to physically access the rock face;
– It makes the record more permanent;
– It is applicable in magnetic environments where conventional compass-clinometer method fails to work

Recent advancements in computing technologies and digital photography have increased the potential of CRTDP to be used in geotechnical engineering for rapid construction of 3D models and rock mass characterization (Sturzenegger & Stead, 2009). Many commercial software packages are available to generate 3D models of the rock face and to extract its structural parameters.

This study characterized rock into weak/fractured and hard/competent rock depending on its relative response to the MWD parameters and then validated the results using CRTDP. MWD data and stereoscopic images were collected from an open-pit mine in Austria, and an algorithm was developed using MATLAB to plot the drilling parameters for the depth of the hole. ShapeMetriX3D (by 3GSM) was used to develop 3D models from stereoscopic images and extract structural information on the rock face to validate the MWD results.

2 METHODOLOGY

This research was based on a literature review, measurement while drilling data, stereoscopic images of the bench face, 3D models and data analysis. Commercial software packages MAT-LAB and ShapeMetriX3D were used to analyze data collected from VA Erzberg's open-pit iron ore mine in Austria.

2.1 *Site description*

VA Erzberg's open-pit iron ore mine is located in Eisenerz, an old mining town of Styria in the central-western part of Austria located about 260 km south-west of the capital, Vienna. Erzberg is estimated to have the largest reserves of iron ore in the country, with approximately 260 million tons of iron ore. Geologically, it is in the greywacke zone, a band of sedimentary rocks that metamorphosed in the Paleozoic era between the Central Eastern and Northern Calcareous Alps of Austria.

The mine is the world's largest deposit of siderite ($FeCO_3$) mineral, mixed with dolomite ($CaMg(CO_3)_2$) and ankerite ($CaFe(CO_3)_2$), and the most common minerals in the deposit are siderite, ankerite, dolomite and calcite. Azurite, malachite and vermilion are also found occasionally. Less common minerals include sideroplesite, chalcanthite, erzbergite, epsomite, rancieite, enargite, dravite and others. Chemical analysis of cutting samples from the mine presents ten (10) different chemical products, including Fe, CaO, SiO_2, MgO, Mn, Al_2O_3,

Na$_2$O, K$_2$O, S and P. Given the presence of these different mineral compositions in the mine, the iron concentration ranges from 22–40%, giving an average value of 33%.

The Erzberg mine has been in operation for more than 1300 years. The deposit was initially mined using underground methods. Later, in 1890, the mining was changed to open-pit, with mining done in benches. In 1986, underground operations were totally ceased and open-pit mining became the only method. As per current production and reserve estimation, the mine can be operating for another 30–35 years.

Currently, The Austrian mining company VA Erzberg is carrying out the mining activity with a workforce of about 250 persons. The mine has a total of 31 benches, of which 21 are currently active. A total of about 12 million tons of rock, including 8 million tons of waste, is mined out annually using conventional drill and blast technique. Because of the varying nature of the ore quality, different short term and long term plans have been made using deposit models to maintain a good balance of iron concentration for processing purposes.

After blasting, the waste is dumped in a nearby dump area, and the ore is hauled to the crushers. Two gyratory crushers (with a capacity of 1200 tons per hour) break the boulders and bigger pieces of rock into a maximum particle size of 15 centimeters. The crushed material is processed further to remove the waste from the ore. This processing phase includes sensor based sorting for the high quality ore (iron content > 30%) and dense media separation for the low quality ore. After removal of the waste, 3 million tons of ore are crushed again to achieve the final product size of 2–10 mm in diameter which are transported to Linz and Donawitz for processing into high quality steel.

2.2 Measurement while drilling

In the Erzberg mine, drilling is done with fully mechanized Epiroc D65 drill rigs equipped with pneumatic Down-The-Hole (DTH) hammers. The Epiroc drill monitoring system retrieves and stores MWD data. The recorded data include time (YYYY-MM-DDThh:mm:ss), depth (m), penetration rate (m/min), feed pressure (bar), rotation pressure (bar), and percussive pressure (water pressure measured by bar). The sampling interval along the borehole is set to 5 cm. On each drill rig MWD data are stored on a USB memory. For this test MWD data were collected from two different bench faces for a total of 14 boreholes. The length of the boreholes was approximately 30 m.

2.3 Image collection

For this study, stereoscopic images were taken using a Nikon D70 s camera with an 18 mm zoom lens. The camera was calibrated and provided by 3GSM as a component of the ShapeMetriX3D software package. At least two images (stereoscopic image pair) are required to generate a 3D model. Several images were taken parallel to the bench face, and the best ones were used for further processing. For the software, the distance between the imaging points (baseline distance) should be about 1/10 to 1/8 of the distance between the imaging point and the rock face (3GSM, 2010). The standard procedure to take stereoscopic images for ShapeMetriX3D is described by 3GSM (2010) and Gaich et al. (2006). Figure 1 shows the image of one of the benches at the mine site.

Range poles with target discs can be seen in the image that are used for referencing and scaling the 3D models. The coordinates of the range poles were determined using GPS and used for referencing the 3D model in a global co-ordinates system.

2.4 Model generation

The software has a special tool, 'Reconstruction Assistant', to convert the stereoscopic image pair into a 3D image. The images were loaded onto the software, and 3D models were generated using this tool. Another tool, 'Surface Trimmer', was used to edit the 3D images to remove the undesired areas from the images. Finally, the software's 'Referencer' tool was used to reference the generic 3D images onto global co-ordinates system. These steps follow the

Figure 1.   Bench face with range poles at Erzberg's open pit mine in Austria.
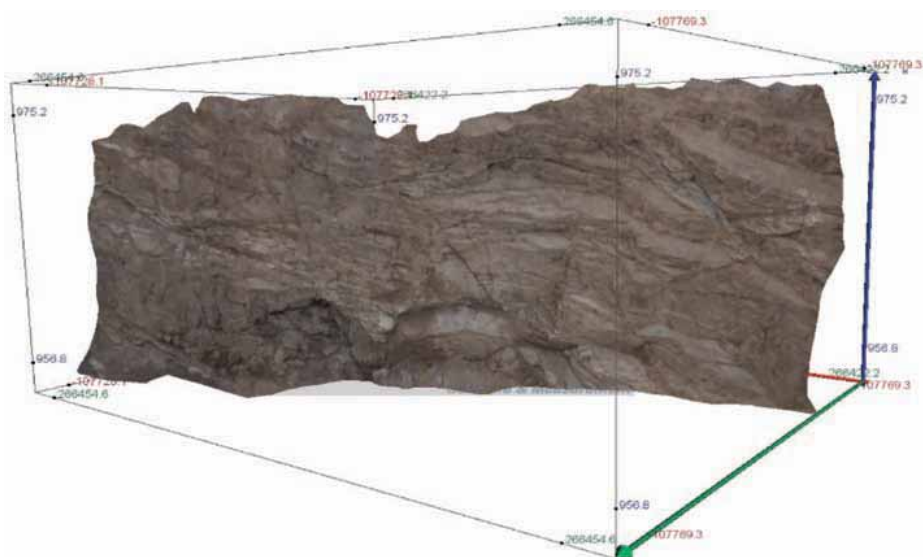
Figure 2.   3D model of a bench face with global co-ordinates at Erzberg's open pit mine in Austria.

standard procedures outlined by 3GSM (2010). Figure 2 shows a 3D image developed using these tools.

3   DATA ANALYSIS

To characterize the rock as weak/fractured or hard/competent rock depending on its relative response to the MWD parameters, the data analysis comprised the following two steps:

1. MWD data analysis
2. Structural data analysis

3.1 *MWD data analysis*

MWD data were collected from the drilling rigs. To extract information from the collected data, an algorithm was developed using MATLAB. The development of the algorithm included:

– Data importation
– Noise reduction
– Parameters extraction
– Variation detection

The drill monitoring system feature three types of files: drill plan (DP), drill quality (DQ), and MWD. The DP file contains the drill plan that were transferred to the drill rig from the mine office. The DQ file gives the status of the drilling process, whether it was successful or if there were any failures during the drilling operation. The MWD file contains penetration rate, percussive pressure, rotation pressure, feed pressure, damping pressure and flush pressure measured during the drilling process.

'Hole ID' and 'Plan ID' from the DQ file and the MWD file were used to import drilling parameters for the required boreholes. Data were imported into MATLAB and filtered to remove noise or faulty MWD samples. Faulty samples included unrealistic values, e.g. negative or abnormally high values for penetration rate or pressure. In addition, variations in drilling parameters during rod changes are not representative samples of the rock behavior during drilling. These unrepresentative samples were removed from the data using the developed algorithm. Figure 3 shows the drilling parameters plotted against the depth of the hole before and after filtering the data.

In Figure 3 (left side), one sampled penetration rate value is more than 2000 m/min; which is an unrealistic value for penetration rate. The figure also shows drops in percussive pressure and feed pressure at 6 m intervals that correspond to adding a new rod after every 6 m. It is important to remove these faulty and unrepresentative samples to get a clear picture of the rock behavior.

Drilling parameters were extracted and plotted against the depth of the borehole using the algorithm. The coordinates of the start and end point of the borehole were stated on the plot, along with the status of drilling activity, i.e. success or fail.

Penetration rate is the most effective drilling parameter to characterize the rock mass using MWD (Khorzoughi, 2013). For example, a fractured rock mass exhibits higher penetration rate and increased rotation pressure (Vezhapparambu, et al., 2018). Penetration rate increases when the drilling encounters a fracture and demonstrates high variation in an extensively fractured rock mass (Schunnesson, 1996). The torque/rotation pressure also shows an increase
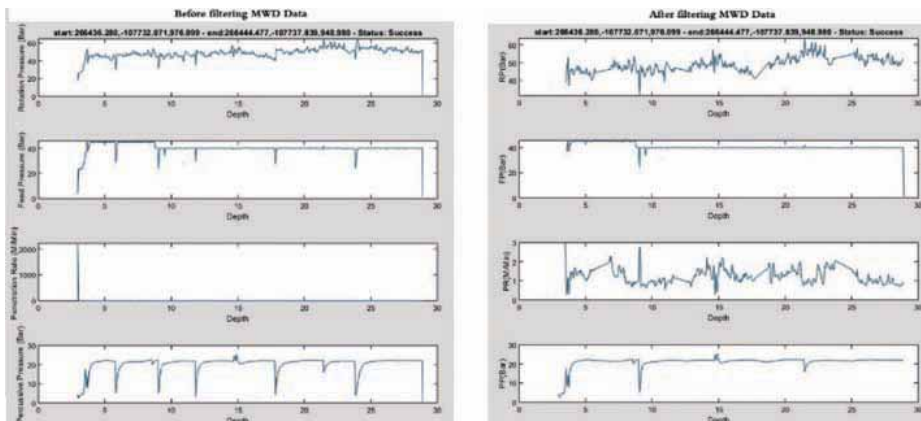
Figure 3.   MWD data before and after filtering unrepresentative samples.
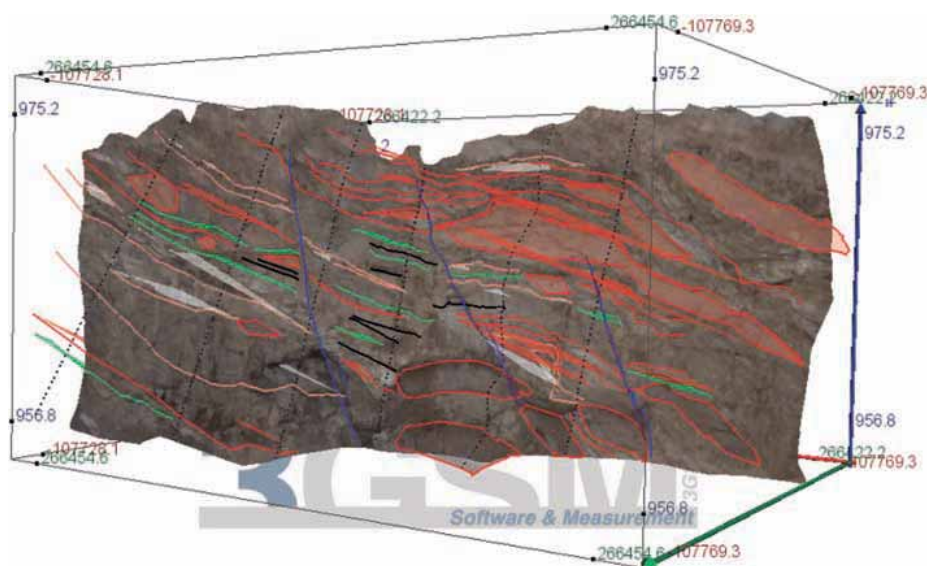
Figure 4.   3D model of a bench face with marked structures and scanlines on the surface.

when drilling through a broken rock mass as it has the tendency to stall the drill bit (Schunnesson, 1996). The Rock strength, fractures and voids can affect the penetration rate (Segui & Higgins, 2002). The peaks on the logs of penetration rate to depth show the presence of fractures, and widths of these peaks indicate the fractures' aperture size (Khorzoughi, 2013). As the drill bit encounters an open fracture, penetration rate increases and rotary torque decreases, as there is no resistance based on the aperture size (Khorzoughi, 2013). The feed pressure and pull down pressure show a slight drop as well, because there is no engagement of the drill bit with the rock mass (Khorzoughi, 2013).

3.2   *Structural data analysis*

The 'SMX Analyst' tool of ShapeMetriX3D, which is very useful tool for present purposes, (Gaich, et al., 2006; Haneberg, 2008; Vasuki, et al., 2014; Beyglou, 2016; Buyer & Schubert, 2017) was used to analyze the structural parameters of the 3D models,. Analysis included the following steps:

– Marking structures on bench face;
– Adding scanlines at borehole locations;
– Determining depth of structures along scanlines.

Figure 4 shows a bench face with marked structures and scanlines. Structures were marked manually using the features of the SMX Analyst tool. Scanlines were drawn at the borehole locations using the coordinates of the boreholes.

The software can generate different structural characteristics like dip, dip direction, spacing, depth of the structures etc. Scanlines were used to extract information on the spacing and depth of the structures along the boreholes.

4   RESULTS AND DISCUSSION

MWD parameters show distinguishable responses to the following:

– Soft or weak rock
– Hard or competent rock
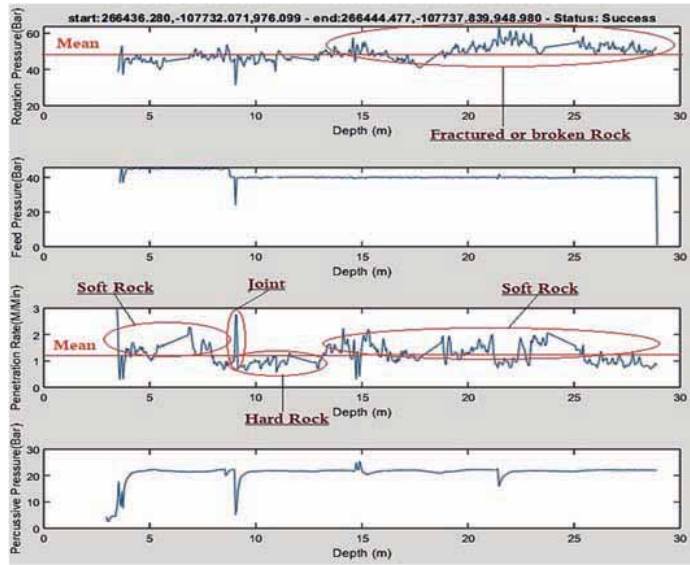
Figure 5. MWD data variations related to different rock types.

– Open joints
– Fractured or broken rock

Two of the drilling parameters, percussive pressure and feed pressure, are controlled by the machine and normally don't respond to the rock behavior (Ghosh, et al., 2017). Variations in these parameters can be seen in Figure 3 for the rod changing process. The other two parameters, penetration rate and rotation pressure, are more sensitive to changes in the rock mass (Schunnesson, 1996). Figure 5 shows the MWD parameters for one borehole, including responses to soft rock, hard rock, open joints and fractured or broken rock.

In the figure, there is a zone of increased rotation pressure compared to the mean value, indicating a rock mass that is highly fractured or broken. This type of rock mass has a tendency to hold or stall the drill bit; therefore, the rotation pressure is increased to maintain the rotation speed. Penetration rate is different for different rock masses. In the figure, penetration rate is higher at the start than the mean, indicating soft or weak rock. Next, a sudden rise indicating open joint, allows the bit to penetrate at a higher speed but only for a moment indicating a narrow aperture size. Following this, a zone with lower penetration rate than the mean indicates hard or competent rock; which was difficult to penetrate than the first zone (with soft rock). At the end, there is another increase in penetration rate with lots of variations indicating weak or soft rock. This zone is highly fractured, a finding confirmed by the rotation pressure.

5 CORRELATION AND VALIDATION

Coordinates of scanlines marked on the bench face and the boreholes from the MWD files were matched to correlate the results. Scanlines were used to determine the depth of the structures visible on the bench face. Information extracted from the 3D image of the bench face with the borehole discussed above suggests similar results. Figure 6 shows the bench face with different rock mass features. At the start, the bench face has weak rock which is removed as back break from the blast but can be seen on the bench face using dip and dip direction values. This material is separated from the competent rock at a depth of 9 m which can be seen as a joint or bedding plane on the bench face. This joint causes a sudden increase in the penetration rate and a drop in the other three drilling parameters indicating an open joint.
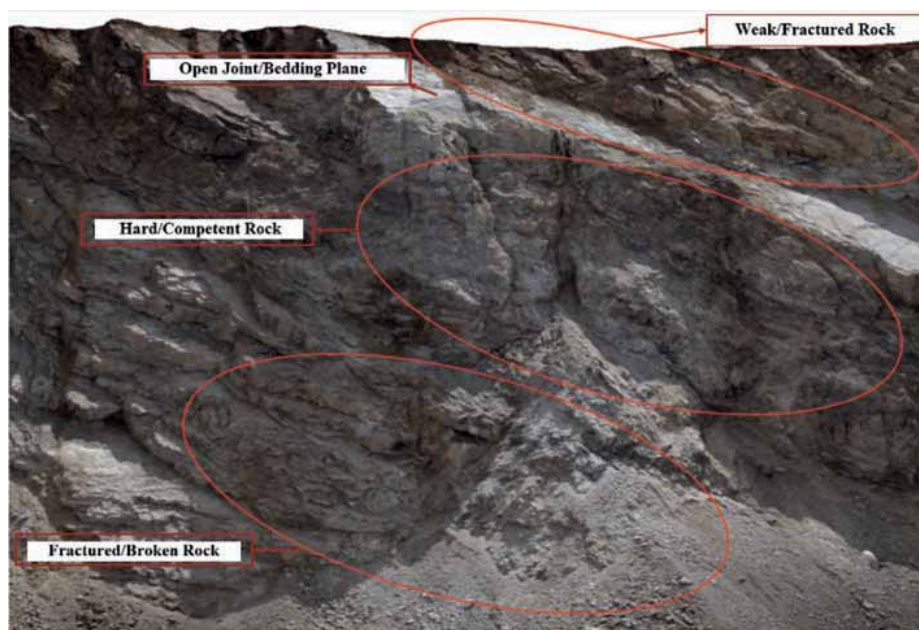
Figure 6. Bench face showing different types of rock mass.

This is followed by a decrease in penetration rate to a depth of 14 m due to the underlying hard or competent rock. At the lower part of the bench face, there is a highly fractured and broken rock mass which causes an increase in penetration rate as well as an increase in rotation pressure in MWD data, as the drill bit has a tendency to stall in such rock conditions. The last part of the MWD data cannot be seen in the image because of the loose material at the toe of the bench face and sub-drilling.

6 CONCLUSION

Results of MWD data and CRTDP data are in close agreement. A higher penetration rate suggests a weaker rock mass and vice versa. A sudden increase in penetration rate suggests the presence of an open joint as closed fractures or joints don't cause the sudden variations seen in the results. Higher rotation pressure suggests a highly fractured or broken rock mass with higher resistance for the bit to rotate. Findings show that the MWD data variations can be used to predict the nature of the rock mass, and this information can be used to optimize the blast design. This will reduce the consumption of explosives in weaker rock mass and improve the stability of the remaining wall by reducing the back break effects.

REFERENCES

3GSM, 2010. *ShapeMetriX 3D, User Manual*. Graz: 3G Software and Measurement GmbH.

Beyglou, A., 2016. *On the Operational Efficiency in Open Pit Mines*, Licentiate Thesis. Luleå: Luleå Tekniska Universitet, Sweden. ISBN: 978-91-7583-699-7 (electronic).

Buyer, A. & Schubert, W., 2017. Calculation the Spacing of Discontinuities from 3D Point Clouds. *Proceedia Engineering* 191(1): 270–278.

Ferrero, A.M., Forlani, G., Roncella, R. & Voyat, H.I., 2009. Advanced Geostructural Survey Methods Applied to Rock Mass Characterization. *Rock Mechanics and Rock Engineering* 42(1): 631–665.

Firpo, G., Salvini, R., Francioni, M. & Ranjith, P.G., 2011. Use of Digital Terrestrial Photogrammetry in Rocky Slope Stability Analysis by Distinct Elements Numerical Methods. *International Journal of Rock Mechanics & Mining Sciences* 48(1): 1045–1054.

Gaich, A., Pötsch, M. & Schubert, W., 2006. Acquisition and Assessment of Geometric Rock Mass Features by True 3D Images. In: *The 41st U.S. Symposium on Rock Mechanics (USRMS), 17–21 June, 2006*. Golden, Colorado: American Rock Mechanics Association.

Ghosh, R., Gustafson, A. & Schunnesson, H., 2018. Development of a Geological Model for Charge-ability Assessment of Borehole using Drill monitoring Technique. *International Journal of Rock Mechanics and Mining Sciences* 109(1): 9–18.

Ghosh, R., Schunnesson, H. & Gustafson, A., 2017. Monitoring of Drill System Behavior for Water-Powered In-The-Hole (ITH) Drilling. *Minerals* 7(121).

Haneberg, W.C., 2008. Using Close Range Terrestrial Digital Photogrammetry for 3D Rock Slope mod-elling and Discontinuity Mapping in the United States. *Bulletin of Engineering Geology & Environment* 67(4): 457–469.

Khorzoughi, M.B., 2013. *Use of Measurement While Drilling Techniques for Improved Rock Mass Characterization in Open-Pit Mines*, Master's Thesis. Vancouver: University of British Columbia, Canada. DOI: 10.14288/1.0073823.

Khorzoughi, M.B., Hall, R. & Apel, D., 2018. Rock Fracture Density Characterization using Measurement While Drilling (MWD) Technique. *International Journal of Mining Science and Technology* 28(1): 859–864.

Leighton, J.C., 1982. *Development of a Correlation between Rotary Drill Performance and Controlled Blasting Powder Factors*, Master's Thesis. Vancouver: University of British Columbia, Canada. DOI: 10.14288/1.0095103.

Piyush, R., Schunnesson, H., Lindqvist, P.-A. & Kumar, U., 2016. Measurement-While-Drilling Technique and its Scope in Design and Prediction of Rock Blasting. *International Journal of Mining Science and Technology* 26(4): 711–719.

Rodgers, M., McVay, M., Horhota, D. & Hernando, J., 2018. Assessment of Rock Strength from Measuring While Drilling Shafts in Florida Limestone. *Canadian Geotechnical Journal* 55(8): 1154–1167.

Schunnesson, H., 1996. RQD Prediction Based on Drill Performance. *Tunneling and Underground Space Technology* 11(3): 345–351.

Segui, J.B. & Higgins, M., 2002. Blast Design Using Measurement While Drilling Parameters. *Fragblast: International Journal for Blasting and Fragmentation* 6(3–4): 287–299.

Sturzenegger, M. & Stead, D., 2009. Close-Range Terrestrial Digital Photogrammetry and Terrestrial Laser Scanning for Discontinuity Characterization on Rock Cuts. *Engineering Geology* 106(1): 163–182.

Van Eldert, J., Schunnesson, H., Johansson, D. & Saiang, D., 2018. Measurement While Drilling (MWD) Technology for Blasting Damage Calculation. In: Håkan Schunnesson and Daniel Johanson (ed.), *12th International Symposium on Rock Fragmentation by Blasting, Luleå, Sweden, 11-13 June 2018*. Luleå: Luleå University of Technology. pp. 139–148.

Van Oosterhout, D., 2016. *Use of MWD Data for Detecting Discontinuities*, Master's Thesis. Delft: Delft University of Technology, Netherland.

Vasuki, Y., Holden, E., Kovesi, P. & Micklethwaite, S., 2014. Semi-Automatic Mapping of Geological Structures using UAV-Based Photogrammetric Data: An Image Analysis Approach. *Computers & Geosciences* 69(1): 22–32.

Westboy, M.J. et al., 2012. 'Structure-from-Motion' photogrammetry: A low-cost, effective tool for geoscience applications. *Geomorphology* 179(1): 300–314.

Vezhapparambu, V.S., Eidsvik, J. & Ellefmo, S.L., 2018. Rock Classification Using Multivariate Analysis of Measurement While Drilling Data: Towards a Better Sampling Strategy. *Minerals* 8(384).

Wolf, P.R. & Dewitt, B.A., 2000. *Elements of Photogrammetry with Applications in GIS*. Third Edition ed. Boston: McGraw Hill Higher Education. ISBN: 0072924543.

Ore grade prediction using informative features of MWD data

S. Liaghat, A. Gustafson, D. Johansson & H. Schunnesson
Division of Mining and Geotechnical Engineering, Luleå University of Technology, Sweden

ABSTRACT: Detailed knowledge of the content and geometrical variation of ore grade is essential in mining operations for production planning and economic analysis. Common ore grade specification methods, sampling and analysis are costly and time consuming. Measurement While Drilling (MWD) technique can directly extract grade information from the drilling process increasing data resolution and reducing cost.

This study introduces a supervised feature selection method based on the Hilbert-Schmidt independence criterion to increase the accuracy of the results and decrease processing time. Potential of the method for recognizing the most effective and non-repetitive dimensions of input data has also been investigated. By exploiting the lower dimension data, a classification model is developed to map the parameter values to ore grade levels.

Evaluation of the model using MWD data from LKAB's Leveäniemi mine proved the effectiveness of the proposed feature selection and classification method.

1 INTRODUCTION

The economic evaluation of possible mining operation for exploring new ore bodies is critical but requires accurate ore grade information (Wellmer et al. 2010). Two common methods for specifying the ore grade are core drilling and drill cutting analysis. The results of core drilling form the basis for investments and long-term production planning. Since the sampling holes are quite far apart, low-resolution data and uncertainty about un-cored areas between holes will be observed (Starr & Ingleton, 1992). Drill cutting analysis extracts information from all production bore holes, but it only provides information on the average grade of a sampled hole (Neff 2003). Both methods provide low resolution data and are costly or time consuming.

Measurement While Drilling (MWD) is a technique of gathering drilling data, which can be employed to characterize the mechanical properties of the penetrated rock mass (Dowell et al. 2006). A holistic analysis of parameters from MWD data gives helpful information on the penetrated rock mass and can be used for several purposes (e.g. to delineate ore from waste). If the parameters include the mechanical properties of the rock, the geology and ore grade levels can be estimated. (Gao et al. 2006). It is also possible to predict other important properties like fragmentation and blast ability based on drilling parameters (Barton et al. 1974, Bieniawski 1995, Deere & Miller 1966).

To facilitate the extraction of different properties from the recorded MWD data, it is necessary to select a proper calculation technique. Machine learning techniques (MLTs) such as neural network, boosting and feature selection are precise and cost efficient for this purpose. MLTs are less time consuming than other experimental methods used for parameter estimation (Kadkhodaie-Ilkhchi et al. 2010). Kadkhodaei et al. (2010) have developed a model to predict rock mass properties by applying pattern recognition (PR) and MLTs to raw data recorded during hole drilling. As the quality of the input data has a significant effect on the model performance, this study aims to improve the results by implementing pre-processing techniques like noise elimination and feature selection on the raw input data. With feature selection, certain features (parameters) that are either redundant or only relevant to the other

features can be removed without loss of significant information. The remaining parameters are called informative features and can be used for modelling.

A common feature selection method is minimum redundancy maximum relevancy (mRMR), an algorithm used to select features which are far apart but still relevant to the classification variable (Laubscher & Jakubec 2001). Another feature selection method is ReliefF, in which the involvement of misclassified values in the feature weight is ascertained by the conditional probability that two values are identical or different, approximated with relative frequencies from the dataset (Kononenko et al. 1997).

Feature selection based on the Hilbert-Schmidt independence criterion (HSIC) is another method able to detect dependencies and complicated relevancies or redundancies in a dataset by employing the "kernel trick." This avoids the explicit mapping that is needed to get linear learning algorithms to learn a nonlinear function or decision boundary. An empirical estimator of HSIC has been generated to lower the required computational time. The criterion in Equation 1 follows the recommendation by Gretton et al. (2005):

$$
\begin{aligned}
HSIC_0\left(K^\alpha, K^\beta\right) &= (m-1)^{-2} \, tr\left(K^\alpha P K^\beta P\right) \\
s.t. \quad K^\alpha &= <\alpha(x), \alpha(x')> \quad \alpha: X \to A \\
K^\beta &= <\beta(y), \beta(y')> \quad \beta: Y \to B \\
P &= I_m - \frac{1}{m} 1_m \cdot 1_m^T
\end{aligned}
\tag{1}
$$

where samples of X and Y are mapped onto spaces A and B based on the kernel functions $\alpha(.)$ and $\beta(.)$; $<.,.>$ shows the inner product of two samples, an indicator for finding similarity; I and m are the identity function and number of samples respectively. In mathematics, if for every row of a square matrix, the magnitude of the diagonal entry in a row is larger than or equal to the sum of the magnitudes of all the other (non-diagonal) entries in that row, the matrix is considered diagonally dominant (Golub et al. 1996). Since the criterion is not accurate for diagonal dominant kernel matrices, Song et al. (2012) suggest the following unbiased empirical estimator of HSIC:

$$
HSIC_1\left(K^\alpha, K^\beta\right) = \frac{(m-4)!}{m!}\left[(m-1)(m-2)\, tr\left(\widetilde{K^\alpha}\widetilde{K^\beta}\right) + 1_m^T \widetilde{K^\alpha} 1_m 1_m^T \widetilde{K^\beta} 1_m\right]
\tag{2}
$$

$\widetilde{K^\alpha}$ and $\widetilde{K^\beta}$ in Equation 2 are the same as the similarity matrices of K^α and K^β when their main diagonal elements are set to zero.

In a diagonally dominant matrix, the vast difference between magnitudes on the main diagonal and the rest of the matrix causes the small ones to be neglected when the data are normalized. Equation 3 can be used to solve the diagonal dominance without removing the main diagonal elements (Liaghat & Mansoori 2016, 2018):

$$
HSIC_2\left(K^\alpha, K^\beta\right) = \frac{1}{(m-1)^2}\sum_i \sigma_i^2
\tag{3}
$$

where, σ_i is the ith eigenvalue of the matrix $e(K^\alpha)^q P(K^\beta)^q P$; q is a random number between 0 and 1; K^α and K^β are gram matrices consisting of the pairwise sample similarities. Using $HSIC_2$ eliminates the diagonal dominance problem of these matrices, and the information on their main diagonal is not removed.

This study introduces a feature selection method based on the $HSIC_2$ with backward elimination search strategy to supervisely identify the informative drill parameters at various depth ranges.

2 METHODOLOGY

In this study, MWD data acquisition is fulfilled to collect raw input data and MLT is used for the pre-processing of the data, model development and model evaluation. Samples

specifications are considered as "features". The study identifies the most informative features from the input MWD data and develops a classification model that can precisely predict the ore grade level of each hole. The recorded MWD data and the ore grade classes are the input and output of the model, respectively.

2.1 *Test site description*

The MWD data and ore grade classes are collected from the Leveäniemi mine. The mine is an open pit operation in the Svappavaara mining area in northern Sweden and is owned and operated by Luossavaara-Kiirunavaara AB (LKAB). The open pit mining method allows maximum ore extraction from the rock with a high degree of safety. The planned annual production of the mine is 12 million tonnes of magnetite ore with an average grade of 44% Fe. The bench height in the pit is 15 m. All production holes in the mine are drilled with fully mechanized SmartROC D65 down-the-hole (DTH) drill rigs. All rigs are equipped with MWD systems that monitor all relevant drill parameters at predefined length intervals during the drilling. These recorded MWD data from six Epiroc D65 drill rigs are used for the analysis in this paper. The rigs have the intelligence and power to drill production blast, pre-split and buffer holes. The study's samples come from 14340 holes; the measured drilling parameters in each hole are penetration rate, percussive pressure, feed pressure and rotation pressure.

2.2 *Classification method*

After proposing a supervised feature selection method to identify the informative properties of data, a classification model is trained by the data extracted from 90% of the whole data (12906 holes) for two purposes:

- To evaluate and compare performance of the suggested feature selection method based on train and test accuracies
- To predict the ore grade class of holes with recorded MWD data in future

Support vector machine (SVM) is the classification method used to model the input MWD data (Cortes et al. 1995). An SVM model is a supervised classification method which divides the points in space, so that the samples of the dispersed categories are classified by a clear gap that is as wide as possible. Also, kernel functions are applied to analyze correlations between input and output data in a higher dimension space which leads to more accurate results (Shawe-Taylor & Cristianini 2004). In this study, *Gaussian kernel* method is used for high dimensional analysis (Nadaraya 1964). This kernel method consider the input data in a space with infinite dimension and gives the opportunity to identify complex dependencies.

2.3 *Model evaluation*

The *k-fold cross validation* method is used to avoid over or under fitting (Kohavi Ron et al. 1995). This model validation technique assesses how the results of a statistical analysis generalize to an independent dataset. Accuracy is the proportion of true predicted labels among the whole number of test samples and it is used to evaluate the feature selection method.

3 DATA PRE-PROCESSING

Since the input data have significant effects on the accuracy of final model, applying pre-processing methods leads to higher accuracy. Noisy samples and non-informative features are removed from recorded raw data using noise elimination and feature selection methods respectively.

3.1 *Noise elimination*

Raw MWD data include noisy or faulty data (Ghosh et al. 2015, Van Eldert et al. 2018). For more reliable results, it is necessary to use a noise reduction method and remove unreliable

data points. A noise reduction method for identifying invalid data has been proposed by the authors based on removing sudden changes in a smooth neighborhood and is described in detail in (Liaghat et al., in prep.). Four types of eliminated samples are:

- Samples recorded at the beginning of each hole (collaring)
- Samples recorded during the rod change process
- Samples related to a sudden peak in a smooth environment
- Samples with a negative or zero drilling parameter value

3.2 *Feature selection*

In previous work, an unsupervised feature selection method was proposed based on $HSIC_2$ (Liaghat & Mansoori 2016, 2018). The feature selection is termed unsupervised when no label is coupled with the data. As the input MWD data have labels, this study proposes a novel supervised feature selection method called S-BAHSIC (Supervised Backward Elimination based on Hilbert-Schmidt Independence Criterion). Equation 4 illustrates the objective function of the suggested method:

$$
\begin{aligned}
&\min\left(HSIC_2\left(K_L^\alpha, K_{G'}^\beta\right)\right) \\
&s.t. \quad X_{G'} = X_G W, \quad W \in \{0,1\}^{n \times n'} \\
&W^T 1_n = 1_{n'}, \ \left\| W 1_{n'} \right\|_0 = n' \\
&K_G^\alpha = <\alpha(x), \alpha(x')> \quad \alpha : X \to A \\
&K_{G'}^\beta = <\beta(x), \beta(x')> \quad \beta : X \to B
\end{aligned}
\tag{4}
$$

where K_L^α is the gram matrix of "labels;" $K_{G'}^\beta$ is the gram matrix of data in the absence of one of the features; W is a mapping function which transfers the original n-dimensional data into a n'-dimensional space ($n' = n-1$).

In the proposed objective function, small value of $HSIC_2$ indicates that the eliminated feature contains important information about the labels and it is an informative feature.

4   MODEL DEVELOPMENT

Using the obtained informative input data, a classification model is developed to precisely predict the *Fe* grade level of each hole. Hence, for each other drilled hole, the mentioned pre-process methods applied on the recorded MWD data of different depth ranges. The obtained reliable and informative data are the input for the trained model. The classification model predict the range of *Fe* grade for the input drilled hole. Hence, the recorded MWD data and the ore grade classes are the input and output of the model, respectively. Figure 1 shows the whole processes during training and testing phases:

As it is depicted in Figure 1 raw MWD data are primarily assessed in the training phase. In this procedure, 90% of the data are exploited to extract reliable data by removing noisy and redundant ones through filtration. Then the proposed feature selection method is applied on filter output in order to find the most informative features which have maximum and minimum relevancy with data labels and other parameters, respectively. Feature selection leads to reduced data which will makes the classification step easier. These data will pass an under-sampling process to create SVM classification, which will be assessed by the 5-fold cross validation method. The final model is developed based on the output of the classification step. The rest of the data (10%) will be utilized in the testing phase to validate the model. In this phase, described noise elimination technique is employed again to remove noises and redundancies in the data. Then, by using informative features from the training phase, important variables will be extracted and used as the input for the developed model to be classified.
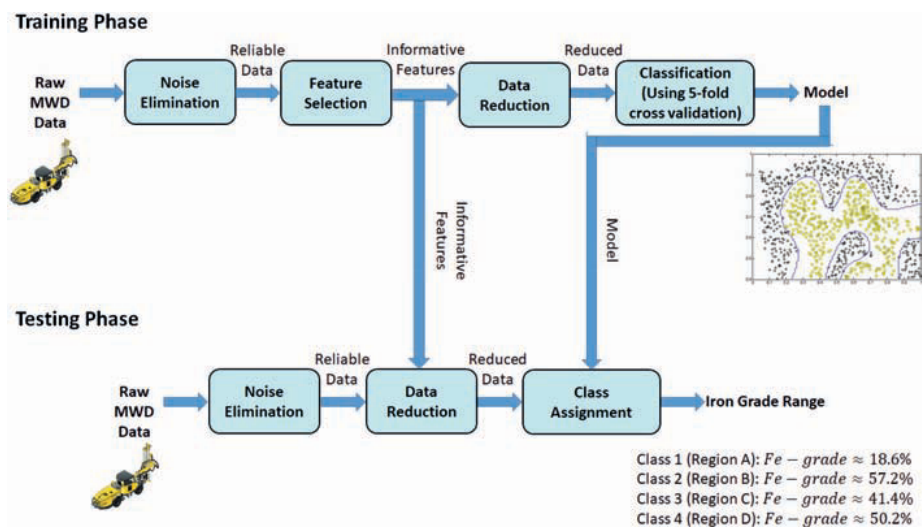
Figure 1. Methodology adopted for model generation, validation and application.
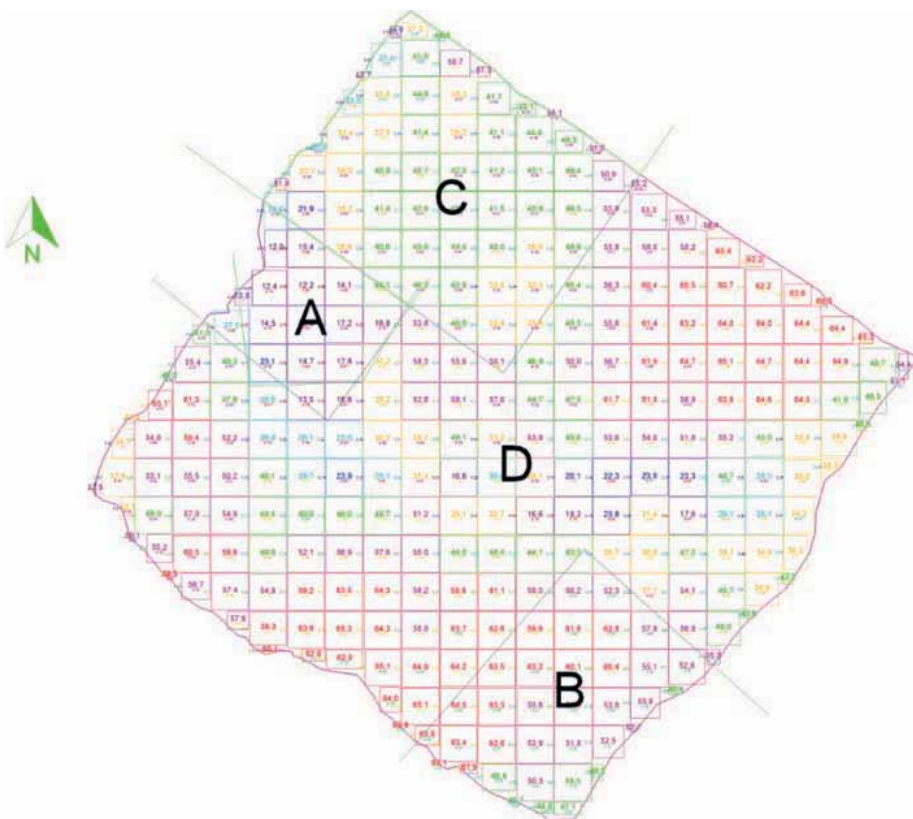
Figure 2. Ore grade percentages of holes in Leveäniemi mine.

The ore grade percentages for the holes in one of the test bench in Leveäniemi mine are shown in Figure 2. The ore in the test bench are delineated in four different ore quality classes defined as:

Class 1 (Region A): $Fe - grade \approx 18.6\%$
Class 2 (Region B): $Fe - grade \approx 57.2\%$
Class 3 (Region C): $Fe - grade \approx 41.4\%$
Class 4 (Region D): $Fe - grade \approx 50.2\%$

After the suggested pre-processing methods are applied to the raw recorded MWD data, an *SVM classification model* is developed based on *Gaussian kernel* method using the supervised processed data. Also, *5-fold cross validation* is used as a performance indicator to validate the achieved model.

5   RESULTS AND DISCUSSION

The effects of noise reduction on the raw input data and drilling data for two holes before and after applying the filter are shown in Figure 2 and Figure 3, respectively.

Since the rod length in the drill string is 6 meters, some of the samples at the depth of 6 m and 12 m are recorded during rod changes. Hence, as observed in Figure 2 and Figure 3, after the noise elimination method is applied, these samples are removed, along with the previously mentioned other three types of noise.

The obtained accuracy in the training phase is showed in Figure 5. After applying S-BAHSIC the samples are classified using SVM and Gaussian kernel. Based on 5-fold cross validation method, the training accuracy is 84%.

In Figure 5, the crosses imply misclassified holes, the circles are the holes classified correctly, and blue, red, yellow and purple colors refers to A, B, C and D regions respectively. A yellow cross outside region C, is assigned to class C, but is considered misclassified since the hole is located outside the defined C area. A yellow circle however represents a hole assigned class C and also located inside region C. The model leads to 50%, 100%, 81.6% and 86.4% accuracies for holes in regions A, B, C and D respectively.

However, looking at e.g. region B the misclassified B holes located in region D are located in direct contact with the B region. Therefore there may be a possibility that the B area is inaccurately delineated rather than a misclassification of the holes. A similar argument can be applied regarding the boundary between region A and C. Hence, the model accuracies presented above may in reality be higher.

The average accuracy using S-BAHSIC is compared with that obtained using the other feature selection methods and shown in Table 1. The suggested feature selection method leads to more classification accuracy among the other common feature selection methods.

In this study, the S-BAHSIC feature selection method solves the diagonal dominance problem. The proposed feature selection method considers the pairwise relations between features in kernel space and assesses the association of each feature with the output. Then, relevancies and redundancies are examined using the accuracy metric. The applied Gaussian
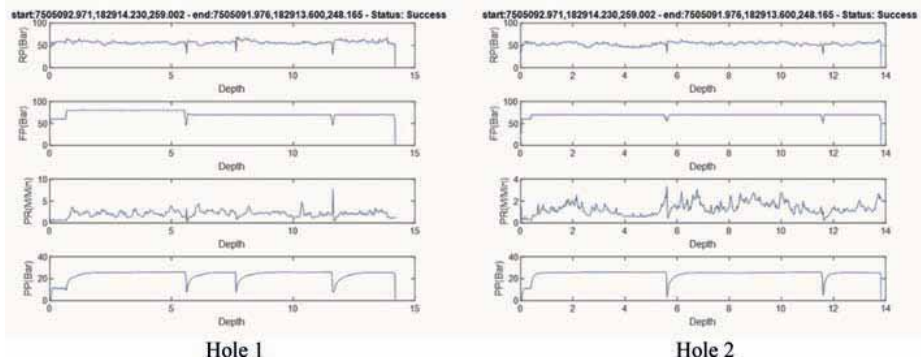
Figure 3.   MWD data before applying noise elimination method.
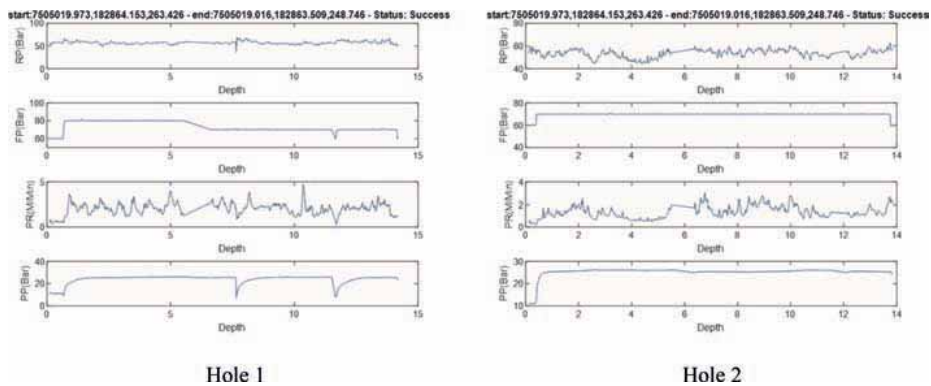
Figure 4. MWD data after applying noise elimination method.
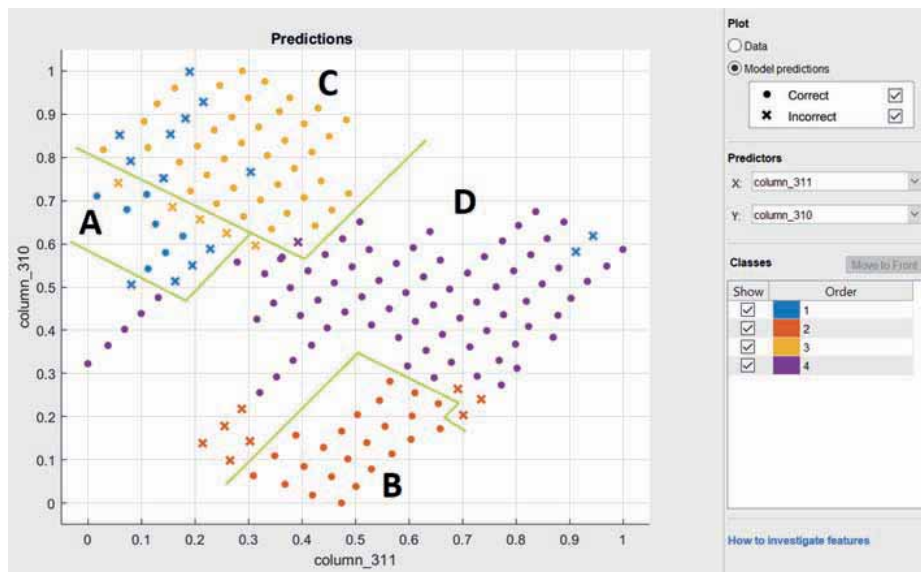
Figure 5. Classified holes.

Table 1. The accuracies obtained by applying different feature selection methods.

Feature selection method	Accuracy (%)
mRMR	63.5 ± 2.1
ReliefF	55.4 ± 3.7
BAHSIC	77.2 ± 2.9
S-BAHSIC	80.1 ± 2.5

function considers the sample similarities in a space with infinite dimensions, thus enabling us to extract complicated dependencies.

In contrast, the results from mRMR are not accurate enough. The method uses the mutual information criterion to investigate the pairwise relations between features and the association of each feature with the output. This criterion is only proficient at identifying linear

232

relations, and it cannot extract non-linear and complicated correlations. The low accuracy of the ReliefF method can be explained in the same way. It does not work based on kernel trick so the complicated dependencies cannot be detected.

Finally, BAHSIC uses the kernel trick. This improves the accuracy of the model, but because $HSIC_1$ is an estimation of the $HSIC_0$ with no bias and high variance, it cannot extract relations precisely. Hence, the resulted accuracy is slightly lower than that obtained by S-BAHSIC. By using the proposed feature selection method on MWD data, the most informative attributes are identified and selected which leads to development of an accurate model. This model predicts mineral content level of a hole based on its MWD data which is available in large quantity and at lower cost as compared to conventional ore grade estimation methods like core drilling and drill cuttings analysis. This model is time-efficient as well, which reduces the time required to estimate the ore grade.

6 CONCLUSION

In this study, the ore grade range of a hole is predicted based on MWD data. To prepare the input data, the raw MWD data and ore grade percentage of each hole are extracted. Since the input data affect the accuracy and performance of a model, MLTs are used for pre-processing the recorded raw data. Applied noise elimination method removes faulty and noisy samples. Drill parameters at various depth ranges are considered features and S-BAHSIC is proposed to identify the most informative features supervisedly. A kernel SVM model is developed based on the reduced MWD data and the 5-fold cross validation method is used to obtain the classification accuracy. The evaluations imply that S-BAHSIC leads to more classification accuracy in comparison with the other common feature selection methods (e.g. mRMR, ReliefF, BAHSIC). Hence, the mineral content level of a borehole could be predicted using the MWD data which are produced in enormous quantity and at a lower cost. Also, the proposed model is time efficient that makes it advantageous over traditional ore grade estimation methods.

REFERENCES

Barton, N., Lien, R., Lunde, J., 1974. Engineering classification of rock masses for the design of tunnel support. *Rock mechanics,* pp. 189–236.

Bieniawski, Z.T., 1995. Classification of rock masses for engineering: the RMR system and future trends. *Rock Testing and Site Characterization,* pp. 553–573.

Corinna, C., Vapnik, Vladimir, N., 1995. Support-vector networks. *Machine Learning.,* p. 273–297.

Deere, D., Miller, R.D., 1966. Engineering classification and index properties for intact rock. *Univ. of Illinois, Tech. Rept.,* pp. 65–116.

Dowell, L., Mills, A., Matt, L., 2006. Drilling Data Acquisition. In: *Drilling Engineering.* s.l.: Society of Petroleum Engineers, p. 647–685.

Gao, T., Cao, J., Zhang, M.Q.J., 2006. *Lithology recognition during oil well drilling based on fuzzy-adaptive hamming network.* s.l., s.n., p. 574–578.

Gene, H., Loan, V., Charles, F., 1996. *Matrix Computations.* 3rd ed. London: The Johns Hopkins University Press.

Ghosh, R., Schunnesson, H., Kumar, U., 2015. *The use of specific energy in rotary drilling: The effect of operational parameters.* s.l., International Symposium on the Application of Computers and Operations Research in the Mineral Industry.

Gretton, A., Bousquet, O., Smola, A.J., Scholkopf, B., 2005. *Measuring statistical dependence with Hilbert-Schmidt norms.* s.l., Springer-Verlag, pp. 63–77.

Kadkhodaie-Ilkhchi, A., Monteiro, S.T., Ramos, F., Hatherly, P., 2010. Rock Recognition From MWD Data: A Comparative Study of Boosting, Neural Networks, and Fuzzy Logic. *IEEE GEOSCIENCE AND REMOTE SENSING LETTERS,* Volume 7, pp. 680–684.

Kohavi, R., San Mateo, Kaufmann, M., 1995. *A study of cross-validation and bootstrap for accuracy estimation and model selection.* s.l., s.n., p. 1137–1143.

Kononenko, I., Šimec Marko, E., Šikonja, R., 1997. Overcoming the myopia of inductive learning algorithms with RELIEFF. *Applied Intelligence,* pp. 39–55.

Laubscher, D.H., Jakubec, J., 2001. The MRMR rock mass classification for jointed rock masses. Underground Mining Methods: Engineering Fundamentals and International Case Studies. *W.A. Hustrulid and R.L. Bullock (eds) Society of Mining Metallurgy and Exploration,* pp. 475–481.

Liaghat, S., Mansoori, E.G., 2016. Unsupervised selection of informative genes in microarray gene expression data. *International Journal of Applied Pattern Recognition,* pp. 351–367.

Liaghat, S., Mansoori, E.G., 2018. Filter-based unsupervised feature selection using Hilbert–Schmidt independence criterion. *International Journal of Machine Learning and Cybernetics,* pp. 1–16.

Nadaraya, E.A., 1964. On Estimating Regression. *Theory of Probability and its Applications.*

Neff, J.M., 2003. Biological effects of drilling fluids, drill cuttings and produced waters. *In Long-term environmental effects of offshore oil and gas development,* pp. 479–548.

Shawe-Taylor, J., Cristianini, N., 2004. *Kernel Methods for Pattern Analysis.* s.l.: Cambridge University Press.

Song, L., Smola, A., Gretton, A., Bedo, J., Borgwardt, K., 2012. Feature selection via dependence maximization. *J. Machine Learning Research,* Volume 13, pp. 1393–1434.

Starr, R.C., Ingleton, R.A., 1992. A new method for collecting core samples without a drilling rig. *Groundwater Monitoring & Remediation,* pp. 91–95.

Van Eldert, J., Schunnesson, H., Johansson, D. & Saiang, D., 2018. *Measurement While Drilling (MWD) Technology for Blasting Damage Calculation.* s.l., 12th International Symposium on Rock Fragmentation by Blasting.

Wellmer, F.W., Dalheimer, M., Wagner, M., 2010. *Economic Evaluations in Exploration.* s.l.: Springer.

Recoverable resource estimation mixing different quality of data

C.R.O. Mariz
Geovariances, Avon, France

A. Prior
Helmholtz-Zentrum Dresden-Rossendorf, Helmholtz Institute Freiberg for Resource Technology,
Freiberg, Germany
Modelling and Valuation Department, Faculty of Geoscience, Geotechnology and Mining, TU
Bergakademie, Freiberg, Germany

J. Benndorf
Faculty of Geoscience, Geotechnology and Mining, TU Bergakademie, Freiberg, Germany

ABSTRACT: Working with different data sets in the mineral resource estimation is a common challenge to be addressed by the industry. Sampling methods, sensor devices, measurement times along the ROM and key variables measured might differ between data sets. These variations are reflected in the quality of each data set. Comparative exploratory data analysis is used to verify if different data sets are sampling the same distribution. Frequently, they show differences in the statistics and variography. This demonstrates that different sets cannot just be merged and used in processes if these are not previously treated. One way of integrating is to attribute a measurement error to the unreliable data set. The methodology proposed enables a resources estimation and risk analysis by considering the variance of measurement error calculated from the cokriging between reliable and unreliable data sets. This paper illustrates an innovative methodology with an application to a sulphide deposit.

Keywords: Geostatistics, Mineral Resource Estimation, Variance of Measurement Error

1 INTRODUCTION

Information about the deposit is essential and scarce. Every sample is important in the process to determine the tonnage, the metal content and the mean grade in the orebody. Often, the global data set contains samples obtained from different sampling methods, with diverse levels of confidence, as qualities, and to estimate using these data sets is a big challenge.

Nowadays, the industry is using sensor technology in order to characterize the mine face. The characterization of this ore presents a metrological problem of instrument calibration. Some of these kinds of instruments compare the signal obtained from in-situ chip samples with reference-signal databases (Van Den Boogaart, 2018). The measurement value will depend on the subjective selection of the reference data set. This represents a source of uncertainty in the modelling. However, both data sets are still important in the estimation process. When this kind of problem is present, a step is added to the estimation process: comparative global and local exploratory data analysis. The goal is to compare the two data sets both at global and local scale, verifying if they are sampling the same distribution in both scales.

The global exploratory analysis involves the calculation of statistics, histograms, variograms, and analysis of statistical profiles by slices (swath plots) for each data set for the key variables. The local exploratory analysis involves comparison of the key variables' behavior at the short-scale for each data set; in other words, to compare the samples localized in the same coordinates. However, normally the information is not known at the same location for the
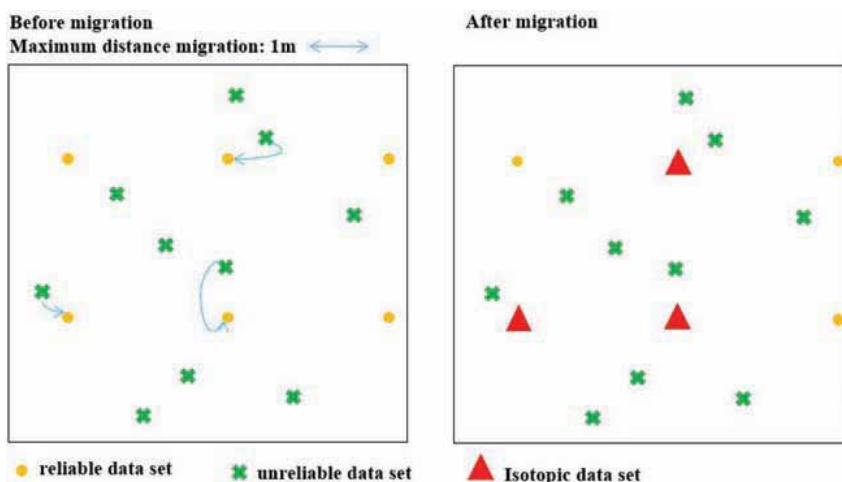
Figure 1. Left – Base map of samples from sampling method NÂř1 (reliable data set, (in yellow) and samples from sampling method NÂř2 (unreliable data set, in green). Right – Base map including the migrated samples forming the isotope data set (in red), bring together the information from sampling method NÂř1 and NÂř2.

same key variable for each data set (entirely heterotopic data). Consequently, the creation of pairs of nearest neighbors for short distances may be necessary. This is obtained by migrating neighboring data to create a partly isotopic data set (Wackernagel, 1998); see Figure 1. The unreliable data (e.g. chip samples) are migrated to reliable data locations (e.g. drillholes) over a short distance. The isotopic data set is used to calculate the cross plots, comparison tests of means and standard deviations, etc.

The results of these operations asses whether both data sets are sampling the same phenomenon. If so, the samples from different sampling methods can be directly mixed and used in the estimation process. Otherwise, an uncertainty is associated with the less reliable data set (Deraisme, 2009) and taken into account in the estimation process.

The aim of this paper is to describe a methodology that allows estimating the recoverable resources using different quality data sets with different confidence levels. This methodology is a combination of resource estimation techniques which uses the concept of measurement error, estimated by cokriging, and geostatistical conditional simulations. The main method used here is called kriging with variance of measurement error (KVME—Chilès, 2012). This technique is a variant of kriging (linear geostatistical method) and can be also adapted to the no-linear geostatistical methods, in particular to the estimation of recoverable resources using conditional simulations. This combination has been successfully applied in different operating mines and commodities such as copper, gold, zinc and bauxite (Deraisme, 2009).

This document is structured presenting a test case study description in Section 2, the methodology implemented in Section 3, the results achieved in Section 4 and the conclusion of this research in Section 5.

2 CASE STUDY DESCRIPTION

The Neves and Corvo massive sulfide deposits are part of the Iberian Belt. The Neves orebody has a maximum thickness of 55 m and measures 700 m by 1.200 m. It consists of massive pyrite and cupriferous massive sulfides with low copper and zinc contents. The Corvo orebody has a maximum thickness of 95 m and measures 1.100 m by 600 m. It is composed of vertically staked lenses of massive cupriferous ores having a lens of barren pyrite and large massive lenses of cassiterite (Chilcott, 2007).

The Neves exploration data consist of 1.982 samples and production data of 16.967 samples; in the Corvo orebody, the exploration data contains 386 samples and the production data 19.322 samples; see Figure 2. The exploration data correspond to drillholes, and the production data set to the chip samples. Each sample interval includes a specific gravity measurement and assay data for different elements, but in this study the focus is copper (Cu). The study was carried out on the Neves and Corvo orebodies; see Figure 3.

The statistics have been calculated on composited exploration and production data taking into account the samples in each orebody. The general statistics of both sets of data is initial evidence concerning the difference between the two data sets; see Table 1. In particular the global mean Cu grade is over-evaluated by production data.
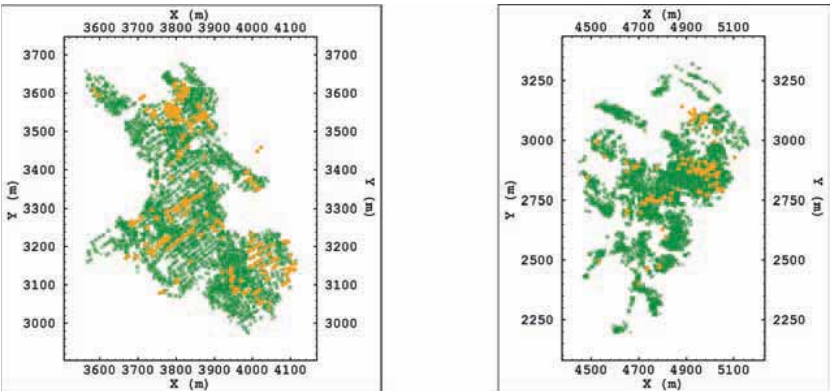
Figure 2. Base map of drill holes header (orange circles) and chip assays (cross green) of Neves (left) and Corvo (right) orebody.
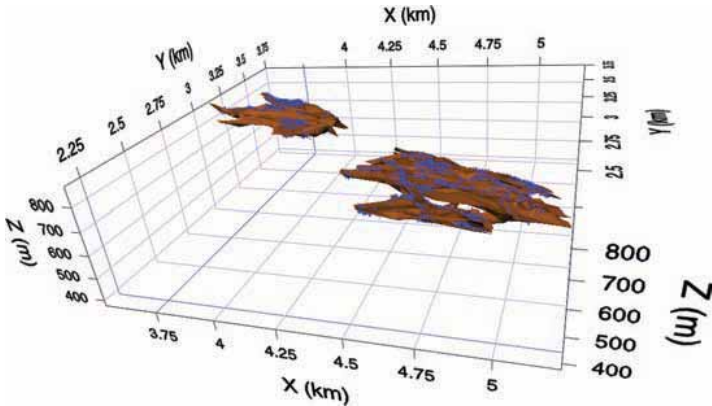
Figure 3. 3D View of drill holes (blue), chip samples (blue) and domain (brown) of Neves (left) and Corvo (right).

Table 1. Statistics on composited exploration and production data for Neves and Corvo, chip samples.

Orebody	Data set	Variable	Count	Min[1]	Max[2]	Mean	Std. Dev.[3]	Variance
Neves	Exploration	Cu	1.982	0,33	18,16	2,53	2,23	5,01
Neves	Production	Cu	16.967	0,04	35,34	3,41	2,91	8,50
Corvo	Exploration	Cu	386	0,09	27,45	4,67	4,27	18,26
Corvo	Production	Cu	19.322	0,04	39,65	6,86	5,87	34,49

[1]for minimum value; [2]for maximum value; and [3]for standard deviation.

237

3 METHODOLOGY

The following section presents the different combination of techniques that has been implemented in this paper. This methodology enables an estimation and risk analysis of the resources of interest from exploration (high quality) and production (low quality) data sets by considering the variance of measurement error associated to the latter one.

The steps followed in the present methodology are:

1. Global and local exploratory data analysis of raw variables for each dataset;
2. Transforming raw variables of the different data sets into their Gaussian equivalent through Gaussian anamorphosis;
3. The calculation of experimental covariances and cross-covariances on Gaussian transformation;
4. Point-wise cokriging from Gaussian exploration data and production data;
5. Turning Bands (TB) conditional simulations with variance of the measurement error from Gaussian variables kriged in (4);
6. Back transformation of the Gaussian variables into raw variables and re-blocking of these to calculate the grade tonnage variables.

The uncertainty derived from the sensor devices usually compromises laboratory analytical error and the sum of all the sampling errors. This information is hardly obtained in mining situations. However, the current methodology also presents an estimation of the uncertainty of the instrument measurement for the production data.

This section contains two subsections. The Subsection 3.1 presents the KVME theoretical basis and the Subsection 3.2 a brief account concerning the Gaussian transformations and the conditional simulation considerations.

3.1 KVME

The mathematical model considered to implement the methodology using a variance of measurement error is based on the idea that the copper grade from each data set is represented by different random functions. The Cu grade from the exploration data set is represented by $Z_1(x)$ and is considered as the main variable in the cokriging (step 4 of the methodology). This is based on the assumption that the measurement error of this variable is nil, since the measurements have been obtained by laboratory analysis. On the other hand, the copper grade from the production data space is represented by $Z_2(x)$ and it is the auxiliary variable in the step 4 of the methodology. This is assumed to have an unknown error $\varepsilon(x)$ from the instrument measurement.

Moreover, these two random functions are informed respectively on two sets of points $S_\alpha = \{x_1, \ldots, x_n\}$ (exploration drillholes locations) and $S_\beta = \{x_1, \ldots, x_m\}$ (chip sample locations). This is a entirely heterotopic data set since both random functions are measured in different locations. The cokriging allows us to use all this information to linearly estimate one or the other of these variables (Wackernagel, 1998),

$$\hat{Z}_{1,\text{Cok}}(x_0) = \sum_{\alpha=1}^{n} \lambda_\alpha Z_1(x_\alpha) + \sum_{\beta=1}^{m} \lambda_\beta Z_2(x_\beta),$$ (1)

where λ_α and λ_β are the cokriging weights assigned to each random function at the data locations.

A general solution to estimate the cross-variogram for heterotopic variables would consist of estimating the cross-covariance model as,

$$\hat{C}_{12}(h) = \frac{1}{2N(h)} \sum_{\alpha=1}^{N(h)} (Z_1(x_\alpha) - m_{Z_1})(Z_2(x_\alpha + h) - m_{Z_2}),$$ (2)

under the assumption of

$$x_\beta - x_\alpha \approx \mathbf{h}$$

where $\mathbf{m}_{Z_1}$ and $\mathbf{m}_{Z_2}$ are mean of Z_1 and Z_2 respectively and $N(\mathbf{h})$ is the number of pairs of points.

Nevertheless, this approach presents one main drawback: the estimation of $\hat{\mathbf{C}}_{12}(\mathbf{0})$ since both random variables are not known at the same location. This problem is addressed by using the statistical correlation between $\mathbf{Z}_1$ and $\mathbf{Z}_{2,\text{Mig}}$ (inexact samples migrated to neighboring exact data location for a short distance; see Figure 1) and the variances of $\mathbf{Z}_1(x)$ and $\mathbf{Z}_2(x)$; or from a weighting between the nugget effect used in the simple-covariance model of $\mathbf{Z}_1(x)$ and $\mathbf{Z}_2(x)$. In this case study the first option will be used.

After obtaining $\hat{\mathbf{Z}}_{1,\text{CoK}}$ by cokriging in the reliable and unreliable data locations, the challenge remains of calculating the instrumental measurement error associated with production data remains. This method proposes to obtain the uncertainty associated to the production data as the variance of kriging of $\hat{\mathbf{Z}}_{1,\text{CoK}}$. Then at the production data locations the measurement error is equal to the kriging variance of $\hat{\mathbf{Z}}_{1,\text{CoK}}$. On the other hand, the exploration data set location is known to have a zero error, because $\hat{\mathbf{Z}}_{1,\text{CoK}}$ is equal to $\mathbf{Z}_1$ and the kriging variance of $\hat{\mathbf{Z}}_{1,\text{CoK}}$ is equal to zero.

$$
\begin{aligned}
\hat{Z}_{1,\text{CoK}}(x) - Z_2(x) &= \in (x) \qquad \forall \qquad x \in S_\beta. \\
\hat{Z}_{1,\text{CoK}}(x) - Z_1(x) &= 0 \qquad \forall \qquad x \in S_\alpha.
\end{aligned}
\tag{3}
$$

The last part of the method consists of performing a kriging combining both data sets but adding to the production one the instrument measurement error $\in (x)$.

In this way, the KVME methodology allows estimating the variable of interest of the deposit by combining different data sets and the uncertainty related to these.

3.2 *Conditional simulations with variance of measurement error*

A measurement error can also be applied to a non-linear estimator such as conditional simulations. Simulation methods are driven by Gaussian assumptions. For that reason, the Gaussian anamorphosis transformation is applied as a first step. This is a nonlinear function that maps a non-Gaussian random field, as $\mathbf{Z}_1(x)$ and $\mathbf{Z}_2(x)$, into a Gaussian space, generating $\mathbf{Y}_1(x)$ and $\mathbf{Y}_2(x)$, both Gaussian variables. Raw variables are converted into Gaussian variables obeying a standard distribution law (mean 0, variance 1). This transformation is one-to-one. It is possible to reverse the process and reconstruct the raw variables from the Gaussian variables. This transformation is calculated, as well as the spatial correlations model of Gaussian variables.

Such as at the KVME, it should be performed a point-wise cokriging from the reliable and unreliable data for the key variables before performing conditional simulations with variance of measurement error.

This paper uses Turing Bands (TB) conditional simulation by integrating the different data sets. TB is the oldest 3D geostatistical simulation method and it simulates a general trend plus a random error (Rossi, 2014). Isatis© has been used to implement this methodology and the variance of measurement error can be implemented only in the TB method.

The TB conditional simulations are obtained using a two-step procedure. The first one is a non-conditional simulation of the specified spatial correlation model, where the number of TB is the only parameter involved at this level, and this should be large enough to ensure the quality of the resulting simulations. The second one is the conditioning to the data with cokriging.

4   RESULTS

The difference between Cu distributions from exploration $\mathbf{Z}_1(x)$ and production $\mathbf{Z}_2(x)$ data is verified to Neves and Corvo for the global and local exploratory data analysis. In Neves and Corvo a slight bias is apparent in the production data, and it is associated with the uncertainty of the instrument measurement for this data. Overall the means and variances

exhibited by the production data are globally consistent with the characteristics of the exploration data (see Figure 4). However, it is necessary to study closely the impact of poor-quality production data.

The Gaussian anamorphosis is performed on both orebodies using the calculated declustering weights estimated from raw variables. These weights are obtained by running a declustering process and this essentially corresponds to cell declustering. It relies on calculating a weighted average grade, with the weights determined by the number of neighbors that a sample contains in a given cell.

Figure 5 and Figure 6 show the experimental Gaussian anamorphosis and anamorphosis estimated models, where $Z_1(x)$ and $Z_2(x)$ raw variables are transformed into $Y_1(x)$ and $Y_2(x)$ Gaussian variables. Raw variables are represented in their cumulative frequency variable form, which constitutes an estimate of the cumulative probability density function (cdf) of the raw grade distribution in the Y axes. The X axes constitute an estimate of the cumulative probability density function (cdf) of the Gaussian grade distribution. The experimental Gaussian anamorphosis (the black curve) is only a discrete one (not all possible Z values have a corresponding values and vice versa), and a continuous modelling (the blue curve) is performed by a mathematical expansion using specific polynomials (the Hermite polynomials).

The Neves and Corvo data set are entirely heterotopic data, $Y_1(x)$ and $Y_2(x)$ are never known at the same location. In this situation it is impossible to use the variogram as a function to characterize the spatial continuity because the cross-variogram cannot be computed. However, one can use the covariance as a spatial model. The only requirement is to assess
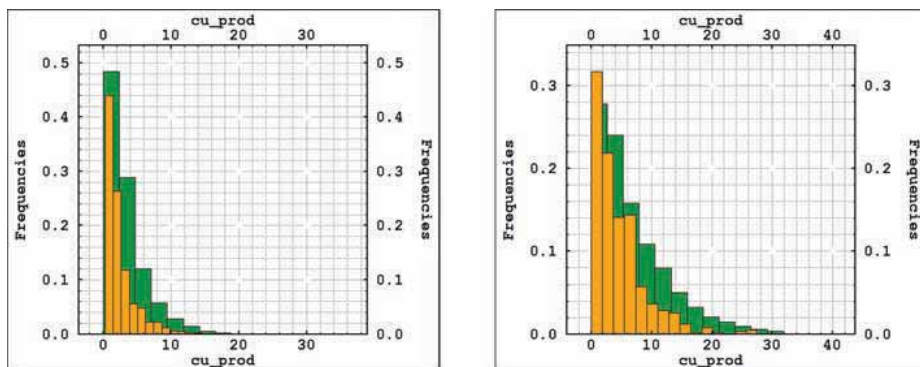
Figure 4. Histogram of exploration data (orange) and production data (green) with declustering weights for Neves (left) and Corvo (right).
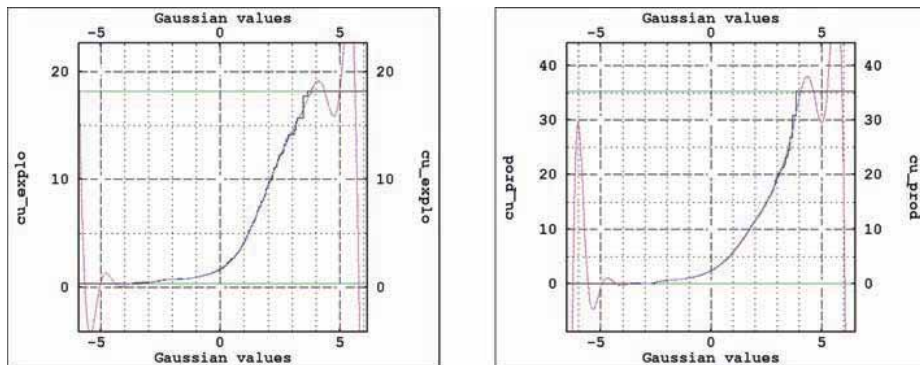
Figure 5. Gaussian anamorphosis of $Z_1(x)$ (left) and $Z_2(x)$ (right) for Neves. In black the experimental Gaussian anamorphosis, in blue the anamorphosis model and in green the boundaries of $Z_1(x)$ and $Z_1(x)$ raw variables.

Figure 6. Gaussian anamorphosis of $Z_1(x)$ (left) and $Z_2(x)$ (right) for Corvo. In black the experimental Gaussian anamorphosis, in blue the anamorphosis model and in green the boundaries of $Z_1(x)$ and $Z_1(x)$ raw variables.

Figure 7. Neves—Experimental and modelled covariance and cross-covariance of $Y_1(x)$ and $Y_1(x)$. Model of $Y_1(x)$ (first column/first row), $Y_2(x)$ (second column/second row), and cross-covariance $Y_1(x)$ and $Y_2(x)$ (first column/ second row). Direction N120 (red); Direction N210 (green) and vertical direction (purple).

the covariance $\hat{C}_{12}(0)$ between the Gaussian variables $Y_1(x)$ and $Y_2(x)$ at the same point (h equal to zero). This covariance can be estimated using the statistical correlation between Y_1 and $Y_{2,\text{Mig}}$ (inexact samples migrated to neighboring exact data location for a short distance; see Figure 1) and the variances of $Y_1(x)$ and $Y_2(x)$.

The experimental covariances and cross-variograms are calculated on $Y_1(x)$ and $Y_2(x)$, respectively Figure 7 and Figure 8; three perpendicular directions are referred to as N120, N210, and N45. Afterwards, covariances and cross-covariance models have been fitted to the experimental covariances and cross-covariance of $Y_1(x)$ and $Y_2(x)$. The same spatial models have been used to perform a point-wise cokriging (step 4 of the methodology) and the TB block conditional simulations (step 5 of the methodology).

Turning Bands block simulations at Selective Mining Unity (SMU) level, of size $4\,m \times 4\,m \times 4\,m$, have been performed for $\hat{\mathbf{Z}}_{1,CoK}$ for each orebody taking into account the variance of the measurement error associated with the production samples and estimated from the kriging variance of $\hat{\mathbf{Z}}_{1,CoK}$. That is to introduce the influence of production data through their re-estimation and the use of a variance of measurement error in the Turning Bands process. Furthermore, for post-processing, a manageable number of realizations have been selected, characterizing the spatial variability of Cu grade in the chosen domain.

For Neves and Corvo, Table 2 presents the global statistics for Cu grade simulated (mean of 100 realizations) from $\mathbf{Z}_1(x)$ and $\mathbf{Z}_2(x)$; i.e. exploration and production data with variance of measurement error for the latter data set. Note that the statistics are presented to $\hat{Y}_1(x)$ and $Y_2(x)$ back-transformed variables (step 6 of the methodology). For Neves and Corvo, the simulated global mean and the mean of each realization are close to the mean of exploration data, $\hat{\mathbf{Z}}_1(x)$, and they respect the local mean.

Figures 9, 10, 11 and 12 show a part of grade tonnage curves for the 100 realizations calculated from TB conditional simulations taking into account the exploration and production data with variance of measurement error for the latter. Through these curves, the Cu mean grade above a given cut-off can be estimated; the same analysis can be done on the tonnage

Table 2. Neves and Corvo global statistics of Cu estimated a by TB conditional simulations with variance of measurement error.

Orebody	Variable	Min[1]	Max[2]	Mean	Std. Dev.[3]	Variance
Neves	Cu	0,35	17,30	2,48	1,53	2,35
Corvo	Cu	0,09	27,45	4,54	3,20	10,22

[1]for minimum value; [2]for maximum value; and [3]for standard deviation.
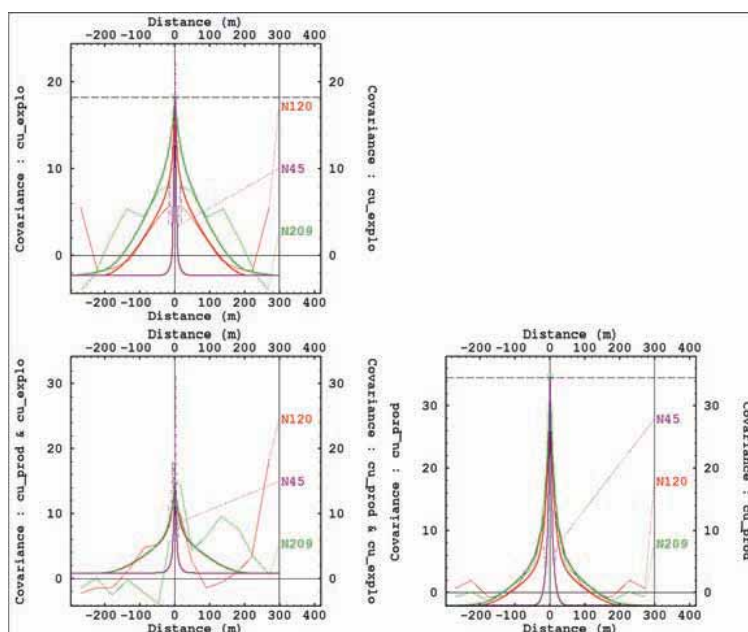
Figure 8. Corvo—Experimental and modelled covariance and cross-covariance of $\mathbf{Y}_1(x)$ and $\mathbf{Y}_1(x)$. Model of $\mathbf{Y}_1(x)$ (first column/first row), $\mathbf{Y}_2(x)$ (second column/second row), and cross-covariance $\mathbf{Y}_1(x)$ and $\mathbf{Y}_2(x)$ (first column/second row). Direction N120 (red); Direction N210 (green) and vertical direction (purple).
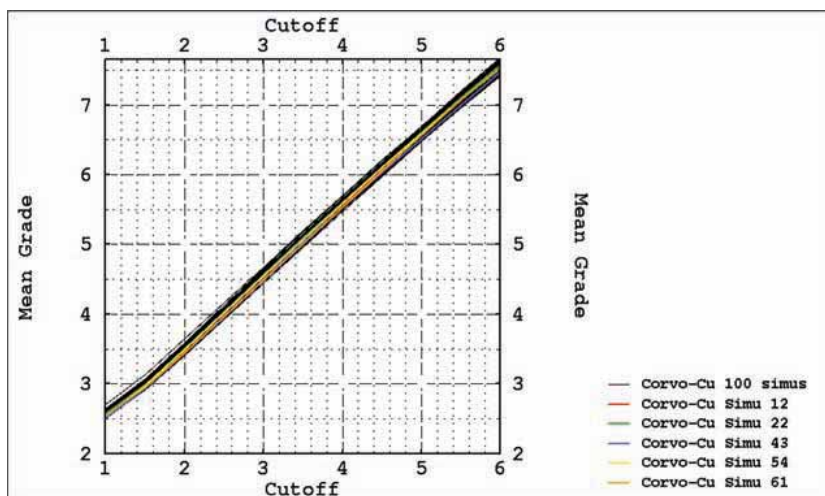
Figure 9. Overlays of Mean grade versus cutoff curves for Corvo orebody for all 100 conditional simulations.
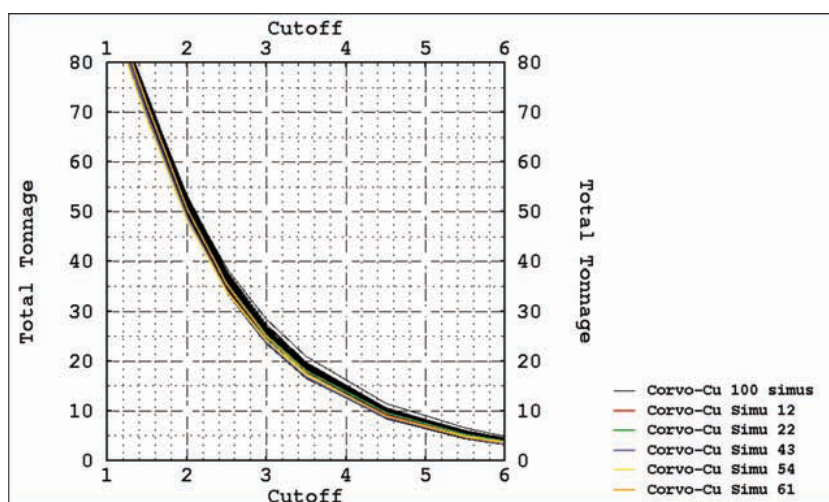
Figure 10. Overlays of Total tonnage versus and cutoff curves for Corvo orebody for all 100 conditional simulations.

and the metal quantity for a given cut-offs. In other words they give the information about the recoverable resources using all data information available to estimation process.

For Neves, for a cutoff applied to Cu grade equal or greater than 4% the global mean grade is approximately 5,55% and for more optimistic scenario is equal to 5,75%, although for the more pessimistic scenario equal to 5,45%. For Corvo, for a cutoff equal or greater than 5% the global mean grade is approximately 7,75% and for more optimist scenario is equal to 8,55%, although for the more pessimist scenario equal to 7,45%.

The methodology described in Section 3 can be performed in multivariate TB conditional simulations, with a variance of measurement error applied on each variable. The point-wise cokriging step (step 4 of this methodology) is run the number of times corresponding to the number of key variables; by changing the main variable to estimate the variance of measurement error for each variable.

243
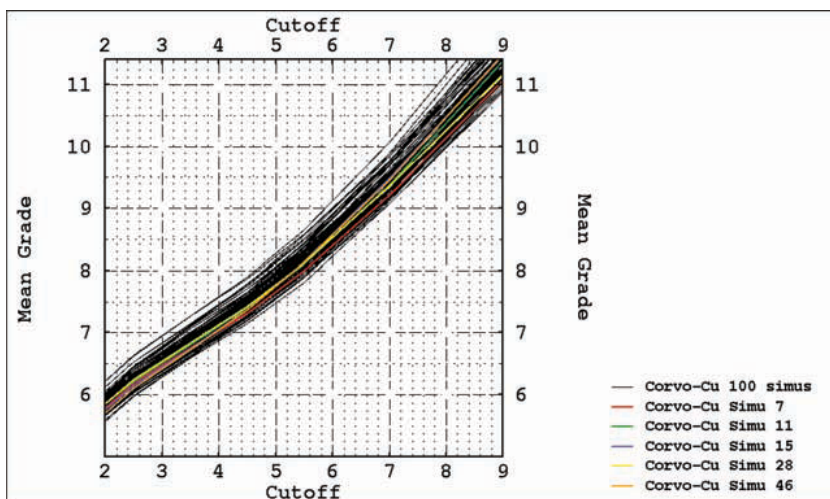
Figure 11. Overlays of Mean grade versus cutoff curves for Corvo orebody for all 100 conditional simulations.
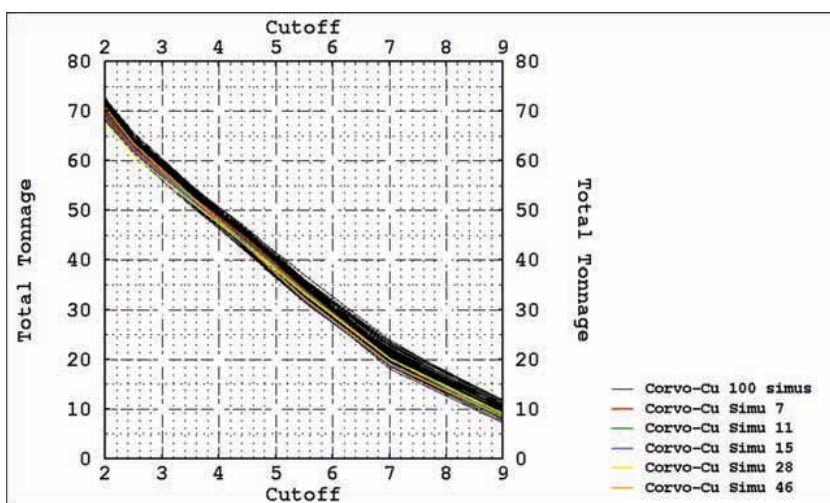
Figure 12. Overlays of total tonnage versus and cutoff curves for Corvo orebody for all 100 conditional simulations.

5 CONCLUSIONS

In the mining industry data can be obtained from different sampling methods, with different support size or where the assays were determined from different technical analytics. In order to assess the different data sets in the same estimation process it is crucial to perform a statistical and geostatistical analysis, at global and local scale. This will determine if the different data sets can be merge directly or not. This paper proposes a methodology used when the different data sets cannot be merged directly. The KVEM combined with TB conditional simulation are two solutions to estimate resources, associating a measurement error to the unreliable or inaccurate data set. The errors are estimated by cokriging from the same element of each involved data set. TB conditional simulations allows going a step further to perform a risk analysis and to calculate the probability that the mean grade of a group of

blocks exceeds a given cut-off. The only obstacle with the methodology presented is that the different data sets are frequently entirely heterotopic for certain elements. In other words, the information is not twined considering the different data sets. In this situation to define the spatial correlation at the same location can be difficult. However, two solution are presented in this document. The methodology presented in this work is illustrated in a polymetallic massive sulphide deposit, where Cu grade is estimated from exploration data (reliable data set) and production sample (unreliable data set). It has been shown that this method improves the quality of the estimation associated with all the available information.

REFERENCES

Bleines, C., Deraisme, J., Geffroy, F., Perseval, S., Rambert, F., Renard, D., Touffait, Y., and Wagner, L. 2018 *Child Development* 65(1): 13–16. Polhill, R.M. 1982. *ISATIS software manual. Geovariances and Ecole des Mines de Paris. 201–206 pp.*

Chilcott, D.L., 2007, Technical Report on the Neves Corvo Mine, Southern Portugal, *Wardell Armstrong International Limited, Ref: WAI/61–0465*: 27–28. Portugal.

Chilès, J.P. & Delfiner, P., 2012, Geostatistics modeling spatial Uncertainty, Second Edition, *Wiley series in probability and statistics*. 216–218, 339.

Deraisme, J. and Strydom, M., 2009, Estimation of iron ore resources integrating diamond and percussion drillholes *Applied Physics of Condensed Matter - 15th International Conference* 2–4. LiptovkÃ. JÃạn, BystrÃạ, Slovakia.

Rossi, M.E. and Deutsch, C.V., 2014, Mineral Resource Estimation *Springer Dordrecht Heidelberg New York London* 171–172.

Van Den Boogaart, K.G. and Tolosana-Delgado, R., 2018, Predictive Geometallurgy: An Interdisciplinary Key Challenge for Mathematical Geosciences. *In Handbook of Mathematical Geosciences, Springer International Publishing,* 673âĂŞ686.

Wackernagel, H., 1998, Multivariate Geostatistics, N. 1997. Recommendations and prejudices, 158, 291. Springer.

Declustering weights as a measure of average sample spacing, applications in mineral resource classification

D.E. Hulse
Gustavson Associates L.L.C., Lakewood Colorado, Colorado

R.C. Bryan
Geostat Systems L.L.C., Golden Colorado, Colorado

ABSTRACT: Mineral resource classification is described in both the SME and CIM Standards for Mineral Resource Reporting. The CIM Standard states "… sampling … is sufficient to assume geological and grade or quality continuity between points of observation", thus is a function of continuity and sample spacing. Continuity can be measured by use of a variogram model, but average sample spacing in three dimensions is more difficult to measure. The declustering algorithms provided with geostatistics software are commonly used to weight data for statistical analysis due to the sometimes-irregular spacing between drill holes during exploration. The weight values are lower when data is closer, reflecting shared influence between samples, and higher for isolated samples reflecting independence. This paper will discuss the potential to use estimates of these declustering weights as an inverse relative measure for average sample spacing to gauge the confidence of the estimate independent of the single nearest sample.

1   INTRODUCTION

Classification of mineral resources and mineral reserves disclosure for stock exchanges is coordinated internationally by a group formed from delegates of various national technical mining associations. The Committee for Mineral Reserves International Reporting Standards (CRIRSCO) includes representatives of the Society of Mining, Metallurgy and Exploration (SME) of the U.S.A., Canadian Institute of Mining Metallurgy and Petroleum (CIM), the Joint Ore Reserves Committee (JORC) of Australia, among others. The authors have chosen to present definitions from the CIM Definition Standards for Mineral Resources and Mineral Reserves (CIM Standing Committee 2014).

> *Measured mineral resource*
> *A Measured Mineral Resource is that part of a Mineral Resource for which quantity, grade or quality, densities, shape, and physical characteristics are estimated with confidence sufficient to allow the application of Modifying Factors to support detailed mine planning and final evaluation of the economic viability of the deposit.*

Geological evidence is derived from detailed and reliable exploration, sampling and testing and is sufficient to confirm geological and grade or quality continuity between points of observation. (CIM Standing Committee 2014). Indicated and Inferred Mineral Resources have similar, however less restrictive definitions. The guideline continues to state that criteria should be applied to define the part of the estimate where the "geological evidence is derived … testing that is sufficient to confirm geological grade or quality …" By this measure the quality of an estimate and hence its classification is based on the availability of data in spatial proximity to make an estimate.

The classification of mineral resources requires some decisions and interpretations be made by the NI43-101 qualified person (QP) or a JORC competent professional (CP). These include

the cell size for declustering and the thresholds for differentiating the mineral resource categories. The classification of mineral resources and reserves has long been a combination of science, past experience and professional judgment of the estimator. All of the definitions are similar and deal with "sample points sufficiently closely spaced to support confidence in the continuity of …" (CIM Standing Committee 2014). There are two challenges to the classification; determining the adequate sample spacing to meet the confidence criteria; and defining which blocks in a model meet those criteria in such a way that the model is useful for reporting and planning.

"Sufficiently closely" has been interpreted in several manners. One method uses the distance between the block estimated and the nearest sample (or samples). Geostatistics gave us the calculation of the estimation variance of the block, an implicit part of the calculation of kriging weights, to account for the confidence in the estimate. A more refined method called "kriging efficiency" has been has been developed to use more aspects of the kriging machinery (Krige 1997). However, kriging efficiency is also sensitive to the estimation variance, thus it tends to generate confidence class patterns that are sensitive to the distance from the closest sample. These methods can result in a pattern called the "spotted dog" where individual samples are surrounded by a higher classification near each sample decaying into pattern of decreasing confidence halos. (Stephenson 2006) In addition to the visual image of the spots, this raises the more practical problem of mine design when the classification changes between measured, indicated and inferred.

These challenges have led to ad hoc methods to classify material within the mining block so larger areas receive a given classification. A popular technique is a multiple search method, where the estimator defines a minimum of number of samples from a minimum number of holes within a nested set of search distance that are used to classify estimates. These specified set of increasing distances are usually proportional to the variogram range. This technique overcomes the spottiness of the closest sample or kriging error.

These manual methods even with the assistance of modern computer programs described by (Seibel and Ligocki 2017) "can be both labor intensive and subjective". Other authors argue that a probability range and confidence interval of the produced grades over a certain time can define the necessary spacing (Verly, et al. 2017), (Reid and Parker 2017). These authors use a 15% relative precision at the 90% confidence interval for annual production to achieve an Indicated Mineral Resource classification and a similar probability range for each quarter to be deemed a Measured Mineral Resource. These methods are computationally intensive and are best utilized by experienced practitioners.

The authors believe that the technique presented herein provides a useful method whereby the needed spacing as determined by the qualified person can be mapped into a pragmatic classification of estimation confidence that is useful for planning and reporting of mineral resources and reserves.

2   DISCUSSION

As described by Stephenson "Block-by-block resource classifications should be smoothed into geologically sensible and coherent zones that reflect a realistic level of geological and grade estimation confidence, taking into account the amount, distribution and quality of data." There is a tool available in much geostatistical software call declustering. The method used herein was made popular by the GSLib software published in 1992 (Deutsch and Journel 1992). Tools for declustering are included in a number of commercial mining software. MicroMODEL (R.K.M. Software 2016), DataMine (Datamine n.d.), MineSight (Hexagon Mining n.d.), and Vulcan (Maptek Inc. n.d.) provide declustering tools. The tool was developed to discount the statistical effect of closely spaced or "clustered" samples. It is often used in the exploratory data analysis stage of a study.

Data clustering can be simply due to the available access where samples points can be collected. It is often due to continually "testing" the continuity of the highest-grade areas of a deposit. The latter can produce biased average grade results from repeated drilling near other high-grade samples. In both cases, closely spaced, interdependent samples can skew the sta-
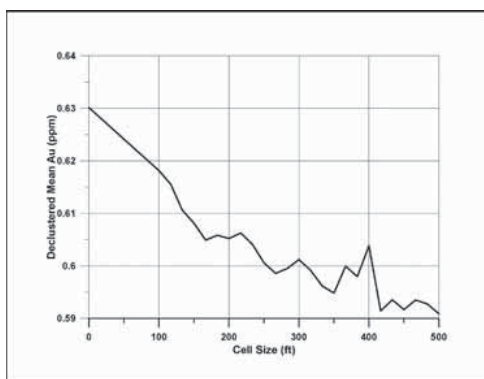
Figure 1. Declustering weight vs. cell size.
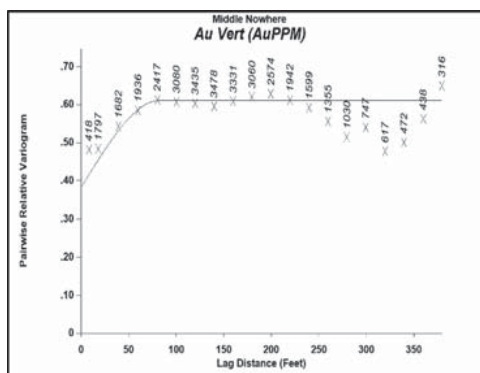
Figure 2. Vertical Gold Variogram - Middle of Nowhere Deposit.

tistical distribution of the data and produce biased estimates. "Declustering" can mathematically compensate for this uneven sample spacing and statistical effects caused by correlated samples.

The GSLib method of declustering calculates weights against a grid overlain on the sample space. This grid goes through a variety of cell sizes to simulate grouping the data into progressively larger cells. At each size, the grid is slid through a pattern of offsets to limit the possibility of a calculation through a chance of the grid position. A condition of the declustering calculation is that the sum of the weights must equal the total number of samples, meaning that individual weights will be either less than or greater than unity.

The objective of the technique is to find the sample spacing that results in the minimum average grade of samples falling within each grid cell which cell, which is by convention a square rectangle defined by the length of one side. In practice, the weighted average grade will decrease until it reaches a plateau. Beyond this point, there is no significant change in the declustered average grade. Beyond a certain cell size and, the declustered mean stabilizes. The resultant declustering weights are thus inversely proportional to the average spacing between samples.

Two hypothetical case studies described later in this paper are used to help illustrate how to apply the technique. The first study represents a gold resource for the Middle of Nowhere gold deposit. The second case study is the Hill Top Iron Ore deposit project in part of a massive magnetite project.

Figure 1 uses the Middle of Nowhere case to illustrate the relationship of reaching the afore mentioned plateau graphically. The graph's y-axis charts the changing declustered average as the cell size changes on the x-axis. Note that the graph drops rapidly until it plateaus when the declustering cell size is at about 160 ft. For reference the sample variogram is shown in Figure 2. This is when the samples taken within a rectangular grid based on 160 foot sides the average declustered grade out at approximately 0.605 ppm. This is an important part of the methodology for classifying the estimated resource, which is described in the next section

3 METHODOLOGY

The technique requires the same steps taken for resource estimation including separating the data into domains. Domain statistics along with the chosen cell size with the calculation of the declustering weights for each sample is calculated. Geostatistical analysis of the variography and the choice of estimation parameters is then done for each domain as well. Grade estimation techniques such as kriging can then used to estimate grades using kriging weights. To alleviate confusion in the multiple usage of the term "weights" for both kriging and declustering, the modifying terms "declustering" and "kriging" will used to differentiate the two types of weights. Declustering weights assigned to the samples by the described

Table 1. Declustering methodology.

Steps	Task description
1	Separate the data into estimation domains as in any estimation.
2	Calculate domain statistics.
3	Run the declustering algorithm. For an iterative algorithm, check the domain statistics with the declustering weights.
4	Perform variography in each domain.
5	Develop estimation parameters.
6	Estimate the grade values.
7	Estimate the declustering weight values with the same search and variogram as the prime variable.
8	Map (or contour) the modeled declustering weights against the sample locations to compare average sample spacing with the weights.
9	Select threshold declustering weights to use for classification.
10	Use results to assist in classifying estimated resources into measured, indicated and inferred.
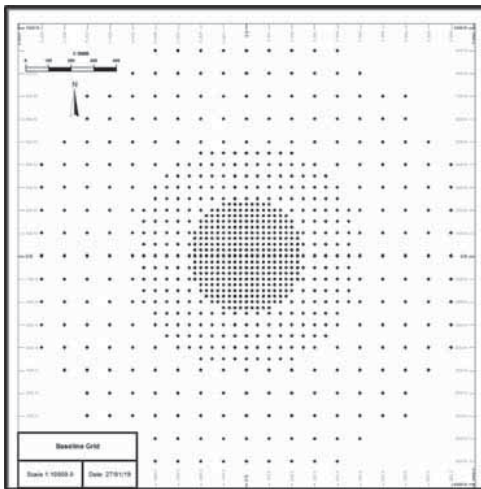
Figure 3. Conceptual sampling grid.
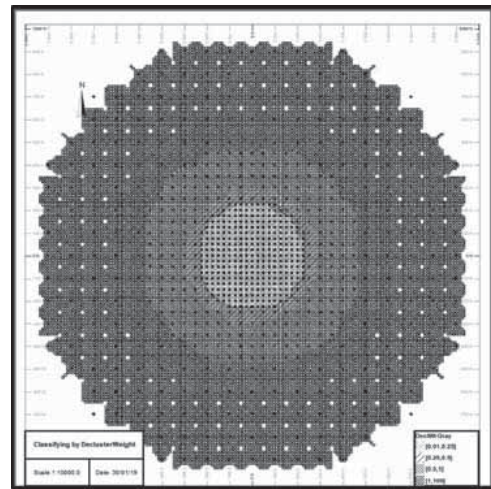
Figure 4. Estimated declustering weights.

method are then estimated into blocks with exactly the same search criteria, method and variogram parameters as those used to estimate the grade values. This insures that the kriging weights used for the estimation of both the grade values and the declustering values are the same. Declustering weight contour maps should be used to help select threshold declustering weights to use for classification

Table 1 indicates a step-by-step procedure. The technique can be easily integrated into most modern mining software's estimation procedures.

4 CONCEPT

To help clarify how the declustering method works, a simplified two-dimensional base grid of was generated. The base is divided into a series of 25×25 unit blocks in size to be estimated by a pattern of sample locations. These sample locations are shown as colored dots in a radially decreasing density, for this example, an isotropic variogram of 100 units is assumed. Shown in Figure 3. Figure 4 shows the model with the decluster weights of each sample

estimated into blocks, and shows the successive halos of higher estimated weights reflecting the decreasing sample density.

5 CASE STUDY 1 – MIDDLE OF NOWHERE GOLD

The Middle of Nowhere is a epithermal gold deposit at the contact of sediments and tertiary volcanics. Additional faulting and fracturing normal to the contact adds structural complexity to the deposit, and a higher-grade domain overprint. The case study will focus on the greater deposit. The drill hole map for a section of the deposit is shown in Figure 5.

Due to the subhorizontal nature of the contact zone and the steep fractures in the deposit, it has been drilled with angled holes in many directions, and the drill density is quite variable through the depth of the deposit.

The declustering cell size selected was 160 ft., and the relationship of cell size to the declustered grade is shown in Figure 1. The corresponding variogram is shown in Figure 2. The cell size represents the initial deflection in the curve and is approximately double the variogram range. The sample spacing on one bench of the model is shown in Figure 5.

The distance to the nearest sample is coded by 35%, 70%, 100% and >100% of the variogram range in Figure 6. The Middle of Nowhere project was originally classified by a multiple search method. The results of this are shown in Figure 7.

Similar results of classification via estimated declustering weights are shown in Figure 8. The thresholds for classification were selected as
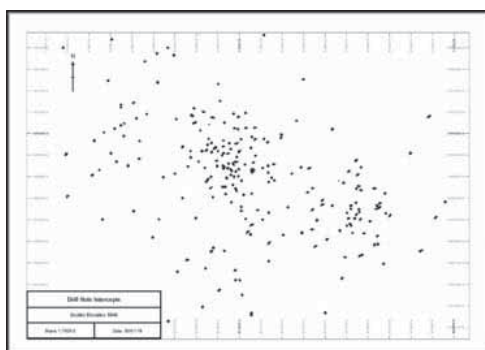
Figure 5. Sample location bench 5840.
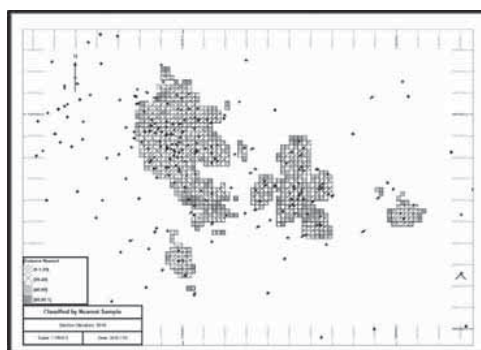
Figure 6. Classification by closest sample.
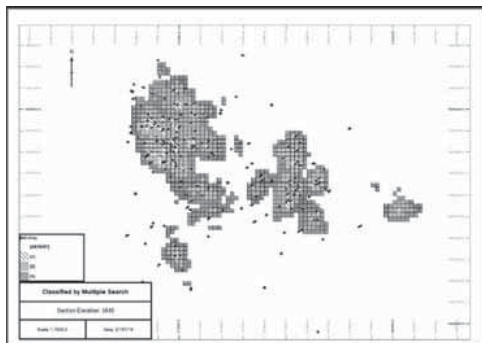
Figure 7. Multiple search classification.
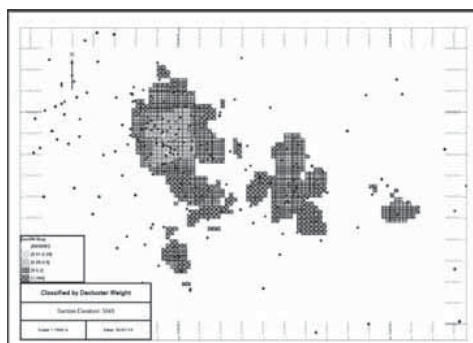
Figure 8. Declustering weight classification.

- Measured <0.5
- Indicated <1.0
- Inferred >1.0

This is visually appropriate and provides similar quantities to the multiple search method, requiring two independent drill holes within 50%, 100%, and 150% of the variogram range respectively.

6   CASE STUDY 2 – HILL TOP

The Hill Top Case Study analyzes a massive magnetite deposit in early stage exploration drilling. The deposit was discovered by aeromagnetic mapping. It is one of several hilltops in an area containing elevated magnetic anomalies.

The empirical variogram with a range of 40 m is shown in Figure 9. Figure 10 shows the average declustered Percent Total Iron [FeTot (%)] grade vs. the cell size. A cell size of 80 m was chosen due to an inflection point on the cell size versus the average FeTot (%) grade curve. Interestingly, 80 meters also happens to be double the variogram range.

Figure 11 shows the distance to the closest sample while Figure 12 shows the corresponding kriging error for a cross section of Hill Top. This study exhibits similar features to the Middle of Nowhere case, in showing the "spotted dog" using nearest neighbor and kriging errors respectively.

The comparison of a multiple search technique and the use of declustering weights in Figure 13 and Figure 14 demonstrate the balancing of declustering weights with differing sample orientations. Both methods still present broad bands of each classification related to the average spacing.
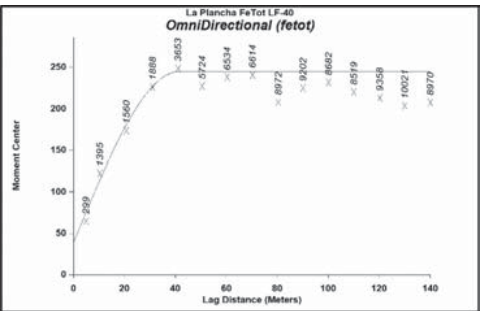
Figure 9.   Hill top empirical variogram.
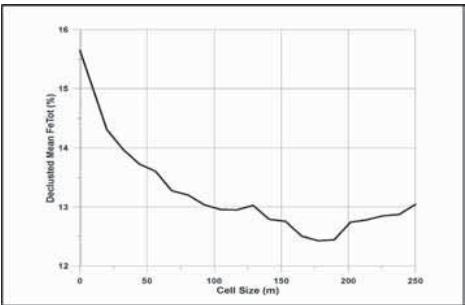
Figure 10.   Hill top declustering analysis.
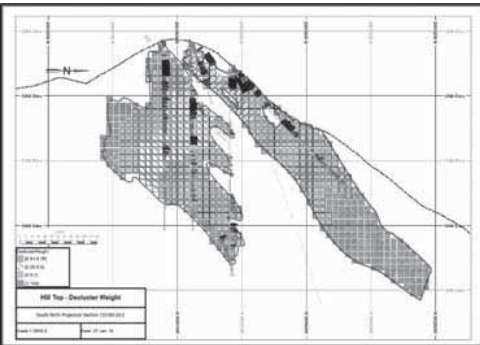
Figure 11.   Hill top nearest sample.
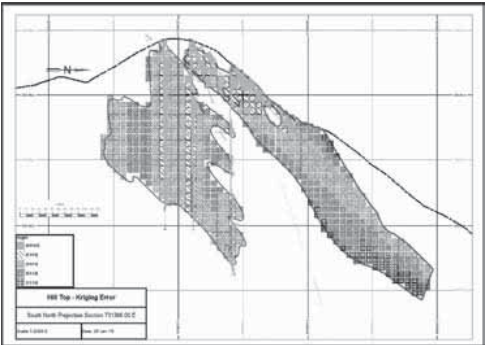
Figure 12.   Hill top kriging error.
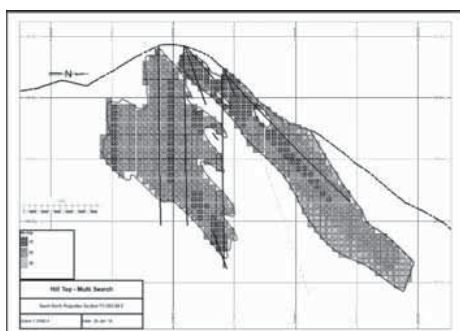
Figure 13.   Hill top multiple search.
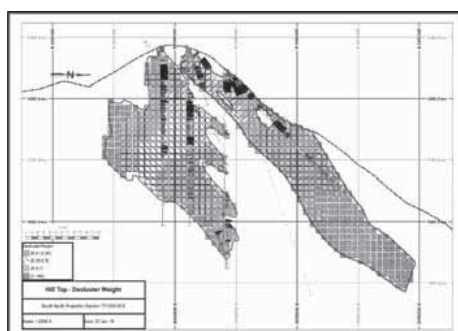
Figure 14.   Declustering weight.

7 CASE STUDY SUMMARY

This paper presented two case studies with client data. Although the projects are not named, the data are real.

In the two case studies, a final cell size of double the variogram range was used. It is uncertain whether this observation can be considered as a "rule-of-thumb", but it is possible that there is a relation of a reasonable declustering cell size to the variogram range. This is a cautious suggestion, and the decision and interpretation is at the discretion of the QP or CP.

There are similarities and differences between the declustering technique under discussion and that of the declustering effect of kriging. The declustering program utilizes the variogram anisotropy to calculate the weights assigned to samples. It only utilizes the geometry, but not the sample-to-sample variance from the theoretical variogram model used in kriging.

Both estimation and declustering require good geological modeling and appropriate assignment of estimation domains. (Verly, et al. 2017) states that "*Complex simulation can be completed as long as the main geological features can be simulated separately*." The simulation study results is defining the sufficient drill hole spacing to achieve adequate confidence. (Reid and Parker 2017) focuses on the density of holes with a Selected Mineralized Zone in each pod of the sandstone hosted uranium deposit. (Jewbali, et al. 2017) utilizes a random search to optimize the cost of infill drilling to achieve adequate drill spacing to convert the resource class of the mineral.

The commonality of most authors is the definition of a necessary spacing to classify the mineral resources. The authors believe that the technique presented herein provides a useful method whereby the needed spacing as determined by the qualified person can be mapped into a pragmatic classification of estimation confidence that is useful for planning and reporting of mineral resources and reserves.

8 CONCLUSIONS

Based on the idea that a mineral resource classification should reflect the average sample density in the local area. It appears that the use of declustering weights as a corollary may be useful. This paper is empirical and is based on general principles used in mineral resource modeling. It is not a theoretical treatment of declustering by kriging during estimation.

The declustering weight method appears to emulate these features of multiple searches and does not require multiple runs to calculate the classifications. It eliminates some of the artifacts such as the floating measured blocks and internal edge effects in the estimated grade.

Like all classification techniques, the final classification needs to be checked against the data density on plans and cross sections. The method is empirical rather than theoretical, and requires that some decisions and interpretations be made by the QP or CP. These include the cell size for declustering and the thresholds for differentiating the mineral resource categories.

When the report is published, the mineral resource classification is solely the responsibility of the QP or CP

REFERENCES

Jewbali, A., D. Silva, R. Inglis, and L. Allan. 2017. "Developing an Optimization Framework for Drill Hole Planning." *Proceedings of the 38th International APCOM.* Golden, Colorado. 2–17 to 2–28.

CIM Standing Committee. 2014. *CIM Definition Standards For Mineral Resources and Mineral Reserves.* Westmount, QC: Canadian Institute of Mining, Metallurgy and Petroleum.

Datamine. n.d. *Datamine Software Help Files.* www.dataminesoftware.com.

Deutsch, Clayton V, and André G. Journel. 1992. *GSLIB Geostatistical Software Library and User Guide.* Oxford University Press.

Hexagon Mining. n.d. "Minesite 3-D." *Hexagon Mining.* https://hexagonmining.com/products/all-products/minesight-3d.

Krige, D. 1997. "A practical analysis of the effects of spatial structure and of data available and accessed, on conditional biases in ordinary kriging." *Geostatistics Wollongong.* 799–810.

Maptek Inc. n.d. "Maptek Vulcan Software Help Files." www.maptek.com.

R.K.M. Software. 2016. *MicroMODEL V9.0l Mine Planning Deposit Software User's Guide.* Lakewood, CO.

Reid, D.P., and H. Parker. 2017. "Confidence Limits Versus Drilling Spacing -- Sandstone Hosted Uranium Deposits." *APCOM 2017, Proceedings of the 38th International Symposium.* 2–17 to 2–28.

Seibel, G0., and L Ligocki. 2017. "Utilizing Probability Assigned Kriging (PACK) and Leapfrog to Construct the Copler Resource Model, East-Central Turkey." *APCOM 2017, Proceedings of the 38th International Symposium.* 15–7 to 15–13.

Stephenson, P.R. et.al. 2006. "Mineral Resource Classification – It's Time to Shoot the Spotted Dog." Society of Mining Exploration and Metallurgy.

Verly, G., H. Parker, C. Artica, H. Kim, and E.L. Bortoletto. 2017. "Classification and Dilution Study by Simulation of a Large Copper Deposit, Peru." *APCOM 2017, Proceedings of the 38th International Symposium.* Golden, CO USA. K-11 to K-18.

Mine planning in digital transformation

Multi stage dumping sequence—a new approach for waste disposal

B.T. Kuckartz & R.L. Peroni
Federal University of Rio Grande do Sul, Porto Alegre, RS, Brazil

ABSTRACT: The mining industry has developed several strategies to optimize ore extraction along past decades. Ore is related to the mine incomes, thus research regarding mine planning focus on ore extraction. However, to mine ore blocks it is necessary to move large volumes of waste material. It is estimated that waste haulage and disposal might represent more than 50% of operational costs, which highlights the importance of integrating waste management in mine planning. Definition of waste dumps can be a complex and difficult task as it relies on several technical and environmental aspects. This paper proposes a new approach for waste disposal called a Multi Stage Dumping Sequence (MSDS), which allocates temporary waste dumps along the way to final dump destination. Although this method demands material re-handling, if well planned, it provides additional time to design and license final waste dump site, and yet, resulting increases in NPV by reducing haulage distances.

1 INTRODUCTION

Mine planning optimization evolved in many aspects in the last decades, aided by mathematical programming and processing software which provide the necessary tools to solve complex and multivariable problems. There are several software and studies regarding mine planning optimization (Li et al. 2012), such as pit limits definition (Dagdelen, 2001, Deutsch et al. 2015, Dimitrakopoulos, 2007; Espinoza et al., 2013) and extraction sequencing (Askari-Nasab et al. 2011, Caccetta et al. 2003; Dimitrakopoulos & Ramazan, 2003, Ramazan & Dimitrakopoulos, 2013, Lambert et al. 2014, Waqar Ali Asad & Dimitrakopoulos, 2012). Profit and incomes are typically related to ore extraction from the mine, thus research regarding mine planning focus on ore optimization and sequencing to maximize the net present value (NPV). However, to get to the ore, it is necessary to remove large mass/volumes of waste material in order to reach ore blocks. The total amount of waste rock depends on stripping ratio and varies from deposit to deposit, nevertheless, it is usually larger than ore quantities.

Waste portions of the mineral deposit do not deliver any profit (Li et al. 2012), given that this material has zero or not enough grade to justify processing. This material is sent to rock dumps which is a necessary mining structure. It is estimated that waste haulage and disposal might represent more than 50% of operational costs (Lizotte & Bonates, 1986). The authors highlight the importance to find ways to reduce transportation cost and integrate the waste management in the mine planning.

Permanent nature of waste dump sites is important to consider not only technical and economic aspects, but also for environmental issues before defining its location (Hekmat et al. 2008). Therefore, dump location is not necessarily the best economical alternative or the one which represents the lower cost option, but a solution that also comply with environmental issues, geotechnical stability, geochemical and physical aspects (Ortiz, 2017, Zinck, 2004). All these factors contribute to make this decision very complex, especially in the early stages of a project, when planners must choose the ideal location in order to avoid re-handling and reduce haulage costs.

Some studies concerning waste rock sequencing and dump optimization (Askari-Nasab & Ben-Awuah, 2011, Fu et al. 2016, Graskoski et al. 2013; Li et al. 2013, Li et al. 2015, Li et al.

2016, Ortiz, 2017) were published in the last few years. These papers found optimum solutions for waste management throughout mixed integer programming (MIP), to solve optimum waste and tailings sequencing in long-term planning, considering multiple dump sites and potential acid drainage issues (Li et al. 2012) and reducing haulage distances. However, in all studies the dumps locations were already defined, and waste rock sequencing would avoid material re-handling in the future.

This paper proposes a new approach for waste disposal called a Multi Stage Dumping Sequence (MSDS), which allocates temporary waste dumps along the way to the final dump destination. This method proposes a planned material re-handling at the beginning of operation, providing additional time to design, prepare and license the final waste dump site (temporary dumps sites also may require license in certain cases, depending on its location), besides reducing waste haulage cost in the first years. Although an increase in unity haulage cost is considered to re-handle material from/to temporary dumps, the NPV increment in the first years, by reducing haulage distances, is still potentially higher. The methodology uses an integrated mine planning and waste sequencing and it is carried out an application to a real case study to demonstrate its applicability.

2 METHODOLOGY

The proposed methodology consists of defining temporary dump sites between the open pit and final dump location. Some variables must be observed to define the number of stages to be used. Variables like haulage and material re-handle costs, distance from pit exit to final dump site and temporary dumps, distance between temporary dumps and waste rate production are considered in this preliminary study.

For explanation purposes and to focus on the differences between conventional and MSDS approaches let's consider a fixed distance "X" from pit exit to final dump location as shown in Figure 1. In conventional approach waste rock would be hauled the whole "X" distance during mine's life, keeping fixed haulage distances outside pit. In MSDS approach two stages will be considered to cover the distance "X", thus haulage distance will be incremental along the mine's life from "Y" to "X". For example, in Figure 1 (where P is the period from mine life) waste rock from P1 (W1) and P2 (W2) will be dumped in a distance "Y" from pit exit. In the P3 (example's last period), W3 is sent all the way to final dump (distance "X") and W1 and W2, located in the first temporary dump stage, are also re-handled to that position ("X–Y" distant).

In the end of the process, total haulage distance is the same for both methods, however in MSDS approach total haulage distance in P1 and P2 (sum of distances) is lesser than conventional method for the same period. The distance reduction in the first periods decreases total haulage cost, even considering an incremental factor for re-handling, which results in NPV increment compared to the base case. Although distance haulage costs reduction in earlier stages will cause an increment in this parameter in later stages, and as NPV is penalized by period (the further is the period, the greater is the penalty), the effect of this increment in operational cost will also be attenuated by period penalization, resulting in higher final NPV.

As a case study, the MSDS methodology was applied to a phosphate mine in Brazil. A block model, from a mine sector, was used to calculate the profit function, which was imported to NPV Scheduler software to build a mathematical open pit and scheduling. Haulage costs were not considered to build the profit function and pit optimization in order to maintain the same number of blocks and NPV potential for comparison purpose. Haulage costs were included afterwards using an Excel spreadsheet, where four MSDS different scenarios were evaluated. Given the waste management purpose of this study and considering that all ore blocks are sent to a fixed processing plant (which represent the same revenue for any tested scenario), all results shown here represent only costs related to waste block.

A base case was considered as the conventional approach. A pit exit and final dump location were established. Inside pit haulage distance and cost were calculated using blocks
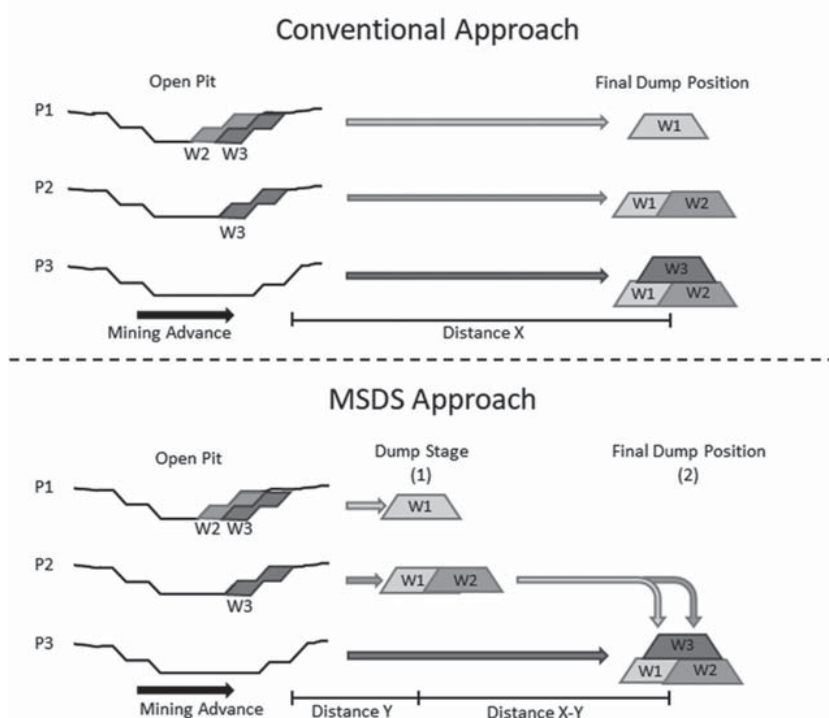
Figure 1. Comparison between conventional and MSDS approaches, where "P" represents the period, "W" the waste material produced in each period and "n" the number of dumping stages.

centroid and pit exit coordinates, while distance between pit exit and final dump were used to calculate outside pit haulage cost. Blocks schedule considers the first 10 years period of production and waste handling, sequenced yearly for each of the five scenarios analyzed.

Four MSDS scenarios were tested with one temporary dump (Dump 1) along the way from pit exit and final dump. In scenario 1 (MSDS 1), the first stage consists of sending waste from years 1 and 2 to Dump 1. In the second stage, waste from years 3 to 10 is sent straight from the pit to final dump, and waste in Dump 1 is re-handled to final dump during the same period (from 3 to 10 years). The other MSDS scenarios are variations of the MSDS 1 scenario regarding when Dump 1 is re-handled to final dump. Re-handling from year 7 to 10 is scenario MSDS 2, from 9 to 10 is scenario MSDS 3, and MSDS 4 consists in re-handling entire Dump 1 in year 10 (Figure 2 represents the workflow for each tested scenario).

Dump 1 location was established close to the pit exit (0.81 km), covering part of 11th year scheduled blocks, thus this temporary dump must be re-handled prior to this period. The Dump 1 area has capacity to accommodate all waste from years 1 and 2 in three benches of 10 m height each. Re-handling costs were considered equal to mining costs and did not considered G&A costs. Final dump is located 3.09 km away from pit exit (according to mine planning), through a haulage road shown in Figure 3. The four MSDS scenarios where chosen in order evaluate how waste re-handling would affect final NPV. MSDS 1 and 4 represent extremes, while 2 and 3 where built according to results found with other two scenarios. As this study proposes a new method of waste management, only a few scenarios where tested, however there are many other possible combinations of re-handling strategies that may be tested in future works.

The necessary number of shovels and trucks to accomplish schedule scenarios were calculated considering utilization factor of 90% and availability of 85%. Average speed during loaded and empty haulage were also estimated in order to calculate trucks production
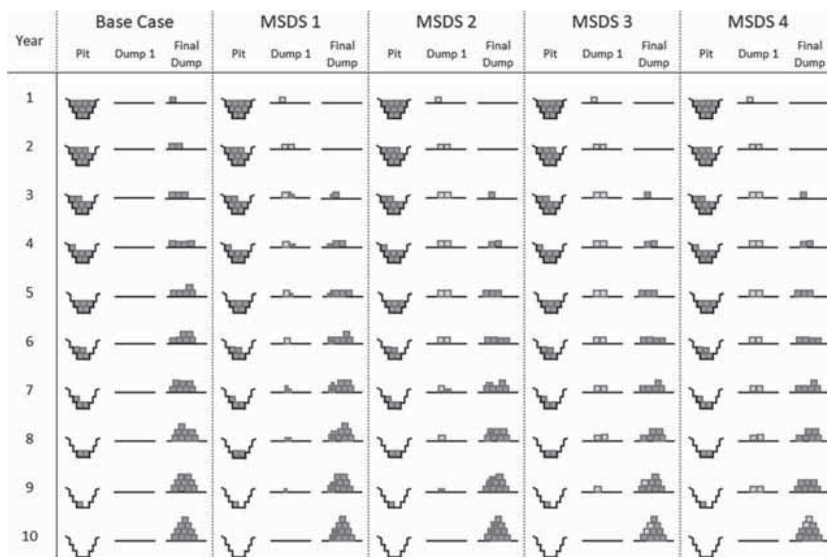
Figure 2. Waste management strategy for all five scenarios analyzed: base case (conventional method) and four MSDS possible scenarios.
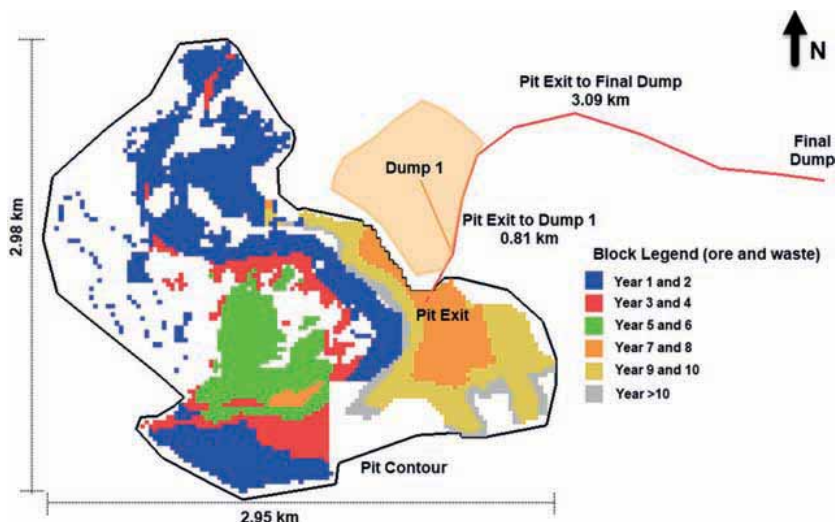
Figure 3. Block schedule for 10 years period and location of pit exit and established temporary dump and final dump.

capacity. Equipment fleets (truck and shovel) were calculated to consider only the waste coming straight from the pit and separately the waste re-handling operation.

3 RESULTS AND DISCUSSION

As mentioned before, all results are regarding total operation costs brought to the present value yearly (NPV), therefore, the smaller negative outcomes represent the better the scenario.

A sensitivity analysis (Figure 4) was made in order to understand how the three main variables (final dump haulage distance (km), loading costs ($/t) and haulage costs ($/t/km)) affect

260
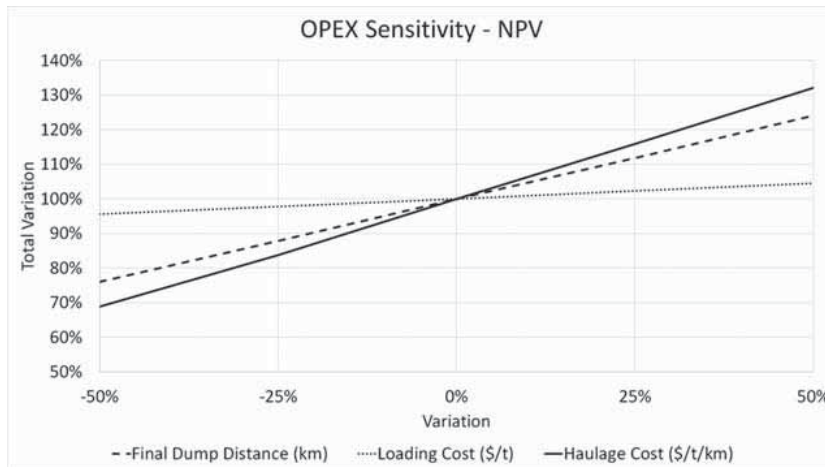
Figure 4. Sensitivity analysis of total OPEX for the base case.

the base case OPEX upon a 50% variation. As expected, haulage cost has the highest influence on final OPEX, closely followed by final dump distance (which is intrinsically related to haulage cost). A 50% variation in haulage cost resulted in +/–30% fluctuation in total OPEX. Final dump distance variation represents a decrease and increase of 14% and 24%, respectively, in total OPEX. Loading cost has a minor effect in total cost variation with +/–4%.

Total waste mass increment between base case (conventional method) and MSDS scenarios is 17%, related to the waste mass increment coming from years 1 and 2. Decision on when and how the temporary dump must be re-handled (main difference between MSDS scenarios) is a key variable to decrease total OPEX.

Starting re-handling in earlier stages, such in MSDS 1, demands an acquisition of less trucks in the first two years, if compared to the fleet necessary to execute the base case scenario. However, acquisition of new equipment for re-handling operation must be done also in earlier stages, which increment investments in periods with lower time penalization. On the other hand, leaving re-handling to the last period (10th year), such in MSDS 4, will require more equipment acquisition (more than MSDS 1) to deal with a larger mass of waste during only one year (10th). However, this late equipment acquisition (investment) is also heavily penalized due to the postponed re-handling, reducing its impact on final NPV. The number of haulage trucks required for each scenario, by year, is presented in Figure 5.

There is only one extra shovel for MSDS scenarios compared to base case (despite MSDS 4, which requires two extra shovels in the 10th year). This extra shovel is used exclusively to Dump 1 re-handling operation (the same is applied to extra trucks). The graph shown in Figure 6 represents total NPV variation (considering OPEX and CAPEX, normalized by final base case NPV) and total waste mass (WM) per year during the 10 years period considered.

The shorter haulage distance in the first two years due to MSDS scenarios results in an equipment fleet reduction of two trucks at the operation start up, which represents 33% costs reduction during this period, compared to base case (but not its final NPV).

Scenario MSDS 1, which starts re-handling in the 3rd year, presents cost increase in all periods from 3rd year ahead, resulting in 1% higher final cost NPV when compared to the base case. Postponing re-handling to the later stages demonstrated better results. Delaying re-handle to the 7th year (MSDS 2) ended with a virtually identical NPV result, with only 0.02% lower cost compared to the base case. Scenarios MSDS 3 and 4, although presented an increment of 50% to 85% in total cost in the last two years (when compared to base case for the same period), presented slightly better results, 0.9% and 0.2% lower total NPV, respectively.

Despite these results did not provide a significant reduction in total NPV cost when compared to base case and its parameters, i.e. final dump distance of 3.09 km, and operational
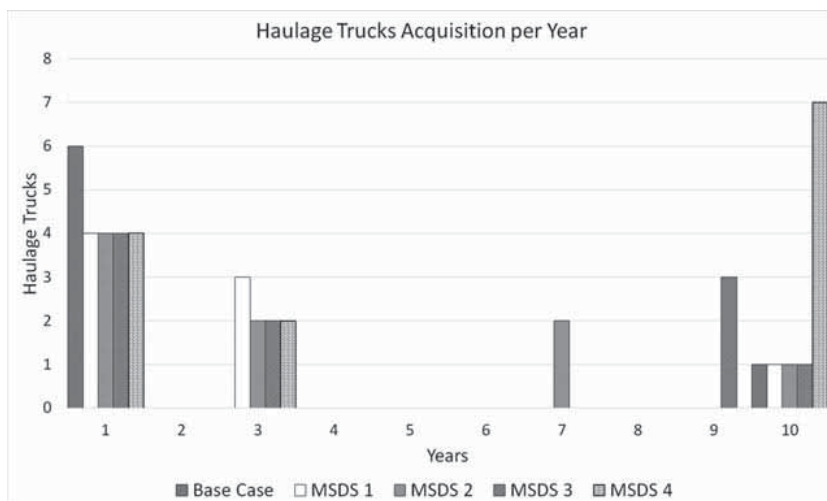
Figure 5. Required number of haulage trucks per year, for each scenario.
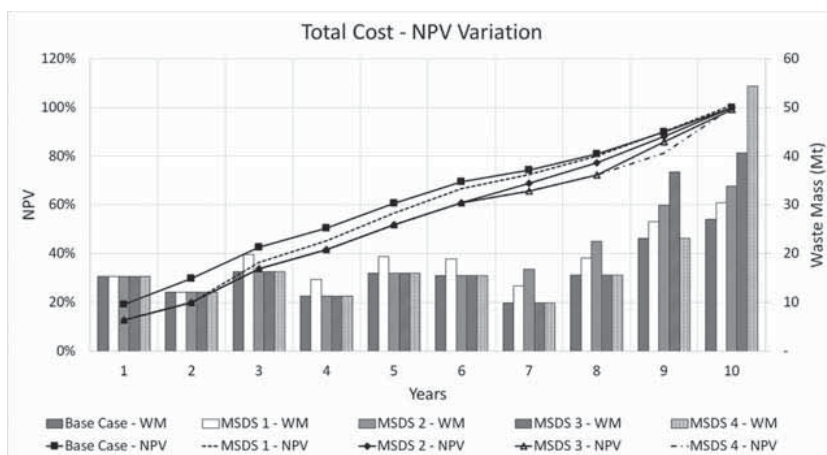
Figure 6. Total amount of waste mass hauled by year for each scenario and OPEX NPV variation.

costs as used, variations on these parameters might turn MSDS scenarios more attractive. Increasing final dump distance to 4.64 km (50% increase) and keeping the same haulage and loading costs result in 2.39%, 3,03% and 2,37% lower NPV costs for MSDS 2, 3 and 4. Meanwhile, if final dump distance reduces to 2.71 km, none of MSDS scenarios tested would result in lower total costs. Same kind of behavior is observed when changing other parameters. It can be observed that there is a limit where one alternative becomes more attractive, economically, than the others.

4 CONCLUSION

Waste re-handling is historically an issue in mining operations, avoided and/or postponed as much as possible due to increase in total operating cost. Moreover, waste re-handling has been always considered to be the worst case scenario by default. However, a planned waste re-handling might impact positively, opening new alternatives for mine operation and planning. Four MSDS scenarios were tested and compared to a base case, and among them, the

3rd one shown the best results, and the 1st one the worst, regarding total NPV costs. It is important to highlight that this work is a preliminary study and, so far, only a few variables were tested, and the next step is to implement an optimization algorithm to determine the best schedule sequence and equipment allocation. However, it provided information that suggests the viability of MSDS method application. Besides the economic and operating aspects analyzed in this study, it is a fact that, MSDS approach provides more time to deal with final dump allocation assessment and selection, environmental permits, and might facilitate management, sequencing and disposal of potential acid forming (PAF) waste rocks.

REFERENCES

Askari-Nasab, H. et al. 2011. A mathematical programming model for open pit short-term production scheduling. *SME annual meeting and exhibit, 113th national western mining conference*: 213–220.

Askari-Nasab, H.; Ben-Awuah, E. 2011. Integration of oil sands mine planning and waste. *35th APCOM symposium, Wollongong, NSW, September*: 24–30.

Caccetta, L.; Hill, S.P. 2003. An application of branch and cut to open pit mine scheduling. *Journal of global optimization* 27: 349–365.

Dagdelen, K. 2001. Open pit optimization—strategies for improving economics of mining projects through mine planning. *Proceedings of the 17th international mining congress and exhibition of Turkey, Ankara, Turkey, June*: 117–122.

González, E.; Williams, M. 2015. Using simulation to quantify uncertainty in ultimate-pit limits and inform infrastructure placement. *Mining engineering magazine, December*: 49–55.

Dimitrakopoulos, R.; Martinez, L.; Ramazan, S. 2007. A maximum upside / minimum down-side approach to the traditional optimization of open pit mine design. *Journal of mining science* 43(1): 81–90.

Ramazan, S. 2003. Uncertainty-based production scheduling in open pit mining. *Transactions of the institutions of mining and metallurgy, section a: mining technology* 316(3): 106–112.

Espinoza, D. et al. 2013. MineLib: a library of open pit mining problems. *Annals of operations re-search* 206(1): 93–114.

Fu, Z.; Topal, E.; Erten, O. 2016. A modified software tool for mine waste rock dump planning. *Ninth AUSIMM open pit operator's conference, Kalgoorlie, WA, November*: 229–242.

Graskoski, S.; Craig, S.; Myburgh, C. 2013. Dynamic pit and waste dump schedule optimization at Tropicana gold mine. *World gold conference, Brisbane, QLD, September*: 121–127.

Hekmat, A.; Osanloo, M.; Shirazi, A. M. 2008. New approach for selection of waste dump sites in open pit mines. *Mining technology* 117(1): 24–31.

Lambert, W.B. et al. 2014. Open-pit block-sequencing formulations: a tutorial. *Interfaces* 44(2): 127–142.

Li, Y.; Topal, E.; Williams, D. 2012. Mathematical approach for better mine waste rock dumping management. *Life of mine conference*, Brisbane, QLD, July: 207–214.

Li, Y.; Topal, E.; Williams, D. 2013. Waste rock dumping optimization using mixed integer programming (mip). *International journal of mining, reclamation and environment* 27(6): 425–436.

Li, Y.; Topal, E.; Williams, D. 2015. A new tool for optimization of mine waste management in potential acid forming. *Tailing and mine waste management for the 21st century,* Sydney, NSW, July: 333–342.

Li, Y.; Topal, E.; Ramazan, S. 2016. Optimizing the long-term mine waste management and truck schedule in a largescale open pit mine. *Transactions of the institutions of mining and metallurgy, section a: mining technology* 125(1): 35–46.

Lizotte, Y.; Bonates, E. 1986. Truck/shovel dispatching rules. *Society of mining engineers, McGill University, Montreal, Canada*.

Ortiz, J. 2017. Methodology for a dump design optimization in large-scale open pit mines. *Cogent engineering* 4(1): 1–11.

Ramazan, S.; Dimitrakopoulos, R. 2013. Production scheduling with uncertain supply: a new solution to the open pit mining problem. *Optimization and engineering* 14(2): 361–380.

Waqar Ali Asad, M.; Dimitrakopoulos, R. 2012. Optimal production scale of open pit mining operations with uncertain metal supply and long-term stockpiles. *Resources policy* 37(1): 81–89.

Zinck, J. 2004. Emerging technologies in mine waste management. *Waste processing and recycling in mineral and metallurgical industries, 5th international symposium, Hamilton, Ontario, Canada*: 49–66.

Parametric analysis of the optimal depth of an open-pit gold mine

R. Motta, C. Porto, D. Machado & O.C. Souto
Universidade Federal do Rio de Janeiro, Rio de Janeiro, RJ, Brazil

ABSTRACT: This paper aims at demonstrating the optimum Percentage of Resource Mined (PRM – mineable reserve divided by total ore resources) by means of a parametric analysis, given three ore body geometries, namely: tabular, cylindrical and pipelike, showing the threshold between open-pit and underground mining, using the so-called Ore Quality Factor (OQF), which will be defined in the text. A conycal open-pit mine was considered to calculate the OQF, the economics of underground mining to go beyond the established limit by underground mining being not considered, which, in the case of the pipelike orebody would be more important. The relative dimensions of the aforesaid shapes were chosen in a way, that resulting volumes are the same and therefore tonnages. The overburden thicknesses considered for the three shapes being the same, the waste-to-ore ratio varies a lot, whether PRM is 10% or 100%. Sensitivity analyses included overburden thickness, ore grades, and slope angles.

1 INTRODUCTION

Open pit mining has often been applied to gold mining worldwide since the low cost of mining allows profitable extraction of low grade ores. In open pit mining the slope angle is an important and conditioning factor to the waste × ore ratio. For example: for pipelike bodies, in order to remove a larger quantity of ore, it is necessary to go deeper, maintaining the same slope angle, while widening the pit (as shown in Figure 1), increasing the waste × ore ratio.

On the other hand, slope stability of a rock masses are governed by factors such as lithologic type, dip angle, degree of rock alteration, structural discontinuities in the rocky body (faults/fractures), among other factors.. Detailed studies are required to evaluate these factors and, there are standards that should be consulted for the geomechanical classification of rocks, such as GSIRMR.

It is important to stress that an optimum angle must be adopted throughout the whole mine life in order to maintain mining operations safe and continuous since large landslides would result in the partial or total closure of activities. Changing slope angle should be avoided as it is a time-consuming operation and could easily cost millions of dollars.
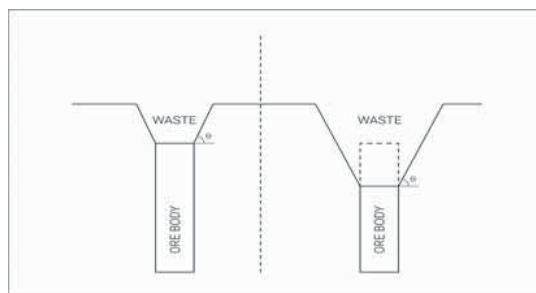
Figure 1.   Increase in waste-to-ore ratio as the pit depth increases.

In this paper a (hypothetical situation is presented where the above mentioned factors are simplified following only the geological type and its theoretical critical pit slope and considering the sound state of the rock. Hard and healthy rocks, such as granite, allow larger angles (e.g. 60°), sandstones intermediate angles (45°) and soft rocks, such as phyllites and schists, smaller angles (30°). The presence of fractures and weathering processes were not taken into account.

According to Evans (1993) the morphology of the mineral deposits considered in this work can be generally classified as discordant with regular contours and confined within a portion of the host rock. As a result, most of these ore bodies are tabular or tubular shaped. Gold bearing veins are generally contained in tabular (or lenticular) bodies that are structurally controlled forming ore shoots. Diamond ores are characteristically hosted in tubular bodies that are known as "pipes" if the pitch is sub-vertical, or pods which are generally referred to for chromite ore seams.

2 BASIC CONCEPTS

Estimation of mineral resource is the first step in the evaluation of mineral deposits. Resources may be subdivided into measured, indicated and inferred, according to the level of confidence in the data acquisition and interpretation. Part of the resources are transformed in reserves if economic viability is demonstrated. Reserves may be proved or probable and as mining progresses only part of the reserves are actually processed as ore (Fig. 3).

It is important to keep in mind that not all the resource is extractable, especially when considering the costs of the operations, with acceptable extraction rates between 10–50% of the deposit (Noble 1993).

Waste, or sterile, is the portion of a mineral deposit with no economic value. Knowing the waste/ore ratio is of paramount importance, since a greater ratio may even make the mine
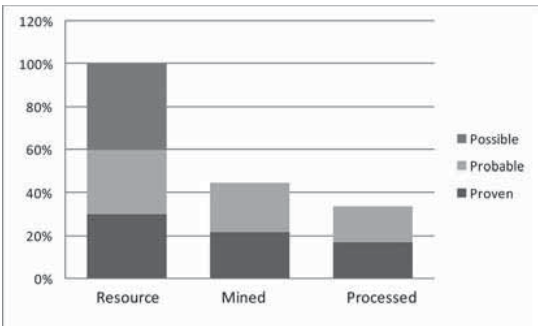
Figure 2.   Typical progression from geologic resources to ore reserves (Noble, 1993).
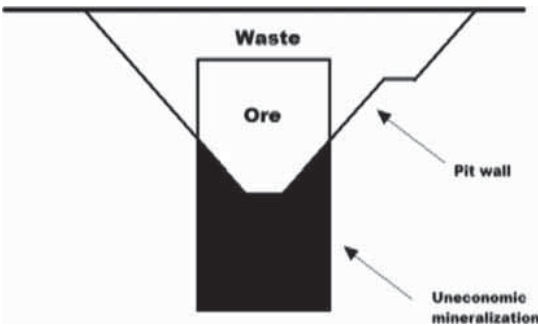
Figure 3.   Open-pit economic limits (adapted from Noble, 1993).

unfeasible. The cutoff grade is the limiting content at which mineral exploitation becomes unpractical, its value involves a series of variables, which must be well studied in order to obtain an ideal value. The choice of cut-off grade can directly affect the profits of a company, since it can modify the economy and even the viability of the deposit by increasing or decreasing the exploitable reserves.

3 CHOOSING THE MODEL

For the present work an open pit mine was chosen. In general, the Open-Pit (OP) method predominates over Underground (Ug) in the world, as it allows greater recovery, flexibility and safety, while the second method is more expensive and dangerous, being mainly used when the bulk mineral is found at greater depths. Some deposits can be mined entirely by one of these methods or by the combination of both. Thus, in order to discover the transition depth (TD – Transition Depth) between one and another, it is necessary to compare the economic efficiencies of its operation, except when the advantages of one of them are totally obvious (Bakhtavar et al., 2002).

The most used way in this evaluation is the waste-ore ratio, also called Stripping Ratio (SR), which represents the amount of non-economic material that must be removed (waste) to remove an ore unit (Hartman, 1992) expressed in m^3/m; t/t; or m^3/t.

The material will be classified as ore if the value of the products exceeds the total costs of processing added to the costs of extraction of the ore and waste as expressed in the formula below (Noble, 1993), the value of the ore is a consequence of these variables.

$$\text{Revenues} \geq \text{Cost}_{PROCESS} + \text{Cost}_{G\&A} + \text{Cost}_{MINE} * (1 + SR) \tag{1}$$

where: Revenues = (Price – Cost – Royalties) * Recovery * Grade

De Carli (2013) indicates three classifications of SR: A) global; B) equilibrium and C) maximum allowed:

A. The overall ratio (OSR) is the ratio of total mass of sterile to total mass of ore (Hartman, 1992), according to the equation

$$OSR = \frac{Tm}{Te} \tag{2}$$

where: T_m = Ore mass; T_e = waste mass;
In order to know the sterile global ore ratio it is necessary first that the boundaries of the ore in the pit is well defined, and from there quantify the ore and the waste within its boundaries. The determination of the maximum depth according to the profitability of the operation requires data on the total costs and revenues that will be received from the sale of the ore and its by-products, if any (Tatiya 2005).

B. The BESR – (Break-Even Stripping Ratio) is calculated to the point at which equilibrium occurs and the required compensation is paid for the net value of the ore (Taylor 1972).

$$BESR = \frac{I - Ct}{Csw} \tag{3}$$

where: I = Revenue per ton ore; C_t = production cost per ton of ore (including all costs up to sale, except for overdraft); C_{sw} = cost per ton of waste. BESR should not be confused with the OSR, which is always inferior, otherwise there would be no profit for the operation (Sodeberg & Rausch, 1968).

C. The maximum permissible ratio (ASR – Allowable Stripping Ratio) is characterized by the highest practiced value in the open pit scenario. The ratio indicated in terms of m^3 of waste per ton of mineral can be determined according to the formula:

$$SR = \frac{Cug - Cop}{Cw} \tag{4}$$

where: C_{ug} = cost of 1ton of ore by underground methods; C_{op} = cost of 1 ton of ore in open pit; C_w = total cost of removing 1 ton of waste in open pit;

Its analysis during the project evaluation stage is of great importance, it can determine the depth where the transition of methods should occur. In order to respect the viability of an open-pit project, the overall OSR ratio of the pit should always be below the ASR (DeCarli, 2013).

4 PROFIT FUNCTION

The PF (Profit Function) benefit function gives the economic value of each block, which should be calculated differently for ore blocks, marginal and waste (Halatchev, 1999). It is the result of the difference between revenues and costs in the mining and processing (for ore) of the block.

$$PF(ORE) = GRADE * R * (PV - CR) - (Cl + CP + CG\&A) \tag{5}$$

where: R = recovery; PV = selling price; C_R = refining cost; C_L = ore mining cost; C_P = processing cost; $C_{G\&A}$ = administrative costs.

The mining costs are not considered in the calculation of the Profit Function for the marginal ore blocks because, regardless of the material to be considered (ore or waste), these costs will be present in the final value of the block. Thus, when the value of the benefit function is positive, the blocks should be treated as oreblocks should be treated as ore.

$$F(MARGINAL) = (GRADE*R*(PV - CR)) - (INC + CP + CG\&A \tag{6}$$

where: INC = incremental cost of the difference between transporting the material to the beneficiation plant relative to the stockpile (if transport distance to the plant is greater than the distance to the stockpile);

While, when the value of the benefit function is negative the blocks should be treated as sterile. Since there is no revenue generation in its removal, the costs considered in the calculation are relative only to the plowing of these sterile blocks.

$$PF(WASTE) = -(CL) \tag{7}$$

5 CUT-OFF GRADE

As stated earlier, the cut-off (Lane, 1964) is the most commonly used criteria in mining to distinguish ore from waste. First the cut-off level (BCOG-Break Even Cut-off Grade) must be determined, the minimum threshold level that pays for all the company's general and administrative costs, as if the profit would be null. (Noble, 1993; Lane, 1964; Hustrulid & Kutcha, 1998)

$$BCOG = \frac{C_L + C_P + C_{G\&A}}{R * (PRICE - C_R - ROYALTIES)} \tag{8}$$

where: C_L = ore mining cost; C_P = processing cost; $C_{G\&A}$ = administrative costs; R = recovery; Price = The sales price of the product; C_R = refining cost; Royalties = the royalties cost;

This formula can be reduced to a Marginal Cut-off Grade (MCOG), in which it considers that the blocks will be extracted in any way, excluding from the calculation the mining costs.

Adding to the formula is the incremental cost INC (Rendu, 2008), which represents the cost difference between mining a block of ore and a block of waste (usually occurs by the variation of transport distance between the plant and the beneficiation or the waste stockpile).

$$MCOG = \frac{INC + C_P + C_{G\&A}}{R * (PV - C_R)} \tag{9}$$

where: Inc = incremental transport cost

The tonnage x cut-off grade curve in Figure 4 shows that for a 0.018 oz/st cut-off grade, there is a 10% reduction in ounces for gold and a 30% reduction in the ore tonnage. These figures, in the article by Noble (1993) are, respectively, 20% and 39%.

Noble (1993) presents the quality factor of the ore (Factor Q), a way to evaluate the stripping ratio for a generic body.

$$Q = \frac{REVENUES - CP - CG\&}{CL} \tag{10}$$

This quality factor was used to test three different geomorphologies of mineral deposits with different waste or overburden thicknesses: 0m (outcropping ore); 36 m and 72 m. Also it was taken into account the geometry and angle of the pit slope (30°, 45° and 60°). Three geometries were chosen: tabular (disc), cylindrical (semi-equilateral) and pipelike (elongated cylinder), their dimensions are proportional, so that the volumes of the three are the same and, consequently, their total tonnages.

Figures 5, 6 and 7 show the general trend of how the percent of Resource Mined referred to Total Resource varies with Ore Quality Factor Q, Overburden thickness, Ore Body Shape, pit slope and ore grade, other parameters remaining equal, for 2 g/t and pit slope 45 degrees.
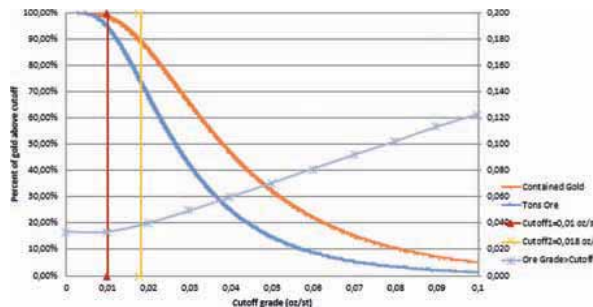
Figure 4.   Tonnage x cut-off grade curve.
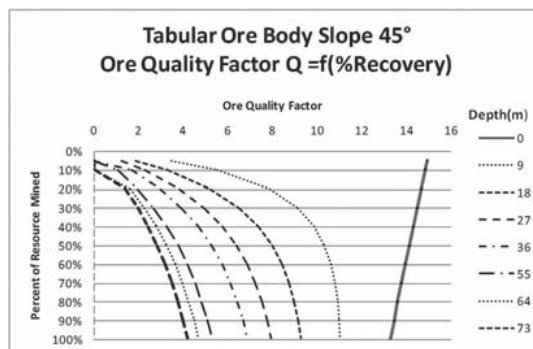
Figure 5.   Percent of resource mined as a function of ore quality factor (Q) overburden thickness (in meters), tabular ore body shape, pit slope 45°, ore grade 2 g/t.
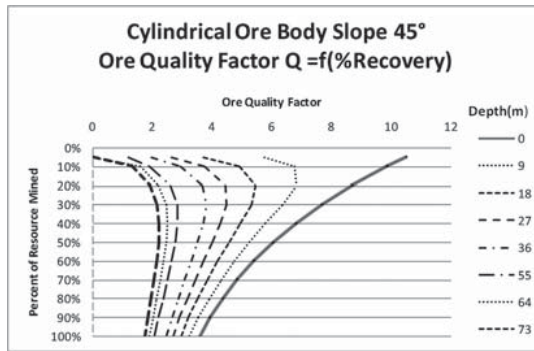
Figure 6. Percent of resource mined as a function of ore quality factor (Q) overburden thickness (in meters), cylindrical ore body shape, pit slope 45°, ore grade 2 g/t.
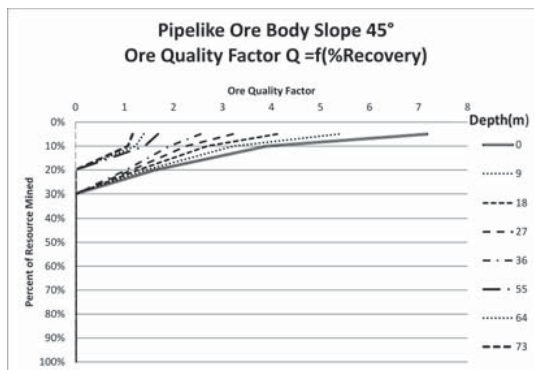
Figure 7. Percent of resource mined as a function of ore quality factor (Q) overburden thickness (in meters), pipelike ore body shape, pit slope 45°, ore grade 2 g/t.

In Figure 5, one can see that, for zero overburden, as open-pit mining goes deeper (bigger PRM), the ore quality factor Q diminishes, although the Q factor lies between 15 and 13, a relatively high index. On the other hand, for maximum (73 m) overburden, as the PRM grows, Q grows as well. This is because the so-called fixed cost of the overburden is diluted, as more and more ore is mined by open-pit mining. The same applies for lines corresponding from 64-m to 9-m overburden depth.

In Figure 6, the general trend is for Q start growing from 0 to 20–30 PRM, and then decreasing or following quasi-vertical lines, up to 100 PRM. It is as if the waste-to-ore ratio would keep approximately constant and therefore keeping Q within narrow limits, for each overburden thickness line. For instance, for the average depth, 36 m, Q grows from 2 to almost 4, at 30 PRM, then decreases to almost 3 at 100 PRM. Differently from Figure 5, in Figure 6, for zero-overburden, Q decreases sharply from o to 100 PRM, that is to say, Q varies from 10 to 4.

In Figure 7, one can see that Q diminishes for all overburden thicknesses, and PRM goes only up to 20–30, even for zero-overburden when adopting open-pit mining, higher PRM leading to underground mining, for a pipelike ore body.

Figure 8 shows the growth of Q with increasing PRM, as the overburden fixed cost is diluted, open-pit mining going deeper. The effect is larger for bigger slopes. Taking a PRM equals 50, Q is respectively 2, 3 and 4, approximately, for pit slopes 30, 45 and 60 degrees.

Figure 9 shows that Q increases with PRM for both Tabular and Cylindrical ore body shapes, decreasing for a pipelike ore body, which is mineable by open-pit only up to PRM 20. Q is smaller for the Tabular ore body shape than for the Cylindrical one, except for PRM equals 100.
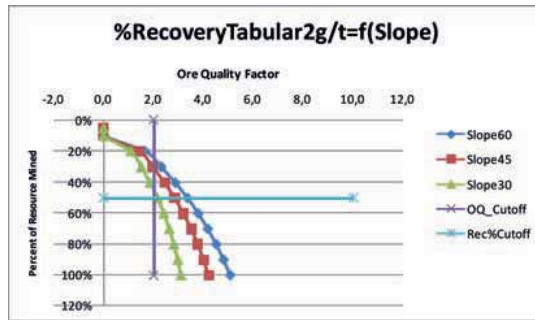
Figure 8. PRM as a function of ore quality factor (Q) considering maximum overburden thickness (73 meters), ore grade 2 g/t and variable pit slope for tabular ore body shape.

Figure 9. PRM as a function of ore quality factor (Q) considering maximum overburden thickness (73 meters), ore grade 2 g/t, fixed pit slope (45°) and variable ore body shape.
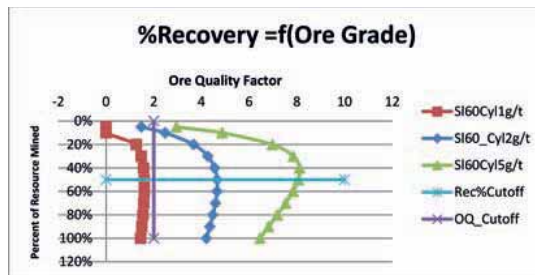
Figure 10. PRM as a function of ore quality factor (Q) considering maximum overburden thickness (73 meters), ore grade 2 g/t, fixed pit slope (60°) Cylindrical ore body shape and variable ore grade.

Figure 10 shows that Q increases with ore grade, as one would suspect (maximum of 2, 4 and 8, respectively, for 1, 2 and 5 g/t). Moreover, Q grows as PRM goes up to 40–50 for all ore grades, decreasing afterwards.

6 CONCLUSION

A valid EXCEL model to do a Parametric Analysis establishing the optimal depth of an open-pit gold mine for three different ore body geometries was built and experiments with the model showed that it responds satisfactorily to a series of different conditions. For pre-feasibility studies, given an ore reserve is to be appraised, the model has not been tested yet, only for some initial conditions. The authors would like to be consulted, under different

conditions, deposits, ore types, in order to test the validity of the model, even if some changes in the original model are required. Additionally, this model may be used for didactic applications at the Geology Department of UFRJ, where the authors are undergraduate students and Professors.

REFERENCES

Bakhtavar, et al. 2002. An approach towards ascertaining open-pit to underground transition depth.

deCarli, C. 2013. Análise de Projetos Limite: lavra a céu aberto vs. lavra subterrânea, Dissertação de Mestrado, UFRGS.

Evans A.M. 1993. Ore Geology and Industrial Minerals—an introduction. Blackwell Scientific Publications, Oxford.

Halatchev, R. 1999. Company Strategy—A basis for Production Scheduling of an Open Pit Complex. Whittle—Strategic Mining Planning, Perth, Whittle Programing Pty. Ltd.

Hartman, H.L. 1992. SME Mining Engineering Handbook. Society for Mining, Metallurgy, and Exploration Inc., 3.

Hustrulid, W., & Kutcha, M. 1998. Open Pit Mine Planning and Design. Rotterdam: A.A. Balkema, 836 p.

Lane, K.F. 1964. The Economics History Review; Tonnages, Medieval and Modern.

Noble, A.C., 1993, Geologic resources vs. ore reserves: Mining Engineering, v. 45 no. 2, 173–176.

Rendu, J.M. 2008. Introduction. An introduction to cut-off grade estimation pp. 1–3. United States of America: Society for Mining, Metallurgy, and Exploration, Inc.

Sodeberg, A., & Rausch, D.O.1968. Surface Mining, 142–143. New York AIME.

Tatiya, R.R., 2005. Surface and Underground Excavations: methods, techniques and equipment. 579 Michigan: A.A. Balkema.

Taylor, H.K. 1972. General Background Theory of Cutoff Grades.160–179.

A procedure to generate optimized ramp designs using mathematical programming

N. Espejo, P. Nancel-Penard & N. Morales

DELPHOS Mine Planning Laboratory, Advanced Mining Technology Center (AMTC)
and Department of Mining Engineering, University of Chile, Santiago, Chile

ABSTRACT: Open-pit mine planners have long relied on optimization models for estimating pushbacks without ramps at the block level. Subsequently, they generate an operational design which includes ramps that are required to access the different parts of the mine. This design depends on the time available and the experience of the planner.

In this paper, we present a procedure that (i) uses mathematical optimization to find a modified pushback, which contains the ramp location at the block level, minimizing the impact on the value of the original pushback, and (ii) produces a designed pushback integrating the operational ramp design at the actual pit profile from the modified pushback.

We apply this procedure on several block models and compare to the original pushback, the modified pushback, and the designed pushback. The results show that the designed pushback are consistently close to the original pushback in terms of value and tonnage.

1 INTRODUCTION

Open pit mine planning is a decision-making process that leads to a realistic and actionable plan to profitably extract mineral resources. Planning can be carried out for a wide range of periods from the very short (next shift) to the very long (life of mine) (Whittle, 2011).

The starting point of the mine planning process is a block model in which the ore body is divided into regular blocks; each block with individual attributes, such as, ore grades, recoveries, and tonnages. The block model is economically valued and the profit is assigned to each block (Bley et al., 2010). This block model together with the geotechnical constraints and the long term economic parameters (costs and commodity prices) is the basic inputs for open pit strategic mine planning.

This models allows to compute, for example, the *ultimate pit* (or *final pit*), which is a set of blocks in the block model that contains the total maximum profit while satisfying the operational requirement (Cacetta & Hill, 2003). Within the ultimate pit, the deposit is divided into nested pits: from the smallest pit with the highest value in terms of profit to the largest pit with the lowest profit value (Dagdelen, 2001) for the purpose of establishing a mining sequence. Nested pits are generated by varying the price of the metals being extracted (Hustrulid et al., 2013b).

However, while the ultimate (and nested pits) are widely used for computation of plans, there are no blocks in real mines. Indeed, these computations are used as a guide in later stages to design actual mine. That is, they are only an approximation of the actual volumes of the pit. Indeed, after obtaining the ultimate pit and nested pits, mine designs which represent real profiles (for example with access ramps) are carried out.

On the one hand, the process for computing the ultimate pit and nested pit rely on optimization techniques that guarantee that an optimal solution will be obtained. On the other hand, the open pit operational design stage is carried out using specialized design software, which are tools to aid the user to make designs faster but they do not ensure the profit optimization. Thus, this stage is mostly a manual process in which the optimality depends on the user.

It follows that the quality of the resulting solution depends on the skills, information and time available for the design phase. Even if there exist some criteria to check the quality (for example, measuring the difference in tonnage and value of the optimal pit shell versus the operational pit design), there is no guarantee that the results would be optimal. In addition, the process itself is very slow and time consuming, making it to analyze the robustness of the obtained design.

Unfortunately, ramps are one of the most important aspects of mine planning and they should be included early in the mine planning process since they do have a significant effect on the reserves (Hustrulid et al., 2013a), because they force the addition of waste and/or reducing the amount of ore from the pit shells.

In this paper, we build on previous work to present a methodology that uses a mathematical model and postprocessing in order to generate a pit design which is as close as possible to the results of the optimization process, but complies with actual design considerations. The mathematical model has been already introduced (see Morales et al. 2017 and Nancel-Penard 2019) starts with the optimized pit (at the block level or support) and generates another profile (also at the block support) with enough space for ramps and so that the impact in value is minimized. The postprocessing, which is the emphasis of this paper, then takes this *proto-design* of the phase and generates a design of the pit and ramp.

1.1 *Review of current practices and related literature in mine designs*

At the mine design stage that consists of converting volumes defined at block level into operational ones, it is necessary to smooth the final pit contour and pushbacks. Mine designs must incorporate all the geometrical components of a slope, which include hauling ramps, where trucks can access each of the phases to transport ore and waste to the final destinations.

Generally, ramps' locations are constructed based on the criteria of the mine planner in charge of the operational mine designs of an open pit. One of the issues faced by the mine planner, which is little written about in the mining literature, is gaining initial access to the ore body (Hustrulid et al., 2013a). Some aspects, which the mine planner must consider when realizing operational designs, are:

- Minimum costs on a net present value basis for the transport of ore and waste throughout the life of mine. The preference is to use of long-life haul roads rather than short-life roads as this reduces overall road construction costs and operating costs (Atkinson, 1992).
- Roads exits from the pit wall. This is dependent upon the crusher location and the dump points (Hustrulid et al., 2013a).
- Optimum number of access points to the pit. More access points mean more flexibility but the added cost could be high (Hustrulid et al., 2013a).
- Optimum number of switchbacks. It is desirable to avoid the use of switchbacks in a pit because they tend to slow traffic, cause greater tire wear and various road maintenance problems (Hustrulid et al., 2013a).
- Minimum traffic congestion (Atkinson, 1992).
- Avoidance of areas where slope stability problems could occur (Atkinson, 1992).

Therefore, the planner must deal with many criteria and considerations to generate a design, which means that the current practice does not necessarily maximizes NPV and minimizes operational costs in pit designs.

2 DESCRIPTION OF THE MODEL AND POSTPROCESSING ALGORITHM

In this section we specify the problem to be solved and describe the mathematical model and postprocessing algorithm.

Figure 1 depicts the whole process. As a first stage, we start with a pushback at the block support (for example the ultimate pit or any nested pit). This pit used as an input for an optimization model that looks for a *pre-design pushback* (also at the block support) so that:

273
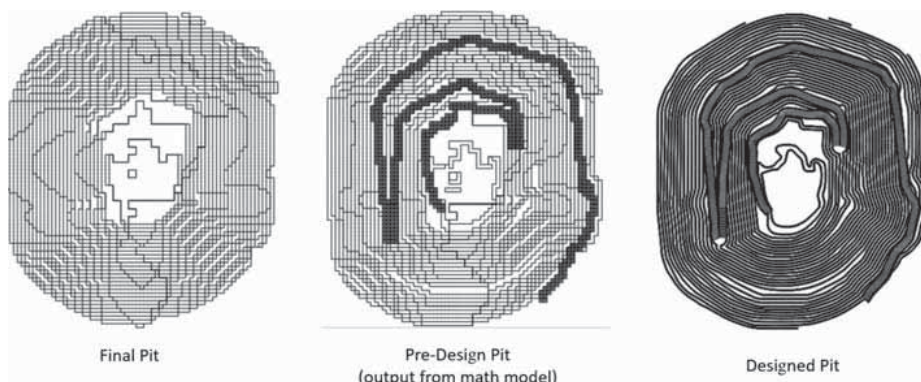
Figure 1.   From ultimate pit to designed ramps.

(i) it contains enough space for the ramps, and (ii) it has a value as close as possible to the original pit. Finally, the postprocessing algorithm transforms the output of the algorithm (i.e. the pre-design pushback plus information about the ramp estimated location) and produces an operational pit profile.

2.1   *Computing the pre-designed pushback*

The pre-designed pushback starts with a block model that includes economic values of the blocks and a pit profile. From this, it will select specific points that aim to estimate the block at which the ramp passes at every level (if the ramp is wider than 1 block, it looks at the outer block). These points can be inside or outside the initial profile, with tolerance distances defined by the user. The model uses these points to estimate the blocks that need to be extracted and generate space for a ramp and from that it estimates the total value of the new volume being computed. The goal is then to maximize the value of that goal.

Further details on the equations of the model can be found in (Morales 2017), and an example of the application of this model in (Nancel-Penard 2018), however it is key to mention that as output, the mathematical model generates the following:

– The set of all blocks that should be extracted.
– A set of control points for the ramp, i.e., a list of blocks that form part of the ramp.

It is also important to notice that, since the model works at the block support, everything has to be approximated by blocks. In particular, for example, the width of the ramp, it's slope, etc.

2.2   *Generating the smooth profile*

This step is an algorithm that aims to fit an operational ramp into the pre-design phase obtained from the block model. For this, the algorithm utilizes not only the profile, but the control points of the ramp at each level and aims to interpolate them using an actual ramp.

The algorithm starts uses the block model and the following standard design parameters: berm and haul ramp widths, global slope angle, bench face angle and interramp angle as depicted in Figure 3 (Left), as well as a number of bencher over which to measure the global slope angle. It also takes as input the result of the mathematical model, which is schematically represented in Figure 3 (Right).

Notice that the algorithm does not consider the ramp slope, as this is already taken into account in the optimization model.

274
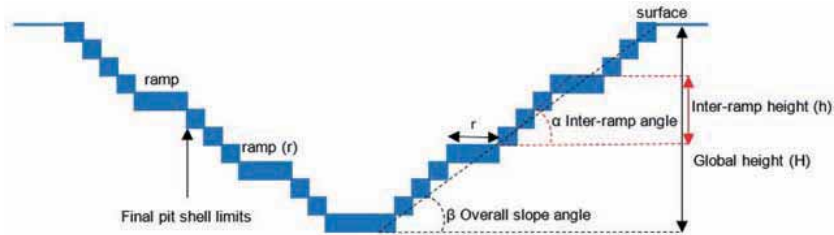
Figure 2. Schematic draw of the pre-design pit at a global scale with the geometrical component of a slope.
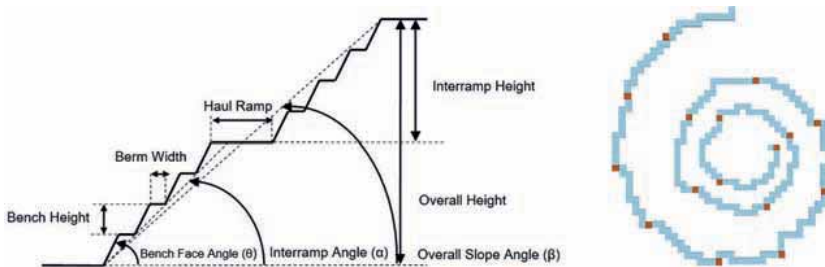
Figure 3. Left: Design parameters for postprocessing algorithm. Right: Output of mathematical model (input for the post processing algorithm). Source: Nancel-Penard et al., In Press.

Table 1. Summary of instances for numerical experiments.

Instance	# total benches	Block size	Global slope angle	Final pit value (MM USD)	Final pit tonnage (MM Ton)
Marvin	30	$15 \times 15 \times 15$	45.6	1,416.2	527.7
Marvin2	30	$15 \times 15 \times 15$	47.4	1,442.3	516.4
KD	18	$20 \times 20 \times 15$	45	647.4	189.9
ZMedium	30	$30 \times 30 \times 15$	45	1,673.7	97.2
ZSmall	14	$15 \times 15 \times 15$	45	1,899.7	541.1

3 NUMERICAL EXPERIMENTS

We consider several block models that are openly available. The models are from the MineLib datasets and provide information not only about block values and coordinates, but also block sizes and precedence arcs.

Table 1 summarizes the main aspects of these instances in terms of number of blocks, benches and block sizes, the global and bench face slope angles, and range of variation of the interramp angles used for different experiments and also information about the ultimate pit in terms of the final pit values and tonnage.

4 RESULTS AND ANALYSIS

Table 2 shows the main results of this article for the 5 instances described before. For each instance, we considered a global slope angle and bench face angle, but different values of interramp angles and a number of benches to control the global angle. We report the differences in terms of tonnage and value after the application of the model and algorithm with

Table 2. Performance of the mathematical model and algorithm in terms of tonnage and value differences.

Instance	Global slope angle	Interramp angle range	# Benches to measure global angle	Max pit tonnage difference math model (%)	Max pit value difference math model (%)	Max pit tonnage difference algorithm (%)	Max pit value difference algorithm (%)
Marvin	45.6	50–55	15–20	3%	1%	1%	1%
Marvin2	47.4	50–55	15–20	3%	1%	3%	2%
KD	45	50–55	5–15	14%	10%	15%	14%
ZMedium	45	50–55	10–20	20%	6%	20%	7%
ZSmall	45	50–55	10–15	12%	6%	15%	11%
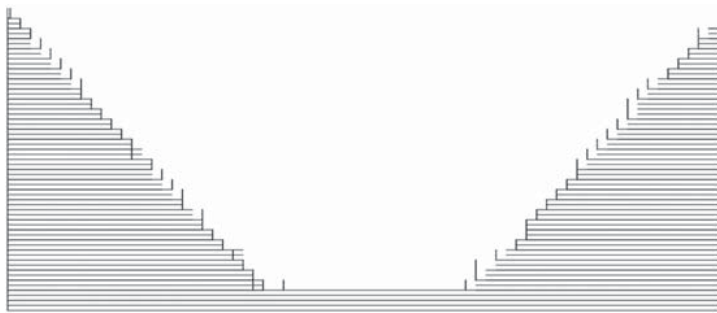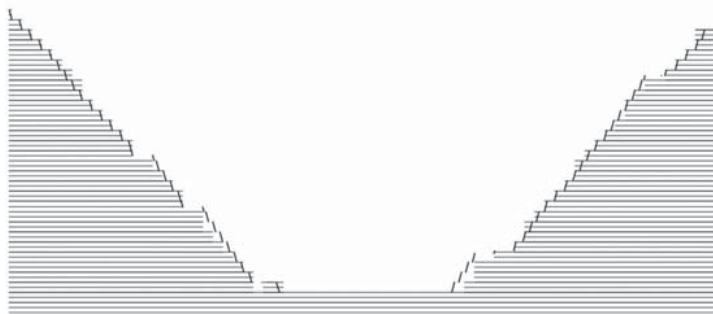
Figure 4. Comparison of profiles for the Marvin instance. From top to bottom: (1) original pit versus model output, (2) model output vs algorithm output and (3) original pit versus algorthm output.

respect to the values in Table 1, however it is worth noting that most of the differences are due to the gap between the original pushback and the result from mathematical model, with the gap for the algorithm being always less than 2% with regards to the model's result.

As it can be seen from the results, the performance of the total variation in terms of value and tonnage can vary significantly from case to case, however the highest difference is introduced by the mathematical model rather than the postprocessing algorithm, which is even capable to reduce the gap sometimes. This is encouraging, because indeed the large differences are mostly due to the several approximations that the mathematical model must perform in terms to *describe* a ramp in terms of blocks, which do not always fit the bench heigh or ramp width.

Figure 4 depicts the profiles obtained for the *Marvin* instance which can be considered as the *best* case. The figure shows the comparison of profiles between the original final pit and the result of the optimization model, the comparison between the result of the optimization model and the output of the postprocessing algorithm, and the comparison between the original pit and the output of the postprocessing algorithm.

Similarly to Figure 4, Figure 5 represents the same comparison between profiles for the *ZMedium* case, which can be considered the *worst performing* scenario in the results.
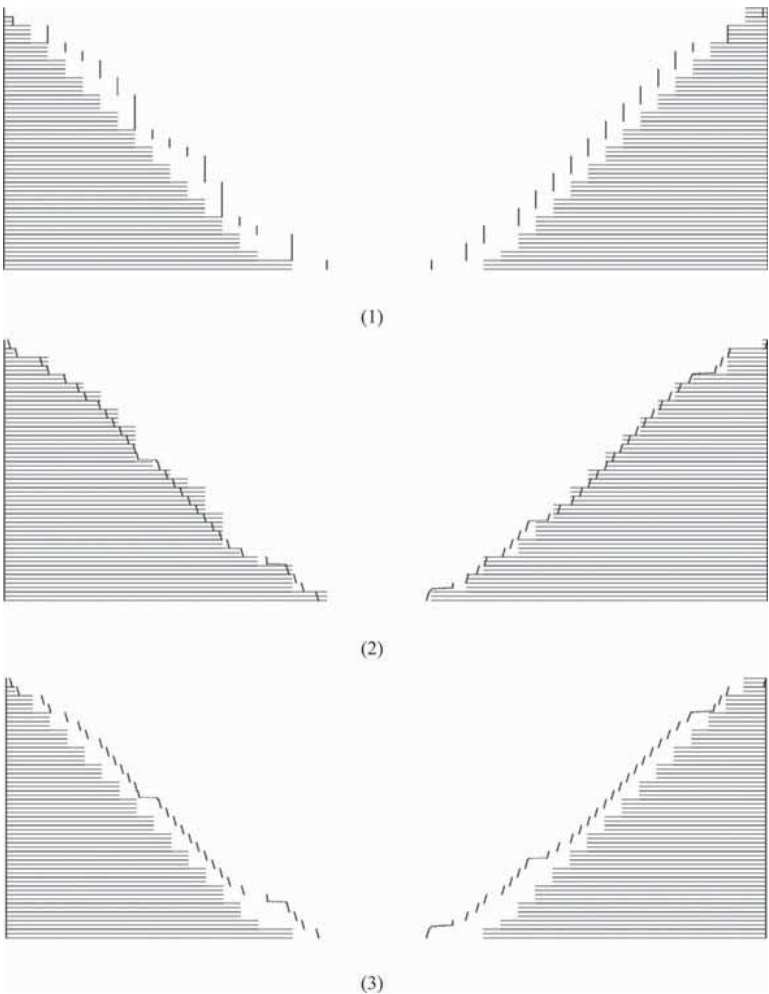
Figure 5. Comparison of profiles for the ZMedium case. From top to bottom: (1) original pit versus model output, (2) model output vs algorithm output and (3) original pit versus algorthm output.

5 CONCLUSIONS

We have presented a methodology that combines an optimization model and a postprocessing algorithm in order to transform an optimized pit profile, computed using block support, into a pit profile that includes an access ramp, and analysed the performance of the methodology over five different block models.

The methodology considers standard design parameters, for which it aims to fit the best ramp so that the total value impact on the initial pit profile is mitigated. Given the operational and design parameters, the methodology is fully automated, therefore providing a valuable tool for constructing the first designs of the mine quickly and therefore allowing to analyse several scenarios with ease.

When evaluated over the different case studies, the methodology shows that it can generate profiles with value and tonnage that are close to the original one, however the differences can be significant, leaving space potential improvement. However, the study also shows that this is mostly due to the difference introduced by the optimization model, which needs to approximate a ramp design using block support. Conversely, the postprocessing algorithm seems very promising in terms of capturing most of the value of the initial solution, even improving it sometimes.

REFERENCES

Atkinson T., 1992. Design and layout of haul roads, in SME Mining Engineering Handbook, 2nd ed., Society for Mining, Metallurgy, and Exploration, Inc., Colorado, USA, 1334–1342.

Bley A., Boland N., Fricke C., Froyland G., 2010. A strengthened formulation and cutting planes for the open pit mine production scheduling problem, Computers & Operations Research, 37, 1641–1647.

Caccetta L., Hill S., 2003. An application of branch and cut to open pit mine scheduling, Journal of global optimization, 27, 349–365.

Dagdelen K., 2001. Open pit optimization—strategies for improving economics of mining projects through mine planning, International Mining Congress and Exhibition of Turkey, Turkey.

Gallagher M.S., Kear R.M., 2001. Split shell open pit design concept applied at De Beers Venetia Mine South Africa using the Whittle and Gemcom software, The Journal of The South African Institute of Mining and Metallurgy, 401–410.

Hustrulid W., Kuchta M., Martin R., 2013a. Geometrical considerations, in Open Pit Mine Planning and Design, Taylor & Francis, eds., Leiden, The Netherlands, 290–408.

Hustrulid W., Kuchta M., Martin R., 2013b. Production planning, in Open Pit Mine Planning and Design, CRC, UK, 504–669.

Lerchs, H. and Grossman, H.C., 1965. Optimal design of open-pit mines, Transactions C.I.M., 58, 47–54.

Morales N., Nancel-Penard P., Parra A., 2017. An Integer Linear Programming Model for Optimizing Open Pit Ramp Design, 38th APCOM proceedings, Session 11, 9–16.

Nancel-Penard P., Morales N., Parra A., Diaz C., Widzyk-Capehart E. In Press. Value-Optimal design of ramps in open pit mining. Archives of Mining Sciences.

Whittle D., 2011. Open-pit planning and design, in SME Mining Engineering Handbook, Published by Society for Mining, Metallurgy, and Exploration, Inc., 877–901.

Williams P., Floyd J., Chitombo G., Maton T., 2013. Design implementation, in Open Pit Slope Design, CSIRO publishing, Australia, 265–326.

Break line and shotpile surfaces modeling in design of large-scale blasts

S.V. Lukichev, O.V. Nagovitsyn & A.S. Shishkin
Mining Institute KSC RAS, Apatity, Russian Federation

ABSTRACT: A software tool for designing open pit large-scale blasts has been developed based on the mining and geological information system MINEFRAME. The given software allows predicting a location of the break line and shotpile surface taking into account the dynamic nature of the rock mass damage and interaction of borehole charges. For this purpose, imitation modelling was used, which allowed mathematical description of the rock mass damage, formation of break lines and shotpile surface of a fractured rock mass. The article describes an algorithm for large-scale blast modelling and shows the examples which confirm a good accordance between the simulation and a real blast.

Keywords: break line, shotpile, open pit large-scale blast, short-delay explosion, imitation simulation, block model

1   INTRODUCTION

At present, damage of rocks by with borehole charge blasting is one of the most common ways of preparing the rock mass to excavation. The costs of loading, transportation and processing of minerals depend on the quality of rock preparation to blasting. At the same time, the blast damage is an integrated and expensive technological process. When designing blasting operations, it is necessary to take into account a significant number of variables, the main ones of which are the elastic-strength characteristics of rocks, the energy characteristics of explosive charges and their spatial arrangement. In this connection, the task of verifying a design solution based on computer modelling of blasting the borehole charges in the rock mass is an urgent issue.

To the moment, in Russia there are two software products which implement the algorithms for 3D simulating large-scale blasts of borehole charges with the formation of rock mass shotpile. These are BLAST MAKER [1] and GEOMIX [2]. The BLAST MAKER's mathematical model of a blast is based on hydrodynamic equations; GEOMIX calculates the blast action of borehole charges by using a velocity field, which is determined based on their potential.

To determine the velocity potential at the charge-rock mass boundary, the time integral is calculated for the dependence that relates the maximum pressure of the blasting products in an explosive cavity with the velocities of detonation, a longitudinal wave in the rock mass and density of explosives and rocks. The pressure in an explosive cavity is calculated on the basis of time dependence, which relates the density and velocity of detonation of explosives, the geometry of the charge and the stemming. The critical value of the rock mass displacement velocity was adopted as a criterion for the rock mass damage.

To implement the 3D design schemes, the authors use a method of forming a regular grid area, for each cell of which the potential is calculated and the area of damage and break line are assessed. At the stage of dispersion of detached rocks along a ballistic trajectory and the formation of a shotpile, the exchange of materials between the individual cells of the grid area is monitored [3].

Despite the use of a rather simplified model of the blast action in the rock mass, the GEOMIX developers managed to obtain a completely realistic large-scale blast model with the formation of break line and geometry of shotpile.

The Mining Institute KSC RAS has studied the issues in the field of borehole rock breaking, including modelling of large-scale blasts, for many decades. At that, the approach developed at the Institute differs significantly from those implemented in both BLAST MAKER and GEOMIX.

Developed on the basis of the mining and geological information system MINEFRAME [4], a set of programs allows dynamical modelling of changes in break line and geometry of shotpile with a short-delay blast of borehole charges in an open pit using simulation modelling tools. Modelling is performed in Geotech-3D software, which is a part of MINEFRAME and is a graphical platform for modelling mining technology objects [5].

Initial data for modeling:

- 3D model of a blasting block,
- Elastic-strength characteristics of rock mass,
- Spatial location of blast boreholes,
- Constructions of borehole charges,
- Energy characteristics of explosive used,
- Scheme of initiation of borehole charges.

These data are formed by the software tools of a module for automated design of borehole breaking [6, 7].

The result of the blast simulation is modified models of a blasting site, containing:

- a wireframe model of the break line surface,
- a wireframe model of the shotpile surface,
- a blocked model of distribution of ore quality in the shotpile.

The algorithm of large-scale blast simulation includes several steps, which are described below.

2 DETERMINATION OF THE DAMAGE ZONE DIMENSIONS AFTER A BOREHOLE CHARGE BLAST

An explosion funnel after the borehole charge blast can only be formed in the case when the zone of radial fissures from the charge goes to the free surface. To calculate the boundaries of the explosion funnel, the dependence is used to calculate the radial stresses in the zone of radial fissures. To obtain the basic calculated values (1, 2) of the blast of an infinitely long borehole charge (r_c – final radius of an explosive cavity, r_g – radius of an overgrinding zone), a two-zone model of the rock mass damage is used, based on the mass-impulse conservation equations in an axisymmetric quasistatic formulation. The validity of the exclusion of the time factor in estimating the size of a damage after the blast of an infinitely long cylindrical charge was proved by comparing the results of an analytical solution in a quasistatic formulation and numerical modelling in a dynamic formulation [8]. To transfer to the calculation of radial stresses after the explosion of borehole charges having the finite length, the authors used the method of replacing a cylindrical charge with equivalent spherical charges located along its axis. The radius of the overgrinding zone after the explosion of an equivalent spherical charge is calculated from the condition of equality of radial stresses on the outer boundary of the damage zone by radial fissures when replacing an infinitely long cylindrical charge with spherical ones.

When transferring to equivalent spherical charges, the sum value of stresses at any point of the 3D space is calculated as the superposition of all radial stresses from equivalent spherical charges, exploded by one delay.

$$r_c = r_o \sqrt[2\gamma]{\frac{P_o}{\sigma_g}\left\{\frac{2\cdot(1+\nu)\cdot\sigma_g}{E_{yu}}\left[(1-\nu)\cdot Ln\left(\frac{\sigma_g}{\overline{\sigma}_p}\right)+1\right]+\left(\frac{r_o}{r_g}\right)^2+\frac{\sigma_g}{K}\cdot\left[1-\left(\frac{r_o}{r_g}\right)^{1,6}\right]\right\}^{0.2}} \qquad (1)$$

where
r_o – radius of explosive cavity (m),
P_o – initial pressure in explosive cavity (MPa),
E_{yu}, K – Young's modulus and uniform compression modulus (MPa),
v – Poisson's ratio,
σ_g, $\bar{\sigma}_p$ – dynamic ultimate compressive and break line strength (MPa).

$$r_g = r_c \cdot \left(\frac{P_c}{\sigma_g} \right)^{2.5} \tag{2}$$

where
P_c – final pressure in explosive cavity (MPa).

Initial and final pressures in explosive cavity are calculated by the formulas (3) and (4) respectively.

$$P_o = K_{ch} \cdot Q_{explosive} \cdot \rho_{explosive} \cdot (\gamma - 1) \tag{3}$$

where
K_{ch} – coefficient of chemical losses,
$Q_{explosive}$ – energy of explosive (J/kg),
$\rho_{explosive}$ – density of explosive (kg/m³),
γ – adiabatic index.

$$P_c = P_o \cdot \left(\frac{r_o}{r_c} \right)^{2\gamma} \tag{4}$$

To find the boundaries of a break line of rocks from the rock mass using the superposition method, the vector of the maximum stress on the free surface from the action of all charges exploded by one delay is calculated. Achieving a critical modulus of the stress vector indicates the penetration of a break line fissure from the charge to the free surface; and the vector itself and its magnitude of stresses are used to calculate the velocity and direction of dispersion of the rock fragments separated from the rock mass.

3 CONSTRUCTION OF A BLOCK MODEL OF THE SIMULATION AREA

To implement the damage simulation algorithm based on a wireframe model of the simulation area (Figure 1), a block model is constructed in the form of a regular structure of elementary
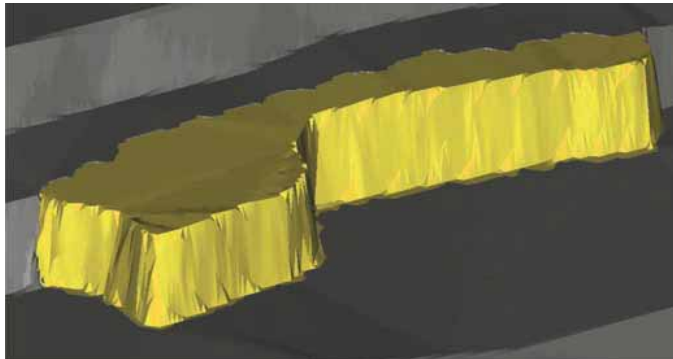
Figure 1. Wireframe model of initial surface (coloured is an area of ore break line).
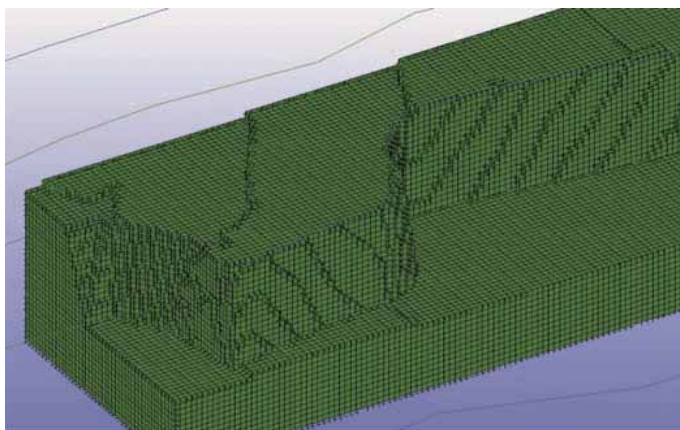
Figure 2. Initial block model of the rock mass.
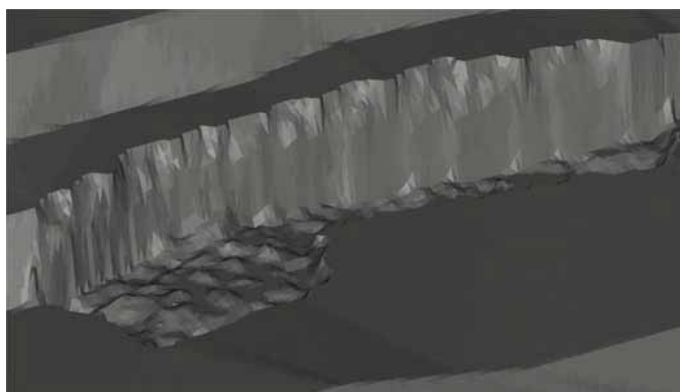
Figure 3. Wireframe model of an open pit sector, changed by the break line surface after the blast.

blocks that are in one of two states: "block – in the rock mass", "block – separated from the rock mass" [9].

The size of the simulation area is set based on possible dispersion of rock fragments separated from the rock mass. Elementary blocks which are not separated from the rock mass, have a shape of a cube of the same size (Figure 2). Elementary blocks which are separated from the rock mass, keep the mass and material composition but moving and increase the volume due to loosening. To accelerate the calculations we give these blocks a spherical shape.

4 MODELLING OF THE BREAK LINE SURFACE IN THE CASE OF SHORT-DELAY EXPLOSION OF BOREHOLE CHARGES

Blasting of a group of boreholes is modelled in accordance with their initiation scheme. When modelling the blast of each subsequent borehole, changes in the free surface geometry made by the blast of previously blown boreholes are taken into account.

The break line surface is formed as follows:

1. For a boundary block that simulates the rock mass surface, the sum vector of radial stresses from spherical charges exploded by one delay is calculated.
2. If the module of the stress vector exceeds the ultimate value of the break line stress, all blocks along the vector line from the boundary block to the charge axis are considered

to be trapped in the explosion funnel. The stress vector specifies the direction of dispersion of a group of these blocks; the initial velocity is calculated taking into account the share of kinetic energy transferred from the energy of the charge explosion to the rock mass.

3. After the formation of a new block boundary of the break line surface, its wireframe model is created (Figure 3), used in the algorithm for modelling the rock mass shotpile.

5 SIMULATION OF THE ROCK MASS SHOTPILE AS A RESULT OF THE BLAST

The shotpile is simulated by modelling the movement of rock fragments separated from the rock mass. At that, a minimum unit of the rock mass volume, for which the displacement and interaction are calculated, is an elementary block. The location of elementary blocks detached from rock mass is calculated at each time point, using the ballistics equations. In a short-delay blast, the trajectories of individual elementary blocks can intersect, and if this happens, the velocity vectors are corrected taking into account the partially inelastic collision mechanism.

When falling onto the surface, the movement of rock fragments is decelerated due to the friction, and the displacement velocity vector is corrected taking into account direction of inclination of the surface at an incidence point. At the end of an elementary block movement, the construction of the shotpile model is completed both in the form of separate elementary blocks (Figure 4), so as the wireframe surface of the shotpile.

The procedure for modelling the shotpile also includes an assessment of the spatial distribution of the material and qualitative composition of minerals (Figure 5).
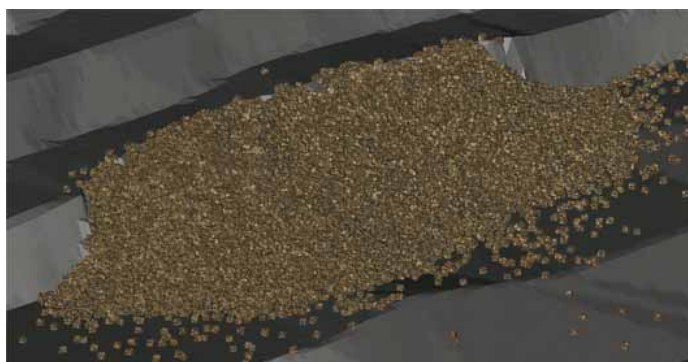
Figure 4. Model of shotpile presented by the ultimate position of elementary blocks detached from the elementary block mass.
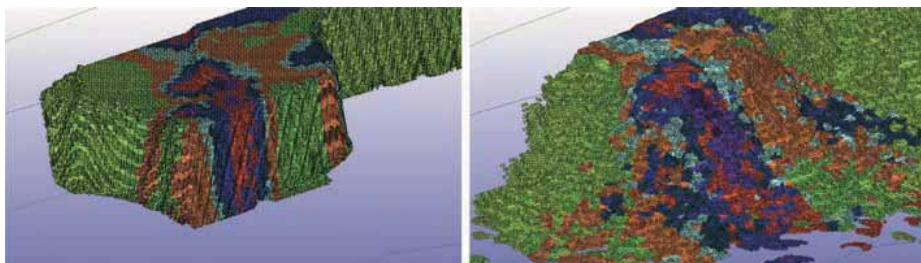
Figure 5. Distribution of mineral contents within an explosive block before and after the blast.

6 ASSESSMENT OF RELEVANCE OF LARGE-SCALE BLAST MODELLING RESULTS

To assess the relevance of the imitation simulation results of the borehole charges explosion, a comparison was made of the calculated and actual break line contours for one of the large-scale blasts at the Zhelezny open-cast mine of Kovdorsky GOK JSC. A comparative analysis of the modelling results with the results of geodetic and geophysical studies in this block was conducted.

In order to comply with the maximum accordance of a real blast and its model, the authors used the results of laser scanning of the block area before the blast, as well as the results of determining the coordinates of the boreholes, their depth and other technological and geological information contained in the large-scale blast project. Figure 6 shows a model of an explosive block with an indicated damage area resulting from the large-scale blast modelling.

As a result of the analysis [10], the actual location of the damage boundaries along the profile of the GPR sounding was obtained. The combination of the predicted and actual boundaries along the sounding profile made it possible to estimate how accurately the modelled boundary of break line reflects the results of a real explosion (Figure 7).

According to the figure, the predicted and actual destruction boundaries for the most part of the profile are close to each other, which suggests the possibility of using the large-scale blast modelling tool to assess the quality of design solutions.
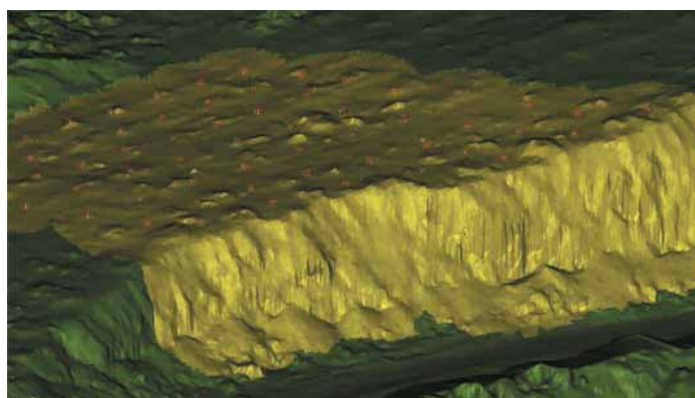
Figure 6.   Model of an explosive block with an indicated damage area resulting from the modelling of a large-scale blast.
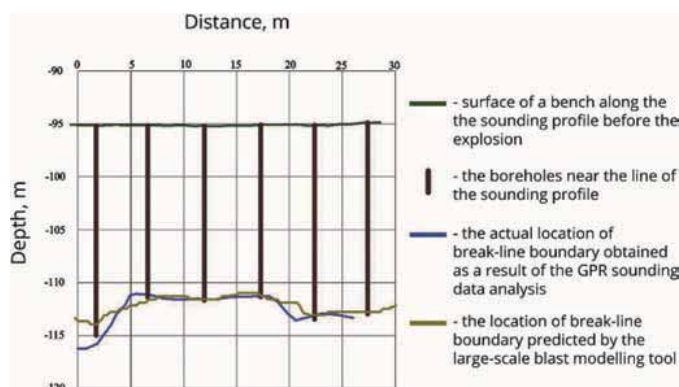
Figure 7.   Cut along one of profiles of GPR sounding of a bench before and after a large-scale blast with indicated predicted and actual boundaries of damage.

7 CONCLUSION

We have implemented a solution for a complex task in the field of design automation of open pit large-scale blasts and the simulation of their results. A software tool for modeling the results of open pit large-scale blasts was developed. The tool allows to predict the results of the project implementation at the design stage, namely:

- geometry of surfaces of break line and shotpile;
- volume of broken rock and mineral content;
- spatial distribution of content in the shotpile;
- losses and dilution of minerals.

Verification of the large-scale blast simulation tool based on a comparison of the results of actual blasts and simulation has shown that they correspond well to each other.

REFERENCES

[1] Tatarchuk S. Yu. Experience in the implementation and operation of BLAST MAKER software// Mining Journal of Kazakhstan. 2013 №11. Pp. 33–36.

[2] Kabelko S.G. Computer modelling of the shotpile an explosive unit and the distribution of the mineral content in the blasted rock mass//Scientific news. 2010, No. 13 (840, Issue 15/1, pp. 84–92.

[3] Volkov Yu. I., Seriy S.S., Dunaev V.A., Gerasimov A.V. GIS GEOMIX for mining industry in Russia and Kazakhstan//Gornyi Zhurnal, 2015(5), 8–13, May 2015.

[4] Lukichev S.V., Nagovitsyn O.V. Automated solution of mining by MINEFRAME software//Mining equipment – 2014, – No. 2., St. Petersburg – pp. 38–42.

[5] Lukichev S., Nagovitsyn O. A system approach to solving the mining technology tasks based on modeling its objects and processes//Proceeding of 38th international symposium APCOM. 2017. August 9–11. P. 5-25-5-29.

[6] Lukichev S.V., Nagovitsyn O.V., Kornienko A.V. Automated design of open pit large-scale blasts in MINEFRAME software//Notes of Mining Institute: "Physical problems of rock destruction". – SPb., T. 171, No. 1. – 2007. – pp. 216–222.

[7] Kornienko A.V., Gurin K.P. Automated design of large-scale blasts in open and underground mining//Proceedings of the 12th international symposium "Development of mineral deposits and underground construction in difficult hydrogeological conditions" "Issues of drainage, geology and geo-informatics, geomechanics, special mining and mining technologies", Belgorod, May 20–24, 2013. pp. 284–295.

[8] Lukichev S.V., Kozyrev S.A. Numerical modeling of the process of dynamic deformation and destruction of rock massif when blasting a single charge or a group of charges//Proceedings of the international scientific conference "Physical problems of explosive destruction of rock massifs". – M .: IPKON RAS, 1999. – pp. 164–168.

[9] Lukichev S.V., Shishkin A.S., Kornienko A.V. Simulation of the process of destruction of rock massif and the formation of break line boundary in a large-scale blast of borehole charges//Mining information and analytical bulletin (scientific and technical journal). 2017. No. S23. Pp. 194–202.

[10] Lukichev S.V., Dyakov A.Yu., Shishkin A.S. Geoinformational methods for analysing the results of geodesic and geophysical studies in assessing the results of open pit large-scale blasts // Problems of Subsoil Use. 2016. № 3 (10). Pp. 89–95.

Incorporation of mineralisation risk into underground mine planning

Rafael Campos Rosado
AngloGold Ashanti, Brasil

João Felipe C.L. Costa
Universidade Federal do Rio Grande do Sul, Brasil

Artur Almgren Saldanha
Geovariances, Chile

ABSTRACT: Underground mine planning aims at determining the amount and sequence of extraction of the mineral resources in order to maximize the deposit profit. It involves multiple sources of information which add risk to the developed plan. Among the risks that can affect the financial return of a mining company, those associated with the geology of the deposit stand out; more specifically the amount of metal contained within the deposits or parts of it.

This risk is mainly due to the complexity of the geological process of the mineral deposits allied to the sparse drilling spacing available used for constructing deterministic models to determine the tonnages and contents of the variable of interest.

This paper aims at develop a methodology to quantify the risk related to the prediction of metal contained in a stope. The risk will be measured based on mine planning constructed through probabilistic models based on geostatistical simulations of the zinc content. Additionally, density is calculated and volume designed for each scenario simulated.

Each designed stope will have its metal content predicted by each simulated model after volume correction using the regression error. Multiple simulations allow to calculate the probability of metal contained at each stope. Based on these results, a risk indicator is proposed to flag the associated risk with the metal contained value in each stope. From this indicator, a rank from low to high risk zones can be taken into account during mining scheduling.

1 INTRODUCTION

Like all economic activities, the ultimate goal of mining is to provide profits for investors.

In addition to economic and market parameters, the profit resulting from a mineral extraction enterprise is directly related to the quantity and quality of the mineral extracted. Therefore, a good knowledge of the deposit is a requirement for attracting investors.

The traditional methods of resources estimation are characterized by providing an unique value for each point or block of the deposit. Thus, it is assumed that each mining block, for example, has a determined value of metal contained in a certain volume of the space and all the financial calculations of return of the investment and even the operational calculations for adjustment of the treatment plant of that ore adopts this information as the ground truth.

Probabilistic models or geostatistical simulation methods were developed to solve this deficiency of the traditional resources estimation methods.

These methods differ in not providing a single modeling solution for the mineral deposit, but infinite solutions equally likely to describe the behavior of the variable under study. In this way, several geological models are generated that represent the deposit under study.

For each model generated, it is applied a transfer function to convert resources into mineral reserves and build the mine plan. From these several plans, it is possible to obtain the probability of a point of the deposit having a certain value and the associated error in the prediction. That is, it is possible to calculate the risks of a particular block does not contain the amount of metal planned.

The simulation algorithms applied to the study of mineral deposits were developed some decades ago and since then several works, not limited only to mining, have been elaborated allowing the improvement of the techniques and the emergence of new methods. These studies present case studies in which the uncertainty associated with the prediction of a geological model and the risks that this uncertainty can bring to a mineral enterprise (Peroni, 2002; Souza, 2007; Diedrich, 2012).

Although the simulation methods allow quantification of uncertainty in the resource estimation, they still have limited application in the mineral industry.

Among the reasons for this low use, three deserve to be highlighted:

 i. Amount of computational time and skilled labor for carrying out the task.
 ii. Lack of technical knowledge among mine planners, regarding the use of simulation techniques.
iii. Mining companies culture, which is still based on deterministic models.

Some studies of underground mine stochastic planning have been developed in recent years, as an example Mello (2015), but, in general, limited to the simulation of the metal content.

In this study, the parameters that map uncertainty regarding the amount of metal contained in a mineral deposit will be evaluated through the construction of probabilistic models.

These models will then be submitted to a transfer function and multiple plans will be created in order to determine the risks associated with the production plan established for the mine.

2 METHODOLOGY

This study aims at developing a methodology to minimize the risk associated with the quantity of metal produced by a mining company and, therefore, to guarantee the stability in producing metal.

The profit (FB) is calculated by the difference between revenue and extraction cost of each stope (Clark; White, 1976).

$$FB = Revenue - Costs \tag{1}$$

Revenue is the arithmetic product of the sale price of the recoverable metal present in the stope and the respective price:

$$Revenue = V \times d \times t \times R \times P \tag{2}$$

where:
V: stope volume
d: rock density
t: metal grade
R: plant global recovery
P: sale price.

The purpose of this study is to evaluate the risks contained in the first three elements of equation (2), that is, the elements that can affect the quantity of metal contained in the forecast.

The sequence of the work to evaluate the geological risk in the underground mine planning is shown in Figure 1.

Figura 1. Sequence of the work.

2.1 *Mine planning*

The mine planning was divided in two parts to carry out the study: design and schedule of the stopes.

Regarding the mining design, there were no changes regarding the market, geomechanical and operational parameters adopted for deterministic planning. The amount of 30 design scenarios required was specified so as not to impact the analysis of results. Thus, 30 designs for each stope were performed in the study area with the optimization tool based on each of the simulated grades through Sequential Gaussian Simulation (SGS).

From this, the density of each stope for each scenario was calculated through a regression with the simulated grades, which is already used in the estimated model and has a high correlation (93%).

Knowing the volume, grade and density for each stope for each simulated scenario, it was possible to construct normal distribution curves of the grade and the contained metal (after confirming their normality) and to determine the standard deviation and the Risk Indicator of the stopes.

The Risk Indicator is calculated as shown:

$$IR = \begin{cases} 1 & se \; Pae > 0,80 \; e \; Pam > 0,50 \\ 2 & se \; 0,50 < Pae < 0,80 \\ 3 & se \; Pae > 0,50 \; e \; Pam < 0,50 \end{cases}$$

where:
IR: Risk Indicator.
Pae: Probability of the metal contained on the stope being above the estimated value.
Pam: Probability of the zinc grade being above the average zinc grade of the mineral reserve (zinc grade = 10,5%).

The risk indicator was calculated for each stope as shown in equation 3. Then, a priority scale was created where stopes classified as 1 should be programmed first, followed by stopes classified as 2 and then stopes classified as 3.

Regarding the production scheduling, it was carried out contemplating three factors:

 i. Mass of ore and metal contained monthly planned for customers (considering only the studied region of the mine).
 ii. Logical scheduling of mining.
iii. Prioritization scale based on the IR.

3   RESULTS AND DISCUSSION

After the validations of the simulations, calculation of the density and design of each stope for each of the 30 scenarios, the evaluations were performed.

Figure 2 shows the results of the simulations in relation to the estimated value. Note, the estimated grade is within the simulated values curve (percentile 5 and percentile 95), as expected.

The results of the metal content and grade simulations for each stope were used on two work fronts:
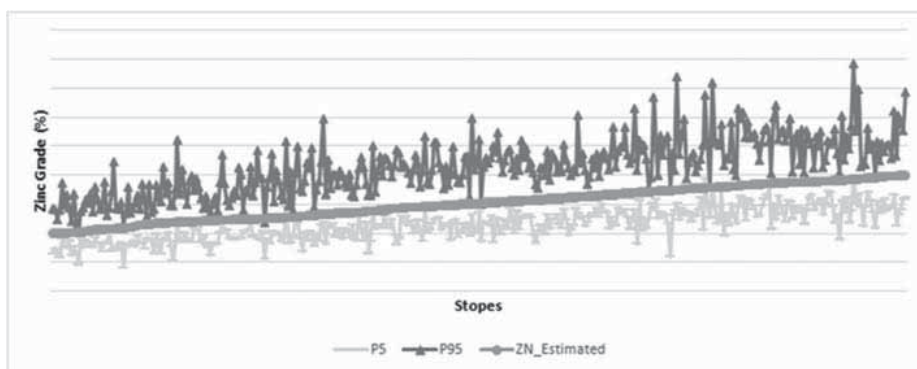
Figure 2. Validation of the simulations.
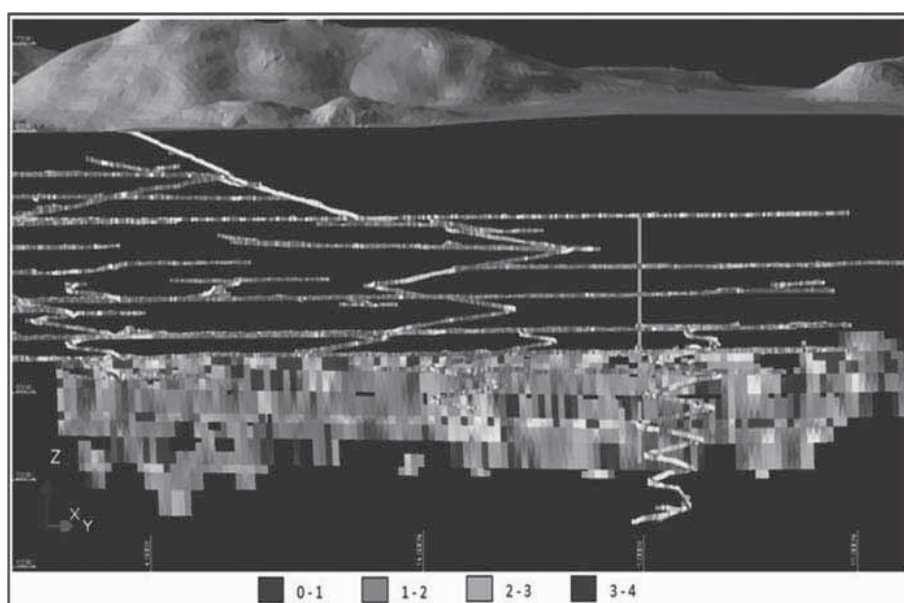
Figure 3. Standard deviation of simulated grades of the stopes.

i. Spatial mapping of areas of greatest variability in order to identify targets for short-term geological mapping prior to the operation, in order to better detail these areas and reduce their uncertainty.

ii. Calculation of the risk indicator that will be used to create the prioritization scale and scheduling the stopes in order to anticipate the lower risk stopes and delay those with higher geological risks.

Figure 3 shows the spatial distribution of variability. Based on this information it is possible to plan in advance detailed exploration of the areas of greatest variability in order to reduce their uncertainty at the time of mining.

Significant changes in the region's mining scheduling are observed, considering or not the scale of prioritization of the stopes, based on the risks and their variability

Figures 4a and 4b show, respectively, the variability of the stopes and the production of metal contained for each monthly period of evaluation based on the results of the simulation of the grades.
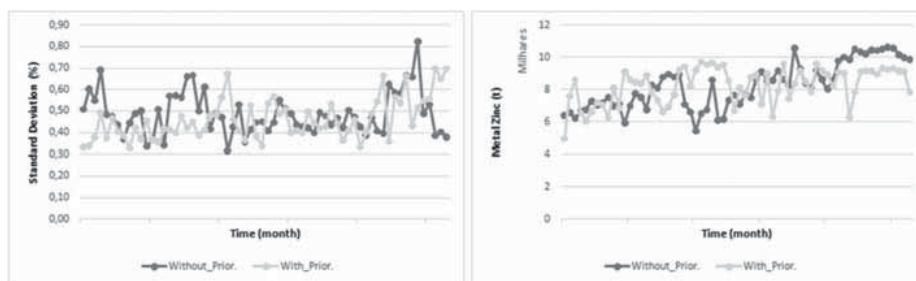
Figure 4. (a) variability of the grades of the stopes. (b) production of metal contained.
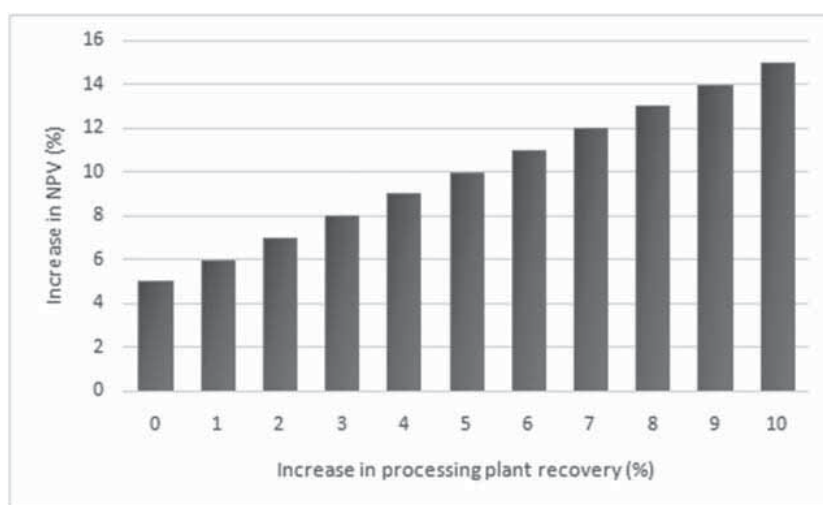
Figure 5. Financial gains due to mill feed stabilization.

It is observed a significant reduction on the variability of grades produced by the mine using the scale of prioritization of the stopes, especially in the first three years of operation (Figure 4a). In addition, changes are observed in the production of metallic zinc by the mine since there are changes in variability between rich and poor regions.

The net present value (NPV) observed for the prioritized scenario presents a result, approximately, 5% above that observed for a scenario without prioritization.

It has historically been observed in this mine that, for more stable mill head grades, the ore processing plant presents significantly higher recovery results and better concentrate specifications. Among the several factors that explain this behavior, is the adequate adjustment of the equipment and systems of the plant to the type of ore processed.

Due to this, it was simulated the impact that a more controlled planning regarding the grade variability can have on the metallurgical recovery of the plant and, consequently, on the financial result.

Figure 5 shows the simulated cash flow results for increments in zinc recovery up to 10% over its average value used in production planning. As can be seen, increases in metallurgical recovery through more stabilized feed would represent significant financial gains.

4 CONCLUSIONS

There are several studies already carried out in mines, especially in open pit mines, regarding the simulation of grades. This study differs in quantifying the uncertainty not only in the

grade variable but also in the density and volume variables for the stopes in an underground mine.

The simulation of the grades was carried out and, from these models, their impact was extended to the calculation of the density by regression and the design of the stopes, that is, to their volume.

It has been demonstrated that it is possible to use this mathematical solution in mining planning of an underground mine and to minimize the risk of not achieving the expected metal production.

For this, a planning scenario was designed for each simulation of grade and calculated value of density. Then the risk indicator for each stope was calculated and a prioritization scale was created in the automatic scheduler, also observing the other restrictions of logical scheduling.

The results showed that when performing the scheduling using the prioritization scale based on the risk indicator, the variability of the stopes is lower in the early years of the plan. In addition, a significant increase was observed in the NPV due to higher grade stopes also present less variability.

As ore feeds the plant with more stable grade, in general, it improves the processing plant recovery. It is expected with the application of the technique herein developed that the financial results are even better than those obtained.

REFERENCES

Clark, I.; White, B. Geostatistical modelling of an orebody as an aid to mine planning. 14th International APCOM Symposium, Pennsylvania, v. 14, p. 1004–1012, out. 1976.

Diedrich, C. Incorporação da variabilidade dos teores para análise de risco de recursos minerais e sequenciamento de lavra. 2012. 187 f. Dissertação (Mestrado em Engenharia) – Programa de Pós-Graduação em Engenharia de Minas, Metalúrgica e de Materiais, Universidade Federal do Rio Grande do Sul, Porto Alegre, 2012.

Mello, P.R.G. Planejamento de lavra sob a incerteza de teores aplicado à lavra subterrânea. 163 f. Dissertação (Mestrado em Engenharia) – Programa de Pós-Graduação em Engenharia de Minas, Metalúrgica e de Materiais, Universidade Federal do Rio Grande do Sul, Porto Alegre, 2015.

Peroni, R.L. Análise da sensibilidade o sequenciamento de lavra em função da incerteza do modelo geológico. 2002. 143 f. Tese (Doutorado em Engenharia) – Programa de Pós-Graduação em Engenharia de Minas, Metalúrgica e de Materiais, Universidade Federal do Rio Grande do Sul, Porto Alegre, 2002.

Souza, L.E. Proposição geoestatística para quantificação do erro em estimativas de tonelagens e teores. 2007. 218 f. Tese (Doutorado em Engenharia) – Programa de Pós-Graduação em Engenharia de Minas, Metalúrgica e de Materiais, Universidade Federal do Rio Grande do Sul, Porto Alegre, 2007.

Economic optimization of rib pillars placement in underground mines

A.B. Andrade & A.R.C. Faria
AngloGold Ashanti, Sabará, MG, Brazil

P.C.B. Rampazzo
Unicamp, Limeira, SP, Brazil

ABSTRACT: Many long hole stoping methods applied in underground mines make use of rib pillars to keep stope stability. It is commonly seen stopes with 30–35 m along strike intercalated by 4–8 m length rib pillars. Depending on the situation (rock mass condition, depth, orebody thickness, etc.) around 15 to 25% of the mine's reserves have to be left as rib pillars, especially when considered retreat methods where, after stoping, pillars are hardly reaccessed. Usually, engineers make use of a standard pattern to place rib pillars along a oredrive. Having the longest stope span possible generally means leaving fewer metal content. However, many orebodies vary along strike in terms of grade and thickness, thus varying in terms of metal content and revenue. As a consequence, regular pattern may not be the best solution. This paper aims to develop a mixed integer linear programming algorithm to optimize rib pillar placement in a sublevel oredrive.

Keywords: mixed integer programming, rib pillars optimization

1   INTRODUCTION

Operational Research is a methodology that makes use of mathematical, statistical and algorithmic models for analysis and decision making (Winston, 2004; Taha, 2017). Problems that can be represented by an optimization model are found in the most diverse areas of applications: transport, communications, energy, mining, petroleum, production, and manufacturing, etc. In all these situations, the objective is to find the best choice within a set of alternatives, respecting the constraints of the problem.

Improper allocation of resources and poorly defined planning processes can lead to loss of time, money, and resources. The optimization is applied to these processes to carry out planning for the sequencing of tasks that respects the constraints of the problem and that results in a more efficient production flow.

As stated by Hustrulid *et al* (1982), sublevel stoping mining method is usually applied to a relatively steeply dipping, competent orebody, surrounded by competent wall rock.

There are some variations of this mine method regarding layout, sequence, orebody dip and width, etc. as detailed and explained by Hustrulid *et al* (1982) and by Linder *et al* (2007), but since it is a method with minimum support, pillars are needed to keep productivity and reasonable dilution levels. Image below shows a standard sublevel stoping design.

Figure 1.   Examples of a typical sublevel stoping layout.

Figure 2. Vertical section (left) showing 5 slices grouped as stopes. In this design, pillars are filtered (blank). At right, a plan section of the same area.

Figure 3. Legend showing grade variability of a sublevel area before picking rib pillars. Gaps in strike are waste zones.

Pillars can be horizontal (sill pillars) or vertical (rib pillars). Since there is less room for changing sill pillars layout, this work focused only in the rib pillars placement.

Among the existing methods to calculate the location and amount of pillars needed, Mathew's stability graph is widely used. It is an empirical method and it should be adapted to each mine's parameters (Melo *et al*, 214). The result of this geotechnical evaluation is the horizontal maximum length of a stope (i.e. stope span) and the minimum horizontal length of a rib pillar, as image below exemplifies. In this case each 5 slices forms a stope. Each slice has a length of a rib pillar.

As orebodies vary in terms of thickness and grade, there is a high chance that geotechnical recommendations for rib pillars placement will not optimize the value extracted and, since rib pillars recovery is an improbable operation (specially in mines applying sublevel with waste rock filling), this value will likely be lost after the mine sequence.

Consequently, optimizing rib pillar placement while satisfying geotechnical constraints could add value with minimum or no operational effort for such mines.

2 METHODOLOGY

The construction of the model implies an attempt to translate the problem into mathematical functions. It is imperative that every study in Operational Research must begin by analyzing the characteristics of the problem and the tools available so that the use of a specific tool can be justified (Taha, 2017). The mathematical model will be implemented in Mathematical Programming software through an algebraic modeling language for writing the objective function to be optimized and the constraints considered in the model. After the implementation of the model, the program is executed by a solver. There are several commercial packages and free packages available to solve optimization problems. In general, they differ from each other by the methods implemented and the types of problems they can solve.

2.1 *Mathematical modelling*

Stopes can be designed with optimization tools such as MSO or manually with vertical strings. Either way, the common practice is that each solid has the length of a rib pillar and some of these solids are grouped between pillars, making a stope. In this project, each of this solid is called a slice. Each slice has a benefit attribute. In the first moment, this is metal content in ounces; $oz[i]$.

After designing a production area, the objective is to define which slices will be flagged as rib pillars, minimizing the amount of value (i.e. metal content) in pillars while satisfying the geotechnical parameters (constraints). This will be outlined as a Mixed Integer Linear Programming (MIP) model (Wolsey, 1998).

Besides a binary variable representing this pillar flag, another variable representing the cumulative size of a stope is created to help writing the constraints. Slices are numbered accordingly to the mining sequence (in this case, in retreat). Therefore, the first slice to be mined will be $i = 0$ and $i = i_{max}$ will be the last slice to be mined.

2.1.1 *Variables*
- *pillar* $[i] \rightarrow 1$ in case the slice i is a rib pillar, 0 otherwise;
- *blksize* $[i] \rightarrow$ positive integer value. Cumulative size of the stope block until slice i. *blksize* $[i] = 0$ in case slice i is a rib pillar.

2.1.2 *Objective function*

$$\text{Minimize} \sum_{i=0}^{i_{max}} oz[i].pillar[i] \tag{1}$$

2.1.3 *Constraints*
The main geotechnical constraint input is the maximum size of a stope in number of slices: *slicemax*. In addition, there will be a constraint to limit the minimum size of a stope, avoiding operationally unpractical stopes: *slicemin*. The other equations are used to control these behaviors.

To model the conditional constraints (*if* constraints) a bigger enough upper bound M is used, as seen in (Taha, 2017; AIMMS, 2018), also known as big-M constraint type.

The following constraints are considered in the model:

- If *pillar* $[i] = 1$ then *blksize* $[i] = 0$, otherwise *blksize* $[i] blksize[i]$ can have any positive integer value:
$$M.pillar[i] + blksize[i] \leq M \tag{2}$$

- If *pillar*$[i] = 0$ then *blksize* $[i] \geq 1$:
$$pillar[i] + blksize[i] \geq 1 \tag{3}$$

- The *blksize* counter has to be less (in case 0) or equal than the previous plus 1:
$$blksize[i] - blksize[i-1] \leq 1 \tag{4}$$

- The *blksize* sequence has to be greater than the previous plus one, unless *pillar*$[i] = 1$:
$$(slicemax + 1).pillar[i] + blksize[i] - blksize[i-1] \geq 1 \tag{5}$$

- If next slice is a pillar, then *blksize* is greater or equal than the minimum allowed (*slicemin*) or *blksize* = 0 (current slice is a pillar):
$$slicemin.pillar[i] - M.pillar[i+1] + blksize[i] \geq (slicemin - M) \tag{6}$$

Since some constraints use the sequence concept (next or previous slices involved), last two constraints are specially defined for the first and last slices.
- If first slice is a pillar, then *blksize* will be 0 and vice-versa:
$$blksize(1) = 1 - pillar(1) \tag{7}$$

- Similarly to equation (6), but for the last slice:
$$M.pillar[i_{max} - 1] + blksize[i_{max} - 1] \leq slicemin \tag{8}$$

The MIP model was implemented in Python 3.7 using the Anaconda distribution. Google OR Tools was used as solver.

At first, the code was written and tested in Jupyter Notebook environment. Then a GUI (graphical user interface) was built using wxFormBuilder. Finally a single.exe application was built with Pyinstaller, making it easier to share with other users.

Main routine ("Optimize rib pillars" button) is the solver for the MIP model. Other three routines (actioned by buttons) were implemented to generate a template file, to import the ounce list and to export the results of the optimization.

Other Python packages used were Numpy and Pandas for file management and MS Excel interface.

The input is an Excel file with slices numbered from 1 to the maximum and an attribute value that will be optimized. For this case, the value of gold troy ounces interrogated for each slice solid.

The output, as shown in figure that follows, is another Excel file with the results for the variables *pillar* [*i*] and *blksize* [*i*].
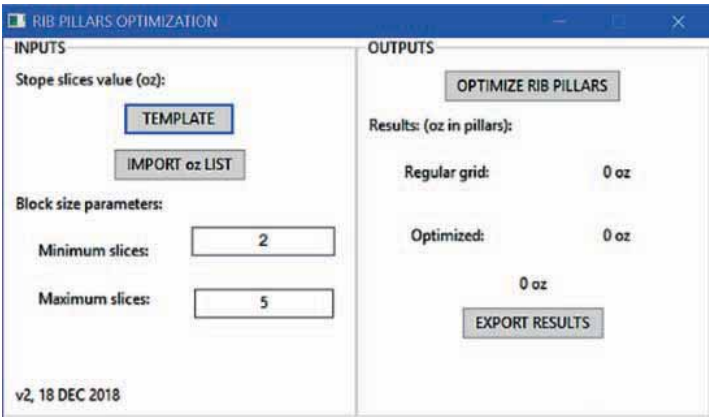
Figure 4. Software main window.

Figure 5. Example of an input file.

295

Slicenum	oz	Pillar	Block size
0	132	0	1
1	166	0	2
2	151	0	3
3	90	1	0
4	93	0	1
5	123	0	2
6	180	1	0
7	241	0	1
8	215	0	2
9	275	0	3
10	207	1	0
11	148	0	1
12	126	0	2
13	110	0	3
14	99	1	0
15	113	0	1

Figure 6. Example of an output file.

3 CASE STUDY

An exercise was performed using data from an underground gold mine in Brazil. Anglogold Ashanti's Cuiabá mine is located in the city of Sabará, state of Minas Gerais, in the Southeast part of Brazil. Nowadays the mine has reached a depth of 1300 m and produces around 1.3 Mtpa.

The mining methods currently being applied in Cuiabá are the Sublevel Stoping and Cut & Fill. The first method is generally used where the orebodies present a dip greater than 37º, and the second method is applied where the orebodies are more flat bedded. For this evaluation, only Sublevel Stoping areas are being considered.

The mine is segmented in two parts based on the orebodies thickness. One part is the Narrow Vein deposit, which is composed by three orebodies (BAL, GAL and CGA) with a thickness of 1–2 m. The other part is called Main Orebodies, composed by two orebodies (FGS and SER) with thickness greater than 5 m.

In order to guarantee the rock mass stability, a combination of sill and rib pillars is used following the geotechnical assumptions and constraints. Normally the sill pillars are left between panels, so that the mining panel length in the vertical direction does not exceed 60 m.

Although, during the short-term, a detailed geotechnical assessment for each stope occurs, in long and medium-terms plans the rib pillars are placed along the oredrives following a general set of geotechnical assumptions regarding pillar and stope span sizes. The rib pillars usually are left with 6 m length. The spans size varies depending on the region of the mine. For the Narrow Veins region, the standard size for the spans are 20 m while in the Main Orebodies a value of 30 m is often applied. The most common approach is to pursue the maximum size of the span and leave the minimum possible number of rib pillars.

A case study considering areas of a year plan was done using the software created and results were compared to the regular pattern solution (which aims minimum number of rib pillars).

With the algorithm, we could compare two different objective functions: maximization of metal content and maximization of profit value (which considers a benefit when less mass is mined for same metal).

3.1.1 *Metal content optimization*
In the first analysis, a comparison between the amount of gold ounces in the regular grid and the optimized grid was made.

All analysis were done for complete sublevel areas or continuous smaller areas where waste zones were present.

3.1.2 *Value optimization*

Instead of gold content, in this second analysis, a profit value was calculated for each slice. This value is a cash flow of the marginal costs of each slice according to unit costs below:

- Gold price: US$ 1,200/oz
- Taxes: US$ 21.60/oz
- Mine and plant costs: US$ 59.60/t

The algorithm approach is the same: minimize the profit left as pillar. Thus, the same software can be used for such analysis.

4 RESULTS AND DISCUSSIONS

Table 1 shows that 20.9% of the oz were being left unmined in the pillars using the regular grid. After the optimization this value reaches 17.9%, resulting in an increase of 5.7 koz in the plan.

The results of the second analysis are presented in Table 2. A comparison between an optimization of gold oz and another of profit value was made in order to verify the effectiveness of each approach.

The optimization in terms of value (profit) shows a result slightly better than the one in terms of oz, with only three areas showing a smaller profit left in pillars. The difference in profit between the two methods is of around US$ 100,000 showing that in this case, both methods present improvements when compared to the regular pillar pattern but they do not present significant differences between each other.

Each mine area represents a software run. Process time was within less than a second for all runs. Hence, even running different scenarios for maximum and minimum number of slices could be practical and done in a reasonable time (seconds).

Table 1. Comparison between oz in regular grid and optimized grid.

	Assumption			oz							Improvement	
MINE AREA	Slicemin	Slicemax	# of slices	Total	Ribs in grid	Mine in grid	% ribs/ mine-Grid	Ribs opt	Mine opt	% ribs/ mine-opt	+oz	diff oz/ mined rid
12 BAL 1	2	3	30	4362	1031	3331	31.0%	950	3412	27.8%	81	2.4%
12 BAL 2	2	3	30	5583	1420	4163	34.1%	1140	4442	25.7%	280	6.7%
12 BAL 3	2	3	26	4235	858	3377	25.4%	858	3377	25.4%	0	0.0%
12 CGA 1	2	6	9	2407	426	1981	21.5%	218	2189	10.0%	208	10.5%
12.1 BAL 1	2	3	26	5876	1475	4401	33.5%	1283	4593	27.9%	193	4.4%
12.1 BAL 2	2	3	26	5857	1404	4453	31.5%	1221	4635	26.3%	183	4.1%
13.1 BAL	2	3	56	12101	3196	8905	35.9%	2664	9437	28.2%	533	6.0%
17.1 FGS	2	5	16	3860	305	3555	8.6%	305	3555	8.6%	0	0.0%
18 FGS 1	2	5	29	15234	2039	13194	15.5%	1882	13351	14.1%	157	1.2%
18 FGS 2-STP1	2	5	10	8647	1432	7214	19.9%	1149	7498	15.3%	284	3.9%
18 FGS 2-STP2	2	5	15	5897	797	5100	15.6%	782	5115	15.3%	15	0.3%
18 FGS 3-STP1	2	5	17	15783	2254	13529	16.7%	2254	13529	16.7%	0	0.0%
18 FGS 3-STP2	2	5	12	6010	951	5059	18.8%	669	5341	12.5%	282	5.6%
18 SER 3	2	5	37	30479	5274	25205	20.9%	3737	26742	14.0%	1537	6.1%
19 FGS SER 1	2	5	61	90944	15256	75689	20.2%	14294	76650	18.6%	962	1.3%
19 FGS SER 4	2	5	41	59104	9615	49489	19.4%	8615	50489	17.1%	1000	2.0%
TOTAL				**276378**	**47735**	**228643**	**20.9%**	**42021**	**234357**	**17.9%**	**5714**	**2.5%**

Table 2. Comparison between oz optimization and value optimization.

MINE AREA	oz				PROFIT (× 1000 US$)			
	Total	Pillar GRID	Pillar OPT oz	Pillar OPT value	Total	Pillar GRID	Pillar OPT oz	Pillar OPT value
12 BAL 1	4362	1031	950	952	3938	925	**841**	**835**
12 BAL 2	5583	1420	1140	1140	5337	1331	1076	1076
12 BAL 3	4235	858	858	858	4011	817	817	817
12 CGA 1	2407	426	218	218	2216	407	205	205
12.1 BAL 1	5876	1475	1283	1283	5543	1426	1183	1183
12.1 BAL 2	5857	1404	1221	1221	5169	1256	1064	1064
13.1 BAL	12101	3196	2664	2754	10910	2874	**2446**	**2387**
17.1 FGS	3860	305	305	305	3673	254	254	254
18 FGS 1	15234	2039	1882	1882	14998	2038	1779	1779
18 FGS2-STP1	8647	1432	1149	1149	8627	1489	1200	1200
18 FGS2-STP2	5897	797	782	782	5085	650	598	598
18 FGS3-STP1	15783	2254	2254	2254	15685	2228	2228	2228
18 FGS3-STP2	6010	951	669	669	5769	898	615	615
18 SER 3	30479	5274	3737	3737	32308	5565	3903	3903
19 FGS SER 1	90944	15256	14294	14294	88642	14851	13906	13906
19 FGS SER 4	59104	9615	8615	8636	61291	10034	**8836**	**8806**
TOTAL	**276378**	**47734**	**42021**	**42134**	**273203**	**47045**	**40953**	**40858**

5 CONCLUSIONS

With a simple rearrangement of pillars, production and money value can be improved with no extra cost or risk. In some circumstances, having smaller spans in lower value areas allowing the best positioning in higher value areas may the optimum decision.

Results are a bit unpredictable and depends on:

- number of pillars to be placed (the bigger the area, the bigger the number of possibilities to optimize);
- orebody variability of each area regarding the standard grid;
- stope span relatively to rib pillar length; and others.

Even with these considerations, 2 to 3% improvement is something that can be achieved.

Profit optimization could use different unit costs as deemed appropriate for a specific mine. In this case study, as gold price, compared to mine costs, was the main driver to the profit calculation results did not differ considerably.

Since it is a quick process and results will be better or equal than the regular pattern, running the optimization will likely became a routine for rib pillars placement.

In short-term plans, after oredrives are fully developed, with detailed mapping of structures and better local knowledge of rock mass, it is usual to have a detailed geotechnical approach, stretching parameters and increasing stope spans having even better results. Even in these cases, the optimization may help with risk assessment, showing the benefit possible with different stope spans or rib lengths.

Future work could be to implement a similar model to a 2D section optimization, whether on a sublevel panel (optimizing sills and rib pillars of different levels) or on a room & pillar method.

REFERENCES

AIMMS B.V. 2018. AIMMS Modeling Guide—Integer Programming Tricks. Haarlem, The Netherlands: AIMMS B.V. https://download.aimms.com/aimms/download/manuals/AIMMS3OM_IntegerProgrammingTricks.pdf.

Hustrulid, W.A. 1982. Underground mining methods handbook. Baltimore, USA: SME.

Linder, U., Smith, M. 2007. Mining Methods in Underground Mining. Örebro, Sweden: Atlas Copco.

Melo, M., Pinto, C.L.L. & Dutra, J.l.G. 2014. Potvin stability graph applied to brazilian geomechanic environment. Rem: Revista Escola de Minas, 67(4), 413–419. https://dx.doi.org/10.1590/0370–44672014670171.

Taha, H.A. Operations Research: An Introduction, 10th ed., Pearson, 2017.

Winston, W.L. Operations Research: Applications and Algorithms, 4th ed., Thomson Brooks/Cole, 2004.

Wolsey, L.A. Integer Programming, John Wiley & Sons, New York, 1998.

APPENDIX I: SOFTWARE REFERENCES

Anaconda: https://www.anaconda.com/.

Google OR Tools: https://developers.google.com/optimization/.

Jupyter Notebook: https://jupyter.org/.

MSO: https://www.dataminesoftware.com/underground-planning/.

Pyinstaller: http://www.pyinstaller.org/.

Python: https://www.python.org/.

wxFormBuilder: https://github.com/wxFormBuilder.

Performance assessment of antithetic random fields in a stochastic mine planning model

G. Nelis & N. Morales
Advanced Mining Technology Center and Department of Mining Engineering, University of Chile, Santiago, Chile

J.M. Ortiz
The Robert M. Buchan Department of Mining, Queen's University, Kingston, Canada

ABSTRACT: Conventional mine planning often relies on parameters estimation to obtain a single production plan. There is no guarantee that these estimations will be accurate in the long term, and this could lead to issues in the mine operation. To deal with this uncertainty, different optimization models have been proposed, which incorporate equally probable scenarios. Unfortunately, the incorporation of uncertainty also imposes a computational challenge: a large number of scenarios is desirable to capture the variability of the uncertain parameters, but each additional scenario increases the computational complexity of the mathematical problem, limiting the cases that can be addressed with stochastic optimization. This paper implements a variance reduction technique in the sequential Gaussian simulation algorithm, which generates grade scenarios with negative correlation, so fewer scenarios can be used without compromising the representation of the grade variability. Our experiments show that using these scenarios achieves the same precision in the objective value of a stochastic optimization problem, but using fewer simulations in the formulation compared with the conventional gaussian algorithm.

Keywords: Antithetic Random Fields, Variance Reduction, Stochastic Optimization, Mine Planning, Geoestatistics

1 INTRODUCTION

Uncertainty in Mine Planning has been a widely studied topic in the last decade. Several works have stated the effect of uncertainty in production plans, and the difficulty in achieving the value predicted based on estimated models (Smith & Dimitrakopoulos 1999 and Dimitrakopoulos et al. 2002). Given this scenario, different methodologies has been proposed to incorporate the uncertainty into the decision making process, using probable future scenarios for the uncertain parameters (costs, prices, grades, etc.). Among these methodologies, several stochastic optimization models has been proposed in the literature, which aim to obtain a production plan considering many scenarios in the formulation in order to obtain a more profitable or robust production schedule. Regarding to geological uncertainty, geostatistics provides simulation techniques, which generates several possible geological scenarios, which can be incorporated into stochastic optimization models. However, the optimization models related to mine planning are often difficult to solve, and this issue is accentuated in the stochastic framework with several scenarios. This poses a clear trade-off: a high number of scenarios is needed to ensure a good representation of the true variability of the uncertain parameter. At the same time, each scenario makes the problem harder to solve, which is a limiting factor to address complex and large mines. Given this scenario, in this paper we evaluate the performance of the antithetic random fields technique, which aims to reduce the number of grade scenarios needed in a optimization problem, without compromising

the representation of the true grade variability, based on generating scenarios with negative pairwise correlation. This technique is tested in a particular stochastic framework, which generates a single production plan based on multiple scenarios.

Scenario reduction has been studied in the last decades with different approaches. One of them is based on selecting a small set that represents the characteristics of a larger set. Usually, the size of the small set is fixed beforehand, and the objective is finding the best subset that minimizes the difference between them considering a relevant attribute for a particular problem. This has been used by Heitsch & Römisch (2003), where they proposed a heuristic to find such subset, defining the relevant distance and adding or subtracting a single scenario aiming to minimize it. A similar methodology was used by Dupačová et al. (2003) and Heitsch & Römisch (2009) in power management. Armstrong et al. (2013) proposed a random search procedure to find a representative subset in an stochastic mine planning problem. They used a proxy variable (ore tonnes above certain cut-off grades) to characterize the differences between scenarios, and the random search procedure proved its usefulness reducing the number of scenarios needed for the stochastic formulation in a real deposit. A similar approach, using proxy variables related to the expected response of a transfer function, has been used by Deutsch & Srinivasan (1996) and McLennan & Deutsch (2005). These proxy variables are used to construct a ranking of realizations to then select a small subset to characterize the uncertainty on the response. This allows to process only a subset of the complete scenarios, typically linked to some key percentiles to represent the variability in the response (Deutsch 2007 and Pereira et al. 2017).

Another approach has been the use of variance reduction techniques, which are procedures to reduce the variance on some estimation without increasing the number of realizations, based on modifications on the algorithm used to generate the scenarios. There are many techniques under this category, and more details can be found in Cheng (1986) and James (1985). In this work, we will use a variance reduction technique known as antithetic variates (Hammersley & Morton 1956), which is based on generating scenarios with negative correlation, expecting that maximizing the difference among the scenarios allows a better representation of the expected variability of the uncertain parameter. An extension of this methodology to a sequential simulation algorithm was proposed by Guthke & Bárdossy (2012). This extension allows to generate an arbitrary number of scenarios negatively correlated in a geostatistical framework. This was used in Nelis et al. (2018) in an stochastic mine planning problem, which achieved a significant variance reduction in the NPV estimation of the mine schedule. In this work, we will use this variance reduction technique in a real case study, using a widely studied stochastic framework, based on the minimization of the deviations from the production targets considering multiple grade scenarios. This framework was first proposed as an optimization problem in Ramazan & Dimitrakopoulos (2007), but many extensions has been proposed such as multiple elements (Benndorf & Dimitrakopoulos 2013), different processing streams (de Freitas et al. 2015) and mining complexes (Goodfellow & Dimitrakopoulos 2016). Specifically, the performance of the antithetic random fields technique will be tested in an optimization model based on Leite & Dimitrakopoulos (2014). This optimization model, along with the antithetic random fields algorithm will be detailed in the next section.

2 METHODS

2.1 *Antithetic random fields*

The antithetic random fields technique is based on the work of Guthke & Bárdossy (2012). They propose a methodology to generate an arbitrary number of scenarios with negative correlation in a sequential simulation algorithm, modifying the generation of the random numbers needed in each scenario. For a conventional sequential Gaussian simulation, each node in the simulation is visited in a random order, and a random number is generated to obtain the simulated value for that node. A new random path is generated for the following scenarios, and the same node is simulated using a different, iid random number. In the algorithm proposed by Guthke & Bárdossy (2012), the same random path is used for all the

scenarios, and the random numbers for each node are drawn beforehand. Moreover, a correlation matrix is imposed to these random numbers to obtain a negative pairwise correlation among every scenario. Then, the negative correlation of the random number transfers to the complete simulated scenarios.

Formally, let m be the number of simulated scenarios required, and n the number of nodes in each scenario. To simulate these m scenarios, m standard Gaussian vectors of size n are needed, one vector for each scenario and one element of these vectors for each node. To achieve the negative correlation between scenarios, a correlation matrix is imposed to these m vectors. Considering Equation (1) as the correlation matrix with α the correlation coefficient. Equation (2) establishes the dependence between the number of scenarios and the correlation coefficient (Guthke & Bárdossy 2012).

$$C_m = \begin{pmatrix} 1 & \alpha & \cdots & \alpha \\ \alpha & 1 & \cdots & \alpha \\ \vdots & \vdots & \ddots & \vdots \\ \alpha & \alpha & \cdots & 1 \end{pmatrix} \tag{1}$$

$$\alpha \geq -\frac{1}{m-1} \tag{2}$$

To impose this correlation matrix between m random vectors, the following algorithm must be followed:

1. Construct Matrix C_m
2. Decompose this matrix in $C_m = BB^T$
3. For each node i to simulate:
   i. A tuple of size m with standard random Gaussian numbers is generated, g_m^i
   ii. Impose the correlation coefficient as $z_m^i = Bg_m^i$
4. The collection of vectors z_m^i form the matrix $R = (z_m^i)^T$. Each column of this matrix is a Gaussian random vector of size n, and each row is a tuple of size m. The correlation matrix among these m vectors is C_m

Then, the sequential Gaussian algorithm is modified to use the same random path for each scenario in the m-tuple and the corresponding random number from matrix R, which allows to generate negatively-correlated scenarios.

For each m-tuple of scenarios:

1. **Random Path:** A random path is generated.
2. **Random Numbers:** Matrix R is constructed.
3. For each scenario s in the m-tuple:
   i. **Simple Kriging:** Visit each node i from scenario s according to the random path and perform a simple kriging estimation using nearby data and any previously simulated nodes.
   ii. **Simulate Value:** Assign the value of this node as:

$$Y(x_i) = Y^{KS}(x_i) + \sigma^{KS}(x_i) R_{i,s} \tag{3}$$

The scenarios obtained by this method are used to solve the optimization problem described in section 2.2, using the convergence analysis described in section 2.3. Notice that these Gaussian random fields are back-transformed to match the original grade histogram.

2.2 *Minimization of deviations*

The optimization model used to evaluate the performance of the antithetic random fields technique is presented in this section. This model is based on Leite & Dimitrakopoulos (2014), and aims to obtain a single production plan maximizing the expected value of the extraction

and, simultaneously, maintaining a consistent production target for every scenario. A cut-off grade is used to classify each block as ore or waste, and since each scenario presents different grades, the same block may have a different classification. Therefore, for the same mine sequence, some scenarios may have a surplus of ore or metal content from the desired target, meanwhile others may have a shortage, which are called deviations. Since the excess and shortage of ore is detrimental for the mining operation, the optimization model incorporates a cost in the objective function accounting for the deviations from the production targets of each scenario. Therefore, the model aims to minimize this cost finding a feasible schedule for all the scenarios at the same time.

Formally, the optimization model is defined as follows: let $\mathcal{B}$ be the set of mining blocks, $\mathcal{T}$ the set of periods of the schedule, $\mathcal{R}$ the set of resources consumed in the extraction process and $\mathcal{S}$ the set of grade scenarios. v_{bt} is the expected profit obtained if block $b \in \mathcal{B}$ is extracted at period $t \in \mathcal{T}$. Each resource $r \in \mathcal{R}$ at period $t \in \mathcal{T}$ has an upper and lower limit which define the production targets, denoted as U_{rt} and L_{rt} respectively. Associated to these targets, parameters c_r^u and c_r^l are the surplus and shortage deviation cost per unit of tonne of resource $r \in \mathcal{R}$ considering that each block $b \in \mathcal{B}$ has a resource attribute of r_{bs} at scenario $s \in \mathcal{S}$. This resource can be denoted as r_b as well, when it is the same amount for all the scenarios. A geological discount rate, ρ_g, controls the cost of deviations through the planning horizon: deviations in an earlier period will have a higher cost than deviations in later periods, which aims to extract blocks with low uncertainty at the beginning of the schedule. Finally, each block $i \in \mathcal{B}$ has a precedence set $\mathcal{P}(i)$ which contains all the blocks that must be extracted before allowing the extraction of block i. The decision variables for this model are defined as follows:

$$
x_{bt} = \begin{cases} 1 & \text{if block } b \in \mathcal{B} \text{ is extracted at period } t \in \mathcal{T} \\ 0 & \text{otherwise} \end{cases} \tag{4}
$$

$$
d_{str}^u = \text{Surplus from production target } U_{rt} \text{ at period } t \in \mathcal{T} \text{ in scenario } s \in \mathcal{S} \tag{5}
$$

$$
d_{str}^l = \text{Shortage from production target } L_{rt} \text{ at period } t \in \mathcal{T} \text{ in scenario } s \in \mathcal{S} \tag{6}
$$

Using these definitions, the stochastic mine planning model to minimize the deviations is defined as:

$$
\max \quad \sum_{b \in \mathcal{B}} x_{bt} \, \bar{v}_{bt} - \frac{1}{|\mathcal{S}|} \sum_{s \in \mathcal{S}} \sum_{t \in \mathcal{T}} \rho_g \left(d_{str}^u c_r^u + d_{str}^l c_r^l \right) \tag{7}
$$

$$
\sum_{b \in \mathcal{B}} x_{bt} \, r_{bs} + d_{str}^l \geq L_{rt} \quad \forall s \in \mathcal{S}, r \in \mathcal{R}, t \in \mathcal{T} \tag{8}
$$

$$
\sum_{b \in \mathcal{B}} x_{bt} - d_{str}^u \geq U_{rt} \quad \forall s \in \mathcal{S}, r \in \mathcal{R}, t \in \mathcal{T} \tag{9}
$$

$$
L_{rt} \leq \sum_{b \in \mathcal{B}} x_{bt} \, r_b \leq U_{rt} \quad \forall t \in \mathcal{T}, r \in \mathcal{R} \tag{10}
$$

$$
x_{it} \leq \sum_{p=1}^{t} x_{jp} \quad \forall t \in \mathcal{T}, j \in \mathcal{P}(i) \tag{11}
$$

$$
\sum_{t \in \mathcal{T}} x_{bt} \leq 1 \quad \forall b \in \mathcal{B} \tag{12}
$$

$$
d_{str}^l \geq 0, d_{str}^u \geq 0 \quad \forall s \in \mathcal{S}, r \in \mathcal{R}, t \in \mathcal{T} \tag{13}
$$

Equation (7) is the objective function. The first term is related to the expected NPV maximization of the schedule, and the second term is the total cost of deviations for every resource considered and for every geological scenario. The base formulation in Leite & Dimitrakopoulos (2014) does not normalize this term by the total number of simulations, but this modification allows to compare the objective function value among instances with a different number of geological scenarios, which is a fundamental part of the convergence analysis. Equation (8) is the Lower Resource Deviation constraint, which accounts for the deviation from lower

production target at scenario $s \in \mathcal{S}$. Since the same block may present a different amount of ore or waste tonnes in different scenarios, each simulation is associated with a different deviation constraint. Similarly, Equation (9) accounts for the excess of production of resource r from the upper production target in each scenario. Since not every resource is allowed to deviate from the production target, Equation (10) represents the capacity constraint for such resources. Equation (11) represents the precedences constraints, which establish a spatial order of the extraction to maintain the pit stability. Equation (12) states that each block can be extracted once. Finally, Equation (13) establishes the bounds for the deviations variables.

2.3 *Convergence analysis*

The performance of the antithetic random fields technique (Section 2.1) in the stochastic mine planning problem (Section 2.2) is evaluated with the following methodology. An *instance* of problem (7) is the set of parameters used to define the objective function and the constraints for a particular case study, such as prices, costs, attributes, etc. More relevant for this study, an instance is defined for the set of scenarios used to represent the grade variability. If the number of scenarios, $|S|$, , is a good representation of this variability, every instance of problem (7) should have a similar optimal objective function value. Equivalently, the dispersion in the objective function value among different instances with the same sample size $|S|$ gives information about the representation of the grade variability for that sample size. Therefore, the evaluation is based on defining several instances of problem (7) with different sample size and different simulation algorithms, and studying their dispersion. The comparison between the results obtained with different simulation algorithms is an indicator of the performance of such algorithms representing the true grade variability of the deposit.

For this case study, the procedure to compare the performance of conventional and antithetic simulations is described as follows:

1. **Scenario generation:** The scenarios necessary to define the instances are generated according to each simulation algorithm:
    i. For the conventional sequential Gaussian algorithm, 600 independent scenarios are generated
    ii. For the antithetic scenarios, 600 realizations are generated in total, but given the nature of this algorithm they are generated in negative-correlated sets of size m. Firstly, 300 sets of $m = 2$ are generated ($\alpha = -1$), which are noted ARF2. Then, 60 sets of $m = 10$ are generated ($\alpha = -0.\overline{11}$), which are noted ARF10
2. **Instance definition:** Using the previously generated scenarios, 30 instances are defined for each simulation algorithm and sample size. The sample sizes $|S|$ chosen for this analysis were 2, 10 and 20. Depending on the simulation algorithm, the definition of these instances is different, which is detailed next:
    i. **Conventional simulations:** 30 sets of $|S| = 2$ are randomly selected from the pool of scenarios, each scenario picked individually. Equivalently, 30 sets of $|S| = 10$ and 30 sets of $|S| = 20$ are selected randomly.
    ii. **ARF2:** For the sample size $|S| = 2$, 30 sets of paired realizations are selected. For $|S| = 10$, each one of the 30 instances is made of 5 sets of ARF2, each set picked randomly. Finally, for $|S| = 20$, 30 instances are defined, each one with 10 sets of ARF2.
    iii. **ARF10:** For $|S| = 2$, 30 pairs of realizations are picked randomly, each one of these pairs is selected from a single set of ARF10. For $|S| = 10$, each instance is defined with a single set of ARF10. Similarly, for $|S| = 20$, each one of the 30 instances is defined by 2 sets of ARF10 picked randomly.
3. **Statistical analysis:** For each case, the 30 instances are solved and the optimal values of the objective function is obtained. The mean value of these 30 instances is an estimator of the true objective function value, while the standard deviation is a measure of the precision of this estimation for each sample size and simulation algorithm. The performance of this antithetic random fields technique is evaluated comparing the standard deviation obtained by using ARF2 and ARF10, and the standard deviation of the conventional simulations.

3 RESULTS

3.1 *Case study*

Drillhole data from a deposit located in Northern Chile were used. The element of interest is copper, with an average grade of 0.28%. The drillhole data cover a total area of 2.0×2.8 km^2 in a pseudo-regular grid of 100 m $\times$ 100 m. For the case study, the central part of the deposit was considered, in a zone of 800×800 m^2. Most of those drillholes are 200 m depth given the mantle disposition of the orebody. General statistics about the data can be found in Table 1

The normal score of the drillhole data was used to perform the point-support Gaussian simulation in a regular grid of $216 \times 216 \times 28$ nodes, with a separation of 3.75 m $\times$ 3.75 m $\times$ 3.75 m between them. A change of support is performed latter, to obtain the final block model with 20412 blocks of $15 \times 15 \times 15$ m^3.

Regarding the optimization model, for each scenario, a cut-off grade was used to calculate the block profit of each block, and later the average of these profits was used as the expected value in the optimization model. Since this calculation can be done prior to the optimization process, 600 scenarios were used for this estimation. For the deviations of each instance, the number of scenarios is variable according to the sample size selection described in section 2.3. The mining capacity is fixed for every scenario and does not allow deviations. On the other hand, the processing capacity allows surplus and shortage deviations from the production target associated with the ore tonnes of each scenario. The scheduling parameters for the optimization model can be found in Table 2.

With these parameters, the methodology proposed in section 2 was implemented, and the results of the dispersion of the NPV values will be presented in the next section.

3.2 *Scheduling results*

The dispersion of objective function value for each simulation algorithm and sample size is shown in Figure 1. The middle line in each boxplot represents the average objective function value of 30 instances for each simulation and sample size, while the size of the box is

Table 1. Basic statistics for the copper content.

Parameter	Value
Mean	0.28%
Maximum	2.74%
Minimum	0.09%
Standard Deviation	0.17%
Data points	15,622

Table 2. Scheduling parameters for the optimization model.

Operational		Economic	
Parameter	Value	Parameter	Value
Planning horizon	5 years	Price	2.5 USD/lb
Mine Capacity	30 MTon	Mining Cost	1.0 USD/Ton
Upper Processing Target	28 MTon	Processing Cost	10 USD/Ton
Lower Processing Target	28 MTon	Selling Cost	0.5 USD/lb
Slope Angle	45°	Recovery	90%
		Economic Discount Rate	10%
		Geological Discount Rate	10%
		Upper Deviation Cost	20 USD/Ton
		Lower Deviation Cost	20 USD/Ton

305
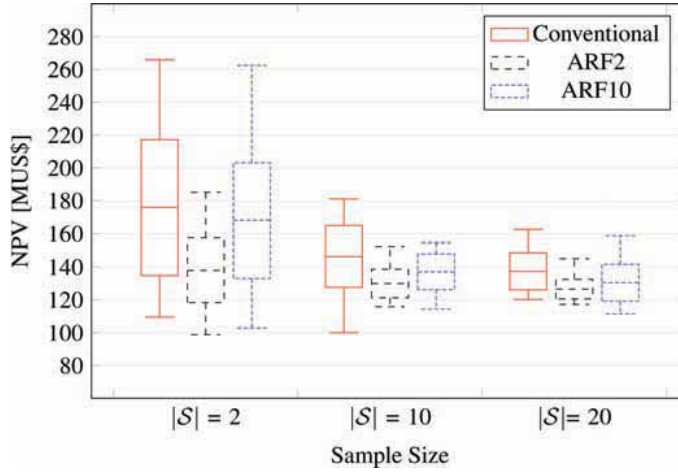
Figure 1. Dispersion of the objective function value.

equivalent to two times the standard deviation of these values, to represent the dispersion obtained for each case. Finally, the upper and lower whiskers show the maximum and minimum value of the objective function.

The first main result is that, for all the types of simulation considered, the larger the sample size $|S|$, the lower the variance of the instances. This result matches the expectation of an improvement in the accuracy on the estimation when a larger sample is taken into account since the true variability of the deposit is represented in a better way. The magnitude of this reduction depends on the type of simulation: Conventional Gaussian simulation achieves a reduction in the standard deviation of 55% from a sample of $|S| = 2$ to a sample of $|S| = 10$, and a reduction of 40% from a sample of $|S| = 10$ to $|S| = 20$. For $ARF2$, the reduction is 56% from a sample of $|S| = 2$ to $|S| = 10$, and 31% from $|S| = 10$ to $|S| = 20$. Finally, for ARF10, the results show an abnormal behavior: a reduction of 69% in the standard deviation is achieved from $|S| = 2$ to $|S| = 10$, which is the highest reduction in this case study, but there is an increase of 4% in the standard deviation from $|S| = 10$ to $|S| = 20$.

This unexpected behavior is explained by the correlation for different sample sizes. In the antithetic random fields technique, the highest the n-tuple to be negatively correlated, the weaker the pairwise negative correlation between the elements of the tuple. For this case, the average pairwise correlation of the elements in a 10-tuple of ARF10 is 0.47. This value is similar to the average pairwise correlation in conventional simulation for this study case, which is 0.52. Therefore, when the sample size is $|S| = 2$, the effect of the negative correlation is weak and a mild reduction in the standard deviation compared with the conventional simulation is presented. This changes with a sample size of $|S| = 10$, where there is a match between the tuple size and the sample size, and therefore the negative correlation allows a good representation with this sample size, explaining the reduction of 69% both for the larger sample size and for the match between sample size and tuple size. This behavior is not present with $|S| = 20$ where the sample size does not match the tuple size and the standard deviation is similar to the conventional case.

Comparing among the different simulation types at the same sample size, the results show that ARF2 achieves the lowest standard deviation for every sample size, even when the sample size does not match the tuple size. This is explained given the strong pairwise antithetic correlation with a tuple of size 2, which for this case study is 0.06. This allows a good representation of the deposit variability even with a sample size of $|S| = 2$, which allows a standard deviation reduction of 52% compared to the conventional simulation algorithm and 44% compared to ARF10, which is similar to the conventional case as it was discussed previously. For a sample size of $|S| = 10$, the tuple does not match the sample size for ARF2, but the average pairwise correlation coefficient of the elements of each sample is 0.38, which is lower

than both the conventional and ARF types of simulations, allowing a better sampling with the same number of scenarios. The reduction in the standard deviation for ARF2 in this sample size is 54% compared to the conventional algorithm and 20% compared to ARF10. Finally, for a sample size of $|S| = 20$, ARF2 achieves the lower standard deviation as well, with a reduction of 47% compared to both conventional and ARF10 simulations.

A possible explanation for these results is related to the nature of the optimization problem. Since the value of the extraction is estimated prior to the simulation process, the geological scenarios are only used to estimate the deviations from the production targets. Since the deviations only consider the classification of the material as ore or waste, the differences among different scenarios are based on whether each block is above or below the cut-off grade. Therefore, a favorable way to sample for this optimization model is focusing on the cases when each block belong to each category, and not necessarily on the complete range of grades for each block. This could explain the performance of ARF2, compared with the rest of the simulation algorithms. Different case studies for this optimization model should be tested to confirm this behavior.

An unexpected result is the difference between the average values of the objective function for each type of simulation and sample size. For every sample size, the average value is lower for ARF2 and higher for the conventional simulation. Moreover, the average value tends to decrease when the sample size is larger. This behavior was not seen in previous works, where the average value was similar for every simulation type (Nelis et al. 2018). The apparent bias is larger with smaller sample sizes, where the average value for conventional algorithm is 22% higher than the average value of ARF2 with $|S| = 2$. This difference decreases with larger sample sizes: for $|S| = 10$, the difference is 11% between the conventional simulations and ARF2 and for $|S| = 20$ gets to 7%. The differences between ARF10 and Conventional are smaller: 4% for $|S| = 2$, 6% for $|S| = 10$ and 5% for $|S| = 20$. Since the true value of the objective function is unknown, it is not possible to establish whether the Antithetic Simulations present a bias. However, it can be seen that the difference between the average value among different simulation types gets smaller with larger sample sizes, so it is expected this difference in the expected value tends to zero with even larger sample sizes. This also could be an indication that even a sample size of $|S| = 20$ is not large enough to guarantee convergence for this case study.

4 CONCLUSIONS

The performance of a variance reduction technique was presented in this work. The results showed that the antithetic random fields implementation achieved a variance reduction in the estimation of the objective value of a particular long-term stochastic optimization model in a case study using real data. A difference between the expected value estimation using this variance reduction technique compared to conventional simulation algorithm was found, but it approached to zero with larger sample sizes. This variance reduction technique shows promising results, and could lead to solve larger cases with fewer scenarios.

REFERENCES

Armstrong, M., Ndiaye, A., Razanatsimba, R. & Galli, A. 2013. Scenario reduction applied to geostatistical simulations. *Mathematical Geosciences* 45: 165–182.
Benndorf, J. & Dimitrakopoulos R. 2013. Stochastic long-term production scheduling of iron ore deposits: Integrating joint multi-element geological uncertainty. *Journal of Mining Science* 49(1): 68–81.

Cheng, R. 1986. Variance reduction methods. *Proceedings of the 1986 Winter Simulation Conference*: 60–68.

de Freitas, M., Dimitrakopoulos, R. & Lamghari, A. 2015. Solving a large sip model for production scheduling at a gold mine with multiple processing streams and uncertain geology. *Transactions of the Institutions of Mining and Metallurgy. Section A: Mining Technology* 124: 24–33.

Deutsch, C. & Srinivasan, S. 1996. Improved reservoir management through ranking stochastic reservoir models. In *Proceedings of the SPE/DOE Improved Oil Recovery Symposium*, Tulsa, OK, USA.

Deutsch, C. 2007. A review of geostatistical approaches for data fusion. In D. Hyndman, F. Day-Lewis & K. Singha. (Eds.), *Subsurface hydrology: data integration for properties and processes* 171 of *Geophysical Monograph Series*: 7–18.

Dimitrakopoulos, R., Farrelly, C.T. & Godoy, M. 2002. Moving forward from traditional optimization: grade uncertainty and risk effects in open-pit design. *Transactions of The Institution of Mining and Metallurgy, Section A: Mining Technology* 111: 82–88.

Dupačová, J., Gröwe-Kuska, N. & Römisch, W. 2003. Scenario reduction in stochastic programming. *Mathematical programming* 95(3): 493–511.

Goodfellow, R. & Dimitrakopoulos, R. 2016. Global optimization of open pit mining complexes with uncertainty. *Applied Soft Computing* 40: 292–304.

Guthke, P. & Bárdossy, A. 2012. Reducing the number of MC runs with antithetic and common random fields. *Advances in Water Resources* 43: 1–13.

Hammersley, J. & Morton, K. 1956. A new Monte Carlo technique: Antithetic variates. *Mathematical Proceedings of the Cambridge Philosophical Society* 52: 449–475.

Heitsch, H. & Römisch, W. 2003. Scenario reduction algorithms in stochastic programming. *Computational Optimization and Applications* 24: 187–206.

Heitsch, H. & Römisch, W. 2009. Scenario tree modeling for multistage stochastic programs. *Mathematical Programming* 118: 371–406.

James, B. 1985. Variance reduction techniques. *The Journal of the Operational Research Society* 36(6): 525–530.

Leite, A. & Dimitrakopoulos, R. 2014. Stochastic optimization of mine production scheduling with uncertain ore/metal/waste supply. *International Journal of Mining Science and Technology* 24: 755–762.

McLennan, J. and Deutsch, C. 2005. Ranking geostatistical realizations by measures connectivity. In *Proceedings of the SPE/PS-CIM/CHOA International Thermal Operations and Heavy Oil Symposium*, Calgary, AB, Canada.

Nelis, G., Ortiz, J. & Morales, N. 2018. Antithetic random fields applied to mine planning under uncertainty. *Computers & Geosciences* 121: 23–29.

Pereira, F., Holden, T., Ibrahim, M. & Porto, E. 2017. Geostatistical reservoir characterization in barracuda field, campos basin: A case study. In *th International Congress of the Brazilian Geophysical Society*, Rio de Janeiro, Brazil,

Ramazan, S. & Dimitrakopoulos, R. 2007. Stochastic optimisation of long-term production scheduling for open pit mines with a new integer programming formulation. *The Australasian Institute of Mining and Metallurgy, Spectrum Series* 14: 359–365.

Smith, M. & Dimitrakopoulos, R. 1999. The influence of deposit uncertainty on mine production scheduling. *International Journal of Surface Mining, Reclamation and Environment* 13(4): 173–178.

A data science model on production level pillar stability at El Teniente mine

R.J. Quevedo & R.F. Quezada
Resident Engineers at El Teniente Mine, Universidad de Santiago, Chile

R.A. Zepeda & S.A. Balboa
Mining Engineers, Department of Geomechanics, CODELCO División El Teniente, Chile

J.P. Vargas & S.A. Pérez
Mining Engineering Department, Universidad de Santiago de Chile, Chile

ABSTRACT: Collapses have been a major geomechanical issue at El Teniente Mine, due to its difficult treatment and the known fact that actually there are neither methodologies nor tools to estimate their possible occurrences or successfully holding their progression. The term "collapse" is understood as a physical process consisting in major large-scale deformations whose later manifestation is the total closure of affected excavations and/or drifts. The objective of this paper is to illustrate the development and results of a pillar vulnerability index, built through a machine learning classification model, in order to estimate collapse-risky areas in production sectors and future projects that are to be put in operation in the coming years, given the 34 years of history of primary ore extraction at El Teniente mine.

1 INTRODUCTION

El Teniente Mine is an underground operation owned by CODELCO, which is located in the first elevations of Los Andes in the central zone of Chile, about 70 km SSE from the capital city, Santiago.

El Teniente mine is a typical porphyry copper-molybdenum deposit, composed mainly by andesite, diorite and hydrothermal breccias of the Miocene eras as the main lithologies.

The main structural feature of the orebody is a stockwork of multi-directional veins and veinlets. The veins are principally cemented with anhydrite, quartz and sulphides.

Geometrically, the deposit is located around a chimney composed of subvolcanic breccias, known as 'Braden Pipe', which postdates the copper-moly mineralization. The hydrothermal mineralization is distributed around this pipe over a variable radial extension of 400 to 800 m, with mineralogical associations of variable strength.

The mineralization shows two distinct forms: the secondary ore is located near the surface and the primary mineralization is located at a greater depth.

The primary ore can be described as a high cohesion and impermeable rockmass. The stock-work veins, containing the original mineralogy, are sealed. According to the geomechanical characterization, the primary ore is harder than the secondary. It's caving results in large fragmentation. Primary rockmass could exhibit brittle, often violent failure mechanisms under a high-stress condition.

2 RESEARCH CONTEXT

Since the beginning of the mining operation in 1982, a series of geomechanical instabilities known as 'collapses' have occurred. A collapse is defined mainly as a progressive deformation

phenomenon, in a scale of mm/day to cm/day, caused by the gradual failure of the rock mass when exposed to high magnitude stresses, usually deriving in the total closure of the affected galleries.

The research studies that analyzed collapse events between 2008 and 2010 in the Esmeralda sector showed that two distinct collapse processes exist in terms of scale. The first one being behind of the caving front and the second being ahead of it, the latter being associated to the presence of major geological structures and their sub-parallel orientation with respect to the caving front.

During the development of the studies and research of this phenomenon under CODELCO's Investigation Project (IP) T13E200 known as: "Desarrollo de Modelo de Diseño Minero para la Mitigación de Colapsos en Mina El Teniente", building a model that allowed the conceptualization of the phenomena was deemed necessary, after studying a series of variables which were determined to be related to it in statistical terms, considering their interdependence, using the information in Esmeralda, Reservas Norte and Dacita (the latter two known collectively as "RENO-Dacita") sectors as a baseline.

Regarding the above and the interdependence of the features previously mentioned, a Gradient-Boosting based Machine Learning algorithm was built in order to obtain an optimal generalization, given the representative elements involved based on previous diagnosis of the collapse processes and using the model's inherent "learning ability" as an opportunity to improve future estimations of damage risks, allowing future and justified decision making.

3 REALIZATION OF COLLAPSES AS AN UNDERLYING PHYSICAL PROCESS

The use of a machine learning model for the estimation of a vulnerability indicator applied to the pillars in a determined production level, is due to the fact that there is no formal analytical expression that allows the definition of the phenomenon as a physical process. Thus, it's occurrence has to be considered as a realization of an underlying process of such characteristics, whose results can be explained by different sets of information.

Considering the above, it's important to point out that, previous to the IP's closure, there is no rigorous definition of the physical process that ends up manifesting as a collapse. On the contrary, only a definition built on the basis of the visible progressive effects produced by the collapse currently exists.

It is then crucial to conceive these collapses as the end-stage of a process that involves a significant interaction between tensional and deformation states which, given the Lamé-Hoek equations for elastic solids, include the stiffness parameters of the rockmass where the support pillar is emplaced.

It is known that the stress solicitations caused by the mining process are fundamentally dependent on the geometry of the caving front and the variant of panel caving method implemented in a determined production sector. On the other hand, mining causes perceivable effects in terms of seismic waves that can cause cumulative damage, thus deriving in the necessity to apply mitigation strategies such as Hydraulic Fracturing (HF). Finally, the mining operation is not a uniform process, given the fact that at any given time different draw points receive a continuous flow of ore priorizing productivity, resulting in the production rate being one of the essential elements in an intent of explaining the load distributions derived from the caving process.

In order to establish the base structure of the model, an experimental design was developed in order to support the information used, which is shown in Fig. 1. It can be noted that the information which feeds the model is subdivided into five information sets, following the previously mentioned criteria.

4 INFORMATION SETS

Given the experimental design shown in Fig. 1, it was determined that the variables serving as the input of the vulnerability model were to be divided into five different sets of information,
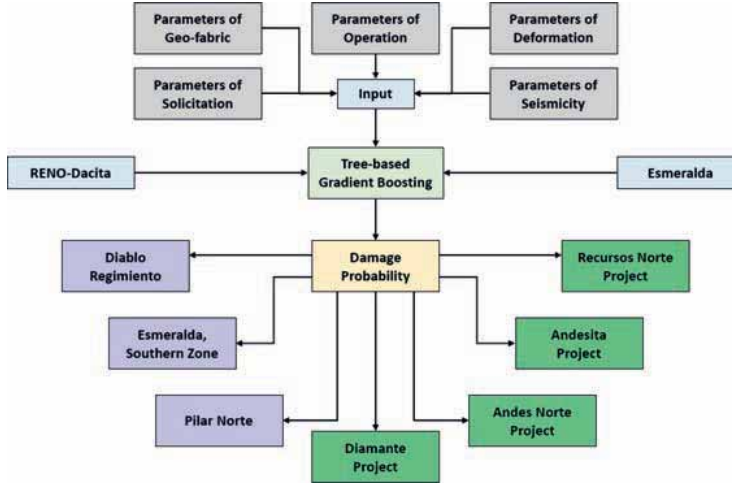
Figure 1.   Experimental design for the vulnerability model.

in order to answer these five key questions in the conceptualization of the genesis of the underlying physical process which in-situ manifestation is the collapse.

On the other hand, since collapses occur as large-scale deformations, it was necessary to introduce a spatial reference to mathematically establish the existence of a collapsed sector as a function of such variables, thus, using the centroids of the pillars in the production level as the element of evaluation.

As a result, the input data has the following structure:

a. Geo-fabric:

These parameters intend to respond the following question: "*How are the pillars shaped and what are they made of?*" They are defined as follows:

i.   Rockmass Geotechnical Zoning: Quantitative characterization of the potential disassembly areas in the rockmass based on the weak veins intensity it has (Millán, 2014) (see Fig. 2).

ii. Effective Pillar Area: Cross sectional area of the pillar in the *XY* plane.

b. Solicitation:

These parameters intend to respond the following question: "*How are the pillars solicited in terms of the tensional field and for how long?*" They are defined as follows:

i.   Pre-mining Vertical Load: The vertical component (σ_{zz}) of the stress tensor in the pre-mining stage along the longitudinal axis of the pillar, based on mine-scale stress numerical modellings (CODELCO, 2015).

ii. Time under Pre-Mining Condition: The amount of time between the pillar's construction and the beginning of the abutment stress influence on it.

iii. Vertical Load in *Abutment-Stress*: The vertical stress over a pillar when it is located in a zone affected by the abutment-stress condition, which has been defined as a 70 m long band extended ahead of the caving front and 30 m behind it (see Fig. 3). It is mathematically defined according to a series of previous studies in Esmeralda (Karzulovic, 2005) as shown in Eq. 1:

$$\sigma_{zz}(a) = f\, C_c\, \sigma_{zz}(p) \tag{1}$$

where $\sigma_{zz}(a)$ is the pillar's vertical load in abutment-stress state; f is the abutment-stress intensity factor (Pardo & Rojas, 2014), which is a function of the panel caving variant used in the analyzed production sector; C_c is a correction coefficient that depends on the curvature of the caving front at a specific point; and $\sigma_{zz}(p)$ is the pillar's vertical load in pre-mining state.

311

Figure 2. Main features of the geotechnical units defined from the rockmass geotechnical zoning.
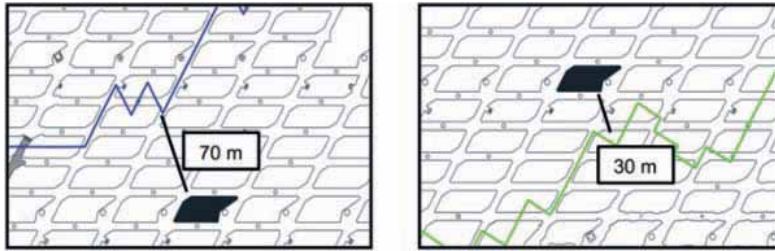
Figure 3. An example of the zone of influence defined by the abutment-stress in the Esmeralda production sector (in blue, the caving front in April, 2000; in green, the caving front in May, 2003). This measuring is applied taking the pillar marked in black as a reference.

iv. <u>Time under abutment-stress condition</u>: The amount of time during which a pillar is under the abutment-stress' zone of influence defined in Fig. 3.

c. Solicitation:

These parameters intend to respond the following question: "How do the pillars actually respond to the existing tensional field?"

The deformation parameters used in the model are referred to the deviatoric components of the stress and strain tensors for an individual pillar, which are strongly dependent on the stiffness which characterizes the mechanic properties of the material. In particular, shear strains correspond to the mechanical response of the rockmass to the shear stresses it is exposed to, without showing changes in its volume, up to the point where the cavity generated by the mining process is at its final stage.

In order to find an expression for the shear strains, starting from the stress tensor, it is necessary to follow a mathematical procedure which is now described: Given the stress tensor for a determined position, expressed in terms of its rectangular coordinates (x,y,z), and assuming an end-stage cavity as a result of the mining process in a rockmass which is characterized as a continuous, linearly elastic and isotropic medium, the shear strain γ_{ij} for the ij plane can be expressed in terms of the respective shear stress τ_{ij} and two constants which describe the mechanical properties of the rockmass, called Young's Modulus E and Poisson's ratio ν as shown in Eq. 2:

$$\gamma_{ij} = \frac{1+\nu}{E} \tag{2}$$

The latter expression is a known result of the Lamé-Hooke Equations for elastic solids. Each lithology has different mechanical properties (and, thus, distinctive characteristics). Given the proportions of these lithologies populating a rockmass where a pillar is emplaced, it is clear that each one has different mechanical conditions.

d. Seismicity:

These parameters intend to respond the following question: "*How is the energy distributed among the pillars?*" They are defined as follows:

i. Relevant Nearby Seismic Events: The number of seismic events with a radiated seismic energy higher than the 1 MJ in a radius of 70 m around the centroid of a determined pillar.

ii. Density of Radiated Seismic Energy (S & P Components): An estimation of the radiated seismic energy per squared distance unit based on the S and P seismic waves for each analyzed pillar. This estimation is done by using an "inverse-square of the distance" assignation, taking the hypocenters of each seismic event with a magnitude M_w larger than zero as the emitting source of seismic radiated energy, assuming these sources as central force fields.

e. Operation:

These parameters intend to respond the following question: "*What do we do during the mining process in terms of operation?*" They are defined as follows:

i. Pre-conditioning Status: A variable that denotes the implementation of the hydraulic fracturing technique in the rockmass where a determined pillar is emplaced. It is expressed as a binary value which is equal to 1 when the pillar is located in a hydro-fractured area, and 0 when it is not.

ii. Mass Flow Rate of Ore: The linear mass density of ore divided per height of extraction column in a determined draw point (the latter known as height of draw), measured in t/m. That being said, since this is a distinctive property of a draw point, it needs to be assigned to the pillars in the same fashion as the seismic radiated energy, making this with an inverse-square estimation for each one of them, using a search radius of 20 m around the analyzed pillar.

5 MODELLING METHODOLOGY

5.1 *Ensemble learning and tree-based gradient boosting technique*

The methodology used for collapse vulnerability modelling was based on a Machine Learning (ML) ensemble learning algorithm. The concept of ML is understood as the science (and art) of programming computers so they can learn from data.

Let us suppose we wish to ask a highly complex question to a random set composed by a thousand people to posteriorly count and sort their answers forming an aggregated answer. In many cases this kind of answer is even more reliable than a single answer given by an expert. This is usually known as "wisdom of the crowd". Similarly, if we aggregate the predictions or estimations of several bad or "weak" learners (information classificators or regressors), we will frequently find better results than we would have obtained with a single learner. This kind of approach is known as an "ensemble" method.

The model was developed based on the "tree gradient boosting" ensemble structure, using binary decision trees as the base weak learners. The empirical binary conceptualization of the pillar state (as target value) was defined as shown as Eq. 3:

$$Y = \begin{cases} 1; & \text{When the pillar is damaged/collapsed} \\ 0; & \text{When the pillar is undamaged/stable} \end{cases} \tag{3}$$

Let Y be the output value of a function to be modelled, while X is the random vector consisting of the sum of the information sets described in section 4, specified for each pillar that is to be analyzed. Then, the problem we wish to model is represented by a joint probability distribution $P(X, Y)$. If the training set is described as $\Lambda = \left\{ \left(x_i, y_i \right) \right\}_{i=1}^{n}$, being (x_i, y_i)
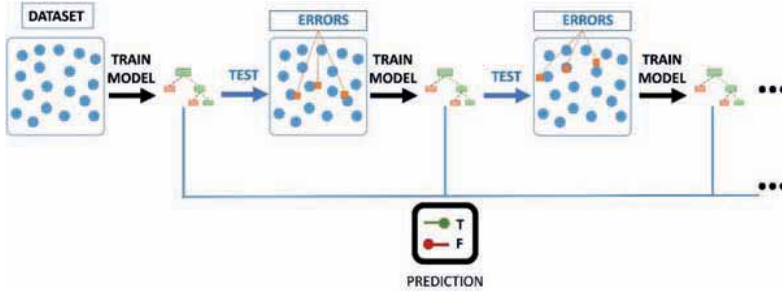
Figure 4.   A simple scheme to explain the gradient boosting technique.

the registered historical data of the problem, then our goal is to find an approximation $\hat{F}(x)$ to the function $Y = F(X)$ that minimizes a measured value of some loss function[1] denoted as $\mathcal{L}(y, F(x))$, so that[2], as shown in Eq. 3:

$$\hat{F}(x) = \arg\min_{D(F)}\left[\mathcal{L}(y, F(x))\right] \qquad (3)$$

In gradient boosting methods, it is assumed that a real value "y" exists, for which we look for an approximation $\hat{F}(x)$ in the form of a weighted sum of functions $h_i(x)$ that belongs to some class $\mathcal{H}$, called weak classifiers (or learners), as shown in Eq. 4:

$$\hat{F}(x) = \sum_{i=1}^{M} \lambda_i h_i(x) + \text{constant} \qquad (4)$$

where $h_i(x)$ is a randomized decision tree, for which it's mth iteration fits the residual values (differences) between the estimator function $\hat{F}_m(x)$, and Y. Let J_m be the number of leaves in the tree; this separates the defined input space by the training set in J_m disjoint regions $R_{1m}, \dots, R_{J_m m}$, and predicts a constant value in each one of them. Using the indicator notation[3], the output of $h_m(x)$ for a given input x can be written as the sum shown in Eq. 5:

$$h_m(x) = \sum_{j=1}^{J_m} b_{jm} 1_{R_{jm}}(x) \qquad (5)$$

---

1. A **loss function** or cost function is a function that maps an event or values of one or more variables onto a real number intuitively representing some "cost" associated with the event. An optimization problem seeks to minimize a loss function. In machine learning, typically a loss function is used for parameter estimation, and the event in question is some function of the difference between estimated and true values for an instance of data.

2. In mathematics, the **arguments of the minimum** (abbreviated as arg min) are the points of the domain of some function at which the function values are minimized. This way, given an arbitrary set X, a totally ordered set Y, and a function $f:X{\rightarrow}Y$, its arguments of the minimum over some subset S of X are defined by

$$\arg\min_{x \in S \subseteq X}\left[f(x)\right] = \left\{x \mid x \in S \land \forall y \in S : f(y) \geq f(x)\right\}$$

3. In mathematics, an indicator function or a characteristic function is a function defined on a set X that indicates membership of an element in a subset A of X, having the value 1 for all elements of A and the value 0 for all elements of X not in A. It is usually denoted by the symbol 1_A, being defined by

$$1_A(x) = \begin{cases} 1; & \text{if } x \in A \\ 0; & \text{if } x \notin A \end{cases}$$

where b_{jm} is the predicted value in the region R_{jm}. Then, the coefficients b_{jm} are multiplied by some value λ_m, chosen to minimize the loss function, which allows us to update the model at each iteration as shown in Equations 6 and 7:

$$F_m(x) = F_{m-1}(x) + \lambda_m h_m(x) \tag{6}$$

$$\lambda_m = \arg\min_{\lambda}\left[\sum_{x_i \in R_{jm}} \mathcal{L}\left(y_i, F_{m-1}(x_i) + \lambda h_m(x_i)\right)\right] \tag{7}$$

Notice that this kind of method corresponds to a heuristic procedure and, by extension, does not generate exact analytical solutions or values for the desired problem, but approximations to such values (in case they exist).

5.2 *Training, validation and application sets*

All the sets of information referred for basis calibration and training, validation and further application of this model correspond to the following production sector and future projects shown in Table 1.

Of the training data, 185 pillars (instances) of the total 866 have suffered collapse damage between the years 2001 and 2017 (132 in Esmeralda, 53 in RENO-Dacita).

5.3 *Quality and precision indicators for the model*

For a binary information classifier, there are a series of metrics that allow us evaluate its quality in terms of the discrimination it makes between the two classes it's supposed to separate.

In this research, three metrics were used listed as follows:

a. ROC Curve:
For any binary information classifier, it is possible to measure its quality in terms of how good it works discriminating both classes in the modelled output. Thus the receiver operating characteristic curve (i.e., ROC curve) is defined as a graphical plot that illustrates the diagnostic ability of the classifier, known as diagnostic potency, as its discrimination threshold is varied. Such threshold, known as cut-off probability or decision boundary, represents the limit value which separates the two mutually exclusive classes of the modelled output. This curve is created by plotting the true positive rate (TPR) against the false positive rate (FPR), both of which are obtained by varying the discrimination threshold of the classifier over the training set. The true positive rate defines how many outcomes correctly labeled as successes exist among all of the observations. On the other hand, the true negative rate defines how many outcomes correctly labeled as failures exist among all of the observations. In ML and statistics, the TPR and FPR are known as sensitivity and specificity, respectively, and, by their very definition, they meet the condition: $0 \leq$ TPR ≤ 1 and $0 \leq$ TNR ≤ 1. When using

Table 1. Training, validation and application sets for the vulnerability model.

Production sector or Project	Type of data	Time interval	N° Pillars
Esmeralda	Training	1996–2010	391
RENO-Dacita	Training	1989–2016	475
Esmeralda, Southern Zone	Validation	2011–2016	357
Diablo Regimiento	Validation	2004–2016	246
Pilar Norte	Validation	2007–2016	70
Recursos Norte Project	Application	2020–2037	748
Andesita Project	Application	2024–2039	382
Diamante Project	Application	2023–2043	830
Andes Norte Project	Application	2023–2055	691

normalized units, the area under the ROC curve (henceforth, AUC) is equal to the probability that a classifier will rank a randomly chosen positive instance higher than a randomly chosen negative one. Since a perfect classifier has an area equal to 1, this means, in praxis, that the AUC informs us about the quality of the classifier: How near is our model from achieving a perfect classification. This is shown in Table 2.

b. Confusion Matrix:

Let us consider a set of pillars that can be separated in terms of the existence or inexistence of damage due to collapse processes. This is a situation for which the output is binary and mutually exclusive, where the presence of damage is considered a "success" and "failure" when otherwise. Thus there are four possible results for such a problem. If the output value is a success while the evaluated instance is also a success (this is, an output value labeling a pillar as damaged when it actually is), then it is called a True Positive (TP). On the other hand, if the output a failure while the evaluated instance is also a failure (this is, an output value that labels a pillar as undamaged when the same pillar is actually undamaged), then it is called a True Negative (TN).

The misclassifications of the model are called False Positives (FP) when the evaluated instance is a failure while the output is labeled as a success (this is, classifying a pillar as damaged when it is actually undamaged), and False Negatives (FN) when the evaluated instance is a success while the output is labeled as a failure (this is, classifying a pillar as undamaged when it is actually damaged). These four outcomes can be formulated in a 2 × 2 matrix, as shown in Table 3.

c. Information Gain Analysis:

Each one of the variables conforming the input of the vulnerability model is able to give a certain amount of information in terms of their contribution to the modelled output (the existence of collapse damage). This way, the degree of influence of a determined variable is

Table 2.   Classification for the accuracy of the AUC.

Classification	AUC
Fail	0.50–0.60
Poor	0.60–0.75
Fair	0.75–0.90
Good	0.90–0.97
Excellent	0.97–1.00

Table 3.   The confusion matrix for a binary classifier.

ESTIMATED CONDITION	REAL CONDITION	
	Damaged	Undamaged
Damaged	True positive	False positive (Type I Error)
Undamaged	False negative (Type II Error)	True negative
	True positive rate or **Sensitivity** $$TPR = \frac{\sum \text{true positive}}{\sum \text{condition positive}}$$	False positive rate or **Fall-Out** $$FPR = \frac{\sum \text{false positive}}{\sum \text{condition negative}}$$
	False negative or **Miss rate** $$FNR = \frac{\sum \text{false negative}}{\sum \text{condition positive}}$$	True negative rate or **Specificity** $$TNR = \frac{\sum \text{true egative}}{\sum \text{condition negative}}$$

estimated in terms of the uncertainty it generates over the output by subtracting each one of the input variables. Thus we can estimate how much information is gained for each feature used as part of the model's experimental design, and how much information is lost when the respective feature is not present in the model (Kullback & Leibler, 1951).

For this purpose, the amount of information gain is calculated considering the ensemble structure and the average depth at which different features fed to the model can be found across the whole set of trees that the algorithm used as weak learners. High importance attributes are usually found near the roots of the binary decision trees, and their information gain values regarding the output can be ordered in a column chart.

6 MODEL RESULTS

The information sets previously described and the features which characterize them, define the training data for a tree-based gradient boosting algorithm called "Extreme Gradient Boosting" (Chen & Guestrin, 2016). The goal of this algorithm is to build a model that optimally captures the interdependence among these variables and the output, thus developing an information classifier that allows us to convey the vulnerability to collapse damage in a production level's support pillars into a probability[4], henceforth being called **Pillar Vulnerability Index (PVI)**.

6.1 *General indicators*

The results obtained by the model in terms of its precision and quality indicators, are shown in Fig. 5.

Regarding the above results, considering there are 185 effectively damaged pillars due to former collapse events in the training set, it should be noted that the sensitivity of the model keeps a stable and discrete decaying up to a 60% cut-off probability, from which its decaying is stronger. The specificity of the model begins with a stable and discrete growing when the cut-off probability is 16%. This highlights a great statistical robustness for the model.

Figure 5. Quality and precision indicators for the vulnerability model.

---

4. This probability doesn't have an analytic formulation. It is obtained by the ensemble structure of the algorithm itself.

On the other hand, it can be noted that, given its ROC curve plot, this curve has an AUC equivalent to 0.91, which means that our model has a diagnostic power of 91%. This implies that there is a 91% probability the model will correctly classify a pillar as damaged, compared to a random guess referred to that same pillar. Given the above, this model has a quality in its classification ability typified as "good".

The most significant variables in the model, in terms of the average information gain over the modelled output, are those referred to the mechanic response of the rock mass in which pillars are emplaced to shear stresses and strains and seismic-nature variables, being the mining process explained as a joint effect whose convergence, given the resulting limit-state values, is a necessary and sufficient condition for collapses to occur.

Finally, it can be noted that the optimal value which discriminates the "damaged" and "undamaged" instances in the model is equivalent to a 34% cut-off probability, which defines a 95% sensitivity and specificity indexes. In order to use multiples of 10 and thus easily partitioning the PVI's interval from 0% to 100%, a threshold discrimination value of 30% was selected. This way, the model has a 96% sensibility and 94% specificity over the training set.

6.2 *PVI Plot over training, validation and application sets*

The results for the plotting of the PVI over the training, validation and application sets, are sequentially shown in Fig. 6.

6.3 *Results discussion*

a. About the model's structure:
Given the threshold discrimination value of 30% cut-off probability, the diagnostic precision indicators are the ones observed in Table 4.

These values are near state-of-the-art at the scale of experimental models and reflect high robustness both from the phenomenon understanding perspective and the associated experimental design.

In terms of each productive sector that conforms the training case, we have:

i. In Esmeralda, the pillars labeled as vulnerable by the PVI correspond to 39% of the total, with an average PVI of 78%. Of the remaining pillars, 61% have been classified as undamaged, having an average PVI value of 4%.
ii. In RENO-Dacita, the pillars labeled as vulnerable by the PVI are 13% of the total, with an average PVI of 75%. The remaining pillars were classified as undamaged, with an average PVI value of 11%.

Regarding the above, the obtained values suggest that a segmentation in terms of obtained PVI values considering the 30% cutoff probability stablished in section 6.1 as well as the average PVI values of the collapsed pillars (see Table 5).

b. About the PVI plot over the production sectors:
Given the results shown in Fig. 6, for the validation set, the following remarks can be acquainted in terms of the pillars labeled as "damaged" by the PVI:

– Diablo Regimiento is a production sector with practically no vulnerable pillars, and it is reasonable to assume the only pillar labeled as vulnerable contained in it as a model outlier, thus being these results an excellent reflection of the present operating conditions of Diablo Regimiento, since this sector actually has the best geomechanical behavior in El Teniente Mine.
– The southern zone of Esmeralda presents three areas that can be labeled as vulnerable, located in the northern, east and central sections of this production sector. Since South Esmeralda is an area which is operated via two separated caving fronts, splitting this sector in two sections called Bloque 1 and Bloque 2 (both separated by a rib pillar denoted locally as "Pilar Interbloques" (P.I.)) it is natural to assume the area labeled as vulnerable over the P.I. (the central one) is associated with unfavorable convex geometries of the induced
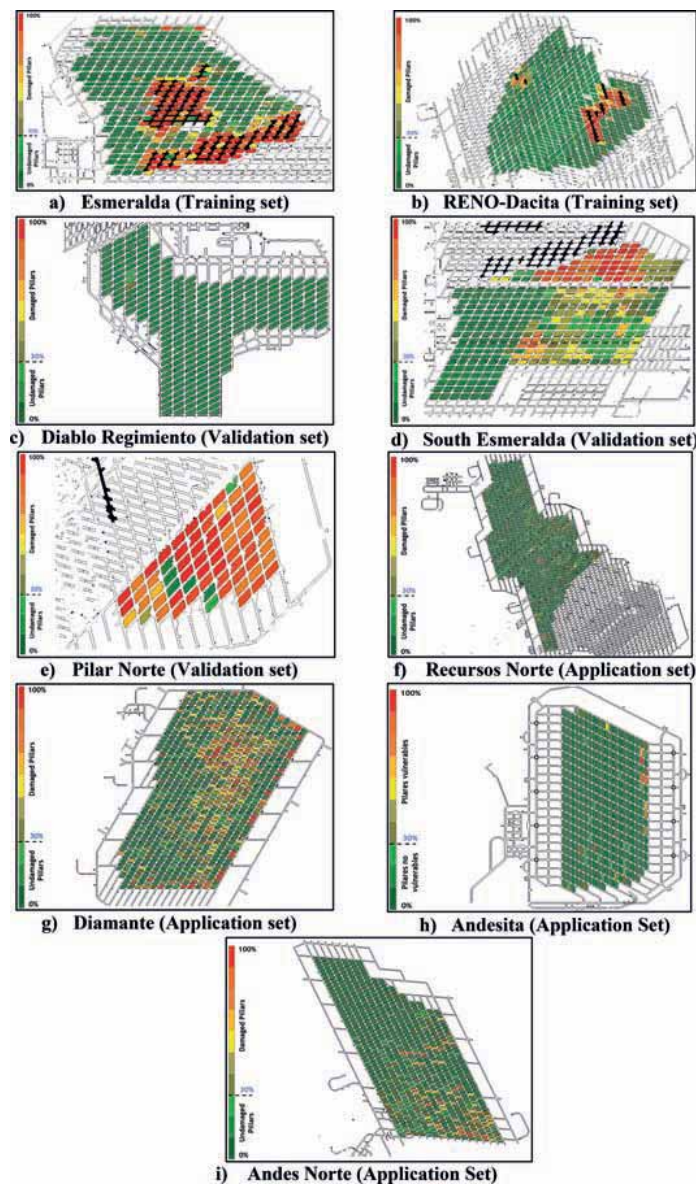
Figure 6.   PVI plot's results for all the production sectors and projects evaluated with the model.

Table 4.   Precision indicators of the vulnerability model over the training set.

	Esmeralda	RENO-Dacita
Sensitivity	95%	96%
Specificity	89%	95%

caving due to this particular situation, generating decompression over the P.I. and allowing further unfavorable deformational states. The northern area labeled as vulnerable in this production sector is reasonable to be assumed as an extension of the collapsed area ahead of the caving front in the northern section of Esmeralda, formerly fed to the model as a training subset. This region is characterized by a high frequency of seismic events, thus

Table 5. Vulnerability categories derived from the PVI.

Pillar State (Label or Classification)	Pillar Vulnerability Index (PVI) Values
Non vulnerable	0%–30%
Semi-vulnerable	30%–70%
Very Vulnerable	70%–100%

existing very high accumulated seismic energy, mostly associated with important presence of geological structures and lithological contacts with high difference of stiffness parameters, being this a known precept of localized seismicity, particularly in zones with regular geotechnical quality, which is the case in this area. This results meet the poor conditions encountered during mining, being this a fair approximation of the reality of this production sector.

– Pilar Norte is mostly a vulnerable sector. Such results are coherent with a series of unfavorable geotechnical conditions that take place on it, having an extensive history of very intense induced seismic activity over the support pillars in its production level, along with a subsequent high radiated seismic energy density per pillar, elevated vertical loads due to the existence of high terrain elevations over the surface, and presence of lithologies whose contact zones are characterized by high difference in stiffness, such as CMET[5]-Diorite and CMET-Andesite. The caving front in Pillar Norte also had a prolonged cease during the 2012–2017 period, having the support pillars in abutment stress state sustained an important amount of damage due to the resulting stress solicitation.

c. **About the PVI plot over projects:**

– Given the support pillars that conform the production level of the northern area of RENO, the western area of Dacita and the Recursos Norte Project, the results show there are 73 pillars labeled as vulnerable by the PVI from a total of 748 (PVI ≥ 30%), which is approximately equivalent to a 10% of the total. All the support pillars labeled as vulnerable located alongside the western and central area of this production level, area associated with unfavorable geological conditions due to the existence of a CMET-Dacite lithological contact, which has a history of individualized seismic response over the mining of RENO-Dacita sector, even with the latter implementation of HF, due to stiffness difference between these lithologies. On the other hand, pillars labeled as vulnerable located in the southeastern side of this production level are associated to high vertical stresses, due to high terrain elevations over the surface. Finally, pillars labeled as vulnerable located in the central and northwestern area of the Recursos Norte project are all associated with the existence of geological structures like faults RN1, RN2, RN3 and RN4, which are all oriented sub-parallel regarding the caving line advancing sequence, being this situation known to have a history of induced high seismic activity in past mining conditions, just like the northern area Esmeralda (fed to the model as a training subset).

– The Diamante Project results show there are 334 pillars labeled as vulnerable by the PVI from a total of 830 (PVI ≥ 30%), which is approximately equivalent to a 40% of the total. Most of these pillars are located in areas which coincide with the existing collapsed zones in the upper production sectors, like Esmeralda (used as a training subset) and Teniente 4 Sur (located above Esmeralda), being the rest generally associated with geological structures with sub-parallel orientations regarding the caving line advancing sequence of Diamante.

– In Andesita Project, the results show there are 18 pillars labeled as vulnerable by the PVI from a total of 338 (PVI ≥ 30%), which is approximately 5% of the total. Most of these pillars are located alongside the CMET-Dacite and CMET-Anhydrite Breccia lithological contacts and in the vicinity of the geological structures present in the southern area of this Project.

---

5. CMET is the acronym of "Complejo Máfico El Teniente" (El Teniente Mafic Complex), which a lithological group mostly conformed by mafic igneous rocks, such as basalts, gabbros, diabases and andesites.

– In **Andes Norte Project**, the results show there are 109 pillars labeled as vulnerable by the PVI from a total of 691 (PVI ≥ 30%), which is roughly 16% of the total. Most of these pillars tend to be located in the vicinities of lithological contacts, such as CMET-Diorite and CMET-Anhydrite Breccia, and in the area where the caving process will be initiated when the Project finally begins its operation. This latter area is coincident with the one where the vertical loads are mostly unfavorable, due to the existence of high terrain elevations over the surface.

7 CONCLUSIONS

According to the previous discussion, the following conclusions can be drawn:

a. Regarding the developed model:
– The algorithmic process carried out using the historical data of El Teniente Mine allowed the construction a model with high predictive capabilities regarding the collapse phenomena.
– The features used in the model development are sufficient to capture the phenomena occurrence via the algorithmic procedure.
– The model has a 91% diagnostic power, based on PVI values and the model's quality, estimated by its ROC curve.
– Based on a PVI cutoff value of 30%, a very high accuracy across the training set is reached, having a 96% value for damaged pillars (sensibility). For undamaged pillars, this value reaches up to 94% (specificity).
– The current model serves as a very good baseline for future accuracy improvements.

b. Regarding the model's application over production sectors currently under development and future projects:
– The results obtained by the model's application are reasonably coherent with the current situation presented in the mine. The diagnosed vulnerable pillars tend to be located in historically known risky areas, which supports the coherence of the whole research.
– The results suggest that there is a significant structural, geological and environmental component aspect regarding the potential occurrence of collapses in pillars.

c. Regarding the global perspective:
– From the individual features used to build the model, the most important aspects are the shear components of stresses and strains for an end-stage cavity as result of the mining process of a production sector and the seismic energy densities in both components, P and S, which shows the significance of the geological discontinuities over collapses occurrences.
– The mining operation can be assumed as a collection of features, each one of them being a necessary but not sufficient condition for a collapse process to occur. This way, only after reaching a series of limit values for each of these features, the collapse process can be triggered, given the environmental conditions of the rockmass where pillars are emplaced.

Finally, the vulnerability model formerly developed has been proposed as a safety criterion, destined to evaluate the limit condition of the explanatory variables formerly defined for this study as representative of the underlying collapse process. This way, for any current or future sector, this tool provides an insight of the regarding environmental and operational conditions that may or may not end in collapse damage for support pillars, allowing the possibility of future decision making processes oriented to modify operational and mining parameters in order to minimize the occurrence of collapse phenomena.

REFERENCES

Araneda, O.A. (2008). Lessons learned in cave Mining: El Teniente 1997–2007. *Proc. 5th International Conference and Exhibition on Mass Mining – MassMin 2008* (pp. 43–52). Luleå, Sweden: Luleå University of technology Press.

Chen, T., & Guestrin, C. (2016). XGBoost: A Scalable Tree Boosting System. *Proceedings of the 22nd ACM SIGKDD International Conference on Knowledge Discovery and Data Mining* (pp. 785–794). San Francisco, United States: ACM. doi:10.1145/2939672.2939785.

CODELCO. (2015). *Características del Modelo Numérico de Esfuerzos a Escala Mina, División El Teniente*. Rancagua, Chile: Codelco Chile, División El Teniente.

Karzulovic, A. (2005). *Efecto de la Geometría de Socavación en los Pilares del UCL, Sector Esmeralda*. Rancagua, Chile: Codelco Chile, División El Teniente.

Kullback, S., & Leibler, R.A. (1951). On Information and Sufficiency. *The Annals of Mathematics Statistics, 22*(1), 79–86. doi:10.1214/aoms/1177729694.

Lundmark, A., Eriksson, K., Johannsen, G., & Kats, A. (2017). Mucin 4 and Matrix Metalloproteinase 7 as Novel Salivary Biomarkers for Periodontitis. *Journal Of Clinical Periodontology, 44*(3), 247–256. doi:10.1111/jcpe.12670.

Millán, J. (2014). *Modelo de Zonación Geotécnica para el Macizo Rocoso en Mina El Teniente*. Rancagua, Chile: Codelco Chile, Dvisión El Teniente.

Mitchell, T.M. (1997). *Machine Learning: An Artificial Intelligence Approach*. McGraw-Hill Science/Engineering/Math.

Pardo, C., & Rojas, E. (2014). *Selección Variante de Explotación, Sector Nuevo Nivel Mina*. Rancagua, Chile: Codelco Chile, División El Teniente.

Pardo, C., Beck, D., Villaescusa, E., & Brzovic, A. (2012). Back Analysis of Intensive Rock Mass Damage at the El Teniente Mine. *Australian Mining Technology Conference*. Perth, Western Australia.

Rojas, E., Gaete, S., Leiva, E., Quiroz, R., Rubio, J., & Seguel, J. (2005). *Task Group for Esmeralda Project (in Spanish)*. Rancagua, Chile: Codelco Chile, División El Teniente.

Wahono, R.S., Herman, N.S., & Ahmad, S. (2014, October). An Analysis on Two Different Data Sets by using Ensemble of k-Nearest Neighbor Classifiers. *Advanced Science Letters, 20*, 1945–1950. doi:10.1166/asl.2014.5640.

Incorporating grade uncertainty into sublevel stope sequencing

Y.A. Sari & M. Kumral
Department of Mining and Materials Engineering, McGill University, Montreal, QC, Canada

ABSTRACT: Uncertainty in mineral deposits causes deviations from the long-term production schedules of mines. As underground mining has high development and operational costs, it is crucial to incorporate the uncertainty in the planning stage. In this research, a new mixed integer linear program that solves the sublevel stope sequencing problem while accounting for the block grade uncertainty is proposed. The new linear programming model incorporates chance constrained programming to manage the risk of the project and to stabilize the expected net present value. In a case study, the effect of varying levels of risk is studied by generating stope sequences for different risk levels. The trade-off between risk and expected net present value is studied. It was found that at higher risk levels the stopes with higher average grade are extracted earlier while at lower risk levels stopes with lower standard deviation are prioritized.

1 INTRODUCTION

Sublevel stope sequencing problem is the long-term planning for sublevel stoping underground mining technique. Conventional stope sequencing approach focuses on ordering of the stope extraction sequence such that mine stability and production requirement constraints will be respected and the profit will be maximized. The expected revenue from a block is calculated from the block tonnage and grade. This approach assumes the ideal condition where the stope average grades are accurately known. In reality, grade information is obtained through estimation or simulation of sparse drill hole samples. Therefore, the estimated/simulated grades deviate from the actual grades. Underground mining has high development and operational costs. Thus, when the plan is made based on the estimated/simulated grades, important loss may occur if the deviation is high. Grade uncertainty can be incorporated into stope sequence planning to minimize this kind of loss. In this paper, a strategy for sublevel stope sequencing that accounts for grade uncertainty is proposed.

2 LITERATURE REVIEW

As the stope sequencing problem does not have as many variables as stope layout planning problem, most approaches make use of the mixed integer linear programming (MILP) method. Chanda (1990) and Trout (1995) are the earliest adapters of MILP to stope sequencing. The objective is profit maximization while accounting for physical stability, minimum production and capacity constraints. However, due to limited computational resources they were not able to obtain results for larger cases.

Nehring, Topal, and Little (2010) combined development, drilling and backfilling phases to reduce the number of variables as the phases have a linear flow. Terblanche and Bley (2015) proposed smoothing the grade data just enough to dissociate feasible regions which allows selective mining. As an alternative to MILP, Manchuk (2008) developed a simulated annealing approach to the problem. This approach starts with a preliminary sub-optimal sequence and at each iteration, it introduces a random change to the sequence. If the resulting sequence is feasible, the updated net present value (NPV) is calculated and

compared to the previous solution. If there is an improvement or with a certain probability, the new solution is accepted as the current solution. The iteration continues from the current solution.

3 METHODOLOGY

The proposed approach is composed of two main stages: (1) First, a stope layout plan is generated. (2) Then, the stope sequence is generated for different risk levels of grade uncertainty. More details to each stage are provided in this section. In the end, the decision is left to the mine managers given all the information.

3.1 *Stope layout plan generation*

There are multiple approaches in the literature for generating the stope layout (Villalba Matamoros and Kumral 2017, 2018; Musingwini 2016; Sari and Kumral 2018b). At this time, the timing of extraction is not known thus the approaches find the portions of the deposit that are economically feasible by maximizing the profit instead of NPV. Also, the mining and mineral processing capacities are not considered for the same reason. Although their methods vary, the output of all approaches is composed of selected stopes in a deposit within the pre-determined height, width and length range. The resulting stopes have a rectangular shape and they are non-overlapping. One of the stope layout generation approaches is used to obtain the location to be sequenced in the next step.

3.2 *Stope sequencing considering grade uncertainty*

A MILP model is proposed for stope sequencing that accounts for grade uncertainty based on Sari and Kumral (2018a). The block grade uncertainty is managed through chance-constrained programming. The average and standard deviation of the block grade among multiple Gaussian sequential simulations of the same deposit are used to control the uncertainty. Chance constrained programming replaces the conventional objective value of NPV maximization with the maximization of the expected NPV and the minimization of the variance of the NPV. The balance between the two objectives is determined using the risk level of the company while assuming normal distribution between different simulations of block grade. The scalar of the risk minimization increases with the lower risk levels. The MILP model is given as below:

Maximize:

$$\sum_{s \in S} \sum_{t \in T} E\left[\frac{\left(g_s yR - C_m - C_p \right) H_s}{\left(1 + d \right)^{t-1}} \right] x_{st} - \Phi_Z^{-1}(\alpha) \sum_{s \in S} \sum_{t \in T} VAR\left[\frac{\left(g_s yR - C_m - C_p \right) H_s}{\left(1 + d \right)^{t-1}} \right] x_{st} \quad (1)$$

Subject to:
Stability requirements:

$$x_{st} + x_{vt} \leq 1 \quad \forall \ s \in S, v \in V, t \in T \quad (2)$$

$$x_{st} + \sum_{b \in B} x_{bt} \leq 1 \quad \forall \ s \in S, t \in T \quad (3)$$

$$\sum_{h=1}^{t} x_{sh} + \sum_{v \in V} x_{sv} \leq 2 \quad \forall \ s \in S, t \in T \quad (4)$$

Extract on one level in one period:

$$x_{st} + x_{dt} \leq 1 \quad \forall \ s \in S, d \in D, t \in T \quad (5)$$

Production requirements:

$$\sum_{s \in S} H_s x_{bt} \leq M \quad t \in T \tag{6}$$

$$\sum_{s \in S} H_s x_{bt} \geq m \quad t \in T \tag{7}$$

$$\sum_{s \in S} Q_s x_{bt} \leq N \quad t \in T \tag{8}$$

Extract once:

$$\sum_{t \in T} x_{st} \leq 1 \quad \forall \; s \in S \tag{9}$$

where x_{st} is the binary decision variable for the extraction of stope s at time t, g_s is the average grade of stope s, y is the ore price, R is the recovery, d is the discount rate, C_m is the mining cost, C_p is the processing cost, H_s is the tonnage of stope s, Q_s is the volume of stope s, α is the risk intolerance level, $\Phi_Z(\cdot)$ is the standard normal distribution function, S is the set of all stopes, T is the set of time periods, V is the set of adjacent stopes, B is the set of vertically aligning stopes, D is the set of stopes on different levels, M is mining capacity per period, m is minimum mining requirement per period, N is backfill capacity per period.

In the given model, chance constrained programming is used to adjust the optimization to a given risk level. The NPV is maximized while the variance in the NPV is minimized at the same time. The two objectives are balanced in the objective function in Equation 1 with the scalar $\Phi_Z^{-1}(\alpha)$, which takes a value according to the risk tolerance level. As the risk intolerance level increases, the balance of the objective function shifts towards minimizing the variance of the NPV. The variance is obtained from the results of multiple Gaussian sequential simulations of ore grades. Equation 2 ensures only one of the adjacent stopes can be mined at a given period. For mine stability, Equation 3 asserts vertically aligned stope mining on different periods and Equation 4 enforces the exposure of a backfilled stope from at most one side. Equation 5 allows the extraction from only one level in a given period. For the production requirements, Equation 6 sets the mining capacity, Equation 7 sets the minimum production and Equation 8 sets the backfill capacity per period. Equation 9 ensures each stope is mined at most once throughout mine life.

4 CASE STUDY

A case study has been conducted to evaluate the effectiveness of the approach. The case study is a gold mine composed of 134,400 blocks. From the drill hole samples, ten different block models were generated using sequential Gaussian simulation. The scheduling period is two months. The mining operation has one waste dump and one mineral processing plant. Other parameters related to the case study are given in Table 1.

Stope layout plan generation step has been performed using the approach proposed by Sari and Kumral 2018b. This approach uses a greedy heuristic approach that is based on dynamic programming. It finds the profit maximizing stope configuration by allocating and solving the sub-problems, then stacking them together. The sub-problems are composed of possible combinations of a certain number of stopes. The solutions to sub-problems are saved in computer memory which reduces the computational time by avoiding solving the same sub-problems multiple times. This way, combinations of a greater number of stopes are generated at each iteration. This is repeated until the maximum possible number of stopes are reached. Then, the stope combination with the highest NPV is selected as the final combination and the overall stope layout. The approach was implemented in C++. The average of the distinct sequential Gaussian simulations were considered as the block grades. The output of the approach consisted of stopes of size 30 m × 30 m × 15 m in X, Y and Z directions.

The resulting stopes, along with the block models generated by the ten sequential Gaussian simulations, and the parameters were used in the stope sequencing considering grade uncertainty step. The MILP model given in the previous section was implemented in CPLEX and used to sequence the case study stopes at the risk intolerance levels 50%, 65%, 75%, 85% and 95%. The resulting plans have been visualized in SGeMS as given in Figure 1. In the figure, the colors of stopes correspond to their extraction period. When the extraction period was compared to the average stope grade and variation, it was observed that at higher risk levels the stopes with higher average grade are extracted earlier while at lower risk levels stopes with lower standard deviation are prioritized.

In Table 2, the objective values for optimized sequences at different risk intolerance levels are given. The value is greater at the higher risk levels and as the risk tolerance decreases, the value also decreases. The lowest value is obtained at the most conservative risk level. At 50% risk intolerance level, the inverse normal distribution function returns zero, canceling out the variation minimization portion of the objective. Hence, the uncertainty model becomes equivalent to the deterministic model at this level.

Table 1. Case study parameters.

Parameter	Value
Number of blocks in X, Y and Z directions	$56 \times 100 \times 24$
Block dimensions in X, Y and Z directions	$5 \text{ m} \times 5 \text{ m} \times 5 \text{ m}$
Ore price	40 $/gr
Mining cost	200 $/tonne
Mineral processing cost	10 $/tonne
Recovery	90%
Discount rate	2%/2 months
Mine life	25 years
Mining capacity	900,000 tons/period
Backfill capacity	500,000 m²/period
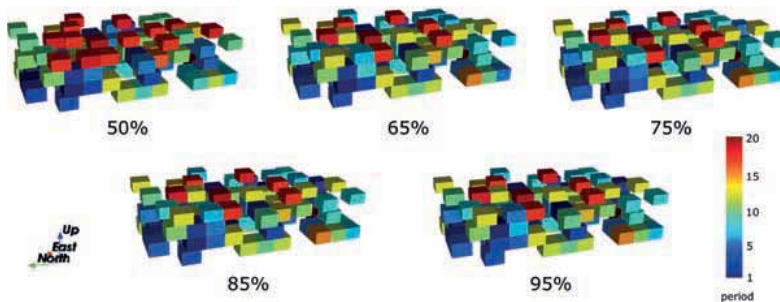
Figure 1. Stope sequences optimized for different risk intolerance levels.

Table 2. Resulting objective values for stope sequences.

Risk intolerance level	Value
50%	1,233 M
65%	756 M
75%	498 M
85%	303 M
95%	123 M

5 DISCUSSION AND CONCLUSIONS

Although many approaches to decrease the grade uncertainty in surface mine planning and scheduling, the subject is not as well studied in the problem of stope sequencing. Conventional stope sequencing MILP models contain mathematical, production requirement and mine stability constraints. In this paper, an approach that incorporates grade uncertainty into stope sequencing has been studied. This approach is composed of two stages; producing the stope layout plan and the sequence with grade uncertainty considerations. Grade uncertainty is incorporated by assessing the variation among different sequential Gaussian simulations and using chance constrained programming. Chance constrained programming modifies the objective function to maximize the average NPV and minimize the variation. The net present value maximization objective of the conventional solution approach is revised with a multi-objective optimization of maximization of the net present value and the minimization of the grade uncertainty. The emphasis on the variation minimization changes with the risk intolerance factor.

The case study has shown that the prioritization of stope extraction was made according to the average stope grades and their variations. In cases where the risk intolerance is higher, in other words, in the more conservative strategies, the objective was lower whereas the risk was lower. On the contrary, in higher risk strategies the objective was higher but the risk of not obtaining the target gains was higher. The sequence selection must be made by comparing the outcomes and taking into account of the company risk taking strategies. Other sources of uncertainty will be considered in the future work.

REFERENCES

Chanda, E.C.K. 1990. "An application of integer programming and simulation to production planning for a stratiform ore body." *Mining Science and Technology* 11 (2):165–72.

Manchuk, John. 2008. "A Framework for Stope Sequence Optimization."

Musingwini, C. 2016. "Optimization in underground mine planning-developments and opportunities." *Journal of the Southern African Institute of Mining and Metallurgy* 116 (9):809–20.

Nehring, M., Erkan Topal, and J. Little. 2010. "A new mathematical programming model for production schedule optimization in underground mining operations." *Journal of the Southern African Institute of Mining and Metallurgy* 110 (8):437–46.

Sari, Yuksel Asli, and Mustafa Kumral. 2018a. "Risk-based stope sequencing optimization for underground mines through chance-constrained programming." In *Manuscript submitted for publication*.

Sari, Yuksel Asli, and Mustafa Kumral. 2018b. "Sublevel stope layout planning through a greedy heuristic approach based on dynamic programming." In *Manuscript submitted for publication*.

Terblanche, S.E., and A. Bley. 2015. "An improved formulation of the underground mine scheduling optimisation problem when considering selective mining." *ORiON* 31 (1):1–16.

Trout, L.P. 1995. Underground mine production scheduling using mixed integer programming. Paper presented at the 25th International APCOM Symposium Proceedings.

Villalba Matamoros, Martha E., and Mustafa Kumral. 2017. "Heuristic stope layout optimisation accounting for variable stope dimensions and dilution management." *International Journal of Mining and Mineral Engineering* 8 (1):1–18.

Villalba Matamoros, Martha E., and Mustafa Kumral. 2018. "Underground mine planning: stope layout optimisation under grade uncertainty using genetic algorithms." *International Journal of Mining, Reclamation and Environment*:1–18.

A spatial clustering algorithm for orebody classification and boundary setting

S. Li, Y.A. Sari & M. Kumral
Department of Mining and Materials Engineering, McGill University, Montreal, QC, Canada

ABSTRACT: Planning of processing capacity and production rates are challenging tasks in mine planning, largely due to the accessibility to the orebody as well as the heterogeneity of ore quantity and grades. In this research, a new approach is proposed to optimize the processing streams and their capacities while considering the block destinations. Destination policies are determined via classification and boundary setting of the orebody. The main objective of this optimization is to design mineral plants such that the deviations from the target grade will be minimized as well as maintaining the balance between the mine production and process capacity. The high initial costs of plant installation are also considered. As the grade distribution within an orebody is largely heterogenous, the optimization is achieved through using spatial clustering techniques to examine the grade distribution throughout the orebody and comparing target grades and mineral processing costs of each possible processing plant. Two similar case studies are presented with possible processing plants to be built along with their costs. The ideal combination of plants is selected while simultaneously determining the plant capacities and block destinations.

1 INTRODUCTION

Block classification is one of the aspects of mine design that has direct impact on the profitability of the operation. Many critical reviews on grade control techniques based on estimation and simulation have been put forward (Verly, 2005, M. Glacken, 1997, Srivastava, 1987, Isaaks, 1990). However, one important factor that is often ignored in open pit mine planning is the impact on the performance processing facilities while having inputs with significant fluctuations in grades. Maintaining a consistent input for processing facilities is imperative as deviations from the target grades of a processing stream lead to unintended losses in recovery, which can be modelled via the Taguchi loss function (Kumral, 2015), a quadratic function that penalizes deviation from a certain target (Taguchi, 1986). It has been proposed that every processing stream maintains a target grade where blocks with exactly the same grade receives no loss from processing, but those with grades different from the target get penalized based on their deviations. Hence minimizing deviations from target grades would lead to reduced loss in recovery and, in turn, increased value of profits from the operation. A more consistent input for processing will also lead to a more uniform product, which tends to be more desirable. Consequently, a spatial clustering technique was put forward to group together the blocks that are spatially adjacent to each other with similar grade attributes in order to form contiguous clusters, which correspond to different processing streams. Clustering algorithms such as k-means could be used to minimize with-in cluster dissimilarities, target grades of each processing stream could then be set to the grade values of each cluster centroid. Capacities of processing streams could be found by counting the number of data points in each cluster. Performance of this technique will be evaluated with the overall profitability of the operation, while taking into account the high costs of constructing additional processing facilities, so that new processing streams are built if and only if the cost more than balances out for the losses in recovery due to deviation from target grades. Inclusion

of the geo-spatial coordinates in the clustering algorithm effectively takes into consideration orebody accessibility and facilities planning of production rates, so that better balances could be achieved between production rates and processing capacities.

2 METHODOLOGY

2.1 K-means clustering algorithm with spatial coordinates as additional variables

The clustering technique used in this paper is the k-means clustering with spatial coordinates as additional variables. i.e. each data point can be written as $x_i^T = [a^T s^T]$ where $a \epsilon R^p$ is the vector of p attributes of interest and $s \epsilon R^d$ represents the vector of geospatial coordinates. The k-means algorithm partitions a given dataset into k prespecified number of clusters in such a way that minimizes the with-in cluster dissimilarity and maximizes the inter-cluster dissimilarity. Various distance measures exist for defining dissimilarity among data points, including the Euclidean distance, the Manhattan distance and many other correlation-based distances. Euclidean distance is chosen in this case as it considers exactly the spatial distance between points. A brief summary of the k-means algorithm is as follows (Kassambara, 2017):

- Randomly select k points as initial cluster centers, with k being a prespecified number

  Until convergence or a maximum number of iterations is reached, repeat the follows:
- Assign each data point to a cluster based on the dissimilarity measure between itself and the cluster centers
- For the k clusters formed, update the cluster centers by taking the average values of all points in each cluster

One common metric used to evaluate the goodness of a k-means clustering is the total with-in cluster sum-of-squares (TWSS), its formula is shown in Equation (1)

$$TWSS = \sum_{i=1}^{k} WSS(i) = \sum_{i=1}^{k} \sum_{j \in C_i} \left(x_j - \boldsymbol{\mu}_i \right)^T \left(x_j - \boldsymbol{\mu}_i \right) \tag{1}$$

where x_j refers to the jth data point, μ_i is the cluster center of the ith cluster and C_i is the set of all points in the ith cluster. Results of the k-means algorithm are known to be sensitive to the selection of k initial cluster centers, hence it is a common practice to start with many different initial allocations and choose the one that performs best. As the number of clusters, k, has to be specified before the algorithm could be run, the optimal number of clusters could be determined by plotting the TWSS against number of clusters (James et al., 2013). Many other clustering algorithms are also available for spatial clustering and will be considered in future studies.

2.2 Economical evaluation of processing scenarios

After using the k-means algorithm to group the data points into k different clusters, the clusters are sorted in ascending order of average grades. A k number of different processing streams is then sampled from n number of total available processing streams without replacement, also in ascending order of recovery, to match the k clusters. Ordering the clusters as well as the processing streams ensures that clusters with higher average grades get sent to processing streams designed to have higher recovery. Therefore, for a given number of k and n, there are in total C_k^n different scenarios for processing. Let the maximum number of clusters be m, then the total number of possible scenarios is given by Equation (2).

$$Number\ of\ scenarios = \sum_{k=1}^{m} C_k^n \tag{2}$$

The idea of 'target grade' is applied in this paper, such that grade deviation from the mean will receive a penalized recovery during processing can be modelled with the Taguchi loss function (Kumral, 2015).

Table 1. List of parameters for revenue and cost calculations.

Parameter	Representation	Unit
a	Vector of attributes	
ρ	Block bulk density	ton/m^3
V	Block volume	m^3
x_j^k	j^{th} block grade of kth attribute	%
N	Total number of blocks	
P_k	Price of kth attribute	$
r_i^k	Recovery from i^{th} processing stream of kth attribute	%
$L(x_j^k)$	Loss of recovery from i^{th} processing stream of kth attribute	%
y_{ji}	Binary variable (1 if j^{th} block sent to i^{th} processing, 0 otherwise)	
p_i	Processing cost of ith processing stream	$/ton
M	Cost of constructing a processing stream	$
m	Total number of clusters/processing streams	
m_c	Mining cost	$/ton

$$L\left(x_j^\gamma\right) = c\left(x_j^\gamma - \mu_i^\gamma\right)^2 \quad \forall x_j \in C_i \tag{3}$$

where x_j^γ is the value of attribute γ of the jth block in the ith cluster, which is denoted by C_i, with μ_i^γ being the value of attribute γ of its center. $L(x_j^\gamma)$ represents the loss in recovery of attribute γ and c is a constant that magnifies the penalization.

Revenue and cost calculations are performed on each scenario and the one that maximizes profit is deemed as optimal. Formulas for calculations of revenue and cost are shown in Equations (4) and (5). Meanings of parameters are shown in Table 1.

$$\text{Total revenue} = \sum_{j=1}^N R\left(x_j\right) = \sum_{j=1}^N \sum_{j=a} x_j^k \times \rho \times V \times P_i \times \left[r_i^k - L\left(x_j^k\right)\right] \tag{4}$$

$$\text{Total cost} = \text{Total cost for processing streams construction} \\ + \text{Total mining cost} + \text{Total processing cost} \tag{5}$$

$$= m \times M + N \times m_c \times \rho \times V + \sum_{j=1}^N \sum_{i=1}^m y_{ji} \times \rho \times V \times p_i$$

3 CASE STUDIES

3.1 Overview

Two case studies were carried out using k-means clustering with spatial coordinates as additional variables. The two datasets were both based on drill hole data, one with easting and northing as x and y coordinates, the other with full x-y-z coordinates. Both datasets contained the same attributes of interest, namely copper and gold grades. Grades of other materials including MgO, CaO etc. were disregarded. 11 options for processing streams were considered and listed in Table 2. List of detailed parameter values is shown in Table 3.

3.2 Case study of a copper and gold dataset with 2D coordinates

Easting and northing were used as x-y coordinates in this dataset. The dataset contained 60 aggregated blocks in total with aggregation having a tonnage of around 100 kilo-tons. The attributes (copper and gold grades) and the geo-spatial coordinates were normalized prior to k-means clustering, so that the scales of the variables would be the same. The TWSS versus

Table 2. List of processing stream options.

Processing stream	Processing cost ($/ton)	Copper recovery (%)	Gold recovery (%)
1	30	54	48
2	40.8	62	53
3	48	68	57
4	55.2	74	63
5	60	79	66
6	67.2	83	71
7	72	85	72
8	74.4	86	73
9	81.6	87	75
10	91.2	88	77
11	100.8	89	78

Table 3. List of profitability parameters.

Parameter	Representation	Unit
M	Cost of constructing a processing stream	$50M
P_{copper}	Price of copper per ton	$5894
P_{gold}	Price of gold per gram	$41
m_c	Mining cost per ton	$50
c	Magnitude of penalization	50
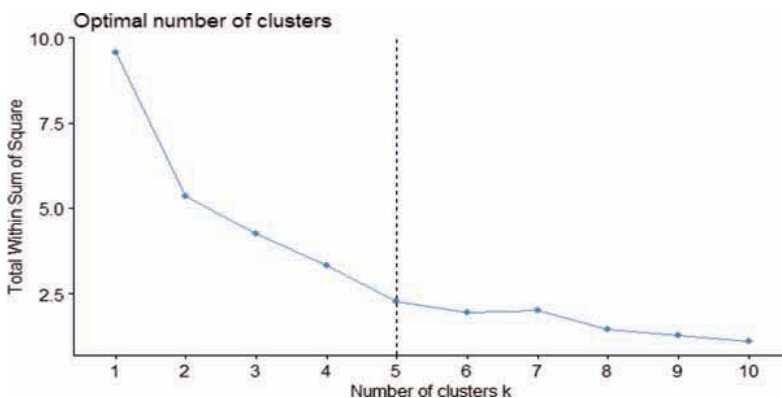
Figure 1. TWSS versus number of clusters (2D dataset).

number of clusters plot is shown in Figure 1. The maximum number of clusters for this dataset was chosen to be 5. As for k > 5, decrease in TWSS per increment of k is significantly lower.

After calculating cost and revenue for each scenario, cluster visualization for the scenario with the maximum amount of profit is shown in Figure 2. Each datapoint is represented by a circular dot, with its color depicting the cluster/processing stream, and size of the dot the normalized copper grade. Spatial k-means produced profit of $1013M. Capacities of each processing stream for results produced by both methods are shown in Table 4.

By observation of the clustering results, spatial k-means is able to provide reasonable interpretations of the data, grouping spatially adjacent blocks with similar grades together.
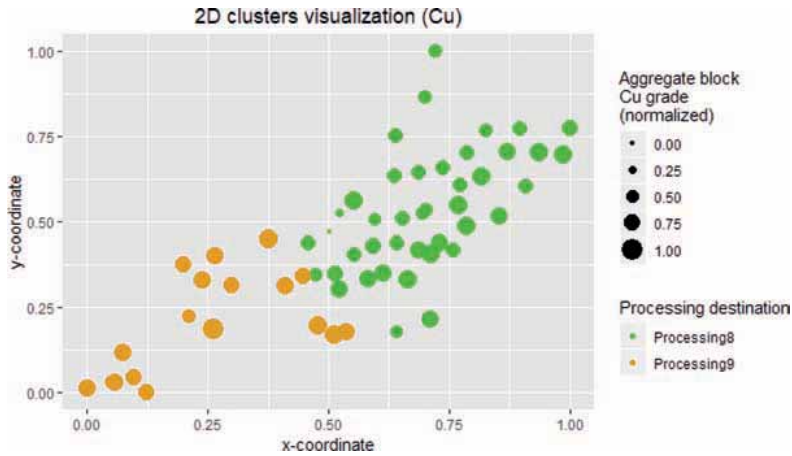
Figure 2.　Cluster visualization for 2D dataset (Copper).

Table 4.　Capacities of processing streams (2D dataset).

Spatial k-means

Processing stream	Number of blocks
Processing 8	42
Processing 9	18
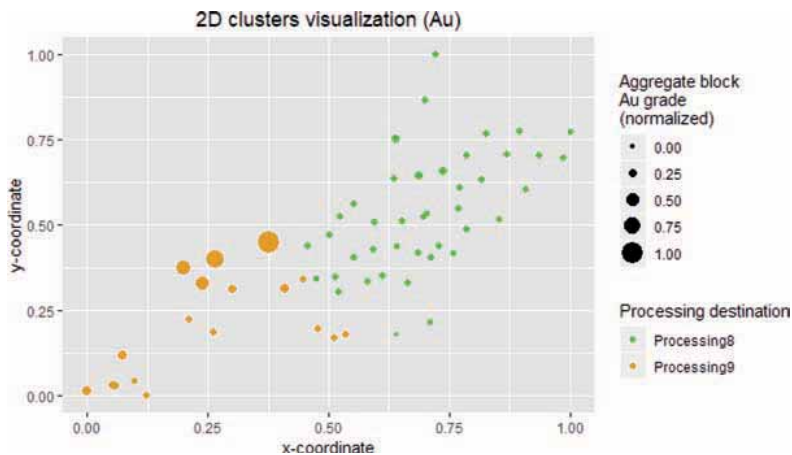
Figure 3.　Cluster visualization for 2D dataset (Gold).

3.3　Case study of a copper and gold dataset with 3D coordinates

The second dataset contained full x-y-z coordinates of 440 aggregated blocks, with each aggregation weighing 40 kilo-tons. Similar treatments were used on the dataset, with the TWSS versus number of clusters plot shown in Figure 4. The maximum number of clusters was selected to be 5.

After performing the k-means algorithm, the optimal scenario was selected based on maximizing profit. Visualization of the optimal processing scenario is shown in Figure 5 and Figure 6, each viewing from a different angle.
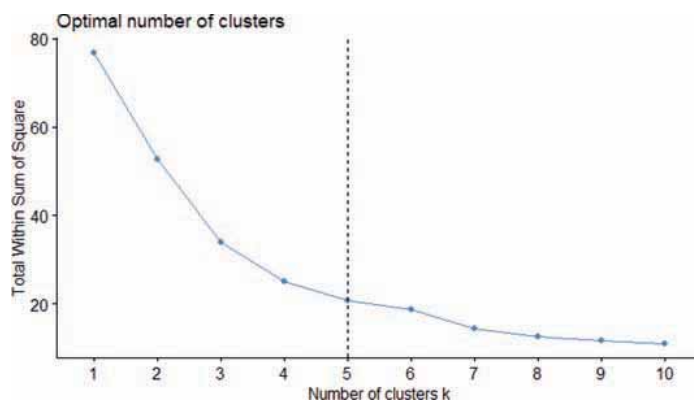
Figure 4.   TWSS versus number of clusters (3D dataset).
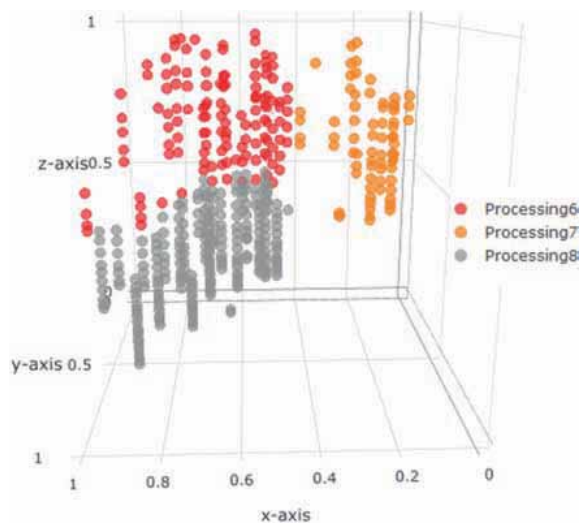
Figure 5.   Clustering 3D visualization view-1.
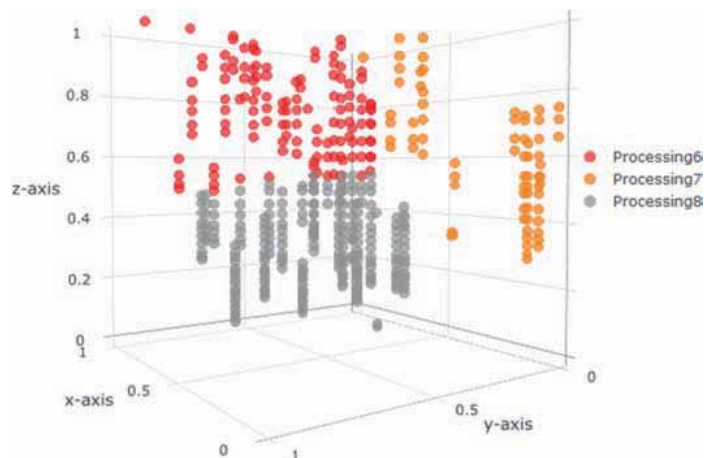
Figure 6.   Clustering 3D visualization view-2.

Table 5. Capacities of processing streams (3D dataset).

Spatial k-means

Processing stream	Number of blocks
Processing 6	129
Processing 7	70
Processing 8	241

For this dataset, a high recovery combination of 3 processing streams yielded the most profitable result for spatial k-means. Spatial k-means produced profit of $878M. Capacities of each processing stream for results produced by both methods are shown in Table 5.

By partitioning the dataset spatially into 3 groups, the spatial clustering method reduced losses in recovery due to variation of grades and provides increased profit while taking into consideration realistic constraints such as over-capacity and geo-spatial locations.

4 CONCLUSION AND FUTURE WORKS

This paper introduces the use of spatial clustering algorithm to generate spatially contiguous clusters, which corresponds to different processing destinations, while minimizing the with-in cluster dissimilarities in mineral grades. Realistic concerns including deviation from target grades and capacities in processing facilities are also taken into consideration, by the penalization of recovery via the Taguchi loss function and calculating the number of data points in each grouped cluster. One of the important factors in the determination of the profit from spatial k-means is the magnitude of penalization of the Taguchi loss function, with better results expected from the clustering method when a high degree of penalization is present. Another influential factor is the overall scale and profitability of the mining operation, with smaller operations being unlikely to balance out the high amount of additional costs of constructing extra processing facilities. In future studies, more sophisticated clustering algorithms will be experimented with, in addition to testing the significance of the loss function with different shapes and scales. Moreover, dissimilarity measures in clustering should explicitly distinguish between the geospatial coordinates and attribute vectors, optimization techniques should also be used instead of listing an exhaustive list of matching scenarios between clusters and processing facilities.

REFERENCES

Isaaks, E.H. 1990. *The Application of Monte Carlo Methods to the Analysis of Spatially Correlated Data.* Stanford University.

James, G., Witten, D., Hastie, T. & Tibshirani, R. 2013. *An Introduction to Statistical Learning: with Applications in R*, Springer New York.

Kassambara, A. 2017. *Unsupervised Machine Learning: Practical Guide to Cluster Analysis in R*, STHDA.

Kumral, M. 2015. Grade control in multi-variable ore deposits as a quality management problem under uncertainty. *International Journal of Quality & Reliability Management,* 32, 334–345.

M Glacken, I. 1997. Change of Support and Use of Economic Parameters for Block Selection.

Srivastava, R.M. 1987. Minimum variance or maximum profitability.

Taguchi, G. 1986. *Introduction to quality engineering: designing quality into products and processes*, The Organization.

Verly, G. 2005. Grade Control Classification of Ore and Waste: A Critical Review of Estimation and Simulation Based Procedures. *Mathematical Geology,* 37, 451–475.

Underground mine planning optimization process to improve values and reduce risks

Hongliang (Henry) Wang
Newmont Mining Corporation, Denver, USA

ABSTRACT: Underground mine planning and optimization has been dramatically improved over the last decade, thanks to a group of innovative tools that have transformed the process. With a case study, this paper is to demonstrate a complete and practical workflow aiming to improve values and reduce risks. The tools applied for this case study include: Stope Optimizer (MSO), Level Designer (PUNO) for rapid mine designs, Hill of Value Model (HoV) for Data Analysis and Strategic Mine Planning Optimization, Schedule Optimization Tool (SOT) and OMP for schedule optimization with multiple layers of constraints.

1 INTRODUCTION

The lack of useful underground mine planning and optimization tools has changed over the last decade or so, thanks to a group of innovative tools that have been developed by researchers, mining software vendors and mining companies[1]. With modern mine design software, mining engineers are moving away from manual digitizing to using automatic design tools, and the majority of the sequence and scheduling can be performed by software with robust rules and logics. Optimization algorithm with fast computer is capable of handling strategic mine planning and very large and complicated underground scheduling problems[2]. However, the whole underground mine planning process, including design, sequence, scheduling and optimization, is still a very time-consuming process, even with the latest tools.

There are challenges between the objectives, such as improving project values, including Net Present Value (NPV), Free Cash Flow (FCF), Internal Rate of Return (IRR), etc., and reducing risks through the validation of operability and practicability of a mining project. Very few literatures have explained how to balance between improving values (optimization) and reducing risks (practicality). And cross the mining industry, there are still misperceptions, inconsistences and ambiguities in regards to what exactly the goal of mine planning optimization is, at various stages of the project or life of the mine.

Underground mine planning and project evaluation processes, as illustrated by the following chart (Figure 1) in the simplest fashion, including studies of the 'rock' – resource and its reliability and uncertainty, 'ore' – economical part of the rock (above certain cut-off grade and 'makes money'), and 'value' – how to make the most money.

This workflow above involves many iterations, with increasing definition of the resource model and updates of the mine plans. A large amount of data can be produced with modern computer and mine planning software. 'Big Data' is great for data analysis and to evaluate multiple options and scenarios, but also requires robust data analysis and powerful algorithms to process the data and identify the best feasible mine plans.

The following sections will show a complete and practical workflow that has improved values and reduced risks for an underground precious metal project. It involved inputs from many other stakeholders, including geologists, resource modelers, metallurgists, open pit engineers, project managers and mine operations. It is believed that some of lessons learned and best practices can be shared by other projects, however, every deposit and operation is also unique, so we cannot simply copy the mine planning process from one project to
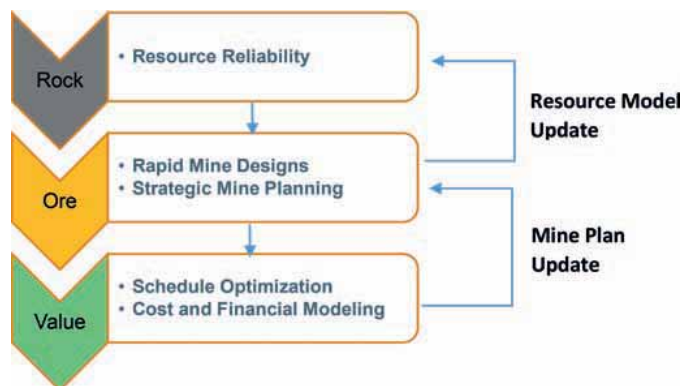
Figure 1.   High level project study workflow.

(a) Au Distribution   (b) S-Index Distribution
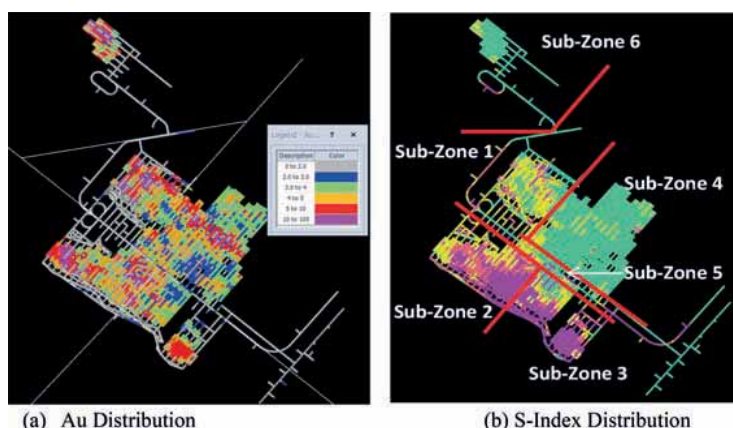
Figure 2.   Distribution of Au and Sulfur grade by sub-zones.

Table 1.   Descriptions of the sub-zones.

Zone	Au grade	Sulfur %	Other conditions
1	Very High to Medium	Medium to Low	Close to the pit wall
2	High to Medium	Very High to Medium	Requires flow through ventilation
3	Medium to Low	High to Medium	Requires flow through ventilation
4	Medium to Low	Low	Large tonnage, close to the pit wall
5	Medium to Low	Medium to Low	It is a pillar between Zone 1,4 and 2,3; last to extract
6	Very High to High	Low	Small tonnage, requires dewatering

another. It is up to the mine engineer to explore the opportunities and understand the limitations of the tools.

One of the most important considerations during the mine planning is to maximize the project values and meet the processing requirements. Great attentions have been paid to grade distributions, including metal (Au, Cu) and geochemistry (S-Index: sulfur contents including elemental sulfur and sulfide sulfur). Based on the relative location to the pit, and the distribution of Au and Sulfur (Figure 2), the underground deposit can be divided into several sub-zones. Table 1 lists the descriptions of the sub-zones, which was the main concern for the mine development layout, especially for the mine ventilation network.

2 UNDERGROUND MINE PLANNING PROCESS

As shown in Figure 1, the project study process involves resource evaluation, mine planning and economic analysis.

2.1 *Resource estimation and grade uncertainty analysis*

Resource modeling is the foundation of mine planning and project economics evaluation. To reduce the risks from the beginning of the process, one needs to understand the resource uncertainties, including risks and opportunities. Conditional simulation has been proven useful to evaluate the resource model. 100 simulation models were created to check the resource model. Simulations of the Au grade were generated using the Turning Bands method. For more details, please refer to a paper published at APCOM 2015[3]. 50 of the 100 simulation models were randomly selected and run through Stope Optimizer or Minable Shape Optimizer (MSO) using the same settings as for the resource model. Simulation results (Figure 3) show that there were about the same amount of metal, but a lesser number of high grade stopes than the resource model predicted.

One recommendation after this analysis was to add additional drilling to the high grade zones and to increase the overall confidence of the model. High grade stopes have the most values. Mine plans after optimization scheduled to mine them in the early years, therefore, any change to the high grade stopes will have more impact on the project values than the low grade ones.

A new block model was produced after additional drillings targeting the high grade zones. It confirmed some of the conclusions from the simulation: there are less high grade stopes than the previous resource model predicted, except at Zone 6, an isolated small area where new drillings have discovered additional high grade ore.

From the results, resource uncertainty can also be upside opportunities—additional high grade at Zone 6 has improve the project financials significantly. However, this also increases some other risks—to recover the high grade ore in the early years and achieve the ounce productions during the ramp up.
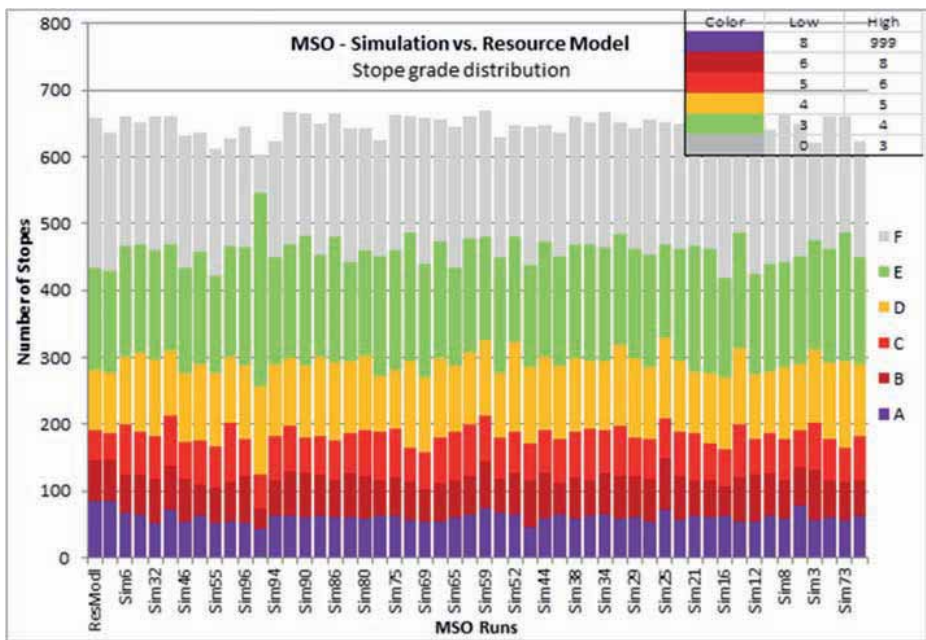
Figure 3.   MSO results for the simulation and resource model.

2.2 *Strategic mine planning*

Strategic mine planning is the process where the mine planning process is integrated with the strategic objectives of the project, which is to optimize the utilization of the principal resources (capital, labor, technology and mineral reserves) and maximize the strengths and opportunities of a mining company, while minimizing its weaknesses and threats[4].

Figure 4 is a simple diagram of the strategic mine planning analysis involves some of the key inputs and outputs. The relationship between project indicators (such as NPV, FCF, life of mine – LOM, production rates) and other inputs and outputs (such as metal prices, cut-off grades, production rate,) can be complicated. Changes in the business environment can affect metal prices and discount rates; mining costs (consumable prices escalation, contracting options) can affect the profitability of the project; production rate, one of the major measurements of a project, is often linked to the processing capacity, which typically requires significantly amount of capital investment. It is important to emphasize that cut-off grade is one of the outputs of the strategic mine planning process, rather than an input. More discussion on this can be found in the following sections. The results of strategic mine planning can also provide guidance to other important questions, such as open pit to underground transition, trucking vs. decline, exploration prioritization, closure strategy, etc.

2.3 *Rapid mine designs*

Strategic mine planning for underground projects is not a recent concept. At a high level, some of the evaluation can be done quickly if actual mine plan inputs are not the main concern. In the past, engineers manually did mine design and schedule, so it was impossible to produce too many mine plans for option analysis. Fortunately, nowadays, the level of details and accuracy has dramatically improved in the last decades, thanks to a suit of innovative tools that revolutionized the process. Rather than relying on assumptions and hypothesis, strategic mine planning now can be built on actual mine designs and schedules.

PRIMO[1] was a R&D project sponsored by Newmont and other major mining companies and software vendors. The goal was to develop an integrated set of underground mine design and scheduling tools for mining engineers. Some of the fruits came out of the PRIMO project (commercialized products) include:

- MSO[5] – fast stope design tool
- PUNO[6] – fast level design tool
- DOT[6] – fast decline design tool
- SOT[7] – schedule optimization tool

The tools have enabled underground mining engineers to improve the key value-adding elements of their work, including the cut-off grade selection, design of underground development and haulage networks, optimization of stope outlines and designs, scheduling and
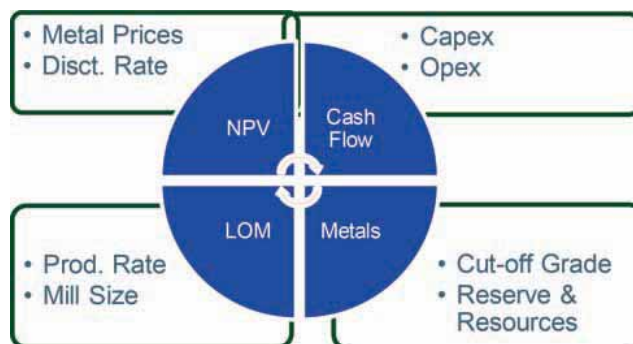
Figure 4.   A simple diagram of the strategic mine planning process.

sequencing of mine development and stoping, and development of production scheduler that maximizes the profitability over the life time of a mine. The PRIMO team developed an integrated set of tools that assists with mine planning at all stages from preliminary assessment through operational planning, with the aim of maximizing the mining project value generated by an underground mine.

- Optimization of stope design – covering strategic, tactical and operational planning
- Increase productivity – fast, effective and efficient engineering designs, relieve engineers from time consuming manual designs and scheduling
- Multiple mine design options can be evaluated quickly for "What-If" analysis
- Increase accuracy – consistent and repeatable design process
- Optimization – hill climbing with rigorous optimization algorithms, case studies since 2011 demonstrated that more ore tons, ounces and higher grade can be achieved with PRIMO than manual designs.

2.4 *Multiple dimensional strategic optimization – hill of value analysis*

Strategic mine planning should be performed before any detailed tactic mine planning, such as long-term or business planning. Strategic mine optimization should 'consider everything'[8]. Hill of Value allows complex relationships between variables to be explored concurrently, for example; cutoff grade, production rate/mill capacity, stope size and gold price. This allows an integrated approach to be taken as part of any options analyses. Simple break-even calculations are not able to capture the impact of the processing constraints.

A high level strategic analysis was conducted for the project using a technique called Hill-of-Value (HoV) model. HoV evaluated a wide range of options and scenarios with high level mine plan and cost assumptions, to study the relationship between cut-off grades, production rate/mill size, life of mine and project NPV/FCF at a strategic level[8]. The goal of this analysis is to provide a guideline or direction to determine some of most important project study outcomes such as cut-off grade and production rate by answering what-if questions and seeking the optimal operation point.

One of the main objectives of this study is to maximize project NPV by evaluating a wide range of options and scenarios. Stope reserve with different cut-off grade, process costs with various mill size/production rate, mining and development costs are the key inputs for the model. The HoV assessment for the project evaluated various production rates, cut-off grades, stope heights and backfill options, as follows:

- Production rate scenarios ranging from 0.5 million tonnes per year (Mtpa) to 1.1 Mtpa, in increments of 0.1 Mtpa, for a total of seven production rate scenarios.
- Cut-off grade scenarios ranging from 2.0 g/t to 7.0 g/t, in increments of 0.5 g/t, for a total of 11 cut-off grade scenarios.
- Stope heights ranging from 20 m to 30 m, in increments of 5 m, for a total of three stope height scenarios.
- Backfill options considered included rock fill, cemented rock fill and paste fill for a total of three fill scenarios.

The varying economic conditions under which the scenarios were tested were as follows:

- Discount rate of 0%, 7%, 9% and 12%, for a total of four discount rate scenarios.
- Gold priced at $1000/oz. to $1600/oz., in increments of $100/oz., for a total of seven gold price scenarios.

Combined, a total of 19,404 different scenarios were tested (in the background) during the HoV assessment. The results from a Hill of Value analysis can be described graphically, with the shape of the "hill" providing as much information as the relative "elevation". A flatter hill demonstrates that the project is more "robust" and/or less "sensitive" to variation in a particular variable whereas a steep peak demonstrates that there is a risk of "falling off" should parameters change. Additional background to the tool itself can be obtained from Brian Hall's book "Cut-off Grades and Optimizing the Strategic Mine Plan"[8].

Figure 5 and 6 are the HoV model result for the project. These graphs plot the NPV (relative value, or NPV Index value) vs. production rate and cut-off grade for the various options. In this case (20 m sub-level, CRF backfill, extract all profitable stope, $1200/ounce au price, single cut-off for all zones), the optimum cutoff is around 5.0 with a production rate of 0.9Mtpa to get the highest NPV, and the optimum cutoff is around 3.0 with a production rate of no more than 0.9Mtpa to get the highest FCF. Adjusting any of the inputs could
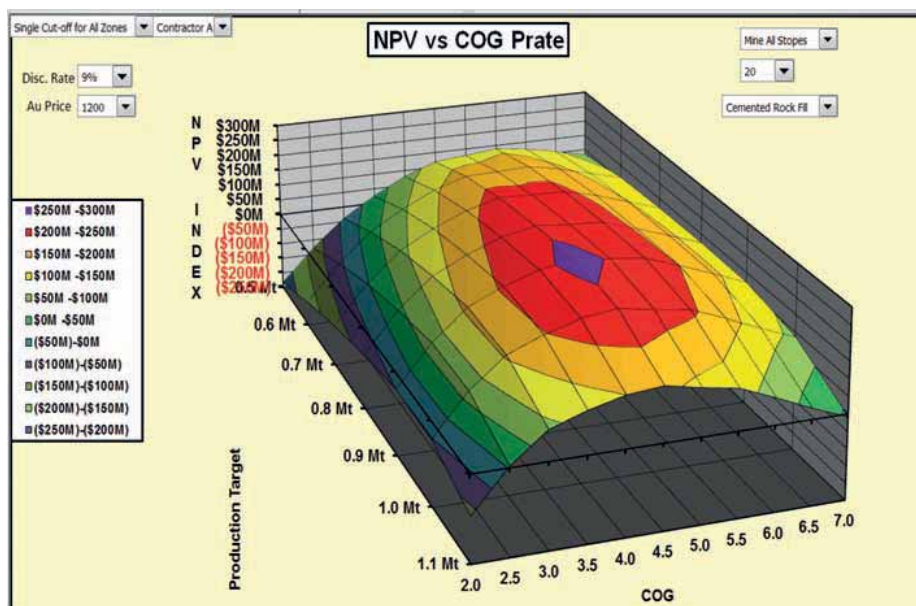
Figure 5. Hill of value result of NPV.
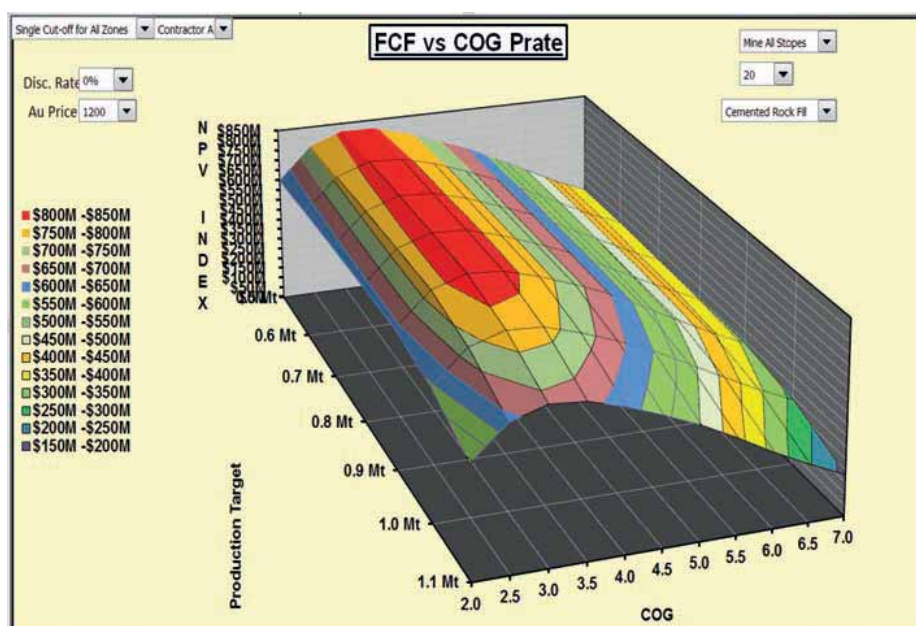
Figure 6. Hill of value result of FCF.

potentially change the outcome: the hill could move up or down, left or right. The shape of the hill can be different with the change of one input, or a combination of a set of changes. This is an important exercise to validate the model, and also to test sensitivities of the major inputs, such as mining methods, metal prices, etc.

Some observations from the HoV analysis:

- Changing the metal price will move the NPV hill up and down, but not left and right. This indicates that the optimal cut-off grade is relatively stable when the metal price changes. By contrast, the cut-off grade calculation with the traditional break-even cut-off grade calculation is directly linked to metal price (linear relationship).
- The profile of the NPV hill is very sensitive to the discount rate. For major capital investment projects, it is important to set up the right discount rate to reduce the risk and generate acceptable rate of turns.

2.5 *Schedule optimization*

HoV provides strategic guidance to the detailed tactical and operational mine planning. With modern commercial mine planning software, mining sequences with predecessors and successors can be systematically set up with rules and logics, to make sure the mine plans are practical, following the proper mining sequences and operational constrains. Resource leveling is a useful scheduling tool and is available through commercial mine planning packages. Resource leveling, by definition, is a technique in which start and finish dates are adjusted based on resource constraints with the goal of balancing demand for resources with the available supply[9]. One of the limitations of resource leveling, as a smoothing tool, is the lack of optimization algorithms, and that the leveled mine plan cannot always follow objectives as identified by the HoV analysis.

A few schedule optimization tools have been applied for this project, named as SOT and OMP[10]. SOT, is commercially available, uses the mine design and sequence as input, including precedence links between development and stoping activities. Mining properties such as duration, length, weight, product grades, activity types and mine area, can be imported into SOT for each mining activity. Mining scenarios, consisting of operational resources and capacities, discount rate, metal prices, operating costs, and capital costs, can be set up in SOT to test various options. SOT uses the heuristics algorithm to optimize the NPV of long term mine schedules[11]. OMP uses Bienstock-Zuckerberg (BZ) algorithm with focus on solving resource constrained project scheduling problems[12]. We tested OMP to produce 'seeds' to speed up the SOT runs.

For this project the mine design has a number of parameters that need to be balanced to determine a viable mine schedule by using SOT, which can be tailored to specific user inputs such as production constraints, targets and mining resources. To avoid peaks and troughs of resource demand and utilization, some of the critical constraints should be applied:

- Geotechnical constraints
- Ventilation constraints
- Equipment resource constraints
- Activity constraints by heading, level and zone
- Mill processing constraints
- Geochemistry value constraints for upper and lower bounds
- Multi-layer constraints to create a reasonable and executable mine plan

In addition to the above constraints, for this particular project, SOT was configured to target high-value stopes in the early years (typically stopes with high gold grades and favorable geochemistry), with lower value stopes in the later years of the mine life. A number of different production rates were tested using SOT, ranging from 700ktpa to 1000ktpa in increments of 100ktpa. For each of the scenarios, different mining and milling costs (and subsequently cut-off grades) must be considered, in order to determine the relative NPV.

The mine planning cut-off grade for the project is dynamic. A "two pass" approach was applied, with mining of high grade ore in the early years to maximize NPV followed by mining of lower grade ore in the later years to improve free cash flow. This "two-pass"

approach was maintained through the project studies, with the corresponding cut-off grades identified as follows:

- 5.0 g/t au in the first seven years (stopes below 5 g/t are excluded from the mine plans)
- 3.0 g/t au for the remainder of mine life (all profitable stopes are included)

Figure 7 is the grade-tonne curve of MSO runs – tonnes, ounces and head grades at various cut-off grades. As suggested by the HoV results (Figure 5), the targeted head grade to maximize NPV (with cut-off grade around 5 g/t) ranges from 8 to 10 g/t; and the targeted head grade to maximize FCF (with cut-off grade around 3 g/t) ranges from 5 to 7 g/t. Figure 8 is the grade profile of the final mine plan. The head grade for the first pass ranges from 8 to 12 g/t; and drops to below 6 g/t in the later years. The SOT mine plan is following the HoV strategies.
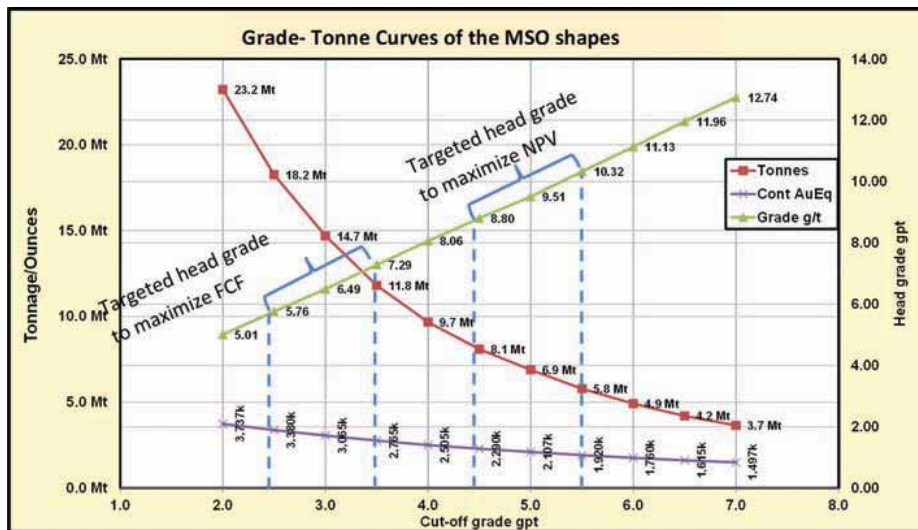
Figure 7. Grade-tonne curve based on the MSO shapes and targeted head grade based on the HoV analysis.
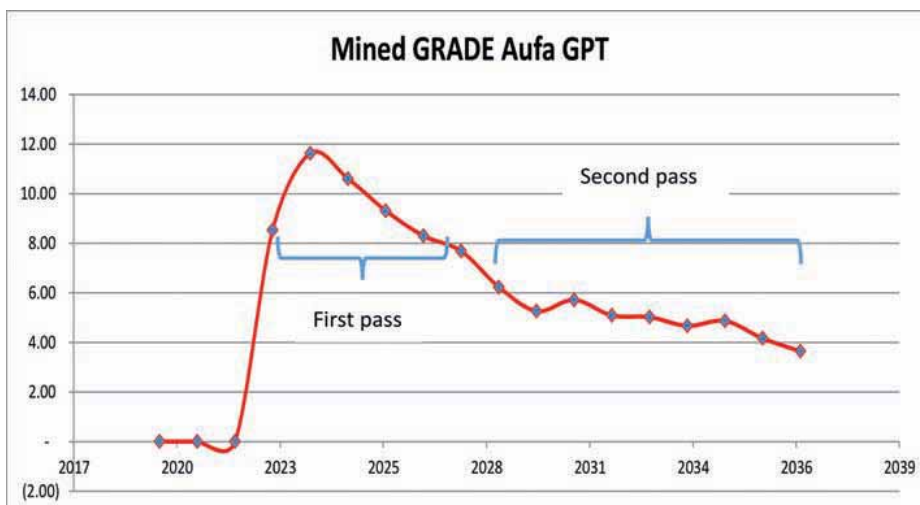
Figure 8. Final mine plan showing the "two pass" strategy.

342

Options analyses performed using both HoV and the SOT demonstrated that the deposit was amenable to a "two pass" approach with respect to the mine planning. In other words, high grade sub-zones can be mined first to maximize NPV, with the subsequent mining of lower grade ore in the later years to improve free cash flow. This two-pass approach was applied to the stope-profit attribute, with SOT configured to target high-value stopes in the early years (typically stopes with high gold grades and favorable geochemistry), with lower value stopes targeted in the later years of the mine.

3 DISCUSSIONS AND CONCLUSIONS

This paper summarized a mine planning optimization workflow implemented for an underground metal mining project. The main contribution of this paper is that it demonstrated a complete and practical underground mine planning optimization process aiming to improve values and reduce risks, with the latest software and analysis tools.

The project has a wide range of metal grades and geochemistry distributions, which makes the mining planning process complicated but also provides flexibility for blending and schedule optimization.

Software tools played a critical role during the mine planning process. Conditional simulation produced a large number of simulation models to validate the resource model. Simulation models after running through Stope Optimizer suggested that there was a fewer number of high grade stopes than the resource model predicted. MSO and PUNO were used for the rapid mine designs, which produced a large amount of data for the HoV strategic mine planning and optimization. HoV analysis identified the value range and provided guidance to cut-off grade and production rate for more detailed scheduling. To improve the project economics and reduce risks, SOT and OMP were applied for schedule optimization with multiple layers of constraints.

A "two pass" mine planning opportunity was recognized with the HoV study. Mining high grade ore in the first seven years to improve NPV, and mining lower grade ore in the later years to maximize free cash flow. This "two-pass" approach was realized with the detailed tactical mine planning.

REFERENCES

[1] PRIMO, AMIRA, Stope Optimization and Stope Layout, 2011 <http://www.amira.com.au/WEB/site.asp?section=projects&page=projectdetails&ProjectLink=2888&Source_ID=1>.
[2] G. Davis, A. Newman, Modern Strategic Mine Planning, 2008, CRC Mining Conference.
[3] A. Jewbali, H. Wang, C. Johnson, Resource Model Uncertainty Analysis and Stope Optimizer (MSO) Evaluation for an Underground Metal Mine Project, APCOM 2015.
[4] Hall A. and Hall B., 2006. Doing the Right Things Right – Identifying and Implementing the Mine Plan that Delivers the Corporate Goals, in Proceedings International Mine Management Conference 2006 (The Australian Institute of Mining and Metallurgy: Melbourne).
[5] C. Alford, M. Brazil, and D. Lee, Stope Optimization, 2007, Optimization in Underground Mining, Handbook of Operations Research In Natural Resources, pp. 561–575.
[6] Fast Level Designer, Decline Optimization <https://mineoptima.com.au>.
[7] Schedule Optimization Tool <http://www.revolutionmining.com/>.
[8] B. Hall, Cut-off Grades and Optimising the Strategic Mine Plan, 2014, Spectrum Series 20 (The Australian Institute of Mining and Metallurgy: Melbourne).
[9] A.B. Szwilski, Advantages of strategic mine planning, 1987, Mining Science and Technology Volume 5, Issue 3, pp. 309–317.
[10] Resource Leveling <https://en.wikipedia.org/wiki/Resource_leveling>.
[11] L. Fava, Heuristic optimization of scheduling scenarios for achieving strategic mine planning targets, MIRARCO Mining Innovation, 2013, 23rd World Mining Congress, Montreal, Canada.
[12] Munoz, G.; Espinoza, D.; Goycoolea, M.; Moreno, E.; Queyranne, M.; Rivera, O., A study of the Bienstock-Zuckerberg algorithm, Applications in Mining and Resource Constrained Project Scheduling, Computational Optimization and Applications. Volume 69, Issue 2, pp. 501–534. March, 2018.

Application of a digital model of deposit in Polish hard coal mines on the example of Polish Mining Group Ltd.

V. Sokoła-Szewioła & M. Poniewiera
Silesian University of Technology, Gliwice, Silesia, Poland

ABSTRACT: The article presents the method of realization of the digital deposit model elaboration, which is used in the Polish Mining Group Ltd. (PGG S.A.). The PGG S.A. has used an integrated package of engineering applications: AutoCAD Civil 3D, Oracle Spatial, EDBJ, GEONET and GEOLISP. The most important element of the system is the GEOLISP software, which allows to automate the process of obtaining data that is important for mining operations, in this it allows for the preparation of surveying—geological documentation in a standard compliant with the law. PGG S.A. mines, starting from introducing data from the resource in an analogue form and direct measurements by developing a graphic visualization of the seam, to use the developed deposit model in the implementation of tasks in the company at each stage of mining production. The above is discussed on the example of one of the mining plants owned by PGG.SA.

1   INTRODUCTION

In the Polish coal mining industry, solutions based on the use of systems enabling the construction of the digital model of the deposit have been used for many years. This is mainly related to applicable legal regulations, which allow the creation of surveying—geological documentation, both measurement, calculation and cartographic documents in a digital form (Klemens, Poniewiera 2010). These documents are used at every stage of mining enterprise operations. In Polish mining enterprises various combinations of IT (Information Technology) and technology environments are used, e.g. SoftMine used to create a deposit model, elaborated by the Geological and Drilling Company in Sosnowiec, Modeller and Reserver from the I/Mine 2000 suite by the Intertech/GSMI, working in MicroStation graphical environment, GoCAD and Grass GIS.

Requirements regarding the functionality of such systems are included in the article (Mertas & Poniewiera 2009). The system that is used in Polish Mining Group Ltd., (PGG S.A.), should be considered the most interesting solution. PGG S.A. is the largest hard coal mining company in the European Union. The construction of the system, which was called the Digital Model of the Deposit (DMD), was started in 2008, (then in the Coal Company Ltd.). Implementation work was carried out by Asseco Poland, Vertical, Geolisp companies and Information Technology Center ROW Ltd. DMD is in fact an information database about mining area and contains information about mining workings, geology, ventilation, mining hazards etc. The PGG S.A. has used an integrated package of engineering applications: AutoCAD Civil 3D, Oracle Spatial, EDBJ, GEONET and GEOLISP. The most important element of the system is the GEOLISP software, which allows to automate the process of obtaining data that is important for mining operations, in this it allows for the preparation of surveying—geological documentation in a standard compliant with the law. The system is systematically enriched with new modules, adapted to the current needs of mining enterprises. This is, among others, while meeting the requirements that allow the creation of measurement, calculation and cartographic documents in an electronic form and the presentation of objects constituting the content of mining maps in accordance with the

requirements of Polish standards—mining maps (Polish Standard) and included in the geodetic and cartographic law Act. The article presents the method of realization of the digital deposit model elaboration, which is used in PGG S.A. mines, starting from introducing data from the resource in an analogue form and direct measurements by developing a graphic visualization of the seam, to use the developed deposit model in the implementation of tasks in the company.

The seam in the model is represented by the set of Triangular Irregular Network. The created surface may be visualized with isolines, hypsometric maps or in 3D. The software automatically completes the values of the appropriate attributes of geological and exploitation conditions, such as field, tonnage, average dip, sulphation, etc. An important advantage of the software is the ability to prepare data for making forecasts of the impact of planned mining exploitation based on the digital model of the deposit. An algorithm of the increased accuracy of prognostic calculations in a disturbed deposit in which folds and faults occur was given. Research in this area was carried out in 2017–2018 at the Silesian University of Technology. The results were used in the software. The above is discussed on the example of one of the mining plants owned by PGG S.A.

2 SYSTEM CHARACTERISTICS

The DMD construction tool is Fusion Middleware SOA Suite software from Oracle company. The software implements the construction of internal integration of applications operating within the system with external applications. The applications operating within the system include programs:

– AutoCAD Civil 3D – this program is a product of Autodesk. The software is a graphical environment of the system, it enables integration with relational databases and ensures topological analyzes.
– Oracle Spatial – this is a relational database software in a spatial format. It provides gathering in one model of the entire PGG S.A. It enables browsing maps from the level of a web browser.
– EDBJ-OPN is a package of programs developed by Jan Białek. The package is used to present the effects of mining works both in the rock mass and on the surface area. It allows forecasting of maximum deformations of the mining area caused also by long-term multiseam exploitation. It also improves documentation regarding surface deformation as a result of conducted exploitation.
– GEONET – it is a package of several dozen programs that implement calculation tasks useful in geodetic and cartographic work. GEONET cooperates with electronic geodetic instruments.
– GEOLISP – is a system for servicing mining digital maps. It works in the AutoCAD system environment. It provides graphic visualization of database objects in a standard consistent with the requirements for creating cartographic documents in mining enterprises.
– Central Module of the Digital Model of Deposit (CMDMD) – application in the Java programming language, used to manage the supply of the Central Data Storage about a Deposit, (CSDoZ), and data from mining maps, CSDoZ searching according to preset parameters and performing analytical reports.
– The Oracle SOA Suite package enables you to run network services in the enterprise as well as from the external internet portals.

The development of the DMD is carried out by the division of tasks in relation to the scope of introduced data. Supervision over the proper conduct of work is performed by the system coordinator. A mining surveyor is responsible for introducing the scope of measurement data, the mining geologist is responsible for introducing the geological data, and the designer of the production preparation is responsible for the data on the newly designed exploitation. The IT data administrator function was also separated, who is responsible for the current data processing, security policy implementation and system operation monitoring.

The implementation work of DMD was carried out in the following stages:

- Scanning and calibration of analog maps.
- Vectorization, adaptation of digital data. Printing and map control.
- Maps update—introducing changes to the model that occurred during the project.
- Creating derivative maps (overview and special). Weaving and control of the derived maps.
- Preparation of surveying—geological documentation.
- Inclusion of surface maps to the system.
- Modeling the effects of mining work in the rock mass and on the surface.
- Construction of a spatial model of mining excavations. Control of a model accomplishment.
- DMD construction. Control and supplementing data. Calculation of hard coal resources.
- Data replication to the Oracle Spatial database. Performing analyzes, reports, queries, documentation.

3 APPLICATION OF DMD ON THE EXAMPLE OF ONE OF THE COAL MINES BEING A PART OF PGG S.A.

3.1 *Data input*

Entering data into the System creating the DMD at the stage of implementation works was preceded by standardization in the scope of data and means of their transmission. Defined, among others the structures of local and network catalogues and virtual disks, the terminology of files, catalogues, objects, thematic layers, etc. The method and scope of assigning permissions for individual user groups were determined. Objects on the given layer were specified. According to the procedure adopted for realization of implementation works, the maps in the analogue format were scanned at 400 dpi (black and white), the remaining 200 dpi. The main format of color files was JPG with the minimum compression set = 10%; for TIFF CCITT Group 4 monochrome raster. Then raster images of the abovementioned maps were calibrated. The degree of polynomial for calibration was chosen according to the rule: with evenly distributed 50 points, the 3rd degree was assumed, below 15 points affine transformation was assumed (first-order polynomial), the remaining ones were calibrated with the second-degree polynomial. In total, during the implementation phase, over 800 basic maps were scanned in the entire company (in the mine presented in the example 100).

Raster images were manually vectorized, obtaining spatial data of the introduced objects. The vectorization process was carried out in the application environment of GEOLISP. During vectorization, the GEOLISP software places individual objects on the right thematic layers, completes the relevant additional data. The digital map is kept in the local coordinate system and, additionally, its copy is created on an ongoing basis in a unified for the entire company, the national coordinate system PL 2000system. The data is updated in the system using the Geonet and GEOLISP softwares. Generally, in the system the point, line, surface and complex objects are distinguished. The facilities have unique codes allowing their unambiguous identification. They are presented by means of conventional marks in accordance with legal regulations and standards specified in Polish Standards—Mining Maps (Regulation 2015, Polish Standard) or conventional designations used on the base maps of the surface. A fragment of the vectorized map of mining excavations, as part of implementation works in the given mine, is shown in Figure 1.

In order to increase the accuracy of the map and the possibility of using objects on the map for direct calculations, more important objects (e.g. geodetic control points) were introduced based on the coordinates from direct measurements. The surface maps were also included to the system. In total, around 7000 geodetic control points, 4000 boreholes, 1500 sections of the basic maps in scales 1: 2000 and 1: 1000 were imported into the system of the entire company. In the given mine, respectively, about 800 geodetic control points, 300 boreholes and about 300 sections of basic maps.

Figure 1. The fragment of a vectorized map of mining excavation (own elaboration).

3.2 *Updating the database—entering changes into the model*

The data introduced by the vectorization method of the raster images were continuously updated with data from indirect field measurements. The system provides the possibility of entering data into the database saved in the files in the DXF and SHAPEFILE formats. The issue of data import is discussed by the authors in the article (Sokoła-Szewioła & Poniewiera 2017). Almost all geodetic calculations can be performed in the graphic edition of the database objects. There are a number of applications, for example, for inserting mining excavations into the AutoCAD program. This allows for automatic creation and joining of excavations. From the operator's side, it is only necessary to enter the coordinates of the point and measurements to the sidewalls. The entered data is subject to ongoing control, using a number of functions available in the software.

3.3 *Preparation of surveying—geological documentation*

The task of the system is to support the work of the surveying—geological departments. GEOLISP software allows to automate the process of creating the overview maps and special mining, geological excavations and the surface maps, in terms of content and the standard compliant with the law. Maps can be generated on the selected scale. The principle was adopted that the objects are entered into the system in the graphic edition, in the scale 1: 1000. Next, the desired scale is being generated keeping the size and shape of conventional signs and descriptions in accordance with the standards. The system allows to generalize the content of the map, the readability of the map, the selection of the optimal location of descriptions.

An important element of the system is the possibility of transformation of spatial data conducted in the local system to the national system, in accordance with the requirements contained in the Regulation (Regulation 2015). This issue was also the subject of research work carried out at the Silesian University of Technology in 2017–2018. As a result, an algorithm for one-stage transformation was developed, allowing for higher transformation accuracy (Sokoła-Szewioła 2017, Sokoła-Szewioła et al. 2018).

One of the important possibilities of the system is the possibility of presenting three-dimensional objects on the plane, such as: the cross-section of an excavation, geological profile, isolines, etc. Flat objects such as isolines or diagrams, as a rule, more clearly and precisely represent the spatial properties of the rock mass than the spatial model.

The chart of the floor of excavation, the dimensioning of the longwall, the cross-section through the excavation is much more convenient to obtain based on the attributes of the map elements than by defining the appropriate surfaces that cross the model in a given place.

The system contains commands related to the creation and editing of longitudinal and transverse cross sections, as well as many typical chart diagrams. Based on the data, a profile of a borehole can also be created (Fig. 3).
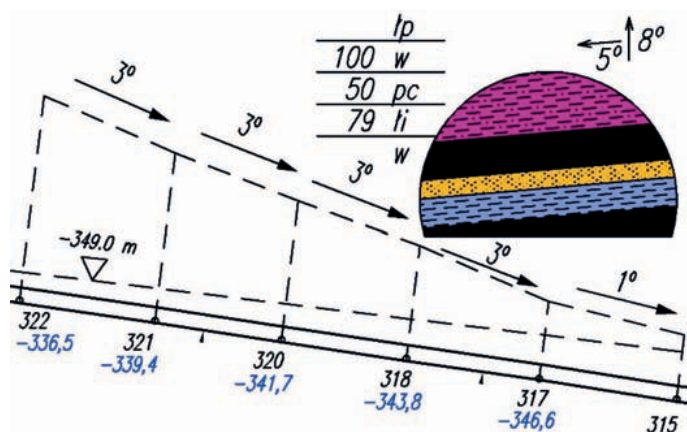
Figure 2. Spatial elements on the plane: geological cross-section of the heading and the projection of an excavation (own elaboration).

Figure 3. The profile of a borehole. Example of a borehole card (own elaboration).

Other important, from the point of view of creating the surveying—geological documentation of the possibilities of the system are to create: the thickness and straightness chart of the wall, a diagram of chemical analysis of water, a rose of cracks, cross-sections through a rock mass and many others. It is essential that it is possible to obtain text and graphics documentation in a traditional form at any time.

3.4 *Effects of mining works in the rock mass and on the surface*

Mining exploitation causes effects on the surface, hence the integration of DMD data with data contained on the maps of the mining area surface is essential. This data has been included in the DMD system. Mining company operations plans must be agreed with the relevant local government units.

Modeling the effects of mining works in the rock mass and on the surface of the area is understood as the possibility of creating the surface of the chosen parameter, (e.g. predicted or observed depressions of the area), adding two surfaces to each other (e.g. the surface of the area and the forecasted declines) and receiving the forecasted sculpture of the surface of the area as a result. Based on the functionality of the DMD system, you can automate the procedure of creating, among others data sets describing mining exploitation, both the parcels and the calculation points, checking and improving these data, various visualization of source data and calculations results, data sets. Such solution enables an immediate obtaining of data on the impact of the planned exploitation on the rock mass and surface,

Figure 4. An example of a generated map of predicted deformations (own elaboration).

which allows to choose the optimal velocity and the shape of conducting works. An example of a map of forecasted area deformations, generated for the area of the given mine is shown in Figure 4.

On the situational and altitude map of the mining area, in addition to the situation and an area development, the categories of the resistance of the objects of the equal or lower category than the category of the mining area within the range of influence of the planned exploitation must be visible. This task can be performed automatically in the DMD system, based on data generated from the EDBJ program.

The legitimacy of the use of the DMD, also at the stage of prognostic calculations, is indicated in the article (Poniewiera 2018). It was found that the results of calculations obtained on the basis of data from the deposit model may differ by a dozen or, in extreme cases, even by several dozen percent from those developed using standard methods. Often a small difference in the calculation results in a large change in the boundary of a deformation category and a part of the structure is classified to the wrong resistance category.

Therefore, it is recommended to create data on exploitation according to the following algorithm.

– Creation of a geometric model of the deposit, including faults and other disturbances.
– Performing of wall topology to avoid errors, e.g. overlapping of neighboring objects.
– Projecting plots on the floor, the walls should have many tops, so that the distance of the parcels from the deposit at any point is as small as possible.
– Collecting remaining data (thickness, start and finish dates, and possibly intermediate dates) from a numeric map, spreadsheet or other database.

3.5 The spatial model of mining excavations

By modeling the network of mining excavations it is understood to create three-dimensional solids of the shape and dimensions selected so that their rectangular projection on the projection plane coincides with the contours of these excavations on the basic map. The system allows to create automatically the solids of excavations based on the objects of the flat map: the lines of the sidewalls, the height angles and the type of the enclosure (Fig. 5). The solids can be made on the basis of the axis of the excavations, i.e. in a simplified way, or on the basis of the sidewalls, thanks to which each cavity is mapped. This functionality makes it possible to improve the implementation of tasks in the field of ventilation, the design of countershaft, the designation of escape routes, etc.

3.6 The use of DMD modeling

Modeling of the Digital Model of the Deposit (e.g. stratigraphic—lithological and tectonic structure of the deposit) in the understanding of the System consists in creating a surface
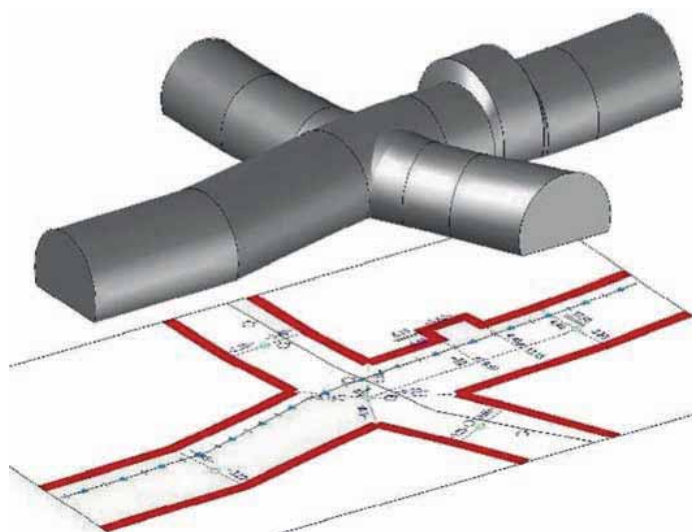
Figure 5.   Modeling of the mining mines network (own elaboration).
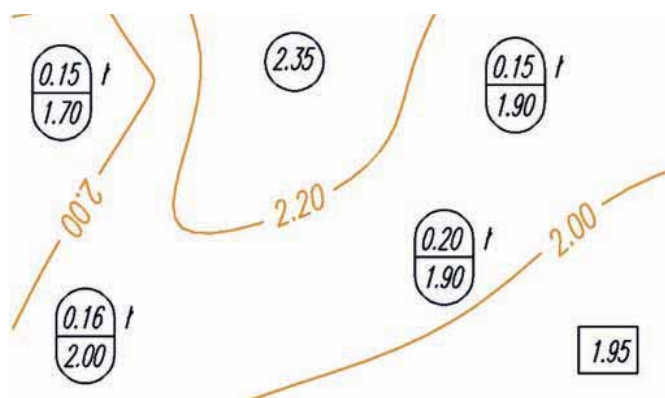
Figure 6.   Isolines of the thickness of the seam (own elaboration).

for any set of data. The surface is understood here as a grid of triangles based on a certain number of points having flat coordinates and a numerical parameter. The surface can be visualized by isolines (Fig. 6), a hypsometric map or a grid of triangles. It is possible to calculate the size between two surfaces (e.g. calculation of hard coal resources according to given criteria). The geological layers are visualized by means of the ceiling surface and the floor of each layer.

It is possible to generate contours based on arbitrarily spaced points. The program for interpolation of contours allows to: take into account breaklines—faults, slopes, ditches, etc., hiding contours under the buildings, slopes, roads, placing descriptions in such a way that they do not coincide with other elements of a drawing, finding wrong places (of a too large height difference).

The biggest problem that we encounter when creating a geometric digital model of a deposit for hard coal deposits is to introduce a discontinuity line: faults, seams junction lines, chocking. In the case of hundreds of small and larger faults that we have in the Upper Silesia Coal Basin mines, the existing methods of introducing the discontinuity line did not pass the test. Therefore, new algorithms were developed (Jelonek et al. 2015):
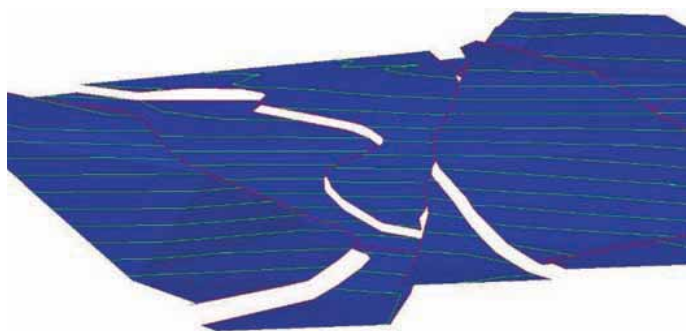
Figure 7. The spatial position of the faults—constant inclination method (own elaboration).

- A method based on calculating the spatial position of the fault based on existing contours that reach it from both sides. In the case of a small number of isolines, tools are used to compact contours.
- The method based on the assumption that the inclination of the seam before and after the fault is constant (Fig. 7).
- With a small number of faults, the entire area is divided along faults into separate parts. Each of these areas is raised by the program by a value equal to the projection of a given fault, obtaining a surface "before tectonics".
- The most accurate way, but requiring a relatively large amount of data, is to create separate surfaces on both sides of the fault. We make surfaces independently and extrapolate using the kriging method. Then, you project the projected wing on the one surface and the projecting one onto the other.
- Another option is to move the fault from the above-lying seam or the carbon ceiling. We place the projection and inclination of the fault between the given seams and we find the intersection of the surface of the fault with the surface of the floor of the next seam.

In the system it is possible to generate the course of the deposit based on the neighboring data concerning neighboring seams. To the surface of the floor, e.g. the above lying seam (including tectonics), we add a surface formed from the differences of a distance at individual measuring points between these neighboring seams. In this way, we obtain the floor of the searched seam.

Using DMD data, you can coordinate activities in the scope of production, transport, enrichment and sales (Fig. 8). It is possible to design production scheduling or exploitation planning (Fig. 9).

3.7 *Performing analyzes, reports, queries, documentation*

The digital model of the deposit can be used to obtain a number of information about plots, such as tonnage, medium ash, or type of coal. As mentioned before, the DMD consists of a series of triangles networks, each of which describes one parameter, e.g. the floor of a seam or total sulfur content. This network of triangles can be cut to any enclosed area, for example, an exploitation wall or a geological plot. In this way we will obtain average and maximum values of all coal parameters for this area. Based on the floor area of the seam, the program can also calculate the inclination of each section of the excavation. The program automatically draws the planned exploitation on the basis of the deposit model and given restrictions (e.g. casing type, legal regulations, etc.).

An important advantage of DMD is that each wall has always current data obtained from the numeric map. Not only dimensions: length, runway, surface, but also, for example, the expected average sulfur content or forecasted fallout of the floor.

The results of analyzes can be saved in files or presented in the form of a printout on plotters and printers. It is possible to print the maps in a rectangular sectional cut, along with the
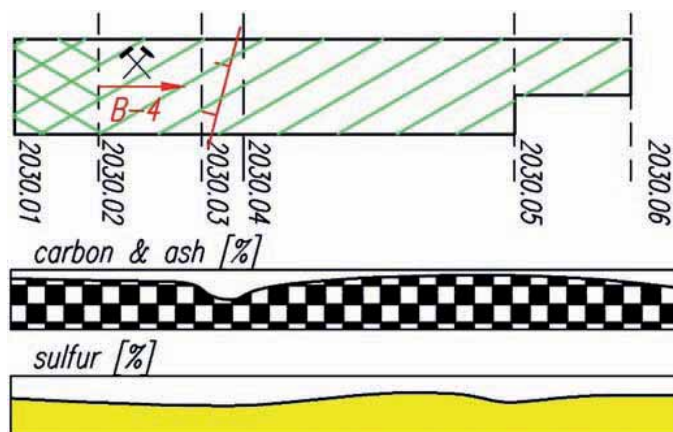
Figure 8. Coordination between production, transportation, coal processing and sales (own elaboration).
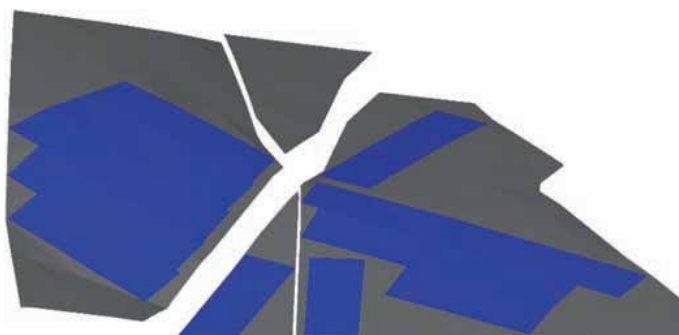
Figure 9. Creation of new exploitation parcel based on digital map (own elaboration).

description of the outside the frame area specified in the Polish Standards—Mining maps or standards for the creation of a base map.

4 CONCLUSIONS

The system presented in the article, used in Polish hard coal mines, to develop a digital model of the deposit, can be considered as a system for documenting and planning hard coal production. It allows for streamlining the implementation of tasks in the field of conducting underground mining plant operations. The proposed solution based on the Fusion Middleware SOA Suite software of the Oracle company, along with application programs, in particular the GEOLISP software is a very good solution, in particular due to the fact that the scope of the functionality of the system was adapted to the Polish conditions of conducting exploitation, while meeting the requirements included in the relevant regulations. It seems that an important advantage of the DMD system is that it is systematically extended with additional functionalities resulting from the current needs of mining entrepreneurs. The article presents only the most important ones. Among the important new solutions used in the system, one should mention the proprietary algorithm of introducing and predicting occurrence of faults, which is of key importance for the design of exploitation and the method of data collection for the purpose of determining the effects of mining works in the rock mass and on the surface.

REFERENCES

Jelonek, I., Poniewiera, M. & Gąsior, B. 2015. The qualitative model of the deposit on the example of the Kompania Węglowa S.A. Part I: Stages in the development of the digital model the deposit. *Schriftenreihe der Deutschen Gesellschaft für Geowissenschaften* Vol. 87: 91. Potsdam: Deutschen Gesellschaft für Geowissenschaften.

Klemens, J. & Poniewiera, M. 2010. Wykorzystanie najnowszych technologii informatycznych do wsparcia procesów mierniczo-geologicznych w Kompanii Węglowej S.A. *Przegląd górniczy* 10/2010: 3–10.

Mertas, J. & Poniewiera, M. 2009. Współczesne funkcje kartografii górniczej. *Conf. Proc. X Dni Miernictwa Górniczego i Ochrony Terenów Górniczych*: 394. Kraków: AGH.

Polish Standards. *Polskie Normy – Mapy górnicze* series PN-G-09000. Polish Committee for Standardization.

Poniewiera, M. 2018. *Wpływ generalizacji danych geometrycznych na dokładność prognoz deformacji terenu górniczego*. Gliwice. BK nr 06/050/BK_18/00. Gliwice. Silesian University of Technology.

Regulation. 2015. Rozporządzenie Ministra Środowiska z dnia 28 października 2015 r. w sprawie dokumentacji mierniczo-geologicznej *Dz.U.* 2015, poz. 1941. Poland.

Sokoła-Szewioła, V. 2017. *Ocena dokładności i opracowanie parametrów transformacji lokalnych układów współrzędnych prostokątnych płaskich stosowanych w przedsiębiorstwach górniczych do układu państwowego z oprogramowaniem w systemie klasy GIS.* BK nr 06/050/BK17/0042. Gliwice: Silesian University of Technology.

Sokoła-Szewioła, V. & Poniewiera, M., 2017. Selected possibilities of the GIS data import in programs AutoCAD Civil 3D and Geolisp. *Geoinformatica Polonica* 16/2017: 69–76. DOI 10.4467/21995923GP.17.005.7192.

Sokoła-Szewioła, V. Poniewiera & M. Pomykoł, M. 2018. Algorithm of transformation between the local system Borowa Góra and the state system PL-2000 on the example of PG Silesia. *IOP Conference Series: Earth and Environmental Science*, Volume 198, conference 1, Sci. 198 012014.

Scheduling and dispatch

Improvements in plan-driven truck dispatching systems for surface mining

M. Samavati, A.W. Palmer, A.J. Hill & K.M. Seiler
Australian Centre for Field Robotics, The University of Sydney, Sydney, Australia

ABSTRACT: Truck dispatching systems have been widely used since the 1970s for truck assignments in open pit mines, in order to coordinate material movement from diggers to process plants and stockpiles. Existing commercial solutions are commonly plan-driven systems, which operate by making real-time truck assignments while maintaining conformance to an established haulage allocation plan. Such systems typically comprise programming models to determine the allocation plan as a set of material flow rates. A significant limitation of these methods is that they optimise flow rates only for instantaneous production. These approaches ignore upcoming events and changes in availability and performance, limiting the ability to optimise flows around such events. The method proposed in this paper extends existing approaches by modelling material flows over a future time-horizon, incorporating upcoming events, disruptions, and changes in resources. Results are presented comparing an established algorithm with the proposed method, showing improved handling of disruption events.

1 INTRODUCTION

Over half of the operating costs of open-pit mines can come from operating the fleet of haul trucks (Alarie and Gamache 2002). Consequently, haul truck dispatching methods that optimally utilise the fleet inside an open pit are of great interest to mining companies. Haul truck dispatching in an open pit mine is the process of coordinating material movement from diggers to process plants and stockpiles, through assigning trucks. Since the 1970s, computer-based truck dispatching systems have been widely used for this purpose. Existing approaches can be classified into: rule-driven heuristics, constrained-assignment approaches, and plan-driven approaches (Munirathinam and Yingling 1994).

   Existing commercial solutions in the mining industry are commonly plan-driven systems, operating by making real-time truck assignments while maintaining conformance to an established haulage allocation plan. These systems consist of two components: the haulage allocation component and the dispatching component (Munirathinam and Yingling 1994). The haulage allocation component designs an allocation plan as a set of material flow rates from diggers to process plants and stockpiles, e.g., kilograms per second of material from a particular digger to specific dumps (i.e., plants and stockpiles). Such plans are designed in a way that the production targets of the company for a certain time horizon (e.g., a 12-hour shift or 24 hours) are fulfilled subject to the operational constraints. Given that the mineral deposit is broken into smaller segments, or blocks, the company's targets are often the amount of material that must be extracted from certain blocks and sent to certain dumps. The dispatching component attempts to achieve the allocation plan through assigning individual haul trucks to haul routes.

   This paper focuses on the haulage allocation component. A variety of methods have been developed to generate optimal flow rates, often comprising a linear programming model. However, a significant limitation of these methods is that they optimise flow rates only for instantaneous production, and do not have an awareness of the production target for the entire time horizon. They are also unable to plan around upcoming disruptions, such as planned maintenance and breaks, or changes in equipment availability (e.g., changes in the number of

available trucks, or digging and dumping capacities). They instead rely on the human dispatch operator to plan the operations around these disruptions with the production plan in mind, and for them to be able to provide their attention at the times where changes are occurring. During particularly busy times, such as the shift changeover and blasts, the operators can easily lose sight on the state of the mine as they struggle to keep up with the large number of manual truck assignments that are required. Ultimately, by considering only a 'local' instantaneous optimisation, they are unable to find 'globally' better solutions across a longer time horizon.

The purpose of this paper is to present a new programming model to explicitly consider the production targets for a full shift, or similar time horizon, and incorporate planned events into a more 'global' or forward-looking optimisation than existing methods. The intent is to allow for non-steady-state behaviour, and to reduce the cognitive load on operators and reliance on their attention at specific points in time. The proposed model also enables feedback control on material quantity targets, allowing re-planning after an unexpected disruption or unusual performance, in order to meet the planned targets rather than relying on the operator to adjust setpoints manually. In this paper, the time horizon considered for the Flow Planner is a 12-hour shift.

The remainder of this paper is structured as follows. In Section 2, we highlight existing work related to the haulage allocation plan component. We describe the problem domain in Section 3, and develop our programming model in the same section. The efficiency of the proposed methodology is judged in Section 4, by testing it on a set of instances and comparing the results to those of an existing technique. This work has been supported by the Rio Tinto Centre for Mine Automation and the Australian Centre for Field Robotics, University of Sydney, Australia.

2 LITERATURE

Haul truck dispatching is well studied in the literature as it is a high-cost aspect of mining. Existing commercial solutions, such as DISPATCH by Modular Mining Systems and SmartMine, in the mining industry are commonly plan-driven systems (Munirathinam and Yingling 1994). White and Olson (1986) and White, Olson et al. (1993) developed a technique that forms the initial basis for DISPATCH (Munirathinam and Yingling 1994), and Subtil, Silva et al. (2011) developed the technique that is the basis of SmartMine. In both studies, the allocation plan component is a Linear Program (LP) that calculates the instantaneous flow rates from diggers such that the productivity of the mine is maximised, subject to constraints such as the number of trucks available, maximum digging rates, the capacity of the dumps, and material blending requirements at the dumps. Bonates and Lizotte (1988) proposed a simplified approach to defining the haulage allocation, where an LP is used to optimally obtain the production rates of all operating shovels such that the production is maximised. The LP is run once a shift to only maximise the production of shovels in both ore and waste without considering the associated value and operational costs. Soumis, Ethier et al. (1989) developed an approach where the entire dispatching procedure is implemented over three stages: equipment plan, operational plan and dispatching plan. The combination of equipment plan and operational plan forms the basis for the haulage allocation plan. Using a heuristic, the equipment plan yields feasible combinations of shovel locations, a subset of which is passed to the operational plan where a mixed integer programming model (MIP) performs the optimisation of production. A number of other existing approaches to the allocation plan component aim to obtain the optimal number of trucks required to service the shovels (Ta, Kresta et al. (2005), Burt and Caccetta (2007), and Upadhyay and Askari-Nasab (2016)).

3 PROBLEM DESCRIPTION AND SOLUTION METHODOLOGY

Mining operations are typically planned as a set of production targets for a given period. For long-term plans these can be quite coarse, however at the time-scale of shifts or days, these production targets typically include: the blocks to be extracted in the period; the dig units

assigned to those blocks; the dumps (crushers, process plants, stockpiles, waste dumps) to which the material should be sent; and the amount, priority and/or order of each such material movement target. Plans (or a process to determine) 'disruptions' to load and haul operations are also often known at this time-scale, including equipment maintenance, availability of equipment and operators, blasting, road maintenance, etc.

A haulage allocation plan specifies the flow rate of material from dig-units to dumps, and is generated as a guide for operations to achieve the planned production targets.

Existing methods optimise instantaneous material flow rates for the current state of the mine. Our proposed system, the 'Flow Planner', extends this planning methodology by generating an optimal haulage allocation plan for a specified time horizon (e.g. shift, day or similar rolling window). The Flow Planner optimises time-varying flows across this longer time horizon, in order to best achieve the overall production targets. This is made possible by incorporating the planned/known events that will disrupt future operations in the short term (maintenance, operator schedules, blasting, etc).

The objective used in existing commercial solutions is to maximise the instantaneous productivity of the mine. Taking a longer-term view of optimisation, our Flow Planner is able to consider more specific objectives, that is, achieving the production targets while minimising operating costs. The truck operating costs are simply modelled as a cost per unit time of operation per truck. The process plant feed cost is incurred when a process plant operates below a minimum desired throughput. The plan failure cost component models the revenue lost due to not meeting the production targets. Combinations of material blocks and target destinations can have different plan failure costs, enabling prioritisation, or speculative 'stretch goals' to be included.

3.1 MIP model

The units of the variables and parameters used in the MIP do not matter as long as they are consistent. While material flows are specified in terms of volume of material, this can be interchanged with material mass without consequence. The indices used in the developed MIP are as follows:

$t \in T$ time periods
$\theta \in \Theta$ truck types
$s \in S$ shovels
$i, j \in L$ locations
$b \in B$ blocks
$i, j \in D$ all dumps (process plants, stockpiles, waste dumps)
$i, j \in C$ process plants

A given shift is divided into a set of time periods $T \in \{0, 1, \ldots, t_{max}\}$. L is the set of locations. The set of blocks is a subset of locations, $B \subset L$. Similarly, $D \subset L$ indicates the set of dumps, $C \subset D$ indicates the set of process plants.

The flow rates in this model represent both the loaded truck flows (from blocks to dumps) and the empty truck flows (from dumps to blocks). For example, suppose that the flow rate from block b to process plant c is 100 kg/s at time period t. This requires an equivalent of 100 kg/s of empty trucking capacity to be arriving (empty) at block b in time period t, in order for it to also be departing (loaded). Therefore the flow of empty trucks (from dumps to blocks) is also calculated. Apart from ensuring this logical consistency, this also allows complementary flows to be discovered; it may be advantageous for trucks to alternate between two cycles that move material in opposing directions (i.e. where the empty haul routes for trucks alternating between the cycles is shorter than the empty haul of trucks remaining on the same cycle).

The following sets are defined in order to aid the description of MIP decision variables. Let N_i be the set of possible destinations for material from a location $i \in L$. If $i \in B$, then $N_i = D$ meaning that loaded trucks leaving a block cannot travel to another block, only dumps. Similarly, if $i \in D$, then $N_i = B$, which indicates that empty trucks leaving any dumps can only travel to blocks to be loaded.

359

Similar to N_i, above M_j represents the set of possible sources for material sent to a location $j \in L$; if $j \in B$, then $M_j = D$, meaning that if the destination is a block, then only empty trucks (from dumps) can travel there. Likewise, if $j \in D$, then $M_j = B$, i.e. if the destination is any dump, the source must be a block.

Decision variable $y_{t,\theta,i,j}$ is a continuous variable indicating the flow rate in time period t for truck type θ from location $i \in L$ to location $j \in N_i$. Variable $v_{t,b}$ is a continuous variable indicating the volume remaining in block b in time period t. The continuous variable $l_{t,i,b}$ denotes the volume of material type b at dump $i \in D$ in time period t. $f_{t,i}$ is a continuous variable representing the flow rate below the minimum desired flow rate into process plant $i \in C$ in time period t. The continuous variable $p_{i,b}$ denotes the gap between the target volume of material b that must be moved to dump $i \in D$ and the achieved volume. $x_{t,b} \in \{0,1\}$ is a binary variable indicating whether block b is being dug in time period t. Finally, $x^s_{t,b} \in \{0,1\}$ and $x^f_{t,b} \in \{0,1\}$ are binary variables representing the start and finish time respectively of block b; they are 0 in all time periods before the start/finish event, and 1 thereafter.

The parameters used in the MIP are as follows:

τ_t — length of time period t

c_θ — operating cost per unit time of truck type θ

ϕ_θ — capacity of truck type θ

$\gamma_{t,\theta}$ — total capacity of truck type θ available in time period t

$\alpha_{t,\theta,i,j}$ — travel time of truck type θ from location $i \in L$ to location $j \in L$ in time period t

$d_{\theta,i}$ — time taken for truck type θ to dump at location $i \in D$

$\beta_{si,\theta}$ — time taken for shovel $s \in S$ located at location $i \in B$ to load truck type θ

π_i — low feed cost of process plant $i \in C$

$\psi_{b,i}$ — cost per unit volume under plan of material $b \in B$ at dump $i \in D$

s_i — shovel allocated to block $i \in B$

$m_{si,t}$ — maximum digging rate of shovel $s \in S$ allocated to block $i \in B$ in time period t

$k_{t,i}$ — maximum flow rate into dump $i \in D$ in time period t

$e_{t,i}$ — minimum desired flow rate into process plant $i \in C$ in time period t

a_b — initial volume of material in block b

$g_{i,b}$ — initial volume of material from block b at dump $i \in D$

$h_{i,b}$ — targeted volume of material from block b to dump $i \in D$

w_b — the block that must be completed before block b

δ_b — number of time periods taken for a shovel to move to block b.

3.1.1 *Objective function*
The developed MIP comprises the cost minimisation objective (1), minimising the overall cost (shortfall, process plant low feed cost, and truck operating cost) of fulfilling a given production targets. The cost coefficients should be \$/unit-volume for the plan failure and process plant low feed costs, and \$/unit-time for the truck operating cost.

$$Z_1 = \min \sum_{b \in B, i \in D} \psi_{b,i} p_{i,b} + \sum_{t \in T, i \in C} \pi_i \tau_t f_{t,i} + \sum_{t \in T, \theta \in \Theta} \frac{\tau_t c_\theta}{\phi_\theta} \left(\sum_{i \in B, j \in N_i} y_{t,\theta,i,j} (\beta_{s_i,\theta} + \alpha_{t,\theta,i,j}) \right.$$
$$\left. + \sum_{i \in D, j \in N_i} y_{t,\theta,i,j} (d_{\theta,i} + \alpha_{t,\theta,i,j}) \right) \tag{1}$$

3.1.2 *Constraints*
The following constraint enforces flow continuity, that is, the sum of the flows going into a location is equal to the sum of the flows leaving a location.

$$\sum_{j \in M_i} y_{t,\theta,j,i} = \sum_{j \in N_i} y_{t,\theta,i,j} \quad \forall t \in T, \theta \in \Theta, i \in L \tag{2}$$

The maximum digging rate of each shovel is enforced by (3). Note that we assume that the maximum digging rate of a shovel varies by time periods; planned maintenance or other

downtimes for the shovel can be incorporated by setting the maximum digging rate to 0 in the relevant time periods, reduced performance, e.g. around shift-change, can be modelled with a reduced maximum flow in those time periods. In (3), the maximum dig rate of the shovel is multiplied by binary variable $x_{t,i}$ indicating whether the block is being dug in that time period. This, in conjunction with constraints (15)–(22), ensures that each shovel can only operate on a single block in any time period.

$$\sum_{\theta \in \Theta j \in N_i} y_{t,\theta,i,j} \le x_{t,i} m_{s_i,t} \quad \forall t \in T, i \in \mathbf{B} \tag{3}$$

Constraint (4) ensures that the maximum flow rate into a dump is not exceeded. Depending on the type of the dump, the maximum flow rate can be either the material rate going into a process plant, or computed based on the time taken by a truck to unload at a dump given the maximum number of trucks that can unload simultaneously at the dump. The extent to which a process plant is operating below its desired minimum flow rate is captured in (5), which is then penalised in the objective function.

$$\sum_{\theta \in \Theta, j \in M_i} y_{t,\theta,j,i} \le k_{t,i} \quad \forall t \in T, i \in \mathbf{D} \tag{4}$$

$$f_{t,i} \ge e_{t,i} - \sum_{\theta \in \Theta, j \in M_i} y_{t,\theta,j,i} \quad \forall t \in T, i \in \mathbf{C} \tag{5}$$

The total capacity of each truck type being used is constrained in (6) to the total capacity available. Note that the total available capacity of each truck type can vary by time periods, as trucks might be removed from the fleet for maintenance, refuelling, shift changes, and breaks.

$$\sum_{i \in B, j \in N_i} y_{t,\theta,i,j} \left(\beta_{s_i,\theta} + \alpha_{t,\theta,i,j} \right) + \sum_{i \in D, j \in N_i} y_{t,\theta,i,j} \left(d_{\theta,i} + \alpha_{t,\theta,i,j} \right) \le \gamma_{t,\theta} \quad \forall t \in T, \theta \in \Theta \tag{6}$$

The initial volume of material in a block is specified by (7), and updated for each subsequent time period in (8).

$$v_{-1,i} = a_i \quad \forall i \in \mathbf{B} \tag{7}$$

$$v_{t,i} = v_{t-1,i} - \tau_t \sum_{\theta \in \Theta j \in N_i} y_{t,\theta,i,j} \quad \forall t \in T, i \in \mathbf{B} \tag{8}$$

The initial volume of each type of material at each dump is specified by (9). The volume of material on the dump in each time period is calculated in (10) by simply integrating the incoming flows over time.

$$l_{-1,i,b} = g_{i,b} \quad \forall b \in \mathbf{B}, i \in \mathbf{D} \tag{9}$$

$$l_{t,i,b} = l_{t-1,i,b} + \tau_t \left(\sum_{\theta \in \Theta} y_{t,\theta,b,i} \right) \quad \forall t \in T, i \in \mathbf{D}, b \in \mathbf{B} \tag{10}$$

The level of conformance with the production targets is computed in (11).

$$p_{i,b} \ge h_{i,b} - l_{t_{\max},i,b} \quad \forall b \in \mathbf{B}, i \in \mathbf{D} \tag{11}$$

In order to prevent undesirable material (e.g. waste) being fed to the process plant, simply to meet its minimum feed, constraint (12) ensures that only the material specified for each dump in the production targets can be dumped at that location.

$$l_{t_{\max},i,b} \le h_{i,b} \quad \forall b \in \mathbf{B}, i \in \mathbf{D} \tag{12}$$

Constraints (13)-(17) ensure that each production target must be completed contiguously by a shovel, i.e. a shovel cannot start excavating a block before finishing the previous block. Γ_s

in Constraint (15) indicates the set of blocks allocated to shovel s. Constraints (18) and (19) ensure that blocks are extracted in the specified order, and that the time taken to move the shovel from one block to another (if any) is accounted for. Constraint (20) forces the entire volume of the target to be removed before it can be marked as finished[1].

$$\sum_{t \in T} x^s_{t,b} \leq 1 \quad \forall b \in B \tag{13}$$

$$\sum_{t \in T} x^f_{t,b} \leq 1 \quad \forall b \in B \tag{14}$$

$$\sum_{b \in \Gamma_s} x_{t,b} \leq 1 \quad \forall t \in T, s \in S \tag{15}$$

$$x_{t,b} = x_{t-1,b} + x^s_{t,b} - x^f_{t,b} \quad \forall t \in T, b \in B \tag{16}$$

$$x_{-1,b} = 0 \quad \forall b \in B \tag{17}$$

$$x^s_{t,b} = x^f_{t-\delta_b,w_b} \quad \forall t \in T \setminus \{0, \ldots, \delta_b - 1\}, b \in B \text{ if } w_b \text{ exists} \tag{18}$$

$$x^s_{t,b} = 0 \quad \forall t \in \{0, \ldots, \delta_b - 1\}, b \in B \tag{19}$$

$$a_b x^f_{t,b} \leq a_b - v_{t,b} \quad \forall t \in T, b \in B \tag{20}$$

4 NUMERICAL RESULTS

To evaluate the performance of the Flow Planner, we run it on a conceptually generated mine. The entire code was written in Python and run on a personal computer with Intel Core i7 CPU at 3.40 gigahertz, 16 gigabytes of RAM, operating under Microsoft Windows 7. Gurobi 7.5 was used to solve our MIP.

While the data for our instance is conceptual in nature, it is based on real operational scenarios with block size, tonnages, grades, resource limitations and sequencing interactions reflective of real-world open pit mining operations.

4.1 *Initial scenario*

The scenario consists of two excavators, five blocks, and five dumps (three process plants and two stockpiles). Blocks B1 and B2 are assigned to one of the excavators, and blocks B3, B4, and B5 are assigned to the other one. The planning time is a 12-hour shift, and blocks B1, B3 and B4 are high priority blocks in that the penalty of not digging them by the end of the shift is higher—in practise, this might be due to the fact that the grade in the block is important in that shift, or it is a waste block that must be removed to reach an important block. The other input data can be seen in Figure 1, which shows the optimal flow rates calculated by Flow Planner.

Figures 1(a) and 1(b) show an upper graph for the total flow rate out of the excavator, and one or more graphs below this for the flow of each block to each dump. The lower graphs sum to the total in the top graph. In Figures 1(a)–1(c), the red lines on dig/dump flow rates indicate the maximum flow rate capacity of the excavator/dump; the flow rates are constrained by this value.

The dashed red line on the summary graph (Figure 1(d)) shows the total truck capacity. The whole system is constrained by this, with the total truck capacity shared amongst all material flows at any point in time. The dashed green line is the total truck utilisation, and in time periods where this is equal to the dashed red line, the system is truck-constrained. The legend in each graph shows, for each flow target: 1) Target: the total target for the shift;

---

1. If block-switching is desirable, small repeated production targets can be specified, or a block specified in the optimisation could represent a local mix of real-world mining blocks.
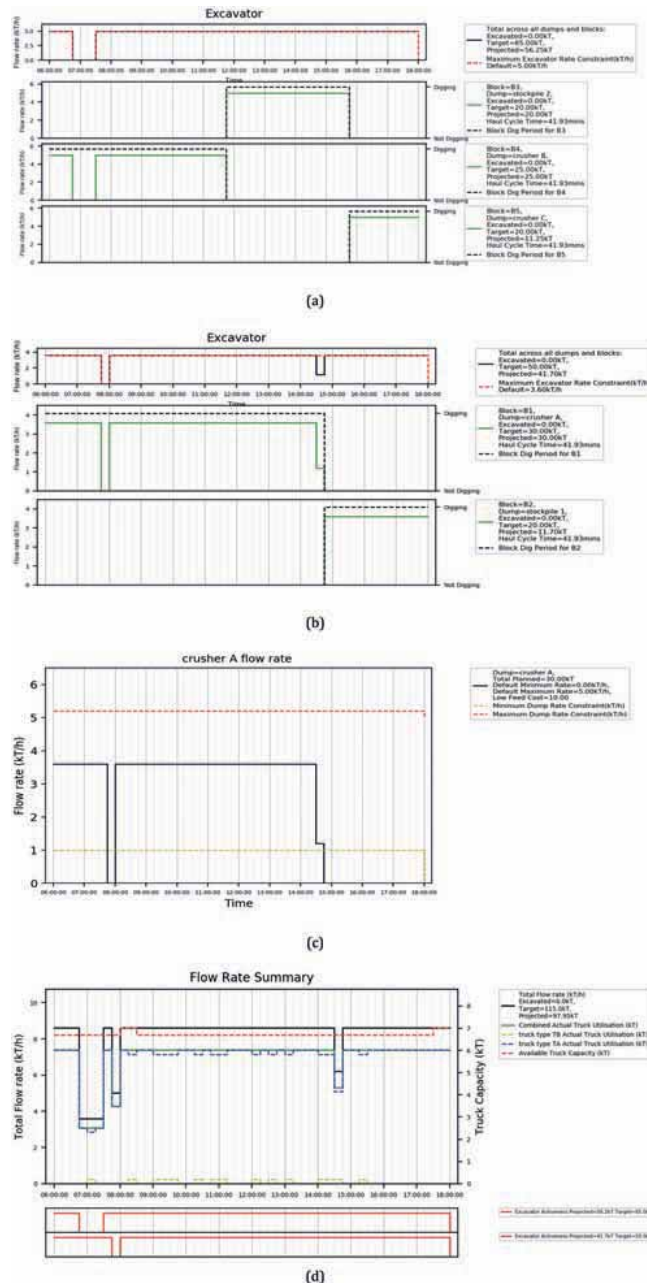
Figure 1. (a) flow rates from blocks B3-B5 to their associated dumps across the shift; (b) flow rates from blocks B1 and B2 to their associated dumps across the shift; (c) flow rates going into process plant 'A' across the shift; (d) sum of all flow rates, available and utilised truck capacities; the lower graph indicates when each digger is active/inactive as a binary up/down state.

2) Excavated: the amount of target already achieved. Flow Planner subtracts this from the given target; 3) Projected: the projection for how much will be achieved by the end of the shift according to the allocation plan. The legend in the summary graph shows these values for the entire shift.

From the summary graph, we have excess truck capacity in this scenario—this is apparent from the dashed green line (truck utilisation) being significantly lower than the dashed red

363

line (truck capacity) across the entire shift. The Flow Planner has largely neglected Truck Type B (which has a smaller tray size). As can be seen in Figure 1(a), the excavator is down from 06:45 to 07:30, and thus the flow rate is zero during this time interval. This excavator digs block B4 from 06:00 until 11:45—apart from the down-time—before starting on B3. Block B5 is the last block due to its lower priority.

Figure 1(c) shows the material flow rate into process plant 'A'. Between 7:45 and 8:00, the excavator digging block B1 is down, and since this is the only block going to process plant 'A', the total incoming rate to this process plant is zero.

4.2 Re-planning (feedback control)

The Flow Planner also enables feedback control on material quantity targets. To demonstrate this, suppose that process plant 'A' unexpectedly breaks down at 13:00. Since unexpected, the generated allocation plan has not taken this downtime into account, and continuing with this plan for the remaining part of the shift may no longer be optimal. In such situations, Flow Planner takes into account the amount already excavated since the beginning of the shift till now, and is re-run to generate a new plan for the rest of the shift. Figure 2 shows the new plan from 13:00 to the end of the shift. The maximum dump rate in Figure 2(a) is zero between 13:00 and 15:00, implying that the process plant is offline. No flows go to process plant 'A' in the new plan, as Flow Planner digs block B2—rather than B1— at 13:00, and the excavator cannot finish B2 by the end of the shift (the projected value for this block is 18 KT, meaning that 18 KT of the block can be extracted by the end of the shift). In the same figure, the excavated value of block B1 is 24.30 KT, meaning that 24.30 KT have already been extracted before 13:00 within the plan in Figure 1, and the remaining 5.70 is never extracted since the excavator only works on B2 after 13:00.

4.3 Comparison

We now examine the improvements that Flow Planner brings to truck dispatching systems by comparing it to the LP developed by White and Olson (1986). Due to the nature of the contributions in Flow Planner, making a fair, meaningful comparison with existing algorithms is difficult; this is mainly because the advantage of Flow Planner over existing methods is generating an optimal allocation plan for the entire shift and incorporating the disruption events, such as maintenance and breaks, and scheduled changes in equipment availabilities throughout the shift. In exiting commercial packages, however, these are handled by a human operator. Nevertheless, we try to mimic the human based process to run the LP of White and Olson (1986) for the entire shift and compare the output with that of Flow Planner. We consider five case studies similar to the one described earlier in this section. All these examples include excavator downtimes and changes in truck availabilities across a 12-hour shift, and the targets are given for the entire shift. The mentioned LP is able to take the targets for the entire shift, but is unable to see the excavator downtimes and truck availability changes as well as the given extraction order of blocks. Therefore, to be able to obtain a plan for the entire shift from the LP, we run it every time one of the following occurs: 1) a block is completed—this is to cope with the fact that the LP does not consider the extraction order, and in practise, a human operator would run the system again to make new decisions for the next block; 2) the truck capacity changes; 3) an excavator goes offline; and 4) an excavator returns online. In every run, the state of the mine (i.e. input data) must be updated manually, e.g., subtracting the amount of material that has already been moved from the total target, and updating equipment availability. The blending of the process plant feed in the LP is controlled through a constraint that ensures the blend of material fed into a process plant is within acceptable bounds (for brevity, we refer the reader to White and Olson (1986) for details on this constraint). To have a fair comparison, we added this constraint to Flow Planner. Since the parameters of this constraint did not exist in our case study data, we generated them randomly.

Table 1 records the outputs of both Flow Planner and the LP on the five case studies. The second column indicates the number of runs needed to obtain a full plan for the entire shift
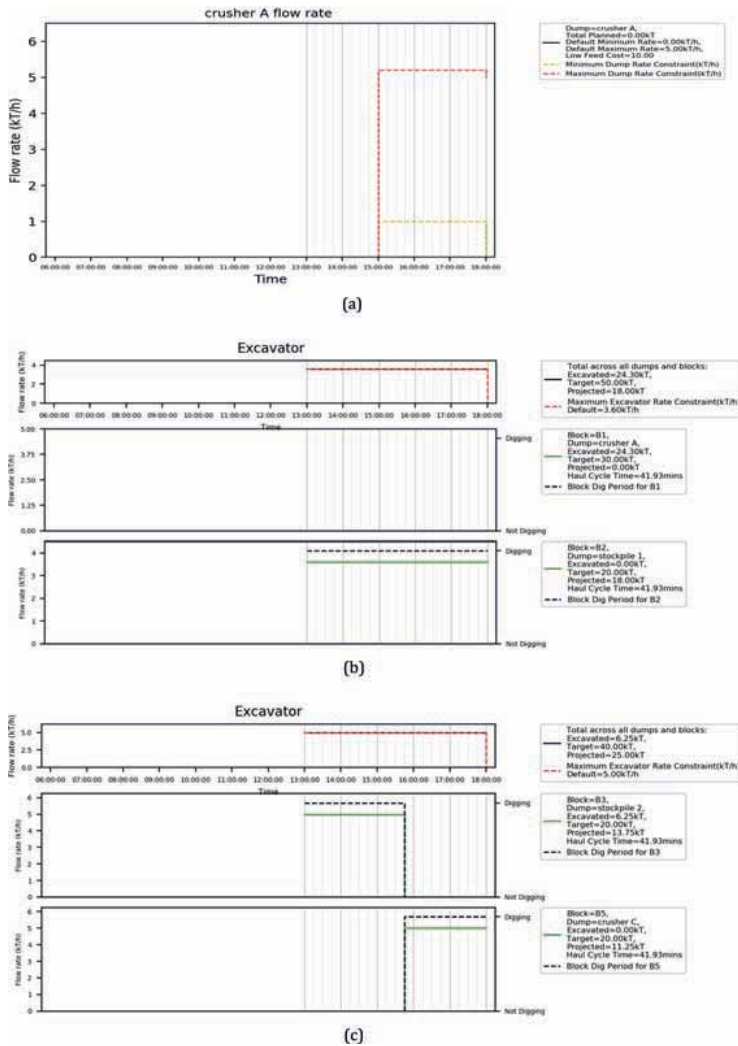
Figure 2. (a) flow rate going into process plant 'A' after re-running Flow Planner at 13:00; (b)–(c) flow rates from blocks to their associated dumps after the re-run.

Table 1. A comparison between the technique developed by White and Olson (1986) and Flow Planner.

Instance	Number of runs needed by LP	Number of runs needed by flow planner	Total target achievement by LP	Total target achievement by flow planner
1	11	1	61.8%	93.4%
2	12	1	58.3%	96.5%
3	9	1	73.6%	98.4%
4	16	1	51.6%	93.7%
5	7	1	68.2%	95.9%
Mean	...	...	**62.70%**	**95.58%**

by the LP. The third column indicates that Flow Planner simply needs to be run only once to provide a plan for the shift. Having to run the LP several times and manually updating the state of the mine across the shift is not the only disadvantage of the old LP; not considering the upcoming events can result in a plan that is far from optimality. The fourth and fifth columns

365

in Table 1 record the percentage of total target that has been fulfilled by the end of the shift by the LP and Flow Planner, respectively (note that the total target given to both algorithms is high enough that is not completely achievable by the end of the shift using the given capacity). From the table, only 61.8% of the target has been met by the LP in the first instance, whereas Flow Planner achieves 93.4%. The average achievement over all instances is only 62.70% by the LP while the average of achievement by Flow Planner is 95.58%. Note that both algorithms are very fast, solving realistic scenarios in seconds, and therefore we did not represent the solution times.

5   CONCLUDING REMARKS

We presented the Flow Planner system to generate haulage allocation plans from production targets. This is the first component of plan-driven dispatching systems in open pit mines. In contrast to existing techniques, the proposed Flow Planner optimises production for the entire shift (or similar period) rather than only instantaneous production, and takes into account upcoming events, such as maintenance and blasts, as well as changes in equipment availability or performance throughout the shift. This allows for better decision making across the full period, reducing the need for an operator to closely monitor and update the plan every time the state of the mine changes. Our Flow Planner additionally considers the flow of empty trucks and enables feedback control on material quantity targets.

The Flow Planner output was described after running it on a conceptually generated, yet realistic, mining scenario. The Flow Planner was compared to an existing plan-driven technique, where five case studies were considered. Our results indicated that an operator would have had to perform the updating and re-running process 7–16 times to be able to cover the entire shift, whereas Flow Planner generated the plan by a single run. The results also showed that the performance of the plan—measured as production target completion—generated by Flow Planner is significantly higher than that of LP; 95.58% of targets were achieved by Flow Planner, whereas the achievement was only 62.70% by the LP.

Future work will consider unexpected disruptions using stochastic and/or robust techniques so that Flow Planner can better prioritise material movements, rather than relying on manual tuning.

REFERENCES

Alarie, S. and M. Gamache (2002). "Overview of solution strategies used in truck dispatching systems for open pit mines." *International Journal of Surface Mining, Reclamation and Environment* **16**(1): 59–76.

Bonates, E. and Y. Lizotte (1988). "A combined approach to solve truck dispatching problems." *Computer Application in the Mineral Industry, Fystas, Collins & Singhal (eds), Balkema, Rotterdam*: 403–412.

Burt, C.N. and L. Caccetta (2007). "Match factor for heterogeneous truck and loader fleets." *International journal of mining, reclamation and environment* **21**(4): 262–270.

Munirathinam, M. and J.C. Yingling (1994). "A review of computer-based truck dispatching strategies for surface mining operations." *International Journal of Surface Mining and Reclamation* **8**(1): 1–15.

Soumis, F., J. Ethier and J. Elbrond (1989). "Evaluation of the new truck dispatching in the Mount Wright Mine." *Application of Computers and Operations Research in the Mineral Industry*: 674–682.

Subtil, R.F., D.M. Silva and J.C. Alves (2011). *A practical approach to truck dispatch for open pit mines.* 35Th APCOM symposium.

Ta, C.H., J.V. Kresta, J.F. Forbes and H.J. Marquez (2005). "A stochastic optimization approach to mine truck allocation." *International journal of surface mining, reclamation and environment* **19**(3): 162–175.

Upadhyay, S. and H. Askari-Nasab (2016). "Truck-shovel allocation optimisation: a goal programming approach." *Mining Technology* **125**(2): 82–92.

White, J. and J. Olson (1986). "Computer-based dispatching in mines with concurrent operating objectives." *Min. Eng. (Littleton, Colo.); (United States)* **38**(11).

White, J.W., J. Olson and S. Vohnout (1993). "On improving truck/shovel productivity in open pit mines." *CIM bulletin* **86**(973): 43–49.

Short-term production scheduling of multiple mines using genetic algorithms

P. Pathak & B. Samanta

Indian Institute of Technology Kharagpur, Kharagpur, West Bengal, India

ABSTRACT: Short-term production scheduling of a mine determines the extraction sequence of blocks on a shorter scale of months, weeks or days. It models the mine operations in great detail and it typically aims to meet the quality and quantity targets of production in each period. Over the years, a number of models have been developed to optimize the short-term production scheduling problem of the mines. However, most of these models were developed for single mines. This paper presents a model to optimize short-term production schedules of mineral value chains comprising of multiple mines. In addition, a genetic algorithm based heuristic approach has been presented to tackle industrial scale instances of short-term production scheduling problem which exact solution techniques cannot solve within a reasonable amount of time. Computational experiments suggest that the presented approach is a promising way to handle complex industrial scale instances of short-term production scheduling problem.

1 INTRODUCTION

Short-term production scheduling plays a pivotal role in optimizing the operations of a mine. It is carried out on a shorter scale with a granularity that typically spans from a week to a month (at maximum) and a horizon which spans from few months to a year (Blom et al. 2018). It seeks to find out, for each short period, the combination of mining blocks which should be extracted, the time at which they should be extracted and the destinations at which they should be sent such that the quality and quantity requirements are met consistently subject to the technical and operational constraints of production. Often, the short-term production scheduling is carried out under the scope of long-term production scheduling and thus the former also plays a key role in linking the operational level activities of a mine to its strategic intent.

Researchers, over the years, have developed a number of models to optimize the short-term production scheduling problem (Sundar & Acharya 1995, Smith 1998, Askari_Nasab et al. 2011, Eivazy & Askari-Nasab 2012, Bakhtavar & Oraee 2012, Mousavi et al. 2014, Kumar & Chatterjee 2016, Matamoros & Dimitrakopoulos 2016, Mousavi et al. 2016, Morales & Reyes 2016). However, most of these models were developed for mineral value chains comprising of a single mine. Also, majority of these models were solved through exact solution techniques which can only handle small scale instances of the problem and are unable to solve industrial scale problems within a reasonable amount of time (Mousavi et al. 2014).

In this study, a generalized mathematical formulation to optimize the short-term production scheduling of mineral value chains comprising of multiple mines has been presented. The formulation nearly models all the relevant technical, practical and operational aspects of short-term production scheduling problem. In addition, a genetic algorithm based heuristic has also been designed to tackle industrial scale instances of the problem.

2 MATHEMATICAL MODEL

The short-term production scheduling problem of mineral value chains comprising of multiple mines has been formulated as a mixed integer linear programming problem (MILP).

It aims to minimize deviations from quality and quantity targets of processing plants, total transportation costs and total rehandling costs subject to all the practical and operational constraints of production. The notation used in the mathematical model follows:

2.1 *Indices*

m: Mine index, m = 1, 2, …, M
p: Processing plant index, p = 1, 2, …, P
s: Stockpile index, s = 1, 2, …, S
w: Waste dump index, w = 1, 2, …, W
d: Destination index, d = 1, 2, …, D
t: Time period index, t = 1, 2, …, T
e: Element index, e = 1, 2, …, E
i_m: block index for mine m, i = 1, 2, …, I_m

2.2 *Parameters*

I_m: Number of blocks in mine m
Pre_{im}:   set of predecessors of block i of mine m
MC_m^t: Mining Capacity of mine m in period t (in tonnes)
$grade_{im}^e$:   Percentage of element e in block i of mine m
$tonnage_{im}$:   Tonnage of block i of mine m (in tonnes)
$tar\_prod_p^t$:   Target production requirement of processing plant p in period t (in tonnes)
$tol\_prod\_pos_p^t$:   Allowed positive tolerance from production target of plant p in period t (%)
$tol\_prod\_neg_p^t$:   Allowed negative tolerance from production target of plant p in period t (%)
$min\_prod_p^t$:   Minimum production requirement for plant p in period t (in tonnes)

$$min\_prod_p^t = \left(tar\_prod_p^t - \left(tar\_prod_p^t * tol\_prod\_neg_p^t\right)\right) \forall p = 1,2,\dots,P; t = 1,2,\dots,T$$

$max\_prod_p^t$:   Maximum production requirement for plant p in period t (in tonnes)

$$max\_prod_p^t = \left(tar\_prod_p^t + \left(tar\_prod_p^t * tol\_prod\_pos_p^t\right)\right) \forall p = 1,2,\dots,P; t = 1,2,\dots,T$$

$tar\_grade_{ep}^t$:   Target grade requirement of element e at plant p in time period t
$tol\_grade\_pos_{ep}^t$: Percentage of positive tolerance allowed for element e at plant p in period t
$tol\_grade\_neg_{ep}^t$: Percentage of negative tolerance allowed for element e at plant p in period t
$min\_grade_{ep}^t$:   Minimum grade requirement of element e at plant p in period t

$$min\_grade_{ep}^t = \left(tar\_grade_{ep}^t - tol\_grade\_neg_{ep}^t\right)$$
$$\forall e = 1,2,\dots,E; p = 1,2,\dots,P; t = 1,2,\dots,T$$

$max\_grade_{ep}^t$:   Maximum grade requirement of element e at plant p in period t

$$max\_grade_{ep}^t = \left(tar\_grade_{ep}^t + tol\_grade\_pos_{ep}^t\right)$$
$$\forall e = 1,2,\dots,E; p = 1,2,\dots,P; t = 1,2,\dots,T$$

$pen\_prod\_pos_p^t$: Penalty cost for positive deviations from target tonnage requirements for plant p in period t (in Rs/tonne)
$pen\_prod\_neg_p^t$: Penalty cost for negative deviations from target tonnage requirements for plant p in period t (in Rs/tonne)
$pen\_grade\_pos_{ep}^t$: Penalty cost for positive deviations of element e from its target grade requirements for plant p in period t (in Rs/tonne)

368

$pen\_grade\_neg^t_{ep}$: Penalty cost for negative deviations of element e from its target grade requirements for plant p in period t (in Rs/tonne)

Inv^0_s : Initial inventory of stockpile s

Inv^t_s : Inventory of stockpile s at the start of period t

Cap_s : Capacity of stockpile s

$min\_grade^t_e$: Minimum acceptable grade of element e at destination d in time period t

$max\_grade^t_{ep}$: Maximum acceptable grade of element e at destination d in time perd t

avg_grade_{es} : Average grade of element e reclaimed from stockpile s

$dist_{ab}$: Distance between element a and element b of the mineral value chain

$haul\_cost$: Cost associated with hauling materials

$rehandling\_cost_{sp}$: Cost associated with reclaiming materials from stock s to plant p

pen_MC_m : Penalty cost associated with violation of production from maximum mining capacity for mine m

2.3 Decision variables

x^t_{imd} : A binary decision variable which takes a value of 1 when block i of mine m is sent to destination d in time period t and 0 otherwise

y^t_{sp} : A continuous decision variable representing the amount of material reclaimed from stockpile s and sent to processing plant p in period t

$dev\_prod\_pos^t_p$: A continuous decision variable representing surplus production from the upper limit of tonnage target of plant p in period t

$dev\_prod\_neg^t_p$: A continuous variable representing shortage in production from the lower limit of tonnage target of plant p in period t

$dev\_grade\_pos^t_{ep}$: A continuous variable representing the tonnage of deviation from the upper limit of grade requirement for element e in plant p in period t

$dev\_grade\_neg^t_{ep}$: A continuous variable representing the tonnage of deviation from lower limit of grade requirement for element e in plant p in period t

$dev\_MC^t_m$: A continuous variable representing negative deviation from maximum possible mining capacity of mine m in period t

2.4 Objective function

Minimize

$$\sum_{t=1}^{T}\sum_{d=1}^{D}\sum_{m=1}^{M}\sum_{i=1}^{I_m}\left(x^t_{imd} * tonnage_{im} * dist_{md} * haul\_\cos t\right) + \sum_{t=1}^{T}\sum_{p=1}^{P}\sum_{s=1}^{S}(y^t_{sp} *$$
$$rehandling\_cost_{sp}) + \sum_{t=1}^{T}\sum_{p=1}^{P}(dev\_prod\_pos^t_p * pen\_prod\_pos^t_p + dev\_prod\_neg^t_p *$$
$$pen\_prod\_neg^t_p) + \sum_{t=1}^{T}\sum_{p=1}^{P}\sum_{e=1}^{E}(dev\_grade\_pos^t_{ep} * pen\_grade\_pos^t_{ep} +$$
$$dev\_grade\_neg^t_{ep} * pen\_grade\_neg^t_{ep}) + \sum_{t=1}^{T}\sum_{m=1}^{M}\left(dev\_MC^t_m * pen\_MC_m\right)$$

(1)

2.5 Constraints

$$\sum_{t=1}^{T}\sum_{d=1}^{D}x^t_{imd} \le 1 \quad \forall m=1,2,\ldots,M; i=1,2,\ldots,I_m \tag{2}$$

$$\sum_{t=1}^{T}\sum_{d=1}^{D}(x^t_{imd} * tonnage_{im}) \le MC^t_m \quad \forall m=1,2,\ldots,M; t=1,2,\ldots,T \tag{3}$$

$$\sum_{t=1}^{T}\sum_{d=1}^{D}(x^t_{imd} * tonnage_{im}) + dev\_MC^t_m \ge MC^t_m \quad \forall m=1,2,\ldots,M; t=1,2,\ldots,T \tag{4}$$

$$\sum_{r=1}^{t}\sum_{d=1}^{D}x^r_{imd} \le \sum_{t=1}^{T}x^t_{jmd} \quad \forall m=1,2,\ldots,M; \left(i,j \in \{1,2,\ldots,I_m\}; i \ne j; j \in pre_{im}\right) \tag{5}$$

$$\sum_{m=1}^{M} \sum_{i=1}^{I_m} (x_{imp}^{t} * tonnage_{im}) + \sum_{s=1}^{S} y_{sp}^{t} - dev\_prod\_pos_{p}^{t} \geq max\_prod_{p}^{t}$$
$$\forall p = 1, 2, \ldots, P; t = 1, 2, \ldots, T \tag{6}$$

$$\sum_{m=1}^{M} \sum_{i=1}^{I_m} (x_{imp}^{t} * tonnage_{im}) + \sum_{s=1}^{S} y_{sp}^{t} + dev\_prod\_neg_{p}^{t} \geq min\_prod_{p}^{t}$$
$$\forall p = 1, 2, \ldots, P; t = 1, 2, \ldots, T \tag{7}$$

$$\sum_{m=1}^{M} \sum_{i=1}^{I_m} \left(x_{imp}^{t} * tonnage_{im} * \left(grade_{im}^{e} - min\_grade_{ep}^{t} \right) \right)$$
$$+ \sum_{s=1}^{S} (y_{sp}^{t} * (avg\_grade_{es} - min\_grade_{ep}^{t})) + dev\_grade\_neg_{ep}^{t} \geq 0$$
$$\forall e = 1, 2, \ldots, E; p = 1, 2, \ldots, P; t = 1, 2 \tag{8}$$

$$\sum_{m=1}^{M} \sum_{i=1}^{I_m} \left(x_{imp}^{t} * tonnage_{im} * \left(grade_{im}^{e} - max\_grade_{ep}^{t} \right) \right)$$
$$+ \sum_{s=1}^{S} (y_{sp}^{t} * (avg\_grade_{es} - max\_grade_{ep}^{t})) - dev\_grade\_pos_{ep}^{t} \leq 0$$
$$\forall e = 1, 2, \ldots, E; p = 1, 2, \ldots, P; t = 1, 2, \ldots, T \tag{9}$$

$$\sum_{m=1}^{M} \sum_{i=1}^{I_m} \left(x_{ims}^{t} * tonnage_{im} * \left(grade_{im}^{e} - min\_grade_{es} \right) \right) \geq 0$$
$$\forall e = 1, 2, \ldots, E; s = 1, 2, \ldots, S; t = 1, 2, \ldots, T \tag{10}$$

$$\sum_{m=1}^{M} \sum_{i=1}^{I_m} \left(x_{ims}^{t} * tonnage_{im} * \left(grade_{im}^{e} - max\_grade_{es} \right) \right) \leq 0$$
$$\forall e = 1, 2, \ldots, E; s = 1, 2, \ldots, S; t = 1, 2, \ldots, T \tag{11}$$

$$Inv_{s}^{0} + \sum_{m=1}^{M} \sum_{i=1}^{I_m} \sum_{r=1}^{t} (x_{ims}^{r} * tonnage_{im}) - \sum_{p=1}^{P} \sum_{r=1}^{t} y_{sp}^{r} \leq Cap_{s}$$
$$\forall s = 1, 2, \ldots, S; t = 1, 2, \ldots, T \tag{12}$$

$$\sum_{p=1}^{P} y_{sp}^{1} \leq Inv_{s}^{0} \quad \forall s = 1, 2, \ldots, S; t = 1 \tag{13}$$

$$\sum_{p=1}^{P} y_{sp}^{t} \leq Inv_{s}^{0} + \sum_{m=1}^{M} \sum_{i=1}^{I_m} \sum_{r=1}^{(t-1)} \left(x_{ims}^{r} * tonnage_{im} \right) + \sum_{p=1}^{P} \sum_{r=1}^{(t-1)} y_{sp}^{r}$$
$$\forall s = 1, 2, \ldots, S; t = 2, 3, \ldots, T \tag{14}$$

$$\sum_{m=1}^{M} \sum_{i=1}^{I_m} \left(x_{imw}^{t} * tonnage_{im} * \left(grade_{im}^{e} - min\_grade_{ew} \right) \right) \geq 0$$
$$\forall e = 1, 2, \ldots, E; w = 1, 2, \ldots, W; t = 1, 2, \ldots, T \tag{15}$$

$$\sum_{m=1}^{M} \sum_{i=1}^{I_m} \left(x_{imw}^{t} * tonnage_{im} * \left(grade_{im}^{e} - max\_grade_{ew} \right) \right) \leq 0$$
$$\forall e = 1, 2, \ldots, E; w = 1, 2, \ldots, W; t = 1, 2, \ldots, T \tag{16}$$

The objective function (Equation (1)) aims to minimize total costs. This include total transportation cost associated with hauling of materials from different mines to different destinations, total rehandling cost associated with reclaiming of materials from stockpiles to different plants and penalty costs associated with violations from target tonnage requirements, target grade requirements and maximum possible mining capacity of the mines. The objective function has to be minimized subject to a number of constraints. The fact that the blocks from each of the mines cannot mined more than once is ensured by constraint (2). Constraints (3) and (4) ensure that the maximum possible production capacity for each mine is met in each period with any deviations from the former being penalized in the objective function. Constraint (5) ensures that the precedence relationships between the blocks for each mine always remain satisfied. Constraint (6) and (7) ensure that the tonnage

targets are met for all the processing plants in each period with any deviations from the upper and lower limits of tonnage requirements being penalized in the objective function. Similarly, constraints (8) and (9) ensure that the target grade requirements for all the elements are met as closely as possible for all the plants in each period. Again, any deviations from the upper and lower limits of grade requirements for every element are penalized in the objective function. Constraint (10) and (11) ensure that the average grade of element e in the material sent to the stockpiles is within the acceptable grade range. Constraint (12) ensures that the inventory of a stockpile at any point cannot exceed its capacity. Constraint (13) and (14) are concerned with the flow of materials from the stockpiles. They ensure that the amount of material reclaimed from a stockpile at a period cannot exceed the inventory of that stockpile at the end of previous period. Constraint (15) and (16) ensure that the average grade of element e sent to the waste dumps is within the acceptable grade range of the dump.

3 GENETIC ALGORITHM BASED SOLUTION APPROACH

The industrial scale instances of short-term production scheduling problem of multiple mines can be a huge problem containing close to thousand to millions of variables and constraints. Such problems cannot be solved by standard solvers within a reasonable amount of time (Mousavi et al. 2014). This paves the way for heuristic techniques which can give suboptimal solutions for such problems within a reasonable amount of computational time. In this section, the popularly known genetic algorithm that has been customized to solve such problems is presented.

3.1 Encoding of schedules

Genetic algorithm relies on encoding of data from phenotype (physical) to genotype (gene) form. In this work, the production schedule i.e. the sequence in which the blocks would be extracted from the mines is expressed as an array of integers (from left to right) with the integers being the ID's of blocks. Also, the time period at which a particular block would be extracted is determined on the basis of its position in the array as well as the mining capacity of the mine. Figure 1 shows the encoding procedure for a sample 2D block model with a mining capacity of 3 blocks per period.

3.2 Generation of initial population

Generation of initial population is the first step in the implementation of any genetic algorithm. In this study, topological sorting technique has been used for the same. In this technique, the block arrangement is first converted into a directed graph with the blocks forming the nodes and the precedence relationships between the blocks forming the arcs. The arcs are directed from a block to all its predecessors. To generate sequences for a mine, a node, of all the nodes having no outgoing arcs, is randomly selected from the graph. The selected node, along with all its incoming arcs, is then removed from the directed graph. This process is then repeated until all the nodes have been removed from the graph. The order in which the nodes are removed gives a sequence for the mine.
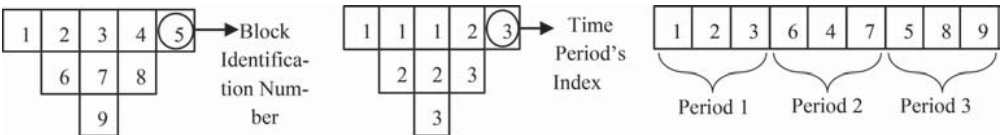
Figure 1. (a) Sample 2D block model; (b) Phenotype representation; (c) Genotype representation.
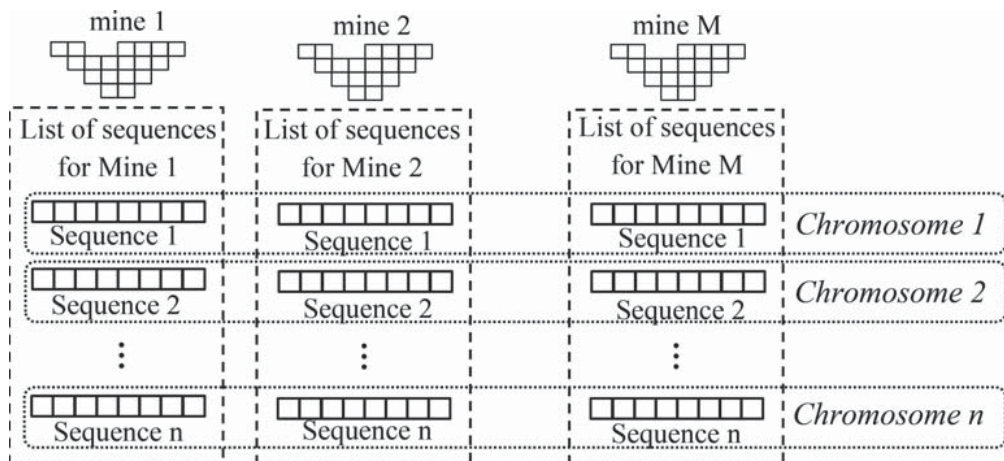
Figure 2.   Chromosomes of the initial population.

The number of chromosomes in the initial population is taken as an input. The afore-mentioned process is then repeated to generate the inputted number of sequences for all the mines. The sequences, one from each of the mine, are then grouped to form chromosomes of the initial population. As shown in Figure 2, the set of first, second and nth sequences of all the mines forms the first, second, and nth chromosome respectively of the initial population.

3.3   *Destination allocation mechanism*

A chromosome stores the sequence in which the blocks would be extracted from all the mines. Once the sequences are known, appropriate destinations have to be ascertained for all the blocks in each chromosome. In this study, CPLEX has been used for this. The allocation of destinations is done on a period wise manner. Thus, in each period, a MILP formula-tion is solved in CPLEX to obtain the destinations for all the blocks in that period. This procedure is then repeated until destinations of all the blocks in all the chromosomes have been found.

3.4   *Fitness assessment*

The next step is concerned with assessment of fitness for all the chromosomes in the popula-tion. For this, a fitness assessment function is required. In this study, Equation (1) has been used to assess the fitness of all the chromosomes at every generation (iteration).

3.5   *Reproduction operator*

The job of a reproduction operator is to emphasize the good solutions and to eliminate the bad ones from the population while keeping the population size constant. In this study, *binary tournament selection operator* has been used for selecting chromosomes to the mating pool. In this operator, a tournament is played between two randomly selected individuals of the population with the fitter individual making it to the mating pool. This operator has been designed in such a way that each individual would participate in the tournament exactly twice. Thus, a chromosome could have either zero, one or a maximum of two copies in the mating pool depending upon its fitness value relative to other chromosomes. This strategy ensures that, at any generation, the worst and the fittest chromosome have zero and two cop-ies respectively in the mating pool.

3.6 *Crossover operator*

The crossover operation produces newer offspring (new chromosomes) from the parents (old chromosomes) by exchanging information (genes) among the latter. A crossover probability decides the number of chromosomes which would undergo crossover at every generation.

In this study, the design of the crossover operator was a tricky task as crossover operators, if normally employed, might produce sequences which violate the precedence relationship among blocks. Keeping this in mind, following crossover operators have been designed:

3.6.1 *Similar before point crossover (SBPX) operator*
The operation of SBPX operator is carried out in two steps. In the first step, a crossover point is randomly selected and all the blocks which lie on left hand side of the point are directly copied from the parents to corresponding offspring i.e. from parent 1 to offspring 1 and from parent 2 to offspring 2. In the second step, the blocks are cross copied i.e. from parent 1 to offspring 2 and from parent 2 to offspring 1 while maintaining the relative order of blocks in the parents to generate new chromosomes.

3.6.2 *Similar after point crossover (SAPX) operator*
SAPX's operation is similar to SBPX except the fact that in the first step, instead of directly copying all the blocks which lie on the left hand side, all the blocks which lie on the right hand side of randomly selected crossover point are directly copied from corresponding parents to the offspring. The second step of its operation is exactly the same as that of SBPX.

3.6.3 *Similar before and after 2 point crossover (SBA2PX) operator*
In this crossover operator, instead of one, two crossover points are randomly selected in the first step. Then, all the blocks which lie on the left hand side and right hand side of the first and second crossover points respectively are directly copied from the parents to corresponding offspring. Again, the second step of its operation is exactly similar to SBPX.

3.7 *Mutation operator*

In mutation operation, the genes of a chromosome are tweaked a little to induce some variations in the same. This invokes and maintains diversity in the population thereby avoiding premature convergence of the algorithm. A mutation probability, similar to crossover, determines the number of chromosomes which would undergo mutation.

Similar to crossover operators, the mutation operator has to be designed in such a way that the precedence relationship between the blocks is always satisfied. Thus, in the designed mutation operator, a block is randomly selected from period 1 and it along with all its successors extracted in period 1 are moved to period 2. The space vacated by the moved blocks is then filled by shifting blocks from period 2 to period 1 from right to left while maintaining the same relative order. The sequence produced after the movement of blocks is then checked for its precedence feasibility. If the generated sequence is feasible, it is accepted and if infeasible, another move is tried between period 1 and 2 until a feasible move is found. This process is then repeated for all the consecutive periods until the blocks are moved between the second last and the last period.

4 CASE STUDY

The proposed model and the solution approach were applied to a real iron ore mine in India. This is a captive mine which supplies iron ore to India's largest steel making company. The mine has 4 pits in operation to meet the quality and quantity requirements of the 2 processing plants. In this case study, 1212 blocks from the 4 pits to be extracted over a horizon of 1 year were taken. The granularity of a time period is one month and thus the problem has

Table 1. Mine parameters.

Parameters	Mine-1	Mine-2	Mine-3	Mine-4
Block Size (x*y*z) (in meters)	20 * 15 * 6	20 * 15 * 6	30 * 24 * 10	30 * 16 * 10
Maximum mining capacity (in kt/month)	119	97	626	475

Table 2. Processing plants parameters.

Parameters	Plant-1	Plant-2
Target production range (in kt/month)	142–157	807–892
Target iron (Fe%) range	60.5–63.5	60–62
Target silica (SiO2%) range	2–4	4–6
Target alumina (Al2O3%) range	3–5	3–5
Penalty cost for tonnage violation (in Rs/tonne)	150	150
Penalty cost for grade violation for Fe, Sio2 and Al2O3 (in Rs/tonne)	50	50

Table 3. Genetic algorithm's parameters.

Parameters	Value
Number of chromosomes in the initial population	20
Crossover probability	0.9
Mutation probability	0.2

Table 4. Comparing genetic algorithm and CPLEX.

Characteristic	CPLEX	Genetic algorithm	Gap (in %)
Objective function value (in million rupees)	26.7	27.6	+3.41%
Computational time (in hours)	29.33	0.93	

been solved for 12 time periods (1 year). The details of some of the important parameters taken as an input to the model are shown in Table 1, Table 2 and Table 3.

The short-term production scheduling problem for the year was then solved using the proposed genetic algorithm to generate month-wise schedules for the pits. In addition, to compare the solution quality and the execution efficiency of the genetic algorithm, the problem was also solved in IBM ILOG CPLEX in a computer having 2.90 Gigahertz of processor and 8GB of RAM. Table 4 shows a comparison between the proposed heuristic technique and CPLEX.

In order to handle the non-linearity associated with stockpiles in CPLEX and to make the model linear, binning approach was used in which each stockpile was further discretized into smaller bins with tight grade ranges for all the elements.

Figure 3 above shows the details of material flow to the two plants. It can be seen that the tonnage requirements of both the plants fall within the upper and lower tolerance limits for almost all the time periods. Similarly, the average Fe% and SiO2% of material fed to both the plants also fall within the tolerance limits in all the time periods. As far as Al2O3% fed to both the plants is concerned, the values fall below the lower tolerance limit for all the time periods. This can be attributed to low in-situ variability of Al2O3% in the deposit.

(a). Tonnage sent to Plant-1

(b). Tonnage sent to Plant-2

(c). Average Fe (%) sent to Plant-1

(d). Average Fe (%) sent to Plant-2

(e). Average SiO2 (%) sent to Plant-1

(f). Average SiO2 (%) sent to Plant-2

(g). Average Al2O3 (%) sent to Plant-1

(h). Average Al2O3 (%) sent to Plant-2
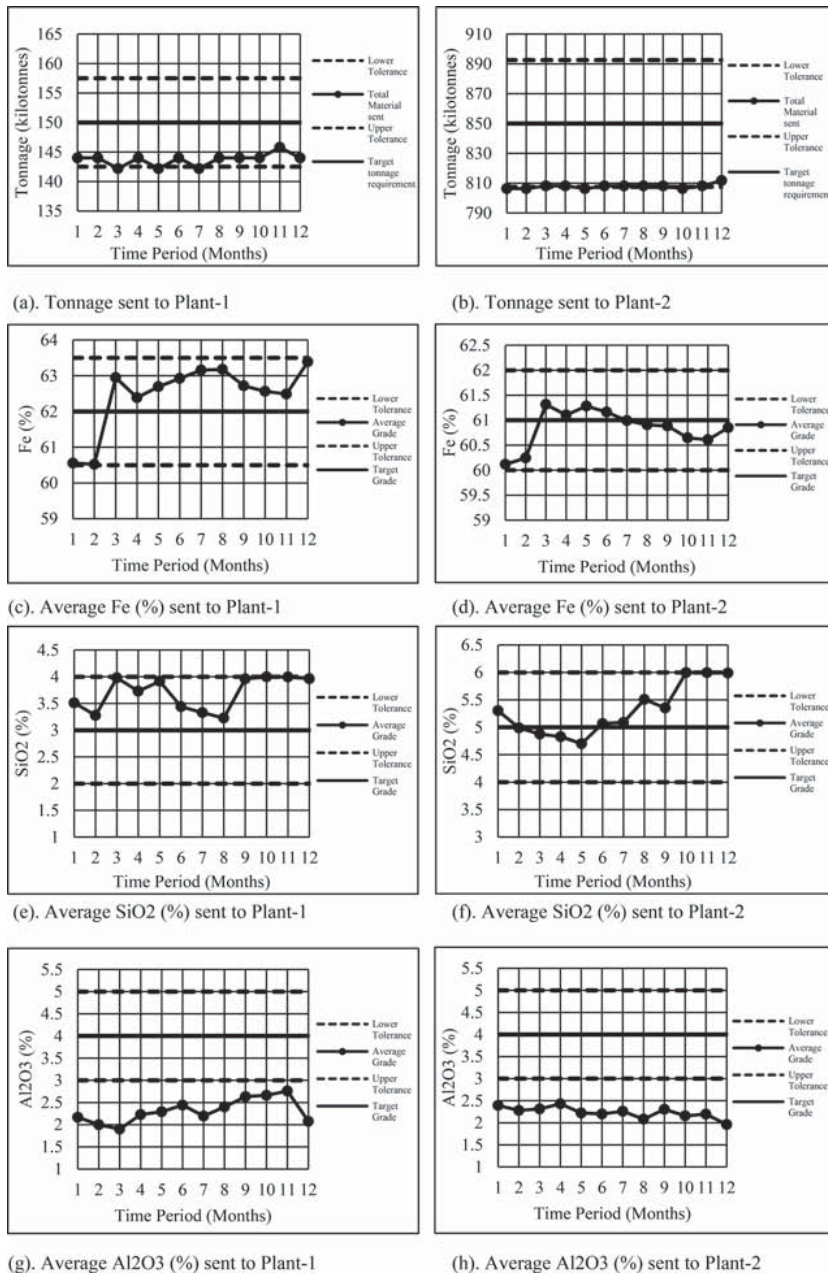
Figure 3. Details of material flow to processing plants given by genetic algorithm.

5 CONCLUSION

This paper presented a new mathematical formulation to model the short-term production scheduling problem of mineral value chains comprising of multiple mines. The model presented here aims to closely meet the quality and quantity requirements of all the processing plants in each period subject to the technical and operational constraints. In addition, a genetic algorithm based heuristic technique was also presented herein to solve industrial scale instances of the problem within a reasonable amount of time. The presented model and the

solution technique were then used to solve short-term production scheduling problem of a real iron ore mine. Also, to compare the solution quality and the execution efficiency of the heuristic technique, the same problem was also solved using IBM ILOG CPLEX. Upon comparison it was found that, in terms of solution quality, the deviation of genetic algorithm from CPLEX was less than 5% and it took CPLEX about 28 more hours to obtain the solution. This suggests that the proposed genetic algorithm based heuristic technique is a promising way to handle industrial scale instances of the short-term production scheduling problem of multiple mines as larger instance would become intractable for CPLEX. Moreover, the heuristic technique allows one to handle the non-linearity associated with the stockpiles and to track the quality of the material sent to and reclaimed from the stockpiles in better way than CPLEX.

REFERENCES

Askari-Nasab, H., Eivazy, H., Tabesh, M., & Badiozamani, M.M. (2011). A mathematical programming model for open pit short-term production scheduling. In *SME Annual Meeting, Denver, Colorado, USA SME. Vol., No. Issue,(2011 of Conference)* (pp. 1–8).

Bakhtavar, E., & Oraee, K. (2012). A Short-term production planning model for dimension stone quarries. In *SME Annual Meeting* (pp. 241–243). Society for Mining, Metallurgy & Exploration.

Blom, M., Pearce, A.R., & Stuckey, P.J. (2018). Short-term planning for open pit mines: a review. *International Journal of Mining, Reclamation and Environment*, 1–22.

Eivazy, H., & Askari-Nasab, H. (2012). A mixed integer linear programming model for short-term open pit mine production scheduling. *Mining Technology*, *121*(2), 97–108.

Kumar, A., & Chatterjee, S. (2016). Open-pit coal mine production sequencing incorporating grade blending and stockpiling options: An application from an Indian mine. *Engineering Optimization*, *273*(December), 1–15.

Matamoros, M.E.V., & Dimitrakopoulos, R. (2016). Stochastic short-term mine production schedule accounting for fleet allocation, operational considerations and blending restrictions. *European Journal of Operational Research*, *255*(3), 911–921.

Morales, N., & Reyes, P. (2016). Increasing the value and feasibility of open pit plans by integrating the mining system into the planning process. *Journal of the Southern African Institute of Mining and Metallurgy*, *116*(7), 663–672.

Mousavi, A., Kozan, E., & Liu, S.Q. (2014). Integrated approach to optimize open-pit mine block sequencing. *Industrial Engineering Non-Traditional Applications in International Settings*, 83–98.

Mousavi, A., Kozan, E., & Liu, S.Q. (2016). Open-pit block sequencing optimization: a mathematical model and solution technique. *Engineering Optimization*, *48*(11), 1932–1950.

Smith, M. (1998). Optimizing short-term production schedules in surface mining: Integrating mine modeling software with AMPL/CPLEX. *International Journal of Surface Mining, Reclamation and Environment*, *12*(4), 149–155.

Sundar, D.K., & Acharya, D. (1995). Blast schedule planning and shiftwise production scheduling of an open cast iron ore mine. *Computers and Industrial Engineering*, *28*(4), 927–935.

A two-stage solution approach for a shift scheduling problem with a simultaneous assignment of machines and workers

Cinna Seifi
Clausthal University of Technology, Clausthal-Zellerfeld, Germany

Marco Schulze
K+S Aktiengesellschaft, Kassel, Germany

Jürgen Zimmermann
Clausthal University of Technology, Clausthal-Zellerfeld, Germany

ABSTRACT: We consider a short-term production scheduling problem in a German potash underground mine where drill-and-blast mining operations have to be assigned to machines and workers and scheduled simultaneously. In addition, several mining-specific requirements have to be taken into account. In order to solve the problem at hand, we propose a two-stage solution approach. In the first stage, we apply a mixed-integer linear program where some time-consuming restrictions are neglected. Afterward, we modify the obtained schedule by integrating the necessary time intervals that were dismissed within the mathematical model. Since an existing heuristic solution procedure for the same problem is currently in use in a German potash mine, we will present results for computational experiments conducted on problem instances derived from real-world data in order to evaluate the performance of the two solution approaches.

1 PROBLEM DESCRIPTION AND LITERATURE REVIEW

This paper addresses a short-term production scheduling problem in a German potash underground mine that was already studied by Schulze & Zimmermann (2017) as well as Schulze et al. (2017) who proposed a rule-based constructive procedure. The extraction of the examined potash mine is done by room-and pillar mining method and the excavation of potash is based on drilling and blasting technique. This kind of underground mining is characterized by eight consecutive sub-steps, i.e., operations, that can be seen as a production cycle: scaling the roof, bolting the roof with expansion-shell bolts, drilling large diameter bore holes, removing the drilled material, drilling blast holes, filling the blast holes with an explosive substance, blasting, and transportation of the broken material to a crusher. For each operation, except blasting, one special mobile machine out of a set of identical or uniform machines is required that is handled by a worker with the corresponding qualification, i.e., skill. Hence, the underlying problem consists of the determination of a shift schedule where (i) a set of jobs[1] has to be selected and determined for execution, (ii) start times of the selected jobs have to be specified, and (iii) machines and workers have to be assigned to the jobs simultaneously while the individual skills of the workers as well as the technological-based precedence relations for the jobs have to be taken into account. The objective is the minimization of the average positive deviation between a predetermined quantity and the amount of extracted crude salt, cumulated over all operations.

Taking the aforementioned characteristics into consideration, we deal with two different problem types that have to be solved simultaneously, that is a machine scheduling problem on the one hand, and an employee timetabling problem on the other hand. The machine

---

1. Note that a job is characterized by the corresponding operation type from the production cycle and the place within the mine where the operation has to be executed.

scheduling problem can be classified as a variant of a so-called hybrid flow shop (HFS) scheduling problem, if we identify each mining operation from the production cycle as a stage, see Schulze et al. (2016). Note that we assume the mining operations as non-preemptable, because an assigned machine stays at the corresponding working place after an interruption (due to workers' breaks or end of a shift) and processing will be resumed at the next possible occasion. In comparison to the classical HFS scheduling problem, due to the short planning horizon of one single working shift, it is not possible to perform all mining operations at all working places. Thus, on the one hand, it has to be decided whether a job at a working place will be processed within the shift under consideration or not, and on the other hand, some possible interruption of the processing of a job at the end of the working shift must be taken into account.

The machines in the problem at hand are mobile and travel from job to job, therefore, no buffers are needed between the stages. Instead, we have to consider driving times between jobs that are processed by the same machine what results in sequence-dependent setup times. In addition, there are so-called technical services that have to be performed for the machines. Before processing the first operation assigned to a machine, a preventive maintenance (first technical services) must be done. After processing the last job assigned to a machine as well as before the end of the working shift if a job has to be interrupted, each machine must be cleaned and fueled (last technical services). Furthermore, for the case in which a worker changes his machine, he has to perform the first technical services for the new machine.

The second problem type, an employee timetabling problem, comprises the assignment of suitable workers to machines within a working shift. We assume that a worker can handle at most one machine at the same time and a machine can be operated by at most one worker at the same time. Since the workers have particular skills on different levels, not all workers can handle all machines. The different skill levels result in different handling times for each machine. Furthermore, the machines on each stage can have different speeds, which means that the processing time of a job depends on both the assigned worker and machine.

In order to generate a schedule that is accepted from the shift supervisor and that meets legal obligations, we furthermore have to satisfy the following mining-specific requirements.

R1: Due to legal regulations, a Δ-minute break for the workers has to be incorporated in the schedule within a predetermined time window. It has to be noted that the break can lead to a delay in the processing of a job.

R2: We have to consider disjunctive constraints for subsets of jobs that are physically close to each other (these jobs "belong" to so-called underground locations). Due to security reasons, it is not allowed that more than one machine is processing there at the same time, i.e., only one job in an underground location can be processed at any point in time.

R3: Although a consistent progress at all working places of the underground locations would be desirable, different excavation states appear, i.e., not the same operation can be performed there. In order to achieve a harmonized state, we prioritize the jobs in an underground location in a way that the progress strives for consistency.

R4: Jobs that are interrupted at the end of the pre-shift have a higher priority than the other jobs within the same underground location.

R5: The operations that symbolize the step drilling large diameter bore holes are non-interruptible. If those operations cannot be finished until the end of the corresponding working shift, they must not be started.

R6: The number of assigned worker to a machine is limited by two. That means no more than two workers can be assigned to a machine and a worker is not allowed to work on more than two machines during a working shift.

In the literature, most works concerning machine scheduling neglect the assignment of workers, while in the field of employee timetabling (i.e., staff scheduling and personnel assignment) the machine scheduling problem is rarely considered. Therefore, we confined our literature review to the integrated employee timetabling and machine scheduling problems. An overview of the studied literature is given in Table 1, where the abbreviations in column *production environment* characterize, whether the authors analyzed a flow shop (FSP), job

	Production environment	Objective function	Formulation
Daniels & Mazzola (1994)	FSP	makespan	time-indexed
Daniels et al. (2004)	FSP	makespan	time-indexed
Huq et al. (2004)	FSP	multi-obj.	seq.-based
Artigues et al. (2006)	JSP	empl. cost	time-indexed
Artigues et al. (2009)	JSP	multi-obj.	seq.-based
Puttkammer et al. (2011)	FSP	multi-obj.	time-indexed
Mencia et al. (2013)	JSP	flow time	
Ramya & Chandrasekaran (2014)	JSP	empl. cost	time-indexed
Frihat et al. (2014)	HJSP	empl. cost	seq.-based
Benavides et al. (2014)	FSP	makespan	seq.-based
Guyon et al. (2014)	JSP	empl. cost	
Agnetis et al. (2014)	JSP	makespan	seq.-based
Campos Ciro et al. (2016)	OSP	flow time	seq.-based
Ahmadi-Javid & Hooshangi-Tabrizi (2017)	JSP	makespan	seq.-based
Santos et al. (2018)	JSP	throughput	time-indexed

shop (JSP), open shop (OSP), or hybrid job shop (HJSP) scheduling problem. Moreover, we indicate what kind of *objective function* as well as *formulation* is considered within the corresponding study.

In brief, our literature review shows that the approaches discussed in the studies are not suitable for the problem at hand what is mainly due to the aspects that we consider (i) a selection of jobs, (ii) setup times for machines and workers, (iii) possible interruption of jobs at the end of the shift, (iv) breaks that could delay the processing of jobs, and (v) that the workers can change their machine within a working shift. In the next section, we introduce a two-stage approach to tackle the problem.

2 TWO-STAGE APPROACH

In our two-stage approach, we first solve a relaxation of the problem described in the previous section using a MIP solver and then, we repair the solution found and generate a feasible one. First, we describe the relaxation (**R-Model**) of our short-term scheduling problem, where some restrictions concerning the breaks or technical services are omitted.

Let J be the set of jobs in the underground mine under consideration. Binary decision variables b_j are 1 if $j \in J$ is processed. Moreover, we introduce binary decision variables x_{jw} and y_{jm} that are 1 if j is processed by worker $w \in W_j$ and machine $m \in G_j$, respectively. G_j and W_j are subsets of the set of available machines G and workers W that can process job j. We also define binary decision variables z_{jwm} that are 1 if worker w and machine m are assigned to job j.

$$\sum_{m \in G_j} y_{jm} = b_j \quad \forall j \in J \tag{1}$$

$$\sum_{w \in W_j} x_{jw} = b_j \quad \forall j \in J \tag{2}$$

$$x_{jw} + y_{jm} \leq 1 + z_{jwm} \quad \forall j \in J, \forall w \in W_j, \forall m \in G_j \tag{3}$$

$$z_{jwm} \leq x_{jw} \quad \forall j \in J, \forall w \in W_j, \forall m \in G_j \tag{4}$$

$$z_{jwm} \leq y_{jm} \quad \forall j \in J, \forall w \in W_j, \forall m \in G_j \tag{5}$$

Let PT_{jwm} be the given parameter that denotes the processing time of job j by worker w and machine m. The actual processing time of job j is then $p_j = \sum_{w \in W_j} \sum_{m \in G_j} z_{jwm} \cdot PT_{jwm}$. In

this paper, we use a sequence-based formulation for our **R-Model**. So, we introduce binary decision variables v_{jr} that are 1 if job j is completed before job r is started.

$$v_{jr} + v_{rj} \leq 1 \quad \forall j, r \in J : j \neq r \tag{6}$$

We have to consider a break for each worker (see **R1**) that leads to the absence of this worker in a specific time. Each worker w has to make a Δ-minute break so that the start time of the break ρ_w lies in a predefined interval $[varphi^\alpha, \varphi^\omega]$. In our relaxation, we do not allow that the processing of a job overlaps the break of the worker who processes this job. However, the break may overlap the drive between two jobs or the technical services that may be executed for a machine.

$$\varphi^\alpha \leq \rho_w \quad \forall w \in W \tag{7}$$

$$\rho_w \leq \varphi^\omega \quad \forall w \in W \tag{8}$$

$$S_j \leq \rho_w + (1 - \omega_j^s)M + (1 - x_{jw})M \quad \forall j \in J, \forall w \in W_j \tag{9}$$

$$\rho_w + \boxtimes \leq S_j + \omega_j^s M + (1 - x_{jw})M \quad \forall j \in J, \forall w \in W_j \tag{10}$$

$$\rho_w \leq S_j + p_j + (1 - \omega_j^e)M + (1 - x_{jw})M \quad \forall j \in J, \forall w \in W_j \tag{11}$$

$$S_j + p_j \leq \rho_w + \omega_j^e M + (1 - x_{jw})M \quad \forall j \in J, \forall w \in W_j \tag{12}$$

$$\omega_j^s + \omega_j^e \leq 1 + \delta_j \quad \forall j \in J \tag{13}$$

$$\delta_j \leq \omega_j^s \quad \forall j \in J \tag{14}$$

$$\delta_j \leq \omega_j^e \quad \forall j \in J \tag{15}$$

If the start time of the break of a worker, who processes job j, is during the processing of j ($\omega_j^s = 1$ and $\omega_j^e = 1$), binary decision variable δ_j takes the value of 1 and a Δ-minute break must be considered for the duration of j, additionally.

At the beginning of the working shift, the first technical services td_m^α must be performed on machine m and the assigned worker drives d_{0jm} time units to the first job.

$$\sum_{m \in G_j} (td_m^\alpha + d_{0jm}) \cdot y_{jm} \leq S_j + (1 - b_j)M \quad \forall j \in J \tag{16}$$

At each working place in an underground location, several operation types must be executed in a specific order related to the prescribed production cycle. Let ul_j be the underground location of j, ml_j be the working place of j in ul_j, and $order_j$ be the position of j in the given order for ml_j. In a working place, always job j with the minimum value of $order_j$ must be completed before any job r with a greater value of $order_r$ can be started.

$$b_r \leq b_j \quad \forall j, r \in J : j \neq r, ul_j = ul_r, ml_j = ml_r, order_j < order_r \tag{17}$$

$$S_j + p_j + \delta_j \cdot \Delta \leq S_r + (2 - b_j - b_r)M$$
$$\forall j, r \in J : j \neq r, ul_j = ul_r, ml_j = ml_r, order_j < order_r \tag{18}$$

For jobs that are processed by the same worker, a precedence relation must be considered. As mentioned in Sect. 1, if a worker changes his machine, he has to go to the new machine (transfer time), has to do the first technical services, and he can drive the machine to the location of the new job. In our relaxed model, we neglect the time for the case, where a worker changes his machine.

380

$$S_j + p_j + \delta_j \cdot \Delta \le S_r + \left(2 - x_{jw} - x_{rw}\right) M + \left(1 - v_{jr}\right) M$$

$$\forall j, r \in J : j \ne r, \forall w \in W_j \cap W_r \tag{19}$$

$$S_r + p_j + \delta_r \cdot \Delta \le S_j + \left(2 - x_{jw} - x_{rw}\right) M + v_{jr} M$$

$$\forall j, r \in J : j \ne r, \forall w \in W_j \cap W_r \tag{20}$$

Moreover, if two jobs are processed by the same machine, a driving time between the jobs must be taken into account.

$$S_j + p_j + d_{jrm} + \delta_j \cdot \Delta \le S_r + \left(2 - y_{jm} - y_{rm}\right) M + \left(1 - v_{jr}\right) M$$

$$\forall j, r \in J : j \ne r, \forall m \in G_j \cap G_r \tag{21}$$

$$S_r + p_j + d_{rjm} + \delta_r \cdot \Delta \le S_j + \left(2 - y_{jm} - y_{rm}\right) M + v_{jr} M$$

$$\forall j, r \in J : j \ne r, \forall m \in G_j \cap G_r \tag{22}$$

After processing the last job on a machine, last technical services must be performed for the machine. Let *Shift* be the duration of the working shift. The following constraints guarantee that if the processing of a job exceeds *Shift* ($id_j = 1$), continuous decision variable $grad_{jwm}$ specifies, which percentage of j is achieved during the shift.

$$S_j + p_j + \delta_j \cdot \Delta + \sum_{m \in G_j} td_m^\omega \cdot y_{jm} \le Shift + id_j M \quad \forall j \in J \tag{23}$$

$$Shift \le S_j + p_j + \delta_j \cdot \Delta + \sum_{m \in G_j} td_m^\omega \cdot y_{jm} + \left(1 - id_j\right) M \quad \forall j \in J \tag{24}$$

$$S_j + \delta_j \cdot \Delta + \sum_{w \in W_j} \sum_{m \in G_j} grad_{jwm} \cdot PT_{jwm} + \sum_{m \in G_j} td_m^\omega \cdot y_{jm} \le Shift + \left(1 - id_j\right) M \, \forall j \in J \tag{25}$$

$$S_j + \delta_j \cdot \Delta + \sum_{w \in W_j} \sum_{m \in G_j} grad_{jwm} \cdot PT_{jwm} + \sum_{m \in G_j} td_m^\omega \cdot y_{jm} \ge Shift \cdot id_j \, \forall j \in J \tag{26}$$

Consequently, if a job is processed ($b_j = 1$) and its duration does not exceed the working shift ($id_j = 0$), $grad_{jwm}$ must take the value of 1.

$$\sum_{w \in W_j} \sum_{m \in G_j} grad_{jwm} \le \left(id_j + b_j\right) M \quad \forall j \in J \tag{27}$$

$$1 - \left(id_j - b_j + 1\right) M \le \sum_{w \in W_j} \sum_{m \in G_j} grad_{jwm} \quad \forall j \in J \tag{28}$$

For the other mining-specific requirements **R2**–**R5**, we formulate the following constraints. Note that we write $j \prec r$ if job j must be completed before job r can be started.

R2:

$$S_j + p_j + \delta_j \cdot \Delta \le S_r + \left(2 - b_j - b_r\right) M + \left(1 - v_{jr}\right) M$$

$$\forall j, r \in J : j \ne r, ul_j = ul_r \tag{29}$$

$$S_r + p_j + \delta_r \cdot \Delta \le S_j + \left(2 - b_j - b_r\right) M + v_{jr} M$$

$$\forall j, r \in J : j \ne r, ul_j = ul_r \tag{30}$$

R3:

$$b_r \le b_j \quad \forall j,r \in J : j \ne r, ul_j = ul_r, j \prec r \tag{31}$$

$$S_j + p_j + \delta_j \cdot \Delta \le S_r + \left(2 - b_j - b_r\right) M \quad \forall j,r \in J : j \ne r, ul_j = ul_r, j \prec r \tag{32}$$

R4:

$$b_r \le b_j \quad \forall j,r \in J : j \ne r, ul_j = ul_r, started_j = 1, started_r = 0 \tag{33}$$

R5:

$$id_j = 0 \quad \forall j \in J : type_j = 4 \tag{34}$$

To realize **R6**, we introduce binary decision variables ma_{wm} that are 1 if w is assigned to m.

$$y_{jm} + x_{jw} \le 1 + ma_{wm} \quad \forall j \in J, \forall w \in W_j, \forall m \in G_j \tag{35}$$

$$\sum_{m \in G} ma_{wm} \le 2 \quad \forall w \in W \tag{36}$$

$$\sum_{w \in W} ma_{wm} \le 2 \quad \forall m \in G \tag{37}$$

Let ton_j be the expected amount of material after processing of job j and ton_k^{pre} be the predetermined quantity (target value) for production step k. We can determine the lower deviation from ton_k^{pre} for each production step by the following constraints.

$$ton_k^{pre} - \sum_{j \in J: type_j = k} \sum_{w \in W_j} \sum_{m \in G_j} grad_{jwm} \cdot ton_j \le dev_k \quad \forall k \in K \tag{38}$$

Our goal is to have a consistent progress so that the following function must be minimized.

$$\sum_{k \in K} dev_k^2$$

If we determine the maximum lower deviation as follows:

$$dev_k \le dev^{max} \quad \forall k \in K, \tag{39}$$

we can then approximate the quadratic objective function by the following linear one.

$$\sum_{k \in K} dev_k + dev^{max} \tag{40}$$

After finding a solution for **R-Model** (Min. (40) s.t. (1)–(39)), the solution is used as an input for Algorithm 1 to generate a feasible solution for the problem instance at hand. In Algorithm 1, we first determine the sequence of the processing of jobs for each machine and each worker. After that, for each machine m, between two consecutive jobs j and r that are processed by different workers, a first technical service must be inserted before starting r. Subsequently, start times of all of the jobs that have to be started after the completion of r must be updated. For each worker w, if w changes his machine and goes from machine m to m', we eventually have to consider last technical services if w processed the last task on m. The worker then goes to the parking location of m', performs first technical services, and drives m' to the location of the next job. Consequently, start times of all of the related jobs must be updated. Then, we check if there are overlaps between breaks of workers and the activities that workers have to perform. In this case, we consider the effect of workers' breaks on start times or durations of jobs and update the start times of all of the affected jobs. The steps above are repeated until there are no more changes in start times of jobs.

Algorithm 1. Repair solution.

1: Input: problem instance D, solution of **R-Model**
2: **repeat**
3:   For each machine, determine the sequence of processed jobs by this machine;
4:   For each worker, determine the sequence of processed jobs by this worker;
5:   **for** all processed jobs j **do**
6:     $S_j^1 = S_j$
7:   **for** all machines m **do**
8:     **if** two consecutive jobs j and r on m are performed by different workers **then**
9:       Insert the time for first technical services for m before S_r
10:      **for** all jobs j' with $v_{rj'} = 1$ **do**
11:        update $S_{j'}$
12: **for** all workers w **do**
13:    **if** two consecutive jobs j and r on w are performed by different machines **then**
14:      Insert the potential last technical services for the machine assigned to j, the transfer time, first technical services for the machine assigned to r, and the driving time from the direct predecessor of r on the assigned machine to r
15:      **for** all jobs j' with $v_{rj'} = 1$ **do**
16:        update $S_{j'}$
17: **for** all workers w **do**
18:    **if** the break of w, who processes job j, overlaps any of the first technical services for the machine assigned to j, driving times to j, the processing of j, or the last technical services for the machine assigned to j **then**
19:      Consider the break of w for S_j or the duration of j
20:      **for** all jobs j' with $v_{jj'} = 1$ **do**
21:        update $S_{j'}$
22: **for** all jobs j with $type_j = 4$ **do**
23:    Eliminate j if the processing of j exceeds the duration of the working shift
24: **until** $S_j^1 = S_j \, \forall_j$
25: Determine the objective value according to the new schedule
26: **return** The feasible schedule

3 COMPUTATIONAL STUDY

To show the suitability of our proposed solution approach, we compare the results of our two-stage approach with the heuristic procedure introduced by Schulze & Zimmermann (2017). For this purpose, we generated 100 test instances based on the case study presented in Schulze & Zimmermann (2017), which depict realistic problems in a German potash underground mine. In Algorithm 2, an overview of the constructive heuristic approach is given (for more details see Schulze & Zimmermann (2017) and Schulze (2016)).

Algorithm 2. Constructive heuristic introduced by Schulze & Zimmermann (2017).

1: **Initialization** (* *construction* *)
2: **Priority-based scheduling**
3: **Staff changes** (* *improvement* *)
4: **repeat**
5:   **Scheduling downstream operations**
6:   **Staff changes**
7:   **Replenishment**
8: **until** total amount of potash cannot be increased
9: **Job reassignment**
10: Insertion of **technical services** (* *post-processing* *)
11: Insertion of **breaks** for workers
12: **return** solution

Table 2. Comparison of the approaches.

	Number of best solutions found	Gap to the best solution found
Two-Stage approach	70	6.1% (20.3%)
Constructive heuristic	30	45.2% (64.6%)

The heuristic procedure is embedded in a multi-start algorithm, where jobs, machines, and workers are chosen based on selection probabilities that are determined by priority values. For the heuristic approach in this paper, we use the setting that is currently used in the underground mine under consideration. In the corresponding assigning method, jobs and workers are randomly chosen, and machines are selected regarding the shortest driving times to the selected job or regarding the shortest processing time based on the selected job and the selected worker.

All tests are executed on an Intel i7–7700 K@4.20 GHz machine with 64 GB RAM under Windows 10. The heuristic algorithm is implemented in Xpress IVE 8.4. For the two-stage approach, we used GAMS 25.1 and GUROBI solver 8.1.0 to solve **R-Model** and C++ to generate a feasible solution with the aid of Algorithm 1. Since we schedule only one working shift, we set an upper time limit of 900 seconds for both approaches that symbolizes a typical duration of a shift handover.

To compare the results achieved by the procedures, we use the value of $\sum_{k \in K} dev_k^2$ that shows how consistent the desired progress could be implemented at the end of the working shift compared to the given state at the beginning of the working shift.

Table 2 presents the number of best solutions found and an average gap to the best solution found. Let S_i^* be the solution found for instance i by procedure * and S^{best} be the best solution found. We calculate $\frac{S_i^* - S^{best}}{S_i^*}$ to determine the gap for instance i (gap$_i$). The numbers presented under "Gap to the best solution found" are obtained by arithmetic averaging over all instances. Note that the number in parentheses is the obtained gap by arithmetic averaging over the number of the instances for which the solution found is not equal to the best solution found (i.e., gap$_i \neq 0$).

We see that the two-stage approach can find for 70 instances the best solution, where the solutions found for the other 30 instances are 20.3% far from the best solution found. On the other hand, the solutions found by the constructive heuristic are on average 45.2% worse than the best solutions found. This number gets significantly worse (64.6%) if we make an average over the 70 instances for which the heuristic could not find the best solution. So, we can conclude that our two-stage approach performs quite promising.

4 CONCLUSION

In this paper, we consider a shift scheduling problem where machines and workers are simultaneously assigned to a selection of the available jobs. We formulate a relaxation of the problem described in Sect. 1 and introduced an algorithm to generate feasible solutions using the solution achieved by the relaxation. The results of a preliminary performance analysis using realistic instances show that the solutions of our proposed two-stage approach clearly outperform the solutions which are currently generated by a constructive heuristic procedure.

Future work concerns the development of good lower bounds for our problem. Moreover, the total output can additionally be taken into account. Considering the trade-off between the presented objective function and the total excavated amount of material could provide new insights.

REFERENCES

Agnetis, A., Murgia, G., & Sbrilli, S., 2014. A job shop scheduling problem with human operators in handicraft production. *International Journal of Production Research* 52(13): 3820–3831.

Ahmadi-Javid, A. & Hooshangi-Tabrizi, P., 2017. Integrating employee timetabling with scheduling of machines and transporters in a job-shop environment: A mathematical formulation and an anarchic society optimization algorithm. *Computers & Operations Research* 84: 73–91.

Artigues, C., Gendreau, M. & Rousseau, L.M., 2006. A flexible model and a hybrid exact method for integrated employee timetabling and production scheduling. In *International Conference on the Practice and Theory of Automated Timetabling* (pp. 67–84). Berlin, Heidelberg: Springer.

Artigues, C., Gendreau, M., Rousseau, L.M. & Vergnaud, A., 2009. Solving an integrated employee timetabling and job-shop scheduling problem via hybrid branch-and-bound. *Computers & Operations Research* 36(8): 2330–2340.

Benavides, A.J., Ritt, M. & Miralles, C., 2014. Flow shop scheduling with heterogeneous workers. *European Journal of Operational Research* 237(2): 713–720.

Campos Ciro, G., Dugardin, F., Yalaoui, F. & Kelly, R., 2016. Open shop scheduling problem with a multi-skills resource constraint: A genetic algorithm and an ant colony optimisation approach. *International Journal of Production Research* 54(16): 4854–4881.

Daniels, R.L. & Mazzola, J.B., 1994. Flow shop scheduling with resource flexibility. *Operations Research* 42(3): 504–522.

Daniels, R.L., Mazzola, J.B. & Shi, D., 2004. Flow shop scheduling with partial resource flexibility. *Management Science* 50(5): 658–669.

Frihat, M., Sadfi, C. & Hadj-Alouane, A.B., 2014. Optimization of integrated employee timetabling and hybrid job shop scheduling under time lag constraints. In *International Conference on Control, Decision and Information Technologies (CoDIT)*, (pp. 282–287). IEEE.

Guyon, O., Lemaire, P., Pinson, E. & Rivreau, D., 2014. Solving an integrated job-shop problem with human resource constraints. *Annals of Operations Research* 213(1): 147–171.

Huq, F., Cutright, K. & Martin, C., 2004. Employee scheduling and makespan minimization in a flow shop with multi-processor work stations: a case study. *Omega* 32(2): 121–129.

Mencia, C., Sierra, M.R. & Varela, R., 2013. An efficient hybrid search algorithm for job shop scheduling with operators. *International Journal of Production Research* 51(17): 5221–5237.

Puttkammer, K., Kleber, R., Schulz, T. & Inderfurth, K., 2011. Simultane Maschinenbelegungs- und Personaleinsatzplanung in KMUs anhand eines Fallbeispiels aus der Druckereibranche. In Sucky, E., Asdecker, B., Dobhan, A., Haas, S. & Wiese, J. (eds), *Logistikmanagement: Herausforderungen, Chancen und Lösungen*: 229–247. University of Bamberg Press.

Ramya, G. & Chandrasekaran, M., 2014. Shuffled frog leaping algorithm approach to employee timetabling and job shop scheduling. *International Journal of Internet Manufacturing and Services 4 & 25* 3(3): 178–203.

Santos, F., Fukasawa, R. & Ricardez-Sandoval, L., 2018. An integrated personnel allocation and machine scheduling problem for industrial size multipurpose plants. *IFAC-PapersOnLine* 51(18): 156–161.

Schulze, M., 2016. Ein hierarchischer Ansatz zur Lösung von Ablaufplanungsproblemen im Bergbau: Darstellung am Beispiel des Örterbaus. Aachen: Shaker.

Schulze, M., Mathiak, T. & Haney, C., 2017. Using operations research techniques to increase efficiency in German potash mining. In *Application of Computers and Operations Research in the Mineral Industry; Proc. intern. symp., Golden, Colorado, 2017* 5: 9–15.

Schulze, M., Rieck, J., Seifi & C., Zimmermann, J., 2016. Machine scheduling in underground mining: An application in the potash industry. *OR Spectrum* 38(2): 365–403.

Schulze, M., Zimmermann, J., 2017. Staff and machine shift scheduling in a German potash mine. *Journal of Scheduling* 20(6): 635–656.

Understanding plan's priorities: Short term scheduling optimization

A.B. Andrade
AngloGold Ashanti, Sabará, MG, Brazil

P.C.B. Rampazzo
Unicamp, Limeira, SP, Brazil

ABSTRACT: Three levels are usually applied to mining planning: Long-term sets the strategy while medium and short-terms aim to achieve main targets (ore production, grades, meters developed, metal production, etc.). Manually scheduling a monthly plan, which is a widely used method, can be a difficult task: A 30-day plan can take days to be elaborated and appropriately validated. In a dynamic mine environment where day-to-day compliance varies, after the first planned day, some of the tasks will not be executed, some might be delayed and some anticipated. It will be needed to review the plan and so next day operation can be correctly prioritized. Most of the time, rescheduling the full plan might not be an option and suboptimal decisions are made. This paper proposes an algorithm for short-term scheduling in underground mines with a flow shop scheduling with parallel machines model, optimizing and automatizing short term planning process.

Keywords: mixed linear programming, short-term scheduling optimization

1 INTRODUCTION

Mining industry, as any capital intensive production system, requires detailed planning to guarantee that resources will be allocated the best way and that returns on investments will happen with predictability.

Usually mine planning is carried out in three different levels. Long-term will set the strategic main targets; medium and short-term, the tactical and operational plans. The focus of this article is the short-term (operational) plan scheduling.

As detailed by Schmidt *et al.* (2000), the operational level schedules operations to assure in-time delivery of final products. Here the question is when to perform a manufacturing task and at which facility so that due dates are met to the fullest extent possible.

In an underground mine context, each production stope has to go through a cycle of activities until ore is finally produced. Thus, we have to schedule machines to each activity of each task (production area) in a way that the final production will be the best.

Consequently, a short-term (operational) plan has to handle with a high level of detail, that is, a greater number of activities compared to tactical or strategic plans. Depending on mining method and other mine specificities, each mine will plan and monitor its own set of activities. Next figure presents an example of AngloGold Ashanti Cuiabá mine in Brazil. In this example, we have the biggest cycle considered, that means, some production areas cycles can skip one or more of these activities.

The basic, and most common approach, to schedule a short-term plan is to do it manually in accordance with the planning and production engineers' experience. Whether done with Gantt based planning tools or with spreadsheets, this method is normally centered on greedy algorithms such as anticipating high grade ore or anticipating lowest duration (easier) tasks. This approach can lead to suboptimum results of the overall production.
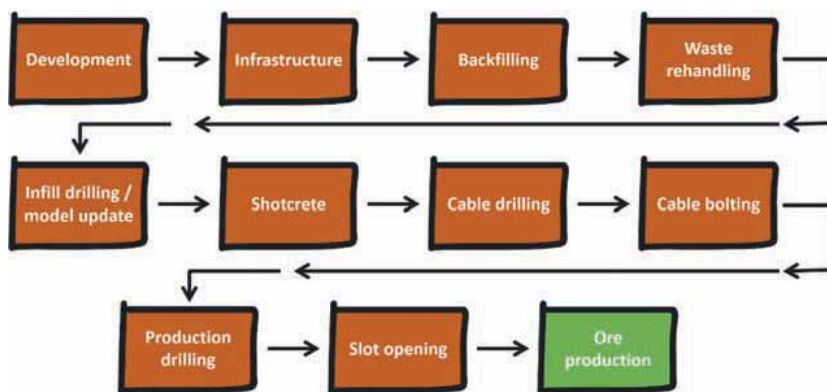
Figure 1. Example of operational activities in each production area plan.

Also, manual schedule is a time-consuming job and limit the possibility of creating scenarios, increasing the risk of having a suboptimal results.

Furthermore, given the dynamicity of an underground mine, short-term plans have to be updated frequently. To guarantee optimal results, these updates should be done for the whole plan, which is rarely achieved, usually being done for smaller periods (e.g. cascading month plans in week, day and shift plans).

Operational Research is a methodology that makes use of mathematical, statistical and algorithmic models for analysis and decision making (Winston, 2004; Taha, 2017). Transportation, communications, energy, mining, petroleum, and manufacturing are some of the areas which problems can be represented by optimization models.

The objective is always to find the optimum (or close enough) choice within a set of possibilities regarding constraints of the problem. Poor decision making and suboptimal resource allocation lead to losses of money and time.

This article proposes an Operational Research algorithm to optimize short-term plans.

2 METHODOLOGY

In an Operational Research study, the main goal is to translate the optimization objective and problem constraints to algebraic equations and thus, build a mathematical model that can be solved by software (a solver).

This process begins by the analysis of characteristics of the problem and the tools available so that the use of a specific tool can be justified (Taha, 2017).

The short-term scheduling problem in underground mines can be considered a subset of the flow shop scheduling problem.

A flow shop scheduling problem is defined (Pinedo, 2016) by the scheduling of n tasks in m machines given that each task has to undergo each machine in the same order, i.e., all tasks has to follow the same process route. The following figure gives an example of a flow shop problem. Here, each task has to be processed by each machine in the same order (green → blue → pink → yellow → red). Each machine can process only one task at time.

The underground mine short-term scheduling problem requires some modifications to the generic flow shop problem. In mines, we have multiple machines doing same activity of a cycle. Thus, the concept of activity and machine has to be split. The cycle will be formed by activities executed by one or more parallel machines.

Although the process route is the same for all tasks, some tasks do not have to go through all activities, following the remaining cycle, e.g. if the task does not have to go through one of the j activities, its processing time for this activity is considered 0, and will be ignored.
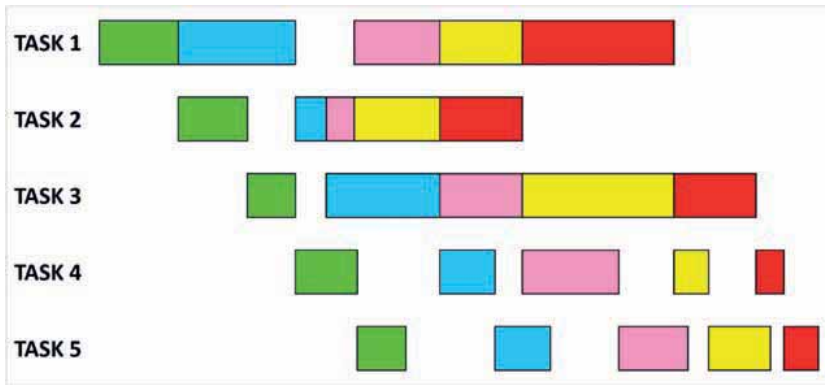
Figure 2.   Example of a flow shop with 5 tasks and 5 machines.
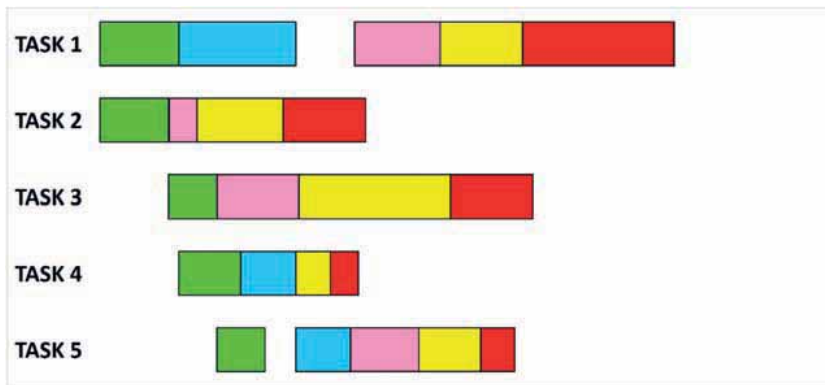
Figure 3.   Example of the flow shop scheduling problem with parallel machines (approach used for the underground mine short-term schedule problem).

Figure 3 below illustrates how five tasks have to go through the same route (green → blue → pink → yellow → red) but tasks 2 and 3 skip the blue activity. Also, activity green can process up to 2 tasks at time, which means two parallel machines can perform green.

Blue, yellow, and red activities also have 2 parallel machines. Pink, only one.

Other modifications considered:

- instead of the commonly applied makespan, objective function was changed to maximize metal production within a given period, in this case, the duration of the plan (e.g., 15 or 30 days). It is considered that, beyond this point in time, we do not have enough tasks or information to schedule the tasks in a complete plan.
- Precedences between tasks activities are allowed and have to be listed. Thus, we can explicitly state that task 2 activity 1 happens only after task 3 activity 4.

2.1   *Mathematical model*

To model and solve this problem a Mixed Integer Linear Programming (MIP) model (Wolsey, 1998) is proposed. The model can be fully described by its inputs, variables (which will also be outputs), objective function and constraints; the latter two described by linear equations.

2.1.1   *Inputs*
- $F \rightarrow$ timeframe within optimization interests;
- $m_j \rightarrow$ array with the number of parallel machines for each activity j;

- h^* → metal production activity index, which we aim to optimize;
- w_i → weights with the value of metal production rate for each task i;
- p_{ij} → matrix with duration of each task i (production areas) to process j activity;
- r_{ij} → matrix with the minimum starting date for each task i in each activity j;
- A_{ijkl} → list with dependencies between a activity j of task i and activity l of task k.

2.1.2 Variables
- pp_{ih^*} → positive integer variable. Process period (duration) of a task i within the F limit for the activity of interest h^*;
- x_{ij} → positive integer variable. Starting period of a task i in activity j;
- x_{ijh} → positive integer variable. Starting period of a task i in machine h of activity j. In case h do not process i, it is equals 0;
- y_{ijh} → binary variable. Equals 1 if machine h of activity j process task i. Otherwise, 0;
- w_{ikj} → binary variable. Equals 1 if task i happens before task k in activity j. Otherwise (k before i), 0;
- z_i → binary variable used to control pp_{ih^*} limits.

2.1.3 Objective function
As previously stated, the objective is to optimize metal production w_i of a within period F. Beyond period F we consider that there is not enough information about the tasks to have a detailed operation plan and hence beyond the scope of the model.

Thus, objective function will be to maximize the sum of the process time pp_{ih^*} multiplied by its metal production rate (weights w_i).

$$Maximize \sum_{i=0}^{n} w_i . pp_{ih^*} \tag{1}$$

2.1.4 Constraints
Following equations model physical constraints currently considered in short-term plans, such as cycle flow, number of activities that can happen at the same time (parallel machines), duration of each task in each activity (machine), starting dates and dependencies between tasks.

$$x_{ih^*} + pp_{ih^*} \leq F + M.z_i \tag{2}$$

$$pp_{ih^*} \leq M.(1 - z_i) \tag{3}$$

$$pp_{ih^*} \leq p_{ih^*} \tag{4}$$

$$x_{ij} \geq r_{ij} \tag{5}$$

$$\sum_{h=1}^{m_j} y_{ijh} = 1 \tag{6}$$

$$x_{ij} + p_{ij} + r_{ij} \leq x_{i(j+1)} \tag{7}$$

$$y_{ijh} + y_{kjh} - w_{ikj} - w_{kij} \leq 1 \tag{8}$$

$$y_{ijh_1} + y_{kjh_2} + w_{ikj} + w_{kij} \leq 3 \tag{9}$$

$$x_{ij} + p_{ij} + r_{ij} \leq x_{kj} + M.(1 + w_{ikj}) \tag{10}$$

$$x_{ij} + p_{ij} + r_{ij} \leq x_{kl} \quad \forall ij, kl \in A_{ijkl} \tag{11}$$

$$x_{ij} = \sum_{h=1}^{m_j} x_{ijh} \tag{12}$$

$$x_{ijh} \leq M.y_{ijh} \tag{13}$$

$$x_{ijh} \leq M.p_{ij} \tag{14}$$

389
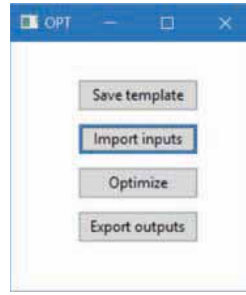
Figure 4.   User interface created to run the algorithm.

To model the conditional constraints (*if constraints*) an upper bound *M* is used, as explained in Taha (2017) and AIMMS (2018), also known as big-*M* constraint type. This can be seen in the constraint pair formed by (2) and (3) and also in constraints (10), (13), and (14).

Constraints (2), (3) and (4) define and limit pp_{ih^*} to 0 if production activity of task i happens after F, to $F - x_{ij}$ otherwise and to p_{ih^*}, since pp_{ih^*} is also the process period of activity h^*.

Equation (5) guarantees that the starting date, x_{ij}, will be greater than starting date constraint, r_{ij}. (6) assures that only one machine will process a activity of a given task. (7) represents the flow of activities for each task.

Constraints (8), (9) and (10) models the relationship between different tasks in parallel machines: if two tasks are processed by the same machine one has to be before other.

Expression (11) models extra dependencies between tasks according to input given. (12), (13) and (14) defines the variable x_{ijh}.

2.2   *Implementation*

The scheduling model was implemented in Python 3.7 with use of Anaconda distribution. The linear programming solver used is Google OR Tools.

The code was written in Jupyter Notebook environment. User interface is done through a spreadsheet where input data can be inserted and output values can be represented as a Gantt chart. A graphical user interface (GUI) was built using wxFormBuilder and then built into a single.exe Windows application with Pyinstaller.

A spreadsheet contains inputs already listed in 2.1.1.

Output is also a spreadsheet that holds all variables results. With x_{ij} values it is possible to create a Gantt chart to validate the result.

3   CASE STUDY

An exercise was performed using data from an underground gold mine in Brazil. AngloGold Ashanti Cuiabá mine is located in the city of Sabará, state of Minas Gerais, in the Southeast part of Brazil. The mine has reached a depth of 1300 m and produces approximately 1.3 Mtpa.

A Cuiabá monthly plan averages 25 tasks and 28 monitored activities. To simplify and generate an easier to understand example, a smaller part of a monthly plan was used considering only 10 tasks and 5 activities.

Inputs were the same listed in Figure 5. Optimized scheduled was then compared to a manual schedule done in advance considering task prioritization according to (*production*)/ (*total duration*) ratio.

Figure 5.   Spreadsheet that holds all input values and do the interface with the algorithm.
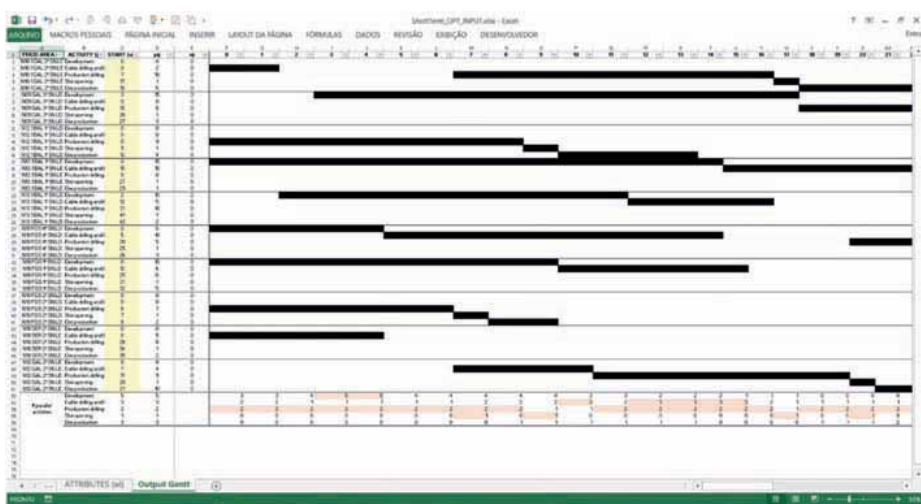
Figure 6.   Output values in yellow cells generating the Gantt chart of the result.

4   RESULTS

Satisfactory results were achieved for the case study: the optimized schedule could achieve 6145 oz while the manual schedule 5039 oz.

It is always hard to compare manual and optimized results, since the manual depends on the experience of the planning engineer and may differ from the scheduling algorithm used (here (*production*)/(*total duration*) ratio).

Optimization processing time was 72 seconds. While this may increase with greater number of tasks and activities (roughly the number of constraints increases with the square of number of tasks) reasonable solving time is expected for practical problems.

5   CONCLUSIONS

Standardizing and automatizing the process increases the flexibility needed to face mine dynamics while always pointing to the best resource allocation, thereby making it easier to create schedule scenarios (for different possible inputs) and having a prioritized task list always updated.

The next step is to implement this optimization algorithm for short-term and operational schedules (monthly to daily plans), allowing plan revisions that dynamically optimize resource allocation according to production results while considering the big picture set by tactical plans.

Although a significant improvement is achieved compared to manual scheduling, this algorithm still has some limitations and does not consider:

- different processing rates for each parallel machine;
- activities being partially done before machine change (preemptions);
- machines performing different activities;
- multiple activities of same task happening in parallel (at same time);
- intangible information of tasks and activities.

It is worth noting that most of these limitations are currently not considered in manual scheduling assumptions and do not represent the general operational procedures (are exceptions).

Future work includes addition of some of this functionality; mainly the use of different machine rates and preemptions.

REFERENCES

AIMMS B.V. 2018. AIMMS Modeling Guide—Integer Programming Tricks. Haarlem, The Netherlands: AIMMS B.V. https://download.aimms.com/aimms/download/manuals/AIMMS3OM_IntegerProgrammingTricks.pdf.

Pinedo, Michael. Scheduling: theory, algorithms, and systems. Springer, 2016.

Schmidt, Günter & Wilhelm, Wilbert. (2000). Strategic, Tactical and Operational Decisions in Multinational Logistics Networks: A Review and Discussion of Modeling Issues. International Journal of Production Research—INT J PROD RES. 38. 1501–1523. 10.1080/002075400188690.

Taha, H.A. Operations Research: An Introduction, 10th ed., Pearson, 2017.

Winston, W.L. Operations Research: Applications and Algorithms, 4th ed., Thomson Brooks/Cole, 2004.

Wolsey, L.A. Integer Programming, John Wiley & Sons, New York, 1998.

APPENDIX I: SOFTWARE REFERENCES

Anaconda: https://www.anaconda.com/.

Google OR Tools: https://developers.google.com/optimization/.

Jupyter Notebook: https://jupyter.org/.

Pyinstaller: http://www.pyinstaller.org/.

Python: https://www.python.org/.

wxFormBuilder: https://github.com/wxFormBuilder.

Simulation and optimization framework for evaluating the mining operations

A. Moradi Afrapoli & H. Askari-Nasab
Mining Optimization Laboratory (MOL), School of Mining Engineering, Department of Civil and Environmental Engineering, University of Alberta, Canada

ABSTRACT: This paper presents a MILP model to solve truck dispatching problem in surface mines. As testing a new technology in mining operation is expensive, simulation is used as a tool to evaluate effects of new technologies in the surface mining operations. However, two significant drawbacks exist in currently available simulation models. The available models ignore the existence of decision-making tools such as mining fleet management systems in mining operations. Also, the available simulation models disregard impacts of processing plants on the mining operation. To test our MILP model, this paper presents an intelligent simulation and optimization framework to mimic the surface mining operations. The given framework covers the drawbacks mentioned above. We implemented the framework in a surface mine case study to compare performance of our MILP model with its in place truck dispatching model. Results of the comparison show more than 10% improvement in production of the case study.

1 INTRODUCTION

Surface mining is an expensive operation. Most of the currently active surface mines implement different decision making tools for making closer to optimal decisions in their daily operations to cut a portion of the expensive operational cost. Several decision making models are developed every day to help in the cost reduction of a surface mine. Testing a new tool and evaluating its performance in a real mining operation is costly. Therefore, simulation modeling has been widely applied as one of the cheapest ways to test a decision making model in surface mining operations since the 1960s. However, the thus far developed simulation models have ignored the critical role of the decision making tools as a component of the surface mining operation system. However, in most of the active mines across the globe, each step of mining is tied closely to the optimal decisions being made by an optimization tool.

In this paper, we present an integrated simulation and optimization framework using which; a surface mining operation can be simulated with as many decision making tools as the mine is using in its daily operation. The framework consists of three major components: the simulation tool, the optimization tool, and the mine's dataset. The components of the framework are linked to each other and information, decisions, and data are transferred between the components during the simulation.

The developed integrated simulation and optimization framework was implemented to simulate a surface mining operation that uses two mathematical models for making optimal decisions in its production optimization and truck dispatching problems. The paper investigates the answer to "what if we replace the current truck dispatching model with a new truck dispatching model?". Based on the drawbacks in currently available truck dispatching decision making models, we developed an Integer linear programming model to solve the truck dispatching problem in surface mines. We substituted currently in place truck dispatching model in the case study with the developed model in the simulation model. Then we compared the performance of the developed model against the in place truck dispatching model.

Next section presents a brief overview of the literature followed by introducing the integrated simulation and optimization framework for simulating mining operation, and the mixed integer linear programming model developed to solve the truck dispatching problem. Afterwards, the application of the integrated framework and the mixed integer linear programming model in a real case study is presented.

2   RELATED LITERATURE

Simulation is the imitation of the operation of a real-world process or system over time (Banks 2001). The power of simulation as a tool to evaluate operating systems has been accepted worldwide. In the literature of the simulation, it origins in a simple mathematical problem called the Buffon's needle dated to 1777. The application of simulation in the mining sector can be traced back to 1940s. However, the credit of the first use of discrete event simulation was given to Rist (1961) who used the Monte Carlo simulation technique to solve the hauling problem in mining operations.

Developments in the capabilities of computers in the 1980s helped researchers conduct studies on the models and observe deficiencies, through the use of computer programs and simulations (Lynch & Morrison 1999). After the first usage of the simulation in the mining operation, several studies have been done by different researches in the field. To evaluate various dispatching techniques and prove positive impacts of implementing dispatching techniques in mining operations Sturgul & Eharisson (1987), Bonates & Lizotte (1988), Forsman et al. (1993), Kolonja & Mutmansky (1994), and Ataeepour & Baafi (1999) implemented simulation modeling.

Awuah-Offei et al. (2003) implemented simulation modeling for determination of fleet size in case of both truck and shovels a mine. To mimic the dynamic expansion of an open pit mine, Askari-Nasab et al. (2007) developed a simulator called open pit production simulator (OPPS). Their study shows that in the cases of modeling dynamicity of the processes and randomness of the input parameters, artificial intelligent simulators can be very efficient and helpful. Fioroni et al. (2008) used discrete event simulation and linked it with an optimization model to deal with the short-term production plan. The goal of the study was to show how simulation and optimization are integrated to achieve a reasonable solution to this problem. To analyze and evaluate the effects of equipment breakdown on the utilization of the resources and production of the operation, Yuriy & Vayenas (2008) combined discrete event simulation with a genetic algorithm based reliability assessment model.

From 2010 to 2015 all simulation studies in the field of truck and shovel mining system including Jaoua et al. (2012), Jaoua et al. (2012), Mena et al. (2013), Ta et al. (2013), Hashemi and Sattarvand (2015), Torkamani & Askari-Nasab (2015), Upadhyay & Askari-Nasab (2017), and Upadhyay & Askari-Nasab (2016) are using the simulation as a tool to evaluate results of the developed optimization algorithm in their studies without incorporating a new component into their system.

Dindarloo et al. (2015) provide a step by step discrete event simulation guideline for truck-shovel mining system equipment selection. The claim in the study is that the framework helps to minimize errors caused by inaccurate assumptions as well as procedures.

In one of the latest simulation study of a truck-shovel mining system, Que et al. (2016) investigated how ignoring the correlation between the input parameters will impact on the results of the study. The research presents a new approach to detect and import correlated parameters into the truck-shovel simulation study. Instead of the independent distributions, the new approach generates a multivariate random vector representing input parameters into the simulation modeling.

Beside all efforts mentioned above, some review studies related to the implementation of the simulation in the mining sector have been done since the late 1990s. Sturgul (1999) provides a historical review of discrete mine system simulation in the United States. Vagenas (1999) present a review of the application of simulations in Canada, and Konyukh et al. (1999) did a review study over the implementation of the simulation in Asia. Raj et al. (2009)

reviewed the application of simulation in production optimization in mines. Hodkiewicz et al. (2010) reviewed the simulation studies in both fields of underground and surface mining and highlighted lack of an integrated mining simulation model which incorporate truck workshop as part of the mining system.

3 MODEL DEVELOPMENT

3.1 *Integrated simulation and optimization framework*

The integrated stochastic simulation and optimization framework developed here consists of four main components: two optimization and two simulation sub models. The two optimization components are decision-making tools in fleet management systems that solve the paths' flow rate and truck dispatching problems (White & Olson 1986, Alarie & Gamache 2002). The simulation components in the framework are mining operation and material flow into downstream processes. Figure 1 shows how the developed framework integrates the four elements.

3.2 *MILP truck dispatching model*

The goal of this paper is to develop a dispatching model that minimizes the cumulative lost time for the entire active material handling fleet including both the loader fleet and the transporter fleet considering operational limitations such as truck capacity, shovel digging rate, and processing plants feed rate requirements while incorporating the truck travel time uncertainties. However, we first present the deterministic model with the objective function, decision variables, and the constraints and introduce the stochastic model in the next subsection. The model shown in this section is a deterministic model with all its input parameters taking deterministic values. It can also be categorized as a mixed integer linear programming model based on the transportation problem. The objective function of the model, presented in Eq. (1), minimizes the cumulative absolute time difference between the times truck t will reach shovel s after dumping it's at dump d (t_{ts}) and the time shovel s will be available to load the next truck (na_s). The second part of the objective function tries to maximize the adjustment factor (AF) encouraging the model to optimize a balanced material delivery to all destinations. AF will be explained later on. Finally, VBN stands for a very big number.

$$\min Z = \sum_{t=1}^{T} \sum_{d=1}^{D} \sum_{s=1}^{S} C_{tds} x_{tds} + VBN(mf - AF) \qquad \forall t \in \{1,...,T\}, \forall d \in \{1,...,D\},$$
$$and \ \forall \ s \in \{1,...,S\} \tag{1}$$

The objective function coefficient for each of the variables is calculated using Eq. (2):
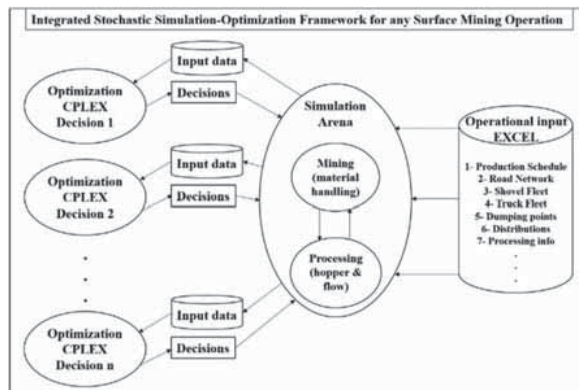
Figure 1. Integration of different components of a mining operation in the developed framework.

$$\begin{aligned}
C_{tds} &= \left| t_{ts} - na_s \right| \\
&= \left| T(t, 3+s) - S(4,s) \right| \\
&= \left| ltt_{td} + qt_{td} + dt_{td} + ett_{tds} - \sum_{t'=1}^{TT} \left(tinq_{t's} + tenr_{t's} \right) \times \left(st_{t's} + lt_{t's} \right) \right| \\
&\forall\, t \in \{1,\ldots,T\}\ \&\, \forall\, s \in \{1,\ldots,S\}\ \&\, \forall\, d \in \{1,\ldots,D\}
\end{aligned} \tag{2}$$

where:

ltt_{td} loaded travel time from current truck t position to dump d

qt_{td} time truck t must spend in the queue at dump d to dump its material

dt_{td} time truck t spends at dump d to back up and dump its material

ett_{ts} time truck t spends to travel empty from the dump location d to shovel s

$tinq_{t's}$ time a truck of type t' that is already in the queue must spend in shovel s queue

$tenr_{t's}$ time a truck of type t' must travel from its current position to reach shovel s

$st_{t's}$ spot time for a truck of type t' at shovel s

$lt_{t's}$ loading time for a truck of type t' at shovel s

Moreover, the decisions need to meet operational constraints such as trucks' and shovels' supply (Eq. (3) and Eq. (4)), destination demand constraint (Eq. (5)), balancing truck distribution over the paths (Eq. (6)), and binary constraints (Eq. (7)).

$$\sum_{d=1}^{D} \sum_{s=1}^{S} x_{tds} \leq 1 \qquad\qquad \forall\, t \in \{1,\ldots,T\} \tag{3}$$

$$\sum_{t=1}^{T} \sum_{d=1}^{D} tc_t x_{tds} \leq sc_s \qquad\qquad \forall\, s \in \{1,\ldots,S\} \tag{4}$$

$$\sum_{t=1}^{T} \sum_{s=1}^{S} tc_t x_{tds} \geq AF \times pc_d \qquad\qquad \forall\, d \in \{1,\ldots,D\} \tag{5}$$

$$0 \leq AF \leq mf \tag{6}$$

$$x_{tds} \in \{0,1\} \quad \forall t \in \{1,\ldots,T\}, \forall d \in \{1,\ldots,D\}, and\ \forall\, s \in \{1,\ldots,S\} \tag{7}$$

where:

x_{ids} binary integer variable to assign truck t to the path connecting shovel s to dump d

tc_t the capacity of truck t

sc_s the capacity of shovel s

pc_d the capacity of dump d (ton)

AF adjustment factor that forces model to distribute extra available trucks among all the possible destinations evenly

mf the proportion of the cumulative available trucks' capacity to the cumulative required path flow rate that can be met using the available trucks

pf_{sd} the required path flow rate for the path from shovel s to dump d based on upper stage decisions

$pmsf_{sd}$ met so far path flow rate for the path from shovel s to dump d

Constraint (3) makes sure that truck t cannot be assigned to more than one shovel. Constraint (4) ensures that summation of the nominal capacity of all the trucks assigned to shovel s does not exceed the shovel's nominal digging rate (capacity). AF in constraint (5) is defined as an adjustment factor. The adjustment factor is a variable that is forcing the model to distribute the truck fleet capacity between all the destinations evenly and is constrained by mf as in Eq. (6). mf is a matching factor that is calculated based on cumulative available truck capacity and cumulative path material handling requirement using Eq. (8). This factor is equal to 1 when the total truck fleet capacity is less than the required path flow rate and is equal to the proportion of the available truck capacity to the full path requirements when

there is extra fleet capacity available. The adjustment factor is constrained by *mf* to uniformly distribute the additional truck fleet capacity among all the needy paths to balance ore and waste production.

$$mf = \max\left\{ 1, \frac{\sum\limits_{t=1}^{T} tc_t}{\sum\limits_{s=1}^{S}\sum\limits_{d=1}^{D} (pf_{sd} - pmsf_{sd})} \right\} \quad \forall t \in \{1,...,T\}, \forall d \in \{1,...,D\}, and \forall\ s \in \{1,...,S\} \quad (8)$$

where:
  tc_t truck capacity for truck t in the fleet
  pf_{sd} the path flow rate for a path linking shovel s to dump d
  $pmsf_{sd}$ The path flow rate for path linking shovel s to dump d that has been met so far

4   APPLICATION TO A CASE STUDY

To test the developed framework in a case study, we need two types of data, the strategic schedule, and the technical and the operational data. However, because of the unavailability of required data from the operating mine, the strategic production schedule was borrowed form Upadhyay (2016), and the operating equipment are assumed. The required distributions for processes of truck and shovel operation were fitted on the historical data using operational data of an existing mine.

4.1   *Mine location and its operational data*

Gol-E-Gohar iron ore mine is located in Kerman Province of Iran. The project lies in the southwest of the province, approximately 50 km southeast of the city of Sirjan. Mining operation in Gol-E-Gohar is being handled by a truck and shovel material handling system.

   The equipment that we assessed consists of five shovels and 31 trucks (Table 1). There are three main dumping points for the loaded trucks including two processing plants and one waste dump.

4.2   *Results of applying the framework in the case study*

The developed simulation and optimization framework was applied to the case study for two times. The first time we ran it for simulating the operation of the case study with its in place truck dispatching system which is the backbone model of the Modular Mining DISPATCH (Modular Mining Systems 2017) developed by White & Olson (1986). Then, we replaced the in place truck dispatching system with the model we developed in this study and reran the simulation. We set up the simulation to run for ten shifts of the operation to capture impacts of the previous shifts on the ongoing or next shifts. We also set up the simulation for 20 replications for reaching the required half widths for the production measurables. After

Table 1.   General specifications of the production fleet.

No.	Loading point	Destination	Starting distance (m)	Loader	Hauler
1	Shovel 1	Plant 1	4129	Hitachi EX2500	Cat 785C
		Plant 2	3626		
2	Shovel 2	Plant 1	4196	Hitachi EX2500	Cat 785C
		Plant 2	3693		
3	Shovel 3	Waste Dump	1930	Hitachi EX5500	Cat 785C
4	Shovel 4	Waste Dump	1850	Hitachi EX5500	Cat 785C
5	Shovel 5	Waste Dump	4295	Hitachi EX2500	Cat 785C

running the simulation models, we compared results of implementing the benchmark truck dispatching model and the MILP truck dispatching model and the results of the comparison are presented in this section.

We first divided the production measurables into two categories: measurables that are used to evaluate how the operation meets the production requirement and measurables that are used to assess the performance of the operation fleet. Table 2 lists the measurable measurables we used to compare our developed MILP truck dispatching model with the in place truck dispatching model in the case study.

The operation runs with two processing plants with 27600 tons/shift feed requirement for each plant. Figure 2 presents a comparison on how the shift-by-shift plant feed requirement is met by implementing the in place truck dispatching model (the backbone of Modular Mining DISPATCH® (Modular Mining Systems 2017)) and the MILP truck dispatching model presented in this paper. The graphs in Figure 2 show that with in place truck dispatching model, current fleet (31 Cat 785C trucks) is not able to meet the plant 1 and plant 2 shift-by-shift feed requirement. However, the same graphs show that by replacing the in place truck dispatching model with the MILP model developed in this study, the current fleet (31 Cat 785C trucks) is capable of meeting the plant 1 and plant 2 feed requirement (dashed blue line). By replacing the in place truck dispatching model with the MILP model the total tonnage of material delivered to the plants improved by more than 10%.

In addition to meeting the plant feed rate requirement, a material handling fleet in surface mine must meet two other essential measurables: stripping ratio and quality of material delivered to the plants (grade). The stripping ratio requirement for the case study is 0.77. This stripping ratio means that for meeting cumulative plants' requirement of 2×27600 tons/shift, the fleet must deliver $2 \times 27600/0.77$ to the waste dump. The graph **a** in Figure 3 shows that during the simulation time, a fleet of 31 Cat 785C is not able to meet the stripping ratio requirement by using the in place truck dispatching model. The same fleet of 31 Cat 785C trucks can meet the stripping ratio requirement if the MILP model developed in this paper is used to make truck dispatching decisions. The material delivered to the plants by the fleet

Table 2. Measurable measurables to compare the performance of the truck dispatching models.

No.	Category	Metric	Unit	Desired target
1	Production	Plant feed rate	Tons/shift	27600 per plant
		Plant head grade	%	60 to 80
		Stripping ratio	–	0.77
2	Fleet performance	Shovel utilization	%	N/A
		Truck wait time	minute	N/A
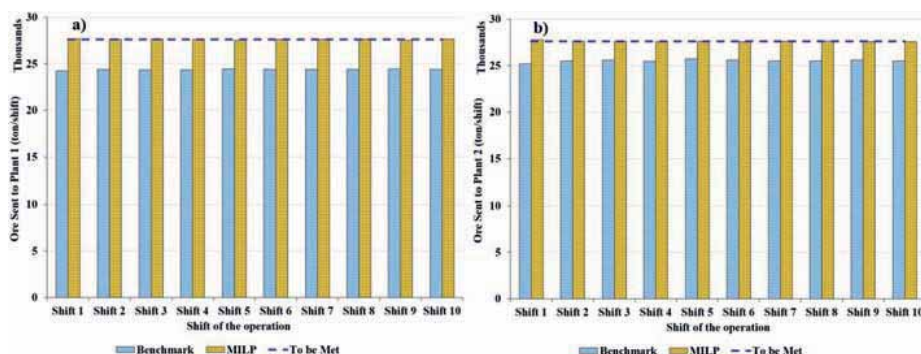
Figure 2. Production measurables, the tonnage of ore delivered to plants in each shift: a) ore delivered to plant 1, b) ore delivered to plant 2.

must follow the plants' head grade requirement. The graph **b** in Figure 3 compares the grade of material delivered to each plant over the simulation run time. Minimum acceptable grade for material to be fed into the plants is 60% and the maximum is 80%. The material delivered to the plants must have grade between 60% and 80% MWT. The graph **b** in Figure 3 shows that during the simulation run time, material delivered to the plants using both truck dispatching models fall into the acceptable range. However, using the MILP truck dispatching model the simulation shows less deviation of the grade from the average head grade compared to the in place truck dispatching model.

The efficiency of the fleet is of high priority in any surface mining operation as it has a direct impact on plant efficiency and the operational costs. Figure 4 depicts a comparison between the performance of active shovels **a** and **b** working trucks in the operation of the case study while using the in place truck dispatching model and replacing it with the MILP model we developed in this research. Figure 4a shows that the in place truck dispatching model sends more trucks to the waste shovels. However, based on Figure 2, the operation is not able to meet the feed rate requirement of the plants. The reason behind sending more trucks to the waste shovels than ore shovels is the decision making model in the in place truck dispatching model. By replacing the in place model with the MILP model, the dispatching decisions are made in a way that the ore shovels are receiving required trucks to feed the plants and the waste shovels are receiving enough trucks to meet the stripping ratio requirement. Another advantage of the MILP model is depicted in Figure 4b. The summation of the time a truck has to spend in queues shows an average of 6.5% improvement by replacing
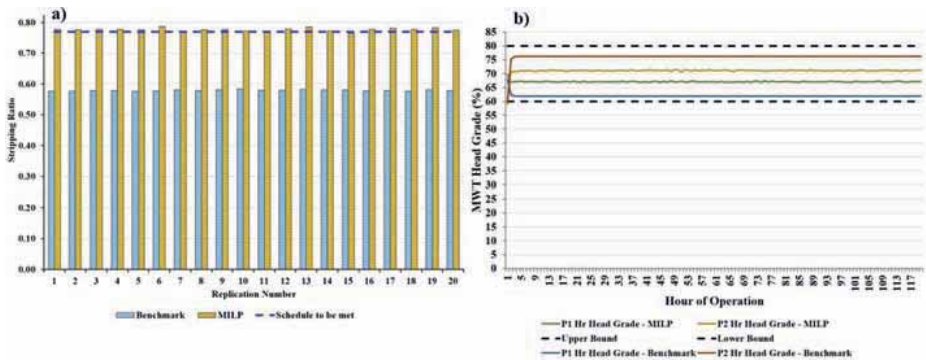
Figure 3.   Production measurables to be met: a) stripping ratio, b) plants MWT grade.
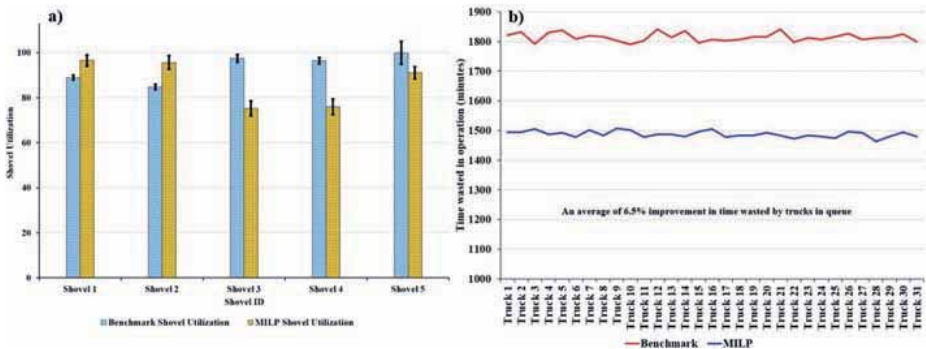
Figure 4.   Equipment measurables: a) shovel utilization, b) cumulative time each truck in the truck fleet wasted in queues.

the in place truck dispatching model with the MILP model. It is because the MILP model considers the time a truck will spend in the queue in its decision making process.

5 CONCLUSIONS

A simulation and optimization framework was presented in this paper to be implemented in the evaluation of surface mining operations. We implemented the developed framework to evaluate the impacts of replacing an in place truck dispatching model with a new truck dispatching model developed by authors in a surface mine case study. The new truck dispatching model was developed based on mixed integer linear programming method covering drawbacks of currently available models. We first simulated the operation of the case study with its in place truck dispatching model. Then, we implemented our MILP model to dispatch trucks in the simulation of the case study. Evaluation of the results shows significant improvement in the production of the case study and performance of the operation fleet. Production of the case study was improved by above 10%. The shovel fleet performed more effectively, and the truck fleet was able to save 6.5% of its time in the operation.

REFERENCES

Alarie, S. & Gamache, M., 2002. Overview of Solution Strategies Used in Truck Dispatching Systems for Open Pit Mines. *International Journal of Mining, Reclamation and Environment*, 16(1), pp. 59–76. Available at: http://www.tandfonline.com/doi/abs/10.1076/ijsm.16.1.59.3408.

Askari-Nasab, H., Frimpong, S. & Szymanski, J., 2007. Modelling open pit dynamics using discrete simulation. *International Journal of Mining, Reclamation and Environment*, 21(1), pp. 35–49. Available at: http://dx.doi.org/10.1080/17480930600720206.

Ataeepour, M. & Baafi, E.Y., 1999. ARENA simulation model for truck-shovel operation in despatching and non-despatching modes. *International Journal of Surface Mining, Reclamation and Environment*, 13(3), pp. 125–129.

Awuah-Offei, K., Temeng, V.A. & Al-Hassan, S., 2003. Predicting equipment requirements using SIMAN simulation—a case study. *Mining Technology*, 112(3), pp. 180–184. Available at: http://dx.doi.org/10.1179/037178403225003609.

Banks, J., 2001. *Discrete-event System Simulation*, Prentice Hall. Available at: https://books.google.ca/books?id=NV1RAAAAMAAJ.

Bonates, E. & Lizotte, Y., 1988. A computer simulation model to evaluate the effect of dispatching. *International Journal of Surface Mining, Reclamation and Environment*, 2(2), pp. 99–104.

Dindarloo, S.R., Osanloo, M. & Frimpong, S., 2015. A stochastic simulation framework for truck and shovel selection and sizing in open pit mines., 115 (March), pp. 209–219.

Fioroni, M.M. et al., 2008. Concurrent simulation and optimization models for mining planning. *Proceedings of the 40th Conference on Winter Simulation*, pp. 759–767.

Forsman, B., Rönnkvist, E. & Vagenas, N., 1993. Truck dispatch computer simulation in Aitik open pit mine. *International Journal of Surface Mining, Reclamation and Environment*, 7(3), pp.117–120.

Hashemi, A.S. & Sattarvand, J., 2015. Simulation Based Investigation of Different Fleet Management Paradigms in Open Pit Mines-A Case Study of Sungun Copper Mine/Symulacje I Badania Różnych Paradygmatów Wykorzystania Floty Pojazdów I Urządzeń W Kopalniach Odkrywkowych. Studium Przypadku: Ko. *Archives of Mining Sciences*, 60(1), pp. 195–208. Available at: http://www.degruyter.com/view/j/amsc.2015.60.issue-1/amsc-2015–0013/amsc-2015-0013.xml.

Hodkiewicz, M., Richardson, S. & Durham, R., 2010. Challenges and Opportunities for Simulation Modelling Integrating. *Australian Mining Technology Conference*, 1, pp. 163–172.

Jaoua, A., Gamache, M. & Riopel, D., 2012. Specification of an intelligent simulation-based real time control architecture: Application to truck control system. *Comput. Ind.*, 63(9), pp. 882–894.

Jaoua, A., Riopel, D. & Gamache, M., 2012. A simulational framework for real-time fleet management in internal transport systems. *Simulational Modeling Practices and Theory 21*, pp.78–90.

Kolonja, B. & Mutmansky, J.M., 1994. Analysis of truck dispatching strategies for surface mining operations using SIMAN. *Transactions—Society for Mining Metallurgy And Exploration Incorporated*, 296, pp. 1845–1851.

Konyukh, V., Galiyev, S. & Li, Z., 1999. Mine simulation in Asia. *International Journal of Surface Mining, Reclamation and Environment*, 13(2), pp. 57–67. Available at: http://dx.doi.org/10.1080/09208119908944210.

Lynch, A.J. & Morrison, R.D., 1999. Simulation in mineral processing history, present status and possibilities. *The Journal of The South African Institute of Mining and Metallurgy*, 99(6), pp. 283–288.

Mena, R. et al., 2013. Availability-based simulation and optimization modeling framework for open-pit mine truck allocation under dynamic constraints. *International Journal of Mining Science and Technology*, 23(1), pp. 113–119. Available at: http://dx.doi.org/10.1016/j.ijmst.2013.01.017.

Modular Mining Systems, 2017. DISPATCH Fleet Management., 2017 (December 4th). Available at: http://www.modularmining.com/.

Que, S., Anani, A. & Awuah-Offei, K., 2016. Effect of ignoring input correlation on truck–shovel simulation. *International Journal of Mining, Reclamation and Environment*, 30(5–6), pp. 405–421. Available at: http://dx.doi.org/10.1080/17480930.2015.1099188.

Raj, M.G., Vardhan, H. & Rao, Y.V, 2009. Production optimization using simulation models in mines: A critical review. *International Journal of Operational Research*, 6(3), pp. 330–359.

Rist, K., 1961. The solution of a transportation problem by use of a Monte Carlo Technique. In *APCOM 1*. Tucson, Arizona, USA: SME.

Sturgul, J.R., 1999. Discrete mine system simulation in the United States. *International Journal of Surface Mining, Reclamation and Environment*, 13(2), pp. 37–41. Available at: http://dx.doi.org/10.1080/09208119908944207.

Sturgul, J.R. & Eharrison, J., 1987. Simulation models for surface mines. *International Journal of Surface Mining, Reclamation and Environment*, 1(3), pp. 187–189.

Ta, C.H., Ingolfsson, A. & Doucette, J., 2013. A linear model for surface mining haul truck allocation incorporating shovel idle probabilities. *European Journal of Operational Research*, 231(3), pp. 770–778. Available at: http://www.sciencedirect.com/science/article/pii/S0377221713005043 [Accessed April 23, 2015].

Torkamani, E. & Askari-Nasab, H., 2015. A linkage of truck-and-shovel operations to short-term mine plans using discrete-event simulation. *IJMME*, 6(2), pp. 97–118. Available at: http://www.inderscienceonline.com/doi/abs/10.1504/IJMME.2015.070367.

Upadhyay, S.P., 2016. *Simulation optimization of mine operations for uncertainty based short term and operational planning in open pit mines*. University of Alberta.

Upadhyay, S.P. & Askari-Nasab, H., 2017. Dynamic shovel allocation approach to short-term production planning in open-pit mines. *International Journal of Mining, Reclamation and Environment*, pp. 1–20. Available at: http://dx.doi.org/10.1080/17480930.2017.1315524.

Upadhyay, S.P. & Askari-Nasab, H., 2016. Truck-shovel allocation optimisation: a goal programming approach. *Mining Technology*, 00(0), pp. 1–11. Available at: http://www.tandfonline.com/doi/full/10.1179/1743286315Y.0000000024.

Vagenas, N., 1999. Applications of discrete-event simulation in Canadian mining operations in the nineties. *International Journal of Surface Mining, Reclamation and Environment*, 13(2), pp. 77–78.

White, J.W. & Olson, J.P., 1986. Computer-based dispatching in mines with concurrent operating objectives. *MIN ENG-LITTLETON*, 38(11), pp. 1045–1054.

Yuriy, G. & Vayenas, N., 2008. Discrete-event simulation of mine equipment systems combined with a reliability assessment model based on genetic algorithms. *International Journal of Mining, Reclamation and Environment*, 22(1), pp. 70–83.

Framework of optimal operational indices for the open pit mines production scheduling problems

M.R. Moghaddam & E. Moosavi
Department of Mining Engineering, South Tehran Branch, Islamic Azad University, Tehran, Iran

ABSTRACT: Understanding the ways in which production scheduling have been done is critical to analyzing existing production scheduling systems and finding ways to improve them. This paper addresses the problem of developing an optimization structure to aid the operational decision-making of scheduling activities in a real-world mining operation. For this purpose, after a brief description of the problem, there is a brief summary of recent advances in constrained—production scheduling optimization for open pit mines. Our contribution in this paper include proposing a production scheduling framework to optimize some data integration issues according to different planning levels. With the correspondence of a better data—based optimization among production scheduling process, we aim to decline some currently used well-established practices to provide more stable and reliable plans This paper not only reviews the range of concepts and approaches used to improve production scheduling but also demonstrates their timeless importance.

Keywords: Production scheduling, open pit mine, Data-based optimization

1 INTRODUCTION

Mining operations begin with exploration of the area that has the potential for mining and continue with exploratory works throughout the region, such as digging, mapping, and geological interpretation. If the open method is confirmed for extraction, the mineral model is expanded through the numerical modeling methods, and mineral reserves are classified into zones that are eventually blocked into millions of 3-D rectangular blocks (Osanloo 2005). The ore element, grade and other necessary information are collected through drilling boreholes in each block and used for economic evaluation of the blocks. Then the mineral mass model, which includes ore distribution and its expected economic value, is used to determine the ultimate pit limit to identify the economic value of the mine.

Production in open pit mines is planned to determine the mine optimal extraction pattern to not only enjoy of the highest economic profit, but also to meet the physical and operational constraints including:

– Extraction capacity constraint,
– Processing plant capacity constraint,
– Processing plant grade(s) constraint,
– Slope angle constraint.

In other words, annual production scheduling is a decision-making problem in which blocks within the pit limit must be extracted so that the highest net present value (NPV) can be obtained, considering the existing constraints. On the other word, the problem is to find the most appropriate way to extract blocks in a volume that can result in the highest amount of NPV. There are many blocks within the ultimate pit limit, for which annual production scheduling should be performed. But production cannot be planned without knowing the ultimate pit limit; in fact, production scheduling requires the economic value of the blocks, calculation of which requires knowledge of the cut-off grades. The relationship among production
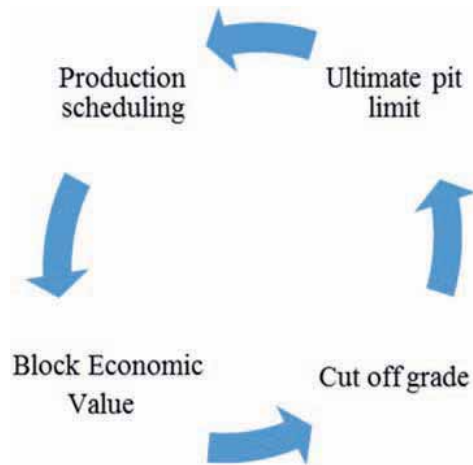
Figure 1. The relationship among production scheduling with the ultimate pit limit, the cut-off grades and the economic value of blocks (Osanloo 2005).

scheduling, the economic value of blocks, the cut-off grades and the ultimate pit limit is similar to a loop like the relationship between chicken and egg (Fig. 1) (Osanloo 2005).

Extensive surveys on different optimization techniques and modeling issues are provided in (Blom et al. 2018; Osanloo et al. 2007; Espinoza et al. 2013). From the literature review, it is found that a number of classical methods have been adopted for solving this problem such as branch and cut method (Caccetta et al. 2003; Bley et al. 2010) mixed-integer programming (MIP) (Gershon et al. 1983; Caccetta, 1998; Ramazan & Dimitrakopoulos 2004; Ramazan et al. 2005; Boland et al. 2009; Bienstock & Zuckerberg 2009; Askari-Nasab et al. 2011; Rimélé et al. 2018), dynamic programming (Roman 1974; Dowd & Onur 1992; Tolwinski & Underwood 1996; Tolwinski 1998; Wang & Chu, 2008), Lagrangian relaxation (Dagdelen et al. 1986; Akaike et al. 1999; Mogi et al. 2001; Gleixner et al. 2008; Boland et al. 2007; Lambert et al. 2013). In the last few years, the dramatic increase in the efficiency of MIP solvers encouraged thorough exploitation of their capabilities and a considerable part of research in this area was directed towards the definition of alternative, more efficient MIP formulations of the problem. Up until now, evolutionary computation techniques have been developed and proposed to solve a wide variety of large-scale problems including production scheduling problem. Specifically, there are Artificial intelligence (Tolwinski & Underwood 1992; Elevli 1995; Ibrahimov et al. 2014), Genetic algorithm (Denby & Schofield 1995; Denby et al. 1998; Zhang 2006; Alipour et al. 2017), simulated annealing (Boucher et al. 2012; Kumral & Dowd 2005), and Particle swarm optimization (Khan & Niemann 2014; Khan 2018).

To reduce the search space in the large-scale problem, and therefore computational time, hybrid methods are efficient than the single methods due to more production efficiency and faster computational time (Shiwei et al. 2012). The hybrid methods are purported to incorporate more complicated constraints and have better quality solutions. Hybrid approaches present several advantages compared to lagrangian relaxation (LR), as thoroughly discussed in (Moosavi et al. 2014). They (i) allow easier integration of additional constraints in the formulation; (ii) Can incorporate more complicated constraints in the model; And (iii) even if optimal results are not available within reasonable time, hybrid solutions usually generate better or equal optimality gaps than ones associated with LR solutions.

In recent times, most of the studies have turned to deal with new solving techniques such as simulation and artificial intelligence techniques. These methods have been proved as a significant forward step in solving production scheduling problems with less computational effort and better results. This paper provides an overview of the recent progress in data-based optimization for production scheduling of open pit mines. Finally, future trends towards the provision of an effective production scheduling problem chart will be discussed.

2 PRODUCTION SCHEDULING METHODS IN MINES

In general, there are three methods for production scheduling in mines:

- The use of trial and error is the first and oldest method in production scheduling. This method is based on the designer, who first considers various options for production of the mine so that all operational and production constraints are satisfied and then the best option with the highest value is selected as the final choice for production scheduling. The proposed program, although practical, is not necessarily economically feasible.
- The use of heuristic methods in production scheduling. In this method, although a good solution can be attained by using optimization techniques and designer's experience, the solution is not necessarily optimal. The floating cone is a heuristic method.
- The use of mathematical programming techniques in optimal production scheduling. Although the proposed program is mathematically optimal, it may be practically impossible to implement because of the lack of direct involvement of the designer in the optimization process.

Therefore, the mine designing and scheduling is a multivariate optimization process and requires a simultaneous solution, which is unfortunately not easily solvable and computable. After three decades of continuous effort, the designing and production scheduling in open pit mines remain unresolved, even considering all aspects at the same time. In this regard, the production designing and scheduling benches of a mine are summarized as follows:

2.1 *Preparation of three dimensional block model of ore deposit*

The increasing use of computers in various scientific topics has led to the idea of developing a block model for minerals. The block model is, in fact, a 3-D display of minerals and rocks in which ores and surrounding rocks are shown as a set of blocks. The best size of blocks complies with geostatistical criteria appropriately and reasonably and is relatively favorable compared to other extractives, technical and economic criteria. As a rule of thumb, the dimensions of the blocks should not be less than one quarter of the distance between the exploratory boreholes, and the height of the blocks usually matches with the height of the extracted benches. Considering the topographic conditions, a number of blocks are usually located in the air that should be eliminated from the calculations. In order to determine the minable blocks, the average grade of each block and the cut-off grades should be calculated using one of the estimation methods. Blocks with a mean grade of greater than or equal to the cut-off grades are considered as minable blocks. In addition to the average grade, weight, discontinuity, water content, mineral type, primary and secondary minerals, mineral processing methods, retrieval rate, revenue, cost, and economic value of the blocks should also be
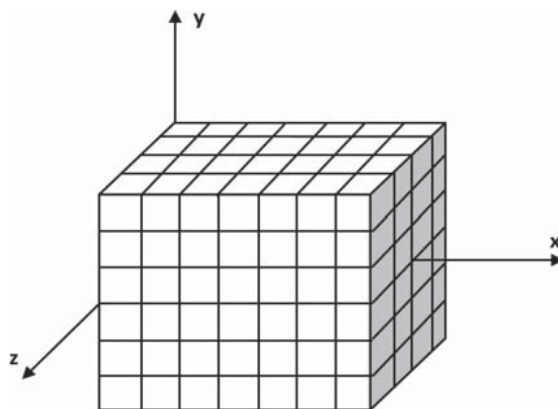
Figure 2.   3-D view of a block model.

calculated for each block. In fact, transforming the ore geological model into an economic block model paves the way to use mathematical optimization methods for mine designing and scheduling. An example of a block model is shown in Fig. 2.

The number of each block along the X, Y, and Z axes indicate the number of columns, rows, and layers or benches and are shown by i, j, and k, respectively.

2.2 Determine of the ultimate pit limit

At this stage, the possible most valuable (optimum) pit is obtained using the Lerch-Grossman 3-D method or the network flow taking into account the safe slope angle in different parts of the mine. This can determine the amount of minable ore reserves.

2.3 Pushbacks design

After designing the ultimate pit limit, extraction of blocks to the ultimate pit limit can be planned using mathematical algorithms. Since the implementation of mathematical models on the whole ultimate pit limit is difficult and impossible in some cases, computerized techniques have been used for extraction from mineral resources in the past two decades, which geometrically resembles to the removal of onion shell from its bulb. Therefore, the blocks in this limit are divided into smaller volumes, which are called pushback. In fact, a pushback refers to the intermediate pits whose successive extraction leads to the extraction of the final pit; in other words, the pushback shows the growth stages of an open pit mine over time. In this method, after determining the ultimate pit limit using the break-even cutoff grade, that limit is converted into a series of smaller pits or pushbacks based on NPV. The initial or central pit, like the core of onion, which has a higher quality than outer shells, has the highest NPV, while NPV is reduced by moving toward the next pushbacks or pits. Depending on the mine size, even 10 pushbacks can be designed for a pit, and the distance between pushbacks or the pushbacks' thickness may vary between 30 to 90 m based on the minable reserve size and the machinery. Each sequence of pushbacks results in a different annual cash flow stream that gives different NPV for a project. Because, a series of pits with different sizes are obtained by generating an economic model at different price for the commodity, cut-off grade, or mining and processing costs (Osanloo 2005, Dagdelen 2000).

2.4 Production scheduling using mathematical algorithms

At this stage, the mathematical model of production scheduling is implemented in the limit of each pushback. Mathematical models not only can determine the pattern of block extraction with maximum profit, but also can guarantee production and geometric constraints.

3 TYPES OF PRODUCTION SCHEDULING AT OPEN PIT MINES

Depending on the time horizon and the intended objectives, production scheduling in mines can be long-term, mid-term, and short-term.

3.1 Long-term production scheduling

Long-term Scheduling is provided to extract and process minerals for a period of 10 to 20 years. The main goal in long-term production scheduling (LTPS) is to prepare the annual (multi-year) plans for all blocks in the ultimate pit limit, but, as already mentioned, since the number of these blocks is very high, all of them cannot be considered for a good annual Scheduling. To solve this problem, the progress should be designed after designing the ultimate pit limit.

The long-term production Scheduling goals are (Steffen 1997):

- Maximizing NPV of the project,
- Minimizing the risk of achieving production goals,
- Maximizing the life-of-mine.

These goals are somewhat contradictory, for example, a program with a maximum NPV may not fit with a plan with a minimum risk; in this case, depending on the risk taking and risk aversion of the designer, a program with a low risk and maximum benefit should be considered for production. Constraints of long-term production Scheduling are as follows (Steffen 1997):

- Minimum and maximum tonnage of ore that must be produced at any time interval.
- Minimum and maximum concentrates to be produced at any time interval.
- The minimum waste tonnage that must be extracted at any time interval in order to have access to sufficient quantities of minable ore in the subsequent periods.
- The maximum number of benches from which extraction is carried out at any time interval.
- The highest and the lowest benches from which extraction is carried out at any time interval.
- Minimum and maximum qualitative parameters related to the mine final product.
- The minimum tonnage of the remaining ore at any time interval.
- The minimum remaining waste at any time interval.
- Slope angle constraint.
- Constraints of ore depos.
- Minimum pit floor width.
- Existence of underground mines or large underground spaces around open pit mines that change the long-term production Scheduling.
- Existence of a waste dump or processing plant waste due to the mining activity that was previously done in that area.
- Existence of transmission lines and roads around the mine.

3.2 Mid-term production scheduling

The length of the production Scheduling horizon varies from one to ten years. It is divided into a range of one to six months, and is special in nature. The mid-term production scheduling (MTPS) are, in fact, the basis for short-term production scheduling (STPS) in mines. The purpose of this plan is to predict production, cost, and revenue. The parameters to be specified in the preparation of this plan are as follows (Steffen 1997):

- The production and operation of shovels and trucks and drilling equipment in one to six months' intervals.
- Grades, retrieval amount, and physical and chemical characteristics of blocks for short-term Scheduling in later stages.
- Prediction of construction and preparation works required in subsequent years (such as roads, opening of a new area of the mine, construction of a rinse lake).
- Waste dumps that should be used to accumulate waste in the future.

3.3 Short-term production scheduling

The length of the scheduling horizon in this case is less than one year and short-term plans are prepared in intervals of one day to one month. Short-term scheduling objectives in mines are (Steffen 1997):

- Providing blending requirements in terms of the quality of materials conveyed to the plant at any time.
- Supplying the required blending site and processing plant to provide the required tonnage for the processing plant.

- Maximum use of mineral equipment capacity.
- Minimizing deviations from long-term production Scheduling.
- Ensuring that the mentioned goals can be achieved in the coming years or months.
- Considering the angles of steady slope in different parts of the mine.
- Providing access to all working benches in the mine.
- Ensuring of the required width for maneuvering the shovel and truck on the benches.

If short-term plans could be prepared for mining to achieve all of the above objectives, it could be claimed that the profits will be maximized. It is worth noting that in the short-term scheduling, the overall capacity of the equipment is considered, but no plan is prepared for the machinery at this stage, meaning that the place and time of equipment use is not determined.

4 DECISION DEPARTMENTS AT OPEN PIT MINES

Given the fact that mining projects are usually long-term projects in which economic problems of current interest have a significant role, an accurate scheduling is required to design and implement them based on different factors. For this purpose, three intervals are considered in open-pit mine production scheduling: long-term, mid-term, and short-term scheduling intervals (Graves 1981).

Fig. 3 indicates a general overview of decision-making methods for extracting minerals. The first area includes production scheduling decision-making in the long-term mine production
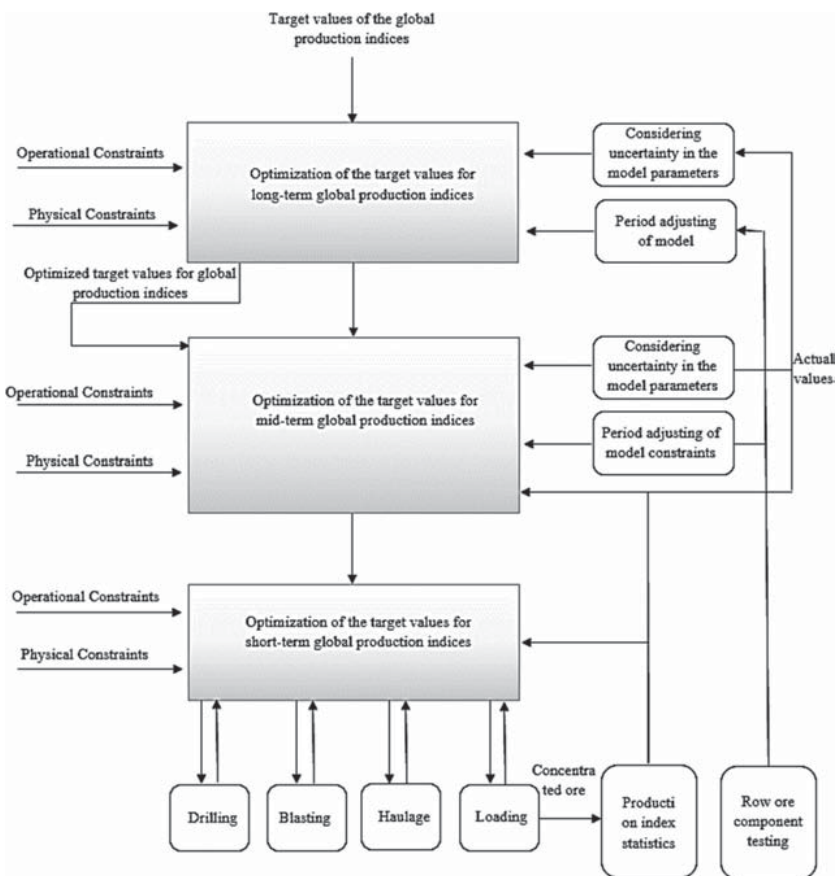
Figure 3. Typical framework for the optimization of operational indices of production scheduling.

scheduling interval. During the years of minerals extraction, scheduling is based on specific information on extraction method, project investment, available mining machinery, mining costs, and geological information of ore deposits in long-term scheduling. After scheduling, it is necessary to determine specialized departments (Drilling, Blasting, Loading, Hauling, etc.), on each of which decisions are made separately. Since the output of each department should be checked, special monitoring seems to be necessary in each section. Finally, technical corrections are taken into account to make the ultimate decisions on each section.

5 STRUCTURE OF THE PRODUCTION SCHEDULING PROBLEM AT OPEN PIT MINES

Production scheduling optimization includes three levels including decomposition of decision-making methods in relation to production indices on different time scales. The high-level decision-making goals include achieving a set of favorable production goals (mainly on a long-term scheduling scale). However, the low-level decision-making goals include conducting more analyses on every specific interval (mainly short-term and daily scales) to achieve the goals of higher levels of decision-making.
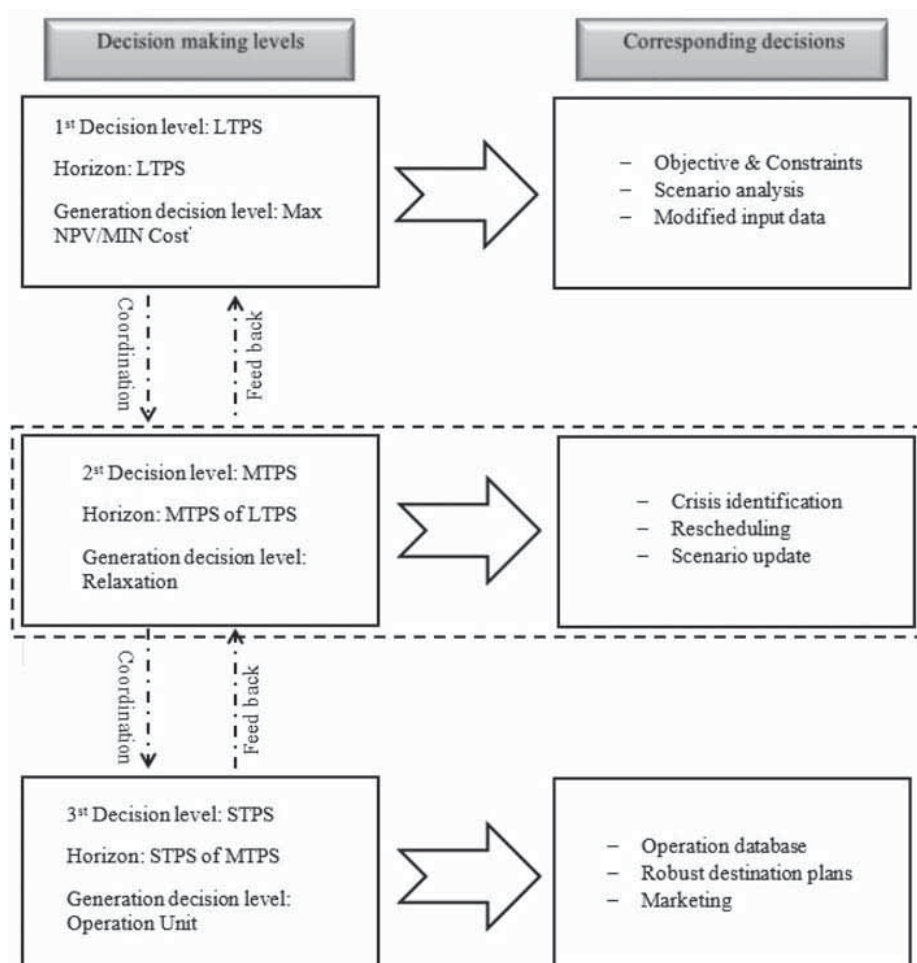
Figure 4.   The proposed structure of level decision making framework.

Production scheduling optimization focuses mainly on decreasing costs and maximizing profits in a specific period of time. Regarding the optimization of production indices, Mohammadi et al. (2017) conducted a study on fineness modulus optimization. Moreover, Xu et al. (2018) carried out a study on the environmental optimization of mine production scheduling. Ramazan (2007) employed three basic algorithms of mine production scheduling to develop a new algorithm based on linear scheduling for the whole blocks of minerals. For this purpose, it was necessary to decrease the number of integer variables and constraints required in the integer scheduling formulation. Likewise, Ahmadi and Shahabi (2018) used the genetic algorithm to optimize the fineness modulus of ores extracted from mines. Yu et al. (2013) proposed a method to provide a raw combination of ore deposits efficiently for decision-making (based on the features of ore deposits). Xu et al. (2018) optimized production indices based on dynamic scheduling. In a study on production scheduling improvement, Taylor defined how production scheduling operated. Janet prepared an appropriate flowchart for the production scheduling problem, and Johnson focused on a mathematic formulation of the scheduling problem (Herrmann et al. 2007). Chai et al. (2011) proposed an integrative optimization method justifying case-based reasoning (CBR) with a multi-objective evolutionary algorithm (MOEA). In their method, CBR decision-making of operational indices was based on the operational experiences of engineers; however, MOEA benefited from the multiple optimization of production indices. Ding et al. (2013) solved a multi-bench optimization problem and proposed a multi-objective optimization solution in order to achieve the appropriate efficiency. In practice, the optimization of operational indices is usually a dynamic problem.

Operational indices result from the decomposition and optimization of production scheduling indices. Based on these indices, there are unknown relationships between existing constraints, evaluation of different scenarios, and input data improvement. Therefore, it is important to coordinate decisions resulting in unique operational indices bringing about production scheduling indices. Fig. 4 indicates an approach along with a typical framework for the optimization of operational indices. It also shows the open-loop optimization structure including long-term, mid-term, and short-term production scheduling intervals.

6 CONCLUSIONS

Over the last decade research into scheduling, particularly in its most common operational form of production scheduling, has risen in importance due to the demands of open pit mine. While much progress has been made on an academic front, doubts remain over the transfer of the science to fit the flexibility requirements of modern production scheduling. Production scheduling has received much attraction in the literature as the solution is made more difficult through the requirement to satisfy the conflicting demands of both objective function and production constraints. All of the production parameters should be optimized for mine production scheduling optimization. For this purpose, the initial structure of the mine production problem was dealt with in this paper to focus on the optimization of mineral production indices. If priorities are identified and complied with correctly in decision-making, it will be possible to modify and improve every operation separately. In fact, technical parameters of production indices are uncertain, and it is important to improve input data in each section. To this end, appropriate structures were proposed to emphasize different sections of description and monitoring problems. It is also recommended that decision-making sections should be integrated with scheduling for the optimization of operational indices, processes, and control in future studies.

REFERENCES

Ahmadi, M.R. & Shahabi, R.S. 2018. cut-off grades optimization in open pit mines using genetic algorithm. *Research Policy* 55: 184–191.

Akaike, A. & Dagdelen, K.A. 1999. Strategic Production Scheduling Method for an Open Pit Mine, *Proc. 28th Symp*. *Application Computers and Operation Research in the Mineral Industry*.

Alipour, A. Khodaiari, A.A. Jafari, A. & Tavakkoli Moghaddam, R. 2017. A genetic algorithm approach for open-pit mine production scheduling. *International Journal of Mining and Geo-Engineering* 51(1): 47–52.

Askari-Nasab, H. Pourrahimian, Y. Ben-Awuah, E. & Kalantari, S. 2011. Mixed Integer Linear Programming Formulations for Open Pit Production Scheduling, *J. Min.Sci* 47.

Bienstock, D. & Zuckerberg, M. 2009. *A New Algorithm for Precedence Constrained Production Scheduling:* Optimization Online.

Bley, A. Boland, N. Fricke, C. & Froyland, G. 2010. A Strengthened Formulation and Cutting Planes for the Open Pit Mine Production Scheduling Problem, *Computer Operation Research* 37.

Blom, C. Pearce, A.R. & Stuckey, P.J. 2018. Short-Term Planning for Open Pit Mines, *A Review, International Journal of Mining Reclamation and Environment*: Published online, DOI: 10. 1080/17480930.

Boland, N. Dumitrescu, I. Froyland, G. & Gleixner, A.M. 2009. LP-Based Disaggregation Approaches to Solving the Open Pit Mining Production Scheduling Problem with Block Processing Selectivity. *Computer Operation Research* 36.

Boland, N. Fricke, C. & Froyland, G. 2007. A Strengthened Formulation and Cutting Planes for the Open Pit Mine Production Scheduling Problem. *Computers and Operations Research* 37.

Boucher, A. & Dimitrakopoulos, R. 2012. Multivariate Block-Support Simulation of the Yandi Iron Ore Deposit. *Mathematical Geosciences* 44.

Caccetta, L. 1998. Open Pit Mine Production Scheduling. *3rd Regional Proceeding of Application Computers and Operation Research in the Mineral Industry*.

Caccetta, L. & Hill, S.P. 2003. An Application of Branch and Cut to Open Pit Mine Scheduling. *Journal Global Optimization* 27.

Chai, T. Ding, J. & Wu, F. 2011. Hybrid intelligent control for optimal operation of shaft furnace roasting process. *Control Engineering Practice* 19 (3): 264–275.

Dagdelen, K. & Johnson, T.B. 1986. Optimum Open Pit Mine Production Scheduling by Lagrangian Parameterization, Proc. *19th Symp. Application Computers and Operation Research in the Mineral Industry*.

Dagdelen, K. 2000. Open pit optimization—Strategies for improving economics of mining projects through mine planning. *Application Computers for Mining Industry*: 125–1.29.

Denby, B. & Schofield, D. 1995. The Use of Genetic Algorithms in Underground Mine Scheduling, Proc. *25th Symp. Application Computers and Mathematics in the Mineral Industry*.

Denby, B. Schofield, D. & Surme, T. 1998. Genetic Algorithm for Flexible Scheduling of Open Pit Operations, Proc. *27th Int. Symp. Application Computers and Mathematics in the Mineral Industry*.

Ding, W.T. Zhang, G.C. & Liu, J.J. 2013. 3' Truncation of the GPD1 promoter in Saccharomyces cerevisiae for improved ethanol yield and productivity. *Appl Environ Microbiol* 79(10): 3273–81.

Dowd, P.A. & Onur, A.H. 1992. Optimizing Open Pit Design and Sequencing, Proc. *23rd Symp. Application Computers and Operation Research in the Mineral Industry*.

Elevli, B. 1995. Open Pit Mine Design and Extraction Sequencing by Use of OR and AI Concept. *International Journal Surface Mining Reclamation Environment* 9.

Espinoza, D. Goycoolea, M. Moreno, E. & Newman, A. 2013. MineLib. A Library of Open Pit Mining Problems. *Annals of Operations Research* 206.

Gershon, M.E. 1983. Optimal Mine Production Scheduling, Evaluation of Large Scale Mathematical Programming Approaches. *International Journal of Mining Engineering* 1.

Gleixner, A. 2008. *Solving Large-Scale Open Pit Mining Production Scheduling Problems by Integer Programming, Master's Thesis*: Technische Universität Berlin.

Graves, S.C. 1981. Multistage Lot—Sizing. An Iterative Procedure. *Technical Report No. 164, Operations Reserch Center, Massachusetts Institue of Technology*. 1979. (To appear in TIMS Studies in Management Science, Multi—Level Productions/Inventory Systems. Teory & Practice, Edited by L.B. Schwarz).

Herrmann, G. Kais, S. Hoffbauer, J. Shah-Hosseini, K. Brüggenolte, N. Schober, H. Fäsi, M. & Schär, P. 2007. *Journal Article|Research Support*. Non-U.S. Gov't: LIF1, SPP382. DNL4, NEJ1, PXR1.

Ibrahimov, M. Mohais, A. Schellenberg, S. & Michalewicz, Z. 2014. Scheduling in Iron Ore Open-Pit Mining, *The Int. J. Advanced Manufacturing Technology* 72.

Khan, A. & Niemann-Delius, C. 2014. Production Scheduling of Open Pit Mines Using Particle Swarm Optimization Algorithm. *Advances in Operations Research*.

Khan, A. 2018. Long-term production scheduling of open pit mines using particle swarm and bat algorithms under grade uncertainty. *The Southern African Institute of Mining and Metallurgy* 118: 361–368.

410

Kumral, M. & Dowd, P.A. 2005. A Simulated Annealing Approach to Mine Production Scheduling. *Journal of Operational Research Society* 56.

Lambert, W.B. & Newman, A.M. 2013. Tailored Lagrangian Relaxation for the Open Pit Block Sequencing Problem. *Annals of Operation Research*, DOI: 10.1007/s10479-012-1287.

Mohammadi, M. Attaran, B. & Malekzadeh, R. 2017. Furazolidone, an Underutilized Drug for H. pylori Eradication, *Lessons from Iran. Digestive diseases and sciences Published. Jun*–02 DOI: 10.1007/s10620-017-4628-5.

Mogi, G. Adachi, T. Akaike, A. & Yamatomi, J. 2001. Optimum Production Scale and Scheduling of Open Pit Mines Using Revised 4D Network Relaxation Method. *Proc. 17th Int. Symp. Mine Planning and Equipment Selection.*

Moosavi, E. Gholamnejad, J. Ataee-pour, M. & Khorram, E. 2014. *A Hybrid Augmented Lagrangian Multiplier Method for the Open Pit Mines Long-Term Production Scheduling Problem Optimization, J. Min.* Sci 50.

Osanloo, M. 2005. *Surface mining methods*. Tehran, Iran: Amir Kabir University of Technology Publication.

Osanloo, M. Gholamnejad, J. & Karimi, B. 2007. Long-Term Open Pit Mining Production Planning. A Review of Models and Algorithms. *International Journal of Mining Reclamation and Environment* 22.

Ramazan, S. & Dimitrakopoulos, R. 2004. Traditional and New MIP Models for Production Scheduling with In-Situ Grade Variability. *Int. Journal Surface Mining Reclamation Environment* 18.

Ramazan, S. Dagdelen, K. & Johnson, T.B. 2005. *Fundamental Tree Algorithm in Optimizing Production Scheduling for Open Pit Mine Design.* Trans: Inst Min Metall.

Ramazan, S. 2007. The new fundamental tree algorithm for production scheduling of open pit mines. *European Journal of Operational Research* 177(2): 1153–1166.

Rimélé, A. Dimitrakopoulos, R. & Gamache, M. 2018. A stochastic optimization method with in-pit waste and tailings disposal for open pit life-of-mine production planning. *Resources Policy* 57: 112–121.

Roman, R.J. 1974. The Role of Time Value of Money in Determining an Open Pit Mining Sequence and Pit Limits. *Proc. 12th Symp. Application Computers and Operation Research in the Mineral Industry*.

Shiwei, Y. Kejun, Z. & Youn, H. 2012. A Hybrid Intelligent Optimization Method for Multiple Metal Grades Optimization. *Neural Computing and Application* 6.

Steffen, O.K.H. 1997. Planning of open pit mines on a risk basis. *The Journal of the South Afrrican Institute of Mining and Metallurgy*: 47–56.

Tolwinski, B. & Underwood, R. 1992. An Algorithm to Estimate the Optimal Evolution of an Open Pit Mine, Proc. 23rd Symp. *Application Computers and Operation Research in the Mineral Industry*.

Tolwinski, B. & Underwood, R. 1996. A Scheduling Algorithm for Open Pit Mines. *IMA Journal of Mathematics Applied in Business and Industry* 7.

Tolwinski, B. 1998. Scheduling Production for Open Pit Mines. Proc. *27th Int. Symp. Application Computers and Operation Research in the Mineral Industry.*

Yu, H.H. Awasaki, T. Schroeder, M.D. Long, F. Yang, J.S. He, Y. Ding, P. Kao, J.C. Wu, G.Y. Peng, H. Myers, G. & Lee, T. 2013. Clonal development and organization of the adult Drosophila central brain. *Curr. Biol* 23(8): 633–643.

Wang, Q. Gu, X. & Chu, D. 2008. A Dynamic Optimization Method for Determining Cutoff Grades in Unerground Mines. *Mineral Resources Management*.

Xu, F.G. Harten, D.J. Diner, A.B. Davis, F.C. Seidel, B. Rheingans, M. Tosca, M.D. Alexandrov, B. Cairns, R.A. Ferrare, S.P. Burton, M.A. Fenn, C.A. Hostetler, R. Wood & Redemann, j. 2018. Coupled retrieval of liquid water cloud and above-cloud aerosol properties using the Airborne Multiangle SpectroPolarimetric Imager (AirMSPI). *Geophys, j. Res. Atmos* 123, 6, 3175–3204, doi: 10.1002/2017 JD027926.

Zhang, M. 2006. Combination Genetic Algorithms and Topological Sort to Optimize Open-Pit Mine Plans. *Proc. 15th Conf. Mine Planning and Equipment Selection*: Torino, Italy.

Mine schedule optimization and mine operational realities: Bridging the gap

A. Chowdu
South Dakota School of Mines and Technology, Rapid City, SD, USA

M. Goycoolea
Universidad Adolfo Ibanez, Peñalohén, Santiago, Chile

A. Brickey
South Dakota School of Mines and Technology, Rapid City, SD, USA

ABSTRACT: Advancement in solution algorithms and computing power continues to drive the adoption of optimization techniques within the underground mining sector. However, limitations in the available data and the choices made during the model setup can create a gap between optimal solutions and operational reality. This paper presents a mining practitioner's guide on effectively utilizing Multi-time Period Knapsack Constraints (MPKC) in scheduling underground mine production, which can close part of that gap. Models with MPKC implemented at different time fidelities, i.e., weekly, monthly and annual, are compared by evaluating solution quality and solver performance. We provide recommendations that can assist in developing both optimal and operationally representative schedules.

Keywords: Underground mining, Production scheduling, Optimization

1 INTRODUCTION

Optimization models are approximate representations of real-world systems. Practitioners often must make simplifying assumptions to ensure feasibility or relax constraints to improve tractability. Any such model's purpose is to provide useful information and improve decision-making abilities. With any model formulation, it is important that the assumptions made do not detract from the model's applicability to the operation. Advances in computation power and solution algorithms have enabled researchers to create and solve model formulations more complex and operationally representative than previously possible. In this paper, we explore some of the recent advances in constructing models with a particular focus on underground mine production schedules.

Williams et al. (1973) were the first to make use of operations research principles to develop an underground production schedule that maximized ore production at a copper operation. The original intent of the project was to formulate a linear program to produce "good" schedules; however, the group was unable to define the qualities that comprised a "good" schedule. Revising their approach, they instead set out to produce a tool to that would help planners evaluate several schedules and then choose the "best" option; while not necessarily achieving optimality, they expected to realize a significant improvement over manual scheduling. As computational power increased with time, researchers began developing integer programs, incorporating binary variables and allowing for 'yes-no' decisions (Trout, 1995; Winkler, 1996). Trout utilized an integer programming model to schedule the operational sequence, i.e., extraction and backfilling, of 55 stopes at the Mt. Isa copper mine in Australia. With over 3500 variables and 6900 constraints, it was substantially larger than

previous attempts. After 200 hours of computation time, the program had not converged on an optimal solution; however, the solution did result in a 24% increase in NPV over the current mine schedule after only 1.6 hours of computation.

Surface mine optimization has been researched and applied to the industry since the 1960s, (Lerchs and Grossmann, 1964; Johnson, 1968). Today, there are numerous commercially available tools utilizing optimization techniques to improve surface operations, e.g., Geovia Whittle Dassault Systèmes (2018), Pit Optimizer Maptek Pty Ltd (2016), MineSight Economic Planner Hexagon AB (2019), to name a few. Over the last two decades, researchers and industry have worked to develop similar tools for underground mine planning. Today, underground mine planners utilize SOT+ (MIRARCO Mining Innovations, 2018), often in conjunction with a 3-dimensional mine design package. SOT+ uses heuristics to develop feasible schedules, iteratively improving over the previously best known solution, that may or may not provide an optimal solution.

Recent research has focused on using deterministic (Brickey, 2015; O'Sullivan, 2014; Little et al., 2008; Topal, 2008; Newman et al., 2003) and stochastic optimization (Carpentier et al., 2016) to produce robust and optimal underground mine schedules. This paper focuses on modeling techniques, existing and new, that can improve the solution quality of deterministic optimization applications to underground production scheduling. A substantive review of underground mine optimization applications can be found in Alford et al. (2007) and Newman et al. (2010).

2 UNDERGROUND MINE PRODUCTION SCHEDULING

Production scheduling is an integral part of the mine planning process. Scheduling underground operations differs from open pit scheduling and is generally considered more challenging and complex (O'Sullivan et al., 2015) to accomplish. Optimizing underground schedules, consequently, also differs significantly from open pit scheduling. Underground excavations are represented as activities, with varying associated tonnages and production rates. Activities can be broadly delineated into (*i*) production, i.e., stopes, top-cuts, under-cuts, (*ii*) development, i.e., ramps, shafts, raises, and (*iii*) auxiliary, i.e., sumps, electric stations.

The traditional production scheduling process endeavors to determine a feasible sequence of these activities such that operational objectives are met (Newman et al., 2010). When optimizing the schedule, the operational goal(s), e.g. maximizing net present value or minimizing costs, is represented by the objective function, while sequencing and resource limitations constrain the model. Operational objectives are often based on corporate goals. Sequencing constraints (or activity precedence) are derived from geotechnical limitations, and physical or operational sequencing. Lastly, resource constraints enforce operational limitations such as equipment capacity, milling capacity and even ventilation requirements.

Production schedules can be categorized on the basis of time horizon as either strategic (long-term) or tactical (short-term). As the names suggest, a strategic schedule is used to provide a big-picture view of the operation, while the tactical schedule aims to inform activity sequencing at a weekly, daily or shift fidelity.

2.1 *The UG-RCPSP model*

An underground production schedule optimization model is used to determine the start dates for a set of activities in order to maximize the operation's value (Net Present Value), while adhering to precedence and resource constraints (King et al., 2017). The Underground Resource Constrained Production Scheduling Problem (UG-RCPSP) model builds on the work of Brickey (2015), a particular case of the resource constrained project scheduling problem (RCPSP). The RCPSP is a known NP-hard problem (Artigues et al., 2013) that consists of scheduling activities over time, subject to precedence and resource availability constraints. The following generalized formulation illustrates the UG-RCPSP.

Indices and sets:

$a \in \mathcal{A}$ set of all activities

$\tilde{a} \in \tilde{\mathcal{A}} \subset \mathcal{A}$ set of activities whose start dates have been predetermined

$\check{a} \in \check{\mathcal{A}}_a$ set of predecessors for activity a

$\overline{a} \in \overline{\mathcal{A}}_a$ set of predecessor activities $\overline{a}$ that must be completed one period in advance of activity a

$r \in \mathcal{R}$ set of resources, such as production and development capacity, whose limits are enforced on a daily basis

$r \in \hat{\mathcal{R}} \subset \mathcal{R}$ set of resources, such as production and development capacity, whose limits are enforced on a monthly basis

$t \in \mathcal{T}$ set of daily time periods

$m \in \mathcal{M}$ set of monthly time periods

$t \in \hat{\mathcal{T}}_m$ set of days contained in month m

Parameters:

c_a monetary value associated with completing activity a [\$]

q_{ra} quantity resource r consumed on a daily timescale when completing activity a [tonnes, meters]

$\hat{q}_{ra}$ quantity resource r consumed on a monthly timescale when completing activity a [tonnes, meters]

$\overline{r}_{rt}$ maximum amount of resource r available on day t [tonnes, meters]

$\hat{r}_{rm}$ maximum amount of resource r available in month m [tonnes, meters]

d_a duration of activity a [days]

$\hat{d}_a$ duration of activity a [months]

$d_{\overline{a}}$ duration, and any associated delay duration, of activity a [days]

δ_t discount factor for period t [fraction]

Decision variables:

X_{at} 1 if activity a is completed by the end of time t; 0 otherwise

$$(\mathbf{Z}) \max \sum_{a \in \mathcal{A}} \sum_{t \in \mathcal{T}} \delta_t c_a \left(X_{at} - X_{a,t-1} \right) \tag{1a}$$

$$\text{s.t.} \quad X_{a,t-1} \leq X_{at} \quad \forall a \in \mathcal{A}, t \in \mathcal{T} \tag{1b}$$

$$X_{at} \leq X_{\overline{a}, t-d_{\overline{a}}} \quad \forall a \in \mathcal{A}, \overline{a} \in \overline{\mathcal{A}}_a, t \in \mathcal{T} \tag{1c}$$

$$\sum_{a \in \mathcal{A}} \frac{q_{ra}}{d_a} \left(X_{at} - X_{a,t-d_a} \right) \leq \overline{r}_{rt} \quad \forall r \in \mathcal{R}, t \in \mathcal{T} \tag{1d}$$

$$\sum_{t \in \hat{\mathcal{T}}_m} \sum_{a \in \mathcal{A}} \frac{\hat{q}_{ra}}{\hat{d}_a} \left(X_{at} - X_{a,t-\hat{d}_a} \right) \leq \hat{r}_{rm} \quad \forall r \in \hat{\mathcal{R}}, m \in \mathcal{M} \tag{1e}$$

$$X_{\tilde{a}1} = 1 \quad \forall \tilde{a} \in \tilde{\mathcal{A}} \tag{1f}$$

$$X_{at} \text{ binary} \quad \forall a \in \mathcal{A}, t \in \mathcal{T} \tag{1g}$$

The objective function (1a) maximizes discounted cash flow. Constraints (1b) and (1c) provide the sequence of activities, i.e., precedence, and enforce when an activity can begin based on predecessor requirements, respectively. Constraint (1d) represents a daily capacity for all resources, whereas constraint (1e) represents a multi-time period resource constraint. The latter constraint is discussed in detail in Section 2.1.1. Finally, constraints (1f) and (1g) enforce start dates for certain predetermined activities (Section 2.1.2) and that the decision variable is binary, respectively. This is a generalized formulation, which can be adapted to suit different operations as required.

Using recently developed linear programming algorithms (Bienstock and Zuckerberg, 2009; Muñoz, 2012), in conjunction with customized rounding (Chicoisne et al., 2012), research has shown that it is possible to solve very large integer problems relatively quickly.

414

Figure 1.   Visualizing a multi-time period knapsack constraint.

Researchers at Adolfo Ibañez University and University of Chile, Santiago, have developed a tool, *OMP Solver* that leverages these new algorithms to solve both surface and underground scheduling problems. The following section presents a special feature that can be used with *OMP Solver* to create models with greater tractability and in producing more operationally representative schedules.

2.1.1   *Multi-Time period knapsack constraints*

Mining operations often use production averages to create strategic and tactical schedules. These averages might reflect the daily, weekly or even monthly production rates for a given mining method or activity, often corresponding to the fidelity of the desired schedule. Considering the highly variable activity durations typically seen at underground mining operations, because of the non-homogeneous nature of the mine design, using averages may leave available production unscheduled. For example, the assigned production rate for stope extraction is 500 tons per day; however, the average mine production requirement over the year may be 1200 tons per day. When using an integer program, this means that the production capacity will be under-utilized by 200 tons per day, assuming that two stopes are available to be scheduled each day. Many practitioners have incorporated continuous variables (Nehring and Topal, 2007; Little et al., 2008), in conjunction with integer variables, to account for this occurrence; yet, there are still challenges associated with solving such large-scale mixed integer problems.

To retain an integer formulation, an alternative was developed that provides the flexibility similar to that seen in mixed integer programs while allowing the use of newer solution methods. We present Multi-time Period Knapsack Constraints (MPKC) that allow practitioners to create schedules with variable production volumes, by achieving a production target or limiting resource capacities measured over multiple time periods. For example, a mine's production output can vary from day-to-day, but the ore production target is set annually. Figure 1 illustrates how the constraints might be implemented. For this example there is a daily production maximum that limits the daily production capacity, but there is also a weekly capacity constraint that limits the weekly production. The weekly constraint might be a production target or might represent a maximum hoisting capacity. In either case, the operation's goal will be to produce a schedule that achieves, but not exceeds, the weekly target while allowing the daily production to fluctuate. Incorporating MPKC reduces the negative impacts of varying durations and production associated with underground activities, while still retaining integrality.

The implementation of MPKC must be carefully considered to achieve the desired benefit. One challenge in effectively utilizing MPKC is in correctly matching the evaluated time horizon to the desired schedule fidelity. To illustrate the effects of MPKC, we present two scenarios with different fidelities of MPKC, annually and monthly. We used the model described in Section 2.1 for these scenarios, each solved for a 10-year time horizon at the daily fidelity. The MPKC was implemented on the ore production capacity while also slightly relaxing the daily ore production capacity, i.e., allowing for more capacity than the average daily production. Annual production targets ramp up through the initial years, leveling off in year 2023. In the case of the monthly fidelity MPKC model, the annual production targets were broken down into equal monthly values.

Figures 2 and 3 show monthly production profiles, subdivided across years (dot-dashed line) and quarters (dashed line). For the annual-fidelity, Figure 2, the solver schedules a majority of the production in the first 9 months of each calendar year. This behavior is
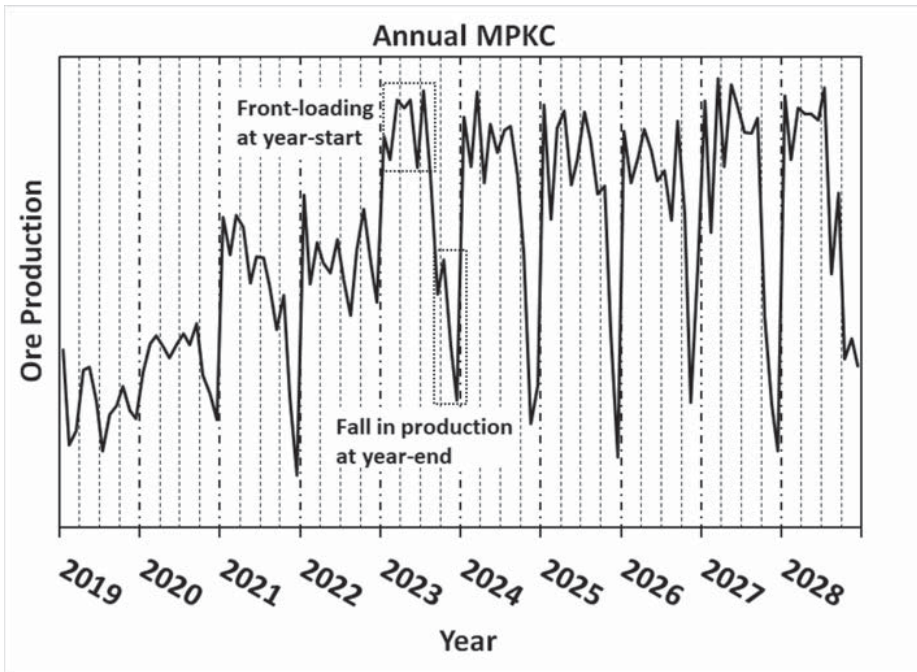
Figure 2. Monthly ore production scheduled over 10 years using annual multi-time period knapsack constraints.
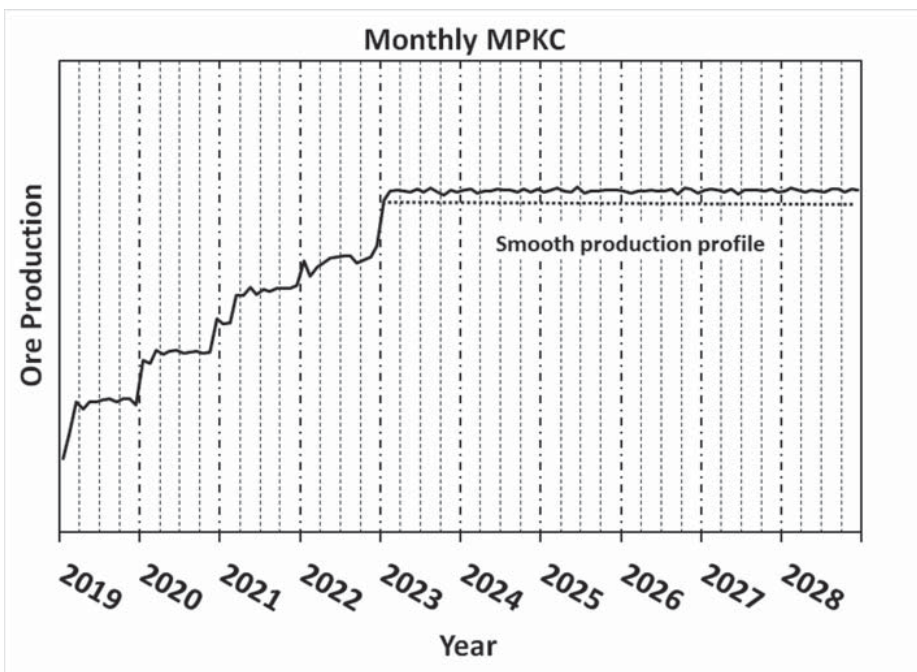
Figure 3. Monthly ore production scheduled over 10 years using monthly multi-time period knapsack constraints.

attributable to the time value of money. Hence, the solver, wanting to maximize operational value, will schedule as much production early in the year as possible, instead of distributing it more evenly throughout the year. We refer to this as "front-loading". Operationally, this "front-loading" is neither feasible, nor desirable. By modifying the MPKC to represent monthly production targets, we see that frontloading is virtually eliminated and the production profile is significantly more consistent. Frontloading may still be occurring within the month which may require using MPKC with shorter time horizons; however, considering the long-term nature of the schedule, this is acceptable accuracy.

2.1.2 *Enforcing start and completion dates*

The desired outcome of an optimized underground production schedule is a collection of activity start dates that maximize value while adhering to precedence and resource constraints. Precedence among activities are used to control activity sequencing and often are associated with operational or geotechnical limitations. For the most part, it is enough to formulate the model with these precedence and resource constraint components to capture the essence of the operation. There may be instances when activity start and completion requirements are needed to satisfy a mine's strategic goals. For example, a new shaft and other associated capital development may need to be completed before the mine's planned expansion can proceed. Disregarding such deadlines creates a less accurate model and may result in improper resource allocation, i.e., equipment, and unrealistic production profiles.

To provide a fixed start date for an activity, we add a "dummy" activity, i.e., an artificial activity that consumes no resources, to create a time delay between the start of the schedule time horizon and the set start date activity. When using the *OMP Solver*, the activity start date can be fixed by pre-defining the decision variable for a given time period as shown in the model (1f) making this process simple and efficient.

To set a completion deadline for an activity, we use MPKC to provide some flexibility as to when the activity can start, while ensuring that the activity is completed by the desired deadline. In many cases, the activity is not necessarily required to be completed on a given date, but that it be completed prior to the deadline. To accomplish this, the activity is evaluated as a unique resource. That resource is constrained by a MPKC where the associated time horizon ends at the required completion date. The use of MPKC allows the schedule flexibility to ensure that the activity is completed while also considering the global scheduling problem.

3 CONCLUSIONS

Improved computation power and solution algorithms have allowed practitioners to formulate and solve increasingly complex models for underground production scheduling. These advances present another opportunity for each practitioner: enhancing model representation to more closely reflect reality. In this paper, we outlined useful tools and guidelines that an underground mine scheduler can use to create more operationally representative schedules. MPKC can overcome the limitations of using averages for constraints and induce some operational flexibility into the schedule, while still retaining integrality and take advantage of the new solution algorithms. In addition, known activity start and completion information should also be incorporated into the model to more closely adhere to the strategic mine plan. Overall, MPKC help improve model and schedule quality, lessening the gap between theory and implementation.

REFERENCES

Alford, C., M. Brazil, and D. H. Lee (2007). Optimisation in underground mining. In *Handbook of operations research in natural resources*, pp. 561–577. Springer.

Artigues, C., S. Demassey, and E. Neron (2013). *Resource-constrained project scheduling: models, algorithms, extensions and applications.* John Wiley & Sons.

Bienstock, D. and D. Zuckerberg (2009). A new LP algorithm for precedence constrained production scheduling. *Optimization Online.*

Brickey, A.J. (2015). *Underground production scheduling optimization with ventilation constraints.* Doctoral dissertation, Colorado School of Mines. Arthur Lakes Library.

Carpentier, S., M. Gamache, and R. Dimitrakopoulos (2016). Underground long-term mine production scheduling with integrated geological risk management. *Mining Technology 125*(2), 93–102.

Chicoisne, R., D. Espinoza, M. Goycoolea, E. Moreno, and E. Rubio (2012). A new algorithm for the open-pit mine production scheduling problem. *Operations Research 60*(3), 517–528.

Dassault Systémes (2018). Whittle.

Hexagon A.B. (2019). Minesight Economic Planner.

Johnson, T.B. (1968). *Optimum open pit mine production scheduling.* Doctoral dissertation, University of California, Berkeley.

King, B.W., M. Goycoolea, and A. Newman (2017). New integer programming models for tactical and strategic underground production scheduling. *Mining Engineering 69*(3), 37–42.

Lerchs, H. and I.F. Grossmann (1964). Optimum design of open-pit mines. In *Operations Research*, Volume 12, pp. B59. Inst Operations Research Management Sciences 901 Elkridge Landing Rd, Ste 400, Linthicum Hts, MD 21090-2909.

Little, J., M. Nehring, and E. Topal (2008). A new mixed-integer programming model for mine production scheduling optimisation in sublevel stope mining. In *Proceedings-Australian Mining Technology Conference.* Twin Waters. The Australasian Institute of Mining and Metallurgy.

Maptek Pty Ltd (2016). Vulcan Pit Optimiser.

MIRARCO Mining Innovations (2018). MIRARCO Mining Innovations.

Muñoz, G. (2012). Modelos de optimizacíon lineal entera y aplicaciones a la minería.

Nehring, M. and E. Topal (2007). Production schedule optimisation in underground hard rock mining using mixed integer programming. In *Project Evaluation Conference 2007*, Volume 2007, pp. 169–175. The Australasian Institute of Mining and Metallurgy.

Newman, A.M., M. Kutcha, and E. Topal (2003). Production scheduling at LKAB's Kiruna Mine using mixed-integer programming. *Mining Engineering 55*(4), 35–40.

Newman, A.M., E. Rubio, R. Caro, A. Weintraub, and K. Eurek (2010). A review of operations research in mine planning. *Interfaces 40*(3), 222–245.

O'Sullivan, D. (2014). *An optimization-based decomposition heuristic for solving complex underground mine scheduling problems.* Doctoral dissertation, Colorado School of Mines.

O'Sullivan, D., A.J. Brickey, and A.M. Newman (2015). Is openpit production scheduling "easier" than its underground counterpart? *Mining Engineering 67*(4), 68–73.

Topal, E. (2008). Early start and late start algorithms to improve the solution time for long-term underground mine production scheduling. *Journal of the Southern African Institute of Mining and Metallurgy 108*(2), 99–107.

Trout, L. (1995). Underground mine production scheduling using mixed integer programming. In *25th International APCOM Symposium Proceedings*, pp. 395–400.

Williams, J., L. Smith, and P. Wells (1973). Planning of underground copper mining. pp. 251–254.

Winkler, B. M. (1996). Using MILP to optimize period fix costs in complex mine sequencing and scheduling problems. *26th Internat. Appl. Comput. Oper. Res. in Mineral Indust. (APCOM) Sympos.* Proc, 441–446.

Optimization model for rostering and crew assignment for train transportation

J. Amaya & E. Molina
Department of Mathematical Engineering and Center for Mathematical Modeling, University of Chile, Santiago, Chile

N. Morales
Delphos Lab., Advanced Mining Technology Center, University of Chile, Santiago, Chile

P. Uribe
Center for Mathematical Modeling, University of Chile, Santiago, Chile

ABSTRACT: This work introduces a model and software for the rostering and crew scheduling problems, for train operation in the mining industry in Chile. The transportation rail network covers most of locations of the industry in the North of the country, including mines, plants and ports. The model possesses particular features due to specific regulations with which train operators in mine material transportation are required to comply. The model and algorithm have been implemented with a user interface suitable for the remote execution of real instances on a High Performance Computing platform. The transportation company regularly uses this computerized tool for planning crew schedules and generating efficient assignments for changing operational conditions. The problem has been partitioned in two steps. Firstly, through a linear mixed integer optimization model, every trip is divided in elemental segments to be served by the crews. Secondly, another optimization model produces the crew assignment to fulfil all the trips demand. The optimization instances are solved by using Gurobi, coded in AMPL and it permits an efficient management of the human resources (drivers), equilibrating the workloads between them.

1 INTRODUCTION

This work introduces two mathematical models that are used together for the rostering and crew scheduling problem, for the operation of trains in the mining industry in a large geographic area located in Chile. The transportation rail network covers most of locations of the industry in the very North of the country, including mines, plants and ports and others.

The problem we are interested on has to deal with two main aspects. Firstly, train trips can be very long, meaning that the same train may have different crew operating it over a the train travel. Therefore, train-stops must be defined at which crew members can be replaced. The location of these stops is limited by several reasons, like nearby location of urban towns, and also they cannot be too far away from each other: in order to allow the crew replacement, a maximum of 10.5 hours limitation, nor they can be too close to each other because that would produce delays and make the transportation company unable to comply with demand. Secondly, the transportation company needs to deal with all the logistics related to the crews: at each train stop, a *fresh* crew takes over the train, so this crew had to be transported from a base or camp; and conversely, another crew leaves for resting and needs to be taken back to base. These crew transportation (from base to train and otherwise) are done using company cars.

The problem described above needs to be solved over the a long time-span that consider in-between resting time of the crew members and overall labor regulations. This gives rise to a very complex instance that involves the partitioning of trips in elemental segments and efficient assignments of crews, to comply with train trips and labor regulations.

In order to tackle this problem, we used mathematical programming to address the two main elements of the problem. For this, the problem has been partitioned in two steps. Firstly, through a linear mixed integer optimization model, every trip is divided in elemental segments to be served by different crews. Secondly, another optimization model produces the crew assignment to fulfil all the trips demand. The drivers must have rest periods (in certain specific camps, whose locations are also decided by the second model.

Figure 1 briefly represents these two problems. The figure illustrates two train trips: Trip 1 goes from West to East and has 9 possible train stops (model selected 3, in black). Trip 2 goes from East to West, has 8 potential stops, but 3 only have been selected. Selected train-stops are points where crew exchanges take place. The figure also represents the schedule of one crew (for simplicity). This crew starts services at Base A (after resting), then it is transported to the first stop or Trip 1 and drives that train to its second stop where it is replaced (by other crew, not depicted in the figure) and transported to Base B. After that it starts its resting time and then starts to work again at Base C, from where it is taken to the first stop of Trip 2, driving that train up its second stop. At that point, the crew is replaced (again by a crew not depicted) and taken to Base A to start a resting period.

It is worth noting that the models and algorithms that we describe have been implemented with a user interface suitable for the remote execution of real instances on a High Performance Computing platform, on an Intel Xeon E5-2660 v2 processor with 10 cores and 48 Gb of RAM. The transportation company regularly uses this computerized tool for planning crew schedules and generating efficient assignments for emerging and changing operational conditions. The optimization models are solved by using Gurobi, coded in AMPL. Many different real scenarios can be tackled by the user, permitting an efficient management of the human resources (drivers) and equilibrate workloads between them.

A similar two-steps approach has been proposed by Drexl et al (2013), but unlike to that paper which focused in an heuristic solution, we focus on integer programming models. A general introduction to this kind of rostering, vehicle and crew assignment models can be found in Ceder (2007), and a practical scheduling model for a crew rotation scheme is solved by Amaya et al (2018), by using a local search optimization strategy. Şahin et al (2011) address the problem of finding a minimal number of crews to carry out a given set of duties (trips), based on a sequential algorithmic procedure. The crew capacity planning problem, to minimize the crew size in railways, is also studied by Suyabatmaz et al (2015).
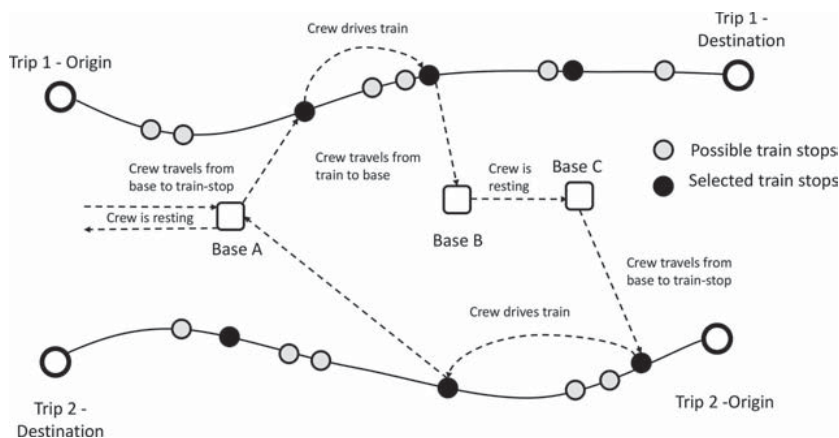
Figure 1. Schematic representation of two train trips and one crew schedule. Train trips and stops are in solid black. Crew schedule is represented by segmented lines.

2 PARTITIONING THE TRAIN TRIP IN ELEMENTAL SEGMENTS

The idea is to divide each trip in elemental sub-trips, in order to generate a list of possible points or locations where the crew replacement can be made. This partition will be used for the crew assignment to the elemental sub-trips, in a second model. Let L be the set of possible locations of change points where the crews can be replaced and $K_t \subseteq L$ all the existing locations along the trajectory of the train t. Each train has a well defined itinerary, that is to say, we know exactly the time of each train at a given location. Furthermore, trains are classified in two types: rotative, whose initial and final point on the trajectory are the same, i.e., as a cycle, and no rotative, whose initial and final point on the trajectory are different. The set of rotative trains is denote by T_c and the no rotative trains T_{nc}, thus, $T = T_c \bigcup T_{nc}$. Moreover we know the following set of parameters:

$k_{t,l}$: Time of train (trip) t at location $l \in K_t$
d^t: Total duration of train t
$d^t_{l,ll}$: Travel time of train t, from location l to ll
$tr_{l,b}$: Travel time for driving a crew from from location l to camb b
$d_{b,l}$: Travel time to drive a crew from location l to the nearest camp

The itinerary of a train induces an order in the set of locations, so we say $l <_t ll$ if $k_{t,l} < k_{t,ll}$. For rotative trains this order doesn't give much information, but for no rotative is really important define it to write its constraints. The binary decision variables are defined below:

$$z_{t,l} = \begin{cases} 1 & \text{if train } t \text{ make a crew replacement at location } l \in K_t \\ 0 & \text{if not} \end{cases}$$

$$v^t_{l,ll} = \begin{cases} 1 & \text{if locations } l, ll \in K_t \text{ are consecutive replacement points for the train } t \\ 0 & \text{if not} \end{cases}$$

In this first model we look for locations that are comparatively near to all bases, in order to minimize the total travel time in cars. The set of constraints to be considered for this problem is described below.

To force a no rotative train to start in a given location $l^t_o = initial(K_t) \in L$, ending at location $l^t_d = final(K_t) \in L$ we impose:

$$\sum_{l \in K_t : l^t_o < l} v^t_{l^t_o,l} = 1, \quad \forall t \in T_{nc} \tag{1}$$

$$\sum_{l \in K_t : l < l^t_d} v^t_{l,l^t_d} = 1, \quad \forall t \in T_{nc} \tag{2}$$

And to connect variables v and z we impose, which means that if train t stops at location l then the train arrives to and leaves that location:

$$\sum_{ll \in K_t : l < ll} v^t_{l,ll} = z_{t,l}, \forall t \in T, \quad \forall l \in K_t \setminus \{l^t_d\} \tag{3}$$

$$\sum_{ll \in K_t : ll < l} v^t_{ll,l} = z_{t,l}, \forall t \in T, \quad \forall l \in K_t \setminus \{l^t_o\} \tag{4}$$

For a rotative train, past constrains turn in:

$$\sum_{ll \in K_t : l \neq ll} v^t_{l,ll} = z_{t,l} = \sum_{ll \in K_t : ll \neq l} v^t_{ll,l}, \quad \forall t \in T_c, \quad \forall l \in K_t \tag{5}$$

The number of daily work hours for crews limited by a given parameter JE_t:

$$v^t_{l,ll} d^t_{l,ll} \leq JE_t, \forall t \in T, \forall l, ll \in K_t, l < ll \tag{6}$$

421

In order to control the number of sub-trips for each train, we include the next constraint in case of no rotative trains:

$$\sum_{l \in K_t} z_{t,l} \leq \left\lceil \frac{d^t}{JE_t} \right\rceil + k, \quad \forall t \in T_{nc} \tag{7}$$

and in case of rotative trains:

$$\frac{d^t}{JE_t} \leq \sum_{l \in K_t} z_{t,l} \leq \left\lceil \frac{d^t}{JE_t} \right\rceil + k, \quad \forall t \in T_c \tag{8}$$

where $k \geq 1$ because the value $\left\lceil \frac{d^t}{JE_t} \right\rceil + 1$ represents the minimal number of sub-trips that fulfill the precedent constraints. This is necessary because the problem may have multiple solutions and we want to keep the one that has a minimal points of crew replacements. In principle, the value $k = 1$ is good if we only consider past constraints, but if we add some additional, as we will show below, the value $k = 1$ could generate infeasibility.

For operational reasons, we need to impose an additional constraint, saying that some changes of crews must be made at a certain prefixed zones (subset of locations). Let $Zc_i \subseteq L, i = 1,..,nz$ the zones where a crew replacement is mandatory. Then,

$$\sum_{l \in K_t \cap Zc_i} z_{t,l} \geq 1, \quad \forall t \in T, i = 1,..,n, K_t \cap Zc_i \neq \varnothing \tag{9}$$

In the context of our specific application, those zones are determined by the capability of the operators (crews) to drive in each geographic; in other words, not all the drivers are authorized to drive train in every zones. The zones (actually, there are three, but this is a parameter of the model) have well defined intersections to ensure feasibility, because changes of crews can be done in the intersections to allow train crossing from a zone to another. The zones are represented by the sets Zc in the model.

Concerning the choice of the objective function, we firstly propose to minimize the total distance between the change points and all rest camp for crews:

$$\min \sum_{t \in T} \sum_{l \in K_t} \sum_{b \in B} tr_{l,b} z_{t,l} \tag{10}$$

Another option is to choose locations at minimal distance to nearest camp:

$$\min \sum_{t \in T} \sum_{l \in K_t} db_l z_{t,l} \tag{11}$$

The result of this model generate an efficient choice of locations for crews changes, as near as possible to the rest camps for crews. In the next section we will introduce a model to generate an optimal crew assignment for the whole set of trains along one week period.

3 THE CREW ASSIGNMENT MODEL

Let us consider a set of M crews (in our specific application, each crew is composed by two operators) and the set V containing all the sub-trips to be fulfilled, defined by the previous model. All those sub-trips have as starting and final stop, two consecutive locations for crew change (in fact, these are points of the timetable for each train). Each one is determined by the variables $v_{l,ll}^t$ having value 1. We also denote D_v the set of days in which the trip v runs (typically $D_v = \{1, ..., 7\}$).

The idea of this model is to connect a sequence of compatible elemental trips to be fulfilled by each specific crew. For this, we need to add two artificial trips v_0 and v_f, to connect with the

initial and final locations of the train, we then define $V_e := V \cup \{v_0, v_f\}$. These two trips will be assigned to fictitious days 0 and 8 respectively. To define compatibility, we use a new variable $d_{v,vv,b}$, corresponding to the duration of the travel from the final location of v to the camp b and then to the origin of trip vv. We also define $h_{v,k}^0$ and $h_{v,k}^f$ as the initial and final times of trip v at day k. The parameter TE denotes the legal maximal duration for the transportation of the crew, from the location to the base camp.

Finally, we define the compatibility parameter $comp_{v,k,vv,kk,b}$ related to two trips. This parameter takes value 1 if the trip v at day k is compatible with trip vv at day kk, having rest camp in base b. In other words, the crew ends trip v at day k, then is transported to camp b and after the rest period the crew is transported to take service at trip vv, day kk.

- A trip can only be compatible with trips in next days, that is to say, if $kk < k$ then $comp_{v,k,vv,kk,b} = 0$.
- All trips are compatible with the fictitious trips v_0 y v_f, that is $comp_{v_0,0,v,k,b} = 1$ and $comp_{v,k,vf,8,b} = 1$.
- Due to the minimum rest time in base camp (10 hours and 20 minutes), we set $comp_{v,k,vv,kk,b} = 1$ if $k < kk$ and $d_{v,vv,b} + 10 + \frac{1}{3} \le h_{vv,kk}^0 - h_{k,v}^f$.
- In other cases $comp_{v,k,vv,kk,b} = 0$.

Finally, we define the main variables for the crew assignment model:

$$w_{v,k,vv,kk,b} = \begin{cases} 1 & \text{if trip } v \text{ day } k \text{ connect with trip } vv \text{ day } kk, \text{ resting time in } b \\ 0 & \text{if not} \end{cases}$$

This variable is set to zero if the two trips are not compatibles. The objective function of this problem corresponds to minimize the total transportation time of crews from trains to base camps and viceversa:

$$\min \sum_{v \in V} \sum_{k \in D_v} \sum_{vv \in V} \sum_{kk \in D_{vv}} \sum_{b \in B} d_{v,vv,b} w_{v,k,vv,kk,b} \tag{12}$$

The constraints correspond to the flows of value 1, from v_0 to v_f. The first two constraints say that from v_0, M trips are connected and in v_f, M trips arrive. This is written as:

$$\sum_{v \in V} \sum_{k \in D_v} w_{v_0,0,v,k,b} = M \tag{13}$$

$$\sum_{v \in V} \sum_{k \in D_v} w_{v,k,v_f,8,b} = M \tag{14}$$

The continuity of the sequence is established as:

$$\sum_{v_1 \in V_e} \sum_{k_1 \in D_{v_1}} \sum_{b \in B} w_{v_1,k_1,v,k,b} = \sum_{v_2 \in V_e} \sum_{k_2 \in D_{v_2}} \sum_{b \in B} w_{v,k,v_2,k_2,b} = 1, \quad \forall v \in V, k \in D_v \tag{15}$$

The last constraint say that operators cannot be transported more than TE hours, from/to locations and camps, in each daily journey. Mathematically, this is expressed as:

$$\sum_{v_1 \in V_e} \sum_{k_1 \in D_{v_1}} \sum_{b \in B} w_{v_1,k_1,v,k,b} tr_{o(v),b} + \sum_{v_2 \in V_e} \sum_{k_2 \in D_{v_2}} \sum_{b \in B} w_{v,k,v_2,k_2,b} tr_{d(v),b} \le TE \tag{16}$$

where $o(v)$ and $d(v)$ denotes the origin and final destination of trip v, respectively.

To include the zones in the model we first define the parameter $Z_v \in \{1,...,nz\}$ which shows the index of the zone to which the trip v belongs to. In this manner, we establish the compatibility between trips belonging to the same zone. Then we need to add to the definition of $comp_{v,k,vv,kk,b}$, the condition:

- If $k < kk$, $Z_v = Z_{vv}$ and $d_{v,vv,b} + 10 + \frac{1}{3} \le h_{vv,kk}^0 - h_{k,v}^f$ then $comp_{v,k,vv,kk,b} = 1$.

Then the model for crew assignment is defined by the objective function (12) subject to Constraints (13), (14), (15) and (16).

If we consider as a set of nodes containing all pairs (v,k), and construct an arc between nodes (v,k) and (vv,kk) if $comp_{v,k,vv,kk,b} = 1$ for any base b, then the model can be seen as a flow problem in this graph, similar to several crew scheduling and rostering models found in bibliography, for example.

4 NUMERICAL EXAMPLE

In this section, we present a numerical instance of a real case, transporting mineral products and supplies between mines and several places (other mines, plants, ports, etc.). The case includes a set of trains running for a 7-days period, say Monday to Sunday. Each train is represented by a code, as follow:

$$T = \begin{Bmatrix} 1203-1204 & 1220-1221 & 1250-1253 & 1701-1702 & 1703-1706 \\ 1709-1714 & 1711-1712 & 201-206 & 207-202 & 208-205 \\ 209-210 & 213-214 & 241-240 & 243-242 & S1101 \\ EMEL & EPAMPA1 & EPAMPA2 & S1201 & S101 \\ DISPAA1 & DISPAA2 & DISPCC \end{Bmatrix}$$

For every train $t \in T$, the set K_t has at least 80 elements (the possible locations for crew replacements), value JE_t is set at value 12 hours or 10.5 hours, depending of t. We only consider cyclical trains, that is to say, $T = T_c$, and every train operate seven days. Moreover, there are 5 camp bases where crews can stay for the 10-hours rest time:

$$B = \{ CAMPCMZ, CALAMA, CAMPMEL, OLLAGU, PNORTE \}$$

The maximal travel time admitted for transportation of crews between bases and locations for replacements is $TE = 2.5$ hours. There are 3 operation zones, Z_1, Z_2 and Z_3, and 2 zones for changes in common areas $Zc_1 = Z_1 \cap Z_2$ and $Zc_2 = Z_2 \cap Z_3$. We test the model for the number of crews $M = 92, 93$ and 94, knowing that for $M \leq 91$ the problem turns infeasible.

The two models, partitioning and crew assignment, run in 4 seconds to find an optimal solution. Obviously, the objective function improves with the number of crews, essentially because as the number of crews increase they can be located closer to camp bases and the marginal cost of hire an additional crew is not included in the models. The number of total crew replacements is the same in three cases because of the number of crew does not affect the partitioning model. This is shown in the following table:

As an example, we show here the scheduling for Crew 6:

Table 1. Comparison.

Total crews (M)	92	93	94
Total change points	83	83	83
Objective function (12)	564.31	544.14	539.58
Time of computing (s)	4.625	4.781	4.781
Crews for zone Z_1	15	16	17
Crews for zone Z_2	56	56	56
Crews for zone Z_3	21	21	21

Table 2. Crew scheduling.

Crew 6	day 1	day 2	day 3	day 4	day 5	day 6	day 7
Segment (sub-trip)	1703–1706_3	1703–1706_3	1711–1712_2	1711–1712_2	1711–1712_2	1711–1712_2	1703–1706_2
Origin – Destination	K49 – CMZ	K49 – CMZ	K97 – MEL	K97 – MEL	K97 – MEL	K97 – MEL	LLANO – K49
Initial time – Final time	07:20–18:09	07:20–18:09	17:22–04:15	17:22–04:15	17:22–04:15	17:22–04:15	22:11–08:30
Initial base for Crew 6	CAMPCMZ	CAMPCMZ	CAMPCMZ	CAMPCMZ	CAMPCMZ	CAMPCMZ	CAMPMEL
Final base for Crew 6	CAMPCMZ	CAMPCMZ	CAMPMEL	CAMPMEL	CAMPMEL	CAMPMEL	CAMPCMZ

5 CONCLUSIONS

The aim of this work was to create a computer software, based on two mathematical models that represent the two main issues for the railway company that transports minerals and supplies in the North region of Chile. The company uses the system to generate the sequence of relay points for crew replacements and then, based on this itinerary, decide the crew assignment to the drivers. The two implemented models are presented in this paper and can be used to generate different efficient feasible solutions very quickly, depending on different scenarios tested by the user. Moreover, the speed of calculations permits the user to generate in some minutes several efficient diagrams (in terms of practical loads for the crews), compared with traditional processes, based on exchanging hand-made files along several weeks of negotiations.

The software tool was developed to provide a friendly environment for user interaction. The computerized tool is currently operating in a train transportation company, but the model could be adapted to tackle other kinds of crew scheduling problems, especially those arising in urban or interurban transportation systems. The main benefit for the company is not only of economic nature, but also the tool permits to facilitate the negotiations between management and the unions, providing objective solutions for the decision-making process.

ACKNOWLEDGMENTS

REFERENCES

Amaya, J. & Uribe, P. 2018. A model and computational tool for crew scheduling in train transportation of mine materials by using a local search strategy. *TOP-Journal of the Spanish Society of Statistics and Operations Research.* 26:383–402.

Ceder, A. (first ed.) 2007. Public transit planning and operation: Modeling, practice and behavior. *CRC press.*

Drexl, M., Rieck, J., Sigl, T., & Press, B. 2013. Simultaneous vehicle and crew routing and scheduling for partial-and full-load long-distance road transport. *Business Research, 6(2)*: 242–264.

Sahin, G. & Yuceoglu, B. 2011. Tactical crew planning in railways. *Transportation Research Part E: Logistics and Transportation Review, 47(6)*: 1221–1243.

Suyabatmaz, A.C., & Sahin, G. 2015. Railway crew capacity planning problem with connectivity of schedules. *Transportation Research Part E: Logistics and Transportation Review, 84.*: 88–100.

Generating pushbacks using direct block mine production scheduling algorithm

C. Aras, K. Dagdelen & T. Johnson
Colorado School of Mines, Golden, CO, USA

ABSTRACT: Traditional mine production scheduling relies on generating pushbacks with price parametrization and aggregating the blocks inside these pushbacks into benches to generate long term annual production schedules. The incremental fashion of obtaining pushbacks fails to incorporate the operational requirements such as multi capacity, multi destinations, blending requirements, truck hours and stockpiles. Since many production schedule plans highly depend on the design of pushbacks, poor designs will prevent the schedules from achieving a maximum NPV or even obtaining a feasible solution. In this paper, block by block yearly schedules will be generated by solving the mine production scheduling problem under the operational requirements and the resulting yearly schedules will be grouped into phases for the pit design. Then, the schedules based on the traditionally generated phases will be compared against the schedules obtained by direct block scheduling guided phase designs.

1   INTRODUCTION

Mine production can be defined as a complex system formed by its elements which are the operational mining system, the blocks to be mined and functions with a goal of maximizing the discounted cash flows of the mining operations. The boundary within which the system functions is expressed by an ultimate pit which contains all the blocks that are profitable to be mined considering only pit slope constraints. This assumes all the resource capacities are unlimited, the mills are free from any kind of blending requirements and the time value of money is ignored. The actual mine production is free of such unrealistic assumptions, therefore understanding the interactions between the mining blocks within this system becomes significant to achieve the objective of maximizing the profit. The factors that delineate these interactions between the blocks and the operational mining system can be commodity price, mining cost, processing cost, grade of the blocks, mineral resource classification categories, cycle times, material type, tonnages mined and processed in a year, total available truck hours, certain blending requirements depending on the material type, multiple processing destinations with different ore recoveries, stockpiles, pit slope angles based on the rock formations, cutoff grades and time value of money. Traditionally, some assumptions are made to reduce the complexity of the system. One of these assumptions is that designating blocks to the most profitable destination results in neglecting factors that influence the block interactions. The decision based on the value at the destination will underestimate the potential profit. It can be illustrated as follows. Let us assume there are two possible processing destinations for an ore block, and that only one more ore block can be sent to a destination where the highest recovery can be achieved. If there are two ore blocks where the lower grade ore block is overlaying the higher-grade ore block, sending the lower grade ore to a destination where less ounces will be recovered will create an opportunity for a high-grade ore to be processed at a destination where more ounces could be recovered. Another common assumption is made based on cycle times. If there are multiple waste dumps to send a waste block, the operator makes a choice based on the lowest cycle time. The fact is waste dumps have limited capacities, therefore if a waste block is required to be mined, the optimizer should be able to send it to an available

waste dump at the time of extraction. Otherwise, the plan generated by an optimizer will be biased on the preselected destinations which will again underestimate the potential profit.

Due to the large scale of block by block mine production scheduling problems, the pushback concept became attractive since it allows scheduling to be done from the sub-pits or nested pits which results in less variables in the optimization model. The pushback design method used to determine a production schedule in an open pit mine starts with determining the ultimate pit limits. Once the ultimate pit limit is obtained, mine planning continues with the goal of finding the optimal extraction sequence of the blocks, which in the end, results in nested pits called as pushbacks. The need for dividing the pit into sub pits arises due to the scale of a block by block production scheduling problem hence, sub-pits or pushbacks are used to schedule the blocks quarterly or yearly. Many heuristic techniques were developed in order to sequence the pushbacks so that the schedules from the pushbacks will be in compliance with the resource capacity and mill blending requirements. Dagdelen and Francois-Bongarcon (1982) determined a series of pushbacks by varying the price of the commodity, cutoff grade, mining or processing costs. Gershon (1987) proposed an algorithm which generates cones with the shape of a pit expanding towards the bottom of the pit with the vertex positioned on each block. The blocks are ranked based on their positional weight and the highest rank block is scheduled first. Whittle's approach (1988) is a commonly used pit parametrization technique which varies the block values incrementally and generates nested pits by implementing the LG algorithm. Seymour (1995) proposed a parameterization algorithm which generates pits as a function of pit volume and pit value. The algorithm is a modified version of the LG algorithm by adding the parametrized variables and allowing sub trees that represent the small pits to be formed (Meagher et al., 2014). The branches are categorized as strong or weak based on the threshold value of their strength which is calculated by dividing the cumulative value of the nodes in the branch by the cumulative mass of the nodes in the branch. Strong branches form the small pits which are sequenced based on their strength value. Ramazan and Dagdelen (1998) developed a minimum stripping ratio pushback design algorithm which is a modified version of the Seymour's algorithm in 1995. The goal of the algorithm is to find pits with the minimum stripping ratio which will lead to a schedule where the ore blocks are mined as soon as possible. Somrit (2011) introduced a phase design algorithm which uses Lagrange parameters to determine the size of the pits in compliance with the annual resource capacity requirements. The usage of Lagrange parameters is similar to the Whittle's pit parametrization technique. The author uses linear interpolation to determine the Lagrange parameters which result in "gap" problems. The methods proposed in the literature follow the incremental fashion of obtaining pushbacks that fail to incorporate the operational requirements such as multi capacity, multi destinations, blending requirements, truck hours, stockpiles and also time value of money. Moreover, the size of the pit has a non-linear relationship with the value of the pit which makes it extremely hard to determine. But the common approach attempts to find the pit size with an assumption of a linear relationship which in the end results with a gap problem. The presence of a gap problem will prevent pushbacks to meet with the capacity requirements. So far, researchers have not found an approach to overcome the stated problems which will in the end produce poorly designed pushbacks. Since many production schedule plans highly depend on the design of pushbacks, poor designs will prevent the schedules from achieving a maximum NPV or even obtaining a solution that meets all of the desired production requirements.

2 METHODOLOGY

2.1 Case study (McLaughlin deposit)

The case study will demonstrate the implementation of the new integer solution algorithm proposed by Aras (2018) on scheduling a data set referred to as the McLaughlin Deposit for 10 years. The schematic description of the assumed mining complex is given in Figure 1. The economic parameters that will be used to derive the block values are given in Table 1. The blocks will be initially subjected to a break-even cutoff grade 0.03 oz/t which will separate
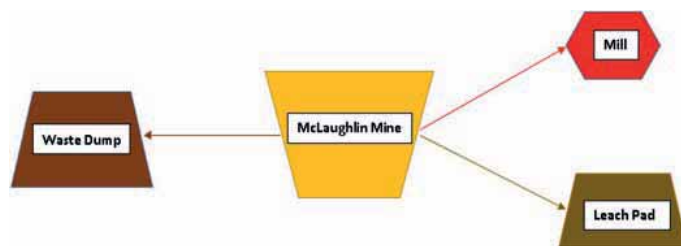
Figure 1.   McLaughlin mine process flow.

Table 1.   Economic parameters.

Parameters	Value
AU	1250 $/oz
MILL COST	12 $/t
LEACH COST	6 $/t
MILL RECOVERY	90%
LEACH RECOVERY	70%
DISCOUNT VALUE	12.5%

Table 2.   Summary of the cutoff grade intervals.

Cutoff	Grades
BREAKEVEN	> = 0.03 oz/t
LEACH	< 0.05 oz/t
UNDECIDED	> =0.05 oz/t AND < 0.08 oz/t
MILL	> = 0.08 oz/t

Table 3.   McLaughlin deposit characteristics.

Material Type	Blocks	Tonnage	AVG Grade
TOTAL	1,922,749	961,374,500	–
WASTE	1,835,583	917,791,500	–
ORE	87,166	43,583,000	0.061 oz/t
MILL	18,144	9,072,000	0.133 oz/t
LEACH	44,634	22,317,000	0.034 oz/t
UNDECIDED	24,388	12,194,000	0.057 oz/t

waste blocks from the ore blocks which carry a recoverable value once processed. Any ore block that has a grade less than 0.05 oz/t will be treated at the leach pads or sent to the waste dump once it is mined. Moreover, an ore block with a grade greater than or equal to 0.08 oz/t will be processed at the mill or sent to the waste dump.

If the grade of a mined ore block is between 0.05 oz/t and 0.08 oz/t, it will be either processed at the mill, treated at the leach pads or sent to the waste dump. The ore blocks in these grade intervals are categorized as "undecided blocks" which means that the process destination is not designated based on a cutoff grade; instead the optimum destination will be determined based on the state of the system. Table 2 presents the cutoff grade intervals adopted for this particular example. Furthermore, the proportions of the blocks in the process stream that belong to different risk categories such as inferred, indicated and measured will be controlled by enforcing risk constraints which are in a form of blending constraints. The deposit characteristics are illustrated in Table 3. It is clear that out of 1.9 million blocks in the block model, only 87 thousand blocks are qualified to be ore blocks with an average grade of 0.061 oz/t. Among the ore blocks, almost half the blocks are leach blocks with an average grade of

0.034 oz/t, and on the remaining half there are 18.1 thousand mill blocks with an average grade of 0.133 oz/t, and 24.4 thousand undecided blocks with an average grade of 0.057 oz/t. Also, Table 4 shows that 19.8% of the blocks are categorized as inferred, 36% as indicated and 44.2% as measured.

2.2   Ultimate pit

Once the block model characteristics are outlined, the next step is to determine the ultimate pit for the McLaughlin Deposit. The mathematical model for the ultimate pit problem requires a single value for a mining decision variable; which means that the destination of a block will be pre-determined. Hence, given a set of possible destinations for a single block, the destination where the highest recoverable value can be achieved will be selected. Moreover, the cone pattern generation technique shown by Aras (2018) is implemented to create arcs between the blocks to accomplish a uniform 45° slope angle. Then the solution to the ultimate pit problem is determined by implementing the pseudoflow algorithm. Table 5 illustrates the number of blocks and tonnage mined in the ultimate pit. It is clear that while the block model consists of 1.9 million blocks, the ultimate pit has only 245.6 thousand blocks. There are about 2 thousand leach blocks that existed in the block model but not mined in the ultimate pit since they are not economical. We can also say that leaving those leach blocks in the ground leads to a decrease in the proportion of inferred blocks about 1.4% as shown in Table 6. Also, there is no observable change in the average grades mined in the ultimate pit. The value of the pit which is calculated with the undiscounted block values determined by picking the most valuable destination was found to be $2 billion in 2018 dollars (USD).

2.3   Optimal mine production schedule

The mine production schedule will be generated to mine the blocks in the ultimate pit under the guidance of production requirements. The life of the mine is 10 years. The mine plan must comply with the yearly production requirements outlined in Table 7. The requirements

Table 4.   Risk profile of the deposit.

RISK CATEGORY	PROPORTION
INFERRED	19.8%
INDICATED	36%
MEASURED	44.2%

Table 5.   Summary of blocks in the ultimate pit.

MATERIAL TYPE	BLOCKS	TONNAGE	AVG GRADE
TOTAL	245,617	122,808,500	–
WASTE	160,445	80,222,500	–
ORE	85,172	42,586,000	0.062 oz/t
MILL	18,140	9,070,000	0.133 oz/t
LEACH	42,737	21,368,500	0.034 oz/t
UNDECIDED	24,295	12,147,500	0.057 oz/t

Table 6.   Ultimate pit risk profile.

RISK CATEGORY	PROPORTION
INFERRED	18.4%
INDICATED	36.7%
MEASURED	44.9%

Table 7. Production requirements for the mine plan.

	PROCESS CAPACITY (TONNAGE)		AVG GRADE (oz/t)		RISK PROPORTIONS		
PERIODS	MILL	LEACH	>= MILL	>= LEACH	<= INF	>= IND	>= MEA
2019	1,500,000	1,500,000	0.062	0.035	20%	10%	35%
2020	1,750,000	1,750,000	0.062	0.035	20%	10%	35%
2021	2,000,000	2,000,000	0.062	0.036	20%	10%	35%
2022	2,750,000	2,750,000	0.062	0.043	40%	10%	25%
2023	3,000,000	3,000,000	0.062	0.043	40%	10%	25%
2024	3,000,000	3,000,000	0.062	0.035	40%	10%	25%
2025	2,750,000	2,750,000	0.062	0.035	50%	10%	25%
2026	2,000,000	2,000,000	0.062	0.035	50%	10%	25%
2027	1,750,000	1,750,000	0.062	0.035	50%	10%	25%
2028	1,500,000	1,500,000	0.062	0.035	50%	10%	25%

Table 8. Summary of the results for the generated mine plan.

		PROCESS CAPACITY (TONNAGE)		AVE GRADE (oz/t)		RISK PROPORTIONS		
PHASES	PERIODS	MILL	LEACH	MILL	LEACH	INF	IND	MEA
PH1	2019	1,500,000	1,500,000	0.196	0.054	7%	27%	66%
	2020	1,750,000	1,750,000	0.149	0.051	6%	39%	55%
PH2	2021	2,000,000	2,000,000	0.124	0.044	9%	40%	52%
	2022	2,750,000	2,750,000	0.089	0.035	13%	38%	49%
	2023	2,999,500	2,999,000	0.075	0.035	11%	40%	49%
PH3	2024	3,000,000	3,000,000	0.063	0.035	19%	37%	45%
	2025	2,750,000	2,750,000	0.062	0.035	25%	35%	40%
PH4	2026	522,000	2,000,000	0.062	0.035	30%	38%	32%
	2027	26,000	1,750,000	0.062	0.035	27%	43%	31%
	2028	63,000	1,500,000	0.074	0.035	41%	34%	25%

Table 9. Summary of the results.

LP NPV @ 12.5%	$1,581,250,000
IP NPV @ 12.5%	$1,581,085,000
OPTIMALITY GAP%	0.01%
SOLUTION TIME	5 h 30 min

include restrictions on the maximum tonnage that can be processed at mill and leach pads, minimum average grade required by mill and leach pads, restrictions on the maximum proportion of the ore blocks that belongs to an inferred category which possess high risk and minimum requirements on the proportion of the ore blocks that belongs to indicated and measured risk categories. Risk proportions basically quantify the risk exposure of the ore blocks in the process flow.

The optimal mine plan is generated by implementing the new integer solution algorithm. The results are shown in Table 8. It is clear that all of the yearly requirements are honored. The yearly schedules are presented on a north-south cross section in Figure 2. In order to assess the quality of the solution, the new integer solution algorithm also provides the theoretical upper bound on a given solution. The theoretical upper bound is calculated by solving the mining problem as a LP problem by using the Bienstock-Zuckerberg (2008, 2009, 2015) decomposition algorithm and then the quality of the integer solution can be measured from the optimality gap. In this case the LP optimal solution is found as $1,581,250,000 and the integer solution is found as $1,581,085,000; as shown in Table 9. The optimality gap is 0.01% and it
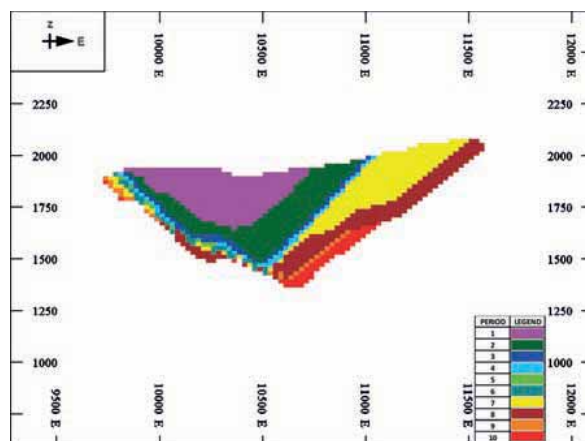
Figure 2. Yearly production schedules on North – 9800 cross section.

took 5 hours 30 minutes to achieve an integer solution. Such a small optimality gap has never been reported in the literature on a problem of this size (~7.3 million variables) with capacity and blending constraints along with multi destinations. Once the optimal yearly schedules are generated, the next step is to use these annual schedules as a guide to design phases as shown in Table 8, where phase 1 consists of first 2 years of the annual schedules, phase 2 consists of years 2021, 2022 and 2023, phase 3 contains years 2024 and 2025, and the schedules of the remaining years 2026, 2027 and 2028 are grouped into phase 4. These 4 phases will be further scheduled bench by bench to generate an optimal and practical mine plan by using Minemax Scheduler for 10 years with the same production requirements outlined in Table 7. The summary of the final schedule is provided in the comparison section.

2.4 Traditional phase design

The traditional approach for generating a life of mine plan for the McLaughlin Deposit would begin by defining phases through a process of incrementally varying block values with commodity price adjustments and solving the problem with the updated block values by using the Pseudoflow algorithm until desired nested pits are obtained. The deposit characteristics of each phase generated by parametrization technique is shown in Table 10. The next step will be generating bench by bench schedules from these phases with a time span of 10 years by using Minemax Scheduler and compared against the mine plan generated by direct block scheduling guided phase schedules.

2.5 Comparison of the schedules generated by guided phase design vs traditional phase design

In this section, the comparison of the two mining plans originating from different phase generating techniques will be outlined. A guided phase design relies on the optimal solution to the problem constrained with the production requirements shown in Table 8. Scheduling these phases bench by bench generated superior results compared to the mine plan based on the traditionally determined phases. It should be noted that both mine plans were able to honor the yearly production requirements. However, the mine plan based on the guided phases produced significantly higher amounts of mill ounces in the first two years of the operation. As it can be seen in Figure 3 and Figure 4, the average grade of the ore blocks processed at the mill is considerably higher in the guided phase schedules than the traditional phase schedules which is due to the quicker production of 166 k recoverable mill ounces in the first two years of the mine plan. It is obvious that the mine plan based on the guided phases prioritizes the high-grade zones in

431

Table 10. Deposit characteristics of the traditional phases.

| MATERIAL TYPE | PHASE 1 | | | |
	BLOCKS	TONNAGE	OUNCES	AVG GRADE
TOTAL	32,111	16,055,500	–	–
WASTE	14,645	7,322,500	–	–
ORE	17,466	8,733,000	718,605	0.082 oz/t
MILL	7,993	3,996,500	557,155	0.139 oz/t
LEACH	9,473	4,736,500	161,450	0.034 oz/t

| MATERIAL TYPE | PHASE 2 | | | |
	BLOCKS	TONNAGE	OUNCES	AVG GRADE
TOTAL	41,199	20,599,500	–	–
WASTE	20,679	10,339,500	–	–
ORE	20,520	10,260,000	806,635	0.079 oz/t
MILL	15,421	7,710,500	717,445	0.093 oz/t
LEACH	5,099	2,549,500	89,190	0.035 oz/t

| MATERIAL TYPE | PHASE 3 | | | |
	BLOCKS	TONNAGE	OUNCES	AVG GRADE
TOTAL	64,638	32,319,000	–	–
WASTE	35,260	17,630,000	–	–
ORE	29,378	14,689,000	763,485	0.052 oz/t
MILL	15,180	7,590,000	519,105	0.068 oz/t
LEACH	14,198	7,099,000	244,380	0.034 oz/t

| MATERIAL TYPE | PHASE 4 | | | |
	BLOCKS	TONNAGE	OUNCES	AVG GRADE
TOTAL	107,763	53,836,500	–	–
WASTE	89,865	44,932,500	–	–
ORE	17,808	8,904,000	334,725	0.038 oz/t
MILL	3,841	1,920,500	108,325	0.056 oz/t
LEACH	13,967	6,983,500	226,400	0.032 oz/t
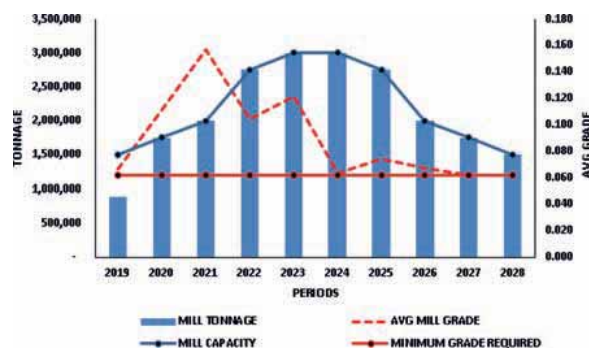
Figure 3. Traditional phase—yearly processed tonnage and the average grade at the mill.

the earlier years of the production in order to prevent the loss in value occurring naturally by the discount factor. Hence, it can be seen clearly in Figure 4 and Figure 6 that both mill and leach average grades are significantly higher in the earlier periods and gradually decrease until they become equal to the minimum yearly average grade required by the process destination. At the
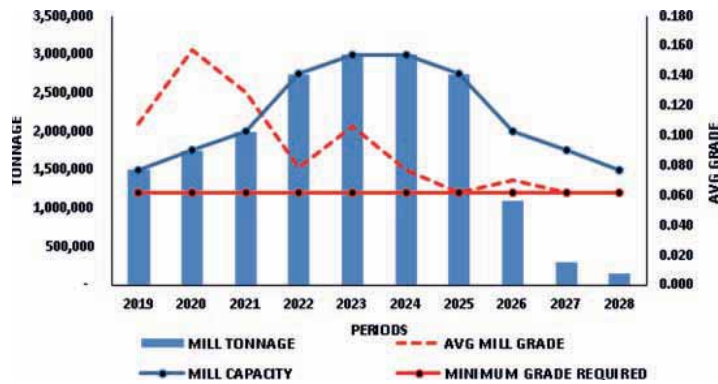
Figure 4.   Guided phase—yearly processed tonnage and the average grade at the mill.
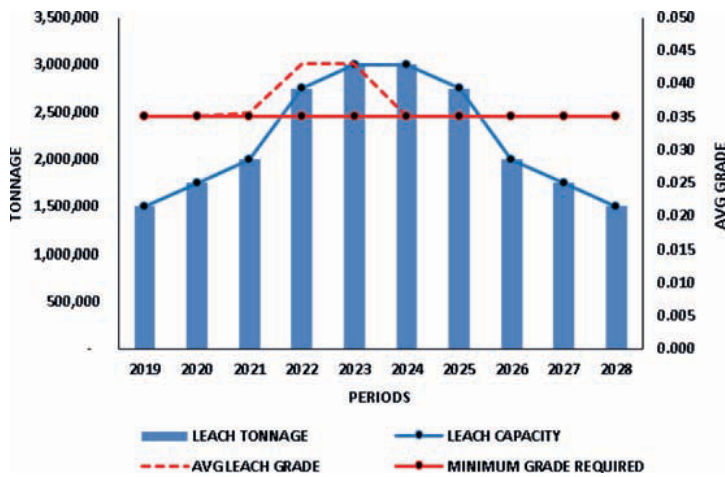
Figure 5.   Traditional phase—yearly processed tonnage and the average grade at the leach pad.
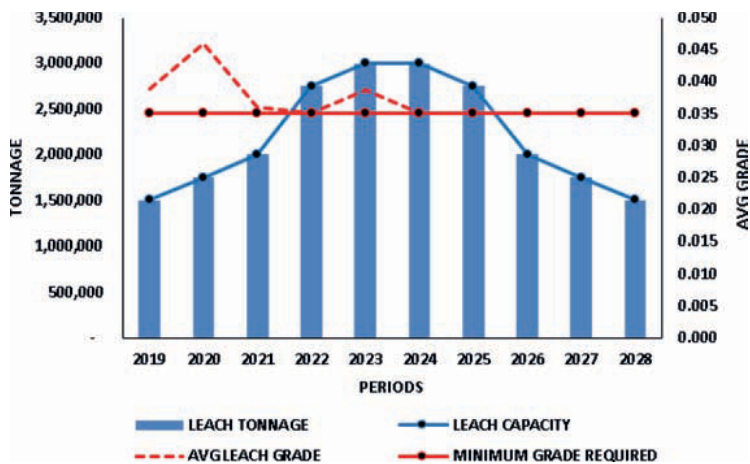
Figure 6.   Guided phase—yearly processed tonnage and the average grade at the leach pad.

same time the schedules based on the traditional phases do not follow the same average grade pattern as shown in Figure 3 and Figure 5 where the mill and leach average grades are fluctuating over the years. The Figure 8 shows the risk behavior of the mine plan based on guided phases over the years. It is apparent that the earlier years of the production, the optimizer can mine the less risky areas from the guided phases since the previously generated block by block schedules already unlocked the less risky areas. This is indeed true in practice where the approved business plan must deliver the number of ounces promised to the shareholders, therefore the confidence level on the processed ore tonnage plays a key role. The riskier areas are postponed to the later years of the production since the confidence level on the riskier areas can be always increased by adding more drill holes later on. However, the schedules based on the traditional phases result in mining ore from the areas that possess high risk in the earlier stages of the production as shown in Figure 7 since the phase designs based on the parametrization techniques do not account for the risk exposure of the ore blocks in the process flow. Finally, the economic evaluation of the two mining plans based on the discounted cumulative cash flow over the life of mine is provided in Figure 9. It is important to highlight the fact that the schedules based on the guided phase design generate $209 million dollar more profit in the first two years of the production and $83 million dollar more profit considering the life of mine production compared to the mine plan based on traditional phases. Since the first two years of the mine plan are the most important years of the production in terms of the business plan as many critical decisions are taken based on the available budget, guided phases also provide maximized cash flow in the earlier stages of the production. Also, the yearly mining shapes of the schedules from the traditional phases are provided in Figure 10 and the guided phases are shown in Figure 11.
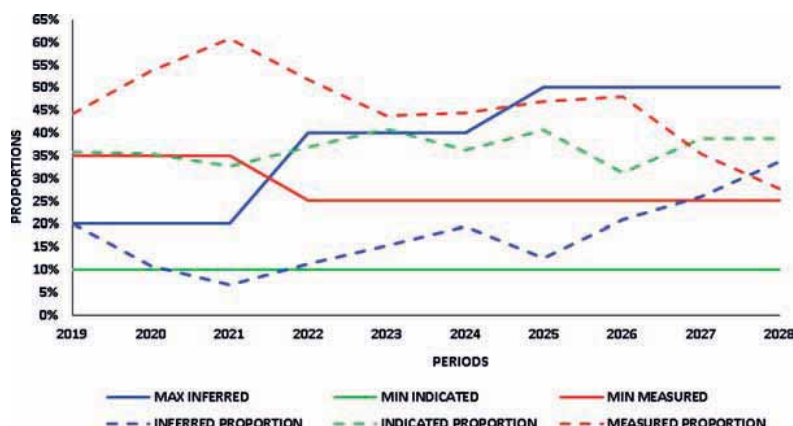
Figure 7.   Traditional phase—risk behavior of the mine plan over the production years.
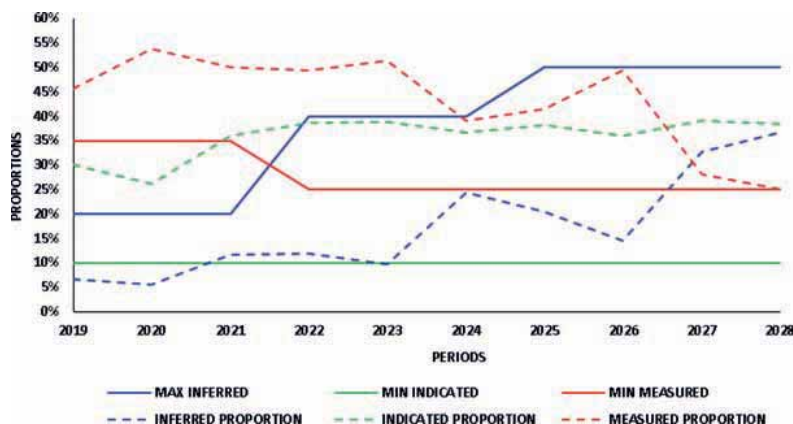
Figure 8.   Guided phase—risk behavior of the mine plan over the production years.

434
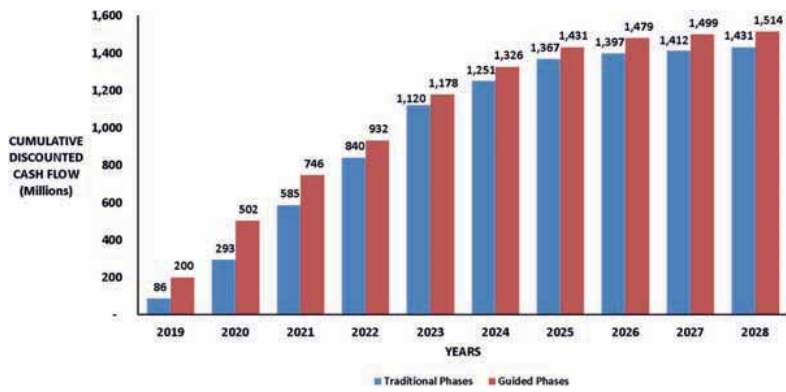
Figure 9.   Cumulative discounted cash flow comparison.
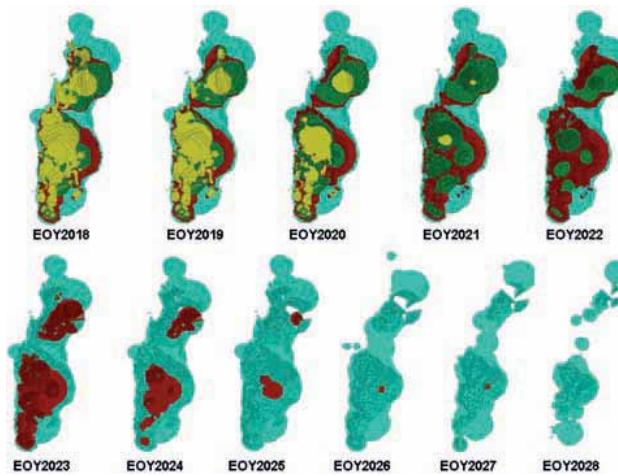
Figure 10.   Traditional phase—annual mining shapes over the production years.
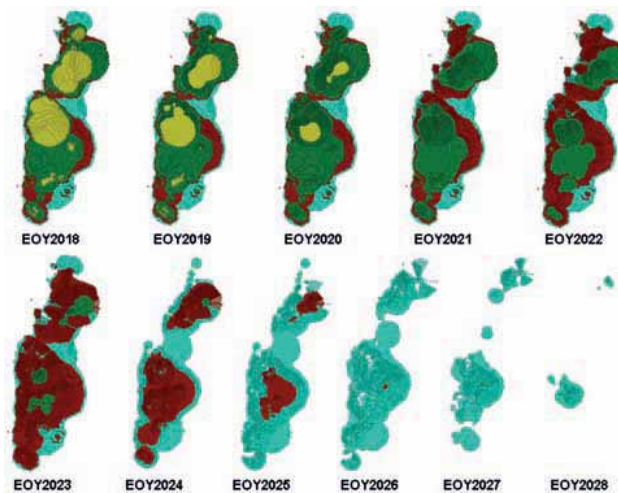
Figure 11.   Guided phase—annual mining shapes over the production years.

3 CONCLUSION

The traditional phase design concept utilizing pit parametrization is widely used in the mining industry. The case study provided in this paper shows that the schedules based on traditional mine phase design could miss a significant number of potential ounces especially in the earlier stages of production that may result in poor cash flows. The underlying reason is mainly the negligence of the operational requirements such as multi capacity, multi destinations, blending requirements, truck hours, and stockpiles together with the time value of money. Given the pre-determined phase shapes, bench by bench scheduling limits the flexibility of the production, therefore block by block scheduling will always generate the most profitable schedules. However, to increase the practicality of the mine plans, the block by block schedules can be grouped into phases for the pit design with haul roads and these phases can be scheduled bench by bench. The novel integer solution algorithm developed at CSM can generate block by block schedules to the mine planning problems modeled with multi capacities, grade blending, grade uncertainty, stockpiles, variable pit slopes, multi destinations and truck hours (Aras, 2018). It should be emphasized that the blocks will not have any pre-determined destinations based on grades, cycle times, material type or some other criteria since the best destination selection per block will be done automatically during the optimization process to maximize the NPV, in other words the dynamic cutoff concept is employed. Another important factor is that the guided phase designs will reflect the risk tolerance of the operator since the underlying block by block schedules already unlocked the regions with the minimal risk exposure in the earlier stages of the production. Therefore, the block by block schedules based on an optimal integer solution will guide the phases towards generating the highest achievable profits both in the earlier stages of the production and the life of mine while honoring the operational and practical requirements. Although not illustrated in the case study, stockpiling the ore material can be easily included in the model.

REFERENCES

Aras, C. (2018). A new integer solution algorithm to solve open-pit mine production scheduling problems. Ph.D. Thesis, Colorado School of Mines, Golden, CO.

Bienstock, D., and Zuckerberg, M. (2009). A new LP algorithm for precedence constrained production scheduling. Industrial Engineering, 1–33.

Bienstock, D., and Zuckerberg, M. (2010). Solving LP relaxations of large-scale precedence constrained problems. Lecture Notes in Computer Science, 1–14.

Bienstock, D., and Zuckerberg, M. (2015). A new LP algorithm for precedence constrained production scheduling. Industrial Engineering, 1–53.

Dagdelen, K., and Francois-Bongarcon D. (1982). Towards the complete double parameterization of recovered reserves in open pit mining. 17th APCOM, 288–296.

Gershon, M. (1987). Heuristic approaches for mine planning and production scheduling. International Journal of Mining and Geological Engineering, 5(1), 1–13.

Johnson, T.B. (1968). Optimum open pit mine production scheduling. Ph.D. Thesis, University of California, Berkeley, CA.

Meagher, C., and Dimitrakopoulos, R., and Avis, D. (2014). Optimized open pit mine design, pushbacks and the gap problem-a review. Journal of Mining Science, 50(3), 508–526.

Ramazan, S. and Dagdelen, K. (1998). A new push back design algorithm in open pit mining. Mine Planning and Equipment Selection, 119–124.

Seymour. F. (1995). Pit limit parametrization from modified 3D Lerchs—Grossmann algorithm. Society for Mining, Metallurgy and Exploration, 95–96.

Somrit, C. (2011). Development of a new open pit mine phase design algorithm using mixed integer linear programming. Ph.D. Thesis, Colorado School of Mines, Golden, CO.

Whittle, J. (1998). Beyond optimization in open pit design. Proceedings of the First Canadian Conference on Computer Applications in the Mineral Industry, 331–337.

Industrial internet of things and gamification applied to fleet and personnel management

Sean Dessureault
MST Global, Tucson, USA

ABSTRACT: The ubiquity of big data, Internet of Things (IoT), and smart devices is radically changing society, our personal lives are being tracked, digitally motivated through gamification, where digital interactions have become an addiction at all income levels, genders, and generations. These forces should not be held at bay in mining, rather we should embrace and take advantage of this phenomenon to improve safety and productivity. Real case studies of these applications of both technology and approach, such as gamification, show that these tracking technologies can bring high visibility and large amounts of data to even the smallest operations and the challenge of making use of the data can be facilitated through the application of gamification. As with our personal smart devices, these technologies are poised to deliver huge improvements in operator feedback, tracking, and performance management, at a much lower cost per unit.

1 INTRODUCTION

Technology has changed every facet of contemporary life in the industrialized world. The universality of mobile phones along with their accompanying mobile apps and social media platforms are rapidly changing and democratizing the developing world. Society has been forced to abandon traditional forms of media, interpersonal interactions, and means of consuming data. Despite the many conferences speeches, journal articles, and research endeavors that extol the benefits of new technology, supervising and motivating personnel, and data utilization has remained relatively unchanged, specifically ever more data is being generated although its utilization rate remains low. However, contemporary life has seen far more transformation than witnessed or experienced in mining.

The forces at work, making our smart devices engaging to the point of addiction, need not be isolated to consumers, rather, an exploration of the key elements of modern technology and demonstrated improvements to modern life can have industrial parallels. The rise of the creativity of crowd or user developed content, the lowering of the cost of monitoring the real activities through the Internet of Things, manipulating human behavior through gamification, and the low-cost of powerful mobile computers. These can all be leveraged in the industrial space to create safer, lower cost mines along with a more engaged workforce.

Industrial Internet of Things (IoT), such as low-cost sensors or imbedded sensing within smart devices such as tablets can provide greatly expanded data collection abilities with low-cost devices with industrial-strength cases. Inertial sensing for detecting movement in the absence of GPS or for vibration monitoring is automatically imbedded in all smart devices, typically for screen orientation and driving games. Bluetooth Low Energy sensors, invented for improved tracking in a retail space, can be repurposed for underground or indoor tracking as well as proximity sensing. Finally, all this sensing can be made ever more useful by creating a highly engaging means of automated work supervision and motivation.

The examples of gamification, inertial sensing, and BLE monitoring were collected with a commercial off-the-shelf system comprising of an iPad, an iPad 'app', and a back-end

data collection environment that includes a web-based configuration console. The data was captured as relational transactional data within an SQL database as well as using big data, namely Javascript Object Notation (JSON) objects generated by the tablet subsequently parsed and loaded into the relational environment.

2 INERTIAL SENSING

Due to economies of scale from consumer-focused products, smart devices have become sophisticated computers packed with sensors. For example, smart devices typically have sophisticated inertial chips where inclination and other movements can be tracked, namely a solid-state gyroscope and tri-axial accelerometer alongside a separate chip that monitors inertial movement and can provide calculated or sensed actions directly within the operating system. For example, the devices automatically detect driving, walking, or 'look at screen' movements, and therefore an app can behave differently, as well, a system can automatically calculate the total time the device was driven, carried on foot, or left on a desk. Direct calculation of triaxial g-forces with a calculated assumed orientation would allow one to capture peak g-forces at a high rate of capture, automatically detecting rough road conditions, including those that could pose a health hazard to the operator driving with the device.

Figure 1 shows the roughness of a roadway wherein a tablet was driven on surface, where the GPS coordinates were also recorded with each maximum acceleration (x,y,z) and a peak vector measure. The heat map shows the vibrations whereas the vertical bars show the speed.

2.1 *How this applies: inertially monitoring true delays*

Knowing inertially, if a machine is moving or immobile provides a far better picture than operator-reported delays or even engine parameters from equipment health monitoring systems. Figure 2 shows a real underground mine outfitted with BLE beacons for tracking and iPads in all haul trucks. The system generated an 'immobility event' every time the machine was immobile longer than a configured 30 seconds. Comparing operator-tracked delays with immobile time over four shifts (by machine, to mask operator behavior), one can see that a large proportion of delays were unreported by personnel.

2.2 *How this applies: inertially monitoring ramp congestion*

Machines such as scoops and trucks should ideally be continuously moving. Any stoppage or reverse movement, especially on a crowded decline, are inefficiencies that should first be monitored, then traffic and dispatching algorithms can be developed specifically for mines according to source (loading areas) rates, sink (dump areas) rates, and the road network connecting them. However, most mines are unaware the of the true ratio between movement and

Figure 1.   Road roughness (heat map) and speed (bars) captured by iPad app, south east Tucson.

Figure 2. Reported vs Unreported Unproductive Time (minutes).
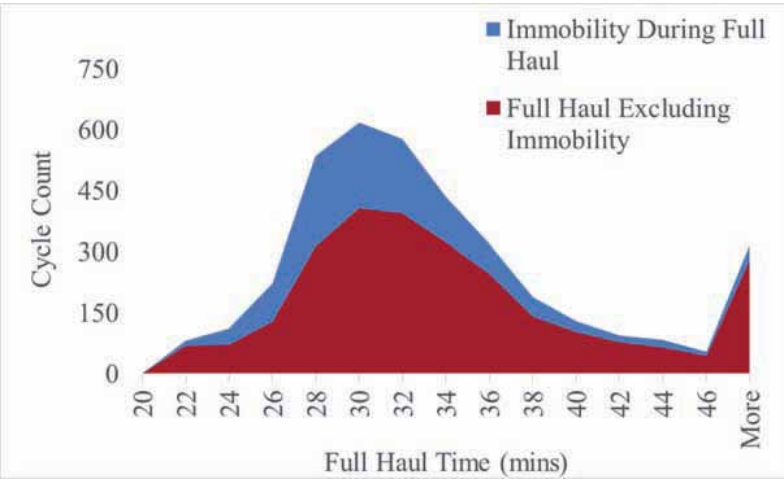
Figure 3. Immobility on the uphill haul while in the ramp.

immobility during haulage. As can be seen from Figure 3, over four shifts, on average, 30% of the loaded up-ramp haul time was spent immobile.

3 BLE BEACON TRACKING

The explosion of the Internet of Things (IoT) at the consumer level has been derived from a combination Big Data and ubiquity of smart devices. Many of the most popular IoT products have a companion app that is used as an additional human user interface as well as a communications bridge to the cloud. This allows a very rich user experience by having most of the data processing and communications infrastructure on the smart device rather than the IoT object. One of the key technologies that could potentially transform mining, especially underground, are nearables. These are usually Bluetooth Low Energy (BLE) beacons, and as the name suggests, uses low-powered Bluetooth chips that are detected by a smart device such as a phone or tablet. The technology was invented as a means of locating people within a retail environment, so that promotional material could be communicated from the

beacon (usually as a URL) to the user holding smart phone. Triangulation and range finding can be used to more accurately position phones. This same technology can be used to replace the far more expensive and inflexible reverse Radio Frequency Identification (RFID) technology used to position personnel in today's mines.

The technology can function as is traditional, where an RFID is sensed by either a fixed detector at key locations connected to infrastructure, or on mobile detectors, in this case the smart device. The most common means is through reverse RFID, where the beacons are placed throughout the mine, broadcasting its ID, which is associated to a known location in a database in the app. The App then transmits the known location if connected wirelessly, to a central location, or stores the movement data and sends when there is connectivity.

The BLE technology provides rudimentary range calculations, where the distance between the beacons can be calculated. Furthermore, since all modern Bluetooth chips have this ability, smart devices can sense the proximity between each other. This means that there is a situational awareness technology that is built into phones and tablets, allowing anyone with a tablet to detect the distance from another tablet or a person having a beacon attached. These beacons can be small, from the size of a coin, to the size of a few AA batteries. Detection and range-finding capabilities of BLE technology is also different from traditional means. Tablets can detect each other, as well as detect beacons up to 300 meters away, meaning, it can sense that there are beacons present, although insufficient signal is available to calculate a distance. When less than 80 meters, the smart device can begin to calculate an actual distance, albeit with some uncertainty (i.e. ±10 m). Traditional technology can detect that a beacon is within 200 meters, and some technology exists where a beacon sets of a secondary Wi-Fi signal when excited by a magnetic field providing an outer and inner zone, but it is still zonal (i.e. it is somewhere within 30 m) but with greater certainty. Therefore, with BLE, positioning location can be achieved without the need for infrastructure, whereas in the current technology, continuous connectivity and sensing of beacons are required to position oneself underground. The tablets can carry all their movements, and detections throughout the day, trigger their cycles based off the loaded map, therefore have the same level of information, improved user experience at the face, all without the infrastructure.

A further benefit of this sensing technology is that the tablets, when broadcasting, can project a small amount of data. In this case, the tablets can broadcast which machine they are currently logged in as, the status (time code), and the state (what activity they are engaged in such as hauling full or empty). When a machine changes status, such as going from 'Ready', to a 'Delay', the other machines within sensing range, can detect the status change. For example, if a truck is waiting in the queue, and the loader operator breaks down, the truck operators would know immediately. Figure 5 shows the sensing of a machine (unit 304) driving by other machines (truck 508, loader 327) and static beacon FL4. As can be seen, all interactions, namely entries (begintime) and exits (EndTime) from the detection zones are recorded, including the state change of hauler 580, and beacon proximity ranges are detected on a 10 second interval, in meters (PointState), the scanning frequency being configurable.

Figure 4.   Underground map for a room and pillar operation.

Equipment Name	Event State Name	Begin Time	End Time
304	Hauler - 580 - Loading - Ready - PRODUCTION-ORE	02/21/19 16:03:00	02/21/19 16:03:47
304	Loader - 327 - Spotting/Hanging - Ready - PRODUCTION-ORE	02/21/19 16:02:52	02/21/19 16:03:10
304	FL4	02/21/19 16:02:47	12/31/69 18:00:00
304	Hauler - 580 - Dumping - Ready - PRODUCTION-ORE	02/21/19 16:02:44	02/21/19 16:03:02

Equipment Name	Time Stamp	Point State	Equipment Model	Work Type Name	Equipment Name
304	02/21/19 16:03:27	29.18	VOLVO A40D	Haulage	580
304	02/21/19 16:03:17	31.99	VOLVO A40D	Haulage	580
304	02/21/19 16:03:07	71.52	CAT980H	Loading	327
304	02/21/19 16:03:07	55.59	VOLVO A40D	Haulage	580
304	02/21/19 15:57:47	46.42	VOLVO A40D	Haulage	573
304	02/21/19 07:29:17	28.85	CAT980H	Loading	327
304	02/21/19 07:29:07	32.87	CAT980H	Loading	327
304	02/21/19 07:28:57	32.6	CAT980H	Loading	327

Figure 5.   Beacon zone entry and exits alongside proximity readings.
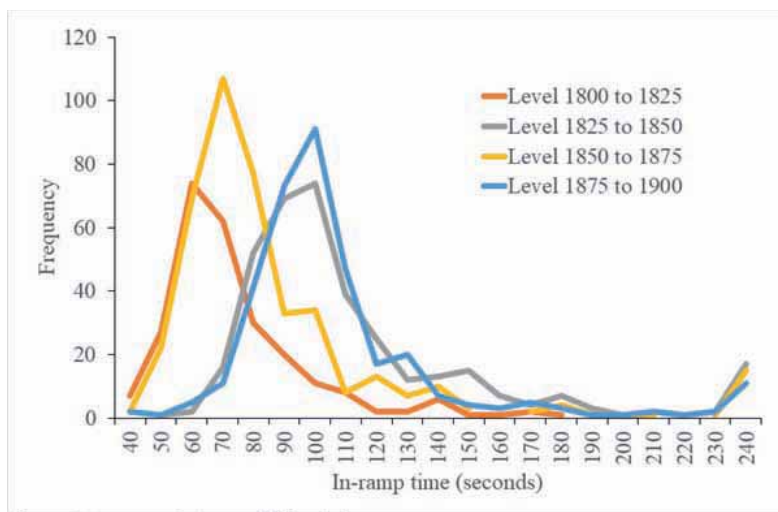
Figure 6.   Ramp travel times uphill loaded.

Since the density of Beacons can be dramatically increased due to their low cost and simplicity in mounting, far more precision and understanding of movements can be achieved. As can be seen in Figure 6, which shows one month of data from an underground mine where beacons were placed throughout a decline. The graph shows the variance, in the form of a histogram, of the average inter-level loaded haulage time in the decline for a hard rock underground mine. As can be seen, significant variance can be observed between levels 1825 to 1850 and 1875 to 1900. Managerial attention should be placed on these areas to reduce both the mean and variance of the cycle time. The activities of the haul trucks were also automatically detected (no operator input necessary) using a web-based user-configured triggering system that combines LE loading-unit sensing (the truck tablet sensing the loader tablet), BLE beacons (configured as a 'loading zone'), GPS (the trucks dumped on surface) and built-in inertial sensors (detecting that the truck came to a stop).

4   MOTIVATION THROUGH GAMIFICATION

The current and incoming generation of mine workers have grown-up using smart devices to manage their personal lives and for entertainment purposes such as video games.

Table 1. Improvements though gamification.

Gamification indicator	Transition	Deployed	Units	Percent improvement
Award for filling-in form within X seconds from shift start	6350	4513	average seconds from start of shift	29%
Award for filling-in form:	2.1	4.9	forms completed per shift	233%
Award for Load Count	21	37	dumps per operator per shift	76%

Gamification is defined as the application of typical elements of game playing (e.g. points, competition, cooperative play, levelling, etc.) to other areas of activity. This is how most of the world now interacts, regardless of culture and country of origin; through smart devices, whose applications typically include gamification elements as a means of creating addiction to an app. This modern nearly-universal human phenomenon can be applied to positive effect by applying a digital points system, levelling, and competition/collaboration mechanics to safety and productivity.

4.1 US coal operation

A gamification application was applied at a coal operation in the United States where the fueling time was subtly added to a leader board, where operators could see their point accumulation throughout the day. Without an explicit improvement program, simply using the gamification program, within a few days of creating the digital "medal" award, the automatically detected fueling events went from an average of 703 seconds to 495 seconds. The leader board included several key performance indicators (KPIs). As can be seen, an improvement of 30% was seen before gamification was applied versus after.

4.2 US underground lead mine

A gamification application was applied at an underground lead mine in the United States, where a transition period occurred where the app had been deployed but no gamification was enacted. Then the operators where introduced to the gamification points and trophies. The system was deployed to improve overall productivity as well as pre-op checklist-form completion compliance. There were a few objectives to the gamification, first in order to improve productivity, a key leading indicator is quicker shift start-ups, where the machine operators should get to their machines, do the pre-check, and begin operating as quickly as possible. Furthermore, by simply filling-out their forms, they could gain points. The gamification awards, that could be seen by the operators directly on their tablets included those in Table 1. The transition period is where the technology was deployed, but without gamification. Deployed was following the deployment of the gamification.

5 CONCLUSIONS

The monumental changes in mobile technology that have transformed nearly all aspects of human communication have not yet had wide reach in the mining industry. Legacy technology providers and have not yet adopted these new technologies because they are specifically target for a much wider mass-market, meaning the profitability margins for the technology are extremely low. However, the change will come as new technology providers recognize the flexibility and inherent capabilities within modern mobile devices and IoT. Furthermore, as new generations of operators begin to join the workforce, they will expect to be engaged in their work.

Short-term open-pit mine production scheduling with hierarchical objectives

F. Manríquez, H. González & N. Morales
DELPHOS Mine Planning Laboratory, Department of Mining Engineering and Advanced Mining Technology Center (AMTC), Universidad de Chile, Santiago, Chile

ABSTRACT: Short-term mine scheduling in open-pit mines consists of meeting the objectives defined by the long-term mine production schedule. Short-term scheduling in open-pit mines has multiple hierarchical objectives to optimize. This work proposes an optimization methodology to generate a short-term open-pit mine production schedule optimizing multiple hierarchical objectives. For the generation of mine schedules, we propose an optimization model based on mixed-integer linear programming. This model considers the usual restrictions of mine sequencing and also takes into account both time and cost of movement between phases of each shovel. In order to optimize the multiple hierarchical short-term objectives, we apply the hierarchical and weighted sum methods in the proposed optimization model. We verify this methodology in a real open-pit mine case study. The results show that both methods generate short-term mine schedules optimizing the different short-term objectives.

1   INTRODUCTION

Short-term mine scheduling in open-pit mines consists of meeting the objectives defined by the long-term mine production schedule. Short-term scheduling in open-pit mines has multiple objectives to optimize. In some mine operations, these objectives are ranked in a descending order which are: (i) the minimization of the deviation between the ore sent to the ore processing plant and the ore processing capacity of the plant per period, (ii) the minimization of the deviation between the metal fines sent to the plant and the fines expected by the ore processing plant, and (iii) the overall minimization of the movement time/cost of the shovel fleet. This work proposes an optimization methodology to generate a short-term open-pit mine production schedule optimizing multiple hierarchical objectives. For the generation of mine schedules, we propose an optimization model based on mixed-integer linear programming (MILP). This model considers the usual restrictions of mine sequencing and also takes into account both time and cost of movement between phases of each shovel. In order to optimize the multiple hierarchical short-term objectives, we apply the hierarchical and weighted sum methods (Grodzevich & Romanko, 2006; Nehring *et al.*, 2018) in the proposed optimization model. We verify this methodology in a real open-pit mine case study. The remainder of this paper is organized as follows. Section 2 briefly reviews the existing literature related to short-term mine production scheduling in open-pit mines. Section 3 presents the proposed optimization model and explains the procedure to perform various objective optimization using both hierarchical and weighted sum methods. In section 4, we describe the open-pit mine case study conducted to generate short-term production schedules optimizing multiple objectives, applying both hierarchical and weighted sum methods. Section 5 reports the results and discussion of the case study. Finally, section 6 presents the conclusions of the work.

2 RELATED WORK

Researchers have mainly applied mathematical optimization to generate short-term production schedules in open-pit mines considering the optimization of multiples objectives. An excellent review of works related to short-term production scheduling in open-pit mines can be found in Blom *et al*. (2018). Smith (1998) describe a model to maximize ore production subject to ore quality constraints. Huang *et al*. (2009) describe a production scheduling tool based on MILP to solve short- and medium-term schedule problems for open-pit mines that involves multiple models, multiple processes, multiple destinations, and blending requirements. Eivazy & Askari-Nasab (2012) develop a MILP model for minimizing the overall cost of open-pit mines, considering multiple destinations. The model incorporates buffer and blending stockpiles, horizontal directional mining and decisions on ramps while controlling operational constraints such as head grade, mining and processing capacities, and mining precedence. L'Heureux *et al*. (2013) propose an optimization model based on MILP to determine the blocks to extract and their order, considering precedence among operational tasks, drilling, blasting, transportation, processing, movement of shovels, drills among others. Blom *et al*. (2014, 2016) propose an optimization problem based on MILP to address the short-term scheduling problem in open-pits networks. The authors also present a rolling-horizon-based algorithm for solving this model. Blom *et al*. (2017) presents a novel variation of the rolling horizon-based algorithm presented in Blom *et al*. (2014, 2016), in which multiple distinct schedules are generated, concurrently, each optimized concerning an ordered sequence of objectives. Matamoros & Dimitrakopoulos (2016) propose a formulation based on stochastic mixed integer programming. The objective function considers terms associated with operating fleet cost, mining cost, and penalty cost to penalize deviation from production target, expected fleet utilization and mining width. Fioroni *et al*. (2008) presented a MILP model to allocate shovels to mine faces and the number of trips that each type of truck fleet have to carry out to these faces, subject to production and blending constraints. The models are called by an open-pit truck-shovel simulation model, whenever a change in the mine operation system occurs, in order to update the allocation of shovels to the new operation state. Upadhyay & Askari-Nasab (2016, 2017, 2018) described a MILP model to allocate shovels to mine faces in order to: maximize production, meet desired head grade and tonnage at crushers and minimize shovel movements. This model is called by an open-pit truck-shovel simulation model, similarly than the work of Fioroni *et al*. (2008).

3 MATERIALS AND METHODS

In this section, we present the optimization model and describe the methodology to generate short-term mine production schedules optimizing various objective optimizations using the hierarchical and weighted sum methods.

3.1 *Optimization model*

The optimization model proposed is a shovel allocation problem based on MILP. The objective of the model is to provide shovel allocations to phases and benches over a one year scheduling horizon. We present the sets & indexes, variables and parameters of the optimization model in Tables 1, 2, and 3, respectively.

Here we describe the constraints of the proposed optimization model. The material extracted by the fleet of shovels of the bench b of the phase f along the planning horizon must be equal to the total material available (Equation 1). The total ore sent to the ore processing plant must be lower than the ore processing capacity (Equation 2). The shovel's operative time plus the shovel's movement time between the phases are lower or equal to the availability of the shovel (Equation 3). In order to assign operative time, a shovel p must be assigned to the bench b of the phase f (Equation 4). When a bench is finished, it cannot be assigned with any shovels (Equation 5). To assign a shovel p in a bench b of a phase f, that

Table 1. Optimization model's sets & indexes.

Symbol	Description
P,p	Set and index for shovels.
F,f	Set and index for phases.
B(f),b	Set for benches of phase f and index for benches.
T,t	Set and index for periods.
R,r	Set and index for routes.
R(f)	Set of routes that contains phase f.
FR(r)	Set of routes which the first phase is equal to the last phase of route r.
FC	Set of consecutive phases (f,f')

Table 2. Optimization model's variables.

Symbol	Description
$x_{p,f,b,t} \in [0,1]$	Time percentage of the period $t \in T$ where shovel $p \in P$ is operative in bench $b \in B$ of the phase $f \in F$.
$\bar{x}_{p,f,b,t} \in \{0,1\}$	Equal to 1 if shovel $p \in P$ is allocated in bench $b \in B$ of the phase $f \in F$ in period $t \in T$, 0 otherwise.
$z_{f,b,t} \in \{0,1\}$	Equal to 1 if bench $b \in B$ of phase $f \in F$ is inactive at period $t \in T$, 0 otherwise.
$\bar{z}_{f,b,t} \in \{0,1\}$	Equal to 1 if bench $b \in B$ of phase $f \in F$ finishes its exploitation in period $t \in T$ or later, 0 otherwise.
$\bar{w}_{p,f,t} \in \{0,1\}$	Equal to 1 if shovel $p \in P$ is allocated on phase $f \in F$ in period $t \in T$, 0 otherwise.
$v_{p,r,t} \in \{0,1\}$	Equal to 1 if shovel p goes through route r in period t, zero otherwise.
$D \in \mathbb{R}^+ \cup \{0\}$	Minimum maximum deviation between the processing plant capacity and the ore send to processing plant
$d_t^- \in \mathbb{R}^+ \cup \{0\}$	Positive deviation between the processing plant capacity and the ore send to processing plant
$G \in \mathbb{R}^+ \cup \{0\}$	Maximum deviation between the processing plant capacity and the ore send to processing plant
$g_t^+ \in \mathbb{R}^+ \cup \{0\}$	Positive deviation between the processing plant capacity and the ore send to processing plant
$g_t^- \in \mathbb{R}^+ \cup \{0\}$	Positive deviation between the processing plant capacity and the ore send to processing plant

Table 3. Optimization model time and cost parameters.

Symbol	Unit	Description
TT	[h]	Total time per period.
$TI_{p,r}$	[%]	Percentage over the nominal time of the period where shovel p needs to move between the phases of route r.
$AV_{p,t}$	[%]	Availability of shovel p in period t.
$CT_{p,r}$	[USD]	Movement cost of shovel p along the phases of route r.
$RM_{p,f,b}$	[t/h]	Maximum throughput of mined material by the shovel p, in the phase f, in the bench b.
$TM_{f,b}$	[t]	Total material to be mined in bench b in phase f.
$OF_{f,b}$	[%]	Percentage of ore material in the bench b of the phase f.
PC	[t]	Total capacity of the ore processing plant.
EG	[%]	Expected grade of the metal by the ore processing plant.
SG	[t/m³]	Rock density.
BH	[m]	Bench height.
$AD_{f,b}$	[m]	Initial operative area of the bench b of the phase f where shovels can operate.
AS_p	[m²]	Minimum operative area of shovel p.
$ML_{f,g}$	–	Maximum number of benches between consecutive phases f and g.
$mL_{f,g}$	–	Minimum number of benches between consecutive phases f and g.

shovel must be allocated in that phase f (Equation 6). To assign operative time in a bench b of a phase f in a shovel p, it must be allocated in that phase f (Equation 7). Bench b of phase f is not finished in period t until all the material are extracted (Equation 8). If a bench b of a phase f is finished in a period t, it remains finished in period $t + 1$. Constraints 10 controls the precedence between benches of the same phase. Thus, to a bench b of a certain phase f can be active, the upper bench must be finished. To assign operative time, the phase-bench must be active (Equation 11). Constraints 12 and 13 controls the precedence between benches of consecutive phases. Constraints 14 to 15 control the area available in the phase-bench in order to allocate shovels. Constraints 16 to 18 models the shovel movements between phases. At most just one route is performed by shovel p in period t (Equation 16). Constraint 17 links the binary variable $\bar{w}_{p,f,t}$ with the variable $v_{p,r,t}$. For each shovel p, the constraint 18 ensures that the route r of period t and the route s of period $t + 1$ are coherent, that is, the last phase f of the r route and the first phase of the s route is the same. The set $FR(t)$ represents the set of all the routes consistent with the r route. That is, the set of routes whose first phase is the same as the first phase of the r route. Constraints 19 and 20 model the deviation between the ore sent to the ore processing plant and the ore processing capacity per period. Constraints 21 to 23 model the deviation between the metal fines sent to ore processing capacity and the expected fines by the ore processing plant per period.

$$\sum_{p \in P, f \in F, b \in B} RM_{p,f,b} \cdot x_{p,f,b,t} \cdot TT = TM_{f,b} \quad \forall p \in F, b \in B(f) \tag{1}$$

$$\sum_{p \in P, f \in F, b \in B} RM_{p,f,b} \cdot x_{p,f,b,t} \cdot TT \leq PC \quad \forall t \in T \tag{2}$$

$$\sum_{f \in F, b \in B(f)} x_{p,f,b,t} + \sum_{r \in R} TI_{p,r} \cdot v_{p,r,t} \leq AV_{p,t} \quad \forall p \in P, t \in T \tag{3}$$

$$\bar{x}_{p,f,b,t} \leq x_{p,f,b,t} \quad \forall p \in P, f \in F, b \in B(f), t \in T \tag{4}$$

$$\bar{x}_{p,f,b,t} + \bar{z}_{f,b,t-1} \leq 1 \quad \forall p \in P, f \in F, b \in B(f), t \in T \tag{5}$$

$$\bar{w}_{p,f,t} \geq \bar{x}_{p,f,b,t} \quad \forall t \in T, f \in F, b \in B(f) \tag{6}$$

$$\bar{w}_{p,f,t} \geq x_{p,f,b,t} \quad \forall p \in P, f \in F, b \in B(f) \tag{7}$$

$$\bar{z}_{f,b,t} \leq \sum_{p \in P, \tau \in \{1...t\}} RM_{p,f,b} \cdot x_{p,f,b,\tau} \cdot TT \quad \forall f \in F, b \in B(f), t \in T \tag{8}$$

$$\bar{z}_{f,b,t} \geq z_{f,b,t-1} \quad \forall f \in F \tag{9}$$

$$z_{f,b,t} \leq \bar{z}_{f,b-1,t} \quad \forall f \in F, b \in B(f), t \in T \tag{10}$$

$$x_{p,f,b,t} \leq z_{f,b,t} \quad \forall p \in P, f \in F, b \in B(f), t \in T \tag{11}$$

$$z_{f,b,t} \geq \bar{z}_{f',\{b'-ML_{f,f'}\},t} \quad \forall (f,f') \in FC, b \in B(f), b' \in B(f'), t \in T \tag{12}$$

$$z_{f,b,t} \leq \bar{z}_{f',\{b'-mL_{f,f'}\},t} \quad \forall (f,f') \in FC, b \in B(f), b' \in B(f'), t \in T \tag{13}$$

$$\sum_{p \in P} AS_p \cdot \bar{x}_{p,f,b,t} \leq AD_{f,b} \quad \forall f \in F, b \in B(f), t = 1 \tag{14}$$

$$\sum_{p \in P} AS_p \cdot \bar{x}_{p,f,b,t} \leq AD_{f,b} + \sum_{p \in P, \tau \in \{1,...,t\}} \frac{RM_{p,f,b} \cdot x_{p,f,b,\tau} \cdot TT}{SG \cdot BH} \forall f \in F, b \in B(f), t \in T \setminus \{1\} \tag{15}$$

$$\sum_{r \in R} v_{p,r,t} \leq 1 \quad \forall p \in P, t \in T \tag{16}$$

$$\bar{w}_{p,f,t} \leq \sum_{r \in R(f)} v_{p,r,t} \quad \forall p \in P, t \in T, f \in F \tag{17}$$

$$\sum_{s \in FR(r)} v_{p,s,t} \geq v_{p,r,t-1} \qquad \forall t \in T \setminus \{1\}, p \in P, r \in R \tag{18}$$

$$d_t^- \leq D \qquad \forall t \in T \tag{19}$$

$$\sum_{p \in P, f \in F, b \in B} RM_{p,f,b} \cdot x_{p,f,b,t} \cdot TT + d_t^- = PC \qquad \forall t \in T \tag{20}$$

$$g_t^+ \leq G \qquad \forall t \in T \tag{21}$$

$$g_t^- \leq G \qquad \forall t \in T \tag{22}$$

$$\sum_{p \in P, f \in F, b \in B} RM_{p,f,b} \cdot x_{p,f,b,t} \cdot TT +$$
$$g_t^- - g_t^+ = \sum_{p \in P, f \in F, b \in B} RM_{p,f,b} \cdot x_{p,f,b,t} \cdot OF_{f,b} \cdot EG \qquad \forall t \in T \tag{23}$$

3.2 *Multiple objective optimization methods*

In this work, we optimize the short-term objectives in the following hierarchical order:

1. Minimize the maximum deviation between ore sent to the ore processing plant and ore processing capacity per period: $f_1 = \min D$
2. Minimize the maximum deviation between metal fines and the expected metal fines expected by the ore processing plant per period: $f_2 = \min G$
3. Minimize overall shovel movement cost: $f_3 = \min \sum_{p \in P, r \in R, t \in T} CT_{p,r} \cdot v_{p,r,t}$

Below, we describe two methods to generate short-term mine production schedules optimizing multiple objectives: the weighted sum method and the hierarchical method.

3.2.1 *Weighted sum method*

The weighted sum method allows the multiple-objective optimization problem to be cast as a single-objective mathematical optimization problem. This single objective function is constructed as a sum of objective functions f_i multiplied by weighting coefficients w_i, hence the name. The coefficients w_i are computed as $w_i = u_i \theta_i$, where u_i are the weights assigned by the decision maker based on the hierarchy of the objectives and θ_i are the normalization factors. In this work, the normalization factors are computed as $\theta_i = z_i^{-1}$, where z_i is the value of the objective function of the optimization problem when solving for the single objective function f_i (Grodzevich & Romanko, 2006). In this way, the weighted sum method consists of two stages. The first one solves i optimization problems (corresponding to the i short-term objectives) in order to obtain the normalization coefficients θ_i. Then, an optimization problem is solved whose objective function corresponds to the weighted sum of all the short-term objectives considered. The coefficients w_i that multiply each of the objectives are calculated using the normalization coefficients θ_i obtained from the first stage and the weights u_i assigned by the decision maker based on the prioritization of the objectives. The following problems need to be solved in the context of the weighted sum method:

- mMDP: Minimize the maximum deviation between ore sent to the processing plant and ore processing capacity per period.
- mMDF: Minimize the maximum deviation between metal fines sent to the processing plant and expected metal fines by the ore processing plant per period.
- mD: Minimize the overall shovel fleet movement cost between phases.
- WS (1,2,3): Minimize the weighted sum of the three short-term objectives considered in this work.

3.2.2 *Hierarchical method*

The hierarchical method allows the decision maker to rank the objective functions in descending order of importance, from 1 to k. Each objective function is then minimized individually subject to a set of additional constraints that do not allow the values of each of the higher

ranked functions to exceed a prescribed fraction of their optimal values obtained on the corresponding steps (Grodzevich & Romanko, 2006). In this work, these sets of additional constraints do not allow the values of each of the higher ranked functions to take no other than the same optimum value obtained on the corresponding steps. In the proposed optimization model, the sets of constraints that impose that the maximum deviation of ore processing capacity per period does not take another value than the obtained in the previously solved problem are 19 and 20. Analogously, the set of constraints that enforce that the maximum deviation of fines per period does not take another value than the obtained in the previously solved problem are 21 to 23. The following problems need to be solved in the context of the hierarchical method:

- mMDP: Minimize the maximum deviation between ore sent to the ore processing plant and the ore processing capacity per period.
- mMDF(mMDP): Minimize the maximum deviation between metal fines sent to the ore processing plant and the expected metal fines by ore processing plant per period, subject to the minimum maximum deviation between ore sent to the processing plant and the ore processing capacity per period.
- mD(mMDF(mMDP)): Minimize overall shovel movement between phases subject to: (i) minimum maximum deviation between ore sent to the processing plant and the ore processing capacity per period, and (ii) the minimum maximum deviation between metal fines sent to the processing plant and the expected metal fines by the ore processing capacity per period.

4 CASE STUDY

A case study of an open-pit copper mine is considered to verify the model. Year 4 is selected as the short-term schedule for the case study. The schedule requires 63.49 [Mt] of ore and 29.55 [Mt] of waste to be mined in year 4 with four phases (1, 2, 3 and 4). Figure 1 depicts the mine layout in year 4 with the road network, one plant crusher and two waste dumps. The plant has an annual ore capacity of 2.51 [Mt]. Plant crusher is desired to have ore with a copper grade of 1.1 [%]. Mine production operations are carried out in two shifts of 12 [h] daily and seven days a week. The mine employs a total of 2 electric shovels. Shovel 1 has a throughput of 4,114 [t/h] and shovel 2 has a throughput of 5,486 [t/h]. Both shovels have an availability of 80.0%. Shovel 1 requires a minimum operational area of 1,239 [m^2], whereas shovel 2 requires 1,491 [m^2]. The shovel average movement velocity is estimated at 0.24 [km/h], due to numerous curves and slopes of the road network for the mine layout case study. The operational cost of shovel movement is estimated at 1.00 [USD/m]. Table 4 shows the distances each shovel needs to travel between phases.

In this case study, the mine operation prioritizes the short-term objectives as shown in section 3.2. We generate a short-term mine production schedules. Comparing the hierarchical

Figure 1. Mine layout with ramps and road network in year 4.

Table 4. Distance between phases.

Phases	1,2	1,3	1,4	2,3	2,4	3,4
Distance [m]	2,800	4,276	3,273	4,813	2,968	1,845

Table 5. Optimization of single optimization problem objectives.

Problem	mMDP	mMDF	mD
Maximum ore processing capacity deviation [%]	1.864%	8.237%	14.500%
Maximum positive deviation of copper fines [t]	6,462	4,967	6,734
Maximum negative deviation of copper fines [t]	6,754	4,967	6,945
Shovel fleet movement time [days]	12.5	9.5	4.0
Shovel fleet movement cost [kUSD]	71.9	54.6	22.8
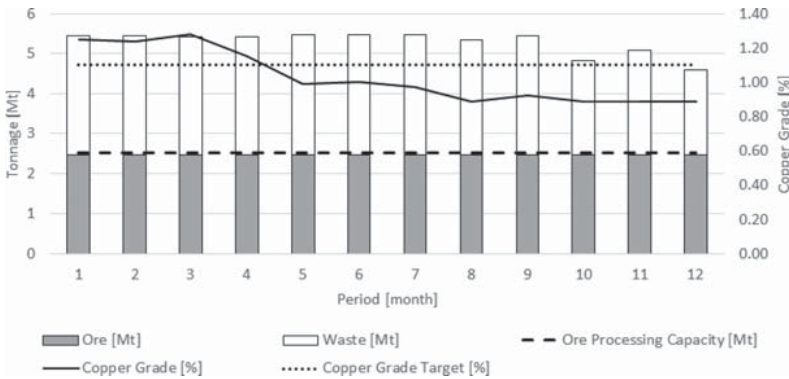
Figure 2. Mine short-term production schedule for the case study.

method with the weighted sum method in terms of: (i) minimum maximum deviation between ore and ore processing capacity per period, (ii) upper and lower maximum deviation between copper fines and expected copper fines in the ore processing capacity per period, (iii) Overall movement cost and time of shovel fleet, and finally (iv) resolution time. In the weighted sum method, the weights u_i assigned by the decision maker for each objective in decreasing order take the values of 10,000; 100 and 10.

5 RESULTS AND DISCUSSION

In the case study, the weighted sum method needs 22.11 [h] to be carried out (resolution of mMDP, mMDF, mD and WS(1,2,3)), while the hierarchical method needs 11.85 [h] (resolution of mMDP, mMDF(mMDP), mD(mMDP(mMDF)). Table 5 shows the results of the mD, mMDP, and mMDF problems.

Figure 2 shows in the final production schedule of the case study, whereas Table 6 compares deviations of plant capacity, deviations of copper fines and overall movements of the shovel fleet for problems associated with the hierarchical method (mMDP, mMDF(mMDP), mD(mMDF(mMDP))) and the problem associated with the weighted sum method (WS(1,2,3)).

From the Table 6 it is verified that each problem of the hierarchical method maintains the objectives imposed by the previous problems and at the same time diminishes or maintains the short-term objective that it wishes to minimize. In effect, it is observed that the mMDP

Table 6. Short-term objectives deviations of case study.

Problem	Hierarchical			Weighted Sum
	mMDP	mMDF (mMDP)	mD (mMDF (mMDP))	WS(1,2,3)
Maximum ore processing capacity deviation [%]	1.864%	1.864%	1.864%	1.864%
Maximum positive deviation of copper fines [t]	6,462	4,484	4,484	4,484
Maximum negative deviation of copper fines [t]	6,754	5,202	5,202	5,202
Shovel fleet movement time [days]	12.5	10.2	10.2	10.2
Shovel fleet movement cost [kUSD]	71.9	58.9	58.9	58.9

problem obtained a maximum deviation of the plant processing capacity of 1.8%, whose level is maintained in the following problems mMDF(mMDP) and mD(mMDF(mMDP)). On the other hand, the problem mMDF(mMDP) decreased the positive and negative deviation of the copper fines concerning the mMDP problem. This deviation is maintained by the post problem mD(mMDF(mMDP)). Also, the problem mMDF(mMDP)) decreased the total days of blade movement obtained by the mMDP problem from 12.5 days to 10.2 days. Finally, problem mD(mMDF(mMDP)) maintained the level of deviations of plant capacity, deviations of copper fines and movement costs and movement times of the shovel fleet obtained by the mMDF problem (mMDP). On the other hand, it is verified that the application of the hierarchical method obtains the same value of the short-term objectives (problem mD(mMDF(mMDP))) than those obtained by the weighted sum method (problem WS(1,2,3)).

6 CONCLUSIONS

Short-term scheduling in open-pit mines needs several objectives to be optimized jointly. In some open-pit mine operations, these objectives are ranked in a descending order of importance: (i) the minimization of the deviation between the ore sent to the ore processing plant and the ore processing capacity of the plant, (ii) the minimization of the deviation between the metal fines sent to the ore processing plant and the metal fines expected by the ore processing plant and finally (iii) the overall minimization of the movement of the shovel fleet. This work proposes an optimization methodology to generate a short-term open-pit mine production schedule optimizing multiple hierarchical objectives. For the generation of mine schedules, we propose an optimization model based on mixed-integer linear programming. This model considers mining sequencing constraints, and also takes into account both time and cost of shovels movement between phases. For the optimization of the various short-term objectives, we apply the hierarchical method and the weighted sum method to a real open-pit mine case study. The results of the case study show that both methods are capable of generating short-term mine schedules by optimizing the various short-term objectives. Additionally, we verified that both methods obtain the same mine production schedule. This article shows the importance and impact of multiple objective optimization methods for the generation of short-term mine production schedules in open-pit mines. This work is part of a Ph.D. research, which was supported by the Advanced Mining Technology Center (AMTC) and the CONICYT Basal Project under Grant FB0809.

REFERENCES

Blom, M., Burt, C., Pearce, A., & Stuckey, P. 2014. A Decomposition-Based Heuristic for Collaborative Scheduling in a Network of Open-Pit Mines. *INFORMS Journal on Computing*, **26**(4), 658–676.

Blom, M., Pearce, A., & Stuckey, P. 2016. A Decomposition-Based Algorithm for the Scheduling of Open-Pit Networks Over Multiple Time Periods. *Management Science*, **62**(10), 3059–3084.

Blom, M., Pearce, A., & Stuckey, P. 2017. Short-term scheduling of an open-pit mine with multiple objectives. *Engineering Optimization*, **49**(5), 777–795.

Blom, M., Pearce, A., & Stuckey, P. 2018. Short-term planning for open pit mines: a review. *International Journal of Mining, Reclamation and Environment*, **0930**, 1–22.

Eivazy, H., & Askari-Nasab, H. 2012. A mixed integer linear programming model for short-term open pit mine production scheduling. *Mining Technology*, **121**(2), 97–108.

Fioroni, M.M., Franzese, L.A.G., Bianchi, T.J., Ezawa, L., Pinto, L.R., & de Miranda, G. 2008. Concurrent simulation and optimization models for mining planning. *Pages 759–767 of: 2008 Winter Simulation Conference*.

Grodzevich, Oleg, & Romanko, Oleksandr. 2006. Normalization and Other Topics in Multi Objective Optimization. *Pages 89–101 of: Fields-MITACS Industrial Problems Workshop*.

Huang, Z., Cai, W., & Banfield, A. 2009. A New Short-and Medium-Term Production Planning Tool - Minesight Schedule Optimizer (MSSO). *Pages 491–495 of: SME annual meeting & exhibit*.

L'Heureux, G, Gamache, M, & Soumis, F. 2013. Mixed integer programming model for short term planning in open-pit mines. *Mining Technology*, **122**(2), 101–109.

Matamoros, Martha E.Villalba, & Dimitrakopoulos, Roussos. 2016. Stochastic short-term mine production schedule accounting for fleet allocation, operational considerations and blending restrictions. *European Journal of Operational Research*, **255**(3), 911–921.

Nehring, M., Knights, P.F., Kizil, M.S., & Hay, E. 2018. A comparison of strategic mine planning approaches for in-pit crushing and conveying, and truck/shovel systems. *International Journal of Mining Science and Technology*, **28**(2).

Smith, Martin L. 1998. Optimizing short-term production schedules in surface mining: Integrating mine modeling software with AMPL/CPLEX. *International Journal of Surface Mining, Reclamation and Environment*, **12**(4), 149–155.

Upadhyay, S.P., & Askari-Nasab, H. 2016. Truck-shovel allocation optimisation: a goal programming approach. *Mining Technology*, **9009**, 1–11.

Upadhyay, S.P., & Askari-Nasab, H. 2017. Dynamic shovel allocation approach to short-term production planning in open-pit mines. *International Journal of Mining, Reclamation and Environment*, **0**(0), 1–20.

Upadhyay, S.P., & Askari-Nasab, H. 2018. Simulation and optimization approach for uncertainty-based short-term planning in open pit mines. *International Journal of Mining Science and Technology*, **28**(2), 153–166.

Mine operation and equipment

A deep learning approach for automated quality control of iron ores

A.K. Gorai & B.C. Balusa
Department of Mining Engineering, National Institute of Technology, Rourkela, India

U. Sameer
Department of Computer Science and Engineering, National Institute of Technology, Rourkela, India

ABSTRACT: The present study aims to design a machine vision system using deep learning algorithm for quality monitoring of iron ores. A total of 53 image samples were used for model calibration and testing. The model was trained using 45 image samples and tested using 9 image samples. The model parameters like the number of nodes and number layers were optimized based on the Root Mean Squared Error (RMSE) values. It was observed that the RMSE was lowest for the network architecture having 5-nodes and 3-hidden layers. The performance of the optimized model was evaluated using four indices including RMSE, Normalized Mean Square Error (NMSE), R-squared, and bias. The RMSE, NMSE, R-squared, and bias of the optimized model were obtained as 8.77, 0.0026, 0.87, and −1.14 respectively. The results indicate that the model gives satisfactory performance in quality predictions of iron ores.

1 INTRODUCTION

The quality of ore in terms of physical (size, shape, strength, etc.) and chemical (composition, grade, etc.) properties specifically defined for the extraction of valuable material through particular treatment process (Ivanov, 1986). The underlying task of predicting a continuous value falls under the category of regression in the field of machine learning. It is the process of studying various characteristics of the data and fitting all the data points into one model. This was performed first by identifying various distinct characteristics of the data known as the features. Then, a regression algorithm such as linear regression (Neter, 1996) or a logistic regression (Hosmer, 2013) was applied, and the regression value of the test data was predicted. The success of these machine learning techniques is hugely dependent on the choice of the features extracted, thus limiting the effectiveness of the regression algorithms. Thus a deep learning algorithm has been designed for prediction of continuous data without any specific feature extraction from the image samples. Deep Learning is an emerging technique for performing representation learning. That is, information from the data is learned using artificial intelligence in the form of a deep neural network. Unlike machine learning techniques which are largely dependent on the features extracted from the data, deep learning techniques learn the features by themselves and perform the necessary prediction task using the learned features. It is the independent nature of deep learning that makes it more effective and superior to machine learning based models when identification and extraction of the feature are not easy. In this work, we perform the task of regression using a deep learning multi-layer network using the raw images of minerals as the input.

Deep learning approach of neural network has been used in many different applications for classification and regression analysis. Baccouche et al. (2011) proposed sequential deep learning for human action recognition. This study developed a fully automated deep learning model, which learns to classify human actions without using any prior knowledge. Yu and

Deng (2011) reviewed deep learning and its applications in signal and information processing. Huang et al. (2014) developed a deep learning model for speech separation. This study explored the use of deep neural networks (DNN) and a recurrent neural network (RNN) for monaural speech separation in a supervised setting. Huval et al. (2015) proposed an empirical evaluation of deep learning on highway driving. In this study, a large data set of highway data was collected and apply deep learning and computer vision algorithms to problems such as car and lane detection. Aliper et al. (2016) demonstrated how deep neural networks trained on large transcriptional response data sets could classify various drugs to therapeutic categories solely based on their transcriptional profiles. Shen et al. (2017) reviewed the recent advances of deep learning to identify, classify, and quantify patterns in medical images. Levine et al. (2018) described a deep learning-based approach to hand-eye coordination for robotic grasping from monocular images. In this study, a large convolutional neural network was trained to learn hand-eye coordination for grasping.

Many researchers used traditional artificial intelligence approaches like artificial neural networks (ANN), support vector machines (SVM), genetic algorithms (GA) for classification ores in the mineral industry. Till date, deep learning neural networks are not used in ore classification in the mineral industry. The present study developed feed forward deep learning neural network model for classifications of Iron ore samples.

2 MATERIALS AND METHODOLOGY

The proposed deep learning algorithm for a machine vision system was developed in three major stages viz. image acquisition, model development, and model evaluation. The steps are represented in a flowchart (shown in Figure 1). The detailed description of each step is given below.

2.1 Image acquisition

A small-scale conveyor-based transportation system was designed and fabricated in the laboratory for image acquisition of iron ore samples. A camera (Logitech HD Webcam c310) was fixed above the conveyor belt for image acquisition. Two sets of LED light were fixed for illumination. These were mounted on 45° inclination to reduce the reflectance, the material to the image capturing device. The conveyor system was powered by a 0.5 horsepower motor made of Crompton Greaves for driving the rollers. The iron ore samples collected from mine were continuously fed at the inlet point of the conveyor belt transportation system. The images of the ores were captured during transportation of ore from the inlet to the outlet point of the belt. A total of 53 images were captured for different types of ore samples (shown in Figure 2). The grade values of the iron ores corresponding to the captured images were estimated using the XRF analyses and summarized in Table 1.

2.2 Model development

The flowchart of the model development is shown in Figure 3. All the captured images were uniformly sized into 64×64 and store as a dataset for learning of the deep network. The deep network was trained with the 80% (44 image samples) of image samples and tested using 20% (= 9) of the image samples.

Image Acquisition → Model Development → Model Evaluation

Figure 1. Broad steps of the proposed work.
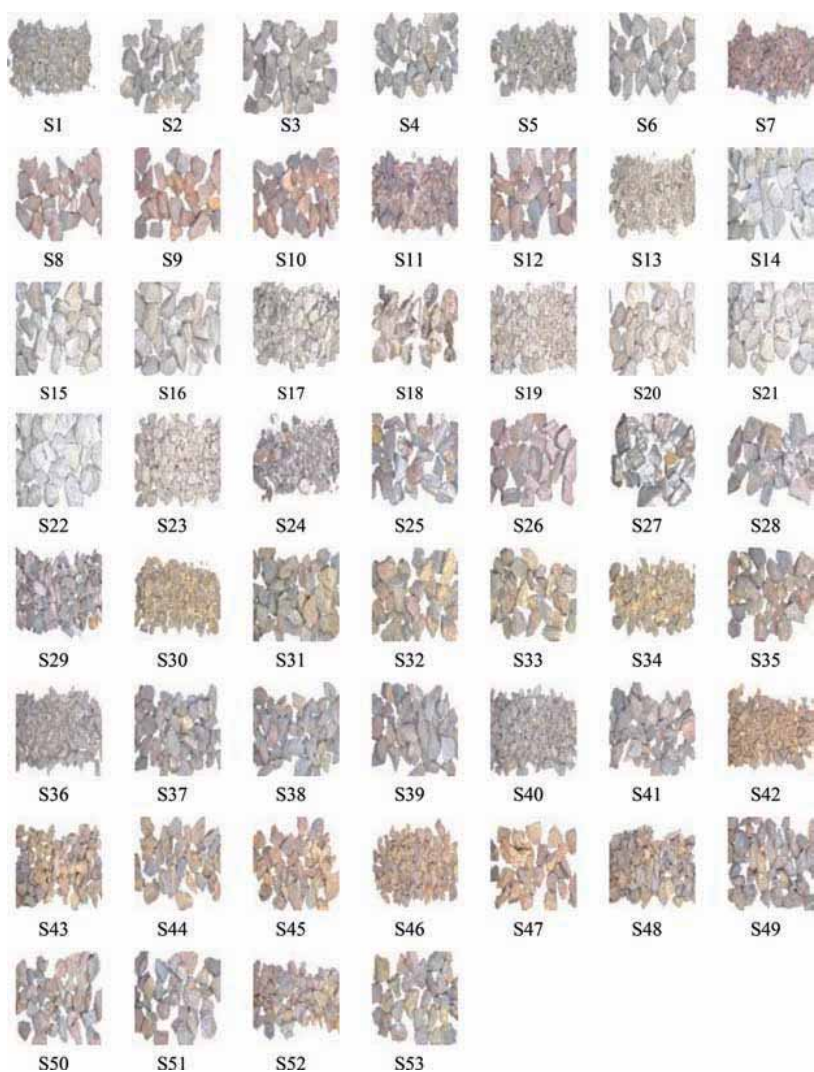
Figure 2.   Images of different types of ore samples.

Table 1.   Observed grade values of iron ore samples corresponding to 53 images.

Sample ID	Grade value	Sample ID	Grade value	Sample ID	Grade value	Sample ID	Grade value	Sample ID	Grade value
S1	59.71	S13	53.73	S25	29.88	S37	28.47	S49	60.06
S2	64.36	S14	58.35	S26	29.49	S38	32.46	S50	65.87
S3	66.57	S15	68.57	S27	37.07	S39	30.06	S51	59.54
S4	62.32	S16	66.32	S28	36.66	S40	28.08	S52	65.96
S5	67.72	S17	68.00	S29	49.64	S41	30.77	S53	67.96
S6	68.03	S18	65.21	S30	30.89	S42	57.14		
S7	61.38	S19	66.20	S31	23.55	S43	68.47		
S8	57.76	S20	59.16	S32	15.75	S44	68.80		
S9	66.43	S21	63.19	S33	13.82	S45	63.79		
S10	67.95	S22	69.54	S34	25.64	S46	66.73		
S11	64.63	S23	68.54	S35	22.77	S47	64.67		
S12	68.74	S24	66.43	S36	48.51	S48	66.58		
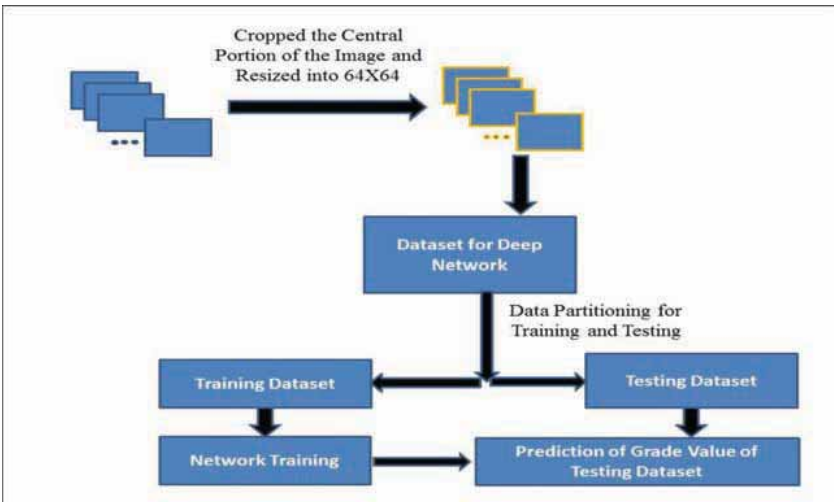
Figure 3.   Flowchart of the model development.
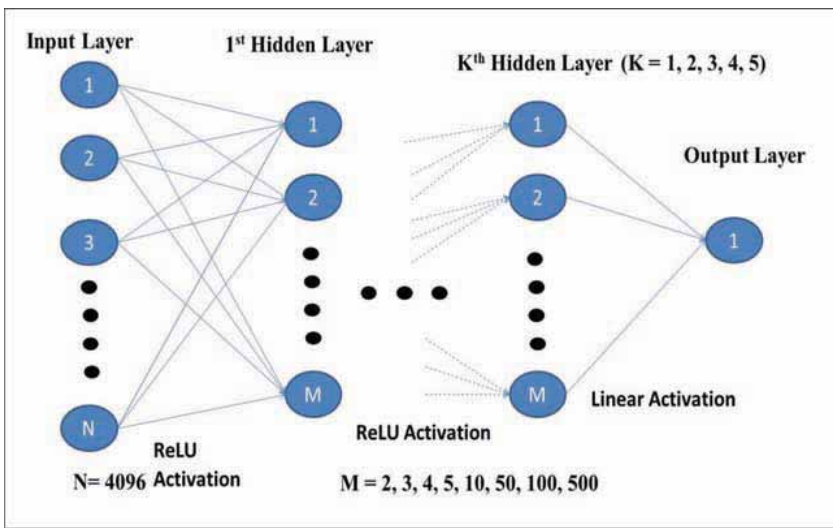
Figure 4.   Proposed network architecture.

In the current study, a multi-layer perceptron (MLP) (Ruck, 1990) based deep neural network was designed for prediction of ore grade. The architecture of the network is shown in Figure 4. The proposed network consists of one input layer, one output layer along with the hidden layers. The number of hidden layers in the network is changed from 1 to 5 for optimization. The input layer process the input data of image samples, the hidden layers are used for feature learning, and the output layer provides the predictions.

The input layer consists of 4096 nodes representing each pixel of the 64×64 image. The network performances are examined for different numbers of nodes (2, 3, 4, 5, 10, 50, 100, and 500) in the hidden layers for optimization of the model. The final layer in the proposed network has a single node to predict the output value for the particular input. Two types of activation functions are used in the network, one with Rectified Linear Unit (ReLU) activation and the other with a linear activation. The ReLU activation (Dahl, 2013) is used for the input layer and all the hidden layers except last. The linear activation function is used for the

458

last hidden layer. The role of an activation function is to produce a non-linear transformation of the input. The ReLU activation is defined as follows:

$$ReLU(x) = \log(1 + e^x) \tag{1}$$

where 'x' represents the input value of a node

In the linear activation, the output is the same as the input. It can be defined as follows:

$$Linear(x) = x \tag{2}$$

The most important module in a deep learning architecture is the role of the optimizer. A deep neural network is initialized with random weights, and the weights are updated iteratively to achieve particular learning (in this case, regression). The weight updating is performed by finding a cost function J(Θ) where Θ is the parameter space of the network. The main function of an optimizer is finding the best values of Θ suitable for the task. Adam optimizer (Kingma, 2014) is used to perform learning. The Adam optimization algorithm is an extension to stochastic gradient descent (SGD) that has maintained a single learning rate for all weight updates, and the learning rate does not change during training. Adam also makes use of the average of the second moments of the gradients (the uncentered variance).

2.3 Model evaluations

The model performance was evaluated with the testing datasets using four error indices viz. root mean square error (RMSE), normalized mean square error (NMSE), R-square, and bias. All the indices were determined from the predicted grade (represent by o) and observed grades (represented by p) of the testing samples using the following respective equations.

$$RMSE = \sqrt{\frac{1}{n_{ts}} \sum_i (o_i - p_i)^2} \tag{3}$$

$$NMSE = \frac{1}{n_{ts}} \frac{\sum_i (o_i - p_i)^2}{\overline{o_i p_i}} \tag{4}$$

$$R^2 = \frac{\left(\sum (o_i - \overline{o_i})(p_i - \overline{p_i}) \right)^2}{\sum (o_i - \overline{o_i})^2 \sum (p_i - \overline{p_i})^2} \tag{5}$$

$$Bias = \frac{1}{n_{ts}} \sum_i (o_i - p_i) \tag{6}$$

where o_i and p_i are the observed and predicted grade of ith samples. n_{ts} represents the number of testing samples. The value of $\overline{o_i}$ and $\overline{p_i}$ can be determined as

$$\overline{o_i} = \frac{1}{n_{ts}} \sum_i o_i \ and \ \overline{p_i} = \frac{1}{n_{ts}} \sum_i p_i \tag{7}$$

3   RESULTS AND DISCUSSION

The proposed deep learning algorithm is based on multi-layer perceptron (MLP). In MLP, the network is initialized with random weights. The input image samples of iron ores are passed through the input layer forming the vector, xi. The random weights at the input layer are multiplied and added to a bias, b. The model used Adam optimizer for learning rate optimization. The resultant vector then passed through an activation function to produce a non-linear value at the end of the layer. The deep learning algorithm is applied to develop a

machine vision system for prediction of quality of iron ores. The iron ore samples were collected from mine using a stratified random sampling method. The samples are collected from the different part of the mine to represent the heterogeneity of the geology present in the specific mine. The images of the iron ore samples are captured in the laboratory by fabricating a pilot conveyor belt transportation system. A total of 53 image samples were captured for the training and testing of the deep network. The grade values of the iron ore samples are estimated using XRF analyzer correspond to each image sample. The grade values ($Fe_2O_3\%$) of the samples are ranged from 19.35% to 97.36%. A wide variation in the grades of iron ores indicates that the quality of ore are varied in the different part of the mine and thus a proper quality monitoring system in the mine is desired.

The deep network was trained using 44 image samples and tested using 9 image samples. The network used ReLU activation function for the input layer and all the hidden layers except last where a linear activation function is used. In the present study, the numbers of hidden layer and the number of nodes in each hidden layer are optimized based on the

Table 2.   Model performance results under different conditions.

Model name	Number of nodes in each hidden layer	Factors	Number of layers				
			1	2	3	4	5
M11 to M15	2	R^2	0.8142	0.8037	0.7983	0.8017	0.8234
		RMSE	10.06	10.16	10.14	10.32	10.24
		Bias	−1.82	−1.27	−1.19	−1.33	−1.32
		NMSE	0.03	0.03	0.03	0.03	0.03
M21 to M25	3	R^2	0.8154	0.8173	0.8217	0.8206	0.8097
		RMSE	9.98	10.00	9.94	10.04	10.10
		Bias	−0.94	−0.84	−1.51	−1.00	−1.78
		NMSE	0.03	0.03	0.03	0.03	0.03
M31 to M35	4	R^2	0.8022	0.7876	0.7826	0.8140	0.8096
		RMSE	10.13	10.36	10.50	10.18	9.99
		Bias	−1.19	−1.47	−1.96	−1.14	−1.84
		NMSE	0.03	0.03	0.03	0.03	0.03
M41 to M45	5	R^2	0.7885	0.8064	0.8701	0.8145	0.8109
		RMSE	10.33	10.13	8.77	9.78	10.08
		Bias	−1.19	−1.55	−1.14	−1.81	−1.31
		NMSE	0.03	0.03	0.02	0.03	0.03
M51 to M55	10	R^2	0.8758	0.8051	0.8134	0.8128	0.8164
		RMSE	9.87	10.15	10.06	10.05	10.21
		Bias	−3.47	−1.44	−1.20	−1.44	−1.77
		NMSE	0.03	0.03	0.03	0.03	0.03
M61 to M65	50	R^2	0.7940	0.8259	0.8542	0.8163	0.8261
		RMSE	10.27	10.21	9.60	10.23	9.78
		Bias	−1.67	−2.25	−0.86	−2.50	−1.53
		NMSE	0.03	0.03	0.03	0.03	0.03
M71 to M75	100	R^2	0.8113	0.8542	0.7662	0.7442	0.7445
		RMSE	10.11	9.69	10.38	10.74	10.52
		Bias	−1.33	−1.99	−1.49	−1.40	−0.98
		NMSE	0.03	0.03	0.03	0.04	0.03
M81 to M85	500	R^2	0.7881	0.8720	0.8546	0.8224	0.7432
		RMSE	10.81	9.59	9.43	10.22	10.30
		Bias	−1.68	−1.23	−1.69	−0.98	−0.37
		NMSE	0.04	0.03	0.03	0.03	0.03
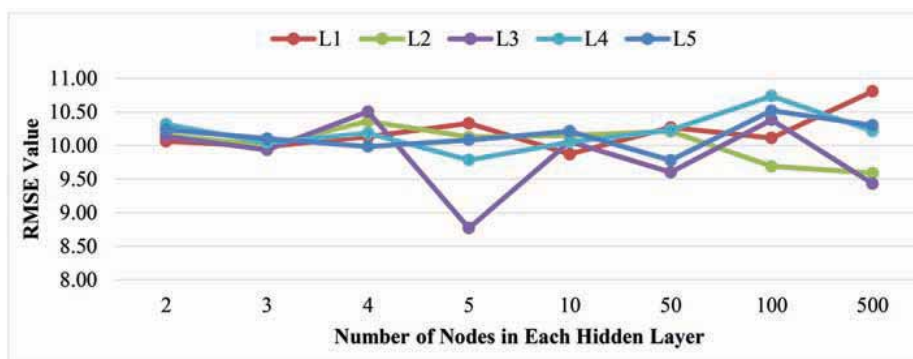
Figure 5.　Trends of RMSE of testing samples for the different model condition.
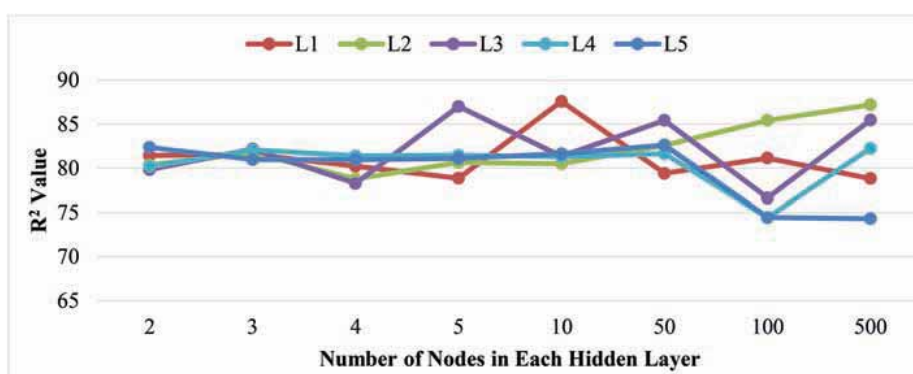
Figure 6.　Trends of R^2 of testing samples for the different model condition.

model performances results. The performance of the network is investigated separately for the different number of hidden layers (1, 2, 3, 4, and 5) with the different number of nodes in the hidden layers (2, 3, 4, 5, 10, 50, 100, and 500). In the present study, 40 Deep network models (M11, M12, …M15, M21,…M25, M31…M35, M41…M45, M51….M55, M61…M65, M71….M75, M81…M85) are trained and tested. The performance of the developed model was evaluated using the four indices (RMSE, NMSE, R2, and bias) as explained in Section 2.4. The model performance indices for different combinations of layer and node are summarized in Table 2.

All the indices are determined using the predicted grades and observed grades of the testing samples. The results indicated that the NMSE value of the model M43 is lowest for the 3-hidden layer and 5-nodes in each hidden layer. The lowest NMSE indicates that the observed grade values are more closely matched with the predicted values. The trend of RMSE and R^2 values are also represented in Figure 5 and Figure 6 respectively. It is observed that the RMSE value is lowest for model M43.The trend of RMSE clearly indicates that the performance of the M43 model is best out of all. Furthermore, the trend of R^2 shows that the regression coefficient of the M43 model (= 0.8701) is nearly equal to the highest R^2 value observed for model M51 (= 0.8758). The R^2 value indicates that the correlation between the observed and predicted values is good for the M43 model. The biases for all the models are found to be relatively high and negative. A negative bias indicates that the model performs with over prediction and thus the models need to be trained and tested using more number of image samples.

4 CONCLUSIONS

The proposed study attempts to develop an MLP-based deep learning network model for prediction of quality of iron ores. The performance of the network is investigated for the different number of hidden layers (1, 2, 3, 4, and 5) and the different number of nodes in each hidden layer (2, 3, 4, 5, 10, 50, 100, and 500). It is observed that the RMSE is lowest for the model having 5-nodes and 3-hidden layers. The performance of the models was evaluated using four indices including RMSE, normalized mean square error (NMSE), R-squared (R^2), and bias. The RMSE, NMSE, and R-squared of the optimized model were obtained as 8.77, 0.0026, and 0.87 respectively. The results indicate that the model gives satisfactory performance in quality predictions of iron ores. The study was performed with less number of image samples, and the performance can be further improved by increasing the number of samples. The proposed technology of quality inspection may be more economical and robust. Thus, the system can play a significant role in automation in the mineral industries. The bias of the optimized model is found to be relatively high (1.14) and negative. A negative bias indicates that the model performs with over prediction and thus the models need to be trained and tested using more number of image samples.

REFERENCES

Aliper, A., Plis, S., Artemov, A., Ulloa, A., Mamoshina, P., & Zhavoronkov, A. (2016). Deep learning applications for predicting pharmacological properties of drugs and drug repurposing using transcriptomic data. Molecular pharmaceutics, 13(7): 2524–2530.

Baccouche, M., Mamalet, F., Wolf, C., Garcia, C., & Baskurt, A. (2011). Sequential Deep Learning for Human Action Recognition. In: Salah A.A., Lepri B. (eds) Human Behavior Understanding. HBU 2011. Lecture Notes in Computer Science, vol. 7065. Springer, Berlin, Heidelberg.

Dahl, G.E., Sainath, T.N., & Hinton, G.E. (2013). Improving deep neural networks for LVCSR using rectified linear units and dropout. IEEE conference on Acoustics, Speech and Signal Processing (ICASSP), 26–31 May 2013, Vancouver, BC, Canada. Doi. 10.1109/ICASSP.2013.6639346.

Hosmer, D.W., Lemeshow, S., & Sturdivant, R.X. (2013). Applied logistic regression, Third Edition, John Wiley & Sons Inc. DOI:10.1002/9781118548387.

Huang, P-S., Kim, M., Hasegawa-Johnson, M., & Smaragdis, P. (2014). Deep learning for monaural speech separation. IEEE conference on Acoustics, Speech and Signal Processing (ICASSP), 4–9 May 2014, Florence, Italy.

Huval, B., Wang, T., Tandon, S., Kiske, J., Song, W., Pazhayampallil, J., Andriluka, M., Rajpurkar, P., Migimatsu, T., Cheng-Yue, R., Mujica, F., Coates, A., & Ng, A.Y. (2015). An empirical evaluation of deep learning on highway driving. arXiv preprint arXiv:1504.01716.

Ivanov, O.P. (1986). Methodological aspects of ore quality control. Soviet Mining Science, 22(3): 207–212.

Kingma, D.P., & Ba, J.L. (2014). Adam: A method for stochastic optimization. arXiv preprint arXiv:1412.6980.

Kunter, M.H., Nachtsheim, C.J., Neter, John, Li, W. (2005). Applied linear statistical models, 5th Edition, McGraw Hill-Irwin, New York, NY, 10020.

Levine, S., Pastor, P., Krizhevsky, A., Ibarz, J., & Quillen, D. (2018). Learning hand-eye coordination for robotic grasping with deep learning and large-scale data collection. The International Journal of Robotics Research, 37(4–5): 421–436.

Ruck, D.W., Rogers, S.K., Kabrisky, M., Oxley, M.E., Suter, B.W. (1990). The multilayer perceptron as an approximation to a Bayes optimal discriminant function. IEEE Transactions on Neural Networks 1(4): 296–298.

Shen, D., Wu, G., & Suk, H.I. (2017). Deep learning in medical image analysis. Annual review of biomedical engineering, 19: 221–248.

Yu, D., & Deng, L. (2011). Deep learning and its applications to signal and information processing. IEEE Signal Processing Magazine, 28(1): 145–154.

Comparison between regression models and neural networks applied to forecast geometallurgical variables

F.G.F. Niquini & J.F.C.L. Costa
Universidade Federal do Rio Grande do Sul, Porto Alegre, Rio Grande do Sul, Brazil

ABSTRACT: Geometallurgical variables are normally forecasted by regression models, which usually shows good results. When non-linear variables need to be predicted, as the metallurgical recovery, accurate and precise forecasts are not always achieved by this technique application. Once neural networks use non-linear activation functions, the predictions for non-linear variables tends to be very accurate. Aiming at comparing the forecasts achieved when regression and neural networks are applied, data from a Brazilian zinc mine was used, where tailings, zinc concentrate and lead concentrate mass recoveries are the variables which compose mass balance. The zinc metallurgical recovery was calculated for zinc and lead concentrates and tailings, aiming at knowing where and how much of the zinc content is going during mineral processing. The results obtained showed the forecast superiority achieved when neural networks were used, in addition to illustrate the possibility to generate a unique model to predict simultaneously six dependent variables.

1 INTRODUCTION

Geometallurgy can be defined as the discipline which analyzes geological, mineralogical, chemical, physical and environmental data collected from a mineral deposit, aiming at explaining the factors affecting ore recovery at a processing plant. It can consider economical parameters, such as ore recoveries and concentrate grades or environmental variables, as water consumption, energy and tailings generation. More often feasibility studies embed geometallurgical variables, having in mind the benefits achieved with this practice: a better financial adherence in a project or in a mine under operation; a better use of the ore; and a better management of environmental impacts caused by the mine or the plant.

Two of the most studied geometallurgical variables are the mass and the metallurgical recovery in the concentrate. Forecast the mass and the metallurgical recovery of non-saleable products, in other words, of tailings, is not a common practice in geometallurgical studies, but it is relevant when the environmental aspects are taken under consideration. Determining tailings mass recovery bring information about how much materials is sent to the tailings dam when a block is mined and processed, making possible to better study the tailings deposition characteristics. Tailings metallurgical recovery reports how much of the economical metal was not sent to the concentrate by the beneficiation process and because of that was discarded, leading to financial losses for the operation. Note that mapping masses of all products (inputs and outputs) and their metallic content gives a better knowledge about the ore that will be processed. These prediction models require a closed sum (mass input = mass output). Fulfilling this premise is not a trivial and is considered as one of the challenges of creating robust geometallurgical models.

Another challenge related to the treatment of geometallurgical data is that most are non-additive (Richmond & Shaw, 2009). Carrasco *et al.* (2008) proved that mass recovery is an additive variable but metallurgical recovery is not and because of that it needs to be studied with prudence. According to Coward *et al.* (2009), additivity is the "property that allows the mean of some variables to be calculated by a simple linear average", or

as described by Carrasco *et al.* (2008), "quantities are said to be additive if the averaged quantity equals the average of the quantities". The non-additivity of an attribute refrains the use linear averages as it would generate biased or inconsistent results according to the studied phenomenon.

One of the most applied techniques to forecast geometallurgical variables is linear regression analysis, uni or multivariate, which uses as independent variables information about *in situ* ore, including grade, grain size distribution or lithology to predict variables such as ore recovery at the processing plant. Examples using this technique in geometallurgy modelling are found in MacMillan *et al.* (2011), Montoya *et al.* (2011), Fernandes (2013), Motta (2014), Vieira (2016), among others. Despite of frequently show good results when applied to forecast geometallurgical variables, when regression models are used to estimate variables which complement themselves, as mass and metallurgical recoveries modeled at each plant output, it is known that not necessarily the predictions sum will bring a perfect closure. Furthermore, once it is a linear estimation, its use to forecast non-additive variables can generate results that do not represent ideally the phenomenon studied.

One alternative to the application of regression analysis, able to overcome the problems describe above, is by using neural networks. Once it uses non-linear activation functions, its use to model non-additive variables is ideal. Another advantage of neural networks is its capacity to estimate simultaneously two or more dependent variables, reducing time during the geometallurgical model elaboration. To compare the results achieved using both techniques herein cited, Nexa Resources provided a database with 49 geometallurgical samples collected at Vazante mine, located in Minas Gerais state, Brazil. The plant under study generates three outputs, being two outputs of saleable products (zinc and lead concentrates) and one tailings output, which are directly sent to the tailings dam. Mass and metallurgical recoveries in each of the outputs are obtained by the application of the following equations:

$$Zn\ Conc.\ Mass\ Recovery = (Zn\ concentrate\ mass/ROM\ mass) \tag{1}$$

$$Pb\ Conc.\ Mass\ Recovery = (Pb\ concentrate\ mass/ROM\ mass) \tag{2}$$

$$Tailings\ Mass\ Recovery = (Tailings\ mass/ROM\ mass) \tag{3}$$

$$Zn\ Met.\ Rec.\ in\ Zn\ Conc. = (Zn\%\ in\ Zn\ conc./Zn\%\ in\ ROM)\ x\ Zn\ Conc.\ Mass\ Rec. \tag{4}$$

$$Zn\ Met.\ Rec.\ in\ Pb\ Conc. = (Zn\%\ in\ Pb\ conc./Zn\%\ in\ ROM)\ x\ Pb\ Conc.\ Mass\ Rec. \tag{5}$$

$$Zn\ Met.\ Rec.\ in\ Tailings = (Zn\%\ in\ Tailings/Zn\%\ in\ ROM)\ x\ Tailings\ Mass\ Rec. \tag{6}$$

Note when the recoveries represented on equations 1, 2 and 3 are summed should add to one and that the same should result to the sum of equations 4, 5 and 6. This occurs once no masses or grades are lost during mineral processing. Presented the dependent variables and their characteristics, the next section shows all data analysis realized.

2 METHODOLOGY

2.1 *Descriptive data analysis*

The database used on this study is composed by 49 samples collected at different zones representing five different geological domains. These samples were analyzed for 28 elements and those are the independent variables under study. Mass and zinc metallurgical recoveries in tailings, zinc and lead concentrates were obtained through flotation tests which reproduce the plant flowchart. Descriptive statistics of the independent and dependent variables are presented in Table 1. Note the lead concentrate mass maximum value is smaller than the smallest value of zinc concentrate and tailings masses recoveries, pointing that the quantity of this material generated by the plant represents a really small portion of the mass processed.

Table 1. Descriptive statistics.

Variable	N	Minimum	Q1	Mean	Median	Q3	Maximum	Std. dev
Zn Met. Rec. in Zn Conc.	49	0.332	0.582	0.713	0.739	0.856	0.943	0.172
Zn Met. Rec. in Pb Conc.	49	0.001	0.005	0.008	0.006	0.010	0.026	0.005
Zn Met. Rec. in Tailings	49	0.047	0.135	0.280	0.258	0.412	0.662	0.171
Zn Conc. Mass Rec.	49	0.032	0.121	0.273	0.262	0.414	0.629	0.174
Pb Conc. Mass Rec.	49	0.002	0.005	0.007	0.007	0.009	0.018	0.003
Tailings Mass Rec.	49	0.364	0.579	0.719	0.733	0.873	0.964	0.173
Zn (%)	49	3.43	7.955	13.544	13.52	18.63	25.66	6.552
C (%)	49	2.170	5.510	6.996	7.010	8.440	11.500	2.171
S (%)	49	0.010	0.020	0.036	0.030	0.040	0.120	0.023
F (ppm)	49	140.000	160.000	196.327	190.000	215.000	310.000	42.558
SiO2 (%)	49	2.430	6.240	8.804	9.240	11.225	14.600	3.169
Ag (ppm)	49	2.860	8.005	14.689	13.050	18.775	44.800	9.363
Al (%)	49	0.160	0.250	0.351	0.290	0.420	0.840	0.166
As (ppm)	49	6.600	25.550	46.910	42.700	64.400	96.900	25.442
Ba (ppm)	49	90.000	155.000	420.204	200.000	720.000	1210.000	364.649
Ca (%)	49	3.520	8.690	11.089	11.150	13.900	18.200	3.795
Cd (ppm)	49	132.500	268.000	396.735	421.000	494.000	666.000	129.494
Co (ppm)	49	22.600	31.700	37.906	35.400	42.200	63.600	8.889
Cr (ppm)	49	12.000	32.500	45.204	44.000	64.000	77.000	18.348
Cu (ppm)	49	15.900	32.750	64.057	45.500	85.750	214.000	46.239
Fe (%)	49	2.500	5.705	12.622	8.880	20.650	26.700	7.878
La (ppm)	49	1.500	2.250	3.071	3.200	3.650	5.200	0.909
Li (ppm)	49	5.300	6.400	7.733	7.900	8.950	10.200	1.392
Mg (%)	49	2.010	5.305	6.848	6.700	8.655	11.400	2.396
Mn (ppm)	49	491.000	565.000	713.776	688.000	822.000	1180.000	166.610
Mo (ppm)	49	0.470	1.370	3.002	2.170	4.500	7.050	1.932
Ni (ppm)	49	15.300	19.500	23.118	23.700	25.700	31.100	3.942
P (ppm)	49	120.000	180.000	251.837	220.000	340.000	410.000	83.583
Pb (%)	49	0.209	0.272	0.314	0.291	0.340	0.481	0.078
Sb (ppm)	49	0.840	3.430	11.285	7.010	21.350	24.900	8.681
Se (ppm)	49	1.000	5.000	12.898	9.000	20.000	35.000	9.549
Sr (ppm)	49	37.900	48.050	56.580	55.100	66.100	82.500	10.590
U (ppm)	49	1.000	2.000	3.910	2.800	6.050	7.700	2.225
V (ppm)	49	9.000	45.500	63.122	58.000	81.500	150.000	31.382

The 49 samples were divided into two datasets: a training set containing 39 samples, where the model was built, and a test set with 10 samples, where the prediction quality of the neural network and of the regression model were evaluated.

2.2 Regression analysis

To define which variables compose each regression model it was used the stepwise algorithm (Hair et al., 2009) considering variable inclusion and exclusion alfa equal to 0.05. For lead metallurgical recovery no statistically significant model was found, showing that none of the 28 independent variables in the database are able to explain this variable variability through regression model. All other dependent variables studied presented valid models, once F test for analyzing model general significance showed a lower p-value than the limit value of 0.05. This means that at least one of the variables inserted in the model can be considered statistically significant. Analyzing the column "P > |t|" presented in Figure 1 it is possible to conclude that all independent variables inserted in the models are statistically significant to explain the variables under study, once all p-values are lower than the significance level determined (0.05).

465

The models created are presented in equations 7 to 11.

$$Zn\ Conc.\ Mass\ Rec. = -0.0717 - 0.0008\ As + 0.0283\ Zn \qquad (7)$$

$$Pb\ Conc.\ Mass\ Rec. = 0.0147 - 0.0004\ Ni - 0.000005\ Ba + 0.000007\ Mn \qquad (8)$$

$$Tailings\ Mass\ Rec. = 1.0624 + 0.0008\ As - 0.0283\ Zn \qquad (9)$$

$$Zn\ Met.\ Rec.\ in\ Zn\ Conc. = 0.2290 - 0.00097\ V + 0.0234\ Zn + 0.00096\ Cu + 0.0224\ Li \qquad (10)$$

$$Zn\ Met.\ Rec.\ in\ Tailings = 0.5218 + 0.0015\ V - 0.0255\ Zn \qquad (11)$$

Analyzing the residual graphs presented in Figure 1 it is possible to conclude that all the five models built have normal distribution of residuals according to Anderson Darling test.

Zn Conc. Mass Recovery

R-squared: 0.986			Adj.R-squared: 0.985	
F-statistic: 1257			Prob(F-statistic): 4.96E-34	
Variable	Coef	Std Error	t	P>|t|
Const	-0.0717	8.29E-03	-8.647	0.000
Zn (%)	0.0283	6.63E-04	42.78	0.000
As (ppm)	-0.0008	1.81E-04	-4.478	0.000

Pb Conc. Mass Recovery

R-squared: 0.386			Adj.R-squared: 0.333	
F-statistic: 7.336			Prob(F-statistic): 0.000611	
Variable	Coef	Std Error	t	P>|t|
Const	0.0147	3.05E-03	4.842	0.000
Ni (ppm)	-0.0004	1.21E-04	-3.591	0.001
Ba (ppm)	-0.000005	1.44E-06	-3.551	0.001
Mn (ppm)	0.000007	3.17E-06	2.234	0.03

Tailings Mass Recovery

R-squared: 0.985			Adj.R-squared: 0.984	
F-statistic: 1160			Prob(F-statistic): 2.07E-33	
Variable	Coef	Std Error	t	P>|t|
Const	1.0624	8.61E-03	123.4	0.000
Zn (%)	-0.0283	6.88E-04	-41.2	0.000
As (ppm)	0.0008	1.87E-04	4.504	0.000

Zn Met. Recovery in Zn Concentrate

R-squared: 0.905			Adj.R-squared: 0.893	
F-statistic: 80.68			Prob(F-statistic): 7.24E-17	
Variable	Coef	Std Error	t	P>|t|
Const	0.2290	9.88E-02	2.317	0.027
V (ppm)	-0.00097	3.61E-04	-2.676	0.011
Cu (ppm)	0.00096	2.95E-04	3.248	0.003
Li (ppm)	0.0224	9.57E-03	2.337	0.03
Zn (%)	0.0234	1.64E-03	14.25	0.000

Zn Met. Recovery in Tailings

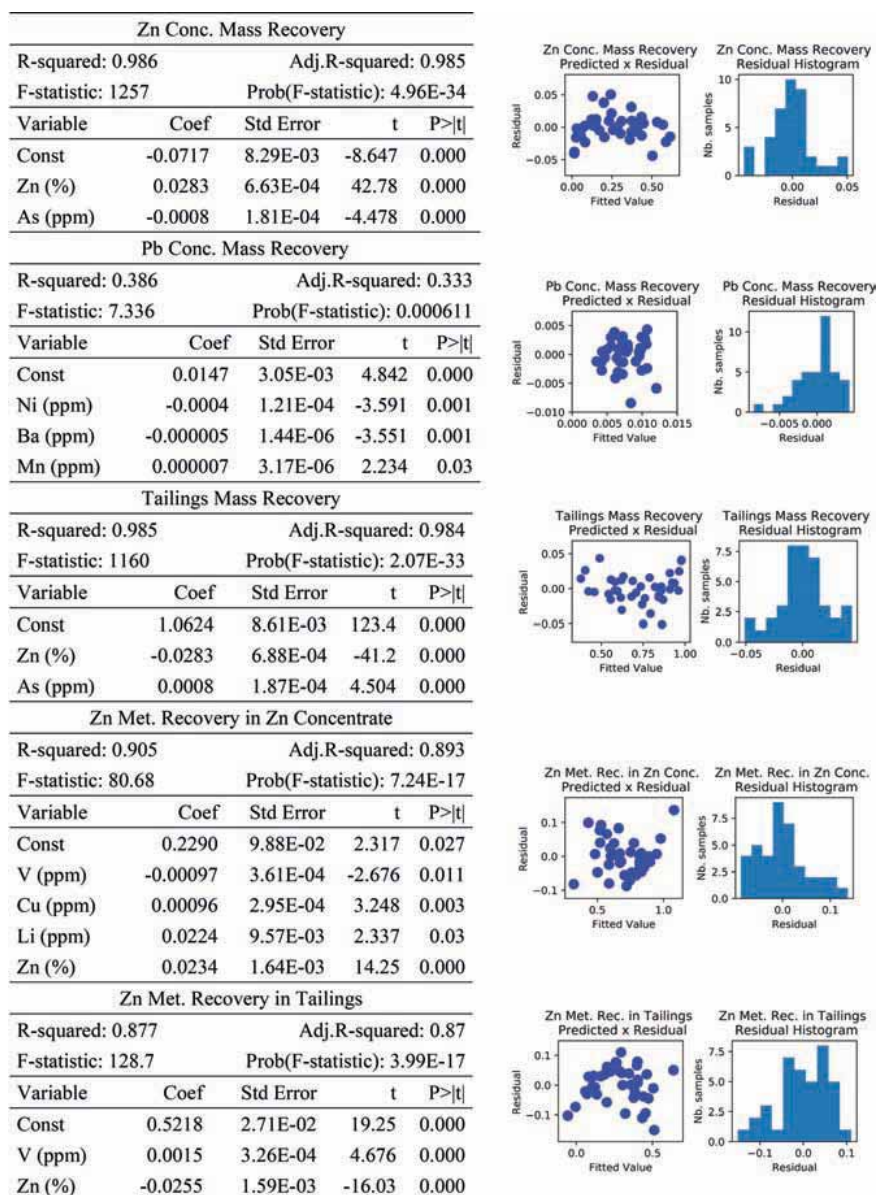|				
R-squared: 0.877			Adj.R-squared: 0.87	
F-statistic: 128.7			Prob(F-statistic): 3.99E-17	
Variable	Coef	Std Error	t	P>|t|
Const	0.5218	2.71E-02	19.25	0.000
V (ppm)	0.0015	3.26E-04	4.676	0.000
Zn (%)	-0.0255	1.59E-03	-16.03	0.000

Figure 1.   Information about the regression models elaborated and residual analysis graphs.

However, a very strong heteroscedastic behavior can be seen when both metallurgical models are evaluated, violating one of the assumptions to create a statistically valid model. The reason for this violation is exactly the non-linear behavior of these dependent variables, as illustrated in Figure 2 graphics A and B where the independent variable Zn was plotted against zinc metallurgical recovery in tailings and in zinc concentrate. When the same variable is plotted against zinc concentrate and tailings mass recoveries, as illustrated in graphics C and D of this figure, it is possible to observe an absence of this non-linear behavior, reinforced that this is a punctual characteristic of the variables related with metallurgical recovery. A possibility to solve this problem is to apply a transformation to those dependent variables and model them in the transformed space. The negative point related to this approach is that the model built will not present a prompt interpretation of results, once all predictions will be in a different scale from the original data, requiring results to be retro transformed. Another alternative is to use a technique able to model data with non-linear relationships, as neural networks. Although the metallurgical recovery models are not statistically the most correct, the decision made was to continue with them aiming at comparing the results obtained using regression models with the ones generated through artificial neural networks.

Using the models created to predict the dependent variables in test set were found correlations near than the ones observed in training set, except for lead concentrate mass recovery, as summarized in Table 2. Consequently, it is possible to conclude that broadly the models built are able to generate good predictions in another dataset different from the one herein used. Even if the result for lead concentrate mass recovery is not as good as the others, it is possible to consider it as satisfactory, once this variable present very reduced masses when compared against the others, in such a way that the financial impact of this material in the mine revenue is minimal.

Figure 3 shows how strong is the correlation between the observed and predicted values in training and test sets. Note on the metallurgical recoveries graphs that there is a non-linear component which was not captured by the models created, resulting in a curved behavior of what should be a linear behavior around the 45° line.

Analyzing mass closure obtained when the three mass recoveries forecasts are summed show closure equal to one in training and test sets, up to two decimal digits. As a regression technique was not able to generate a model to predict zinc metallurgical recovery in lead concentrate, it was not possible to calculate the metallurgical closure. However, it is possible to see 15 out of the 39 samples in the training set summing one without consider
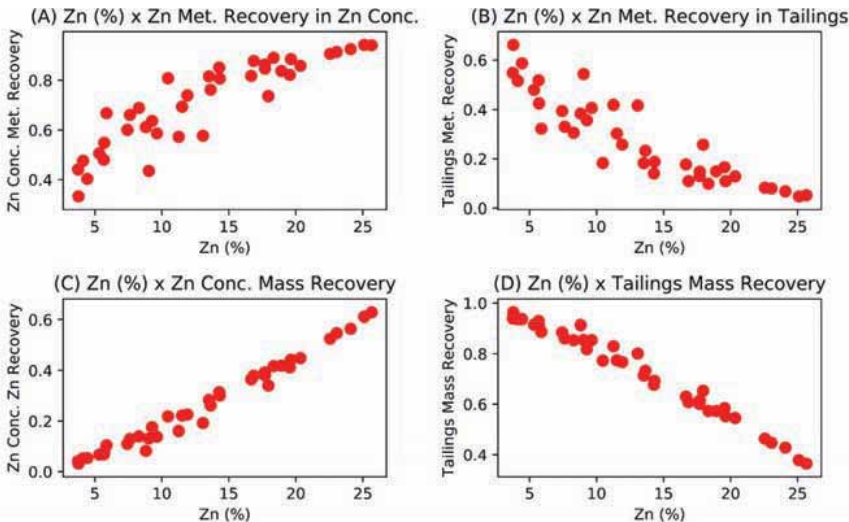

Figure 2. ROM grades plotted against tailings and zinc concentrate masses and metallurgical recoveries.

Table 2. Observed against predicted correlations using regression models.

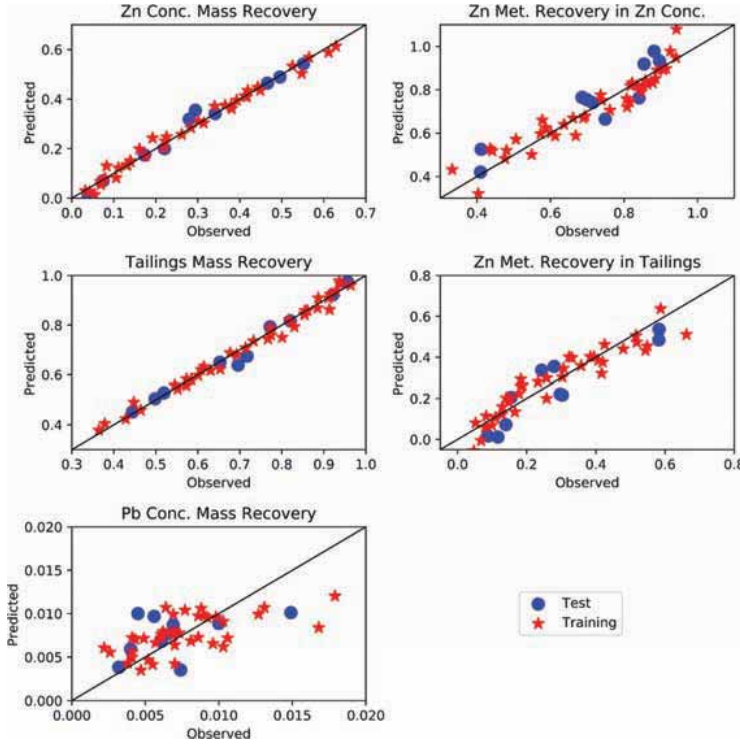| Variable	Training set	Test set
Zn Conc. Mass Recovery	0.993	0.989
Pb Conc. Mass Recovery	0.621	0.442
Tailings Mass Recovery	0.992	0.989
Zn Met. Recovery in Zn Conc.	0.951	0.928
Zn Met. Recovery in Tailings	0.937	0.913

Figure 3. Observed values against predicted thru the use of the models built.

zinc metallurgical recovery in lead concentrate. The same behavior is observed in the test set, where 3 out of the 10 samples showed sum above one. Furthermore, it was identified two negative values for zinc metallurgical recovery in tailings and one prediction above one for zinc metallurgical recovery in zinc concentrate. These results show the need to do a post processing before using them in practice.

2.3 Artificial neural networks

2.3.1 Background theory
The mathematical representation of a neural network with one hidden layer, such as the one used in this study, is presented below starting with the equations representing the input and hidden layer connections:

$$v_j = \sum_{i=0}^{d} \beta_{ji} x_i \tag{12}$$

$$z_j = \varphi(v_j) \tag{13}$$

where d is the number of input variables, x_i represents the input variables, β are the weights which connect the input nodes to the hidden nodes, v represents the hidden layer linear combiner, φ is the activation function used in the hidden layer and z represents the hidden node value. The weight with zero index is the bias element which is related to $x_0 = 1$. The reader should refer to Izenman (2008) for more details.

The equations representing the connections between the hidden layer and the output layer can be written as:

$$v'_k = \sum_{j=0}^{m} \alpha_{kj} z_j \tag{14}$$

$$\hat{y}_k = \varphi'(v'_k) \tag{15}$$

where m is the number of hidden nodes, α are the weights which connect the hidden nodes with the output nodes, v' represents the output layer linear combiner, $\hat{y}$ represents the output node estimate and φ' is the activation function for the output layer. The weight with zero index is the bias element introduced in each output node, which is related to $z_0 = 1$.

It is possible to write all four equations above as one, presented below:

$$\hat{y}_k = \varphi'\left(\sum_{j=0}^{m} \alpha_{kj} \varphi\left(\sum_{i=0}^{d} \beta_{ji} x_i\right)\right) \tag{16}$$

The most popular method for estimating the network parameters is the "backpropagation"-of-errors algorithm (Izenman, 2008), which was applied to neural networks by Werbos (1974). The backpropagation generates the first derivatives of an error function with regard to β and α weights and through the application of the gradient-descent optimization method these derivatives are used to estimate the weights by minimizing the error function under study.

The choice of activation functions can be decisive in elaborating either a robust network or one with poor predictive quality. The activation function can assume several forms and produce outputs in the 0 to 1 or −1 to 1 range or even in a real numbers set. The most widely applied activation functions are the threshold, signal, rectifier, hyperbolic tangent, sigmoid and linear, being the last two mentioned the ones used in this study and represented respectively on equations 17 and 18:

$$Sigmoid\ function: \varphi(v) = \frac{1}{1 + exp(-v)} \tag{17}$$

$$Linear\ function: \varphi(v) = v \tag{18}$$

Once all basic concepts necessary to understand neural networks were presented, the next step is to elaborate a network for the data available in this study.

2.3.2 *Neural network elaboration*

In order to make possible to compare the results obtained using regression analysis and neural networks, the variables chosen to be used as input in the network were the same used to create the regression models, so, the neural network input variables were: Mn (ppm), Ni (ppm), Ba (ppm), As (ppm), Zn (%), V (ppm), Li (ppm) and Cu (ppm).

The first step to elaborate a network with these variables was to transform the independent variables aiming at making all of them varying within the same range, once the biggest part of the elements was analyzed in ppm and the Zn variable was analyzed in percentage. Two transforms were tested: standardization for zero mean and unit variance and a transformation to put all values varying in the 0 to 1 range. Analyzing the results obtained when both transforms were applied, it was possible to conclude that the standardization presented better results.

To identify which set of parameters generate the best forecasts for mass and metallurgical recovery in all plant outputs, it was tested several combinations, as described below.

The first step is to define which is the best learning rate to be used in the backpropagation algorithm (details in Izenman (2008)). It was tested values between 10^{-6} and 10^{-1} and for 0.05 best results were obtained.

The activation functions tested in the hidden layer were: linear, sigmoid, hyperbolic tangent, relu and softplus; being the sigmoid function (equation 17) the one that presented the best results. For the activation function in the output layer no tests were realized, once it is necessary to have an output inside the real numbers set, what can be achieved only using the linear function (equation 18).

The test for hidden nodes number was realized considering networks with 2 to 15 nodes. The 14 nodes network gave the best results.

Finished the parameter tests it was defined that the neural network should use a learning rate of 0.05, sigmoid activation function in the hidden layer, which should have 14 nodes, and linear activation function in the output layer. Figure 4 showed the network structure.

Table 3 illustrates the correlation between the observed data and the forecasts obtained through the application of the network created. Analyzing the results, excellent correlations (>0.90) are seen in the training and test sets, except for lead concentrate mass recovery and zinc metallurgical recovery in lead concentrate, but even for these variables the results can be considered good.
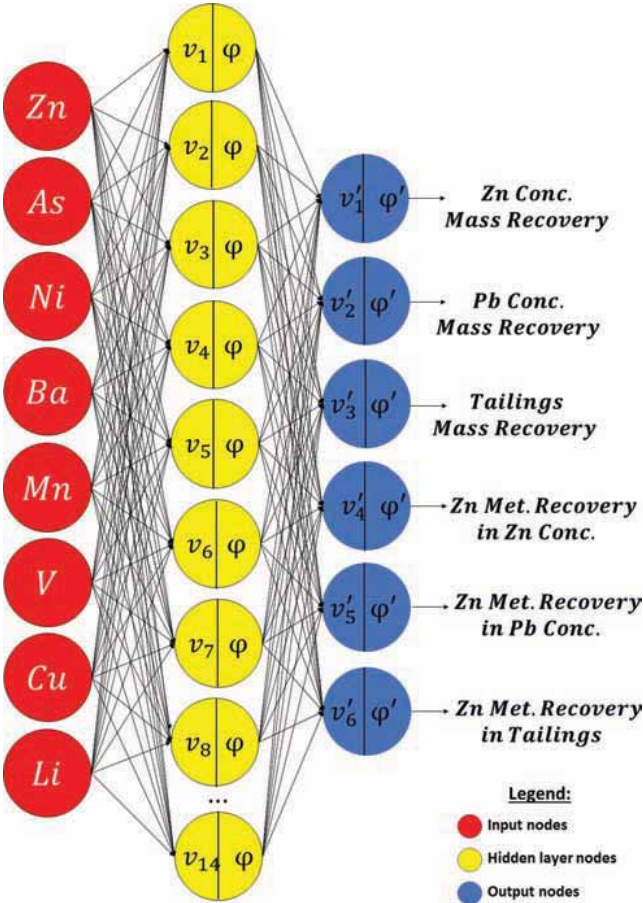

Figure 4. Neural network built to forecast mass and metallurgical recovery.

Table 3. Observed against predicted values correlation using neural networks.

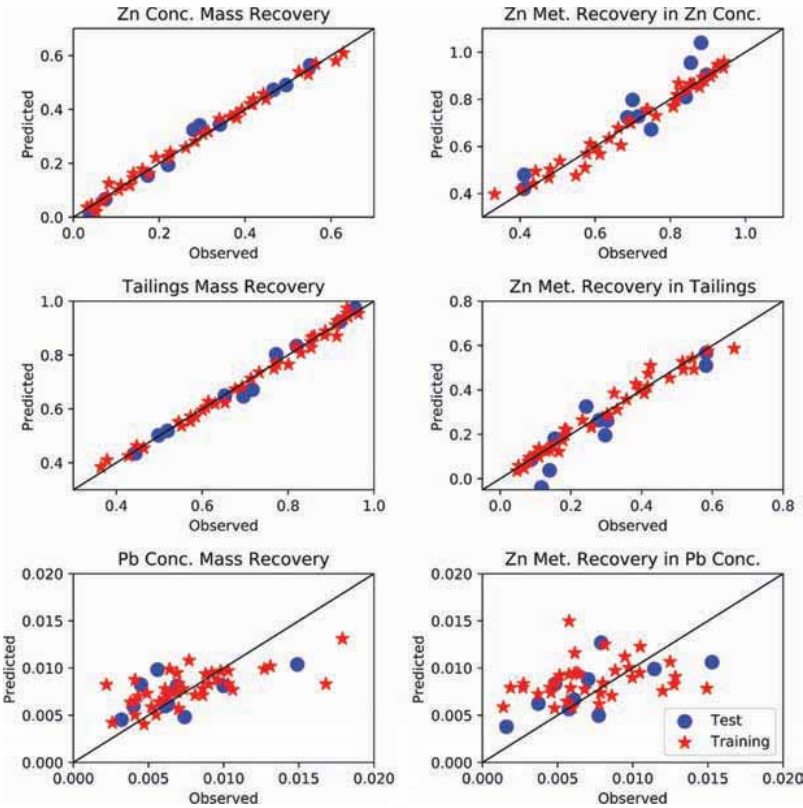| Variable	Training set	Test set
Zn Conc. Mass Recovery	0.996	0.992
Pb Conc. Mass Recovery	0.662	0.585
Tailings Mass Recovery	0.995	0.991
Zn Met. Recovery in Zn Conc.	0.985	0.936
Zn Met. Recovery in Pb Conc.	0.512	0.660
Zn Met. Recovery in Tailings	0.983	0.932

Figure 5. Observed values against predicted through the use of neural networks.

Figure 5 illustrates the correlations presented in Table 3. The non-linear behavior obtained when the regression model was applied cannot be seen when neural networks are used, showing that this technique is able to capture the variability of those variables.

Analyzing the forecasts made through the neural network built it is possible to observe a metallurgical closure equal to one for all samples in the training and test sets. Excepting for one sample in the training and test sets, the mass closure was equal to one, considering two decimal digits. One negative forecast was observed for zinc metallurgical recovery in tailings and one prediction greater than one was observed for zinc metallurgical recovery in zinc concentrate.

The results show that neural networks also need a post processing before been used in practice, even if the number of wrong results were lower than the number observed when data was forecasted using regression models.

Table 4. Correlation comparison between real and predicted data using regression and neural networks.

Variable	Neural networks		Regression	
	Training set	Test set	Training set	Test set
Zn Conc. Mass Recovery	0.996	0.992	0.993	0.989
Pb Conc. Mass Recovery	0.662	0.585	0.621	0.442
Tailings Mass Recovery	0.995	0.991	0.992	0.989
Zn. Met. Recovery in Zn Conc.	0.985	0.936	0.951	0.928
Zn Met. Recovery in Pb Conc.	0.512	0.660	–	–
Zn Met. Recovery in Tailings	0.983	0.932	0.937	0.913

3 CONCLUSIONS

Table 4 summarizes the results obtained using both techniques herein presented. All variables showed better correlations between the predicted and real values when neural networks were applied. For the metallurgical recovery variables this advantage is more noticed, considering that regression analysis was not able to create a statistically valid model to forecast zinc metallurgical recovery in lead concentrate.

Neural networks do not require any statistical assumption as residuals normality and homoscedasticity and showed facility to model simultaneously 6 dependent variables, making this technique more practical then regression analysis in several aspects. Another advantage observed is related to mass and metallurgical closure, which is better obtained compared to the one seen when regression analysis was used. This reduces the time spent in post processing the results. Artificial neural networks generated better results and is a less laborious technique, showing that it is a viable alternative in geometallurgy data modelling.

REFERENCES

Carrasco, P., Chilès, J.P., Séguret, S. 2008. Additivity, metallurgical recovery and grade. Geostats 2008, Santiago, Chile, p. 237–246.

Coward, S., Vann, J., Dunham, S., Stewart, M. 2009. The Primary-Response Framework for Geometallurgical Variables. Seventh International Mining Geology Conference, Perth, WA, 17–19 agosto, p. 109–113.

Fernandes, F.G. 2013. Estudo do Melhor Método de Extrapolação de Regressão Múltipla para Construção do Modelo Geometalúrgico de uma Mina de Fosfato Brasileira. Dissertação de Mestrado – Universidade Federal de Ouro Preto, 160 p.

Hair, J.F., Anderson, R.E., Tathm, R.L., Black, W.C., Babin, B.J. 2009. Análise Multivariada de dados. 6ª edição, New Jersey, Prentice Hall, p. 145–220.

Izenman, A.J. 2008. Modern Multivariate Statistical Techniques. New York, Springer, p. 336.

MacMillan, E., Ehrig, K., Liebezeit, V., P Kittler, P., Lower, C. 2011. Use of Geometallurgy to Predict Tailings Leach Acid Consumption at Olympic Dam. The first AUSIMM International Geometallurgy Conference. Brisbane, QLD, p. 93–102.

Montoya, P.A., Keeney, L., Jahoda, R., Hunt, J., Berry, R., Drews, U., Chamberlain, V., Leichliter, S. 2011. Techniques Applicable to Prefeasibility Projects – La Colosa Case Study. The first AUSIMM International Geometallurgy Conference. Brisbane, QLD, p. 103–111.

Motta, E.G.M. 2014. Definição de Domínios Mineralógicos em Minério de Ferro Utilizando Krigagem de Indicadores. Dissertação de Mestrado – Universidade Federal do Rio Grande do Sul, 223 p.

Richmond, A., Shaw, W.J. 2009. Geometallurgical Modelling – Quo Vadis? Seventh International Mining Geology Conference. Perth, WA, p. 115–118.

Vieira, M.C.A. 2016. Metodologia para Prever Recuperação de Zinco em Planta de Beneficiamento. Dissertação de Mestrado – Universidade Federal do Rio Grande do Sul, 176 p.

Werbos, P.J. 1974. Beyond regression: new tools for prediction and analysis in the behavioral sciences. Ph.D. dissertation, Harvard University, 454 p.

The simulation of the excavation sites of coal mines

K.N. Kopylov
JSC SUEK, The Russia

S.S. Kubrin & D.I. Blokhin
Institute of Comprehensive Exploitation of Mineral Resources Russian Academy of Sciences, Russia

ABSTRACT: In the conditions of high-performance working faces should be used methods of operational management of the fully- mechanized, allowing organizing the maximum performance during the technological processes of breaking and transportation of coal, including taking into account the forecast of methane concentration within the bay. Based on the actual data on the work of the mine "Polysaevskaya" was developed a simulation model of the search's optimal mode of control of the feed rate of the harvester. Because of the uneven loading of the flight conveyer reduces the efficiency use of technological equipment. With the help of mathematical modeling, the optimal feed modes of the combine found, which provide an increase in the productivity. Based on the model of operational management can be determined modes of operation of the complex, providing maximum performance.

1   INTRODUCTION

The main products of the coal mine provides the excavation site which is influenced by many factors: mining and geological (conditions of occurrence of the coal seam, the properties of coal and host rocks, etc.), mining (method of preparation, ventilation scheme, the applied means of mechanization, the intensity of development of reserves of the excavation site). The efficiency of the excavation site is determined by the operating time of the installed equipment for coal extraction and the degree of use of the installed capacity, which depends mainly on the feed rate of the combine. It based on its value that the design load on the treatment face planned. There are various methods of determining the average maximum permissible load on the working face in methane mines (Ruban et al. 2009). They allow quite accurately determine the load in different mining and geological conditions, taking into account the technological schemes of mining coal reserves and ventilation schemes. Unfortunately, these methods cannot applied in the operational management of the mechanized complex, because they differ in the complexity of calculations, the presence of many factors, including empirical ones, which have different values along the length of the working face.

  The most promising approach is to determine the parameters of the mechanized complex based on the use of mathematical modeling of technological processes (Samarskij & Mihajlov 2001). The excavation site as a whole is a complex system, which influenced by the coal seam and host rocks, the applied means of mechanization, the state of the mine atmosphere and the intensity of methane emission. In recent years, several developed mathematical models describing the work of the excavation site have presented in scientific publications. In (Tkachev & Bublikov 2015) substantiated the algorithm of automatic control of the feed speeds and cutting from the standpoint of stabilization of the loading and performance of the Executive bodies. Of interest is: the mathematical description of the forecast of methane release from the surface of the coal seam exposure taking into account the high rate of advance of the preparatory face (Kachurin et al. 2011); the methodology of the forecast of the maximum permissible load on the treatment face by the gas factor (Slastunov et al. 2015), based on the solution of differential equations in partial derivatives of methane mass transfer;

a mathematical description for predicting field concentrations of methane in breakage face (Borshchevich et al. 2010); the relationship that allows to predict the methane release from the broken coal in the preparatory workings with the speed of face advance (Kachurin et al. 2014); the results of studies of gas emission from broken coal during high-performance treatment systems (Shevchenko & Livinskaya 2015); model parameter optimization of the extraction of the stratum "Fourth" mines of JSC "Vorkutaugol" (Kazanin & Sufiyarov 2014).

2 FORMALIZATION OF THE TASK

In practice, it is required quickly determine the modes of operation of complex-mechanized faces in specific current conditions. Of particular importance is the correct choice of the program of operational management and monitoring of technological operations for the timely detection of deviations from the selected mode, adjustment of the established current modes of operation of technological processes and the development, and if necessary, the implementation of measures aimed at reducing the risks of accidents (Kopylov et al. 2016, Kopylov et al. 2018, Kopylov et al. 2017). The analysis of the works considered above shows that the results given in them are not suitable for the development of a model of the technological process characterizing the main operations of the extraction complex: the beating and transportation of coal.

When creating a mathematical model of the excavation complex, the input factors are: the feed rate of the combine, the speed of the flight conveyor, loader, crusher, belt conveyor, the concentration of methane at the inlet and outlet of the treatment face, the relative methane content of the developed layer; the output parameter is the performance of the combine. To formalize the task, it is necessary to make the transition from verbal description to quantitative relations between input and output parameters. The first verbal description that needs to formalize defines two actions – "the destruction of the coal seam and the movement of coal to the flight conveyor."

To represent these actions in a mathematical model, it is required to specify additional variables (the location and time of the combine relative to the face), which are determined based on input parameters. When considering the problem, when the feed of the combine carried out at a constant speed, there are no special problems. However, in practice, the harvester along the lava moves at variable speed and often with stops. Therefore, in general case the motion of the excavation of the harvester along the line of slaughtering is carried out with the same velocity, V_k, is given by an arbitrary (specified by the operator of the harvester) the law $V_k = V_k(t)$. Then the location of the harvester is determined as the $x(t)$ coordinate and is found from the solution of the differential equation

$$\frac{dx}{dt} = V_k(t) \tag{1}$$

With the constant movement of the harvester, its location changes with time $x_k = x_k(t)$. Using the parametric setting of the combine location coordinate, that is, expressing the time, you can go through the coordinate to the equation

$$\frac{dx}{dt} = V_k(x(t)) \tag{2}$$

Thus, the number of additional variables reduced; however, this will not be correct, since if the dependence $x_k = x_k(t)$ is unambiguous, then the dependence $t = t(x_k)$ is unambiguous only with the constant movement of the harvester. If it stops or moves backwards, the certainty is lost. This is the first feature of the task to taken into account.

The second feature arises when trying to quantitatively, using mathematical notation, formalize the second verbal description of the mechanized complex – "coal, getting on the flight conveyor moves along the face." At a constant rate of flow extraction processor, the amount of repelling them coal will be permanent. The current filling of the flight conveyor with coal

at the point $x_k = x_k(t)$ is determined by the volume dv of the beaten coal during dt, depending on the working thickness of a seamh, the length of the screw l and the feed rate of the harvester and will be equal to $dv = hlV_k dt$. Taking into account the specific weight of coal γ, the weight of the beaten coal volume will be $dM = h\gamma l V_k dt$. Defined in this way, the volume of dv coal weighing dM moves within the bay on the flight conveyor at a speed of V_{sk}. Then the time to move it to the exit of the bay is determined from the equation

$$\frac{dx}{dt} = -V_{sk}(t) \qquad (3)$$

by the ration

$$T_i = -\frac{1}{V_{sk}} \int_{x=x_i}^{x=x_0} dx \qquad (4)$$

here $V_{sk} = const$ – the speed of the flight conveyor, x_i place of the breaking portion of the coal dM, x_0 – coordinate of flight conveyor from belt entries. Total weight of broken coal in the bay at time t_j defines the integration of elementary portions broken coal, for which the condition – travel time from point of cutting to conveyor drift does not exceed the transportation time by flight conveyor:

$$Q = \int_{i=1}^{i=n} dM_i \qquad (5)$$

for i satisfying the condition:

$$t_j - t_0 \leq -\frac{1}{V_{sk}} \int_{x=x_i}^{x=x_0} dx \qquad (6)$$

or

$$\int_{x_i}^{x_j} \frac{dx}{V_k} - t_0 \leq -\frac{1}{V_{sk}} \int_{x=x_i}^{x=x_0} dx \qquad (7)$$

If the feed rate of the harvester is constant ($V_{sk} = const$), then the integral disappears in the left part of the condition, and an easily calculated ratio

$$\left(x_j - x_i \right) \Big/ V_k$$

is obtained. Then, knowing the speed of the combine harvester and flight conveyor is not difficult to determine the weight of coal in the bay.

When considering the general case-determining the volume of coal on the flight conveyor, it is enough to use a simplified scheme of its operation (Fig. 1). The flight conveyor is shown by a horizontal line. The point x_0 corresponds to the joint of the crusher and flight conveyor. Let during the cutting of coal, the harvester moves along the face line with some varying feed rate $V_k(t)$. The coal repulsed by the combine is loaded on a flight conveyor, which in turn moves at a constant speed $V_{sk} = const$. By the time the approach the excavation of the harvester to the point with coordinates of x_i as the result of blasting, loading of coal harvester and moving the flight conveyor with submerged him coal, at time t_i flight conveyor loaded with coal, the volume of which (in Fig. 1 conditionally shown in gray) is described by the function $\varphi = \varphi(x)$. After a period of time dt flight conveyor moved the entire volume of coal to the side of the conveyor belt (the lower part of the Figure 1). In this case, part of the coal (after the point x_0) is overloaded to the next equipment in the transportation line (shown by a
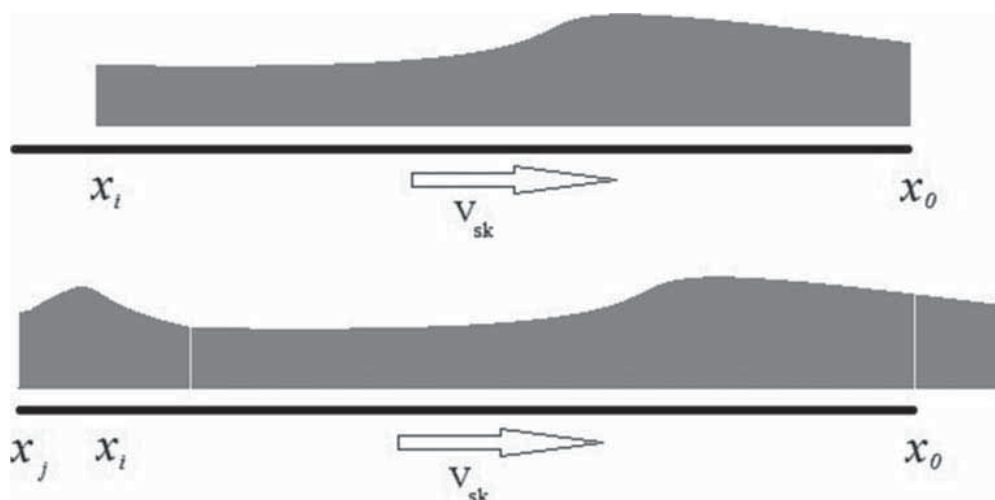
475

Figure 1.   Scheme of movement of coal flight conveyor.

separated element on the right outside the flight conveyor). In turn, the extraction processor continues the breaking of the coal has shifted to the point x_j, and for the time dt has uploaded to flight conveyor coal, the amount of which is conventionally shown on the left.

The upper part corresponds to the loading of the flight conveyor with coal at the time t_i.

The lower part corresponds to the loading of the flight conveyor with coal at the time $t_j = t_i + dt$.

Coordinate x_0 – the place of articulation of the flight conveyor with crusher, x_i is the location of the excavation of the harvester at time t_i, x_j location of excavation harvester at time t_j, V_{sk} – speed flight conveyor.

The analysis of the described process indicates that. Firstly, there is simply a shift in the volume of coal towards the conveyor drift at the speed of the flight conveyor, secondly, there is a replenishment of the volume of coal in proportion to the feed rate of the extraction combine, and, thirdly, there is a removal of the volume of coal poured onto other theological equipment. It should note that the process has the property of irreversibility. Thus, because the data on the volumes of coal to reload to the following process equipment are lost, it is necessary to additionally save data on the volumes of coal overloaded from the flight conveyor to be able to describe the process with a reversible time. The operation of shifting the volumes of coal along the scraper conveyor does not allow the description in the final form. In other words, in mathematics there are no such transformation operators $D(\varphi) = D\varphi$ (x), for which the action on the function should depend on the values of its arguments. That is, the action of such an operator on the function φ, should be different and allow to describe the processes (coal loading, coal movement, coal handling). In this case, the scope of the operator, at the x coordinate, changes when moving the harvester. Thus, with the help of functions of continuous description of the coal distribution on the flight conveyor, it is impossible to obtain a formal description of the processes of "loading coal by the extraction combine on the flight conveyor", "moving coal by the flight conveyor", "transshipment of coal from the flight conveyor".

Using a discrete representation of the volume of coal, that is, considering the numerous portions of coal that are "loaded by the extraction combine on the flight conveyor", "moved by the flight conveyor", "overloaded from the flight conveyor", it is necessary to introduce the equations of motion of each portion into the problem. In this case, the weights of the coal portions loaded by the combine on the flight conveyor will be different ($dM_i \neq dM_{i+k}$). Therefore, in the condition (left side) of determining the portions of coal that are in the bay, it is necessary to use an integral, which leads to the fact that for each portion it is necessary to know its current location, for which it is necessary to solve a set of equations of motion

of each portion. This approach leads, firstly, to a sharp increase in the dimension of the problem by several orders of magnitude. Secondly, a need to constantly generate dependencies describing the movements along the face of the newly repulsed portion of coal by the flight conveyor, and after the overload of the elementary portion from the flight conveyor to remove these dependencies. All this leads to the fact that the discrete formulation of the problem of describing the process of complex-mechanized face today is not solved.

All these circumstances leave only one way to represent the length-distributed loading of the scraper conveyor in the form of selective different actions on the elements of the function φ. This should increase the dimension of the distribution function of coal on the scraper conveyor, adding time t presenting it as $\varphi = \varphi(x, t)$.

Then, the increase in the volume of coal by the extraction combine on the flight conveyor is written by the expression $\varphi = \varphi(x_k, t) = \varphi(x_{ki}, t_i) + dM = \varphi(x_{ki}, t_i) + h\gamma lVk\ dt$. Moving cargo flight conveyor (with speed V_{sk}) – shift operation – transformation function $\varphi(x, t)$, which is described by the expression $\varphi(x_i, t + dt) = \varphi(x_i - V_{sk}\ dt, t)$. In this case, the part of the conveyor, which is located at the top of the road, and is a section that appeared in the time interval dt and remains empty $\varphi(x_n \div x_n - V_{sk}\ dt, t + dt) = \varphi(x_i - V_{sk}\ dt, t) = 0$.

Coal, which was on the flight conveyor at the bottom of the bay, is overloaded to the following process equipment. This volume of coal is $\varphi_{out}(x_k, t) = \varphi(x_1 \div x_1 + V_{sk}\ dt, t)$. Similar to the flight conveyor as a streaming device for moving the rock mass, a loader, a crushing plant, and a belt conveyor work.

The ratios describing the technological process of moving the combine harvester, rock mass, with the help of technological equipment of complex-mechanized face the following.

Submission of the combine along the face (1).

The flow of coal

$$
\begin{cases}
\varphi_{sk}(x_i, t_i) + dM = \varphi_{sk}(x_i, t_i) + \gamma hlV_k dt(x_i = x_k) \\[2ex]
\varphi_p(x_i, t_i) + dM = \varphi_p(x_n \div x_n - V_p dt, t_i) = \varphi_{sk}(x_1 \div x_1 + V_{sk} dt, t_i)\dfrac{V_{sk}}{V_p} \\[2ex]
\varphi_d(x_i, t_i) + dM = \varphi_d(x_n \div x_n - V_d dt, t_i) = \varphi_p(x_1 \div x_1 + V_p dt, t_i)\dfrac{V_p}{V_d} \\[2ex]
\varphi_{lk}(x_i, t_i) + dM = \varphi_{lk}(x_n \div x_n - V_{lk} dt, t_i) = \varphi_d(x_1 \div x_1 + V_d dt, t_i)\dfrac{V_d}{V_{lk}}
\end{cases}
\tag{8}
$$

Coal movements

$$
\begin{cases}
\begin{cases}
\varphi_{sk}(x_i, t + dt) = \varphi_{sk}(x_i - V_{sk} dt, t), if(x_i \prec x_n - V_{sk} dt) \\
\varphi_{sk}(x_n \div x_n - V_{sk} dt, t + dt) = 0, if(x_i \geq x_n - V_{sk} dt)
\end{cases} \\[2ex]
\begin{cases}
\varphi_p(x_i, t + dt) = \varphi_p(x_i - V_p dt, t), if(x_i \prec x_n - V_p dt) \\
\varphi_p(x_n \div x_n - V_p dt, t + dt) = 0, if(x_i \geq x_n - V_p dt)
\end{cases} \\[2ex]
\begin{cases}
\varphi_d(x_i, t + dt) = \varphi_d(x_i - V_d dt, t), if(x_i \prec x_n - V_d dt) \\
\varphi_d(x_n \div x_n - V_d dt, t + dt) = 0, if(x_i \geq x_n - V_d dt)
\end{cases} \\[2ex]
\begin{cases}
\varphi_{lk}(x_i, t + dt) = \varphi_{lk}(x_i - V_{lk} dt, t), if(x_i \prec x_n - V_{lk} dt) \\
\varphi_{lk}(x_n \div x_n - V_{lk} dt, t + dt) = 0, if(x_i \geq x_n - V_{lk} dt)
\end{cases}
\end{cases}
\tag{9}
$$

Transshipment of coal to the following process equipment

$$
\begin{cases}
\varphi_{out} \to p^{(x,t)} = \varphi_{sk}\left(x_1 \div x_1 + V_{sk}dt, t\right) \\[2mm]
\varphi_{out} \to d^{(x,t)} = \varphi_{p}\left(x_1 \div x_1 + V_{p}dt, t\right) \\[2mm]
\varphi_{out} \to lk^{(x,t)} = \varphi_{d}\left(x_1 \div x_1 + V_{d}dt, t\right) \\[2mm]
\varphi_{out}(x,t) = \varphi_{lk}\left(x_1 \div x_1 + V_{lk}dt, t\right)
\end{cases}
\tag{10}
$$

3 SIMULATION RESULT

For the conditions of the bay 17 – 49 mine Polysaevskaya conducted simulation of techno-logical processes of breaking and transportation of coal at a nominal constant feed rate of the harvester 6 m/min (Fig. 2). The parameters of the bay are as follows: the seam thickness of 1,74 m, angle of seam dip12 – 17°, cutting resistance 140 kg/cm², volume weight of coal 1,29 t/m³, face length 300 m, the number of mechanized support unit 177; length of the auger shearer 1 m, the cutting mode of the shearer uni-direction cutting, production per cycle 675 tons, production 7–10 thousand tons/day, the actual gas content of the forma-tion 3 – 6 m³/t, flight conveyor speed 1,32 m/s, combined ventilation scheme. In this case, the volume of coal on the flight conveyor increases linearly. The maximum loading of the conveyor is achieved only at the end of the working passage, at the top of the face, and is equal to 50 tons of coal. On all bay there will be slightly more than 70 tons of coal. For Fig. 2 shows the uneven loading of equipment. To improve the efficiency of the technical resource it is necessary to find the optimal mode of change in the feed rate of the combine harvester, providing the highest performance with the accepted limitation of the volume of coal in the bay.

The result of using a mathematical model to determine the optimal mode of change in the feed rate of the combine is shown in Fig. 3. On the Fig. 4 shows the mode of change in the feed rate of the combine, along the face. Because the time of passage of the harvester has decreased (from 50 minutes 42 seconds to with 37 minutes 31 seconds) the performance increased by 26%. Taking into account the idling time of the combine for cleaning at a feed rate of 20 m/min for about 15 minutes, the productivity increase will be 19%.
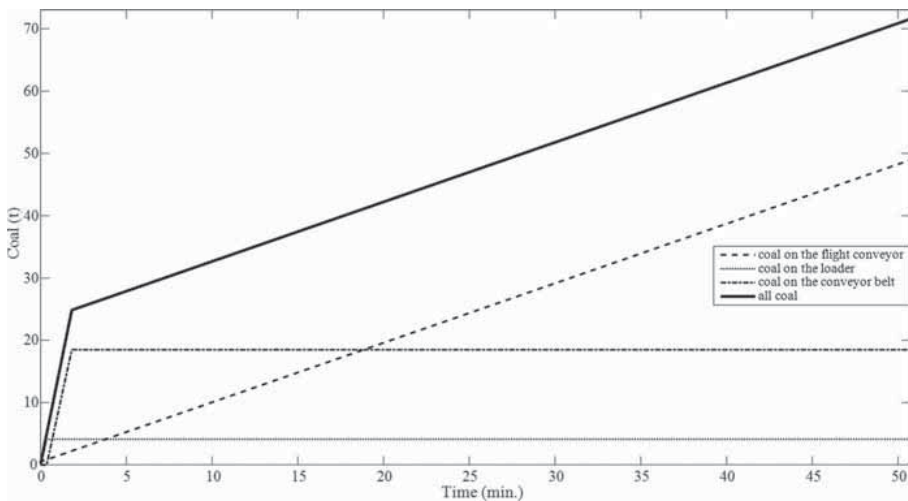

Figure 2.   The volumes of coal at the excavation bay with constant feed speed of the harvester 6 m/min.
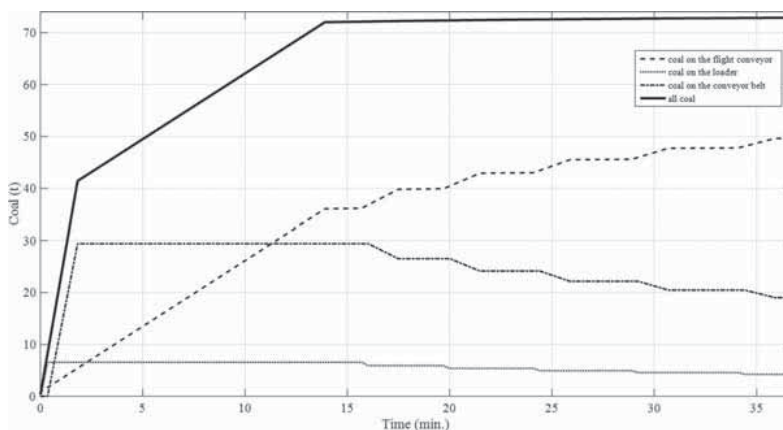
Figure 3. The volumes of coal at the excavation bay with optimum feed speed of the harvester.
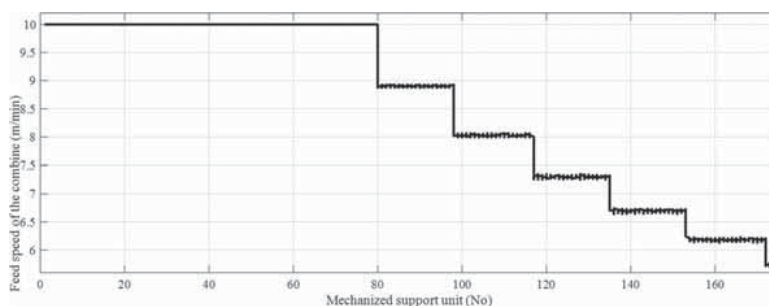

Figure 4. The optimal mode of change in the feed speed of the combine on the location of the mechanized support unit.

4 CONCLUSION

Thus, it proved that it is impossible to formalize the work of complex-mechanized face based on the use of continuous or discrete final description of the processes of loading, movement and unloading of coal by the technological equipment of the excavation site.

A mathematical model of the complex—mechanized face based on the separation of the processes of loading, movement and unloading of coal technological equipment of the excavation site. The presented model adequately describes the main technological processes at the excavation site.

The presented mathematical model of formalization of the main technological processes taking place at the excavation site—breaking, loading, moving and unloading of coal can used to determine the effective modes of operation of complex-mechanized face, in order to achieve maximum productivity of the excavation site and to ensure trouble-free operation of the installed equipment.

REFERENCES

Borshchevich, A.M., Kovalev, R.A., Buhtiyarov, A.A., Sarycheva, I.V. 2010. Ogranichenie nagruzki na ochistnoj zaboj po gazovomu faktoru. *Izvestiya Tul'skogo Gosudarstvennogo universiteta. Estestvennye nauki* (1): 232–239.
Kachurin, N.M., Kaledina, N.O., Kachurin, A.N. 2011. Vydelenie metana s poverhnosti obnazhennogo ugol'nogo plasta v podgotovitel'nuyu vyrabotku. *Izvestiya Tul'skogo Gosudarstvennogo universiteta. Nauki o Zemle* (1): 80–84.

Kachurin, N.M., Vorob'ev, S.A., Kachurin, A.N., Sarycheva, I.V. 2014. Matematicheskie modeli metanovydeleniya v podgotovitel'nye vyrabotki i ochistnye zaboi iz otbitogo uglya. *Izvestiya Tul'skogo Gosudarstvennogo universiteta. Tekhnicheskie nauki* (1): 158–164.

Kazanin, O.I., Sufiyarov, A.M. 2014. Ocenka vliyaniya dliny lavy na harakter gazovydeleniya na vyemochnyh uchastkah shaht OAO «Vorkutaugol'». *Zapiski Gornogo instituta* 207: 36–40.

Kopylov, K.N., Kubrin, S.S., Reshetnyak, S.N. 2018. Aktual'nost' povysheniya urovnya energoeffektivnosti i bezopasnosti vyemochnogo uchastka ugol'noj shahty. *Ugol'*: (10): 66–67.

Kopylov, K.N., Kubrin, S.S., Zakorshmennyj, I.M., Reshetnyak, S.N. 2017. Eksperimental'nye issledovaniya parametrov raboty ochistnogo kombajna ugol'noj shahty pri razlichnyh skorostyah podachi. *Gornyj informacionno-analiticheskij byullyuten'* (12): 48–55.

Kopylov, K.N., Zakorshmennyj, I.M., Kubrin, S.S. 2016. Voprosy upravleniya ochistnym kompleksom pri otrabotke vysokogazonosnyh plastov na primere shahty «Polysaevskaya AO «SUEK-Kuzbass». *Ugol'* (12): 32–34.

Ruban, A.D., Artemiev, V.B., Zaburdyaev, V.S., Zaburdyaev, G.S., Rudenko, Yu.F. 2009. *Problemy obespecheniya vysokoj proizvoditel'nosti ochistnyh zaboev v metanoobil'nyh shahtah*. Moscow.

Samarskij, A.A., Mihajlov, A.P. 2001. *Matematicheskoe modelirovanie: Idei. Metody. Primery*. Moscow: Fizmatlit.

Shevchenko, L.A., Livinskaya, S.N. 2015. Gazovydelenie iz otbitogo uglya pri intensivnoj otrabotke ugol'nyh plastov. *Vestnik KuzGTU* (1): 164–166.

Slastunov, S.V., Karkashadze, G.G., Mazanik, E.V., Lupij M.G. 2015. Nauchno-tekhnicheskoe obespechenie metodologii prognoza maksimal'no dopustimyh nagruzok na ochistnoj zaboj pri otrabotke gazonosnyh ugol'nyh plastov. *Gornyj zhurnal* (3): 4–8.

Tkachev, V.V., Bublikov, A.V. 2015. *Ispol'zovanie imitacionnogo modelirovaniya dlya issledovaniya sistemy avtomaticheskogo upravleniya dobychnym kom-bajnom: monografiya*. Donetsk: NGU.

An operational data based framework for longwall shearer performance measurement

E. Yilmaz & M. Erkayaoglu
Middle East Technical University, Ankara, Turkey

ABSTRACT: Coal is an important part of the energy mix in today's world. In most countries, the deposits that can be economically extracted using surface mining techniques are becoming scarcer, resulting in underground mining, especially longwall operations, providing a larger share of total coal production. Optimisation of longwall operations should take equipment performance into consideration to understand the efficiency of the system and utilize it continuously as part of decision-making. In this study, the effects of the operational factors on the shearer performance in a longwall operation, and the total productive time of the shearer for a shift, were investigated. Data were collected from a longwall operation on site as input to a simulation model that allows the factors affecting the efficiency of the system to be investigated. The results of this study defines a suggested framework for the collection, analysis, and interpretation of longwall mining related operational data for the measurement of shearer performance.

1 INTRODUCTION

Coal is one of the most commonly utilized energy source for primary electricity generation in many countries. According to the research conducted by the World Energy Council (2016), energy production from coal-based resources increased by 64% between 2000 and 2014. Today, approximately one-third of world electricity is provided by coal-based energy production in the world, and coal is expected to maintain its importance in energy production in the next 30 years (World Energy Council 2016).

Coal can be extracted from the earth crust by applying underground mining methods or surface mining methods. Surface mining methods are applied to deposits having shallow depths due to technical and economic reasons. As the shallow depth coal deposits are extracted with the increase in energy demands of the humankind, underground mining activities have become more common for the extraction of coal deposits for the near future.

Production efficiency in mining activities was of secondary importance in production planning in the past since the companies were available to extract high-grade deposits. However, as the amount of high-grade deposits decreased due to extraction, mining industry was directed to lower grade deposits. Therefore, production efficiency become more critical for companies.

Mining engineers are challenged with different operational problems during production. Some researchers approached these problems by applying mathematical techniques including linear (Lamghari et al. 2015), nonlinear programming, genetic algorithm (Azimi & Osanloo 2011) and integer programming (Zhang & Xia 2015). However, as the mining problems are mostly composed of stochastic processes, deterministic approach might not be applicable to certain problems that involve uncertainties. On the other hand, discrete event simulation (DES) technique can be successfully applied to systems having stochastic processes such mining activities, by utilizing data collected either manually or automatically.

Increase in the availability of computational power provides engineers the flexibility to implement several simulation languages that have been developed to date. Currently, SIMAN and GPSS/H are two of the most commonly used simulation languages in modelling of mining activities. These programming languages have been implemented into various software

packages such as Arena® Simulation Software and GPSS/H with Proof Animation. These software packages provide visual and easy-to-use interfaces to the end user. In the mining simulation literature, several researchers implemented discrete event simulation technique to different stages of production by using these software packages. Ozdemir & Kumral (2018) investigated the feasibility of the production target of an open pit mine by considering the stochastic structure of the mine by using of Arena® Software. Que et al. (2016) studied the efficiency consideration of a ground articulate pipeline system and shovel interaction by using of Arena® Software. Tarshizi (2014) conducted a research on simulating evacuation scenarios, places of rescue chambers and equipment used in rescue operations of an underground mine by using of GPSS/H. Tarshizi et al. (2015) analyzed the environmental impact of a coal mine having two pit operations considering haulage performance and production target of the mine by using of GPSS/H.

Main objective of this study is to implement discrete event simulation to an underground Longwall Top Coal Caving Mine (LTCC) in Turkey to investigate the shearer performance of the longwall operation by considering the amount of coal produced in a shift (8 hrs). In the study, duration of the shearer delays, time between arrivals of the shearer durations, cutting speed of the shearer, flit speed of the shearer, and reversal time of the shearer drum have been considered for the evaluation of the shearer performance.

2 METHODOLOGY

Methodology of this study covers modelling of the mine and analysis of the simulation model.

2.1 *Longwall top coal caving*

Coal seams are sedimentary deposits that commonly have large longitudinal extents and uniform thicknesses. The longwall mining method has been developed to take advantage of this sedimentary deposit property. In longwall mining method, rock properties of the hanging wall and footwall might be considered as non-critical concepts since the hanging wall is artificially supported. In fact, longwall mining method can be applied in cases where the hanging wall and footwall are weak or competent. Mechanization can be easily adapted in longwall mining method (Hustrulid & Bullock 2001) and depends on the uniformity of the deposits related to geological condition of the region. Thus, uniformity of the deposits is one of the main challenges in mechanized longwall mines. In mechanized longwall mines, shearers are used for cutting the coal especially for thick coal seam extraction. Major elements of longwall systems are presented in Figure 1.

The LTCC method is a type of thick coal seam extraction method that can be implemented in coal seams with thickness and cutting height of 20 m and 5 m, respectively. The recently improved two-stage LTCC methodology can be adapted to up to 41° dip angles. In the first stage, the lower portion of the coal seam excavation operations similar to classical longwall operations are performed. In the second stage, upper portion of the coal seam, top coal, is caved behind the shields. In LTCC mines, two conveyor systems are commonly constructed, front conveyors used for the transportation of face coal material from the longwall face and rear conveyors used for the transportation of top coal behind the shields. LTCC method is considered as a cost-efficient
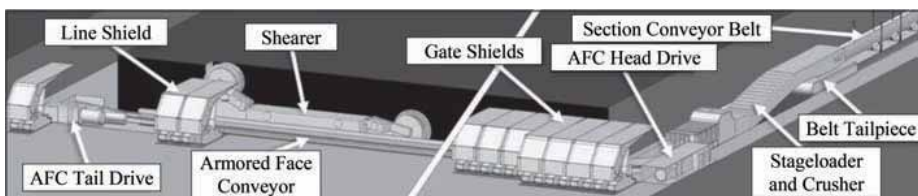

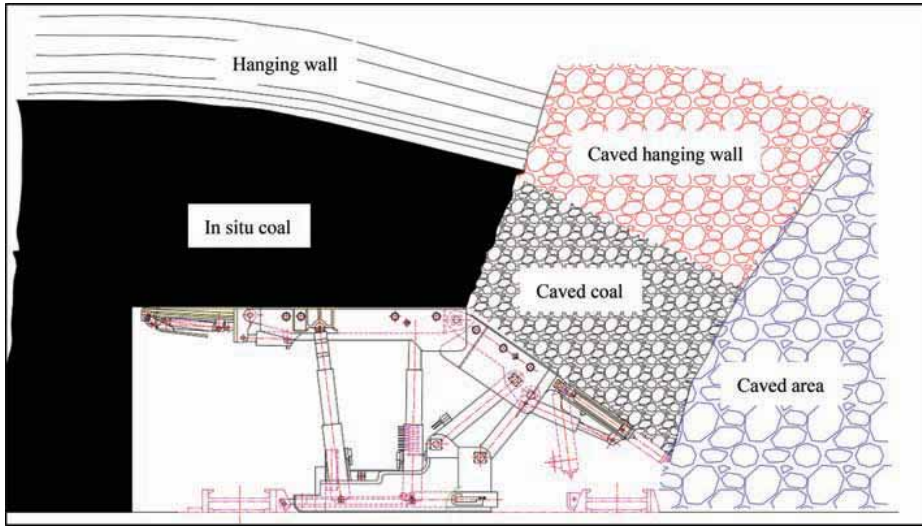Figure 1. Major elements of longwall systems (Darling 2011).

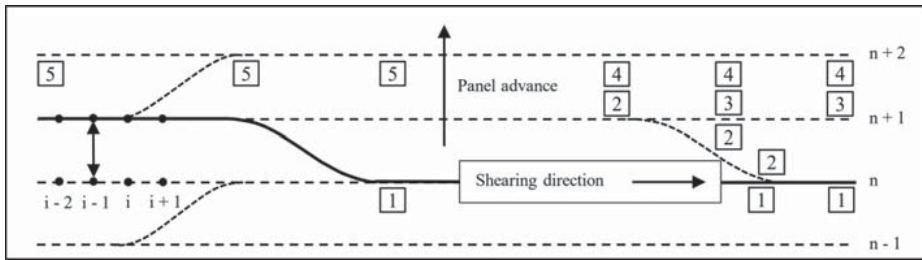Figure 2. Cross-sectional view of LTCC method (Xie & Zhao 2009).

Figure 3. Bi-directional cutting sequence (Reid et al. 2003).

mining system since the major part of the coal seam is excavated with the aid of gravity (Le et al. 2017). Cross-sectional view of the LTCC method is represented in Figure 2.

Cutting system of the shearer is bi-directional where the sequence is initiated by the shearer cutting the coal two times at the each gate for the completion of the shearer advance. Bi-directional cutting sequence is represented in Figure 3. The numbers indicate the operation sequence in the cutting process.

2.2 Discrete event simulation

Discrete event simulation is based on modelling of a system having stochastic, dynamic and discrete processes. Stochastic processes have uncertainties that can be defined by statistical distributions. The statistical structure of the system leads to a variety of outputs in every simulation run. In fact, statistical data analysis and the determination of replication number can be considered as an important part of the simulation study. Dynamic processes define the evolution of the model according to the time whereas in discrete processes, change in the system occurs in discrete points of time (Banks et al. 2010). Models in discrete event simulation predict the outputs of the stochastic processes (Y) according to the system parameters (p) and inputs (x) (Que et al. 2016).

$$[Y_1, Y_2, \ldots Y_i] = f\left(p_1, p_2, \ldots p_{j_k}, x_1, x_1, \ldots x_{j_m}\right) \tag{1}$$

483

In the scope of the study, production and transportation system of a longwall top coal caving operation was modelled by using of discrete event simulation technique.

3 CASE STUDY OVERVIEW

In this case study, data were collected from an operation located in Soma, Turkey. The available data infrastructure in the mine control room was accessed and a manual entry dump of the shearer and shield movement was created. The geology of the research area is introduced as it is one of the crucial parameters that affect the performance of the longwall equipment.

3.1 *Geology of the study area*

The LTCC mining operation is located in Soma Basin, Turkey. The stratigraphic sequences of the rock formation from bottom layer to top layer are Pre-Neogene rock formations, Neogene sediments, and Post Neogene sediments (Nebert 1978). Pre-Neogene rock formation is the oldest formation in the region and is composed of grey greywacke, meta-sandstone, arkose, schist and conglomerate (Nebert 1978). The Neogene rock formation is composed of two different units, Miocene aged series and Pliocene aged series. Miocene aged series are composed of intermediate level lignite formation, limestone-clay-gravel bands Gastropoda fossils formation, marl (leaf traces) formation, bottom level lignite formation and clay-sand-gravel formation. On the other hand, Pliocene aged series are composed of fine-grained silicified limestone-tuff formation, conglomerate-sandstone-clay formation, marl-tuff-clay-limestone-leaf fossils formation, top-level lignite formation, and clay-sandstone-banded sericite (mottled) formation (Nebert 1978). Pleistocene aged and Holocene aged rocks form the Post-Neogene unit that mostly involves reddish coloured, blocky-coarse conglomerates and pebbly sandstones (Nebert 1978). Stratigraphy of Soma Basin and rock units forming different ages in the region are presented in Figure 4.
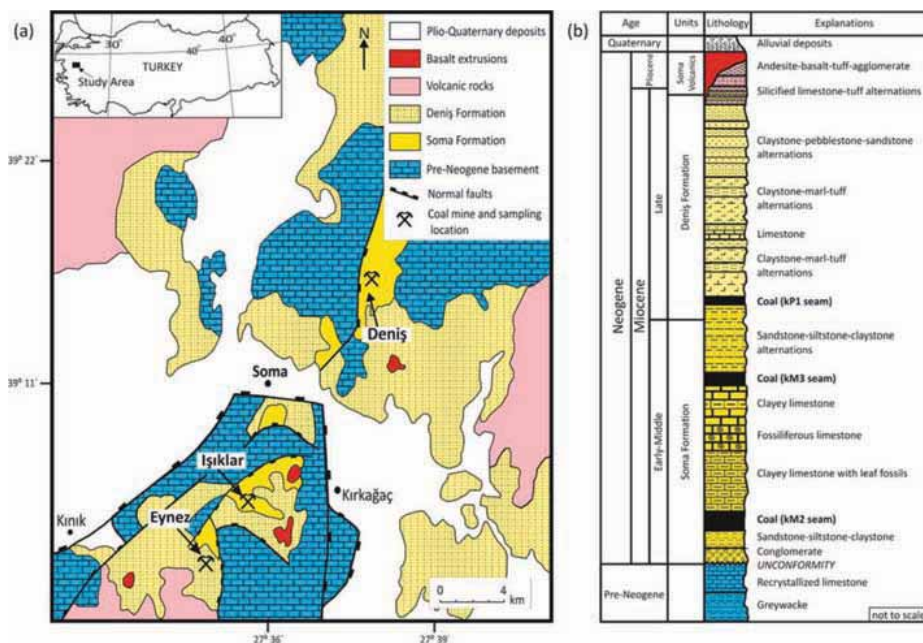

Figure 4. Stratigraphy of Soma Basin (Karayiğit et al. 2017).

Coal reserves in the region are estimated as 800 million tonnes and the general properties of the coal in the Soma Basin are summarized in Table 1.

Many faults intersect the coal formation in the region and these faults are mostly high angle oblique-slip normal faults. Strikes of these faults NW-SE, NE-SW, and E-W directions (İnci 2002).

3.2   *Modelling of the LTCC operation*

The excavation and transportation systems of an LTCC operation located in western Turkey were modelled in Arena® Software. Although operations were performed in two production panels, only one of them was modelled. Cutting parameters in the modelled panel are presented in Table 2 and the equipment used in the coal excavation operations are given in Table 3.

Transportation of the coal from the face is achieved by an AFC, RC, BSL and three different belt conveyors (BC-1, BC-2, and BC-3). Specifications of the conveyors are presented in Table 4.

Table 1.   Properties of coal reserves in Soma Basin (Nebert 1978).

Property	Value	Unit
Calorific value	4000–5000	kCal/kg
Moisture content	10–20	%
Ash content	40–50	%
Thickness of the coal seam	15–35	m
Inclination of the coal seam	08–25	º

Table 2.   Properties of the modelled panel in the mine.

Parameter	Length (m)
Face length	159.25
Depth of cut	0.80
Shearer cutting height	3.00

Table 3.   Equipment in the mine.

Equipment type	Equipment name	Total number
Shearer	CAT EL1000 (2 m drum-width)	1
Shield	95 Zhengzhou (1.75 m × 3.20 m)	91
Armoured face conveyor (AFC)	CAT AFC PF4	1
Rear conveyor (RC)	CAT AFC PF4	1
Beam stage loader (BSL)	BSLPF4 with SK111 Crusher	1

Table 4.   Conveyor specifications.

Parameter	AFC	RC	BSL	BC-1	BC-2	BC-3
Length (m)	159.25	159.25	41	600	1025	1800
Velocity (m/sec)	1.14	1.14	1.29	3.2	3.2	3.8
Capacity (tph)	1000	1000	1500	1600	1600	2500

In the simulation model, three main algorithms were constructed. The first algorithm provides the coal flow in the system. According to the first algorithm, face coal enters the system and is transported out of the mine by using of AFC, BSL, BC-1, BC-2, and BC-3, respectively. On the other hand, top coal enters the system and is transported out of the mine by using of RC, BSL, BC-1, BC-2, and BC-3, respectively. The second algorithm determines the shearer movement in bi-directional cutting sequence. According to the second algorithm, the production of face coal and top coal is determined. The third algorithm determines whether there is enough space on the AFC and RC for face coal entities and top coal entities for the transportation to BSL. With the aid of this algorithm, different delay times can be assigned to every entity entering the system. The simulation model allows transportation time of face coal entities and top coal entities on the AFC and RC to be estimated.

The operational data based framework for LTCC mining is represented in Figure 5.

The framework is based on the utilization of operational data that can either be classified as process type or relational type of data. Underground mining equipment is commonly generating process type of data that is characterized by high frequency and small size data packets that provide information about instantaneous sensor readings. SCADA systems and PLCs can be considered as additional data sources that could be integrated on a semantic layer, such as a data warehouse. Safety records that are recorded either manually or automatically generate relational type of data and should also be taken into consideration within a framework defined for LTCC operations. The integrated data should be used to develop visualizations and reports utilized by mine management for decision making, daily mine management, and performance measurement. The integrated data could also be used to prepare the input parameters of a discrete event simulation model. This model would be analyzed on a regular basis and the simulation results would be integrated back to the data warehouse. This way, simulation output and the integrated layer of operational data will be used to develop various tools that will aid engineers and managers on site. For this case study, the available
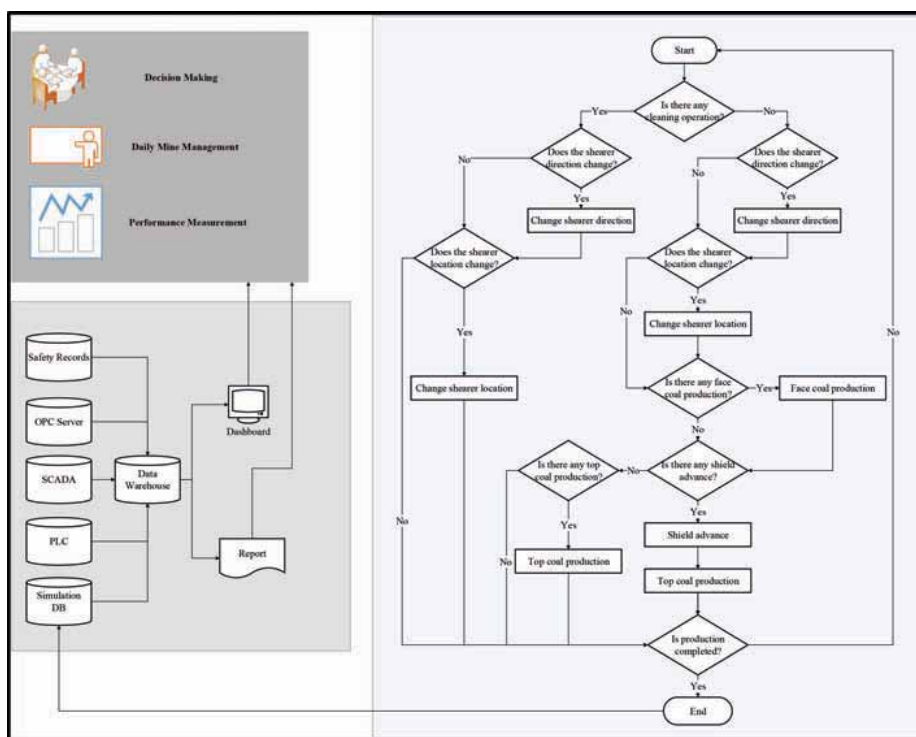

Figure 5.   Operational data based framework for LTCC operations.

Table 5. Statistical distributions in the study.

Parameter name	Unit	Distributional expression
Duration of the shearer delays	min	WEIB (8.61, 0.48)
Time between arrivals of the shearer delays	min	LOGN (3.67, 5.40)
Flit speed of the shearer	m/min	1.00 + 25 * BETA (2.27, 10.80)
Cutting speed of the shearer	m/min	1.00 + 13 * BETA (1.81, 8.08)
Reversal time of the shearer drum	min	LOGN (0.30, 0.20)

data were provided by OPC servers but could not be accessed or integrated with other data sources. Operational data were collected manually.

In the mine, cleaning operations are performed in the conditions where basement of the coal face is not cut properly or rocks from the hanging wall fall off the longwall face. In the model, it is assumed that there is no coal production during the cleaning operations. In addition, top coal production in the model is performed after shields are moved forward. In the model, time between arrivals and duration of the shearer delays are randomly assigned based on the collected data and the statistical distributions that were fit by using Arena® Input Analyzer. In the model, all the shearer stoppages have been defined as delays irrespective of their causes. Similar to the determination of time between arrivals and duration of the shearer delays, cleaning operation, shearer movement, shield advance, conveyor operations, and top coal production processes were also individually modelled to build up the simulation model that represents the coal production for the LTCC operation. The statistical distributions used in the model are presented in Table 5.

The duration of the shearer delays was analyzed and represented by a Weibull distribution with a scale parameter of 8.61 and shape parameter of 0.48, which could be considered as a failure rate that decreases over time. A lognormal distribution with a mean of 3.67 and standard deviation of 5.40 was fit to the data related to the time between arrivals of the shearer delays similar to the distribution fit to the reversal time of the shearer drum with a mean of 0.30 and standard deviation of 0.20. The flit speed with shape parameters of 2.27 and 10.80 and the cutting speed of the shearer with shape parameters of 1.81 and 8.08 were considered as Beta distributions where the peak in the probability density functions are expressed.

4 RESULTS AND DISCUSSION

The selection of mining method for an underground coal deposit is mainly related to the geology by means of the existence of multiple seams, the coal thickness, and especially the cavability of the hanging wall. A simulation model representing the operational delays of a top coal caving operation was developed as the cutting operation is of major importance for this method affected by the face advance rate, shield alignment, and other parameters. The geology of the study area led the simulation study to handle the problem in two separate domains, face coal production and top coal caving both modeled in Arena®. In the scope of this study, data were collected from the mine, and modeled in Arena® Input Analyzer. After statistical analysis, 20 different scenarios were assessed in the model. The confidence level in the study is chosen as 95% and the replication number in the simulation models is selected as 150 as it was observed that beyond this limit, no significant changes occurred.

4.1 Verification and validation of the simulation model

The simulation model was verified by checking the accuracy of the model outputs under certain condition of the inputs. On the other hand, validation of the model was performed by a comparison of the model outputs with the real operational data. The model outputs and actual production of the mine in a shift are presented in Table 6.

As it can be seen in Table 6, the outputs of the simulation model are compatible with the results of the real operational data. After validation processes were completed, alternatives were tested in the same simulation model.

4.2 *Evaluations and results of the simulation model*

Model outputs show that the face coal production was 228.15 tonnes per shift, top coal production was 2984.43 tonnes per shift, and as a result, total production in the mine was 3212.58 tonnes per shift. In the context of this study, sensitivity analysis on face coal production was performed to investigate shearer performance. Distributional parameters of the alternatives were re-determined for every simulation run. The results of the sensitivity analysis are presented in Figure 6.

The operational delays defined in this study were considered regardless of their causes due to the available data that were accessible on site and the lack of level of granularity of data to categorize delays based on their sources. As it can be inferred from Figure 6, time between arrivals of the shearer delays, flit speed of the shearer, and cutting speed of the shearer were directly proportional to shearer production rate in a shift. When the time between arrivals of the shearer delays, flit speed of the shearer and cutting speed of the shearer were seperately reduced by 20%, shearer production rate in a shift decreased by 27.70%, 22.00%, and 14.24%, respectively. When their values were separately increased by 20%, shearer production rate in a shift increased by 13.96%, 13.99% and 1.45%, respectively. Duration of the shearer

Table 6. Comparison of model outputs and operational data in a shift.

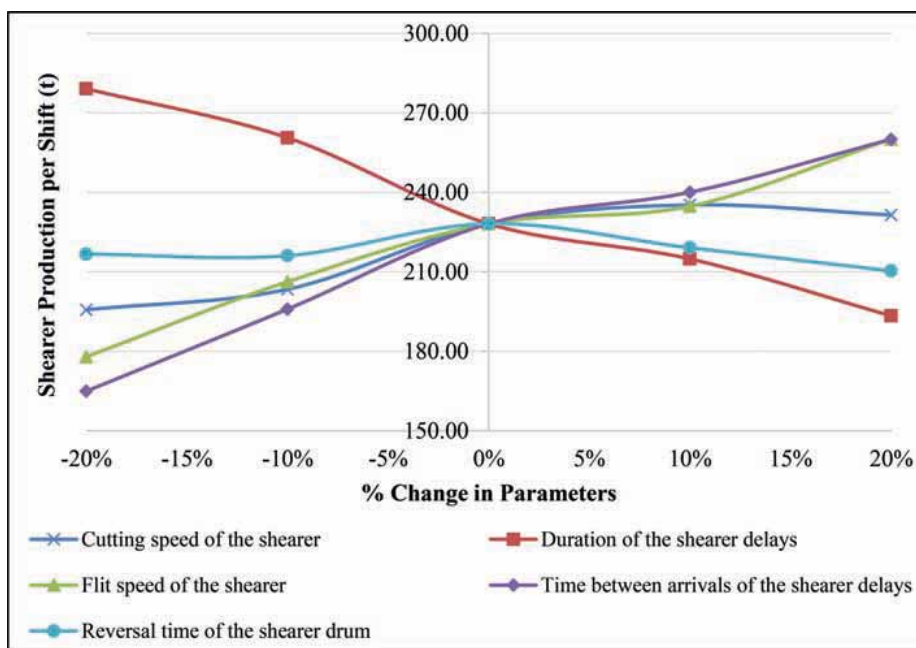| Outputs in average	Face coal	Top coal	Total
Model Output (t)	228.15 ± 21.13	2984.43 ± 262.53	3212.58 ± 283.66
Actual Production (t)	197.25 ± 65.51	2491.35 ± 827.41	2682.60 ± 892.92

Figure 6. Sensitivity analysis on shearer production per shift.

delays were inversely proportional to shearer production rate since the shearer production rate decreased when non-operational time of the shearer was increased, as expected. When the shearer delays was decreased to 80% of its actual values, shearer production rate in a shift was increased by 22.34%. On the contrary, and increase of 20% of its actual values led to a 15.23% decrease of shearer production rate in a shift. On the other hand, reversal time of the shearer drum had almost no effect on shearer production rate. Two main reasons that led to this situation are that the shearer having very short drum reversal times and there were few drum reversal operations in a shift.

5   CONCLUSION

The mining industry relies on complex systems with numerous variables that affect the production in the system. Within the scope of the study, a model that represented a fully-mechanized LTCC system was developed and the shearer performance was investigated in one production panel of a real operation located in Soma, Turkey. According to the sensitivity analysis performed on the shear production rates, time between arrivals of the shearer delays were the most effective variable for the developed simulation models. This conclusion is based on the change of shearer production with respect to the variation in the operational duration of the shearer. In other words, shearer operation was interrupted continuously in the mine affecting the production rate. Conveyor systems used for the transportation of coal in the mine are subject to "operational delays" that can be related to breakdowns that occur in any section of the system and cause an interruption of the whole operation. The main aim of engineers on site is to increase the system efficiency and in order to achieve better system efficiency, operational delays have to be decreased. Operational delays can be minimized by utilizing operational data and making it part of the decision making process in daily mine management. The data collected for this study were limited and could be increased by creating an easy-to-access environment for engineers. This way, operational data of the LTCC operation would be utilize to track the performance of the equipment in real time. Additionally, training of the operators (decrease in cleaning operation in the mine) and following a pre-determined maintenance strategy for the machines in the operations (decrease in breakdowns of the machines) are crucial for an efficient LTCC operation.

Future studies are planned to compare bi-directional cutting system with the uni-directional cutting system on the efficiency consideration of the mine and integrating the available data on-site for further analysis of the operation.

REFERENCES

Azimi, Y. & Osanloo, M. 2011. Determination of open pit mining cut-off grade strategy using combination of nonlinear programming and genetic algorithm. *Archives of Mining Sciences* 56(2): 189–212.
Banks, J., Carson, J., Nelson, B.L. & Nicol, D. 2010. *Discrete-Event System Simulation*. NJ: Prentice Hall.
Darling, P. (ed) 2011. *SME Mining Engineering Handbook*. SME.
Hustrulid, W.A. & Bullock, R.C. (eds) 2001. *Underground Mining Methods: Engineering Fundamentals and International Case Studies*. SME.
İnci, U. 2002. Depositional evolution of Miocene coal successions in the Soma coalfield, western Turkey. *International Journal of Coal Geology* 51(1): 1–29.
Karayiğit, A.İ., Littke, R., Querol, X., Jones, T., Oskay, R.G. & Christanis, K. 2017. The Miocene coal seams in the Soma Basin (W. Turkey): Insights from coal petrography, mineralogy and geochemistry. *International Journal of Coal Geology* 173: 110–128.
Lamghari, A., Dimitrakopoulos, R. & Ferland, J.A. 2015. A hybrid method based on linear programming and variable neighborhood descent for scheduling production in open-pit mines. *Journal of Global Optimization* 63(3): 555–582.
Le, T.D., Mitra, R., Oh, J., & Hebblewhite, B. 2017. A review of cavability evaluation in longwall top coal caving. *International Journal of Mining Science and Technology* 27(6): 907–915.

Nebert, K. 1978. Linyit içeren Soma Neojen bölgesi, Bati Anadolu. *Mineral Research and Exploration Institute of Turkey (MTA) Bulletin* 90: 20–69.

Ozdemir, B. & Kumral, M. 2018. Appraising production targets through agent-based Petri net simulation of material handling systems in open pit mines. *Simulation Modelling Practice and Theory* 87: 138–154.

Que, S., Awuah-Offei, K. & Frimpong, S. 2016. Optimising design parameters of continuous mining transport systems using discrete event simulation. *International Journal of Mining, Reclamation and Environment*, 30(3): 217–230.

Reid, D.C., Hainsworth, D.W., Ralston, J.C., McPhee, R.J. & Hargrave, C.O. 2003. Inertial navigation: enabling technology for longwall mining automation. *Proceedings of the 4th International Conference of Computer Applications in the Mineral Industries, Calgary, Alberta, Canada, 8–10 September 2003.*

Tarshizi, E.K. 2014. *Multiple Discrete-Event Simulation and Animation Models to Assist Modern Mining Operations.* Doctoral Thesis in Geoengineering. University of Nevada, Reno, USA.

Tarshizi, E.K., Sturgul, J.R., Ibarra, V. & Taylor, D. 2015. Simulation and animation model to boost mining efficiency and enviro-friendly in multi-pit operations. *International Journal of Mining Science and Technology* 25: 671–674.

World Energy Council 2016. World Energy Council|Resources. Retrieved January 23, 2019, from https://www.worldenergy.org/wp-content/uploads/2016/10/World-Energy-Resources-Full-report-2016.10.03.pdf.

Xie, Y.S. & Zhao, Y.S. 2009. Numerical simulation of the top coal caving process using the discrete element method. *International Journal of Rock Mechanics and Mining Sciences* 46(6): 983–991.

Zhang, L. & Xia, X. 2015. An integer programming approach for truck-shovel dispatching problem in open-pit mines. *Energy Procedia* 75: 1779–1784.

The digital mine eco-system

Willem A.S. Fourie
Information, Communication and Technology, Komatsu Mining Corporation, Warrendale, Pennsylvania, USA

ABSTRACT: Komatsu's business focus is to provide surface and underground mining operations with superior equipment, solutions and direct service. The goal is to deliver the lowest cost per unit of production over the life cycle of the equipment while prioritizing safety. To achieve these results, Komatsu utilizes data, prognostics and analytics in applications throughout Smart Solutions centers around the globe to improve production, refine operations, detect pre-mature failures and implement preventative strategies. The smart connected products of a Joy longwall system include a shearing machine, Armored Face Conveyor (AFC), roof supports, stage loader, crusher, and mobile belt tailpiece. While monitoring longwall operations, the ongoing aim is to detect patterns and systematic relationships amongst the operator inputs, control system parameters, sensor data and alarm/event information. Statistical techniques, such as regression analysis, and single and multi-variables analysis are utilized to optimize cutting speed, detect roof cavities and improve roof support cycle times. Predictive diagnostics and analytic rules are implemented to analyze real-time data and provide notifications and alerts of changing longwall characteristics.

Keywords: JOY, RS20s, FaceBoss, Longwall systems, Shearers, Analytics

1 INTRODUCTION

Over the past several years, we have seen mining companies use machine learning and deep learning to support longwall mining. The internet, big data and improvements in processing power have allowed the mining industry to measure, monitor and analyze more information than ever before. To help customers make the most of this new technology, Komatsu has pioneered processes to capture machine data and transform it into knowledge that allows customers to make the best decisions possible.

This paper will discuss how digital technologies allow mines to transition from a reactive, unit-based monitoring approach, to a proactive method that utilizes modern technologies. System and performance monitoring enable users to link various data sources including operator performance, maintenance, logistics and safety systems.

2 SMART CONNECTED PRODUCTS

2.1 Longwall mining

A longwall system consists of a shearer, powered roof support system, armored face conveyor, belt conveyor, power supply and pump stations all of which are linked together. As the longwall system moves forward in the mine, it extracts an average of 2,200 tons of material per hour, filling a 100-ton railcar in less than three minutes. A Joy automated longwall system monitors and controls important aspects of the system such as roof support leg pressures, electric motor currents, voltage speeds, temperature, vibration, and many other things. It also transmits data between individual pieces of equipment, as well as up to the surface.

Komatsu has ushered in the age of smart, connected longwall products, complementing them with advanced analytics to create a digital equivalent of their physical counterparts. The goal of this is to detect patterns and systematic relationships among the operator inputs, control system parameters, sensor data and alarm/event information. Statistical techniques, such as regression analysis, are utilized to optimize cutting profiles, detect roof cavities and improve roof support cycle times. Predictive diagnostics and rule use cases are implemented to analyze real-time data and provide notifications and alerts of changing longwall characteristics.

The ability to store the longwall system data and correlate it with event trigger points, enables data analysts to provide effective and efficient feedback to mining operations. State of the art systems are fundamental for analyzing data from 7,000 plus sensors to determine critical conditions likely to trigger an event. All of Komatsu's smart connected products' information is centrally stored in a cloud storage environment. This enables Komatsu to schedule and manage data mining around the clock, allowing analysts to collaborate in a virtual environment to provide customers with solutions as soon as they need them.

Komatsu's data analytics capabilities drive value into the mining process by turning volumes of sensor data into actionable information used to make real-time decisions to optimize efficiency, reduce downtime and provide the customer with improved profit margins.

3 MAKING STRATEGIC DATA-DRIVEN DECISIONS

The automated longwall with select user inputs has the ability to operate autonomously with the shearer cutting coal pass by pass, achieving in excess of 1 million tons per month. Komatsu's approach to data-driven decisions is unique and provides a significant value add. Some common questions about this method are:

Which set of smart, connected product capabilities and features should be pursued?
- Komatsu is pursuing extensive product capabilities at multiple levels. Customers can monitor, control, and optimize performance and operation of their equipment. Komatsu is also in the process of developing a fully autonomous system.

How much functionality should be embedded in the product and how much in the cloud?
- Komatsu chose to build functionality into both the product and the cloud. Certain safety features are embedded in the machine (for example, emergency shut downs), but others are managed in the cloud (cavity detection), enabling the equipment to be operated more safely in challenging underground conditions.

Is this an open or closed system?
- Komatsu employs proprietary, closed systems, reflecting the need for deep design integration involving all the machines in the product system.

Should we develop a full set of smart, connected product capabilities and infrastructure internally or outsource to vendors and partners?
- Komatsu has chosen to outsource parts of the technology stack while building others in-house in cases where mining-specific circumstances are critical.

What data must be collected to capture, secure, and maximize the value of its offering?
- Komatsu is capturing data from all our products pertaining to their condition, performance, and service needs. This is necessary to optimize performance, support predictive maintenance, and enable autonomous operation.

How do we manage ownership and access rights to product data?
- Komatsu gathers and securely manages the data it is collecting from machines in the cloud. Its ability to ingest this data is part of the value proposition and is well accepted by customers. The product data is not shared with outside parties. Komatsu has nondisclosure agreements with its customers that allow them to access the machine data. Komatsu

has always sold and provided direct service of its machines in-house and is now able to optimize that service at a new level. The direct service model enables the Company to be connected directly to the mine and directly to its centers of technology around the world without going through an intermediary or third-party dealer.

Additionally, Komatsu has been providing the mining industry with innovative technologies to enhance safety for the better part of a century. For underground mining operations, the personal proximity detection system for Joy longwall systems provides operators with the individualized safety features and protection they deserve. The system is connected to a personal identification tag, worn by all personnel on the longwall face, which tracks an employee by name and/or job function. It then transmits radio signals and uses relative RF signal strength, as well as an accelerometer, to accurately track the operator's position and communicate the information over Joy's FaceBoss control system for powered roof supports (PRS). The radio signals transmitted by the individually identified tag are actioned by the PRS mimic to protect workers against automated advancing shields.

4 PROGNOSTICS AND DATA ANALYTICS

4.1 *Smart technologies employed to improve safety*

Komatsu has been working to develop systems that will enable mine personnel to be located away from the mining face. One such option is a Remote Management Center (RMC), an information and control station located a distance away from the longwall system, positioning the operator in a more secure environment while still giving the operator access to critical information, camera images and control over the key components of the operation.

Inbuilt automation of individual components of the longwall system is well-developed and proven by technologies such as roof support automation and advanced shearer automation (ASA), which help facilitate and allow for smooth remote operation. Still, the level of achievable remote operation is largely dependent on the site, as adverse geology and unpredictable seams cannot always be detected during the mining process, meaning the number of manual interventions will rise and fall from longwall to longwall. Should an operator encounter an extreme situation, the RMC allows the operator to make manual interventions remotely using the information and images provided.

4.2 *Monitoring roof support operation and performance*

With prognostics and data analytics, Komatsu is able to identify and report on roof supports that are failing to achieve required set level of pressure after advancing. This pressure failure could lead to a lack of support to the roof, resulting in failure of strata above and forward of the
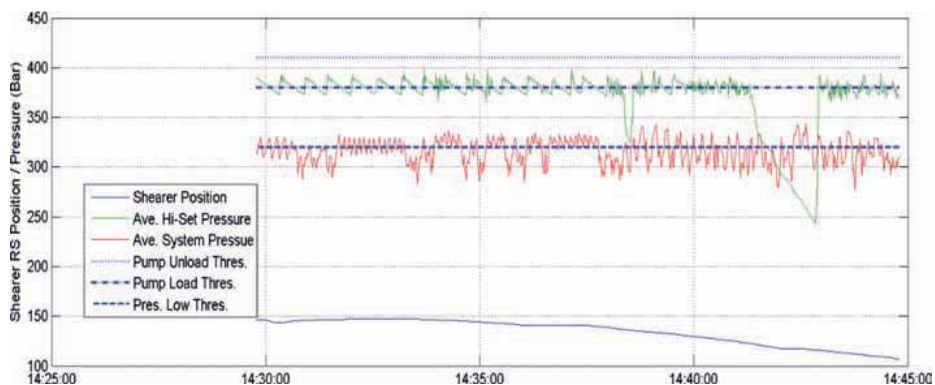

Figure 1.   Insufficient high set pressure leads to roof cavity forming.

longwall as well as the formation of cavities. A large cavity has the potential to halt production for periods in excess of 36 hours and can create harmful situations for operators. In addition, poor performing roof supports will slow the overall mining operation by reducing the production rate.

By using analytical techniques, the Smart Solutions team can provide the mining crew the proper guidance to manage, and more importantly, resolve, dangerous situations such as the presence of failing roof cavities. Long-term data can help operations realize inherent production improvements, ultimately resulting in a safer work environment—a key outcome for every mining operator. Through cloud systems and edge-analytics, Komatsu is able to improve the response time for notifications and alerts that are sent to mine personnel via machine control or portable electronic devices.

4.3 Shear cycle optimization

Longwall systems can consist of approximately 210 roof supports with a face length in excess of 430 m. Coal seam thickness can vary from 1.7 m to 7 m. The optimization of the roof supports' lower, advance, set and shearer cycle speed provides data that allows process optimization through the Faceboss RS20s and ASA automation systems.

Figure 2 highlights data points from multiple shears. Data analytics shows that roof support set times are slower than the previous cycle by 15.5% when cavities are present on the face.

Below, Figure 3 shows the results of a comparison between two consecutive longwall blocks based on different levels of automation. By managing the extraction height and minimizing deviations, you can see that ASA provides advantages to mine operators from one longwall block to the next. Aggregating data in the cloud is critical to allow Komatsu's team of prognostics engineers to implement complex data mining rules and utilize real-time data streaming.

When automation engineers at the mine need to investigate parameter changes on machines, they rely heavily on Komatsu's data scientists and their analysis based on information gathered over many cycles.

Figure 4 below highlights results of investigations that have been concluded when shearer speed is analyzed to determine the most optimum speed settings for mine cutting conditions. Factors that influences the cutting conditions are strata pressure, coal hardness, drum design to name only some of the factors. In this analysis the results demonstrate that operating at a lower speed setting there is more variation that occurs across the face and with higher settings the shearer will operate more consistently across the face.

It is important to note that analysis of automation parameters is continuously needed to ensure that the best performance is achieved within the specific mine operating parameters.
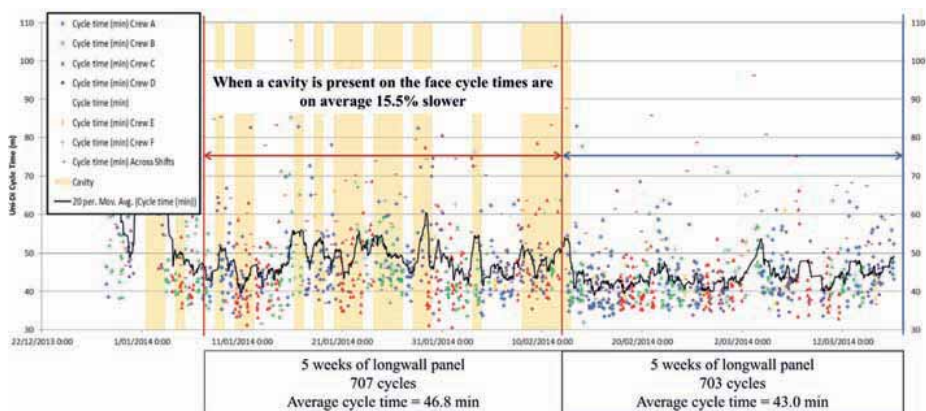

Figure 2.   Cycle time performance optimization.

Additional longwall recovery realized by reducing variation when
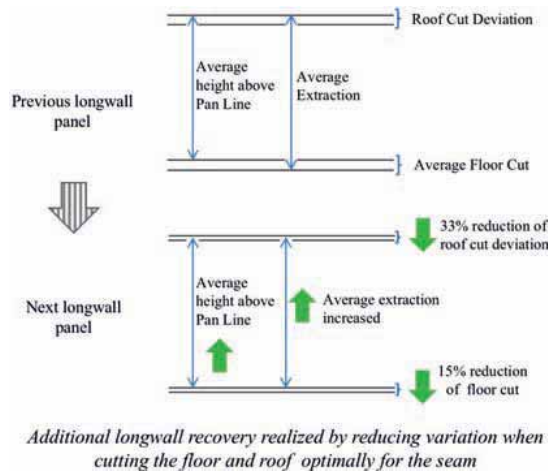cutting the floor and roof optimally for the seam

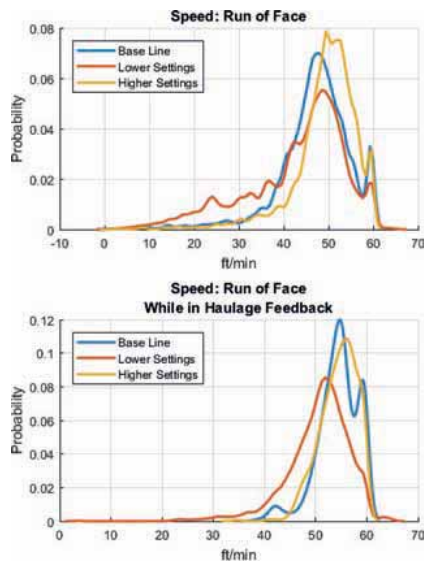Figure 3.   Extraction optimization.

Figure 4.   Shearer shearing speed analysis.

By using data mining and communicating with customers, Komatsu is able to assist mines
in minimizing overtime costs while helping them operate machines at optimum performance
setpoints to prevent unscheduled maintenance.

5   CONCLUSION

Through data analytics and prognostics, Komatsu has evolved its focus from optimizing
the performance of individual pieces of mining equipment to optimizing the systems across the
fleet of equipment deployed in the mine. When the Joy Faceboss products are connected to the
cloud analytics framework, Komatsu is able to drive the continuous improvements that result in
lower operating costs, increased productivity and improved safety throughout the mine.

Based on market feedback the following are key enablers to help our customers reduce total cost of ownership (TCO):

1. Automation – **reduce** the number of **people** in high risk areas and improve consistency
2. Data analytics – provide customers access to **product performance**
3. Optimized mining methods – **increase** extraction **ratio** and **reduce waste**
4. Smart connected products – complete insight into the value chain, even third-party machinery, to get insight on key **performance indicators** for all aspects of the business

REFERENCES

Porter, M.E., Heppelmann, J.E., How smart connected products are transforming competition, Harvard Business Review, November 2014.
Hill, T. & Lewicki, P. (2007). STATISTICS: Methods and Applications. StatSoft, Tulsa, OK.
*Komatsu, Joy, and Faceboss are trademarks of Komatsu Mining Corp. or one of its affiliates.

Application of DEM-FEM methods in tests of loads on idlers

B. Doroszuk, R. Król & L. Gładysiewicz
Faculty of Geoengineering, Mining and Geology, Wrocław University of Science and Technology, Wrocław, Poland

ABSTRACT: The effectiveness of optimization and modernization activities of a belt conveyor depends largely on the accuracy of the description of the conveyed material stream. The loads from the belt alone can only be determined with the use of laboratory experiments. Such experiments, however, are scarce and could be supported with the help of DEM-FEM techniques. The paper presents the application of discrete element method for modeling the conveyed bulk material and determining the forces exerted on a belt from transported material. Coupling discrete and finite element methods allows to extract the forces acting on the belt in DEM simulation and import them to FEM analysis. The finite element method with the use of a hyperelastic model for the belt, loaded with imported forces is applied to determine the contact zone between the belt and idlers and the forces transmitted from the belt to the idlers.

1 INTRODUCTION

Effective optimization and modernization of belt conveyors largely depends on accurate description of the stream of transported material. Information on forces acting on idlers is used to analyze the durability of bearings and idlers (Król 2017), to determine optimal solutions allowing the support of the upper run with idler sets (Gładysiewicz et al. 2016), and also to calculate resistances to motion (Kawalec & Kulinowski 2007). The resultant data showing actual loads acting on the conveyor belt may be used to determine stress concentration in the conveyor belt core (Bajda et al. 2016) or to define safety factors in modern diagnostic systems (Błażej et al. 2018). Idlers are subjected to a wide range of loads varying from limited forces exerted when the conveyor does not transport any material to significant forces exerted when the conveyor is fully loaded with material. Loads due to belt alone are determined solely with the use of empirical methods based on the results of laboratory tests (Grabner et al. 1999). Only a limited number of measurements have been performed to supplement theoretical knowledge on idler loads (Gładysiewicz et al. 2019, Geesmann 2001).

Loads acting on idlers may be also determined in models constructed with the use of Discrete Element Method (DEM) techniques and based on the analysis of interactions between the bulk material and the conveyor belt, as observed during the transportation process. For example, in order to improve methods used in calculating loads on conveyor idler rolls and increase accuracy in predicting the energy loss due to the bulk solid flexure, (Ilic & Wheeler 2016) proposed a number of laboratory experiments and simulations on a moving belt conveyor, where the pressure acting on the surface of the belt due to the interaction with the bulk solid was measured for the first time using pressure sensors. Direct analysis of the load, the deformation and the stresses inside the element interacting with the bulk solid is also possible by employing coupled FEM-DEM simulations. The use of coupled FEM-DEM simulations for pure numerical analysis of the interaction between bulk material, belt and idler was described in (Dratt et al. 2015). In this approach, a simplified FEM model for a fabric belt is combined with a calibrated DEM model for cohesionless grit. This simulation approach also allowed determining loads acting on idler sets (Dratt et al. 2015).

This article presents a methodology for simulation research, in which DEM is used to model bulk solid and calculate forces acting on the conveyor belt due to the mass of the

transported material. This information was subsequently used in further FEM analyses. Using a hyperelastic model for a belt loaded with known forces in FEM allowed simulating the contact zone between the belt and the idler, as well as the interaction forces between these elements in various loading scenarios. The validity of the parameters assumed in the model was verified by comparing the obtained results of radial loads acting on idlers with the analytical results based on the theory of bulk solids.

2 PREPARING OF NUMERICAL EXPERIMENTS

The model used in the numerical calculations was a three-roller carrying idler set comprising $\phi 133 \times 465$ mm rollers formed into a trough with an angle of 30°. Figure 1 shows the constructed model of the idler set fixed in support. The analysis covered a support system for the upper run of the conveyor belt having width B = 1200 mm and a spacing of 0.83 m.

The numerical experiments were performed for an assumed GT EP 1600/4 B-1200 conveyor belt which has a transverse flexibility of 400 mm (Hardygóra & Woźniak, unpubl.). This parameter was established in laboratory tests, according to the current standard (PKN 2008), for a sample having an average thickness of 15.1 mm. The manufacturer's specification of the analyzed conveyor belt (FTT WOLBROM 2015) was used to calculate its volume density with allowance for the thickness of the core and of the covers. The density assumed for the model test was $\rho = 1400$ kg/m³. The belt was modeled as a uniform body having constant mean density.

Identification of stress state in elastic materials (e.g. steel) with the use of Finite Element Method requires only Young modulus E and Poisson's ratio v (Jaszak 2016). In the case of a conveyor belt, the task is more complicated, as rubber displays a nonlinear stress-strain relationship in the range of strain exceeding 5% (Fig. 2) (Jaszak 2016). This relationship is detailed in an equation in (Jaszak 2016):

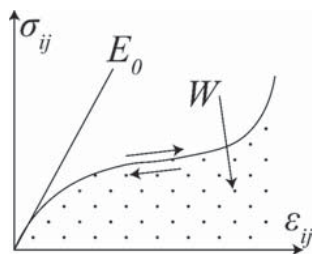Figure 1.   CAD model of the idler set with the support.

Figure 2.   Stress-strain characteristic curves for typical hyperelastic materials and the area below the curve representing the amount of energy stored in a hyperelastic material. Based on (Jaszak 2016).

$$\sigma_{ij} = \frac{\partial W}{\partial \varepsilon_{ij}} \qquad (1)$$

where σ = stress; ε = strain; and W = strain energy density in a volume unit of material.

The behavior of a hyperelastic material is closely related to strain energy function (SEF), which may be typically described with three strain invariants I_1, I_2, and I_3. Strain energy density of rubber may be described with many polynomials (Ali et al. 2010). The most popular models used in simulating hyperelastic materials include: Mooney-Rivlin model, Neo-Hookean model, Full Polynomial model, Yeoh model, Ogden model and Arruda-Boyce model (Jaszak 2016, Shahzad et al. 2015).

In order to simulate the actual behavior of a conveyor belt, attempts were made at implementing all of the above models in the FEM environment and eventually the Ogden model was chosen as the tool most accurately representing the sag of the belt during its transverse flexibility tests (Shahzad et al. 2015). The Ogden model is characteristic in that it is a phenomenological model based on principal stretches instead of invariants (Shahzad et al. 2015). The model, described in Equation 2, correctly captures the upturn (stiffening) of a stress-strain curve and as a result allows a precise representation of large rubber deformations (Shahzad et al. 2015):

$$W = \sum_{i=1}^{N} \frac{2\mu_i}{\alpha_i^2} \left(\bar{\lambda}_1^{\alpha_i} + \bar{\lambda}_2^{\alpha_i} + \bar{\lambda}_3^{\alpha_i} - 3 \right) + \sum_{i=1}^{N} \cdot \frac{1}{D_i} \left(J_{el} - 1 \right)^{2i} \qquad (2)$$

where D_i = material constant related to the bulk modulus; J_{el} = determinant of the strain gradient tensor; N = number of terms in strain energy function; λ_i = the deviatoric principal stretch; and μ_i, α_i = material constants.

The model of the conveyor belt was based on a set of coefficients for rubber, as presented in Table 1. In order to verify the hyperelastic model of assumed density, a simple numerical simulation was proposed. The belt sample was modeled with two rigidly fixed fasteners. The fasteners could rotate around their axes and one of them could additionally slide in a horizontal plane (Fig. 3). The belt model was discretized with the use of four-node quadrilaterals 20 mm in size. The fastener was modeled with default, software-implemented parameters for steel: ρ = 7850 kg/m³, v = 0.3 and E = 2E+11 Pa. The curved mesh of the fasteners was composed of three-node elements having one side at least 2.45 mm in length. In a model according to such a design, standard tests of transverse flexibility could be fully simulated.

The sag of the sample determined in the numerical simulation was by approx. 1.5% different from the sag observed in laboratory tests. This result was accepted as satisfactory and the model was used in further analyses.

In the next step, simulations focused on a fragment of belt resting on three idler sets (Fig. 4a). The model of the belt was discretized with four-node quadrilaterals having elements 100 mm in size, and the models of the idlers were also meshed with four-node quadrilaterals, but the elements were not larger than 50 mm. In the case of the middle idler set, the sides were set as not longer than 30 mm. The idlers were defined as fixed steel cylinders. The belt comprised two symmetrical fragments rigidly connected in the middle plane. The connection plane of the two belt elements was defined as rigid and subjected only to downward

Table 1. Coefficients of Ogden material model, N = 3. Based on (Shahzad et al. 2015).

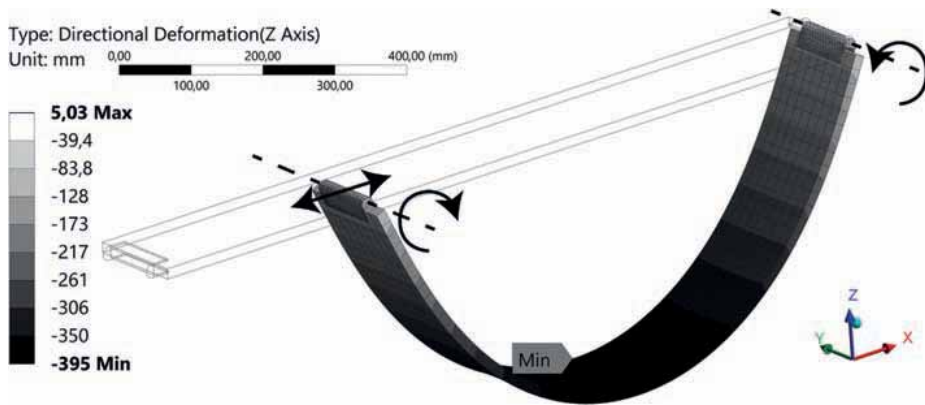| i	μ_i	α_i	D_i
	MPa	–	1/MPa
1	0.445	−0.224	1.82E-3
2	3.290	4.375	4.60E-5
3	2.892	−2.783	−7.34E-7

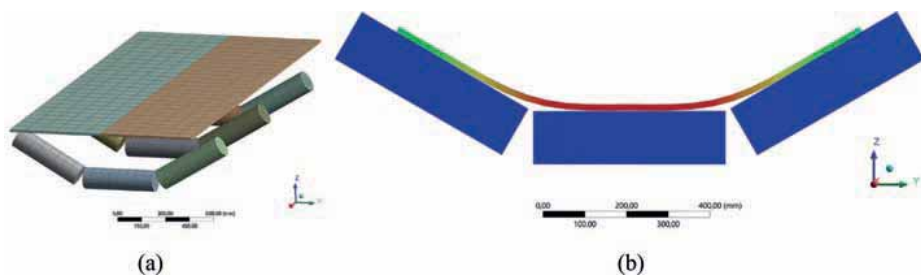Figure 3. Results of FEM-based belt analysis with the Ogden model.

Figure 4. Conveyor belt: (a) prior to resting on the idler sets; (b) cross-section through the middle set after positioning the belt.

movement until the belt contacted the idler. Thus positioned on the idler sets, the belt was used to determine its cross-section in the middle idler set. This cross-section in turn served to generate a CAD solid body of a belt resting on idlers with zero loading (Fig. 4b).

3 MODEL TESTS

For the sake of the model development, the conveyor belt's trough was filled with DEM-simulated ore extracted from an underground mine. Parameters describing ore particles and their contact with the rubber of the conveyor belt came from own original research. The measurable parameters describing the ore and its contact with steel and rubber were examined. The examined parameters were averaged and then calibrated using a flow property test (Doroszuk et al., in press). The ore particles on the belt were modeled to be approximately 5 cm in size (Fig. 5).

A model of a belt section 2.5 m in length was positioned symmetrically on 3 idler sets. The mesh of the outer idler sets was not altered. The middle idler set and the belt were discretized with three-node elements 20 mm and 100 mm in size, respectively. The belt model was discretized with an algorithm for mesh refinement in the contact zone with the middle idler set. The support of the middle idler set is shown in Figure 6. The belt ends on both sides were defined as fixed supports in order to meet the condition of maximum allowable belt sag.

The resulting model with mesh refined in the contact zone with the idler set was imported into the EDEM computer application in order to perform DEM-based simulations. The model which served as a probing area was extended with a longer belt fragment (Fig. 7), in which ore particles were automatically generated and accelerated to belt speed $v = 2$ m/s.
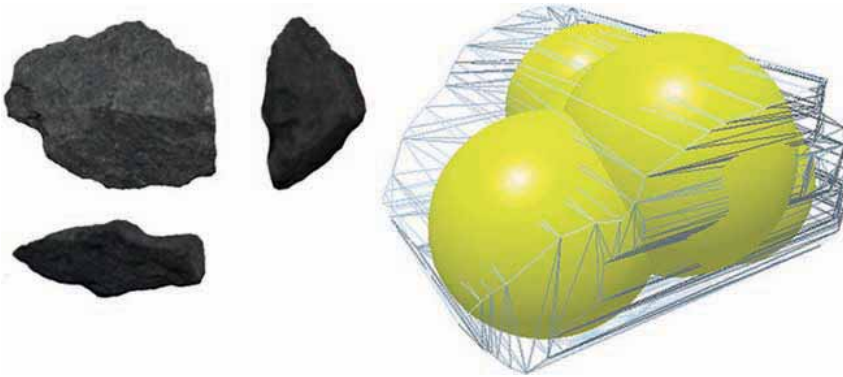
Figure 5. Representation of ore particles with spheres and a 3D model.
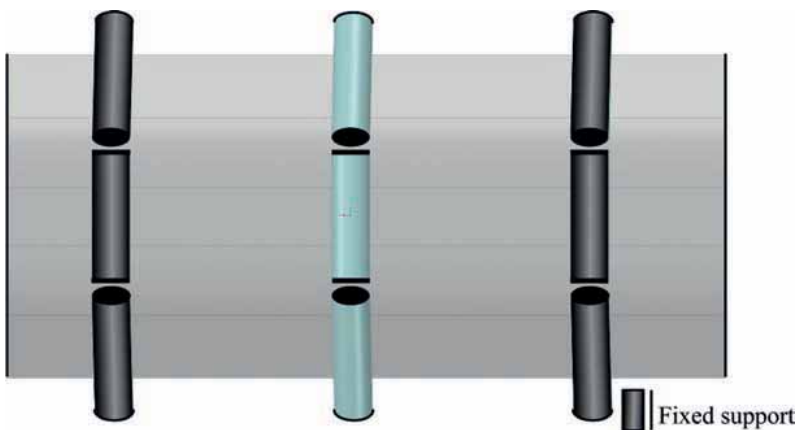

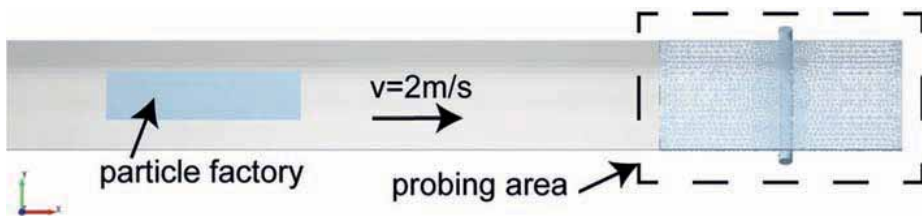Figure 6. Model of the belt support system.

Figure 7. Geometry of the model used in DEM analysis.

Using relationships described in (Gładysiewicz 2003), the nominal capacity of the conveyor was defined at 457.24 kg/s. This value was accepted as the nominal belt load degree $k_z = 1$.

The intensity of particle production in EDEM was increased by 25 kg/s at 10-second intervals (Fig. 8), in the range from 25 kg/s to 500 kg/s (Fig. 9). The capacity was measured at a distance equal in length to the accepted idler set spacing (0.83 m) within the probing area.

As the DEM environment does not allow hyperelastic properties to be attributed to the elements of the system, belt loads were exported to the FEM environment. In addition, the Finite Element Method allows an analysis of material deformation resulting from the interaction between the material and the belt's own mass. Therefore, belt loading was exported from EDEM as force vectors (Fig. 10).
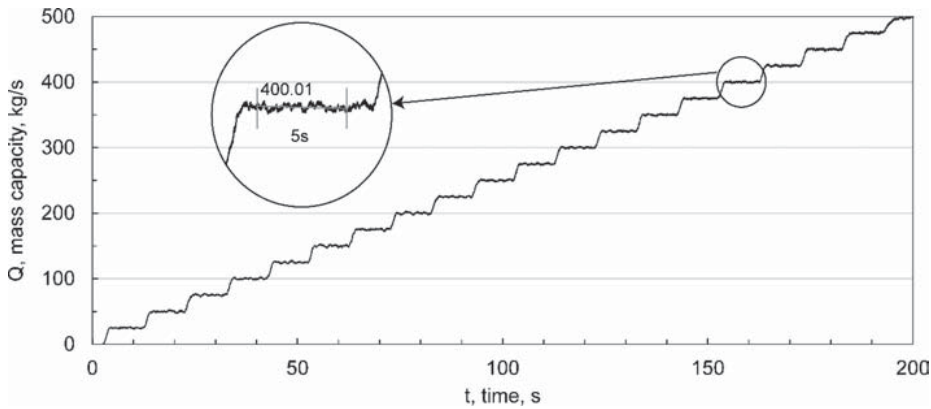
Figure 8. Ore stream simulated in the DEM environment.

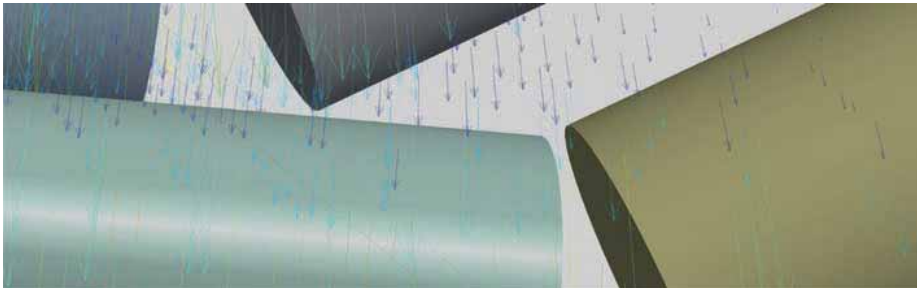Figure 9. Models of belt loading at a capacity of 25 kg/s and 500 kg/s.

Figure 10. Imported forces acting on the belt.

The load range assumed for the calculations was obtained by averaging the measurements which were recorded in DEM simulations at 5-second intervals and during which the ore stream was approximately constant (Fig. 8).

The conveyor belt was simply supported on the idler sets and was loaded within a set force range. This configuration allowed recording the forces acting on the idler supports and determining the contact zones with the idlers.

The values of forces recorded in the idler supports (Fig. 11) served to calculate radial loads on idlers (Fig. 12). The measured reactive forces on the supports of the modeled idlers allow for their mass and account only for the reactive forces due to the belt and the transported material. The contact zone, on the other hand, was approximated by employing the exported belt mesh geometry deformations (Fig. 13).

The forces acting on the pickup idlers were analytically determined in the QNK-TT computer system, which employs motion resistance calculation algorithms based on elementary resistances method (Gładysiewicz 2003). The system has been designed on the basis of object-oriented modeling for a set conveyor route configuration, belt properties and conveyor structural characteristics and is used in calculations of forces acting on the belt, motion resistances
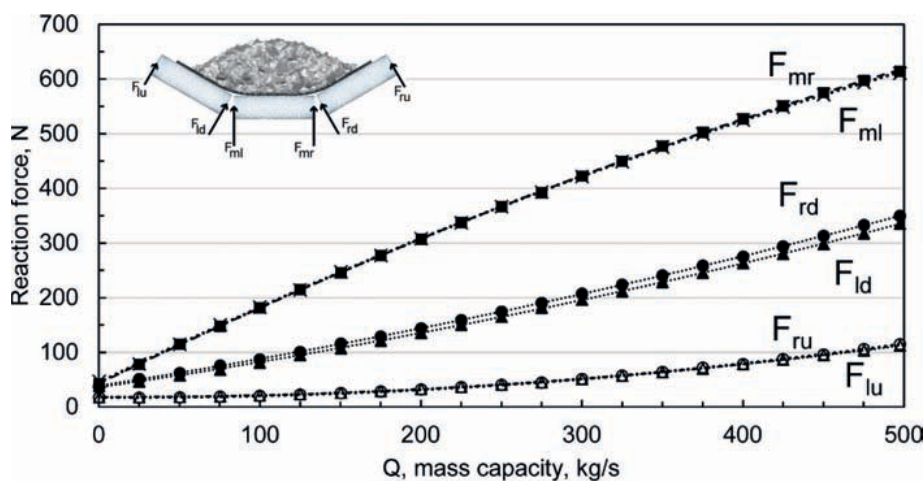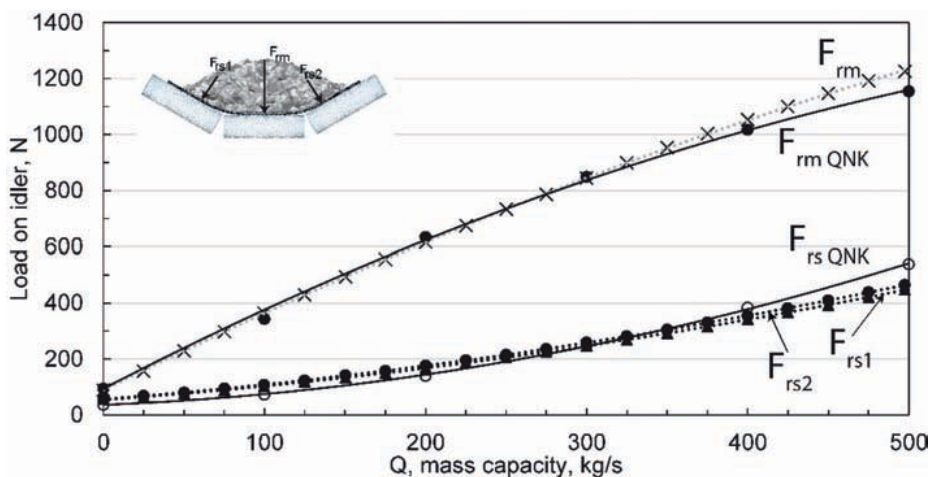
Figure 11.   Reaction forces on idler supports.

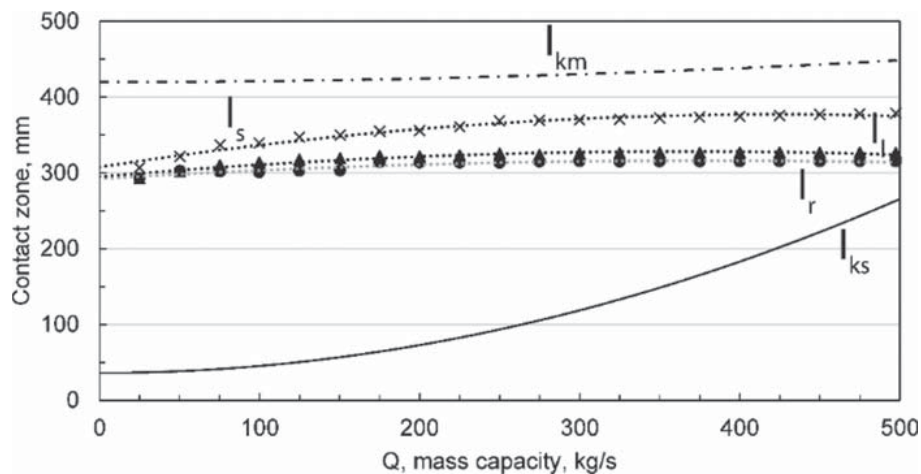Figure 12.   Radial loads on idlers.

Figure 13.   Contact zones.

Table 2. Polynomials describing trend curves.

Parameter	Y	A_1	A_2	A_3	Adj. R^2
Reaction at the upper support of the left idler	F_{lu}	4E-4	8.3E-3	18.17	1.00
Reaction at the upper support of the right idler	F_{ru}	4E-4	1.3E-2	17.74	1.00
Reaction at the lower support of the left idler	F_{ld}	3E-4	0.43	35.90	1.00
Reaction at the lower support of the right idler	F_{rd}	3E-4	0.47	38.64	1.00
Reaction at the right support of the middle idler	F_{mr}	−6E-4	1.44	44.58	1.00
Reaction at the left support of the middle idler	F_{ml}	−6E-4	1.44	42.93	1.00
Radial load on the right idler	F_{rs2}	7E-4	0.45	56.38	1.00
Radial load on the left idler	F_{rs1}	7.E-4	0.42	54.15	1.00
Radial load on the middle idler	F_{rm}	−11E-4	2.86	89.16	1.00
Radial load on the side idler (QNK-TT)	$F_{rs\,QNK}$	16E-4	0.23	36.51	1.00
Radial load on the middle idler (QNK-TT)	$F_{rm\,QNK}$	−17E-4	2.99	93.92	1.00
Contact zone on the right idler	l_r	−2E-4	0.13	292.26	0.90
Contact zone on the left idler	l_l	−3E-4	0.18	295.00	0.93
Contact zone on the middle idler	l_m	−4E-4	0.33	307.70	0.97

and the power of the main drive mechanism. The system also allows for the random influence of belt and material wandering on idler loading.

The analyzed contact zones were compared with the zones analytically defined on the basis of equations from (Gładysiewicz 2003):

- for the middle idler:

$$l_{km} = B \cdot \left(0,35 + 0,02 \cdot k_z^2\right)$$ (3)

- for the side idler:

$$l_{ks} = B \cdot \left(0,03 + 0,16 \cdot k_z^2\right)$$ (4)

where B = belt width; and k_z = dimensionless belt loading coefficient.

Matching functions of curves to the data as shown in the graphs are described with second-degree polynomials, according to the equation

$$Y = A_1 + A_2 Q + A_3 Q^2$$ (5)

where Y = parameter to be calculated; Q = mass capacity; and A_1, A_2, A_3 = coefficients of Table 2 along with matching coefficients R^2.

4 CONCLUSION

A stream of ore representing fine bulk material was used to make a comparison between radial loads on idlers obtained with the DEM-FEM method and the analytical results based on the theory of bulk solids (Gładysiewicz 2003). The two methods proved highly consistent, demonstrating that the model is based on valid assumptions.

However, the DEM-FEM method allows constructing models of belt loaded with a non-uniform stream of material, which is a typical situation in the transportation of ore lumps highly varying in size (and mechanical parameters resulting from varying lithological composition). Equations based on the bulk solids theory do not allow for such configurations.

The FEM belt model requires further studies on the representation of its layer-based design, which would provide parameters for belts of uniform core design but varying thicknesses of covers and/or reinforcement layers (e.g. in the breaker-type belts).

The results obtained from the model for the contact zones between the belt and the idlers deviate significantly from the calculated results, which are based on approximated empirical relationships. These relationships do not allow for the transverse stiffness of the belt and for the material parameters. The methodology here presented may be used to deliver more accurate data in calculations of resistances to motion in belt conveyors. In the future coupling DEM-FEM simulations will allow modeling the loads of a diverse and randomly variable stream of ore, typical for rock mass with wide range of granulation. Such possibilities today are not provided by analytical methods based on the theory of bulk solids.

ACKNOWLEDGEMENTS

REFERENCES

Ali, A., Hosseini, M. & Sahari, B.B. 2010. A Review of Constitutive Models for Rubber-Like Materials. *American Journal of Engineering and Applied Sciences* 3(1): 232–239.

Bajda, M., Błażej, R. & Hardygóra, M. 2016. Impact of selected parameters on the fatigue strength of splices on multiply textile conveyor belts. *World Multidisciplinary Earth Sciences Symposium (WMESS 2016); Proc. intern. symp.,* Prague, 5–9 September 2017. IOP Publishing.

Błażej, R., Jurdziak, L., Kozłowski, T., & Kirjanów, A. 2018. The use of magnetic sensors in monitoring the condition of the core in steel cord conveyor belts—tests of the measuring probe and the design of the DiagBelt system. *Measurement: Journal of the International Measurement Confederation* 123: 48–53.

Doroszuk, B., Walker, P. & Król, R. 2019. Badania własności zróżnicowanej litologicznie rudy miedzi na potrzeby modelowania DEM. CUPRUM—Czasopismo Naukowo-Techniczne Górnictwa Rud 90(1): 5–19 (in press).

Dratt, M., Katterfled, A. & Wheeler, C.A. 2015. Determination of the bulk flexure resistance via coupled FEM-DEM simulation. *The 8th International Conference for Conveying and Handling of Particulate Solids; Proc. intern. Symp.*, Tel-Aviv, May 2015.

FTT WOLBROM, 2015. *Taśmy przenośnikowe tkaninowo—gumowe trudno palne* [Online]. Available at: https://fttwolbrom.com/tasmy-przenosnikowe-trudno-zapalne/ (Accessed: 21 October 2018).

Grabner, K., Grimmer, K.-J. & Kessler, F. 1999. Research into Normal-Forces Between Belt and Idlers at Critical Locations on the Belt Conveyor Track. *Bulk Solids Handling* 13(4): 727–734.

Geesmann, F.O. 2001. *Experimentale und Theoretische Untersuchungen der Bewegungswiderstaende von Gurtfördernanlage.* PhD Thesis. University of Hannover.

Gładysiewicz, L. 2003. *Przenośniki taśmowe: teoria i obliczenia*. Wrocław: Oficyna Wydawnicza Politechniki Wrocławskiej.

Gładysiewicz, L., Kawalec, W. & Król, R. 2016. Dobór rozstawu krążników górnych przenośnika taśmowego z uwzględnieniem losowo zmiennej strugi urobku. *Eksploatacja i Niezawodność* 18(1): 32–37.

Gładysiewicz, L., Król, R. & Kisielewski, W. 2019. Measurements of loads on belt conveyor idlers operated in real conditions. *Measurement: Journal of the International Measurement Confederation* 134: 336–334.

Hardygóra, M. & Woźniak, D. 2008. Sprawozdanie z badań nr LTT/39/14 Badanie elastyczności poprzecznej taśm przenośnikowych wg PN-EN ISO 703:2008. Wrocław: Politechnika Wrocławska—Instytut Górnictwa Laboratorium Transportu Taśmowego.

Ilic, D. & Wheeler, C. 2016. Measurement and simulation of the bulk solid load on a conveyor belt during transportation. *Powder Technology* 307: 190–202.

Jaszak, P. 2016. Modelowanie gumy za pomocą metody elementów skończonych. *Elastomery* 20 (3): 31–39.

Kawalec, W. & Kulinowski, P. 2007. Obliczenia przenośników taśmowych metodą podstawową oraz oporów jednostkowych w zintegrowanym środowisku programowym. *Transport Przemysłowy* 1: 59–64.

Król, R. 2017. Studies of the Durability of Belt Conveyor Idlers with Working Loads Taken into Account. *World Multidisciplinary Earth Sciences Symposium (WMESS 2017); Proc. intern. symp.,* Prague, 11–15 September 2017. IOP Conference Series: Earth and Environmental Science 95(4).

PKN (Polish Committee for Standardization), 2008, *PN-EN ISO 703:2008 Taśmy przenośnikowe: Elastyczność poprzeczna (zdolność do układania się w nieckę): Metoda badania.* Warszawa: PKN.

Shahzad, M., Kamran, A., Siddiqui, M.Z. & Farhan, M. 2015. Mechanical Characterization and FE Modelling of a Hyperelastic Material. *Materials Research* 18(5): 918–924.

Comprehensive, experimental verification of the effects of the lock-up function implementation in LHD haul trucks in the deep underground mine

Tomasz Kaniewski
OZG Lubin, KGHM Polska Miedz SA, Lubin, Poland

Paweł Śliwiński
KGHM Polska Miedz SA, Headquarters Lubin, Poland

Justyna Hebda-Sobkowicz & Radoslaw Zimroz
Faculty of GeoEngineering, Mining and Geology, Wroclaw University of Technology, Wroclaw, Poland

ABSTRACT: Large haul trucks cooperating with wheel loaders are used on a large scale for horizontal hauling in underground mines of KGHM Polish Copper. Most of the population of LHD trucks are machines with a capacity of up to 25 tons produced by KGHM ZANAM. The latest products include the TB series of trucks: CB4-20TB, CB4-24TB. These are modern machines, equipped with a monitoring system that acquires many operational parameters according to the KGHM data acquisition standard. They are developed in close cooperation with users. Thanks to the data from the onboard monitoring system, machines have been equipped with the Lock-up system, which is closely related to the operation of the gearbox. The article describes the effects analysis of the use of the "lock-up" function in the CB4 20TB machine, based on monitoring data analysis. The Lock-up function is automatically activated by the digital transmission controller under certain conditions. For specified operating ranges, the gearbox mechanically blocks the hydraulic torque converter. This action improves the efficiency of the transmission, which translates into fuel consumption, exhaust emissions, reduction of heat emission by the converter. It improves the efficiency of engine-based braking, reducing the load on the friction-based braking system thus prolonging the lifespan of the brakes and the safety of the users. In the paper, the technical and economic benefits and the improvement of machine operation safety are analyzed. They are expressed by reducing the load on braking systems, reducing the temperature of the oil in the gearbox and reducing the fuel consumption.

1   INTRODUCTION

Mining concerns and companies that produce machine systems for mining, especially underground, face many challenges. Extreme environmental conditions, deteriorating parameters of exploited deposits, a radical increase in the demand for mineral resources related to the development of modern technologies and the globalization of raw material markets cause huge interest of enterprises in improving the efficiency of processes in every possible element [1–9].

Improvements in efficiency could be achieved in many ways, in this paper we consider technical solutions only. One of such innovations recently introduced to underground mines is lock up system installed in mobile machines such as loaders or trucks. The concept of lock up system is well known in the automotive industry, especially in heavy duty mobile machines. The basic tasks of lock up are to block the torque converter in order to increase efficiency of driveline (the transmission) and/or to enable effective engine-based braking. A typical usage of lock up system is (for efficiency increase) vehicle moving at a constant speed on straight sections of the road or (for engine braking) heavy vehicles moving on slopes,

for saving brakes—typical for heavy tipper trucks, mine vehicles etc. [10–19]. Unfortunately, in mining conditions, many innovative solutions commonly used in other industries do not meet or do not fully meet demands. It can also be said that in many cases determining the cost-effectiveness of implementation of a given innovation is difficult which also does not favor the introduction of new solutions.

In this paper, we present results of a simple test done in the underground mine, as well as the methodology that allows to evaluate the impact of the lockup system on efficiency of machines noticed from several perspectives. The procedure is based on analysis of data from on-board monitoring system that has been successfully implemented and now there are more than 120 machines covered by efficiency monitoring program in considered underground mines [4–9]. The paper is organized as follows: first we present a machine selected for the experimental work, then basic features of on-board monitoring system will be introduced, next we will briefly recall the idea of lock up system used in this machine and finally the results of the experiment will be presented and be discussed.

2 ON-BOARD MONITORING SYSTEM DESCRIPTION

2.1 *Machine description*

The machine used in the experiment is a haul truck CB4-20TB produced by KGHM ZANAM. Basic parameters of the truck are: Lenght:10 300 mm, Width: 3 350 mm, Height (cabin in position): 1900/2000/2100 mm, Total weight: 26000 kg, Box capacity: 11,1 m³, Nominal payload: 20,0 t, Power rating: 149 kW, Driving speed: up to 20 km/h. Photo of the machine is shown in Fig. 1.

2.2 *Monitoring system description*

According to the standard of data monitoring [2,7] developed in the frame of internal KGHM Group project, there is a list of parameters measured on the machine. Depends on the machine type, the list may contain different parameters. During the experiment, we were able to acquire several variables listed in Table 1. They are related to the various component, have different dynamics (low-frequency processes such as temperature, high-frequency processes such as pressure, etc.) and have different robustness. From this paper perspective, only some of available data will be used. All data are sampled with 1Hz frequency.

2.3 *Lock up system used in mining machine*

The extremely exacting environment in deep underground mine requires innovative solutions. One of such technical solution is haul truck CB4-20TB produced by KGHM Zanam. This machine consists of efficient components including Diesel engine (model Cummins QSB6.7) with power 149 kW and torque 950 Nm at 1500 rpm, hydraulic transmission integrated into the gearbox – (Dana Spicer HR32000 that is fully-reversed, switchable under load and electrically controlled system), additive drive system that consists of hydraulic motors built into the hubs of the load box with power distribution (70/30 respectively: front/rear) and operator-actuated drive—switched off automatically when gear 2 is engaged. The selected innovations used in the machine are illustrated in Fig. 2.

Figure 1.   Photo of investigated Haul Truck machine.

Table 1. A list of monitored parameters for Haul Truck.

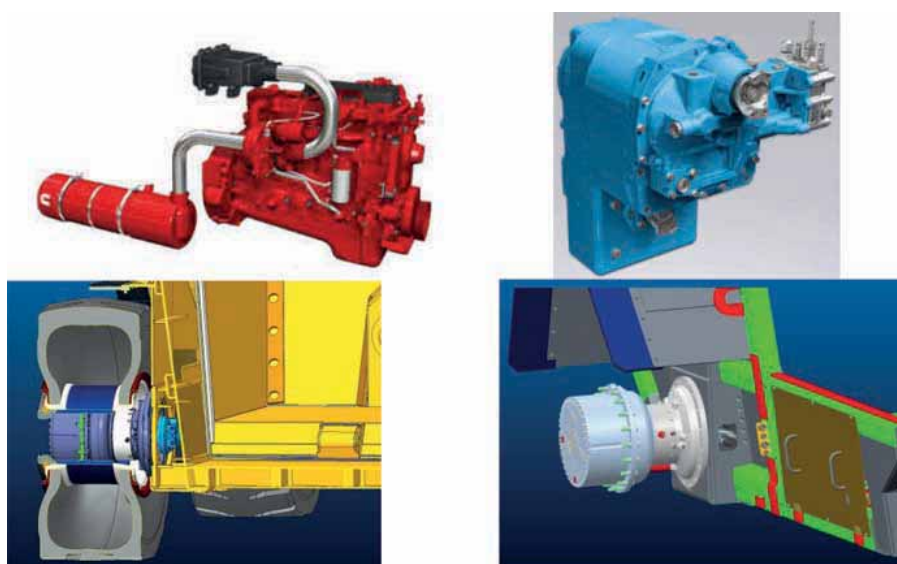| Variable name	Description
'BREAKP'	breaking pressure
'ENGCOOLT'	temperature of the cooling liquid of the internal combustion engine
'ENGHOURS'	number of operating hours of the internal combustion engine cumulatively
'ENGOILP'	oil pressure of the internal combustion engine
'ENGRPM'	engine speed
'ENGTPS'	deflection of the gas pedal
'FUELUS'	instant fuel consumption
'GROILP'	Transmission oil pressure
'GROILT'	oil temperature of transmission and torque converter
'HYDDRV'	attached additional hub drive
'HYDOILP'	pressure in the hydraulic system
'HYDOILT'	hydraulic oil temperature
'INTAKEP'	engine boost pressure
'INTAKET'	air temperature at the engine's intake
'SELGEAR'	direction and current gear
'SPEED'	average speed every 1s
'SWITCHMOVE'	switching the direction of travel under load
'TRNBPS'	position of the brake pedal; 0–100%
'TRNLUP'	lock up on/of

Figure 2. Powertrain components of Haul Truck CB4-20TB.

The design of the machine is systematically improved—among others thanks to installed monitoring systems and cooperation with users. An additional APC controller has been introduced in the drivetrain system, which provides the following functions (Fig. 3):

- protects gearboxes against overloads,
- allows driving in automatic mode,
- controls the lockup function which has been implemented to increase the efficiency of engine braking while driving on a slope.
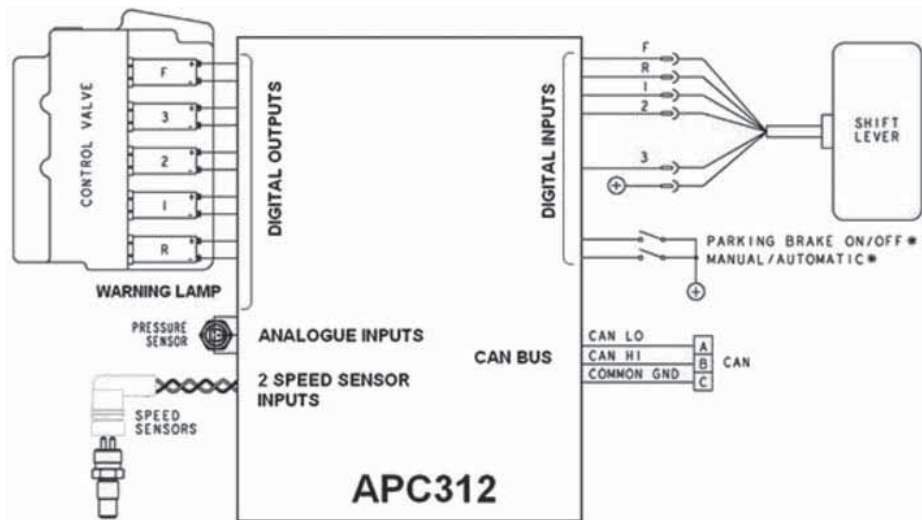
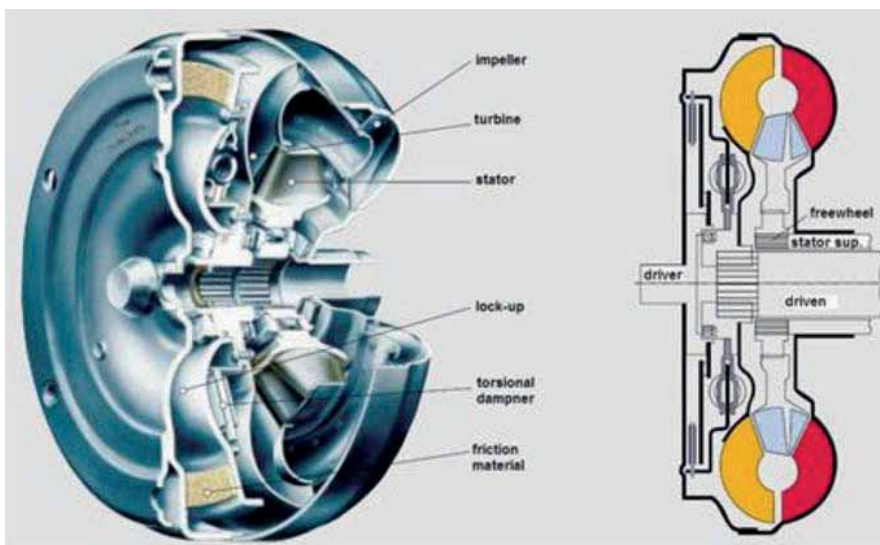Figure 3.   A block scheme of the APC312 system.

Figure 4.   The idea of hydraulic transmission with lock up system.

The converter has a mechanical clutch (lockup), which, when the load is stable, locks the converter pump mechanically.

2.4   *Plan of experimental work*

In order to prove the efficiency of lock up system, a plan for experimental works has been prepared. An identification of lock up system's influence on machine operation in real environment was the main target. We would like to check if the usage of the lock up system affects:

- Fuel consumption
- Averaged speed of machine during transporting materials
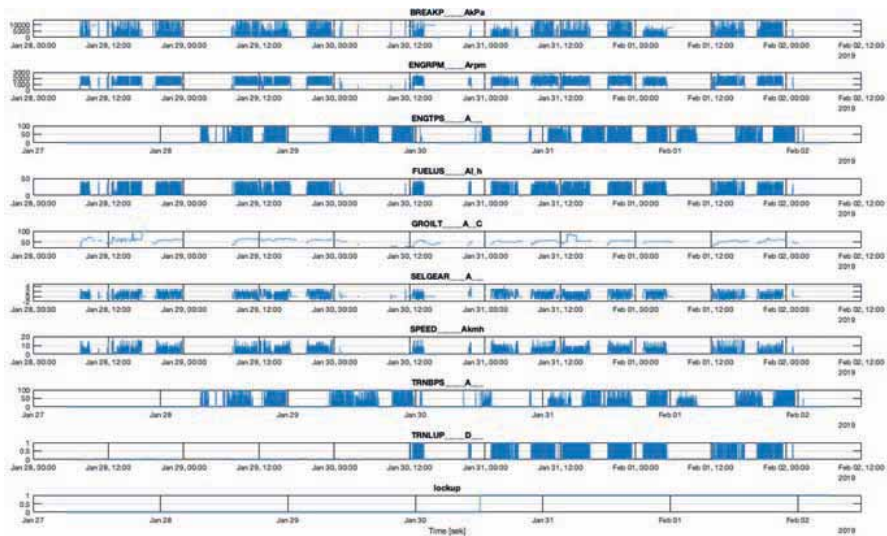- braking performance of the engine

Figure 5.   A raw data monitoring system– an example used in calculations.

- loading of brake system
- oil temperature in the drivetrain (gearbox torque converter)

The experiment was conducted over a period of two weeks. First, a data sample was collected for a machine with an active lock-up function. Then, the lock-up function was blocked in the transmission control software. In both cases data have been acquired by already mentioned on board monitoring system.

2.5   *Presentation of acquired data*

In the Fig. 5 a raw data from on-board monitoring system are presented. The analysed data are related to such factors as breaking pressure, engine speed, position of the gas pedal [0–100%], instantaneous fuel consumption, oil temperature of transmission and torque converter, direction and current gear, average speed in every 1s, position of the brake pedal [0–100%] and lock up on/off. Based on these data some basic (primary) and indirect (secondary) KPIs will be calculated. By visual inspection of raw data it is very hard to estimate the influence of lockup system on temperature or fuel consumption. According to our experience, high variability of the data, their streaming character, random disturbance in the signal during acquisition in real mining conditions etc., requires practically advanced signal processing and analysis including validation, pre-processing, calculating basic features [5] and finally high-level performance indicators [4, 5, 6, 8, 9].

3   METHODOLOGY

3.1   *The lock up system and operational efficiency analysis—a brief review*

The reason for installation of the lockup system in regarded machines was to improve effective engine-based braking while driving on underground workings with a high slope and to minimize energy losses during stationary part of the process i.e. driving at constant speed on straight, flat road.

The main purpose of these experiments was to verify whether the lock up will really provide the effects for loaded machine driving and how big this impact is. The mechanical blocking of the converter's rotors should improve the efficiency of power transfer to the wheels, and consequently reduce the fuel consumption. The use of lockup for heavy, low-speed machines

has been negligible till now, but recently such technological innovations have been installed in some construction and mining machines (eg. OptiShift transmission from VOLVO). For this purpose, a research method based on data from the onboard monitoring system installed on the machine is proposed. The software of the on board monitoring system has been modified as additional variables have been introduced to signal lockup activation.

3.2 *Experimental data processing*

The machine operation in underground mine is a very complex process that depends on many factors [8]. To compare two machines and conclude on their efficiency one has to carefully plan the experiment and recognise what parameters have the influence on final results. To make such comparison reasonable, careful data selection has been done first [9]. The procedure consists of three main steps:

1. **Selection of data samples** to ensure comparability of machine working conditions. Based on the data from the operators' work records in the IT environment HR-TM (module of the SAP system), we choose similar daily services. We rely on the following criteria:
   - Mining unit ordering work,
   - Place of work for a given machine,
   - Type of work performed by a given machine,
   - Length of the distance between mining face and mining screen.

2. **Calculation of basic operational indicators** for each shift based on monitoring data:
   - **Engine run time**, using ENGRPM signal we count samples recorded in every 1 second and the result is divided by 3600 [1h]. It is estimated for: total time, neutral gear, driving of loaded machine—all in [hours],
   - **Fuel consumption,** variable FUELUS is used, we sum up the samples of the signal recorded in every 1 second, the result is divided by the 3600 [1h], so finally we obtain: total consumption [dm³] and consumption for driving [dm³],
   - **The distance** traveled by the machine, variable SPEED is used, we sum up the samples recorded in every 1 second, the result is divided by the 3600 [1h], so finally we obtain the total distance [km],
   - **Oil temperature** for the driving system: average oil temperature in [°C].

3. Calculation of indirect, operational **key performance (efficiency) indicators for each work shift:**
   - **Total fuel** consumption per **distance traveled** [dm³/km],
   - Fuel **consumption for driving** mode (a more reliable indicator) [dm³/km].

3.3 *Discussion*

The machines WO20TB with the lockup function have been used for over two years so far. The solution has been proved to be failure-free and the cost of its installation (considering cost of the whole machine) seems to be low, however, surprisingly the end-users have not ordered machines with the lockup function. In our opinion, there was no measurable evidence to support the economic justification for introducing this modification. Thanks to the use of the described method, measurable effects related to the reduction of fuel consumption have been confirmed. Moreover, we also showed positive impact on usage of brake (lower temperature of oil suggests that operator used engine-based brake rather than conventional friction-based braking system to slow down that will increase life time of a brake).

4 RESULTS

In this section, step by step, the results of the proposed procedure will be presented and discussed. First, in Fig. 6 we show that the efficiency of the transmission is better when using the lockup function, because the average fuel consumption (FUELUS) is smaller and even

the speed of the machine is higher (samples are average values for 15-minute blocks). The calculation done for context: BRAKP = 0, SPEED> 1, GEAR 2 ÷ 3.

Figure 7 present data for the case when a machine is operated and frequently retarding braking is used. In the figure one may notice that the efficiency of the engine braking with activated the lockup function is better, i.e. the average engine RPM is higher. (average values for 15-minute blocks). The analysis have been done with assumed context: BRAKP> 100, SPEED> 1, GEAR –2, –1,1,2,3,4.

Figure 8 presents average oil temperature in the driving system. The graphs show that when using the lockup function, the average oil temperature in the drive system is lower with parameter of the engine speed as well. (average values for 15-minute blocks). It means that brakes are less used due to more effective usage of engine-based braking.
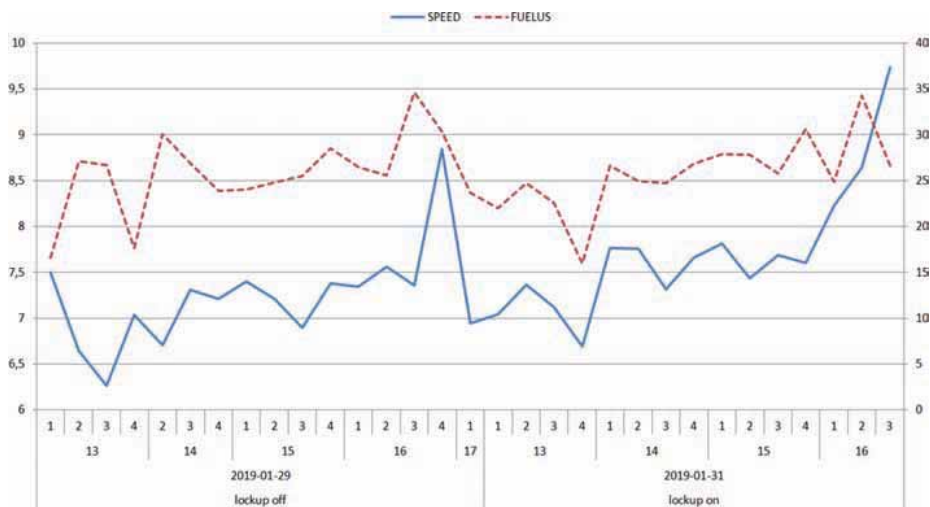

Figure 6.   Influence of LOCK UP system on fuel consumption.
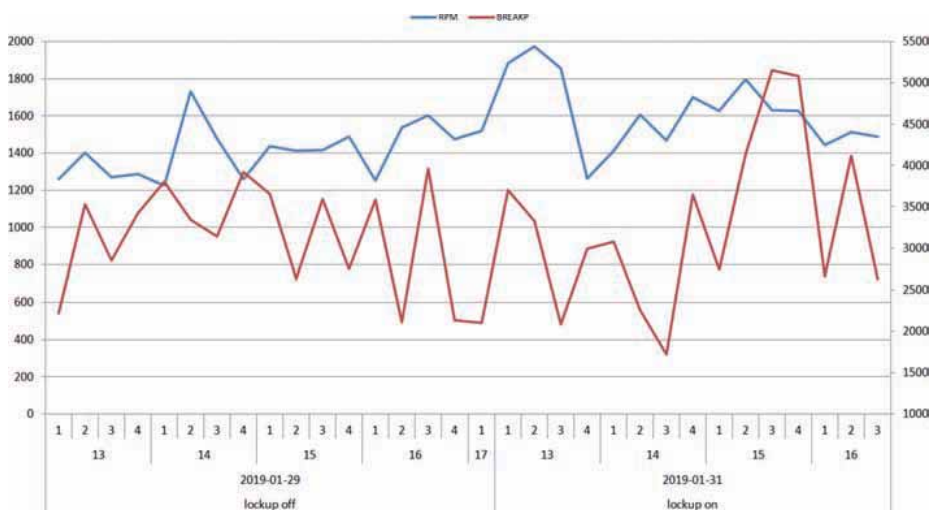

Figure 7.   Influence of LOCK UP system on brake usage and engine speed.

Figure 8.   Influence of lock up system on oil temperature.

Table 2.   Comparison of results for WO 168L, CB4 20TB with lockup.

Parameter	Lockup off	Lockup on
Engine operation [h]	70,13	57,04
distance[km]	101,45	129,70
Fuel consumption in total [l]	411,33	478,91
Fuel consumption (idle) [l]	38,82	53,85
Averaged fuel consumption/1 km [l/1 km]	4,05	3,69
Averaged fuel consumption/1 km without idle [l/1 km]	3,67	3,28
Averaged fuel consumption/ h of engine operation [l]	10,86	9,8
Averaged operation time/day (24h) [h]	13,06	12,76
Operation with lockup [%]	0	68%
Averaged save in total		8,93%
Averaged save for driving machine only		10,74%
Averaged temperature of oil	60,14	54,74

5   CONCLUSIONS

In the paper a selected issues of efficiency of underground machines have been discussed. The main purpose of the work was to propose a procedure to confirm that utility of the installation of lock-up system in underground machines operated in deep copper ore mine is technically and economically reasonable. We have proposed the plan of an experiment and procedure of data analysis to obtain a set of performance indicators, that could confirm benefits of using lock up system.

It has been found that the indicators extracted based on operating parameters, in particular related to fuel consumption, are significant smaller (8.93% overall) for used lockup. If one consider the machine regime "driving" only, savings are at a level of 10.74%. It allows to achieve real economic effects (there are more than 1000 machines in the taken into consideration company). It is also important that decreased fuel consumption results also in reducing the amount of exhaust gas emitted by the machine. It might be considered as a significant benefit taking into account ventilation cost and geometry of mining works (tunnels).

It was also confirmed, that while using lock up, RPM engine speed is higher, that means more efficient engine-based brake.

Finally, it has been found that using lock up system allows to decrease temperature of oil in brake system (less usage of brake due to using engine for deceleration—using retarding instead of conventional friction-based braking system)

REFERENCES

[1] McBain, J. & Timusk, M.: Software Architecture for Condition Monitoring of Mobile Underground Mining Machinery A framework Extensible to Intelligent Signal Processing and Analysis. In: 2012 IEEE Conference on Prognostics and Health Management, PHM, pp. 1–12 (2012), doi:10.1109/ICPHM.2012.629954.

[2] Kicki, J. & Dyczko, A.: The concept of automation and monitoring of the production process in an underground mine. In: New Techniques and Technologies in Mining—Proceedings of the School of Underground Mining, pp. 245–253 (2010).

[3] Gustafson A., Schunnesson H., Galar D. & Kumar U. The influence of the operating environment on manual and automated load-haul-dump machines: a fault tree analysis. International Journal of Mining, Reclamation and Environment, Vol. 27, 2013, p. 75–87.

[4] Wodecki, J. et al. Technical condition change detection using Anderson–Darling statistic approach for LHD machines–engine overheating problem 2018 International Journal of Mining, Reclamation and Environment 32(6), pp. 392–400.

[5] Zimroz R., Wodecki J., Król R., Andrzejewski M., Śliwiński P. & Stefaniak P. Self-propelled mining machine monitoring system-data validation, processing and analysis. In: Drebenstedt C., Singhal R. (eds) Mine Planning and Equipment Selection. Springer, Cham, 2014, p. 1285–1294.

[6] Stefaniak P. et al. An Effectiveness Indicator for a Mining Loader Based on the Pressure Signal Measured at a Bucket's Hydraulic Cylinder Procedia Earth and Planetary Science 15, 797–805.

[7] Dyczko A., et al.: Koncepcja monitoringu i transmisji danych technologicznych pracy samojezdnych maszyn górniczych w KGHM Polska Miedź S.A. unpublished technical report prepared for KGHM PM SA (in Polish).

[8] Stefaniak P. et al. (2016) Multidimensional Signal Analysis for Technical Condition, Operation and Performance Understanding of Heavy Duty Mining Machines. In: Chaari F., Zimroz R., Bartelmus W., Haddar M. (eds) Advances in Condition Monitoring of Machinery in Non-Stationary Operations. CMMNO 2014. Applied Condition Monitoring, vol 4. Springer, Cham.

[9] Wyłomańska, A. & Zimroz, R. Signal segmentation for operational regimes detection of heavy duty mining mobile machines—a statistical approach Diagnostyka 2014. Vol. 15, No. 2.

[10] Kugimiya, T., Mitsui, J., Yoshimura, N., Kaneko, H., Akamatsu, H., Ueda, F., Nakada, T., (...) & Akiyama, S. Development of automatic transmission fluid for slip-controlled lock-up clutch systems (1995) SAE Technical Papers. doi: 10.4271/952348.

[11] Tohyama, M., Ohmori, T. & Ueda, F. Anti-shudder mechanism of ATF additives at slip-controlled lock-up clutch 1999 SAE Technical Papers.

[12] Adachi, K., Ochi, Y., Segawa, S. & Higashimata, A. Slip control for a lock-up clutch with a robust control method (2004) Proceedings of the SICE Annual Conference, art. no. TAI-9-1, pp. 893–898.

[13] Sivertsson, M. & Eriksson, L. Optimal Powertrain Lock-Up Transients for a Heavy Duty Series Hybrid Electric Vehicle 2017 IFAC-PapersOnLine 50(1), pp. 7842–7848.

[14] Li, C., Xi, J., Gu, H. & Chen, H. A Research on Lock-up Process Control Strategy for Torque Converter Based on Dual Objectives 2018 Qiche Gongcheng/Automotive Engineering 40(10), pp. 1200–1205.

[15] Wellmann, T., Govindswamy, K., Orzechowski, J. & Srinivasan, S. Influence of Automatic Engine Stop/Start Systems on Vehicle NVH and Launch Performance (2015) SAE International Journal of Engines, 8 (4). doi: 10.4271/2015-01-2183.

[16] Kurnia, J.C., Sasmito, A.P., Wong, W.Y. & Mujumdar, A.S. Prediction and innovative control strategies for oxygen and hazardous gases from diesel emission in underground mines 2014 Science of the Total Environment 481(1), pp. 317–334.

[17] Heikkilä, M., Huova, M., Tammisto, J., Linjama, M. & Tervonen, J. Fuel efficiency optimization of a baseline wheel loader and its hydraulic hybrid variants using dynamic programming 2018 BATH/ASME 2018 Symposium on Fluid Power and Motion Control, FPMC 2018.

[18] Wellmann, T., Govindswamy, K. & Tomazic, D. Impact of the Future Fuel Economy Targets on Powertrain, Driveline and Vehicle NVH Development 2017 SAE Technical Papers 2017-June.

[19] Moawad, A. & Rousseau, A. Impact of Electric Drive Vehicle Technologies on Fuel Efficiency to Support 2017–2025 CAFE Regulations (2014) SAE International Journal of Alternative Powertrains, 3 (2), pp. 163–175. doi: 10.4271/2014-01-1084.

Analysis of dynamic external loads to haul truck machine subsystems during operation in a deep underground mine

Paweł Śliwiński & Tomasz Kaniewski
KGHM Polska Miedz SA, M. Skłodowskiej-Curie, Lubin, Poland

Justyna Hebda-Sobkowicz & Radoslaw Zimroz
Faculty of Geoengineering, Mining and Geology, Wrocław University of Science and Technology, Wybrzeże Wyspiańskiego, Wrocław, Poland

Agnieszka Wylomańska
Faculty of Pure and Applied Mathematics, Wrocław University of Science and Technology, Wybrzeże Wyspiańskiego, Wrocław, Poland

ABSTRACT: The rough shape of the road surface in an underground deep copper ore mine is a source of external excitations to many systems and components of the underground mobile machines. Moreover, the geometry of mining corridors, driver's skills and habits (dynamics of driving style), machine conditions etc., might have a serious influence on the overall dynamic load of such a machine. As a result, the construction of the mining machines used in the mines of KGHM Polska Miedź SA is exposed to extreme conditions. This applies to both operation close in mining face and driving in underground tunnels. There are cases of serious construction node damages in the machine due to the above-mentioned reasons. Thanks to some implemented onboard monitoring systems a lot of various types of data are acquired on regular basis with 1 second sampling frequency. In general, the purpose of the monitoring system was related to the daily production evaluation, maintenance, etc. In addition, it allows to analyze processes in the long term. However, due to mentioned factors, there are many transient events that negatively affect operation and condition of the machine and these situations are hard to identify using data acquired by the onboard system in the current configuration. In this work, we installed a portable vibration acquisition device (a smartphone) in a couple of machines to check if it is possible to identify experimentally the influence of road surface quality to dynamics and condition of the machine sub-systems (especially joints of components) and driver's behavior (style of driving). First trials proved that while using vibration data we are able to parametrize and compare the daily activity of haul truck machine.

1 INTRODUCTION

The Mining production in an underground mine is a very complex process. It requires a significant support from machines, automated mechanical systems or even robots. Extreme, harsh conditions, gas hazard, the presence of aggressive environment (salt, dust, water), high temperature (primary rock temperature might be c.a. 45C) – all these factors cause that the performance of human beings as well as machines is limited. Indeed, in the case of machines, their life time is much shorter in comparison to surface mining. The rough shape of the road surface in underground deep copper ore mine is a critical issue from a tires maintenance perspective, however, it is also a source of external excitations to many systems and components of the underground machines. Room and pillar technology results in a network of corridors (tunnels). Due to imperfection of blasting technology, the geometry of mining corridors, mentioned road surface shape, elevations of corridors, but also driver's skills and

habits (dynamics of driving style), machine conditions etc., might have a serious influence on overall dynamic load of such a machine. Obviously, it will also affect the wear/degradation of the machine and overall efficiency of the machine.

The paper is a kind of introductory work. First, we have done several experiments using the regular car and two examples of the road–results appeared very promising [1]. Other authors also have tried to use mobile phones to measure some parameters and use them to evaluate of quality of roads [2, 3, 4, 5, 6, 7, 8, 9]. However, in the deep mine using heavy duty machines is a challenging issue. In order to "control" experimental work during regular activities of the machine (ore transport from mining face to mining screen–i.e. unloading point), we combined vibration data with existing onboard monitoring system used in the mine. From that system, one might measure speed, fuel consumption, current gear, and many other parameters. It helps us to link vibration level with machine operational regimes, acceleration, deceleration, changing driving direction, etc.

The paper is organized as follows: first, we briefly present a machine, describe the experiment and the data from the onboard monitoring system. Then we propose a simple methodology, that is based mostly on a simple statistical analysis and—on this stage–a visual inspection of the data rather than an advanced algorithm. Some basic conclusions are drawn at the end of the paper.

2 MACHINE AND EXPERIMENT

2.1 *Machine description*

The machine used in the experiment is a Haul Truck CB4-20TB produced by KGHM ZANAM. Basic parameters of the truck are: length: 10300 mm, width: 3350 mm, height (cabin in position): 1900/2000/2100 mm, total weight: 26000 kg, box capacity: 11.1 m3, nominal payload: 20 t, power rating: 149 kW, driving speed: up to 20 km/h. Photo of the machine is shown in Fig. 1.

The machine is commonly used in KGHM underground mines for ore transport from mining face to mining screen (unloading point). The Haul Truck is used if the distance is longer than a couple of hundred meters, for shorter distances usually loaders are used.

2.2 *Monitoring system description*

According to the standard of data monitoring for underground machines developed in the frame of internal KGHM Group project, there is a list of parameters measured on the machine [10, 11, 12]. Depending on the machine type and the version of the monitoring system, the list may contain different parameters. During the experiment, we are able to acquire 19 variables listed in Table 1, the names of the parameters usually are associated with the information which they represent. They are related to the various component, have different dynamics (low-frequency processes as temperature, high-frequency processes as pressure) and have different robustness.

All data are sampled with 1 Hz. All measurements are stored in the memory of the device until the machine will go back to the so-called "heavy machinery chamber" (kind of underground garage) for routine maintenance procedures or fueling. In the mentioned chamber, an

Figure 1.   Photo of investigated Haul Truck machine.

Table 1. A list of monitored parameters for Haul Truck.

Variable name	Description
'BREAKP'	breaking pressure
'ENGCOOLT'	temperature of the cooling liquid of the internal combustion engine
'ENGHOURS'	number of operating hours of the internal combustion engine cumulatively
'ENGOILP'	oil pressure of the internal combustion engine
'ENGRPM'	engine speed
'ENGTPS'	deflection of the gas pedal
'FUELUS'	instant fuel consumption
'GROILP'	transmission oil pressure
'GROILT'	oil temperature of transmission and torque converter
'HYDDRV'	attached additional hub drive
'HYDOILP'	pressure in the hydraulic system
'HYDOILT'	hydraulic oil temperature
'INTAKEP'	engine boost pressure
'INTAKET'	air temperature at the engine's intake
'SELGEAR'	direction and current gear
'SPEED'	average speed every 1 s
'SWITCHMOVE'	switching the direction of travel under load
'TRNBPS'	position of the brake pedal; 0–100%
'TRNLUP'	lock up on/off

Figure 2. Map of the part of the mine with highlighted route in green of the examined machine.

ICT infrastructure is installed, and data are automatically transferred via WIFI protocol to the central database. They are processed and reported on a daily basis.

During the experiment the mobile phone (smartphone) was additionally installed on the window of the machine (see Fig. 3) and using freeware application the vibration data have been acquired and stored to *.csv file. The first assumption was to measure vibration with the highest available sampling frequency. Finally, the data have been pre-processed (down-sampled) to 1 Hz sampling frequency as in onboard monitoring system to easily synchronize all data together.

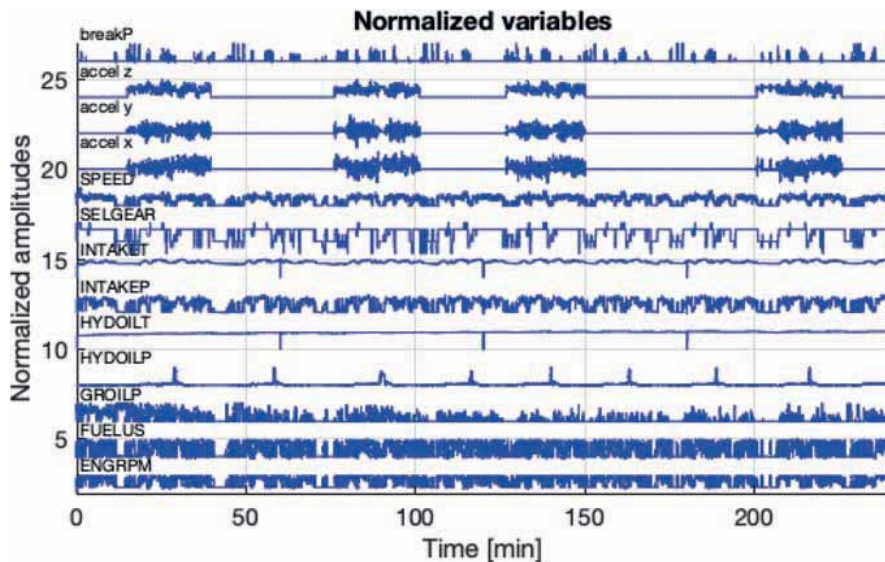Figure 3. The location of the smartphone in the cabin.

Figure 4. Raw data acquired from Haul Track during one shift.

2.3 *Experiment in the mine*

The experiment has been performed in one of the mining units in the underground mine. A route for hauling the ore is presented in green on the map in Fig. 2. A specific feature of this part of the mine is a serious change of elevation (several dozen meters) that significantly influence the operation of the machine (more load going up, playing with breaking system going down). Due to extremely harsh conditions, signals acquired on mining machines have to be carefully inspected, validated and preprocessed before they are subjected to proper analysis [12, 13].

As mentioned, the smartphone was installed in the operator's cabin (see Fig. 3). For data safety reasons, after one cycle of the haul truck, data acquisition was stopped for data saving and restarted again to obtain separate data files.

In fact, several experiments have been done for various types of LHDs, Haul Trucks and Self-propelled Transport Trucks (for transport of people). In Fig. 4 there are an exemplary signals acquired on the machine from onboard monitoring system as well as 4 segments related to measurements of accelerations from a smartphone. For consistent, graphical presentation all data have been normalized to obtain 0–1 range data. Some of the data (mostly temperatures) are useless for the considered context of analysis, so they will not be taken into account in the further part of the paper. An important variable is Hyd_Oil_P that informs about unloading, so one may easily identify the loaded and unloaded Haul Truck.

3 METHODOLOGY

Dynamics of external excitations during acceleration, deceleration, loading or unloading processes are "natural" and expected. These parts of the process could be extracted and parametrized in the sense of number of events, length, maximum of excitation, etc. However, in
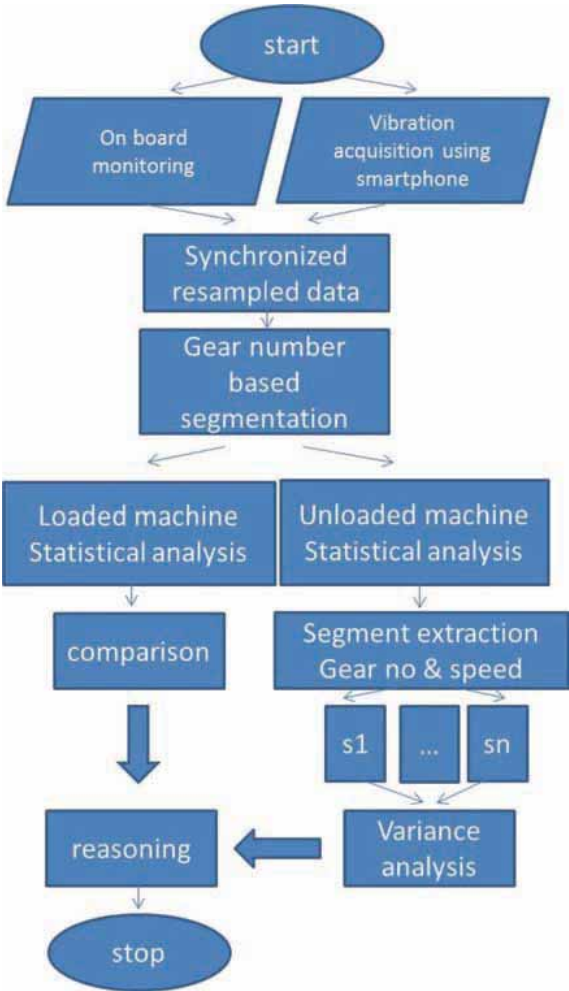

Figure 5. Proposed algorithm for data analysis.

this paper we would like to focus on seemingly "stationary" parts of the process and dynamic phenomena occurring during these periods. "Stationary part" means that number of factors that could influence dynamics is minimized.

Signals acquired from the machine are extremely nonstationary, thus the primary idea here is to make the problem simpler by selection of the most stationary part of data. In theory, there are several possible ways to select "stationary" segments, however, based on some preliminary investigation it was decided that best solution is to use gear number 2, mostly used for driving from mining screen to mining face and back. Using other variables (speed, fuel consumption) is complicated due to the nature of the variability of these parameters.

It is worth mentioning that data has been standardized in sense of sampling frequency (all variables with 1 Hz). After mentioned segmentation (selection of samples for gear number = 2 only), data were grouped into segments of the loaded and unloaded machine and statistically analyzed. It was found that due to the influence of other operational parameters (speed, rpm) global (calculated for all segments with gear = 2 and unloaded box) statistical measures are not effective. It is due to influence of other factors that on this stage of research have not been precisely identified yet. It was previously stated that due to complexity of the problem, analysis of data acquired from LHD machines should take into account many variables, i.e. should be multidimensional [14, 15]. Therefore, in the second phase of segmentation, part of signals with the same gear and similar speed have been investigated for the unloaded machine. Analysis of variance [14] of these segments has allowed recognizing the change in vibration for various road roughness. At this stage, there is no automatic procedure to achieve final results (i.e. road recognition system) but it has been proved that identification of road surface might be possible based on vibration analysis. Overview of the proposed idea is shown in Fig. 5.

4 RESULTS

In this section the preprocessed data and the results of our investigations are presented. In Fig. 6 one may notice that even if we select samples for gear = 2 (as potentially criterion of stationarity of data), the "engine RPM" and the "fuel consumption" data are still very nonstationary—it means that some external factors influence on behavior of the machine. It might in some sense explain why results presented in Figure 7 are not promising.
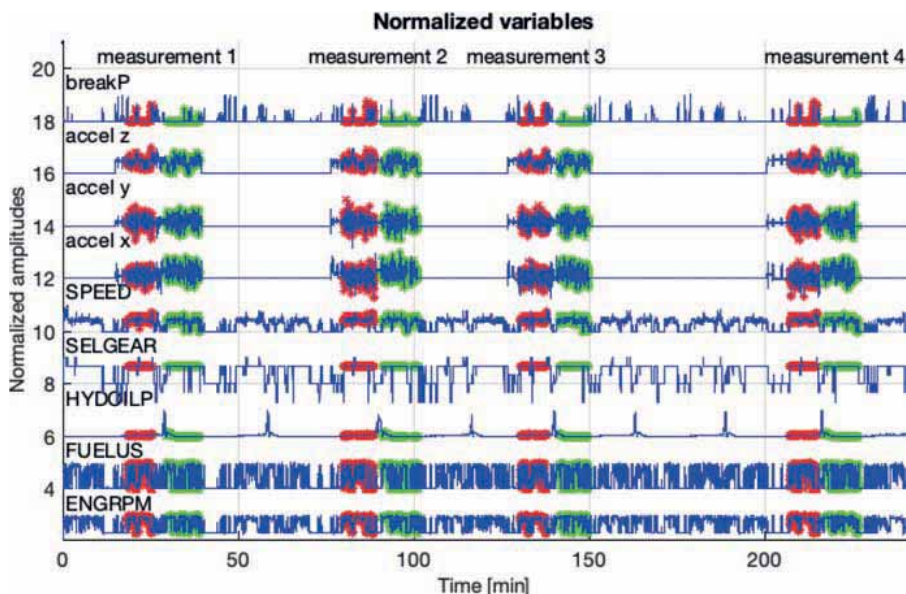

Figure 6.   Results of signals segmentation for gear = 2 (samples in red color selected).
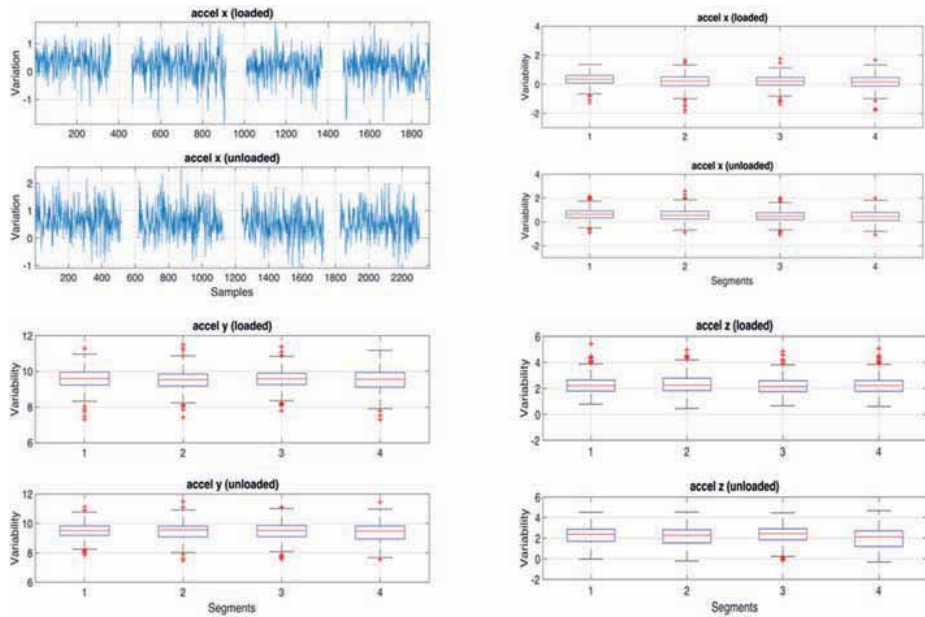
Figure 7. Statistical analysis for pre-segmented vibrations measured in direction XYZ.

Fig. 7 presents statistical analysis using box plots: namely vibration signals and their boxplots for vibration measurement in direction X for loaded and unloaded machine (no difference between vibrations these two experiments) and next the boxplots for vibration measurement in direction Y and Z (again no serious difference).

4.1 *Detailed analysis of signals for unloaded machine case*

The deeper analysis of Fig. 6 leads to a conclusion that apart from FuelUs and EngRPM also breakP and Speed reveal significant variability that obviously influences vibrations. To confirm our hypothesis that road surface influence on the external excitation in the machine we propose to investigate in details part of the data presented in Fig. 8. By red, vertical lines we manually highlighted 3 segments: segment 1 – with nearly constant EngRPM, FuelUs and Speed (no breakP) with Gear = 2, just after unloading process (unloading might be precisely recognized by hydraulic oil pressure analysis [16]). It can be interpreted as a regular drive from unloading point to mining face. As it is close to unloading point, the condition of road is relatively good.

Segment 2 is the next part of the signal after change of gear and return to Gear = 2. One can notice some variation in EngRPM, FuelUs and Speed (especially at the end of Segment 2 the perturbation is related to use of break). In general, we may assume that mentioned factors have similar values to segment 1. Segment 3, again, consists of data for Gear = 2 (after some combination of gear changes), nearly stationary speed (similar to segment 1 end segment 2), no break usage, and some variation in FuelUs and EngRPM (it might be related to variation in slope of the road). Fig. 9 shows another example of manual segmentation (segments marked by arrow).

Fig. 10 shows vibration signal (extracted segments according to discussed above method) for measurement 2 and measurement 4. It is clearly seen that variation for both measurements for first signal is small, for segment 2 and 3 – the signal variations are high. It is related to quality of the road (closer to mining face, worse road quality). The next step provides a statistical description of these processes, starting from the processes' variance. However, as it was highlighted to use statistical analysis, we should exclude deterministic factors first. From Fig. 10 as well as from earlier figures one may see a lot of deterministic low-frequency processes that should be extracted and explained. At this phase of investigations, we try to
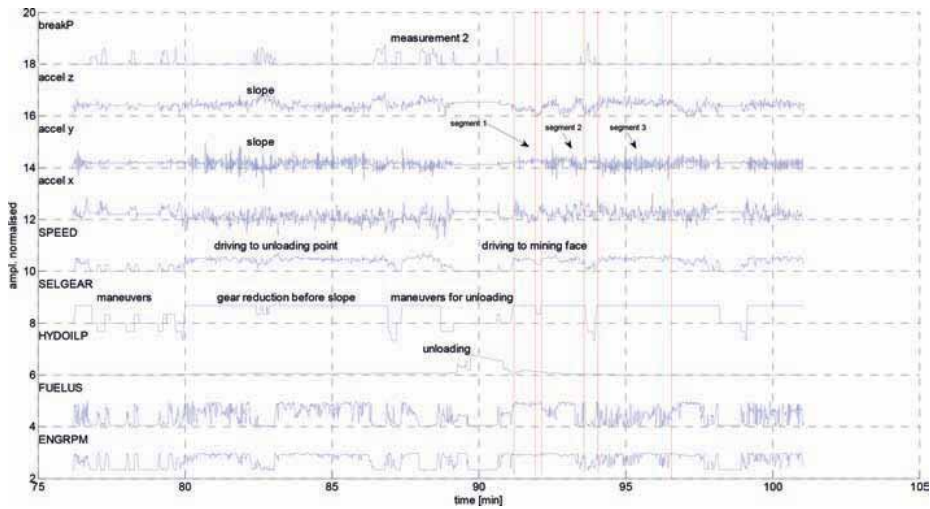
Figure 8. Measurement number 2 – speed, EngRMP and FuelUs inspection—influence of road quality on vibrations.
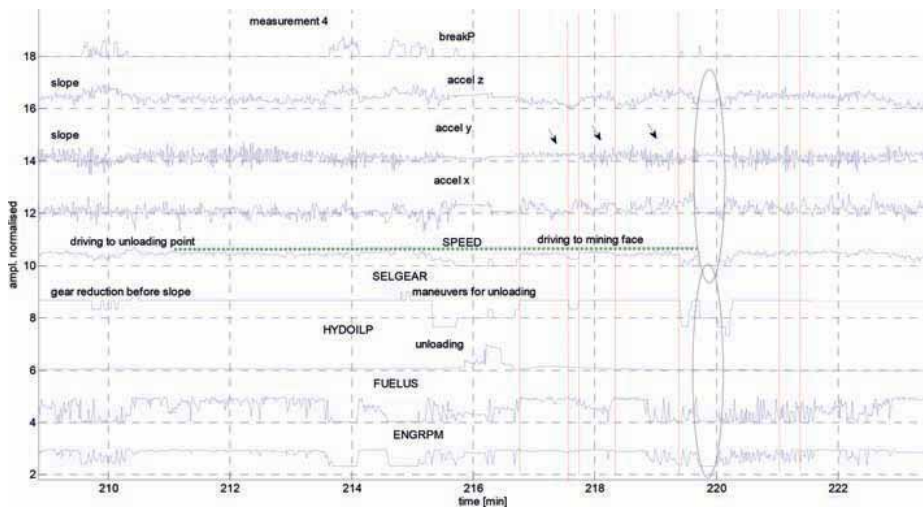

Figure 9. Measurement number 4 – speed context inspection—influence of road quality on vibrations.

understand what information we can extract from measurements and if really, we can use vibration analysis for road surface evaluation.

Signals segmentation strategy should take into account many factors. It has been found that it should be multilevel strategy. One of conclusions may be that during drive on gear 2 the operator can use a break and it will affect the vibration signal (not related to road surface). Fig. 11 presents break pressure data extracted according to gear = 2. It is clearly seen that for a machine with an empty box there are several situations that the operator tries to slow down machine by brake. For loaded machine (box filled with ore) usage of brake is much more intensive. It significantly will affect analysis—this is the reason we have selected drive with the empty box. In general, the preprocessing of data (for statistical analysis) should be done very carefully.
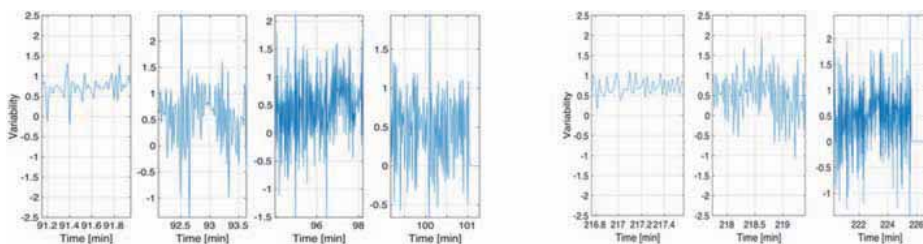
Figure 10. vibration data for pre-segmented measurement 2 and measurement 4 (after unloading) a) First segment with good road (close to unloading point), 2nd-4th segments rough surface b) First segment with good road (close to unloading point), 2nd-3rd segments rough surface.
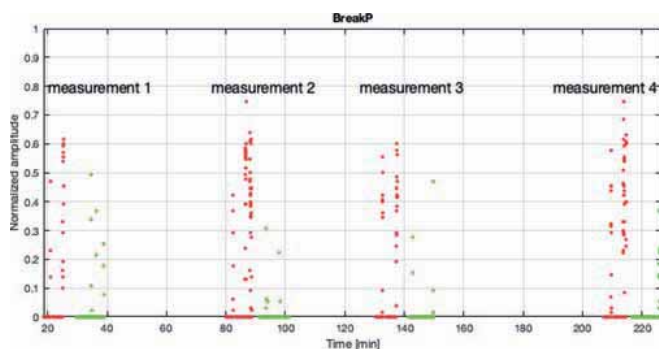

Figure 11. The hydraulic pressure signal for loaded and unloaded machine operated under Gear 2.

5 CONCLUSIONS

In the paper the results of preliminary analysis on dynamic excitation to Haul Truck operated in deep underground mine have been presented. It was shown that signals are extremely nonstationary, depend on several groups of factors. To deduce from the data, the analysis should be done according to the context, i.e. before interpretation, one should make sure that the impact from other factors is minimized. The main purpose of this work is to examine the external excitation used in the machine, which is related to the uneven surface. External excitation might be related to the payload (weight of material carried by the truck box), several operational parameters (speed, rpm, gear), environmental factors (mud, water) as well of the geometry of the corridor (elevations, falls, turns, intersections) and finally skills of the operator. In order to really investigate influence of road surface and simplify the analysis, we introduced gear number context—only data acquired during driving on gear number 2 have been analyzed. Gear = 2 is the most used gear for "stationary" driving. It has been found that basic statistical analysis is not able to recognize differences between vibration for the loaded and unloaded machine. We have proposed additional criteria for segmentation, namely the speed, the fuel consumption and the EngineRPM speed.

Detailed analysis of acceleration in three XYZ directions allows identification of some typical behavior of an operator/machine. We have confirmed, that close to mining screen, vibration registered by sensors are smaller (in sense of variance of vibration), while close to mining face the are much intense. It is related to road quality (closer to mining face—worse road quality). In this paper, we completely ignore highly transient regimes when the operator is changing the gear during acceleration or deceleration. This issue will be considered in the future research.

REFERENCES

[1] Zimoz, R., Wodecki, J., Hebda-Sobkowicz, J., Wyłomanska, A., Stefaniak, P., Sliwinski, P., Kaniewski, T., Mobile based vibration monitoring and its application to road quality monitoring in deep underground mine, Vibroengineering PROCEDIA, Vol. 19, 2018, p. 153–158. https://doi.org/10.21595/vp.2018.20211.

[1] Thompson, R.J. et al. Mine road maintenance management using haul truck response measurements. Institution of Mining and Metallurgy. Transactions. Section A: Mining Technology 115(4), 123–128 (2006).

[3] Wang, H., Huo, N., Li, J., Wang, K., Wang, Z. A road quality detection method based on the mahalanobis-taguchi system. IEEE Access, Vol. 6, 2018, p. 29078–29087.

[4] Tai, Y.-C., Chan, C.-W., Hsu, J.-Y.-J. Automatic road anomaly detection using smart mobile device. Conference on Technologies and Applications of Artificial Intelligence, Hsinchu, Taiwan, 2010.

[5] Sandberg, U. S. Road macro-and megatexture influence on fuel consumption. Surface Characteristics of Roadways: International Research and Technologies, 1990).

[6] Eriksson, J., Girod, L., Hull, B., Newton, R., Madden, S., Balakrishnan, H. The pothole patrol: using a mobile sensor network for road surface monitoring. Proceedings of the 6th International Conference on Mobile Systems, Applications, and Services, 2008, p. 29–39.

[7] Forslöf, J. Continuous road condition monitoring with smartphones. Roadroid AB, 2014.

[8] Astarita, V., Caruso, M.V., Danieli, G., Festa, D.C., Giofrè, V.P., Iuele, T., Vaiana, R. A mobile application for road surface quality control: Uniqualroad. Procedia-Social and Behavioral Sciences, Vol. 54, 2012, p. 1135–1144.

[9] Gustafso, A., Schunnesson, H., Galar, D., Kumar, U. The influence of the operating environment on manual and automated load-haul-dump machines: a fault tree analysis. International Journal of Mining, Reclamation and Environment, Vol. 27, 2013, p. 75–87.

[10] Dyczko, A., et al.: Koncepcja monitoringu i transmisji danych technologicznych pracy samojezdnych maszyn górniczych w KGHM Polska Miedź S.A. unpublished technical report prepared for KGHM PM SA (in Polish).

[11] Kicki, J. & Dyczko, A.: The concept of automation and monitoring of the production process in an underground mine. In: New Techniques and Technologies in Mining—Proceedings of the School of Underground Mining, pp. 245–253 (2010).

[12] Zimroz, R. et al. 2014 Self-propelled Mining Machine Monitoring System—Data Validation, Processing and Analysis. In: Drebenstedt C., Singhal R. (eds) *Mine Planning and Equipment Selection*. 2014. p. 1285–1294. Springer, Cham.

[13] Kępski, P., Barszcz, T.: Validation of vibration signals for diagnostics of mining machinery. *Diagnostyka* 4(64), 25–30 (2012).

[14] Wyłomańska, A., Zimroz, R. Signal segmentation for operational regimes detection of heavy duty mining mobile machines—a statistical approach *Diagnostyka* 2014. Vol. 15, No. 2.

[15] Stefaniak, P. et al. (2016) Multidimensional Signal Analysis for Technical Condition, Operation and Performance Understanding of Heavy Duty Mining Machines. In: Chaari F., Zimroz R., Bartelmus W., Haddar M. (eds) *Advances in Condition Monitoring of Machinery in Non-Stationary Operations. CMMNO* 2014. *Applied Condition Monitoring*, vol 4. Springer, Cham.

[16] Stefaniak, P. et al. An Effectiveness Indicator for a Mining Loader Based on the Pressure Signal Measured at a Bucket's Hydraulic Cylinder *Procedia Earth and Planetary Science* 15, 797–805.

Selection of variables acquired by the on-board monitoring system to determine operational cycles for haul truck vehicle

Paweł Śliwiński & Marek Andrzejewski
KGHM Polska Miedz SA, Head Quarters M. Skłodowskiej-Curie, Lubin, Poland

Tomasz Kaniewski
OZG Lubin, KGHM Polska Miedz SA, Lubin, Poland

Justyna Hebda-Sobkowicz & Radoslaw Zimroz
Faculty of Geoengineering, Mining and Geology, Wrocław University of Science and Technology, Wybrzeże Wyspiańskiego, Wrocław, Poland

ABSTRACT: Self-propelled Mining Machines (LHD—Load Haul Dump, Haul Truck) are the basic technical resource used in copper ore mines in KGHM PM S.A. Machine operation costs: depreciation, service, consumables, remuneration of operators, etc., account for over 30% of the technical costs of copper ore production. To optimize the cost machines and processes are monitored. The aim of the article is to select variables available in the Haul Truck monitoring system for operational regimes identification. The development of indicators for evaluation of the organization of work in the production process, e.g. number of machine cycles, average cycle time, deviations from the average cycle time, starting/finishing of machine operation for work shift, etc. may be considered as the first step to optimize the cost of the process. A method for counting work cycles for LHD loaders has been already developed, using the pressure signal from the actuator in the hydraulic system. However, in the case of Haul Truck, the nature of data is different and the new algorithm is needed. Moreover, in practice, there are limitations in the use of the pressure based indicator due to the loss of data caused by the pressure sensor's susceptibility to mechanical damage. Based on these experiences, we will improve the method, thanks to the use of sensors that are not so susceptible to damage. The article will present the results of analyses regarding the possibility of using other registered physical variables (engine revolutions, instant fuel consumption, speed, the pressure in the braking system, etc.), which are much more reliable and resistant to interference.

1 INTRODUCTION

The rapid development of industrial electronics makes monitoring of mining equipment operating underground mines, effective. Mobile machines such as loaders, haul truck, drilling/bolting machines are very specific and their usage and maintenance are demanding. A lot of efforts have been put in that field [1–6]. The onboard monitoring system is used in underground KGHM mines in more than 100 mining machines (loaders, truck, drilling/bolting machines). After a successful pilot phase, a lot of data measured in every 1 s is stored on the machines and transmitted to the data warehouse every day. One might conclude, that data acquisition problem has been overcome. Unfortunately, the problem of data validation, processing, analysis and finally reporting are still challenges for such industrial BIG DATA case [7–8]. There are already many reports prepared on regular basis. However, there is an increasing need for reliable information for various levels of management staff in the mine. In this paper, we will discuss an important problem how to automatically transform raw data from haul truck onboard monitoring system into operational information about production effectiveness, namely number of cycles of haul truck performed underground in a single shift. This issue has been partially solved for LHD

loader [9], however, it was done using hydraulic oil pressure signal (*Hyd_Oil_P*). Unfortunately, we may adjudge, that after a couple of years of experience, there is a need to increase reliability/robustness of the procedure and end-user suggested to use data other than pressure signal (as the pressure sensor is sensitive and often is broken due to very harsh conditions). In the paper, we will propose a methodology for informative signals selection for the defined task (i.e. estimation of a number of cycles). First, we briefly describe the monitoring system used in haul truck and present exemplary data set for 1 shift. Then a proposed methodology will be presented and applied to 3 days data set from the haul truck monitoring system.

2 ON-BOARD MONITORING SYSTEM DESCRIPTION

2.1 *Machine description*

The machine used in the experiment is a haul truck CB4-20TB produced by KGHM ZANAM. Basic parameters of the truck are: Lenght:10 300 mm, Width: 3 350 mm, Height (cabin in position): 1900/2000/2100 mm, Total weight: 26000 kg, Box capacity: 11,1 m³, Nominal payload: 20,0 t, Power rating: 149 kW, Driving speed: up to 20 km/h. Photo of the machine is shown in Fig. 1.

2.2 *Monitoring system description*

According to the standard of data monitoring for LHD machines [10] developed in the frame of internal KGHM Group project, there is a list of parameters measured on the machine.

Figure 1. Photo of investigated Haul Truck machine.

Table 1. A list of monitored parameters for haul truck.

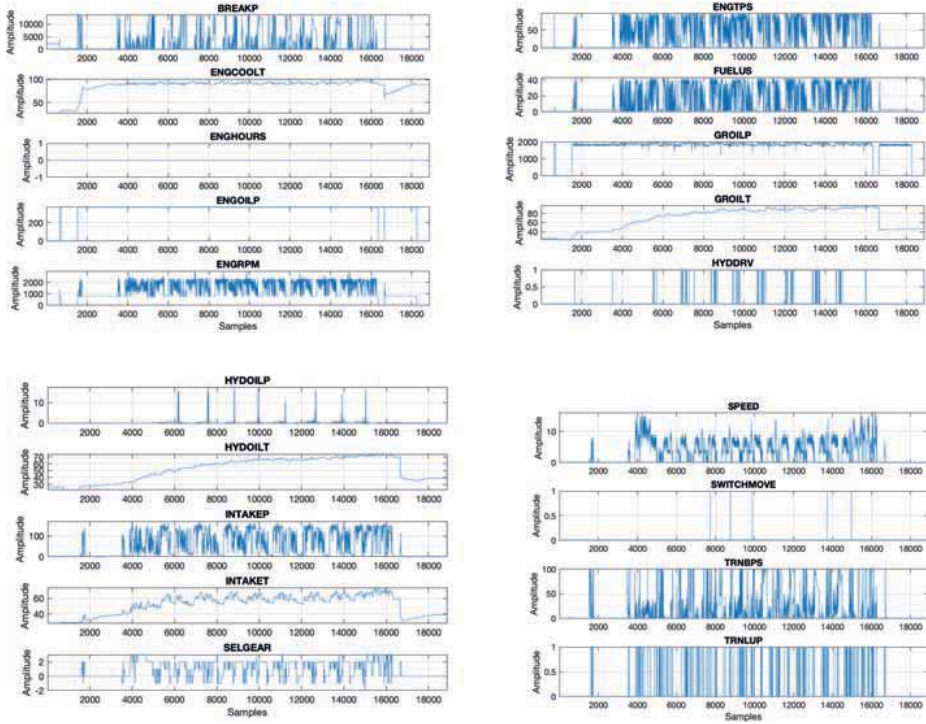| Variable name	Description
'BREAKP'	breaking pressure
'ENGCOOLT'	temperature of the cooling liquid of the internal combustion engine
'ENGHOURS'	number of operating hours of the internal combustion engine cumulatively
'ENGOILP'	oil pressure of the internal combustion engine
'ENGRPM'	engine speed
'ENGTPS'	deflection of the gas pedal
'FUELUS'	instant fuel consumption
'GROILP'	Transmission oil pressure
'GROILT'	oil temperature of transmission and torque converter
'HYDDRV'	attached additional hub drive
'HYDOILP'	pressure in the hydraulic system
'HYDOILT'	hydraulic oil temperature
'INTAKEP'	engine boost pressure
'INTAKET'	air temperature at the engine's intake
'SELGEAR'	direction and current gear
'SPEED'	average speed every 1 s
'SWITCHMOVE'	switching the direction of travel under load
'TRNBPS'	position of the brake pedal; 0–100%
'TRNLUP'	lock up on/of

Figure 2. A raw data from 1 shift—an example.

Depends on the machine type and basic or advanced version of the monitoring system, the list may contain different parameters. During the experiment, we were able to acquire 19 variables listed in Table 1. They are related to the various component, have different dynamics (low-frequency processes as temperature, high-frequency processes as pressure, etc.) and have different robustness. All data are sampled with 1 Hz.

2.3 *Exemplary data presentation*

In Fig. 2 one might see raw data acquired by the system from a regular shift in an underground mine. As mentioned, the most interesting and clear signal is in sub-plot 11 (variable called *Hyd_Oil_P*). The usage of alternative variables is not intuitive. The preliminary selection was done by mining engineers based on the physics of the machines and processes (operations). However, we look for information-based criteria for selection of variables.

3 INFORMATIVE VARIABLES SELECTION METHODOLOGY

3.1 *General description of the approach*

Extraction of information from multidimensional data from multi-channel monitoring system is a well-known problem in data analysis [11,14,15]. It could be done by selection or transformation [14–15]. In the case of selection, the most critical issue is the criterion of selection. From a signal processing perspective, searching for indicators describing the effectiveness of the haulage process is the discovery of a cyclic pattern in acquired signals. The Haul Truck (HT) is used for transport of copper ore from the vicinity of mining face (ore is provided by loader) to mining screen (unloading point, next ore is transported by the belt conveyors to the shaft). This operation is cyclic, the daily scenario may be as follow: on the

beginning of the shift, the machine is going to the mining face, after loading by LHD, the HT goes to unloading point, release ore and goes back to mining face. The whole process may take (depending on distance) c.a. from several to dozen minutes. Due to a number of machines operating in given mining departments and other factors related to "normal" operation of the underground mine, the transportation process might be disturbed for each cycle (HT must stop for a while because the loading process appeared more complicated, or unloading process is blocked due to oversized ore pieces etc.). Such disturbances mean that cycles may have some variation in time and it brings extra complexity during analysis. Anyway, the cyclic nature of the process is the basis for further analysis in this paper.

3.2 *Autocorrelation function*

Autocorrelation function (ACF) describes the correlation of a signal with a delayed copy of itself as a function of delay. In other words, it measures the similarity between observations as a function of the time lag between them. The analysis of autocorrelation might be considered as a mathematical tool for finding repeating patterns (i.e. operational cycle for haulage).

In our analysis we use the empirical autocorrelation function that for the vector of observations of the stationary process $x_1,\ldots,x_n$ for lag k is defined as:

$$\rho(k) = \frac{\gamma(k)}{\gamma(0)}, \tag{1}$$

where the $\gamma(\cdot)$ is the empirical autocovariance function defined as [13]:

$$\gamma(k) = \frac{1}{n}\sum_{i=1}^{n-k}(x_i - \overline{x})(x_{i+k} - \overline{x}), \tag{2}$$

where $\overline{x} = \frac{1}{n}\sum_{i=1}^{n}x_i$ is a sample mean.

3.3 *Clustering of autocorrelation functions*

The idea proposed here is to select (in the first stage) variables that have similar behavior as the most intuitive signal (HydOilP). So, we "cluster" all ACF function to find groups of ACFs that are very similar and very different than ACF of *HydOilP* variable. First, it was done by the visual inspection. Finally, we proposed to calculate residuals between ACF of the given variable and ACF of *HydOilP*, and for each residual signal, we calculated the sum of squared samples. One may conclude that for a smaller value of such feature, the difference between ACFs is smaller, too, that means signals are similar.

3.4 *A selection procedure*

The whole procedure is illustrated in Fig. 3. As mentioned, we rely on the assumption that the cyclic nature of the process could be estimated via ACF. If processes (as temperature) are not varying in the same way, for sure they are not suitable for the cycle estimation. The hydraulic oil pressure signal is used as a reference signal here.

Then the second phase of the procedure is based on some engineering assumptions related to knowledge about the process. It is clear, that unloading process requires a machine with a stationary position (no driving speed), and it is (for safety reason) related to usage of neutral gear (Gear = 0). To unload haul truck, there is a need to "push out" the ore from the box, so one might expect some fuel consumption (we assumed it as – minimum – 10% of max fuel consumption during the shift). For all these 3 conditions, we clear out samples for all signals (we put zeros instead of real values).

In the case when we "clear" completely signals by removing samples for predefined above rules, we remove the whole signal. Finally, we compare our reference signal with remaining signals. In this paper this comparison was visual, but it might be again energy-based criterion, the distance between vectors, etc. It will be further investigated.
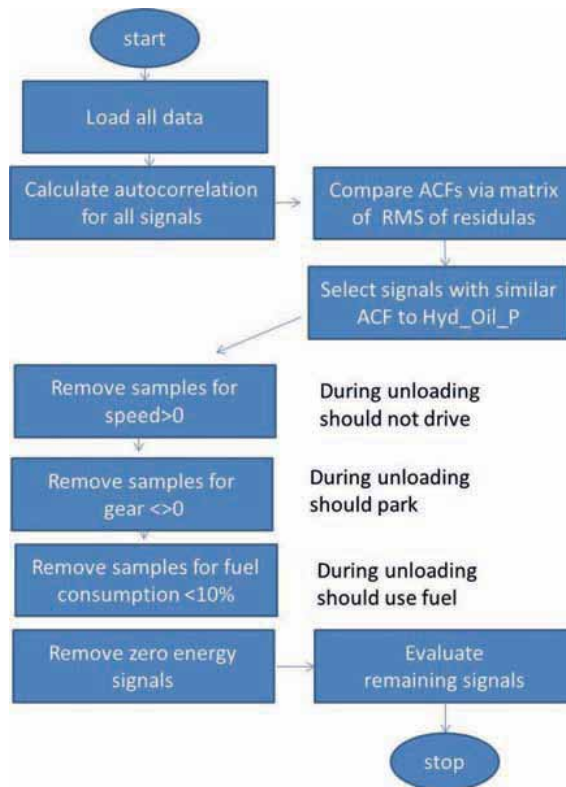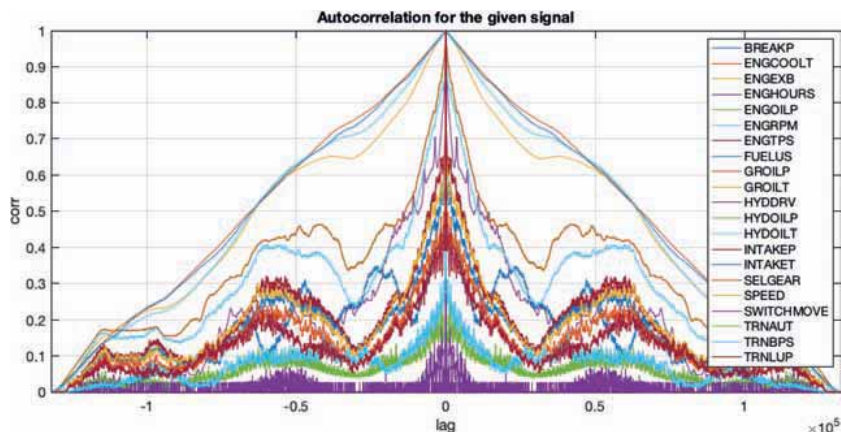
Figure 3.   A procedure for variable selection.

Figure 4.   Normalized Autocorrelation functions of all signals.

3.5   *Discussion*

It might appear that the final selection of signals will bring some redundant data. There are two possible ways: we can reduce the number of signals via selection of one of them or "fuse" data by simple aggregation to increase the power of recognition of hidden pattern. At this stage, there is no simple answer what option is better. From an implementation point of view, fewer variables are better, however, data fusion is commonly used to increase the robustness

of the algorithm. We believe that it requires more tests on the large data set and the final decision should be made on effectiveness analysis.

4 RESULTS

In this section results of the proposed procedure will be presented and discussed step by step. First, in Fig. 9 we present Normalized Autocorrelation functions of all signals. One can see that there is a group of ACF that are similar to each other however it is totally different than hydraulic oil pressure. So, a good example of such a class is a set of 4 temperature signals. Fig. 5 presents ACFs grouped into 6 class, Fig. 6 similarly as Fig. 5 shows signals plotted in such classes.

Figs. 7,8 and 9 show the results of each step of data cleaning by plotting samples fulfilling predefined conditions. First is related to removing (clearing) samples for time instances where speed is non-zero (the machine cannot drive during unloading). The second step is related to clearing samples for nonzero gear number (machine should have neutral gear, i.e. zero, during unloading). Finally, the unloading process is energy consuming, so it is assumed that fuel consumption will be high (here we assumed that will be higher than 10% of max fuel use). From Fig. 8 one might notice that several signals reveal very cyclic behavior—synchronized to the hydraulic oil pressure signal. It means that they could be used as input data for cycle estimation. In order to make data more smooth, a moving window summing up data have been applied, see Fig. 9. It has appeared that {*breakP and TRNBPS*} as well as {*FuelUs, ENGTPS, intakeP*} are significantly interdependent. It could be expected as *Break Pressure* and *position of brake pedal* are linearly dependent; similarly as *fuel consumption, engine boost pressure* and *deflection of the gas pedal.* So it makes the possible further simplification of the problem.
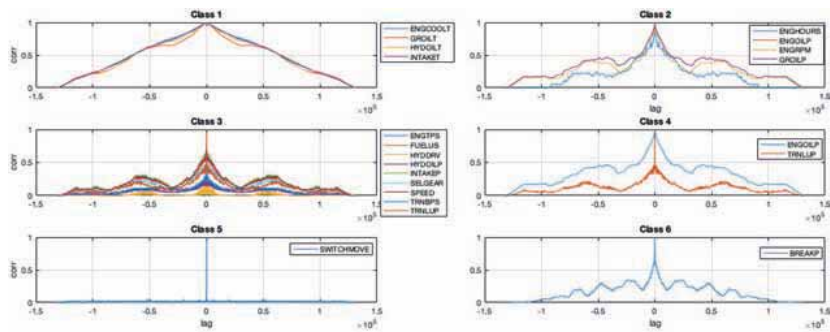

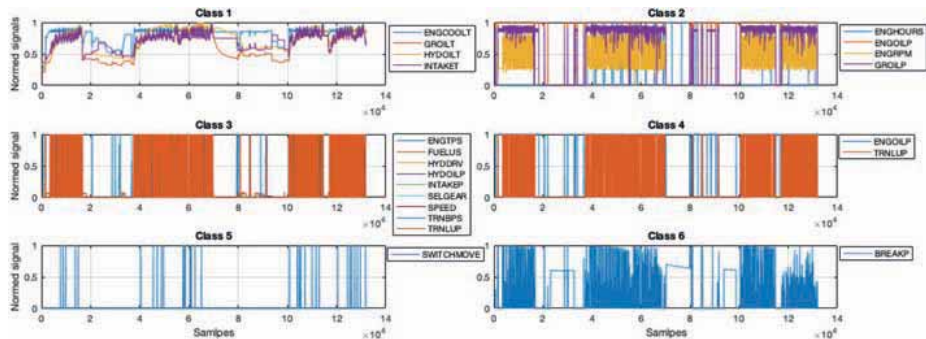Figure 5.   Results of ACF clustering (6 classes).

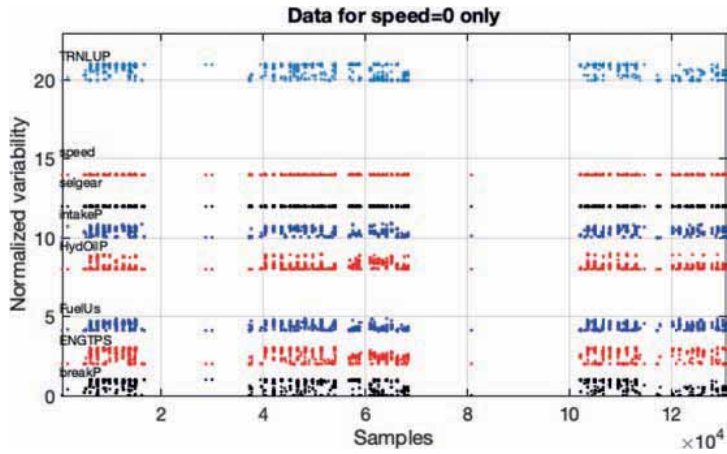Figure 6.   Plots of clustered signals.

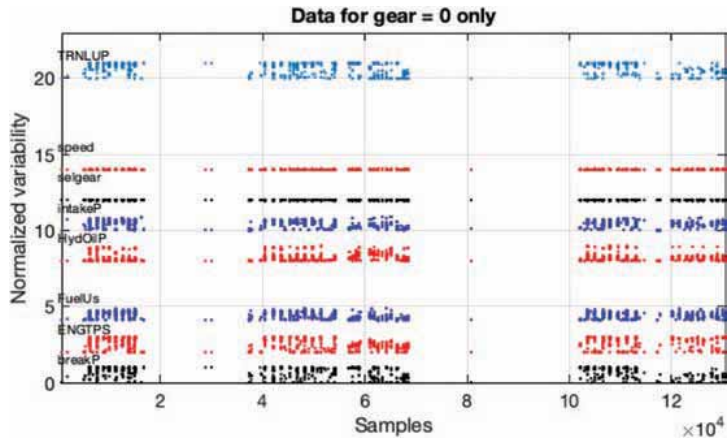Figure 7.   Cleaning the signal by removing samples for speed<>0.

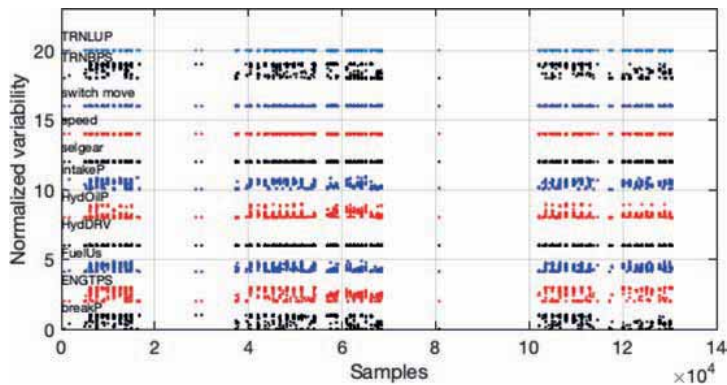Figure 8.   Cleaning the signal by removing samples for gear <>0.

Figure 9.   Final cleaning of data for fuel consumption >10% max fuel consumption.
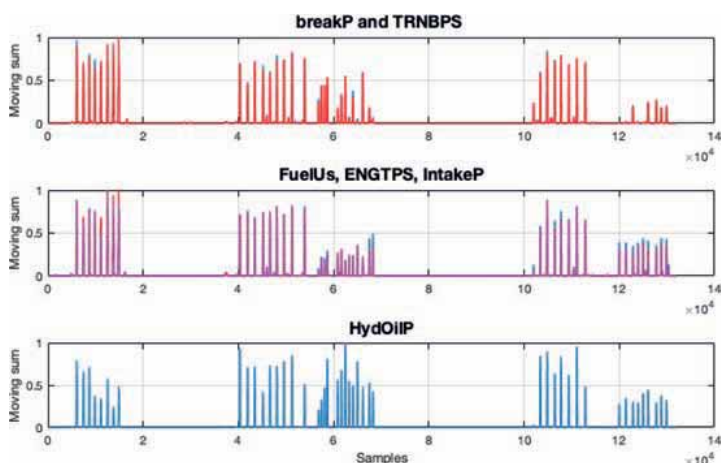
Figure 10.   Final picture of variable selection.

5   CONCLUSIONS

In the paper, a procedure for variable selection for operational cycles identification has been proposed. The basic idea is simple, as we expect to have cyclic nature of the process, we should receive some repetitive pattern in the observed data. It is clearly seen in hydraulic oil pressure data (*HydOilP*). However, due to extremely harsh condition in the mine, this measurement channel is frequently broken and there is a need to substitute this variable. So, to find some expected cyclic pattern we decided to use simple tool for dependency analysis in the data, i.e. autocorrelation function. Similarities in autocorrelation functions (ACF) estimated for all variables are valuated and based on simple energetic criterion (RMS of residual signal between *HydOilP* and others) preselection of variables has been done. After this stage we obtained 11 variables with similar ACFs. It should be highlighted, that similar ACF does not mean an exact similarity in the signal—they may be shifted in time and have the same cyclic nature. So, the next step of processing is needed.

The second phase of the procedure is based on some engineering assumptions related to the knowledge about the process. It is clear, that the unloading process requires a machine with a stationary position (no driving speed), and it is (for safety reason) related to the usage of neutral gear (Gear = 0). To unload a haul truck, there is a need to "push out" the ore from the box, so one might expect some fuel consumption (we assumed it as >10% of max fuel consumption during the shift). Such simple 3 rules "clear" the remaining channels significantly and it allows to notice that {*breakP and TRNBPS*} as well as {*FuelUs, ENGTPS,intakeP*} are interdependent. Finally, it seems to be obvious*: Break Pressure* and *position of brake pedal* are linearly dependent; similarly as *fuel consumption, engine boost pressure* and *deflection of the gas pedal*.

So finally we might conclude that to identify operational regimes of haul truck one need following variables: *speed, gear number* and one of {*breakP, TRNBPS, FuelUs, ENGTPS, INTAKEP*} or ideally *HydOilP*. To improve the robustness of the recognition procedure data fusion approach could be used that will be the next research task for our team. Comparative study and effectiveness will be also tested on a wider population of signals.

REFERENCES

[1] McBain, J., Timusk, M.: Software Architecture for Condition Monitoring of Mobile Underground Mining Machinery A framework Extensible to Intelligent Signal Processing and Analysis. In: 2012 *IEEE Conference on Prognostics and Health Management, PHM*, pp. 1–12 (2012), doi:10.1109/ ICPHM.2012.629954.

[2] Kohler, J.L., et al.: On-board electrical diagnostic system to improve the availability of continuous mining machines. *Mining Engineering* 46(8), 987–990 (1994).

[3] Thompson, R.J. et al.: Mine road maintenance management using haul truck response measurements. *Institution of Mining and Metallurgy. Transactions. Section A: Mining Technology* 115(4), 123–128 (2006).

[4] Kicki, J. & Dyczko, A.: The concept of automation and monitoring of the production process in an underground mine. In: New Techniques and Technologies in Mining—Proceedings of the School of Underground Mining, pp. 245–253 (2010).

[5] Gustafson A., Schunnesson H., Galar D., Kumar U. The influence of the operating environment on manual and automated load-haul-dump machines: a fault tree analysis. International Journal of Mining, Reclamation and Environment, Vol. 27, 2013, p. 75–87.

[6] Wodecki, J. et al.: Technical condition change detection using Anderson–Darling statistic approach for LHD machines–engine overheating problem 2018 International Journal of Mining, Reclamation and Environment 32(6), pp. 392–400.

[7] Zimroz R., Wodecki J., Król R., Andrzejewski M., Śliwiński P., Stefaniak P. Self-propelled mining machine monitoring system-data validation, processing and analysis. In: Drebenstedt C., Singhal R. (eds) *Mine Planning and Equipment Selection*. Springer, Cham, 2014, p. 1285–1294.

[8] Kępski, P., Barszcz, T.: Validation of vibration signals for diagnostics of mining machinery. *Diagnostyka* 4(64), 25–30 (2012).

[9] Stefaniak P. et al.: An Effectiveness Indicator for a Mining Loader Based on the Pressure Signal Measured at a Bucket's Hydraulic Cylinder *Procedia Earth and Planetary Science* 15, 797–805.

[10] Dyczko A., et al.: Koncepcja monitoringu i transmisji danych technologicznych pracy samojezdnych maszyn górniczych w KGHM Polska Miedź S.A. unpublished technical report prepared for KGHM PM SA (in Polish).

[11] Stefaniak P. et al. (2016), Multidimensional Signal Analysis for Technical Condition, Operation and Performance Understanding of Heavy Duty Mining Machines. In: Chaari F., Zimroz R., Bartelmus W., Haddar M. (eds) *Advances in Condition Monitoring of Machinery in Non-Stationary Operations. CMMNO 2014. Applied Condition Monitoring*, vol 4. Springer, Cham.

[12] Wyłomańska, A. & Zimroz, R. Signal segmentation for operational regimes detection of heavy duty mining mobile machines—a statistical approach *Diagnostyka* 2014 Vol. 15, No. 2.

[13] P.J. Brockwell, R.A. Davis, Introduction to Time Series and Forecasting, Springer, 2002.

[14] Bartkowiak, A., Zimroz, R. Dimensionality reduction via variables selection—Linear and nonlinear approaches with application to vibration-based condition monitoring of planetary gearbox 2014 Applied Acoustics 77, pp. 169–177.

[15] Bartkowiak, A., Zimroz, R. Data dimension reduction and visualization with application to multidimensional gearbox diagnostics data: Comparison of several methods 2012 Solid State Phenomena 180, pp. 177–184.

An integrated simulation model for opportunistic maintenance

O. Golbasi
Middle East Technical University, Ankara, Turkey

M. Olmez Turan
Colorado School of Mines, Golden, USA

C. Karpuz
Middle East Technical University, Ankara, Turkey

ABSTRACT: Maintenance policies embody various work packages with different intention of implementation. When and how to perform these work packages for which equipment is always a problem that needs to be solved specific to the machine itself. Since a surface mining operation is carried out generally in demanding working conditions and multiple equipment hold an operational dependency to accomplish a production cycle, it may be tough to constitute the scope and content of the related maintenance policy. Although the literature on maintenance modelling commonly concentrates on corrective repairing and preventive replacement, opportunistic maintenance that investigates whether an opportunity exists for the proactive maintenance of a running component in case of failure of another dependent component is not discussed as required. Indeed, opportunistic maintenance is practically observed at mine sites. In this basis, the current study aims to develop an integrated simulation model that considers mathematical interaction of corrective, preventive and opportunistic maintenance, and their effects on stochastic uptime and downtime behavior of systems. A numerical example applied for multiple shovels is also provided to highlight the outcomes of the developed model.

1 INTRODUCTION

Maintenance policy modelling may be defined as obtaining and comparing feasible solutions in the policy content with an objective function that intends to maximize equipment availability or minimize direct, indirect or combinational cost factors. In such a model, the model constraints may cover various factors such as, inventory limits, budget, reliability threshold, and production target. At this point, the model scope highly depends on the type of equipment to be maintained, and the maintenance activities that need to be practical and beneficial against the deterioration in equipment components.

The relevant literature generally classifies maintenance implementations in two main groups as corrective and preventive. Corrective maintenance has a run to failure strategy, and be applied after failure occurrence. It may be divided into two subcategories as immediate and deferred corrective maintenance. They are valid for the cases where the negative consequences of a component failure should be removed immediately or maintenance may be delayed since the damaged component is not operationally critical, respectively. On the other hand, preventive maintenance requires a scheduled and/or technological interference for the upcoming failures to prevent both component and production damages beforehand. Maintenance implementation with predetermined time intervals, condition-based maintenance, and opportunistic maintenance are considered as the branches of preventive maintenance. In this basis, preventive repairing or replacement of specific components in predetermined time intervals may be financially feasible in some circumstances. On the other hand, some

operational symptoms of components that may be obtained from vibration, pressure and noise may be good indicators of an impending failure; and condition-monitoring system may be conformed to such a condition. In another case, corrective repairing or replacement of a component may give an opportunity for proactive control and maintenance of the other components. As it is understood from the variety in maintenance work packages, different equipment may require different maintenance policies, which serve in compliance with the working environment of equipment, and need to be applicable in financial and practical manner.

In this sense, the current study correlates the stochastic operating and maintenance behaviors of a system with an integrated maintenance model including corrective maintenance, opportunistic maintenance and regular preventive inspections. The developed model allows examining the effects of changeable parameters in a maintenance policy to the downtime attitude of the system.

2 THE DEVELOPED MODEL

2.1 General methodology

The model evaluates mutual interactions between the downtime and uptime behaviors of subsystems in operation, and manages lifetime and maintenance duration dataflow to decide one or multiple of corrective, preventive, and opportunistic maintenance activities in the actualized timeframe. In the model, various modules run for the integration of opportunistic maintenance to a policy that activates a proactive maintenance for deteriorated subsystems in case of corrective maintenance of any other subsystem failing during working hours. A decision is given for the subsystem deterioration considering the expert opinions such that a defect giving any sign for a forthcoming failure is considered as detectable during the inspections if this signing period overlaps with any nearby inspection duration. For a better mimicking of system maintenance, administrative breaks were also considered in the model. The general simulation methodology can be viewed in Figure 1.
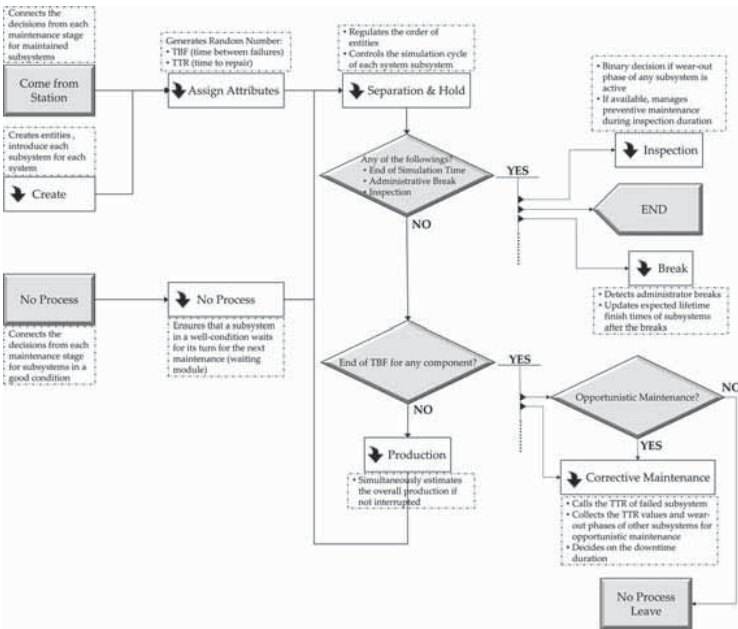

Figure 1. Methodology of the simulation model.

2.2   *Steps of the model*

A mining operation requires coordinated movements of different machineries with an intention of fulfilling any of drilling, blasting, loading, and hauling activities. Deterioration of components/subsystems in an equipment may change depending on the operation type where it is involved. Therefore, characterization of a mining equipment as a whole is not practical. A system needs to be decomposed into its subsystem; and failure records should be clustered regarding the subsystems. A subsystem is a collection of multiple components that gathers to perform a specific task in a system. Therefore, any exposure to failure and the related failure modes may be explained more explicitly following a failure and/or maintenance data classification based on the subsystems. The current model uses random variables to evaluate functional conditions of subsystems anywhere in the timeframe by using a probabilistic approach. For instance, in a specific simulation time, one subsystem may be detected as failed where another subsystem may be in a deterioration, i.e. wear-out, period without any complete failure. In such a case, failure of a subsystem may create an opportunistic time span to maintain the deteriorated but not failed subsystems. If there is not such an opportunity, the same deteriorated subsystem may be diagnosed during regular inspections. In this basis, the following model steps evaluate the functional abilities of subsystems, and give the resultant maintenance decisions by using discrete event simulation:

  i. Generating random numbers: They are generated from the probability density functions of surviving, i.e. time between failures (TBF), and repairing, i.e. time to repair (TTR), durations. These numeric values provide a stochastic uptime and downtime characterization in compliance with the natural operating behavior of system.
 ii. Ordering subsystems: For each simulation time, subsystems are evaluated and ordered considering their failure conditions since opportunistic maintenance can only take place once another subsystem fails. Therefore, subsystems with a near-failure condition is located at the top of list with a priority. This module also ensures the completion of simulation cycle for all subsystems for the active simulation time to provide a holistic and complete view on the system.
iii. Checking deterministic thresholds: Three main types of deterministic thresholds are used: Target simulation time, inspection points, and administrative breaks. In case that any of these values is arrived at the active simulation time, the related modules are activated. The simulation is ended if the active simulation time is equal to target simulation time. In any inspection, the subsystems with a probability of being detected as deteriorated during the inspection duration are revealed, and these subsystems are preventively maintained. In case of any preventive maintenance, a new random TBF is generated for the component. Administration breaks are the scheduled breaks where the production is interrupted due to shift changes or any other administrative decision.
 iv. Evaluating subsystem failure period: If the active simulation time does not give any sign about the deterministic thresholds discussed above and if a failure is detected during anytime in the operation, this period is evaluated not just for the failed component but also for the other subsystems in an operating condition. Because, the production interruption caused by a subsystem failure may create an opportunistic time span for the proactive maintenance of other subsystems. Randomly generated TTR value of the failed subsystem is compared with the random TTR values of other subsystems. If any subsystem is in a wear-out period and if it is decided that proactive maintenance for that subsystem can be performed within the assigned corrective maintenance duration, then an opportunistic maintenance is applied preventively. Any subsystem exposed to either of preventive (proactive) and corrective maintenance gets a new random TBF right after the maintenance activity.
  v. Estimating production amount: System production is interrupted in a) regular inspections, b) subsystem failures that require corrective maintenance during normal operation time, and c) administrative breaks. Other than these conditions, system is assumed to have a production with a specific cycle time. Length of the cycle time and production amount are introduced in compliance with the nature of production. Discrete production amounts are gathered cumulatively to find out the total production throughout the target simulation time.

3 NUMERIC EXAMPLE

3.1 *Input dataset*

The proposed model was implemented for multiple cable shovels operating in an opencast mine. The datasets were retrieved from a study by Roy et al. (2001), and include reliability and maintenance probability distribution functions for the subsystems of three shovels in the same mine (Table 1). It was stated in the research that a total number of 224, 200, and 154 failures were observed for three shovels for an operation period of 2 years. Initially, the shovels were decomposed into subsystems as air system (SHA), boom mechanism (SHB), crowd mechanism (SHC), dipper system (SHD), electrical system (SHE), hoist mechanism (SHH), lubrication system (SHL), magneto torque system (SHM), operator cabin and structure (SHO), power take-off unit (SHP), steering mechanism (SHS), and undercarriage unit (SHU). Among the identified subsystems, SHA, SHC, SHD, SHE and SHH were determined to be the main contributors to the failure breakdowns. Therefore, reliability and maintenance data of the remaining subsystems were grouped under other subsystems (OTH).

In the detection of subsystems to be maintained preventively in the regular inspections, delay-time concept is used. This concept assumes that a component or subsystem in a wear-out period may give some indications for the forthcoming failure, such as anomalies in sound, vibration or pressure levels or some mechanical impairments that may cause a failure in a near future. If such an indication is observed, it is assumed that the related defect can be detected during an inspection by the maintenance crew, and maintained preventively without waiting for the lifetime finish, i.e. failure, time. These kinds of indications can be captured by an experienced maintenance crew or condition-monitoring systems if available. In this study, some percentile numbers were assumed (Table 2) by comparing with the values in a study by Golbasi

Table 1. Shovel TBF and TTR datasets to be used in the simulation.

| | Code | Time Between Failure (TBF) | | Time to Repair (TTR) | |
		Best-fit	Parameters	Best-fit	Parameters
Shovel 1	SHA	Weibull	$\beta = 1.169$; $\eta = 522.9$	Lognormal	$\mu = 10.14$; $\sigma = 8.26$
	SHC	Exponential	$\lambda = 880.3$	Exponential	$\lambda = 32.5$
	SHD	Exponential	$\lambda = 60.16$	Lognormal	$\mu = 11.12$; $\sigma = 17.36$
	SHE	Weibull	$\beta = 0.871$; $\eta = 111.1$	Lognormal	$\mu = 28.73$; $\sigma = 62.76$
	SHH	Weibull	$\beta = 1.684$; $\eta = 485$	Lognormal	$\mu = 13.3$; $\sigma = 15.91$
	OTH	Weibull	$\beta = 0.856$; $\eta = 191.3$	Lognormal	$\mu = 26.09$; $\sigma = 45.08$
Shovel 2	SHA	Exponential	$\lambda = 384.3$	Exponential	$\lambda = 16$
	SHC	Weibull	$\beta = 1.562$; $\eta = 146.83$	Lognormal	$\mu = 26.92$; $\sigma = 47.8$
	SHD	Weibull	$\beta = 1.115$; $\eta = 57.17$	Lognormal	$\mu = 10.93$; $\sigma = 13.58$
	SHE	Weibull	$\beta = 1.119$; $\eta = 87.64$	Lognormal	$\mu = 17.25$; $\sigma = 19.34$
	SHH	Weibull	$\beta = 1.226$; $\eta = 130.44$	Exponential	$\lambda = 12.36$
	OTH	Exponential	$\lambda = 116.3$	Lognormal	$\mu = 20.71$; $\sigma = 38.23$
Shovel-3	SHA	Weibull	$\beta = 1.177$; $\eta = 506.14$	Lognormal	$\mu = 18.54$; $\sigma = 46.45$
	SHC	Exponential	$\lambda = 220.6$	Lognormal	$\mu = 46.79$; $\sigma = 102.6$
	SHD	Weibull	$\beta = 1.108$; $\eta = 79.23$	Lognormal	$\mu = 15.79$; $\sigma = 25.28$
	SHE	Exponential	$\lambda = 96.5$	Lognormal	$\mu = 35.33$; $\sigma = 82.94$
	SHH	Weibull	$\beta = 1.029$; $\eta = 206.43$	Lognormal	$\mu = 17.76$; $\sigma = 23.75$
	OTH	Weibull	$\beta = 1.361$; $\eta = 301.16$	Exponential	$\lambda = 76.5$

Table 2. Assumed deterioration threshold values for the Shovel subsystems.

Subsystems	SHA	SHC	SHD	SHE	SHH	OTH
Threshold values (%)	75	90	90	95	90	90

and Demirel (2017). The subsystems give an alert in the model after the percentile proportion of its assigned random lifetime, i.e. threshold values, is passed over in the active simulation time.

3.2 *Simulation results for the three shovels operating independently*

As discussed previously, the simulation simultaneously checks the corrective, preventive, and opportunistic maintenance conditions of subsystems, and makes an evaluation on their repairing and the future operating performances if any maintenance is decided in single or multiple subsystem. In case that a subsystem is detected not to need any preventive maintenance during an inspection, a regular inspection is performed. This regular inspection turns subsystem into as bad as old condition. It means that failure probability just before and after inspection for that subsystem will be equal to each other for that subsystem. Figures 2 and 3 illustrate the sample views of the monitoring module that reveals the comparative conditions of shovel subsystems during inspection and working hours, respectively. Figure 2 shows that subsystems in yellow are having a preventive maintenance in inspection since they are in a wear-out period, and will turn to a failure if not interfered. As seen in Figure 3, corrective maintenance for Shovel-1 SHE gives an opportunity for proactive maintenance of SHD in a deterioration period.

The algorithm also allows understanding the effect of time between inspections, i.e. inspection interval, to corrective maintenance profile of the system. It should be noticed that
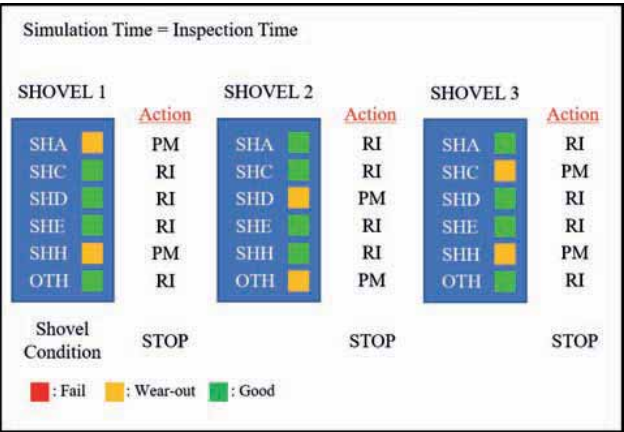

Figure 2. Maintenance behavior of subsystems during inspection hours.
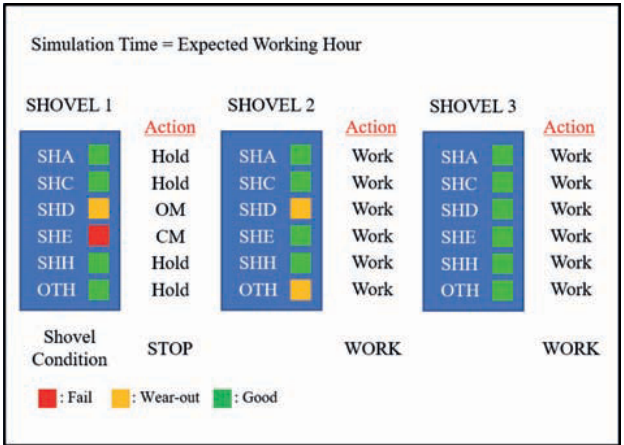

Figure 3. Maintenance behavior of subsystems during working hours.

elimination of regular inspections from maintenance policies or increasing the inspection intervals might cause a remarkable jump in the deterioration and failure rates of components and subsystems. Correlation between inspection intervals and corrective maintenance statistics for the shovel subsystems can be investigated in Table 3.

Sensitivity of inspection intervals to corrective maintenance, given in Table 3, was also explained by nonlinear regression equations in Table 4, and plotted in Figures 4 and 5. In the equations, x, y, and z refer to the time between inspections-TBI (h), total corrective repairing time (h), and total corrective repairing number of the shovels, respectively. In addition, MSE and S stand for the mean sum of squared errors and the standard error that are used to measure the accuracy of fitted equation. Ranges of the equation parameters, i.e. the equation constants Pr1 and Pr2, for the upper and lower bounds for 95% confidence interval were also given in the table. This ranges help to identify a forecasting area instead of a single point in the line, as shown in Figures 4 and 5 with the dashed lines. The plotted figures reveal that the length of inspection interval has a remarkable effect on the failure behaviors of subsystems.

Table 3. Effect of time between inspections on the corrective maintenance profile of the subsystems.

| | Subsystems | Time between Inspections (h) | | | | |
		40	80	120	160	200
Shovel 1 — Repair Time (h)	SHA	2.6	5.4	6.8	7.6	9.2
	SHC	38.0	64.9	89.0	100.6	107.0
	SHD	201.6	239.1	248.3	258.5	258.4
	SHE	264.4	308.1	327.0	334.7	348.0
	SHH	19.7	40.7	63.0	70.1	71.3
	OTH	132.5	172.2	187.9	190.7	193.7
Shovel 1 — Repair Number	SHA	0.7	1.4	1.8	2.0	2.4
	SHC	2.3	3.8	5.0	5.6	6.0
	SHD	43.8	51.6	53.4	55.3	55.4
	SHE	24.8	29.0	30.2	30.7	31.3
	SHH	1.8	3.8	5.2	5.9	6.2
	OTH	23.5	29.9	32.4	33.0	33.6
Shovel 2 — Repair Time (h)	SHA	23.1	39.5	48.5	58.5	62.8
	SHC	96.8	130.8	146.5	151.0	156.1
	SHD	269.2	298.1	309.8	314.2	319.1
	SHE	250.6	276.1	282.1	283.8	285.0
	SHH	123.7	151.5	163.5	167.7	170.9
	OTH	213.5	240.2	248.8	257.1	256.9
Shovel 2 — Repair Number	SHA	3.1	5.0	5.9	7.0	7.4
	SHC	16.5	21.7	24.0	24.7	25.4
	SHD	65.5	72.5	75.3	76.4	77.1
	SHE	57.7	63.7	65.0	65.3	65.7
	SHH	27.1	32.8	34.9	35.8	36.3
	OTH	54.9	61.8	63.7	65.4	65.8
Shovel 3 — Repair Time (h)	SHA	14.8	27.1	32.8	38.6	41.8
	SHC	110.5	133.1	142.5	147.7	146.1
	SHD	279.0	317.5	332.2	338.0	346.6
	SHE	219.6	236.8	244.1	245.7	246.0
	SHH	24.7	38.9	43.1	45.6	46.4
	OTH	191.1	292.5	334.1	359.4	376.5
Shovel 3 — Repair Number	SHA	3.0	5.0	5.8	6.6	7.1
	SHC	24.7	29.5	31.5	32.7	32.3
	SHD	47.2	52.9	55.3	56.1	57.1
	SHE	43.9	47.3	48.8	48.9	48.9
	SHH	5.8	9.0	9.9	10.3	10.5
	OTH	11.7	17.9	20.2	21.5	22.3

Table 4. Nonlinear regression equations for the corrective repairing behaviors.

|	Equation	Model accuracy	Parameters in 95% CI
Shovel 1	$y = 1170.97x^{-6.22/x}$	MSE:35.4792 S:5.9564	Pr1: (1144.49, 1198.07) Pr2: (−6.70, −5.74)
	$z = 146.85e^{-16.60/x}$	MSE:0.08 S:0.29	Pr1: (145.93, 147.78) Pr2: (−17.13, −16.06)
Shovel 2	$y = 1348.27/(x + 15.12)$	MSE:6.11 S:2.47	Pr1: (1339.47, 1357.18) Pr2: (14.44, 15.81)
	$z = 304.51x − 3.231/x$	MSE:3.67 S:1.92	Pr1: (297.22, 311.97) Pr2: (−3.71, −2.76)
Shovel 3	$y = 1353.16x/(x + 24.14)$	MSE:27.26 S:5.22	Pr1: (1331.52, 1375.48) Pr2: (22.23, 26.15)
	$z = 194.27x/(x + 16.72)$	MSE:1.14 S:1.07	Pr1: (190.41, 198.28) Pr2: (14.61, 18.96)
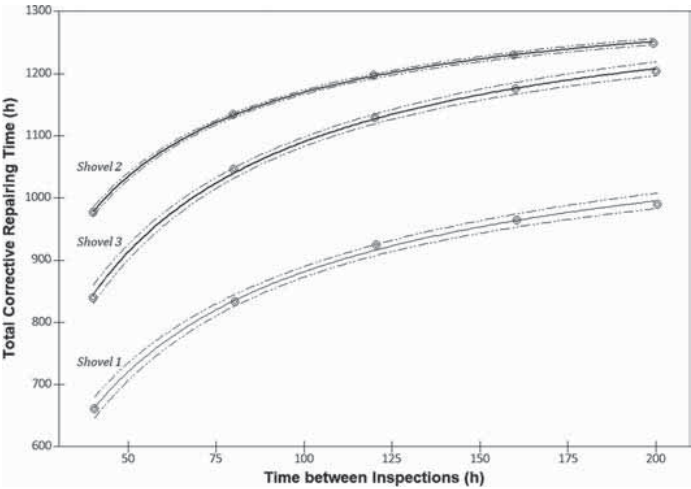
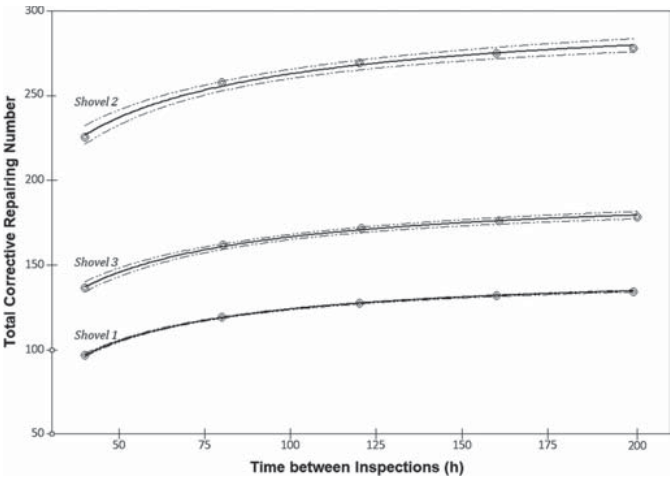Figure 4. Effect of time between inspections to total corrective maintenance time.

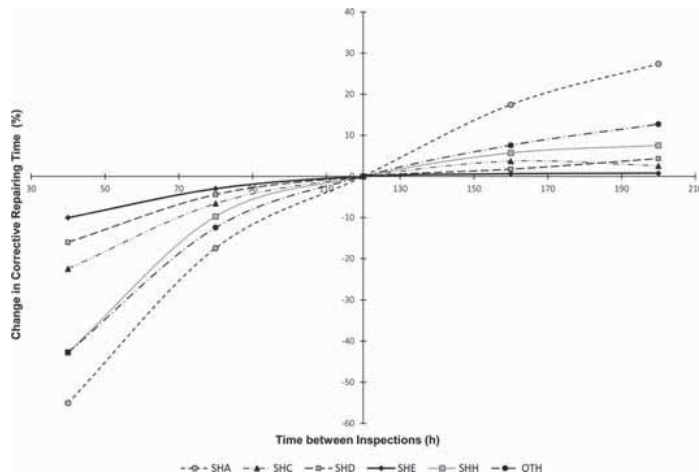Figure 5. Effect of time between inspections to total corrective maintenance number.

Figure 6.   Sensitivity of total corrective maintenance time of shovel 3 subsystems to inspection interval.

Excessive failure occurrences cause frequent interruption in production and deterioration of system components before their expected useful lifetimes. The simulation was performed up to an inspection interval of 200 h. The generated equations can be used to make a forecasting for higher inspection intervals.

The simulation results also help to understand sensitivity of subsystems to the changing inspection intervals. Figure 6 presents a representative graph for the subsystems of Shovel 3. Inspection interval of 120 h was taken as a reference point; and increase or decrease in the total corrective maintenance times for different inspection intervals were shown comparatively in the figure. It is concluded from the graph that corrective maintenance profiles of SHA and SHE are the most and the least sensitive to the changes in inspection intervals, respectively.

4   CONCLUSION

Effectiveness of a maintenance policy reserves a high uncertainty stemming from the stochastic lifetime behaviors of components and subsystems in the maintained systems. In addition, what to implement in planned and unplanned activities may change the financial and operational benefit of the maintenance policy. This paper describes a simulation model that integrates corrective, preventive and opportunistic maintenance to the stochastic repairing and operating behavior of a working system. Once the integration was achieved, the model was tested for different inspection intervals since inspections are critical in mines especially for operationally important loading and hauling machines. In this basis, the model was tested for three shovels. Operating and repairing stochasticity in the shovel subsystems was introduced to the model for a better understanding of system behavior. The simulation outputs were used to reveal the sensitivity of subsystems to the changeable inspection intervals. In a sample sensitivity graph plotted for Shovel 3, it was seen that SHA shows the highest sensitivity to inspection intervals where it is the least for SHE. Effect of opportunistic maintenance to the overall maintenance cost will be considered in a future study.

REFERENCES

Gölbaşı, O. & Demirel, N. 2017. A cost-effective simulation algorithm for inspection interval optimization: An application to mining equipment. *Computers and Industrial Engineering*, *113*, 525–540. https://doi.org/10.1016/j.cie.2017.09.002.

Roy, S.K., Bhattacharyya, M.M., & Naikan, V.N.A. 2001. Maintainability and reliability analysis of a fleet of shovels. *Mining Technology*, *110*(3), 163–171. https://doi.org/10.1179/mnt.2001.110.3.163.

Approach of mining equipment performance with simulation of the use of autonomous trucks

W.S. Felsch Jr.
Federal University of Ouro Preto, Brazil
CSN Mining, Brazil

A.F. Oliveira & C.E.A. Ortiz
Federal University of Ouro Preto, Brazil

ABSTRACT: The research has focused on evaluating different mine scenarios using good practices of operational improvements with the use of autonomous equipment. The study was developed at Casa de Pedra Mine, located in Brazil. The data was extracted from the electronic dispatch system and a software simulator of mine operations was used. A simulation was developed with the scenario of autonomous transport operation, with the objective of comparing the benefits of technology with the traditional scenario using operators. The productivity of the autonomous system increased by an average of 6.4% to 15.6% and the effective use of the transport fleet increased from 3% to 7% The simulation allows the verification of effective gains in the transport fleet. The Autonomous Haulage System (AHS) has a relatively high cost, so it is necessary to carry out a financial feasibility study in order to verify the effectiveness of these equipment in each type of mine.

1 INTRODUCTION

The demands for increased competitiveness, associated with the adoption of new technologies and knowledge, are increasingly common factors in companies and organizations of all segments. In the specific case of mining employment, increased productivity and decreased costs are possible whenever new knowledge and techniques are introduced for the execution of work.

At the same time, security has become more and more paramount in the face of mining operations. In this scenario, there are opportunities to expand automation to the most critical and costly operations for the mining industry.

Automation is related to operations where human interference is minimal or not present, thus being more stable, safe and continuous processes. The automation in mining operations consists in the control of operations at a safe distance through joysticks and cameras and, in the case of transportation of materials, autonomous operations where a computer controls the equipment through specialized software. The most relevant benefit would be the withdrawal of people from potential areas of risk in mining.

One of the first areas being explored as a candidate for automation in an open pit mine operation is that of mine haulage trucks. AHS trucks are receiving increased attention from the industry, with both Komatsu and Caterpillar as leading manufacturers of haulage trucks creating the first systems being used in mining (Parreira, 2013).

In the field of mining operations, the processes of greatest interest to automate are drilling, loading and the material transport system. Self-propelled drills and trucks are being used in large mines and have positive results related to increased productivity, increased utilization, shorter downtime, and increased operational safety. In material transport, Rivera (2014) estimates that the productivity gain for autonomous operations can be up to 20% and the

equipment utilization gains are between 10–20%. For the same author, the expectation is that the use of autonomous trucks will also reduce operating costs and extend the life of some components such as the braking system and tires and reduce fuel consumption and gas emissions.

In addition to the gains related to equipment and operation, the automation of the transport system also reduces the losses associated with human factors by overlapping the variability of each operator's equipment, shutdowns due to physiological needs, shift changes and absenteeism. In this way, the operation becomes more continuous, stable and safe.

Many parameters can affect the efficiency of the fleet in open pit mining, such as: (Australian Gov, 2010; Curi et al., 2013): mine plan and mine layout; speed, payload and cycle time; tire wear and rolling resistance; age and maintenance of the vehicles; dump site design; idle time; engine operating parameters and transmission shift patterns;

According to Baloo (2008), and to Curi et al., (2013), the mine haulage truck selection was based on the following criteria: Loading tool match required for mining ore and waste; availability of capital and delivery dates; productivity rate to achieve the mine plan; pit geometry and haulage routes.

Mines with design problems, access maintenance conditions, crossings and excess auxiliary equipment would probably not be able to obtain the indicated gains stipulated in the initial project of implantation of autonomous trucks. Pre-analysis of mine conditions is necessary to maximize equipment performance, avoiding unnecessary downtime.

Figure 1 identifies the factors that most impact on productivity of mine load and transport equipment (machine, administration and operation factor), according to a survey conducted in North America (2013 – M&T Magazine apud Curi et.Al.):

According to the research data, the operation factors "Disobeying rules", "Inattention" and "Malpractice" amount to 48% of the reasons of low productivity listed and are directly related to the monitoring and guidance of the activities carried out and with the technical expertise of the drivers of the equipment.

How a person drives will differ according to his or her skills, abilities, motivation, chemical influences, etc. These differences may account for a decrease in work performance, and/or an increase in operational costs and number of accidents (Clarke et al, 1999).

According to Rasmussen (1997), by virtue of the dynamics of the current working world, the human-machine system suffers the stress of intense rhythms of technological modifications, competitive markets and pressures from different backgrounds in the workplace.

Knowledge about position and speed of the vehicle (especially relative to other vehicles) can prevent accidents and reduce the cost of maintenance and replacement. While driverless
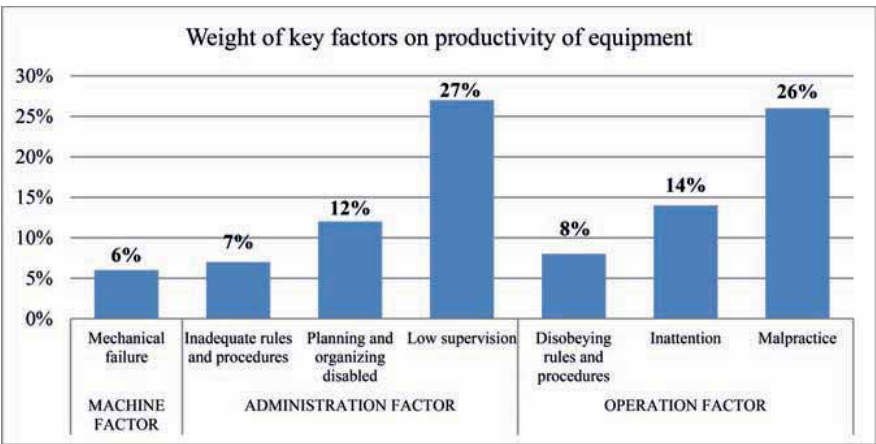

Figure 1. Percentages relating to weights of key factors that impact directly the productivity of the equipment.

haulage trucks are not immune to breakdowns, increased consistency and scheduled maintenance will improve the lifetime of machine components, leading to longer periods between maintenance, and so, costs associated with maintenance will decline. Lost production can be minimized or eliminated as unpredicted breakdown frequency will also decline (Bennink, 2008).

To predict future results, it is important to know the degree to which an autonomous haulage system can approach or exceed a manual system. As a result, simulation softwares can be used to help predict benchmarked KPIs as well as discover new KPIs that might be better at measuring future changes with new technology.

2 LITERATURE REVIEW

Simulation has become a useful and versatile tool for analyzing, through a computer, the behavior of complex systems involving several variables. Prado (2014) states that "simulation is the technique of solving a problem by analyzing a model that describes the behavior of the system using a digital computer." In the same line of reasoning, Cassandras & Lafortune (2010) says that the term simulation can be understood as the process of designing and creating a computer model of the actual or proposed system, with the purpose of conducting numerical experiments to provide a better understanding of the behavior of the system for a given set of conditions.

For Sakurada & Miyake (2009), discrete event simulation (DES) encompasses the study of simulation models whose variables change state instantaneously at specific points of time, in contrast to continuous models whose variables can change state continuously over time.

Sturgul (2001) also highlighted important applications of simulation in mining operations for open pit mines: ore handling; fleet dimensioning; loading and transport; allocation of equipment; among others.

Parreira (2013) notes that the conventional transport fleet in a mine can be adapted to an autonomous operating system. However, for this to happen it is necessary to invest in a wireless network and digital mapping of the mine, as well as precision GPS systems in each transport equipment.

Trucks with autonomous technology are equipped with high precision GPS systems, so we can track their position in real time and manage them from the control room. They are also equipped with wireless communication systems, which allow a continuous flow of information with the control room. The equipment has obstacle detection sensors, allowing the detection of the presence of other equipment and people working around it and judging in which case it should slow down or stop completely (Rivera, 2014).

Through the use of a simulation software, the authors Parreira and Meech (2012) applied the simulation in an open pit to compare some performance indicators between the system of autonomous trucks and conventional trucks; Tan et al. (2012) developed and applied a computational optimization-simulation model to support the management of operations in an open-pit copper mine; and Guimarães et al. (2007), developed a computational simulation model with the objective of validating the results obtained by the application of a mathematical programming model for dynamic truck allocation in order to meet quality and production targets in open pit mines.

3 METHODOLOGY

The data used to conduct the research were taken from the database of the electronic dispatch system of the company CSN Mineração. The system used is the Intellimine© version 5, developed by the company Modular Mining Systems ©. The data sent by the mine equipment are stored in a server, being able to make frequent queries and generate reliable information. The system database has the operation logs and through predetermined queries, developed in SQL language, customized reports are generated on the data collected during the operations, in real time.

The software used to perform the simulations was the Delphos Open Pit Simulator©
(DSIM), which is a discrete event simulation tool, developed by the Advanced Technologi-
cal Mining Center (AMTC) at the University of Chile. DSIM© can estimate the production
of a mining plan from three basic elements: mine layout (topography, operation fronts and
routes); fleet of cargo and transportation equipment, detailed production plan.

First, a simulation was performed in order to validate the actual operation compared to
the DSIM© information.

The information regarding a day of operation of the study target mine with a duration of
24 hours was imputed in the simulator. The following variables were inserted in the software:
detailed production plan by origin and destination; operational losses (reasons for stopping
the equipment); MTBF; MTTR; average speed; distributions of values related to loading
times, download time and queue time.

For the day considered in the simulation, the layout of the mine consisted of 9 mining
fronts and 12 destinations, among them 2 crushers and 1stock. The topography and routes
used are shown in Figure 2. In addition to these points, the layout also included a parking lot.
From the parking lot, the trucks leave after the shift.

100 replicates were performed in Simulation 1 and their results can be identified in Figure 3
and Table 1. The deviations identified in the indicators mass and hours worked in the trans-
port fleet were satisfactory and representative. The model was validated and new simulations
were carried out.

Table 1 illustrates the deviations identified between the data related to actual operation
and data obtained using the simulator.

After the validation of the model, two more simulation scenarios were compared, which
will be compared with scenario 1.

3.1 *Simulation 2*

Operation with speed stipulated through the 3rd quartile.

This scenario consists of the simulation of operational improvements to be performed in
the mine, arising from the process of implementation of the autonomous technology, which
directly impact the average speed of the trucks. The simulated scenario depicts the activities
necessary to be carried out in a preliminary way to the beginning of the process of implantation
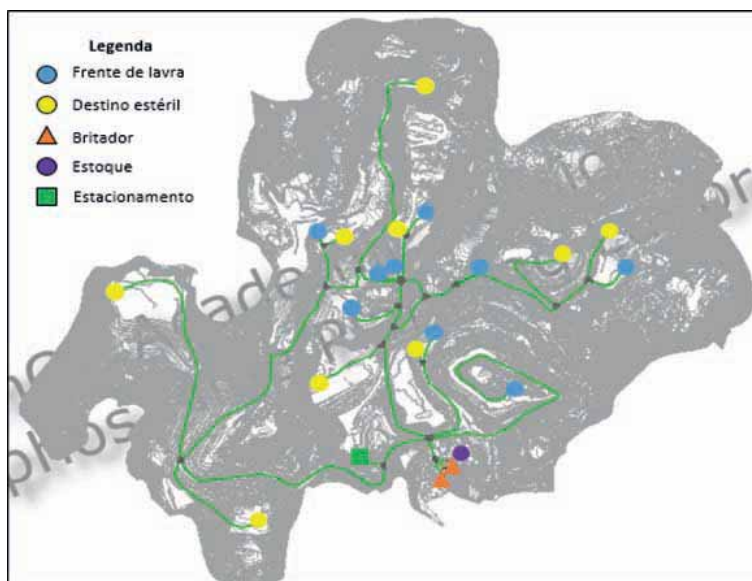

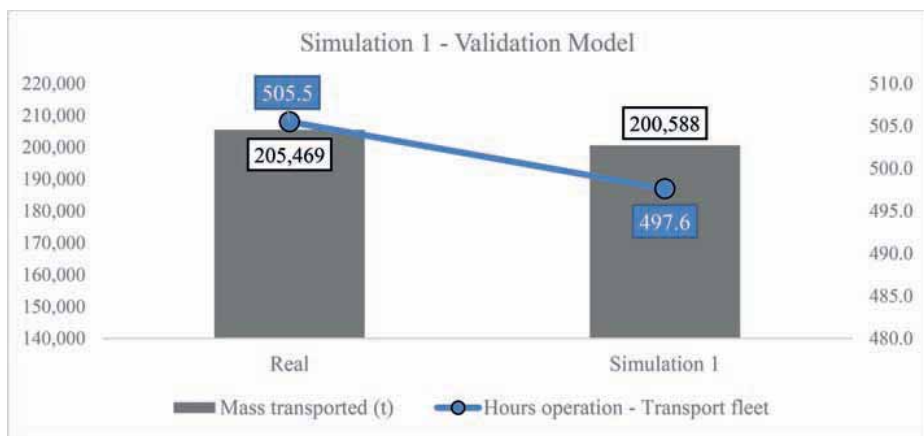Figure 2.   Topographic map of the mine with the paths used.

Figure 3.　Results of simulation 1.

Table 1.　Result of simulation 1 and model validation.

Indicator	Δ (1/real)
Mass (t)	−2,4%
Hours—transport fleet	−1,6%

Table 2.　Average speed performed on different transport profiles.

Average speed						
	Empty truck			Loaded truck		
	Lower level	Plane	Upper level	Lower level	Plane	Upper level
Average speed (km/h)	25,26	26,75	25,02	16,98	17,83	15,23
3rd quartile (km/h)	29,13	30,85	28,85	19,35	20,32	17,35
% operators 3rd quartile	12,39%			15,31%		

of the autonomous technology. Through statistical analysis, the average fleet speed was stratified for each mine operator, being calculated through the normal distribution the value of its 3rd quartile, according to Table 2.

It can be verified that there are several operators that already practice simulated speed through the 3rd quartile. In addition to the improvements of the mentioned conditions, the training of the operators is shown with great importance to leverage the results.

3.2　*Simulation 3*

Autonomous operation with speed stipulated through the 3rd quartile.

The autonomous operation was designed in the simulator through the exclusion of operational stops of the trucks that have direct relation with the use of operators. The stop motives that have been changed are: Turn shift; Fog; Meeting; Meal; Lack of operator; Inspection of the operator; Operator displacement; Stop for physiological needs; Operator sleepy. These operational stops were replaced by hours of equipment operation.

4 CASE STUDY

This paper is a case study in a mine located in the iron quadrangle, the "Casa de Pedra" mine, a division of CSN Group, located in the city of Congonhas, in the Brazilian state of Minas Gerais.

The company stands out for the extraction of iron ore of high content and for having an integrated system of distribution of its production formed by [mine—railroad—port] that supports the attendance of all the current operations from the production, transport and shipment of the ore for export. The method of mining is open pit, with mining of the waste material; drilling, rock clearing, ore loading and transportation. The extraction is carried out in descending order, in horizontal levels, in benches of 13 m of height and berms of 8 m of width. The slope angles vary between 36 and 45° depending on the lithology and relevant geotechnical parameters.

The objective of the research is to simulate three different mine scenarios, between operational improvements and autonomous operation. The results obtained will be analyzed through mine operational indicators, such as: Transported mass (t); Utilization (%) and Productivity (t/h) of load and transportation equipment; Index of queues in loading (%); Idle index of loading equipment (%).

The technology used by the manufacturers of autonomous equipment uses presence sensors and positioning projection, as well as analyzing the information of the embedded telemetry system. Occurrences such as high braking rate, pressure variation between the suspensions and high rolling resistance can cause speed reduction and even equipment shutdown.

For the implementation of a future project of autonomous equipment in mining, it is necessary to avoid possible problems that the technology can cause. Unnecessary equipment stops can occur in situations where the technology identifies risks to the equipment. The main factors to be analyzed at the beginning of the project are:

- Width of loading locations;
- Construction, design and maintenance of access roads;
- Clovers and crosses;
- Impact of the presence of auxiliary equipment in the mine (tractors, motor graders, vans);
- Drainage plan;
- Operational interventions (displacements, quality control, detonations, among others).

The work of adequacy of these mine parameters is fundamental to maximize the future results of the implementation of an autonomous mine project.

5 RESULTS

The results of the simulations can be verified in Figures 4, 5 and 6.

Simulation 2 resulted in a 5% increase in the mass moved in the simulated period of one day of operation and a 4% reduction in the effective use of transport equipment. Simulation 3 was 16% more productive, with a 6% increase in the actual use of the trucks.

The results related to the transport equipment can be verified in Figure 5. It can be analyzed that the indicator of queues in the load rises as the mass increases. This means that there is an excess of trucks used in the operation and, therefore, there is a possibility of reducing the transport fleet. This effect related to queues can also be verified in transport productivity. The indicator increases 6% in simulation 2, but reduces 2% in comparison with the autonomous scenario, influenced by the increase of the queues.

The use of the load equipment increases 17% with the implementation of the autonomous equipment fleet. This result shows that the current operation, characterized by simulation 1, has a larger dimensioning in loading and excessive equipment available. The loading productivity increased 25%, influenced by the 31% reduction in equipment idleness.

Table 3 shows the final result of the tests, with the comparison of the simulated scenarios.
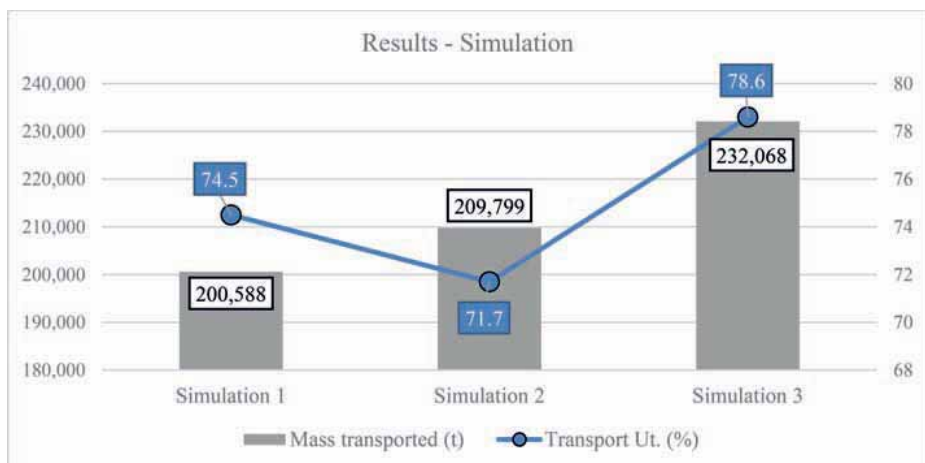
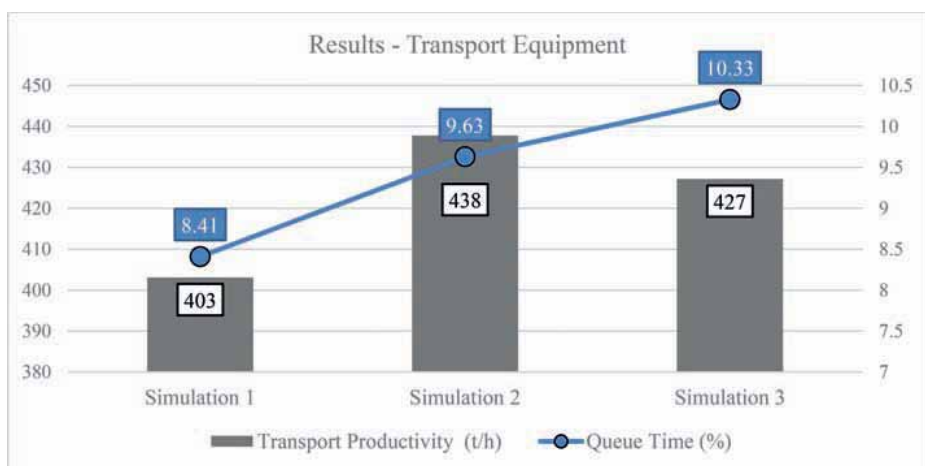Figure 4. Results related to mass (t) and use of transport equipment (%).

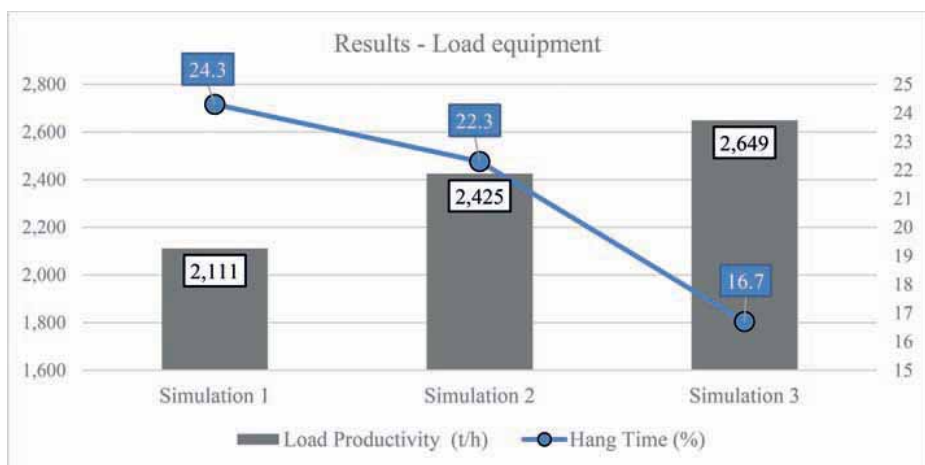Figure 5. Results related to transport equipment.

Figure 6. Results related to load equipment.

Table 3. Results of the simulations and their respective variations.

Results—Simulation	Simulation 1	Simulation 2	Simulation 3	Δ (%)		
				Δ (2/1)	Δ (3/1)	Δ (3/2)
Mass transported (t)	200.588	209.799	232.068	5%	16%	11%
Transport productivity (t/h)	403	438	427	9%	6%	−2%
Transport Ut. (%)	74,5	71,7	78,6	−4%	6%	10%
Queue time (%)	8,41	9,63	10,33	15%	23%	7%
Load productivity (t/h)	2.111	2.425	2.649	15%	25%	9%
Load Ut. (%)	55,7	63,3	65	14%	17%	3%
Hang time (%)	24,3	22,3	16,7	−8%	−31%	−25%

6 CONCLUSIONS

Due to advances in technology and its incorporation in the mineral sector, the study of the automation of transport systems in open pit mines is very relevant.

The objective of the three simulations was to evaluate the potential gains with the implantation of autonomous equipment in its operation.

The maximization of the results from the implementation of the autonomous technology requires some adjustments and standardization of projects in the mine layout, such as accesses, square widths, operational stops and number of auxiliary equipment that travel concomitantly with the production equipment.

The results show significant gains related to increased productivity and use of transport equipment. Another point of great importance is the possibility of reducing the number of equipment sized to execute the production plan. It is necessary to perform a technical-economic analysis of each site, in a way to make the implementation of autonomous transport systems feasible.

The main benefit of the technology is the elimination of manual incidents and accidents that are originated from the distraction and fatigue of the operators. The economic value of the system is also maximized by reducing maintenance costs because the equipment is used more consistently and is better managed under software control.

Each mine project has unique variables, such as climatic and geotechnical conditions, types of material, size of equipment, volume of production, among others. As a result, different setpoints are required for each project.

REFERENCES

Australian Government. 2010. Department of Resources, Energy and Tourism, Analyses of Diesel for mine haul and transport operations, A case study, Australia, 2010.

Baloo, D.T. 2008. Equipment selection at Tenke Fungurume Mining. *Proceedings of Seventeenth International Symposium on Mine Planning and Equipment Selection*, Beijing, China, pg. 269–278, Ed. Univ. Laval/Int.Journal of Mining, Rec. Env.

Bennink, C. 2008. Trucks & transportation—take steps to cut vehicle fuel costs; a proactive approach can add up to major savings. *Equipment Today*, 44(6).

Cassandras, C. & Lafortune, S. 2010. Introduction to Discrete System. 2ª edição.

Catterpilar. Cat Autonomous trucks Haul 1b Tonnes. Available <http://www.mining.com/web/cat-autonomous-trucks-haul-1b-tonnes/>. Access in: 21 Nov. 2018.

Clarke, R., Goodman, M., Perel, M. and Knipling, R. 1999. Driver performance and ivhs collision avoidance systems: a search for design-relevant measurement protocol. *National Highway Traffic Safety Administration*. Office of Crash Avoidance Research National Highway Traffic Safety Administration.

Curi, A., Felsch Jr., W.S., Meireles., B.P., Rodovalho, E.C. 2013. Evaluation of Haul Trucks Performance in a CSN Mine. *International Conference on Mine Planning and Equipment Selection*. MPES 2013. Dresden, Germany.

DELPHOS. DSIM Manual Open Pit v1.2. 2016. Available: < http://delphoslab.cl/index.php/software-es/manuales/99-dsim-open-pit>. Access in: 10 jul. 2018.

Guimarães, I.F.; Souza, M.J.F.; e Pantuza Jr, G. 2007. Modelo de simulação computacional para validação dos resultados de alocação dinâmica de caminhões com atendimento de metas de qualidade e de produção em minas a céu aberto. *XIV Simpósio de Engenharia de Produção (SIMPEP)*.

Hucka, V.J., Tu, J.H. 1985. Analysis of open pit truck haulage system by use of a computer model. *CIM bulletin*, 78:879, p. 53–59.

Komatsu. Komatsu Celebrates 10th Anniversary of Commercial Deployment of AHS. Available <http://www.komatsu.com.au/AboutKomatsu/NewsAndPublications/News/Pages/Komatsu-celebrates-10th-anniversary-of-commercial-deployment-of-Autonomous-Haulage-System-(AHS).aspx>. Access in: 21 nov. 2018.

Parreira, J. 2013. An Interactive Simulation Model to Compare an Autonomous Haulage Truck System with a Manually-Operated System. 212 p. Published Doctoral Dissertation. The University of British Columbia, Vancouver, BC, Canada. 2013.

Parreira, J.; Meech, J. 2012. Simulation of an Open Pit Mine to Study Autonomous Haulage Trucks. Norman B. Keevil Institute of Mining Engineering, The University of British Columbia, Vancouver, BC, Canada, V6TZIZ4. 2012.

Prado, D. 2014. Teoria das Filas e da Simulação, 5ª ed. Nova Lima: Falconi, 2014a.

Rasmussen, J. 1997. Risk management in a dynamic society: a modeling problem. *Safety science*, v.27, n.2 e 3, p.183–213.

Rivera, J.R.M. 2014. Efectos de la Incorporación de Tecnologías Autònomas em el Diseño y la Planificación Minera. Faculdade de Ciências Físicas e Matemáticas, Departamento de Engenharia de Minas, Universidade do Chile, Santiago de Chile, 2014.

Sakurada, N.; Miyuke, D.I. 2009. Aplicação de simuladores de eventos discretos no processo de modelagem de sistemas de operações de serviços. 2009. *Revista Gestão e Produção*, São Carlos, v. 16, n. 1, p. 25–43, jan.-mar.

Sturgul, J.R. 2001. Modeling and Simulation in Mining—Its Time Has Finally Arrived, SIMULATION: Transactions of the Society for Modeling and Simulation International; 76: 286, 2001.

Tan, Y.; Chinbat, U.; Miwa, K. Takakuma, S. 2012. Operations Modeling and Analysis of Open Pit Copper Mining Using GPS Tracking Data. Proceedings of the 2012 Winter Simulation Conference. C. Laroque, J. Himmelspach, R. Pasupathy, O. Rose, and A.M.Uhrmacher, eds.

Modelling and forecasting geometallurgical recovery at a phosphate mine

L.B. Andrade & I.E. Cabral
Federal University of Ouro Preto, Brazil

J.F.C.L. Costa
Federal University of Rio Grande do Sul, Brazil

ABSTRACT: As human population grows, so does the pressure to improve the efficiency on the use of mineral resources which are finite, nonrenewable and fundamental to human existence and its development. Lately there has been a growth in the application of geometallurgy models, an instrument that allows the connection between ore characteristics and mineral processing in a predictive model that is essential for mine planning. Integrated control of the quality of the ore from its mining to its final product can be accomplished by building a geological-typological model, establishing the spatial relationships at the deposits to the different ore-type categories. This article presents an ore-type model built using clustering and indicator kriging to identify and map the domains. Additionally, the metallurgical recovery within each domain is predicted using a multivariate linear regression model. The results were compared against real recovery proving the accuracy and precision of the predictions derived from the model. The methodology is illustrated at a major phosphate deposit

1   INTRODUCTION

Geometallurgy is a field based on a multidisciplinary approach aimed at integrating geological, mineralogical and metallurgical information and yielding a spatial quantitative predictive model for production management (LISHCHUK, 2015). The favorable characteristics of an ore body that require a geometallurgical model are high variability, low mineral grade and complex mineralogy. The phosphate deposit studied in this article is an Alkaline-carbonate complex, situated at Serra do Salitre with an average P_2O_5 lower than other active phosphate mines, where intense weathering has occurred, forming new mineral formations and creating a complex mineralogical environment. The concept of geometallurgy fits the problem definition, since it furnishes expected plant performance depending on the feedstock, integrating the quality control of the ore and decreasing the uncertainty that surrounds recovery performance.

  The metallurgical recovery information can be achieved experimentally at a pilot plant or by lab tests, that require time and money. One way to reduce the cost of the experiments is to identify chemical components, currently analyzed in the ore, with possible correlation with the metallurgical recovery. To identify patterns according to ore's x-ray features, a machine learning technique was applied; to predict its behavior, whereby regression equations were established. In addition, to model the ore-type boundaries the concept of Indicator Kriging was proposed. Machine learning is a method of data analysis that automates analytical model building. It is a branch of artificial intelligence based on the idea that systems can learn from data, identify patterns and make decisions with minimal human intervention. The Machine Learning technique applied in the study was the Hierarchical Cluster Analysis, which involves grouping unsupervised data points without including targets, so we do not tell the system where to go, the system must understand itself from the data given. In this way,

the clustering algorithm classifies each data point into a specific group, relating samples in a way that the most similar are grouped together.

Indicator Kriging (IK) involves the linking of an indicator to a geological domain, in this case to a cluster domain, providing the probability of each unsampled location of belonging to each cluster domain and becomes theoretically possible to predict, for a given oxides grade the recovery expected for that block/region.

Identifying ore classes and distinguishing their behavior on the processes, anticipates the expected behavior for these ore types when mine planning. Estimating how they are spatially distributed helps mine planners to strategically schedule their operations. maximizing the use of the resource.

2 MATERIALS AND METHODS

The sampled data consisted of 734 samples from 62 rotary drilled holes with a sample length of 2.5 m and arrangement in a grid with an average spacing of 90 x 90 m that belongs to a medium plan region from the pit.

2.1 *Geometallurgy*

Geometallurgical programs can be divided into three approaches: traditional, proxies and mineralogical. In the traditional approach, the metallurgical response of an ore in the mineral processing plant is calculated from the chemical assays using mathematical functions. The proxies approach uses geometallurgical tests for many samples and the mineralogical approach includes quantitative mineralogical information. For our study, a traditional approach was taken considering correlation between the elemental grades: CaO, Fe_2O_3, MgO, SiO_2, TiO_2, Na_2O, K_2O, MnO and geometallurgical tests were performed, as well as prediction being done through a mathematical function. A total of 361 samples were bench tested according to an industrial flowsheet, and the all the batch flotation test results were averaged. On MINITAB® their recovery responses were correlated with their ore chemical components and fitted into a regression equation.

2.2 *Clustering analysis*

Machine Learning is a method of data analysis that automates the construction of an analytical model. The purpose of machine learning is to develop computational techniques that allow the simulation of the learning process and the construction of systems capable of gaining knowledge automatically (Mitchell, 1997). Hierarchical cluster analysis (HCA) is a machine learning technique that seeks to build a hierarchy of clusters, one by one, until clustering all points into a single group. One of the HCA features is to display the data in a two-dimensional space in order to display the groupings as one dendogram. The distance between the points reflects the similarity of its properties, being useful to determine the similarity between objects. In theory, data points that are in the same group should have similar properties and/or features, while data points in different groups should have highly dissimilar properties and/or features. In other words, all clustering is done with the goal of maximizing the homogeneity within each cluster and maximizing the heterogeneity between clusters.

2.3 *Indicator kriging*

Lithological domains were coded and then their indicator variables were elaborated, one for each unit. In this step, a value of 1 was assigned to indicate the presence of a domain, and 0 to indicate the unit absence.

$$I(x) = \begin{cases} 1 & if \ x \in Cluster \\ 0 & otherwise \end{cases}$$

For each indicator variable, 3 semi variograms were calculated, two in the XY plane (horizontal) and one with a 90° dip (vertical). All experimental semi variograms were performed by a simple spherical structure

3 RESULTS AND DISCUSSIONS

3.1 *Clustering*

The hierarquical clustering classified classes according to their similarity considering the variables. When the of dissimilarity increases, we reach a level where we are grouping groups that are already homogeneous. Automatic truncation uses these criteria to decide when to stop adding observations. In this study the clustering stopped at 4 groups, as shown at Figure 1.

It is possible to highlight that the class 2 is the most different from the others, since it presented a high dissimilarity with the other cluster from the first division. This is confirmed by the class centroids presented at Table 1.

Class 2 have the lowest values for SiO_2, CaO, MgO and K_2O, and on the other hand has the biggest grades for Al_2O_3, Fe_2O_3 and TiO_2. The great advantage of using Clustering techniques is that, when grouping similar data, it is possible to describe in a more efficient and effective way the peculiar characteristics of each of the identified groups. This statement can be confirmed on the boxplot for the P_2O_5 Recovery which allowed to highlight some distinct trends for certain classes, as shown on Figure 2.

Class 2 presents the lower interval for the metallurgical recovery, highly distinct from others performance intervals. On the other hand, smaller distances between classes, which means more similarity between them, is validated by the fact that Classes 1 and 4 have the lowest distance separating their class centroids and are the ones with better metallurgical performances. Class 3 is mid-term, since from all classes, it is are the one that has the smallest aver-
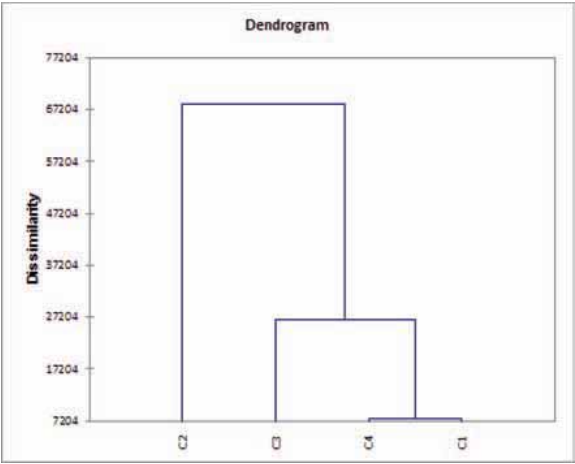

Figure 1.   Final Dendogram representing the clustering analysis.

Table 1.   Class centroids.

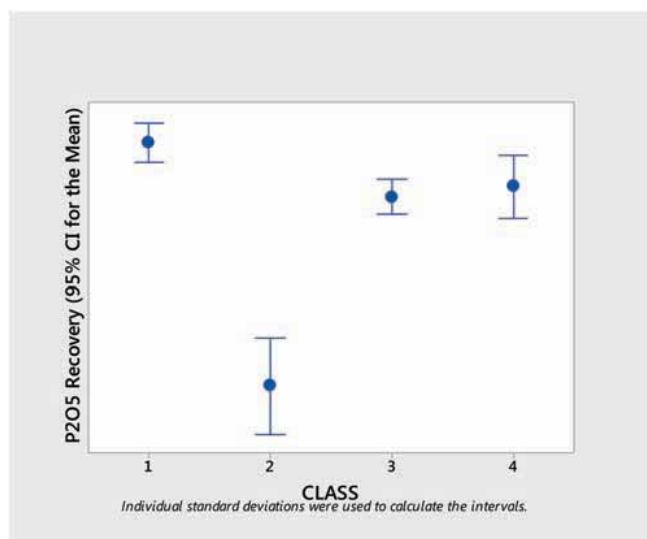| Class	SiO$_2$	Al$_2$O$_3$	Fe$_2$O$_3$	CaO	MgO	TiO$_2$	P$_2$O$_5$	Na$_2$O	K$_2$O	MnO	LOI
1	33.491	3.299	16.880	18.574	9.098	7.724	3.825	0.858	1.513	0.255	3.303
2	13.411	8.862	35.938	6.628	1.537	17.821	5.221	0.101	0.604	0.469	7.078
3	26.500	5.867	23.666	12.613	5.144	11.563	5.589	0.273	1.606	0.360	5.118
4	39.994	5.316	16.192	12.213	7.929	6.680	2.779	0.969	2.765	0.258	3.660

Figure 2.   Boxplots presenting P$_2$O$_5$ recovery for different classes.

age distance between other classes. Comparing performances, it does not present results as good as those of 1 and 4, or the lower ones that class 2 presents. Using Minitab, the same elemental grades were considered as "X", aiming to predict P$_2$O$_5$ Recovery, the "Y" and 4 linear equation

3.2   *Indicator kriging*

As for the variographic modeling, the estimation of the contents was performed individually for each class, considering 4 domains. After merging the probability for each block belonging to each class, it became possible to define the ore-types boundaries. Aiming to validate the estimate different strategies were taken like visual inspection, cross validation and frequency distribuition. Visually, the block model resulted keeps the class pattern observed on the drill-holes, having more representants from class 2 on first horizons, than class 3 and then 1 and 4. Cross validation method showed 80% of matching samples between the real and estimated. At last the class frequency was from the block model was compared with the one from the database and is presented on Figure 3.

When comparing database frequency distribution for the classes and block model, is reasonable to validate the estimate as per their histograms. Class frequency distribution continues about the same, as confirmed by the average. The validations of the estimation performed indicated a good adherence between the actual and estimated values, making it valid and reliable the model generated in this work. With the different domains established, the regression equation for each class was applied for each block, and based on their chemical components, their metallurgical recovery was predicted.

Metallurgical recovery region (below 30%) so it becomes achievable for mine planners to restrict class 2 from mine planning, since it presents lower quality for the plant performance.

Ore-types domains from classes 1 and 4 have high correlation with the better performance regions, being class 1 more representative than class 4. This is the high quality ore for the plant.

Ore-type domain from class 3 is mid-term regarding the dendogram classification, presenting most medium performance blocks, with a few blocks having good results and a few with bad results. It is suggested that for this class, hierarchical clustering be repeated and another geometallurgical test campaign performed in order to better understand the behavior since only this class resulted as a heterogeneous one.
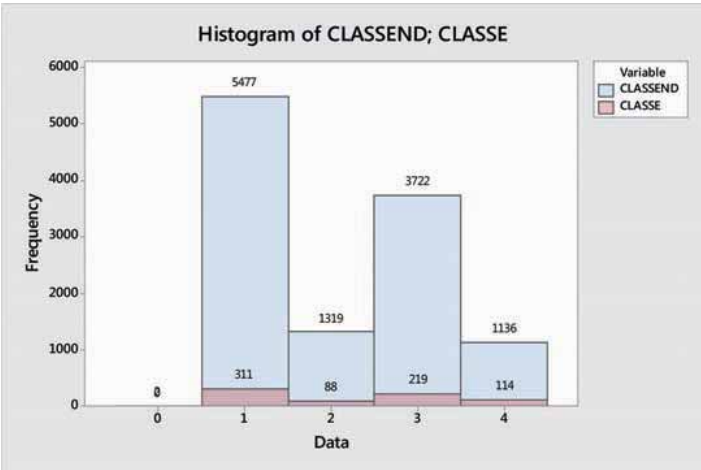
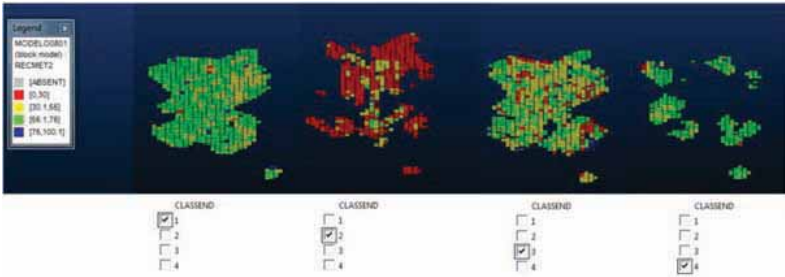Figure 3. Estimate validation comparing database and block model.
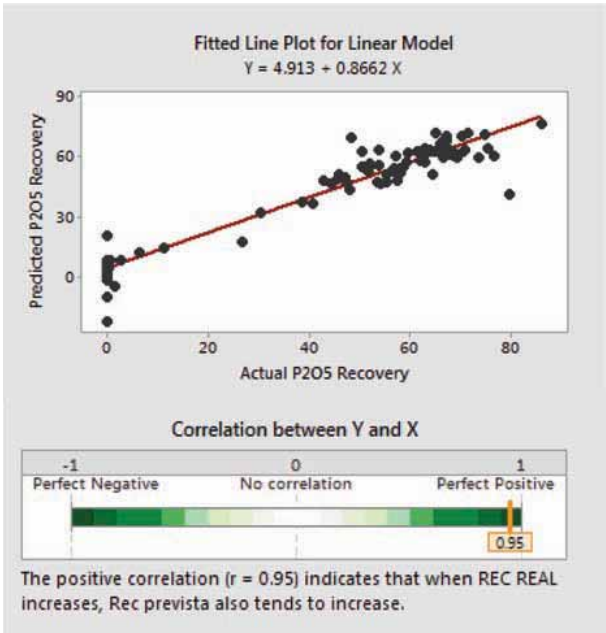

Figure 4. Geometallurgical domains.

Figure 5. Regression and correlation between P2O5 recovery predicted and actual one.

3.3 *Geometallurgical model reconciliation*

The best way to test the Geometallurgical Model created should be to perform a comparison between actual plant performance for each ore-type. Once the plant considered for the methodology was commissioned during this study, the reconciliation could be affected. By that, the Geometallurgical check was applied on a group of new samples tested on a lab scale, through the same flowsheet. They were classified into the 4 ore-types, based on the clustering algorithm, and had their performance predicted, considering the regression equation for their classification. The results between real metallurgical recovery and the predicted one shows high correlation for the model created as presented in the figure.

The prediction quality was assessed with a positive correlation of 95% compared to the virtual truth, with 91.54% of the results explained by the linear model created, that is, for each expected recovery value, the equation (Y = 4.913 + 0.8662x) should be applied to correct the predicted value. Therefore, it can be concluded that the model is valid to estimate samples not used in its construction.

4 CONCLUSION

The methodology created to identify domains applying to metallurgical recovery shows effectiveness since it was able to establish the boundaries of the ore-types and had good correlation to the metallurgical recovery. This metallurgical forecast could act as an assumption for the production planning, since it was able to identify the domain of worse metallurgical recovery that should be restricted from the feeding of the beneficiation plant.

The combination of clustering analysis and Indicator Kriging can be applied to create and model ore types for different process parameters like the work index, Soda consumption,% fines or density moisture linking performance at the plant to its domain locations at the mine and having an integrated quality control through the production chain.

REFERENCES

Arroyo Ortiz, C.E. Caracterização geometalúrgica e modelagem geoestatística da Mina de Brucutu—Quadrilátero Ferrífero (MG). 2014. 206 f. Tese (Doutorado em Evolução Crustal e Recursos Naturais) – Escola de Minas, Universidade Federal de Ouro Preto, Ouro Preto, 2014.

Biondi, J.C. Processos Metalogenéticos e os depósitos brasileiros. São Paulo, Oficina de Textos, 2003. 528p.

Born, H., Kahn, H. Caracterização geológica e mineralógica voltada ao aproveitamento de jazimento fosfáticos. In: Encontro Nacional De Rochas Fosfáticas, 5, São Paulo, 1990. Anais... São Paulo: IBRAFOS, 1990.

Dunham, S., Vann, J. Geometallurgy, Geostatistics and Project Value—Does your block model tell you what you need to know? In: Project Evaluation Conference, Melbourne, 2007. Proceedings... Melbourne: Australasian Institute of Mining and Metallurgy, 2007. p. 189–196.

Goovaerts, P. Geostatistics for natural resources evaluation. New York: Oxford University Press, 1997. 483 p.

Lishchuk, V. Geometallurgical Programs: critical evaluation of applied methods and techniques. 110 p. 2016. Thesis [Minerals and Metallurgical Engineering] – Luleå University of Technology, Lulea, 2016.

Metz, J. Interpretação de clusters gerados por algortimos de clustering hierárquico. Dissertação [Ciência da computação e matmática computacional] – Universidade de São Paulo, 2006.

Mitchell, T.M. (1997). Machine Learning. McGraw-Hill Series in Computer Science.

Schouwstra, R.P.; De Vaux, D.V.; Snyman, Q. Further development of a chemistry proxy for geometallurgical modelling at the Mogalakwena mine. J.S. Afr. Inst. Min. Metall., Johannesburg, v. 117, n. 7, p. 719–726, July 2017.

Artificial intelligence using real-time data

L.-P. Campeau & M. Dubois
Newtrax Technologies, Montreal, Canada

ABSTRACT: Great changes have been taking place in the underground mines of the world for several years now. More and more data is being collected at each stage of the extraction process, at ever-increasing frequency and accuracy. In this context, the use of this data poses new challenges in analysis and prediction. This presentation will discuss the various Machine Learning techniques used by Newtrax to extract value out of this data and examples of concrete applications of these techniques.

1 INTRODUCTION

The digitalization of underground mines has recently opened a whole new area of possibilities in safety, automation and optimization of operations. One of these applications is in the field of predictive maintenance, where the connectivity of equipment can be leveraged to greatly improve maintenance policies. This article will present the recent progress and applications made by Newtrax in the field of predictive maintenance of underground mobile equipment using real-time data and Artificial Intelligence (AI). First, an introduction to the research context and definitions will be presented, followed by a description of the models used, and their application's results.

2 CONTEXT AND DEFINITIONS

Given that the audience of this paper comes from many different backgrounds and that it brings together notions that might not be familiar to all of them, the first part of this article will be dedicated to defining the context of this research and the important concepts.

2.1 Newtrax system

Newtrax provides Internet-of-Things (IOT) solutions for real-time data collection in underground hard rock mines. It supplies the hardware required to collect and transmit the data as well as the software solutions for safety and productivity applications. The big data collected through the system come from a large variety of sources. The positioning data of personnel is collected through tracking-enabled cap lamps (personal safety devices), environmental data is collected through geotechnical and ventilation instruments and vehicle data like positioning and sensor telemetry is collected through a large number of sensors that are adapted to all equipment brands and models. The resulting contextualized data raises interest for Machine Learning applications for many reasons, for example: the goal of the operation is very simple (extract ore), the system is relatively isolated underground, the granularity of data is high (samples every second), years of historical labels exist, and more. The Newtrax system has been collecting data now for many years across all continents at more than 75 mine sites. Figure 1 illustrates the personnel tracking solution.

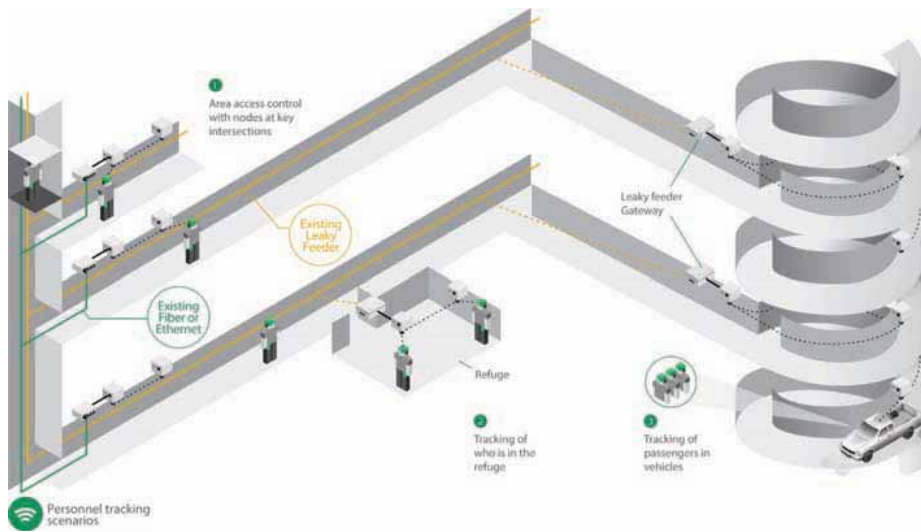Figure 1.   Newtrax personnel tracking solution.

2.2   *Predictive maintenance*

Maintenance strategies generally fall into three large categories, namely corrective, preventive or predictive. The first one, corrective, is the equivalent of having no strategy and consists of performing maintenance operations on equipment only at times of failure. The second one, preventive maintenance, corresponds to performing maintenance operations at fixed time intervals on equipment with no regards to the conditions of the equipment. This strategy has the advantage of preventing many costly failures through a somewhat "excessive" maintenance protocol but has the drawback of requiring many more maintenance operations than needed, as demonstrated by (Hashemian and Bean 2011). Finally, predictive maintenance relies on equipment condition indicators to perform maintenance operations only when needed i.e. when conditions indicating an imminent failure are detected. This has the advantages of needing less maintenance operations and catching failure events from fast degradation that could fall in between scheduled preventive maintenance. It is also very valuable as it allows for the maintenance to be planned when it disrupts the least the production. In practice, maintenance strategies consist most often of preventive maintenance with the addition of predictive maintenance where indicators are available, and some unplanned corrective maintenance occasionally.

There is a lot of literature on the subject of predictive or condition-based maintenance and the point here is not to review it all, but such review can be found in the article of (Peng, Dong, and Zuo 2010). (Schwabacher and Goebel 2007) also published a review specifically on the subject of artificial intelligence in predictive maintenance and a state of the art of the wider field of maintenance optimization can be found in the work of (Sharma, Yadava, and Deshmukh 2011).

For mobile equipment in underground mines, to the best of the author's knowledge, no publications about predictive maintenance using AI are available. A probable cause of this is the scarce availability of data in such contexts. This does not however mean that maintenance improvements are not studied in underground mines. For example (Mkemai 2011) uses two mine sites to evaluate maintenance practices and possible improvements for their underground mobile fleet. Another example of this are the preliminary results presented by (Laukka et al. 2016) who use vibration data from specifically installed accelerometers to try identifying potential faults on mobile equipment. The paper concludes that more data is required in order to achieve results and that a wireless data transfer system would help solve the problem.

2.3 *Supervised and unsupervised learning*

Machine Learning (ML) can be described as an application of Artificial Intelligence (AI), based on the idea that algorithms can autonomously "learn" from data in order to make predictions or help decision-making without being explicitly programmed. Predictive maintenance algorithms development by Newtrax take advantage of two general categories of machine learning algorithms; supervised and unsupervised learning. The supervised approach is based on the idea that by training the algorithms with labeled data, it will "learn" to differentiate between the characteristics of the different labels and acquire the ability to predict the right label for new entries. A classic example of this is character recognition, where a model is trained on labeled images of character e.g. a picture of a handwritten four labeled "4", to develop the ability to read number and letters from pictures. See (Yalcın 2018) for a simple and visual example. Applications of supervised learning to predictive maintenance can be found in the work of (Li et al. 2014) and (Susto et al. 2015).

Unsupervised learning, on the other hand, is based on the idea that by simply looking at the unlabeled data, the model will be able to split entries in different categories based on the similarity of their characteristics. A common example of this is in customer segmentation, where these algorithms are used to regroup customers into a limited number of categories in order to develop tailored marketing strategies for each of them. (Vivek 2018) display simple and visual example of the problem. An application to predictive maintenance is illustrated in the article from (Beghi et al. 2014).

Each of these approaches has advantages and inconveniences and cannot be applied in all situations. For instance, supervised techniques generally require a lot of labeled data for their training, which can pose problems in the case where few or no data are available for certain labels or can require a lot of preliminary work only to label the data. That being said, if unsupervised techniques do not require any label, their results are generally much more uncertain since the characteristics of each group formed cannot be known in advance.

3 MODELS AND RESULTS

This section will discuss the different techniques used by Newtrax in the context of predictive maintenance and some of its applications. Before they are put into the machine learning algorithms, the different channels of information undergo a series of transformations specific to each algorithm including but not limited to: rolling window mean/max/min/standard deviation, categorization, Principal Component Analysis (PCA), standardization and special events identification.

3.1 *Supervised learning*

Newtrax uses supervised learning for specific events detection that have already been observed in historical data e.g. engine or transmission failures. The labeling for the various equipment failure is derived from maintenance logs supplied by our clients. The algorithms used for this type of task are classifier, meaning that they classify the real time data coming from the equipment in different categories. Support Vector Machines (SVM) and Neural Network (NN) are used for this type of application. Put in really simple terms, the way SVM works is that it finds the best hyperplane (e.g. a line in two dimensions) that separates the points from different categories based on the training data. Once trained, the algorithm makes predictions for new data by simply looking at which side of these hyperplanes the new points are located. As for neural networks, they make use of a network of mathematical "neurons" and find the best setting for these neuron parameters by optimization with the training data. Predictions are made by passing new data through this optimized neuron network which returns an answer.

One of our most prominent result in supervised learning was in the area of truck engine failure detection. The engine, taken as a whole, is definitely the most critical component of a haulage truck since a failure will stop the truck for extended periods of time and require costly

repairs. As an example, Table 1 show conservative estimates of the costs of an engine failure event. The parts and labor cost is based on the difference between the exchange value with the manufacturer of a blown engine and the exchange value of a used engine i.e. an engine that has reached its maximal engine hours without suffering a major failure. The engine life loss is the dollar equivalent of the average proportion of engine life lost from the engine not reaching its maximal engine hours. Truck and Fleet production are the equivalent revenu lost by the affected truck and revenu lost around the affected truck by the fleet. These numbers were all based on actual cost taken from underground mines and conservative estimates. Looking at the numbers, it is easily understood why preventing engine failure can be very beneficial to a mine operation.

In order to train the model, historical data from truck engine failure was collected and many different combinations of algorithms and transformations were tested. In this case, SVMs prooved to be the most accurate at classifying data into "normal condition" or "imminent failure" categories. Different prediction horizons were also tested i.e. the time length of the imminent failure warning, and the best results were achieved with a two weeks warning.

Figure 2 shows the results of a real-life example of a haulage truck that occurred during the course of a pilot project made in collaboration with a mining company. The X axis is a timeline and Y is a unitless value extracted from our machine learning algorithms. In simple terms, on the one hand, the more negative the value is, the more the algorithm is confident that everything is running normally. On the other hand, when the value goes above 0, it means that a problem is occurring, with more and more confidence as the value rise. As the graph shows, our algorithm detected a sudden change in the operating conditions of the engine in the first week of October 2018. A little over two weeks later, the truck was brought in for maintenance and it was found that one of the crankshaft bearings had come apart due to a manufacturing defect. Even if the defect was noticed relatively quickly, many mobile pieces on the engine still had to be changed, damaged by the operation of the truck with the broken part. Figure 2 clearly shows that our algorithm had detected the fault two weeks earlier.

Table 1. Examples of costs for engine failure events.

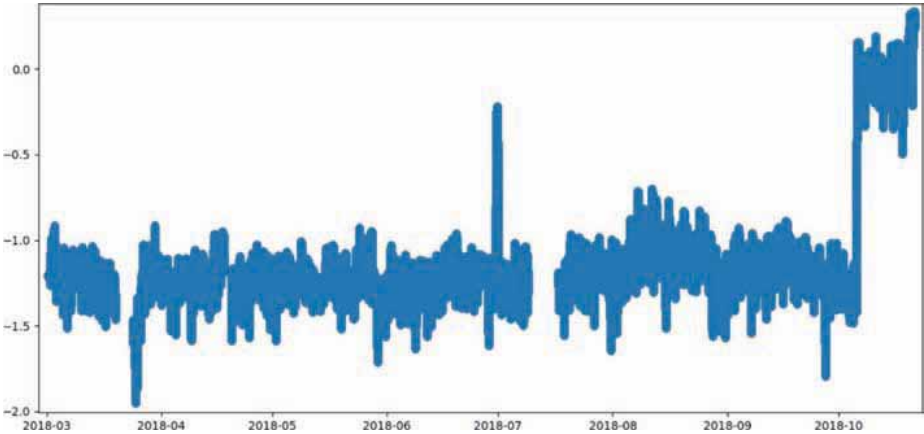| Details	Cost (USD)
Parts and labors	50 000
Engine life loss	6 000
Truck production loss	40 000
Fleet production loss	26 000
Total	121 000

Figure 2. Real life example of engine failure prediction.

3.2 *Unsupervised learning*

One of the many possible applications of unsupervised learning is in the field of outlier detection. It allows the user to identify outliers automatically within a series of data, that is, points that have different characteristics from the rest of the distribution. The two algorithms mainly used for this are One Class Support Vector Machine (OCSVM) and isolation forests. The first one is a variation of the classical SVMs where instead of finding the best separating hyperplane between different categories, it finds a hyperplane that includes most of the data, effectively defining what is normal data. On the other hand, isolation forest randomly split the data in two containers, and repeat the process until all data points are in different containers. By repeating the separating process multiple times, the algorithm can identify outliers by finding the points that in average takes the least splits to be singled out.

These algorithms are currently used with data generated from each sensor individually, e.g. rolling average etc, in order to detect faulty behavior. It was found that sensors that produce more outliers then average are almost always in a faulty condition. This might sound trivial for some faults where for example the sensors simply do not transmit any value anymore, but prove to be a very valuable tool for situations where sensors are simply off by a few percent or vary abnormally. When the integrity of each sensor is confirmed, combinations of sensors are then tested to detect many more faults, like transmission, engine power or battery problems. The advantage of these algorithms is that no labeling effort needs to be put in and that they are more likely to detect never-before-seen failures.

4 CONCLUSION

This article presented the results of the application of machine learning technique to predictive maintenance of mobile equipment for underground mines. It showed that the combination of real-time data and Machine Learning helps create large savings for underground mine operations by detecting multiple different failures in advance. Even though these results are very promising, they represent only one of the possible fields of application of AI in mining. The authors think that other applications will also soon start creating value, for instance in the area of short interval control and real-time planning optimization. Early results have been achieved in these fields promising great improvements in day-to-day operations.

REFERENCES

Beghi, A., L. Cecchinato, C. Corazzol, M. Rampazzo, F. Simmini, and G.A. Susto. 2014. "A One-Class SVM Based Tool for Machine Learning Novelty Detection in HVAC Chiller Systems." *IFAC Proceedings Volumes (IFAC-PapersOnline)* 19: 1953–58. https://doi.org/10.3182/20140824-6-ZA-1003.02382.

Hashemian, H.M., and Wendell C. Bean. 2011. "State-of-the-Art Predictive Maintenance Techniques." *IEEE Transactions on Instrumentation and Measurement* 60 (10): 3480–92. https://doi.org/10.1109/TIM.2009.2036347.

Laukka, Arto, Juhamatti Saari, Jari Ruuska, Esko Juuso, and Sulo Lahdelma. 2016. "Condition-Based Monitoring for Underground Mobile Machines." *International Journal of Industrial and Systems Engineering* 23 (1): 74–89.

Li, Hongfei, Dhaivat Parikh, Qing He, Buyue Qian, Zhiguo Li, Dongping Fang, and Arun Hampapur. 2014. "Improving Rail Network Velocity: A Machine Learning Approach to Predictive Maintenance." *Transportation Research Part C: Emerging Technologies* 45: 17–26. https://doi.org/10.1016/j.trc.2014.04.013.

Mkemai, Rashid. 2011. "Maintenance Procedures and Practices for Underground Mobile Mining Equipment," 1–76.

Peng, Ying, Ming Dong, and Ming Jian Zuo. 2010. "Current Status of Machine Prognostics in Condition-Based Maintenance: A Review." *International Journal of Advanced Manufacturing Technology* 50 (1–4): 297–313. https://doi.org/10.1007/s00170-009-2482-0.

Schwabacher, Mark, and Kai Goebel. 2007. "A Survey of Artificial Intelligence for Prognostics." *AAAI Fall Symposium*, 107–14. http://www.aaai.org/Papers/Symposia/Fall/2007/FS-07-02/FS07-02-016.pdf.

Sharma, Anil, G.S. Yadava, and S.G. Deshmukh. 2011. "A Literature Review and Future Perspectives on Maintenance Optimization." *Journal of Quality in Maintenance Engineering* 17 (1): 5–25. https://doi.org/10.1108/13552511111116222.

Susto, Gian Antonio, Andrea Schirru, Simone Pampuri, Seán McLoone, and Alessandro Beghi. 2015. "Machine Learning for Predictive Maintenance: A Multiple Classifier Approach." *IEEE Transactions on Industrial Informatics* 11 (3): 812–20. https://doi.org/10.1109/TII.2014.2349359.

Vivek, Sowmya. 2018. "Clustering Algorithms for Customer Segmentation – Towards Data Science." 2018. https://towardsdatascience.com/clustering-algorithms-for-customer-segmentation-af637c6830ac.

Yalcın, Orhan Gazi. 2018. "Image Classification in 10 Minutes with MNIST Dataset." 2018. https://towardsdatascience.com/image-classification-in-10-minutes-with-mnist-dataset-54c35b77a38d.

LTE, 4G & 5G – Broadband mobile communications in mining applications

W. Santos

R&D Automation, Epiroc Rock Drills AB, Sweden

ABSTRACT: Wireless connectivity is a key element in the journey towards the digital mine where more and more industrial devices are expected to be connected to this new productivity web. For many years, private high speed wireless networks in industry have been possible thanks to the largely worldwide deployed standard IEEE802.11, popularly known as *Wi-Fi*. This paradigm is now about to change, and it's changing rapidly. This paper aims to offer a high level overview of this new technology called LTE, how Epiroc will interact with it and why it is becoming so popular especially amongst big mining operators.

1   INTRODUCTION

The rapid development of industrial and communication technologies in recent years have increasingly benefit mining activities and operations around the globe. Many companies are rapidly deploying these new tools and applications such as telemetry, wireless sensors, remote operation, etc., in order to gain the associated productivity and financial benefits. This trend, often referred to as the *4th industrial revolution*, is heavily dependent on integrating automation and data exchange in manufacturing technologies, which in turn requires ubiquitous and reliable connectivity to effectively support these technologies. This paper presents and discusses in brief what LTE, 4G and 5G are, the basic components and architecture as well as why it is being considered a more suitable long-term wireless technology for mining applications.

1.1   *What is it?*

LTE is short for Long Term Evolution and is part of a global initiative standardization group called 3GPP (3rd Generation Partnership Project). The work on LTE was initiated in 2004 with the overall aim of providing a new radio-access technology focusing on packet-switched data only[1]. Additionally this standard included targets on peak data rates, user/system throughput, spectral efficiency as well as backwards compatibility with legacy technologies. LTE is commercially known as 4G, the fourth generation of mobile broadband technologies.

LTE is considered the first truly *universal* standard and the very first *data-centric*, *packet-switched*, *IP-based*, mobile broadband technology. It can operate in many different frequency bands (mostly licensed spectrum) as well as features various mechanisms for load balancing, congestion control and traffic prioritization.

Through LTE much higher peak bit rates can be achieved under much lower latency compared to previous 3G standards. From its first release in 2008 (3GPP Release 8) the expected downlink peak bit rate was of 300Mbps thanks to a number of features and mechanisms aimed to efficiently utilize the available radio spectrum.

---

1. Previous mobile standards were purely circuit-switched and voice-centric. This started to change in 3G.

Figure 1. 3GPP logos.

Release 10 (completed late 2010) marks the start of the LTE evolution and is often referred to as *LTE-Advanced*. Then during late 2015, release 13 would bring even more features encompassing new scenarios and improved specifications. This release is called *LTE-Advanced Pro* and sometimes commercially dubbed *4.5G* and seen as an intermediate technology between 4G, defined by the first releases of LTE and the upcoming new 5G air interface.

1.2 *What is it meant by 5G?*

Simply put 5G[2] – the fifth generation of mobile broadband technology – is a set of 3GPP LTE releases created to define a new radio access network (RAN). This new work started in late 2016 and it is been very recently released in late Q2 2018 under the name Release 15 or 5G NR (New Radio). Additional features, improvements and amendments are already underway in Release 16 (5G phase 2). This work is expected to be done by the end of 2019.

The main focus for 5G has been to improve further the radio access network, aiming for reliably supporting even more connected devices, with even higher bit rates and with even lower latency.

So 5G is not a totally different technology but a continuation of the work started by 3GPP with the release of LTE. As often illustrated by the 3GPP's LTE logos (Fig. 1), 5G is the next step after LTE Advanced Pro.

Commercial 5G networks are expected to be launched during 2019 and 2020.

2 SYSTEM ARCHITECTURE

The LTE system consists of an *Access* part and a *Core* part. The *Access* consists of an E-UTRAN (Evolved Universal Terrestrial Radio Access Network) and the *Core* is formed by the EPC (Evolved Packet Core). Altogether they form the so called EPS (Evolved Packet System).

Below on Fig. 2 a high-level representation of an EPS is depicted. Next a quick overview of each block is given in order to aid understanding of the main functions.

2.1 *E-UTRAN*

Here is where all radio access to the network is handled. E-UTRAN or simply *RAN* (Radio Access Network) is consisted of an *eNodeB* (E-UTRAN Node B, or just eNB) which for simplicity can here be seen as the "*base station*". The *UE* or User Equipment, is the LTE mobile device (for ex., a smartphone, a modem or a sensor) that connects to the eNB.

The eNodeB is a comprehensive logical implementation part of the RAN, responsible for many important functions such as roaming decision of an UE between base stations, scheduling, radio-resource handling, retransmission protocols, coding and various multi-antenna schemes.

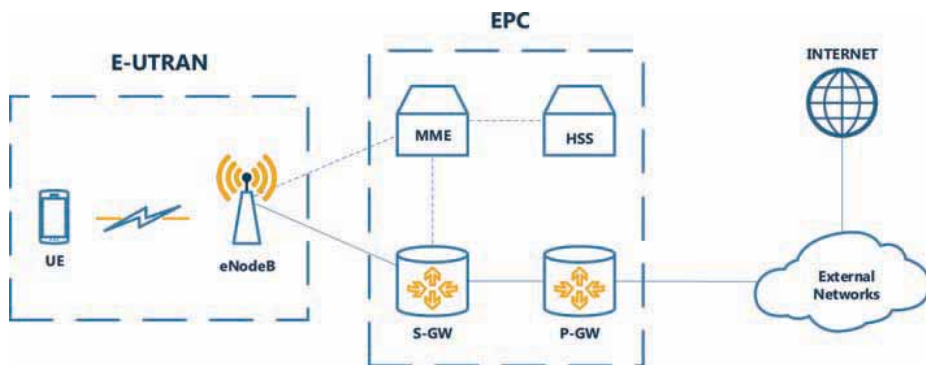2. Not to be confused with 5GHz ISM frequency band.

Figure 2.   The Evolved Packet System.

2.2   *EPC*

The EPC supports access to the packet-switched domain, the Internet and other networks. It consists of different types of nodes which are briefly described below:

- *MME,* the *mobility management entity*, is the <u>control-plane</u> node of the EPC. It's responsible for connection/release of bearers (prioritization mechanism in LTE) to a device, handling of idle to active transitions and handling of security keys.
- *S-GW*, or *serving gateway*, is the <u>user-plane</u> node connecting the EPC to the RAN. It acts as a mobility anchor when devices move between eNBs as well as a mobility anchor for other 3GPP technologies (GSM/GPRS and HSPA). Collection of information and statistics necessary for charging is also handled by the S-GW.
- *P-GW (PDN gateway or P-GW),* is the *packet data network gateway* which connects the EPC to the Internet and/or external networks (for example a mine's LAN infrastructure). Allocation of the IP address for a specific device is handled by the P-GW, as well as, QoS (Quality-of-Service) enforcement according to the policy controlled by the PCRF[3]. The P-GW is also the mobility anchor for non-3GPP radio-access technologies such as CDMA200, connected to the EPC.
- *HSS,* is the home subscriber service, a database containing subscriber information.

Important detail to know here is that these nodes are *logical* nodes. That means that in a physical implementation, these functions and nodes could very well be combined into a single physical node.

NOTE: the so-called *Core Network* can be consisted of one or several *EPCs*. A typical scenario for mining though could be a single core (*EPC*) with multiple *eNBs* or even one single *eNB* with several remote radios connected to it. On Fig. 3 a general deployment diagram consisted of one *EPC* and a *RAN* with several *eNBs*.

2.3   *Spectrum*

The radio spectrum is a finite and limited resource that cannot be reinvented. Only utilized more efficiently. LTE operates mainly in licensed spectrum in the microwave range being 25 of them FDD (Frequency Division Duplexing) bands and 12 TDD (Time Division Duplexing) bands. Starting with 5G, milimeterwave bands may be introduced for some applications.

FDD bands require pairs of channels for UL (uplink) and DL (downlink) while TDD bands only require a single channel for both directions.

Radio spectrum is an expensive asset often owned by governments and telecom operators so anyone willing to deploy a LTE system will most likely need to apply for a license. This

---

3. Policy and Charging Rules Function, another logic node, neglected in the diagram.
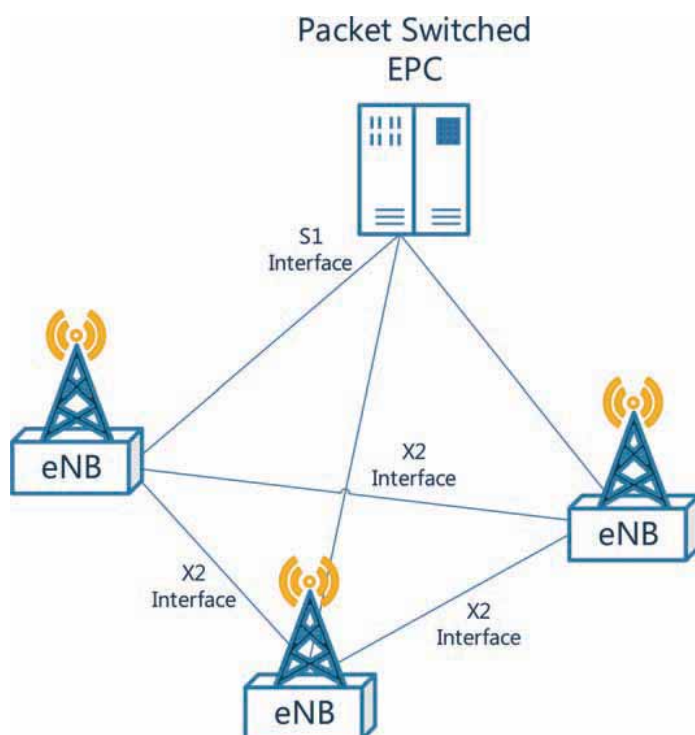
Figure 3.   LTE network with several eNBs.

has been one of the reasons why the industry, specially mining, has been reluctant to mobile broadband technologies. Moreover, since IEEE802.11 (Wi-Fi) operates on a narrow unlicensed band it became easily the first choice for mine sites looking for supporting wireless connectivity at a reasonable price and requires no dependency on extra contracts and licenses.

3   THE CASE FOR MINING

3.1   *The inherent shortcomings of Wi-Fi*

IEEE802.11 (Wi-Fi) as well as other wireless technologies have been serving the mining industry for many years now. Great advances have been made within the Wi-Fi standard so it rapidly became ubiquitous and a relatively easy, standardized, way to provide good wireless connectivity with *some* mobility.

The problem is now that the demands for reliable and more scalable wireless communication systems in mining applications are increasing[4] at the same time that the Wi-Fi technology seems to have reached its limit. With a very limited and narrow spectrum, low power devices (which forces densification and added installation/maintenance costs), single channels for both downlink and uplink as well as no possibility to traffic and congestion control whatsoever, seems to have turned Wi-Fi into a less likely long term technology for the current and future aspirations of the mining industry.

Of course Wi-Fi still has its own areas of use however for those scenarios where capacity, low latency and high reliability are non-negotiable pre-requisites (for ex time-critical

---

4. Especially when it comes to mission-critical applications.

applications such as remote operation of mining machinery), LTE seems to have better means to fulfil these requirements.

3.2 *The expected benefits of LTE*

Although LTE is a relatively new communications technology for the mining industry, a number of technical aspects and late improvements have turned it into a very interesting and promising option for the digitalized mining operation. The main aspects and benefits are:

- LTE is an IP/Data-centric network solution
- Possibility to tailored private core network (EPC) deployments
- SDN (Software-Defined Networks) allowing for virtualization of core network functions that can be run on generic hardware
- Better traffic control through scheduling and QoS mechanisms
- Better coverage and interference control
- Better security mechanisms
- Multiple services can reliably share the same infrastructure
- Possibility to accommodate low-power/low-throughput devices in standard LTE bands (for ex LTE-CAT-M1 and NB1), laying out the platform for the IIoT (Industrial Internet of Things) where all kinds of sensors can potentially be wirelessly connected to the same network.

There are though a number of potential "cons" when choosing a mobile broadband technology as the main wireless communications solution. As stated, LTE is a relatively new technology and there is so much we still do not know. Tele-operators, equipment manufacturers, system integrators, IT departments, machinery manufacturers and mining operations staff will all have to come together to make the implementation and operation of the network successfully. Technical support and the right competences in place are mandatory pre-requirement in order to obtain the full benefits. Probably a totally different business model is needed, tailored for mining customers only?

Many of these aspects are being evaluated right now through two main collaboration projects where Epiroc (aka Atlas Copco) has been actively involved, PIMM DMA (https://www.simsmining.eu/) and SIMS (https://www.simsmining.eu/).

4   WHERE DOES EPIROC FIT IN ALL THIS?

Epiroc as OEM, supplying heavy machinery but also automation and telematics solutions will inevitably have a role to play in this new scenario.

The machines will need to be equipped with an UE device that withstands the harsh environment as well as have the correct electrical characteristics to be onboard of a machine. Also the UE needs to fulfil the performance requirements of the application, depending if it is for simple data collection and file transfer (Certiq, RRA) or if it is for time-critical applications (tele-remote).

Figure 4 illustrates the typical integration points between Epiroc's solutions and the LTE network. This is a possible scenario but not the *only* scenario.

The OP-Station (tele-remote control station), usually physically located in a control room will be connected to the mine site's OTN or Operation Technology Network (usually physically and logically separated from the corporate business network). Servers like the RRA (Rig Remote Access) server and the LBO (Local Backoffice) will most likely be connected to the OTN as well.

In turn, the OTN connects to the EPC through the *P-GW*. The EPC can be a local deployment (so-called a *private core*) or it can be supplied as a remote deployment, where the EPC service is provided by a telecom operator or a system integrator. The drawback with the latter is that the system will most likely rely on a WAN connection for the RAN (E-UTRAN) in order to reach the EPC which may increase latency and impose capacity and reliability issues.

The possibility to run the EPC as a *private core deployment* is certainly one of the main aspects that's made possible for mine sites to deploy LTE. This because WAN connectivity
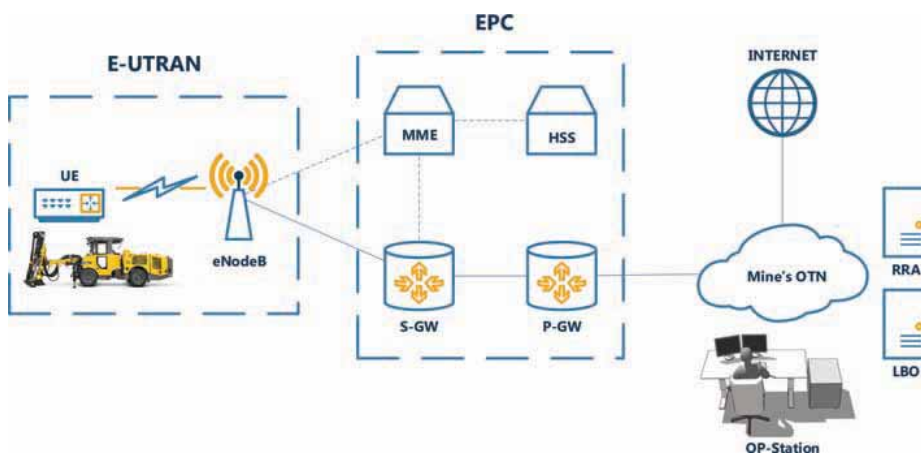
Figure 4. Integration to an LTE network.

(Wide Area Network, often the Internet access line) to and from mine sites are *usually* very limited. Besides, hence the OTN is specifically designed for control systems and production tasks it wouldn't make sense to have all this sensitive traffic to leave the mine site, even though link data encryption mechanisms are available for that purpose.

5 CONCLUSIONS

LTE is a wireless communication technology that promises better traffic control, higher bit rates and low latency. Tailored solutions and the possibility for mining operators to deploy their own private LTE core and RAN has turned this technology into a very interesting long term option for all industries, including mining.

As OEMs and system integrators we need to adapt, learn and collaborate in order to ensure proper operation and outstanding performance of our connected machines and automation systems.

FURTHER READING

SIMS, Sustainable Intelligent Mining Systems (https://www.simsmining.eu/).
PIMM-DMA, Pilot for Industrial Mobile Communication in Mining – Digitalized Mining Area https://www.sics.se/projects/pimm.
LTE bands and spectrum – http://niviuk.free.fr/lte_band.php.
LTE throughput calculation – https://tools.pedroc.co.uk/4g-speed/

REFERENCES

Dahlman, E., Parkvall, S., Sköld, J., *4G LTE-Advanced Pro and The Road to 5G*, Academic Press, 2016.
3GPP, The Mobile Broadband Standard (www.3gpp.org).
Various, Compilation, *Communications engineering desk reference*, Academic Press, 2009.
GMG – Global Mining Guidelines Group, Underground Mine Communications Infrastructure (https://gmggroup.org/projects/underground-communications-infrastructure/).
Wireless standards chart, National Instruments, (www.ni.com/rf).

Development assumptions of a data and service management centre at KGHM S.A.

Paweł Pyda
KGHM Polska Miedź S.A. o/COPI, Lubin, Poland

Paweł Stefaniak
KGHM Cuprum Research and Development Centre, Systems Analytics Unit, Wrocław, Poland

Helena Dudycz
Wrocław University of Economics, Department of Information Technology, Wrocław, Poland

ABSTRACT: The aim of this paper is to present the premises and assumptions for the construction of a platform intended to collect, process, and analyse large data sets, as well as to make business services available in a large industrial enterprise such as KGHM Polska Miedź. In particular, the analysis covered issues related to Data Governance and SOA Governance. Consideration is also given to IT architecture and organisational structure as elements necessary to build the Competence Centre for Data Analyses and Processing.

1 INTRODUCTION

After three major industrial revolutions (mechanisation, electrification, and digitisation) we are in the fourth stage, referred to as Industry 4.0. The result of the third revolution, i.e. Industry 3.0, was the digitisation of enterprises, which opened the possibility to process data on a large scale; also, micro-controllers were created to control machines, and the level of automation increased. Management, planning, and control systems were set up to facilitate coordination in the area of production. Industry 4.0 goes one step further with its goal of integrating people, digitally controlled machines connected to the Internet (IoT – Internet of Things), and information systems. Translating these premises into reality requires designing an appropriate IT infrastructure, implementing appropriate IT tools, and introducing organisational changes.

The term Industry 4.0 was used for the first time at the Hanover trade fair in 2011 (Industrie 4.0. 2011). In April 2013, a group led by Siegfried Dais of Robert Bosch GmbH in cooperation with Henning Kagermann (acatech – Deutsche Akademie der Technikwissenschaften) presented a final report to the German Federal Government containing guidelines for the implementation of the Industry 4.0 concept (in German: Industrie 4.0) (Kagermann, H. & Wahlster, W. & Helbig, J. 2013). In Poland, with a press release dated May 31, 2017, the Ministry of Digitisation announced the establishment of Polish Industry Platform 4.0 (Ministerstwo Rozwoju. 2017). Further work on the platform resulted in the development of a draft law on the Future Industry Platform Foundation, which was adopted by the Council of Ministers on October 16, 2018 (Kancelaria Prezesa Rady Ministrów. 2018).

The concept of Industry 4.0 was also adopted by KGHM Polska Miedź S.A. In 2018, KGHM 4.0 Programme was launched, which includes key projects from various areas of the company (production safety, management, information, and maintenance of machinery and devices). In order to ensure effective implementation, this programme was divided into three areas: Industry, ICT (Information and Communication Technologies) and support projects. The ICT area comprises two key projects: "Implementation of Service Oriented Architecture (SOA)" and "Development of Data Governance Processes, including policies and standards for data processed within business areas". These projects are closely related to the subject of this paper.

Enterprise Architecture with a specific architecture framework may be helpful in introducing strategic changes. One of the most recognisable tools for building a given architecture is TOGAF belonging to The Open Group industrial consortium. TOGAF perfectly harmonises with the premises of Data Governance with respect to building a management and data processing architecture, as well as with the premises of SOA Governance with respect to building a service-oriented architecture. Both concepts will be used under the above-mentioned projects to build an appropriate ecosystem, which will be one of the key elements of the Industry 4.0 Platform.

The aim of the article is to present the premises and assumptions related to the data processing centre under construction as part of KGHM 4.0 Programme being implemented at KGHM Polska Miedź. The structure of the article is as follows. The first part of the paper discusses the concepts of Data Governance and SOA Governance, as they constitute the basic solutions of the data processing centre under development at KGHM Polska Miedź. Next, the identified problem related to the processing, management, and analysis of very large data sets as well as reporting thereof in a large industrial enterprise, i.e. KGHM Polska Miedź, is presented. In particular, the analysis covered issues related to Data Governance and SOA Governance. Consideration is also given to IT architecture and organisational structure as elements necessary to develop a data and services governance centre. The article ends with a summary.

2 THEORETICAL FOUNDATIONS OF DATA GOVERNANCE

2.1 Data governance organisations

Large organisations such as KGHM operate relying on a number of area-specific systems (e.g. ERP, CRM, BPM, Contract Management System, Procurement Support System, GIS, industrial systems, etc.). Each of these systems stores and generates considerable amounts of data, and Large-scale data processing is a daily reality. The management responsible for individual business areas, as well as the Management Board itself, expect the information on which decisions are based to be reliable (of high quality), consistent, and available in a timely manner. The role of information in the decision-making process has increased in importance and is just as important as material or human resources. It is essential that information is stored and managed in a transparent manner, that it has a specific owner, that supervision of access to information is ensured, and that the source and flow of data can be identified. A wide range of activities according to specific standards and rules is defined by the term Data Governance, which means the management and supervision of data. The implementation of the Data Governance concept is not trivial and, depending on the level of maturity the organisation wants to achieve, it may take from 2 to 5 years. During the implementation, it is possible to take advantage of international non-profit organisations' ready-made architectural frameworks. The most important of these are:

- DAMA International, DAMA (Data Management Association),
- Data Governance Professionals Organization (DGPO),
- The Data Governance Society,
- The Data Governance Council,
- Enterprise Data Management Council,
- IQ International – The International Association for Information and Data Quality,
- Data Governance Australia.

It is also worth mentioning that in addition to organisations that promote their approach independent of suppliers, software manufacturers themselves provide their own architectural frameworks such as:

- SAS Data Governance Framework,
- SAP Master Data Governance,
- IBM Data Governance Framework,
- Oracle Enterprise Data Governance.

The guide DAMA International contains a set of processes in specific thematic areas (specialisations) related to data management provided in the form of good practices. The concept of data governance comprises processes such as planning, specification, creation, acquisition, maintenance, use, archiving, acquisition, control, and cleaning of data (Dama International. 2017). These processes mesh and interact. The DAMA organisation distinguishes 11 thematic areas (Figure 1):

- Data Governance – planning, supervision, and control over data management.
- Data Architecture – full structure of data and sources of this data as an integral part of the enterprise's architecture.
- Data Modelling & Design – analysis, design, creation, testing, and maintenance.
- Data Storage & Operations – deployment and management of physical data structures.
- Data Security – ensuring privacy, confidentiality, and appropriate access.
- Data Integration & Interoperability – acquisition, extraction, transformation, transfer, delivery, replication, federation, virtualisation, and ongoing support.
- Documents & Content – storing, securing, indexing and providing access to data from unstructured sources (files and physical records) and making this data available for integration and interoperability with structured data (databases).
- Reference & Master Data – shared data management aiming to reduce redundancy and ensure better data quality by standardising definitions.
- Data Warehousing & Business Intelligence – managing the processing of analytical data and providing support for decision making based on reporting and analysis of data.
- Metadata – collecting, categorising, maintaining, integrating, controlling, managing, and providing metadata.
- Data Quality – defining, monitoring, and maintaining data consistency, as well as improving data quality.

Each of these areas logically groups activities according to a given issue, with the Data Governance area being the central element that connects the others.
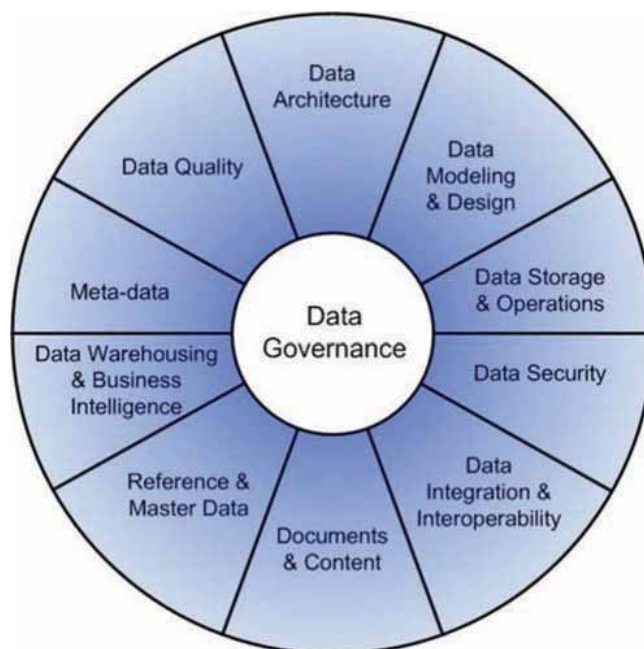

Figure 1.   Thematic areas according to DAMA-DMBOK Guide. Source: Dama International. 2017.

3 THEORETICAL FOUNDATIONS OF SOA GOVERNANCE

3.1 *The definition of SOA governance*

Governance means defining, implementing, and monitoring rules, principles, standards, procedures, and processes that allow organisations to manage their business by assigning appropriate roles to employees (Torry, H.). It is also the establishment of responsibility, decision-making rights, as well as communication and escalation channels (Torry, H.). SOA Governance is an extension of IT Governance and EA Governance (EA – Enterprise Architecture). Figure no. 2 presents these relationships.

The acronym SOA stands for Service Oriented Architecture. SOA defines the possibilities of integrating applications and business processes through related services often referred to as Web Services. The SOA architecture allows one to think in a natural way about the services that exist in the organisation and its environment. Depending on the role of SOA in the organisation and context (related to business, architecture, implementation, or operation), the following definitions can be distinguished:

- from a business perspective, SOA defines a set of business services that can comprise other services, providing a certain value that an organisation wants to pass on internally or externally to its clients or partners,
- from an architectural perspective, SOA is an architectural style that supports service orientation,
- from an implementation perspective, SOA defines infrastructure standards as well as the programming and technology models used to implement services,
- from the usage (application) perspective, SOA contains a set of relationships and arrangements between service consumers and their providers, which determine the quality of service (Keen, M. & Adamski, D. & Basu, I. & Chilcott, P. & Eames, M. & Endrei, M. & Fagalde, B. & Raszka, R. & Seabury. S.D. 2007).

3.2 *Expected benefits of SOA Governance implementation*

SOA Governance implementation is a difficult process that requires appropriate preparation both business-wise and from the IT department. For implementation to be successful, the focus must be on four areas. The 4P principle, well known from the ITIL (Information
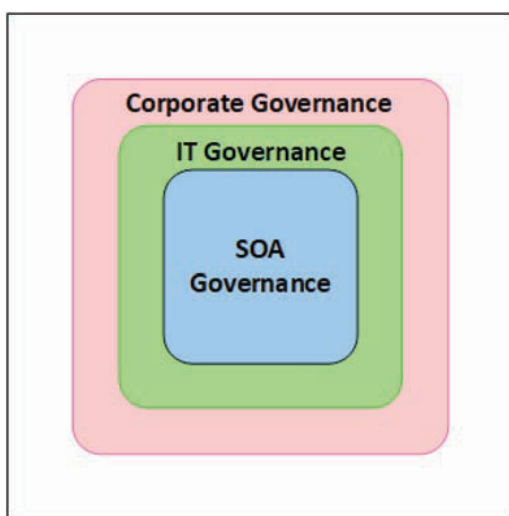

Figure 2.   Dependencies between concept models. Source: Implementing Technology to Support SOA Governance and Management. 2007. Redbooks.

Technology Infrastructure Library) methodology, which is a set of best practices in IT service management (Cabinet Office. 2011), defines them as follows (The Art of Service. 2009):

- People – human resources, knowledge, skills, communication, and awareness;
- Processes – organisation of management and work through an appropriate process model;
- Products – technologies, hardware, and software;
- Partners – cooperation with internal and external clients (between all interested parties).

A well-conducted implementation of SOA Governance can benefit the company's IT department and, consequently, the entire organisation.

From the IT point of view, the following expected benefits from the implementation of SOA Governance in the company can be distinguished:

- integration of applications is possible regardless of the platform;
- access to resources (services) is easier;
- breaking away from the "round robin" approach to integration development;
- easy maintenance and development of services;
- system functionalities are made available in the form of services.

From the business point of view, the following expected benefits can be named (Erl, T. 2007, Yoon, T. & Carter, P. 2007):

- reduction of the Total Cost of Ownership (TCO);
- reduction of product delivery time;
- greater business agility;
- increased customer satisfaction;
- increased flexibility of business processes;
- improved flow of and access to information from various sources within the company.

To sum up, well-conducted SOA Governance implementation helps reduce redundant services and enables better use of hardware resources, while the "re-usability" of services allows reducing the costs associated with the production of new functionalities responding to the management staff's new business needs. Additionally, the time of delivering new products to the business is also shortened, and it is possible to react more quickly to changes.

4 DATA GOVERNANCE AND SOA GOVERNANCE AS THE BASIS FOR THE ARCHITECTURE MODEL AT *KGHM POLSKA MIEDŹ*

4.1 *Identified difficulties pertaining to data management and software development at KGHM Polska Miedź*

KGHM Polska Miedź is a large industrial enterprise with several branches. These are:

- Head Office of the Company;
- Accounting Services Centre;
- "Rudna" Mining Facility;
- "Lubin" Mining Facility;
- Mining and Smelting Rescue Unit;
- "Polkowice-Sieroszowice" Mining Facility;
- Ore Enrichment Facility;
- Hydrotechnical Plant;
- "Legnica" Copper Smelter;
- Main Centre for Information Processing;
- "Cedynia" Copper Smelter;
- "Głogów" Copper Smelter.

KGHM is a company constituting a capital group comprising several dozen companies. Its operation is based on a number of domain-specific systems. Some of them are standard

software solutions supplied by leading manufacturers, to which all branches of the company have common access. Due to the activities conducted by KGHM, there are also IT systems tailored to specific business needs. Some of them are applied at one branch only, but there are also those used by several branches. The least desirable situation is when several branches work on different systems within the same business area while using "own" rather than shared information resources, e.g. each branch applies a different reporting tool, based on its own databases. Figure 3 presents an example situation.

Very often, people who develop reports, as well as their recipients, use concepts which they understand in slightly different ways. The lack of a standardised glossary of business terms that can be used by the interested parties contributes to misunderstandings. Another aspect is access to data necessary to perform analyses or complex calculations using advanced models. First of all, access to data is hampered by the fact that they are located in dispersed systems and there is, therefore, a risk of data inconsistency. Secondly, it is difficult to carry out complex calculations because there are problems with data storage (lack of sufficient space for data) and processing (poorly performing computer) on an employee's workstation. Further important issues are software development and the adaptation of existing systems to new business requirements.

KGHM Polska Miedź S.A. uses several hundred different IT systems. In addition, new software development needs are constantly appearing, which will cover new business areas of the Company as well as the Capital Group. In other words, new business needs are identified that require new IT systems' functionalities that will streamline work and provide access to relevant information. In order to meet these challenges, the Company carries out further projects, and therefore more and more project teams and external companies are working on new IT systems. The number of simultaneously undertaken IT initiatives covering various issues and business areas is very large, which is why very often project groups doing their work are unaware that at the same time someone else is developing (or has already developed) a similar functionality to solve a similar problem using the same data. As a result of work carried out by various design teams across the Company, new IT systems providing similar functionalities are created, which often leads to the production of duplicate IT solutions or parts thereof (e.g. system modules). As a result, KGHM incurs additional costs resulting from, among other things, improper use of human resources, carrying out similar solutions. Figure 4 presents a target model of shared data and services.
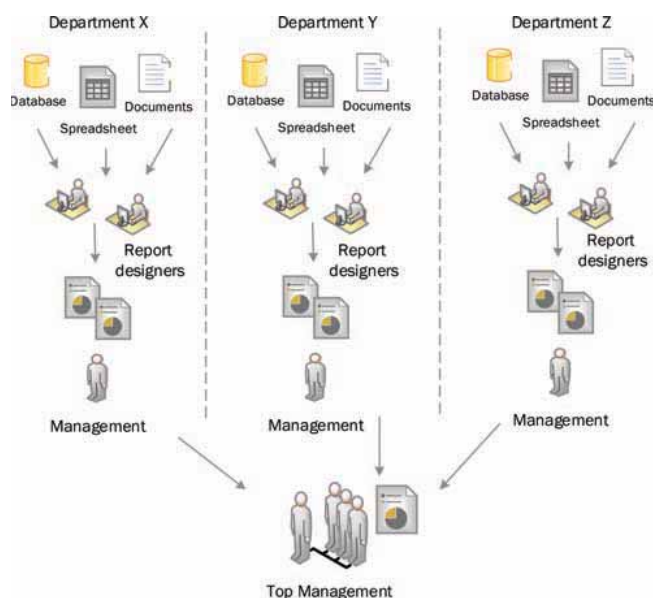

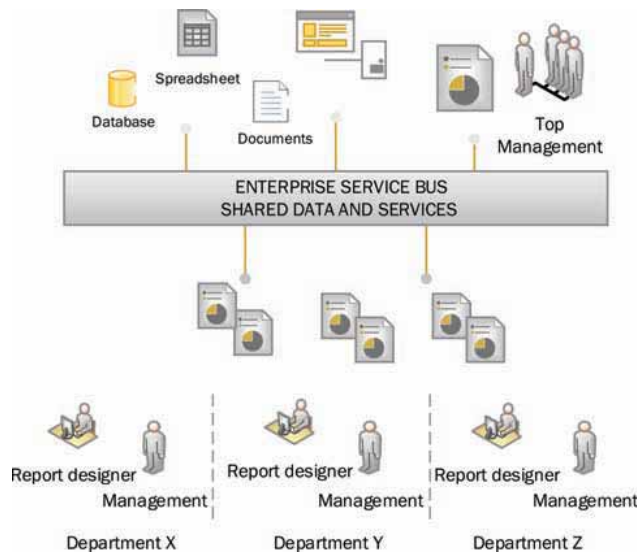Figure 3.   Distributed data sources. Source: Own work.

Figure 4.   Shared data and services model. Source: Own work.

4.2   *A proposal for a data and service management platform to integrate data and systems across KGHM Polska Miedź*

On the basis of projects launched under the KGHM 4.0 programmes named "Implementation of Service Oriented Architecture (SOA)" and "Development of Data Governance Processes, including policies and standards for data processed within business areas", project tasks were initiated. Work on the model is being carried out in accordance with the premises of the Data Governance and SOA Governance concepts. The key components that will make up the centre should be named as parts of the data processing and integration platform.

In the area of data management, the following types of tools can be distinguished:

- reporting and data presentation tools;
- advanced data analysis tools (prediction, modelling, etc.);
- data modelling tools;
- tools for creating ETL (Extract Transform Load) processes;
- tools supporting Data Governance processes;
- data warehouses.

The Data Governance Policy involves the creation of many organisational roles and the definition of procedures with a view to handling business processes. Thus, in our model, using tools that support ETL processes, the programmer creates appropriate data flows which supply data warehouses. A multi-thematic data warehouse stores data logically grouped according to business domain Data Marts) (Chodkowska-Gyurics, A. 2009). Using appropriate software, analysts use the data stored in the warehouse to build complex mathematical models. The results of these calculations are stored back in the database. Then, designers use the reports to create breakdowns for the management. The Data Steward uses relevant tools to ensure the correctness of Data Governance processes.

In the area of data integration, the following elements can be distinguished:

- ESB (Enterprise Service Bus),
- corporate services repository,
- service management tools (availability rules, authorisations, and monitoring),
- tools securing services (encryption, authentication, authorisation, etc.),
- tools for developing services (development environments).

As is the case with Data Governance, the SOA Governance policy assumes the creation of many organisational roles and support for tasks related to maintaining services of an appropriate standard. As a consequence, it enables the implementation of business processes. Clients of the service can search the repository to use a service of their choice. Analysts and architects design new services and modify current ones. Programmers write a code responsible for the implementation of the business process. Administrators ensure that services are secure and available. Business owners of the services supervise them.

4.3 *A proposed extension of the IT system architecture model at KGHM Polska Miedź based on big data tools*

The IT system *architecture model at KGHM Polska Miedź* discussed in the previous section, enables efficient handling of business processes in terms of storage, processing, analysis, integration, and making data available in the form of reports. The scope of data is limited to thematic warehouses. The amount of data is relatively small, and data loading processes usually take place once a day (or more frequently, in individual cases).

The demand for the collection and processing of large amounts of data in real time is expected to increase in the near future due to ongoing and planned projects. There is discussion on the implementation of new systems in the field of mining, mechanics, geology (geodesy) or the widely understood concept of IOT (Internet of Things) (Perry, L. 2018) related to the handling and analysis of data from industrial equipment (water pumps, sensors of self-propelled mining machines, belt conveyors, sensors of seismic vibrations, etc.). In addition to typical structural data, there is also a need to collect unstructured data, such as images from CCTV cameras or sounds produced by rock masses or machinery. To analyse this type of data, we could employ algorithms, methods and tools of artificial intelligence (Ford, M. 2018), data mining (Han, J. & Kamber, M. 2006), and machine learning (Dean, J. 2014). They are able to process and analyse signals (e.g. image recognition) in real time and, on that basis, to take appropriate decision-making steps. A decision-making system may be helpful in such a case by sending a message to a device (e.g. an air-conditioning fan) about its stoppage while simultaneously notifying relevant services (report, e-mail, text message, etc.).

The extension of the IT system architecture model at KGHM Polska Miedź by adding new Big Data tools does not interfere with the implementation of Data Governance and SOA Governance principles. After the model has been extended with Big Data tools, processes and people will be supervised by these solutions.

5 CONCLUSIONS

The challenges posed by the Industry 4.0 concept make companies introduce appropriate organisational, legal, and technological changes. In the several years to come, the implementation of the Industry 4.0 concept will constitute a "to be or not to be" case. It allows not only to gain a competitive advantage, but it is also the foundation of a stable company. KGHM Polska Miedź certainly aspires to be one of the companies aiming at full compliance with the concept of Industry 4.0. The first steps have been taken, which is reflected in the launch of the KGHM 4.0 Programme, comprising many key projects implemented in various areas of the company's operation. This article sets out to present plans to build a data and service management centre as one of the main elements of Platform 4.0. The work has already started on two projects: "SOA-oriented architecture" and "Development of Data Governance processes, including policies and standards for data processed within business areas". Plans for the first stage involve implementing mainly analytical tools, while the second phase will consist in introducing Big Data tools that will enable the analysis of industrial data as well as the processing of data from sources including spatial information systems.

In accordance with the guidelines of the Data Governance and SOA Governance concepts, tasks related to the implementation of IT tools, procedures and organisational changes are performed. The result of this work is expected to be an environment enabling efficient

processing and management of data and services for the entire KGHM Group located in one place.

REFERENCES

Ankam, V. 2016. Big Data Analytics. Packt Publishing.

Cabinet Office. 2011. ITIL® Service Strategy, The Stationery Office.

Chodkowska-Gyurics, A. 2009. Hurtownie danych, Wydawnictwo Naukowe PWN.

Dama International. 2010. The DAMA Guide to the Data Management Body of Knowledge (DAMA-DMBOK). Technics Publications.

Dama International. 2017. DAMA-DMBOK: Data Management Body of Knowledge (2nd Edition). Technics Publications.

Dean, J. 2014. Big Data, Data Mining, and Machine Learning. Wiley: Hoboken.

Erl, T. 2007. SOA Principles of Service Design (The Prentice Hall Service-Oriented Computing Series from Thomas Erl).

Erl, T. 2014. SOA Koncepcje, technologie i projektowanie. Helion.

Ford, M. 2018. Architects of Intelligence: The truth about AI from the people building it. Packt Publishing.

Han, J. & Kamber, M. 2006. Data mining: concepts and techniques. Morgan Kaufmann Pub.

Industrie 4.0. 2011. Mit dem Internet der Dinge auf dem Weg zur 4. industriellen Revolution.

Kagermann, H. & Wahlster, W. & Helbig, J. 2013. Recommendations for implementing the strategic initiative INDUSTRIE 4.0. National Academy of Science and Engineering.

Kancelaria Prezesa Rady Ministrów. 2018. Projekt ustawy o Fundacji Platforma Przemysłu Przyszłości. (https://bip.kprm.gov.pl/kpr/wykaz/r90792432089,Projekt-ustawy-o-Fundacji-Platforma-Prze-myslu-Przyszlosci.html).

Keen, M. & Adamski, D. & Basu, I. & Chilcott, P. & Eames, M. & Endrei, M. & Fagalde, B. & Raszka, R. & Seabury. S.D. 2007. Implementing Technology to Support SOA Governance and Management. International Business Machines Corporation.

Kumar, V.N. 2018. Modern Big Data Processing with Hadoop: Expert techniques for architecting end-to-end Big Data solutions to get valuable insights. Packt Publishing.

Ladley, J. 2012. Data Governance: How to Design, Deploy and Sustain an Effective Data Governance Program. Morgan Kaufmann.

Menken, I. 2012 ITIL Foundation Complete Certification Kit – Fourth Edition: Study Guide Book and Online Course. Emereo Publishing.

Ministerstwo Rozwoju. 2017. Powstanie Polska Platforma Przemysłu 4.0. (https://www.mpit.gov.pl/media/38857/PowstaniePolskaPlatformaPrzemyslu4_0.pdf).

Perry, L. 2018 Internet of Things for Architects: Architecting IoT solutions by implementing sensors, communication infrastructure, edge computing, analytics, and security. Packt Publishing.

Pulier, E. & Taylor, H. 2005. Understanding Enterprise SOA. Manning Publications.

Sen, H. 2018. Data Governance: Perspectives and Practices. Technics Publications.

The Art of Service. 2009. ITIL V3 Foundation complete certification kit. The Art of Service.

The Open Group. (https://www.opengroup.org/).

Torry, H. A guide to SOA Governance. Torr Harris Integration Solutions.

Yoon, T. & Carter, P. 2007. Investigating the Antecedents and Benefits of SOA Implementation: A Multi-Case Study Approach, AIS Electronic Library (AISeL).

Mineberry—remote monitoring of abandoned shaft openings

B. vom Berg, F. Schmachtenberger & B. von Gruchalla
Technische Hochschule Georg Agricola, Bochum, North Rhine-Westfalia, Germany

F. Wollnik, S. Klaß, A. Koschare, S. Schnell & J. Schliebs
RAG Aktiengesellschacht, Herne, North Rhine-Westfalia, Germany

ABSTRACT: In the German regions of Saarland and the southern Ruhr area in particular one can find surface openings which are in part centuries old and relics of past hard-coal underground mining activities. In order to minimise possible risks and hazards which may result from those openings, RAG AG has been monitoring around 7,300 of those openings and is currently restoring at least 35 of them. In addition, an innovative monitoring system is to be developed and established that will allow for an improved monitoring of this huge legacy. In close collaboration with RAG AG, the Research Institute of Post-Mining and the Faculty of Electrical Engineering, Information Technology and Industrial Engineering at THGA University of Applied Sciences have been designing and implementing suitable and continually working monitoring systems that use state-of-the-art sensor and transmission technology and will be developed further.

1 THE MINEBERRY SYSTEM

The principal idea of these system, called Mineberry system, is to develop modular solutions that can work independently for almost any kind of abandoned mining objects. To make this possible, it was necessary to merge opportunities provided by the Internet of Things (IoT) with solutions relying on established and proven technology. In such cases, the components which are lowered and mounted into the shafts do not only need to withstand the adverse environmental conditions, but (in parts) also meet the requirements of explosion protection. Special attention is being paid to ensuring a long durability of each system while generating high cost-efficiency.

The smallest of the system which are currently being developed consists of sensors, a solar generator and a micro-controller which transmits the data directly into a cloud storage using the Sigfox network (a low-power wide-area network for small data volumes). In a simple scenario, the sensors monitor the vertical movement of the column with which the abandoned shaft has been filled. The data gathered in this way are continually displayed and saved in the cloud storage used and, if needed, transmitted to a pre-set reporting chain.

If, in addition to the measuring data, stills are needed of the current local situation, a Raspberry Pi system will be used. Using an infrared camera, this system is able to record images night and day and thus enables the user to carry out a visual assessment of the local conditions. An-other option is to measure not only the vertical movement of the filling column, but also its precise depth. This system transmits the data generated here using a UMTS connection (mobile telecommunications network) to upload and send configurable emails.

The people in charge can use an adjustable depth limit value in order to receive immediate information if a significant change in the surface opening occurs. In this case, if the pre-set value is exceeded, another messages is sent per email and text message, e.g. to an engineer or a technician who can then assess the situation and take the necessary steps needed.

This innovative concept for monitoring abandoned mining objects is currently being tested at different locations in the field.

2 THE BASIC CONCEPT

Figure 1 shows some recent examples of surface openings of abandoned hard-coal mining (anti-clockwise): a surface caving, a restored abandoned shaft and a restored abandoned shaft with an end fitting that serves as a flame trap (Protego cap):

As a first application, the (sudden) vertical subsidence of the filled shaft column is to be recorded and pertinent warning and alarm signals are to be transmitted to a central point.

For that purpose, suitable sensors are mounted on the shaft cover or the surface which record essential shaft parameters, see Figure 2.

The measuring values recoded are transmitted to a micro-processor station (monitoring station) where they are processed and sent to a central cloud storage using a wireless network. From that cloud storage, the data are transferred to the user.

Figure 1.   Examples of some surface openings of abandoned hard-coal mining.
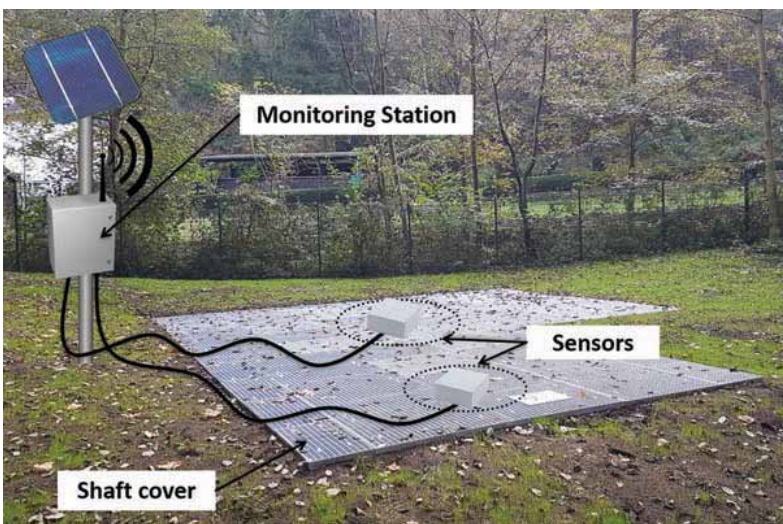
Figure 2.   Sensor system on the shaft cover and central monitoring station with wireless data transfer and solar generator.

Depending on the individual profile requirements of the monitoring, currently two different monitoring concepts (two development stages) can be implemented.

3 DEVELOPMENT STAGE 1: THE SIGFOX SYSTEM

Figure 3 shows the principal design of the first development stage of the monitoring system (Sigfox system) using an abandoned shaft that has already been restored by RAG as an example (hereinafter called "sample shaft").

Two weights of 1 kg mass each are placed on the shaft column of the filled shaft which needs to be monitored; these two weights are connected with the pull-cable switches SZS1 and SZS2 using appropriate steel cables (stainless steel V2A, diameter 2 mm).

In order to implement alarm levels of different grades regarding the subsidence of the shaft column, the cables on the filling column have additional rope loops of different lengths, a short one for SZS1 and a long one for SZS2.

Usually, the weights and the wound rope loops lie on top of the shaft column. Now, if the shaft column is sinking vertically, the additional rope loops are unwound. First, the short rope is tensioned and thus actuates pull-cable switch SZS1. This action is recorded by the monitoring station and immediately transmitted as a warning (e-mail and/or text message) to the central point or a selected circle of individuals.

Here, the decision can be made which further steps are necessary to stabilise the shaft or the shaft column. If the shaft column continues to sink further, the second, longer rope is tensioned and pull-cable switch SZS2 is activated. This action initiates another immediate signal by the monitoring station (e-mail and/or text message) which is interpreted as a highest-level alarm or hazard message by the users and which requires immediate measures to stabilise the shaft or the shaft column.

This actuation using two switching points was selected to help the user distinguish between a slow subsidence of the filling column and a spontaneous, larger sinking of the filling column. The respective limit values depend on the parameters of the object to be monitored and are individually defined for each shaft.

To monitor the overall functionality of the monitoring station, the station sends cyclical life signs at preset intervals (every 15 minutes including recording the current status of the pull-cable switches) to the central monitoring point. For the individual design of an entire monitoring unit (monitoring station, sensor system and auxiliary components) used to monitor the filled shaft, one aspect is indispensably to be observed:
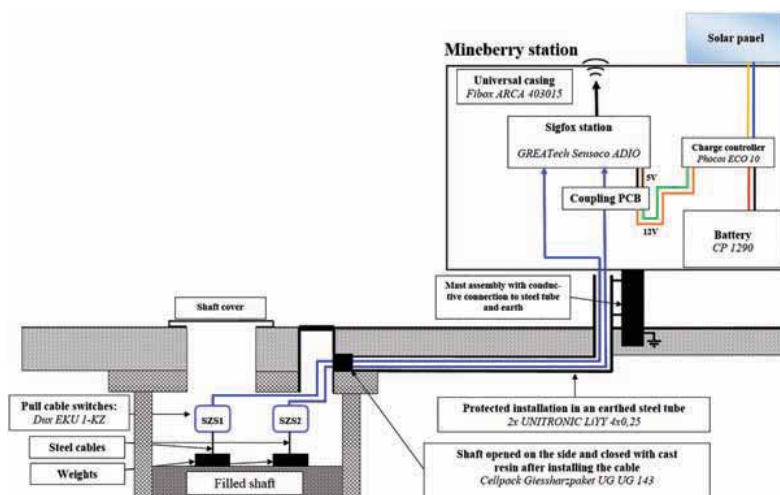

Figure 3. Design of the Sigfox system used for monitoring the sample shaft.

Depending on the shaft type and the conditions inside the shaft and its immediate sur-roundings, there can be a release of different and in certain cases explosive gas mixtures. Therefore, all monitoring systems installed of any kind must comply with the requirements of explosion protection. That means that the electrical and electronic systems in use must full-fil the requirements of the type of protection Intrinsic Safety according to EN 60079ff. It needs to be checked in each case whether measures of explosion protection have to be taken at the shaft to be monitored or not. Thus, the following explanations will point out any additional components that need to be installed at the specific points that are critical regard-ing intrinsic safety.

Figure 3 above shows an overview of the installation of a monitoring unit that is used to monitor our sample shaft. First, the two pull-cable switches SZS1 and SZS2 are installed in the upper part of the shaft wall as shown in Figure 4.

The two pull-cable switches are simple end-of-line units with a break and a make contact. Ac-cording to EN 60079-11, a switch is a simple electrical apparatus and thus does not need to comply with the standards of explosion protection. Here, the switch has a plastic casing which is directly connected to the shaft wall and thus to earth by means of a conductive connection.

Moreover, if an intrinsically safe electrical installation becomes necessary, the electrical power supplied to the pull-cable switches is additionally limited by appropriate Zener barri-ers. The proof of intrinsic safety of the pull-cable switches and the Zener barriers is provided in a pertinent document for intrinsic safety.

The connecting cables of the two pull-cable switches SZS1 and SZS2 are led to the outside through a drill hole in the shaft wall. The hole itself is closed again by cast resin. Outside the shaft, two cables are installed protected inside a steel tube until they reach the nadir of the monitoring station, see Figure 5.

The earthed steel mast tube to which the monitoring station is fastened is used to continue the installation of the cables to monitoring station. Inside the monitoring station, the signals are transmitted directly to the micro-controller system (Sigfox station).

A coupling PCB is used to implement the necessary voltage supply of the pull-cable switches.

However, if the entire monitoring unit needs to be assembled as intrinsically safe, the intrin-sically safe circuit (shaft range with pull-cable switches and connecting cables) is separated
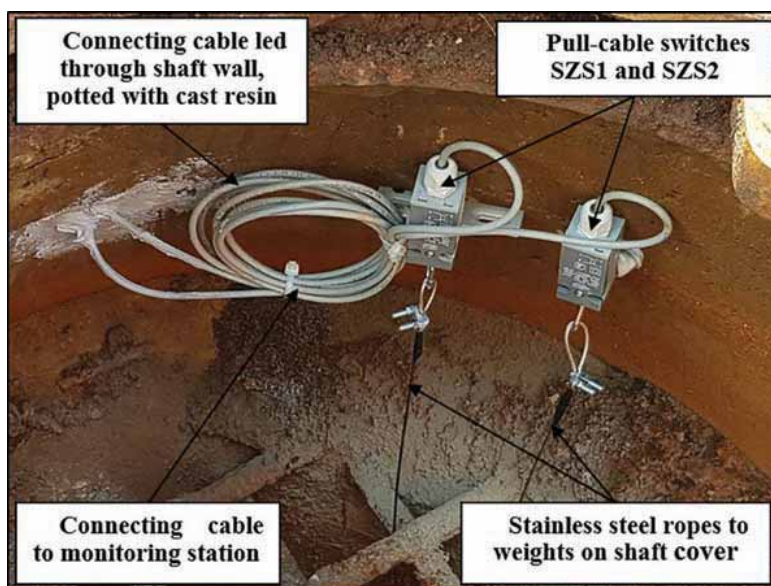

Figure 4.   Installation of the pull-cable switches SZS1 and SZS2.

Figure 5.   Installation of the connecting cables for the pull-cable switches.
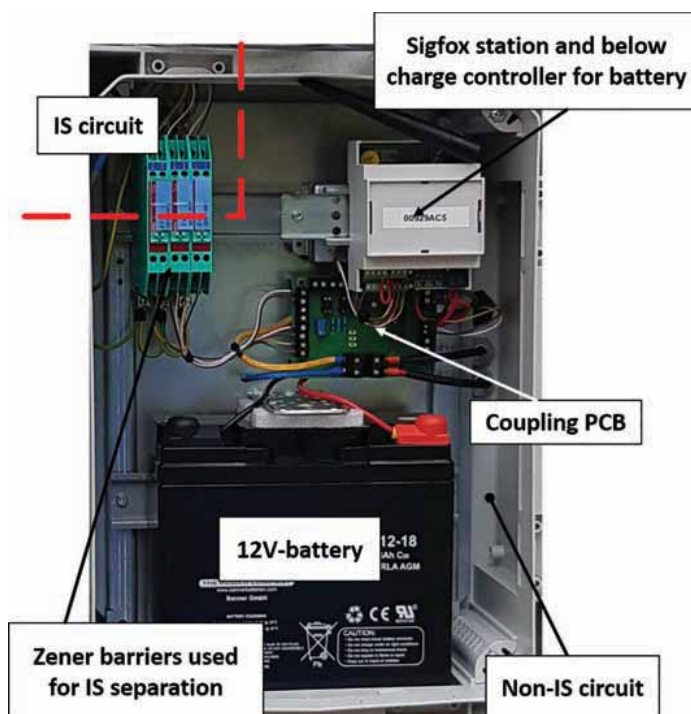

Figure 6.   Assembly of monitoring station with circuits being intrinsically safe (IS) separated by Zener barriers.

from the non- intrinsically safe circuit (monitoring station and surrounding) at this point by using appropriate Zener barriers, see Figure 6 overleaf.

The Zener barrier Z710 made by Pepperl + Fuchs is used as a safety barrier in explosion protection. Their task is to prevent any incendiveness of the circuits which are used in

Figure 7. The entire monitoring unit at the sample shaft.

an explosive atmosphere. These barriers are used in conjunction with the simple pull-cable switches to ensure a safe use of the system in areas where standards of explosion protection do apply. The sample shaft, however, is not one of those.

The conditions pull-cable switches recorded by the Sigfox station in this way are then trans-mitted via the Sigfox network (a part of the Internet of Things, IoT) to the Sigfox cloud; from there, the user(s) can access and retrieve the data and can also visualise it.

A solar generator (consisting of a solar panel, charge controller and rechargeable battery) is used for the independent power supply of the entire monitoring unit 24 hours a day and 365 days a year.

Figure 7 shows the entire monitoring unit of the sample shaft monitoring.

4 THE USER DASHBOARD

The measuring values recording are stored in the Sigfox cloud via the global Sigfox network; from there, they can be display on the user's PC, laptop, tablet or Smartphone as shown in Figure 8.

The layout of this dashboards can be freely configured and thus perfectly adapted to individual needs. Here, the following is displayed on the dashboard:
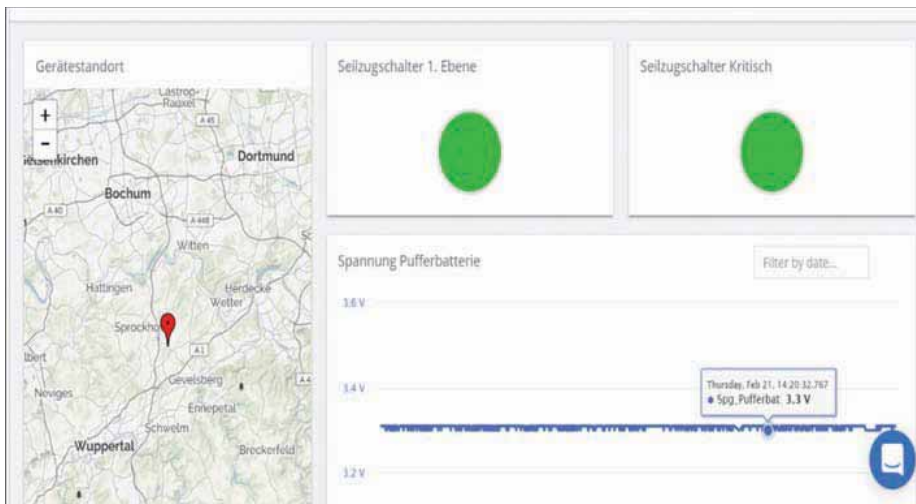
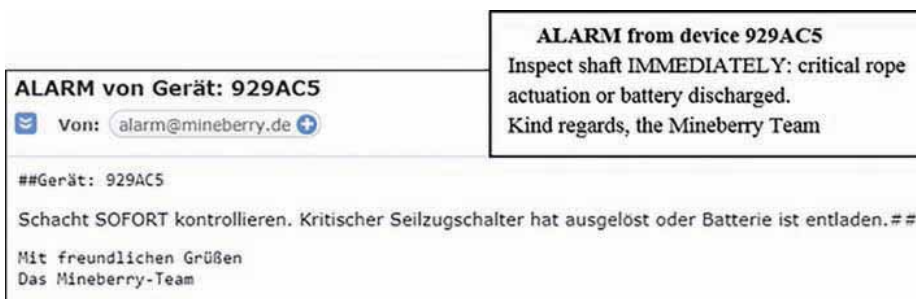Figure 8.   The user dashboard displaying the sample shaft.

Figure 9.   Original e-mail from the Sigfox system with English translation.

- The two LEDs signalise the switching mode of the two pull-cable switches:
  - GREEN: pull-cable switches not actuated
  - RED: pull-cable switches actuated (pulled)
- The line graph shows the monitored voltage run of an internal buffer battery.
- The location indicator on the left shows the rough position of the shaft (here only used for information purposes as the shaft is not moving).

If the pull-cable switches are actuated, this can be immediately seen on the dashboard. Additionally, warning and alarm emails/text messages are sent to any number of persons as shown in Figure 9.

5   DEVELOPMENT STAGE 2: THE RASPBERRY PI SYSTEM

In the second development stage of the monitoring system, the Raspberry PI micro-computer system, which has a more powerful computer core, will be used for the monitoring station.

This computer enables not only the connection of additional sensor and actuator units, but it also allows for the set-up of an infrared camera to generate images of the shaft surroundings day and night and to transfer these images. Here, the UMTS mobile network will be used for the data transfer.

6 EXTENSIONS

The monitoring stations of both development stages can be flexibly extended by additional components such as:

- Connection of a rope path receiver to measure the current depth of the shaft column in cm/m in order to record even the smallest slow changes in the vertical position of the column. Additionally, exact depth limit values can be pre-set now: if these values are reached, warning and alarm messages can be generated.
- LED signal light and siren in order to generate warn and alarm messages directly on the spot if the shaft column is sinking.

The monitoring stations of both development stages have been in use at different abandoned shafts in the Ruhr area and the Saarland; they show a high level of reliability and provide optimal support to RAG in their online monitoring of surface openings of abandoned hard-coal mining. Further areas of use, e.g. the monitoring of mine dewatering shafts, are being planned.

Optimization of material logistics by using leading edge electronic Information and Communication Technologies (ICT) in underground coalmine

Max Thomas Stöttner
Formerly senior planning engineer at RAG Anthrazit Ibbenbüren GmbH, Ibbenbüren, Germany

ABSTRACT: Ibbenbüren Anthracite mine was owned and operated by RAG Anthrazit Ibbenbüren GmbH, a subsidiary of RAG AG enterprise in Essen/Germany. Mine's capacity was 2 Million tons per year, average employment before mine was closed in 2018 was about 2,500. Product sales went into an 838 MW power plant at mine site and in heating markets. From 2011 until 2014 RAG's Ibbenbüren mine was participant at international research project "OPTI-MINE" co-funded by the Research Fund for Coal and Steel (RFCS) of European Commission. First, a redundant fiber optic network in meshed ring structure and consisting of standardized intrinsically safe network components (switches) with coal mining ATEX approval was installed. After elimination of the initial difficulties, it was fully functional and operated reliably. With this new network, a reliable high bandwidth data transfer and control of production facilities could be achieved. Based on this network and by integration of RFID and WLAN products systems for personnel communication via hand-held, remote control for machine operations and material tracking and logistics support were designed and created.

1 INTRODUCTION

RAG Anthrazit Ibbenbüren covered Working Package 2 of OPTI-MINE research project. Objectives of WP 2 were as follows:

- To optimize the overall mining process in a remote production area by unified personal communications
- To speed up and optimize material logistics by introduction of a network integrated automatic material tracking system
- To enhance mine safety by unified network communications and by using the network for a later integration of results from RFCS EMTECH project.
- To improve mining process efficiency by optimized conveyor belt skew sensors and integration of controls The overall budget granted for the RAG Anthrazit mine was € 1.350 Million.

This paper is restricted to give a review about the logistic task of the OPTI-MINE project.

The first step was setting up a meshed fibre optic network. The network was exploited for the regular operation in the working section Beustfeld and technically adjusted to future changes. On the basis of this network infrastructure and by deployment of standardized network components consisting of standardized WLAN and passive RFID components Mining Infrastructure Computers (MIC's) developed by MineTronics, IT-systems for container tracking, material tracking, container management and for locomotive information could be built up and successfully operated. Thereby a higher transparency regarding locations of operating resources in the logistics field could be demonstrated. In connection with these results a higher logistics efficiency and respectively cost reductions due to an optimized use

of transport units and transport means have been reached. The FO-Network and the system for material logistics were in use until mine was closed down in 2018.

2 SETTING UP A FIBER OTPIC NETWORK

From 2011 until 2014 the network structure with fiber optic cables (FOC) has been installed in the working section "Beustfeld". In total around 5,000 m FO cables were laid (24 FO cables, 12 FO break out cables with and 12 without plug) and 20 required FOC hubs were installed under-ground, see Figure 1. Moreover, 19 IPC-PLC (industrial grade PC–Programmable Logic Controller) controllers were used for operating underground facilities. 10 MIC's (Mining Infrastructure Computers) were installed as active components in the network infrastructure, consisting of a managed fiber optic switch, a WLAN accesspoint and application software for handling of location tracking and to read RFID information for material logistics.

The topology of the gigabit Ethernet network consists of a redundant ring. The ring stretches out underground over North Shaft, area Ostfeld to Oeynhausen Shaft and back again to North Shaft. An additional ring connects Oeynhausen Shaft with North Shaft on surface over 6 km distance, see Figure 2.

The complete underground network structure is connected to the above ground network by redundantly designed Cisco switches on surface. It is divided into three logic virtual networks: VLAN process and control net, VLAN camera net and VLAN logistics net.

After elimination of the initial difficulties as they appear frequently at the introduction of new unproven technologies (like overheating of MIC's or excessive data streams), and after optimization the network was fully functional and reliably operated.

By the set-up as redundant network using a meshed ring structure and by the use of standardized network components (switches) with ATEX approval in the underground area, a higher system stability concerning data transfer and control of production facilities, compared to the previous copper-wire star structure, could be successfully demonstrated.
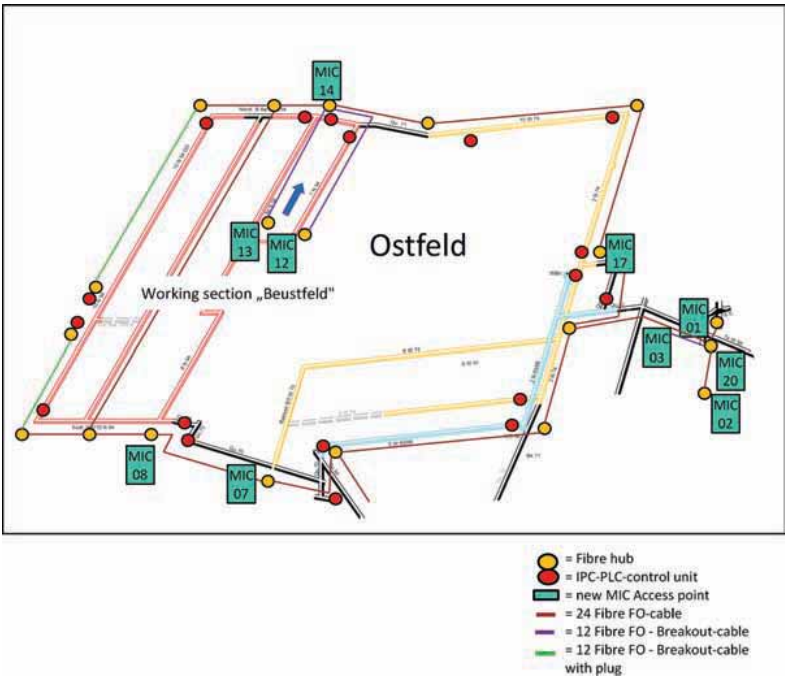

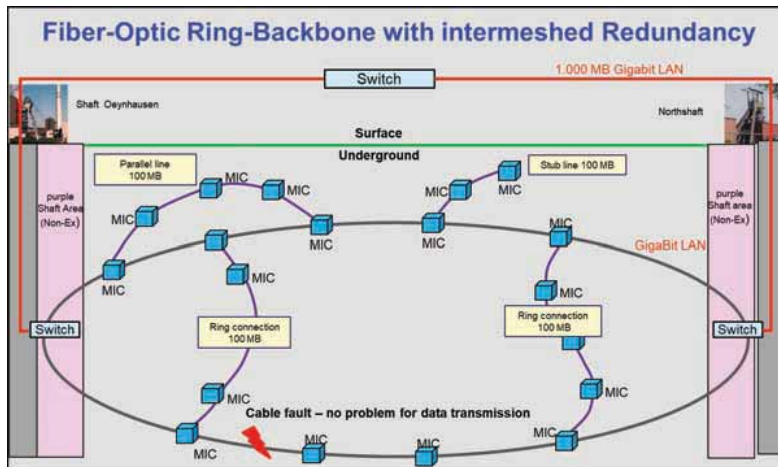Figure 1.   Fiber optic network, underground expansion status in end of 2014.

Figure 2. Network infrastructure with new ICT components at Ibbenbüren mine.
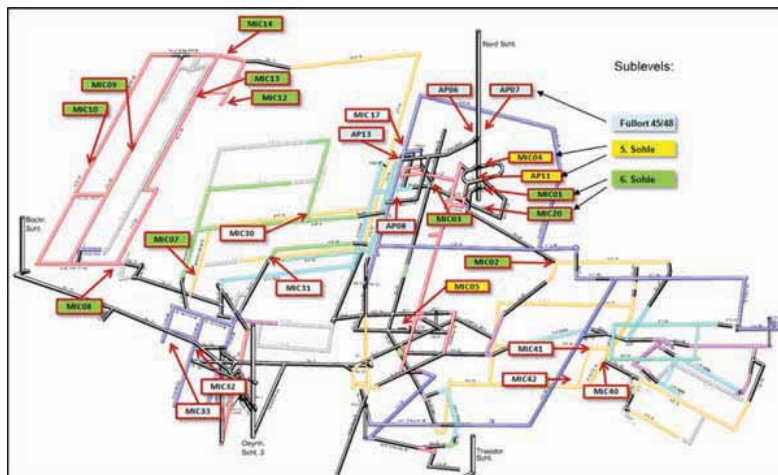

Figure 3. MIC's and RFID-Access points for material tracking.

Moreover, it met the expectation to enable operation of several different IT applications using different kinds of hard- and software from different manufacturers, only within one universal network system.

3 OPTIMIZATION OF MATERIAL LOGISTICS

The underground MIC's are equipped with intrinsically safe passive RFID readers. Thereby it is possible to detect and utilise passive long range RFID tags, which are affixed to the operation facilities (transportation units/containers).

Based on the experience of a former RFID project and in the course of the project OPTI-MINE, the MIC's positions and thereby the RFID reader's positions were optimised. The access points/MIC's (RFID readers) were distributed in the shaft areas of North Shaft and in the working section Beustfeld. The south part of the mining field was only partly equipped with this technique, see Figure 3. In the shaft close-up range, at the different levels (draw points 45/48, 5th level and 6th level) the RFID readers could be straightened out. Multiple readings at shunting of locomotives were thus eliminated.

The system is used to track containers and materials during the entire transport chain from the container loading position on the surface to the active underground workings.

After commissioning the ordered material in the SAP system, the material is loaded into transportation units (containers) on the above ground loading area. For each material commission barcode labels are printed by the SAP system which during loading process the loader attaches to the containers. Each material commission in the container is identified by such a label which can be electronically identified by an individual barcode. If multiple material commissions are loaded into the same container, multiple labels are placed on the container side.

At the same time all containers are equipped with two passive long range RFID tags on either side of each container. Both material commission numbers and container RFID tag numbers are known by the material handling database, see Figure 4.

After loading, the transportation units are pushed on a track through a small shack ("linking station") before they arrive at the shaft, Figure 5. Inside the linking station, an RFID reader detects the container tag. Thus the stored container number and the container type are known. At the same time, a barcode reader records the barcode label on the container, which indicates the commission number. Thereby the information on material content, commission and transportation unit are fitted together (linked) and thus the content and destination of each transportation unit are known. Next time, each transportation unit is detected via RFID at the shaft entrance before being lifted down to the mine. Another RFID reader at the shaft exit detects the containers returning from the underground installations. Ana-
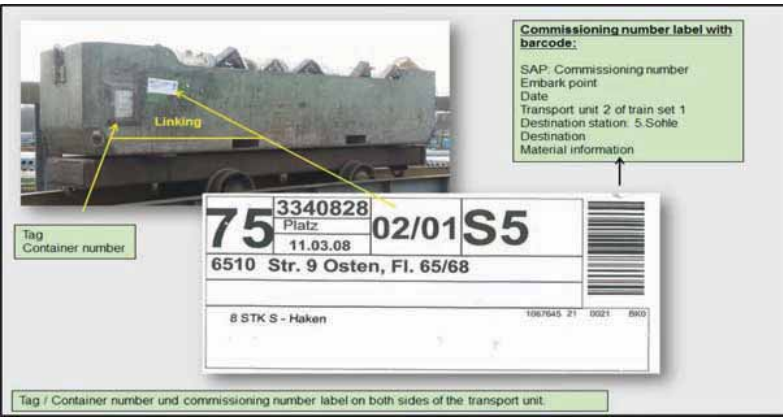

Figure 4.   Material Label and RFID tag on the container.

Figure 5.   "Linking Station" to connect material commissions with transportation container numbers.

logically the detection at the stations on the different underground mining levels takes place during the transport to the longwall operations and road headings, see Figure 6.

In the underground installations the containers are transported by monorail trains. In order to organize and keep track of the monorail locomotives these were also equipped with passive RFID tags similar to those used on the containers. This was the precondition to identify a particular train in order to create analysis about the equipment usage.

An existing container management software was upgraded to show the locations of containers as well as to improve the container handling. The visualization basically performed the following analyses:

- Access point scheme (illustration 'when' an access point reported last time).
- In time tracking of individual containers, respectively container types and material commission numbers (see figure 7).
- Current locomotive information and their transport units.
- Analysis of transport volume/container types at shaft entry/shaft exit.
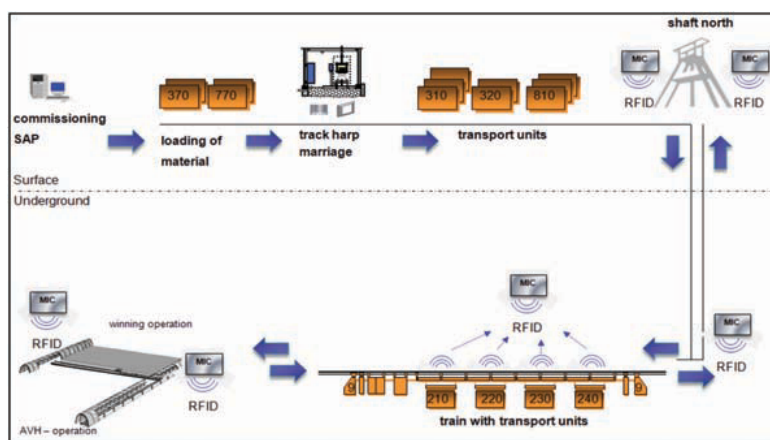

Figure 6.   Illustration of material and container tracking.
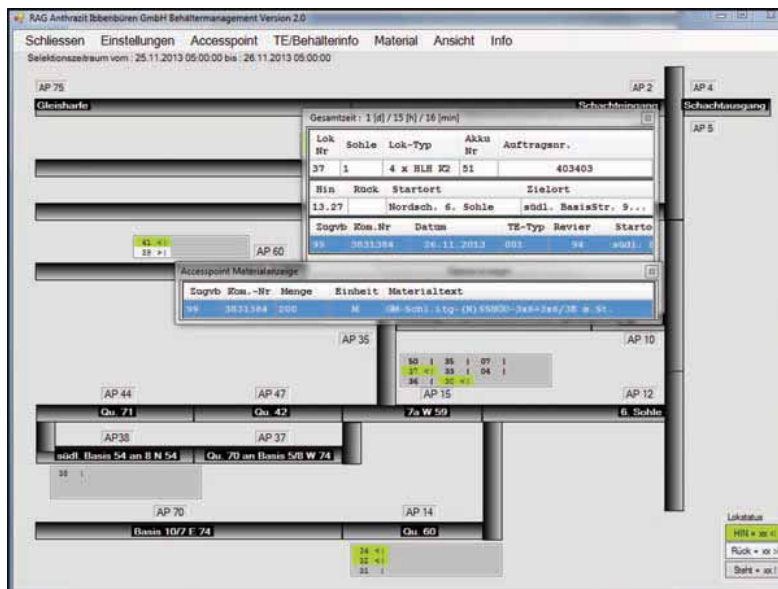

Figure 7.   Screen with container and material commission tracking and localization.

During the entire project, Key Performance Indicators (KPI's) were measured together with academic partners. For this part of the project, the KPI was defined and measured for RAG Anthrazit mine as a "TPI" (Transport Performance Indicator) measuring the achieved productivity gain in the field of container transport. For this KPI the number of transport units transported per day was compared to the number of man shifts in transport per day. At the end of the project, this KPI showed for transportation processes an increase in productivity of 30%.

4 CONCLUSION

A meshed fiber optic network infrastructure was installed at RAG Anthrazit hard coal mine. The active components conformed multi purpose units ("MIC–Mining Infrastructure Computers") which were used for on the basis of a meshed fiber optic network infrastructure which at the same time was also used for many other purposes and by the deployment of standardized network components, with standardized RFID and WLAN components inside the MIC's developed the company MineTronics, IT-systems for container tracking, material tracking, container management and for locomotive information could be built up and successfully operated. System was in use for regular operation in the production area of RAG Anthrazit mine in Ibben-büren/Germany for four years. Thereby a higher transparency regarding locations of operating resources in the logistics field could be demonstrated. In connection with that results a higher logistics efficiency and respectively cost reductions due to an optimized use of transport units and transport means.

All applications introduced during OPTI-MINE project add a certain value to the mines that make use of them. They either provide an information base for further process optimization (Material tracking and logistics), ease the communication with under ground workforce (Messaging, VoIP networks and legacy device integration) or reduce acquisition as well as configuration and maintenance costs (Automation, VoIP networks and legacy device integration, Machine to Machine communication). Further on, the whole under ground network installed in the participating mines follows open specifications and industry standards. Thus, it provides end-to-end communication without a vendor lock-in and therefore, the under ground network behaves like well known above ground technology, making network administration and network maintenance easier and more cost-reasonable. Dissemination of developed ICT technology to other potential users is considerable and possible.

REFERENCES

Bendrat, M., and Dauber, C. "Key Performance Indicators—A tool to assess ICT-applications in underground coal mines", Aachen International Mining Symposia 2014.
"Demonstration of Process Optimization for Increasing the Efficiency and Safety by Integrating Leading Edge Electronic Information and Communication Technologies (ICT) in Coal Mines", Final Report of research project OPTI-MINE, European Commission, Research Programme of the Research Fund for Coal and Steel, Reporting period: 01 July 2011–30 June 2014.
Kuschel, B., Misz, T.: OPTI-MINE, 4th Coordination meeting, Presentation "RFID transport capacity tracking and longwall control underground", Osnabrück, 2013.
Mueller, C., Huebner, A.: OPTI-MINE, 5th Coordination meeting, "MineTronics activities by work packages", Madrid, 2013.

Taylor & Francis
Taylor & Francis Group
http://taylorandfrancis.com

Mine safety in digital transformation

Development of blast-induced ground vibration wireless monitoring system

Ragam Prashanth & D.S. Nimaje
National Institute of Technology, Rourkela, India

ABSTRACT: In recent decades, the ground vibration induced by blasting is an inevitable outcome and severely damages surrounding structures. Hence, it is essential to monitor the ground vibration to evaluate and control the adverse consequences of blasting. Several conventional instruments were widely adopted to measure vibration in terms of Peak Particle Velocity (PPV). The major limitation of the conventional system is wire-based, expensive, and cannot transfer real-time seamless information. To mitigate, proposed a novel real-time, low-cost wireless vibration system. In this context, design and implement an economical wireless system to monitor PPV effectively. Further, discuss the overall architecture, integrating of hardware, and implementation of software protocols in the process of making the wireless system. Developed prototype having an accelerometer, Radio Frequency (RF) module, and microcontroller unit. The system was installed at different locations in Mine-A, India and obtained results ensure that PPV values are varied from 0.191 to 8.60 mm/sec.

1   INTRODUCTION

Drilling and Blasting (DAB) are the most pervasive excavation operations for rock fragmentations in the mining industry. Explosives are a valuable source of energy used to breakage, excavation, and displacement of the rock mass. During the time of explosive detonates, a large quantity of energy was realized. Only 20% of energy can be utilized for fragmenting the rock and remain wasted away in the form of ground vibration, air blast, fly rock, and back breaks (Ragam 2018a). The adverse effects of blast-induced ground vibration are the collapse of nearby trees and live hood, get cracks in mine office buildings, and chances to failure overburden dumps. Recently, the complaints are rapidly increased given by mine resident people owing to the effects of ground vibrations due to blasting. Thus, it is necessary to monitor and control ground vibration. Usually, ground vibration can be expressed in terms of peak particle velocity (PPV) and the units are an mm/s. Limit values for Blast-Induced Ground Vibration (BIGV) are recommended in the standard by Directorate General of Mines Safety (DGMS) circular No. 7 of 1997 in India. The permissible PPV of ground vibration at a sensitive structure should be below 5 mm/s (Ragam 2018b). Researchers, academicians, and scientists are widely used conventional type seismographs to measure the PPV in various mine case studies. The conventional systems such as Instantel Blast mate-III, Minimate Plus, Minimate Pro, UVS1500, MR 202-CE etc. are installed to evaluate ground vibration levels (Nimaje 2019) in open cast mines (Fig. 1). The presently used conventional instruments have one to three geophone sensors to measure PPV (mm/sec) and one microphone sensor for air blast measurement (dB). The prices of the available systems are starting from US $4500–7000 dollars.

1.1   *Limitations of existing systems*

The conventional devices like Instantel Blast mate-III, Minimate Plus, Minimate Pro, UVS1500, MR 202-CE used for measuring the PPV are cable-based communication system

Figure 1.   Various types of seismographs installed in mines.

type and have limitations such as (Ragam 2018c): Susceptible to failure due to breakage in the wire; Wire impedance owing to the length of wire not possible to extend; Cannot transfer the measured data in real-time; Expensive systems; Limited storage memory; Need an expert to operate; Tedious and time-consuming process.

To mitigate the aforementioned limitations, proposed and developed an economical and reliable wireless sensor network (WSN)-based system. In recent years, Information and Communication Technologies (ICT) has been used extensively and inexpensive Micro-Electro-Mechanical-System (MEMS) technology has enabled in the applications of environmental and industrial monitoring. In addition, these sensors are embedding within the WSN. As a result, the embedded of both MEMS sensors and RF modules were enhanced transmission abilities for the application of BIGV monitoring with novel methods such as the utilization of WSNs for the realization of low-cost monitoring systems. The main objective of integrating various MEMS sensors within the WSN has initiated by researchers in the new millennium. Moreover, the price of a MEMS accelerometer sensor may be just 10% or less over the commercially available conventional accelerometer along with the signal condition unit. MEMS accelerometer has become a ubiquitous part of everyday life owing to their small dimension (currently even less than 2mm), easy to integrate with any electronic devices, high shock-resistance, high reliability, high accuracy, low power consumption, and low cost (Luczak 2017).

Few researchers (Kim 2013) already remarked the advantages of WSN technology over conventional monitoring systems. It covers a wide range of objects from various embedded operating systems and micro-controller units to wireless protocols. The intelligent internet-based network connects ubiquitous devices to the internet to exchange seamless data and communicating via sensing devices according to agreed protocols. It accomplishes the aim of intelligent identifying, locating, tracking, monitoring, and managing things. It is used to establish communication from person to person as well as things and things. In this WSN paradigm, various things surrounding us should be attached to networks in one form or another. WSN has three main characteristics and as follows (Chen 2014):

1.1.1   *Comprehensive perception*

Sensor devices, radio frequency identification (RFID) tags, and barcode are providing the information of objects at any time and anywhere which will be a great opportunity. By using it, sensing information and communication system can be invisibly embedded in the environment. Wireless sensor network enables us to interact with real-world remotely. Objects and locations are identified using identification technologies. Identification and recognition of the physical world is the basic foundation of developing overall perception.

1.1.2 *Reliable transmission*

Sensing object information can be available at any time through multiple radio networks, telecommunication, and the internet. Communication technology includes wire, wireless transmission, switching, and gateway technologies. Further, WSN provides an interactive platform among the real physical world, the digital world, and the machine to machine (M2M). The important technology of networks of things is established and communicated between M2M as well as machine to human.

1.1.3 *Intelligent processing*

After receiving the information, it stores in the database including computing technology like cloud computing. The available network service providers process the billions of messages immediately using cloud computing technology. Thus, this technology is the main promoter of WSN applications.

In this context, the main aim of this study is to help mine administrations, blast experts, and nearby residing community to obtain real-time information such as BIGV data from an end user (sink node) through wireless sensor nodes. A Global System for Mobile (GSM) RF module has been placed in the sensor node as an RF protocol conversion in between blasting point to end users such as mine managers, experts of blasting as well as rural peoples who live in and around the mine area. The designed wireless system was installed successfully at different locations in Mine-A, India and monitored the vibration levels (in terms of PPV) over a period of eleven days.

2 SYSTEM ARCHITECTURE

Usually, ground vibration due to blasting is a low frequency and low amplitude waves. Thus, it is very difficult to capture. An accelerometer sensor is used as a sensing device which captures the vibration as well as earthquake waves. It is essential to measure low frequency and low amplitude signals, choose high sensitivity and low noise density MEMS-based accelerometer sensor. The proposed system consists of three layers and depicted in Figure 2. The layers are (Akyildiz 2002):

1. Sensing Layer
2. Network layer
3. Application layer

The first layer of the proposed system is the sensing layer and the main role of it is to collect the physical characteristics data. Sensor nodes are deployed in the unmanned dynamic environment in and around the blasting site at different vulnerable distances. Sensor nodes are configured by a star/mesh topology network to exchange information in a network layer section.
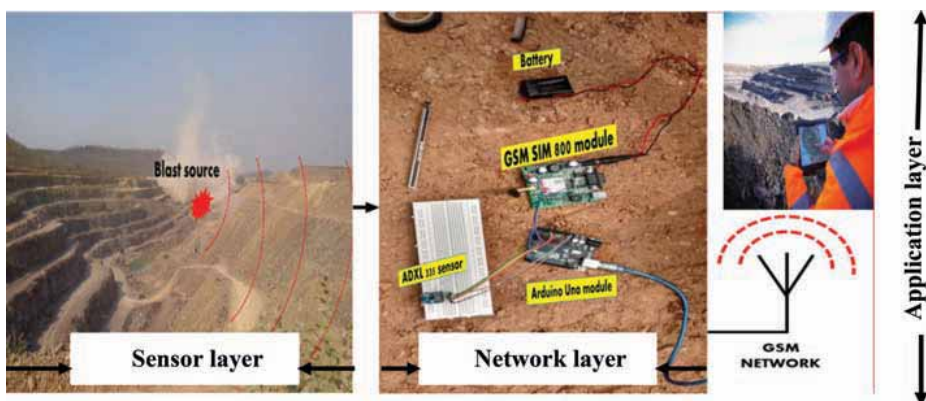

Figure 2.   System architecture.

2.1 *Sensor node*

Sensor node consists of a microcontroller unit (MCU), an analog-to-digital converter (ADC), RF module along with an accelerometer sensor shown in Figure 3. Each sensor node has to be placed at various distances from the blasting point. For instance, sensor node 1 is deployed at a 100 m distance from the blast source. Similarly, Sensor node 2 and node 3 might be placed at other distances (200 m, 250 m, and 300 m. etc.). After blasting, the generated waves are captured by each accelerometer sensor of respective sensor nodes and converts into appropriate electrical (voltage) signals. Every sensor node is to collect and send the sensed data to the Global System for Mobile communication (GSM network layer) RF module.

Similarly, the main function of the network layer is to transmit the information from the sensor layer to application layer using GSM module receives the sensor nodes 1, 2 and 3 data sequentially and convey to end user using AT commands (Fig. 2). In the end, the end user can retrieve the information to analyze in the application layer. Finally, the sensed data from sensor node 1, 2 and node 3 must be displayed in the system (PC) as well as tablet/phone (if required) using SMS (Fig. 4).
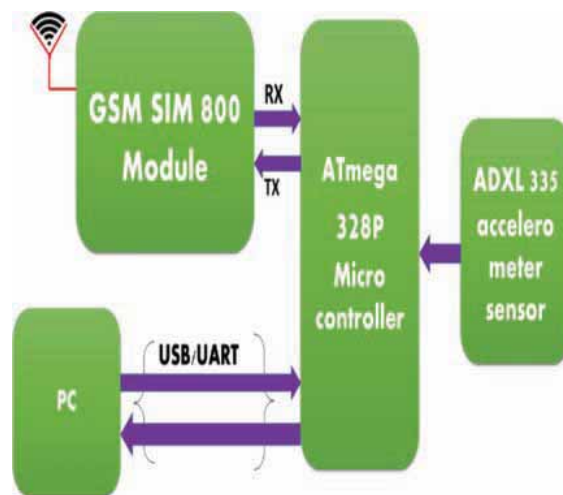

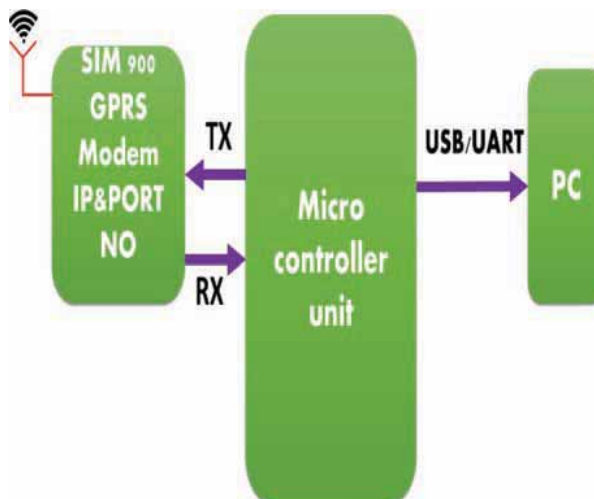Figure 3. Architecture of the sensor node (mote).

Figure 4. Architecture of receiver node.

Figure 5. Integration of ADXL 335 accelerometer with Arduino microcontroller board and GSM.

3 DEVELOPMENT OF WIRELESS SENSOR SYSTEM

The system consists of MEMS accelerometer (ADXL 335), RF module (GSM), and Arduino Uno microcontroller board as shown in Figure 5. ADXL 335 is inexpensive 3-axis accelerometer having moderate sensitivity range lies between 270–330 mV/g and low noise density varies from 150–300 μg/√Hz rms. It was used to measure tilt, acceleration, rotation, and vibration with a range of ± 3 g. These MEMS-based accelerometers have an advantage over the conventional accelerometers that they are capable of measuring the acceleration due to gravity (Manjiyani 2014). Arduino Uno is an open-source single-board using ATmega328P microcontroller considered as a processing unit. It provides sets of digital and analog I/O pins that can be interfaced to various expansion boards and other circuits. The boards feature serial communications interfaces, including USB on some models, for loading programs from personal computers. For programming, the microcontrollers, the Arduino platform provides an integrated (IDE) based on the processing project, which includes support for C, C++ and Java programming languages.

GSM 800 device is used as an RF module to establish wireless communication. Three outputs of the accelerometer sensor are plugged into the standard expansion headers on the Arduino Uno development board represented in Figure 5. The software program was implemented in the Arduino Integrated Development Environment or Arduino Software (IDE) which contains a text editor for writing code, a message area, a text console, a toolbar with buttons for common functions and a series of menus. The testbed has been designed and developed by interfacing Arduino Uno with triaxial accelerometer ADXL 335 and GSM module SIM 800. The accelerometer needs a power source of 5 V and Grounding. GSM SIM 800 RF module requires a power supply of 9–12 volts along with proper grounding. The transmitter (Tx) section of Arduino Uno board is connected to the receiver of GSM module so that Arduino can send the accelerometer readings to GSM module and therefore the GSM 800 shall send the data obtained from Arduino to any displaying device i.e, mobile phone or personal computer (PC).

4 FIELD EXPERIMENT

The designed system has been installed at different vulnerable and strategic locations from the blast site as depicted in Figure 6. The investigation has been carried out in Mine-A with a longitude of 83°32'57.4" and latitude of 21°41'24" located in India. It is fully mechanized limestone mine operated by DAB to primary breakage and rock fragmentation. Atlas Copco makes D50 and Sandvik make TITON 500 drill machines are widely used for DAB

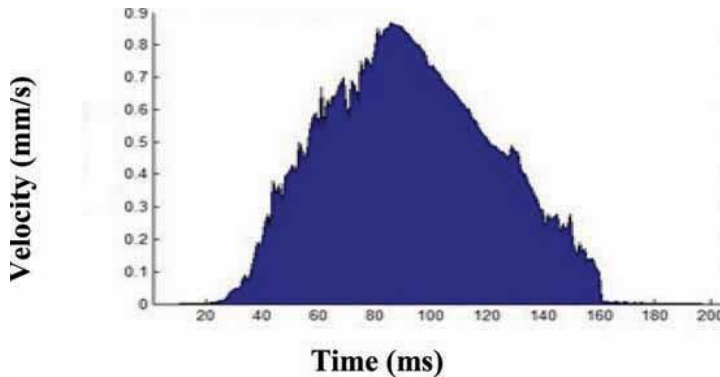Figure 6.   Installation of test bed in Mine-A.

Figure 7.   Recorded PPV using accelerometer based test bed at 600 distance.

operations with around 9 to 10 m bench height. Burden varies from 3–3.5 m, the spacing between 4–5 m, and quantity of charge per hole between 40–60 kg for 115 mm hole diameter. Accordingly, the stemming column in the blast holes also varies between 2.5–3 m. Staggered pattern and the square grid pattern of holes are drilled. The blast hole depth is 10 meter including 10% subgrade drilling.

The non-electric (NONEL) system of initiation (TLDs 17/250 ms and 25/250 ms) is being used for blasting work in combination with ANFO and cast booster weighing 150 gm. In case of watery hole during the rainy season and in the lower bench, large diameter slurry explosive cartridges (Aquadyne and super gel) were used for blasting. Each blast is monitored for ground vibration and fragmentation and necessary care has been taken based on the report obtained. Minimate plus device is used for measurement of ground vibration in the field survey. In blasting, two to three rows of holes are blasted at a time and maximum of 60 holes are blasted at a time with proper initiation, charging pattern and charge per delay. Delay is set in such a way that each hole gets the adequate free face and blasted at a time. Hence optimum fragmentation with reduced ground vibration is achieved. So practically the charge per delay is only the amount of explosive placed in a single hole, i.e. 40–60 kg.

The developed system was installed in Mine-A. Eleven PPV values were captured at each measured point using a test bed along with Minimate Plus seismograph. The obtained PPV values are varied owing to the distance between the blast point and the monitored location and other parameters such as a charge per hole, number of holes, spacing, burden, and hole depth. The test setup was placed at different monitoring locations (distances) every day to
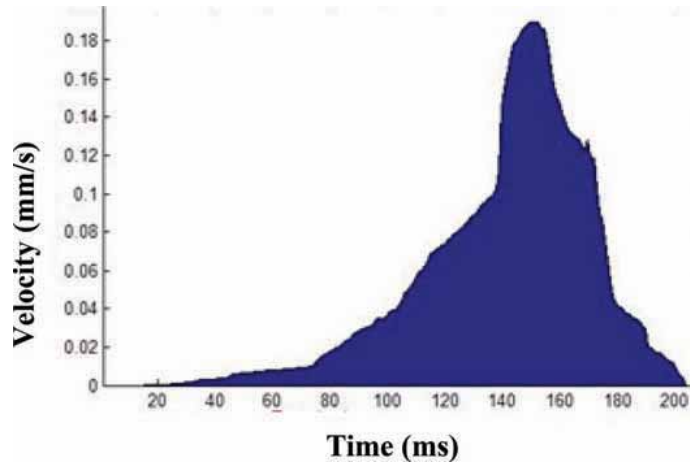
Figure 8.   Recorded PPV using accelerometer based test bed at 750 distance.
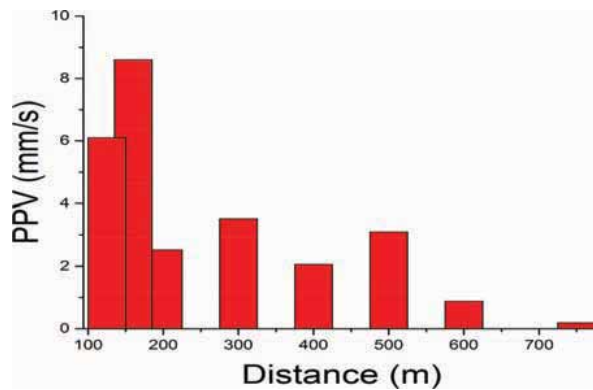

Figure 9.   Measured PPVs with respect distances.

detect blast event PPV while blasting operation. On the first day, the testbed was installed at a 125 m distance from blast face and the observed PPV as 6.02 mm/s. Similarly, the next day the PPV was observed 8.25 mm/s at 150 mm distance. Each of the recorded PPV value is plotted in MATLAB 12(b) software as shown in Figures 7–8. The same process had been carried out for remaining days (total of eleven recorded values) and depicted in Figure 9. The obtained results are plotted in MATLAB software to easily analyze and observation of PPV ranges.

5   CONCLUSIONS

In this investigation, a system was developed for monitoring the peak particle velocity induced by blasting. Three-axis ADXL 335 accelerometer sensor was employed as a sensing device and GSM 800 RF module for establishing communication between test setup source to the authorized mobile user. The following conclusions were drawn from the field investigation:

1. Developed an inexpensive system by integrating an accelerometer sensor, GSM RF module to Arduino UNO microcontroller board. Software programming has been implemented in Arduino IDE open source software and installed in Mine-A, India.
2. The investigation has been conducted a period of eleven days and recorded eleven PPV values at different locations (distances) from the blast point.

3. The obtained results were revealed that minimum PPV observed as 0.191 mm/sec at a distance of 750m from blast source to the monitoring point. On the contrary, maximum PPV value (8.6 mm/sec) detected at a 150m distance.
4. The rigorous investigation should be required to monitor the BIGV at various locations from the blast source to monitor PPVs with the developed system.

6 FUTURE SCOPE

A number of PPVs values obtained by installing more accelerometer sensors (sensor nodes) which monitor a larger area within a low budget. The GSM RF module has an added feature i.e., it can be used as a warning system by giving the alarm. Thus, it was utilized for alerting through the audio signal to the persons working in the mines. LoRa is an RF module which has a coverage range around 2–15 km. However, integration of IoT with LoRa RF can be implemented for accessing monitoring data from anywhere in the world which is an emerging area.

REFERENCES

Akyildiz, I.F., Su, W., Sankarasubramaniam, Y., & Cayirci, E. 2002. Wireless sensor networks: a survey. Computer Networks, 38(4):393–422.

Chen, S., Xu, H., Liu, D., Hu, B., & Wang, H. 2014. A vision of IoT: Applications, challenges, and opportunities with china perspective. IEEE Internet of Things journal, 1(4):349–359.

Kim, J., Kwon, S., Park, S., & Kim, Y. 2013. A MEMS-based commutation module with vibration sensor for wireless sensor network-based tunnel-blasting monitoring. KSCE Journal of Civil Engineering, 17(7):1644–1653.

Łuczak, S., Grepl, R., & Bodnicki, M. 2017. Selection of mems accelerometers for tilt measurements. Journal of Sensors, 2017:1–13, Doi:10.1155/2017/9796146.

Manjiyani, Z.A.A., Jacob, R. T., Keerthan Kumar, R., & Varghese, B. 2014. Development of MEMS based 3-axis accelerometer for hand movement monitoring. International Journal of Scientific and Research Publications, 4(2):1–4.

Nimaje, D.S., & Prashanth, R. 2019. Application of MEMS-Based Accelerometer Wireless Sensor Systems for Monitoring of Blast-Induced Ground Vibration and Structural Health: A Review. IET Wireless Sensor Systems, Doi:10.1049/iet-wss.2018.5099.

Ragam, P., & Nimaje, D.S. 2018a. Evaluation and prediction of blast-induced peak particle velocity using artificial neural network: A case study. Noise & Vibration Worldwide, 49(3):111–119.

Ragam, P., & Nimaje, D.S. 2018b. Monitoring of blast-induced ground vibration using WSN and prediction with an ANN approach of ACC dungri limestone mine, India. Journal of Vibroengineering, 20(2):1051–1062.

Ragam, P., & Nimaje, D.S. 2018c. Selection and Evolution of MEMS Accelerometer Sensor for Measurement of Blast-Induced Peak Particle Velocity. IEEE Sensors Letters, 2(4):1–4.

Increased safety in deep mining with IoT and autonomous robots

F. Günther & H. Mischo
TU Bergakademie Freiberg, Institute of Mining and Special Civil Engineering, Freiberg, Germany

R. Lösch & S. Grehl
TU Bergakademie Freiberg, Institute of Computer Science, Freiberg, Germany

F. Güth
TU Bergakademie Freiberg, Institute of Electronic and Sensor Materials, Freiberg, Germany

ABSTRACT: 'Safety first' – all miners know the importance of this slogan. Personal protective equipment, automated or remote-controlled machinery and safety instructions all help to avoid accidents underground. However, there are still many dangerous mining situations where the risk to human life is too high. Modern technologies can help to overcome this obstacle. Researchers at the TU Bergakademie Freiberg are working with autonomous robots and the Internet of Things in underground mining. A mobile autonomous robot, in combination with a wireless sensor network, can help to explore unknown or inaccessible areas. These could be in abandoned or active mines, where hazardous situations occur with unpredictable risks too severe for human activity. This paper will focus on development and application possibilities of this technology, especially regarding mine safety. The first test results from the prototypes will be presented from the viewpoint of a mining engineer, with respect to benefits and limitations for mine operators.

1 INTRODUCTION

The feasibility of a mining project is determined not only by its profitability, but also by the fact that work must be carried out safely. In contrast to other branches of industry, mines seem to be a particularly unsafe workplace due to the special environmental conditions. Lack of light, confinement, danger of falling rocks, and the occurrence of dangerous gases are just some of the factors. Today, almost all accidents can be avoided through targeted actions. If we consider only the accident statistics of the BGRCI (German Social Accident Insurance Institution) for the raw materials and chemical industry as an example, we can see that both in 2010 (13.9) and in 2017 (10.4) the lowest number of accidents per 1,000 full-time workers were reported in the mining sector compared to the other branches of industry represented in the BGRCI (Ø 2010: 19.2 and 2017: 18.1) (Berufsgenossenschaft Rohstoffe und chemische Industrie 2010, 2017). These figures show a positive downward trend. Nevertheless, the Saxon Mining Office recorded a total of 70 reportable accidents at work in 2017. Of these, 21 were caused by falling rocks or other objects (Sächsisches Oberbergamt 2017).

The goal for research and development in mining should therefore always be to increase occupational safety, so that even more accidents can be avoided. Increasing the automation level and the use of autonomous robots within the mining process is just one way to achieve this goal. Another approach is a significant increase in sensory data acquisition and the use of intelligent evaluation algorithms. Large mining companies, for example, are already using autonomous trucks for underground mining (Mining Magazine 2016). However, technologies that can be used in unknown and non-instrumented underground mining environments are not yet fully developed or commercialised. Forgotten, abandoned or historic mines can all be found in the Saxony Ore Mountains. When damage occurs to the surface, such mines must

be remediated and supported by specialised mining companies. Unawareness of the exact locations, extent and conditions of such mines can be a great danger to workers.

Scientists of the TU Bergakademie Freiberg investigate technologies in a number of projects and implement prototypes to support those activities. In the following, the project ARIDuA, its possible use-cases, requirements and challenges are shown in two examples. The researchers focus on the practical aspects during the implementation and deployment phase. In specific one may see that besides the increasing safety underground, robots and sensors themselves can become a source of danger.

2 PROJECT OVERVIEW

Robotics and IoT technologies are research targets of the ARIDuA-Group (Autonomous Robots and Internet of Things in underground mining) at TU Bergakademie Freiberg (Germany). These junior research group, founded in 2017, has an interdisciplinary structure in order to benefit from synergies through the combination of technology concepts. Six PhD students from the disciplines of computer science, materials science, mine surveying and mining, develop interdisciplinary concepts and prototypes with the aim of progressive digitization and automation in underground mines.

The ESF-funded project (European Social Fund), which runs until mid-2020, aims to develop an autonomous moving robot for the installation and maintenance of underground IoT infrastructure (Lösch et al. 2018b). The mining robot "Julius" from the previous project "Mining-RoX" (Grehl et al. 2017) id used as a platform and will be developed further. Among other things, a wireless sensor network (WSN) is installed. To further benefit from this structure, mobile sensor box integrate a communication layer and act as nodes within this network, instrumenting the mine itself. These sensor boxes should be able to record relevant ventilation data using sensors and connect wirelessly both to the Internet and other devices. In addition, evaluation algorithms for predicting dangerous events using neural networks based on the acquired sensor data will be developed. In parallel, a classification algorithm for the detection of ore veins based on optical characteristics will be created (Varga and Grehl 2018), so that all technologies together are a first step to a unmanned mine. The universities own research and teaching mine "Reiche Zeche" in Freiberg is available as a unique test environment (Mischo 2015). Sections of the mine (depth: 150 m) are used for underground tests in a real-world environment.

3 POSSIBLE APPLICATION SCENARIOS AND TASKS

Before developing and installing underground wireless networks, neuronal networks, autonomous mining robots or mobile sensor boxes, the question of the purpose for which these technologies are to be used must be answered. As a boundary condition for the ARIDuA project, the sites should be limited to underground mines. Within the framework of the project, the focus will be on mines in Saxony, Germany. Both the research and training mine "Reiche Zeche" and the abandoned mines in the Ore Mountains (Erzgebirge) are former ore mines, where mainly silver, non-ferrous metals and uranium were mined. In these mines, active mining was stopped at the latest in the second half of the 20th century. Today, they are mostly used for tourism. In total, there are 52 mines open to visitors in Saxony (Sächsisches Oberbergamt 2016). Other historic mines have been partly abandoned since the Middle Ages and their existence or condition is poorly known. The only three active underground mines in Saxony are located in Niederschlag (fluorspar), Seilitz (kaolin) and Hammerunterwiesenthal (marble) and are managed by small companies (Sächsisches Oberbergamt 2014). While there is a large number of remediation work underground in old and abondened former mines.

The resulting technologies can be also used in regular operation, for scheduled monitoring or maintenance of the mine. Possible tasks include the automated sensoric measurement of environmental conditions. In addition to ventilation data such as gas concentrations or

Table 1. Environmental parameters of particular interest in "Reiche Zeche".

Gases	Air	Mine water		Flora & Fauna
Rn	Temperature	pH-value		Fungi
CO	Humidity	Sulphate content		Bacteria
CO_2	Air pressure	Electrical conductivity		
NOx	Air velocity	Flow volume		
O_2		Content Cr, Cu, Ni, Cd, Co, Pb, Zn, Cl, Fe, C, As		
H_2S		Water level		
CH_4		Redox potential		

temperature, this also includes information about mine water. Table 1 provides an overview of the environmental conditions of particular interest in the "Reiche Zeche". It is possible to integrate systems for personnel or machine tracking via a wireless data network. The precise location of workers and visitors underground is of considerable interest, especially in hazardous situations. This IoT instrumentalisation of a mine, comparable with the functionalities of "Smart Home" solutions for private houses, can be installed and maintained by workers or a robot. Further robotic tasks can be mapping, providing 3D scans for calculations and virtual mine models, as well as colour images and video recordings of the drifts. This can be done both in addition to human inspection and data recording, but also especially in those areas of the mine that are unknown or inaccessible. At the same time as the environmental conditions are recorded, robots and WSN can also be used to explore abandoned mining areas.

In the case of incidents such as a major gas blowout, an explosion or an unexpected roof collapse, information about the current condition of the mine and the ventilation conditions underground is rarely available. Under these dangerous conditions, people must explore the situation on site slowly and with measuring instruments, without endangering their own health. Especially in such situations, the first ascent after the event and collection of relevant data without endangering human life is of high interest. A robot could remotely or autonomously access and explore all hazardous areas accessible even only through small openings. Either the data is transmitted directly to the surface or to a safe area, or the robot first returns and the data can be evaluated. In addition to being used after an event or incident, it is also conceivable that IoT and robotics could be used together with the mine rescue team to prevent hazards and for rescue operations. As well as for preliminary exploration in front of the team, a robot could also be used to transport material and establish a communication link to the incident command. In addition to voice transmission, video transmission to the surface can also be beneficial for more detailed mission planning. Further task scenarios are of course imaginable for the individual mines. It should also be considered that not all tasks can be performed simultaneously by one robot, thus a number of robots can be deployed simultaneously.

4 ADVANTAGES

The advantages of using this type of modern equipment are a massive improvement in work safety for the miners. If machines can be sent to unknown or potentially dangerous areas instead of people, numerous dangers to human health can be avoided. In addition to risks of rock fall or water entry, these include the dangers of toxic or non-respirable air and natural radioactivity. Moreover, descent into the mine can be avoided in areas with inadequate ventilation or high temperatures.

Robotic map creation of previously unmapped areas benefits work planning, the deployment of mine workers and is basis for ventilation planning. In an emergency, a tracking system shows the position of people underground and, if necessary, their direction of movement. This allows rescue operations to be coordinated more efficiently. The installation of (wireless) communication networks by the robots, mobile or fixed, is an advantage for the

entire mine operation. Today, communication during an incident or rescue operation is often only possible via a few permanently installed telephones. Once an overall network exists, devices can be integrated to transmit voice or text messages. This enables workers to get help faster, be informed about events or receive instructions quickly.

A massive increase in sensor data collection, in addition to, or even in combination with, an intelligent evaluation algorithm, can detect increased gas concentrations or other deviations from the normal value at an early stage. Occupational safety actions can be initiated more quickly to prevent accidents. Besides the higher frequency of automatic data acquisition in contrast to manual measurements, it is also easier to store relevant digital data for documentation. These can be used for later assessment or as a data basis for improvements in operation.

In addition to numerical sensor data, image data also reflect the state of the environment. By recording point clouds and various camera and video images, mine workings which are difficult to access can also be seen without human on site-inspection. The data can be used for pure visualization, inspection, documentation or to create models. 3D mine models are an excellent basis for training, e.g. for learning machine handling or for simulators. At the TU Bergakademie Freiberg, for example, a mine rescue simulator was developed from the data recorded in the "Mining-RoX" project from a section of "Reiche Zeche" mine (Schmieder 2017). In this simulator the students train to handle rescue operations in a team, while sitting in front of laptops. They are using software, which is designed like a computer game and they control virtual mine rescuers in a simulation of the 'Reiche Zeche'. This is the preparation for trainings in the real section in the mine. Additionally such simulations can be extended to virtual reality environments, with the expectation of a much more higher learning effect.

Therefore, not only the health protection of the workers but also the higher efficiency and accuracy are valuable factors for the application of these new technologies. Machines can also work in cooperation with employees but at a constant quality, independent of break times.

5 CHALLENGES FOR REALIZATION

Despite the significant advantages the progressive automation and digitization with the long-term target of an unmanned mine are confronted with numerous difficulties. In particular, these difficulties result from the special nature of the mine environment in contrast to surface industrial facilities, legal issues, the handling of large amounts of data and the individual requirements of prospective users. Furthermore, each mine must be considered separately for each application. The following sections give an overview of possible problems and challenges, although it is not an exhaustive list.

5.1 *Underground environmental conditions*

Underground mines are artificial cavities created for the purpose of extracting raw materials. The environmental conditions in a mine highly depend on the depth of the mine; the mineral extracted, the surrounding rock and geology, the mining technology or current use of the mine and several other factors, and are unique to each mine. Temperatures range from cool to very high (typically from 8°C to 50°C). This defines high requirements on material durability. Materials behaviour during temperature changes should also be considered, e.g. when entering or leaving the mine. Ore mines in particular are characterised by a very high relative humidity, up to 100%. Often there is dripping or stagnant water on the floor, and the mine water often has very low pH values, causing corrosion or short circuits. In general, no natural light is available underground, hence without artificial light absolute darkness exists. Specifically, for the use of detection algorithms based on optical features, the very different lighting conditions represent a problem. The outgassing of CH_4 in some pits can create explosive environments, so potential ignition sources must be avoided. Depending on the extraction method and raw material, a lot of dust is generated during driving, which can contaminate sensors and equipment and make them unusable.

5.2 *Difficulties for construction*

In contrast to above-ground facilities, mines are defined in their maximal spatial extent. They are bound to the place of the deposit and active operations continue to develop dynamically. There are at least two entrances to the mine, sometimes more. However, these shafts or ramps have a limited cross-section. This limits the maximum dimensions of the equipment that can be transported underground. The same applies to the mine workings in which they are used. The transport possibilities in a mine are restricted by the dimensions of the relevant machines. The equipment must be transportable with the available machinery and be loadable or even drivable. Vibrations or bumps may occur during transport which may cause damage to the construction or electronics. For the construction of mobile robots, the necessary ground clearance of the device and a suitable mode of transport must also be selected. Obstacles can be rails, uneven floors, installations and support, standing or flowing water and rock masses. Mobile devices must have independent power supply, i.e. sufficient battery capacity. When rechargeable batteries are used, safety during charging must be ensured. The main hazards here are explosion or ignition of the battery in the event of defects. None of the devices must block escape routes in the event of a defect. Furthermore, protection of workers from mechanical hazards such as jamming or falling over of the device must be ensured by the constructive design in advance.

5.3 *Challenges for autonomous navigation*

Autonomous driving for street vehicles is already well advanced above ground. However, the findings can only be applied to a limited extent in autonomous underground navigation. The biggest difference is the lack of GPS or a similar localization system on an industrial level. As a minimal requirement any autonomous robot needs information about its surrounding area, i.e. by the method of laser scans. Its geo-reference inside the mine however is more a nice-to-have feature, from which especially the robots mapping algorithms will benefit. Particularly in unknown or non-instrumented mine environments, it is a challenge to link the local map of the robot with the real-world coordinates. A similar problem arises for determining the exact depth at which the robot is located. Other factors such as the uneven floor, reflections on water surfaces or changing cross sections, challenge the autonomous navigation. Besides this independent operation mode, the robots activities may always be overwritten by a human operator at any given time, ideally remotely either from underground or outside of the mine.

5.4 *Data transmission and further processing*

The establishment of data networks in mines is much more difficult than in other closed environments. It is possible to transmit wired data; however, this is only practicable for permanently installed sensors. Due to the continuous dynamic development of the mine and the mining process, installation and extension work of the corresponding infrastructure is continuously necessary. The use of wireless networks is also advantageous with regard to the integration of numerous mobile sensors and devices. However, the expansion of radio waves underground is massively restricted due to the small cross-sections, massive walls of rock, unevenness of the walls, supports and installations in the route, layout of the drifts and others. In some cases, data can only be transmitted over a few meters or, in most cases, only with a visual connection (line of sight, LOS). The selection of a suitable radio network is crucial for its performance underground. The use of electromagnetic waves underground must be checked in advance with regard to explosion protection and blasting work. Through automation, digitization and monitoring, the number of sensors and therefore the acquired data increases immensely. The collection and further processing of data must comply with legal regulations. The extent to which personal data may and must be collected has to be considered in the same way as the anonymization of data in individual cases. The large amounts of data still pose a problem. In order to manage this, they have to be selected, evaluated, processed and stored using suitable algorithms. Questions like these have to be solved before the data acquisition starts.
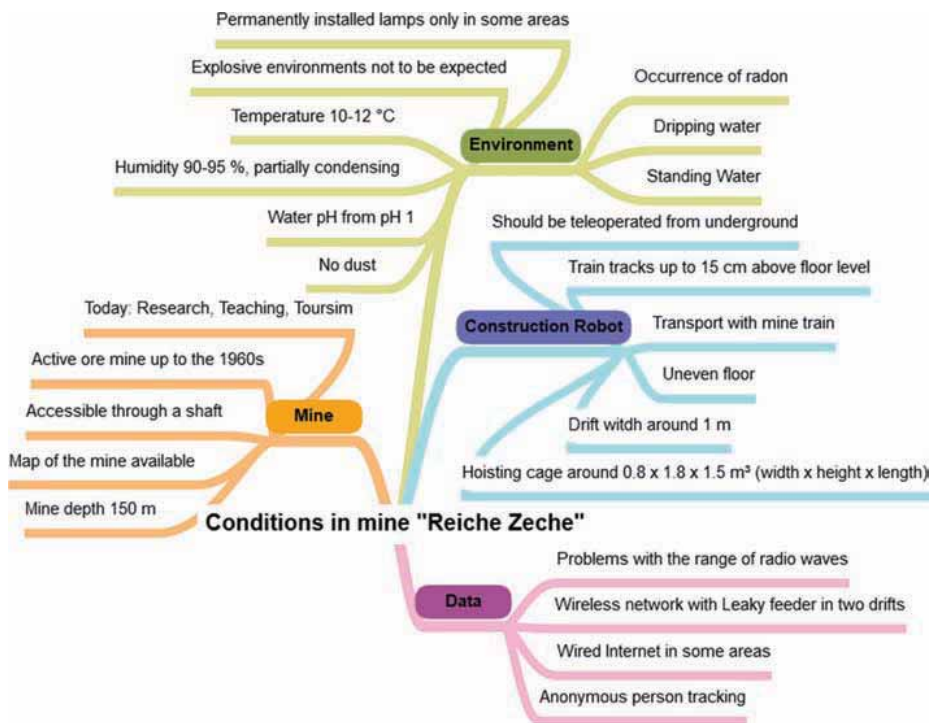
Figure 1.   Conditions in the research and teaching mine "Reiche Zeche".

5.5   *Integration into mine operations*

The scepticism of mine operators and especially miners regarding IoT technologies and robotics is usually very high. The operability of the equipment must be adapted to the training level and capabilities of the workers. This also includes ergonomic design. Currently there are still difficulties in answering legal questions regarding the use of autonomous machines together with humans. This concerns health protection but also liability issues in the event of accidents involving autonomous technology. In spite of the benefits for employees in terms of increased safety, smaller companies in particular have to ask themselves whether investments in these new technologies are economically viable. The applications presented are not primarily aimed at increasing productivity or output. Furthermore, qualified specialists must also be available for installation and maintenance.

5.6   *Conditions in the research and teaching mine "Reiche Zeche"*

A review of some of the challenges addressed in the previous sections was carried out for the Research and Training Mine "Reiche Zeche". The technologies researched in the ARIDuA project will initially be adapted for the test cases in this particular mine. Knowledge of the conditions there became necessary for the prototypes presented as examples in Chapter 6. The representation of some aspects can be seen in Figure 1.

6   RESULTING PROTOTYPES

So far, a large number of devices and algorithms have been developed in the ARIDuA project. Two focal points of the project work, the robot and the WSN, are described in detail in the following chapters as excellent examples of the research work. It is also shown how the challenges described in chapter 5 were solved, in particular how they were adapted to the special

challenges of the "Reiche Zeche" (see 5.6). In addition, excellent work has been done in the field of data evaluation, automated geological mapping, robotic manipulation and navigation, which is here not further discussed.

6.1 *Wireless Sensor Network (WSN)*

The developments within the project regarding the WSN have focussed so far on two aspects: the identification of a wireless data transmission technology suitable for the layout of the Research and Teaching Mine and the implementation of sensors for relevant variables as listed in Table 1. Suitable equipment for both tasks were selected from commercially available components with special emphasis on low energy consumption, small form factor and freely accessible data interfaces. This approach enables the assembly of tailor-made and battery powered sensor nodes from parts by various manufacturers for specific measuring tasks. All sensor nodes consist of at least four functional units: a power supply, a microcontroller, a wireless transceiver and the sensors. One example of a sensor box for gas concentration measurements is shown in Figure 2. The microcontroller has a LoRa (Long Range) modem for wireless data transmission at a frequency of 868 MHz offering very high receiver-sensitivity and hence long range at low power consumption (Centenaro et al. 2016). In an experiment a range of 240 m in a straight drift and 85 m in an angled drift was achieved which is far superior to tests with WLAN and Bluetooth. A second design using a 6LoWPAN (IPv6 over Low power Wireless Personal Area Network) based mesh-network-topology operating at 868 MHz has been described in (Güth 2018). While the achievable range in this case is smaller than with LoRa, the mesh approach allows data to be forwarded by each unit of the network, which increases the maximum distances. These sensor boxes (see Figure 3) use sensors for the measurement of environmental variables such as temperature, humidity and air pressure. The hardware is made by Texas Instruments (Texas Instruments) and the software by Thingsquare (Thingsquare). Two weeks of continuous measurements in a selected part of the mine resulted in no measurable degradation of the sensors and electronics, i.e. over that time span, their functionality was not impaired by the environmental conditions. In a lab trial, the nodes wirelessly transmitted data every five minutes for 162 days, powered by two AA batteries with a total capacity of 3000 mAh at 3 V. Future work will focus on the combination of the LoRa standard and the mesh network topology while including more relevant sensors into the WSN.

6.2 *Robot "Julius" and autonomous navigation*

The aforementioned robot is based on a platform by Innok Robotics and is depicted in Figure 4. Due to the environmental conditions and the research objectives, the chassis was upgraded to protection standard IP67 and optical sensors as well as a robotic hand and arm, whose protection is increased by a rubber sleeve and glove, were added. The robot's
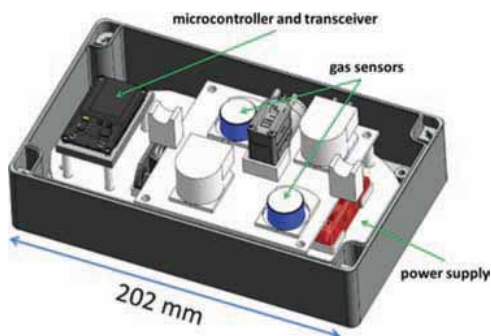

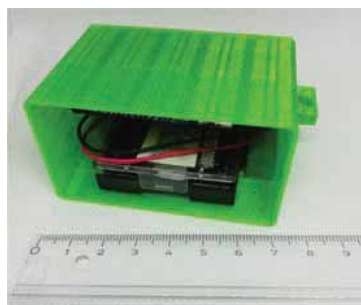Figure 2. CAD model of the gas sensor box without lid.

Figure 3. Photograph of one 6LoWPAN sensor box without lid. The electronics including microcontroller and sensors are in the black housing.
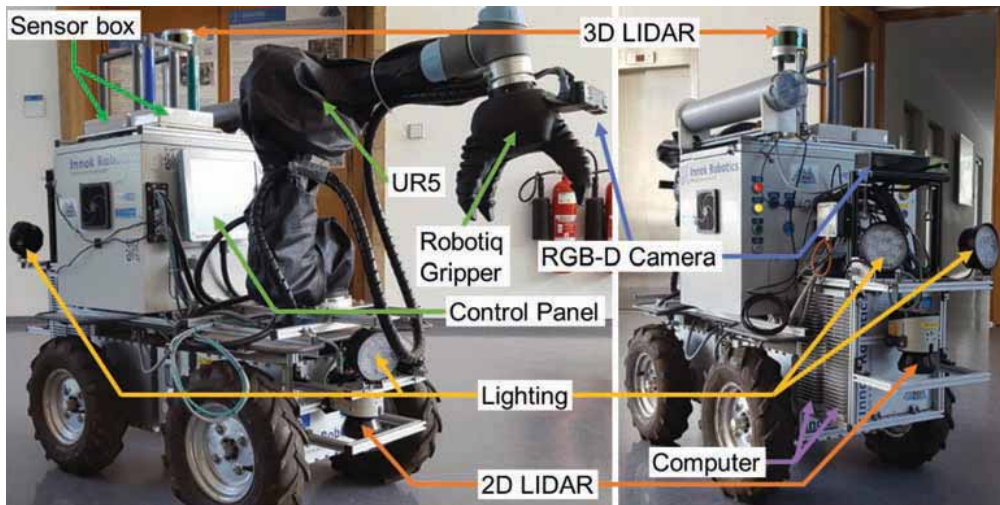
Figure 4. The research robot "Julius", which was retrofitted to withstand the mine's environment and suffice ARIDuA's objectives. In particular, its robotic arm and hand are protected by a rubber covering. Furthermore, it comprises LED spotlights, optical sensors e.g. 2D laser scanners, a 3D laser scanner and colour and depth cameras. Several sensor boxes are carried on top. Adapted from (Lösch et al. 2018a).

footprint is about 0.65 times 1.42 metres and it measures 1.3 metres in height (without arm). It is powered by a four-wheel-drive and the whole robot weights roughly 160 kilogrammes. More details about the platform, its sensor setup and navigation capabilities can be found in (Lösch et al. 2018a).

With its sensors and computational power, the robot is able to drive autonomously, i.e. it is able to steer and accelerate automatically and detect obstacles. Members of ARIDuA tested two types of navigation strategies: absolute and relative navigation. The former requires mapping an area beforehand and placing points on the map. With these preconditions, the robot is able to localise itself in the map and drive autonomously from one point to another. The mapping algorithm uses the front camera and therefore depends on light. The latter navigation strategy does not require a map and uses the robot's environment for orientation and navigation. The implemented algorithm uses the 3D laser scanner and thus does not depend on light.

7 SUMMARY AND OUTLOOK

For the underground use of autonomous machine, data networks and various sensors there is a wide range of applications in underground mining, especially for unknown and non-instrumented areas. In particular, the avoidance of accidents in the future by pre-exploration or by the autonomous work of a robot in potentially dangerous environments is very important. The loss of a machine compared to the health of life of a human being is negligible. However, the special environmental conditions underground also place challenging demands on the developers of the technology, and successful solutions from aboveground applications cannot simply be duplicated. In the ARIDuA project, however, both a robot and a first WSN were developed and successfully tested. The findings from the first experiments, which were not all error-free, offer interesting hints for the further development of the technologies. The goal is to be able to offer concrete solution ideas for the development of products at some point in the future.

The next steps will be to improve existing developments, in particular robust autonomous navigation and a mobile wireless sensor network with increased ranges. As soon as this has been achieved, the individual technologies will be connected. In the future, the robot should be able to set up the sensor network with its arm autonomously and the data should be

evaluated automatically. After stable test operation, the final step will be to test the technologies in other mines as well.

REFERENCES

Berufsgenossenschaft Rohstoffe und chemische Industrie (Ed.) (2010): Auf einen Blick 2010. Aktuelle Zahlen der BG RCI. Available online at https://www.bgrci.de/fileadmin/BGRCI/Downloads/Publikationen/Auf_einen_Blick_2010.pdf, checked on 1/30/2019.

Berufsgenossenschaft Rohstoffe und chemische Industrie (Ed.) (2017): Auf einen Blick 2017. Aktuelle Zahlen der BG RCI. Available online at https://www.bgrci.de/fileadmin/BGRCI/Banner_und_Artikelbilder/Presse_und_Medien/Publikationen/AufEinenBlick2017_finalDeutsch.pdf, checked on 1/30/2019.

Centenaro, Marco; Vangelista, Lorenzo; Zanella, Andrea; Zorzi, Michele (2016): Long-range communications in unlicensed bands: the rising stars in the IoT and smart city scenarios. In *IEEE Wireless Commun.* 23 (5), pp. 60–67. DOI: 10.1109/MWC.2016.7721743.

Grehl, S.; Mischo, H.; Jung, B. (2017): Research perspective–mobile robots in underground mining. Using robots to accelerate mine mapping, create virtual models, assist workers and increase safety. In *BULLETIN MAGAZINE* (02), pp. 44–47.

Güth, Frederic (2018): Autonomous Robots and the Internet of Things in Underground Mining. With assistance of Steve Grehl, Robert Lösch, Bernhard Jung, Sebastian Varga, Nasrin Rezaei-Abadchi, Franziska Günther et al. In Otto (Ed.): Proceedings of the 12th Smart Systems Integration Conference 2018: International Conference and Exhibition on Integration Issues of Miniaturized Systems. Smart Systems Integration. Dresden, 11.04.-12.04.2018: Mesago Messe Frankfurt GmbH, pp. 215–222.

Lösch, Robert; Grehl, S.; Donner, M.; Jung, Bernhard; Buhl, Claudia (2018a): Design of an Autonomous Robot for Mapping, Navigation, and Manipulation in Underground Mines. In *IEEE/RSJ International Conference on Intelligent Robots and Systems (IROS), Madrid, Spain*.

Lösch, Robert; Grehl, Steve; Güth, Frederic; Günther, Franziska; Rezaei-Abadchi, Nasrin; Jung, Bernhard (2018b): Roboter und Internet der Dinge zur Umgebungsdatenerfassung unter Tage. In *Acamonta–Zeitschrift der Freunde und Förderer der Technischen Universität Bergakademie Freiberg* 25, pp. 41–45.

Mining Magazine (Ed.) (2016): Volvo tests driverless trucks at Kristineberg. Available online at https://www.miningmagazine.com/fleet/news/1263537/volvo-tests-driverless-trucks-kristineberg, updated on 9/8/2016, checked on 8/27/2018.

Sächsisches Oberbergamt (2014): Der Bergbau in Sachsen. Bericht des Sächsischen Oberbergamtes und des Landesamtes für Umwelt, Landwirtschaft und Geologie (Referat Rohstoffgeologie) für das Jahr 2013. Available online at http://www.oba.sachsen.de/download/2014_09_24_JB2013_web.pdf, checked on 1/23/2019.

Sächsisches Oberbergamt (2016): Der Bergbau in Sachsen. Bericht des Sächsischen Oberbergamtes und des Landesamtes für Umwelt, Landwirtschaft und Geologie für das Jahr 2015. Available online at http://www.oba.sachsen.de/download/2016_11_09_JB2015_Druckfassung.pdf, checked on 1/23/2019.

Sächsisches Oberbergamt (2017): Zahlen und Fakten. Available online at http://www.oba.sachsen.de/278.htm, updated on 12/13/2018, checked on 1/23/2019.

Schmieder, T. (2017): Research project Mining-RoX—From 3D mine scans to a mine rescue simulator. In *GeoResources Journal* (1), pp. 41–42.

Texas Instruments: Information on SensorTags by Texas Instruments. Available online at http://www.ti.com/ww/en/wireless_connectivity/sensortag/tearDown.html, checked on 4/23/2018.

Thingsquare: Website. Available online at http://www.thingsquare.com, checked on 4/23/2018.

Varga, Sebastian; Grehl, Steve (2018): ARIDuA—Autonome Roboter und Inernet der Dinge n untertägigen Anlagen. In Jörg Benndorf (Ed.): 19. Geokinematischer Tag. Freiberg, 17.-18.05.2018. Nossen: Wagner Digitaldruck und Medien GmbH (Schriftenreihe des Institutes für Markscheidewesen und Geodäsie an der Technischen Universität Bergakademie Freiberg, 2018-1), pp. 147–158.

Coupled CFD-DEM modelling of mine dust dispersion in underground roadway

Lihai Tan & Ting Ren
School of Civil, Mining and Environmental Engineering, University of Wollongong, NSW, Australia

ABSTRACT: Dust particles floating inside roadways are characterized by various sizes. However, it is difficult to replicate the dust environment with such factors taken into consideration in laboratory experiments. Fortunately, computational technology provides an alternative way for that. In this study, in order to investigate the movement mechanism of dust with different diameters from heading face in the underground roadway, a three-dimensional CFD-DEM coupling numerical model is presented using the Eulerian-Lagrangian method. A numerical roadway model based on a practical engineering case has been established for the purpose of studying the dust diffusion under single-forced ventilation condition in roadway underground. The study suggests that particle size has a significant effect on dust dispersion. The results demonstrate that CFD-DEM coupling computational simulation can be an effective approach for the investigation of dust issues in underground engineering.

1 INTRODUCTION

Dust pollution is one of the most serious issues in coal mining underground. With the popularity of mechanical mining, dust is becoming a major hazard threating worker's health and equipment safety (Petsonk et al., 2013). Various dedusting methods have been developed in order to solve the dust concentration problem, among which ventilation is regarded as one of the most practical ways for dust reduction. Undoubtedly, understanding the migration and distribution of dust particles is of great importance for dust control by ventilation. It has long been known that both the hazard level of dust on human health and explosion risk largely depend on the size of dust (Sapko et al., 2007). Dust with smaller sizes is more likely to enhance the explosion risk, especially for those whose particle diameter is less than 200 um.

Various dedusting methods have been developed in order to solve the dust concentration problem, among which ventilation is regarded as one of the most practical ways for dust reduction. Undoubtedly, understanding the migration and distribution of dust particles is of great importance for dust control by ventilation. As an alternative methodology, Computational Fluid Dynamics (CFD) numerical simulation has been extensively employed; as it can investigate the dust dispersion and airflow overall, and is easy to replicate practical cases and ventilation conditions with much less geometry and size constraints. Over the past years, extensive studies have been performed on dust dispersion in coal mines using the CFD method. Toraño investigated the evolution of airflow and dust flow field in a roadway with forced-exhaust ventilation system using the CFD method whose feasibility and accuracy have been perfectly proved by in-site measurements (Toraño et al., 2011). Wang numerically investigated the dust movement and dust distribution with hybrid ventilation system and the results show an uneven distribution of dust in the laneway (Wang et al., 2015). Kurnia employed the CFD method to evaluate various methods used for mitigating dust dispersion from the mining face and determined the most effective one (Kurnia et al., 2014). Wang simulated the dust in a roadway with a curtain of air curtain installed on the shearer using the CFD method and the results show that the air curtain can effectively reduce the dust concentration on the side of the operator (Pengfei et al., 2011). Parra examined three different types of ventilation systems

(blowing, exhaust and mixed ventilation) using the CFD method and this numerical study was validated by the measurements taken in a real mine gallery (Parra et al., 2006).

All of the above studies using the CFD method show that the distribution and movement of dust are affected obviously by the airflow field. However, most of them mainly pay their attention to the dust dispersion at a macro-scale; as the CFD method is difficult to reveal the movement characteristics of particles from a microscopic viewpoint. Recently, CFD-DEM (computational fluid dynamics and discrete element method) coupling method has been under development for numerical simulation with fluid-solid two-phase flows involved. Using this method, the airflow is simulated and investigated by the traditional CFD method while the simulation of particles is performed by the DEM method; thus allowing the interaction between fluid and solid to be considered. Therefore, the motion of any particle in the airflow can be tracked and its migration can be accurately determined. Moreover, this method requires less empirical parameters and affords the ability to clearly present the particle trajectory and the interaction between particle and fluid (Yu et al., 2018).

In this study, an airflow-dust model was established using a CFD-DEM coupling method. The dispersion process of dust particles in a roadway installed with single-forced ventilation system was numerically simulated and the effect of particle size on dust dispersion and distribution was analysed. The aim of this study is to improve the understanding of dust dispersion mechanism and present the performance of the CFD-DEM coupling method on studying the particle migration in airflow.

2 NUMERICAL MODELLING OF AIR-DUST COUPLED FLOW

In this study, Eulerian-Lagrangian method was employed to track the particle trajectory in the airflow. As the total volume of particles was far smaller than that of the fluid, which caused little force of dusts on airflow, one-way coupling modelling was employed, which means that the influence of dusts on airflow was not taken into consideration. As the sphere is the most typical shape of dust, spherical dust particles with different sizes were considered. Spherical particles with diameters of 20 um, 40 um, 60 um and 80 um were created to analyse the size effect.

The prototype of the numerical roadway model was a typical three-centred arch roadway underground in a coal mine. The dimension of the roadway was 3.7 m × 3.4 m × 40.0 m
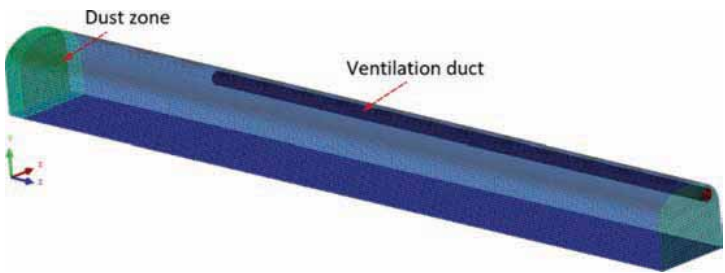

Figure 1. The numerical model of the roadway.

Table 1. Parameters for the CFD-DEM coupling simulation.

Properties		Values	Properties	Values
Dust	Density	1400 kg/m^3	Ventilation velocity	15.33 m/s
	Poisson's ratio	0.5	Turbulent intensity	5.0%
	Shear modulus	1×10^8 Pa	Time step (CFD)	1.0×10^{-4} s
Air	Density	1.225 kg/m^3	Time step (DEM)	1.2×10^{-7} s
	Viscosity	1.789×10^{-5} m^2/s	Gravity	9.8 m/s^2

(width × height × length). Single-forced ventilation system was used for dust removal in the roadway. The ventilation duct with a diameter of 0.6 m, whose centre axis was 2.6 m away from the floor and 1.2 m away from the tunnel centre axis along Z axis, was 10.0 m away from the heading face. Forced air capacity was 260 m³/min, affording a ventilation velocity of 15.33 m/s. The initial dusts were assumed to be distributed statically and uniformly inside the dust zone within 1.0 m of the heading face.

The time-step, which has a positive correlation with particle's size and density and a negative correlation with particle's stiffness, must be small enough for an accurate result. In this study, the DEM time-step was set as 1.2×10^{-7} s in accordance with the smallest particle. k-ε model was used to describe the air turbulent flow in the airflow field. The interaction of particle to particle was described by the Hertz-Mindlin (no slip) model and the interaction between particles and wall by the Hertz-Mindlin with JKR model. Other key parameters are listed in Table 1. Before CFD-DEM coupling with dust created, the ventilation was performed for 120 seconds and the airflow field was stable.

3 ANALYSIS OF RESULTS

3.1 Airflow field

The velocity streamlines for the airflow at the dispersion time of 0.0s are presented in Figure 2. According to Yu's research, the airflow field was suggested to be classified into three regions: vortex region, multi-direction turbulence region and stable region (Yu et al., 2018). This classification method is also applied in this study. As shown in Figure 2, air was jetted out from the ventilation duct rapidly, forming a high-velocity strip airflow field extending to the heading face, and then the airflow flowed against the heading face to the other side and turned back towards the roadway exit. The region between the heading face and ventilation duct was regarded as the vortex region. In this region, the airflow slowed down quickly with ventilation velocity decreasing from 15.33 m/s to about 3.5 m/s due to energy loss. Afterwards, air flowed into the multi-direction turbulence region with a length of about 16.0 m,
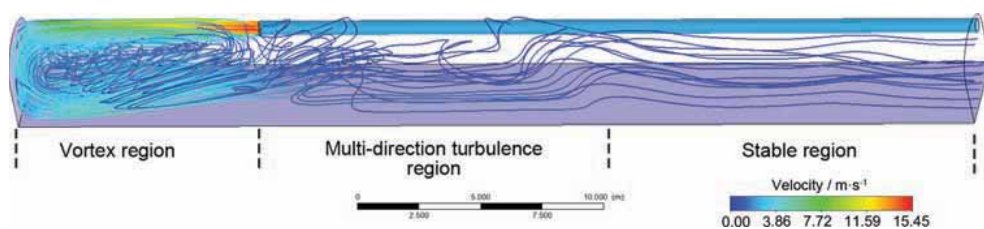

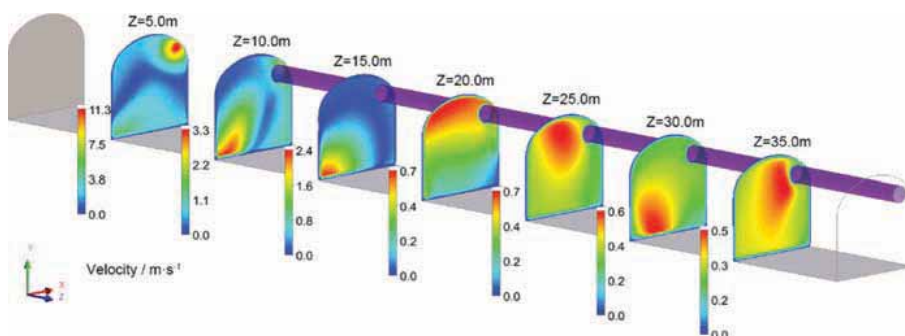Figure 2. Velocity field of airflow in the roadway.

Figure 3. Velocity field sections of airflow in the roadway.

where the airflow was somewhat disordered and decelerated continuously. Eventually, the airflow decelerated to the lowest level of less than 0.5m/s, becoming stable and parallel to the axes of the roadway in the stable region.

As shown in Figure 3, in the vortex region, the ejected air resulted in the high-speed airflow concentration in front of the outlet of the ventilation duct, then the rebounded airflow formed another high-speed airflow concentration in the lower area close to the floor (Z = 5.0 m). In the turbulence region, high-speed airflow firstly concentrated at the side opposite to the ventilation duct and then migrated to the upper area of the roadway (Z = 15.0 m and Z = 20.0 m). In the stable region, the velocity of airflow had been slowed down to the lowest level (Z = 30.0 m and Z = 35.0 m).

3.2 *Migration of particles with different sizes*

In the numerical model, the positive direction of the Z axis denotes the direction from the heading face to the roadway exit along the long axis of the roadway. Therefore, the dispersion velocity for different kinds of dust particles was defined as their average Z velocity. The dispersion velocity of spherical dust particles with different sizes is presented in Figure 4. It can be seen that the dispersion velocity of all particles soared dramatically at first and reached a climax of about 3.7 m/s when dispersion time was roughly 2.1 s. Subsequently, the average dispersion velocity dropped sharply to the lowest level for all dust particles. It should be noticed that average dispersion velocity for participles with diameter of 20 um and 40 um turned to be negative for a while with lowest velocity of −0.67 m/s and −0.33 m/s, respectively. At post-peak stage, obvious velocity fluctuation can be observed for particles with diameters of 20 um and 40 um. However, the post-peak dispersion velocity of dust particles with greater diameters (60 um and 80 um) was much stable and levelled off at about 0.4 m/s.

The difference of dispersion velocity caused different dust dispersion distances, which is shown in Figure 5. Turning points for dusts with different sizes appeared simultaneously when dispersion time was 5.0 s, which lagged behind the time when dispersion velocity reached its peak. Each dispersion evolution curve can be divided into two parts. Before the turning point, dispersion curves rose quickly and almost coincident with each other. When dispersion time reached the turning point, the curves began to get flatter and went up linearly. The average distance gap between dust particles also widened gradually. In general, dust particles with greater sizes migrated further along the long axis of the roadway than those with smaller sizes. When dispersion time was 30.0 s, the average dispersion distance for dust particles with diameter of 80 um was 22.2 m while for those with diameter of 20 um was only 15.7 m.

Figure 6 presents the distribution of dust particles with different sizes at different dispersion times. The particles with different diameters are represented by different colours. As the
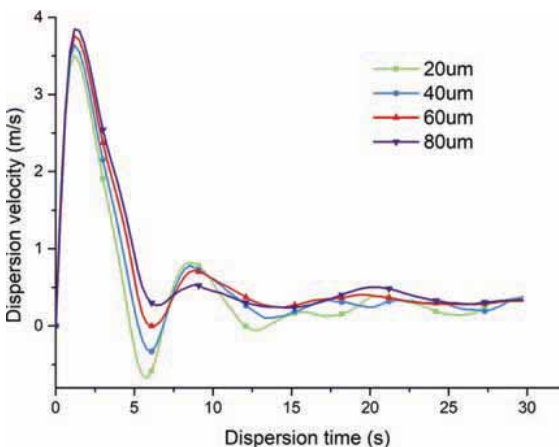

Figure 4. The dispersion velocities of spherical dust particles with different sizes.
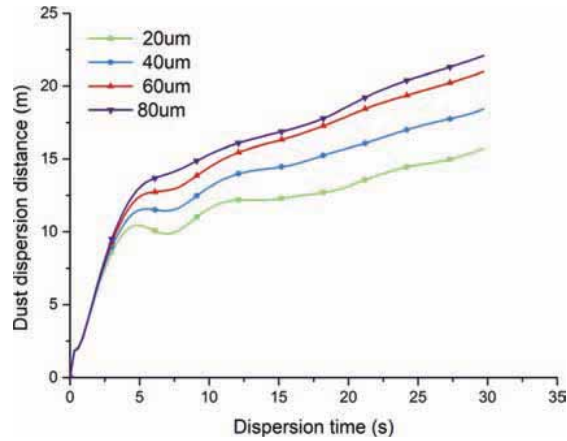
615

Figure 5. The average dispersion distance of spherical dust particles with different sizes.
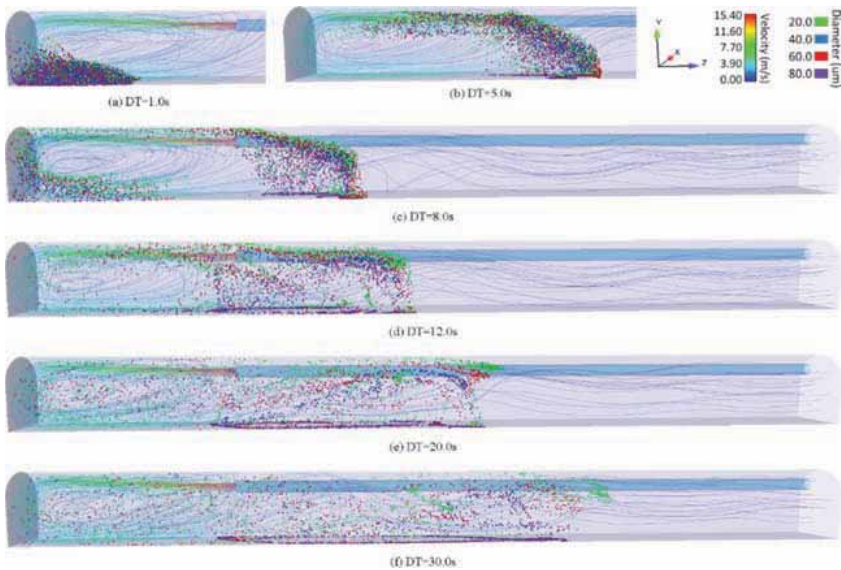

Figure 6. The migration of dust particles with different sizes at typical dispersion times.

size of dust particles was far smaller compared with that of the roadway, all the dust particles had been amplified for better observation. For the purpose of better understanding the dust distribution characteristics, the projection of dust distribution in the XY plane and ZY plane are presented in Figure 7 and Figure 8 respectively.

At the beginning of dispersion (DT = 1.0 s), all particles near the heading face were dragged down and moved forward with the rebounded airflow. When DT = 5.0 s, some dust particles, the majority of whom were small particles with diameters of 20 um and 40 um, were sucked into the airflow ejected from the ventilation duct and then dragged back to the vortex region because of the strong negative pressure around the outlet of the ventilation duct. Afterwards, more and more dust particles were dragged back when approaching to the outlet of the ventilation. When DT = 8.0 s, a dust backflow loop had been formed. The backward dust particles flew with the ejected airflow and repeated the trajectory from the heading face. There was a possibility for them to get rid of the vortex region at the end of the circulation. With the increase of dispersion time, an increasing
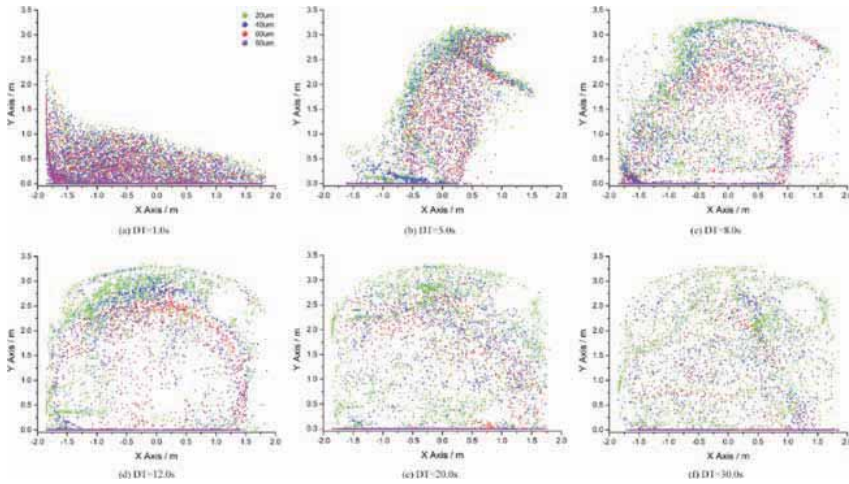
Figure 7.   The projection of dust distribution on XY plane at typical dispersion times.
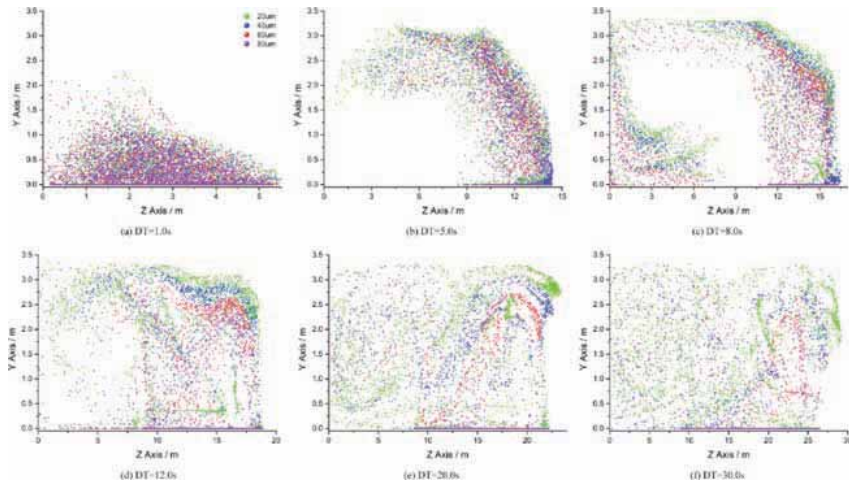

Figure 8.   The projection of dust distribution on ZY plane at typical dispersion times.

number of dust particles had escaped from the vortex region and entered the stable region. When DT = 30.0 s, most dust particles had been got out of vortex region while only few of them, which were mainly small particles with diameters of 20 um and 40 um, were still flowing in the circulation.

The plane projections clearly illustrate the distribution difference between dust particles with different sizes. Smaller dust particles were more likely to flow above larger dust particles. During dispersion time from 8.0 s to 30.0 s, we can see that dust particles could be roughly divided into four height levels with the smallest particles with diameter of 20 um migrating at the highest level and the largest particles with diameter of 80 um at the lowest one. It is also obvious that the influence of gravity over particles was sensitive to particle size. As shown in Figure 8, when DT = 1.0 s, a considerable portion of dust particles with diameter of 80 um settled on the floor, then rose again with strong airflow. Overall, settled dust particles, most of whose diameter was 80 um, were mainly distributed in the area more than 9.0 m away from the heading face. There was no obvious settlement of dust particles with diameters of 20 um and 40 um.

4 DISCUSSIONS AND CONCLUSIONS

According to the evolution of dust dispersion velocity, four stages in the process of dispersion can be classified under the single-forced ventilation condition as shown in Figure 9. The scattered points denote the velocities of different kinds of dust particles and the black dash line denotes their average value.

1. Accelerative dispersion stage
High-speed airflow ejected from the ventilation duct and rebounded when reaching the heading face, forming a vortex airflow field between ventilation duct and heading face. Therefore, at the beginning of dispersion, the dust particles near the heading face accelerated rapidly because of the strong drag force from the rebounded airflow.
2. Deceleration dispersion stage
The velocity of the rebounded airflow suffered a sharp decrease in a short distance. Accordingly, the dust particles slowed down rapidly. Moreover, in this period, a number of particles were sucked into the circulation in the vortex region. Consequently, the overall dispersion velocity experienced a drastic drop.
3. Fluctuant stage
In this stage, a large proportion of the dust particles had migrated into the turbulence region and the rest of them was still bound in the vortex region. Overall, the dispersion velocity was fluctuant at a lower level.
4. Stable dispersion stage
As the airflow flew into the stable region, most of the dust particles began to migrate in a stable dispersion velocity until flowing out from the roadway.

For the dust particles investigated in this study, particles with greater diameters were easier to disperse forward than those with smaller diameters. This may be attributed to their better motion stability in the airflow. The smaller dust particles are more susceptible to the airflow characterized by instability before entering the stable region. As a result, their motion is less orderly. It has been observed in this study that the smaller dust particles are more likely to be affected by the entrainment effect of the high-speed ejected airflow and therefore there is a high possibility of getting incorporated into the dust circulation for them.

Dust particles mainly settled in the multi-direction turbulence region and stable region where the airflow speed was much less than that in the vortex region. In this study, for larger dust particles with diameters of 60 um and 80 um, they were more likely to migrate at a lower height and settle compared with those of diameters of 20 um and 40 um due to the effect of gravity, which means that smaller dust particles are more responsible for dust pollution.

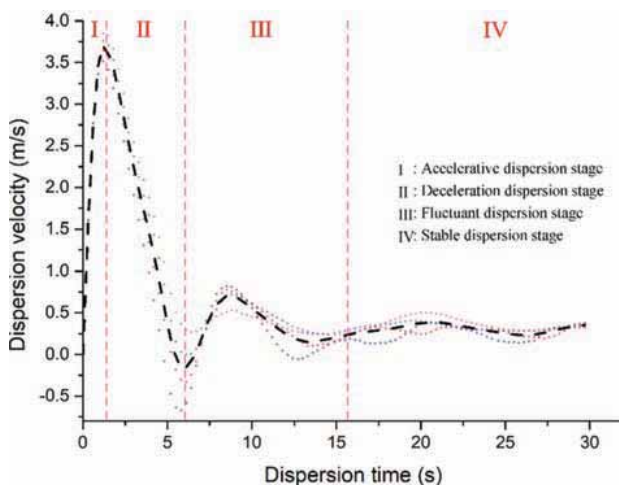
Figure 9. The average dispersion velocities of all dust particles.

REFERENCES

Kurnia, J.C., Sasmito, A.P. & Mujumdar, A.S. (2014). Dust dispersion and management in underground mining faces. *International Journal of Mining Science and Technology,* 24, 39–44.

Parra, M., Villafruela, J., Castro, F. & Mendez, C. (2006). Numerical and experimental analysis of different ventilation systems in deep mines. *Building and Environment,* 41, 87–93.

Pengfei, W., Tao, F. & Ronghua, L. (2011). Numerical simulation of dust distribution at a fully mechanized face under the isolation effect of an air curtain. *Mining Science and Technology (China),* 21, 65–69.

Petsonk, E.L., Rose, C. & Cohen, R. (2013). Coal mine dust lung disease. New lessons from an old exposure. *American journal of respiratory and critical care medicine,* 187, 1178–1185.

Sapko, M.J., Cashdollar, K.L. & Green, G.M. (2007). Coal dust particle size survey of US mines. *Journal of Loss Prevention in the Process Industries,* 20, 616–620.

Toraño, J., Torno, S., Menéndez, M. & Gent, M. (2011). Auxiliary ventilation in mining roadways driven with roadheaders: validated CFD modelling of dust behaviour. *Tunnelling and Underground Space Technology,* 26, 201–210.

Wang, Y., Luo, G., Geng, F., Li, Y. & Li, Y. (2015). Numerical study on dust movement and dust distribution for hybrid ventilation system in a laneway of coal mine. *Journal of Loss Prevention in the Process Industries,* 36, 146–157.

Yu, H., Cheng, W., Xie, Y. & Peng, H. (2018). Micro-scale pollution mechanism of dust diffusion in a blasting driving face based on CFD-DEM coupled model. *Environmental Science and Pollution Research*, 1–21.

Proximity detection of explosive methane clouds in longwall mines

J.F. Brune, H.S. Düzgün, G.E. Bogin Jr., A. Juganda, C. Strebinger,
T. Nguyen, E. Isleyen & C. Demirkanr
Colorado School of Mines, Golden CO, USA

ABSTRACT: Methane detection in underground coal and other gassy mines traditionally done with point-type sensors or by certified examiners using handheld meters. To provide a sufficient margin of safety, machine-mounted point sensors shut down equipment at methane concentrations of 1 or 1.5%, yet many mine fires and explosions have shown that point sensors may not be capable of detecting explosive methane clouds. The 2010 explosion at the Upper Big Branch mine in West Virginia, USA, is one such example that killed 29 miners. Researchers are using multi-point methane readings, CFD, and 3-D modeling to produce the real-time methane distribution cloud and visualization through virtual and augmented reality (VR and AR). Knowing the position of the shearer, shields and other ignition sources creates a proximity detection model for the methane cloud that will automatically shut off the shearer or other equipment before an explosion can happen.

1   INTRODUCTION

The 2010 methane and coal dust explosion at the Upper Big Branch Mine in West Virginia, United States, killed 29 miners. Investigators (Page, 2011) found that worn cutter bits on the drums of the longwall shearer likely ignited a cloud of flammable methane-air mixture that had migrated into the face area from the gob fringe behind the shields. As Brune and Sapko (2012) demonstrated, it is easily possible that flammable or explosive mixtures form near the cutter bits that remain undetected by the methane sensors mounted on the shearer body, the headgate and tailgate drives. This calls into question the validity of point-type methane readings that have long been used worldwide to protect miners from methane explosions, as this was likely a contributing cause of the Upper Big Branch explosion.

Figure 1 is a depiction of methane emanating from a fissure in the coalbed from Kissell (2006). It shows that the ventilation flow quickly dilutes methane through the explosive range, yet the Kissell's figure does not provide a scale or airflow quantity—it is merely a sketch.
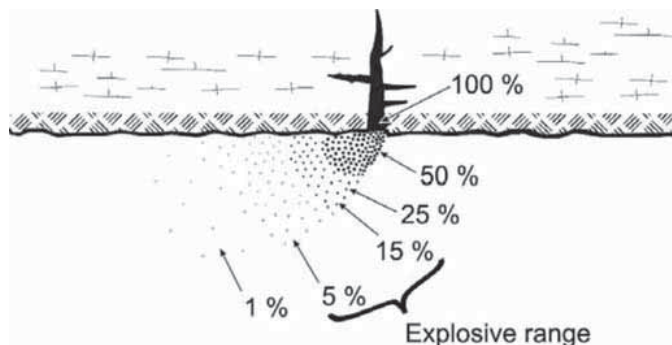

Figure 1.   Dilution of methane emanating from a fissure in the coalbed (Kissell, 2006).

The U.S. Mine Safety and Health Administration (MSHA) issued guidance (MSHA, 2013) for certified mine examiners to test for methane with handheld detectors "within 5 feet of the face and at least 12 inches from the roof, face, ribs, and floor." Reasons for these distances are not specified but one can assume that the 12-inch (0.3m) standoff relates to the dilution depicted in Figure 1 while the 5-foot (1.5 m) standoff from the face is designed to keep the examiner from traveling beyond the last row of roof support.

In the United States the limit for methane detected is 1.0%. At this level, all "electrically powered equipment in the face shall be de-energized and other mechanized equipment shall be shut off" (30 CFR §75.323). This applies regardless whether the methane is detected using a handheld or machine-mounted sensor. MSHA may permit up to 1.5% CH_4 in the longwall face, provided that certain enhanced methane monitoring provisions are met. In this case, the shearer will alarm and must be de-energized at this level and corrections made to reduce CH_4 below 1.5%. Automatic power shutdown must occur at 2% CH_4 (see U.S. regulation 30 CFR §75.323 and §27.24). In most cases, machine-mounted sensors are directly linked to de-energize the equipment automatically. If 1.5% or more methane is detected in a working place, all persons must be removed from the affected area except those required to restore ventilation. U.S. law also permits up to 1.5% or even up to 2.0% in specific return air courses.

These methane limits are common to many countries. Most countries require mine-wide atmospheric monitoring systems, but such systems are not currently mandated in U.S. coal mines. In any case, all methane and atmospheric monitoring systems rely on point-type detectors placed at strategic locations to test both the fresh air and the exhaust airways.

2 METHANE DISTRIBUTION IN THE LONGWALL FACE

Researchers at the Colorado School of Mines (CSM), with funding from CDC NIOSH, have conducted extensive work with computational fluid dynamics (CFD) studying airflow distribution, leakages between the face and the gob, and methane distribution patterns. From a CFD modeling perspective, a longwall face ventilation is quite complex. Shearer and face conveyor are moving obstructions, and the shield support, hydraulic hoses, cables etc. are difficult to model in sufficient detail. Therefore, in another project funded by NIOSH, CSM researchers are constructing a 1:40 scaled longwall model for physical airflow and explosion testing.

Figure 2 shows the plan view of the CFD longwall model with airflow velocity contours shaded in color according to the legend provided. These contours are valid for approximately 1.5 m above the mine floor. This is a bleeder ventilation system typical for a U.S. coal mine, with layout, geometry and airflow quantities adopted from an actual mine. In the model, the
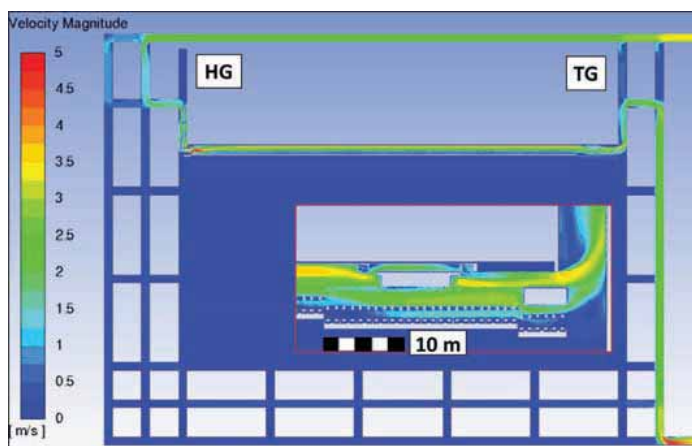

Figure 2. Plan view of face airflow velocity contours. C = curtain, HG = headgate, R = regulator, S = seal, TG = tailgate. Arrows indicate direction of flow.

shearer is cutting near the tailgate (TG) and located between shield numbers 140 and 148 of 152 shields on the face. The inset in Figure 2 provides a detailed view of the flow velocity distribution around the shearer and near the tailgate. Flow obstructions marked in grey represent the coal face, the shearer body, tailgate drive and shield hydraulic jacks.

Figure 2 illustrates the complexity of air flows in the face area. It clearly shows the turbulences caused by sharp turns and obstacles in the flow path. The reference plane 1.5 m above the coal floor was chosen arbitrarily. It should be noted that different flow patterns may occur in other reference planes.

Figure 3 depicts three reference zones where methane content was studied: Zone M1 represents the walkway underneath the support shields where mine examiners typically take air velocity and methane readings using handheld instruments. Zone M2 is in the path of the shearer body, above the face conveyor. Shearer-mounted methane sensors are typically located at the top of the shearer body and operate in this zone. Zone M3 is the top corner area where the concentration of methane released from the freshly cut coalbed is highest and the cutter bits are in contact the roof rock. Zone M3 is a likely location to ignite methane explosions, especially if worn cutter bits leave streaks of hot metal on the roof rock. Zone M3 shifts during the cutting process: prior to cutting coal, M3 is closer to the shields, while after cutting out, M3 shifts away from the shields until the shields are pulled up for the next cut.

Figure 4 shows the average methane mole fraction in percent for each of the three reference zones based on CFD modeling results with the sharer positioned at the tailgate, shield
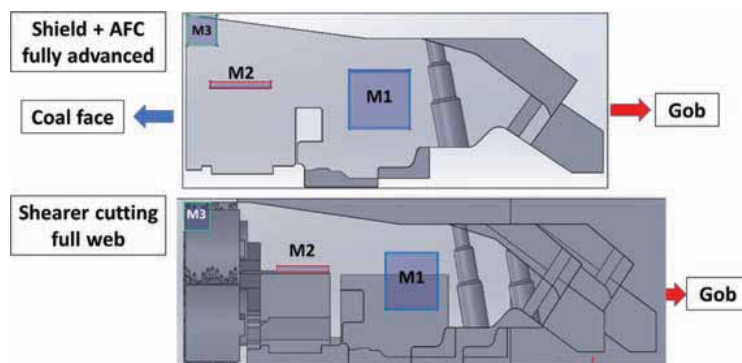
Figure 3. Cross section of the longwall face showing three reference zones for methane detection. Zone M1 is 1 m squared. The top image shows zone M3 after cutting out the coal, while to bottom image shows the same location with the shields advanced for the next cut. View is towards the tailgate.

Figure 4. Average methane content in each of the reference zones, plotted over the length of the longwall face from headgate (shield no. 1) to tailgate (shield no. 152).

150. In the CFD models, methane was emitted from the exposed coal face area only. In future models, researchers will include methane emissions from the freshly cut coal on the face conveyor as well as emissions from the gob. The CFD models include realistically represented cutting drums that rotate but do not yet include water sprays. Fresh air entering the longwall face is assumed to have no methane.
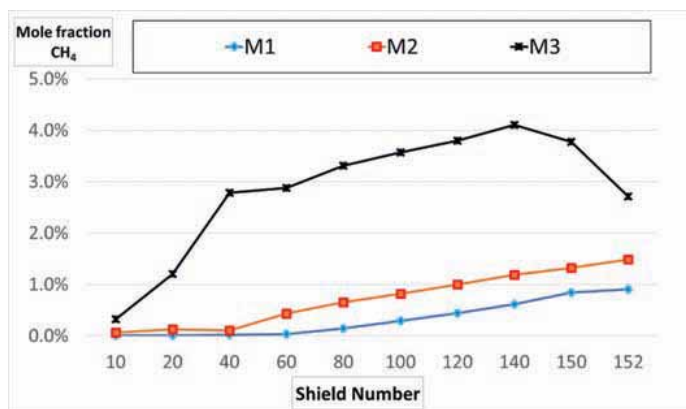
From the CFD models, researchers note several key observations about the methane distribution in the tailgate area of the longwall face:

1. Methane concentration increases over the length of the face from headgate to tailgate, following the ventilation air stream. This is caused by two additive effects: the face air quantity decreases over the length of the face because some air leaks into the bleeder ventilated gob. At the same time, methane emissions along the face are cumulative, leading to increasing methane volume over the length of the face. Researchers note that methane distribution may be different for progressively sealed or bleederless gobs as the leakage patterns are different, but the general trend of increasing methane concentrations from headgate to tailgate remains.
2. Referring to Figures 3 and 4, the average methane concentrations are lowest in zone M1. This is expected as M1 is farthest away from the methane source. Based on the CFD model, machine-mounted sensor readings in zone M2 may read 2 to 7 times higher than concentrations measured with handheld instruments in zone M1 at the same shield location. Researchers have yet to study the impact of boundary layer effects on top of the shearer body to determine their impact on machine sensor readings.
3. Methane concentrations in zone M3 are highest. It should be noted that both M3 locations coexist on the longwall face. M3 is assumed to always be in the top left corner of the face, as viewed from the headgate, but its distance to the other zones varies depending on the shearer cut. Both M3 locations are represented in the graph in Figure 4. The M3 location shifts as the shearer cuts, until the shields advance following the shearer cut.
4. Based on the CFD model, methane concentrations in zone M3 are 3 to 30 times higher than those measured in M1. In the current scenario, a handheld examination under shield no. 140 would read 0.6% methane while the concentration in the shearer cutting zone M3 exceeds 4%. It is likely that the shearer would not alarm as it travels towards the tailgate past shield no. 140 where the M2 average does not exceed 1.5%.
5. The peak methane concentration in Zone 3 occurs around shield 140. Methane concentration drops towards the tailgate because the shearer partially obstructs the airflow and increases turbulent mixing and dilution. In addition, the gob plate that prevents gob rubble from entering the face at the tailgate, further obstructs the flow and increases face air velocity, as the inset in Figure 2 shows.

Figure 5 shows a projection of Figure 4 data with methane amounts increased by 25%. With the shearer located at shield 140, the methane sensor in location M2 still would likely
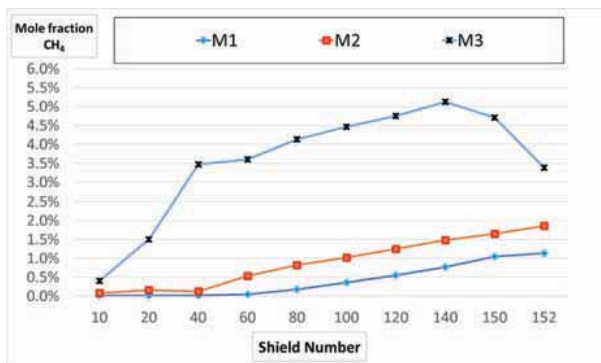

Figure 5.   Methane concentrations as presented in Figure 4, with methane inflow increased by 25%. At Shield 140, M2 concentration is 1.5% while M3 is explosive.

not alarm, as the M2 concentration is just below 1.5%. As the shearer continues to travel towards to tailgate, the M2 concentration will exceed 1.5%. Considering that the time lag of the machine-mounted sensor may be 20 seconds or more (see Taylor et al., 2010), the shearer may be well on its way back and snaking in for the next pass by the time the sensor responds. At a speed of 1 m/s, the shearer would advance 10 shields in 20 s. This puts the headgate-side cutter drum near the explosive zone at shield 150, where an explosion hazard exists. At this location, the M3 methane concentration is exceeding 4.5%. It should also be noted that hand-held methane readings in this scenario would read around 1.0% which may not raise concerns if the ventilation plan allows up to 1.5% in the longwall face.

3 A METHANE EXPLOSION HAZARD PROXIMITY MODEL

Rather than relying on one or two point-type methane detectors, future methane monitoring are expected to utilize real-time CFD modeling, supported by remote infrared detectors combined with multiple, strategically positioned point-type sensors. Researchers at the Colorado School of Mines propose a methane hazard proximity model that can detect a cloud of explosive or flammable methane-air mixture and track the explosive zones as they form and move through the face.

Figure 6 shows an MSHA artist's rendering of a flammable methane-air cloud that migrated into the tailgate area of the longwall face at the Upper Big Branch mine, resulting in the 2010 explosion when it reached the shearer as it was cutting sandstone roof with dull bits. The envisioned real-time CFD model of the longwall face would continuously recalculate the air quality distribution in the face area using data from a larger number of point-type and infrared sensors to compute "shells" of the cloud that mark defined methane concentrations limits of interest as the shearer cuts the face area. Using the sensor information, the model computes the source(s) of methane and projects direction of flow and proximity to potential ignition sources such as the cutter drums of the shearer. If the model determines proximity of a flammable gas mixture, specific equipment such as shearer, shields and conveyors will lock out. Lock-outs can be released as soon as ventilation improves and/or the hazardous cloud has passed.

Figure 7 shows a snapshot CFD depiction of the longwall tailgate area with the shearer, drums rotating. The blue shaded envelope marks methane concentrations ranging from 1–2% while the green area illustrates the 2–4% methane range. Near the cutting drums, there are small areas of red shading that indicate concentrations above 4% methane.

The CFD model further confirms that the green and red zones are not "visible" to either the sensor mounted on the shearer or a sensor that would typically be mounted on the tailgate drive and would not be detected with current methane monitoring equipment. Figure 8 shows a different rendering of the CFD model referencing the locations of machine-mounted
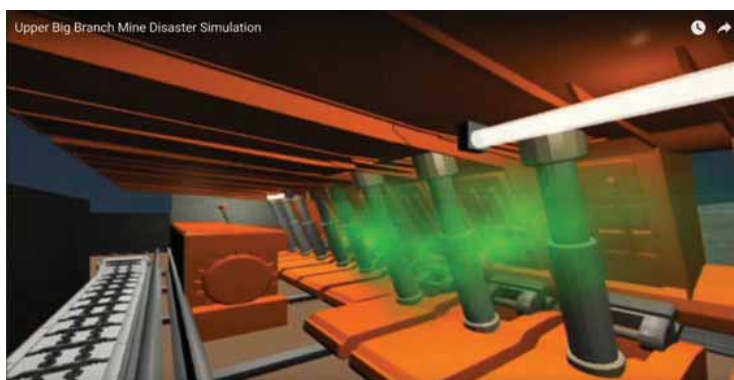

Figure 6.   Simulated, flammable methane-air could, depicted in green, migrating towards the tailgate of the longwall at Upper Big Branch mine. MSHA.
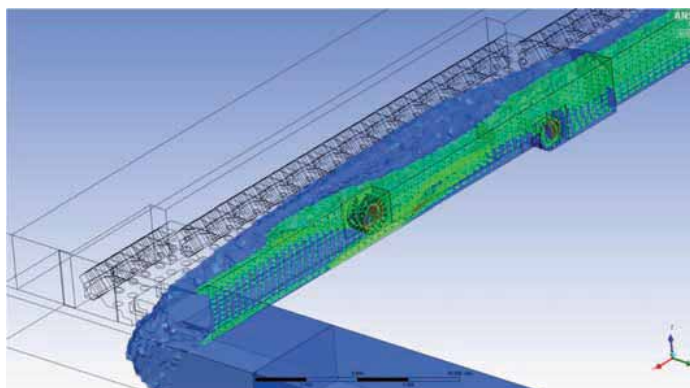
Figure 7.   Methane cloud forming around a longwall shearer cutting in the tailgate area. Blue shading indicates methane concentrations between 1 and 2%, green, 2–4% and red, above 4%. Shearer is static with drums rotating and cutting towards the tailgate.
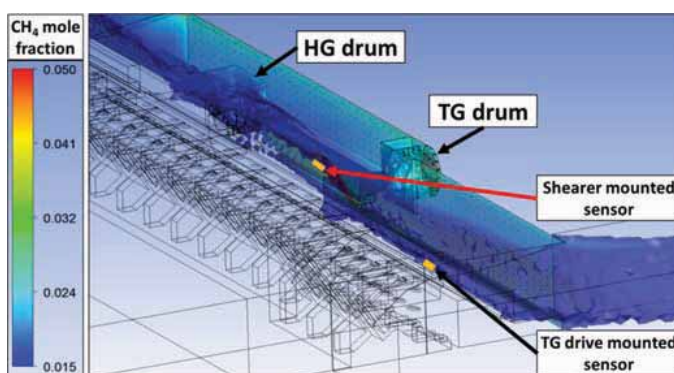

Figure 8.   Methane-air cloud around the shearer with mole fractions between 1.5% and 5%, with colors indicated in the legend. The machine mounted and tailgate drive mounted sensors will not alarm as they are not "seeing" concentrations above 1.5%.

sensors on both the shearer and the tailgate drive. The sensor locations were taken from Page et al., 2011). Figure 8 shows that both sensors are outside the colored cloud that marks methane mole fractions between 1.5% and 5%. In this model scenario, neither sensor would alarm as they are both in concentrations below 1.5%. A handheld methane reading taken in Zone M1 would indicate a concentration below 1%.

4   SUMMARY AND CONCLUSIONS

CFD modeling of longwall ventilation and methane concentrations confirms that current practices of manual methane readings as well as machine-mounted methane sensors are likely not capable of detecting explosive methane air-mixtures near the shearer cutting drums. This may explain frequent face ignitions in U.S. longwall mines (Verma and Brune, 2010) and also provide insight into circumstances that led to the 2010 Upper Big Branch mine explosion. Current limits of 1 or 1.5% in the shearer path and/or walkway are not suitable indicators to warn of methane ignition and explosion hazards in the longwall face.

Researchers at the Colorado School of Mines have developed detailed Computational Fluid Dynamics (CFD) models that depict airflow and methane concentrations in the longwall face and generated predictive envelopes of possible methane concentrations around the

shearer. These methane envelopes suggest more meaningful strategic locations where methane sensors should be mounted to provide a more accurate warning of methane explosion hazards. In the near future, as sufficient computing power becomes available, such CFD models will be available in real-time and provide the underpinnings for a proximity detection model where the shearer and other ignition sources can be shut off automatically as an explosive methane cloud approaches. To provide sufficient calibration for the real-time CFD models, researcher recommend to mount methane sensors in the tips of all shields, in zone M3 shown in Figure 3. In addition, directional infrared sensors should be added to provide further calibration for the real-time CFD model that serves to inform of explosion hazards.

Future research also needs to re-visit the methane triggers of 1.0% or 1.5% commonly accepted in the coal industry worldwide. As real-time methane distribution models become reality, mine operators can monitor methane in the mining face to much greater detail. With sensors mounted in locations where their indication is truly meaningful, it may be justifiable to set the alarm and shut-off at higher levels while still providing greater safety and protection against methane ignitions and explosions.

5   FUTURE RESEARCH

CFD real-time methane distribution models will be visualized through virtual and augmented reality (VR, AR) where miners can "see" hazardous methane clouds on display screens and in their heads-up displays. (Sebnem to add a paragraph or two).

ACKNOWLEDGEMENT

REFERENCES

Brune, J.F. and Sapko, M.J. 2012. A Modeling Study on Longwall Tailgate Ventilation, Proceedings, 14th North American Mine Ventilation Symposium, Salt Lake City, UT, June 2012, 6 p.

Kissell, F.N. 2006. Handbook for Methane Control in Mining, CDC NIOSH IC9486, Pittsburgh 2006.

MSHA 2011. Clip from Upper Big Branch Mine Accident Scenario Video, MSHA web site https://arlweb.msha.gov/Fatals/2010/UBB/PerformanceCoalUBB.asp, accessed 12-17-18.

MSHA 2013. Program Policy Letter No. P13-V-06, Reissue of P11-V-8; Tests for Methane at the Working Face, Using Extendable Probes or Other Acceptable Means, U.S. Mines Safety and Health Administration, Arlington VA, 2013.

Page NG et al. 2011. Mine Safety and Health Administration, Coal Mine Safety and Health, Report of Investigation—Fatal Underground Mine Explosion April 5, 2010, Arlington VA, December 2011.

Page, N.G. et al. 2011. Mine Safety and Health Administration, Coal Mine Safety and Health, Report of Investigation—Fatal Underground Mine Explosion April 5, 2010, Arlington VA, December 2011.

Taylor, C.D., Chilton, J.E. and Goodman, G.V.R. 2010. Guidelines for the Control and Monitoring of Methane Gas on Continuous Mining Operations, CDC NIOSH IC9523, Pittsburgh, 2010, 69 p.

United States Code of Federal Regulations, 2019. Title 30 Mineral Resources, U.S. Government Printing Office, 2019.

Verma, A., Brune, J.F. 2016. Face ignitions in US coal mines and prevention technologies. Preprint no. 16–132, SME 2016 Annual Meeting, Phoenix AZ February 2016.

Evaluation of trackless mobile machine collision management systems

H.A. Hamersma & P.S. Els
Department of Mechanical and Aeronautical Engineering, University of Pretoria, South Africa

C.E. Doran
Mitacom Pty Ltd., Brisbane, Australia

ABSTRACT: Recent changes in the Mine Health and Safety Act in South Africa require employers at any mine to take reasonably practicable measures to ensure that persons are prevented from being injured due to collisions between Trackless Mobile Machines (TMMs) and between TMMs and pedestrians. This has resulted in numerous suppliers of Collision Management Systems (CMS) entering the market, often with products that are not sufficiently tested or developed to address the significant challenges associated with the practical implementation of such systems. As a result, a test methodology was developed in consultation with the South African mining industry based on machine stopping performance. This paper presents the test methodology, describing the specific test configurations, testing equipment, success criteria and sample test results. To date, eighteen lab-scale tests have been conducted on systems intended for implementation in all sectors of the mining industry in South Africa. Finally, some key findings and recommendations are made. These findings are based on some common challenges encountered by CMS suppliers during the evaluation tests and lessons learnt by the test laboratory during the development of the evaluation procedure.

1 INTRODUCTION

Informal discussions between mining houses in 2004 proposed the idea of improving earth moving equipment safety. As a result, the Earth Moving Equipment Safety Round Table (EMESRT) was established in 2006, facilitated by the University of Queensland (EMESRT, 2018). EMESRT took the initiative in accelerating the development and adoption of technology to minimise the health and safety risks associated with earth moving equipment. With this objective, a performance requirement was developed (EMESRT, 2016). The performance requirement sets out interaction scenarios between machines, machines and pedestrians, and between machines and the environment.

The Minister of the South African Department of Mineral Resources amended the regulations relating to machinery and equipment, as documented in the Government Gazette published on 27 February 2015 (South Africa., 2015). The amendments to the regulations pertaining to machinery and equipment require that employers take reasonably practicable measures to ensure that pedestrians are prevented from being involved in collisions with TMMs. Where significant risks exist that TMMs may collide with pedestrians or with each other, these measures must at least include the automatic detection of the presence of a pedestrian or TMM within its vicinity. The operator of the TMM(s) and the pedestrian (if applicable) must be warned. In the event where no action is taken to prevent such a collision, the TMM(s) must be retarded to a safe speed where after the brakes of the TMM must be automatically applied without human intervention (South Africa, 2015).

Recently, the International Council on Mining and Metals (ICMM) launched an initiative to eliminate fatalities on mining sites (ICMM, 2018). The ICMM reports that TMMs

are involved in between thirty and forty per cent of industry fatalities. The ICMM is thus coordinating the development of a knowledge hub to be used by the entire mining sector. The ICMM hopes to eliminate these fatalities by making existing controls more reliable and by introducing new controls such as collision avoidance technology (ICMM, 2018).

The development of technology to reduce the risks associated with earth moving equipment and its interaction with each other and with pedestrians is thus of global importance and receiving attention on a large scale. This has presented an opportunity for developers of collision management systems (CMS) to enter the market, not only in South Africa, but globally. Multiple suppliers have made use of this opportunity, often with products that are not sufficiently tested or developed to address the significant challenges associated with the practical implementation of such systems, with a negative impact on production and unintended consequences (possibly even resulting in less safe working conditions) as a result.

The Minerals Council of South Africa's (MINCOSA) Mine Occupational Safety and Health (MOSH) Technical Specification Guideline (Minerals Council of South Africa, 2018a) was developed to guide mines and CMS suppliers in the development and implementation process. The MINCOSA MOSH Technical Specification Guideline (Minerals Council of South Africa, 2018a) provides information for the development of operation-specific technical specifications for CMS solutions. It expands on the nine (9) Control Levels introduced by EMESRT in their performance requirement (EMESRT, 2016). Control Levels 7 through 9 are applicable to CMS. The Control Levels are defined as:

- Control Level 7 (L7) – Operator Awareness (where the operator is alerted to the proximity of another TMM or person)
- Control Level 8 (L8) – Advisory Controls (where the operator is advised as to the appropriate action to be taken)
- Control Level 9 (L9) – Intervention Controls (where control is taken from the operator and the TMM is brought to a safe stop)

The MINCOSA MOSH Technical Specification Guideline (Minerals Council of South Africa, 2018a) recommends a technology development path for CMS solutions. The recommended development path includes several stage gates that involve lab-scale tests, single machine and multiple machine tests before full roll-out of the CMS solution can commence. The objective of this paper is to present a test methodology with which such collision management systems can be evaluated at lab-scale and single machine level, along with some sample results.

2 TEST METHODOLOGY

Along with the MINCOSA MOSH Technical Specification Guideline, a Test Evaluation Guideline was developed (Minerals Council of South Africa, 2018b). The Test Evaluation Guideline describes the specific test configurations to be carried out to test a CMS solution's capability. This section focuses on the lab-scale tests with brief explanations outlining the extension of the approach to single machine tests to be conducted on actual TMMs at a pilot site that is representative of the end user operating environment. The intention of the lab-scale tests is to test the CMS solution's capability and not its integration with an actual TMM. The integration and adaptation of the CMS to an actual TMM is tested during the single machine tests.

2.1 *Test scope*

The first step in evaluating CMS performance is defining the test scope. This scope comprises scenarios, machine speeds and directions, and control levels. The scenarios are based on the interaction scenarios defined by EMESRT (EMESRT, 2016). The speeds are chosen by the CMS vendor and is ideally based on the risk assessment of the intended end user (the mine). The control levels are based on the CMS vendor's own stated capability. An example of a test scope is shown in Figure 1, indicating the scenarios (see first column, based on EMESRT scenarios), the movement direction and speed (see top rows) and the control level the CMS

Scenario	Interaction Type	CMS Scope (Target)										Cross-Reference Scenario to uTCxx											
		Speed (km/h)										Applicable Control Levels											
		Reverse				MI	Forward					Test Configuration											
		REV4	REV3	REV2	REV1		FWD1	FWD2	FWD3	FWD4		uTC1	uTC2	uTC3	uTC4	uTC5	uTC6	uTC7	uTC8	uTC9	uTC10	uTC11	uTC12
		REV-50	REV-30	REV-10	REV-3	MI-0	FWD-3	FWD-10	FWD-30	FWD-50													
L1-Head-on	V-V	·	·	·	·	9	9	9	9	8				7+									
L2-Reverse-on	V-V	·	·	9	9	9	·	·	·	·					7+								
L3-Backup	V-V	·	·	9	9	9	·	·	·	·					7+								
L4-Dovetailing	V-V	·	·	·	·	9	9	9	9	9					7+								
L5-Passing Head-on	V-V	·	·	·	·	·	7	7	7	7						7+							
L6-Passing Reverse-on	V-V	·	·	7	7	·	·	·	·	·					7+	7+							
L7-Overtaking	V-V	·	·	·	·	·	9	9	9	8						7+							
L8-Blind Approach	V-V	·	·	·	·									7+									
T1-Merge	V-V	·	·	·	·	9	9	9	9	8			7+										
T2-Crossover	V-V	·	·	·	·	9	9	9	9	8		7+											
T3-Junction	V-V	·	·	·	·	9	9	9	9	8		7+											
T4-Intersection	V-V	·	·	·	·	9	9	9	9	8		7+											
O1-Obstacle	V-E	7	8	9	9	9	9	9	9	8										7+			
P1-Person (direct)	V-P	7	8	9	9	9	9	9	9	8										7+	7+		
P3-Person (indirect)	V-P	7	7	7	7	7	7	7	7	7											7+	7+	7+
V1-Void	V-E	·	·	9	9	9	9	9	9	8								7+					
V4-Loss of Control	LoC	·	·	8	9	9	9	9	9	8								7+					
V6-Congested Area	V-V	·	·	8	9	9	9	8	7	7						7+							
C1-Curving Dovetail	V-V	·	·	·	·	·	9	9	7	7							7+						
C2-Curving Head-on	V-V	·	·	·	·	·	9	9	7	7									7+				
C3-Curving Reverse-on	V-V	·	·	·	·	·	9	9	7	7									7+				
R1-Swing	V-V	·	·	·	·	·	·	·	·	·													
R2-Drop	V-V	·	·	·	·	·	·	·	·	·													
P4-Access & Egress	V-P	·	·	·	·	·	·	·	·	·													

Figure 1.   Example of nominated scope.

solution will achieve for each scenario and speed combination. The test configurations pertaining to each scenario are also shown in Figure 1 and discussed in Section 2.2.

It is important to note that the CMS solution is tested for its safety and for its impact on production. This involves testing the CMS to ensure that there are no false negatives (i.e. situations where an unwanted event will occur but no intervention is triggered) and that there are no false positives (i.e. situations where there is no unwanted interaction but an intervention is triggered). For this reason tests such as Test Configuration 3 (Head-head) and Test Configuration 6 (Passing (Straight)) are performed. The success criteria for false positive and false negative tests are different, and is discussed in Section 2.4. The false positive test configurations may provide insight into the impact a CMS solution may have on production.

2.2   Test configurations

Thirteen (13) test configurations are recommended by the Test Evaluation Guideline. Of the thirteen test configurations, the first eleven (11) are indicated for both surface and underground mining equipment (SME & UME). The remaining two are only indicated for UME.

Figure 2 shows schematic representations of the test configurations. Each schematic in Figure 2 shows the position of the two objects (local object (LO) and remote object (RO)) and the motion direction of each object (v_{LO}, v_{RO} and FWD or REV, if applicable). The schematics also include the stopping distance (D'), stop gap (G_{min}) or following gap (F) or passing gap (P), the distance where the CMS signal is generated (S), the offset when objects are passing each other (X) when applicable, and the radius of curvature (R).

The scenarios selected in the scope guides the test configurations to be performed. Some scenarios rely on a single test configuration, while other scenarios are seen as combinations of test configurations. Figure 1 cross-references the scenarios to test configurations.

The test configurations are applicable to the lab-scale tests and single machine tests stage gates of the MINCOSA technology development path. Several speed combinations are performed for each test configuration, with each speed combination repeated three times for the lab-scale tests. When performing the single machine tests, the number of tests may be reduced in the interest of time and the resulting impact on production on the pilot site where the tests are conducted. During both lab-scale and single machine tests, only two test vehicles/ machines are used (LO and RO).
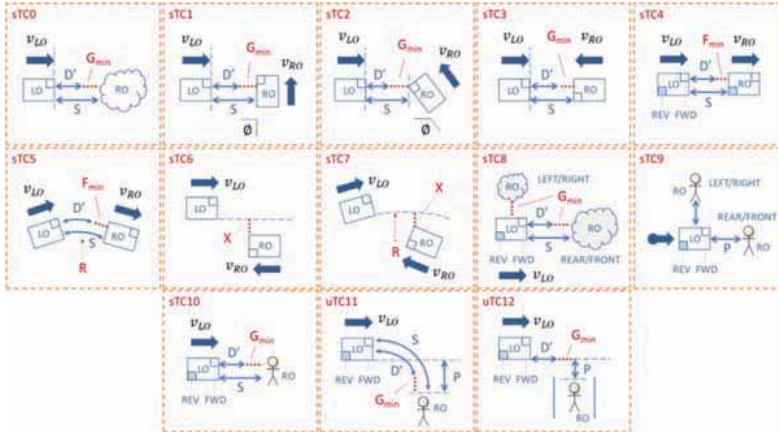
Figure 2. Test configurations recommended by the MINCOSA MOSH Test Evaluation Guideline (Minerals Council of South Africa, 2018b).

2.3 *Test equipment and site*

The lab-scale tests are conducted with two light vehicles. Each vehicle is instrumented with the following equipment:

- Brake pedal robot and controller (developed at the University of Pretoria)
- Racelogic VBOX 3i Dual Antenna RTK differential GPS with IMU (Racelogic, 2014)
- dSPACE MicroAutoBox II embedded real-time computer (dSPACE GmbH, 2016)
- Complete CMS solution from third party vendor (the solution being tested)

The brake pedal robot consists of a linear actuator and controller that controls the brake pedal position on each vehicle. When a L9 intervention signal is generated by the CMS, the test vehicle's deceleration is controlled by a feedback control system. Deceleration is measured with the Racelogic VBOX 3i system and controlled by adjusting the brake pedal position. The deceleration is configured before the tests are conducted and is based on recommendation from the CMS vendor. In the absence of a recommendation from the CMS vendor, a relevant standard is used to derive the deceleration to be applied during the tests. Standards such as ISO3450:2011 (International Organisation of Standardisation, 2011) and SANS1589-1:2012 (South African Bureau of Standards., 2012) are then recommended, based on the CMS solution's intended application.

The use of a feedback control loop and brake pedal robot to control the deceleration of the test vehicles results in braking performance that is equivalent to that of a TMM. This is illustrated in the following equation showing the demand forces acting on a vehicle (Gillespie, 1992):

$$F_{demand} = -F_{brakes} - F_{drag} - F_{gradient} - F_{rolling\ resistance}$$
$$\Rightarrow ma_x = ma_{brakes} + ma_{drag} + ma_{gradient} + ma_{rolling\ resistance}$$
$$\therefore a_x = a_{brakes} + a_{drag} + a_{gradient} + a_{rolling\ resistance}$$

where F represents a force, m is the mass of the TMM, and a is the deceleration. By controlling a_x, the deceleration of the TMM as a system, the impact of friction coefficient (represented by a_{brakes}, aerodynamic drag (a_{drag}), gradient ($a_{gradient}$, and rolling resistance ($a_{rolling\ resistance}$) are lumped together and taken into account.

The vehicle positions, orientations, speeds and accelerations are measured with the Racelogic VBOX 3i Dual Antenna RTK differential GPS system (Racelogic, 2014). The Racelogic VBOX 3i system is a differential GPS that provides absolute positional accuracy of ± 2 cm and speed accuracy of 0.1 km/h at a sampling rate of 100 Hz. A RTK GNSS base station

is used to improve the absolute accuracy of the GPS and a Kalman Filter enabled inertial measurement unit (IMU) is used to smooth the measurements and deals with GPS signal dropouts. Furthermore, the VBOX is equipped with a telemetry system that allows for communication between the vehicles. Data transmitted between the machines is configurable, but can consist of among others, vehicle speed, relative positions and orientations.

Control of the brake pedal robot, logging of the VBOX data and the interface between the test vehicle and the CMS solution is achieved with the dSPACE MicroAutoBox II (dSPACE GmbH, 2016). Data is logged at 1000 Hz and the interface is run in real-time. The dSPACE MicroAutoBox II can interface with the 3rd party CMS solution via a CAN bus or via a Digital I/O interface or both. The dSPACE allows for rapid prototyping and is easily adaptable to the CMS vendor's interface.

Lab-scale tests are conducted at Gerotek Test Facilities (Armscor Defence Institutes SOC). Gerotek Test Facilities is a proving ground with multiple test tracks located to the west of Pretoria, South Africa. Tests are conducted on both asphalt and concrete surfaces and are all performed on level roads. This ensures that tests results are repeatable. Tests are mainly conducted on the Straight Track—a one kilometre straight concrete track that is 30 m wide at the widest part—and on the Dynamic Circle—a 100 m radius circular track that has a test section that is approximately 90 m wide and 50 m long. Straight line tests are conducted on the Straight Track and intersection and curved tests are conducted on the Dynamic Circle.

Figure 3 shows a schematic representation of the test setup and Figure 4 shows the test vehicle, brake pedal robot and measurement instruments on the test track at Gerotek Test Facilities.

2.4 *Success criteria*

The lab-scale test mainly tests the CMS solution's decision making, although the sensing capability is also inherently tested. During all of the tests at Gerotek Test Facilities, line-of-sight
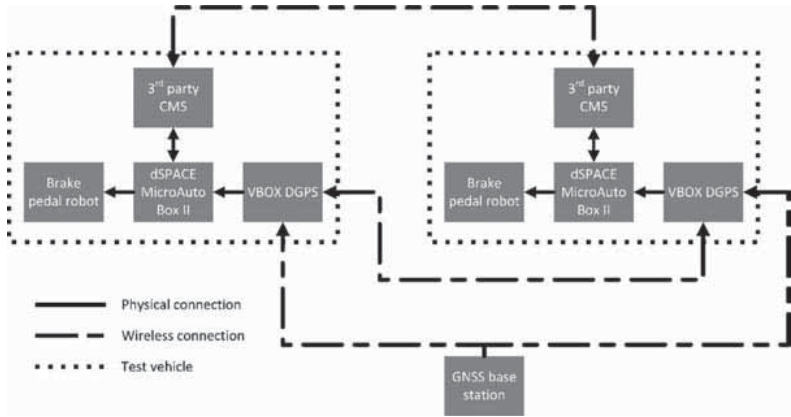

Figure 3. Schematic representation of test setup, showing components used for lab-scale tests and single machine tests.

Figure 4. Test vehicle (left) and brake pedal robot (right).

is maintained. Ideally, the sensing capability should be tested in a site that is representative of the intended operating environment. The integration and adaptation of the CMS to an actual TMM is tested during the single machine tests. However, the overall success criteria are similar for both.

In the absence of regulated/standardised performance requirements, the onus is placed on the CMS vendor to nominate the distance values according to which they will be tested. The L7 and L8 criteria are thus distances at which the appropriate signals will be triggered and the L9 criteria is the distance at which the machine will reach the safe braking speed and finally stop.

The CMS vendor is also asked to specify a tolerance, which is then applied to these distances. This tolerance is to account for delays in the system that may be attributed to sensing, decision making, communication, and interface delays. Finally, a measurement tolerance based on the measurement equipment is added on top of the tolerance specified by the CMS vendor. Figure 5 shows an example of the test criteria used for sTC3 – Head-head (Straight).

The success criteria needs to be specified for each test configuration (shown in Figure 2) and each speed combination that is tested. The results of each test configuration are then used along with the scenario-test configuration cross-reference of Figure 1 to determine whether the CMS solution passes a specific speed for a specific scenario.

For both the lab-scale and single machine tests, the system must pass all of the test runs at a speed combination for it to pass the test configuration at that speed.

2.4.1 *False negative criteria*

The false negative success criteria requires that the applicable control levels are triggered. The L7 and L8 success criteria are based on the distances (gap) between LO and RO when the L7 and L8 Control Level signals will be triggered. The L9 success criteria is based on the TMM reaching a pre-defined speed (which may be zero) at a specified distance. Defining the L9 control strategy before testing commences is thus of utmost importance, due to the multitude of approaches of applying L9 intervention control encountered in the industry.

A requirement of the L9 intervention control, as stipulated in Chapter 8 of the Mine Health and Safety Act of South Africa (South Africa., 2015), requires the TMM to be brought to a safe and controlled stop. This is in practice difficult to achieve consistently, due to the complex vehicle dynamics involved in stopping a TMM and the intricacies of braking systems found on TMMs.

Generally (although there are some exceptions), the approach has been to define a safe braking speed below which the emergency brake system can be used to safely bring the vehi-

Local Object Speed (v) Code	Remote Object Speed (v) Code	Test Parameter	Head-on Distance [metre]	Pass/fail minimum [metre]	Pass/fail maximum [metre]
FWD1	FWD1	Stop Gap (G)	10.2	9.2	13.3
FWD1	FWD1	Alert 7	17.4	15.7	22.7
FWD1	FWD1	Stop 8	14.4	13.0	18.8
FWD1	FWD1	Stop 9	11.4	10.3	14.8
FWD2	FWD1	Stop Gap (G)	15.9	14.3	20.7
FWD2	FWD1	Alert 7	32.3	29.0	42.0
FWD2	FWD1	Stop 8	25.8	23.2	33.5
FWD2	FWD1	Stop 9	16.9	15.2	22.0
FWD3	FWD1	Stop Gap (G)	20.0	18.0	26.0
FWD3	FWD1	Alert 7	69.1	62.2	89.8
FWD3	FWD1	Stop 8	54.1	48.7	70.3
FWD3	FWD1	Slow 9	39.1	35.2	50.8
FWD3	FWD1	Stop 9	21.0	18.9	27.3
FWD4	FWD1	Stop Gap (G)	29.4	26.5	38.2
FWD4	FWD1	Alert 7	137.6	123.8	178.9
FWD4	FWD1	Stop 8	112.6	101.3	146.4
FWD4	FWD1	Slow 9	87.6	78.8	113.9
FWD4	FWD1	Stop 9	31.0	27.9	40.3

Figure 5.   Sub-set of pass/fail criteria for sTC3.

cle to a standstill. This requires that the CMS vendor and the OEM must agree on a safe L9 intervention strategy and is crucial to the success of CMS in practice. A problem encountered with this approach is reducing the machine speed to this pre-defined safe brake speed. There are multiple approaches employed by OEMs to achieve this, chief among which is de-rating or de-throttling the power unit. This introduces a multitude of variables that influence the distance required to reach the safe braking speed from the operating speed. These variables include the grade of the road the TMM is travelling on, the payload of the TMM, gear selection of the TMM and the driveline type. For the lab-scale tests, the type of intervention above and below the safe braking speed is agreed upon *a priori* in the form of an acceleration set point, with the test vehicles then matching this performance using the brake robot. For the single machine tests on actual TMMs, the CMS vendor needs to take the variance in braking performance into account.

Nevertheless, the success criteria for L9 intervention can be summarised as follows:

- The CMS may not generate a L9 Stop signal above the safe braking speed.
- The LO must slow down to the safe braking speed at a distance from the RO not less than the distance at which the L9 Stop signal is expected.
- Once the LO and RO are stationary, the gap between the two objects must be greater than a specified value.

For the majority of the test configurations, the distance is measured between the two test vehicles/machines. Due to the complexity associated with the intersection test configurations, the distance is measured in these cases to the anticipated intersection point. Because of the variability when performing intersection tests, the measurement tolerance is increased for these test runs. Typical measurement tolerance is ± 0.5 m which is then increased to ± 2 m for intersection tests.

2.4.2 *False positive criteria*
The false positive success criteria differs from the false negative criteria, because in the false positive tests the triggering of warnings or interventions is undesired. False positive warnings or interventions may hamper production and have a negative impact on the mining activity. Test configurations that involve false positive tests are Test Configurations 6, 7, 9, and 12. In these test configurations, the objects are separated an agreed upon distance and the tests then conducted. The triggering of control levels when the objects are not on a collision course will then be registered as failed test runs.

2.5 *Reporting*

The final step in the test methodology is reporting on the results. This is of the utmost importance, as this provides the CMS vendor with a thorough report on the performance of the system and it may be used by mines to compare the CMS capability with their requirement. The report contains a description of the scope of the tests (the scope is nominated by the CMS vendor prior to testing) and the actual tested capability. An example of the scope is shown in Figure 1 and tested capability is shown in Figure 6. The report thus gives the reader insight into the maturity of the CMS solution and the vendor's own understanding of the capabilities and limitations of the solution.

3 SAMPLE TEST RESULTS

Figure 7 shows an example of the test results for Test Configuration 3 – Head-head (Straight) and Figure 8 shows an example of the test results for Test Configuration 1 – Crossing (90°). The two objects' speeds are shown in the 'a) Object speed' plots and the objects' positions are shown in the 'b) Object position' plots. Also shown in these figures are the positions where the different control levels were triggered.

Scenario	Interaction Type	CMS Scope (Capability)								
		Speed (km/h)								
		Reverse				MI	Forward			
		REV4	REV3	REV2	REV1		FWD1	FWD2	FWD3	FWD4
		REV:50	REV:30	REV:10	REV:3	MI:0	FWD:3	FWD:10	FWD:30	FWD:50
L1-Head-on	V-V	-	-	-	-		9	8	9	
L2-Reverse-on	V-V	-	-	9	9		-	-	-	-
L3-Backup	V-V	-	-	9	9		-	-	-	-
L4-Dovetailing	V-V	-	-	-	-		9	9	9	8
L5-Passing Head-on	V-V	-	-	-	-	-	7	7	7	7
L6-Passing Reverse-on	V-V	-	-	7	7	-	-	-	-	-
L7-Overtaking	V-V	-	-	-	-	-	9	9	9	8
L8-Blind Approach	V-V	-	-	-	-					
T1-Merge	V-V	-	-	-	-		9		8	
T2-Crossover	V-V	-	-	-	-			9		
T3-Junction	V-V	-	-	-	-			9		
T4-Intersection	V-V	-	-	-	-			9		
O1-Obstacle	V-E			9	9		9	9	9	8
P1-Person (direct)	V-P			9	9		9	9	9	9
P3-Person (indirect)	V-P			7	7		7	7	7	7
V1-Void	V-E	-	-	9	9		9	9	9	8
V4-Loss of Control	LoC	-	-	9	9		9	9	9	8
V6-Congested Area	V-V	-	-	9	9		9	8	7	
C1-Curving Dovetail	V-V	-	-	-	-	-	9			
C2-Curving Head-on	V-V	-	-	-	-	-	9	9		
C3-Curving Reverse-on	V-V	-	-	-	-	-	9	9		
R1-Swing	V-V	-	-	-	-		-	-	-	-
R2-Drop	V-V	-	-	-	-		-	-	-	-
P4-Access & Egress	V-P	-	-	-	-		-	-	-	-

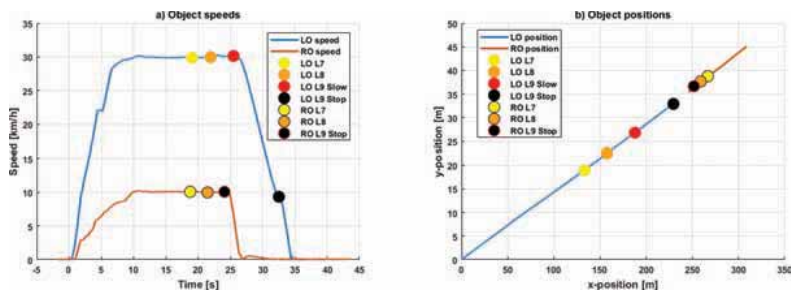Figure 6.   Example of tested capability contained in the report.

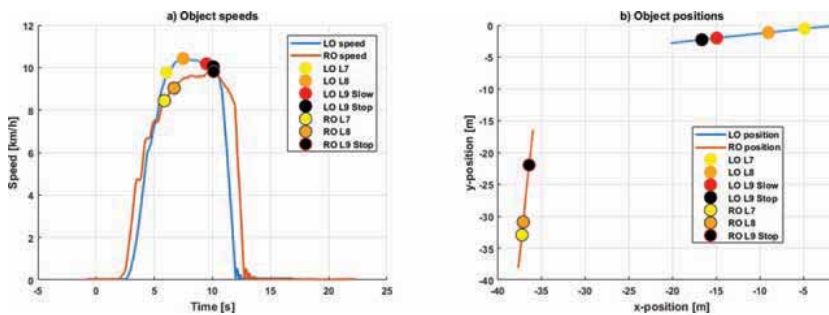Figure 7.   Test configuration 3 – Head to head test results.

Figure 8.   Test configuration 1 – Crossing (90°) test results.

4   DISCUSSION

At the time of writing, twenty-one (21) evaluations had been conducted on systems intended for implementation in all sectors of the mining industry in South Africa, twenty (20) at lab-scale level and one at single machine level. The twenty-one (21) evaluations have been conducted on twelve (12) different CMS suppliers. During the course of these evaluations, several refinements and improvements were made to the evaluation procedure before arriving at its current form. Some of the lessons learnt so far include:

- A large test area is needed. It is important that the test vehicle is at the intended speed well before the first control level will be triggered, hence appropriate run-up is needed.
- It is important that the CMS distances are known before starting the test. This includes understanding the intervention strategy the CMS will apply.
- Controlling the speed at the intended speed is important to ensure accurate performance of the CMS.
- Communication between the drivers of the two test vehicles is of vital importance.
- CMS suppliers often have not discussed the expected system performance with their customers (the mine). This complicates matters, as CMS suppliers often are not mining experts with limited exposure to the day-to-day operations of a mine. Very often there is very little guidance from the customer to guide and influence the development of the CMS.
- The test report must be written for a non-technical audience, failure to do so may result in readers questioning the veracity of the report.

Feedback from the CMS suppliers after conducting tests have been positive, with the following a summary of the feedback:

- The testing is extremely thorough;
- CMS suppliers have underestimated the complexity involved;
- Tests have contributed significantly to improving the offerings of CMS suppliers; and
- The evaluation procedure has provided a better understanding of the environment within which CMSs will be used.

5 CONCLUSION

An evaluation procedure was developed in cooperation with the MINCOSA which thoroughly tests the performance of CMSs. This evaluation procedure has been found to be a game-changer in the development process to improve technology readiness levels.

ACKNOWLEDGEMENT

REFERENCES

Armscor Defence Institutes SOC Gerotek Test Facilities.
Dspace GMBH (2016). dSPACE.
EMESRT (2016) Vehicle Interaction Systems.
EMESRT (2018) The EMESRT Story.
Gillespie, T.D. (1992) *Fundamentals of vehicle dynamics,* Warrendale, PA, SAE International.
ICMM (2018) Vehicle Interaction Controls.
International Organisation of Standardisation (2011) ISO 3450:2011 Earth-moving machinery – Wheeled or high-speed rubber-tracked machines – Performance requirements and test procedures for brake systems. Geneva, Switzerland.
Minerals Council of South Africa. (2018a) *Collision Management Systems Technical Specification Guideline* Johannesburg, South Africa, Minerals Council of South Africa.
Minerals Council of South Africa. (2018b) *Collision Management Systems Test Evaluation Guideline,* Johannesburg, South Africa, Minerals Council of South Africa.
Racelogic (2014) VBOX 3i v3 100 Hz GPS Data Logger.
South Africa. (2015) Mine Health and Safety Act, 1996 (Act No 29 of 1996): Amendment of Chapter 8 of the regulations relating to machinery and equipment (Proclamation No. R. 125). *Government Gazette 38493:22.*
South African Bureau of Standards. (2012) SANS1589-1:2012 – The braking performance of trackless mobile mining machines Part 1: General requirements. Pretoria, South Africa.

A sensitive carbon monoxide monitoring system for forecasting coal spontaneous combustion

Z.W. Wang, Y.F. Li, T.T. Zhang, Y.B. Wei & T.Y. Liu
Laser Institute, Qilu University of Technology (Shandong Academy of Sciences), Jinan, China

ABSTRACT: The coal spontaneous combustion has been recognized as one of the major hazards in coal mine production. The fiber optic Raman scatter-based Distributed Temperature Sensor (DTS) is an effective approach for coal spontaneous combustion monitoring, which provides a convenient means to monitor the temperature distribution of coal area over time. Recently, as the most important characteristic gas, Carbon Monoxide (CO) can be used for early detection of coal spontaneous combustion in mine goafs. In this work, a sensitive and stable CO monitoring system was developed by using a Distributed Feedback (DFB) laser operating at 2.33 µm and a Herriott-type multi-pass gas cell with a 20-m optical length, taking advantage of the in-situ monitoring, excellent accuracy and simple structure available from direct absorption spectroscopy. The results obtained have validated the potential use of such a CO monitoring system in a practical monitoring application, such as the coal spontaneous combustion monitoring.

1   INTRODUCTION

There are a great variety of health and safety hazards in the coal mines, such as water flooding, rock roof collapse, methane gas explosion, and coal mine combustion *etc* (Liang et al., 2016). According to the published statistics, the coal mine combustion has been recognized as one of the major hazards in coal mine production, which can be classified as coal spontaneous combustion and electrical fault (Lieberman and Hewitt, 2004). The coal spontaneous combustion is due to the slowly oxidized process of coal residue in the goaf. Because of the highly exothermic oxidized process, the great heat accumulated in turn accelerate the coal combustion and thus causes fire. So far, the fiber optic Raman scatter-based distributed temperature sensor (DTS) is an effective approach for coal spontaneous combustion monitoring, which provides a convenient means to monitor the temperature distribution of coal area over time (Yuan et al., 2012). However, the DTS fiber cable cannot be directly mounted in coal oxidization zone. Hence, the monitored temperature by the DTS technology is not an actual temperature of coal oxidization zone.

More recently, multi-gas monitoring technology has attracted more and more attention to forecasting coal spontaneous combustion (Zhang et al., 2011). The oxidization process is characterized by presence and increase of many kinds of gases, such as carbon monoxide (CO) at initial phase of oxidization, ethene (C_2H_4) when the oxidization gets severe, and ethyne (C_2H_2) where its presence means fire is imminent. By monitoring the concentrations of each gas within the mixed gases, the early warning signal can be issued before coal spontaneous combustion. Among these characteristic gases, CO is the most important gas for early detection of coal spontaneous combustion. Typical detection sensitivity of CO present in goaf area is 1 part per million (ppm) by volume.

Conventional gas analysis system for coal mine combustion monitoring is chromatography-based gas tubing bundles system, which suffers from long time delay due to the longer distance (10 km or longer) between goaf and the underground gas analysis system (Liu et al., 2018). As a cutting-edge technology for gas detection, tunable diode laser absorption

spectroscopy (TDLAS) shows the advantages and potential for real time on-line monitoring, offering high selectivity and sensitivity, long-term stability and excellent reliability.

Because of the stronger absorption of the CO first overtone band, a CO sensor using a laser diode operating around 2.3 μm can provide sensitive detection. In this work, a sensitive and stable CO monitoring system was developed by using a distributed feedback (DFB) laser operating at 2.33 μm and a Herriott-type multi-pass gas cell with a 20-m optical length, taking advantage of the in-situ monitoring, excellent accuracy and simple structure available from direct absorption spectroscopy. The detection accuracy of system was about ±0.1 ppm when as low as 1 ppm CO gas was detected. Further, a long-term continuous monitoring evaluation has clearly demonstrated the long-term stability and reliability of the monitoring system. The results obtained have validated the potential use of such a CO monitoring system in a practical monitoring application, such as the coal spontaneous combustion monitoring.

2 PRINCIPLE

A distributed feedback (DFB) laser operating at a specific wavelength of 2330.18 nm was employed to target the strong absorption line of CO first overtone band, a wavelength where the corresponding absorption intensity is 3.39×10^{-21} cm^{-1}/(mol × cm^{-2}). The Herriott-type multi-pass gas cell (MGC) has an effective optical length of 20 m, with a base volume of 0.57 L. Both sides of the inside of the gas cell were dielectric coated, providing a broadband transmission over the wavelength range from 2290 nm to 2370 nm. The transmitted laser beams were detected by using the RT extended-InGaAs photo-detector installed within the system. Using a current driver and temperature controller, the emitting laser wavelength can be tuned with a sawtooth wave. The intensity of the laser decreases when the laser light is passed through CO gas-filled MGC and as a result, the measured small dip in the background line creates the gas absorption signal. According to the Lambert-Beer law, the CO gas concentration can be obtained using following formula (Paynter, 2010):

$$C = \frac{A}{PS(T)L} \tag{1}$$

$$A = \int_{-\infty}^{\infty} -\ln\left(\frac{I}{I_0}\right) d\lambda \tag{2}$$

where C is the volume concentration of the measured CO gas sample, I_0 is the initial light intensity, I is the light intensity due to the absorption, λ is the laser wavelength, L is the length of the optical path, P is the total pressure of the gas medium and $S(T)$ is the intensity of the characteristic spectral lines (which show a temperature dependence).

3 RESULTS

In the experiment carried out, the CO gas, at a concentration of 30 ppm, was mixed with pure nitrogen (99.999% N$_2$) to create various CO gas samples at different nominal concentrations: 3 ppm, 1 ppm, 0.5 ppm, 0.3 ppm, and 0.1 ppm. These gases were successively filled into the gas cell with a constant flow rate of 1000 mL/min. The monitored raw data were recorded during the whole process and these are illustrated in Figure 1. At the same time, the measured raw data were smoothed using a 10-points moving average method, in order to show the trends more clearly. As depicted, the results show that the CO monitoring system could detect CO gas samples with excellent precison and stability. And it can readily sense the presence of CO gas, at a concentration as low as 0.1 ppm. As illustrated in Figure 1, data monitored can be used to determine that the detection accuracy of system was about ±0.1 ppm when as low as 1 ppm CO gas was detected and the detection limit of system could be estimated to be 0.1 ppm
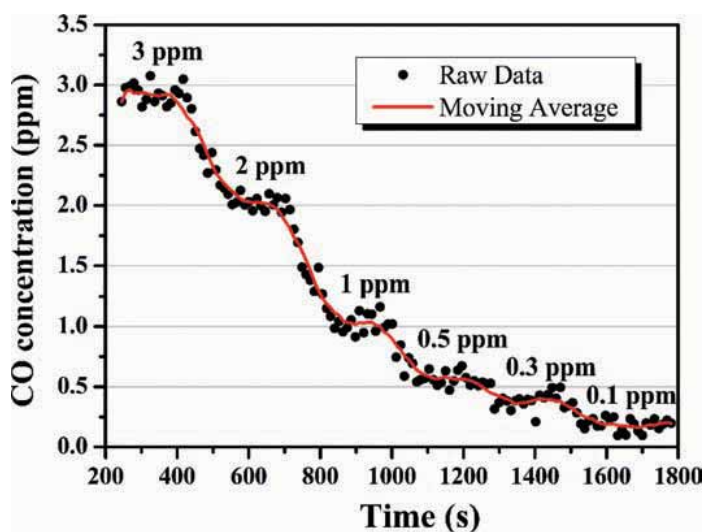
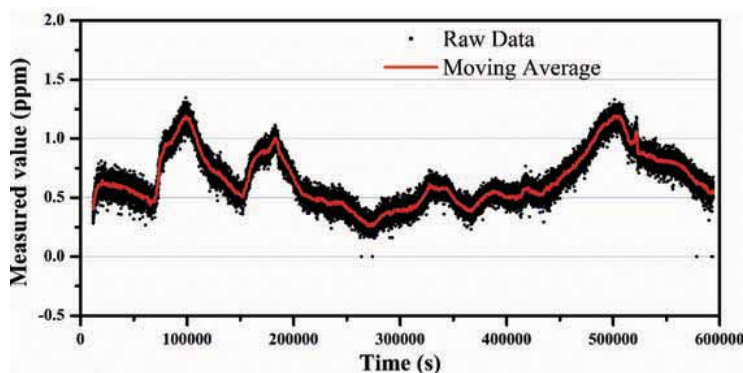Figure 1. Measured CO concentrations determined from the monitoring system developed.

Figure 2. The measured CO concentration using the monitoring system developed.

in this work. Due to extremely small amount of impurity of pure N_2, the measurement accuracy of CO monitoring system decreased when 0.1 ppm CO gas was detected.

To evaluate the stability and reliability of CO monitor developed, the system operated continuously for over 600,000 second in an ambient atmosphere, as shown in Figure 2. In order to enhance the stability of system, the measured raw data were smoothed using a 30-points moving average method. As can be seen from the Figure 2, the actual fluctuations of the CO gas concentration in the ambien air could be measured by using the CO monitoring system developed. Looking at these closely, the first 'rogue peak' resulted from the leaking CO gas from another experiment being carried out in the same place. Figure 2 has clearly demonstrated the long-term stability and reliability of monitoring system. More importantly, there is no cross interference seen in the monitoring of ambient air. The results obtained have validated the potential use of such a CO monitoring system in a practical monitoring application, such as the coal spontaneous combustion monitoring.

4   CONCLUSION

In summary, multi-gas monitoring technique is an effective approach for coal spontaneous combustion monitoring, in addition to fiber optic Raman scatter-based DTS. Conventional

gas analysis system for coal mine combustion monitoring is chromatography-based gas tubing bundles system, which suffers from long time delay. As a cutting-edge technology for gas detection, tunable diode laser absorption spectroscopy (TDLAS) shows the advantages and potential for real time on-line monitoring, offering high selectivity and sensitivity, long-term stability and excellent reliability.

As the most important characteristic gas, CO gas can be used for early detection of coal spontaneous combustion in mine goafs. In this report, a sensitive and stable CO monitoring system was demonstrated by using a 2.33 μm distributed feedback (DFB) laser and a 20-m Herriott-type multi-pass gas cell, taking advantage of *in-situ* monitoring, excellent accuracy, simple structure and lower cross interference available from direct absorption spectroscopy. The detection accuracy of system was about ±0.1 ppm when as low as 1 ppm CO gas was detected. Data monitored can be used to determine that the detection limit of system was about 0.1 ppm. Moreover, a long-term continuous monitoring evaluation has clearly demonstrated the excellent stability and reliability of monitoring system developed. The results obtained have validated the potential use of such a CO monitoring system in a practical monitoring application, such as forecasting coal spontaneous combustion.

ACKNOWLEDGEMENT

REFERENCES

Liang, Y., Hou, X., Luo, H., Tian, F. & Yu, G. 2016. Development countermeasures and current situation of coal mine fire prevention & extinguishing in China. *Coal Science & Technology*.

Lieberman, H. & Hewitt, C. 2004. Innovative Techniques for Detection and Control of Underground Spontaneous Combustion of Coal. *Communications of the Acm,* 26, 419–429.

Liu, T., Wei, Y., Song, G., Hu, B., Li, L., Jin, G., Wang, J., Li, Y., Song, C. & Shi, Z.J.M. 2018. Fibre optic sensors for coal mine hazard detection. 124, S0263224118302239.

Paynter, R.W. 2010. Modification of the Beer–Lambert equation for application to concentration gradients. *Surface & Interface Analysis,* 3, 186–187.

Yuan, L., Tao, L., Wei, Y. & Sun, Z. Application of Distributed Optical Fiber Temperature Sensing System Based on Raman Scattering in Coal Mine Safety Monitoring. Photonics & Optoelectronics, 2012.

Zhang, X.H., Wen, H., Deng, J., Zhang, X.C. & Tien, J.C. 2011. Forecast of coal spontaneous combustion with artificial neural network model based on testing and monitoring gas indices. *Journal of Coal Science & Engineering,* 17, 336.

Application of laser methane sensor in on-line monitoring of gas pipeline

G.X. Jin & H. Meng
Shandong Micro-Sensor Photonics Ltd., China

G.H. Jia & W.W. Wang
Xinwen Mining Group Zhaoguan Energy Ltd., China

H. Zhang & Z.D. Shi
Shandong Micro-Sensor Photonics Ltd., China

T.Y. Liu
Laser institute, Shandong Academy of Sciences, China

C.X. Song
Shandong Micro-Sensor Photonics Ltd., China

Y.N. Ning
Laser institute, Shandong Academy of Sciences, China

ABSTRACT: Laser methane sensor has the characteristics of wide measurement range, low measurement error, fast response, long period between every calibrations, long service life, no gas cross-interference and convenient maintenance in the operation. Based on the VCSEL laser technology, the methane sensor using a self-adaptive, multi-band spectral absorption technology realizes ultra-low power laser spectral detection. Operation at temperature ranging from –10°C to 50°C and pressure ranging from 30 kPa to 200 kPa, the new Laser methane sensor greatly improves the accuracy and reliability of methane measurement on a gas pipeline. By introducing Internet of Things technology, the connection between sensor and computer/mobile terminal and remote real-time monitoring can be realized, and the data of gas drainage pipeline can be monitored and viewed at any time. In this presentation, the design of the VCSEL laser methane sensor and the measured results will be shown, the further improvements will be discussed.

Keywords: Gas drainage, Laser methane sensor, Temperature and Pressure Compensation, Internet of things

1 INTRODUCTION

The implementation of Chinese Government's policy of "purging gas before mining" at all high gas mines is one of the fundamental solutions to prevent gas accidents in the process of coal mining. The coal mine gas drainage and utilization not only enable the high gas mines to be mined at a low gas concentration state, avoiding the gas-induced disasters during coal mine production, but also can prevent the methane gas from being released to environmental, reducing the green gas emission (Provisional Standards). Because the concentration of methane in the pipeline fluctuates greatly during the gas drainage process, it is necessary to use a special gas distribution pipeline network to mix the extracted gas to maintain gas concentration at a high and stable value. In this process, it is necessary to monitor the methane

gas concentration in the gas pipeline. However, there are a number of challenges in monitoring methane in the pipeline system, first, in order to operate gas extraction system safely, a large amount of water mist is usually sprayed into the pipeline, resulting in a high humidity condition in the pipeline; secondly, the methane concentration during the extraction process varies considerably, this requires the methane sensor can be operated over a large concentration range; thirdly, during the extraction process the pipeline leakage to may occurs, and it is very danger if the leakage occurs in a confined area, as the methane gas would explode if its concentration reaches to a range of 5%–16% (Xu), this requires that the methane monitoring sensor needs to have a accuracy over large concentration range; fourthly, the gas drainage pipelines are usually laid out over a long distance and the surrounding environment along the pipeline is very complicated for monitoring system to be installed.

Currently the methane gas sensors used in coal mines mainly are based on the technologies such as catalytic combustion, thermal conductivity, optical interference and infrared absorption. These detection methods have some shortfalls and disadvantages in methane pipeline monitoring. For instance, the measured results with the use of those gas sensors are easy to drift; the measurement range is relatively small, they can be easily affected by the water or mist in the pipeline, and resulting low precision and poor reliability; also it is easy to be poison at high gas concentration, etc. Whilst for the Infrared absorption sensors, the measured results can be easily interfered by different other gases presented in the extracted gas (Chen, Liu, Ye). To overcome the difficulties encountered with traditional methane sensors, fiber optic sensors based on laser spectral absorption becomes an alternative solution to offer accurate measurements over a large operational range of methane concentration. The features of insensitive to water and other gases make it more suitable to be employed in real time and in harsh environments such as online monitoring of gas pipelines (Liu, Wang). The laser methane sensor has the characteristics of large measuring range, low measuring error, fast response time, long calibration period, long service life, no gas cross interference and easy maintenance. Comparing with several other sensors, the laser methane sensor has considerable advantages in terms of stability and reliability, which make these sensors to be particularly suitable for being used in harsh environments such as gas drainage pipes in coal mines.

Due to the large variation of gas pressure and ambient temperature in the extraction pipeline, it greatly affects the accuracy of the measured value of gas concentration. In order to improve the measurement accuracy, this paper introduces a new laser methane sensor based on VCSEL as its light source has been developed. This sensor can be operated over a wide range of temperature and pressure variation. With the use of Internet of Things technology, it can achieve remote real-time gas concentration monitoring.

2 WORKING PRINCIPLE OF THE LASER MECHANE SENSOR

It is well know that methane can be measured based on the principle of gas spectral absorption. According to Lambert-Beer's law, one parallel light of light intensity $I_0(\lambda)$ passes through a gas chamber which contains gas to be measured; if the light source spectrum covers one or more absorption lines of the gas, the relationship between the transmitted light intensity $I(\lambda)$, the incident light $I_0(\lambda)$ and gas concentration C is given by the following equation (Xu)

$$I(\lambda) = I_0(\lambda) exp\left[-\alpha(\lambda)CL\right] = I_0(\lambda) \exp\left[-PS(T)\phi(\lambda)CL\right] \tag{1}$$

where $\alpha(\lambda)$ is the absorption coefficient of the gas; L is the length of the light passing through the gas; P is the total pressure of the gas; $S(T)$ is the line intensity of the characteristic spectral line of the gas, indicating the absorption intensity of the spectral line, which is a function of gas temperature; $\phi(\lambda)$ is a linear function that represents the shape of the measured absorption spectral line and is function of gas temperature, total pressure, and the mixture of each components contented in the gas.

By performing logarithm operation on both sides of equation (1), integrating over the entire frequency domain, it becomes

$$PCS(T)\phi(\lambda)L = \int_{-\infty}^{\infty} -\ln\left(\frac{I}{I_0}\right) d\lambda = A \tag{2}$$

Therefore, the gas concentration can be directly calculated by the following formula

$$C = \frac{\int_{-\infty}^{\infty} -\ln\left(\frac{I}{I_0}\right) d\lambda}{PS(T)\phi(\lambda)L} = \frac{A}{PS(T)\phi(\lambda)L} \tag{3}$$

In the case where parameters such as pressure P, absorption line intensity $S(T)$ and effective length of gas absorption L are known, the integrated value of $-\ln(I/I_0)$ in the frequency domain is brought into the equation (3) and the gas concentration value C can be finally obtained. Normally, the spectral absorption signal is integrated after a corresponding linear function is used for fitting the measured data. The integral value is then accurately calculated from the line fitting data and the influence of the measurement error cane reduced. Assuming that the pressure and absorption line of a gas are a constant in the actual sensor design and the concentration of the gas can be measured only by measuring the change of the light intensity before and after the gas absorption. In order to improve the accuracy and reliability of the measurement, temperature and pressure compensation are required (Li, Zhao).

3 PIPELINE WIRELESS LASER METHANE SENSOR MONITERING SYSTEM

The Internet of Things (IoT) is an important part of the new generation of information technology and an important development in the era of information. The use of IoT technology in gas drainage pipelines is also an advancement and new area. To obtain the gas concentration data of gas drainage pipelines at any time and at anywhere it very important for coal mine industry.

3.1 System structures

The system consists of three sections: a sensor probe, a control PC with a user server terminal, and a mobile terminal. The sensor probe employed is a mine wireless laser methane sensor; the device terminal is composed of a computer terminal, a mobile phone and other mobile device terminals; the User server is used to connect the sensor to the computer terminal/mobile phone; GPRS is employed to communicate between sensor probe and the other terminals to achieve the real-time gas concentration monitoring.
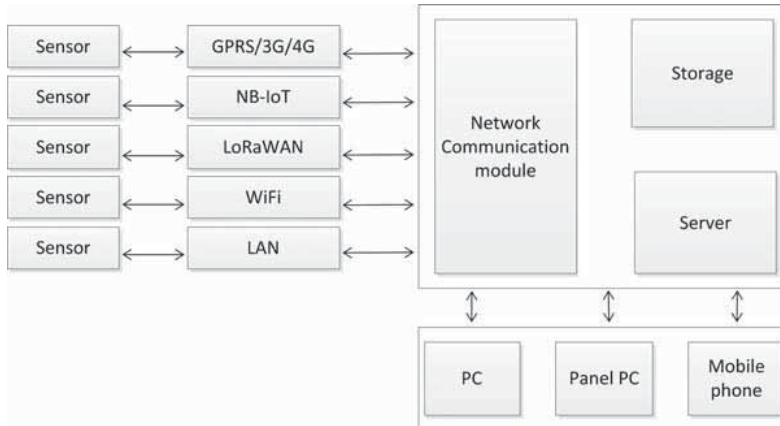

Figure 1. System block diagram.

3.2 *Research on temperature compensation technology*

For a traditional methane sensor, its operating temperature range is 0–40°C, which is suitable for underground coal mine environments. In gas drainage monitoring applications, a wider operating temperature range is required for outdoor use. The laser methane sensor based on DFB requires a laser temperature control unit hence the range of temperature control is limited, generally in the range of ±20 degree. It is more difficult to further increase the operating temperature range as more power is needed to maintain at high or low temperatures.

From equation 3, it can be seen that there is a parameter of (λ), which is a linear function that represents the shape of the measured absorption spectral line and is function of gas temperature, total pressure, and the mixture of each components contented in the gas. Hence, the variation of $\phi(\lambda)$ due to temperature or/and pressure changes needs to be compensated in order to obtain an accurate measurement.

An adaptive multi-band spectral absorption technology is innovated based on VCSEL laser technology, by which a wide operational temperature range can be achieved, in addition, this technology enable an accurate gas concentration measurement with an ultra-low power consumption.

The measurement results of the laser methane sensor in the range of –10 degree to 50 degree are shown in Table 1.

The measurement results of 20% of methane gas over the temperature range of –10C to 50C with the use of the laser methane sensor are shown in Figure 2 (the blue and red dots are the methane concentration before and after the temperature compensation.

Table 1. Laser methane sensor temperature compensation data (under 20% methane).

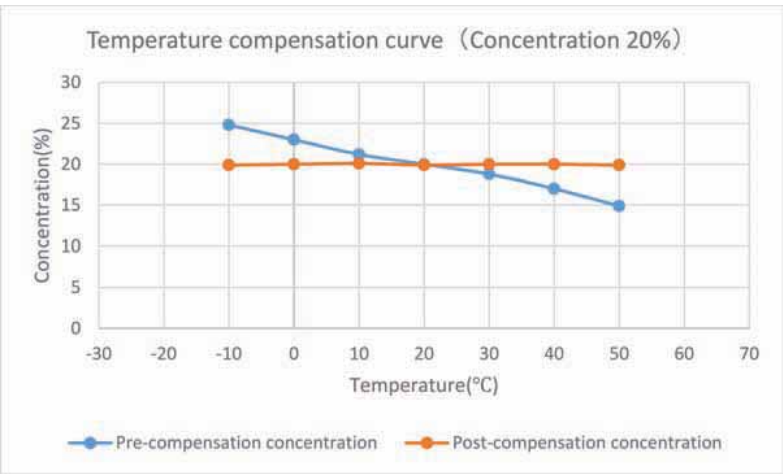| No.	Temperature (°C)	Concentration before temperature compensation (%)	Concentration after temperature compensation (%)	Deviation
1	–9.5	24.3	20.1	0.37%
2	1.1	23.0	20.2	0.78%
3	12.3	21.1	20.0	0.00%
4	21.4	20.0	20.0	–0.24%
5	31.2	18.9	19.9	–0.80%
6	40.8	17.6	19.9	–0.75%
7	50.5	16.6	19.9	–0.87%

Figure 2. Methane concentration curve before and after the temperature compensation (at 20% methane).
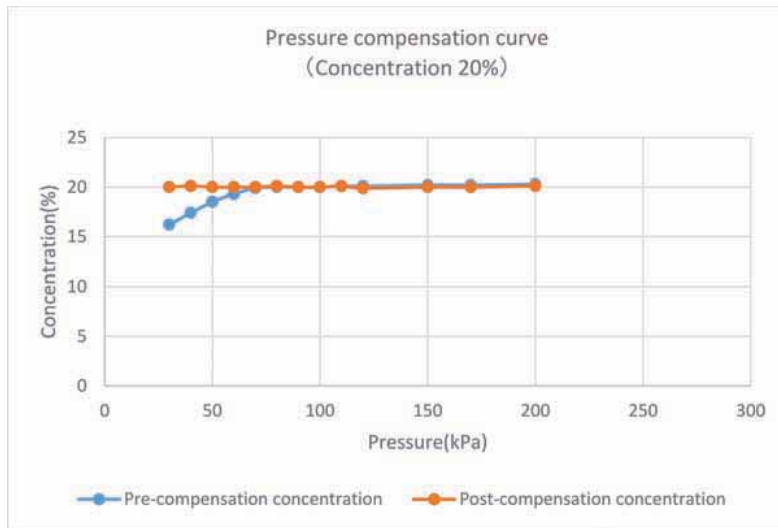
Figure 3. Compression of the measured methane concentration data before and after the pressure compensation (at 20% of methane concentration).

Table 2. The measured methane data with the use the pressure compensation scheme (at 20% of methane concentration).

No.	Pressure (Kpa)	Pre-compensation concentration (%)	Post-compensation concentration (%)	Deviation
1	202.9	20.4	19.9	–0.09%
2	181.5	20.3	19.9	–0.07%
3	159.0	20.3	19.9	–0.06%
4	140.4	20.2	19.9	–0.07%
5	119.1	20.1	19.9	0.09%
6	100.4	19.9	20.0	0.18%
7	90.3	19.8	20.0	0.17%
8	80.3	19.6	19.9	0.09%
9	70.8	19.4	19.9	0.04%
10	59.6	18.9	19.9	–0.09%
11	51.2	18.5	19.9	–0.18%
12	39.4	17.4	19.9	–0.25%
13	31.3	16.2	20.0	0.17%

The current design of the sensor can be operated at the temperature range of –15°C~55°C for coal mine applications. It is possible to extend the operational temperature range of –30°~70°C for other application requirements.

3.3 *Research on pressure compensation technology*

The conventional methane sensor is used at pressures range of 50 to 150 kPa in gas drainage applications. In the some applications, a wider pressure range is required. In this case, it is necessary to adopt a pressure compensation scheme to eliminate the measurement error induced by the pressure variations. To this end, a pressure high-precision compensation technology is innovated and developed based on using VCSEL laser technology, with the use this pressure compensation scheme, an accurate measurement within the pressure range of 30–200 kpa was achieved.

The measured methane concentration curves before and after the pressure compensation (at 20% methane) over a pressure range from 30 kpa to 200 kpa are shown in Figure 3.

It can be seen that the measurement accuracy is improved with the use of the pressure compensation within the pressure range of 30–200 kpa.

4 FIELD TRIALS AND RESULTS

As shown in Figure 4, in order to reduce the water and dust effect is the test, a water and dust filter device is used before the sensor that is installed in the field.

The NB-Internet of Things communication scheme is employed in order to achieve a real-time monitoring of the sensor data. This mine wireless laser methane sensor monitoring system establishes the connection between the sensor and the remote monitor devices such as a mobile phone, and the real-time monitoring of each sensor in the field can be achieved, as the result, the real-time data of every sensor can be queried through the internet anywhere in the world.

The data of the measured results are shown in Table 4 below.

The mine laser methane sensor accurately measures methane concentration, temperature and pressure, and the measured results can be view globally with the use a mobile phone. After a long-term operation, sensor system operation is stable and no abnormalities such as data mutations and disconnections during the operation.

From the on-site operational results, it can be seen that the laser methane sensor developed here is an ideal solution for gas drainage pipeline applications. The system has very good advantages when used in coal mine applications, especially where the installation location is remote.

Figure 4.   Field installation diagram.

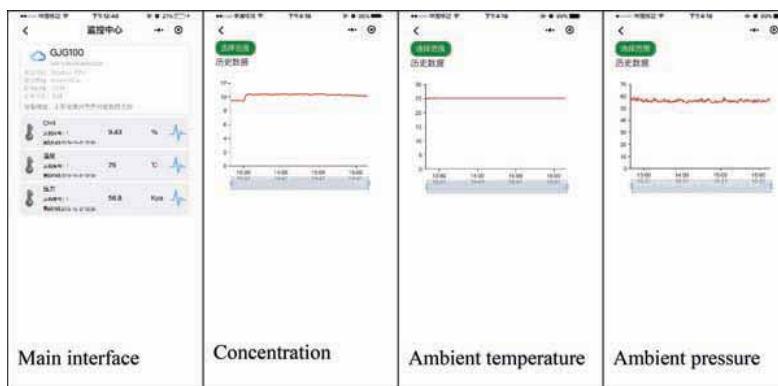Table 4.   The recorded operational data (pressure, temperature and methane concentration).
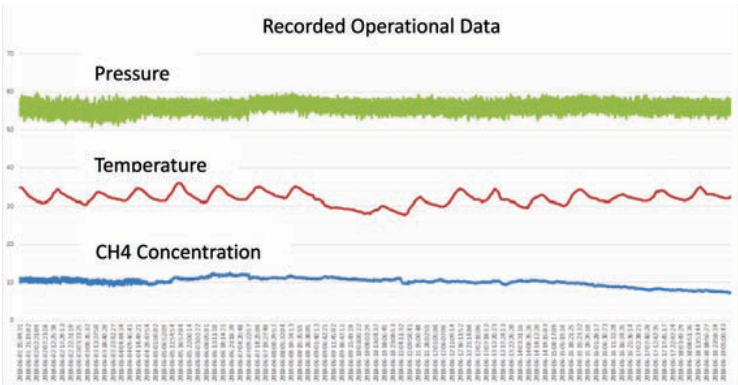
Figure 5. Mobile phone data display.

5 CONCLUSION

This paper describes a novel laser methane sensor, which is based on VCSEL laser technology to use temperature and pressure compensation schemes to achieve a large operational temperature range and a large pressure range. The laser methane sensor accurately measured the methane concentration in the temperature range of –15°C~55°C, at a pressure range of 30~200 kpa, and is suitable for gas drainage monitoring. The monitoring system employs the NB Internet of Things technology to achieve remote real-time monitoring anytime and anywhere in the application of gas drainage pipelines.

REFERENCES

Cheng Y.P., etc. 2006. Practice and application of coal mine gas control "drainage before mining". *Journal of Mining and Safety Engineering, 2006, 23 (4): 389–392*.
Liu J. Safety Guarantee Technology for Pipeline Transportation of Low Concentration Gas in Coal Mines. *Shanxi Coal, 2011, 31 (5): 65–66*.
Liu W.Q. etc. High sensitive differential absorption spectroscopy for air quality monitoring. *Optical technology, 2005 (3): 288–291*.
Li Y.F. etc. Gas extraction pipeline safety monitoring system based on optical fiber sensing technology, *Shandong Science 2014*.
Provisional Standards for Gas Drainage in Coal Mines. (http://www.safehoo.com/Laws/Trade/Coal/201110/202475.shtml). *Safety Management Network*.
Wang Y.J. Research on harmful gas measurement technology based on optical fiber spectral absorption. *Yanshan University, Qinhuangdao, 2007*.
Xu Z. 2011. Development of methane detector in coal mine gas detection. *Wuhan University of Science and Technology*.
Ye X.F. etc. Research on CH4 Gas Optical Fiber Sensor. *Semiconductor Photoelectric, 2000, 21 (3): 218–220*.
Zhao Y.J. etc. Application of optical fiber methane monitoring system based on spectral absorption in gas extraction. *Spectroscopy and spectral analysis, 2010, 30*.

Fibre optic sensor for coal mine combustion detection

T.Y. Liu
Laser Institute, Shandong Academy of Sciences, China

X.J. Meng & F.Q. Wang
Yankuang Coal Mine Group, China

R.C. Li
Shandong Micro-Sensor Photonics Ltd., China

M.Y. Hou & Z.W. Wang
Laser Institute, Shandong Academy of Sciences, China

J. Hu
Shandong Micro-Sensor Photonics Ltd., China

Y.F. Li
Laser Institute, Shandong Academy of Sciences, China

L.Z. Ma
Shandong Micro-Sensor Photonics Ltd., China

Y.B. Wei
Laser Institute, Shandong Academy of Sciences, China

S.X. Zhang
Shandong Micro-Sensor Photonics Ltd., China

ABSTRACT: Spontaneous combustion is a major safety hazard in underground coal mines. Conventional technology is based on tubing bundle gas sampling system and chromatography based gas monitoring instrument, which is typically located on the ground monitor centre and suffering from long delay time, being cumbersome to maintain and inaccuracy due to possible tubing leakage. An intrinsically safe fibre optic distributed temperature sensor and interrogator for based on multimode fibre and Raman scattering principle have been developed. The fibre optic cables are laid down in the long wall ventilation tunnels and left embedded inside the goaf. The interrogator is typically installed in the underground power station with data transmitted to the ground monitor centre. Protection procedures have been developed so that the fibre optic cables have high probability of survival inside the goaf and sealed area of the underground coal mines. Early warning and location of spontaneous combustion hazards have been successfully demonstrated and fire hazard was prevented.

Keywords: Fiber Optic Distributed Temperature Sensor, Coal Combustion, Laser Gas Sensor, Hazard, Detection

1   INTRODUCTION

Coal mine naturally affects the safety of coal mine production. Traditional monitoring means mostly use bundle tube system. Usually, analytical instruments are placed in the ground

monitoring room and pumped to the ground by long-distance bundle tube for chromatographic analysis. Because of the long distance between bundles and pipes, many pipe joints, air leakage often occurs, and the measurement error is large, the maintenance cost is high. More importantly, it is impossible to locate the fire source effectively. In this paper, distributed optical fiber temperature measurement technology is proposed to monitor coal mine goaf ignition, and the instrument adopts intrinsically safe design, and has outstanding advantages of safety, convenience and other advantages, and has been successfully applied in the field. The environment of goaf is bad, so the construction and protection of optical cable is particularly important.

2 COAL MINE FIRE MONITORING

Coal mine fires are mainly divided into internal fires and external fires. Internal fires are mainly caused by coal self-ignition and external fires are mainly caused by equipment or electric cable short circuits. Distributed optical fiber temperature measurement technology offers advantages of inherent safety, wide monitoring range, accurate positioning in solving mine fires.

2.1 *Coal mine self-ignition*

2.1.1 *Scheme*
As shown in the figure, the temperature-sensitive optic cable is laid along two lanes of the roadway, and the end of the cable is connected to the demodulator. The demodulator is installed in the nearest substation. The demodulator is responsible for optical signal output and detection, temperature demodulation and data transmission. It is transmitted to the ground server which includes a network distribution software via the ring network switch [3].

2.1.2 *Protection of optical cable*
Due to the harsh environment of the goaf, the selection and protection of the cable is very important. The armored and high-strength flame-retardant fiber optic cable is selected. The protection of the fiber optic cable is implemented by buried laying, steel pipe protection and spring structure stainless steel. Connect the spring tube at the joint to prevent the cable from being deformed by extrusion. According to the specific actual conditions of the coal mine, it can also be laid along the supply air supply pipeline and the gas drainage pipeline, and laid on the side of the pipeline. Once the coal mine roof collapses, the support of the pipeline can be used for protection.

2.2 *Fire monitoring of belt conveyor and cable*

The distance between the belt conveyor and the cable is wide, and the traditional point type monitoring is difficult to implement. The distributed optical fiber temperature measurement technology is specially suitable for this occasion. The fire monitoring of the belt conveyor and the cable focuses on solving the laying problem of the optical cable, and can be along the belt conveyor. Cables are laid along the cable or cable surface for temperature sensing. The belt conveyor idler is a hot spot. It is recommended to wind the cable at the roller bearing and increase the protection of the cable. The monitoring effect is better [4].

3 HOST DISIGN

3.1 *Hardware design*

An embedded, high-performance, low-power processor is used as the control core. In view of the limitations of current intrinsically safe power performance specifications, two intrinsically safe power supplies are used for whole system's power supply [2]. One power load includes pulse
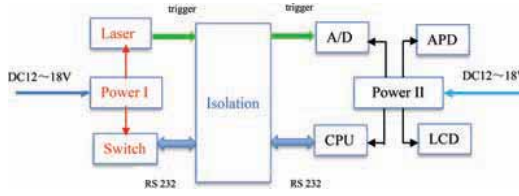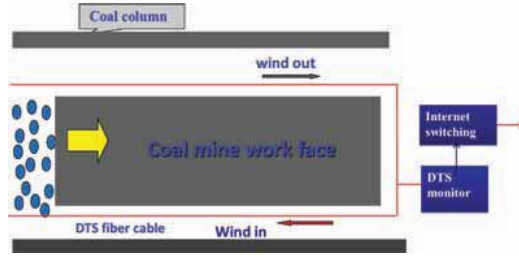
Figure 1. DTS hardware schematic.

Figure 2. Coal mine sel-ignition monitor system.

laser source and an optical switch, and the other power load includes processor, A/D card, APD detector and LCD display; the two loads are electrically isolated as shown in Figure 1.

The MOPA-structured pulse laser has a large starting current, The instantaneous startup of pulse laser easily caused the intrinsically safe power supply to shut down. The internal circuit grading start method is used to reduce the impact current, and the parameters of other circuit board controller capacitors and inductors are determined to meet the requirements of the intrinsically safe circuit.

3.2 *Software design*

The embedded Linux system is used to develop the system's lower computer software, including data acquisition, data processing, temperature demodulation, display, storage, data transmission, etc. Multi-threaded and multi-tasking processing is adopted, and QT language is selected for software interface development. A standard modbus communication protocol data communication is adopted and the upper computer is implemented by WEB software.

When calculating temperature, internal optical fibers can be selected as reference. The concrete formulas are as follows:

$$\frac{1}{T_m} = \frac{1}{T_0} - C_{hk} * \ln\left[\frac{N_s(T_0) N_a(T_m)}{N_a(T_0) N_s(T_m)}\right]$$

T_0 is the temperature of the reference region, T_m is the temperature of a certain position of the optical cable, $N_s(T_0)$ is the average value of the Stokes curve intensity in the reference region, $N_a(T_0)$ is the average value of the anti-Stokes curve in the reference region, $N_a(T_m)$ is the anti-Stokes intensity at a certain point of the optical cable, $N_s(T_m)$ is the Stokes intensity at a certain point of the optical cable, and C_{hk} is the constant.

4 TYPICAL DATA ANALYSIS

The following figure is the change curve of monitoring data of spontaneous combustion in a goaf of a mine. Figure 3, From the curve, the temperature in the 200–450 m area increases
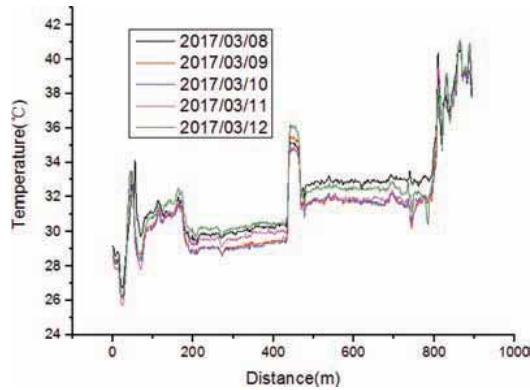
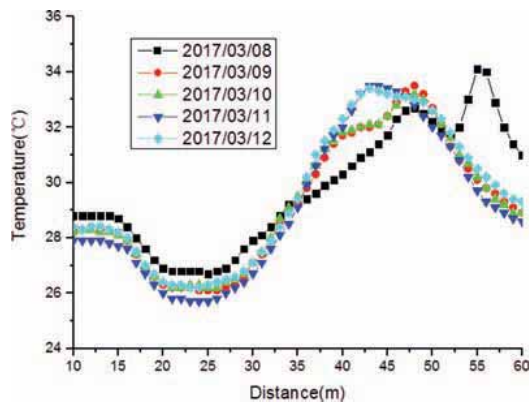Figure 3. Natural warming data of coal mine.

Figure 4. Translation of the highest point of oxidation zone.
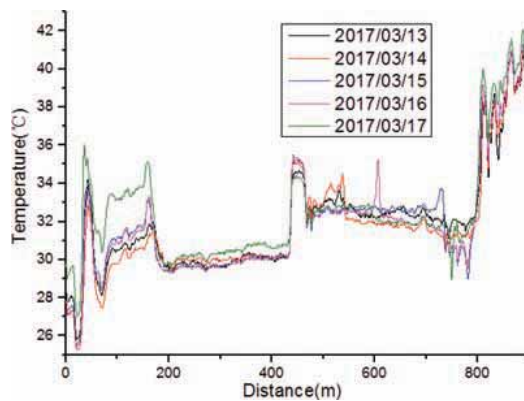

Figure 5. Change data after fire extinguishing.

gradually. Although the local temperature only increased by 2–3°C, the overall temperature curve was rising. There is a tendency to get angry. In the front part of the curve throughout the day, the high temperature point gradually shifts from 58 meters to 42 meters.

We can also deduce the possible distribution of "three zones" in coal mines according to the change of temperature. We can magnify the temperature data from 10 meters to 60 meters further. Some interesting conclusions can be found. Figure 4, the high temperature point gradually shifts from 58 meters to 42 meters.

Figure 5 After the open fire was discovered, fire extinguishing and sealing treatment began on March 13. From the curve, the temperature of the front and rear end of the sealed optical cable increased obviously. Especially after the first 200 meters and the back 800 meters.

5   CONCLUSION

Coal mine fire affects safe production. The use of distributed optical fiber temperature measurement technology has obvious advantages for coal natural ignition monitoring. The design of intrinsically safe type further reduces power consumption and optimizes product reliability. Further promote the application of fire monitoring in coal external causes.

REFERENCES

[1] Li Yongjun. Ren Meiqing. Hao Yu Application of Optical Fiber Temperature Measurement Technology in Goaf. Shaanxi Coal. 2018.02.0076-04.
[2] Li Jun, Mo Zhigang, Zhang Shulin Design and Realization of Mine Intrinsically Safe Distributed Optical Fiber Temperature Measurement. Automation Technology and Application. 1003–7241 (2018), 10-0016-05.
[3] Xie Junwen, Lu Xi. Distributed Optical Fiber Temperature Measurement Technology for Flammability at High Inclination Angle Application of spontaneous combustion monitoring in goaf of coal seam. Coal Mine Safety 2014, (11):118–121.
[4] Zheng Xiaoliang, Hu Yelin. Underground Electricity Based on Distributed Optical Fiber Temperature Measurement Technology Design of Cable Temperature Monitoring System. Design Technique. 2009, (9):19–21.

IoT and robotics

Lithological hyperspectral characterization for UAV sensor selection

F.S. Beretta, A.L. Rodrigues, R.L. Peroni, S.B. Rolim & J.F. Costa
Federal University of Rio Grande do Sul, Porto Alegre, RS, Brazil

ABSTRACT: The definition between lithologies is vital for a successful mine planning. new field data is constantly collected to feed the reconciliation process. Whilst performing with the traditional approach, the professional is exposed to weather conditions, dust, risks with the moving equipment and bench highs. This task can benefit from the automation of boundaries detection between materials. The use of Unmanned Aerial Vehicles (UAVs) and automated classification using Machine Learning (ML) techniques improved in the last few years. However, non-visible wavelengths are still rarely used for materials classification. Other electromagnetic frequencies can be captured by specific sensors so the automatization process could use these data as training and test in a supervised classification. The characterization of materials that are similar in visible wavelengths can be useful to understand the behavior of the electromagnetic bands to clearly differentiate materials, so the correct sensor can be plugged onto the aerial vehicle.

1 INTRODUCTION

The identification of contacts between lithologies and ore/waste short term mapping is the basis to short term mine planning, geological model updating and reconciliation between the projected and the actual production. Automated lithological classification can grant safety to the geologist, increases the model updating frequency and accuracy of the georeferenced contacts. The input models are created from photogrammetric air-born point clouds, whose points carry any local information detected by unmanned aerial vehicles (UAVs) and their sensors.

Photogrammetric topographic reconstitution is already established in the mining industry, as presented by Salvani et al. (2016), Hugenholtz et al. (2013) Silva et al. (2016), Peroni (2016), Westoby et al. (2012) and Beretta et al. (2017). Using machine learning (ML) techniques on 2-D images, Dalm et al. (2017), Ehrenfeld et al. (2017), and Bamford et al. (2017) presented mineralogical differentiation, metallurgical classification and granulometric characterization, respectively. Automated lithological classification already being used based on 3-D point clouds on the visual specter range, such as red, green and blue (RGB) components acquired by ordinary cameras, as presented by Beretta et al. (2019). Figure 1 shows the input RGB point cloud along with the training/test selected dataset feeding the resulting classified model for the selected ML algorithm and the sample size.

When the materials are visually similar, sensors that detect other electromagnetic wavelengths are necessary to detect differences that the human eye cannot distinguish. For example, long-wave infrared or any other wavelength that highlights the contrast between materials for ML supervised classification of the 3-D point cloud. Dense point clouds are generally huge, as such, excessive data can be laborious, slow and computationally time demanding. In order to assess the importance of information for every kind of material of interest, a prior characterization with exploratory data analysis using feature engineering is essential to select the correct electromagnetic wavelength bands that behave differently for each pair of lithologies.
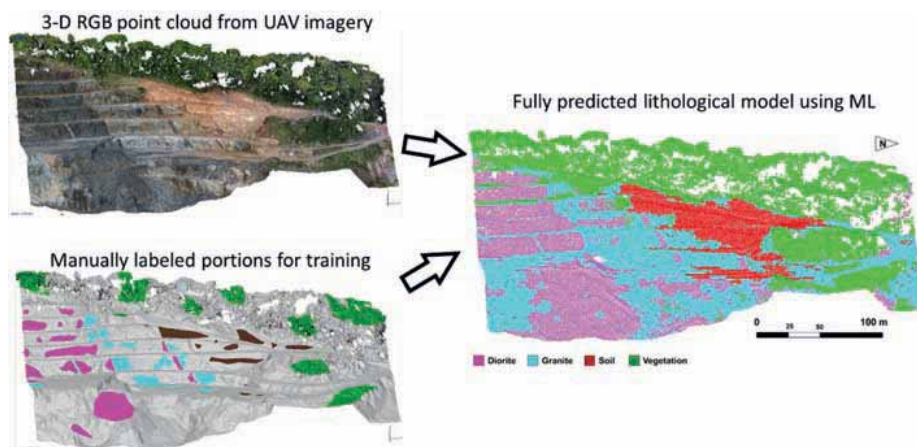
Figure 1. Automatic classification on a 3-D point cloud using ML techniques.

2 MATERIALS AND METHOTDS

2.1 *Site selection*

The mining face intended for the characterization had to be selected considering the number of in situ different materials that are mined separately, due to their different qualities or economic interest, and that are visually similar. Also, the mining face selected should ideally stay untouched until the sensor is selected and a flight performed to register the mineral characteristics using an UAV. To cover those requirements, a phosphate mining face has been selected for the samples collection. It is located in the Tapira mine, nearby Araxá, Brazil.

2.2 *Sampling*

In total, 25 samples have been collected, identified, georeferenced and kept in appropriate bags to preserve their original characteristics, such as moisture and granulometric distribution.

The transition zone between the ore, called base isalterite, and top isalterite, which has analogous constitution to the base, but with higher titanium grade. Both lithologies present similar color when their moistures are alike. However, during the dry season, the waste retains more water, making the visual contrast between materials more evident. Also, other materials present colors that could bewilder when considering only RGB, such as aloterite (upper clay) and deeper, less weathered ore. Figure 2 shows the sampling location on the mining face.

The samples collected on the elevation 1,280 m represent aloterite region, typically a waste zone. On elevation 1,270 m, 15 samples were taken in a transition zone between the high-Ti top isalterite and the ore zone. In the high-Ti zone, the material tends to be more moisturized and composed by silt and does not preserve any remaining structure from the original rock. It is constituted by anatasium and Fe and Al oxi-hidroxides, crandalite, magnetite, caulinite and quartz. The mineralized zone presents more preserved structures from the original rock with higher apatite content, reflecting on P_2O_5 grades higher than 5% and TiO_2 lower than 10%.

On the 1,240 m bench, six samples were taken in the transition zone between the weathered and the semi-compact ore, with more granular material. This presents a decrease of the P, Ti and Fe contents. Minerals such as anatasium, vermiculite, titanium-rich magnetite and iron oxi-hidroxides are less frequent as the elevation decreases. On the other hand, carbonates and phlogopites are more abundant.
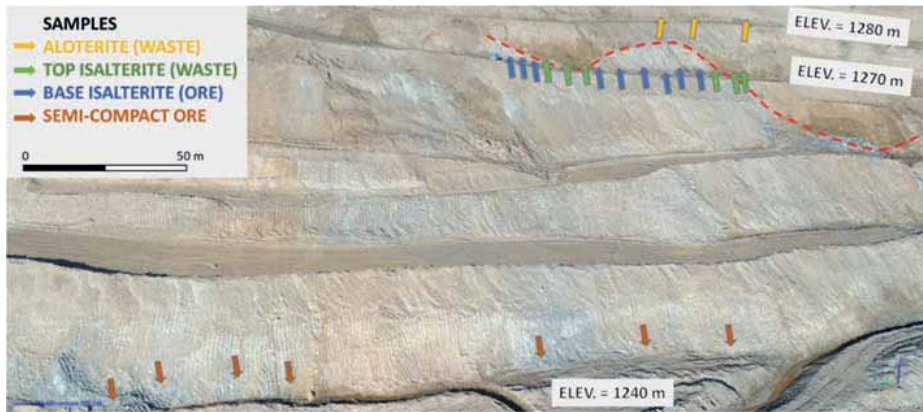
Figure 2. Location of the different materials sampling on the mining face.

2.3 *Sample analysis*

To characterize the samples, the moisture content was preserved with appropriate sampling bags. This ensures that the field conditions would be represented during the analysis, as the aim of this work is to identify the bands that differentiates in situ materials.

An ASD's FieldSpec® bench spectroradiometer was used to measure the reflectance from 2,151 bands for wavelengths between 350 and 2,500 ηm. The samples were analyzed in appropriate lab conditions of controlled temperature and interference, guaranteeing that the equipment was calibrated with white surface for each sample before the reading.

The feature engineering phase is the act of creating new variables from the original ones. In addition to the reflectance values new variables were constructed: the difference between the reflectance values. These values were calculated in wavelength order, to be similar to a numerical derivative.

3 RESULTS AND DISCUSSION

3.1 *Hyperspectral reflectance*

The equipment took five measures in each sample and the average reflectance was considered for each hyperspectral band, giving 25 spectral results from 350 ηm to 2500 ηm. The samples were colored according the description made by the geologist giving the separation in the four different lithologies. Figure 3 presents the results compiled for all the analyzed samples.

As the top isalterite retains more water, its whole spectrum presents lower reflectance when compared with the base isalterite. Also, the semi-compact lithology presents lower curves due to the lower weathering condition and more granular texture.

The band around 2,300 ηm presents a feature only for the ore lithologies, either semi-compact or base isalterite. This is due to Fe and Mg hidroxides contents. Similar behaviour is observed on the band around 2,210 ηm, due to Al hidroxides. This last feature differentiates the semi-compact ore from the other materials.

These direct reflectance results suggest that sensors on those two bands would indicate more clearly binary contrasts between ore and non-ore materials (band 2,300 ηm) and semi-compact ore from the others (band 2,210 ηm).

3.2 *Spectral exploratory data analysis*

With only a few samples (25) it is not appropriate to do supervised learning. The exploratory data analysis provides helpful insights regarding the possibility of differentiating the rocks
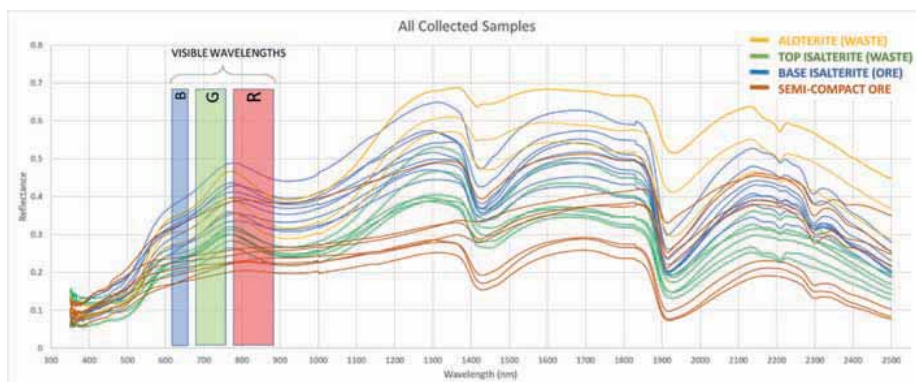
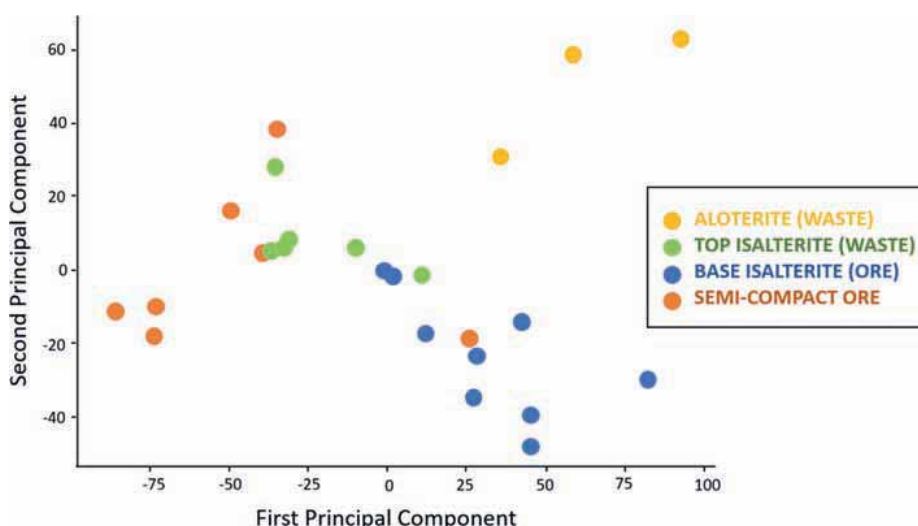Figure 3. Spectral measures for the collected samples.

Figure 4. Two principal components for the collected samples considering all the hyperspectral information.

lithology. In this study the analysis was made using the dimension embedding technique principal component analysis (PCA) which represents all the variables in a lower dimension (2-D for our study). The PCA method does not discard or eliminate variables but create two (for 2-D embedding) new variables which are linear combinations from the originals.

When all the hyperspectral bands information is considered, Machine Learning techniques can be applied to differentiate the materials. PCA was performed and the two first components are shown in Figure 4.

For the wavelengths where the materials behavior differs, the bands data were isolated and the PCA was ran once again. Figure 5 presents the two principal components when only the 2,300 ηm band is selected (a) and clearly shows the clustered ore dots.

The PCA results suggest clusters that could be modelled by machine learning algorithms, such as Random Forrest, or Support Vector Machine, for instance. This means that if a hyperspectral sensor is attached to the UAV, the resulting images and photogrammetric point cloud could be modelled using all the information, or at least, the principal bands that represent the materials behavior.
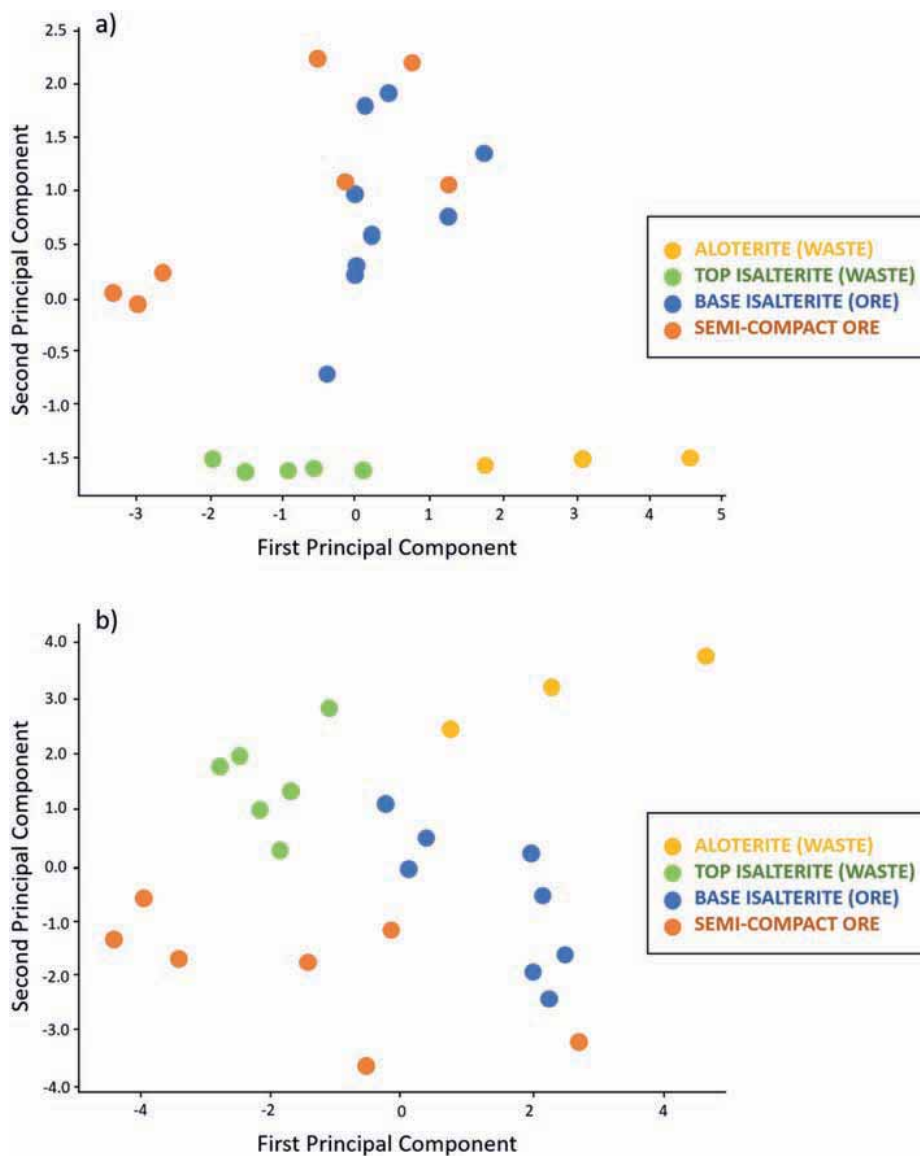
Figure 5. PCA for the collected samples when 2,300 ηm band (a) and for 2,300 ηm + RGB (b).

4 CONCLUSION

The appropriate sensor helps evidencing the contrast between materials in an open pit mine, even in non-visible wavelength when attached to an UAV. For each group of lithologies that should be segregated, an adequate wavelength must be selected. Hyperspectral cameras are useful to differentiate materials according to their element's composition. However, too many data can make the computational process too slow and expensive. Also, a hyperspectral sensor might be prohibitively expensive.

Specific wavelengths can be selected through spectroscopic data analysis and the important bands can be used to show differences among materials. For the samples collected and analyzed, ore materials are clearly separable from the waste by PCA. One sort of ore is separable from the other lithologies too. Thus, with a few selected electromagnetic bands, the lithologies can be classified when the appropriate data is acquired.

For future work, the authors aim to purchase the appropriate sensors that cover the indicated bands through statistical analysis.

REFERENCES

Bamford, T., Esmaeili, K., Schoellig, A. 2017. Aerial Rock Fragmentation Analysis in Low-Light Condition Using UAV Technology. In: *38th Application of Computers and Operations Research in the Mineral Industry*. Golden. p. 4_1–4_8.

Beretta, F., Peroni, R., Costa, J.F. 2017. Stockpile volumetric survey using aircraft imagery in comparison with traditional methods. In: *38th Application of Computers and Operations Research in the Mineral Industry*. Golden, p. 4_9–4_15.

Beretta, F., Rodrigues, A., Peroni, R., Costa, J.F. 2019. Using UAV for Automatic Lithological Classification of Open Pit Mining Front. *REM—International Engineering Journal*. v. 72 N.1.

Dalm, M., Buxton, N., Ruitenbeek, A. 2017. Discriminating ore and waste in a porphyry copper deposit using short-wavelength infrared (SWIR) hyperspectral imagery. *Minerals Engineering*, v.105: p. 10–18.

Ehrenfeld, A., Egaña, A., Guerrero, P., Liberman, S., Hanna, V., Voisin, L., Adams, M. 2017. Geometallurgical variables characterization using hyperspectral images and machine learning technics. In: *38th Application of Computers and Operations Research in the Mineral Industry*, Golden, p. 6_1–6_6.

Hugenholtz, C.H., Whitehead, K., Brown, O., Barchyn, T., Moorman, B., LeClair, A., Riddel, K., Hamilton, T. 2013. Geomorphological Mapping with a Small Unmanned Aircraft System (sUAS): Feature Detection and Accuracy Assessment of a Photogrammetrically-Derived Digital Terrain Model. *Geomorphology* v. 194, p. 16–24, Retrieved (http://dx.doi.org/10.1016/j.geomorph.2013.03.023).

Peroni, R. 2016. *Aplicações de mapeamento e modelagem de terreno com uso de VANTs em áreas de mineração (Application of mapping and modelling using UAV in mining areas).* Universidade Federal de Santa Catarina. Relatório de Pós-doutorado (Post-PhD. Report). 136p.

Salvini, R., Esposito, G., Mastrorocco, G., and Seddaiu, M. 2016. Using a Remotely Piloted Aircraft System (RPAS) to Analyze the Stability of a Natural Rock Slope. *EGU General Assembly 2016*, 18:4409.

Silva, C., Duarte, C., Souto, M., Santos, A., Amaro, v., Bicho, C., Sabadia, J.A. 2016. Avaliação da acurácia do cálculo de volume de pilhas de rejeito utilizando VANT, GNSS e LiDAR (Accuracy volumetry evaluation of tailings using UAV, GNSS and LiDAR), *Boletim de Ciências Geodésicas*, v. 22, p. 73–94.

Westoby, J., Brasington, J., Glasser, N., Hambrey, M., Reynolds, J. 2012. 'Structure-From-Motion' photogrammetry: A low-cost, effective tool for geoscience applications. *Geomorphology*, v. 179, p. 300–314.

High-resolution modeling of open-pit slopes using UAV and photogrammetry

R. Battulwar, J. Valencia, G. Winkelmaier, B. Parvin & J. Sattarvand
University of Nevada, Reno, Nevada, USA

ABSTRACT: Accurate detection and characterization of tension cracks for stability analyses purposes in open-pit mines requires high-resolution terrain models of the mine. This paper presents several contributions to the field of remote sensing of mines using Unmanned Aerial Vehicles (UAVs). A multivariate linear regression model for battery power consumption of drone has been derived by conducting an empirical study in various flight scenarios. The model has also been validated using data from a test flight. A genetic algorithm for solving the problem of flight planning and optimization have been proposed. The developed power consumption model has been used as the fitness function in this algorithm. A novel Android application has been developed for autonomous drone flights to follow mine terrain and capture high-resolution images. These images will be stitched together to be used for crack detection. A case study has been presented showcasing the ability of the developed software to achieve high-resolution imaging of an area.

1 INTRODUCTION

The past decade has witnessed an unparalleled augmentation in the field of UAVs. Their presence can be seen in modern mining operations throughout the world. With the increased availability of cost-effective drones and skilled personnel, many drone companies are looking for potential applications of drones in the mining industry. Considering the vast nature of mines and their hazardous environment, UAV technology is the perfect tool to be applied in these operations. As a result, many mining giants like Rio Tinto, BHP Billiton, Newmont, and Barrick have already been using drones for surveying, volumetric analyses, and monitoring purposes. Transforming these tasks into an aerial task gives a big advantage in terms of time and man power.

Despite advances in slope monitoring, identification of tension cracks remains a laborious task on the part of geotechnical engineers. Some of the drawbacks of the current slope monitoring practices which are addressed through this research work are as follows. (i) The radar-based scanners essentially monitor the slope movement but cannot identify cracks which are useful for numerical modeling of slope stability. Further, their deployment is expensive and unaffordable for small mining operations. The price of an SSR can go as high as 450,000 USD which includes installation as well as training cost (Hannon, 2007). (ii) The process of installing instrumentation in a moving wall to monitor the expansion of each crack is firstly unsafe and dangerous. Secondly, this task is slow and time-consuming.

In this study, it is proposed to utilize (i) a UAV for imaging and mapping the open-pit mines, and (ii) state-of-the-art machine learning techniques for automated identification of cracks and characterizing their dynamics. The results will be an early-warning system that alerts the geotechnical engineers about the location of potential failures so that the necessary safety steps can be executed.

The availability of up-to-date high-resolution terrain models of a mine is a crucial bottleneck for achieving accurate detection of tension cracks or any other useful purposes like volumetric analysis or designed vs actual survey of ramps and benches. This problem is

addressed in this paper by creating a novel application to generate sub-millimeters resolution three-dimensional models of mine terrain as well as presenting an algorithm to optimize the drone path. With the advent of commercial drones for civil use, may software companies have developed software packages/applications for flight planning and autonomous flight execution of the UAVs. There are two stages of flights in this study. Firstly, an area mapping flight is conducted over a new mine with ground control points to create accurate three-dimensional models of the mine. Since the position of benches and walls keep changing in the mine (which is not updated in the Google Maps frequently), this stage helps to create a current map of the mine. Secondly, the surface terrain obtained in the first stage is used as an input to fly the drone over the mine benches.

2 LITERATURE REVIEW

Photogrammetry is the science of measuring the 3-D coordinates of physical world object from their photographs. Torrero et al. (2015) have presented a methodology for generating high-resolution orthomosaic of an active landslide area using a micro UAV fitted with an image sensor. Structure from Motion (SfM) is another technique of estimating the 3-D form of a scene from a series of 2-D digital images (Hartley & Zisserman, 2000). Lucieer (2011) showed the use of Sfm for generating a 3D point cloud of topography in a real-world coordinate system with an accuracy of 3 cm from overlapping UAV photographs of the terrain. Zarco-Tejada (2018) explains how UAV equipped with normal thermal and multi-spectral imaging sensors guided by autonomous navigation using GPS has overcome successfully the financial and technical challenges of Satellite sensors and derived quantitative remote sensing products on crop stress and water spills. Visockienė (2016) and Di Franco & Buttazzo (2016) presented the mathematical relations for flight planning and estimating the parameters of flight for taking overlapping photos of an area. It is industry wide recommended to have 85% forward overlap and 70% side overlap for dense vegetation and fields (PIX4D, 2018).

Due to the limited amount of battery onboard a drone, it is important to fly through the waypoints in an optimized way. The optimization problem is such that the drone should start from a starting point, fly and take photos at each waypoint exactly one and return to the starting point in the shortest amount of energy consumed. Such an optimization problem is typical of the travelling salesman problem (TSP). The TSP is one of the well-known problems in the field of combinatorial optimization. It is basically a minimization of the total distance traveled by the salesman while touring all cities exactly once and returning to the starting city (Hussain et al., 2017). The TSP is a nondeterministic polynomial-time hard problem.

Different approaches have been suggested in the literature for solving the TSP, such as simulated annealing (Kirkpatrick, 1985), neural networks (Bhide, 1993), and Tabu search (Glover, 1990). Integer linear programming methods have also been proposed with ways to eliminate subtours (Miller, 1960). However, as the number of points increases up to more than 100, integer programming becomes impractical. Meneses (2017) has presented an application of a genetic algorithm for solving the 3-D variation of the TSP. The advantage of deploying this kind of evolutionary algorithm is that the speed of reaching the solution can be increased by using metaheuristics for estimating the initial solution.

Ergezer (2013) has presented a way of using a genetic algorithm for path planning for multiple drones in a 3-D coordinate system. The problem was to plan the flight of drone through some desired areas while avoiding some undesired areas. Portas et al. (2010) have designed an evolutionary trajectory for multiple UAVs in a military environment which can work online as well as offline. The objective function in their work tries to minimize the risk to the UAV from enemy's missiles and includes constraints based on drone's dynamics and environment. To improve the speed of path planning using a genetic algorithm, Pehlivanoglu & Abdurrahman (2007) proposed a vibrational mutation operator based genetic algorithm. It also helps in escaping the local minima which the genetic algorithms are more prone to reach on.

3 UAV PATH PLANNING AND OPTIMIZATION

3.1 *Empirical study*

A power consumption model of UAV considering the effect of wind is necessary for optimizing the battery performance of drone. Studies in the literature proposed that there are two main approaches to power consumption models of a drone. (i) White-box model approach: In this approach, a microscopic behavior model for each drone is derived from a comprehensive study of the motor performance, aerodynamic environment, and battery systems. Such a model requires a lot of aerodynamic parameters relating to the body of the drone and sophisticated experimental setups. This is also specific to that particular drone (Kim et al., 2013). (ii) Black-box model approach: In this approach, a multivariate regression model for the power consumption of a drone is derived by doing empirical studies (Cappiello et al., 2002). Such a model is more flexible and acceptable for flight mission optimization. Further, this approach is more desirable as it is based on parameters which are more easily measurable. This makes it more suitable for the mining industry as most of the companies use commercial drones which usually don't come with a development kit (Tseng et al., 2017).

In this study, the black-box model approach has been utilized for the estimation of the energy consumption. In a drone, most of the battery is consumed in powering of motors to lift the UAV's body in the air. Further, the energy is used in the movements of the UAV in the air. Experiments have been conducted for studying the performance of the battery when the drone flies in different directions and wind speeds. Each drone has three main motions: hovering, horizontal moving, and vertical moving. A flight of a drone is a combination of these three motion types. In each experiment, the drone is programmed to ascend and descent repeatedly at its maximum speed in a vertical direction. Then, it is moved horizontally without altering its altitude at maximum speed. To understand the effect of wind on battery performance, another set of experiments have been conducted in which the drone flies in the same direction as wind and vice versa repeatedly. The experiments have been conducted for three wind speed cases including 17.28 km/hr, 18 km/hr, and 19.8 km/hr. A commercially available drone with a camera sensor, DJI Mavic Pro has been used as a test platform equipped with a windspeed meter.

DJI Mavic Pro has a maximum flight time of 27 minutes and camera resolution of 12 MP (DJI, 2018). The frequency of wind measurements is 2 sec. The flights were made at a local park on different days to consider the different wind speeds and make the study more comprehensive.

Figure 1 depicts the recorded telemetry of the first set of experiments of the test drone DJI Mavic Pro. It has been observed that the power consumption steadily increases as the
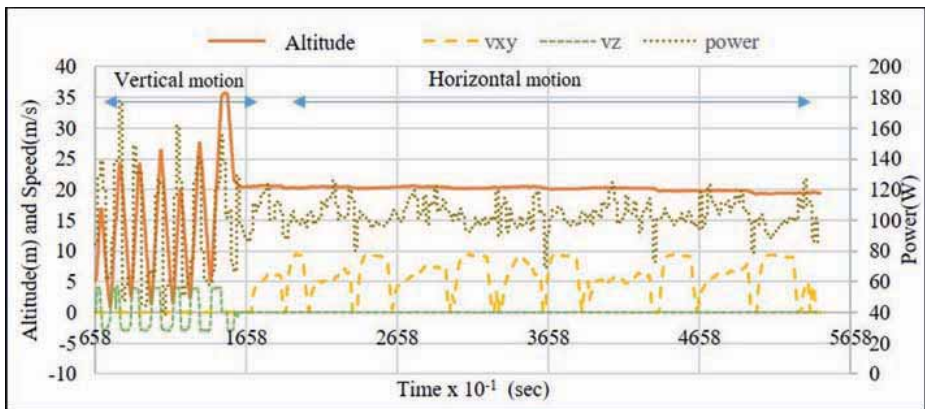

Figure 1.   Battery power consumption of DJI Mavic pro with different motions.
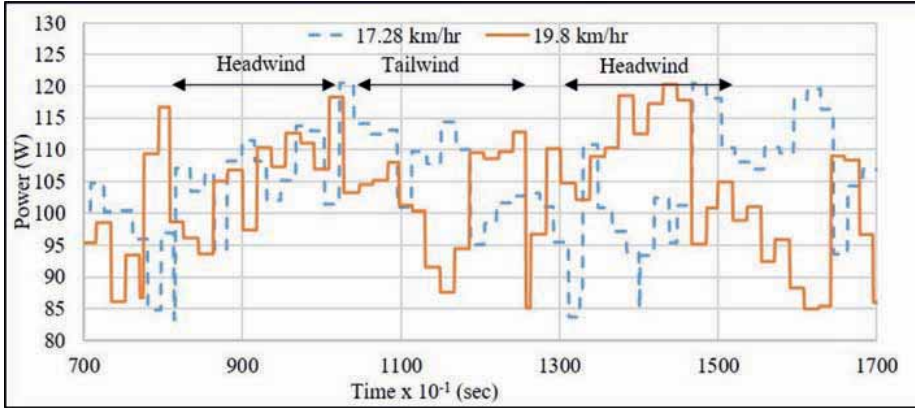
Figure 2. Battery power consumption of DJI Mavic Pro under different wind conditions.

drone ascends and decreases as it descends. During these motions, the drone also accelerates to reach its maximum speed in a vertical direction. The horizontal speed data generated due to GPS errors has been filtered. During the horizontal motions with constant altitude, the power consumption is relatively stable. The power consumption between the two motions has also been recorded which account for the hovering motion.

From Figure 2, it can be concluded that for DJI Mavic pro, as expected, the power consumption steadily increases when it flies in headwind direction and decreases in the tailwind direction. However, the relation is not linear. According to the aerodynamics, when flying into the headwind, the power consumption slightly decreases due to the relative airflow over the propellers increases and hence the translational lift increases (FAA, 2016). However, at higher wind speeds, the aerodynamic drag could outweigh the translational lift. In our setting, the drone is flying at its maximum speed and hence flying into the headwind is adding more drag to the aircraft leading to more power consumption.

3.1.1 *Regression model of power consumption for DJI Mavic Pro*

The collected data (as described in the previous section) was used for deriving the coefficients of a multivariate linear regression model which is given in Eq. (1). The regression analysis has been done in Minitab (Mintab, 2018). The estimated battery power consumption power P (W) is given by:

$$
P = 103.67 + \begin{bmatrix} 0.9 \\ 0.048 \\ 0.204 \\ 0.128 \end{bmatrix}^T \begin{bmatrix} v_{xy} \\ v_{xy}^2 \\ v_{xy}.a_{xy} \\ v_{xy}.wind \end{bmatrix} + \begin{bmatrix} -0.764 \\ 0.006 \\ -0.505 \\ 0.034 \end{bmatrix}^T \begin{bmatrix} a_{xy} \\ a_{xy}^2 \\ a_{xy}.a_z \\ a_{xy}.wind \end{bmatrix} + \begin{bmatrix} -2.54 \\ -2.359 \\ 1.167 \\ 1.987 \end{bmatrix}^T \begin{bmatrix} v_z \\ v_z^2 \\ v_z.a_z \\ v_z.wind \end{bmatrix}
$$

$$
+ \begin{bmatrix} -2.493 \\ -0.016 \\ -0.075 \\ -0.08 \end{bmatrix}^T \begin{bmatrix} a_z \\ a_z^2 \\ wind \\ wind^2 \end{bmatrix} \tag{1}
$$

where v_{xy} and a_{xy} are the magnitudes of speed and acceleration vectors in horizontal direction. v_z and a_z are the magnitudes of speed and acceleration vectors in vertical direction. *wind* is wind vector in horizontal direction. If the wind and speed are considered constant, the total energy consumed within a flight with duration T can be estimated by *P.T.*

664

3.1.2 *Model validation*

A test flight has been conducted for validating the power consumption model the same platform DJI Mavic Pro. It has been programmed to fly in the vertical direction with maximum capacity repeatedly and then horizontally in headwind and tailwind direction with maximum speed. The wind speed is 5.76 km/hr during this period of flight.

It has been observed that the average error of estimation is 0.7% with the standard deviation of 0.11. Since the final goal is to optimize the entire flight of the drone, a total energy consumption of the flight has been estimated which can be shown in Figure 3(b). The model can accurately predict the energy consumption of the drone at a wind speed of 5.76 km/hr. The error in estimating the total energy consumed at the end of the flight is 0.6%. The estimated model is also able to capture the trends of power consumption with respect to the wind speed and direction of movement as proved by Figure 3.

3.2 *Genetic algorithm*

Genetic algorithms (GAs) are based on Darwin's theory of evolution which states that the survival of an organism is defined by "survival of the fittest" rule and was developed by Goldberg (Gen & Runwei, 1997). In the given optimization problem, the UAV has to visit each point exactly one and return to the same starting point such that the cost of the entire trip is minimum. This is the classic travelling salesman problem (TSP) which is NP-Hard. In section 2, genetic algorithms have been presented to solve the UAV path planning and optimization problems. In this study, instead of using a simple distance function as in a typical TSP, an energy consumption model of the drone has been used in the fitness function. Figure 4 presents the general flow of the proposed algorithm whereas its main components are discussed in the next sections. The objective of the algorithm is to minimize the energy
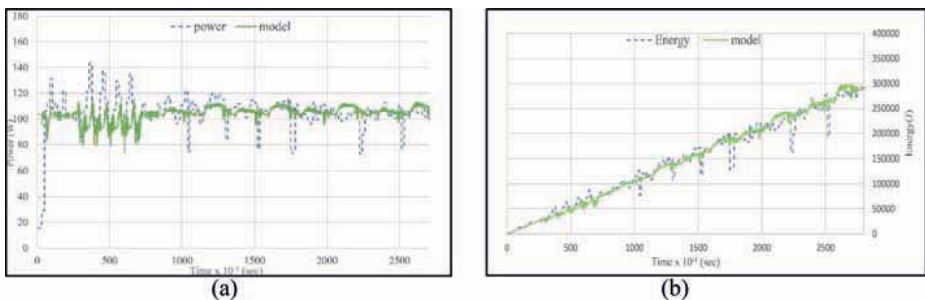

Figure 3.   Measured and modelled (a) power and (b) energy consumption for DJI Mavic Pro.
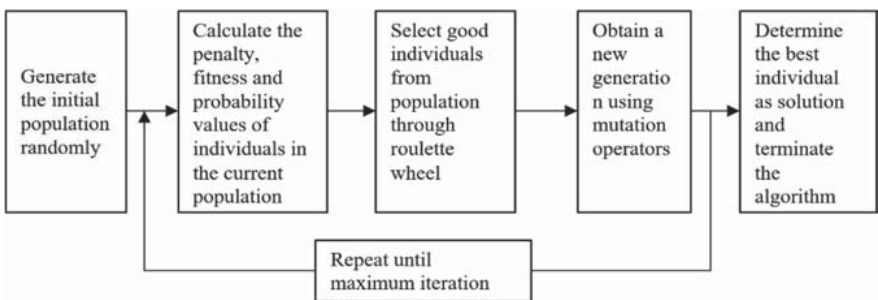

Figure 4.   Proposed genetic algorithm.

consumed in each path as well as to fulfill the constraints of a traveling salesman problem. An image sensor is fitted at the bottom of the UAV to take photos at each point in the tour. If i, j, and k are three consecutive points in a proposed route, then the fitness of that route can be determined by Eq. (2).

$$\text{Fitness Function} = \sum E_{ij} + \alpha.\theta_{ijk} \tag{2}$$

where $E_{i,j}$ is the energy consumed by the UAV in moving from waypoints *i* to *j*, and $\theta_{i,j,k}$ is the vector angle between path segments (*i*, *j*) and (*j*, *k*). During our preliminary studies, it was observed that the output route has a lot of sharp turns and the drone takes some time and energy in changing its yaw direction. In order to avoid it, the parameter α is a weight added as the penalty for sharp turns. If the sharp turns are desired, then the value of α should be input low and if the sharp turns are not desired then its value should be considered high.

The chromosome structure is represented in the form of a sequence of waypoints, which defines a point with latitude, longitude, and elevation in the WGS 84 coordinate system. This type of representation is referred to as "path representation" and possibly the most natural representation of a tour (Larranaga, 1999). This representation also facilitates the use of many popular genetic operators like PMX, cycle crossover, order crossover, and genetic edge recombination crossover (ER).

3.3 *Results*

A case study has been developed by deriving the centerlines of benches for a mine in Nevada. The centerlines have been extracted using Surpac (Dassaults, 2018) by digitizing the strings between two contours of the mine. The centerlines are then elevated further 36.75 m above the ground as the required resolution for the images is 1.27 cm. These centerlines are then fed to the GA for finding the optimum path. Currently, the algorithm has mutation operators such as swap, flip and slide. For a 317-points length path, the algorithm takes 15 minutes to reach the solution. As much as 60% of the times goes for calculating the initial distance and search matrices. In the algorithm, the population size of 100 has been used with swap, flip and slide as mutation operators. The stopping criteria which are the conditions at which the algorithm stops running are set as the maximum number of iterations. The number of iterations has been set at 100,000 dues to the complexity of the problem and to ensure that the solution is as near-optimal as possible. The experiments have been conducted on a PC with 6GB RAM.

It has been observed in the experimental studies that the cost of the best route planned by the algorithm is 96 which is very close to the optimal route whose length is 80. However, on an average, the solution provided by the proposed algorithm is almost double the optimal solution. The experimental verification has been conducted for the presented path planning algorithm. However, being an NP-Hard problem, no evidence has been found that this is the best solution for this kind of problems.

4 ANDROID APPLICATION: DEVELOPMENT AND EVALUATION

In this section, the development and working of an Android flight control application have been explained. For this application, Android Studio V.3.1.4 has been used as developing environment, DJI Android SDK (DJI, 2018) has been used for interaction with UAV's flight controller, and Google Maps Platform's Maps API (Google, 2018) has been utilized for navigation. The latest versions of all three kits have been accessed from the websites and implemented in JAVA. DJI Mavic Pro has been used for conducting test flights using the application during the development and testing stages. The android application is running on a 1.3 GHz CPU with 2 GB RAM capacity.

The initial interface of the application has been designed as shown in Figure 5. The Application has been designed to import the 3-D terrains models from Photoscan as a reference for the user. Further, it will allow the user to plan and edit mapping operations based on the imported terrain. Then the user can set the speed, altitude, return home commands and so on. The application then uploads the path to the drone's controller which will execute the mission (imaging of the benches) and bring the drone back to its initial launch position. The images taken by the drone during the mission will be uploaded to the server where they will be processed for the next stages.

4.1 Evaluation of the android application

A test flight has been conducted at the East Keystone Trail Head, Reno, NV to validate the ability of the developed application to conduct terrain following missions. This site is considered appropriate for this experiment because of its hilly terrain. Ground control points (GCPs) have been laid over the area approximately 0.09 km2 as shown in Figure(a). These points are made with survey grade spray paint with a bright color like orange as shown in Figure 6(b). The size of the X-mark is 1 m × 1 m. A wooden peg has been installed at the center of the X-mark to be used as a point of the survey. A wooden stick with ribbon, as shown in Figure 6(c), has been placed near the GCPs to help them spot easily. Once the points have been marked, each of them could be surveyed using Trimble R8 as receiver and Trimble TSC3 as a data collector.

The entire exercise of laying down the point and surveying them took 1.5 hours. The stage 1 flight has been conducted over the area with Phantom 4 Pro. Once that the aerial imagery has been collected, it has been processed in PhotoScan to generate 3-D models. The software was running on a PC with 32 GB RAM and Nvidia GeForce GTX 1080 graphics card.

The generated models have been imported into the designed application to conduct the stage 2 flight with the terrain-aware feature enabled. The flight characteristics for stage 1

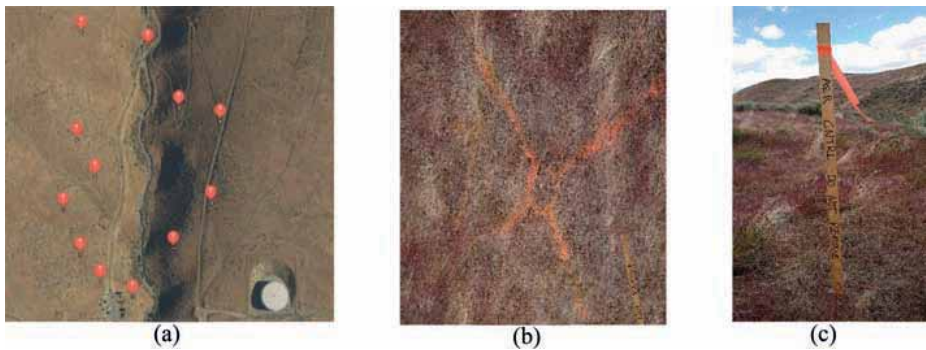Figure 5.   Mission planning interface.

Figure 6.   (a) Ground control points at Keystone Trailhead; (b) X-mark as GCP; (c) Survey Stakes.

and stage 2 flights have been shown in Table 1, and the estimated parallel path for this mapping operation has been shown in Figure 7(a). The altitude has been set to lower values for generating high-resolution models in PhotoScan. It can be observed in Figure 7(a) that the imported terrain map of the test site generated from PhotoScan has been overlaid on the Google Maps to aid the user in flight planning. Since the terrain-aware feature has been enabled, the flight planning will be based on the altitude values derived from the terrain. DJI Mavic Pro has been used for this test flight.

It can be observed from Figure 7(b) that the UAV was able to follow the terrain by maintaining the altitude of 36.5 m above the ground throughout the flight. This feature makes the drone increase its altitude as it approaches the hill. Without terrain-awareness, if the drone was flying at 36.5 over the same area, it would crash into the hill. The advantage of flying at lower altitudes is evident in Figure 8. The resolution of the DEM is almost equal to the theoretical GSD when the flying altitude of a UAV is 36.5 m. Further, the resolution of both DEM and orthomosaic has been significantly increased compared to the stage 1 flight (Figure 8 (a) and (b)). This is a significant advantage that even though the imaging sensor of Mavic Pro is smaller than Phantom 4 Pro (20 MP resolution), the former generates higher resolution models. An orthomosaic with a resolution of 6.3 mm/pix is reasonably sufficient for crack detection and drill hole accuracy measurements.

Table 1. Flight planning for stage 1 and stage 2.

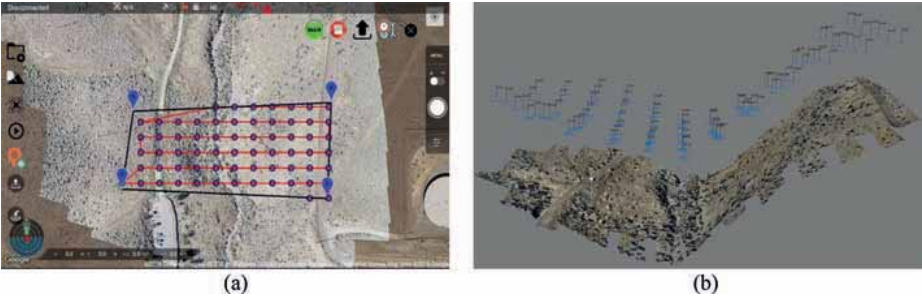| Parameters	Stage 1	Stage 2	Parameters	Stage 1	Stage 2
Altitude (AGL)	60 m	36.5 m	Forward overlap	80	80
Area	0.0658 km²	0.0104 km²	Side overlap	80	80
Max. speed	7 m/s	5 m/s	Terrain-aware	No	Yes
Flight time	15 min	7 min	No. of images	119	84

Figure 7. (a) Parallel flight for stage 2 and (b) Generated point cloud with the location of images.
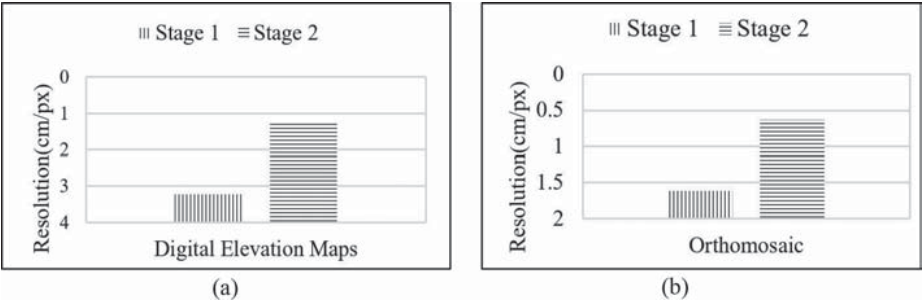

Figure 8. Comparison resolutions of (a) DEMs & (b) Orthomosaic of stage 1 and stage 2 flights.

5 CONCLUSIONS

Geo-referenced three-dimensional models of a mine can be generated from the nadir aerial imagery with resolution comparable to other scanning methods. Resolution of the generated point cloud and orthomosaic from the first stage flight is not sufficient to be used for measuring tension cracks. Resolution of the models can be improved by increasing the size of image sensor resolution or decreasing the flight altitude or both. Therefore, a second terrain-aware flight has been planned for getting high-resolution images in this study.

An empirical study was performed to model the battery performance of a test UAV considering various flight circumstances. This way, a linear regression model for the power consumption of the drone was derived and validated for a test scenario. Further, an optimization algorithm was proposed to solve the problem of path planning which resulted in a path which consumes the least battery power. A case study based on an open pit mine from Nevada was presented. The algorithm was tested to find out the optimum path for high resolution imaging of the benches of the given mine. It is safe to conclude that the proposed algorithm can generate tours which are near-optimal considering the stochastic nature of the algorithm. The suggested algorithm can also be studied for online implementation to maximize the area mapped in a mine with one single battery of the UAV. Considering the huge size of open-pit mines, the algorithm can also be implemented for the case of path planning for multiple drones.

An android application has been designed using Android Studio, Google Maps API and DJI Android SDK. The application is able to plan and execute area mapping operations for remote surveying of any area with UAVs. The application can also import the 3-D terrain models generated from photogrammetric software. A terrain-aware feature has been implemented inside the application to maneuver the UAV over a non-planar terrain. This feature enables the drone to fly at altitudes as low as 10 m to take high definition images of an area. It is able to accomplish this task with two stages of flight. Stage 1 flight is a traditional high-altitude mapping operation which outputs 3-D models of the area. Stage 2 flight is being planned to use these models making the drone to adjust its flying altitude based on the ground elevation. The result is the UAV which is capable of flying closer to the ground and taking high-resolution images. The entire method was tested and validated at site in Reno, Nevada. The resolution of the models was compared to arrive at the conclusion that the stage two flight generates a high-resolution 3-D model of a given area.

REFERENCES

Bhide, S., John, N. & Kabuka, M.R. 1993. A Boolean Neural Network Approach for the Traveling Salesman Problem. *Computers, IEEE Transactions on,* 42:1271–1278.

Cappiello, A., Ismail, C., Edward, N., Alessandro, L. & Maya, A.Z. 2002. A Statistical Model of Vehicle Emissions and Fuel Consumption. *Proceedings of the IEEE 5th International Conference on Intelligent Transportation Systems*:801–809.

Dassualt systemss. 2018. *Geovia Surpac.*

Di Franco, C. & Buttazzo, G. 2016. Coverage Path Planning for UAVs Photogrammetry with Energy and Resolution Constraints. *Journal of Intelligent & Robotic Systems,* 83(3):445–462.

DJI. 2018. *DJI Developer*. [Online] Available from: https://developer.dji.com/mobile-sdk/.

Ergezer, H., Kemal, L. 2013. Path Planning for UAVs for Maximum Information Collection. *IEEE Transactions on Aerospace Electronic Systems,* 49:502–520.

Gen, M. & Runwei, C. 1997. *Genetic Algorithms & Engineering Design.*

Glover, F. 1990. Artificial intelligence, heuristic frameworks and tabu search, Managerial & Decision Economics. 365–378.

Google. 2018. Google Developer. [Online] Available from: https:// developer.android.com/studio/.

Google. 2018. *Google Maps Platform*. [Online] Available from: https://cloud.google.com/maps-platform/maps/.

Hartley, R. & Zisserman, A. 2000. *Multiple view geometry in computer vision.* Cambridge University Press.

Hussain, A., Muhammad, Y.S., Nauman Sajid, M., Hussain, I., Mohamd Shoukry, A. & Gani, S. 2017. Genetic Algorithm for Traveling Salesman Problem with Modified Cycle Crossover Operator. *Computational Intelligence and Neuroscience,* 2017:7.

Kim, E., Jinkyu, L., & Kang, S. 2013. Real-time prediction of battery power requirements for electric vehicles. *Proceedings of the ACM/IEEE 4th International Conference on Cyber-Physical Systems, ICCPS 2013*:11–20.

Kirkpatrick, S. & Toulouse, G. 1985. Configuration space analysis of travelling salesman problems. *http://dx.doi.org/10.1051/jphys:019850046080127700,* 46.

Larranaga, P., Kuijpers, C., Murga R., H., Inza, I. & Dizdarevic S. 1999. Genetic Algorithms for the Travelling Salesman Problem: A Review of Representations and Operators. *Artificial Intelligence Review,* 13:129–170.

Lucieer, A., Sharon, R. & Darren, T. 2011. Unmanned Aerial Vehicle (UAV) Remote Sensing for Hyperspatial Terrain Mapping of Antarctic Moss Beds based on Structure from Motion (SfM) point clouds.

Meneses, S., Cueva, R., Tupia, M. & Guanira, M. 2017. A genetic algorithm to solve 3D traveling salesman problem with initial population based on a GRASP algorithm. *Journal of Computational Methods in Sciences and Engineering,* 17:1–10.

Miller, E., C., Tucker, A.W. & Zemlin, R.A. 1960. Integer Programming Formulation of Traveling Salesman Problems. *J. Acm,* 7:326–329.

Mintab, 2018. *Minitab 18*. [Online] Available from: http://www.minitab.com/en-us/.

Pehlivanoglu, Y. & Abdurrahman, H. 2007. Vibrational Genetic Algorithm Based Path Planner for Autonomous UAV in Spatial Data Based Environments. *Proceedings of the 3rd International Conference on Recent Advances in Space Technologies, RAST 2007*:573–578.

PIX4D. 2018. *How to verify that there is enough overlap between the images*. [Online] Available from: http://support.pix4d.com/hc/en-us/articles/203756125-How-to-verify-that-there-is-enough-overlap-between-the-images.

Portas, E., Torre, L., Cruz, J. & Toro, B. 2010. Evolutionary Trajectory Planner for Multiple UAVs in Realistic Scenarios. *Robotics, IEEE Transactions on,* 26:619–634.

Sužiedelytė-Visockienė, J. 2016. Unmanned Aerial Vehicles for Photogrammetry: Analysis of Orthophoto Images over the Territory of Lithuania. *Journal of Aerospace Engineering,* 2016:9.

Torrero, L., Seoli, L., Molino, A., Giordan, D., Manconi, A., Allasia, P. & Baldo, M. 2015. The Use of Micro-UAV to Monitor Active Landslide Scenarios. *Engineering Geology for Society and Territory—volume 5*, Cham:701–704.

Tseng, C., Chau, C., Elbassioni, K. & Khonji, M. 2017. Autonomous Recharging and Flight Mission Planning for Battery-operated Autonomous Drones. *arXiv preprint arXiv:1703.10049*.

US Federal Aviation Administration. 2016. Remote Pilot—Small Unmanned Aircraft Systems Study Guide.

Zarco-Tejada, J., P., Berni, J., Suarez, L. & Fereres, E. 2018. A new era in remote sensing of crops with unmanned robots. *SPIE Newsroom*: pp. 2–4.

Enhancement of explosive energy distribution using UAVs and machine learning

J. Valencia, R. Battulwar, M. Zare Naghadehi & J. Sattarvand
Department of Mining and Metallurgical Engineering, University of Nevada, Reno, USA

ABSTRACT: Blasting engineers need right information at the right time to achieve safe and productive blasting. This paper explains how to use Image Processing (IP) and Machine Learning (ML) to compensate the drilling inaccuracy through adjustment of the drillhole explosives in order to enhance the Explosive Energy Distribution (EED). Accordingly, images of the drilled blasting site are collected by a specially programmed Unmanned Aerial Vehicle (UAV) and processed by a photogrammetry software to provide orthomosaic map and Digital Elevation Model (DEM) of the site. Subsequently, the models are analyzed to identify as-built locations of the drillholes, and finally, an optimization model is run to manipulate the amount and configuration of the charges in each drillhole in order to reach the most uniform explosive energy distribution in the rock mass. Current paper's focus is on the process of models generation and identification of the exact locations of the drillholes.

1 INTRODUCTION

The final position of blast holes still is a task that is not completely controlled in mine sites. The best control for this purpose would be surveying, but usually the surveyors in the mines are dedicated to many other activities and do not exclusively control drillholes. Although majority of new drill rigs have accurate GPS devices, but comparison of the designed patterns with the results of surveyed drillholes in some case studies surprisingly shows a considerable difference (Valencia López et al, 2015). These errors can be attributed to a number of sources such as the loss of signal, improper coverage in the site, malfunctioning hardware, etc. Therefore, blasters may not reach the perceived goals without knowing of the correct as-built drillhole locations and all the analysis, calculations, modeling and simulation would therefore be based on incorrect information. However, the time-consuming task of surveying of all drillholes is a challenging procedure which cannot be easily accommodated in an open pit mining operation. Present study proposes a solution to control the final drillhole locations using Drone Imaging, Image Processing and Machine Learning. This is a running research with some uncompleted components and the paper will be focused on the process of data collection (imaging) and generating the blast site models as well as the automated drillhole location identification.

Previous modelling results have indicated that changes in post-blast fragment strength significantly influences the performance of the SAG mill, producing up to a 20% increase in throughput (Michaux & Djordjevic, 2005). However, the effective explosive energy represents only around 26% of the total available energy (Sanchidrián et al, 2007). In order to obtain an optimal EED, it is crucial to keep a good control of the drilling accuracy.

General procedure of the developed technology is depicted in Figure 1. The process starts with taking high resolution images from the drilled site. A conventional off-the-shelf drone such as DJI products can be used for this purpose, however, in order to take high-resolution pictures (few mm/pixel) the drone needs to get close to the ground and take images at 20 to 30 meters above the ground level. A special ground control application is programmed to accomplish this step. Next, a commercial photogrammetry software is used to process the

Figure 1.   Main steps of the technology.

images and stich those together in order to generate a large RGB photo of the site called orthomosaic map. Photogrammetry also uses the differences between pixels on overlapping areas to generate a three dimensional model of the surface called DEM. A DEM is a gray-scale picture that the values of pixels represent the altitude at the location of pixels. These two models are then processed by machine learning algorithms to find the exact locations of the drillholes automatically. Although a high accuracy of the coordinates can be achieved by photogrammetry using ground control point and surveying of their locations, however, the process can return the accurate relative locations without ground control points too. Finally, a binary optimization model is built and solved in order to adjust the amount of the charges in each drillhole to reach the most uniform energy distribution.

2   STEPS OF ENERGY DISTRIBUTION OPTIMIZATION

2.1   *Drone imaging and photogrammetry*

The presence of UAV has been drastically increased in the past decade by enhancing their technological features and the cost-effectiveness at the same time. Drones have facilitated the process of data acquisition from inaccessible and dangerous areas of the mines and a new application for this valuable data appears in the industry every day. The images needed for analysis of the blasting sites in current study were captured using a DJI Phantom 4 Pro at the altitudes of 40 ft. (12.2 m), 60 ft. (18.3 m) and 100 ft. (30.5 m) Above Ground Level (AGL). For photogrammetry purposes, the pictures were taken with 80 to 90 percent overlap and processed using a commercial package called Agisoft Photoscan. Consequently, the Digital Elevation Models (DEM) and Orthomosaic maps of the drilling areas were generated. Then, Matlab is used for processing the generated models and implementing machine learning algorithms in order to identify exact locations of the drillholes.

2.2   *Drillholes identification image processing*

Initially, procedural image processing is used to identify drillhole locations on the orthomosaic map. Images from a case study blasting site are captured from an open pit operation in Nevada. Pictures are taken at different altitudes of 40 ft (12.2 m), 60 ft (18.3 m) and 100 ft (30.5 m) AGL with a completely vertical gimbal angle. Figure 2 shows one of the pictures taken at 100 ft AGL. Then different image processing algorithms are tested to reduce the information, build the structural presentation and finally extract the information from structural presentation.

Grey-scale conversion is the initial step in many image analysis algorithms. The process essentially simplifies (i.e., reduces) the amount of information in the image by weighted summation of the red, green, and blue channels (Solomon & Breckon, 2011). Thresholding is a simple transformation that can generate good results in some applications. It produces a binary image from a grey-scale or color image by setting pixel values to 1 or 0 depending on whether they are above or below the threshold value. This is commonly used to separate or segment a region or object within the image based upon its pixel values (Solomon & Breckon, 2011). Different threshold values were tried (0.1, 0.2, 0.3, 0.4, and 0.5) but the best results were reached with 0.193 which was still noisy for identification of drillholes.

Different algorithms such as Roberts, Prewitt, Sobel, Gray Thresholding, Laplacian and Laplacian of Gaussian were tested with minimum success to find the appropriate image processing methodology of drillhole identification.

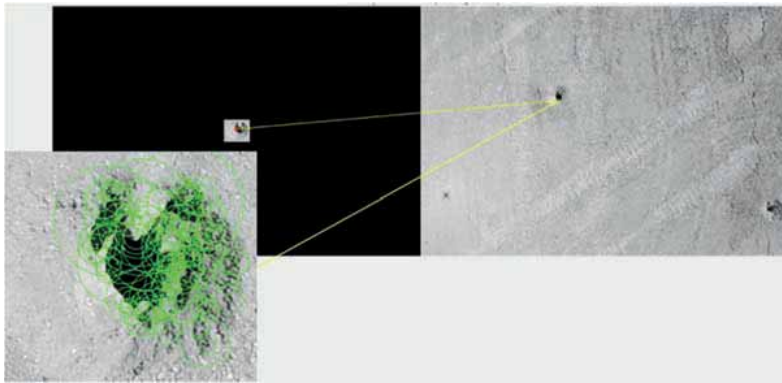Figure 2.   Aerial image of drilling site at 100 ft (30.5 m) AGL.

Figure 3.   Use of strongest features of a single hole to detect drillholes in aerial images using the programming and numerical analysis software.

2.3   *Drillholes identification using machine learning*

Although the traditional machine learning recommended to contain between 100–10,000 samples and 1,000,000 samples for deep learning (Kim, 2017), because of close similarity of drillholes in our case, we used a total of 136 drillhole samples.

For the detection of the strongest features of a drillhole, the "Object detection in a cluttered scene using point feature matching" methodology was used(2018b). This approach involves finding point correspondences between the reference, in our case a drillhole and the target aerial image containing several drillholes (Figure 3).

Furthermore, a supervised machine learning process is tested. It starts annotation of the Regions of Interest (ROI) using an Image Labeler application (app). Figure 4, over the pictures taken from different altitudes AGL (2018a). Then, training of the network is done using Aggregate Channel Features (ACF) object detector algorithm. The time to complete the training process was 406 seconds. Parallel pool option is used to optimize the computation of training processes. After training, some of the images were chosen and bounding boxes (bboxes) perceived by ACF detector were checked. The results, Figure 5, showed that the drillholes are very well recognized with a high confidence level using the Machine Learning algorithm.
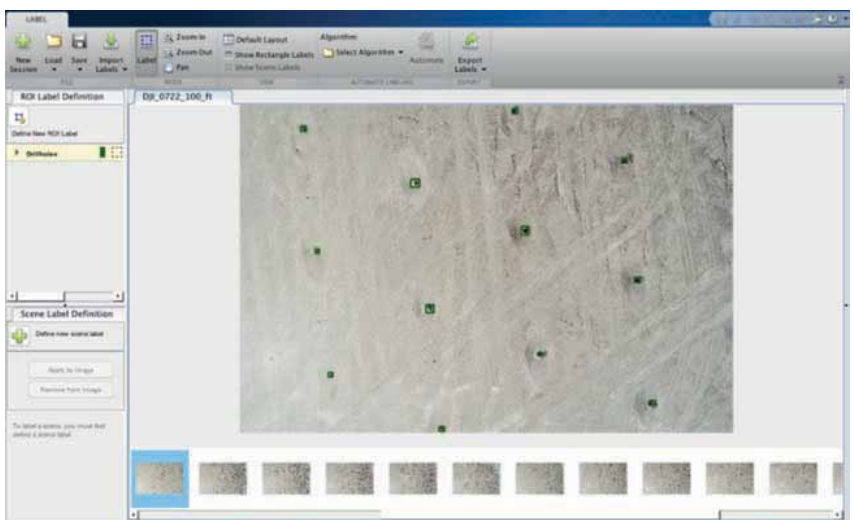
Figure 4.   Labeling drillholes at 100 ft (30.5 m) altitude in the image labeler app.

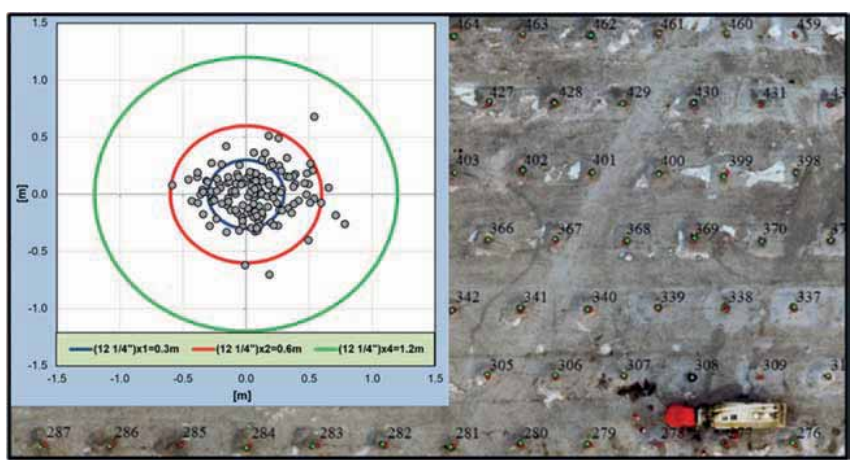Figure 5.   Drillholes detected using an image captured at 60 ft (18.3 m) AGL including confidence percentage.

Figure 6.   Graphical Comparison between real drillholes (red) and designed drillholes (green).

2.4 *Drilling accuracy*

The detected drillholes by Image Processing and/or Machine Learning are compared against their designed locations. Figure 6 shows the deviations of the as-built drilling operation from the designed configuration. The real drillholes and their designed locations are displayed in red and green respectively. It reveals that the errors can even reach to the level of 1 meter in the case study.

3 EXPLOSIVE ENERGY DISTRIBUTION (EED)

Simulation of EED is a known process for blasters to analyze blasting performance and ensure its safety and productivity. In contrast with sophisticated thermodynamically/thermo-physical models, blasting engineers have a simplified approach based on the powder factor which is also used in current research project. Generally, the powder factor is just an average for the entire blast, and do not clearly reflects variations in burden, spacing, bench height, hole diameter, charge length or explosive energy in particular areas of the blasting. In this approach, a small portion of the charge is considered and its resulting explosive energy concentration at point P at the distance of r from the charge segment is calculated using Eq. (1) (JKTech, 2012).

$$P = 187.5 \frac{\rho_e}{\rho_r} D^2 \frac{1}{h^2} \left(\frac{L_2}{r_2} - \frac{L_1}{r_1} \right) \tag{1}$$

where L_1, L_2, h and l are the distances illustrated in the Figure 7, D is drillhole diameter, and ρ_e and ρ_r are the densities of the explosive and rocks respectively. Eventually, the total energy concentration at this point can be calculated by integration of all energy contributions from different charge segments.

Figure 8 illustrates a simple calculation based on the Equation (1) for a single drillhole. In this case, drillhole diameter of 12 ¼" (311 millimeters), rock density of 2.65 g/cm³, and explosive density of 1.33 g/cm³ are considered.

3.1 *EED optimization*

A completely uniform EED can never be reached from a blasting operation. Even in a completely uniform drilling pattern there will be much higher energy levels at the vicinity of
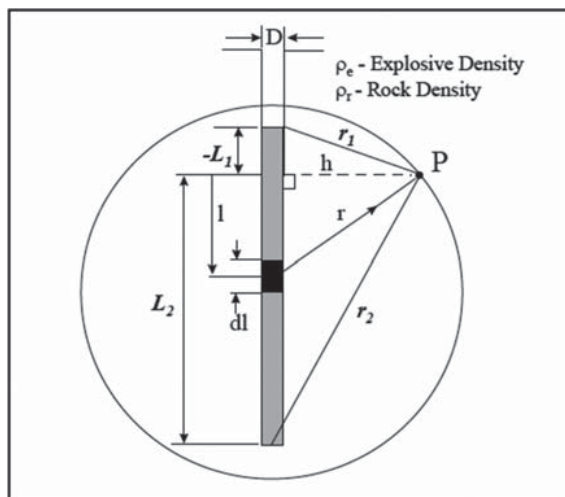

Figure 7. Explosive energy concentration around explosive charges (JKTech, 2012).
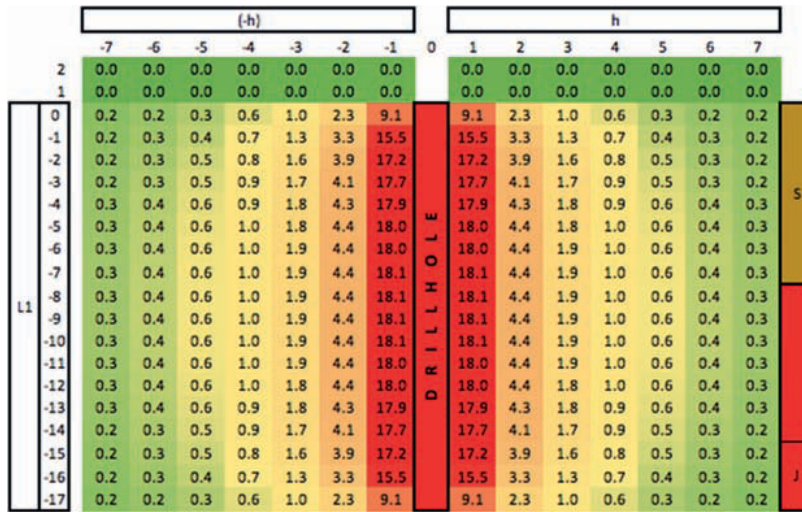
			(-h)									h				
		-7	-6	-5	-4	-3	-2	-1	0	1	2	3	4	5	6	7
	2	0.0	0.0	0.0	0.0	0.0	0.0	0.0		0.0	0.0	0.0	0.0	0.0	0.0	0.0
	1	0.0	0.0	0.0	0.0	0.0	0.0	0.0		0.0	0.0	0.0	0.0	0.0	0.0	0.0
	0	0.2	0.2	0.3	0.6	1.0	2.3	9.1		9.1	2.3	1.0	0.6	0.3	0.2	0.2
	-1	0.2	0.3	0.4	0.7	1.3	3.3	15.5		15.5	3.3	1.3	0.7	0.4	0.3	0.2
	-2	0.2	0.3	0.5	0.8	1.6	3.9	17.2		17.2	3.9	1.6	0.8	0.5	0.3	0.2
	-3	0.2	0.3	0.5	0.9	1.7	4.1	17.7		17.7	4.1	1.7	0.9	0.5	0.3	0.2
	-4	0.3	0.4	0.6	0.9	1.8	4.3	17.9		17.9	4.3	1.8	0.9	0.6	0.4	0.3
	-5	0.3	0.4	0.6	1.0	1.8	4.4	18.0		18.0	4.4	1.8	1.0	0.6	0.4	0.3
	-6	0.3	0.4	0.6	1.0	1.9	4.4	18.0		18.0	4.4	1.9	1.0	0.6	0.4	0.3
	-7	0.3	0.4	0.6	1.0	1.9	4.4	18.1		18.1	4.4	1.9	1.0	0.6	0.4	0.3
L1	-8	0.3	0.4	0.6	1.0	1.9	4.4	18.1		18.1	4.4	1.9	1.0	0.6	0.4	0.3
	-9	0.3	0.4	0.6	1.0	1.9	4.4	18.1		18.1	4.4	1.9	1.0	0.6	0.4	0.3
	-10	0.3	0.4	0.6	1.0	1.9	4.4	18.1		18.1	4.4	1.9	1.0	0.6	0.4	0.3
	-11	0.3	0.4	0.6	1.0	1.9	4.4	18.0		18.0	4.4	1.9	1.0	0.6	0.4	0.3
	-12	0.3	0.4	0.6	1.0	1.8	4.4	18.0		18.0	4.4	1.8	1.0	0.6	0.4	0.3
	-13	0.3	0.4	0.6	0.9	1.8	4.3	17.9		17.9	4.3	1.8	0.9	0.6	0.4	0.3
	-14	0.2	0.3	0.5	0.9	1.7	4.1	17.7		17.7	4.1	1.7	0.9	0.5	0.3	0.2
	-15	0.2	0.3	0.5	0.8	1.6	3.9	17.2		17.2	3.9	1.6	0.8	0.5	0.3	0.2
	-16	0.2	0.3	0.4	0.7	1.3	3.3	15.5		15.5	3.3	1.3	0.7	0.4	0.3	0.2
	-17	0.2	0.2	0.3	0.6	1.0	2.3	9.1		9.1	2.3	1.0	0.6	0.3	0.2	0.2

Figure 8   Schematic representation of EED profile with different energy levels.
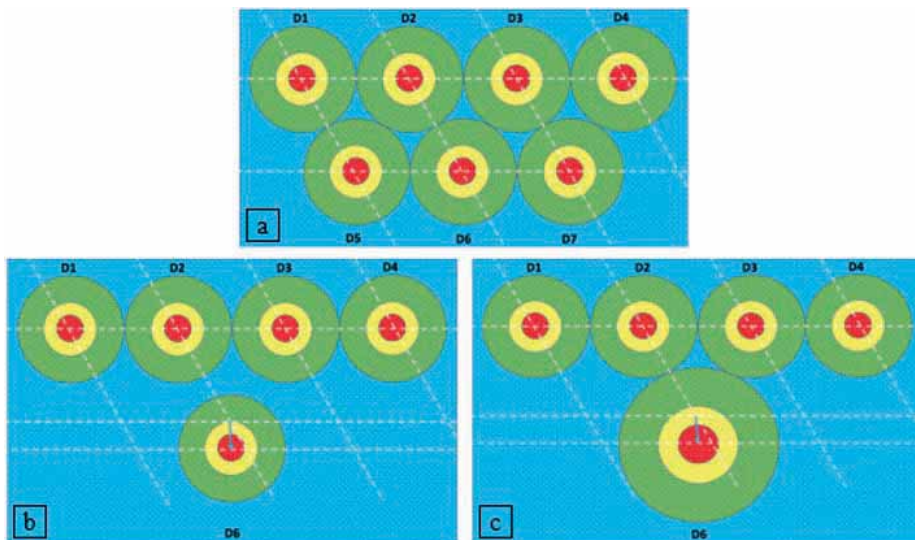

Figure 9.   (a) Ideal EED for a staggered drilling pattern: (b) Impact on EED from the error in D6 positioning; (c) Adjustment of the charge in D6 to compensate drilling error.

charges compared to the middle of the drillhole pattern (Figure 9a). This is the ideal EED that can be obtained from a blasting operation. Figure 9b shows the effect of a one-meter error in locating drillhole number D6. Clearly, the areas between drillholes number D2, D3, D6 will not receive sufficient energy and would lead to a poor fragmentation, excessive vibration, and potential flyrock. A potential solution has been shown in Figure 9c where adding more explosive to D6 or using higher energy explosives has compensated the drilling inaccuracy and provided sufficient energy to all zones.

For the EED optimization purpose, a 3D block model of the blast zone is going to be built and 4D dynamic calculation will be used to find the energy concentration of each block. Then a cost function will be considered for optimization purpose for penalizing of the deviations of the energy concentration from their average value. Decision variables of this opti-

mization model will be the amount of charge in each drill hole. Optimization model will be solved using a metaheuristic algorithm and the result will determine the required changes in charging of each drill hole in order to maximize energy distribution uniformity.

4 CONCLUSIONS

Despite using relatively accurate technologies, drilling of the blast holes on their designated coordination is still an issue in open-pit mining. The problem arises from the fact that blasters are not usually aware of the magnitude and direction of this error due to the operational restrictions in surveying of all drillholes. The paper explains a new automated methodology in order to measure the deviation of the as-built drillholes from their desired locations and adjust the charges of individual drillholes to compensate materialized errors.

The offered approach consists of taking a series of high resolution images from the blasting site and using photogrammetry to generate big picture (orthomosaic) and surface elevation model of the site. Then, an image processing/machine learning approach is used to automatically measure drilling errors. Finally, an optimization model is solved to calculate how to compensate the drilling inaccuracy by adjustment of the charges in each drillhole in order to reach the best possible EED.

REFERENCES

JKTech (2012) 2DRing, Underground Blast Design, User Manual.
Kim, P. i.-y. n. (2017) *MATLAB deep learning: with machine learning, neural networks and artificial intelligence* [eBook]. Place of publication not identified. New York, NY: Apress, Distributed to the book trade worldwide by Springer Science+Business Media New York.
Michaux, S. & Djordjevic, N. (2005) Influence of explosive energy on the strength of the rock fragments and SAG mill throughput. *Minerals Engineering*, 18(4), 439–448.
Sanchidrián, J.A., Segarra, P. & López, L.M. (2007) Energy components in rock blasting. *International Journal of Rock Mechanics and Mining Sciences*, 44(1), 130–147.
Solomon, C. & Breckon, T. (2011) *Fundamentals of Digital Image Processing: A Practical Approach with Examples in Matlab*. New York, UNITED KINGDOM: John Wiley & Sons, Incorporated.
Valencia López, J.P., Contreras Moreno, E.H. p. g. & Universidad de Santiago de Chile. Departamento de Ingeniería en, M. (2015). Evaluación de alternativas de perforación y tronadura para el mejoramiento de la fragmentación en Mina Los Filos, Estado de Guerrero, México. Santiago.

The concept of walking robot for mining industry

B. Dębogórski, P. Sperzyński, M. Fiedeń, T. Ursel & A. Muraszkowski
Faculty of Mechanical Engineering, Wrocław University of Science and Technology, Wrocław, Lower Silesia, Poland

ABSTRACT: The article describes briefly actual state of the art of unmanned vehicle for mining industry, from inspection robot to automatic train for ore transport. Concept of unconventional walking robot for inspection is presented and comparison with standard wheel and track solutions is shown with theirs advantages and disadvantages as well. Main advantages of author's solution are limiting the number of motors to two, simplifying control algorithms and increasing durability through displacing sensitive systems like motors, electronic, from legs to the body of the robot. Several results with different optimization parameters for geometric synthesis of used leg mechanism in different environmental condition are shown. The authors heuristic method of geometric synthesis is briefly presented, that can be used not only for walking mechanisms.

1 INTRODUCTION

In the mining industry, the reliability and dependability of the applied solutions acts a special role. Due to the difficult conditions under the surface of the ground, most activities are performed by man. A few major threats to people's health and life can be distinguished: climatic, methane explosion, seismicity or rock burst. Underground, air temperatures often reach over 30°C, with high relative humidity ranging from 70% to even 100% (Drenda, 2012). Another important risk factor underground is the atmosphere itself. While ore in a coal mine is extracted, a methane deposits can be released, hence the risk of an explosion is created. Accordingly, even spark-ignition engines are not used underground. Respectively suitable protection of the workplace of people, throughout securing of the heavy equipment or the mine passageway have to be prepared, due to seismic or rock burst hazards. Therefore, the research of the possibility of replacing human work by autonomous or remote controlled machines has begun.

Recently, Robotic solutions replacing human work, were built as a prototypes for the needs of scientific research, which were highly defective. Increasingly, however, these solutions become implemented as ready to market products. On Figure 1, examples of mobile robots constructed for research purposes, intended mainly for inspection has been presented. The consortium of Emag-Piap Institutes (Poland) has constructed the MPI mobile platform (Figure 1a). The robot is intended for help in a mine rescue station. For this purpose, the robot, with special instrumentation has been equipped, allowing to work in potentially explosive conditions, where humans cannot be present at. MPI weights of approx. 1100 kg and reaches a maximum speed of 0,7 m/s (Kasprzyczak, 2016). Another example is the second prototype of the OmniBot II inspection robot (Figure 1b). The robot has a caterpillar track drive, which allows to move at a speed of 0,5 m/s. Additional arms, equipped with caterpillars as well, increase robot mobility, when overcoming obstacles. The robot is controlled via tele-operation, using a fiber optic spool, placed on the platform (Wang, 2014). Following example is TeleRescuer (Novák 2018) inspection robot. The Robot (Figure 1c) consists of the main chassis with four independent tracked arms, main components are placed in a flameproof
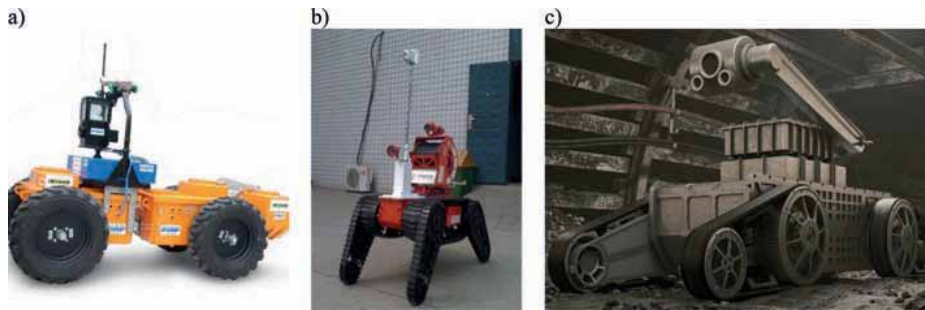
Figure 1. Mobile robots created in term of inspection use, a) MPI platform, b) Omnibot II, c) Telerescuer.

Figure 2. Exemplary autonomous heavy equipment used in iron ore mine in West Australia, Pilbara region.

housing. For inspection purposes, a 3D vison system is mounted on a scanner arm to build a map of a mine.

Mine work automation programs, from remote machine operation to fully autonomous drilling rigs and spoil transport vehicles are being developed all over the world. Mining robotics development programs are conducted, among others in Europe, Canada, Australia, South Africa or Chile.

In Western Australia, Rio Tinto built an iron mine that used robotic control systems in such operations as drilling or transporting ore(Figure 2). An example is a man-operated drilling rig (Figure 2b.), which can be switched to automatic mode depending on the terrain and the conditions in which it operates. The next operation which has been automated is the transportation of ore. This is done using the fully autonomous Komatsu 930E vehicles (Figure 2a) or centrally controlled train (Figure 2c) (Grad, 2010).

2 CONCEPT

2.1 *Analysis of existing solutions*

Currently, the most widespread drive system for mobile platforms are wheel drive solution. It is used mainly due to the highest energy efficiency from all types of drives. For this reason, it is also the most thoroughly tested system. It is very accurately described in the control theory that provides many control algorithms. The biggest disadvantage of this system is the difficulty in overcoming terrain obstacles, especially when they are larger than half the diameter of the wheel and passing on loose ground. It works best on an even, paved surface. An additional problem is the risk of tire damage on the sharp edges of the rocky surface.

Another type of drive is a track drive. It significantly increases the ability to move in difficult terrain. The ability to overcome obstacles is much greater if additional wheels placed above the others inside the track are used. The disadvantages of this solution are the low

efficiency of the system, making it impractical when traveling over greater distances, much larger dimensions, both occupied space in the vehicle and a large weight. The track system significantly hampers autonomous steering when performing a turn maneuver due to slippage. This type of drive significantly degrades the ground on which it moves, so it cannot be used in some tasks, for example patrolling farmlands or forests.

The walking drives solve the problem of overcoming obstacles. With a properly designed structure, the platform can enter the obstacle, raising the leg accordingly. The problem with moving on loose ground is solved by proper foot structure and control algorithm that minimizes the longitudinal force between the foot and the ground. Consumption of materials in contact with the ground is also significantly reduced. It results from a larger contact surface than in the case of wheels, different characteristic of the distribution of contact forces between the vehicle and the ground. The risk of damage to the surface is also reduced. In the case of a walking system it is also possible to choose the place where the foot is applied to the ground, with less risk of damage to the foot or to control of grip before transferring the entire load to the foot. The cost of transport is larger than for wheels but smaller than in a tracked drive. For example, energy efficient DURUS robot has 1,5 COT (cost of transport), Boston Dynamics ATLAS ca. 20 COT, Boston Dynamic Cheetah 0,5 COT, a car 0,05–0,25 COT, tracked vehicle like BWP-1 has 3,5 COT, Leopard 2 A4 6,5 COT. For comparison human during walk has 0,2 COT.

The walking drives also have disadvantages. Currently the biggest problem is maintaining balance, especially when moving on uneven terrain. Currently, a strong emphasis is put on developing control algorithms that allow moving vehicles in difficult conditions, which makes them very complex. For this purpose, leg mechanisms with several degrees of freedom are being developed. In addition, feet with two, sometimes three, active degrees of freedom are used. Most often, the drives are mounted in the legs, making them heavy, expensive and additionally sensitive to damage. In order to increase the efficiency of the drive, the weight of the legs is minimized by slimming the supporting structure, which simultaneously increases the susceptibility to damage or is made of lighter materials, which in turn increases the cost of the construction.

2.2 *Proposed solution*

The use of the Klann mechanism allows to eliminate some problems of anthropomorphic drives. Stabilization is achieved by the use of eight legs. Thanks to that, the robot has four foot on the ground all the time. In the basic version, all legs are powered by two motors. This significantly reduces the cost of the robot's limb. In addition, motors are placed in the body, which significantly reduces the weight of the limbs, which consist only of construction elements and susceptibility to mechanical damage. In the case of damage, replacement of the leg is much cheaper, because sensitive elements such as motors, sensors, control electronics or power and control wires are placed in the body. The disadvantage is the number of required legs for the mechanism to work properly. Because of this, the inertia of the mechanism is quite large, but it is evenly distributed, reducing the amplitude of load torque on the motor. When the platform moves at a constant speed, the motor also rotates in one direction at a constant speed. Because the walking trajectory is predetermined by the geometry of the mechanism, with varying terrain, the efficiency of movement is lower than in the case of mechanisms with more degrees of freedom. The clan mechanism is a plane mechanism, so when the platform turns, there are large slides on feet, just like in a track drive. The stability of the vehicle is not affected, however, they cause major disturbances in odometry systems. These slides are necessary for the proper execution of the turn maneuver and result from the construction of the mechanism. For this reason, when the platform moves on a surface with high adhesion, large lateral forces are created in the limbs, which impede movement and additionally burden the structure. With a loose or low-adhesion surface like a solid rock, this should not be a problem.

The Klann linkage mechanism in 1994 was developed, as an analogy to animal limbs. An implementation of a gait motion, as a replacement for wheel vehicle drive, was the goal

design. The limb mechanism structure is planar (Figure 3), which includes a triangle frame, a crank, two rocker arms connected directly to the frame and two couplers, all connected by revolute joints.

Fundamental dimensions of the mechanism's links are defined in order to optimize the H-point trajectory (foot) whilst crank is performing a half of a revolution, as a rectilinear path. The remaining crank rotation allows to raise the foot to a certain height before returning to the initial condition and repeating the cycle of a gait. Two identical limbs coupled on a one crankshaft and rotated in phase by half a crank revolution cycle, enables to the vehicle to move in parallel to the ground. To maintain static gait stability, connecting four such pairs of limbs (eight at total), two at the front and two at the rear of the vehicle and similarly on the sides, is required (Figure 4).

The decisive influence on the movement of a walking robot on uneven terrain has a way of moving his foot. The ability to overcome obstacles depends, among other, on the height on which the robot is able to raise the foot, and on what period of step the height reaches the maximum. The Klann mechanism allows the generation of many different foot trajectories with one degree of freedom, changing only parameters such as the length of individual parts, and the angles between them. The shape of the trajectory should be determined by the
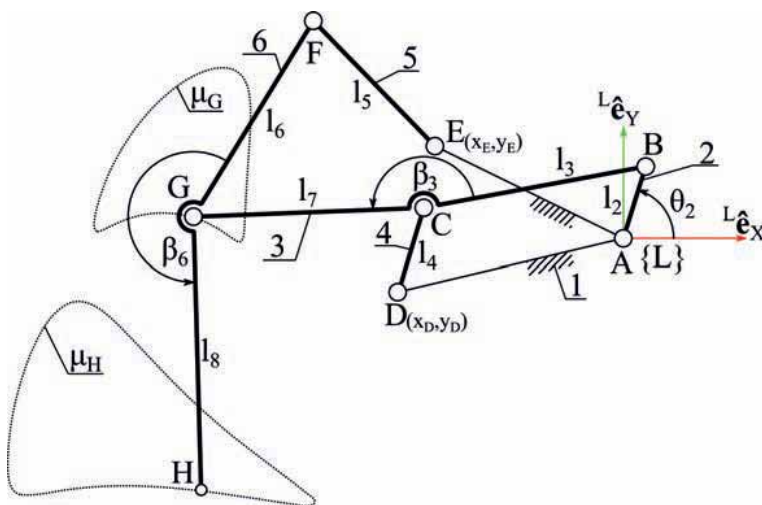
Figure 3. Kinematic scheme of Klann mechanism.

Figure 4. Visualization of robot with Klann mechanism.

conditions of environment in which the robot moves. Depending on the type of terrain, various configurations of the Klann mechanism are optimal.

Under varied surface conditions, the robot should be able to overcome many different obstacles. The universal trajectory that allows effective moving on a flat surface, and overcoming small irregularities is a trajectory with a symmetrical shape (Figure 5).

The universalism of this trajectory comes from the possibility of overcoming the same obstacles regardless of the direction of the robot's movement and the linear trajectory of the step. With similar dimensions of the mechanism changing only one parameter, you can get a higher trajectory at the expense of its length. The obtained trajectory is suitable for overcoming the higher terrain obstacles, but at the same time the robot will move more slowly (Figure 6). The trajectory can also be extended and flattened (Figure 7) to increase the speed of the robot at the same crank speed, however this trajectory works best on a flat surface.

The disadvantage of the symmetrical trajectory in the case of the Klann mechanism is that it achieves a maximum height in the middle of the lead, while at the ends of the trajectory the height is relatively small. This allows you to overcome obstacles much lower than the maximum height at which the foot is raised. In order to eliminate these disadvantages, a trajectory reaching its maximum near one of the extremes can be used, Figure 8.

Such a trajectory allows to overcome obstacles that are not much lower than the maximum height at which the foot is raised. In the case of a steady slope of the surface, the orientation of
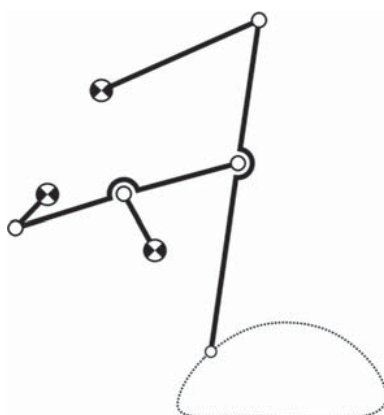

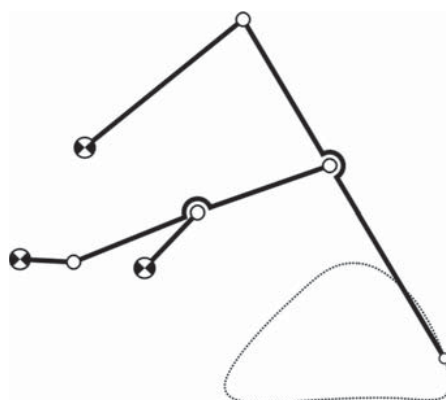Figure 5.   Symmetrical trajectory of Klann mechanism.

Figure 6.   Increased height of symmetrical trajectory of Klann mechanism.
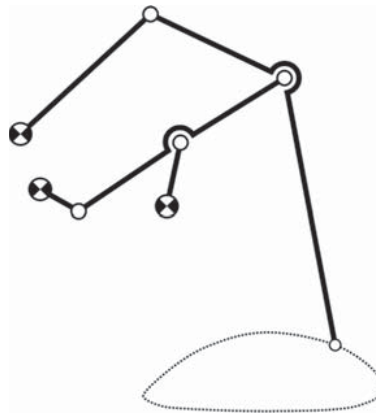
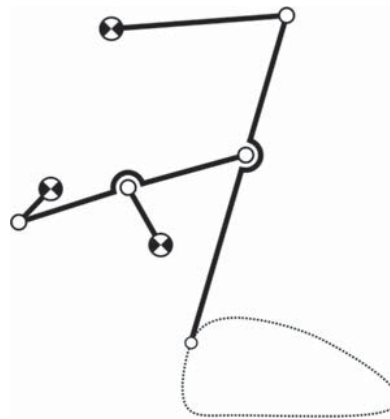Figure 7.   Extended trajectory of Klann mechanism.

Figure 8.   Asymmetrical trajectory of Klann mechanism with maximum on one side.
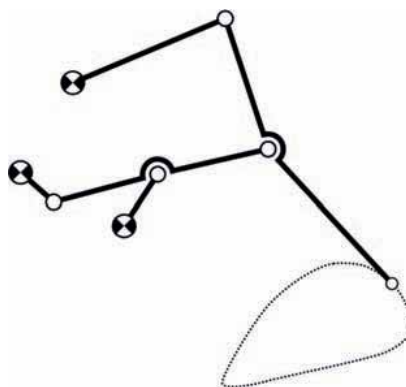

Figure 9.   Trajectory of Klann mechanism with rotated orientation.

the trajectory can be changed as shown in Figure 9. The change in orientation allows overcoming higher obstacles under a constant slope, ex. a robot with such a trajectory is able to walk effectively up the stairs, but this solution does not work on a flat surface.

Designing the right lengths of the parts and the angles between them in the Klann mechanism to obtain the desired trajectory shape is a complex task requiring the optimization of

683
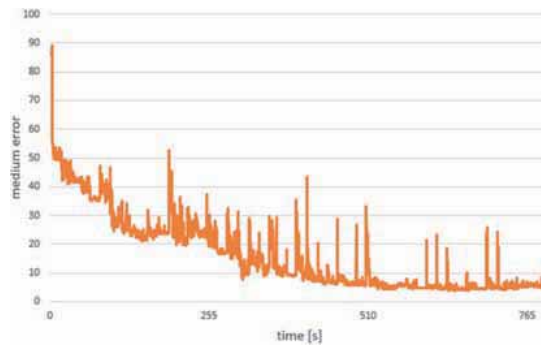
Figure 10. The value of error function over time of modified heuristic method for geometric synthesis of Klann mechanism.
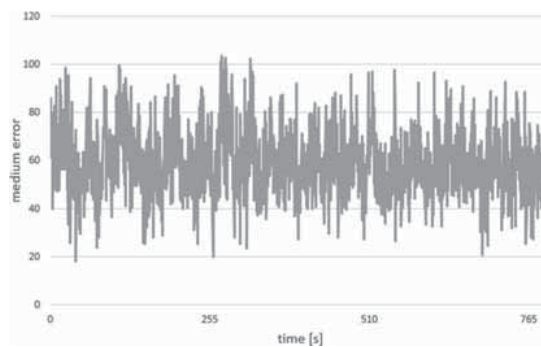

Figure 11. The value of error function over time of classical genetic algorithm for geometric synthesis of Klann mechanism.

thirteen parameters in a wide range. To calculate the parameters of the mechanism, a heuristic method of geometric synthesis based on the genetic algorithm was developed. Due to the large number of parameters in the case of synthesis of the Klann mechanism, the classic genetic algorithm is not practical. The developed method allows to achieve a sufficiently low level of error in time allowing the practical application of the method. Figure 10 shows the average error rate over time for the developed method during optimization of the Klann mechanism, Figure 11 shows the same process for the classical genetic algorithm.

3 CONCLUSION

After analyzing the Klann mechanism, it seems reasonable to apply it to a walking platform moving in difficult mine conditions. It has functionalities that allow to build a robot with durable limbs, and low cost to repair at the same time. All important systems, drives, electronics, sensors are mounted in the body, so they are protected against mechanical damage. Currently, work is underway to eliminate disadvantages of the mechanism that reduce the efficiency of its use. First of all, the use of eight legs, which significantly increases the mass of moving parts. Optimization is carried out to reduce leg mass. Another problem is the occurrence of slips and high lateral forces during turns. Modifications of the walking mechanism are being developed to minimize these properties. Simultaneously, the first prototype is being built.

REFERENCES

Drenda, J. 2012, Ocena klimatycznych warunków pracy górników w polskich kopalniach węgla kamiennego i rudy miedzi, Górnictwo i Geologia, Vol. 7(3).

Grad P. 2010, Running with Robotics. Engineering and Mining Journal; Jacksonville Vol. 211, Issue 1, pp. 34–36.

Kabiesz, J., Knechtel, J. & Krause, E. 2016, Górnicze zagrożenia naturalne. GZW w XXI wieku, XXIII Międzynarodowa Konferencja Naukowo-Techniczna z cyklu GÓRNICZE ZAGROŻENIA NATURALNE.

Kasprzyczak, L., Szwejkowski, P. & Cader, M. 2016, Robotics in mining exemplified by Mobile Inspection Platform, Mining – Informatics, Automation and Electrical Engineering, No 2(52, 6) J, pp. 23–28.

Novák, P., Kot, T., Babjak, J., Konečný, Z., Moczulski, W. & López, Á.R. 2018, Implementation of Explosion Safety Regulations in Design of a Mobile Robot for Coal Mines, Applied Sciences, Vol. 8(11).

Ralston, J.C. & Hainsworth, D.W. 1998, The Numbat: A remotely controlled mine emergency response vehicle. Field and Service Robotics; Springer: London, UK; pp. 53–59.

Wang, W., Dong, W., Su, Y., Wu, D. & Du, Z. 2014 Development of search-and-rescue robots for underground coal mine applications. J. Field Robot., 31, pp. 386–407.

State-of-the-art mechatronic systems for mining developed in Poland

Dariusz Jasiulek, Małgorzata Malec, Bartosz Polnik, Krzysztof Stankiewicz & Stanisław Trenczek
Institute of Mining Technology Komag, Gliwice, Poland

ABSTRACT: Each year intelligent control and automation systems, i.e. the systems capable for adaptation and learning, gain much wider group of users. Distributed monitoring, control and automation systems, data transmission networks, electric energy storage and management systems are more widely used in present industrial practice. Especially due to the necessity of continuous improvement of work safety, as well as the need of increasing production effectiveness and operational reliability, the scope of smart systems, which are currently under implementation in the Polish hard coal mining industry, is also constantly growing. KOMAG Institute of Mining Technology develops state-of-the-art, intelligent mechatronic systems, which increase safety in the mining industry, reduce energy consumption of technological processes of coal production. Its innovative solutions, oriented onto an improvement of mining processes, are presented in the paper. Assumptions of an IoT (Internet of Things) and direct communication M2M (Machine to Machine) have a strong impact on the structure and functionality of machinery control systems, shaping the ideas of Industry 4.0. All control systems, in accordance with the IoT, use communication networks, often with a high degree of complexity, combining various components, modules, actuators and sensors. KOMAG researchers noticed and proposed a solution to the problem of self-organizing communication paths in a complex sensors network. In order to create and optimize the communication structure an algorithm of SA class (Swarm Algorithm) is proposed. Another innovative solution, presented in the paper, includes Shield Support Monitoring System (SSMS), which enables monitoring of roof condition in real time, by monitoring the parameters of shield support (such as shield support geometry, hydraulic pressure parameters and tip to face distance). SSMS provides data to Longwall Mining Conditions Prediction System (LMCPS) for a prediction of roof fall hazards and a generation of information about indispensable corrective measures. The developed projects include automation, monitoring and visualization, technologies of artificial intelligence and systems of recording, which perfectly fit the present development trends of mining mechanization systems described, among others, in the foresight project entitled "Scenarios of technological development of the hard coal mining industry".

1 INTRODUCTION

At present in Poland the underground mining industry faces a big challenge resulting from a perspective of maximal use of hard coal in the power sector, of coking coal in the metallurgical industry, copper ore for a production of copper as well as silver and gold. In each of these cases, it is indispensable to increase efficiency of minerals' production at keeping occupational safety conditions of miners on a highest possible level.

1.1 *Mining 4.0*

The only way, enabling to reach this objective, includes an engagement of the Polish mining industry in the activities of the Industry 4.0 which becomes more and more popular in

Europe. Tests of key sectors for the German and European economy have shown (Berger 2015) that a progress is possible due to a digital transformation, having the following basic factors: digital data, automation, communication and a digital access of consumers (Fig. 1).

Broadly understood, underground mining industry starts its transformation under the name Mining 4.0. This name includes a development of such fields as: Internet of Things, Mechatronics, Telematics and Distribution of Products.

The first field – Internet of Things – aims at including all the equipment in the network of systematic monitoring, smart and mainly remotely controlled from the internal level of a mining entrepreneur, but also from the external level of a supplier/producer/service-man of machines and equipment. From the point of view of safety and economics, it is essential to combine production processes (Fig. 2) with business processes (Zieliński 2012) using appropriate software due to which all the fields are interconnected with one another. Other advanced modules, enabling so called "treating" of collected data from the point of view of an assessment, drawing conclusions and suggesting solutions can be added to typical monitoring systems.

When it is also combined with economics based on the same multi-level approach to a problem, then it is possible to obtain rational information about conducted production and business processes (Zawiła-Niedźwiecki 2013).

The second field – Mechatronics – includes elements of Mechanics, Electronics, Control and Information Technology – and it is used, among others, for designing of state-of-the-art automated and robotized machines and equipment, including industrial robots. According to the definition approved by the International Federation for the Theory of Machines and Mechanisms, Mechatronics is "a synergic combination of Fine Mechanics, Electronic Control and Systematic Thinking while designing products and production processes" (Sztucki 2000). Within the mechanical field, virtual prototyping methods are used (Winkler & Tokarczyk 2010). Products of mechatronics and mechatronic systems should be characterized by multifunctionality, flexibility and a possibility of an easy configuration, as well as by an adaptation ability and operational simplicity. It can be stated explicitly, that in fact this subject-matter has been developed for a dozen or so years by scientists and manufacturers of products working for the mining industry, which will be illustrated with some examples in a further part of this paper.

A significant part of the mechatronics is telematics. The subject matter of telematics covers (Wydro 2005):

– structural solutions, in which electronic gaining and processing of information are integral elements of telecommunication system,
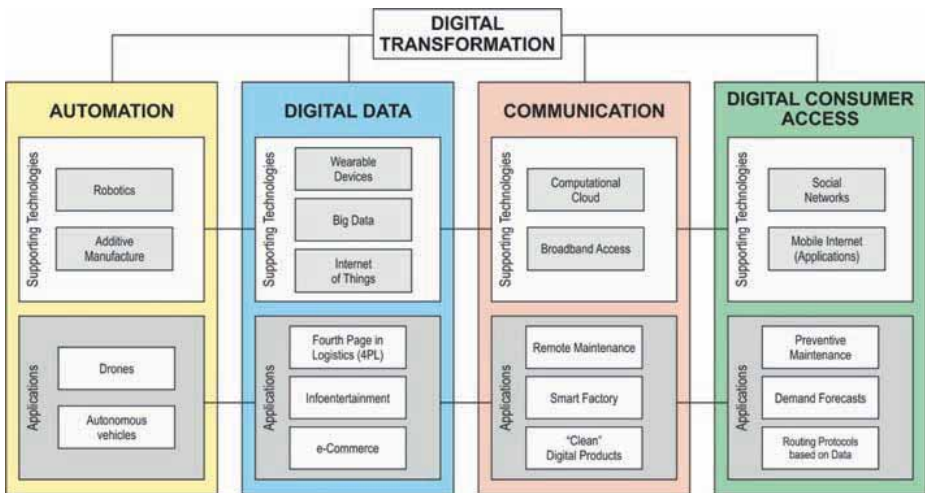

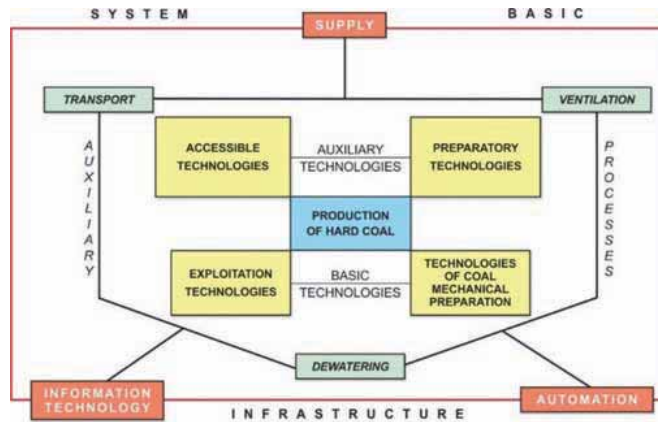Figure 1. Development factors of industry digital transformation.

Figure 2. Schematic diagram of infrastructure – process interconnections (Trenczek 2009).

– technical solutions integrating general – purpose telecommunication and information systems.

In principle telematics determines new telecommunication systems connected with the information technology, which in the mining industry relates to teleinformation systems integrating telecommunication with information technology used in these systems (Wojaczek 2017). The last one of the fields – a distribution of products is oriented onto a final recipient, but a distribution itself is an element of logistic activities in an enterprise (Witkowski 1995).

Due to the continuous striving to increase the safety of mining crews (Latos & Stankiewicz 2015) and to improve the efficiency of mining, transport and coal processing, many R&D units aim at the research projects on implementation of state-of-the-art control systems as well as a wireless network of sensors which can cooperate with the distributed control systems (Tanenbaum & Stehen 2006, Jonak et al. 2010). However, the design of self-organizing, distributed wireless sensors networks and control systems requires a development of an alternative method for power supply of its components through harvesting energy available in its vicinity, e.g., the energy of mechanical vibrations, thermal energy (Woszczyński & Świder 2014, Wischke et al. 2011, Stankiewicz & Woszczyński 2010, Mitcheson et al. 2008, Radkowski et al. 2012), and the energy of rotational movement or electromagnetic radiation. Self-powered sensors are more commonly used in ventilation or air-conditioning systems and in monitoring the migration of animals and also in the systems monitoring technical parameters.

Artificial intelligence is more and more commonly used for control and communication in the mining industry as well as for monitoring and diagnostics of subassemblies and component wear (Prostański & Jonak 2003, Bartoszek et al. 2013). According to KOMAG's experience, three hardware and software components of the discussed solutions are most important as regards operational reliability: self-powering sensors, distributed control systems, and self-organizing communication network gathering these components to the system.

2 STATE-OF-THE-ART MECHATRONIC SYSTEMS FOR MINING

2.1 *Self-powered sensors*

Self-powered sensors are equipped with generators, converting the energy in its vicinity into electric energy. Depending on the generator design, the self-powered sensors can be supplied by energy of light, gas flow, mechanical vibrations, or electromagnetic radiation. Electromagnetic or piezoelectric generators are most often used for a conversion of mechanical vibration energy (Gilbert & Balouchi 2008).

Energy harvesting enables a recovery of energy, securing the communication between wireless sensors. Research on wireless sensors, which does not require a fixed source of energy, was intensively developed in the last decade (Jasiulek et al. 2013, Jasiulek 2014). The investigations are carried out in the following three main directions:

– the organization of radio communication,
– the minimization of energy consumption by electronic components, and
– power supply system.

Self-powered sensors communicate with master devices through radio transmission systems of low energy consumption (usually it is Bluetooth Low Energy standard).

2.2 *Intelligent computer communication networks*

Future mining of seams with high methane content, threatened by bumps and high temperatures, forces the designers to develop autonomous systems to withdraw personnel from dangerous zones and to reduce its role mainly to supervision activities. Operational problems, described above, have an impact on control systems and safety of mine transportation. Results of research projects aiming at increasing the reliability of those machines and at permanent monitoring are known (Batko et al. 2008). Work on a development of technical solutions that enable a reliable supervision of the transportation machines is also carried out (Gładysiewicz 2011). Information on the rotational speed, vibrations, and temperature of critical nodes of machines and monitoring in real time is of key importance for work safety in underground workings, especially as regards fire hazards.

After the acquisition, a wireless communication system between the machines (Ad Hoc communication), transferring data to the central computer is the last stage of the measuring cycle. In such grids, routing protocols based on artificial intelligence technology and methods are used more frequently.

2.2.1 *Routing protocols in Ad Hoc networks*

A routing protocol ensures the passage of data packages from the source node to the target node. Bearing in mind the mentioned limitations of an Ad Hoc network, the realization of this task is not easy. Many different routing protocols, which can be implemented in Ad Hoc mobile networks, are available. The existing solutions can be classified as follows (Boukerche 2009, Sarkar et al. 2012, Słoczyński 2004):

– Proactive protocols, where routes are stored in routing tables.
– Reactive protocols are also known as routing protocols on demand.
– Hybrid protocols combine the properties of proactive and reactive protocols.

2.2.2 *The self-organizing structure of sensor network*

The self-organizing communication structure, named SSKIR (Stankiewicz 2014), is based on one of the artificial intelligence technologies, "swarm intelligence," which is a direct implementation of phenomena and behaviour in nature among organisms living in large groups. Their behaviour, to some extent, can be transferred to the operation of routing protocols. The system structures developed by humans (irrespectively of real implementation), using the swarm algorithm, have high possibilities for adaptation and high operational reliability. In 1987, during the SIGGRAPH conference, the programmer Craig Reynolds, in the paper entitled "Flocks, Herds, and Schools: A Distributed Behavioural Model," suggested three basic rules of self-organization based on observed groups of animals, as follows (Reynolds 1987):

– Collision avoidance is a control eliminating a local concentration of individuals. Collision avoidance eliminates accumulation of hardware and decision structures.
– Flock centrings are actions towards the average behaviour of local groups of individuals.
– Velocity matching rules are actions towards the average objective of local groups of individuals. Velocity matching enables an individual to adapt its actions to other individuals from its local group.

Basing on the above rules, a creation of a communication system made of a sensor network in which routing is based on a swarm algorithm was suggested by KOMAG. Each data frame transferred by the Measure Transmission Unit (MTU) is marked by a quality coefficient WP specifying the transmission priority referring to the effectiveness of data transmission to the main transceiver stations. This coefficient can take a value that conforms to one of connections or path metrics (Feeney 2009).

2.3 *Distributed control system*

A distributed control system (DCS) is a specially designed automated control system that consists of geographically distributed control elements over the plant or control area. It differs from the centralized control system wherein a single controller at a central location handles the control function, but in DCS each process element or machine or group of machines is controlled by a dedicated controller. DCS consists of a large number of local controllers in various sections of plant control area which are connected via a high speed communication network. R&D projects, realized at KOMAG, enabled a development of distributed control system modules under the trade name KOGASTER. KOGASTER is a good example of a system which is able to include and unite, mentioned above, self-powered sensors and wired/wireless computer communication networks, and is implemented in a harsh mining environment.

The KOGASTER control and diagnostic system is a distributed system using CAN bus and CANopen protocol (Bartoszek et al. 2013, Bartoszek et al. 2014), for communication. It is used for local control in mining machines and equipment (Jura et al. 2015, Jura & Bartoszek 2017). Use of CAN bus and CANopen protocol causes that it is an open system. The characteristic features of the KOGASTER control system are as follows:

– distributed structure,
– intrinsically safe, redundant CAN bus,
– intrinsically safe manufacture of system modules.

2.3.1 *Structure of distributed control system*

The structure of the distributed control system consists of control modules, inputs-outputs, measuring transducers, actuating components and digital interface, connected with digital CAN bus. The possibility of power supply and data transmission in one bundle of wires is an advantage of this solution.

The reliability of distributed system is achieved by the redundancy of CAN bus and doubling the modules and transducers, which increases unit manufacture cost but enables to decrease costs resulting from possible breakdowns caused by machine failure. A battery powered locomotive equipped with two independent control panels and two drives is a good example.

2.4 *Systems for measuring the operational parameters of roof support*

On the market there are measuring systems enabling measurements of roof support selected parameters. The systems have different functionalities. They differ in technical solutions as regards data transfer method and feeding systems. An analysis of the existing solutions indicates that wire and wireless systems for measuring the pressure in legs are available. Pressure measurements are used for a control of roof support load-bearing capacity as well as for a verification of proper roof support selection to in-situ mining conditions (Płonka et al. 2017). In the scope of roof support geometry measurements wire systems are available.

2.4.1 *Concept of measuring system*

At present a progress in the field of automation of longwall systems does not include monitoring of roof behaviour and preventing against disadvantageous phenomena associated with roof behaviour, such as roof falls to the longwall face or lack of roof fall behind the

shield support. Development of Shield Support Monitoring System (SSMS), which enables monitoring of roof condition in real time, by monitoring the parameters of shield support, as well as development of Longwall Mining Conditions Prediction System (LMCPS) for a prediction of roof fall hazards and a generation of information about indispensable corrective measures, is the PRASS III project objective.

2.4.2 *Shield Support Monitoring System (SSMS)*

Shield Support Monitoring System (SSMS) includes geometrical parameters of shield support, hydraulic pressure parameters, tip to face distance and new wireless communication system. SSMS enables monitoring and recording roof support operational parameters in real time and it is the basis for a development of the Longwall Mining Conditions Prediction System (LMCPS). For monitoring geometrical parameters of powered roof support, SSMS includes a set of sensors enabling a determination of an absolute position of each powered roof support component. All the devices of SSMS meet the requirements of the ATEX Directive.

2.4.3 *Longwall Mining Conditions Prediction System (LMCPS)*

It is assumed that by monitoring both shield support behaviour (leg pressures, geometry and tip to face distance) and geotechnical conditions in longwall in real time, warnings can be given for significant improper shield support behaviour and the formation of roof instabilities, such as roof cavities/falls or shield closure, several hours in advance. This advance warning allows miners to take a preventive action (such as improvement of roof strata stability by injections or improvement of the shield support behaviour by increase/decrease of leg pressure, change of shield geometry etc.) which in turn can reduce longwall downtime and hazards.

Presented scope of work is realized within the PRASS III (Productivity and safety of shield support) project coordinated by KOMAG.

2.5 *Monitoring of gases*

An exploitation of deeper seams, while using the existing ventilation systems, forces miners to limit, and in extreme cases completely eliminate internal combustion engines from work in these areas. Alternatively, machines with an internal combustion engine can be powered electrically. They are powered from traction or batteries. Mining machinery with battery powered drive is used more widely. The lead-acid cells emit hydrogen in the charging or recharging process at specified concentrations, which is an explosive gas. When evaluating the required ventilation, the concentration of electrolyte gases should be less than 2%, to avoid the risk of ignition.

Due to the problems mentioned above, KOMAG developed the MONITOR H system which is simple, safe and reliable. The compact design enables an easy installation in existing battery cases. The system can be configured to suit user's individual needs.

The monitoring system enables a continuous measurement of the cell temperature inside the cell battery compartment and a continuous measurement of the hydrogen concentration emitted from the battery while charging and recharging. These measurements are made using two temperature sensors and two catalytic sensors for measuring flammable gases. An important aspect is an ability to measure hydrogen concentration in two ranges – low to 100% LEL and high above 100% LEL. This measurement method is required due to a need of the approval for an operation in the potentially explosive areas. An integration of the developed MONITOR-H system with the battery-operated control system via a suitable relay enables to:

– protect cells from damage caused by hydrogen emissions and the presence of high temperatures,
– extend their service life by limiting the adverse effect of their gasification and the presence of high temperatures,

– maintain the desired battery status by recording on-line actual battery capacity,
– improve operator's safety by interacting with the battery management application.

2.6 *Power supply system of roadheading mining machines*

Roadheading machines are commonly used in the Polish coal mining industry, for activities related to proper maintenance of the false floor in the roadway workings. They are self-running machines on a track electro-hydraulic drive chassis. During drilling, a hydraulic pump, driven by an electric motor, powered by a drop-down cable is connected to the mine power network. The disadvantage of this solution consists in a limited mobility and an exposure of the cable to mechanical damages, so research work has been undertaken by KOMAG (Polnik 2018) in cooperation with the mining machinery manufacturer HYDROTECH S.A. to develop a drive system powered by batteries cell.

In order to increase machine operational availability, it is planned to power the machine with electricity through so-called electric hybrids. It is a system based on wired network power from the mine network and additionally on independent power supply from cell batteries. The machine works on battery power. When the battery is discharged, it is possible to supply the machine from the mine network, thus continuing the work while simultaneously charging the battery cells.

During the tests, a correct operation of the battery charging and discharging module as well as the control and safety system were checked. In the result of these tests, no irregularities were found. The current when charging cell batteries is 30 A, allowing to charge the battery in about 3 hours, which fulfils technical and technological assumptions. The combined control and safety system guarantees that every irregularity, created in the power module model is detected and blocked by the developed security system. When the power module model did not confirm a connection of the mobile machine's electrical motor during testing, only the output voltage and communication of the power electronic converter were verified during the tests.

2.7 *Remote control mining system*

Mining operations are deployed with sophisticated industrial controls and sensors for safety and operational efficiency. These sites must work around the clock to be operationally efficient and productive and must experience minimal downtime due to communication failures. At severe environmental conditions underground, the networking of mining areas requires rugged, anti-vibration specifications of devices to ensure complete control of loading operations while transferring data securely. KOMAG developed Bluester to meet these requirements. The Bluester system (Fig. 3) is designed to control mining machines such as: locomotives, suspended monorails, hoists. It has two important functions to improve the operator's work and improve safety: wireless control and control of security procedures application. The combination of these two functions in one device is an innovative solution.

Figure 3. A view of Bluester system (Juszczyk et al. 2015).

The Bluester system is adapted to work in mine workings classified as "a", "b" and "c" of the danger of methane explosion as well as class A and B of coal dust explosion hazard. The MLA charger is intended for use in non-hazardous areas. The main advantages of the Bluester System are:

– Wireless remote control increases operator's mobility and work safety.
– Versatility – it can be adapted to operate with any device.
– It can work in methane and/or coal dust explosion hazard areas.
– The range of the operational distance eliminates a possibility of an uncontrolled departure of the machine from the operator.
– Control function – checking compliance with safety procedures set by the manufacturer or the supervising mine authorities by remote reading of RFID markers.
– Reduction of operational costs.

3 SUMMARY

Control and monitoring systems, capable of adaptation and learning, are used in industrial practice on a larger scale. Internet of Things (IoT) techniques and direct communication M2M (Machine to Machine) have an impact on the structure and functionality of control systems used in machines, shaping the idea of Industry 4.0.

A practical use of energy harvesting is possible due to an implementation of electronic circuits with low energy demands, which enable energy management coming from low power sources to supply wireless sensors operating in self-organizing networks.

An example of a control system with a distributed architecture is the KOGASTER control system based on the CAN bus and the CANopen protocol. The use of intrinsically safe devices in the KOGASTER system enables its implementation to control machines and devices operating in zones where there is a risk of methane and coal dust explosions.

The method of the self-organization of the communication system, based on a swarm algorithm enables an implementation of the state-of-the-art and effective routing technology in the networks of mesh topology, including those used in underground mines, especially in diagnostic and monitoring systems, as well as for a protection of machines. Subassemblies of the networks equipped with MTU nodes can be treated as components of a measuring swarm. It is particularly important for operational safety in underground mines due to the reliability of mesh networks.

REFERENCES

Bartoszek S., Jagoda J., Jura J. System diagnostyczny ładowarki bocznie wysypującej bazujący na iskrobezpiecznej magistrali CAN. Szybkobieżne Pojazdy Gąsienicowe (32) nr 1, Ośrodek Badawczo – Rozwojowy Urządzeń Mechanicznych OBRUM sp. z o.o., Gliwice 2013.

Bartoszek S., Jagoda J., Jura J., Latos M. Systemy wbudowane w zespołach sterowania, diagnostyki oraz wizualizacji dla górnictwa. Monografia KOMTECH 2014, Instytut Techniki Górniczej KOMAG, Gliwice 2014, ISBN 978-83-60708-83-5.

Batko W., Borkowski B., Głocki K. Application of database systems in machine diagnostic monitoring. Eksploatacja i Niezawodność – Maintenance and Reliability 2008; 1: 7–10.

Berger R. The digital transformation of industry, BDI, 2015, s. 20, https://www.rolandberger. com/media/pdf/Roland_Berger_digital_transformation_of_industry_20150315.pdf.

Boukerche A. Alhorithms and Protocols for Wireless and Mobile Ad Hoc Networks. Wiley. Ottawa 2009.

Feeney L.M. A Taxonomy for Routing Protocols in Mobile Ad Hoc Networks. SICS. Technical Report T99/07. Kista 1999.

Gilbert J.M., Balouchi F. Comparison of Energy Harvesting Systems for Wireless Sensor Networks. International Journal of Automation and Computing 05(4), October 2008, 334–347.

Gładysiewicz L, Król R, Bukowski J. Tests of conveyor resistance to motion. Eksploatacja i Niezawodność – Maintenance and Reliability 2011; 3: 17–25.

Jasiulek D. Propozycje zastosowania czujników samozasilających się w przemyśle wydobywczym, Przegląd Górniczy vol. 1/2014.

Jasiulek D. Bartoszek S., Latos M., Jagoda J., Jura J., Stankiewicz K. System wibrodiagnostyczny maszyn górniczych. Innowacyjne techniki i technologie dla górnictwa. Bezpieczeństwo – Jakość – Efektywność. ITG KOMAG 2013. p. 347–363.

Jasiulek D., Stankiewicz K., Jagoda J. Możliwości zastosowania czujników samozasilających się przeznaczonych do pracy w podziemiach kopalń. Mechanizacja i Automatyzacja Górnictwa. Nr 8(519), 73–80 (2013).

Jonak J., Prostański D., Jasiulek D., Rogala-Rojek J., Puchała B. Koncepcja adaptacyjnego układu sterowania w kombajnach chodnikowych REMAG SA. Problemy bezpieczeństwa w budowie i eksploatacji maszyn i urządzeń górnictwa podziemnego. Monografia pod redakcją Krzysztofa Krauze, Centrum Badań i Dozoru Górnictwa Podziemnego sp. z o.o., Lędziny 2010 115–123.

Jura J., Bartoszek S., Jagoda J., Krzak Ł. Magistrala CAN w zastosowaniach górniczych. Szybkobieżne Pojazdy Gąsienicowe, Biul. Nauk.-Tech. 2015 nr 2 s. 67–78, ISSN 0860-8369.

Jura J., Bartoszek S. KOGASTER - instalacja elektryczna napędów spalinowych. Masz. Gór. 2017 nr 4, 41–51, ISSN 2450-9442.

Juszczyk D., Konsek R., Krzak Ł. Bezprzewodowy system sterowania maszynami górniczymi Bluester, Proceedings of KOMTECH 2015, p. 266.

Latos M., Stankiewicz K. Studies on the effectiveness of noise protection for an enclosed industrial area using global active noise reduction systems. Low Frequency Noise, Vibration and Active Control Journal, 2015, vol. 34, nr 1, 9–20.

Mitcheson P.D., Rao G.K., Green T.C. Energy Harvesting From Human and Machine Motion for Wireless Electronic Devices. Vol. 96. No. 9, September 2008. Proceedings of the IEEE.

Płonka M., Rajwa S., Lubosik Z. Ocena pracy obudowy zmechanizowanej na podstawie danych z monitoringu ciśnienia i postępu sekcji. Przegląd Górniczy nr 4/2017. 25–33.

Polnik B. An Innovative Power Supply System Dedicate for Roadheading Mining Machines, ECS Transactions, 87 (1) 2018, pp. 349–362.

Prostański D., Jonak J. Sieci neuronowe w badaniach procesu urabiania skał stożkowymi nożami obrotowymi, Monografia, ITG KOMAG, Gliwice 2003.

Reynolds C.W. Flocks, Herds, and Schools: A Distributed Behavioral Model. SIGGRAPH. Anaheim 1987.

Radkowski S., Lubikowski K., Piątak A. Vibration Energy Harvesting in the Transportation System: a Review. Diagnostyka – Applied Structural Health, Usage and Condition Monitoring' 4(64)/2012.

Sarkar S. K, Basavaraju T. G, Puttamadappa C. Ad Hoc Mobile Wireless Networks. Principles, Protocols, and Applications. Second edition. CRC Press. Taylor & Francis Group. Boca Raton 2012.

Słoczyński J. Untypical routing algorithms. Master's thesis. Lodz University of Technology 2004.

Winkler T., Tokarczyk J. Multi-Criteria Assessment of Virtual Prototypes of Mining Machines. Proceedings of the World Congress on Engineering and Computer Science 2010 Vol II. WCECS 2010, October 20–22, 2010, San Francisco, USA. ISSN: 2078-0958.

Stankiewicz K., Woszczyński M. Metody odzyskiwania i przetwarzania energii cieplnej. Maszyny Górnicze nr 1, 39–46 (2010).

Stankiewicz K. Self-organization of network structure based on swarm algorithms. Problemy Eksploatacji – Maintenance Problems 2014; 2: 5–14.

Sztucki T. Marketing przedsiębiorcy i menedżera. Agencja Wydawnicza Placet, Warszawa 2000.

Tanenbaum A.S., Stehen M.V. Systemy rozproszone. Zasady i paradygmaty. Klasyka informatyki. WN-T, Warszawa 2006.

Trenczek S.: Kierunki rozwoju infrastruktury systemowej zasilania, informatyki technicznej i automatyki. Mechanizacja i Automatyzacja Górnictwa 2009, Vol. 9, 9–15.

Wischke M., Masur M., Kröner M., Woias P. Vibration harvesting in traffic tunnels to power wireless sensor nodes. Smart Materials and Structures Volume 20 Number 8. 2011.

Witkowski J. Rodzaje działań w zakresie strategii logistycznej przedsiębiorstwa. AE we Wrocła-wiu, Wrocław 1995.

Wojaczek A. Telematyka w podziemnych zakładach górniczych. Mining – Informatics, Automation and Electrical 2017, Nr 7, 27–34.

Woszczyński M., Świder J. Use of the System for Energy Recuperation and Control in Diesel Machines. Machine Dynamics Research, 2014, Vol. 38, No 1.

Wydro K.B. Telematyka – znaczenie i definicje terminu. Telekomunikacja i techniki informacyjne 2005, Nr 1–2, s. 116–127.

Zawiła-Niedźwiecki J. Zarządzanie ryzykiem operacyjnym w zapewnianiu ciągłości działania organizacji. Wyd. Edu-Libri, Kraków, 2013.

Zieliński J. Co to jest proces biznesowy. http://it-consulting.pl/autoinstalator/wordpress/2012/ 09/28/ business-process-manifesto/, 2012.

Designing top layer in Internet of Things for underground mines

S. Feng & E. Ding
National Joint Engineering Laboratory of Internet Applied Technology of Mines, China University of Mining and Technology, Xuzhou, China
IoT Perception Mine Research Center, China University of Mining and Technology, Xuzhou, China

ABSTRACT: The booming development of IoT for mines requires the planning of the mining technology from the top layer. This paper interprets the "top layer design of mine internet technology" compiled by the State Administration of Work Safety. This paper analyzes the technical background and the core content of the top-level design from several aspects, including the design idea, the development status, the challenges, the strategic goals, the core technology, the implementation route and the supporting measures. This provides a reference that helps the scientific researchers and the technological managers in the mining industry to understand and use the ideas of "top layer design". The demonstration project in Jiahe coal mine proves the feasibility and the effectiveness of the ideas.

1 INTRODUCTION

The Internet of Things (IoT) for mines can support the mining enterprises to realize ubiquitous perception of the mine and intelligent decision. It is an important basis for industry administration departments to improve supervision and law enforcement and management level (Ding & Zhao, 2015). Since the beginning of the 2010, the concept of IoT for mines has been widely recognized by the government, the academia and the enterprises (Han, 2016). Its connotation and extension continue to expand and deepen. Some solutions with the characteristics of IoT for mines have been constantly put forward and gradually put into operation. There have been some demonstration applications in several large mining industry groups across the country. The productivity and safety level of the mine have been greatly improved (Hu, et al., 2016). At the same time, the IoT for mines gives birth to a large number of emerging industry clusters, which helps create a clear economic and social value for the society.

Although the IoT for mines has made certain achievements in the theoretical system, the technical framework, the product development, the application and the popularization, there are still a lot of room for improvement in the different aspects, including the means of perception, the link between the objects, the information mining, the standard construction, the service and the big data analysis. We need to view the overall situation of the national industrial development and solve the difficult problems we are facing systematically. We need to avoid the old ways and make the scientific plans for the future development. There are several problems with the old ways. For instance, each system was treated mutually independent. The development lacked the standards and the investment was duplicated. The ecosystem was fragmented. To provide the scientific guidance for the future development of IoT for mines is the internal driving force of the top-level design of IoT technology for mines. This paper interprets the design idea, the main contents, the key fields and the implementation of the top-level design of IoT for mines. This provide a reference for the scientific researchers in the mining industry and technological managers to read, understand and use the ideas of "top layer design".

2   THE IDEA OF THE DESIGN

For a long time, in the process of mine production in China, the new information technology failed to be integrated into the core business and process of safety production. Besides, the business flow and information flow failed to reach the deep fusion and connection, which affected the effect of the work on informatization to some extent (Zhang et al., 2010). It is difficult to collect the information of mine safety production effectively. It is difficult to guarantee the accuracy of the data as various kinds of safety data and information are filled manually. The authenticity of information and the accuracy of data are difficult to be guaranteed. The mine safety monitoring data has not been effectively utilized and mined. A large amount of data is wasted.

At present, the new energy technology revolution, Industry 4.0 and China Manufacturing 2025 all profoundly affect the various aspects of coal production. For the mine safety, the advanced perception based on the IoT should be achieved. The safety equipment develops toward the direction of "big, micro and intelligence". The sensing part and the perception part should be strengthened emphatically. We need to bring the concept of network virtualization, that is, software defined network. The information security is a part of mine safety. At present the mine lacks the unified perception and the high efficient service. We need to expand the interdisciplinary content, refine the key technology on the foundation of fusion and clarify the difference between the IoT for mines and the comprehensive automation. For designing the top layer of the IoT for mines, we need to consider the current situation and make plans for the future. We also need to consult the experts and provide the platform based services. Specifically speaking, the guidelines include several aspects. Firstly, we must clarify that the goal of the top-level design of the IoT for mines technology is to start the overall design from the high end of the mine. Secondly, we need to avoid several problems, e.g. the network independence, the lack of unified planning and standards, the duplication of investment, the isolated system in the applications of IoT for mines. Thirdly, the overall planning and design is not aimed at a particular mine. It only puts forward the general goal of the design. Fourthly, we need a unified and open platform for IoT services (Zhang & Zhang, 2013) to achieve the interoperability and seamless links between the people and the objects and between the object and the object. We need to implement the real-time control system of the mine and achieve the accurate managements and scientific decision-making. Meanwhile, the platform can be used to support the researchers from different disciplines to carry out research work, and can be accessed by different service providers. Finally, the IoT for mines, which is essentially about the service, is a platform to support the services (Yao et al., 2016). All kinds of mine applications aim to provide the services on this platform. The supporting technologies for these application services include the network technology, cloud computing, artificial intelligence, big data and so on.

3   THE MAIN CONTENTS OF TOP LAYER DESIGN

3.1   *The architecture of the contents*

Figure 1 shows the main contents of top layer design of IoT technology for mines, including the development status, the opportunities and challenges in the development of IoT for mines, the strategic goals, the key development areas of IoT for mines, the safeguard measures and construction routes. Among them, the development status, opportunities and challenges are the starting point of design. The strategic goals are the blueprint. The key development areas are the core. The safeguard measures and the construction roadmap are the implementation strategies.

3.2   *The development status and challenges of IoT for mines*

To clarify the development status of the IoT for mines is the premise of the top layer design. Although the IoT for mines has shown good adaptability to the mines and has the broad application prospects, the overall status is more about "sensing" and "transmission". There are too few studies on "awareness" and "application". We need to broaden and deepen the research on the perception level, the transport layer, the application layer and the public technology.
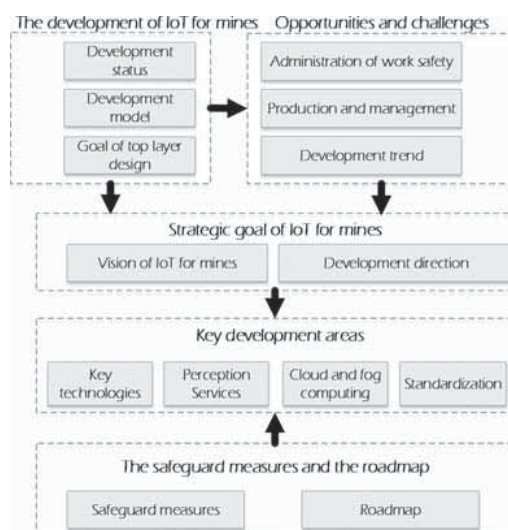
Figure 1.   The main content of top layer design of IoT for mines.

The perception layer is the forefront of the IoT for mines and is responsible for the task of perceiving data (Hu et al., 2014). However, the sensors in the current mine are still limited to the specific subsystems. The lack of distributed and networked mine sensing technology and applications make it impossible for us to achieve distributed monitoring and control. This kind of "islanding" implementation method makes it difficult to achieve perceptual data fusion and reduces the trustworthiness of perceptual data. This is contrary to the interconnection in the IoT. At the same time, there are few novel sensing technologies in the perception layer. We also lack the networked and distributed monitoring theory and methods. Thus, we cannot really meet the requirements of connecting everything and ubiquitous perception of things in the IoT for mines, resulting in an opaque state of mine production to a large extent.

The transport layer is a "neural" channel for the steady and reliable transmission of information. It is the key to connect the perception layer and the application layer. It generally includes two main parts, i.e. the backbone network and the perceptual network. However, the backbone network of each mine is the 1000 M (10 G for individual coal mine) of industrial automation network. These industrial Ethernet networks do not have the capability of accurate time synchronization for the whole network. Thus, they cannot provide the time-based services, such as the real-time tracking and management of events occurring in the whole mine. Therefore, it is impossible to describe the mine production process from the aspects of space and time. The time synchronization of the entire network needs to be carried out. The WiFi and WSN are widely used for the perceptual network. However, it is difficult for these wireless communication technologies to meet the needs of long-distance multi-hop transmission, multi-service bearer, self-organizing network on demand and reconstruction after disasters. It is necessary to develop a new kind of network. We need the new communication technologies and the perception network. At the same time, the use of 6LoWPan should be encouraged to promote the transition from IPv4 to IPv6 in order to manage and efficiently use the massive terminals deployed in these mines.

The application layer is the ultimate goal of IoT for the construction of the mines. The applications are important tools for data presentation, operation management, decision support and service provision. Although the integrated automation system of mines realized the integration of the functions of each subsystem, it only realized the linkage between a few systems. The deep information mining and integration of applications among multiple systems were not achieved. From the point of view of mine safety, the single factor reveals only one-sided reasons for disasters. We should deploy a number of subsystems and focus on the important observations in order to achieve the fusion analysis. Only in this way can we fully reveal the multi-coupling of disasters and achieve the accurate and timely pre-disaster warning.

For the public technologies in the IoT for mines, there are still many problems that need to be solved (Colakovic & Hadzialic, 2018). In particular, there are not enough research on the standards that can be used to promote the development of the IoT for mines. The overall situation should be considered from different aspects, e.g. the description of the thing and the interoperability. Moreover, we need to work on a series of mine standards for the IoT.

3.3 *The strategic goals of IoT for mines*

There are several strategic goals of IoT for mines. Firstly, the new sensors and intelligent things of mining will rapidly grow to form a semantic Web in around a decade of development. Secondly, the cloud computing and big data for the mines are widely used to form the "cloud" or "fog" computing service platform. Thirdly, the new service system and the value chain gradually improve and the sustainable mining ecological environment is initially formed. The core contents of the strategic goals are to construct the semantic mine and develop the mine service platform, and make the mine development sustainable.

There are a large number of objects in the mine environment. These objects and production processes continually generate a large number of events. Using the IoT technologies to interconnect these things helps them work together to create the new applications and services. Through the application of new sensors, distributed measurement and energy harvesting technology, the mine monitoring and control without blind zone can be realized. Through the technologies such as ubiquitous sensing, the software defined network and post-disaster reconstruction of network, we can achieve the seamless connection between the objects in the mines. With a priori model and the expert knowledge, we can achieve that the technology of IoT for mines evolves from the sensing to the context awareness. The mine production process gradually becomes transparent.

We aim to achieve the semantic expression, information fusion, knowledge mining and semantic description of the mine through the unified IoT platform, cloud computing service and big data technology. In this way, the information will be effectively used. In particular, we can empower the system with the capability of early safety warning and the virtual reproduction of events. Thus, we can significantly improve the efficiency of mine production and safety level. Meanwhile, through the construction of IoT for mines, an open and networked platform for the applications will be formed to provide the mines with the professional services.

3.4 *The key development areas of IoT for mines*

In view of the strategic goals of IoT for mines, we need to make breakthroughs in the key technologies, and provide the perception services, and build the "cloud" and "fog" platforms to promote the work on the standardization.

3.4.1 *Key technologies*
The key technologies include developing miniaturized intelligent devices, clarifying the detailed rules of radio wave propagation in the mine roadway, exploring the construction strategy of cloud computing platform and big data platform, working on the semantics (Aguilar et al. 2018), studying the security mechanism and the strategy of privacy protection and constructing a reliable network.

3.4.2 *Perception services*
The perception services of IoT for mines will focus on four aspects, i.e. "human, machine, environment and management".

1. The human perception. The IoT for mines needs to provide the context-aware service for the people. The safety of the people is the most important aspect in the mine production process. The surveillance system needs to be developed for the workers' localization, the activity recognition and intelligent decision-making.
2. The equipment perception. The status of the equipments needs to be monitored in real-time.

3. The disaster perception. The mine disaster is the biggest factor affecting the mine production. Based on the traditional mine mechanism research, we should collect the various disaster precursor information, such as hydrology, stress strain and gas, to establish the danger identification model based on IoT for mines. We need to develop the technology and the equipment for intelligent prediction of the danger and the disaster.
4. The environment perception. The mining resources and the environment are very important for the sustainable development of mining enterprises. Therefore, we should develop the technology and method of real-time monitoring of ecological environment in the mining area.
5. The management perception. We should build a cloud platform for the integrated service management. This platform can provide the real-time, accurate and scientific decision-making service for the mine operation and management.

3.4.3 *The cloud platform and the fog platform*
Implementing the cloud platform and the fog platform for the management and services of the mine is the necessary step for IoT for mines to exert its full potential. Through the cloud service platform, the field data of each mine is storged and analyzed. The specialized service can be provided through the high performance computing center. The researchers located in different places, such as research institutes and government agencies, can conduct the on-demand analysis of data on this platform to provide specialized analysis reports for enterprises, as shown in Figure 2.

The fog computing platform is known as the mine micro-cloud in a single mining enterprise. The fog computing extends the network computing model that features cloud computing, migrating the data, data processing, and applications to the local devices at the edge of the network, rather than concentrating on the data center. This makes it more widely used in different applications.

3.4.4 *Standardization*
Standardization is the necessary step to ensure the orderly and healthy development of IoT for mines and to ensure the open interconnection of the products. At present, the State Administration of Work Safety has organized the compilation of the standard of information exchange for the mine safety production, which mainly solves the problems of the
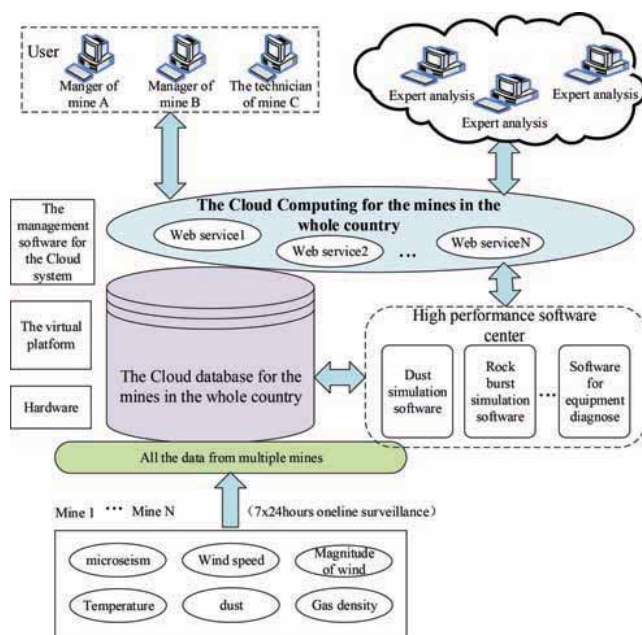

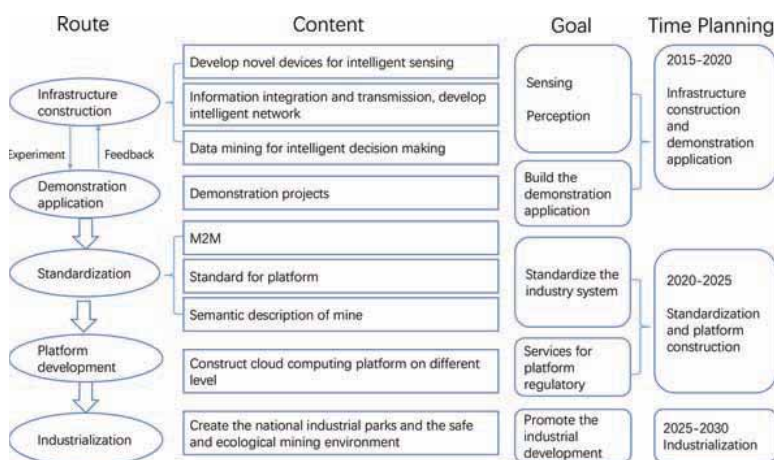Figure 2.   The architecture of the cloud service for IoT for mines.

Figure 3. The roadmap for the construction of IoT for mines.

interconnection of the equipments and information exchange in the IoT. However, this work is still far from enough. It is necessary to speed up the development of overall common standards, perceptual standards, transport standards and application-layer standards.

4 THE IMPLEMENTATION OF THE ROUTE AND SAFEGUARD MEASURES

For the implementation of the IoT for mines, we need an overall planning and design, and move on step by step. Figure 3 shows the recommended roadmap for the top layer design. It covers various aspects, including infrastructure construction, demonstration application, standard setting, platform construction and industrialization. It requires research in politics, industry and academia. We need to intensify the financial support and strengthen the financing policies support, the tax policy support and the industrial policy support. We also need to cultivate the talents and develop the international cooperation. In this way, we can establish the IoT ecosystem for the mines, and work together for the theoretical and technological breakthroughs, the equipment development and industrial applications.

5 EXPERIMENT—THE DEMONSTRATION PROJECT IN JIAHE COAL MINE

The Jiahe coal mine is located in Xuzhou, Jiangsu province. The demonstration project was funded by the government. The research group headed by Prof. Enjie Ding spent about one month conducting a field study and prepared the blueprint for the project in Jiahe coal mine. The researchers determined the subsystems of the whole system and the indicators of the performance, as well as the specifications for data exchange. The group made a plan to integrate the subsystems. The system was tested in the real-world environment. After the software debugging, the system ran successfully and the performance was greatly improved.

The whole system was composed of three subsystems, i.e. the human monitoring subsystem, the equipment monitoring subsystem and the environment monitoring subsystem. As shown in Figure 4, the moving targets including the miners and the vehicles were being tracked. Meanwhile, the environment were being monitored. For example, when the temperature was too high, the alarm was activated, indicating an emergency. The underground equipment monitoring system is shown in Figure 5 We can see whether the equipment was working properly or not.

According to the geological conditions of Jiahe coal mine, the microseismic monitoring system was set up. It was composed of the data collection subsystem, the recorder subsystem, the analyser and the demodulation measurement probes. The system shown in Figure 6 successfully helped monitor the microseism in the underground mine.
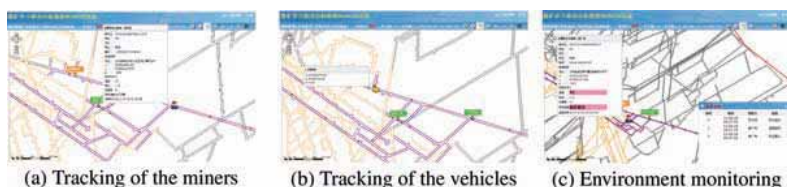
(a) Tracking of the miners   (b) Tracking of the vehicles   (c) Environment monitoring

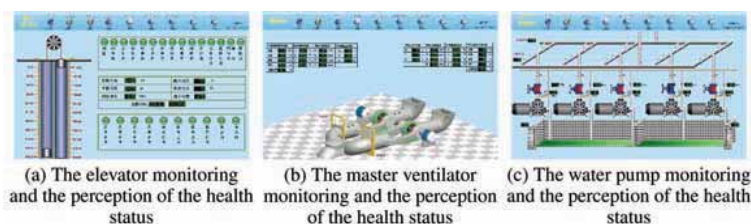Figure 4. The moving targets tracking and the environment monitoring for the underground surveillance.

(a) The elevator monitoring and the perception of the health status   (b) The master ventilator monitoring and the perception of the health status   (c) The water pump monitoring and the perception of the health status

Figure 5. The underground equipment monitoring system.

(a) Data collection   (b) The recorder   (c) The analyser   (d) The probes
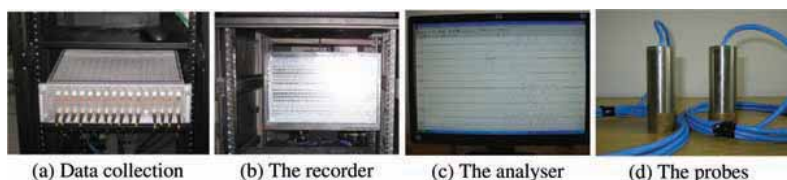
Figure 6. The microseismic monitoring system consists of the DLM-SOS data collection system, the recorder, the analyser and the demodulation measurement probes.

6 CONCLUSIONS

Designing the top layer of IoT for mines is an important measure taken by the State Administration of Work Safety for the overall development of China's mining industry. It is used to guide the sustainable and healthy development of the IoT technology and to ensure the efficient and safe production in mines. We need to fully understand the development status and the challenges of IoT for mines, and clarify the strategic development goals. Besides, we must accurately make the plans for the development of the key technologies, and formulate a clear roadmap of the development. The top layer design of IoT for mines is a good opportunity for cooperation. It points out the direction of the future development of IoT for mines. The demonstration project in Jiahe coal mine proves the feasibility and the effectiveness of the ideas of the top layer design.

REFERENCES

Aguilar, J., Jerez, M. & Rodríguez, T. 2018. CAMeOnto: Context awareness meta ontology modeling, *Applied Computing and Informatics*, 14(2):202–213.

Colakovic, A. & Hadzialic, M. 2018. Internet of Things (IoT): A review of enabling technologies, challenges, and open research issues. *Computer Networks*, 144: p. 17–39.

Ding, E. & Zhao Z. 2015. The current situation of IoT for mines and the development trend. *Industry and Mine Automation*, 41(5):1–5.

Han, J. 2016. The research on the key technologies for the construction of shenhua intelligent mine and the demonstration. *Journal of China Coal Society*, 41(12):3181–3189.

Hu, Q., Wu L. & Zhang, S. 2014. Deployment and energy consumption analysis of locating WSN in coal mining surface. *Journal of China University of Mining Technology*, 43(2):351–355.

Hu, Q., Zhang, S. & Wu, L. 2016. The localization of moving targets in the coal mine: challenges, current situation and trends. *Journal of China Coal Society*, 41(5):1059–1068.

Ramamurthy S.R. & Roy N. 2018. Recent trends in machine learning for human activity recognition—A survey. *WIREs Data Mining Knowl Discov*, e1254.

Yao, J., Ding, E. & Zhang, S. 2016. The vision of perception IoT for mines and developing trends. *Industry and Mine Automation*, 42(9):1–5.

Zhang, S., Ding, E. & Xu Z. 2010. The second talk on the IoT and perception mine—perception mine, digital mine and integrated automation of the mine. *Industry and Mine Automation*, 36(11):129–132.

Zhang, S. & Zhang, T. 2013. On the structural platform and service platform of mining material networking. *Industry and Mine Automation*, 39(1):34–38.

Emerging technology and synergies from other industries

Development of optimized processes in construction management supported by Building Information Modeling (BIM) with special focus on procurement: Case study at HOCHTIEF Polska

Klaus Boede
HOCHTIEF Polska S.A., Poland

ABSTRACT: Construction is struggling with innovation, which is mainly due to intense price competition and low margins. A next innovation wave seems to come with BIM. BIM, which stands for Building Information Modeling, is a method where the building is constructed digitally first, thereby occurring problems like mistakes in the design and clashes at the building site can be prevented. Further building sequences can be optimized, which, in consequence saves time and money. Besides technical implementation working with BIM is process driven, thereby standard processes on site for packaging and procurement, information management and works preparation must be developed and adopted by project staff to apply BIM technology as efficiently as possible. This paper describes the standard processes in construction and develops simplified adaptation of main processes for a large construction site in Poland.

1 INTRODUCTION

The construction Industry is one of the most important industries of today and has a great impact on the economy of any nation. In general, construction produces 5–10% of GDP in western countries. Any piece of building, infrastructure or real estate erected is undertaken by segments of the construction industry. However, as construction being a mature, highly competitive industry with limited scope for knowledge externalities it has a comparatively low level of investment in innovation. For instance, the productivity index of the production industry in Germany increased within the last 25 years substantially, whereas the construction industry remained almost without any productivity increases[1].

There is increasing pressure to become more innovative and deliver better value for money for clients. However, certain characteristics of the industry—e.g. low margins leaving less capital for innovation—appear to slow progress and make innovation difficult. Further, the combination of individual procurement of heterogeneous products by clients and increasing specialization and subcontracting (procuring) within the industry significantly limits the scope and potential for positive knowledge externalities, as argued by Dubois and Gadde (2002)[2]. At the same time the pressure on time and costs is substantially increasing, which can be seen in a strongly growing number of low cost offers and increasing importance of claim-management. To cope with this increasingly difficult environment good solutions are needed[3].

Literature research as well as practical experiences in the industry show that the construction industry seems to change radically. The change in technology delivers new opportunities to improve the execution of projects which become more and more complex. This is also valid for the environment in which the projects are performed. The growing density of requirements

---

1. Statistisches Bundesamt, Fachserie 18, Reihe 1.5, 2013.
2. Dubois, A. and Gadde, L.-E. (2002) The construction industry as a loosely coupled system: implications for productivity and innovation, Construction Management and Economics, 20, 621–631.
3. Swiss Association of Consulting Engineers (USIC), Nr. 22, 03.062016.

to sustainability leads to the circumstance that better quality needs to be performed on less space.

Under the key word "Industry 4.0" the construction industry is facing increased digitalization. Major innovation is seen with the introduction of BIM—Building Information Modelling. With this method a building will be fully geometrically visualized in a (virtual) 3D Computer model before construction and allowing all parameters to be retrieved for the execution phase from the model. The conventional 2D plans will subsequently be replaced. In addition, 4D models including construction scheduling, and 5D models with a full set of construction costing estimates will be able to generate significant benefits.

A holistic view to projects and processes is required to achieve full benefit of the desired innovation. This means that

- Digitalization in the construction industry leads to a comprehensive and integrated approach to projects and connected processes. Looking at life cycle cost becomes increasingly important. Design, procuring and execution is no longer seen as a separate service. Their leverage gains importance from planning over project realization to handover and operation.
- Needs drive change. The industrial construction industry is driven by the need to a sustainable Return on Investment (ROI), so in principle is owner driven.
- Planning and design is of the essence. The more we know and as early as possible and, in consequence, the more finite our investment strategies become the more we will demand predictable outcomes.
- Processes are in focus: Changes in Construction are influenced much less by what we could do (technology) by what we must do (process)[4].

2   IMPORTANCE OF WORK PACKAGING

One of the advantages offered by BIM to the construction industry is the capability to virtually plan and build a project before actual execution of work. BIM provides a completed model of final deliverables, offering visual foresight of access, site layout, crane staging, and various other construction sequencing challenges, enabling the formation of a more robust execution plan[5]. The adoption of BIM leads to an increase of design capabilities and the early definition of work packages which require additional specialist knowledge in the design teams. A work package is a suitable, i.e. manageable work unit with detailed outline of the partial (sub) construction projects in terms of scope, purpose and sequences. The package includes a budget that meets the budgetary limits set by the company or client and scheduled plan that includes material, workforce, machinery, equipment and partially further outsourced support. Finally, for each work packages tenders are obtained, and orders placed[6].

Numerous papers have been written on this topic. One simplified and straightforward method is presented by Geoff Ryan as "Advanced Work Packaging". This method integrates three multifaceted components of Work Packaging, Information Management and Work Preparation. Work Packaging and Work Preparation are overlapping processes, where Information Management is the interface between them. As a prerequisite, more attention must be given to the processes during execution to optimize the integration of the advanced (BIM) technology into the work processes on complex construction sites. Figure 1 shows the connection of the components.

4. "Even More Schedules for Sale/Advanced Work Packaging for Construction Pr." by G. Ryan, AuthorHouse 2017, P. 7.
5. https://www.workpackaging.org/single-post/2017/06/21/Using-Building-Information-Modeling-BIM-to-enhance-Work-Packaging-for-Piping.
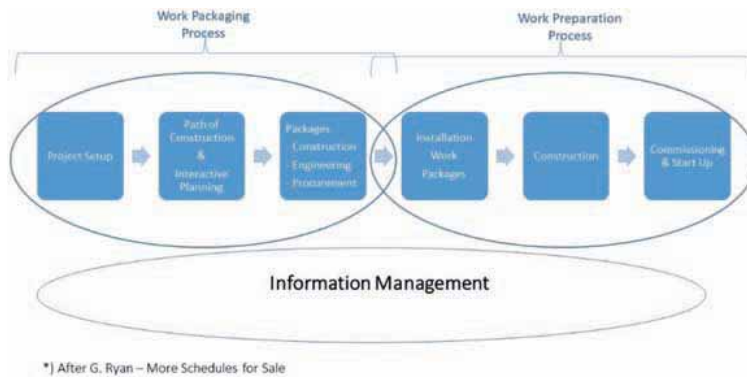6. https://www.designingbuildings.co.uk/wiki/Construction_work_packaging.

Figure 1. Work packaging, information management and work preparation[7].

The guiding principle is that we can significantly reduce our construction schedules, optimize our safety and quality performance, minimize cost and make construction projects predictable by being organized[8] in a more efficient way. This implies to plan as much as possible before starting the works on site, which is in practice very difficult to do. Often reasons for failed projects are lack of design and effort and usually not missing knowledge. In consequence, data and data management becomes the central element of this method.

3 THE PROCESS

Work packaging starts at project onset (generally at tendering), identifying suitable construction work packages in terms of scope, purpose and sequences and aligning them with engineering (scheduling, drawings, calculations, etc.) and procurement work packages (materials, deliveries, etc.)[9]. This populates the construction work packages with all the drawings and materials and gets them ready to be carved into installation work packages by the construction team[10]. In general, for a typical construction manager individual subcontractor work allocation is seen as package in present daily routines. On large complex projects Work Packaging should be supported by a packaging manager, who is charged with leading the department, creating the overall strategy and developing an overall culture of work packaging, taking the package "from cradle to grave".

The management of information is a strategy that addresses the matter of reliable and efficient flow of information between all project participants. Therefore, the target of the strategy is to design systems and interfaces that align the source data with the users. The desired outcome is to ensure that all the right people have access to the data they need, which is compatible with others project data and is formatted to be interoperable. As a result, all project participants should always have access to the data they require[11]. An information manager should be appointed to influence the development of rules and standards for information generation and exchange.

---

7. G. Ryan, p. 10.
8. G. Ryan, p. 2.
9. Construction Work Package (CWP) – A single discipline of a CWA that defines a logical division of construction work. Engineering Work Package (EWP) – An engineering deliverable, single discipline that contains all the engineering data required for a single Construction Work Package: Scope of Work, Drawings, Vendor Data, Bill of Materials and Specifications. Procurement Work Package (PWP) – A procurement deliverable, that contains all the materials required to satisfy a single CWP.
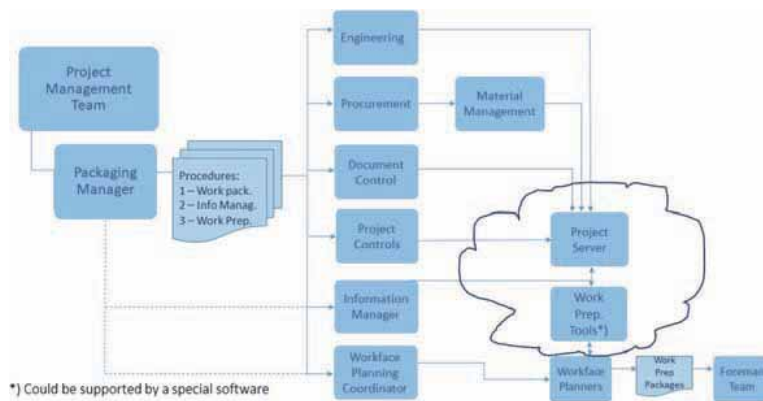10. G. Ryan, p. 14.
11. G. Ryan, p. 15.

Figure 2. Work packaging, information management and work preparation in a flow chart[12].

The workface is that geographic point on site where people implement materials into a building facility or plant, i.e. where the actual construction works are carried out. Work preparation is the process of identifying what the work force on site needs and what must be done to get the right material and right equipment in the right quantity and the right point of time to them. The works on site can be initiated by the appointment of a work preparation specialist at the start of detailed engineering design. Figure 2 describes the whole process in a flow chart.

4 PROCUREMENT AND SUBCONTRACTOR INVOLVEMENT

Procurement is an essential key process of strategic importance for a typical construction manager as around 80–85% of the annual turnover is directly procured in form of individual subcontracts or materials. Procurement needs constant attention to maintain company's profitability, bearing in mind that a construction company is a commodity business with comparably low profit margins. As an example, for a typical construction manager, HOCHTIEF Polska manages around 20 large projects with an average project size of approx. EUR 30 m, each project having an average of approx. 220 suppliers/subcontractors with about 465 concluded subcontracts/amendments.

The procurement process in construction is decentralized and complex. Buildings are constructed in remote places as a design construct service where individual work pieces (packages) are constructed or assembled. In turn, the general contractor sells individually priced commodities which are either manufactured on site or in fabrics. First pricing of the bid and later manufacturing or procuring the individual parts or services of a building is a complex, however standardized process.

Every savings made in procurement leads to a direct reduction of expenditure of the business and increases the profits. This directly impacts the quality of the purchasing process and the company's profits. As a result, consistent purchasing processes conducted in the extended interaction and networked with partnering units can guarantee the company's continued success.

If packages are carried out as own work the procurement team must identify all the materials and labor required for a specific Construction Work Package (CWP) as a unique package of works for themselves. This allows to manage fabrication and material purchases and to be on site at the required point of time. In parallel the engineering team establishes the Engineering Work Package with information like material matrix[13] and fabrication

---

12. After G. Ryan, p. 16.
13. Material matrix: As an extract from the Engineering Work Package (EWP) the material matrix shows a list of all materials required to construct the CWP, the organization responsible to procure the components, the Fabricator/Supplier and Required on Site (RAS) date (CWP Start Date).
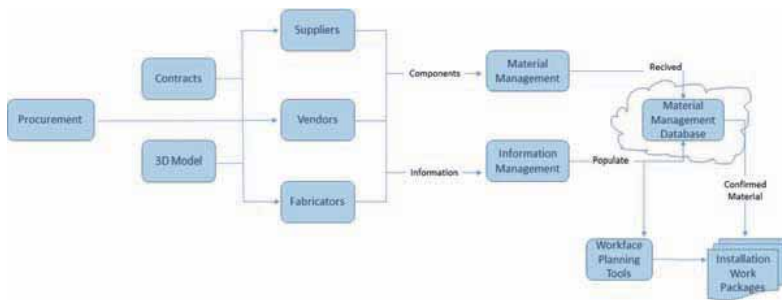
Figure 3. Procurement process.

drawings[14] to create a Procurement Work Package. In the next step the procurement team generates quantity take offs (QTO's) from the entire model, leading to an order of raw materials to site. A Procurement Work Package can also be allocated as a lumpsum package to subcontractors transferring all risks in relation to execution of the package to the engaged subcontractor.

Contents of a Procurement Work Package are in principle detailed specifications of requirements for suppliers and vendors consisting of

– Scope statement[15],
– Material Matrix,
– Fabrication Drawings and
– 3D Model.

To satisfy the data requirements for a fully attributed 3D model, the procurement team will need to establish contractual obligations for vendors, suppliers and fabricators to supply comprehensive data along with their products. Figure 3 shows a simplified chart of the procurement process[16].

This described holistic approach requires optimized involvement of subcontractors into the processes, which must be contractually secured. The subcontractors need to participate in general contractor sponsored work schedule coordination for design and execution of all works. The program starts before actual construction on site or in its initial phase and later shortly before installation of the specific works in a more detailed manner. In principle there are three variants procuring with BIM:

4.1 *Variant 1 – Standard tendering with quantities and BIM*

On the base of a BIM—planning model the Bill of Quantities (BoQ) will be established under consideration of partial lists/extracts from modelling as a base. The BIM BoQs differ from classical BoQs as they are more detailed. This can cause additional expenditure for the subcontractors, if they are not used to tender modules. The advantages for the general contractor is that he receives a module price and could "play" with the quantification derived from the data base accordingly. With this rather trivial kind of tendering the possibilities of BIM would be used rather rudimentary[17]. At present this variant works for all earth and raw construction works.

---

14. Fabrication drawings: A component of the EWP that is the complete list of equipment steel or pipe drawings that need to be fabricated for a single CWP.
15. Scope Statement: A description of the procurement scope and strategy for the acquisition of components and the fabrication of any kind of equipment, steel or pipe, along with the common delivery date.
16. After G. Ryan.
17. Projektmanagement im Hochbau, von Hans Sommer, Springer-Verlag Berlin Heidelberg, 2016, p. 152.

4.2 *Variant 2 – Modular tendering*

With this variant the tendering would take place as in Variant 1. In addition, the subcontractors receive a production and time orientated set of data with the offer. In this case the subcontractors should support the production planning to optimize the project. As a prerequisite the subcontractors need to have suitable BIM skills or need to procure the support of a BIM (planning) manager[18]. This variant could be applied for earth works and raw/structural construction works, but also partially for MEP works.

4.3 *Variant 3 – IPD (Integrated Project Delivery)*

With a planning- and optimization process under BIM involvement the available possibilities can be used best of all when all partners, i.e. all essential executive companies—are integrated at a very early stage into the process and maintain a high level of BIM skills and extensive knowledge of methodology and processes involved. This early and comprehensive involvement of the executing companies is called IPD and requires that the subcontractors receive a production and time orientated set of data with the offer as in Variant 2. The subcontractors should support the production planning to optimize the project supported by a capable BIM (planning) manager[19].

The biggest challenge for IPD is to allocate contracts for the execution of construction if the contents of the building works are not defined at all. It must be proven that the best value for money is maintained. A lot of trust for the client has to be built up for this variant, because a competitive situation is maintained only during the selection procedure. It has to be made sure that the best in the market is selected for a specific job. Therefore, great importance has to be given to the selection procedure under the direction of the project management. The trust of the client into the know—how, the experience and the integrity of the project manager has to be earned[20].

5   CASE STUDY AT HOCHTIEF POLSKA

HOCHTIEF Polska started to implement BIM by end of 2016 with initial staff training and development of general guidance for BIM use. In a next step BIM was piloted on a design & build project in Warsaw, followed by application for structural design in the Technical Office of the Warsaw Branch. These steps enabled to implement BIM as a pilot for project execution starting April 2018.

A suitable project was found with acquisition of Airport Traffic Control Centre in Poznan. The project comprises design & build of a two-story office building with basement, Gross Floor Area (GFA) 10.000 m². Structural construction, partly executed with prefabricated concrete elements and steel structures, all M&E works (without equipment and external services) and roads were included in the contract (lump sum EUR 20.5 m).

The client Polish Air Navigation Services Agency (Polska Agencja Żeglugi Powietrznej, PAZP) is responsible for functional description of the works, HOCHTIEF for full execution design.

The proposed project execution period of 19 months consists of:

- 8 months for successive preparation of complete execution design including
  - 3 months for building permit design preparation (including all required approvals) and 2 months for receiving of building permit
- 9 months for works execution (one shift per day anticipated)
- 3 months for take-over procedure and receiving of occupancy permit.

---

18. Ibid., p. 152.
19. Ibid., p. 152.
20. Ibid., p. 153.

During the main design phase between September and December 2018 weekly design meetings took place. HOCHTIEF and subcontractors developed 15 individual BIM Models for structural, architectural, ventilation (4 models, 1 each floor), electrical (2 models), plumbing, mechanical, tele techniques, gas piping, air conditioning (2 models), canalization, and heating. 11 models were based on REVIT software, 4 models for ventilation design were based on VENTPACK software featuring special duct design algorithms. VENTPACK models can be easily downloaded with REVIT and IFC (Industry Foundation Classes) formats.

HOCHTIEF coordinated the design meetings by synchronizing the models with BIM COLLAB software. In addition, the SOLIBRI Model checking software was applied. To save time, in parallel to the design works site preparation, excavation works, and piling were carried out. Design and coordination meetings will be continued with adequate frequency during execution phase.

During the design phase more than 250 design inconsistencies (classified as issues, faults, clashes, requests for information, enquiries, remarks and arrangements) could be identified and clarified. By end of December 2018 the client received a full set of 2D drawings and the contractually agreed MEP Model components for approval. In parallel the structural model was further developed for Quantity Take Off's (QTO's) for site excavations, animation of sequencing for concrete works, checks for completeness and QTO's of slabs, modeling of external roads, sidewalks and parking places. In addition, responsible subcontractors developed their schedules for MEP works.

5.1 *Main experiences gained from the project*

Work Breakdown Structure (WBS): Important for a frictionless information flow is the formation of a uniform nomenclature starting with a Work Breakdown Structure (WBS), which is a hierarchical representation of a complete project (based on work). The WBS forms a direct alignment between work, time and cost by serving as the basis for work packaging, procurement, schedule development, work preparation and cost accounting[21]. The information can be collected and shared under the same numbering/headings. As a result, a standardized WBS is seen as a prerequisite for optimized site processes. On the PAZP project the numbering system focused solely on BIM elements without further synchronizing cost control, procurement, scheduling etc. In consequence, development of a uniform meaningful numbering system is seen as a comprehensive task involving several departments/functions and should be developed soon.

Procurement: Quantities and specifications for ground works and structural works (foundation, slabs, etc.) could be partially determined based on a simplified initial BIM Model. Tender calculations were based on received subcontractor offers and on prices achieved on currently executed similar projects. Advanced key subcontractors like all M&E works, façades, steel structure, etc. had to be procured before execution design was complete. For these works a standardized package approach was chosen to minimize exposure to claims. Letters of Intent were signed for M&E works (43% of CV) with selected subcontractors. Final contracts were concluded lump summed based on "back to back" contract conditions.

SharePoint: Implementation of a uniform share point system for frictionless sharing of all necessary information between all project parties is a critical issue. Adequate access rights to be developed to protect sensitive information.

Scheduling: General practice at HOCHTIEF Polska is to prepare project execution schedules for tendering, for the contract, and before execution of works with special information on procurement and design. Regular updates of schedules during execution are carried out monthly in line with standard project reporting obligations. On this project proper schedule update procedures in conjunction with the BIM model are to be further developed during the execution phase.

---

21. The different levels of WBS are recorded in a WBS library, defined with (among others) Plan, Construction Work Area, CWP, EWP, PWP, MWP (Module Work Package), IWP (Installation Work Package).
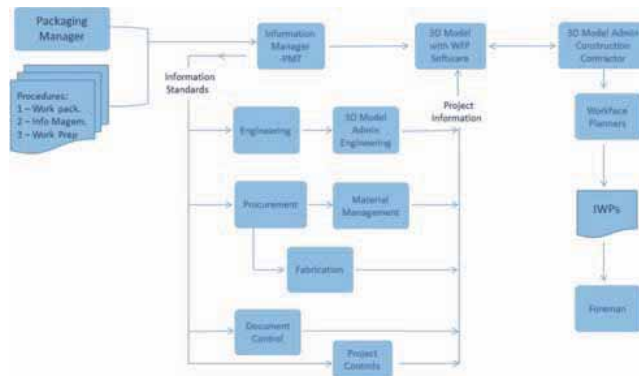
Figure 4. Information management[22].

Shifting of Tasks and Responsibilities: Tasks and responsibilities of team members change with use of BIM and specials roles must be defined. In consequence, an appropriate set of project job descriptions are to be defined before and during project execution.

Development of Standard Procedures: With BIM a digital twin of the projects with the expectations of substantial productivity gains for planning, design and execution of the project can be created. However, working with BIM is process driven. A target for this project was to develop a set of standard processes based on existing work procedures and as close to standard daily routines as possible, adopting or tailoring them carefully to BIM requirements. At first three simplified standardized procedures were developed for Work Packaging, Information Management, and Work Preparation.

Procedure 1 – Work Packaging contains a definition of the Work Breakdown Structure, definition of packages, works scheduling and procurement regulations. Further, tasks and responsibilities of the project management team are defined.

Procedure 2 – Information Management contains Data/Nomenclature, Information Storage/Processes, Data Exchange conventions (SharePoint/document control)/formats and further details for job descriptions for Information Manager/3 D Modeler/Cost Controller. A general process description is presented in Figure 4.

Procedure 3 – Work Preparation contains definitions and scope of the installation work package. This includes regular updates of schedules (weekly/monthly plan), including delivery schedule of subcontractor works and materials, constraint management and performance measurement.

6 CONCLUSIONS

6.1 *Case study*

- The implementation of BIM at HOCHTIEF Polska is expected to improve efficiency in daily construction management practice. However, widespread and comprehensive implementation needs to be accelerated.
- In the case study standard patterns and processes for efficient operational use of BIM could be developed and imbedded into practical project execution.
- Key requirement for successful BIM adaptation in construction is the introduction of standardized easy to use processes for packaging, information management and work preparation as close to common construction environment as possible to guarantee comprehensive BIM use on site and to achieve desired efficiency gains. In addition, the proc-

22. https://insight-awp.com/wp-content/uploads/2017/10/2.0-Information-Management-Procedure-Insight-AWP-2017.pdf.

esses must be built into daily work routines, to use them in a rather intuitive manner to avoid previously used "conventional" work patterns.

- Standard processes and templates developed in the case study can be used for further roll out, trainings, acquisition, and for public relation.
- Full roll out time is estimated with 2–3 years. This time frame is needed for further improvement/refinement of processes, trainings and necessary standardization.
- For efficient use of BIM, it is very important to define which information in what quality and format must be available to make decisions based on secured information and proper risk assessment. No more information as necessary should be generated.
- Substantial efficiency gains in design are observed using BIM compared to conventional 2D design. However, efficiency loss during implementation phase must be considered.
- Management involved gains easy access to technical data through central data management and data exchange platforms.

6.2   *Main benefits of BIM are summarized as follows*

- Main arguments for the implementation of BIM are avoidance of planning and execution mistakes (collision or clash identification, detection of omissions and their proper management.
- Generation of 3D MEP plans during execution can create efficiency gains during implementation of work packages on site.
- Improved sequencing through visualization during execution for all packages can lead to shorter project execution.
- Improved procurement with better specifications and accurate QTO's for procurement packages can generate substantial cost reductions.
- Overall performance/progress control for project and, in detail, improved control of subcontractor works during project execution in terms of completeness, time and quality.

6.3   *Most important internal and external constrains for BIM implementation are*

Internal

- Construction project execution is a complex and interdisciplinary management task, coordinated by senior and well experienced site managers. Construction is based on extensive personnel experience; generally new working methods are only adopted if the managers feel that it works, i.e. they do not like "experiments with unknown outcomes". The reluctance to change is based on experience that any disruption of the construction process can cause project failure. In consequence, existing and experience-based project management processes and tools must be adopted and tailored for efficient BIM application on sites.
- Construction is a low margin business, which makes it difficult to bear the cost for implementation of BIM by management contractors, unless the client pays for it.
- In many cases there are insufficient IT and BIM skills available (quality of personnel and high costs associated). Especially subcontractors and partially external designers are lacking suitable IT skills.

External

- Generally, a kind of "container based" work environment rules on construction sites. Every project participant is owner of their (own) data. Implementation of BIM will change this practice and force information exchange with improved cooperation.
- Architects/designers complain that BIM bears high cost for them. In addition, more planning and design work must be carried out in earlier project phases, which is often not paid due to fixed and phase-based remuneration concepts for planners and architects[23].
- There is a lack of guiding legislation to adopt BIM for public and private projects in Poland.

---

23. Example: HOAI—Remuneration guideline for Architects and Engineers in Germany.

- Common general business environment in construction causes a strong segregation of architects/designers and contractors for planning and execution.
- In some cases, architects/owners are hesitant to share their knowledge and rather protect their "ruling knowledge". This goes in line with copyright issues.
- Common and appropriate levels of detail for model set up must be developed and agreed.

6.4 *Way forward with BIM*

- BIM should be understood as a part of a comprehensive digitalization strategy in construction and should be seen as an important management tasks.
- General approach of large contractors is to handle design and BIM management themselves. They are developing strategic BIM-Management capabilities in their companies and have a strong desire to connect with BIM experts and partners in design and planning offices. In turn, large construction management companies will develop further competitive advantage.
- Principle rule is first planning and design followed by construct: This should not be valid only for large projects but for all construction projects.
- For every project a BIM-project execution plan needs to be developed, defining the requirements for cooperation and workflow (could be attached to contracts).
- BIM changes work culture in construction, requiring different contract models, solutions like partnering or alliancing can be adopted, which are partially used in Anglo American countries.
- The value chain will change radically. Owners/developers, planners, general contractors and suppliers/manufacturers will experience substantial change of rolls and with different task profiles. Possible are direct links to manufacturers with different improved design capabilities.
- Main elements for any successful digitization strategy must contain[24]:
- Renewal of organizational structure with flat hierarchies and interdisciplinary cooperation throughout the company. The employees must be heard and included in the reforms, i.e. BIM partially needs to come from bottom up as an evolutionary approach. The specialist staff working with BIM drives the process to a vast extent.
  - Creation of separate innovation units to develop new ideas in a "protected space".
  - "Trial and error" instead of perfectionism must be allowed.
  - Digitization requires strong partnering concepts.
  - Keeping the contact with the client, demonstrate the increase of service quality for the customer.
  - "Digital innovation yes, but not digital only", meaning that the traditional structures should not be destroyed—because digitization works best if both worlds, the old and the new way of business dealings, can coexist.

---

24. Handelsblatt, 19.11.2018.

Development of a low-cost Proximity Warning System for mine equipment using smartphone and bluetooth beacons

J. Baek & Y. Choi

Department of Energy Resources Engineering, Pukyong National University, Busan, Korea

ABSTRACT: This study developed a low-cost Proximity Warning System (PWS) that can be used to prevent collisions in underground mines or road tunnels. The PWS receives signals from Bluetooth beacons attached to mine workers and equipment via smartphones mounted in vehicles and provides the drivers with a primary (caution) alert and a secondary (warning) alert in stages according to the intensity of the signal. After identifying suitable RSSI threshold values for the caution and warning zones based on the results of a preliminary experiment, a field test was conducted in an underground tunnel. From the results of 50 experiment repetitions, the accuracies of the first and second alert occurrences in the caution zone and warning zone were found to be 93% and 95%, respectively. The Bluetooth beacon–based PWS can be used effectively in mine safety management because it is relatively inexpensive, its functions can be easily extended using the smartphone application.

1   INTRODUCTION

Collisions not only between pieces of equipment but also between equipment and mine workers frequently occur inside underground mines, which are narrow and dark (CDC 2019a). According to mine disaster statistics issued by the Centers for Disease Control and Prevention (CDC), accidents involving mining equipment inside underground mining sites in the United States have accounted for 37 deaths since 1984, and 16 workers have been killed in crashes involving shuttle cars and buckets between 2000 and 2010 (CDC 2019b). Moreover, nearly 47% of all deaths that have occurred in underground mines between 2011 and 2015 have been caused by collisions between equipment and workers (CDC 2019c).

To prevent the occurrence of said collisions between pieces of equipment as well as between equipment and workers inside underground mines, proximity warning systems (PWSs) involving the use of electromagnetic- or magnetic-field sensors have been developed and used in the past (Schiffbauer 2002). A PWS provides collision risk warnings when workers and equipment come within a certain distance of each other (Ruff 2019). The National Institute for Occupational Safety and Health (NIOSH) in the United States has performed numerous studies concerning the development of PWSs using radio-frequency identification (RFID) technology and magnetic-field sensors for mining sites (Ruff 2000, Ruff 2001a, Ruff 2001b, Schiffbauer 2002).

Recently, attempts have been made to develop PWSs using Bluetooth low energy (BLE), which corresponds to Bluetooth 4.0 wireless communication technology. Based on the IEEE 802.15.1 communication standard corresponding to the 2.4-GHz frequency band, the use of BLE serves to reduce power consumption as well as packet size, thereby enabling faster data transmission (Jung & Choi 2017, Baek et al. 2018).

The purpose of this study was to develop a low-cost proximity warning system for mine equipment using smartphone and Bluetooth beacons for use in underground mines. A smartphone application that provided drivers with progressive collision-risk alarms based on the status of a received signal strength indicator (RSSI) was developed. The said alarms were issued after the receipt of signals—transmitted by Bluetooth beacons attached to workers and equipment inside an underground mine—by a smartphone mounted on a moving

equipment. This paper describes the development of the proposed system along with the presentation of results obtained during field tests performed inside an underground tunnel.

2 DESIGN OF PROPOSED PROXIMITY WARNING SYSTEM

As already mentioned, the proposed PWS system received signals from Bluetooth beacons and provided drivers with progressive collision alerts (Figure 1). Inside an underground mine, Bluetooth beacons were installed on the safety helmets of workers, the rears of vehicles, and at potentially dangerous locations. In addition, "caution" and "warning" zones, wherein the first and second alerts, respectively, are to be provided, were defined along the direction of motion of a vehicle equipped with a smartphone. Signals transmitted from pedestrian workers, the preceding vehicle, and Bluetooth beacons installed at dangerous locations were received by the smartphone mounted on the vehicle so that the primary (caution) and secondary (warning) alerts could be provided to the driver progressively, in accordance with corresponding RSSI values.

2.1 Design of BLE transmitter units using bluetooth beacons

The transmission characteristics of Bluetooth beacons may vary depending on their orientation Installation. Signals propagating to the front and back of the beacon exhibit directionality, whereas those propagating to the side exhibit omnidirectionality. The proposed PWS was designed to use omnidirectional signals generated from the sides of beacons, accomplished by attaching Bluetooth beacons in a horizontal orientation.

The Bluetooth beacons were installed on a worker's helmet, on the back of a vehicle, and at a potentially hazardous location. Bluetooth beacons attached to workers' helmets help drivers recognize workers approaching the caution and warning zones, even in dark workspaces, thereby preventing collisions. Inside underground tunnels, where vehicles move linearly along a fixed path, Bluetooth beacons can be installed on the rear of each vehicle, with a smartphone installed at the front to prevent collisions between vehicles.

2.2 Design of BLE receiver units using smartphones

The smartphone application for the PWS was developed using the MIT App Inventor to work on the Android operating system. The database stores media access control (MAC)
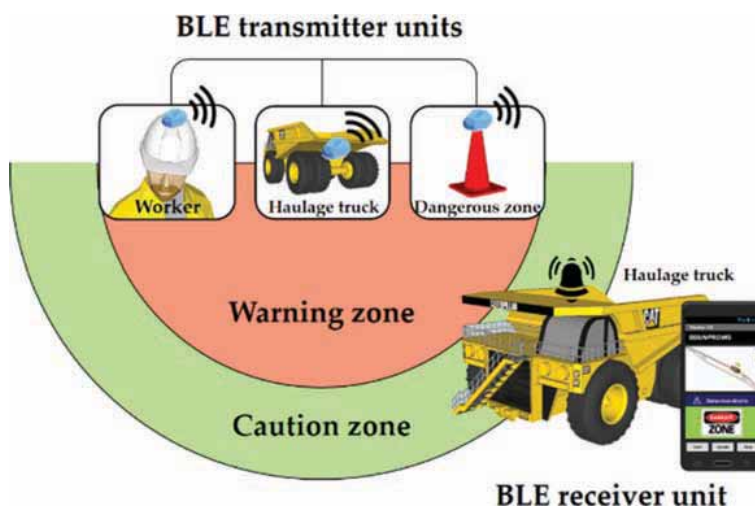

Figure 1. Conceptual diagram depicting Bluetooth Low Energy (BLE) transmitter and receiver units of the proposed low-cost Bluetooth beacon-based proximity warning system.

addresses of all Bluetooth beacons installed inside the underground mine, as well as alert images corresponding to each beacon.

PWS separately manages information pertaining to Bluetooth navigation beacons for identifying current locations of equipment mounted with a smartphone, along with information concerning Bluetooth PWS beacons for detecting the approach of workers and other equipment.

When a smartphone receives a signal from a PWS beacon, the primary/caution and/or secondary/warning alert images are displayed based on the RSSI value. In other words, a primary/caution alert is issued if the PWS beacon's signal strength exceeds the RSSI threshold for the caution zone. Likewise, a secondary/warning alert is issued if the said signal strength exceeds the RSSI threshold for the warning zone. Users can manually set RSSI thresholds for the caution and warning zones based on the characteristics of the workplace.

3 FIELD EXPERIMENT METHOD

The in-field applicability of the PWS was evaluated via experiments performed inside the Yeonhwa underground tunnel (35°12′55″N, 129°13′20″E) located in Gijang-gun, Busan, Korea. Nine Bluetooth navigation beacons were installed on tunnel walls at 20 m intervals, starting from the point of entry into the underground tunnel (0 m) up to 160 m. In addition, Bluetooth PWS beacons were attached to the safety helmets of pedestrian workers as well as to the rear of vehicles, as depicted in Figure 2.

To configure the application so that it would issue corresponding alerts when the caution and warning zones were located approximately 20 m and 10 m away from transmitting beacons, respectively, signals were received for five minutes from locations 10 m and 20 m away from Bluetooth beacons, and the corresponding RSSI value distributions were analyzed (Table 1). Because the purpose of the PWS was to prevent collisions inside underground tunnels, the RSSI thresholds for the caution and warning zones were set conservatively, with the set values representing a 5% cumulative percentage. Thus, the set threshold values equaled −99 dBm and −91 dBm for the caution and warning zones, respectively.
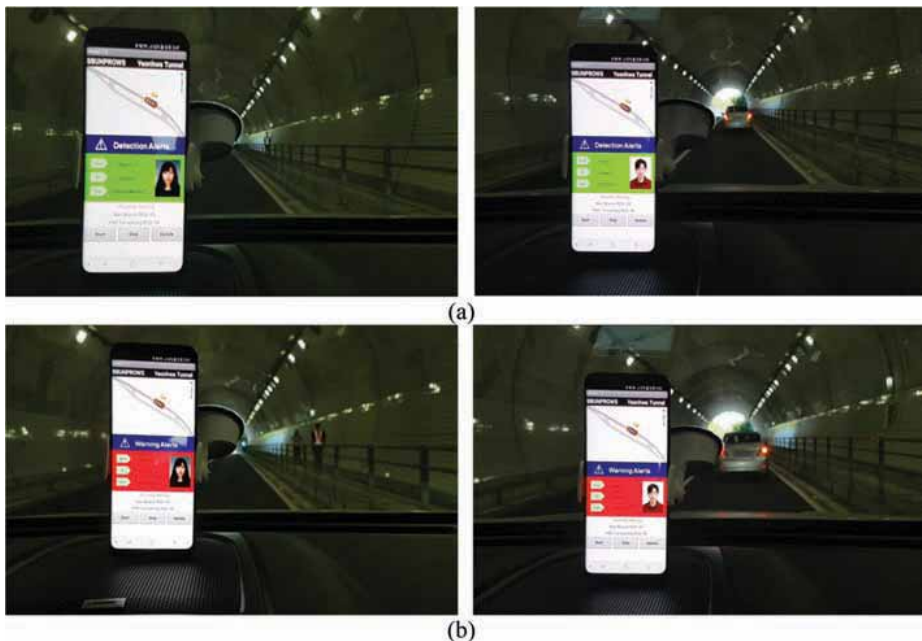

Figure 2. Results of filed experiments, the smartphone application displayed (a) primary/caution alert and (b) secondary/warning alert ahead of a worker (left images) and a passing vehicle (right images).

717

Table 1. Results of the statistical analysis of RSSI distributions.

Transmitted power (dBm)	Range (m)	Statistics (dBm)						
		Max	Min	Mode	Mean	First quartile	Second quartile	Third quartile
4	10	−76	−95	−81	−83	−84	−82	−81
	20	−85	−100	−98	−96	−99	−97	−94

Table 2. Accuracy assessment of alerts issued by the smartphone application.

Type of alert	Primary/Caution alert	Secondary/Warning alert
No. of trials	50	50
No. of true positives	50	50
No. of true negatives	43	45
No. of false positives	7	5
No. of false negatives	0	0
Accuracy (%)	93	95
Recall	1	1

4 RESULTS

Figure 2 depicts how the smartphone application performed on a smartphone-mounted vehicle when a worker wearing a PWS-beacon-mounted helmet was located in the study site along with a preceding vehicle. Until the worker entered the caution (20 m) or warning (10 m) zones near the vehicle, only the navigation image with vehicle position inside the tunnel was displayed on the smartphone screen. As the vehicle moved further and the worker entered the caution zone, a primary/caution alert was issued to the driver. Likewise, as the worker approached the warning zone, a secondary/warning alert was issued. It was also confirmed that when two vehicles approached each other, both primary/caution and secondary/warning alerts were issued to the driver in steps, based on the degree of proximity.

To analyze the accuracy of alerts issued to the driver by the smartphone application, the above experiment was repeated 50 times for the case in which a vehicle approached a pedestrian worker. Lengths of the caution and warning buffer zones were set in the range of 20–30 m and 10–20 m, respectively, ahead of the vehicle along its direction of motion.

During the 50 repetitions of the above-described experiment, 50 true-positive primary and secondary alert scenarios were observed, whereas the number of false positives equaled 7 and 5 with regard to issuance of primary and secondary alerts, respectively. Zero false negatives were observed. The above results are summarized in Table 2. In accordance with these results, the observed accuracy of the proposed smartphone application with regard to the issuance of primary/caution and secondary/warning equaled 93% and 95%, respectively.

5 CONCLUSIONS

The proposed study reports the development of a low-cost proximity warning system capable of receiving signals from Bluetooth beacons installed on the bodies of pedestrian workers, equipment, and at dangerous locations inside underground mines, which provide potential collision-risk alerts based on RSSI values of signals received. Field experiments were performed using the proposed PWS inside an underground tunnel in Busan, Korea. The results of said experiments demonstrate that when a pedestrian worker or vehicle installed with a Bluetooth beacon enters a caution or warning zone, the extent of which typically starts from 20 m and

10 m upstream of the vehicle, respectively, the system successfully issues primary (caution) and secondary (warning) alerts to drivers. Furthermore, the said experiment was repeated 50 times, thereby demonstrating that the accuracy of issuance of the primary and secondary alerts corresponding to entry into the caution and warning zones equaled 93% and 95%, respectively.

The proposed Bluetooth-beacon-based PWS possesses the following advantages over the existing PWSs employed in underground tunnels:

1. Bluetooth beacons that transmit BLE signals do not require an external power source, because they receive power from a coin battery. Therefore, no additional infrastructure is required for supplying power to underground mines.
2. The system is cost competitive because Bluetooth beacons are inexpensive, and there is no need to set up a separate signal reception terminal, since smartphones are used as receptors.
3. Existing systems necessitate the installation of large and heavy antennas as part of production equipment and mining structures for installing wireless signal transmitters. However, Bluetooth beacons, being small and lightweight, can be easily installed anywhere inside underground mines. In addition, Bluetooth beacons are made of sturdy materials and are less vulnerable to humidity; this makes them especially suitable for use in underground mining sites.
4. The proposed PWS system can be extended by adding new functions using the Bluetooth beacon software development kit (SDK) and Android application programming interface (API).
5. The smartphone application can be shared as open source. Therefore, it is expected that the proposed Bluetooth-beacon-based PWS can effectively be introduced at low cost for use in underground tunnels and safety management.

Although the proposed smartphone application has been successfully tested for use in underground tunnels, the results obtained do not guarantee that it can be reliably used in underground mines. This is because operating conditions in underground mines are significantly different from those in underground tunnels. Therefore, further experimental research must be performed concerning the use of the PWS in underground mines.

REFERENCES

Baek, J., Choi, Y., Lee, C. & Jung, J. 2018. Performance Comparison of Bluetooth Beacon and Reverse RFID Systems as Potential Tools for Measuring Truck Travel Time on Open-pit Mines: A Simulation Experiment. *Geosystem Engineering* 21(1): 43–52.
CDC. 2019a. Number and Rate of Occupational Mining Fatalities at Underground Work Locations by Year, 2006–2015. Available from: https://www.cdc.gov/niosh/mining/UserFiles/statistics/15g09uaa.svg. [Accessed 21 January 2019].
CDC. 2019b. Mining Topic: Proximity Detection. Available from: https://www.cdc.gov/niosh/mining/topics/ProximityDetection.html. [Accessed 21 January 2019].
CDC. 2019c. Number and Percentage of Occupational Fatalities by Accident Class Underground Mining Locations, 2011–2015. Available from: https://www.cdc.gov/niosh/mining/UserFiles/statistics/15g06uaa.svg. [Accessed 21 January 2019].
Jung, J. & Choi, Y. 2017. Measuring Transport Time of Mine Equipment in and Underground Mine Using a Bluetooth Beacon System. *Minerals* 7(1): 1–10.
Ruff, T.M. 2000. *Test Results of Collision Warning Systems for Surface Mining Dump Trucks.* National Institute for Occupational Safety and Health (NIOSH). Report Number: 9652.
Ruff, T.M. 2001a. Application of Radio-frequency Identification Systems to Collision Avoidance in Metal/nonmetal Mines. *IEEE Transactions on Industry Applications* 37(1): 112–116.
Ruff, T.M. 2001b. *Test Results of Collision Warning Systems on Off-Highway Dump Trucks: Phase 2.* National Institute for Occupational Safety and Health (NIOSH). Report Number: 9654.
Ruff, T.M. 2019. Overview of Proximity Warning Technology and Approaches. Available from: https://www.cdc.gov/niosh/mining/userfiles/workshops/proximityworkshop2010/ruff-niosh-pdworkshop2010-508.pdf. [Accessed 21 January 2019].
Schiffbauer, W.H. 2002. An Active Proximity Warning System for Surface and Underground Mining Applications. *Mining Engineering* 54(12): 40–48.

Version control system applied to resource modeling projects

C.Z. da Silva, Á.L. Rodrigues, J.F.C.L. Costa, J.L. Alves & A.M. Amaral
Universidade Federal do Rio Grande do Sul, Porto Alegre, Brazil

ABSTRACT: Resource modeling projects generally are performed by a team and involve many stages in which several different documents are generated. To better efficiency and productivity there is the need to organize and track all the modifications made by the team on the project as they happen. To track all the changes in real time can be challenging. The solution proposed is the use of a version control system, which is the management of changes made to a collection of information, such as documents and computer programs. The version control system use is well established in software development. So, in a versioning system all the modification history of the files generated by different people on the team are saved for a later analysis of the chronological development of the project. Also, the version control system provides metrics such as number of files added by each user and amount of modifications made on each document to determine the contribution of each team member during the project progress. An experiment was performed using a *Git* platform to manage a resource modeling project executed by a group of students to verify the quality control and efficacy of the version control system applied to resource modeling projects. All the metrics available are used to evaluate the performance of each team member. Additionally, the project manager can examine, accept and reject all modifications made as they occur in real time, permitting a better control of information for further report.

1 INTRODUCTION

Resource modeling is a complex procedure and involves several different stages, from the sampling process to resource classification. In practice, each phase in a resource modeling project is carried out by a distinct group of people, specialized in a certain step of the process. At the end, all products brought out by each team form the final model presented to the client. Mining/oil projects produce a large number digital data, such as parameter files, digital models, staff reports and so on. The larger the project, the more files are created and edited and more people are working on the same files. One can easily imagine that without a proper method to track all changes made in each file may lead to confusion, errors and delays. Therefore, in major organizations, document management plays an essential role. For that reason, an appropriate methodology of storage and availability of these documents, is of the uppermost importance. A company can make every stage of development of a team's task available throughout its structure. Monitoring all documents through a system that provides essential information on project progress, reports changes and status of the designated programs. A rudimentary method of collaborative work is the transmission of a document by physical or electronic media, such as e-mail (Figure 1). In this scenario, the first user creates the document and transfers it to another user who in turn adds data and passes it on to another user. This is a case of a document where collaboration is performed in a serial way, meaning each user edits the document at a given time. The problems associated with this approach are that it is not possible to automatically track the latest version, leading to confusion among team members. Also, documents with multiple authors cannot be modified simultaneously. This method can be slightly evolved using a file server, such as *Dropbox*™ or *Google Drive*™. In this type of server the files are stored in a place of general knowledge. However, the issue of simultaneous editing will not yet be considered. For example, user A

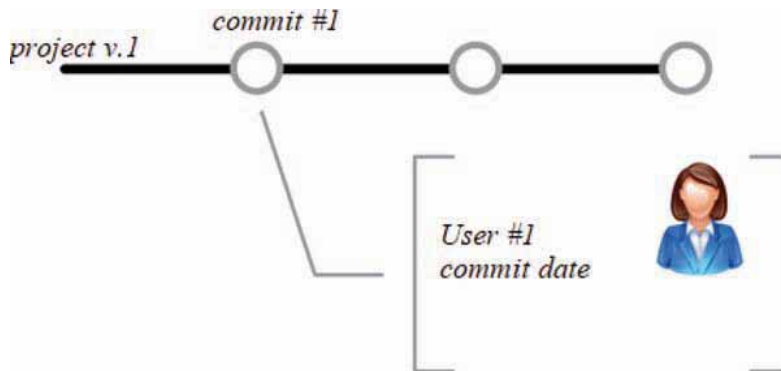Figure 1.   Collaboration through a serial manner.

Figure 2.   Project evolution through users insertions called *commit*.

opens the file located on the server. While the file is edit by user A, a user B also downloads the same document located on the server. Now, user A saves the modified file and uploads it to the file server. When user B saves its version of the file, the work performed by user A will be discarded, because user B opened the document at a time when there were no changes made by user A. The scenarios shown indicate that a strategic file or document must be integrated with a tool that makes the document easily available to employees and at the same time allows the submission of modifications in a non-serial way.

1.1   *Versioning Control System (VCS)*

In computer science the need for a logical way to control modifications made to documents is extremely important, therefore, the most complex versioning systems are those used by software's developers, where people may edit files concurrently. A file versioning system is a repository in which modifications are tracked (in the sense of being cataloged) (O' Sullivan and Bryan, 2009). But, there is still a hierarchy of permissions, for example, the project manager may accept or reject a modification made by a user, and, may even choose who can read the content of the project. Revision control systems manage all changes made on a set of data (files) over time, capable of tracking a complex structure of data, including binary files. In VCS generally the data is stored on a server or *repository* which is accessible to all users. When a modification is needed the user may *check out* the data from the repository, creating a *working copy* for the user. This avoids the changes to immediately affect the project. Only when all changes are made, the user uploads the updated file version to the repository. The uploaded version creates a *commit* on the project. This commit may be kept, rejected or even merged with commits of other users. Examples of projects that use a versioning system are: Linux kernel (www.kernel.org) and Wikipedia (www.wikipedia.org). As the project evolves according to the addition of commits, all modifications will be registered along with the user identification, date of submission and a line of information written by the user explaining briefly what was modified (Figure 2).

721

The interaction of a user with the system is through synchronization of data to update the project (Figure 3). As seen in Figure 3, the system operation begins with a synchronization of the project files with the server. Then, the user performs his work with a parameter file for a given task, for example, exploratory data analysis, variography, kriging (Matheron, 1963), simulation (Verly, 1983; Isaaks, 1990), etc. When the user decides that the parameter file is able to be integrated into the project and be used by other team members, the user inserts a commit.

Also, the project manager is responsible for administering the repository, by granting permissions to specific users to read and write on project data, create branches (with different tasks or copies of the entire project) in order to test out different solutions to eventual problems. Also, the manager can merge a branch to the main project (Figure 4), accept and reject commits inserted by the team (Figure 5), evaluate the appropriate models and solutions
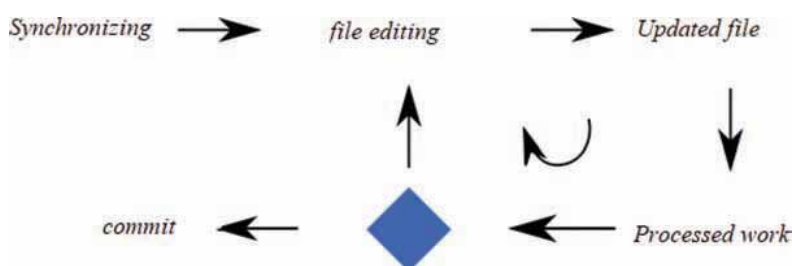
Figure 3.   User's interaction with the VCS platform.
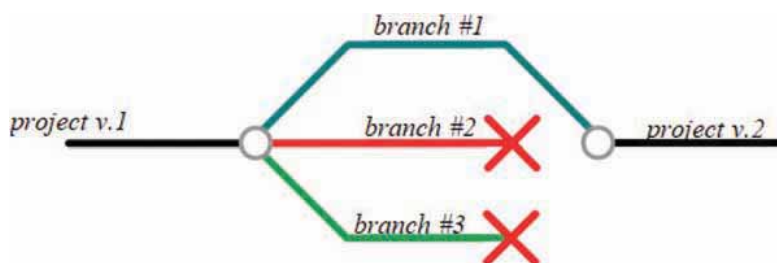
Figure 4.   Creation of different branches and subsequent annexation of the best solution to the project.
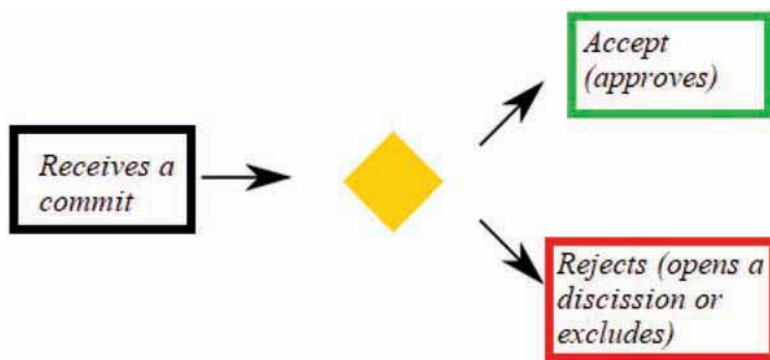
Figure 5.   Commit analysis performed by the project manager. A commit can be accepted or rejected, a rejection can be the source of a discussion with the commit creator in order to be accepted the next time.
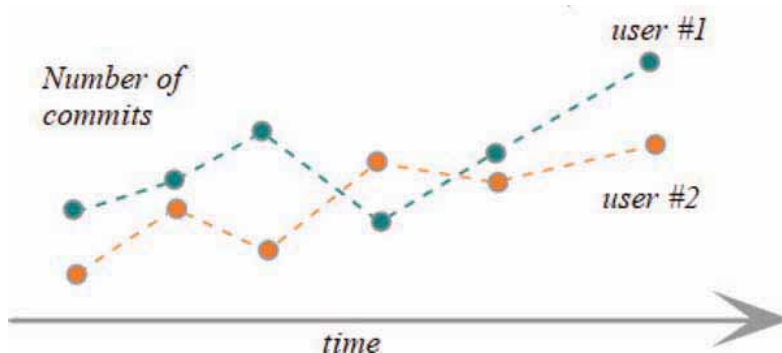
Figure 6. Index of accepted and rejected commits of users 1 and 2.

developed as the project evolved. An important aspect of VCS is the possibility of returning to a former version of the data in project, therefore, all decisions may be reviewed at later time.

Another feature of VCS is the opportunity to create productivity reports. Since a track record of commits generated is retained by the system, this information may be used to access each user's performance throughout the project, which supports decisions and project directions. Some examples of reports are: number of commits per user in a time frame (Figure 6).

2 METHODOLOGY

The project was developed on a git repository, which consists in a folder that contains all the repository data. The folder can be navigated as in any usual computer folder, but to switch between branches and other facilities on the platform, one must run the git command tool. The repository process to generate figures and results is summarized in three stages:

1. In the first stage a pre-processing of the repository is performed. At this point, a clone of the repository where all binaries files are extracted and the corresponding histories deleted;
2. The second stage consists in processing the repository (using a python script). In this stage all commits are examined and the metadata information put in a database. This stage is required to create custom fields necessary for the project's specification;
3. The third stage is to scan the database generated, so one may compute the desired statistics and create the final results in form of figures.

A test run of VCS was performed within the Laboratório de Pesquisa Mineral e Planejmaneto Mineiro (LPM) at Universidade Federal do Rio Grande do Sul (UFRGS) to evaluate its applicability in the mining industry environment.

The experimental use of VCS involved two graduate students who are in the initial period of their masters. These two students had an assignment relative to a course of the masters program, that should be developed together by both. The given assignment emulates a resource evaluation project, in which the two students are to elaborate, as a team, through the VCS platform. The test run involves part of the protocol of a resource evaluation project. Specifically, the phases of exploratory data analysis, spatial continuity analysis, the generation of a simulated grade model and the validation of the built model. The students project covered a manifold of exercises, each on different simulation methodologies. To perform each and every one of the project tasks the students used typical geostatistical software, such as: GsLib (Deutsch and Journel, 1998) and Ar2tech's software Ar2 gems®. Also, as the project evolved, both students should update a text report of each task concluded. The files referring to the project should be committed to the VCS platform. This way, the course teacher is able to verify, demand corrections and approve models as they were generated. On top of that, the teacher can also obtain an *on fly* a report of each student's performance throughout the project.

2.1 *The students project*

As mentioned previously, the project developed by the students is relative to a graduate's course from the masters program at the mining engineering department at UFRGS. Throughout the course the students are presented several simulation methodologies used in resource evaluation. From this set of methodologies, three are picked out to be handed as an exercise at the end of the course for grading purposes. In this case the methodologies which should be included on the final report were:

- Sequential Gaussian Simulation (Isaaks, 1990);
- Sequential indicator simulation (continuous variable) (Goovaerts, 1997; Seifert and Jensen, 1999);
- Sequential indicator simulation (categorical variable) (Goovaerts, 1997).

To apply such methodologies on any data set, it is common practice to perform exploratory data analysis, variogram modeling, sample search strategy definition and the validation process.

The students were assigned each one a different simulation approach to use, and one that should be performed concurrently between them. Every step of the simulation process should be *checked in* or committed to the VCS platform for evaluation and progress control.

There were two students involved in the project's development. They will be addressed in this paper as user 1 and user 2.

2.2 *GitHub*

The platform chosen as a VCS was the GitHub™ platform, which is a hosting system widely used amongst programmers that allows for any remote contributor (anywhere in the world) to make changes, add and review files from a project. Through GitHub™ is also possible to access the amount of total commits inserted on the project by each user and the total amount of changes made on the project and its different branches (created and merged) throughout time (Figure 7).

2.3 *Metrics*

The chosen metrics are the key element to track and evaluate a project. The metrics are divided by its information source:

- Information from the commit itself. It includes hash unique code, branch, author, committer, date of creation, date of commit, insertions and deletions;
- Information inserted by an external agent. This agent may be the project's manager or a supervisor. The information is retrieved from the above mentioned custom metrics. In this study the custom metrics are grade, importance and a total project's completion percentage. And its values assigned by a manager.

These two types of information are gathered in the database to be post-processed. As examples of custom metrics we used grade and a project's completion index. The grade
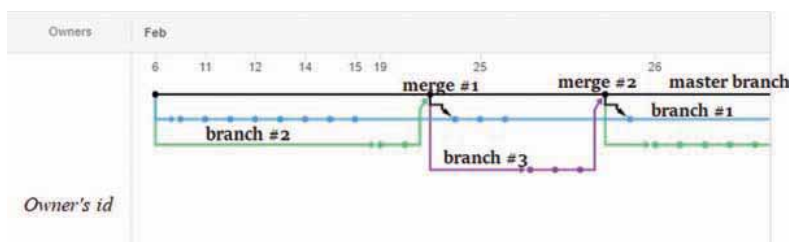

Figure 7. Example of project evolution trough time (figure modified from www.github.com).

custom metric is an input by the manager to any quantity of commits in the project. In post-processing phase it can be generated the mean and standard deviation of some user's grades or the global grade's statistics. It can be generated also a time-series grade for each user or the entire project for any time frame. The total completion index metric is also inserted by a manager which oversees the project. In any desired commit the manager may insert a number representing how much of the project is completed. This number usually increases over the time but it can decrease following the manager's discretion.

While operating, this input is made when the repository is scanned and the database is generated. After that, the manager may fill in the desired fields.

Another information that can be extracted is the authoring activity for a specific file or folder. This file filtering can show the same graphics and statistics as the complete set of project's commits and it is a valuable resource to the micro management of the project. One example is how the final report file is going, or an important result data file. The tracking works with a specific folder also.

3 RESULTS

In this section presents some metrics gathered in the test project. As stated before, for an overall evaluation of the users one must not rely on only a few metrics. For this case the metrics used were: number of commits, number of insertions, number of deletions and the activity. Additionally, two custom metrics are shown: grade and importance of a commit. The grade metric represents how right or wrong a commit is, ergo, a quality measure. On the other hand, importance of a commit measures the impact of the such commit in the project. These two presented custom metrics are represented by a value between 0 and 10 and can be assigned to any commit, it is not required to assign a value to all commits. The analysis is made using only the commits with any value.

3.1 *Metrics results throughout the project's time frame*

Here are presented results gathered in all project's time frame.

In Figure 8 is shown the number of commits by author. Figure 9 shows the amount the insertions by author in all project, in this case is taken into account the binaries files committed into the project, such as figures. The number of insertions for a binary file is 64 bytes in the file, for binary files do not have the concept of text lines. This feature may lead to distortions in the user's evaluation so a project with binary files stripped from its logs were created
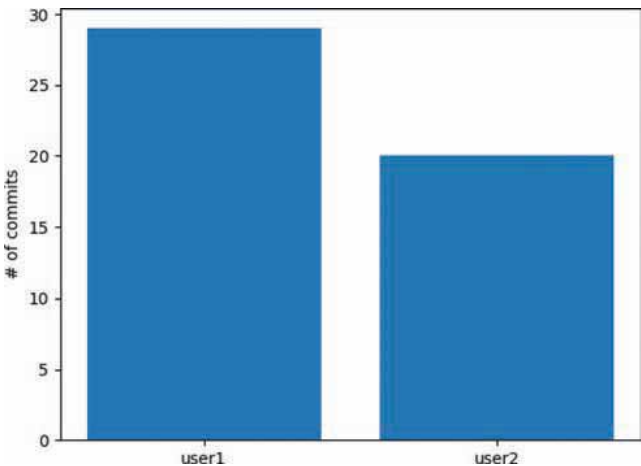

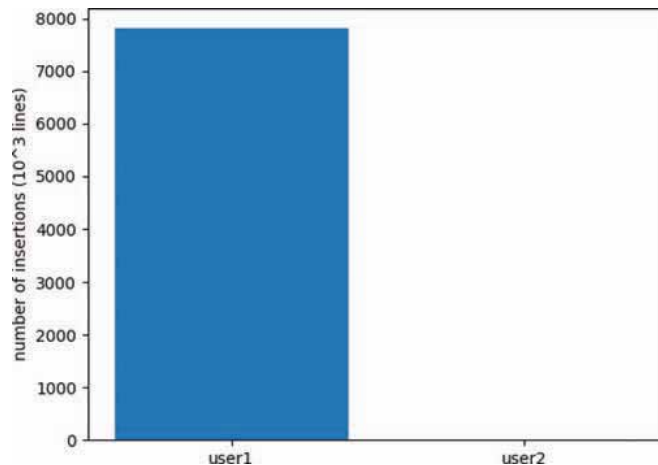Figure 8.   Number of total commits by author.

Figure 9. Number of total insertions by author when taken into account the binary files. In this case is visible the distortion of the user's interactions in the project due to the addition of binary files by user1.
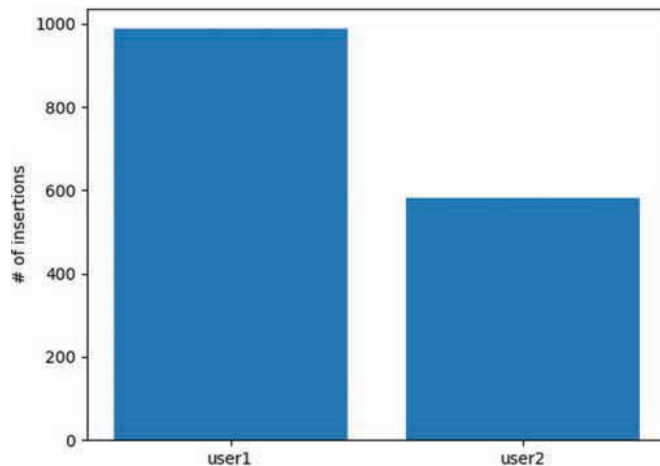

Figure 10. Number of total insertions by author. This result is correspondent to the project without binary files in the history.

and the result is shown in Figure 10. This binary file distortion issue was addressed also using the custom metrics defined by the manager.

From Figure 9 it can be noted the total number of commits favours the user 1. The number of commits in this case does not make the distinction if the file is binary, therefore, favouring user 2, which may have inserted many. PNG files to the server.

On the other hand, in Figure 10, when the binary files are not taken into account, the amount of commits, ergo, contributions to the project made by each user is actually not as disparate as it seemed in Figure 9.

The grade's results and the importance results are handled including the binary files. These custom metrics are a chance to the manager to evaluate the commits, not only by the amount of data inserted or deleted, but through the meaning and importance of each commit.

The Figure 11 is presented the histogram for the metric grade. It is important to highlight that the amount of graded commits is not the same as the amount of total commits in the project. The manager chooses the amount of commits that will receive grade (which also applies to the metric importance). The histogram for the importance metric results is shown in Figure 12.
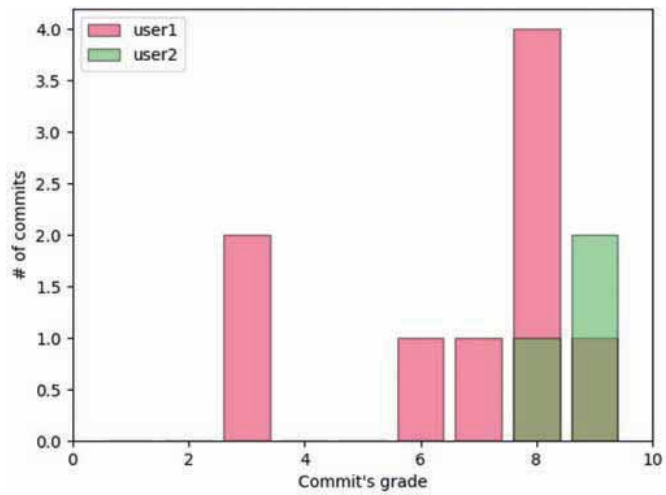
Figure 11. Commit's grade histogram. The histograms for each user are superimposed (transparency was applied).
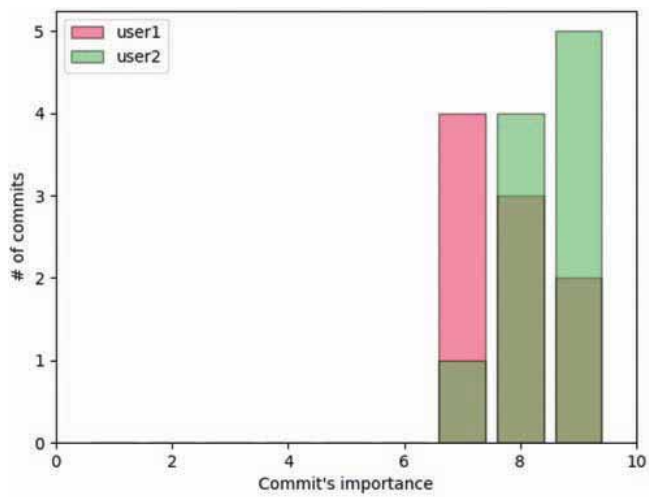

Figure 12. Commit's importance histogram. The histograms for each user are superimposed.
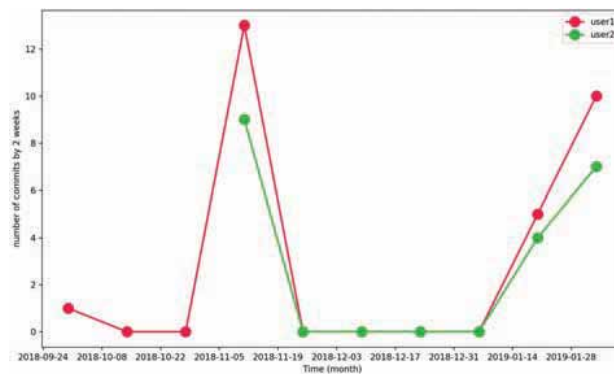

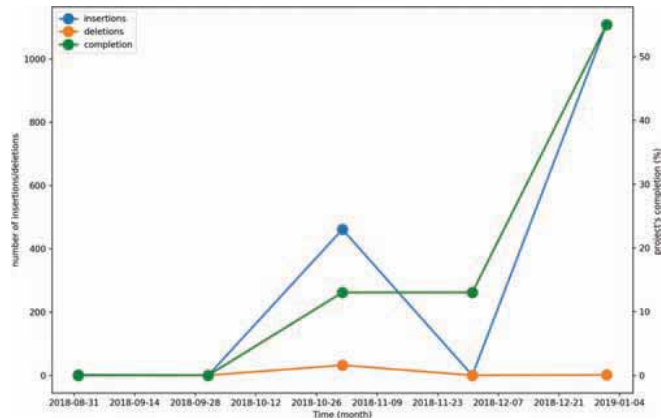Figure 13. Time series for number of commits by 2 weeks period.

Figure 14. All author's insertions and deletions time series by month (y axis to the left) and the project's completion (y axis to the right). These metrics are related to the project's history excluding the binary files.
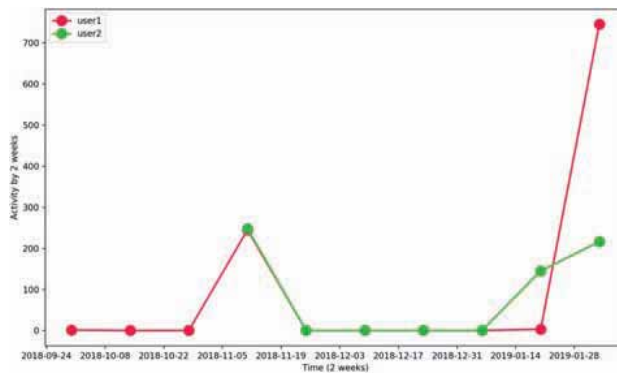

Figure 15. Activity time series using a 2 week time window. The activity is comprised of the number of insertions plus the number of deletions in the project's history excluding the binary files.

3.2 *Temporal series results*

The temporal series results denote the temporal analysis of the project's characteristics. In Figure 13 is presented the number of commits submitted using a 2 week time frame. Figure 14 shows insertions, deletions and the project's percentage of completion in a monthly period. The percentage of the project's completion is another custom metric assigned by the manager to any commit. The temporal re-sampling in one month time period considers the maximum percentage of completion value in each period. Again, these results are related to the project's version without considering the binary files. The activity (insertions plus deletions) is shown in Figure 15.

4 CONCLUSIONS

This study shows an experiment to register and track the development of a geostatistical project using a versioning system (VCS) (O' Sullivan and Bryan, 2009). This methodology is focused on the project manager, which is the person that decides for which custom metrics to use and how to analyse each metric. And, finally summarize the most important results in reports.

The workflow was automated using python scripts. The manager experience can be improved by the transformation of these script into a graphical software.

As pointed out in the results section, an important discussion of the versioning system utility in a geostatistical projects is the treatment of binary files, when measuring the user's interaction. This study suggests that to address this issue the methodology must use additional resources as:

1. Analysis of the binary stripped version of the project, or a file filtered version of the project;
2. Custom metrics such as this study suggests: Grade and importance of commits.

As the system (VCS Git) is capable of any customization there are numerous git capabilities, such as a specific file or folder tracking, that were not fully explored. However, the use of the VCS system in a geostatiscal project showed great control of the files generated, in the sense that a previous state could be restored to the project. Also, the open possibility to develop custom metrics gives rise to all kinds of analysis and interactions with respect to the team as well as the company's productivity.

REFERENCES

Deutsch, C.V. and Journel, A.G. (1998). *Geostatistical software library and users guide.* Oxford Univeristy Press, New York.

Goovaerts, P. (1997). *Geostatistics for natural resources evaluation.* Oxford University Press, Oxford.

Isaaks, E.H. (1990). *The application of Monte Carlo methods to the analysis of spatially correlated data.* PhD thesis, Stanford University.

Matheron, G. (1963). Principles of geostatistics. *Economic Geology,* 58(8):1246–1266.

O'Sullivan, B. and Bryan, O. (2009). *Mercurial: The Definitive Guide.* O'Reilly Media, Inc.

Seifert, D. and Jensen, J.L. (1999). Using sequential indicator simulation as a tool in reservoir description: Issues and uncertainties. *Mathematical Geology,* 31(5):527–550.

Ver1y, G. (1983). The multigaussian approach and its applications to the estimation of local reserves. *Journal of the International Association for Mathematical Geology,* 15(2):259–286.

From machine construction to mechatronic system design: Digital Transformation is changing the way of thinking!

Szymon Kochanik
MT-Silesia Sp. z o.o., Wroclaw, Poland

Piotr Dudzinski
Wroclaw University of Technology, Wroclaw, Poland

Christoph Mueller
MobileTronics GmbH, Ladbergen, Germany

ABSTRACT: During Digital Transformation, an increasing part of machine functionality is moving into electronics and software: With increasing demands on functional safety, assistance systems and autonomy, software is becoming the most expensive part in development of new machines. Therefore, identical software needs to be reused in as many machines or components as possible. This paper shows practical approaches to a modern, function based and modular system design mirroring the component based software approach into the machine's structural concept. Prior to any traditional construction work, this comprises of an overall cross competence functional design, and a detail design using multi criteria decision making techniques followed by a detail design and implementation, whereas all digital systems are implemented simultaneously to the mechanic design. This assures that there is sufficient time for software implementation and the risk of surprises, redesign and delay during start up is very limited.

1   INTRODUCTION

Traditional machine construction as practiced since beginning of industrialization starts with creating mechanic structures, calculating the static and dynamic behavior meaning everything classically connected to mechanic construction. Historically, innovative machine construction often was regarded "art of engineering" (Hellige 2008), the chief constructor with all of his experience was seen as the master of this art.

Over time, many procedures changed and in general there is a much more open approach today. However, especially with traditional machine builders the legacy procedures are still obvious: Working in customers projects related to automated machines during the past years it could often be heard: "It's not your turn yet, the control system we start later, first we need to solve all the issues in mechanics and hydraulics..." (Dudzinski 1994, Bürkel 2013).

This results in a project timeline similar to a construction project, where later crafts are starting their work later in sequence with the construction process. This is shown in Fig. 1. In this timeline, the time needed to design and implement the control system often is dramatically underestimated leading to the consequence that the programming is performed in hectic, it cannot be well tested and it is completed during commissioning and start up of the machine. Resulting delays in delivery and quality problems especially related to the control system are only one consequence; When during control system design the necessity for changes in mechanics or hydraulics shows up, dramatic delays in project completion are obvious as parts have to be redesigned followed by delivery time for the new parts etc. Often deficits in mechanics and hydraulics also have to be covered by workarounds in the control system leading to unnecessary functional limitations or a more complicated operation.

Figure 1.   Traditional machine design timeline (symbolic).

Also it was observed by the authors during the past years that machine structures could have been designed much more simple if the control system designers would have been involved from the beginning of design: Often it is much more simple, more reliable and more cost efficient to solve a function in software than e.g. implementing a logic interlock by using hydraulic valves.

This has been understood by new players entering the traditional machine building market like Google with autonomous cars or players like "Street Scooter" – a spinoff from the RWTH Aachen supplying Deutsche Post and others with electrically powered distribution vehicles. Their time to market often is surprisingly short if compared to companies traditionally active in the respective market.

2   NEW REQUIREMENTS ON MACHINE SAFETY

Now, legislative and normative demands are in force which require structured analysis on safety and risk of the machine and the machine in it's operation environment. The "Failure Mode and Effects Analysis" (FMEA) concerns the entire design and operation of the machine thereby also including functional aspects which in traditional machine design "are solved later".

However consequently following these demands gives the chance to identify potential dangers and also functional problems of the machine at an early stage of design if these analyses are carried out in an interdisciplinary way involving all subsystems of the machine and ideally also experts from operation and service. This makes the functional safety analysis at an early design stage an important input to the entire, interdisciplinary overall machine (or better mechatronic system) design process. A precondition for being able to carry out the FMEA in a goal oriented way is therefore also the existence of an interdisciplinary functional predesign of the planned mechatronic system.

From the FMEA safety demands are resulting which need to be addressed by the entire design team. Also in this context different alternative solutions are possible for every identified item: They can be addressed in an alternative way e.g. by mechanic design or by functional safe software or by organizational measures. If more complex decisions need to be made, a structured and reproducible decision making process is recommended as described below.

For marketing machines in Europe the legislative basis of the EC Machine Directive has to be followed in order to be allowed to CE-mark the product. Consequently, all functional safe software controlling the machine has to be developed in accordance to EN 13849-1 and validated in accordance to EN13849-2. The resulting control function development has to follow the so called V-Model and sets high demands on documentation, verification and structured validation. It can be estimated that the effort for safety related software development is about four times the effort needed for non safety related software.

It is easy to understand that a late change in the machine design may cause an avalanche effect downstream the entire development process, especially when taking into account the traditional development process as outlined in Fig. 1.

731

At the same time, machine manufacturers now are facing a large number of new challenges connected to digital transformation in the industry, which is regarded a "Paradigm Change" (Andersch 2015) affecting all industry.

Especially smaller machine manufacturers are used to regard everything related to software as "not their main competence" or "just needed to make it work", which also is shown by the fact that for historic reasons the development of automation ("PLC") software is performed within the electric department. The consequences are significant:

- In many cases the quality of the control software is very low
- No or only basic routines for software version management are implemented in the company
- A structured configuration management is not available
- Software modifications are made "on the fly" for every individual machine built resulting in a large number of software branches with only minor modifications
- Difficulties in functionality and service resulting from items above

Consequently, the software always has to follow all the changes and modifications made for every individual machine: When the purchasing department finds a cheaper sensor for one individual machine, this sensor will be used—Never taking into account the fact that the software change together with the required new version handling causes cost exponentially higher than what was saved on the sensor!

At the same time the end customers of mobile machines are demanding new functions:

- Driver Assistance systems
- Fully automatic or autonomous operation
- Data controlled operation
- Data communication
- Operation reports
- Remote Service and remote supervision
- Black Boxes
- Maintenance support

Most machine manufacturers still today are handling such demands only in a reactive way, meaning that they implement functions only if a customer demands them. In this case a quick and cheap implementation is needed as "it is only for one particular project". Such solutions are characterized by the fact that they are prone to functional problems as they never can be fully tested, they are subject to delivery delays and finally they never are profitable. Therefore, many machine manufacturers find themselves in a vicious circle concluding that software and automation "only creates problems".

And on top, in "digitalized" machinery, the share of value created by software based solutions is steadily increasing (Andersch 2015). Nowadays, software development is the most expensive part of machine design and development. Standardization of the software modules is precisely as important as proactively offering digital functionality to the end customers. In terms of information exchange the information exchange formats have to be standardized in order to save the effort for individually adjusting interfaces. In mining using the IREDES standard is a good template for exchange of standardized machine information.

Also the trend towards autonomous and highly automated machines sets new demands on the overall machine design. It is not enough to declare that a machine is "autonomous ready" or "automation ready" simply by having a PLC controller on board. Also leaving the higher level automation to a third party company has to be seen critical as any modification of the machine automatically voids the certification (in Europe CE marking) of the machine because the machine is not any longer in the status as it once was certified. The third party providing the higher level automation may not be able to re-certify the machine to full extend due to lack of information from the underlying machine as by example the brake and steering calculations for a mobile machine.

In order to be able to provide profitable modern, "digital" solutions, machine builders have to proactively provide customer oriented solutions rather than to react on "sudden" customer demands to win the order for a particular delivery.

Also a fully automated machine from the beginning should be designed for this purpose rather than relying on "addon" systems: An automated machine requires a much higher reliability and precision of the underlying mechanics, hydraulics and electrics than a manually operated machine: For a driver it does not matter whether the machine briefly stops, he applies a reset and operation continues. Also he is able to intuitively compensate for hydraulic and mechanic play via his "manual" control loop. An automated machine however needs to apply timeouts and consistency checks of the accuracy. It stops e.g. for timeout and requires human attention.

Frequent stops however are mainly caused by wear and inaccuracies in the mechanics or by assembly issues in cabling and other details which are presumed "*unimportant*" during conventional machine design and production.

All these details have to be taken care of from the beginning of the design in order to assure a successful automation. What sense does an autonomous machine make if it needs service support several times a day?

4   A SYSTEM ORIENTED APPROACH

As software in modern machine design conforms the most expensive part of machine development, the way how a machines manufacturer looks on machine development needs to be changed towards a holistic system approach. This approach also has to take care of the interfaces between the subsystems and of the interaction between all the subsystems: A related statistic confirms, that best in class manufacturers start resolving integration issues early in design (80%) as well as during the verification and test phase (100%) (Aberdeen 2006).

A symbolic timeline of a modern mechatronic system development sequence is shown in Fig. 2. After freezing the Business Requirement Specification the Systems Architecture phase is the most important change. In this phase the functional design of the entire mechatronic system is carried out.

This means that interdisciplinary specialists from all involved subsystems are working together in order to jointly decide about the machine setup, the components and subsystems to be chosen etc. This cooperation assures, that all design relevant aspects of the entire system are taken into account. In this phase, a special emphasis is put on all the interfaces between the subsystems, regardless whether these interfaces are mechanically (fastenings, drive shafts,...), hydraulically, pneumatically, electrically or related to the information exchange in the control system. After concluding the functional design phase by freezing the System Architecture, all subsystems and the related interfaces shall be clearly defined by their general parameters.

Already during the Systems Architecture the FMEA is carried out in order to determine the safety measures and the safety functions to be taken care of in the control system design.

An important factor in this phase is the re-usability of software. Already during System Architecture unknowingly the decision is made whether or not the future automation of the machine will be cost efficient or not:

Figure 2.   Mechatronic system design timeline.

If the new design covers an entire family of machines of the same type or if the design of the new machine will be a future basis for derivatives, then the System Architecture has to take into account to cover all machines of similar type and all derivatives by a single, reliable and well tested software. This means that in the future only one single software source code has to be maintained and all differences between the single products are handled via configuration changes. Another consequence is that later addons to the software can be easily implemented retroactively on already existing machines without having to change machine specific software versions.

Today, software is developed in an object and component oriented way. This is a perfectly modular approach also for mechatronic system design, however it requires a strict functional modularity which is set up in a way different from the traditional thinking in different competence disciplines like Mechanics, Hydraulics, Electrics and Control System. This is explained in the following example:

Assumed, a new underground loader is being designed. Independently from size and dimensions there shall be the following subsystems on an abstracted level:

1. Power Supply (independently from Diesel, Battery or whatever)
2. Traction
3. Steering
4. Boom lifting/lowering and scoop functions
5. Cabin and/or autonomous guidance
6. Auxiliary aggregates (cooling, lights, whatever)

All these systems have interfaces to each other, be it the mechanic fastening of components, the hydraulic pressure needed to operate cylinders or motors, the electric power or electronic control system interfaces. If all these interfaces are clearly defined and independent from a specific implementation, then the functional components or even entire subsystems can be exchanged without or with only limited changes in the controlling software.

According to this definition the Steering system covers the hydraulic steering cylinders, the valves, the steering related sensors and all steering related software modules as well as the pages dedicated to steering on the visualization screen. Observe that the hydraulic supply is not part of the steering, as also other systems may need hydraulic power like the boom actuation. So the hydraulic supply is within a separate functional subsystem or combined with the general power supply: The steering subsystem is not interested in the fact where the pressure comes from. The main thing for the steering is that sufficient pressure is supplied. However, all hydraulic parts dedicated to steering (valves, accumulators, cylinders etc) are part of the Steering functional subsystem!

Consequently, when certain components are used in common by different subsystems (like the joystick is used for steering and for boom control at the same time), such component may be part of another subsystem (e.g. "Cabin") hosting those components. This requires a generic interfaces between these subsystems.

Interface definitions between the subsystems shall be generic. In terms of software they shall consist of physical SI-Values, percentages or status information rather than using raw sensor values or other system specific or component specific and encoded legacy information. This is a significant difference to traditional control system setup and simplifies system maintenance and interchangeability of components at minimized effort for software changes.

Following this rule, the traction system requests a certain power (ideally in kW) from the Power Supply when the driver pushes the acceleration pedal. The process is similar when the driver is sending a steering command: The relative value coming from the joystick is turned into a (machine specific) steering angle which is maintained by the steering system.

If this functional and strictly layered structure of the subsystems is maintained, then generic functions can be prepared in the software to control the particular subsystem, even independently from the particular hardware used on a specific machine. This means that the core software for an entire product portfolio can be maintained by just one single software version. At today's amount of memory available even in small control computers, individual
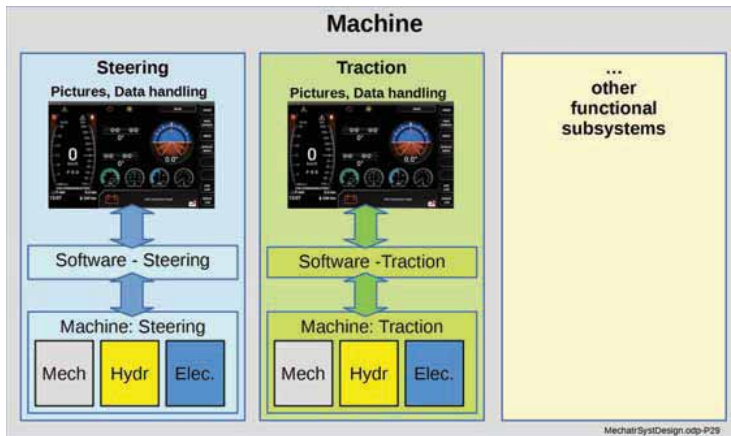
Figure 3. Design in functional subsystems.

functions applicable only to a single machine type can be handled in the same software version and activated/deactivated by configuration parameters.

This principle is of special importance to those parts of software which are relevant to functional safety which causes them to be validated in accordance to EN13849-2, as these functions can be precisely assigned to the functional subsystems of a machine. Whenever those functions are changed, a complete re-validation is needed. As better and smaller the safety software is designed, as lower the effort for (re-)validation. Facing the fact that such validation easily may take multiple days for several people reducing this effort to a minimum by software design is a real cost cutting measure:

From the risk analysis (FMEA) it becomes clear, which functions have to be implemented in the control system as safety functions. The software designers have to keep these functions as small as possible in order to limit the amount of re-validation needed in case of changes needed.

This functional mechatronic system design philosophy needs more time for specification and functional design with system architecture and FMEA. A disadvantage of this design philosophy may be that the development time until "something real is visible", meaning some concrete mechanical elements show up in the workshop is longer than in traditional "hands on" approaches. However like in software design it shows that every hour spent in structured design pays off by several hours or even days saved in implementation, testing and subsequent problem solving.

5 STRUCTURED DECISION MAKING

During functional design, a number of complex decisions with a high impact on machine functionality and economy of the product have to be made. Such design decisions are complex because of a multitude of dependencies to other systems. In general there is a limited number of alternative solutions and a number of—in many cases undocumented—criteria the decision is basing on. After technical design decisions in a later stage of use of the product or in case of problems during implementation or testing often the question is asked "why did we make this decision, why did we not use alternative xy".

A good method for making design decisions is a simplified "Multi Criteria Decision Analysis" (MCDA or MCA). This is a decision-making process in which a set of criteria are defined, ranked in terms of relevance and importance, and evaluated consistently. After a set of criteria have been defined and ranked by stakeholders and decision makers, each alternative is evaluated against the same set of criteria, creating an assessment of value for each alternative (Brixner 2017).

The result is a ranking of the design alternatives, which of course is dependent on the individual ranking and evaluation of the applied criteria. In technical matters it is a good idea to

have different people evaluate the criteria against each other. If the resulting ranking of the alternatives shows a clear trend, then the decision may be regarded valid to a very high degree.

A further advantage of such procedure is that not only technical but also organizational and economic design criteria can be part of the decision making process. Typical criteria for technical decisions beside the task specific technical criteria are: development cost, development time, production cost, serviceability, software design effort, component availability, safety.

It is important that in this analysis the details of cost and effort do not need to be known in detail. There is just an estimation being made resulting in a relative ranking against the preset importance ("weight") of the different criteria.

The MCDA is applied to the entire functional module or subsystem of the machine as a whole, meaning that complete alternatives including the mechanics, hydraulics, electrics, and control system including software. This way the complete effort and cross dependencies for different alternatives of the entire steering system, traction system etc are evaluated in their completeness!

6   CONCLUSION

In traditional machine design the development of a new machine followed the specialist division based design sequence of mechanics first, then hydraulics or pneumatics, electrics and control system development.

Digital Transformation however changes the way of designing machines: From the specialist division based approach to a functional module approach. In the System Architecture, the functional modules are defined together with all their interfaces of whatever kind: Mechanic, hydraulic, electric, data and even multimedia. In the following design these modules are detailed in cooperation of interdisciplinary design teams with the goal of finding the technically best and most economic solution for the entire scope of the particular subsystem.

Following this approach, all detail design—including the control software—is designed simultaneously, potential problems are identified at an earliest possible stage and the safety analysis is accompanying the design. This approach leads to efficient machine design, timely delivery of the design and mechatronic systems which easily can be modified and new machine types can be easily derived from original developments. This approach is a precondition to efficiently use the functionality of the control software which conforms a steadily increasing share of the machine value. A further advantage is the cost efficiency as a highest possible reusability of subsystems and software modules can be assured by design.

REFERENCES

Aberdeen 2006, The Mechatronics System Design Benchmark Report, Aberdeen Group Inc,. Boston MA, USA, 2006.

Andersch 2015, Paradigmenwechsel im deutschen Maschinen- und Anlagenbau, Study, Andersch AG, Frankfurt / M., 2015.

Brixner 2017, Applying Multi-Criteria Decision Analysis (MCDA) Simple Scoring as an Evidence-based HTA Methodology for Evaluating Off-Patent Pharmaceuticals (OPPs) in Emerging Markets, Brixner D. et al, Elevier 2017.

Bürkel 1993, Process-Optimized Sytem Functionality of Mobile Work Machines, Bürkel M., Busterud B.E., Czabanowski R., Diefenbach M., Dudziński P., Heuckeroth M., Konieczny A., Kosiara A. Lommatsch J., Skurjat A., Stefanow D.: EU Project report SME-2013-606227-PROSYMA.

DfCLG 2009, Multi Criteria Analysis: A manual, Department for Communities and Local Government, London 2009.

Dudzinski 1994, Gummilaufwerke – Projektierung eines Musterlaufwerkes, Piotr Dudzinski, IAMT - Ingenieurgesellschaft für allgemeine Machinentechnik mbH, Projektnummer 2192–20, Plauen 1994.

Hellige 2008, Wissenschaft vs. Design: Konstruktionslehren für den Maschinenbau, den Computer und die Software im historischen Diskursvergleich, Hans D. Hellige, artec paper No. 158 ISSN 1613–4907, Universität Bremen, Germany, 2008.

Rethinking mining transport: Trackless trains for mass transport in mining

George Biro & C. Mueller
MobileTronics GmbH, Ladbergen, Germany

M. Juzwiak & G. Tabak
MT-Silesia Sp. z o.o., Wroclaw, Poland

ABSTRACT: Mass transport of excavated materials in mining today is performed by LHD's and Trucks, rail bound trains or conveyor belts. While the use of trucks is very flexible but resource consuming, conveyor belts are stationary but highly efficient. Rail bound trains need dedicated driveways or tunnels in an underground mine causing high cost and time needed for construction. Enabled through "Digital Transformation" trackless trains running on flat surface in coexistence with standard vehicle traffic are available now as a new option. Trackless trains consist of a number of mechanically interconnected rubber tired cars whereas all axles are actively electronically steered so they precisely follow the track of the leading axle. A computer controls the train like it would be running on a "virtual rail". Like standard vehicles and in contrast to rail bound trains, VirtuRail trains are able to run steep inclines and declines. Proven in tunneling operations, this technology also becomes available for mass transport in mining.

1 INTRODUCTION

Traditionally, conveyor belts, conventional trains and trucks are the major methods for transport of supply and bulk materials in mining. All these transport systems have their particular advantages and disadvantages and the choice of the transport system has a major impact on the overall cost of a mining operation.

While trucks are flexible and able to run on ramps with steep graded inclines and declines, trains and conveyor belts are lacking of this capability to different degree. On the other hand, conveyors provide a means of large capacity continuous transport however on very static routes. Trains are able to transport large amounts of material from a limited number of loading points to a limited number of unloading points, whereas the limitation depends on the rail network infrastructure. Also the physics of steel wheel–rail contact limits the use of trains on steel rails to low grades compared to standard rubber tired vehicles. In addition, train traffic mostly needs a separate driveway, which does not allow the simultaneous use of standard vehicles on a flat surface. This often requires an interrupted transport with changing the load from truck to train. In addition, significant cost have to be calculated for maintaining the rail network.

Also conveyor belts especially in underground installations limit the tunnel profile available for vehicles and mining machines to pass. Therefore, in many underground installations, separate tunnels are excavated for conveyor belt transport or even dedicated transport levels are needed for train transport with significant impact on cost and time needed for excavating the transport infrastructure prior to mining operations being able to start.

In commercial tunneling the situation is similar when it comes to the supply of materials like pre-cast concrete elements, shotcrete or other materials to a Tunnel Boring Machine: The traditional rail bound transport is limited to low grade inclines and declines. The alternative

Figure 1. Schematic view of the five car train: Left: TBM side.

is a transport by trucks or special "Multi Service Vehicles" ("MSV"). These vehicles are running in "dead end" applications, where turning the vehicle at it's destination is impossible. Thus, the vehicle has to be equipped with two driver cabins at either end. The vehicle length is limited due to the impossibility to steer the combination of multiple connected vehicles around narrow curves. Certain fully mechanical designs to solve these limitations have shown that these designs always are limiting the length of the "train". This is the reason why these vehicles are built as vehicles with very high load per car causing special vehicle designs with respectively high cost. Certain fully mechanical designs to solve the steering problem have shown that these designs always are limiting the length of the "train".

Therefore, an ideal solution for cost effective and flexible transport of heterogeneous materials is a train on rubber wheels consisting of multiple cars which keep running on a single track. The solution presented here is using the VirtuRail® system for safe and automatically guided vehicle control which is successfully in operation since 2016 at the Ahrental construction site of the Brenner Base Tunnel close to Innsbruck in Austria operated by the joint venture of STRABAG/Salini Impregilo.

Three trains of five cars at a total train length of abt. 65 m and a gross weight of 130t are used for regular supply of pre-cast (concrete) elements, shotcrete and other consumables. One train of three cars is used for shotcrete and other material supply as well as for special operations like extension of the conveyor belt or the medium voltage cable. The trains consist of four axle cars at 40t gross weight and two axle cars at a gross weight of 20t.

The trains in this application are powered by Diesel-hydraulic traction; Every second of the 14 axles is powered, all wheels are braking, the maximum service speed is 25 km/h.

The driving trajectory consists of a 2.5 km long access tunnel at a decline of 11,6% followed by a 90° curve of 30 m radius and a straight section excavated by drill-and blast down to the starting cavern of the TBM. From there the TBM excavated tunnel starts, which reached 13 km in February 2019. Inside the TBM backup the minimum lateral clearance is 18 cm which requires a very high driving precision of the automatic steering.

2 DIGITAL RAILS

The reason why since over 150 years trains are running on steel rails is the fact that the steel rails mechanically assure track stability. Road vehicles however perform a smaller curve radius with every trailing axle added to the vehicle. This fact in combination with the width of roads especially in curves is limiting the length of the truck-trailer combination.

Inspired by an application in commercial tunneling (see below), the idea was to create a train of a number of single cars on rubber wheels, whereas all axles in the train keep the same track, precisely as if they would be guided by mechanic steel rails.

The mechanic preconditions for such system are:

- All axles of all cars in the train have to be mechanically steerable
- All steering has to be electronically controlled with e.g. electrohydraulic actuation
- A control computer generates a "virtual rail" and generates the steering commands for all axles in the train so they precisely follow the "virtual rail".

Thereby the software transforms the steel rails into a "virtual rail" inside the train's control computers in order to keep all axles on an identical track–as if they were running on steel rails. This "virtual rail" enables the train to pass narrow curves. Furthermore the rubber-tired surface contact assures the ability to drive up-and downhill on steep ramps at much more than 10% grade, precisely like a truck.

This principle enables a train of connected cars to run on flat driving surface without the need of any mechanic guidance like e.g. steel rails. This enables mixed traffic with standard vehicles and eliminates the need for separate train driving space.

The software is divided into two main functions:

1. The "Track Follow Mode" which means that all trailing axles are precisely following the track of the first–leading–axle.
2. The "Guidance Mode" which additionally to the "Track Follow Mode" automatically guides the first axle

3   TRACK FOLLOW MODE

The so called "track follow mode" is the basic functionality of the control software. It enables the wheels on all axles precisely follow the first axle in the train. In manual operation, the first axle is controlled by the driver manually using an electronic multi functional joystick. In this way, the driver is steering the leading axle like on a traditional road vehicle. The steering commands determine the driving trajectory of the leading axle and thereby also the "position of the tracks" on the driveway which all following axles precisely have to drive on.

The control software moves a map along the train, which together with a number of sensors e.g. for the steering angles, issues the control commands to keep every axle precisely on the track determined by the first–leading–axle. This is performed using most modern mathematic algorithms which by far are exceeding the complexity of controlling an airplane.

Therefore, all axles precisely follow the track of the first axle without negotiating a narrower curve radius–which would be the case with a traditional truck/trailer combination. As all axles are on the same track, very narrow curves can be passed. The minimum curve radius is therefore only determined by the maximum steering angle and the width/length of the longest vehicle in train. The lateral deviation of the last axle in a five car train of ca. 70 m length after running through a 30 m radius curve is less than 10 cm.

The Track Follow Mode causes a driving behavior which is substantially different from a truck-trailer combination. The drivers must get used to the fact that driving the biggest possible curve radius with the front axle (like they would do with a truck-trailer) is not necessary and can be rather counterproductive. The drivers get used to this behavior very quickly when driving curves in manual mode.

4   AUTOMATIC, INFRASTRUCTURE FREE GUIDANCE

Due to the fact that many driving situations are rather complex, the software provides additional driver support functions which make the driver feel more like operating a locomotive of a traditional train rather than driving a rubber-tired vehicle:

Certain driving situations require a very high degree of precision, like in the first application the 70 m long train negotiating a 30 m radius curve or docking precisely into the TBM backup system so the fast unloading devices are able to grip the pre-cast concrete elements loaded on the train by a lateral tolerance of only 2,5 cm from the optimal track.

This automatic guidance is achieved by an additional software layer which automatically guides the first axle in respect to the route section or the location of the train. Different guidance principles are used for guidance of the first axle:

- Outside the tunnel in free space high precision (cm level) GPS is used in combination with on board sensors
- Inside the tunnel on board sensors like Laser Scanners (LIDAR) and RADAR are used to determine the tunnel walls and the available driving space in front of the train.

In the basic system, the guidance is implemented as driver assistance function. It enables the driver to just select a particular route section inside the tunnel e.g. "access tunnel downhill", "curve inbound", "TBM tunnel" or "TBM docking". The guidance computer then

Figure 2.   Perfect alignment inside the backup.

automatically assigns the respective driving regime by setting the maximum allowed speed which the driver is not able to exceed. Also, the "position" of the "virtual rail" inside the tunnel is assigned as to be e.g. "1,8 m from the right tunnel wall" or "in the middle of the tunnel". The guidance system is equipped with LIDAR and RADAR based sensors on either end of the trains. The signals from these and more sensors are fusioned and processed by very advanced mathematical guidance algorithms to automatically steer the train, so it precisely follows the preset speed and track.

During Auto-Steering mode, the driver always has the possibility to manually take over the steering simply by intuitively moving the joystick left or right. He can return to Auto–mode any time simply by pushing a related button on the joystick. For safety reasons high speed driving at 25 km/h is only possible in auto-steering mode when the system assures the sufficient amount of clearance in front and to the sides of the train.

Nearly all special situations like narrowed roadways due to works in the existing tunnel, meeting other trains or cars etc. are handled automatically by the driver assistance system without the need of driver intervention. The system may, depending on the available space, limit the driving speed to a level regarded safe for the available space. When two trains meet in the comparatively narrow exploration tunnel in the first application, it was planned during design that the outbound train would stop and have the inbound train pass. In practice it has shown that both trains pass at slow speed using the automatic guidance functions.

This system also works reliably in special situations like under smoke or fog conditions. Laser and Radar sensors are using different physical principles which are ideally supplementing each other. Due to the different characteristics of the sensors and the resulting physical diversity, the detection is very reliable. However due to the different physics and the resulting deviating timing behavior of the sensors, the software needs to use very complex sensor fusion algorithms. When only one single sensor system is supplying reliable data, the train speed is limited.

The functionality of the guidance was proven by several fire drills using a special train for self-rescue and a fire brigade train used for emergency operations. In these drills, the tunnel was set under artificial smoke; The trains were running very reliable on reduced speed using the automatic guidance.

Inside the tunnel there are no infrastructure elements needed like inductive loops or positioning tags buried in the floor. In certain cases and depending on the tunnel wall structure, radar reflectors made of simple steel plates may be needed at certain positions.

To automatically switch the route sections, simple passive RFID tags may be mounted in the tunnel walls. The rough locations of the trains can be estimated via their WLAN associations so the logistics can be followed up from a central location.

5 FUNCTIONAL SAFETY

Electronic steering of mobile machines and vehicles ("Steer-by-wire") as well as electronically controlled braking ("Brake-by-wire") is subject to strict safety regulations to exclude and prevent accidents.

To be allowed to market a machine in the European Union (EU), the producer has to assure "CE conformity" and respective product safety by following the EC Machine Directive. This can be achieved by following the applicable harmonized norms and their subordinated normative references. For underground equipment this is the EN1889 "Mobile machines working underground. Safety. Rubber tyred vehicles". Parts of these regulations and subordinated (referenced) norms are covering the electronic control of safety relevant machine functions requiring a design in accordance to EN13849-1 and a validation of the entire mechatronic systems, potentially together with their operative environment in accordance to EN13849-2.

These norms require detailed risk analysis and set very high demands on the quality and documentation of all safety relevant functions on the machine: Software design, implementation and verification/validation must be carried out in accordance to the so called "V-Model" assuring the correct implementation and validation of the functionality on all levels of design, implementation and testing.

As every new version of safety software must be run through the full validation routines before being released for operation, the amount of safety software is kept at the lowest possible level covering the routines needed for basic steering, braking, parking brake, speed control and Safety Stop.

The system is set up in a way that every car in the train forms a single, intrinsically functional safe unit. All functions are implemented on approved Safety Controller Hardware using certified software development systems for development of the safety functions.

Such Safety Controller hardware is available on the market as "Fail safe" devices. This means that the controller enters a safe state and all outputs are going to a defined safe level when the power is switched off or if any hardware failure is detected. However, on a vehicle driving at over 7 m/sec it is not enough to simply switch off an output as the steering still has to work during the distance needed for braking. Therefore, a so called "fail operational" setup is needed which assures full functionality of brake and steering when the controller enters the fail-safe state.

Accordingly, two controllers are used per car which permanently supervise each other. Both controllers are connected to dedicated redundant sensors and actuators for the safety relevant functions. In case one controller detects an error and switches to fail safe state, the other controller takes over with no delay and the safety functionality is fully assured, so steering and braking are still possible.

Also the further operation of the train is allowed when one controller is not available e.g. due to a failure caused by sensor problems or cable breaks. In such case the maximum speed is limited to a value which does not need the redundancy to be active. This function enhances the reliability and prevents from downstream standstill of the production.

Following this principle every car in the train is an independent functionally safe unit. A safe operation has been assured for over 200.000 km in the first application without any accident or safety relevant incident.

The fail-safe controllers are also controlling non-safe functions on the train. These controllers allow to upload new or changed non-safe functions to the controller without the necessity to re-validate the safety functions of the machine. This interference free design saves significant time during startup and in case changes in the non-safe parts of the system are required at a later stage.

6   OPERATION EXPERIENCE

The VirtuRail® system was first used on the RowaTrains supplying the Tunnel Boring Machine excavating the exploration tunnel for the Brenner Base Tunnel in Austria. The Tunnel Boring Machine is operated from the Ahrental construction site close to Innsbruck and run by a joint venture of STRABAG/Salini Impregilo.

The system is in operation since May 2016 on six trains, whereof four are used for supply of the Tunnel Boring Machine, one is a standby train for self-rescue of the TBM crew and another one is used as fire brigade train.

Three trains of five cars at a total train length of abt. 65 m and a gross weight of 130t are used for regular supply of pre-cast (concrete) elements, shotcrete and other consumables. One train of three cars is used for shotcrete and other material supply as well as for special operations like extensions the conveyor belt and medium voltage cable. The trains consist of four axle cars at 40t gross weight and two axle cars on a gross weight of 20t.

The trains in this application are powered by Diesel-hydraulic traction; Every second of the 14 axles is powered, all wheels are braking, the maximum service speed is 25 km/h.

The driving trajectory consists of a 2.5 km long access tunnel at a decline of 11,6% followed by a 90° curve of 30 m radius and a straight section excavated by drill-and blast down to the starting cavern of the TBM. From there the TBM excavated tunnel starts, which reached 13 km in February 2019. Inside the TBM backup the minimum lateral clearance is 18 cm which requires a very high driving precision of the automatic steering.

A special advantage of this application is the availability of the driving surface for standard trucks and vehicles; so emergency services and crews can access the TBM and all intermediate workplaces by individual car transport which saves time and resources compared to the need for an organized rail bound transport.

Furthermore, the flexibility of driving on the loading area is highly appreciated by the construction site, since the mixed traffic of trucks, cars and mobile machines is not disturbed

Figure 3.   Four axle car loaded with pre cast concrete elements.

by steel rail installations. Thereby, VirtuRail® trains enable the use in narrow, shared traffic areas. And it saves all cost for rail system maintenance which also is very significant.

On the other hand, it has to be mentioned, that such highly automated equipment requires a higher maintenance effort compared to "simple" railroad cars. However, the operational advantages are by far overcompensating the higher maintenance effort, especially when the saving of the track maintenance and the operational advantages of simultaneous car traffic are considered. The maintenance of the electronic systems is supported by MobileTronics via operational black boxes on board the trains which can be remotely accessed and an event reporting system which reports all events to a central server at MobileTronics. This server generates an operational statistic for every week of operation, which especially in the beginning was an essential guideline for the reactive and preventive on site mechanic maintenance.

Since startup, the VirtuRail® trains have completed a total of more than 200.000 km of operation without any significant automation problems. The system also showed its reliability by a seamless supply of the TBM during the daily advance world record of 61 m during 24 hours on May 17th 2017 (BBT 2018).

An unexpected result of the startup was that the drivers were subjectively feeling safer than with the traditional vehicles used in the beginning, especially with respect to the braking behavior at full load on the 11,6% decline access tunnel.

7 AUTONOMOUS OPERATION IN MIXED TRAFFIC ENVIRONMENT

Due to the good experience with the VirtuRail functional setup and the reliability, a showcase was performed on Dec 03, 2018 demonstrating the fully autonomous drive of one train all the way into the TBM backup (STRABAG 2018).

As the modular software including the auto-steering is prepared by design for autonomous operation, only minor modifications were needed for the train's on board electronic systems in order to perform this showcase. The main change was the installation of section readers and transponders to identify related landmarks in the tunnel at the places where the operator during regular – driver assisted–operation has to switch over to the next route section. This successful autonomous drive has shown that the system is able to cope with all kinds of special situations without driver interaction: Opposing traffic, driving around obstacles, sharing the road with manually operated cars etc.

Another important result of the autonomous demonstration was the fact that all acceleration and braking actions of the train are much smoother and much more machine friendly compared to the manual actions of a human driver. This matches results from other autonomous operation of mining machinery and allows the conclusion that the autonomous operation will lead to a further reduction of energy consumption and maintenance cost, a fact which however at this point of time cannot be verified.

It must be emphasized that this autonomous operation did not take place in closed/fenced or specially prepared area! All tests for the autonomous drive as well as the showcase demonstration itself took place in the regular working environment of the tunneling construction site. In autonomous vehicle terminology this demonstration thereby was carried out in a so called "mixed use environment", which makes this demonstration very highly respected also outside the tunneling industry as a leading edge autonomous vehicle proof-of-concept!

Extending the existing application to a fully autonomous system working safely in the tunneling environment from the technical point of view would not require more than 3–4 months. The main effort would be to install a central supervision workplace which provides a central overview of the locations and status of the trains together with live video and the possibility for the remote operator to restart and manually maneuver in exceptional situations.

However, for future autonomous operation the availability of a mechanic vehicle design originally intended for fully automatic operation with an optimized technical reliability of the underlying mechanic and hydraulic systems is an essential precondition. Furthermore, a fully electric operation is needed due to higher demands on emissions and environmental compatibility. This would also save significant cost for tunnel ventilation compared to Diesel

operated machines. Also, the operation cost can be reduced due to higher energy efficiency of the electric vehicles. In following projects extensive experience was gained in integration of battery and hybrid powered heavy electric vehicles.

In the following project MobileTronics already has demonstrated the successful integration of electric drivetrains, which shows a much higher energy efficiency and a much better controllability of the traction system due to the fast and precise behavior of the frequency converters.

8 MINING APPLICATIONS

The future VirtuRail® trains and vehicles therefore will be modular products designed for highest reliability in daily service to allow autonomous operation. This design for reliability has to cover all subsystems as mechanics, hydraulics, electrics or the control system, which also the manual operation will strongly benefit from. Manual operation is then possible from two cabins as shown or from only one single driver comfortable driver cabin.

In mining, rubber tired software controlled trains can be used for bulk material transport as a new alternative to trucks, conveyor belts and rail bound trains: personnel cost optimized high volume transport over longer distances in underground and open pit mines e.g. to transport ore from the production areas to the shaft or directly to the preparation plant via a ramp.

For such applications, the train cars can be designed to automatically unload to the side. For this purpose the train moves through an unloading installation overhead a bunker similar to those used with rail bound trains: Each care frame is locked inside an unloading rack while the bucket tips to the side during a slow move of the train through the unloading rack.

As the software is not locked to certain setups of the cars in terms of number of axles, car dimensions and loads, the mechanic design can be made very flexible also including standard heavy truck buckets as well as special designed buckets and undercarriages.

A big advantage of such applications in mining is the fact that all the expensive tunnel infrastructure is not usable exclusively to rail bound train traffic only. Due to the flat driving surface all tunnels also can be used for other transport purposes.

Some underground mines are today organizing mass transport by a separate train transport level which is located underneath the production level of the mine. Such train transport level conforms a huge investment which has to be started and performed long time before ore excavation can be started on the new production level. This means that enormous amount of capital is bound in the transport level. The new technology running trains right on the production level has several advantages, even if taking into consideration that separate tunnels for the train traffic may be needed:

- No early capital binding in a dedicated transport level
- Transport tunnel infrastructure can be extended "just in time" with the progressing production

Figure 4. VirtuRail Bulk Material Train draft.

- Mass transport can be performed up/down ramps thereby connecting different mine levels
- The transportation tunnels can be used for other traffic; in coming applications also in coexistence with autonomous trains and vehicles in mixed traffic setups

First studies for such applications are already under way showing the positive impact on operations and economy of underground mines. Also in surface mining, VirtuRail trains have the potential to become an alternative to conveyor belt installations or traditional truck transport. Other areas of interest cover any transport applications on private ground e.g. container transport in harbors.

REFERENCES

BBT 2018, Press Release "The Brenner Base Tunnel: The Tunnel Boring Machine is breaking world speed records through the mountain", BBT SE, Wien, 2018.
STRABAG 2018, Press Release "World's first autonomous supply of a Tunnel Boring Machine using trackless VirtuRail trains", STRABAG SE, Wien, 2018.

Interaction of man and machine: Lessons learned from aviation

Finn Hovgaard
Airline Captain (SAS), Denmark

Christoph Mueller & George Biro
MobileTronics GmbH, Ladbergen, Germany

ABSTRACT: In aviation, accidents and incidents are followed up and investigated much more thoroughly than in any other industry. This is why the aviation industry should call the attention from other industries when it comes to draw experiences from the consequences of combining highly automated systems with human operators. Based on examples from aviation the paper transfers experience from modern aircraft to highly automated machines in mining and tunneling and gives suggestions to the engineers and developers mainly proposing them to avoid implementing automation which can bypass and/or distract the human control in a complex situation where a human brain must interact with advanced computer programming, instead of taking over full and direct control in order to solve an emergency situation.

1 INTRODUCTION

Modern vehicles, machines and also aircraft are equipped with computer based automated control to a steadily increasing extend. A major reason for automation often is often the aim to reduce the number of human errors and to relieve the operator from "*repetitive or non-rewarding tasks for which humans are less suited*" (Skybrary 2018).

By automation therefore, the number of operator inputs is reduced as the automation takes care of most routine tasks, but this, in turn, makes the impact of every remaining human decision on the entire operation much higher (Mueller 1986), as by example:

- In an aircraft a single wrong manual control input is simply compensated by the next manual command; However an undetected wrong waypoint input into the Flight Management System defining the entire route may have severe consequences.
- A wrong input from the operator to lower the cutting board of a harvester results in cutting the plants too low, but it is easy and uncomplicated for the operator to detect and then compensate by a simple corrective input. A wrong preset value in the auto-level electronics results in an entire field to be cut wrongly if undetected or ignored.
- Drilling one hole from at a slightly wrong position when operating a Drill Rig manually has less impact on operations than running an automatic rig on a completely wrong electronic drill pattern.

The more automation is involved in operation, the more the human operator gets uncoupled from the basic operation of the equipment: Every driver of a car using "Driver Assistance Systems" knows how long time it takes to realize what was happening when suddenly an aural warning informs about the unavailability e.g. of the distance cruise control or the lane departure assistant due to e.g. heavy rain, snowfall or simply a failure of the system. If this happens while driving at 120 km/h (about 33 m/second) on a road lane which is only 3,5 m

wide, you certainly do not want to spend unnecessary time with recognition and analyzing as you most likely need to act intuitively, swift and with full manual control in order to save your expensive new car with all the built-in electronic features and gimmicks.

Such comparable situations would even be worse during remote operation, as a remote operator is uncoupled from all local impressions which the pure data based automation is not able to provide to the operator (e.g sound, smell, vibration, visual surroundings or environmental impressions not related to the machine itself).

In case of a severe failure or an emergency, a car driver often have the option to stop at the roadside and call assistance. This option is not available to pilots flying through extremely cold thin air at a speed of 800 km/h at an altitude of 10.000 m. The pilots must keep controlling the aircraft and at the same time begin to evaluate error messages, analyze the root cause behind the situation, exclude non-essential consequentially derived warnings, apply relevant checklists and procedures while handling communication with the passengers, cabin crew and ATC. On top of this comes decision making about a possible diversion and a lot of other challenges. Spending too much time with performing everything by the book in such situations can in some cases even worsen the situation as valuable time is lost: Especially during emergencies timely behavior often is much more important than reaching the absolute precision (King 2016). "*Get the people down, the rest we organize during descend*" according to a main aviation principle of "*Aviate – Navigate – Communicate*".

From the above it is obvious that the more clear and unmistakable the situation can be presented to the pilot (operator), and the less complicated a direct control can be established the less time is needed to recognize and analyzing the situation, which in turn can save lives.

Reviewing only a few accidents from the past 30 years, as outlined below, a subjective impression arises that these important principles slowly are covered by complex procedures, increased automation and in some situations, an extreme information overflow, which is far away from the capacity of any human operator.

The experience from aviation as the industry with best incident and accident investigation is of major interest for operation of any kind of highly automated machinery. Understanding the consequences may help also in mining to design highly automated machines as well as remote operation centers that, in the best possible way, put the human operator into the center of every possible situation no matter the level of automation. This principle will maybe sometimes lead to a decision not to implement areas of automation in a "Man-Machine" context which however might be the right solution. (European Agency for Safety and Health at Work identifying "the human machine interface as an emerging risk" EU-OSHA 2009).

2 HUMAN – MACHINE INTERACTION RELATED AVIATION ACCIDENTS

In order to be able to draw conclusions from examples a few typical aviation accidents shall be briefly discussed with their influence of the Human-Machine Interface:

2.1 *QF32 near Singapore 2010*

Quantas flight 32 was a passenger flight from London to Sydney via Singapore on November 4th 2010served by an Airbus A380 aircraft. Shortly after takeoff from Singapore Changi Airport it suffered an uncontained engine failure and returned to Singapore to make an emergency landing.

During the emergency which caused a large number of aircraft systems to fail, the information management in the cockpit became a major issue: The "Electronic Centralised Aircraft Monitoring" (ECAM) system gathers data from 250,000 sensors and parameters to manage 1320 checklists (de Crespigny, 2018). It requires the pilots to work these checklists in an order prioritized by the ECAM system. "We actioned 100 checklists in the air and another 20 on the ground … The result was that the cockpit was one of the most stressful environments it's possible to imagine." (de Crespigny, 2018). On this flight, 5 experienced pilots were on the flight deck (ATSB 2013). Nevertheless, "it took about 50 minutes for the flight

crew to complete all of the initial procedures associated with the ECAM messages" (ATSB 2013). The Australian Transport Safety Bureau (ATSB) later spent 966 days investigating what exactly happened. Captain de Crespigny states about this situation: "We faced what felt like an overwhelming barrage of urgent checklists, some replaced so quickly by the next one that we didn't have time to take them in." (ATSB 2013).

Fortunately, the plane was controllable and they had time to work with this flood of messages as they nevertheless had to burn off fuel to reduce safety risk by lowering the weight and thereby runway length needed for landing.

2.2 *AF447 over the South Atlantic 2008*

Air France Flight 447 was a scheduled passenger flight from Rio de Janeiro, Brazil, to Paris, France, which crashed on 1 June 2009. The Airbus A330 stalled at high altitude and did not recover, eventually crashing into the Atlantic Ocean. All 228 passengers and crew died.

According to the final investigation report (BEA 2012) the plane encountered inconsistencies between the airspeed measurements most likely caused by ice crystals blocking the pitot tube sensors. The autopilot disconnect as a result. Then the crew reacted incorrectly and ultimately caused an aerodynamic stall from which it was not able to recover.

The design of the Airbus Flight Guidance System is designed to alter between different "LAWS" depending on the available sensor input to the three Air Data Computers and Autopilot. In this case the Flight Management System had changed from "NORMAL LAW" to "ALTERNATE LAW". This change of "law", which have a huge impact on the redundancy systems and the flight envelope protective system is not directly displayed to the pilot but must be interpreted by the pilot via some missing information and "X" marks in the corners of the instruments. One of the consequences of the automatic transition from "NORMAL LAW" to "ALTERNATE LAW" is that the automatic aircraft stall protection is lost.

The final investigation report explicitly mentions "The lack of a clear display ... of the airspeed inconsistencies identified by the computers" as well as "the absence of any training, at high altitude, in manual aeroplane handling" (BEA 2012) and in related airspeed inconsistency situations. Some systems generated failure messages only about consequences but never mentioned the pitot tubes as the origin of the problem.

2.3 *JT610 Lion Air Flight near Jakarta 2018*

The Lion Air flight JT610 was a domestic flight from Jakarta to Pankal Pinang in Indonesia. The nearly brand new Boeing 737 Max 8 aircraft crashed into the Java Sea 13 minutes after takeoff. Nobody of the 189 people on board survived.

A preliminary investigation report reveals flight control problems noticed by passengers and crew on previous flights and problems with the airspeed and angle-of-attack sensors:

The airplane was equipped with a new stall protection system. This system may have been supplied by wrong data from the faulty Angle-of-Attack sensor which caused the stall protection system to initiate a dive. This system was overriding the contradictory (correct) human inputs to recover from the dive. The plane crashed into the sea. (AVHerald 2019).

2.4 *LH044 Hamburg 2008*

The flight from Munich to Hamburg was operated by an Airbus A320 on March 1st 2008 in significant gusting crosswind conditions following a major storm system in Europe. The left main gear touched the runway but lifted off again, the right hand wing rose rapidly causing the left wing tip to strike the runway surface and the aircraft veer to the left before the airplane was recovered by the crew and a go around commenced (AVHerald 2010).

The investigation report states: "The investigation has shown, that not a single mistake by involved persons, not a malfunction of the airplane and not a deficiency in the organisation led to the wing contacting the ground, but a combination of multiple factors that all such incidents and accidents have of course" (AVHerald 2010).

Related to the Man-Machine Interface the investigation report mentions the fact that the standard Airbus flight control system, per design, is modulating manual pilot flight control inputs in different ways, depending on the flight situation. This means that a given manual input will have different impact on the control surfaces depending on whether the plane is airborne, in flare (shortly before landing) or in ground mode.

Both pilots made compensating inputs to the controls, however due to the first ground contact the movements of the control surfaces were limited making it impossible to compensate the roll. The manufacturer stated that "Had the sidestick input been applied 1,5 seconds earlier, … the left hand bangle would have been limited to 10 degrees" and thus no ground contact would have occurred (AVHerald 2010).

As stated above, this incident investigation could not point out a single factor as the main reason for the ground contact. The pilots did what was expected from them and the Airbus Flight Control System did exactly what it was designed to do, but in between, there might have been a lack of closed loop between "man and machine".

2.5 IT148 Air Inter near Strasbourg 1992

The flight was a scheduled passenger service from Lyon to Strasbourg in France. On 20 January 1992, the aircraft in darkness crashed in the Vosges Mountains while circling to land at Strasbourg Airport. 87 of the 96 people on board were killed.

The investigation showed that the pilots most probably made a wrong input into the Flight Control Unit (FCU). With the, at that time new, autopilot system, pilots were able to select different flight path modes: A vertical speed displayed as a two digit number where the first digit represented the whole thousands and the second digit represented the hundreds of feet the pilot wanted the aircraft to climb/descend with. (rate of climb/descend). Or a Flight Path Angle mode (FPA) where a specified angle could be set, e.g. a 3.3 degrees angle of descend. This value was set in the same readout window as the rate of descend and the only difference in the two very different situations was the "dot" between the two digits. That means that a set value of "33" gave an input to the Flight Director to climb or descend with 3300 ft./min. whereas "3.3" was a command to follow a flight path angle of 3.3 degrees.

Both modes share the same selector knob as well as the display and have only a small push button to toggle the modes and also similar mode indicators "V/S" versus "FPA". (Johnson 1995).

It is anticipated that the pilots were typing in "33" while the FCU was in Vertical Speed Mode, which means 3300 ft/min vertical speed rather than selecting "3.3" in Flight Path Angle mode in order to achieve the regular approach slope of 3,3°. During darkness, in turbulent conditions and under high workload it is understandable that such details as a tiny dot between two digits and a small text ("VS" contra "FPA") can bee overseen by two humans under a considerable stressful working pressure.

Motivated by this accident an experimental study was carried out by the Aeronautical Systems Laboratory of the Massachusetts Institute of Technology in 1995 about the flight crews mode awareness (Johnson 1995). The study was carried out in simulator experiments and resulted in the conclusion that out of 12 pilots 10 were not able to detect an error in the descent rate caused by unintended activation of the Vertical Speed mode before significantly deviating from the glide path.

Later, the aircraft manufacturer modified the display so it now shows 33oo in Vertical Speed mode. This modification is a clear indication of the originally wrong user interface design.

2.6 Classification

In the above mentioned examples the Human-Machine-Interface was at least a contributing factor to the accidents and incidents or it caused additional workload and distraction of the human from the essential tasks.

From these examples of aviation accidents we are trying to classify Human – Machine Interface (HMI) related accidents and incidents into the following causal categories, whereas

accidents and incidents mostly are multi causal and seldom only fall only into one single category:

1. Designed behavior of the automation different from what the operator would intuitively expect as in examples IT148, LH044, JT610, QF32.
2. Errors in the automation system and the impossibility of the human operator to couteract as the automation prohibits or rejects the "intuitive" inputs as wrong as it was the case probably in JT610.
3. Lack of in depth training in handling the rare situations, where the automated system will provide the pilot with e.g. false flight guidance display inputs. Such situations often calls for the pilot to act against what he has been trained to do during his basic pilot education and resulting wrong behavior of the human in extraordinary situations as in the AF 447 example; Sometimes even in combination with blindly following the advises of the automation system, even when they originate from wrong sensor data as in AF 447.
4. Distraction from the essential tasks and mental overload caused by the automation in extraordinary situations (QF32).
5. Unquestioned believe in the computer instruments "What the computer tells us should be right" as in AF447.

In all cases it can be said that the highly automated systems, which are designed to help in safeguarding the aircraft and even take up for most human errors, suddenly either fails or end up in special situations none of the software designers ever have foreseen could happen. In these rare cases the pilot is expected to, in a very short time, both recognize, analyze and apply countermeasures which he never have been trained nor faced before in his career.

3   AUTOMATION AND MANUAL OPERATION

Several accident investigations with lucky outcome revealed that the pilots were mainly relying on their experience from operation of non or less automated airplanes. In the above mentioned examples this applies especially to the QF32 case. The captain of the QF32 flight, Richard de Crespigny states: "… I figured there had to be another way out of this mess. Sometimes we have to create our own novel solutions." (de Crespigny, 2018). He then landed the aircraft using routines from his earlier air force training. With respect of testing the function of all remaining systems needed for landing he states "… this is not something that would normally ever be done in an aircraft with passengers aboard, but we were a long way from normal" (de Crespigny, 2018).

Another example is the famous and well known glider landing of the A320 in the Hudson river in 2009: The pilots were sure about they couldn't make it to one of the airports, so based on their expertise (Cpt. Sullenberger also had glider experience) they regarded this as the best possible solution (NTSB 2010). Would a computer ever have chosen this option?

Both crew finally made their decisions following the "TLAR" principle, because they realized that the situation never had been foreseen by the automation designers and thereby rendering the pilots alone with the problem.

"TLAR" means "That Looks About Right". Based on your experience it allows you "to take action quickly without having to first make precise calculations. In all of life, timeliness is often better than perfection. Striving for perfection can sometimes lead to paralysis and inaction, and distract from situational awareness" (King 2016).

In several reports it is also stated that the computers gave distracting warnings while the crews were trying to recover. Some felt distracted but ignored them like QF32 during landing (de Crespigny 2018, AISB 2013). Other crews followed the wrong warnings into the disaster, not realizing that these alarms were basing on erroneous sensor data like in AF447 (BEA 2012).

An important aspect in this context is the operator training and the ability of operators to correctly assess a situation. Operators of manual machines are aware of and know by their experience and in the end by "intuition" ("TLAR") how to handle the actuators, regardless

whether actuators are control surfaces of an airplane or hydraulic cylinders of a drill boom or on an excavator.

Operators of automated equipment however are trained to precisely follow procedures or checklists and how to make the correct inputs so the automated machine can perform it's tasks according to the programmed routines. Therefore an operator of a drill rig who only drills in auto mode only has very limited skills in manually controlling the feed or in moving the booms manually to a new position.

Automation moves the tasks of the operator from being an active part in the control loop into the role of a human monitoring function. This in turn also results in the inability of the human to take over manually within the shortest possible amount of time as he needs some time to regain full situational awareness which is required for a correct action in an extraordinary situation. This also requires training together with maintaining manual operation skills (FAA 2013).

In 2013, the American Federal Aviation Administration (FAA) issued a "Safety Alert for Operators" ("Operators" meaning airlines in this context) with the purpose "to promote manual flight operations when appropriate" (FAA 2013).

The background of this Safety Alert is described as follows: "A recent analysis of flight operations data (including normal flight operations, incidents, and accidents) identified an increase in manual handling errors. The Federal Aviation Administration (FAA) believes maintaining and improving the knowledge and skills for manual flight operations is necessary for safe flight operations."

Under regular operating conditions, modern aircraft are not designed to be operated "fully manual", meaning with manual control of the control surfaces and, using manual thrust control and, in many cases, switching off the Flight Directors which normally gives steering inputs to the primary flight display (PFD). Consequently, following this safety alert by training manual flying during regular flights would mean to intentionally switch off certain systems. Such an action normally only would be performed in simulator training, as it may be regarded a safety risk during regular operations.

In some critical situations the automation system even prevents the pilot from counteracting an unwanted aircraft behavior by taking over the controls with full authority and direct correlation between the manual input and the movement of the control surfaces (Lionair 2018, LH044). Such situations can occur, either because of software sequences intended for safeguarding the aircraft (LH044) or because the electronics rely on insufficient or wrong sensor input (Lionair 2018).

In such situations it is very difficult for the pilot to recognize and analyze the reason why the aircraft suddenly behaves in an unwanted way. Every pilot will instinctively try to counteract with taking over manually and regain a safe flightpath with his controls, but in some cases this is impossible because the electronics has deselected or modified the manual control inputs from the pilot. Therefore the pilot must locate and disconnect the switches for e.g. the air data computers on the overhead panel in order to regain control over the aircraft. To locate and switch off such systems craves that the pilot divert his attention totally from the flight instruments and the look-out. Such a task can be rather challenging, especially if the aircraft is in an almost vertical dive at low altitude!

In a fully human centered design, despite of all technological advance, machine learning, artificial intelligence etc., the pilot or operator must have the full authority, at any time, to regain a regular and unobstructed manual operation mode without diverting his attention from his primary controls and instruments. If this is not possible, it should be considered not to include a human operator in the process at all, because the risk of Man-machine related errors then will be too high.

4   HUMAN CENTERED AUTOMATION DESIGN

Already in 1996, NASA outlined in a technical memorandum the principles for Human Centered Automation Design (Billings, 1996):

1. Responsibility and command authority: "Automation is able to limit the operator's authority, and in some cases it is not obvious to the operator that this has occurred." and further: "If the human operator cannot effectively oversee and retain management authority over his tools, he has lost authority over the entire operation".

2. Operators must be involved: As long as machines are not completely autonomous, no one questions the necessity for operator involvement at some level; the questions relate to the degree of involvement. Operators often become preoccupied by details at the expense of loosing "the big picture" of their operation. The background is the design philosophy "If it is technically and economically feasible to automate a function, automate it" (Douglas 1990, cit. by Billings 1996).

3. Operators must be informed: Glass Cockpit technology has all but erased the problem of insufficient data in the system. "Data, however is not information. It becomes information only when it is appropriately transformed and presented in a way which is meaningful to a person who needs it in a given context."

4. Humans must be able to monitor the automation: This sounds obvious, however often automation is "strong and silent" about it's work, leaving humans to wonder about what it is doing. The "quiet and dark cockpit" also known as "Black Panel Technology" reflects this philosophy by giving an indication only when something is not operating properly. However due to the fact that automation moves human decisions to a higher, strategic level, the automation also needs to inform the operator positively about what it is doing in order to enable the operator to supervise it's correctness.

5. Automation must be predictable: Because of the logical complexity of modern digital systems, they may fail in ways that are quite different from "physical" systems. This increases the probability that the operator's mental model will not fully account for it's actual performance. Only if an automation's normal behavior is predictable, operators are able to detect subtle signs of failure. This fact emphasizes the importance of building the mental models during training and the importance of simplicity in functional design.

6. Automation must monitor the human: Just as machines are prone to failure also the human is subject to making erroneous decisions. Human error contributes to roughly 80% of all aviation accidents. Audible beeps are frequently used; In order to shorten the time to re-gain situational awareness, audible clear text voice output would be optimal.

7. Communication of intent: Cross monitoring between man and machine and vice versa can only be effective if the monitoring agent – whether human or machine – knows what the monitored agent is trying to accomplish, and in some cases, why! These intentions must be explicit and communicated to the other intelligent agents in the system. While communication from the machine to the human technically can be achieved by quite simple computer peripherals, communicating the true intention from a human to the machine can be a big challenge or even impossible as the computer software has to be prepared (programmed) for every – foreseeable – case.

Applying these principles to the aviation accidents in the first chapter it can easily be questioned whether the principles of Human-Centered Automation Design are met by the design of modern airplane automation systems.

5 HOW ARE THINGS PRESENTED – THE ROLE OF DISPLAYS

As long as partly automated machines in dialog with human operators will be used in any industry, the interaction between human and machine will be a crucial factor.

Especially in the IT148 accident misleading display information played an important role as factor contributing to the accident which was confirmed during the related MIT study (Johnson 1995).

During regular operation, displays have to show relevant information, not raw data. In case some information has to be deemed unreliable (e.g. due to a sensor defect), it may be better to

show no value at all rather than showing wrong or "last available" values, possibly together with a small "unreliable" indication. No value at all may intuitively trigger the human to use common sense or other available information for decision making.

Humans tend to believe more in electronic displays than in their personal impression. And this becomes more and more visible as more the human is uncoupled from the manual control tasks. Consequently, a wrong value on the display not questioned by common sense may lead to wrong decisions.

Similar the situation of the error messages. According to the Human Centered Automation principles, data "becomes information only when it is appropriately transformed and presented in a way which is meaningful to a person who needs it in a given context." In the QF32 accident it can be questioned, whether all the "information" shown on the displays was really "meaningful to a person who needs it in a given context". The context was a multi system failure situation beyond the design of the automation system. So working all these checklists caused a lot of questionable additional stress to the crew. In case of QF32 the crew worked 50 minutes on 100 ECAM checklists (ATSB 2013), being lucky that they had control of the plane. In case of the need for an immediate landing only about an average of 17 minutes are available to bring the plane on the ground.

6   AUTOMATION OF A NEW MOBILE UNDERGROUND TRANSPORT SYSTEM

During the past three years, MobileTronics was developing the VirtuRail® system for rubber tired track-in-track trains for applications in mining and tunneling. In order to have all axles precisely following the first axle using electronic control systems and for automatic guidance of the train in tunnel environments, this system uses complex computer systems. In addition, safety requires that electronic brake and steering functions have to be fail-operational requiring automation system redundancy.

Steering all 18 or more axles manually to follow on one single "virtual rail" simply is impossible to be carried out manually. This means that this function only can be provided by a fully electronic system. From the beginning it was clear, that the operator has to be in the focus of the design in order to support him to maintain situational awareness under all operational conditions, even when he is not able to see along all the train. Compared to an airplane this is a simple application; However the system needs to be absolutely reliable and usable for mining and construction environments.

The Human Centered Design of the user interface was therefore developed with assistance from an aviation professional, covering his experience from operation of "traditional" airplanes, from the design of simulator training and from the operation of modern highly automated aircraft.

The goal of the automation system was to allow manual operation, driver assisted operation and ultimately also fully autonomous operation. A basic recommendation from aviation and consequence from partly confusing status information on modern aircraft was the clear and unambiguous design of the operation modes easy to understand for the operators together with a clearly visible mode indication on the electronic display:

- Autonomous: Steering and speed controlled automatically, no driver interaction needed
- Automatic: Steering of all axles is performed automatically basing on the route section selected by the driver, speed controlled manually – electronic speed and steering angle safety limits apply depending on the route section parameters
- Manual: Manual steering of the first axle, the trailing axles are controlled by the track follow algorithms
- Alternate: One of the redundant automation systems is inoperable, driving is possible at reduced speed, track follow system active potentially with reduced availability
- Service: No interlocks, only accessible to maintenance staff

Steering of the trains is – like in modern aircraft – fully electronic. For steering the driver uses a safety certified electronic joystick which also contains buttons and dials for the most

Figure 1.   Screenshot of a modern E-Drive vehicle.

used operational functions. During driving, regardless whether manual or automatic, the driver does not need to take the hand from the joystick to handle all driving related functions.

For control of speed and operational brake in the first system electronic pedals were used like in a car. On pilot recommendation this was changed in the second generation to a throttle (speed) lever left of the driver seat which integrates (electric) traction, energy recuperation and brake actions.

During machine startup, the display shows an electronic check list for the checks the operator has to perform prior to start driving; The system cross checks the load on all cars to determine the correct brake pressures for each individual car and informs the driver about possible discrepancies.

While driving, the display only shows the information essential for driving like speed, energy flow, battery status. All information which is regarded normal and within the regular operation envelopes is not shown on the display. According to the "Black Panel" technology, irregularity information is only communicated when needed. For this purpose, easy to understand graphic symbols are used together with a clear traffic light like color code.

In Automatic mode, when the guidance system automatically steers the train in the tunnel the driver does not have to move the joystick. However, when the driver deems it necessary e.g. to prepare for meeting opposing traffic which is not yet within visibility of the sensors, the automation falls back from Automatic to Manual mode. When the driver wishes to return to Automatic, he intentionally has to push the corresponding button in the joystick.

Due to this cleanliness of design and operation, drivers only need a short training, despite of the system complexity of 12 networked controllers, guidance computers and guidance sensors. At the same time the operation experience of close to 3 years and over 200.000 km shows that no incidents or Human-Machine interaction related issues occurred in this safety related automation system.

7   CONCLUSIONS

As long as humans are interacting with automated machines of any kind, the interaction between man and machine remains the most critical part in operation (EU-OSHA 2009). The examples from aviation lead to the hypothesis that manual operation with well trained operators is safe as well as fully automatic/autonomous operation under well defined and foreseeable conditions. The mixed operation however may be problematic if the principles of Human Centered Automation Design are not met.

A skilled operator should always have the possibility to override and take over manually and if needed bypass the automated systems in order to obtain full manual control. Related to a disabled underground vehicle it may be important to be able to move it out of the way to keep the emergency escape routes clear similar to an aircraft always need to be able to land safely.

Automation system designers should learn from related experience and design not only the displays but also the entire interaction with the operator around the people, a way of design which is significantly different from the traditional engineering centered approach.

With today's artificial intelligence and machine learning it is also possible to learn electronically from operational data recorded during manual operation. A precondition for this however is that during machine learning an experienced operator is controlling the machine in a way not obstructed by computer interaction.

REFERENCES

ATSB 2013, Inflight uncontained engine failure Airbus A380-842 VH-OQA, Final report AO2010-089, Australian Transport Safety Bureau, 2013.

AVHerald 2019 Crash: Lion B38M near Jakarta on Oct 29th 2018, aircraft lost height and crashed into Java Sea, wrong AoA data, online at www.avherald.com.

AVHerald 2010 Report: Lufthansa A320 at Hamburg on Mar 1st 2008, wing touches runway in cross wind landing, online at www.avherald.com.

BEA 2012, Final Report on the accident on 1st June 2009 to the Airbus A330-203 registered F-GZCP operated by Air France flight AF447 Rio de Janeiro – Paris, Bureau d'Enquêtes et d'Analyses pour la sécurité de l'aviation civile, Paris 2012.

Billings, C. Human-Centered Aviation Automation: Principles and Guidelines, NASA Technical Memorandum 110381, February 1996.

de Crespigny, R. 2018 Inside the cockpit of QF32: How Australia's worst aviation disaster was averted, online at: news.com.au, retrieved 2019-01-21.

EU-OSHA 2009 The human machine interface as an emerging risk, European Agency for Safety and Health at Work, DOI 10.2802/21813.

FAA 2013, Safety Alert For Operators SAFO 13002, issued 2013-01-04.

Johnson, E. 1995, EXPERIMENTAL STUDY OF VERTICAL FLIGHT PATH MODE AWARENESS, ASL of the MIT, Camebridge MA, 1995.

King, J. 2016 Why learning to fly by TLAR is important, in: Flying Magazine October 2016.

Mueller, C. 1986 "Elektronik an Landmaschinen", Diploma Thesis, Osnabrück 1986.

NTSB 2010 Aircraft Accident Report … US Airways Flight 1549, document number NTSB/AAR-10/03 PB2010-910403, Washington DC 2010.

Skybrary 2018 Cockpit Automation – Advantages and Safety Challenges, online at www.skybrary.aero retrieved 2019-01-21.

Taylor & Francis
Taylor & Francis Group
http://taylorandfrancis.com

Author index

Proceedings in Earth and geosciences series

The *Proceedings in Earth and geosciences* series contains proceedings of peer-reviewed international conferences dealing in earth and geosciences. The main topics covered by the series include: geotechnical engineering, underground construction, mining, rock mechanics, soil mechanics and hydrogeology.

1. Tunnels and Underground Cities: Engineering and Innovation meet Archaeology, Architecture and Art
   Edited by Daniele Peila, Giulia Viggiani & Tarcisio Celestino
   ISBN: 978-1-138-38865-9 (Hbk + USB)
   ISBN: 978-0-429-42444-1 (eBook)
2. Geotechnics Fundamentals and Applications in Construction
   Edited by Rashid Mangushev, Askar Zhussupbekov, Yoshinori Iwasaki & Igor Sakharov
   ISBN: 978-0-367-17983-0 (Hbk)
   ISBN: 978-0-429-05888-2 (eBook)